ІНСТИТУТ МОЛЕКУЛЯРНОЇ БІОЛОГІЇ І ГЕНЕТИКИ
НАЦІОНАЛЬНОЇ АКАДЕМІЇ НАУК УКРАЇНИ

Кваліфікаційна наукова праця на правах наукової доповіді за сукупністю статей

Мошинець Олена Володимирівна

УДК 579.2+579.6+606+616-095+616-03

ДИСЕРТАЦІЯ

Біотехнологічні і структурно-функціональні особливості і клінічні аспекти біоплівок грамнегативних бактерій

03.00.20 - біотехнологія (біологічні науки)

Подається на здобуття наукового ступеня доктора біологічних наук

Дисертація містить результати власних досліджень. Використання ідей, результатів і текстів інших авторів мають посилання на відповідне джерело.

О. В. Мошинець

Київ

2025

Присвячується пам'яті мого дорогого вчителя та великого друга,
видатного мікробіолога і дослідника еволюції,
і просто неймовірної людини,
з якою мені пощастило працювати сімнадцять з половиною років,
доктора Ендрю Спайрса

Dedicated to the memory of my dear teacher and great friend,
an outstanding microbiologist and evolutionary scientists,
and simply an incredible person with whom I was fortunate to work for seventeen and a half years,
Dr. Andrew Spiers.

АНОТАЦІЯ

Мошинець О. В. Біотехнологічні і структурно-функціональні особливості і клінічні аспекти біоплівок грамнегативних бактерій. - Кваліфікаційна наукова праця на правах наукової доповіді за сукупністю статей.

Дисертація на здобуття наукового ступеня доктора біологічних наук за спеціальністю 03.00.20 «Біотехнологія» (біологічні науки). – Інститут молекулярної біології і генетики Національної академії наук України, Київ, 2025.

Протягом майже всього періоду розвитку клінічної мікробіології за виключенням останніх тридцяти років бактерії сприймались виключно як індивідуальні організми мікроскопічного розміру з індивідуальними властивостями щодо патогенезу, колонізації різноманітних екологічних ніш та стійкості до антибактеріальної терапії. Втім сучасна фундаментальна мікробіологія змінила своє уявлення щодо «персоналізації» бактерій. Починаючи із 1994 року вийшла серія робіт Costerton J.W. в яких було систематизоване уявлення про біоплівки як форму колонізації еконіші при інфекційному процесі. З того часу, традиційні уявлення щодо існування популяцій мікроорганізмів стали змінюватись. Принаймні, стало зрозуміло, чому хірургічна санація осередків інфекції в організмі здатна значно підвищувати ефективність лікування на тлі антибіотикотерапії, чому багато антибіотиків, до яких бактерії чутливі на клітинному рівні, залишаються малоефективними *in vivo* та чому досить старий метод лікування гайморитів введенням розчинів трипсину мав ефективність. Причина всіх цих явищ – здатність бактерій до колективної поведінки, в наслідок якої утворюються надклітинні просторові агрегації – біоплівки.

Біоплівка – просторове угрупування бактеріальних клітин, які міцно вбудовані в шари позаклітинного високополімерного матриксу. Біоплівка з екологічного погляду представляє собою нову, створену бактеріями, еконішу, яка виконує головну функцію – захист бактеріальних клітин від зовнішніх стресів. Перепади температур, посуха, атаки хижаків та токсинів – все це суттєво знижує ефективність стресора якщо ті самі бактерії встигли побудувати біоплівку. Але, біоплівка є динамічною структурою, саме тому в певний час свого онтогенезу вона стає перенаселеною та токсичною для своїх мешканців, тому частина популяції біоплівки переходить у рухливу форму. Таким чином, існує циклічність розвитку біоплівки – від сталої до рухливої форм, а їх існування – від нерухливи прикріплених форм до планктонної популяції. Таке чергування прикріпленої та рухливої форм, або біоплівки та планктону є життєвим циклом бактерії. Фактично біоплівки – це форма існування бактерії та форма колонізації нею еконіші. Біоплівки можуть мати різноманітну локалізацію,

зокрема, на межі розподілу фаз (повітря-рідина, рідина-тверда поверхня), або у товщі рідини.

На клітинному рівні біоплівка є складним багатокомпонентним утворенням. Схематично її можна розділити на дві фракції – на клітини та позаклітинний полімерний матрикс. Біоплівки бактерій утворюються в результаті численних і різноманітних фізичних взаємодій. Бактеріальні клітини всередині біоплівки взаємодіють один з одним шляхом тісних, проміжних і далеких взаємодій за участю клітинних поверхонь, поверхневих структур (наприклад, джгутиків та пілей), компонентів матриксу біоплівки та різноманітних поверхонь розподілу фаз (наприклад, розподіл фаз повітря-рідина).

До складу матриксу біоплівки входять різноманітні полімери, які мають різні ступені специфічності. Наприклад, у складі біоплівки грам-позитивних бактерій часто домінують білки, а у грам-негативних дуже важливим полімером є різноманітні полісахариди. Цікаво, що структура біоплівки сильно залежить від температурних умов. Так, у представників *Proteobacteria* целюлозний оперон (сукупність генів, що відповідають за продукцію целюлози) репресується при 37ºС та активується за умов 28ºС і нижче. Це відбувається тому, що протеобактерії із патогенними властивостями здатні використовувати дві альтернативні екологічні стратегії колонізації: целюлоза їм не потрібна для побудови біоплівки при патогенній колонізації тканин пацієнта, але вона дуже вдало допомагає депонувати вологу та протистояти низькій вологості при вільному сапрофітному існуванні. Дуже розповсюдженими структурними елементами біоплівок всіх бактерій є екзоклітинна ДНК, або еДНК. Цей полімер виконує функції первинного адгезину, депонування поживних речовин та власне структурного полімеру. Для деяких бактерій, наприклад, для *Pseudomonas aeruginosa*, еДНК може бути головним полімером матриксу біоплівки протягом перших 48 годин розвитку. Багато бактерій також використовують функціональні амілоїдні фібрили для первинного прикріплення до поверхні та до компонентів матриксу біоплівки. Не дивлячись на те, що амілоїди є білками, вони є хімічно та біологічно стійкими, малорозчинними та добре адгезуються до еДНК, стабілізуючи таким чином каркас біоплівки.

Феномен біоплівки має дуже велике фундаментальне та прикладне значення для розуміння різноманітних бактеріальних процесів. Зокрема, розуміння біоплівки важливо для очищення поверхонь від небажаних біоплівок, розуміння існування вільноіснуючих (сапрофітних) біоплівкових спільнот та підбір ефективної терапії інфекційного процесу. Біоплівки суттєво знижують діапазон ефективних антибіотиків серед тих, які виявили ефективність у класичних мікробіологічних тестах. Так, треба мати на увазі, що завдяки

великому вмісту еДНК біоплівки *P. aeruginosa* знижують свою чутливість до катіонних пептидів та аміноглікозидів в сотні разів. Таж сама еДНК в біоплівках *Staphylococcus epidermidis* суттєво знижує біодоступність ванкоміцину. Біоплівка – врівноважена система, яка адаптується до зовнішніх стресорів. Через це, ефективний контроль над інфекційним процесом, який так чи інакше асоційований із біоплівкою збудника, можливий за умов комплексного підходу, а саме, раціонального підбору антибіотику та максимального механічного усунення біоплівки. Інфекційні ускладнення, пов'язані із утворенням біоплівки на інертних поверхнях – катетерах, імплантах, металевих конструкціях тощо, потребують усунення інертної поверхні (видалення катетеру, імпланту) та максимальне видалення інфікованих тканин (парапротезна інфекція, остеомієліт).

Такий новий погляд на різноманітні бактеріальні процеси через розуміння біології біоплівок відкриває нові можливості для біотехнологічних і біомедичних технологій. Зокрема, залежність інфекційного процесу від утворення біоплівки залишає вікно можливостей для розробки специфічної антибіоплівкової терапії та створення нових матеріалів із зниженим потенціалом по прикріпленню бактерій та їх колонізації, а використання механізмів регуляції утворення біоплівок може бути використано в різноманітних біотехнологіях, зокрема, аграрного напрямку.

Метою цієї роботи було вивчити структурно-функціональні особливості окремих грамнегативних бактерій, дослідити можливості використання деяких властивостей грамнегативних бактерій в біотехнологіях і клінічно-лікувальній практиці.

В представленій роботі було проаналізовано структурну роль целюлози в біоплівках *Pseudomonas fluorescens* SBW25, зокрема, екотипу (похідного штаму) Wrinkly Spreader (WS) та досліджено роль целюлози в утворенні біоплівок диким ізолятом *Bordetella avium* 197N. Біоплівки *P. fluorescens* SBW25 є популярною моделлю для досліджень в області експериментальної еволюції та молекулярної біології. З'ясовано, що адаптивна колонізація у статичних мікрокосмах призводить до утворення мутантного штаму-суперпродуценту біоплівки WS, який колонізує зону меніску (інтерфаза повітря-рідина) і основним компонентом якого є целюлоза. В такому модельному статичному мікрокосмі екосистемна інженерія перших диких колоністів створює нову екологічну нішу для подальшої еволюції популяції і її більш успішної колонізації. На молекулярному рівні до утворення суперпродуценту WS призводять випадкові мутації, які шляхом відбору призводять до селекції мутантів, що накопичують вторинний клітинних месенджер c-di-GMP, що призводить по посиленого синтезу целюлози і утворення міцної біоплівки а зоні меніску. Це у свою чергу дозволяє штаму WS перехоплювати більше кисню, що дифундує в стовп

рідини, і обмежують зростання конкурентів нижче. Можливо, бактеріальна целюлоза виконує не тільки структурні функції, а й використовується для утворення невеликих біоплівок у водоймах, утримуючи бактерії на інтерфейсу повітря-рідина або для утримання їх на твердих поверхнях проти течії води. Целюлозні волокна можуть протистояти стресу висихання в середовищах з обмеженим вмістом води або навіть забезпечувати захист від хижаків протистів і нематод. Звичайно можливо, що целюлоза виконує ряд функцій, якими можна пояснити широке поширення оперону синтезу целюлози серед *Proteobacteria*, які мешкають у різноманітних середовищах.

Синтез целюлози у *Proteobacteria* забезпечується оперонами бактеріальної целюлозосинтази (bcs, від bacterial cellulose synthase), які є широко поширеними. Цікаво, що субодиниці, необхідні для часткового ацетилювання полімеру, здається, обмежені кількома ґрунтовими, асоційованими з рослинами та фітопатогенними псевдомонадами групи ɣ, включаючи *P. fluorescens* SBW25 та кілька патоварів *Pseudomonas syringae*. Однак, оперон bcs із субодиницями ацетилювання також анотований у неспорідненому респіраторному патогені b-групи *B. avium* 197N. Наше порівняння послідовностей білків субодиниць і аналіз вмісту GC підтверджує велику подібність між *B. avium* 197N і оперонами псевдомонад, що дає змогу припустити, що в обох випадках субодиниці синтази целюлози та субодиниці ацетилювання були придбані як одна одиниця. Використовуючи статичні рідкі мікрокосми, ми підтвердили, що *B. avium* 197N експресує низькі рівні целюлози в біоплівках, що утворюються на повітряно-рідинному інтерфейсі, і що міцність біоплівки та рівень прикріплення можна збільшити шляхом підвищення рівнів c-di-GMP, як у псевдомонад. Втім, ми також показали, що сама целюлоза не є критичною для утворення самої біоплівки. Виявлення того, що B. *avium* 197N здатний виробляти целюлозу за допомогою висококонсервативного, але відносно рідкісного оперону bcs, ставить питання про те, яку функціональну роль цей модифікований полімер відіграє під час інфікування верхніх дихальних шляхів або виживання між хазяїнами, і які сигнали зовнішнього середовища регулюють виробництво целюлози.

Ще один важливий компонент біоплівок грамнегативних бактерій – амілоїдні фібрили. Для дослідження цього важливого компоненту було розроблено новий високочутливий (у порівнянні із класичним) зелений випромінюючий водорозчинний амінокетоенольний барвник AmyGreen. Цей барвник майже не флуоресціює у розчині, але дає яскраве зелене випромінювання в присутності амілоїдних фібрил білків. AmyGreen теж є слабо флуоресцентним в присутності біомолекул, які є компонентами клітин, екзоклітинного матриксу або середовища, зокрема в присутності нуклеїнових кислот, полісахаридів, ліпідів,

білків. Таким чином, флуоресценцію AmyGreen використали для візуалізації амілоїдних компонентів екзоклітинного матриксу в біоплівках *Escherichia coli, Klebsiella pneumoniae, P. aeruginosa, B. avium* і *Staphylococcus aureus.* Ефективність

AmyGreen порівнювали з традиційним чутливим до амілоїду барвником Thioflavine T. З'ясувалось, що основною перевагою AmyGreen (концентрація 10^{-5} М) є більш висока чутливість для візуалізації амілоїдних компонентів в біоплівкіх у порівнянні з Thioflavine T (10^{-4} М). Крім того, AmyGreen має меншу селективність до нуклеїнових кислот, що було продемонстровано як в експериментах у розчині, так і при фарбуванні еукаріотичних мезенхімальних стовбурових клітин людини, які було використано як негативний контроль. Таким чином, новий барвник має менший ризик хибнопозитивної відповіді при визначенні амілоїдних компонентів бактеріальних біоплівок. Комбіноване фарбування біоплівки барвником AmyGreen і чутливим до целюлози барвником Calcofluor White демонструє диференційне забарвлення та різну локалізацію забарвлених компонентів, що вказує різноманітність локалізацій полісахаридів та амілоїдів у досліджених біоплівках.

Головним структурним компонентом біоплівки *P. fluorescens* SBW25 WS є целюлоза, але як саме фібрили целюлози інтегруються в успішний матрикс біоплівки було невідомо. В нашій роботі ми також з'ясували, що Також було продемонстровано, що амілоїди також відіграють певну структурну роль в біоплівці *P. fluorescens* SBW25 WS та досліджені мембранні везикули і їхній білковий склад.

Успішність бактеріальної колонізації складних еконіш вимагає індивідуальної відповіді на зміни умов на мікрорівні так само як і кооперацію на рівні угруповання для продукції таких великомасштабних структур як біоплівки. Координація індивідуальних відповідей і відповідей угруповання може бути досягнута шляхом зв'язування внутрішньоклітинних сенсорних і регуляторних систем, опосередкованих біс-(3′,5′)циклічним димерним гуанозинмонофосфатом (c-di-GMP) та іншими сполуками індивідуумів із міжклітинною регуляцією – почуттям кворуму (ПК), що контролює популяцію. Накопичується все більше доказів того, що формування біоплівки багатьма псевдомонадами регулюється як внутрішньоклітинними, так і міжклітинними регуляторними системами, хоча в разі модельної *P. fluorescens* SBW25 WS, у котрій мутації, що підвищують рівні c-di-GMP, призводять до створення міцної целюлозної біоплівки на кордоні розділу фаз повітря–рідина, не було виявлено ніякого свідоцтва залучення кворумзалежної регуляції. Проте наш огляд геному *P. fluorescens* SBW25 виявив потенційний ПК-залежний регуляторний шлях та інші ПК-залежні гени, пов'язані з гомеостазом c-di-GMP, а молекули ПК-сигналінгу було ідентифіковано в культурі. Ці дані

свідчать про можливий зв'язок між c-di-GMP-регуляцією і ПК у *P. fluorescens* SBW25, що дозволяє проводити більш складний і гнучкий контроль продукції целюлози і утворення біоплівки за колонізації ґрунтів і еконіш, асоційованих з рослинами, – природними середовищами існування *P. fluorescens* SBW25.

Утворення біоплівок має велике феноменологічне значення в патогенезі різноманітних інфекційних процесів. Відомо, що захворювання пародонту пов'язані з полімікробними біоплівки та активацією запалення. Було досліджено під'ясенний цитологічний (мікро) ландшафт при пародонтиті, з'ясовано роль езоклітинної ДНК (еДНК) при пародонтиті та запропоновано концепцію ролі імунної еДНК господаря в запаленні при пародонтиті, що може покращити наше розуміння механізмів важких форм пародонтиту. Аналіз під'ясенної біоплівки за допомогою модифікованого методу Холодного виявив низький вміст бактеріальних амілоїдів та високий рівень еДНК в пародонтних біоплівках. Встановлено, що еДНК бактерій становить менше третини загальної еДНК в цитологічному ландшафті при пародонтиті. Вірогідно, що переважна кількість еДНК при пародонтиті вивільняється з нейтрофільних позаклітинних пасток і може мати велике значення у розвитку біоплівок, що викликають пародонтит. Таким чином, еДНК активованих імунокомпетентних клітин господаря може бути основним фактором персистенції бактерій і розвитку патологічного запалення при пародонтиті.

Розуміння патогенетичної ролі біоплівок інфекційних ізолятів відкриває нові фармакологічні можливості для створення альтернативних терапевтичних протоколів, заснованих на антибіоплівковій терапії. Більш того, з'ясовано, що нові комбінації деяких класичних антибіотиків можуть діяти синергічно, що призводить до пригнічення розвитку множинної антибіотикорезистентності. Втім, важко передбачити, яка саме комбінація антибіотиків буде успішною. Стандартний тест на антимікробну чутливість може не виявити таких синергідних ефектів через особливість інфекційного процесу. Крім того, існує фізіологічна різниця між планктонними вільно існуючими та прикріпленими, захищеними біоплівкою, бактеріальними клітинами і, відповідно, чутливість до антибіотиків у таких різних субпопуляцій теж буде відрізнятись. На прикладі номінально стійкої до макролідів бактерії *K. pneumoniae* ATCC 10031 було продемонстровано ефективність кількох макролідів у пригніченні росту біоплівки і здатність азитроміцину підвищувати ефективність таргетного антибіотику метансульфонату колістину при біоплівкових інфекціях, спричинених *K. pneumoniae*, Ця синергетична дія також була підтверджена на колекції госпітальних ізолятів *K. pneumoniae* із високою резистентністю. Ця сама

терапевтична комбінація азитроміцину і метансульфонату колістину була досліджена на розробленій модель рани *in vitro*. Розроблена модель складалась з
тривимірної колагенової губчастої основи, засіяної епітелізованими HEK293 клітинами, яку було занурено в рідинне середовище, що імітує ексудат ранового дна. В цій моделі було підтверджено високу терапевтичну ефективність комбінації азитроміцину з метансульфонатом колістину у пригніченні високорезистентного штаму *K. pneumoniae*. Використання азитроміцину для пом'якщення важкості інфекційного процесу та у комбінації із таргетним антибіотиком було продемонстровано у лікуванні пацієнта, який отримав бойові поранення та обширні ранові інфекції, спричинені мультирезистентними та панрезистентними штамами. Зокрема, пацієнта було успішно вилікувано комбінованою терапією азитроміцином з меропенемом. Отримані результати підкреслюють необхідність пошуку нових ефективних протимікробних терапевтичних підходів як альтернативні стратегії лікування інфекцій із високою резистентністю.

Іншою стратегією протидії розвитку антимікробної резистентності є пошук нових антимікробних речовин методами біомедичної хімії і раціонального драг-дизайну. Втім треба пам'ятати, що специфічні інгібітори із антибактеріальними властивостями для обраних інфекційних штамів можуть мати неочікувані стимулюючі ефекти для інших патогенів. Більш того, такі ефекти мають бути перевірені не тільки в класичних біомедичних моделях, тобто, на рівні рідкої культури (планктонна субпопуляція) і на рівні агаризованих колоній (штучні мікробні агрегації), а і в наближених до умов реального інфекційного процесу умовах – на біоплівках. Відштовхуючись від цього уявлення було досліджено нову антистафілокову речовину. Зокрема, 2-(2-аміно-3-хлор-бензоїламіно)бензойну кислоту, яка здатна інгібувати сортазу А *S. aureus* із папаметрами IC 50 59,7 мкМ. Антибактеріальний і антибіоплівковий аналізи також підтвердили високу специфічність сполуки проти двох стандартних штамів і трьох госпітальних ізолятів *S. aureus*. Втім, було досліджено, що ця сама речовина не впливала на рівні планктону двох грам-негативних штамів, зокрема, *P. aeruginosa* PA01 і *K. pneumoniae* ATCC 10031. Цікаво, що ця речовина не впливала на розвиток біоплівки *P. aeruginosa* PA01, але стимулювала чотирикратний ріст біомаси біоплівки *K. pneumoniae* ATCC 10031. Таким чином, при дослідженні нових антимікробних речовин важливими є дослідження неочікуваних стимулюючих ефектів на альтернативні збудник інфекцій.

Біоплівки є не тільки прямим патологічним фактором, а ще й опосередкованим через підтримання пулу генів антибіотикорезистентності, який динамічно розвивається в Україні. Війна, що триває в Україні, додатково погіршила стан із антибіотикорезистентністю

грамнегативних бактерій. Наші дані свідчать про зміну моделей резистентності, особливо серед аміноглікозидів і колістину, порівняно з попередніми даними. У той час як карбапенемази типу NDM і OXA-48 продовжують домінувати, ідентифіковано широкий діапазон інших генів резистентності. Значна частка фенотипово резистентних штамів без виявленого генотипу, пов'язаного з резистентністю, також свідчить про те, що в популяції українських грамнегативних інфекцій домінують додаткові механізми резистентності.

Саме через те, що біоплівки підтримують пул генетичних факторів резистентності, вибір ефективних біоцидів, які використовуються в рутинній лікарняній практиці, повинен враховувати роль дезінфікуючих засобів у підтримці та розвитку місцевого резистому.
Деякі біоциди гіпотетично можуть впливати на перенесення генів резистентності до антибіотиків у лікарняній мікробній популяції. шляхом сприяння горизонтальному генному переносу та подальшому зберіганню генів антибіотикорезистентності в навколишньому середовищі. В нашій роботі ми дослідили чим відрізняються біоциди по дії на еДНК із зрілих біоплівок двох опортуністичних модельних штамів *P. aeruginosa* ATCC 27853 і *S. aureus* ATCC 25923. Дія чотирьох груп біоцидів, зокрема, спиртів, перекису водню, сполук четвертинного амонію та полімерний біоцид полігексаметиленгуанідин гідрохлорид (PHMG-Cl) досліджували із використанням біоплівок *P. aeruginosa* ATCC 27853 і *S. aureus* ATCC 25923. Більшість біоцидів, за винятком PHMG-Cl і 70% етанолу, викликали значне вивільнення еДНК. Було показано, що PHMG-Cl блокує розвиток біоплівки при використанні в концентраціях 0,5% і 0,1%. Це може бути пов'язано з утворенням комплексів ДНК–PHMG-Cl. За допомогою молекулярного докінгу запропоновано модель зв'язування PHMG-Cl з парами основ A-T. Було виявлено, що PHMG-Cl зв'язується з високомолекулярною ДНК і плазмідною ДНК, інактивація еДНК на поверхнях продовжується навіть після 4 тижнів після обробки поверхні біоцидом. PHMG-Cl також ефективно інактивував еДНК у вигляді гену стійкості до антибіотиків, пов'язаного з біоплівкою, що було знайдено в еДНК полірезистентного штаму *K. pneumoniae*.

Утворення біоплівки, або мікрообростання, є основною стратегією бактерій для колонізації поверхні та може відбуватися на поверхні будь-якої природи, де присутні бактерії. Вплив на структуру біоплівки може бути ефективною стратегією зниження мікрообрастання поверхонь. Досліджено декілька шляхів модифікації матеріалів, які призводили до зниження мікрообрастання. Зокрема, запропоновано і досліджено новий термічно стійкий полімерний біоцид полігексаметиленгуанідин 2-нафталінсульфонат, який додано до поліаміду. Було підтверджено антибіоплівкову активність проти

умовнопатогенних бактерій *S. aureus* ATCC 25923 та *E.coli* K12 для полімерів, що містили 7% та

10% полімерного біоциду. Ще один полімерний катіонний біоцид 1-додецилпіридинію додецилбензолсульфонат (PyrC 12-DBS) був синтезований і протестований як потенційний протибіоплівковий компонент як додаток до комерційної алкідної фарби РР-115 (Україна). Модифіковані покриття РР-115/PyrC 12 –DBS, що містили 8% і 16% PyrC 12 –DBS, проявили суттєві антибіопівлівкові властивості проти *S. aureus* ATCC 25923 і *P. aeruginosa* PA01. Також було досліджено можливості зниження мікрообрастання металевих поверхонь шляхом їхньої лазерної модифікації. Така модифікація призвела до суттєвого зниження біомаси біоплівок *P. aeruginosa* PA01 і *S. aureus* ATCC29423.

Втім, феномен біоплівок може також бути використано у створення нових агробіотехнологій. Відомо, що кілька модельних рослин реагують на молекули бактеріального почуття кворуму, зокрема, зміненим ростом коренів і експресією генів, а також розвитком індукованої стійкість до патогенних захворювань рослин. Сполуки почуття кворуму можуть представляти нові активні речовини, які можна застосовувати як праймери для насіння рослин для підвищення стійкості зернових культур до хвороботворних мікроорганізмів та абіотичного стресу та підвищення врожайності. В нашій роботі було досліджено ефекти гексаноїл гомосерин лактону (ГГЛ) на проростання насіння пшениці озимої *Triticum aestivum* L., розвиток рослин та їхню продуктивність на прикладі двох українських сортів пшениці озимої Володарка та Ятрань 60. Досліди проростання *in vitro* показали, що праймування насіння ГГЛ мало невеликий, але значний позитивний вплив на рівень схожості (1,2 х збільшення), розвиток колеоптиля та корінця (1,4-кратне збільшення). В польових дослідженнях протягом двох вегетаційних періодів (2015–16 та 2016–17) також продемонстровано значні покращення біомаси на стадії кущіння (збільшення в 1,4 рази), а також покращення структури посівів. Зокрема, врожайність зерна (збільшення в 1,4–1,5 рази) та якість (1,3-кратне збільшення хорошого зерна). Ці польові результати показують, що бактеріальні ацилгомосерин лактони, такі як ГГЛ, можна використовувати для покращення врожаю зернових культур.

Ключові слова: біоплівка, грам-негативні бактерії, целюлоза, амілоїди, еДНК, почуття кворуму, регуляція, інфекція, біоциди, антибіотикорезистентність, азитроміцин, терапія, праймування рослин.

SUMMARY

Moshynets O. V. Biotechnological and structural and functional features, and clinical aspects of biofilms of gram-negative bacteria. - Qualification scientific work in the form of a scientific report based on research articles.

Thesis for a degree of Doctor of Biological Sciences (D.Sc.) in Biology, speciality 03.00.20 - Biotechnology (biological sciences). - Institute of Molecular Biology and Genetics of the National Academy of Sciences of Ukraine, Kyiv, 2025.

During almost the entire period when clinical microbiology exists, with the exception of the last thirty years, bacteria were perceived exclusively as individual organisms of microscopic size with individual properties regarding pathogenesis, colonization of various ecological niches and resistance to antibacterial therapy. However, modern microbiology has changed the idea of the "personalization" of bacteria. Starting from 1994, a series of works by Costerton J.W. was published, in which the idea of biofilms as a form of colonization of the econiche during the infectious process was systematized. Since then, traditional ideas about microbial populations began to change. At least, it became clear why surgical sanitation of foci of infection in the body can significantly increase the effectiveness of treatment against the background of antibiotic therapy, why many antibiotics to which bacteria are sensitive at the cellular level remain ineffective *in vivo* and why a rather old method of treating sinusitis by introducing trypsin solutions was effective. The reason for all these phenomena is the ability of bacteria to collective behavior, as a result of which supracellular spatial aggregations called biofilms are formed.

Biofilm - a spatial group of bacterial cells that are firmly embedded in the layers of the extracellular high-polymer matrix. From an ecological point of view, biofilm is a new econiche created by bacteria, which performs the main function - protecting bacterial cells from external stresses. Temperature changes, drought, attacks by predators and toxins - all this significantly reduces the effectiveness of the stressor if the same bacteria have managed to build a biofilm. However, a biofilm is a dynamic structure, which is why at a certain time in its ontogenesis it becomes overpopulated and toxic to its inhabitants, so part of the biofilm population passes into a mobile form. Thus, there is a cyclicity of biofilm development - from fixed to mobile forms, and their existence - from immobile attached forms to a planktonic population. This alternation of attached and mobile forms, or biofilm and plankton, is the life cycle of the bacterium. In fact, biofilms are a form of existence of the bacterium and a form of colonization of the ecosystem by it. Biofilms can have various localizations, in particular, at the phase interface (air-liquid, liquidsolid surface), or in the liquid column.

At the cellular level, a biofilm is a complex multicomponent aggregation. It can be schematically divided into two fractions - cells and an extracellular polymer matrix. Bacterial biofilms are formed as a result of numerous and diverse physical interactions. Bacterial cells within a biofilm interact with each other through close, intermediate and long-range interactions involving cell surfaces, surface structures (e.g. flagella and pili), components of the biofilm matrix and various phase distribution surfaces (e.g. air-liquid phase distribution). The biofilm matrix includes a variety of polymers that have different degrees of specificity. For example, proteins often dominate the composition of the biofilm of gram-positive bacteria, while in gram-negative bacteria, various polysaccharides are a very important polymer. Interestingly, the structure of the biofilm is highly dependent on temperature conditions. Thus, in representatives of *Proteobacteria*, the cellulose operon (a set of genes responsible for the production of cellulose) is repressed at 37ºC and activated at 28ºC and below. This is because proteobacteria with pathogenic properties are able to use two alternative ecological colonization strategies: they do not need cellulose to build a biofilm during pathogenic colonization of patient tissues, but it very successfully helps to deposit moisture and withstand low humidity during free saprophytic existence. Very common structural elements of biofilms of all bacteria are extracellular DNA, or eDNA. This polymer performs the functions of primary adhesin, nutrient deposition and the structural polymer itself. For some bacteria, for example, for *Pseudomonas aeruginosa*, eDNA can be the main polymer of the biofilm matrix during the first 48 hours of development. Many bacteria also use functional amyloid fibrils for primary attachment to the surface and to components of the biofilm matrix. Despite the fact that amyloids are proteins, they are chemically and biologically stable, poorly soluble and adhere well to eDNA, thus stabilizing the biofilm framework.

The phenomenon of biofilm is of great fundamental and applied importance for understanding various bacterial processes. In particular, understanding biofilm is important for cleaning surfaces from unwanted biofilms, understanding the existence of free-living (saprophytic) biofilm communities and selecting effective therapy for the infectious process. Biofilms significantly reduce the range of effective antibiotics among those that have shown effectiveness in classical microbiological tests. Thus, it should be borne in mind that due to the high content of eDNA, *P. aeruginosa* biofilms reduce their sensitivity to cationic peptides and aminoglycosides by hundreds of times. The same eDNA in *Staphylococcus epidermidis* biofilms significantly reduces the bioavailability of vancomycin. A biofilm is a balanced system that adapts to external stressors. Therefore, effective control of the infectious process, which is somehow associated with the pathogen biofilm, is possible under the conditions of a comprehensive approach, namely, rational selection of an antibiotic and maximum mechanical removal of the biofilm. Infectious

complications associated with the formation of a biofilm on inert surfaces - catheters, implants, metal structures, etc., require the removal of the inert surface (removal of the catheter, implant) and maximum removal of infected tissues (paraprosthetic infection, osteomyelitis).

Such a new view of various bacterial processes through understanding the biofilms opens up new opportunities for biotechnological and biomedical technologies. In particular, the dependence of the infectious process on the formation of a biofilm leaves a window of opportunity for the development of specific anti-biofilm therapy and the creation of new materials with a reduced potential for bacterial attachment and colonization, and the use of mechanisms for regulating the formation of biofilms can be used in various biotechnologies, in particular, in the agricultural direction.

The aim of this work was to study the structural and functional features of individual gramnegative bacteria, and to investigate the possibilities of using some properties of gram-negative bacteria in biotechnology and clinical practice.

In the presented work, the structural role of cellulose in the biofilms of *Pseudomonas fluorescens* SBW25, in particular, the ecotype (derived strain) Wrinkly Spreader (WS), and the role of cellulose in the formation of biofilms by the wild isolate *Bordetella avium* 197N was analyzed. *P. fluorescens* SBW25 biofilms are a popular model for experimental evolution and molecular biology studies. It has been shown that adaptive colonization in static microcosms results in the formation of a mutant WS biofilm superproducer strain that colonizes the meniscus zone (air-liquid interface) and whose main component is cellulose. In such a model static microcosm, ecosystem engineering of the first wild colonists creates a new ecological niche for further population evolution and more successful colonization. At the molecular level, the formation of WS superproducers is led by random mutations, which, through selection, lead to the selection of mutants that accumulate the secondary cellular messenger c-di-GMP, which leads to enhanced cellulose synthesis and the formation of a strong biofilm in the meniscus zone. This in turn allows the WS strain to intercept more oxygen diffusing into the liquid column and limit the growth of competitors below. It is possible that bacterial cellulose serves not only structural functions but is also used to form small biofilms in water bodies, holding bacteria at the air-liquid interface or to hold them on solid surfaces against the flow of water. Cellulose fibers may resist desiccation stress in water-limited environments or even provide protection against protist and nematode predators. It is certainly possible that cellulose serves a number of functions that could explain the wide distribution of the cellulose synthesis operon among *Proteobacteria* living in a variety of environments.

Cellulose synthesis in *Proteobacteria* is mediated by bacterial cellulose synthase (bcs) operons, which are widely distributed. Interestingly, the subunits required for partial acetylation of the polymer appear to be restricted to a few soil, plant-associated, and phytopathogenic ɣ-group pseudomonads, including *P. fluorescens* SBW25 and several pathovar *Pseudomonas syringae*. However, the bcs operon with acetylation subunits is also annotated in the unrelated b-group respiratory pathogen *B. avium* 197N. Our comparison of subunit protein sequences and GC content analysis confirm the high similarity between *B. avium* 197N and the pseudomonad operons, suggesting that in both cases the cellulose synthase subunit and the acetylation subunit were acquired as a single unit. Using static liquid microcosms, we confirmed that *B. avium* 197N expresses low levels of cellulose in biofilms formed at the air-liquid interface, and that biofilm strength and attachment can be increased by increasing levels of c-di-GMP, as in pseudomonads. However, we also showed that cellulose itself is not critical for biofilm formation. The discovery that *B. avium* 197N is able to produce cellulose via the highly conserved but relatively rare bcs operon raises the question of what functional role this modified polymer plays during upper respiratory tract infection or host survival, and what environmental signals regulate cellulose production.

Another important component of Gram-negative bacterial biofilms is amyloid fibrils. To study this important component, a new highly sensitive (compared to the classical) green emitting water-soluble aminoketoenol dye AmyGreen was developed. This dye almost does not fluoresce in solution, but gives bright green emission in the presence of amyloid fibrils of proteins.

AmyGreen is also weakly fluorescent in the presence of biomolecules that are components of cells, the extracellular matrix or the environment, in particular in the presence of nucleic acids, polysaccharides, lipids, proteins. Thus, the fluorescence of AmyGreen was used to visualize amyloid components of the extracellular matrix in biofilms of *Escherichia coli*, *Klebsiella pneumoniae*, *P. aeruginosa*, *B. avium* and *Staphylococcus aureus*. The efficiency of AmyGreen was compared with the traditional amyloid-sensitive dye Thioflavine T. It was found that the main advantage of AmyGreen (concentration 10^{-5} M) is the higher sensitivity for visualization of amyloid components in biofilms compared to Thioflavine T (10^{-4} M). In addition, AmyGreen has a lower selectivity for nucleic acids, which was demonstrated both in experiments in solution and when staining human eukaryotic mesenchymal stem cells, which were used as a negative control. Thus, the new dye has a lower risk of false positive response when determining amyloid components of bacterial biofilms. Combined staining of biofilms with AmyGreen dye and cellulose-sensitive dye Calcofluor White demonstrates differential staining and different localization of the stained

components, indicating the diversity of localizations of polysaccharides and amyloids in the studied biofilms.

The main structural component of the *P. fluorescens* SBW25 WS biofilm is cellulose, but how exactly cellulose fibrils are integrated into a successful biofilm matrix was unknown. In our work, we found that amyloids also play a structural role in the *P. fluorescens* SBW25 WS biofilm and investigated membrane vesicles and their protein composition.

Successful bacterial colonization of complex econiches requires individual responses to changing conditions at the microscale as well as cooperation at the community level for the production of large-scale structures such as biofilms. Coordination of individual and community responses may be achieved by linking intracellular sensory and regulatory systems mediated by bis-(3′,5′)-cyclic dimeric guanosine monophosphate (c-di-GMP) and other compounds of individuals with intercellular regulation, quorum sensing (QS), which controls the population. There is increasing evidence that biofilm formation by many pseudomonads is regulated by both intracellular and intercellular regulatory systems, although in the case of the model *P. fluorescens* SBW25 WS, in which mutations that increase c-di-GMP levels lead to the formation of a strong cellulose biofilm at the air–liquid interface, no evidence of quorum sensing has been found. However, our overview of *P. fluorescens* SBW25 genome revealed a potential QS-dependent regulatory pathway and other QS-dependent genes involved in c-di-GMP homeostasis, and QS signaling molecules were identified in culture. These data suggest a possible link between c-diGMP regulation and QS in *P. fluorescens* SBW25, allowing for more complex and flexible control of cellulose production and biofilm formation during colonization of soils and plant-associated econiches, the natural habitats of P. *fluorescens* SBW25.

Biofilm formation is of great phenomenological importance in the pathogenesis of various infectious processes. Periodontal diseases are known to be associated with polymicrobial biofilms and the activation of inflammation. The subgingival cytological (micro)landscape in periodontitis was investigated, the role of extracellular DNA (eDNA) in periodontitis was elucidated, and the concept of the role of host immune eDNA in inflammation in periodontitis was proposed, which may improve our understanding of the mechanisms of severe periodontitis. Analysis of subgingival biofilms using a modified Kholodny method revealed a low content of bacterial amyloids and a high level of eDNA in periodontal biofilms. It was found that bacterial eDNA accounts for less than a third of the total eDNA in the cytological landscape in periodontitis. It is likely that the majority of eDNA in periodontitis is released from neutrophil extracellular traps and may be of great importance in the development of biofilms that cause periodontitis. Thus, eDNA of activated

immunocompetent host cells may be a major factor in bacterial persistence and the development of pathological inflammation in periodontitis.

Understanding the pathogenetic role of biofilms of infectious isolates opens up new pharmacological possibilities for the creation of alternative therapeutic protocols based on antibiofilm therapy. Moreover, it has been found that new combinations of some classical antibiotics can act synergistically, which leads to the suppression of the development of multiple antibiotic resistance. However, it is difficult to predict which combination of antibiotics will be successful. Standard antimicrobial susceptibility testing may not detect such synergistic effects due to the specificity of the infectious process. In addition, there is a physiological difference between planktonic free-living and attached, biofilm-protected bacterial cells and, accordingly, the sensitivity to antibiotics in such different subpopulations will also differ. Using the nominally macrolide-resistant bacterium *K. pneumoniae* ATCC 10031, the efficacy of several macrolides in inhibiting biofilm growth and the ability of azithromycin to enhance the efficacy of the targeted antibiotic colistin methanesulfonate in biofilm infections caused by *K. pneumoniae* were demonstrated. This synergistic effect was also confirmed in a collection of hospital isolates of *K. pneumoniae* with high resistance. The same therapeutic combination of azithromycin and colistin methanesulfonate was investigated in a developed *in vitro* wound model. The developed model consisted of a three-dimensional collagen sponge base seeded with epithelialized HEK293 cells, which was immersed in a liquid medium that mimics wound bed exudate. In this model, the high therapeutic efficacy of the combination of azithromycin and colistin methanesulfonate in inhibiting a highly resistant strain of *K. pneumoniae* was confirmed. The use of azithromycin to mitigate the severity of the infection process and in combination with a targeted antibiotic was demonstrated in the treatment of a patient who received combat injuries and extensive wound infections caused by multidrug-resistant and pandrug-resistant strains. In particular, the patient was successfully cured by combination therapy with azithromycin and meropenem. The results obtained emphasize the need to find new effective antimicrobial therapeutic approaches as alternative strategies for the treatment of infections with high resistance.

Another strategy to combat the development of antimicrobial resistance is the search for new antimicrobial substances using biomedical chemistry and rational drug design methods. However, it should be remembered that specific inhibitors with antibacterial properties for selected infectious strains may have unexpected stimulating effects for other pathogens. Moreover, such effects should be tested not only in classical biomedical models, i.e., at the level of liquid culture (planktonic subpopulation) and at the level of agar colonies (artificial microbial aggregations), but also in conditions close to the conditions of the real infectious process - on biofilms. Based on this idea, a

new antistaphylococcal substance was investigated. In particular, 2-(2-amino-3-chlorobenzoylamino)-benzoic acid, which is able to inhibit sortase A of *S. aureus* with IC 50 parameters of 59.7 μM. Antibacterial and antibiofilm assays also confirmed the high specificity of the compound against two standard strains and three hospital isolates of *S. aureus*. However, it was investigated that this same substance did not affect the planktonic levels of two gram-negative strains, in particular, *P. aeruginosa* PA01 and *K. pneumoniae* ATCC 10031. Interestingly, this substance did not affect the development of the *P. aeruginosa* PA01 biofilm, but stimulated a fourfold increase in the biomass of the *K. pneumoniae* ATCC 10031 biofilm. Thus, when studying new antimicrobial substances, it is important to study unexpected stimulatory effects on alternative pathogens. Biofilms are not only a direct pathological factor, but also an indirect one through the maintenance of the antibiotic resistance gene pool, which is dynamically developing in Ukraine. The ongoing war in Ukraine has further worsened the situation with antibiotic resistance of gramnegative bacteria. Our data suggest a change in resistance patterns, particularly among aminoglycosides and colistin, compared with previous data. While NDM-type and OXA-48-type carbapenemases continue to dominate, a wide range of other resistance genes have been identified. The significant proportion of phenotypically resistant strains without a genotype associated with resistance also suggests that additional resistance mechanisms dominate the Ukrainian Gramnegative infection population.

Because biofilms support a pool of genetic resistance factors, the selection of effective biocides used in routine hospital practice should take into account the role of disinfectants in maintaining and developing the local resistance system. Some biocides may hypothetically affect the transfer of antibiotic resistance genes in the hospital microbial population by promoting horizontal gene transfer and subsequent maintenance of antibiotic resistance genes in the environment. In our work, we investigated the differences in the biocides' effects on eDNA from mature biofilms of two opportunistic model strains *P. aeruginosa* ATCC 27853 and *S. aureus* ATCC 25923. The effects of four groups of biocides, in particular, alcohols, hydrogen peroxide, quaternary ammonium compounds, and the polymeric biocide polyhexamethyleneguanidine hydrochloride (PHMG-Cl), were investigated using *P. aeruginosa* ATCC 27853 and *S. aureus* ATCC 25923 biofilms. Most biocides, with the exception of PHMG-Cl and 70% ethanol, caused significant release of eDNA. It was shown that PHMG-Cl blocks biofilm development when used in concentrations of 0.5% and 0.1%. This may be due to the formation of DNA–PHMG-Cl complexes. A model of PHMG-Cl binding to A-T base pairs was proposed using molecular docking. PHMG-Cl was found to bind to high molecular weight DNA and plasmid DNA, and eDNA inactivation on surfaces continued even after 4 weeks of surface treatment with the biocide.

PHMG-Cl also effectively inactivated eDNA in the form of a biofilm-associated antibiotic resistance gene found in the eDNA of a multidrug-resistant strain of *K. pneumoniae*.

Biofilm formation, or microfouling, is a major strategy for bacteria to colonize surfaces and can occur on any surface of any nature where bacteria are present. Influencing the structure of the biofilm may be an effective strategy to reduce microfouling of surfaces. Several ways of modifying materials have been investigated that have resulted in reduced microfouling. In particular, a novel thermally stable polymeric biocide, polyhexamethyleneguanidine 2-naphthalenesulfonate, was proposed and tested, which was added to polyamide. Antibiofilm activity against the opportunistic bacteria *S. aureus* ATCC 25923 and *E. coli* K12 was confirmed for polymers containing 7% and 10% of the polymeric biocide. Another polymeric cationic biocide 1-dodecylpyridinium dodecylbenzenesulfonate (PyrC 12-DBS) was synthesized and tested as a potential antibiofilm component as an additive to the commercial alkyd paint PP-115 (Ukraine). Modified coatings PP115/PyrC 12 –DBS containing 8% and 16% PyrC 12 –DBS showed significant antibiofilm properties against *S. aureus* ATCC 25923 and *P. aeruginosa* PA01. The possibility of reducing microfouling of metal surfaces by their laser modification was also investigated. This modification led to a significant decrease in the biomass of *P. aeruginosa* PA01 and *S. aureus* ATCC29423 biofilms.

However, the biofilm phenomenon can also be used to create new agrobiotechnologies. Several model plants are known to respond to bacterial quorum sensing molecules, in particular by altered root growth and gene expression, as well as the development of induced resistance to plant pathogens. Quorum sensing compounds may represent new active substances that can be used as plant seed primers to enhance the resistance of cereal crops to pathogens and abiotic stress and increase yield. In our work, the effects of hexanoyl homoserine lactone (HHL) on seed germination of winter wheat *Triticum aestivum* L., plant development and their productivity were investigated using two Ukrainian winter wheat varieties Volodarka and Yatran 60 as an example. *In vitro* germination experiments showed that priming of seeds with HHL had a small but significant positive effect on the germination rate (1.2 x increase), coleoptile and root development (1.4-fold increase). Field studies during two growing seasons (2015–16 and 2016–17) also demonstrated significant improvements in tillering biomass (1.4-fold increase), as well as improved crop structure, in particular, grain yield (1.4–1.5-fold increase) and quality (1.3-fold increase in good grain). These field results show that bacterial acylhomoserine lactones, such as HHL, can be used to improve crop yields.

Keywords: biofilm, gram-negative bacteria, cellulose, amyloids, eDNA, quorum sensing, regulation, infection, biocides, antibiotic resistance, azithromycin, therapy, plant priming.

СПИСОК ПУБЛІКАЦІЙ ЗДОБУВАЧА

Наукові праці, що розкривають основні наукові результати дисертації:

1. Pallett S.J.C., Morkowska A., Woolley S.D., Potochilova V.V., Rudnieva K.L., Iungin O.S., Sgro V., Boyd S.E., Reece N., Lambert Z.L., Tan N.K., Mughal N., Moshynets O.V., Moore L.S.P., O'Shea M.K. Evolving antimicrobial resistance of extensively drug-resistant Gram-negative severe infections associated with conflict wounds in Ukraine: an observational study. Lancet Regional Health - Europe. 2025 Mar 20;52:101274. https://doi: 10.1016/j.lanepe.2025.101274 **[IF 13,6; SCOPUS, WoS; SCImago Q1 – 2024 Public Health, Environmental and Occupational Health]** (Особистий внесок здобувача: збір колекції ізолятів, обговорення результатів, написання рукопису).

2. Pallett S.J.C., Morkowska A., Woolley S.D., O'Shea M.K., Moore L.S.P., Moshynets O. Severe conflict-associated wound infections complicated by the discovery of carbapenemasecoproducing Pseudomonas aeruginosa in Ukraine. Lancet Microbe. 2024 Dec 6:101046. https://doi.org/10.1016/j.lanmic.2024.101046 **[IF 20,9; SCOPUS, WoS; SCImago Q1 – 2023 Infectious diseases, Microbiology (medical)]** (Особистий внесок здобувача: збір колекції ізолятів, обговорення результатів).

3. Pallett S.J., Mistry R., Lambert Z.L., Woolley S.D., Abbara A., Breathnach A.O., Lamb L.E., Williams A., Mughal N., **Moshynets O.**, Hughes S.J., O'Shea M.K., Moore L.S. (2024) Conflict and catastrophe-related severe burn injuries: A challenging setting for antimicrobial decision-making. Journal of Infection 89 (3): 106224. https://doi.org/10.1016/j.jinf.2024.106224 **[IF 14,3; SCOPUS, WoS; SCImago Q1 – 2023 Infectious diseases]** (Особистий внесок здобувача: аналіз національних підходів у веденні опікових пацієнтів в Україні).

4. Slobodianyk-Kolomoiets M., Khlebas S., Mazur I., Rudnieva K., Potochilova V., Iungin O., Kamyshnyi O., Kamyshna I., Potters G., Spiers A.J., **Moshynets O**. (2024) Extracellular host DNA contributes to pathogenic biofilm formation during periodontitis. Frontiers in Cellular and Infection Microbiology 14: 1374817. https://doi.org/10.3389/fcimb.2024.1374817 **[IF 4,6; SCOPUS, WoS; SCImago Q1 – 2023 Infectious diseases]** (Особистий внесок здобувача:

концептуалізація, планування та адміністрування роботи, аналіз літератури, проведення лабораторних досліджень, аналіз результатів, написання рукопису).

5. Rogalsky S., **Moshynets O**., Dzhuzha O., Tarasyuk O., Hubina A., Darabut A.M., Lobko Y., Morozovska I., Protasov O., Bardeau J.F. (2024) Preparation and characterization of new antifouling coating based on alkyd paint modified with hydrophobic cationic biocide. Journal of Coatings Technology and Research 21: 939-953. https://doi.org/10.1007/s11998-023-00862-8 **[IF 2,3; SCOPUS; SCImago Q2 – 2023 Surfaces, coatings and films]** (Особистий внесок здобувача: проведення антибіоплівкових досліджень, аналіз результатів, написання рукопису).

6. Gnilitskyi I., Rymar S., Iungin O., Vyshnevskyy O., Parisseg P., Potters G., Zayats A.V., **Moshynets O**. (2023) Femtosecond laser modified metal surfaces alter biofilm architecture and reduce bacterial biofilm formation. Nanoscale Advance 5(23): 6659–6669. https://doi.org/10.1039/D3NA00599B **[IF 4,6; SCOPUS, WoS; SCImago Q1 – 2023 Materials Science]** (Особистий внесок здобувача: проведення антибіоплівкових досліджень, проведення мікроелементного аналізу, скануюча електронна мікроскопія зразків, аналіз результатів, написання рукопису).

7. Kryzhevskyi V., Strokous V., Lifshyts Y., Rybianets Y., Oberniak A., Krikunov A., Iungin O., Potochilova V., Rudnieva K., Petakh P., Kamyshnyi A., **Moshynets O.** (2023) Case report: Azithromycin-meropenem combination therapy as a low-cost approach to combat PDR gramnegative infections of war wounds in Ukraine. Frontiers in Medicine, 10:1264492. https://doi.org/10.3389/fmed.2023.1264492 **[IF 3,1; SCOPUS, WoS; SCImago Q1 – 2023 Medicine]** (Особистий внесок здобувача: концептуалізація, аналіз літератури, ведення пацієнта, аналіз результатів, графічне представлення динаміки показників, написання рукопису).

8. **Moshynets O.V**., Baranovskyi T.P., Iungin O.S., Krikunov A.A., Potochilova V.V., Rudnieva K.L., Potters G., Pokholenko I. (2023) Therapeutic potential of an azithromycin-colistin combination against XDR *K. pneumoniae* in a 3D collagen-based in vitro wound model of a biofilm infection. Antibiotics 12: 293. https://doi.org/10.3390/antibiotics12020293 **[IF 4,3; SCOPUS, WoS; SCImago Q1 – 2023 Pharmacology]** (Особистий внесок здобувача: концептуалізація, аналіз літератури, планування та адміністрування роботи, дослідження

біоплівок в умовах моделі ранової інфекції, порівняльний аналіз антибіоплівкової дії антибіотиків, аналіз результатів, написання рукопису).

9. **Moshynets O.V.**, Baranovskyi T.P., Cameron S., Iungin O.S., Pokholenko I., Jerdan R., Kamyshnyi A., Krikunov A.A., Potochilova V.V., Rudnieva K.L., Spiers A.J. (2022) Azithromycin possesses biofilm–inhibitory activity and potentiates non-bactericidal colistin methanesulfonate (CMS) and polymyxin B against *Klebsiella pneumonia*. PLoS ONE 17(7): e0270983. https://doi.org/10.1371/journal.pone.0270983 **[IF 3,7; SCOPUS, WoS; SCImago Q1 – 2022 Multidisciplinary]** (Особистий внесок здобувача: концептуалізація, аналіз літератури, планування та адміністрування роботи, дослідження біоплівок, порівняльний аналіз антибіоплівкової дії антибіотиків, порівняльний аналіз синергідної дії антибіотиків за методом Кірбі-Бауера, аналіз результатів, написання рукопису).

10. **Moshynets O.V**., Pokholenko I., Iungin O., Potters G., Spiers A.J. (2022) eDNA, Amyloid fibers and membrane vesicles identified in *Pseudomonas fluorescens* SBW25 biofilms. International Journal of Molecular Sciences 23: 15096. https://doi.org/10.3390/ijms232315096 **[IF 4,9; SCOPUS, WoS; SCImago Q2 – 2022 Molecular biology]** (Особистий внесок здобувача: концептуалізація, планування та адміністрування роботи, проведення комбінованого дослідження біоплівок, мікроскопічні дослідження біоплівок, виділення мембранних везикул, проведення трансмісійної електронної мікроскопії зразків везикул, спектрофотометричні дослідження, виділення і аналіз білків матриксу біоплівок і білків мембранних везикул, аналіз отриманих результатів, написання рукопису).

11. **Moshynets O.V.**, Baranovskyi T.P., Iungin O.S., Kysil N.P., Metelytsia L.O., Pokholenko I., Potochilova V.V., Potters G., Rudnieva K.L., Rymar S.Y., Semenyuta I.V., Spiers A.J., Tarasyuk O.P., Rogalsky S.P. (2022) eDNA inactivation and biofilm inhibition by the polymeric biocide polyhexamethylene guanidine hydrochloride (PHMG-Cl). International Journal of Molecular Sciences 23(2):731. https://doi.org/10.3390/ijms23020731 **[IF 4,9; SCOPUS, WoS; SCImago Q2 – 2022 Molecular biology]** (Особистий внесок здобувача: концептуалізація, аналіз літератури, планування та адміністрування роботи, отримання моделей біоплівок, підбір біоцидів для порівняльних досліджень, виділення ДНК, спектрофотометричний аналіз, аналіз якості ДНК, аналіз пролонгованості дії полімерного біоциду ПГМГ-ГХ, аналіз результатів, написання рукопису).

12. Volynets G.P., Barthels F., Hammerschmidt S.J., **Moshynets O.V**., Lukashov S.S., Starosyla S.A., Vyshniakova H.V., Iungin O.S., Bdzhola V.G., Prykhod'ko A.O., Syniugin A.R., Sapelkin V.M., Yarmoluk S.M., Schirmeister T. (2022) Identification of novel small-molecular inhibitors of *Staphylococcus aureus* sortase A using hybrid virtual screening. Journal of Antibiotics 75: 321–332. https://doi.org/10.1038/s41429-022-00524-8 **[IF 2,1; SCOPUS; SCImago Q2 – 2022 Drug discovery]** (Особистий внесок здобувача: проведення досліджень на біоплівках, аналіз результатів, написання рукопису).

13. **Moshynets O.**, Chernii S., Chernii V., Losytskyy M.Y., Karakhim S., Czerwieniec R., Pekhnyo V., Yarmoluk S., Kovalska V. (2020) Fluorescent β-ketoenole AmyGreen dye for visualization of amyloid components of bacterial biofilms. Methods and Applications in Fluorescence 8(3). DOI 10.1088/2050-6120/ab90e0 **[IF 2,3; SCOPUS; SCImago Q1 – 2020 Instrumentation]** (Особистий внесок здобувача: проведення мікроскопічних досліджень на біоплівках, аналіз результатів, написання рукопису).

14. **Moshynets O.**, Bardeau J.F., Tarasyuk O., Makhno S., Cherniavska T., Dzhuzha O., Potters G., Rogalsky S. (2019) Antibiofilm activity of polyamide 11 modified with thermally stable polymeric biocide polyhexamethylene guanidine 2-naphtalenesulfonate. International Journal of Molecular Sciences 20: 348. https://doi.org/10.3390/ijms20020348 **[IF 4,9; SCOPUS, WoS; SCImago Q1 – 2019 Organic chemistry]** (Особистий внесок здобувача: проведення антибіоплівкових досліджень, аналіз результатів, написання рукопису).

15. **Moshynets O**., Babenko L., Rogalsky S., Iungin O., Foster J., Kosakivska I., Potters G., Spiers A. (2019) Priming winter wheat seeds with the bacterial quorum sensing signal N-hexanoylL-homoserine lactone (C6-HSL) shows potential to improve plant growth and seed yield. PLoS ONE, 14 (2): e0209460. https://doi.org/10.1371/journal.pone.0209460 **[IF 3,7; SCOPUS, WoS; SCImago Q1 – 2022 Multidisciplinary]** (Особистий внесок здобувача: концептуалізація, планування та адміністрування роботи, проведення мікробіологічних досліджень, курація польових і лабораторних досліджень, обрахунок результатів, аналіз результатів, написання рукопису).

16. **Moshynets O.V.**, Foster D., Karakhim S.A., McLaughlin K., Rogalsky S.P., Rymar S.Y., Volynets G.P., Spiers A.J. (2018) Examining c-di-GMP and possible QS regulation in *Pseudomonas fluorescens* SBW25: links between intra and inter-cellular regulation benefits

community cooperative activities such as biofilm formation. Ukrainian Biochemical Journal 90(3): 17-31. doi: https://doi.org/10.15407/ubj90.03.017 **[SCOPUS; SCImago Q4 – 2018 Biochemistry]** (Особистий внесок здобувача: концептуалізація, аналіз літератури, біоінформатичний аналіз, написання рукопису).

17. McLaughlin K., Folorunso A.O., Deeni Y.Y., Foster D., Gorbatiuk O., Hapca S.M., Immoor C., Koza A., Mohammed I.U., **Moshynets O.**, Rogalsky S., Zawadzki K., Spiers A.J. (2017) Biofilm formation and cellulose expression by *Bordetella avium* 197N, the causative agent of bordetellosis in birds and an opportunistic respiratory pathogen in humans. Research in Microbiology 168: 419-430. https://doi.org/10.1016/j.resmic.2017.01.002 **[IF 2,5; SCOPUS, WoS; SCImago Q3 – 2019 Microbiology]** (Особистий внесок здобувача: дослідження структури біоплівок штамів *B. avium*, аналіз отриманих результатів, написання рукопису).

18. Koza A., Kusmierska A., McLauglin Kimberley, **Moshynets O**., Spiers A.J. (2017) Adaptive radiation of *P. fluorescens* SBW25 in experimental microcosms provides an understanding of the evolutionary ecology and molecular biology of A-L interface biofilmformation. FEMS Microbiology Letters 364 (12). **[IF 2,2; SCOPUS, WoS; SCImago Q3 – 2017 Microbiology]** (Особистий внесок здобувача: аналіз літературних джерел, написання рукопису).

19. **Moshynets O.V.,** Spiers A.J. (2016) Viewing biofilms within the larger context of bacterial aggregations. In "Biofilms", p. 3-22, InTech Press. DOI: 10.5772/62912. (Особистий внесок здобувача: аналіз літератури, концептуалізація, написання рукопису та підготовка глави монографії до друку).

20. **Moshynets O.**, Boretska M., Spiers A.J. (2013) From Winogradsky's column to contemporary research using bacterial microcosms. In Harris C.C. (eds.) "Microcosms: Ecology, Biological Implications and Environmental Impact"; p. 1-27, April, Nova Publisher. (Особистий внесок здобувача: аналіз літератури, концептуалізація, підготовка і проведення досліджень, підготовка ілюстративного матеріалу, написання рукопису та підготовка глави монографії до друку).

21. Spiers A.J., Deeni Y., Folorunso A.O., Koza A., **Moshynets O.,** Zawadzki K. (2013) Cellulose expression in *Pseudomonas fluorescens* SBW25 and other environmental pseudomonads. In: van de Ven T. & Godbout L. (eds.) "Cellulose – Medical, Pharmaceutical and

Electronic Applications", p. 1-26, InTech Press, 2013. – 304 p. DOI: 10.5772/53736 (Особистий внесок здобувача: аналіз літератури, написання рукопису та підготовка глави монографії до друку).

Публікації, що засвідчують апробацію матеріалів дисертації:

1. **Moshynets O.,** Slobodianyk-Kolomoiets M., Khlebas S., Mazur I., Rudnieva K., Potochilova V., Iungin O., Potters G., Spiers A. J. Extracellular host DNA contributes to pathogenic biofilm formation during periodontitis. Eurobiofilms 2024, oral presentation O-14, Copenhagen, Denmark, 24-29 June 2024. (Особистий внесок здобувача: тези і доповідь засновані на результатах отриманих здобувачем або під його керівництвом, здобувач написав тези конференції та безпосередньо представив усну доповідь).
2. **Moshynets O.**, Gnilitskyi I., Rymar S., Iungin O., Vyshnevskyy O., Potters G. Laser modification of metal surfaces alters biofilm architecture and reduce bacterial biofilm formation. Eurobiofilms 2024, poster presentation PG2-62, Copenhagen, Denmark, 24-29 June 2024.
(Особистий внесок здобувача: тези і доповідь засновані на результатах отриманих здобувачем або під його керівництвом, здобувач написав тези конференції та безпосередньо представив стендову доповідь).
3. **Moshynets O**., Iungin O., Rymar S., Gnilitskyi I., Potters G. Nano-microstructured metal surfaces demonstrated alteration in biofilm architecture and reduction in biofilm formation. The 9th Thesinge biofilm meeting on biomaterial-associated infections May 13-14, 2024, Thesinge, The Netherlands. (Особистий внесок здобувача: тези і доповідь засновані на результатах отриманих здобувачем або під його керівництвом, здобувач написав тези конференції та безпосередньо представив стендову доповідь).
4. **Moshynets O.**, Iungin O., Potochilova V., Rudnieva K. Azithromycin mitigates PDR phenotype and improves sensitivity to meropenem in PDR *Klebsiella pneumoniae* biofilms. 34th European Congress of Clinical Microbiology & Infectious Diseases ESCMID-Global, Abstract/ePoster Number: 4227/P0182, 27 – 30 April 2024, Bacelona, Spain. (Особистий внесок здобувача: тези і доповідь засновані на результатах отриманих здобувачем або під його

керівництвом, здобувач написав тези конференції та безпосередньо представив стендову доповідь).

5. **Moshynets O.**, Kryzhevskyi V., Strokous V., Lifshyts Y., Rybianets Y., Oberniak A., Iungin O., Potochilova V., Rudnieva K. The alternative low-cost approach to combating PDR gram-negative infections of war injuries in Ukraine using a combination of azithromycinmeropenem. 34th European Congress of Clinical Microbiology & Infectious Diseases ESCMIDGlobal, Abstract/ePoster Number: 06182/P4128, 27 – 30 April 2024, Bacelona, Spain. (Особистий внесок здобувача: тези і доповідь засновані на результатах отриманих здобувачем або під його керівництвом, здобувач написав тези конференції та безпосередньо представив стендову доповідь).

6. **Moshynets O**., Baranovskyi T., Iungin O., Pokholenko I., Potochilova V., Krikunov A., Spiers A., Rudnieva K. Adaptation to azithromycin mitigates PDR phenotype and restores sensitivity to meropenem in PDR *Klebsiella pneumoniae*. 33rd European Congress of Clinical Microbiology & Infectious Diseases, Abstract/ePoster Number: 3094/P0461, 15 – 18 April 2023, Copenhagen, Denmark. (Особистий внесок здобувача: тези і доповідь засновані на результатах отриманих здобувачем або під його керівництвом, здобувач написав тези конференції та безпосередньо представив стендову доповідь).

7. **Moshynets O**., Rudnieva K., Potochilova V., Iungin O., Baranovskyi T., Spiers A., Krikunov A., Pokholenko I. Biomimetic wound surface model using collagen-based 3D scaffolds seeded with HEK293 cells show azithromycin-colistin combination treatment highly effective against XDR K. pneumoniae infection. 33rd European Congress of Clinical Microbiology & Infectious Diseases, Abstract/ePoster Number: 2720/P1021, 15 – 18 April 2023, Copenhagen, Denmark. (Особистий внесок здобувача: тези і доповідь засновані на результатах отриманих здобувачем або під його керівництвом, здобувач написав тези конференції та безпосередньо представив стендову доповідь).

8. **Moshynets O**. Azithromycin in a combined application of antibacterials against PDR *K. pneumoniae*: does it influence antibiotic bioavailability and permeability?", "Molecular basis of antibiotic permeability in Gram-negative bacteria" Workshop, 21-24 June 2022, Hamburg, Germany. (Особистий внесок здобувача: тези і доповідь засновані на результатах отриманих

здобувачем або під його керівництвом, здобувач написав тези конференції та безпосередньо представив усну доповідь).

9. **Moshynets O**., Rudnieva K., Baranovskyi T., Potochilova V., Iungin O., Pokholenk I., Spiers A.J. Azithromycin reveals biofilm–inhibitory activity and potentiates non-bactericidal colistin methanesulfonate against *Klebsiella pneumonia*. Proceedings of the All-Ukrainian Conference on Molecular and Cell Biology with international participation, dedicated to the heroic struggle of the Ukrainian people against the Russian invaders, p. 61, 15-17 June 2022, Kyiv, Ukraine. (Особистий внесок здобувача: тези і доповідь засновані на результатах отриманих здобувачем або під його керівництвом, здобувач написав тези конференції та безпосередньо представив усну доповідь).

10. Pokholenko I., Rudnieva K., Baranovskyi T., Potochilova V., Iungin O., Spiers A., Krikunov A. A., **Moshynets O.** Biomimetic 3D model to reproduce wound-associated biofilmrelated infectious process *in vitro*. Proceedings of the All-Ukrainian Conference on Molecular and Cell Biology with international participation, dedicated to the heroic struggle of the Ukrainian people against the Russian invaders, p. 53, 15-17 June 2022, Kyiv, Ukraine. (Особистий внесок здобувача: тези і доповідь засновані на результатах отриманих здобувачем або під його керівництвом, здобувач написав тези конференції та безпосередньо представив усну доповідь).

11. **Moshynets O.V.**, Baranovskyi T.P., Iungin O.S., Kysil N.P., Metelytsia L.O., Pokholenko I., Potochilova V.V., Potters G., Rudnieva K.L., Rymar S.Y., Semenyuta I.V., Spiers A.J., Tarasyuk O.P., Rogalsky S.P. Biocides contribute to antibiotic resistance spread by increase eDNA release from biofilms. – 00365. The 32nd European Congress of Clinical Microbiology and Infectious Diseases, No 365, 23 - 26 April 2022, Lisbon, Portugal. (Особистий внесок здобувача: тези і доповідь засновані на результатах отриманих здобувачем або під його керівництвом, здобувач написав тези конференції та безпосередньо представив усну доповідь).

12. **Moshynets O**., Krykunov O., Iungin O., Jerdan R., Filonenko G., Spiers A. Azithromycin possesses biofilm-inhibitory activity against Klebsiella pneumonia and potentiates colistin to combat klebsiella-associated infection. - 051-DKMP. 6 th Joint Conference of DGHM & VAAM, 8-11 March 2020, Leipzig, Germany. (Особистий внесок здобувача: тези і доповідь засновані на результатах отриманих здобувачем або під його керівництвом, здобувач написав тези конференції та безпосередньо представив стендову доповідь).

13. **Moshynets O**., Chernii S., Snihirova Y., Czerwieniec R., Chernii V., Yarmoluk S., Kovalska V. AmyGreen is a new amyloid-sensitive stain for biofilm research - 101-MCBP. 6 th Joint Conference of DGHM & VAAM, 8-11 March 2020, Leipzig, Germany. (Особистий внесок здобувача: тези і доповідь засновані на результатах отриманих здобувачем або під його керівництвом, здобувач написав тези конференції та безпосередньо представив стендову доповідь).

14. **Moshynets O**., Iungin O., De Baere K., Meskens R., Leyn M., Bardeau J.F., Tarasyuk O., Makhno S., Cherniavska T., Dzhuzha O., Potters G., Rogalsky S. Polyhexamethylene guanidine salts as an effective biofouling and DNA inhibitor for polymeric articles and protective coatings. 8th Congress of European Microbiologists, July 7-11, 2019, Glasgow, UK. (Особистий внесок здобувача: тези і доповідь засновані на результатах отриманих здобувачем або під його керівництвом, здобувач написав тези конференції та безпосередньо представив стендову доповідь).

15. **Moshynets O**., Spiers A. Identification of extracellular DNA in *P.fluorescens* SBW25 airliquid interface biofilms. 8th Congress of European Microbiologists, July 7-11, 2019, Glasgow, UK. (Особистий внесок здобувача: тези і доповідь засновані на результатах отриманих здобувачем або під його керівництвом, здобувач написав тези конференції та безпосередньо представив стендову доповідь).

16. **Moshynets O.V**., Vodianyk A.A., Krykunov O.A., Spiers A.J. Azithromycin-colistin as a new combination therapy against carbapenem-resistant *Klebsiella pneumoniae* infection: antibiofilm activity and treatment effectiveness. Setting our sights on infectious diseases Conference, 12-15 May 2019, University of Dundee, UK. (Особистий внесок здобувача: тези і доповідь засновані на результатах отриманих здобувачем або під його керівництвом, здобувач написав тези конференції та безпосередньо представив усну доповідь).

17. **Moshynets O.,** Spiers A., Krykunov A. Azithromycin-colistin as a new combination therapy against carbapenem resistant *Klebsiella pneumonia* esepsis: anti-biofilm activity and treatment effectiveness. – P2461. The 29th Congress of Clinical Microbiology & Infectious Diseases, 13-16 April 2019, Amsterdam, the Netherlands. (Особистий внесок здобувача: тези і доповідь засновані на результатах отриманих здобувачем або під його керівництвом, здобувач написав тези конференції та безпосередньо представив стендову доповідь).

18. **Moshynets O.**, Babenko L., Foster, J., Kosakivska I., Iungin O., Potters G., Rogalsky S., Jerdan R., Bamanga, R, Spiers A. The quorum-signal N-hexanoyl-L-homoserine lactone applied as a winter wheat seed primer has a phytostimulative effect. – 166 B. 17th Symposium of International Society on Microbial Ecology, ISME, 12-17 August 2018, Leipzig, Germany.

(Особистий внесок здобувача: тези і доповідь засновані на результатах отриманих здобувачем або під його керівництвом, здобувач написав тези конференції та безпосередньо представив стендову доповідь).

19. **Moshynets O.,** Bardeau J.F., Tarasyuk O., Makhno S., Cherniavska T., Dzhuzha O., Rogalsky S. Antibiofilm activity of polyamide 11 modified with cationic biocide. – P2085. The 28th European Congress of Clinical Microbiology and Infectious Diseases, 21 - 24 April 2018, Madrid, Spain. (Особистий внесок здобувача: тези і доповідь засновані на результатах отриманих здобувачем або під його керівництвом, здобувач написав тези конференції та безпосередньо представив стендову доповідь).

20. **Moshynets O**., Babenko L., Foster, J., Kosakivska I., Iungin O., Potters G., Rogalsky S., Jerdan R., Bamanga R, Spiers A. The quorum-sensing molecule N-hexanoyl-L-homoserine lactone applied in seed priming effects phytosphere microflora, chlorophyll levels and crop yield of winter wheat. – EMV30. Annual Conference 2018 of the Association for General and Applied Microbiology, VAAM 2018, March 17-20, Wolfsburg, Germany. (Особистий внесок здобувача: тези і доповідь засновані на результатах отриманих здобувачем або під його керівництвом, здобувач написав тези конференції та безпосередньо представив стендову доповідь).

21. **Moshynets O**., Rogalsky S., Iungin O., Voychuk S., Tarasyuk O., Potters G. Cationic biocides as potential antifouling agents for polymeric coatings/plastic systems. Annual Conference 2018 of the Association for General and Applied Microbiology, VAAM 2018, March 17-20, Wolfsburg, Germany. (Особистий внесок здобувача: тези і доповідь засновані на результатах отриманих здобувачем або під його керівництвом, здобувач написав тези конференції та безпосередньо представив стендову доповідь).

22. **Moshynets O.**, Babenko L., Karakhim S., Kharkhota M., Kosakivska I., Rogalsky S., Shcherbatiuk M., Suslova O., Spiers A. N-acyl-L-homoserine lactones are inter-kingdom signalling molecules controlling quorum sensing in the Gram-negative bacteria and priming plants increasing stress adaptation. P.5.4-035, Abstract of the 42-nd Congress of Federation of European

Biochemical Societies, Jerusalem, Israel; 10–14 September 2017. (Особистий внесок здобувача: тези і доповідь засновані на результатах отриманих здобувачем або під його керівництвом, здобувач написав тези конференції та безпосередньо представив стендову доповідь).

23. **Moshynets O.,** Rogalsky S., Irodov D., Karakhim S., Tarnavsky S., Kharhota M., Volynets G., Spiers A. *Pseudomonas fluorescens* SBW25 uses N-octanoyl-L-homoserine lactone as a quorum sensing molecule. Abstract No 691 of the 7th Congress of European Microbiologists, July 9-13, 2017, Valencia, Spain. (Особистий внесок здобувача: тези і доповідь засновані на результатах отриманих здобувачем або під його керівництвом, здобувач написав тези конференції та безпосередньо представив стендову доповідь).

24. Babenko L.M., Rogalsky S.P., Suslova O.S., Shcherbatiuk M.M., Kosakivska I.V., **Moshynets O.V.** The quorum-sensing molecule N-hexanoyl-L-homoserine lactone used for presowing wheat seed priming reveals phytostimulated activity and affects the rhizosphere microflora. Book of Abstracts of the 14th Symposium on Bacterial Ecology and Genetics, 4-8 June 2017, Aberdeen, UK. – P.102-103. (Особистий внесок здобувача: тези і доповідь засновані на результатах отриманих здобувачем або під його керівництвом, здобувач написав тези конференції та безпосередньо представив стендову доповідь).

25. **Moshynets O.V**., Rymar S.Y., Rogalsky S.P., Kisyl N.P., Spiers A.J. Biocides as a causative agent of the emergence of pan-drug resistance: biocidal effects on DNA structure and biological activity. The 27th European Congress of Clinical Microbiology and Infectious Diseases, 22 - 25 April 2017, Vienna, Austria. (Особистий внесок здобувача: тези і доповідь засновані на результатах отриманих здобувачем або під його керівництвом, здобувач написав тези конференції та безпосередньо представив стендову доповідь).

26. **Moshynets O.V.,** Rogalsky S., Karakhim S.O. Spiers A.J. Evidence of quorum sensing in the biofilm-forming soil and plant-associated *Pseudomonas fluorescens* SBW25. Biofilms 7, 2628 June 2016, Porto, Portugal – P1: 62. (Особистий внесок здобувача: тези і доповідь засновані на результатах отриманих здобувачем або під його керівництвом, здобувач написав тези конференції та безпосередньо представив стендову доповідь).

27. Protasov A., Bardwau J.F., MorozovskayaI., Guryanova G., Metelytsia L., Kalashnikova L., Kopernyk I., Kipnis L., Tarasyuk O., **Moshynets O**., Rogalsky S. New antifouling coating containing polymeric biocide polyhexamethylene guanidine molybdate. 18th International Congress on Marine Corrosion and Fouling, 19-24 June 2016, Toulon, France – P.219.

(Особистий внесок здобувача: тези і доповідь засновані на результатах отриманих здобувачем або під його керівництвом, здобувач написав тези конференції та безпосередньо представив стендову доповідь).

28. **Moshynets O.V**., Rogalsky S.P., Babenko L.M., Shcherbatiuk M.M., Spiers A.J. Quorum sensing in Gram-negatives: from a biofilm to the plant immunity. II International Scientific Conference "Microbiology and Immunology – the development outlook in the 21st century", 1415 April 2016, Kiev, Ukraine. (Особистий внесок здобувача: тези і доповідь засновані на результатах отриманих здобувачем або під його керівництвом, здобувач написав тези конференції та безпосередньо представив стендову доповідь).

29. **Moshynets O**., Rogalsky S., Bellenberg S., Boretska M., Irodov D., Kararhim S., Spiers A. *Pseudomonas fluorescens* SBW25 uses two signaling pathways utilizing N-acylhomoserine lacton and alpha-hydroxy ketones. Proceedings of the 6th FEMS2015, 7-11 June 2015, Maastricht, The Nitherlands. – FEMS-1379 (Особистий внесок здобувача: тези і доповідь засновані на результатах отриманих здобувачем або під його керівництвом, здобувач написав тези конференції та безпосередньо представив стендову доповідь).

30. **Moshynets O.**, Rogalsky S., Pokholenko J., Irodov D., Kararhim S., Spiers A.J. *Pseudomonas fluorescens* SBW25 reveals AHL-dependent quorum sensing behaviour in culture and biofilms. Proceedings of the Biofilms 6, International Conference on Microbial Biofilms, 1113 May 2014, Vienna, Austria. – P. 46.

ЗМІСТ

Перелік умовних скорочень……36

Вступ……37

РОЗДІЛ 1. Огляд літератури……. 47

РОЗДІЛ 2. Матеріали і методи досліджень…….. 96

2.1. Робота з бактеріями……. 96

2.1.1. Штами бактерій і плазміди ……..… 96

2.1.2. Умови культивування ……. 98

2.1.3. Визначення антимікробної чутливості ……. 100

2.1.4. Отримання біоплівок …….. 101

2.1.5. Дослідження антибіоплівкових властивостей поверхонь……..... 103

2.1.6. Комбінований аналіз біоплівки ……. 105

2.1.7. Вплив антибіотиків на біоплівки і планктон *Klebsiella* spp……. 106

2.1.8. Дослідження виходу еДНК ……... 107

2.1.9. Виділення еДНК біоплівки …… 107

2.1.10. Вплив ПГМГ-ГХ на еДНК і плазмідну ДНК pC1-L. ……. 108

2.2. Робота з еукаріотичними культурами…… 108

2.2.1. Культури, що використовувались в роботі ……. 108

2.2.2. Життєздатність еукаріотичних клітин після впливу антибіотиків…… 109

2.2.3. Вплив різних культуральних і клітин HEK293 на ріст *K. pneumoniae* UHI 1090……..…… 109

2.2.4. Аналіз прикріплення еукаріотичних клітин ……. 109

2.3. Конфокальна лазерна скануюча мікроскопія ……. 110

2.4. Аналіз колокалізації ……111

2.5. Флуоресцентна гібридbзація *in situ* (FISH) ……. 111

2.6. Полімеразна ланцюгова реакція (ПЛР) …….……. 112

2.7. Виділення мембранних везикул …….……. 113

2.8. Характеристика білків матриксу біоплівки ……. 113

2.9. MALDI-TOF мас-спектрометрія та ідентифікація білків …….…… 114

2.10. Скануюча і трансмісійна електронна мікроскопія ……..… 114

2.11. Модель ранової поверхні ……..……. 115

2.11.1. Підготовка колагенового матриксу ……...…. 115

2.11.2. Підготовка моделі рани ……...…. 115

2.12. Біоциди, що було використано у роботі ……..…… 116

2.13. Дослідження поверхонь на здатність бактеріальної колонізації …… 116

2.13.1. Підготовка поверхонь та біоцидів. ……. 116

2.13.2. Налаштування лазера та текстурування поверхні ……. 116

2.13.3. Синтез полімерного біоциду ПГМГ-ГХ ……. 117

2.13.4. Приготування та характеристика композитних плівок ПА-11/ПГМГ-НС ……..…. 118

2.13.5. Синтез катіонного біоциду 1-додецилпіридинію додецилбензолсульфоната (PyrC12-DBS) …….……. 119

2.13.6. Підготовка антиобрастаючого покриття ……..……. 120

2.13.7. Характеристика нових покриттів ……..……. 121

2.13.8. Вплив пластикової поверхні, обробленої ПГМГ-ГХ,

на еДНК……. 122

2.14. Синтез C6-HSL. ……..……. 122

2.15. Робота з рослинами ……..……. 124

2.15.1. Сорти озимої пшениці ……..……. 124

2.15.2. Підготовка насіння ……. 124

2.15.3. Дослідження схожості насіння .……. 124

2.15.4. Дослідження посівів …….……. 125

2.15.5. Дослідження рівнів хлорофілу та каротиноїдів …….……. 125

2.15.6. Мікробіологічна характеристика …….……. 125

2.16. Біоінформатичний аналіз ……. 126

2.17. Молекулярний докінг-аналіз …….……. 126

2.18. Статистичні методи ……. 127

2.19. Етичні умови ……. 128

2.20. Відбір пацієнтів х періодонтитом ……..……. 128

РОЗДІЛ 3. Структурні та екологічні особливості біоплівок грамнегативних бактерій…… 130

3.1. Роль целюлози у структурі біоплівок *Pseudomonas* spp …….……. 130

3.2. Роль целюлози у структурі біоплівок *Bordetella* spp. ……..……. 159

3.3. Роль екзоклітинної ДНК, амілоїдних фібрил і мембранних везикул у біоплівці *P.fluorescens* SBW25. ……. 174

3.4. Роль амілоїдогенезу в біоплівках грам-негативних бактерій. ……. 214

3.5. Фізіологічна роль почуття кворуму у *P.fluorescens* SBW25. …..……. 230

РОЗДІЛ 4. Роль біоплівок у розвитку інфекційних ускладнень. …….……. 248

4.1. Патогенез опосередкований біоплівками як результат взаємодії патогенів з імунною системою хазяїна при пародонтиті……. 248

4.2. Біоплівки *Klebsiella pneumoniae* як форма інфекційного процесу та комбінована анти-біоплівкова терапія клебсієльозів ……..…. 267

4.3. Неспецифічна біоплівко-стимулююча активність фармакологічних молекул……. 315

РОЗДІЛ 5. Роль біоплівок як джерела генів резистому у госпітальному середовищі..... 329

5.1. Розповсюдженість генів антибіотикорезистентності в українській популяції грам-негативних госпітальних інфекцій. ……..……. 330

5.2. Роль біоцидів у підтриманні пулу генів стійкості до антибіотиків у госпітальному середовищі. …….....…. 343

5.3. Розробка нових матеріалів із анти-біоплiковою та анти-ДНК діями для вирішення проблем персистування генів стійкості до антибіотиків у госпітальному середовищі. ……..... 365

РОЗДІЛ 6. Біотехнології на основі біоплівок грамнегативних бактерій для Вирішення завдань у агропромисловості…….....… 412

Висновки. …….....……. 431

Список літературних джерел …….....……. 433

Додаток 1. Список публікацій здобувача ……....……. 448

Перелік умовних скорочень

АГЛ – ацилгомосеринлактони

ВООЗ – Всесвітня організація охорони здоров'я

вДНК – внутрішньоклітинна ДНК, iDNA

ГАР – гени антибіотикорезистентності

ГГЛ – гексаноіл-L-гомосерин лактон

ГПГ – горизонтальний перенос генів

еДНК – екзоклітинна ДНК, eDNA

ПК – почуттям кворуму

П-Р інтерфейс – повітря-рідина інтерфейс

Р-Т інтерфаза – рідина-тверда поверхня інтерфейс

суб-МІК – субмінімальні інгібіторні концентрації

ТЕМ – трансмісійна електронним мікроскопія

AWaRe – Access, Watch, and Reserve, доступ, нагляд і резерв

Bcs – bacterial cellulose synthase, бактеріальна целюлозосинтази

c-di-GMP – біс-(3′,5′)-циклічний димерний гуанозинмонофосфат

ECDC – European Centre for Disease Prevention and Control, Європейський центр профілактики та контролю захворювань

eDNA – extracellular DNA, екзоклітинна ДНК

iDNA – intracellular DNA, внутрішньоклітинна ДНК

MDR – multidrug resistant, мультирезистентний

PDR – pandrug resistant, повністю резистентний

PHMG-Cl - polyhexamethylene guanidine hydrochloride, полігексаметиленгуанідин гідрохлорид

PNAG – Poly-β-1,6-N-acetyl-D-glucosamine, полі-N-ацетилглюкозамін (PNAG)

PyrC 12-DBS – 1-dodecylpyridinium dodecylbenzenesulfonate, 1-додецилпіридинію додецилбензолсульфонат

WS – Wrinkly Spreader

XDR – extensively drug-resistant, з роширенною резистентністю

Вступ

Обґрунтування вибору теми дослідження. Протягом майже всього періоду розвитку клінічної мікробіології за виключенням останніх тридцяти років бактерії, як збудники інфекційних хвороб, сприймались виключно як індивідуальні організми мікроскопічного розміру з індивідуальними властивостями щодо патогенезу, колонізації та стійкості до антибактеріальної терапії. Втім сучасна фундаментальна мікробіологія, змінила своє уявлення щодо «персоналізації» бактерій. Починаючи із 1994 року вийшла серія робіт Costerton J.W. в яких було систематизоване уявлення про біоплівки, як форму колонізації еко ніші при інфекційному процесі (1, 2). З того часу, традиційні уявлення щодо існування популяцій мікроорганізмів стали змінюватись. Принаймні, стало зрозуміло, чому хірургічна санація осередків інфекції в організмі здатна значно підвищувати ефективність лікування на тлі антибіотикотерапії, чому багато антибіотиків, до яких бактерії чутливі на клітинному рівні, залишаються малоефективними *in vivo* або, навпаки, неочікувано мають підвищену ефективність, та чому досить старий метод лікування гайморитів введенням розчинів трипсину мав ефективність (3-5). Причина всіх цих явищ – здатність бактерій до колективної поведінки, в наслідок якої утворюються над клітинні просторові агрегації – біоплівки.

Біоплівка – просторове угрупування бактеріальних клітин, які міцно вбудовані в шари позаклітинного високополімерного матриксу. Біоплівка з екологічного погляду представляє собою нову, створену бактеріями, еконішу, яка виконує головну функцію – захист бактеріальних клітин від зовнішніх стресів. Перепади температур, посуха, атаки хижаків та токсинів – все це суттєво знижує бактеріолітичний ефект якщо ті самі бактерії встигли побудувати біоплівку (5, 6). Але, біоплівка є динамічною структурою, через що, в певний час свого онтогенезу, вона стає перенаселеною та токсичною для своїх же мешканців. З іншого боку, бактерії, які були настільки успішні, що змогли побудувати свою біоплівку при заданих умовах, можуть претендувати і на подальшу колонізацію простору. Але робити це шляхом розростання біоплівки не є достатнім, адже проблема накопичення токсинів та недостатність поживних речовин в біоплівці залишається, що стимулює подальше розповсюдження колонізації через активацію планктонного способу життя. Таким чином, існує циклічність розвитку біоплівки – від сталої до рухливої форм. Таке

чергування прикріпленої та рухливої форм, або біоплівки та планктону є життєвим циклом бактерії.

На молекулярному рівні переключення двох альтернативних метаболічних форм реалізується через регуляцію концентрації головного вторинного месенджера - циклічного ді-гуанілмонофосфату, або ц-ді-ГМФ, а ферменти, які відповідають за його накопичення та утилізацію структурно подібні до системи регуляції адреналіну (для вивільнення останнього необхідне підвищення рівню циклічного аденозинмонофосфату, або цАМФ.). Біоплівкова (прикріплена) форма існування створюється на фоні підвищеного рівня ц-ді-ГМФ, а планктонна – за умов низького рівня ц-ді-ГМФ. Цікаво, що рівні ц-ді-ГМФ бактерії у більшості випадків корелюються через популяційний гормональний сигналінг – почуття кворуму. Концентрація сигнальних месенджерів в популяції, тобто в міжклітинному просторі, визначає рівень ц-ді-ГМФ в кожній окремій клітині. Через відчуття рівня сигнальних месенджерів, в популяції, бактерії координують свою генетичну програму та здатні таким чином до колективної поведінки (8-10).

Формування і властивості боплівок залежить від індивідуальних характеристик штаму, адже для протистояння висиханню та утримання на поверхні рідини або супротиву току рідини на рівні зануреної поверхні необхідні різні механізми. Важливо пам’ятати, що існування бактерій у біоплівці, яка є природнім угрупуванням, дуже відрізняється від існування тих самих бактерій за умов існування їх колоній на агаризованому середовищі, яке за своєю суттю є штучним. Саме через ці відмінності у природніх і штучних угрупованнях, тобто у біоплівках і колоніях, не дозволяють використовувати агаризовані колонії як універсальну модель дослідження чутливості бактерій до антибіотику.

На клітинному рівні біоплівка є складним багатокомпонентним утворенням. Схематично її можна розділити на дві фракції – на клітини та позаклітинний полімерний матрикс. Біоплівки бактерій утворюються в результаті численних і різноманітних фізичних взаємодій. Бактеріальні клітини всередині біоплівки взаємодіють один з одним шляхом тісних, проміжних і далеких взаємодій за участю клітинних поверхонь, поверхневих структур (наприклад, джгутиків та пілей), компонентів матриксу біоплівки та різноманітних поверхонь розподілу фаз (наприклад, розподіл фаз повітря-рідина).

До складу матриксу біоплівки входять різноманітні полімери, які мають різні ступені специфічності. Наприклад, у складі біоплівки грам-позитивних бактерій часто домінують

білки, а у грам-негативних, дуже важливим полімером, є різноманітні полісахариди. Цікаво, що структура біоплівки сильно залежить від температурних умов. Так, у представників *Proteobacteria* целюлозний оперон (сукупність генів, що відповідають за продукцію целюлози) репресується при 37ºС та активується за умов 28ºС і нижче. Це відбувається тому, що протеобактерії із патогенними властивостями здатні використовувати дві альтернативні екологічні стратегії колонізації: целюлоза їм не потрібна для побудови біоплівки при патогенній колонізації тканин пацієнта, але вона дуже вдало допомагає депонувати вологу та протистояти посусі при вільному сапрофітному існуванні (11-13). Дуже розповсюдженими структурними елементами біоплівок всіх бактерій є екзоклітинна ДНК, або еДНК (14-18). Цей полімер виконує функції первинного адгезину, депонування поживних речовин та власне структурного полімеру. Для деяких бактерій, наприклад, для *Pseudomonas aeruginosa*, еДНК може бути головним полімером матриксу біоплівки протягом перших 48 годин розвитку. Багато бактерій також використовують функціональні амілоїдні фібрили для первинного прикріплення до поверхні та до компонентів матриксу біоплівки. Не дивлячись на те, що амілоїди є білками, вони є хімічно та біологічно стійкими, малорозчинними та добре адгезуються до еДНК, стабілізуючи таким чином каркас біоплівки.

Біоплівки – це форма колонізації поверхні, зокрема, і критичних поверхонь, захист яких є важливим для реалізації технологічних процесів. Так, захист поверхонь металів в тому числі і вкритих фарбами, та різноманітних пластиків, в тому числі і пластиків медичного призначення є важливим напрямом розвитку нових матеріалів.

Феномен біоплівки має дуже велике значення для терапії інфекційного процесу. Біоплівки суттєво знижують діапазон ефективних антибіотиків серед тих, які виявили ефективність у класичних мікробіологічних тестах. Так, треба мати на увазі, що завдяки великому вмісту еДНК біоплівки *P.aeruginosa* знижують свою чутливість до катіонних пептидів та аміноглікозидів в сотні разів. Таж сама еДНК в біоплівках *Staphylococcus epidermidis* суттєво знижує біодоступність ванкоміцину. Біоплівка – врівноважена система, яка адаптується до зовнішніх стресорів. Через це, ефективний контроль над інфекційним процесом, який так чи інакше асоційований із біоплівкою збудника, можливий за умов комплексного підходу, а саме, раціонального підбору антибіотику та максимального механічного усунення біоплівки. Зокрема, інфекційні ускладнення, пов’язані із утворенням

біоплівки на/в тканинах пацієнта обов'язково потребують максимального усунення біоплівки шляхом розтину та санації абсцесів (тонзилярні, паратонзилярні та інші абсцеси), призначення розріджувачів мокроти (пневмонії) або хірургічне видалення інфікованих тканин (панкреатити, ендокардити). Інфекційні ускладнення, пов'язані із утворенням біоплівки на інертних поверхнях – катетерах, імплантах, металевих конструкціях тощо, потребують усунення інертної поверхні (видалення катетеру, імпланту) та максимальне видалення інфікованих тканин (парапротезна інфекція, остеомієліт). Втім, така залежність інфекційного процесу від якості біоплівки залишає вікно можливостей по розробці специфічної антибіоплівкової терапії та розроблення нових матеріалів із зниженим потенціалом по прикріпленню бактерій та їх біозростанню.

Наша робота поглиблює та систематизує знання про біоплівки, зокрема, біоплівки грам-негативних бактерій, та додає нові дані про роль целюлози, екзоклітинної ДНК, амілоїдних фібрил і мембранних везикул та почуття кворуму у біоплівках грам-негативних бактерій та можливості використання сигнальних месенджерів у біотехнологіях для захисту рослин. Окремо досліджується роль біоплівок у розвитку інфекційних процесів та обговорюється та доводиться можливість антибіоплівкової терапії у пацієнтів із множинної резистентністю та роль біоплівок як джерела генів резистому у госпітальному середовищі.

Мета та завдання дослідження. *Метою* роботи було дослідити біотехнологічні і структурно-функціональні особливості і клінічні аспекти біоплівок грамнегативних бактерій. Для досягнення цієї мети поставлено наступні *завдання*:

1. Дослідити роль целюлози у структурі біоплівок *Pseudomonas* spp загалом та, зокрема, в структурі біоплівок *Bordetella* spp;
2. Дослідити роль амілоїдогенезу в біоплівках грам-негативних бактерій;
3. Дослідити роль екзоклітинної ДНК, амілоїдних фібрил і мембранних везикул у біоплівці *P.fluorescens* SBW25;
4. Проаналізувати фізіологічну роль почуття кворуму у *P.fluorescens* SBW25;
5. Вивчити особливості патогенезу запальних процесів, опосередкованих біоплівками, зокрема, на прикладі взаємодії біоплівок пародонтопатогенів із імунною системою хазяїна при пародонтиті;
6. Дослідити особливості біоплівкотворення госпітальним патогеном *K. pneumoniae* та розробити засади до комбінованої анти-біоплівкової терапії клебсієльозів;

7. Проаналізувати вірогідність неспецифічної біоплівко-стимулюючої активності нових фармакологічних молекул;
8. Вивчити роль біоплівок як джерела генів резистому у госпітальному середовищі, зокрема, роль біоцидів у підтриманні пулу генів стійкості до антибіотиків;
9. Розробити нові матеріали із анти-біоплівковою та анти-ДНК діями для вирішення проблем персистування генів стійкості до антибіотиків у госпітальному середовищі;
10. Дослідити можливість використання бактеріальних сигнальних месенджерів для вирішення завдань у агропромисловості.

Об'єкт дослідження – механізми утворення біоплівок грам-негативними бактеріями, компоненти біоплівок.

Предмет дослідження – бактеріальна целюлоза, амілоїди, мембранні везикула, сигнальні месенджери, екзоклітинна ДНК, патологічні біоплівки і їхня фенотипова чутливість до антибіотиків, терапія полірезистентних грам-негативних інфекцій, антибіотикорезистентність, резистом, нові функціональні матеріали з антимікробними властивостями, нові екологічні біотехнології на основі бактеріальних сигнальних месенджерів.

Методи дослідження. В роботі було застосовано набір загальноприйнятих методів досліджень, зокрема:

– мікробіологічні методи досліджень: культивування мікроорганізмів та їх біоплівок, вивчення їх морфології методами світлової, флуоресцентної та конфокальної лазерної скануючої мікроскопії, сканувальної та трансмісивної електронної мікроскопії (СЕМ та ТЕМ), вивчення спектрів чутливості до антимікробних препаратів методами дискової дифузії та бульйонних розведень, дослідження біоплівок методом комбінованого аналізу біоплівок.
– генетичні й генно-інженерні методи досліджень: отримання і вивчення рекомбінантних штамів бактерій, виділення хромосомної, плазмідної та екзоклітинної ДНК, горизонтальний гель-електрофорез ДНК, полімеразна ланцюгова реакція (ПЛР), напівкількісна полімеразна ланцюгова реакція із зворотною транскрипцією, флуоресцентна гібридизація in situ (FISH).

- біохімічні методи досліджень: виділення білку, кількісний і якісний аналіз білкового складу проби методом MALDI-TOF Mac-спектометрії, виділення мембранних везикул з біоплівки і планктонної популяції, діаліз, отримання колагену і колагенового матриксу, вимір хлорофілу і каротиноїдів.
- цитологічні/культуральні методи: культивування лінії HEK293 та ADSC першого пасажу, оцінка життєздатності еукаріотичних клітин.
- хімічні методи: синтез полімерного біоциду ПГМГ-ГХ, синтез композитних плівок ПА-11/ПГМГ-НС, синтез катіонного біоциду 1-додецилпіридинію додецилбензолсульфоната, характеристика полімерів, синтез C6-HSL.
- робота з рослинами: підготовка насіння, дослідження схожості насіння, дослідження посівів.
- біоінформатичний аналіз: ідентифікація гомологів бактеріальної синтази целюлози в геномах протеобактерій, молекулярний докінг-аналіз.
- статистичні методи.

Наукова новизна отриманих результатів. В роботі вперше продемонстровано роль целюлози як структурного компоненту біоплівок бордетел та показано її адгезивні властивості при утворенні біопілівки на абіотичній поверхні. Вперше досліджено структурну роль функціонального амілоїдогенезу в біоплівках грам-негативних бактерій, зокрема в госпітальних штамах *Klebsiella* spp., продемонстровано генеторегенність амілоїдогенезу у госпітальних клебсієл. Вперше досліджено структурно-функціональну роль функціональних амілоїдів та екзоклітинної ДНК в біоплівках *P. fluorescens* SBW25, доведена важливість еДНК в адгезії і міцності біоплівок. Також детально досліджено утворення мембранних везикул планктонною та біоплівковою субпопуляціями *P. fluorescens* SBW25, порівняно їхній білковий компонент та встановлено, що фізіологічний стан бактеріальної популяції впливає на білки відповідних везикул. Вперше проаналізовано здатності *P. fluorescens* SBW25 до почуття кворуму. Вперше детально досліджено механізми утворення патологічних мультикультурних біоплівок при пародонтиті, встановлено важливу роль екзоклітинної ДНК хазяїна в персистуванні таких біоплівок і підтриманні запалення. Вперше проаналізовано біоплівки госпітальних штамів *K. pneumoniae*, отриманих від українських пацієнтів. Вперше розроблено засади антибіоплівкової терапії полірезистентних інфекцій *K. pneumoniae.* Досліджено

неспецифічні біоплівко-стимулюючі активності нових анти-стафілококових фармакологічних молекул, націлених на сортазу А стафілококу. Вперше досліджено біоплівки грам-позитивного і грам-негативного штамів як джерело контамінації генами антибіотикорезистентності простору госпітальної палати через використання різноманітних госпітальних дезінфікуючих засобів. Вперше розроблено нові матеріали із анти-біоплівковою та анти-ДНК дією для деконтамінації лікарняного простору. Вперше доведено можливість використання бактеріальних сигнальних молекул для підвищення врожайності українських сортів озимої пшениці.

Практичне значенні отриманих результатів. Протягом виконання роботи було запропоновано новий інструмент для дослідження бактеріальних амілоїдів, який згодом було використано для дослідження різноманітних біоплівок, зокрема й патологічних біоплівок пародонту. Було проаналізовано здатність різних біоцидів, що використовуються у повсякденній практиці в українських лікарнях, до посилання контамінації простору генами антибіотикорезистентності та встановлено, які біоциди є найсильнішими факторами контамінації. Було встановлено унікальність структури патологічних біоплівок, що утворюються при пародонтиті, що дає змогу змінити парадигму лікування пацієнтів із хронічним пародонтитом. Було встановлено, що макролідний антибіотик азитроміцин здатний до пригнічення біоплівок звичайних та полірезистентних штамів *K. pneumoniae.* На основі цього феномену було розроблено принципово новий підхід для лікування полірезистентних інфекцій *K. pneumoniae*, який було успішно застосовано для лікування критично хворого пацієнта. Запропонований методи терапії внесено до локального стандарту операційних процедур (СОП) ряду лікарень і успішно застосовується в рутинній практиці для лікування важких полірезистентних грам-негативних інфекцій. Матеріали дисертації увійшли в навчальний посібник (Котов О.В., Корпусенко І.В., Міхно С.П., Мошинець О.В., Котов В.О. Основи антибактеріальної терапії та профілактики для хірургів. Навчальний посібник – Кривий Ріг: Видавець Чернявський Д.О., 2024, - 224 с., з іл.) та використовуються у навчальних курсах мікробіологічного та лікувального профілю для студентів медичних спеціальностей ВНЗ України та протягом курсів післядипломної медичної освіти. Запропоновано нову технологію праймування насіннєвого матеріалу і рослин продуктивних сортів з метою захисту від різноманітних комплексних стресорів та для підвищення врожайності.

Особистий внесок здобувача. Роботи здобувача, представлені в цій дисертації, засновані на результатах отриманих нею особисто, або за її безпосередньої участі чи під її керівництвом. Мету і задачі дослідження, а також висновки було сформульовано особисто. Огляд літератури, зокрема, аналіз біоплівок як форми бактеріальних агрегацій та аналіз робіт Виноградського було проведено разом з доктором Ендрю Спайрсом (Dr Andrew Spiers), університет Абертей Данді, Данді, Велика Британія). Вивчення ролі целюлози та екзоклітинної ДНК в культурах *Pseudomonas* spp., *Bordetella* spp., *P. fluorescens* SBW25 також було проведено у співпраці із доктором Ендрю Спайрсом. Роль амілоїдогенезу в біоплівках грам-негативних бактерій було проведено разом із к.б.н. С. Черній під керівництвом д.б.н. В. Ковальської (відділ біомедичної хімії Інституту молекулярної біології і генетики НАН України, Київ, Україна). Роботи по дослідженню біоплівок при пародонтиті було проведено у співпраці із к.м.н. М. Слободяник-Коломоєць та д.м.н. І. Мазур (кафедра стоматології НГУ імені Шупика, Київ, Україна). Роботи із дослідження ефектів біоцидів і нових матеріалів із біоцидними властивостями було виконано у співпраці із к.х.н. С. Рогальським (лабораторія модифікації полімерів Інститут біоорганічної хімії та нафтохімії імені В.П. Кухаря НАН України, Київ, Україна) і проф. Гіртом Поттерсом (Geert Potters), Морська академія Антверпену, Антверпен, Бельгія, а роботи із вивчення властивостей модифікованих металевих поверхонь з PhD Ярославом Гнилицьким, ТОВ “NoviNano lab”. Дослідження молекулярно-генетичних механізмів антибіотикорезистентності проведені у співпраці із майором доктором Скоттом Паллеттом (Scott JC Pallett) з лікарні Челсі та Вестмінстеру Фонду NHS і Королівського центру оборонної медицини, Лондон, Велика Британія.

Зв’язок роботи з науковими програмами, планами, темами. Робота виконувалась в Інституті молекулярної біології і генетики НАН України в рамках різноманітних наукових проектів. Роботу було виконано в межах різних наукових проектів, зокрема, науково-дослідного проекту “Розробка біотехнології праймування пшениці на основі бактерійних сигнальних молекул класу ацилгомосеринлактонів для підвищення стійкості і врожайності” (№ держреєстрації 0115U004178) в рамках мультидисциплінарної програми НАНУ “Молекулярні та клітинні біотехнології для медицини, індустрії та аграрних наук” та науково-дослідної роботи “Вплив бактеріальних сигнальних молекул на врожайність та рослинні мікробні асоціації” у співпраці з Julius Kühn-Institut Federal Research Centre for

Cultivated Plants (JKI), Німеччина (№ держреєстрації 0119U103436), прикладного біотехнологічного проекту «Розробка комплексного препарату комбінованої дії на основі похідних колагену для лікування раневих поверхонь» (№ держреєстрації 0120U101290), науково-технічної роботи 2020.02/0246 «Розробка комбінованої терапії важких *Klebsiella pneumoniae*–асоційованих нозокоміальних інфекцій для подолання їхньої антибіотикорезистентності» за підтримки НФДУ за програмою "Підтримка досліджень провідних та молодих учених" (№ держреєстрації 0120U104850), індивідуального гранту на дослідження за проектом "Etiology of extracellular DNA in pathogenic biofilms associated with periodontitis" що профінансовано програмою УНТЦ для стипендіальної програми віртуального залучення українських науковців (STCU program for Virtual Scientist Engagement Fellowship Program for Ukrainian Scientists) (Grant Agreement #2008-VSE) та проекту за програмою NATO Science for Peace and Security multi-year project SPS G6053 "Inhibition of Bacterial Settlement and Biofilm Formation through Physical Control of the Environment (PHYBI)" (№ держреєстрації 0124U002389).

Апробація результатів дисертації. Основні результати дисертації доповідалися та обговорювалися на міжнародній конференції з мікробних біоплівок Biofilms 6, Відень, Австрія (2014); на шостому конгресі європейських мікробіологічних товариств FEMS2015, Маастріхт, Нідерланди (2015); на II міжнародній науково-практичній конференції «Мікробіологія та імунологія – перспективи розвитку у 21 столітті», Київ, Україна (2016); на 18-му міжнародному конгресі з морської корозії та обростання, Тулон, Франція (2016); на міжнародній конференції з мікробних біоплівок Biofilms 7, Порто, Португалія (2016); на 27-му Європейському конгресі з клінічної мікробіології та інфекційних хвороб 27th ECCMID, Відень, Австрія (2017); на 14-му симпозіумі з бактеріальної екології та генетики BAGECO 14, Абердин, Сполучене Королівство (2017); на сьомому конгресі європейських мікробіологічних товариств FEMS2017 Валенсія, Іспанія (2017); на 42-му конгресі Федерації європейських біохімічних товариств, Єрусалим, Ізраїль (2017); на щорічній конференції асоціації загальної та прикладної мікробіології VAAM, Вольфсбург, Німеччина (2018); на 28-му Європейському конгресі з клінічної мікробіології та інфекційних хвороб 28th ECCMID, Мадрид, Іспанія (2018); на 17-му симпозіумі Міжнародного товариства мікробної екології ISME 2018, Лейпциг, Німеччина (2018); на 29-му Європейському конгресі з клінічної мікробіології та інфекційних хвороб 29th

ECCMID, Амстердам, Нідерланди (2018); на Setting our sights on infectious diseases Conference, Данді, Велика Британія (2019); на восьмому конгресі європейських мікробіологічних товариств FEMS2019, Глазго, Велика Британія (2019); на шостій спільній конференції DGHM & VAAM, Лейпциг, Німеччина (2020); на 32-му Європейському конгресі з клінічної мікробіології та інфекційних хвороб 32th ECCMID, Лісабон, Португалія (2022); на всеукраїнській конференції з молекулярної та клітинної біології з міжнародною участю, присвячена героїчній боротьбі українського народу проти російських загарбників, Київ, Україна (2022); на воркшопі "Molecular basis of antibiotic permeability in Gram-negative bacteria", Гамбург, Німеччина (2022); на 33-му Європейському конгресі з клінічної мікробіології та інфекційних хвороб 33th ECCMID, Копенгаген, Данія (2023); 34-му Європейському конгресі з клінічної мікробіології та інфекційних хвороб ESCMID-Global, Барселона, Іспанія (2024); дев'ята нарада в Тесінге з питань біоплівки щодо інфекцій, пов'язаних із біоматеріалом, Тесінге, Нідерланди (2024); конференція Eurobiofilms 2024, Копенгаген, Данія (2024).

Публікації. За матеріалами дисертації опубліковано 51 наукові роботи, з них 1 робота у науковому фаховому виданні України та 20 у закордонних наукових журналах, проіндексованих в міжнародних наукометричних базах даних Scopus і Web of Science, 30 тез доповідей на вітчизняних та закордонних наукових конференціях. Серед цих робіт: 11 експериментальних статей у журналах, що належать до Q1 SCImago; 4 експериментальних статей у журналах, що належать до Q2 SCImago; 2 експериментальні статті у журналах, що належать до Q3 SCImago та одна стаття у журналі з Q4 категорії SCImago; та три розділи монографій видавництв InTech Press і Nova Publisher.

Структура та обсяг дисертації. Дисертаційна робота є кваліфікаційною науковою працею на правах наукової доповіді за сукупністю статей, викладена на 459 друкованих сторінках. Дисертація складається з наступних структурних підрозділів: вступу, огляду літератури, розділу матеріалів і методів досліджень, основної частини, висновків, переліку використаних джерел та додатку. Розділами дисертації є публікації здобувача наукового ступеня в виданнях високого рівня. Список використаної літератури включає 1422 джерел, з яких 1250 є в публікаціях здобувача. Робота загалом містить 142 рисунка і 21 таблицю, опублікованих в працях здобувача.

РОЗДІЛ 1. Огляд літератури

Бактеріальні біоплівки як форма «мікробних міст» домінує в нашому розумінні існування бактерій в відповідних екологічних нішах протягом останніх 30 років. Біоплівки бактерій відомі дослідникам і спостерігачам під різноманітними дефініціями, зокрема це й активний мул, згустки, колонії, флокули, мати, плівки, плоти, шлами, зооглеї тощо. Концепція моделі біоплівки як форми інфекційного процесу було вперше сформульовано Костертоном у (1, 2), де автор представляв розвиток біоплівки як серію пов'язаних подій, починаючи з прикріплення вільно існуючих планктонних бактерій до зануреної у рідину твердої поверхні, зростання мікроколоній у вигляді простих конічних структур та подальше дозрівання у вигляді більшої грибоподібної структури, які були передбачені як «мікробні міста». Це розуміння біоплівок досить швидко стало домінуючим у клінічній мікробіології і стало використовуватись для розуміння перебігу інфекційного процесу і оцінки ефективності антимікробної терапії, хоча все ще не вийшло на практичний рівень персоналізованих досліджень (19). Втім, саме таке домінуюче розуміння агрегацій мікробних клітин обмежило його використання у найширшому масштабі, тобто, в різноманітних екологічних аспектах. Саме дослідженню феномену біоплівок як універсальної природньої агрегації мікробних клітин, який протистоїть штучній агрегації мікробних клітин – колоніям на агарі з одного боку і рухливій вільно існуючій субпопуляції бактеріальних клітин – планктону з другого боку присвячений аналіз, проведений автором (20).

Дослідження таких різноманітних біоплівок, які сформувались в комплексних екологічних нішах – нетривіальне завдання, яке має поширити наші розуміння про цитологічно-екологічні аспекти взаємодій бактеріальних біоплівок з компонентами еконіші. Велика заслуга у таких екологічних методах дослідження належить засновнику екологічної мікробіології Сергію Виноградському (1856 – 1953), роботи якого про спостереженню бактеріальних біоплівок в різноманітних екологічних умовах були продовжені автором і представлені через аналіз біографії і робіт Виноградського та аналіз власних досліджень (21).

Viewing Biofilms within the Larger Context of Bacterial Aggregations

Olena V. Moshynets and Andrew J. Spiers

Additional information is available at the end of the chapter

http://dx.doi.org/10.5772/62912

Abstract

The 'Microbial Cities' vision of bacterial biofilms has dominated our understanding of the development and functioning of bacterial aggregations for the past 20 years, during which active sludge, clumps, colonies, flocs, mats, pellicles, rafts, slimes, zooglea, etc. have been largely forgotten or ignored. Although the medically inspired developmental model of human pathogen biofilms has merits including providing a rationale for the development of anti-biofilm therapeutics, it fails to provide links to other types of bacterial aggregation that are commonly found in a wide range of natural and man-made environments. Possibly as a result, applied and environmental microbiologists tend to avoid the term 'biofilm' and use others such as 'microbial mats' instead. Here we challenge the simplistic planktonic (independent and free-swimming bacteria)-biofilm (sessile and co-operative bacteria) dichotomy, and consider biofilms within the larger context of bacterial aggregations. By placing biofilms into context, which we see as a continuum of aggregations or communities with varying abiotic and biotic properties, fundamental physical, biological, and evolutionary ecological processes that effect community development and function can no longer be considered unique to biofilms, but may also be important in other aggregations that develop over time and change in nature depending on prevailing conditions. By doing this, we will be better able to distinguish those processes which govern bacterial colonisation and ecological success in a wider sense from those that are unique to particular environments and specialised strategies.

Keywords: Bacterial aggregations, Biofilms, Colonies, Communities, Planktonic and sessile bacteria

INTECH
open science | open minds

© 2016 The Author(s). Licensee InTech. This chapter is distributed under the terms of the Creative Commons Attribution License (http://creativecommons.org/licenses/by/3.0), which permits unrestricted use, distribution, and reproduction in any medium, provided the original work is properly cited. CC BY

1. Introduction

Modern biofilm research often acknowledges the seminal reviews of Costerton et al. [1,2] in which a conceptual model of biofilm development and structure was first presented. In this model, biofilm development is described as a series of linked events, from the attachment of free-swimming planktonic bacteria to a submerged solid surface, the growth of microcolonies in simple conical structures, and subsequent maturation as larger mushroom-shaped structures which have been envisioned as 'Microbial Cities' (this appellation may derive from reviews entitled 'City of Microbes' and 'Microbial Metropolis' [3,4], but we are unsure). Equally important to this description was the dichotomous differentiation between independent free-swimming planktonic bacteria with the co-operative and co-ordinated communities of sessile bacteria forming biofilms, and the somewhat teleological suggestion that surface-attached communities allowed growth in harsh conditions which planktonic bacteria could not survive [2]. This view of complex bacterial behaviour and growth strategies was in contrast with the apparently contemporary idea that bacteria were unsophisticated organisms [5].

Since the publication of the Costerton et al. reviews, our understanding of biofilms has developed through the study of model bacteria as well as of natural communities forming multispecies biofilms (we direct the reader to the reviews cited in the following sections as a means of accessing recent biofilm research and current understanding). Model human pathogens forming biofilms important for virulence include *Escherichia coli* [6], *Pseudomonas aeruginosa* [7], *Salmonella enterica* [8], *Staphylococcus aureus* [9], *Vibrio cholera* [10], etc., though the archetype is probably *P. aeruginosa*, an opportunistic pathogen of the human respiratory tract and a key factor in cystic fibrosis patient mortality [11]. As a result of an understanding of pathogen biofilm formation, critical points in the developmental processes are now being scrutinised as possible targets for anti-biofilm therapeutics [7]. Biofilms are also recognised as having importance in a range of other natural and man-made environments, impacting on crop productivity, food technology, metal corrosion, veterinary medicine, etc. [12–15], and microbial mats, a term seemingly preferred by applied and environmental microbiologists, are found on rock surfaces, in caves, wetlands, sediments, salt marshes, lakes and seas, thermal springs, hypersaline ponds and lagoons, methane and petroleum seeps, oil wells, etc. [16–21]. Comparisons between pathogenic and environmental biofilm-forming bacteria highlighting commonalities suggest that biofilm developmental pathways or responses may not be unique to species or particular environments.

Investigations of biofilm-forming bacteria have revealed key sensory-regulatory pathways, including intercellular communication and intracellular regulation, required to control biofilm development by altering motility and attachment behaviour, physiology and metabolism, the production of extracellular polymeric substances (EPS) forming the matrix of biofilms, and dispersants required to release bacteria from mature structures [22–27]. The use of a variety of different experimental systems, including in vitro flow cells, microtitre plates, static microcosms, etc., as well as animal models [28–31], has also identified the impact of abiotic factors such as liquid flow and mass transport; O_2 and nutrient diffusion; surface physical-chemistry and topology; and biotic interactions between bacteria, surfaces, and matrix components; and

http://dx.doi.org/10.5772/62912

so on, on biofilm formation and structure [23–26,32]. In addition, research focussed more on medical and environmental microbiology, rather than on biofilm formation per se [33–37], as well as on evolutionary ecology and social microbiology [11,38–41], are increasingly providing explanations for the role or function of biofilms in different environments and evidence of their ecological success.

Despite the obvious diversity in biofilm research as evidenced by publications in journals covering a wide range of disciplines including microbiology, microbial biotechnology, environmental science, and medical microbiology, our general understanding of biofilms is nonetheless dominated by a few human pathogens and the submerged solid-surface interface biofilms they produce in flow cells or microtitre plates [28,29,31] (here we refer to these as liquid-solid surface (L-S) interface biofilms to differentiate them from other types of biofilms or bacterial aggregations). Of these, the medically inspired developmental model of *P. aeruginosa*, often chosen to represent the 'Microbial Cities' vision, is perhaps the most persuasive, with bacteria growing in these structures almost exclusively compared to free-swimming planktonic bacteria. We are growing concerned that this vision is beginning to dominate biofilm research in a negative manner.

2. A continuum of aggregations

In this opinion piece, we challenge the simplistic planktonic-(sessile) biofilm dichotomy and advocate the inclusion of biofilms within the larger context of bacterial aggregations. We believe that by recognising biofilms within a continuum of aggregations or communities with varying properties, it will enable a more extensive investigation of bacterial colonisation, and in particular, allow us to distinguish those processes governing general colonisation and ecological success from those unique to particular environments and specialised strategies.

Costerton et al. [2] defined biofilms as 'matrix-enclosed bacterial populations adherent to each other and/or to surfaces or interfaces ... (and) includes microbial aggregates and floccules and also adherent populations within the pore spaces of porous media'. Although this definition is broad (i.e. sensu lato), there is a presumption by current researchers that biofilms are those structures formed on submerged solid surfaces (i.e. at the L-S interface) and that other structures associated with surfaces or interfaces are somehow different or inconsequential. We would suggest that L-S interface biofilms as observed in flow-cells and microtitre plates are a means to investigate biofilm formation independently of natural environments or context, as it is difficult or impossible to extrapolate from these simple in vitro systems to the more complex natural environments from which the bacteria of interest were first isolated [29–31]. We note that in some later reviews, the description of biofilms is extended with more examples. However, this has also lead to a more relaxed *(sensu amplo)* definition in which 'biofilm' is frequently used as a synonym of 'aggregation', even though the former is often defined by the latter (e.g. [42]). As a matter of etymology, 'aggregation' which originates in late Middle English (1150–1500 AD) should take precedence over 'biofilm' whose usage largely stems from the 1990s.

As an example of how the biofilm definition has been extended following the definition of Costerton et al. [1,2], we consider the inclusion of air-liquid (A-L) interface biofilms and agar plate-grown colonies as suggested by Branda et al. [42].

3. Biofilms at the air-liquid interface

Material, including bacteria, accumulates at the air-liquid interface of sea or fresh water to form surface films often subject to highly variable conditions [19]. A-L interface biofilms also form on the surface of static liquids in experimental microcosms, and are sometimes referred to as pellicles or floating biofilms. These are produced by a wide range of bacteria, including *Bacillus subtilis* [43], *Gluconacetobacter xylinus* (formerly known as *Acetobacter xylinum* and since reclassified as *Komagataeibacter xylinus*) [44], as well as numerous enteric bacteria and pseudomonads [44–46].

Although A-L interface biofilms may look superficially similar, the diversity of bacteria which form them would suggest that they vary in structure and other characteristics as well. We have been investigating this by comparing biofilms produced by environmental *Pseudomonas* spp. isolates, using relatively large static microcosms in 30-ml glass universal vials containing liquid growth medium [44,47,48]. These allow us to undertake combined biofilm assays which determine growth, attachment to the vial walls, and biofilm strength [49–51]. Using this approach, we have been able to quantitatively differentiate biofilms produced at the meniscus and A-L interface [50,52]. These include biofilms limited to the meniscus region, attached biofilms which extend across the A-L interface, and unattached 'floating' biofilms (as well as 'invisible' attached biofilms too thin or transparent to see by eye [52]). It is possible that the floaters and attached biofilms represent substantially different colonisation strategies, with the former recruiting planktonic cells directly from the liquid column to the A-L interface and growing from multiple loci, and the latter developing from sessile cells attaching in the meniscus region and subsequently growing out across the A-L interface [52].

Although floating biofilms have been reported in which buoyancy is the result of trapped CO_2 released by respiration (e.g. *G. xylinus* [44]), the two different A-L interface biofilms produced by our model environmental pseudomonad, *P. fluorescens* SBW25, known as the viscous mass and Wrinkly Spreader biofilms, are not buoyant per se and readily sink when disturbed [49,53,54]. It is likely that they are maintained at the A-L interface by hydrophobic cell surfaces, matrix components, and surfactant which pierce or weaken the A-L interface [53,54]. Interestingly, we have recently found that for the Wrinkly Spreader, a class of adaptive mutants of the wild-type strain which evolves in static microcosms, drip-fed glass bead columns, and soil [48,51,55], attached A-L interface biofilm growth can be seamlessly linked to swarming motility and colony growth using 'transitional microcosms' in which a layer of agar is set along the side of the vial, providing both liquid and dry agar surfaces for colonisation (C. Immoor, O. Moshynets , A. Spiers, Unpublished Observations).

In these transitional microcosms, we wonder whether there is more than just planktonic bacteria growing in the liquid column and a single, distinct structure colonising both the liquid and agar surfaces in these simple environments, as suggested by the simplistic planktonic-

http://dx.doi.org/10.5772/62912

(sessile) biofilm dichotomy. Instead, we think it is likely that there are different types of aggregation including L-S interface biofilms attached to the vial walls at the meniscus, attached biofilms extending out across the liquid surface, confluent colonies growing on the agar surface, and microcolonies developing in the swarm-front as bacteria move up the agar surface and away from the liquid media. We are interested in identifying which abiotic and biotic factors drive growth at different points across the transitional zone, and understanding how these might alter behaviour and gene expression patterns to produce the structures we can observe within a few hours and over several days.

4. Colonies are not biofilms

Whilst we approve of the inclusion of A-L interface biofilms in the *sensu amplo* Costerton et al. [1,2] definition, we resist the suggestion that colonies grown on agar plates should be included too, despite the fact that investigations of colony morphology have been presented as biofilm research (e.g. [43,56–61] etc.). In contrast, we have investigated the colony morphologies of Wrinkly Spreader mini-*Tn* mutants on agar plates as a means to identify the genes required for biofilm formation; importantly, we also tested the mutants in static microcosms to determine the impact on biofilm formation to confirm the identity of these genes as important in biofilm formation [48].

Our objection to the inclusion of colonies as biofilms is based on a consideration of the O_2 and nutrient gradients established in these aggregations, as well as liquid flow (**Figure 1**). Rather than argue that these are insignificant differences, we would suggest that colonies, A-L and L-S interface biofilms would be better presented within a larger continuum of aggregations in which O_2 and nutrient gradients (and other chemicals including communication signals and waste, etc.), and liquid flow can be used to differentiate between types of aggregation. In this way, it now becomes reasonable to ask whether the parallel O_2 and nutrient gradients observed

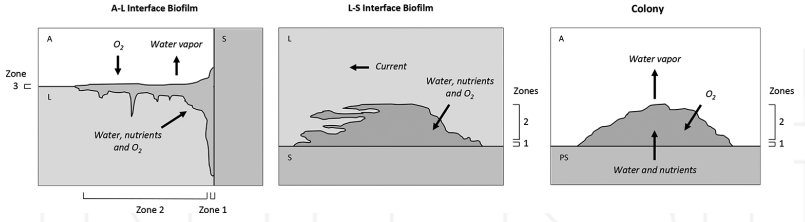

Figure 1. Bacterial aggregations include biofilms and colonies with significant similarities and interesting differences. Liquid-solid surface (L-S) interface biofilms (middle) are subject to physical stress and establish various chemical gradients. Similarly, air-liquid interface (A-L) biofilms (left) or colonies (right) also experience physical stress and establish gradients. In each type of aggregation, a layer of cells is attached to the solid surface (Zone 1) with distal regions are held in place by cell and matrix component interactions (Zone 2). In A-L interface biofilms, cells and matrix components may also break through the interface (Zone 3). However, nutrients are supplied by capillary flow (mass transport) from beneath colonies, whereas in A-L and L-S interface biofilms, they are transported or diffuse from the surrounding liquid. (A, air; L, liquid; PS, permeable or porous solid; S, solid.)

in L-S interface biofilms present a substantially different set of conditions for bacteria than the opposing gradients found in colonies. Similarly, it would be interesting to compare liquid flow within biofilms subject to external liquid currents, with the evaporation- and capillary-driven liquid flow within colonies subject to different drying regimes.

Notably, colonies show different growth patterns, have highly structured morphologies, are sometimes surrounded by EPS, and may show co-operative behaviour, so it is not unreasonable to consider that they are responding to abiotic and biotic conditions as do biofilms [6,42, 43]. In soil, water availability, often described by the matrix potential, is a significant factor restricting bacterial motility, the formation of aggregations, and colonisation through the pore network [62–64]. In such systems it is highly likely that contiguous bacterial populations colonise non-permeable solid surfaces covered or linked by thin films of water with slimes or swarms; permeable solids through which water is available with microcolonies and colonies; and partially and fully saturated pores with A-L and L-S interface biofilms, slimes, and planktonic bacteria.

5. Aggregations respond to different conditions

We would argue that bacteria colonising a range of environments should develop into different aggregations in response to local conditions and opportunities. These aggregations might appear to be superficially similar (e.g. A-L and L-S interface biofilms) or substantially different (cf. a colony), depending on bacterial responses and colonisation strategies aimed at maximising ecological success, as well as on our ability to recognise which abiotic and biotic factors have the greatest impact on the developing population.

Our observations of linked Wrinkly Spreader A-L interface biofilms and colonies in the transitional microcosms might suggest that these are very similar aggregations used to colonise two interfaces (the liquid and agar surfaces) which do not pose significantly different challenges to bacterial growth. However, competitive fitness assays in each environment suggests that Wrinkly Spreaders achieve substantially different levels of ecological success in colonising liquid and agar surfaces: they have a fitness advantage in static microcosms but are at a disadvantage in colonies compared to wild-type *P. fluorescens* SBW25 [65–68]. These fitness differences suggest that environmental conditions probably change across the transitional zone, with the initial Wrinkly Spreader population responding to these changes to colonise the A-L interface and agar surfaces in different manners.

We speculate that the fitness advantage of Wrinkly Spreaders is determined by the subtle trade-off in energy expenditure needed to produce A-L interface biofilms in static microcosms and the increased access to O_2 biofilm formation allows. The growth of *P. fluorescens* SBW25 is limited by O_2 and it drives the evolution of the Wrinkly Spreaders [69]. Relative small numbers of wild-type colonists rapidly generate an O_2 gradient through respiration, converting the homogeneous liquid column into a shallow upper zone having normal levels of O_2 and a deeper lower zone with rapidly diminishing O_2 levels (these colonists are in effect environmental engineers) [69]. As this population rapidly expands, random mutation results in

Wrinkly Spreader genotypes which are recruited to the A-L interface through the expression of attachment factor and cellulose which provides the main matrix component for the biofilm [49,53,68]. Those bacteria localised to the A-L interface have access to higher levels of O_2, compared with those lower down, and consequently grow faster [69]. Higher levels of O_2 might also induce a SOS response via reactive oxygen species (ROS) leading to the expression of an error-prone DNA polymerase, as in the case of *P. aeruginosa* PA01 [70], increasing mutation rates and the appearance of Wrinkly Spreader mutants.

As a result of access to higher levels of O_2, Wrinkly Spreaders have a fitness advantage over non-biofilm-forming competitors [69]. We speculate that in colonies where Wrinkly Spreaders still express attachment factor and cellulose, these components have no essential function and therefore pose a fitness cost to the growing population, explaining why the Wrinkly Spreaders are poorly adapted to growing on agar surfaces. Interestingly, improved O_2 access has also been suggested as an explanation for the wrinkled colonies produced by *P. aeruginosa* PA14. However, it appears that a more complex level of redox control regulating the use of different electron donors, including O_2 diffusing into the colony from above and redox-active phenazines produced by bacteria located at the base of the colony, may govern metabolism in *P. aeruginosa* PA14 and other bacteria producing wrinkled colonies including *B. subtilis* [57,71,72].

More generally, O_2 gradients determine the distribution of aerobic and anaerobic bacteria in a wide range of environments, including water columns, sediments and soils, where it effects growth, gene expression patterns and metabolism, and along with other competing electron acceptors, help define aerobic, micro-aerobic (transitional) and anaerobic niches [73–76]. It is therefore not surprising if O_2 gradients also played a central role in the development and function of a wider range of bacterial aggregations, and not just in biofilms and colonies.

6. Other terminology

As a slight digression, we present a non-exhaustive selection of vernacular and scientific terminology used to describe bacterial aggregations which includes active sludge, biofilms, clumps, colonies, flocs, mats, pellicles, rafts, slimes, zooglea, etc. (**Table 1**). We would expect that a more extensive review of the early microbiology literature, including French, German, and Russian publications, and of current microbiology, microbial biotechnology, environmental science, and medical microbiology publications, would result in more terms being identified. Although the first observations of biofilms (dental plaque) were made by van Leeuwenhoek (1683–1708) [34], microbial mats appeared much earlier, and are identified today as the fossilised remains of 3.5-billion-year-old stromatolites [77]. Arguably the first observation by a microbiologist was made by Pasteur (1864) [34], and by the end of the nineteenth-century, environmental microbiologists were investigating them as well (we list several early observations following Pasteur in **Table 2**). For example,Winogradsky (1895) [78] described jelly-like masses of bacteria as 'zooglea', whilst Egunov (1895) [79]) and Sorokina (1938) [80] more obviously referred to biofilms in the current sense, using terms that translate into bacterial 'plate' or 'plane', and 'film', respectively.

Abscesses, inclusion bodies and metastasis	A mass of bacteria growing within another structure, including sediments, soils, plant and animal tissues.
Active fluids	Formed by motile bacteria moving together at high density in a liquid.
Active sludge	A complex mixture or community of bacteria and other microorganisms produced and used in wastewater treatment.
Aggregates, blobs, clumps, colloids, lumps and masses	A mass of bacteria (and other microorganisms) having some sort of physical cohesion; these may have developed by growth, or they may be the result of physical mixing or disturbance.
Bacterial plates	A layer of bacteria formed in a water column at a certain depth depending on oxygen levels.
Biofilms	A mass of bacteria enclosed in a protective matrix of EPS and associated with a surface or interface; most often used to refer to liquid-solid surface (L-S) interface biofilms such as those developing in flow-cells and in microtitre plates.
Biolaminites, microbialites, stratifera and stromatolites	Living and fossilised microbial mats which may trap and bind sediments and/or cause mineral precipitation, sometimes intercalated by sediment laminae; sometimes referred to as microbial-induced sedimentary (MIS) structures.
Clusters	A zone of physiologically synchronised bacteria within a lager aggregation, or a small mass of bacteria such as a colony or floc.
Collapsed cakes	Formed by the collapse of clumps or flocs on membranes during filtration.
Colonies, macro- and micro-colonies	A mass of bacteria having some sort of physical cohesion and having developed by growth on a solid dry surface; micro-colonies are those associated with the biofilm development process on submerged solid surfaces, or small aggregations of bacteria not noticed as colonies unless observed with magnification on leaf surfaces, detritus, or agar plates.
Communities and consortia	A complex mixture of multiple bacterial species (or genotypes) and possibly other microorganisms in which biotic interactions define structure and function.
Crusts, dust particulates and aerosols	Microbial communities developing on the surface of soils and dessert sand; also the dried remnants of colonies etc.
Deposits and sediments	Mass or body of bacteria that accumulate on dry or submerged surfaces due to wind or water movement.
Desert varnish	A dark stain or coating covering rock surfaces and colonised by bacteria.
Filamentous structures and streamers	Long strands of material stretching out from the main mass of a biofilm subject to liquid flow.
Films, layers, planes, plates, volumes and zones	A thin layer or volume containing bacteria which may or may not be physically connected to one another, solid surfaces, or other interfaces, and occurring in liquids, porous or permeable solids.
Flocs and snow	Masses of bacteria formed by growth, self-association, hydrophobic interactions, or by attachment to suspended inert particles; flocs in sea water are referred to as snow.
Floaters	Biofilms at the air-liquid interface having no appreciable attachment to a solid surface; these may be localised at the liquid surface by buoyancy, penetration of the interface, or by hydrophobic surfaces.
Foams	Air-water emulsions containing high concentrations of bacteria and compounds such as polymers and surfactants, which may help stabilise the structure.
Granules	A mass of bacteria growing on small solid particles.

Jellies and zooglea (or zoogloea)	A slimy mass of bacteria encased in a gel-like material, often found floating in water or found on plant stems or leaf litter.
Laminae	Layers of microbial mat generations, or microbial mats overgrowing sediments.
Mats	Microbial communities, often with clear layering or stratification, found in streams, lake or sea beds; these may also contain, algae and plants, and trap small particles including sand and stones.
Meniscus growth	A mass of bacteria adhered to a solid surface in the meniscus region of static liquids (the air-liquid-solid surface (A-L-S) interface).
Microcenosis, microbial cenosis	Microbial communities formed in a particular niche or site.
Micro-zones and pelogens	Microbial communities growing in thin layers structurally segregated with different characteristics or activities in sediments or silt.
Pellicles	A thin film or gel-like coating surrounding of individual bacteria, as well as air-liquid (A-L) interface biofilms.
Phlegm balls	Flocs found in underground streams.
Plaque	Dental biofilms formed largely by anaerobic bacteria on the surfaces and cavities in teeth.
Rafts	Flat sections on the edges of colonies, often associated with twitching motility, or flat pieces of un-attached biofilm found at the air-liquid interface.
Remains and remnants	A mass of bacteria and cellular debris found at a site at which they probably did not develop or a portion of a larger mass which has been removed by physical disturbance, predation or decay.
Sediments	Bacteria from liquids no longer in suspension, or microbial communities developing in sediments or silt.
Slimes, glycocalyx and viscous liquids	Viscous liquids or regions of a larger volume of liquid containing high densities of bacteria and EPS.
Snottites and snoticles	Pendulous or dripping masses of bacteria developing on cave walls or at the bottom of stalactites, especially limestone cave speleothems.
Swarms	Bacteria showing a particular form of surface-associated motility, moving in high densities across moist or wet surfaces.

This is a non-exhaustive list where terms, meanings and usage varies between contexts, and grouped terms may not be synonymous.

Table 1. Vernacular and scientific terminology used to describe bacterial aggregations

1864 Pasteur describes slimy material called Mother of Vinegar [34].

1887 Winogradsky observed bacterial growth in ring-like structures in a liquid microcosm containing H_2S and covered with a glass slide to restrict O_2 diffusion [86].

1893 Beijerink observed bacteria growing in zones of enriched water microcosms, the positions of which could be altered depending on O_2 and H_2 levels. Described 'Bakterienniveau' or 'niveau' as an aggregation formed by motile bacteria [87].

1895 Winogradsky observes bacterial zoogleas on potato slices [78].

1895	Egunov observed bacterial plates forming in microcosms containing Black Sea sediments, the position of which depended on anaerobic conditions, O_2 and H_2S levels. Some of these bacteria were motile, and Egunov asked what forces drove them to form a stationary aggregation [79,88].
1900	Egunov describes bacterial attachment during plate formation, and his 'bioanisotropy' concept for environments (continuous matter exchange between an organism and its surroundings) [89].
1914	Isachenko describes 'pink water' caused by the aggregation of purple bacteria in sea water as well as bacteria forming cloud-like structures in liquid microcosms [36].
1933	Henrici observed that bacteria mostly grow on submerged surfaces, not in free flowing water [34].
1935	Zobell describes marine bacteria attachment to surfaces [34].
1938	Sorokina describes a bacterial film forming on a submerged slime surface in a liquid microcosm [80].

Table 2. Early observations of bacterial aggregations.

More recently, pendulous and dripping snottites have been described on cave walls and stalactites [81] and collapsed cakes are a problem in filtration [82]. More interesting, perhaps, are the reports that bacterial remains have been misidentified as dinosaur soft tissues [83] and desert varnishes are being used to train sensors for future planetary explorations [84]. Regrettably, we also note that a chance to create a more evocative science fiction term for biofilms on the International Space Station was missed [85].

We argue that such an extensive collection of terms used to describe bacterial aggregations should not be considered a plethora, but rather an indication that the diversity of aggregations we are aware of may reflect the multitude of ways bacteria to respond to differing ecological opportunities. However, we do not suggest that each of the terms are unique, as quite evidently different types of aggregations may be associated closely or more distantly from one another, depending on which abiotic or biotic factors are considered.

7. Key features linking aggregations

Bacteria interact with abiotic and biotic factors by responding to physical and chemical cues according to behavioural and adaptive strategies under constant selection to maximise fitness. When these cues and strategies are considered in the context of a larger continuum of aggregations, it is possible to identify key features that link aggregations within a larger continuum (**Table 3**). Here we briefly indicate how physical interactions, diffusion radii, and increasing genetic diversity might be used to compare different types of aggregations.

Chemical gradients	Controlling the behaviour of individuals and groups, defining zones of optimal and restricted growth, providing information about local conditions; of nutrients, O_2 and other electron acceptors and metabolites, chemosensory, regulatory and communication compounds, and waste.
Competition	Between genotypes or lineages for resources, drives adaptation, allows investment in public goods but also results in cheaters.
Complexity	Of abiotic and biotic interactions, of genotypes, metabolism, structures, etc.

Communication, co-operation and co-ordination	Linking individuals into a group through the exchange of communication signals and/or response to the same environmental signals, resulting in similar behaviours or activities, and the production of common goods such as EPS and other secreted products.
Developmental pathway	Guiding the behaviour individuals and groups through a series of defined stages and resulting in a specific type of aggregate; responding to abiotic and biotic factors including communication signals.
Environmental conditions and modification	Abiotic chemical and physical factors, biotic factors; niche, opportunities, substrates, resources, stress, variation and instability; local, large-scale and irreversible changes, depletion, contamination.
Gene expression	Controlling behaviour, communication, metabolism, the production of compounds required for the formation of aggregations, etc.
Genotypes and diversity	Aggregations may arise from a single individual or founder population of the same genotype, but diversity will develop over time with radiation and immigration; single or multi-species aggregations; cheaters, invaders and persisters.
Liquid flow	Around and within aggregations, effecting the development of the physical structure, deformation and breakage, boundary layers, mass transport and diffusion of molecules, as well as the movement of bacteria.
Mobility	Of individual bacteria, small groups and larger aggregations, over small and large-scale distances, across interfaces, surfaces and volumes, and through environments.
Physical interactions	With interfaces, surfaces, bacteria, EPS, etc., in terms of strength, elasticity or resilience, distances, duration and reversibility.
Resilience	To chemical and physical stress, external competition, predation, and in terms of physical structure.
Sensory zones	The ability of individuals to detect the presence of others using altered chemical gradients, metabolites and communication signals (diffusion radii), and the distance separating individuals or groups.
Stratification	From homogeneous mixtures to clustered or layered differences resulting from age, metabolism, diversity and function.
Structure and rheology	Aggregations having properties similar to Newtonian liquids, visco-elastic gels and solids.
Succession	The diversity and function of aggregations will develop over time and with changing environmental conditions.
Time	The time-scale for the development, presence or persistence of aggregations may vary considerably, effecting population size, radiation, succession, aggregation structure and stratification, and environmental impact.

Table 3. Features linking bacterial aggregations within a larger continuum.

Physical interactions involving bacterial surface coatings, appendages and matrix, solid surfaces and interfaces within A-L and L-S interface biofilms are known to be complex (**Figure 2**), but there is no reason to believe that all types of interactions are unique to these particular aggregations. We therefore propose that one feature of the continuum of aggregations could be expressed by a scale going from no interactions with solid surfaces or other interfaces, as in the case of a population of planktonic bacteria, through short-term, weak, or distant physical contacts with surfaces, interfaces, or material, to the complexity of interactions seen in A-L and L-S interface biofilms, and presumably in other aggregations such as flocs, granules, and snow.

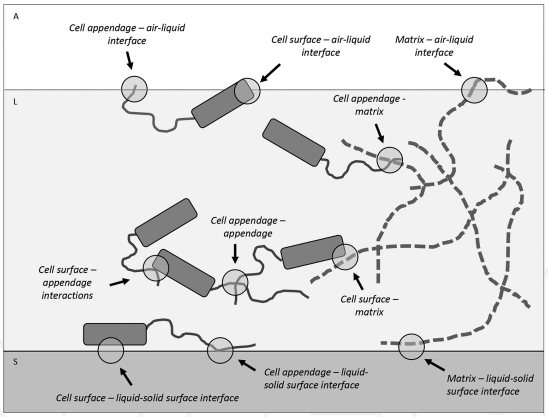

Figure 2. Bacterial aggregations are constructed by numerous and varied physical interactions. Bacterial cells within aggregations will interact with one another through close, intermediate, and long-range interactions involving surface coatings and extended appendages (e.g. flagella), matrix components, solid surfaces and interfaces (e.g. the air-liquid interface). (Key: A, air; L, liquid; S, solid; Matrix components or fibres are artistically depicted by dashed lines and bacteria as bacilli with a single flagella.)

Interactions with surfaces and interfaces also clearly limit the ability of an aggregation to develop, so the ability to expand across surfaces or to penetrate volumes, along with altered mass transport and diffusion characteristics, also present other scales with which to compare aggregations (**Figure 3**). In particular, diffusion radii will determine the ability of individual bacteria to detect the proximity of others and to respond competitively or with co-operation. Clearly, low-density planktonic and surface-attached bacteria may be beyond detection distances, but as bacterial numbers increase, their individual and collective impacts on local environmental conditions will lead to a situation where they are now within the same micro-environment, and similar conditions may result in coordinated changes in gene expression

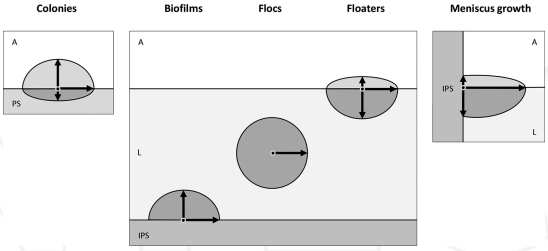

Figure 3. Bacterial aggregations develop at interfaces, within liquids, porous solids, and visco-elastic materials. Colonising bacteria may develop into communities restricted primarily by diffusion or liquid flow (mass transport) of chemicals and the ability to expand across interfaces or into spaces (radial arrows). Shown here (left to right) are colonies growing on and into a solid, biofilms growing on a solid submerged surface, flocs developing from a suspended particle, floaters forming at the air-liquid interface, and meniscus growth occurring at the air-liquid-solid surface interface. (Key : A, air; IPS, impermeable solid; L, liquid; PS, permeable or porous solid; S, solid; arrows indicate expansion radii and the opposite direction indicates diffusion gradients that limit growth.)

http://dx.doi.org/10.5772/62912

patterns, behaviour, and metabolism. We propose that separation distance, scaled in terms of chemical gradients, will also be a useful means of comparing and differentiating bacterial aggregations.

Aggregations developing over significant periods of time will also gain diversity by radiation and immigration, leading to multispecies communities subject to ecological succession, driven by internal competitive and co-operative interactions and changing environmental conditions (**Figure 4**). We propose that both diversity in terms of genotype or species composition and community function could also be used to consider bacterial aggregations, and this perspective is complementary to understanding the physical interactions and the molecular biology underlying the development of these structures.

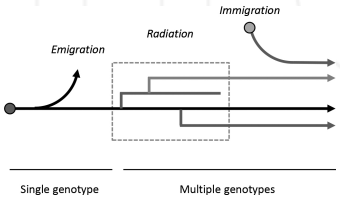

Figure 4. Bacterial aggregations gain diversity over time. An aggregation developing from a single genotype will gain diversity through radiation (mutation), immigration, and succession. Stochastic events and changing selective pressures will result in different genotypes within the community; some genotypes may become extinct and diversity may fall. (Key: Time progresses from left to right; colonising genotypes are shown as circles; mutation events as vertical lines; successful genotypes are indicated by arrows and an extinction event by a truncated line.)

By considering the ability of individual bacteria to respond to their local environments via different growth and colonisation strategies, the impact of abiotic conditions on individuals and the structures they create, and the longer-term development of the community, it is possible to speculate how altered environmental conditions and circumstance can lead to the cycling between different types of aggregation (**Figure 5**). The ability of bacteria to move between different types of aggregation with changing conditions or to exploit new opportunities will clearly differentiate those able to colonise a wide range of environments with those adapted to very specific niches.

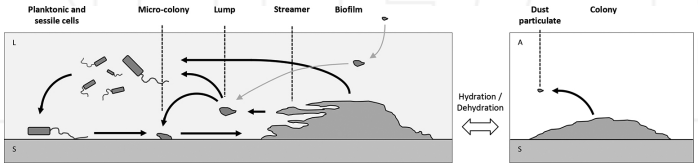

Figure 5. Bacterial aggregations change nature with altering environmental conditions. Although aggregations may develop and persist in one site, conditions may change resulting in an aggregation with a substantially different nature. The archetypal L-S interface biofilm developmental process is shown on the left. Biofilms may dry out to form slimes and colonies, and further drying might result in dust particulates which may rehydrate to form aggregations. (Key: A, air; L, liquid; S, solid; bacteria are artistically depicted as bacilli with a single flagella.)

8. Conclusion

In this opinion piece, we advocate the inclusion of biofilms within the larger context of a continuum of bacterial aggregations. We do this because we are growing concerned that the 'Microbial Cities' vision originating from the seminal reviews by Costerton et al. [1,2] is beginning to dominate biofilm research, and that such a narrow view limits our ability to better understand bacterial colonisation of a variety of different environments. In this continuum, we consider A-L and L-S interface biofilms to be biofilms, but argue that other aggregations such as colonies are significantly different and should not be referred to using this particular term. It is also possible that applied and environmental microbiologists prefer to refer to microbial mats rather than to biofilms, because the latter is too closely associated with experimental L-S interface biofilms produced in flow-cells or microtitre plates, and too far removed from the aggregations found in natural and other man-made environments.

We believe that the advantages of taking a wide view will allow us to distinguish those processes governing general colonisation through the formation of aggregations and ecological success, from those unique to particular environments and specialised strategies (as an apologia, we remind readers of the sensu lato definition of biofilms, secundum Costerton et al., which was inclusive of a number of different aggregations). By suggesting that biofilms are better considered as one of a variety of different aggregations, the simplistic planktonic-(sessile) biofilm dichotomy is also challenged, and perhaps the best reference or comparator for different aggregations will not always be logarithmic phase planktonic bacteria.

Author details

Olena V. Moshynets[1] and Andrew J. Spiers[2*]

*Address all correspondence to: a.spiers@abertay.ac.uk

1 Cell Regulatory Mechanisms Department, Institute of Molecular Biology and Genetics of the National Academy of Sciences of Ukraine, Kiev, Ukraine

2 School of Science, Engineering and Technology, Abertay University, Dundee, United Kingdom

References

[1] Costerton JW, Lewandowski Z, DeBeer D, Caldwell D, Korber D, James G. Biofilms, the customized microniche. J Bacteriol. 1994; 176:2137–2142.

[2] Costerton JW, Lewandowski Z, Caldwell D, Korber D, Lappin-Scott HM. Microbial biofilms. Annu Rev Microbiol. 1995; 49:711–745.

[3] Watnik P, Kolter R. Biofilm, City of Microbes. J Bacteriol. 2000; 182:2675–2679.

[4] Wimpenny J. Microbial metropolis. Adv Microbial Physiol. 2009; 56:29–84.

[5] Ben-Jacob E, Levine H. Self-engineering capabilities of bacteria. J. R. Soc. Interface 2006; 3:197–214.

[6] Hufnagel DA, Depas WH, Chapman MR. The biology of the *Escherichia coli* extracellular matrix. Microbiol Spectrum 2014; 3:MB-0014-2014.

[7] Tolker-Nielsen T. *Pseudomonas aeruginosa* biofilm infections: from molecular biofilm biology to new treatment possibilities. APMIS Suppl. 2014; 138:1–51.

[8] Simm R, Ahmad I, Rhen M, Le Guyon S, Römling U. Regulation of biofilm formation in *Salmonella enterica* serovar Typhimurium. Future Microbiol. 2014; 9:1261–1282.

[9] Archer NK, Mazaitis MJ, Costerton JW, Leid JG, Powers ME, Shirtliff ME. *Staphylococcus aureus* biofilms. Virulence 2011; 2:445–459.

[10] Teschler JK, Zamorano-Sánchez D, Utada AS, Warner CJA, Wong GCL, Linington RG, Yildiz FH. Living in the matrix: assembly and control of *Vibrio cholerae* biofilms. Nat Rev Microbiol. 2015; 13:255–268.

[11] Folkesson A, Jelsbak L, Yang L, Johansen HK, Ciofu O, Høiby N, Molin S. Adaptation of *Pseudomonas aeruginosa* to the cystic fibrosis airway: an evolutionary perspective. Nat Rev Microbiol. 2012; 10:841–851.

[12] Kumar CG, Anand SK. Significance of microbial biofilms in food industry: a review. Int J Food Microbiol. 1998; 42:9–27.

[13] Clutterbuck AL, Woods EJ, Knottenbelt DC, Clegg PD, Cochrane CA, Percival SL. Biofilms and their relevance to veterinary medicine. Vet Microbiol. 2007; 121:1–17.

[14] Bogino PC, de las Mercedes Oliva M, Sorroche FG, Giordano W. The role of bacterial biofilms and surface components in plant-bacterial associations. Int J Mol Sci. 2013; 14:15838–15859.

[15] Li K, Whitfield M, Van Vliet KJ. Beating the bugs: roles of microbial biofilms in corrosion. Corros Rev. 2013; 31:73–84.

[16] Taylor-George S, Palmer F, Staley JT, Borns DJ, Curtiss B, Adams JB. Fungi and bacteria involved in desert varnish formation. Microb Ecol. 1983; 9:227–245.

[17] Dupraz C, Visscher PT. Microbial lithification in marine stromatolites and hypersaline mats. Trends Microbiol. 2005; 13:429–438.

[18] Edwards KJ, Bach W, McCollom TM. Geomicrobiology in oceanography: microbe–mineral interactions at and below the seafloor. Trends Microbiol. 2005; 13:449–456.

[19] Wotton RS, Preston TM. Surface films: areas of water bodies that are often overlooked. BioScience 2005; 55:137–145.

[20] Franks J, Stolz JF. Flat laminated microbial mat communities. Earth-Science Rev. 2009; 96:163–172.

[21] Bolhuis H, Cretoiu MS, Stal LJ. Molecular ecology of microbial mats. FEMS Microbiol Ecol. 2014; 90:335–350.

[22] McDougald D, Rice SA, Barraud N, Steinberg PD, Kjelleberg S. Should we stay or should we go: mechanisms and ecological consequences for biofilm dispersal. Nat Rev Microbiol. 2011; 10:39–50.

[23] Renner LD, Weibel DB. Physicochemical regulation of biofilm formation. MRS Bulletin 2011; 36:347–355.

[24] Busscher HJ, van der Mei HC. How do bacteria know they are on a surface and regulate their response to an adhering state? PLoS Pathogens 2012; 8:e1002440.

[25] Guttenplan SB, Kearns DB. Regulation of flagellar motility during biofilm formation. FEMS Microbiol Rev. 2013; 37:849–871.

[26] Mhatre E, Monterrosa RG, Kovács AT. From environmental signals to regulators: modulation of biofilm development in Gram-positive bacteria. J Basic Microbiol. 2014; 54:616–632.

[27] Donné J, Dewilde S. The challenging world of biofilm physiology. Adv Microb Physiol. 2015; 67:235–292.

[28] Pamp SJ, Sternberg C, Tolker-Nielsen T. Insight into the microbial multicellular lifestyle via flow-cell technology and confocal microscopy. Cytometry Part A 2009; 75A:90–103.

[29] Coenye T, Nelis HJ. In vitro and in vivo model systems to study microbial biofilm formation. J Microbiol Meth. 2010; 83:89–105.

[30] Bjarnsholt T, Alhede M, Alhede M, Eickhardt-Sørensen SR, Moser C, Kühl M, Jensen PØ, Høiby N. The in vivo biofilm. Trends Microbiol. 2013; 21:466–474.

[31] Roberts AEL, Kragh KN, Bjarnsholt T, Diggle SP. The limitations of in vitro experimentation in understanding biofilms and chronic infection. J Mol Biol. 2015; 427:3646–3661.

[32] Belas R. Biofilms, flagella, and mechanosensing of surfaces by bacteria. Trends Microbiol. 2014; 22:517–527.

[33] von Rosenvinge EC, O'May GA, Macfarlane S, Macfarlane GT, Shirtliff ME. Microbial biofilms and gastrointestinal diseases. Pathog Dis. 2013; 67:25–38.

[34] Römling U, Kjelleberg S, Normark S, Nyman L, Uhlin BE, Åkerlund B. Microbial biofilm formation: a need to act. J Internal Med. 2014; 276:98–110.

[35] Yaron S, Römling U. Biofilm formation by enteric pathogens and its role in plant colonization and persistence. Microb Biotechnol. 2014; 7:496–516.

[36] Isachenko BL. Investigations on bacteria from Artic Ocean. [In Russian] Proceedings of the Murmansk Scientific-Enterprise Expedition 1906. Agriculture Department, Petrograd, 1914.

[37] Rybtke M, Hultqvist LD, Givskov M, Tolker-Nielsen T. *Pseudomonas aeruginosa* biofilm infections: community structure, antimicrobial tolerance and immune response. J Mol Biol. 2015; 427:3628–3645.

[38] Parsek MR, Greenberg EP. Sociomicrobiology: the connections between quorum sensing and biofilms. Trends Microbiol. 2005; 13:27–33.

[39] West SA, Griffin AS, Gardner A, Diggle SP. Social evolution theory for microorganisms. Nat Rev Microbiol. 2006; 4:597–607.

[40] Nadell CD, Xavier JB, Foster KR. The sociobiology of biofilms. FEMS Microbiol Rev. 2009; 33:206–224.

[41] Burmølle M, Ren D, Bjarnsholt T, Sørensen SJ. Interactions in multispecies biofilms: do they actually matter? Trends Microbiol. 2014; 22:84–91.

[42] Branda S, Vik Å, Friedman L, Kolter R. Biofilms: the matrix revisited. Trends Microbiol. 2005; 13:20–26.

[43] Vlamakis H, Chai Y, Beauregard P, Losick R, Kolter R. Sticking together: building a biofilm the *Bacillus subtilis* way. Nat Rev Microbiol. 2013; 11:157–168.

[44] Spiers AJ, Deeni YY, Folorunso AO, Koza A, Moshynets O, Zawadzk K. Cellulose expression in *Pseudomonas fluorescens* SBW25 and other environmental pseudomonads. In: De Ven V, Godbout L, editors. Cellulose – Medical, Pharmaceutical and Electronic Applications. Rijeka: InTech Publishers, 2013. p. 1–26.

[45] Römling U. Characterization of the rdar morphotype, a multicellular behaviour in Enterobacteriaceae. Cell Mol Life Sci. 2005; 62:1234–1246.

[46] Armitano J, Méjean V, Jourlin-Castelli C. Gram-negative bacteria can also form pellicles. Environ Microbiol Rep. 2014; 6:534–544.

[47] Moshynets O, Boretska M, Spiers AJ. From Winogradsky's column to contemporary research using bacterial microcosms. In: Harris CH, editor. Microcosms: Ecology, Biological Implications and Environmental Impact. Microbiology Research Advances Series. New York: Nova Publishers, 2013. p. 1–27.

[48] Spiers AJ. A mechanistic explanation linking adaptive mutation, niche change and fitness advantage for the Wrinkly Spreader. Int J Evol Biol. 2014; 2014: Article ID 675432, 10 pages.

[49] Spiers AJ, Bohannon J, Gehrig SM, Rainey PB. Biofilm formation at the air–liquid interface by the *Pseudomonas fluorescens* SBW25 Wrinkly Spreader requires an acetylated form of cellulose. Mol Microbiol. 2003; 50:15–27.

[50] Ude S, Arnold DL, Moon CD, Timms-Wilson T, Spiers AJ. Biofilm formation and cellulose expression among diverse environmental Pseudomonas isolates. Environ Microbiol. 2006; 8:1997–2011.

[51] Udall YC, Deeni Y, Hapca SM, Raikes D, Spiers AJ. The evolution of biofilm-forming wrinkly spreaders in static microcosms and drip-fed columns selects for subtle differences in wrinkleality and fitness. FEMS Microb Ecol. 2015; 91:fiv057.

[52] Robertson M, Hapca SM, Moshynets O, Spiers AJ. Air–liquid interface biofilm formation by psychrotrophic pseudomonads recovered from spoilt meat. Antonie van Leeuwenhoek 2013; 103:251–259.

[53] Spiers AJ, Rainey PB. The *Pseudomonas fluorescens* SBW25 wrinkly spreader biofilm requires attachment factor, cellulose fibre and LPS interactions to maintain strength and integrity. Microbiology 2005; 151:2829–2839.

[54] Koza A, Hallett PD, Moon CD, Spiers AJ. Characterization of a novel air–liquid interface biofilm of *Pseudomonas fluorescens* SBW25. Microbiology 2009; 155:1397–1406.

[55] Gómez P, Buckling A. Real-time microbial adaptive diversification in soil. Ecology Lett. 2013; 16:650–655.

[56] Ray VA, Morris AR, Visick KL. A semi-quantitative approach to assess biofilm formation using wrinkled colony development. J Vis Exp. 2012; 64:e4035.

[57] Dietrich LE, Okegbe C, Price-Whelan A, Sakhtah H, Hunter RC, Newman DK. Bacterial community morphogenesis is intimately linked to the intracellular redox state. J Bacteriol. 2013; 195:1371–1380.

[58] Cairns LS, Hobley L, Stanelly-Wall NR. Biofilm formation by *Bacillus subtilis*: new insights into regulatory strategies and assembly mechanisms. Mol Microbiol. 2014; 93:587–598.

[59] Espeso DR, Carpio A, Einarsson B. Differential growth of wrinkled biofilms. Phys Rev E Stat Nonlin Soft Matter Phys. 2015; 91:022710.

[60] Hobley L, Harkins C, MacPhee CE, Stanley-Wall NR. Giving structure to the biofilm matrix: an overview of individual strategies and emerging common themes. FEMS Microbiol Rev. 2015; 39:649–669.

[61] Wang X, Wang G, Hao M. Modelling of the *Bacillus subtilis* bacterial biofilm growing on an agar substrate. Comput Math Methods Med. 2015; ID 581829.

[62] Or D, Phutane S, Dechesne A. Extracellular polymeric substances affecting pore-scale hydrologic conditions for bacterial activity in unsaturated soils. Vadose Zone J. 2007; 6:298–305.

[63] Or D, Smets BF, Wraith JM, Dechesne A, Friedman SP. Physical constraints affecting bacterial habitats and activity in unsaturated porous media – a review. Water Res. 2007; 30:1505–1527.

[64] Dechesne A, Or D, Gülez G, Smets BF. The porous surface model, a novel experimental system for online quantitative observation of microbial processes under unsaturated conditions. Appl Environ Microbiol. 2008; 74:5195–5200.

[65] Rainey PB, Travisano M. Adaptive radiation in a heterogeneous environment. Nature 1998; 394:69–72.

[66] Spiers AJ. Wrinkly-Spreader fitness in the two-dimensional agar plate microcosm: maladaptation, compensation and ecological success. PLoS One. 2007; 2:e740.

[67] Green JH, Koza A, Moshynets O, Pajor R, Ritchie MR, Spiers AJ. Evolution in a test tube: rise of the wrinkly spreaders. J Biol Educ. 2011; 45:54–59.

[68] Spiers AJ, Kahn SG, Travisano M, Bohannon J, Rainey PB (2002). Adaptive divergence in *Pseudomonas fluorescens*. 1. Determinants of Wrinkly Spreader fitness and the cause of an evolutionary transition. Genetics 2002; 161:33–46.

[69] Koza A, Moshynets O, Otten W, Spiers AJ. Environmental modification and niche construction: Developing O_2 gradients drive the evolution of the Wrinkly Spreader. ISME J. 2011; 5:665–673.

[70] Sanders LH, Rockel A, Lu H, Wozniak DJ, Sutton MD. Role of *Pseudomonas aeruginosa dinB*-encoded DNA Polymerase IV in mutagenesis. J Bact. 2006; 188:8573–8585.

[71] Kempes CP, Okegbe C, Mears-Clarke Z, Follows MJ, Dietrich LE. Morphological optimization for access to dual oxidants in biofilms. Proc Natl Acad Sci USA. 2014; 111:208–213.

[72] Okegbe C, Price-Whelan A, Dietrich LE. Redox-driven regulation of microbial community morphogenesis. Curr Opin Microbiol. 2014; 18:39–45.

[73] Brune A, Frenzel P, Cypionka H. Life at the oxic-anoxic interface: microbial activities and adaptations. FEMS Microbiol Rev. 2000; 24:691–710.

[74] Fenchel T, Finlay B. Oxygen and the spatial structure of microbial communities. Biol Rev Camb Philos Soc. 2008; 83:553–569.

[75] Härtig E, Jahn D. Regulation of the anaerobic metabolism in *Bacillus subtilis*. Adv Microb Physiol. 2012; 61:195–216.

[76] Bettenbrock K, Bai H, Ederer M, Green J, Hellingwerf KJ, Holcombe M, Kunz S, Rolfe MD, Sanguinetti G, Sawodny O, Sharma P, Steinsiek S. Towards a systems level understanding of the oxygen response of *Escherichia coli*. Adv Microb Physiol. 2014; 64:65–114.

[77] Noffke N, Christian D, Wacey D, Hazen RM. Microbially induced sedimentary structures recording an ancient ecosystem in the *ca*. 3.48 billion-year-old dresser formation, Pilibara, Western Australia. Astrobiology 2013; 13:1103–1124.

[78] Winogradsky SN. On free atmospheric nitrogen assimilation by microbes [In Russian]. Arch Biological Sci, Imperial Institute of Experimental Medicine in St. Petersburg, 1895; 3:293–351.

[79] Egunov MA. Sulfur bacterium of Odessa estuaries. [In Russian] Arch Biological Sciences, Imperial Institute of Experimental Medicine in St. Petersburg. 1895; 3:378–393.

[80] Sorokina VA. Exchange of substance between slime and water, as influenced by the formation of a bacterial film on the surface of the slime. [In Russian] Microbiology 1938; 7:579–591.

[81] Johnson DB. Geomicrobiology of extremely acidic subsurface environments. FEMS Microbiol Ecol. 2012; 81:2–12.

[82] Guo W, Ngo H-H, Li J. A mini-review on membrane fouling. Bioresource Technol. 2012; 122:27–34.

[83] Kaye TG, Gaugler G, Sawlowicz Z. Dinosaurian soft tissues interpreted as bacterial biofilms. PLoS One. 2008; 3:e2308.

[84] Malherbe C, Ingley R, Hutchinson I, Edwards H, Carr AS, Harris L, Boom A. Biogeological analysis of desert varnish using portable Raman spectrometers. Astrobiology. 2015; 15:442–452.

[85] Kim W, Tengra FK, Young Z, Shong J, Marchand N, Chan HK, Pangule RC, Parra M, Dordick JS, Plawsky JL, Collins CH. Spaceflight promotes biofilm formation by *Pseudomonas aeruginosa*. PLoS One 2013; 8:e62437.

[86] Winogradsky SN. On sulfur bacteria. [In German] Botanical Newspaper. 1887; 45: 489–610.

[87] Beyerink NW. On breathing characteristics of moving bacteria. [In German] Central Journal of Bacteria and Parasites 1893; XIV:827.

[88] Egunov M. On a plate of sulphur bacteria in the Black Sea. [In Russian] Findings of the Odessa Agricultural Institute 1926, II:49–60.

In: Microcosms
Editor: Christopher C. Harris
ISBN: 978-1-62618-661-3
© 2013 Nova Science Publishers, Inc.

The license for this PDF is unlimited except that no part of this digital document may be reproduced, stored in a retrieval system or transmitted commercially in any form or by any means. The publisher has taken reasonable care in the preparation of this digital document, but makes no expressed or implied warranty of any kind and assumes no responsibility for any errors or omissions. No liability is assumed for incidental or consequential damages in connection with or arising out of information contained herein. This digital document is sold with the clear understanding that the publisher is not engaged in rendering legal, medical or any other professional services.

Chapter 1

FROM WINOGRADSKY'S COLUMN TO CONTEMPORARY RESEARCH USING BACTERIAL MICROCOSMS

Olena Moshynets[1], Mariia Boretska[2] and Andrew J. Spiers[3]*

[1]Laboratory of Microbial Ecology, Institute of Molecular Biology and Genetics,
National Academy of Sciences of Ukraine, Kyiv, Ukraine
[2]Department of General and Soil Microbiology,
D. K. Zabolotny Institute of Microbiology and Virology,
National Academy of Sciences of Ukraine, Kyiv, Ukraine
[3]The SIMBIOS Centre and School of Contemporary Sciences,
University of Abertay Dundee, Dundee, UK

ABSTRACT

The fast pace of scientific research often means that contemporary investigators are unaware of critical developments resulting from the work of previous generations of scientists. We were superficially aware of Sergei Winogradsky (1856 – 1953) through his columns, currently in teaching to illustrate aspects of microbial succession and community function, but were unaware of his importance as the founder of microbial ecology and the first to use microcosms to study bacterial physiology. Here we take the opportunity to remind fellow microbiologists of his work, presenting in homage columns constructed using water and sediments from the Dnipro (Dnieper) collected close to his place of birth. We then provide a review of our own research using microcosms to investigate aspects of plant-bacterial interactions, bacterial evolution, biofilm-formation, and soil colonization, as well as recent advances in developing plastic and transparent soils to investigate root development and fungal hyphae invasion in soil pore networks, to show that more than one hundred years after the invention of the microcosm, they are still being used profitably in microbial research.

* E-mail address: a.spiers@abertay.ac.uk.

INTRODUCTION

The science of medical microbiology was established through the pioneering work of scientists such as Louis Pasteur (1822 – 1895), Ferdinand Cohn (1828 – 1898), Heinrich Koch (1843 – 1910), and others in the last part of the 19th century. Pasteur made significant breakthroughs investigating the cause and prevention of diseases, Cohn instigated bacterial classification based on morphology, and Koch became famous for his postulates defining pathogens. During this period, the early isolation and characterisation of bacteria relied on the use of universal growth media and the presumption that all microbial activity was the result of specific isolates functioning alone. In contrast, the pioneering work of the environmental and ecological microbiologists, Martinus Beijerinck (1851 – 1931) and Sergei Winogradsky (1856 – 1953), are often overlooked and are perhaps unfairly overshadowed by their contemporaries who studied human disease. Beijerinck and Winogradsky investigated the biochemical role bacteria play in important natural processes, including nitrification, nitrogen fixation and sulfur[1] oxidation. Winogradsky emphasised repeatedly that the objectives of ecological microbiology differed from those of medical microbiology [109, 110]. He pioneered the use of the selective[2] approach to study biological processes in contrast to the universal medium used by Koch and others to isolate and characterise pure strains (see the quote from Winogradsky [105, 106] in [109]), as well as the realisation that in order to understand some biological processes, communities of bacteria needed to be studied rather than single cultures. Winogradsky is often described as the father of microbial ecology, and is considered the founder of contemporary ecological microbiology in Russia where his approach led to the Winogradsky School of Microbiology[3] [2, 17, 109, 110]. More relevant to this book is that Winogradsky was one of the first to use and promote microcosms in microbial research.

S. N. WINOGRADSKY

Sergei Nikolaevich Winogradsky[4] was born in 1856 into a wealthy family in Kyiv (Kiev), then part of Russia (a photograph of him is presented in Figure 1). He appeared to have had a troubled education, selling his golden graduation medal from the Second Kyiv Gymnasium (a secondary or grammar school) in 1873 in response to what he felt was an '*uninteresting, disagreeable, physically and morally humiliating style of teaching*' (Selam Waksman, quoted in [17]). He entered the University of Kyiv in 1873 to study law following his brother and father, but transferred to the natural sciences within a month before leaving the university altogether. He spent a year at the St. Petersburg Academy of Music studying piano, before finally entering the University of St. Petersburg in 1877 to study the natural sciences and microbial physiology with Andrey Famintsyn.

[1] We adopt the spelling convention for sulfur and sulfur compounds as recommended by the Royal Society of Chemistry Nomenclature Committee.
[2] Winogradsky referred to this as 'elective'.
[3] In comparison, Beijernck's Delft School of Microbiology was relatively well-known to non-Soviet microbiologists and historians of biology.
[4] Also transliterated from the Russian (Виноградский) or Ukrainian (Виноградський) as 'Vinogradskii'.

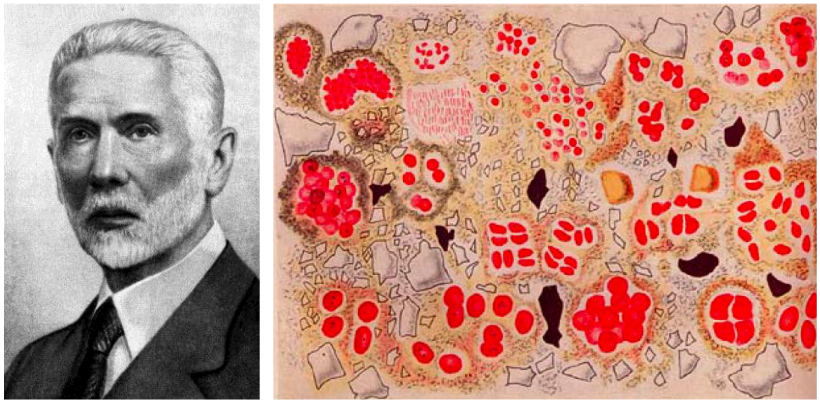

Figure 1. S.N. Winogradsky and soil landscapes. (Left) Photograph of Winogradsky (c. 1936). (Right) Winogradsky drew 'soil landscapes' to show the relationship between soil microorganisms and particles (Brie soil sample, ~100 µm wide; c. 1924). Images are from Winogradsky [105] and Seliber [82].

An outline of his impressive professional career is provided in the table at the end of this Chapter, and several relevant areas of his work are described in this section (the details summarised here are compiled from various references including [1, 2, 3, 17, 75, 78, 82, 104, 109, 110]; we do not cite Winogradsky's research publications here as they can be accessed through the references provided). In Famintsyn's laboratory, Winogradsky examined the nutritional and physiological properties of the yeast, *Candida vini*, originally known as *Mycoderma vini*[5]. *C. vini* is a pathogen of sugar beet (*Beta vulgaris*), which was causing problems for the developing European sugar industry, and it is also an etiological agent of wine illness or mould. Winogradsky used Geissler chambers to investigate the growth of *C. vini* cultures under different conditions. Detailed descriptions of this apparatus originally used by Pasteur [61] and its use by Winogradsky can be found in [2, 17]. In his biography of Winogradsky, Waksman suggests that these investigations of *C. vini* are the '*first careful investigations ever made on the influence of controlled environment on the growth of microorganisms in pure culture, under well-defined experimental conditions*' (Waksman, quoted in [17]). They may also be the first significant use of microcosms in the study of microorganisms, and Famintsyn's approach of coupling nutritional and physiological experiments with microscopic observations became Winogradsky's *modus operandi* [17]. Having completed his Master of Science degree at the University of St. Petersburg, Winogradsky joined Anton DeBary at the University of Strasburg in 1885 where he studied the filamentous sulfur-oxidizing bacterium *Beggiatoa*[6]. He was initially assigned a project to determine whether microorganisms were monomorphic or pleomorphic[7]. Winogradsky chose to investigate this using *Beggiatoa*, but could not prove the case that it was monomorphic as he was unable to isolate sufficiently pure cultures from sulfur springs in Switzerland and Germany. However, he became interested in the ability of *Beggiatoa* to accumulate intracellular sulfur granules and the role of sulfur metabolism in the growth of this bacterium.

[5] For a description of the *Candida* see [86].
[6] For a description of the *Beggiatoa* see [98].
[7] At the time there was a significant debate as to whether microorganisms exhibited multiple forms (i.e. pleomorphic) or whether they only had one form (i.e. monomorphic) (now the current view). However, to prove monomorphism, pure cultures where required for investigation.

During this period Winogradsky also '*reconfigured his technical repertoire …* (adding) *new variations of slide microcultures and, most important, artificial environments*' to investigate bacteria in their natural state, allowing him to bring the '*field into his laboratory*' [2].

Winogradsky demonstrated that the *Beggiatoa* oxidized H_2S (hydrogen sulfide) to S^0 (sulfur) to release energy and formed the sulfur granules[8] as a result of that process, referring to this form of metabolism as 'inorgoxidation' (the oxidation of inorganic compounds). By observing the behaviour of *Beggiatoa* cells under a cover-slip, Winogradsky was able to demonstrate that the cells migrated to a narrow interface where both H_2S and O_2 (oxygen) co-exist, O_2 being required for the oxidation of H_2S. This was also an early demonstration that motile organisms will choose an optimal position along chemical gradients where the most efficient metabolism and rapid growth is possible. A corollary of this is that simple microcosms with two chemical gradients can provide a habitat choice to which organisms can respond. From his studies of the oxidation of H_2S by *Beggiatoa*, Winogradsky formulated the theory of chemolithotrophy in which inorganic substrates, usually of mineral origin, are used to obtain reducing equivalents for biosynthesis or respiration. Many chemolithotrophic pathways are now known in which a wide range of inorganic substances, such as H_2S, NH_3 (ammonia), Fe^{2+} (ferrous iron), etc., are used by bacteria as a source of energy. For a range of reviews on this subject, see [23, 24, 28, 39, 42, 85]. Winogradsky then moved to the Swiss Polytechnic Institute in Zurich in 1888 where he developed his physical chemistry and bacterial skills in association with Ernst Schultz and Otto Roth (Winogradsky had a very poor opinion of Roth, see the quote in [17]). At Zurich, he studied the chemolithotrophy of sulfur and iron bacterium. Winogradsky also began his '*monumental studies on nitrification that provided clear evidence for the process of bacterial autotrophy and for its roles in the cycles of Nature*' [17] for which he is most famously remembered. He was the first to isolate and characterize nitrifying bacteria that oxidized NO_2^- (nitrite) to NO_3^- (nitrate), and confirmed that the oxidation of nitrogen in soil was a two-step biological process: NH_4^+ (ammonium) to NO_3^- and NO_3^- to NO_2^- (nitrite), with each step being performed by different organisms. This finding led directly to the concept of sulfur and nitrogen cycling in nature. For recent reviews on nutrient cycling and the roles of microorganisms, see [11, 20, 22, 24, 47, 49, 76, 85].

Winogradsky also reported the first example of chemoautrophy in which the energy gained from NO_2^- oxidation is used to fix CO_2 (carbon dioxide) to make organic compounds for growth or energy. The significance of this was that it was the first demonstration as an alternative to photosynthesis in which the energy from light is used to fix CO_2 (for a description of the different modes of energy conversion used by bacteria, see [79]). Dworkin [17] suggests that at this stage in the 1890's, Winogradsky began to recognize the need to re-examine and reinterpret laboratory observations with what actually happens in soils and elsewhere, marking the true beginning of the field of microbial ecology. It is noteworthy that Ernst Haeckel first defined ecology (œkologie) in 1868 as '*the science of all the relations of organisms with the external world, with the organic and anorganic conditions of existence; … the mutual relations of all organisms living in one and the same place, their adaptation to environmental circumstances, their transformations in the struggle for life …*' (Haeckel, quoted by [4]). Winogradsky returned to St. Petersburg in 1891 to be the Head of the General Microbiology Department of the Imperial State Institute of Experimental Medicine,

[8] He also determined that S^0 was further oxidized to SO_4^{2-} (sulfate) to release even more energy. The SO_4^{2-} is excreted as H_2SO_4 (sulfuric acid).

eventually becoming the Director in 1902. During this period he made a number of important discoveries, including the first isolation of the free-living anaerobic nitrogen fixer, *Clostridium pasteurianum*, originally known as *C. pastorianum*. This anaerobic bacterium could grow under N_2 (nitrogen) gas but not under normal aerobic (oxygenated) conditions. He subsequently showed that his original isolation of *C. pasteurianum* in flasks was successful because he had purified it in the presence of two contaminating aerobic organisms. These were able to reduce O_2 levels sufficiently to allow *C. pasteurianum* to grow anaerobically. In soils, the co-existence of different species having different nutritional requirements and activities underpins community function, and once again, Winogradsky's experiments with simple microcosms demonstrates that important ecological interactions can be identified and experimentally tested. In 1896 he presented a lecture at the Institute of Experimental Medicine '*On the role of microbes in the general cycle of life*' in which he visualized the activity of microbes as regulating the circulation of chemicals between the organic and inorganic realms throughout the world [2].

In 1905 Winogradsky resigned as Director of the Imperial State Institute of Experimental Medicine and retired to his estate in Gorodok in the Ukraine. However, he was forced to flee in the aftermath of the Russian Revolution in 1921. He spent the last thirty years of his life at the Pasteur Institute, which at that time was the centre of European microbiology, '*formulating the ideas and precepts of what was to become known as microbial ecology*' [17]. Central to this was the 'Direct' method which included microscopy and microphotography to '*gain direct access to the microscopic landscapes of soils*' [2]. In Figure 1 we present a soil landscape drawn by Winogradsky published in the 1920's[9] showing the distribution of microorganisms and particles of soil in a sample obtained from the Brie region of France [105, 106] (his soil landscapes have an artistic appeal that are lacking modern soil images, *cf.* Figures 5, 6 and 7, but in turn, his images lack the quantitative detail expected in contemporary research). During this period, another early pioneer of soil microbiology working in Kyiv, Nikolai Cholodny, developed the famous buried glass slide method to sample soil microorganisms whilst maintaining some spatial detail [12, 13]. He also realized that soil microorganisms could be studied by microscopy under natural conditions, using small transparent soil chambers where the influence of soil treatments could be studied experimentally. The innovative aspect of Winogradsky's Direct method, including contributions from others such as Cholodny, was that it did not rely on *in vitro* cultures but rather allowed investigation of microorganisms directly in the complexity of their natural environment. Edward Russell working at the Rothamsted Agricultural Experimental Station in the UK[10] corresponded with Winogradsky whom he called '*the founder of soil microbiology*', discussing the application of the Direct method in their work. Russell's colleague, Henry Thornton, began to combine it with their statistical approach to investigating soil microbiology. However, to link microbial distributions in soils with biochemical processes, Thornton maintained that there was still an essential place for the investigation of *in vitro* cultures in soil microbiology [2], a view that was ultimately accepted by Winogradsky in the development of his Direct method. During his career, Winogradsky was transformed from plant physiologist, to microbiologist and then to the first ecological

[9] It is worth mentioning that the first 35mm camera produced by Leica was not available until 1925, so hand-drawn microscopic observations were routinely used at the time of Winogradsky's soil studies.

[10] Apropos nothing at all, Andrew Spiers has a link with Rothamsted as some relatives live nearby.

microbiologist [3, 17]. In 1949 he published *Microbiologie du Sol: Problèmes et Méthodes, Cinquante ans de Recherches* (Soil Microbiology: Problems and Methods, Fifty Years of Investigations) [105, 106], a compendium of his research which included an essay describing the synthesis of microbiology and ecology into the new discipline of microbial ecology, and the development of soil microbiology. In this, his direct method had evolved into a synthetic approach that accommodated the biological, chemical and physical characteristics of soils. He argued that to study soil microbiology, a combination of techniques were required and that the biological, physical and chemical components should be thought of as parts of a single system [2]. In his biography Waksman concludes, in a somewhat understated manner, that Winogradsky had made '*significant contributions to the sciences of plant physiology, microbiology, soil science, and ecology*' and that '*his work unites these fields in a novel way*' [104]. Winogradsky published his last paper in 1953 and died the following year aged 97.

FROM GEISSLER CHAMBERS TO THE WINOGRADSKY COLUMN

Winogradsky began his observations of *Candida vini* using Geissler chambers which allowed him to make prolonged microscopic observations of the growing cells for up to eight months at a time. The Geissler chamber[11] was a section of glass tube that had been flattened to provide a small growth zone or microcosm through which different media could be passed (see [2, 17, 61]). These were probably the first flow chambers for the direct observation of microorganisms, very similar to the pedoscops capillary system proposed almost a century later [65], and analogous to current flow systems used in combination with CLSM (Confocal laser scanning microscopy) (e.g. [95]). Winogradsky went on to use larger microcosms to study sulfur bacteria, inoculating 3 – 5 litre flasks with pieces of muddy *Butomus umbellatus* (flowering or grass rush) rhizome which were then maintained for up to 6 weeks whilst measuring H_2S production and sampling for bacteria. He also used small glass cylinders and Petri dishes containing silica gels soaked with different nutrients to maintain and examine soil cultures. Winogradsky used glass cylinders filled with sulfur spring water and sediments to grow *Beggiatoa*. He subsequently used them to describe a variety of organisms, including purple photosynthetic bacteria[12]. These cylinders, now known as Winogradsky's columns, containing various mixtures of sand, soil, sediments, and water, are ideally suited to introducing microbiology students to selective culture methods, microbial community succession, and stratification along chemical and physical gradients (e.g. [6, 74, 77, 78]).

Winogradsky's columns are easily constructed and microbial changes are observable within weeks (as an example, see Figures 2 and 3 showing the construction of a pair of columns using river water and sediments collected from the banks of the Dnipro in Kyiv and their development over a period of several weeks). A further refinement of the Winogradsky column includes the use of agar to semi-solidify aqueous layers containing different nutrients to allow the isolation of bacteria.

[11] The 'Geissler tube' was the name given to early gas discharge tubes invented by the physicist Heinrich Geissler in 1857. It is not clear how the Geissler chamber used by microbiologists might relate to this, though it was used by Pasteur in the 1860's [61].

[12] Winogradsky was unaware at the time that they were capable of anaerobic anoxygenic photosynthesis [78].

Figure 2. Constructing Winogradsky's columns. We produced Winogradsky's columns using river water and sediments collected from the banks of the Dnipro. (Top left) The snow and ice-covered Dnipro in Kyiv in January 2013. (Bottom left) Sediment samples diligently collected by two of the Authors. (Right) Mariia Boretska (left) and Olena Moshynets (right) adding sediments and water to a glass cylinder to produce the Winogradsky's column. See Figure 3 for a series of images taken of these columns over a period of several weeks. Images are from Mariia Boretska and Olena Moshynets.

Figure 3. Microbial development of the Winogradsky's columns. The Dnipro river sediment and water columns were maintained at room temperature (~20°C) for several weeks under anaerobic conditions during which microbial colonisation and stratification occur. Shown here are a series of photographs of two columns; the left-hand one was incubated in the dark, and the right-hand one exposed to natural light. (Left to right) Immediately after construction; after 13, 23 and 37 days. Images are from Mariia Boretska and Olena Moshynets.

In a study of the cycling of H_2S and SO_4^{2-} in Black Sea coastal waters, another early pioneer of environmental microbiology, Mikhail Egunov, observed the development of a

bacterial film[13] between the upper SO_4^{2-}–rich layer and the lower H_2S–rich layer[14], and concluded that such a region occurred in the Black Sea at a depth of 200 m [18]; a sketch of Egunov's column was reproduced in a later publication by Winogradsky's only student, Vasily Omeliansky [57]). Although Winogradsky obtained his *Beggiatoa* from sulfur springs, they have also been recovered from the Black Sea and other marine environments, including deep-sea hydrothermal vent environments where they oxidize H_2S to S^0 and S^0 to SO_4^{2-}. In a study of the mechanism and rate of sulfide oxidation in water, Yury Sorokin used an experimental column to model the vertical gradient of the oxidation-reduction (redox) potential of sea water and bacteria in the Black Sea in which he also cited Egunov's earlier work [87]. After a period of two weeks Sorokin observed the stratification of bacteria in two principal regions of the column. The upper one contained H_2S–oxidizing *Acidithiobacilli*, formerly known as *Thiobacilli*, between the upper O_2–rich water layer and the lower H_2S–rich anaerobic water layer. The lower region was directly above a layer of agar at the bottom of the column, containing sulfide and sulfates which diffused upwards into the water column. In this lower region, sulfate-reduction was observed by the development of a ring of black sulfate-reducing colonies on the cylinder walls. Sorokin's column supported all of the biological functions required for a complete sulfur cycle, despite being structurally a very simple microcosm. Investigations of Black Sea microbiology continues today, almost 120 years after Egunov's original work, and now includes modern approaches such as metagenomics (reviewed by [96]). The ability to obtain bacterial sequences from environmental samples, such as particulate matter or marine snow, can provide information on bacterial diversity and community function. Sequences obtained from snow samples recovered from the suboxic zone of the Black Sea suggest that the interior of these sinking aggregates might support Mn (manganese) and SO_4^{2-} reduction as well as H_2S and S^0 oxidation [25]. Although the redox gradient might be the most obvious large-scale chemical gradient in the Black Sea, it is clear that there are smaller, local chemical gradients that might also affect bacterial activity and help define micro-habitats. Micrometre–scale gradients also exist within sediment and soil pore networks and aggregates where they help define micro-habitats and community function.

CONTEMPORARY USE OF MICROCOSMS IN BACTERIAL RESEARCH

It is humbling to summarize the achievements of the founder of contemporary ecological microbiology, albeit in such a superficial manner and without direct reference to his scientific publications, but it is also a useful exercise to show the early development and use of microcosms in microbiology. A microcosm can be simply defined as '*a community, place, or situation regarded as encapsulating in miniature the characteristics of something much larger*' [63]. They have been used by biologists from a variety of disciplines to study physiology, processes, and interactions over a range of scales, from single cell-traps to laboratory cultures, aquaria, field trials, to the management of national parks, entire river systems, lakes, coastal regions, and islands.

[13] A 'bacterial plate' may be a more accurate translation of 'бактериальная пластинка' [18].
[14] This is similar to Winogradsky's observations of *Beggiatoa* behaviour under a cover-slip.

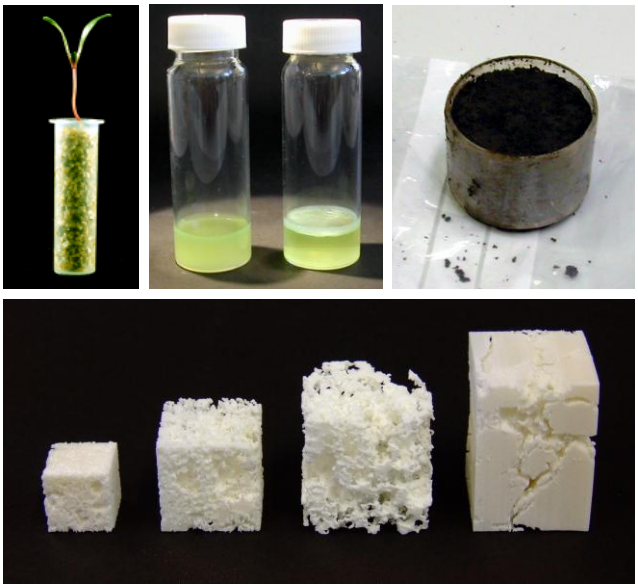

Figure 4. Microcosms have been used to investigate aspects of microbiological ecology, adaptation and evolution. (Top left) Plant-specific induction of *Pf.* SBW25 gene expression has been examined using sugar beet seedlings grown in a vermiculite – compost mixture (the plastic tube has a 1 cm diameter). (Top middle) Bacterial evolution and biofilm-formation have been investigated using glass vials containing liquid growth media (the glass vial has a 2.75 cm diameter). The microcosm on the left contains wild-type *Pf.* SBW25 that grows in the liquid column, and in the microcosm on the right, the evolved Wrinkly Spreader mutant forms a biofilm at the air-liquid interface. (Top right) The impact of bacterial surfactant expression on water distribution within soil pore networks has been investigated using sterile repacked soil aggregate cores (the core ring has a 37 mm diameter). (Bottom) Soil pore structures visualized by X-ray CT have been printed out at a larger scale in plastic to allow the investigation of fungal and bacterial colonization processes (the smallest cube is 1.8 cm wide). Images are from Andrew Spiers and Ruth Falconer.

Although the use of microcosms in research has important caveats, most often associated with the limited complexity of the system or the application of results to large-scale systems, they nonetheless provide a very powerful experimental system for biological research. As an example of this, we take the opportunity here to briefly present the research that colleagues and ourselves have undertaken in this field over the last 15 years, utilizing artificial growth media in glass vials and petri dishes, plants and repacked soil aggregate cores, and most recently, plastic and transparent soils, to investigate aspects of microbial ecology, adaptation and evolution (see Table 1 and Figure 4). Much of this work has involved the use of the soil and plant-associated fluorescent pseudomonad, *Pseudomonas fluorescens* SBW25 (referred to henceforth as *Pf.* SBW25), as a model organism in experimental evolution and biofilm studies (e.g. [44, 72, 92, 93]) and plant-microbe interactions (e.g. [26, 27, 69, 83]). *Pf.* SBW25 was isolated from a leaf of a sugar beet crop grown at the University Farm at Wytham, Oxford, UK (SBW stands for Sugar Beet Wytham) [71]. Like other fluorescent pseudomonads, *Pf.* SBW25 is a benign, plant growth-promoting bacterium, colonizing the leaves and roots of a wide variety of crop plants and weeds. In general, *P. fluorescens* strains are not considered plant pathogens [64], though like some other plant growth-promoting bacteria, *Pf.* SBW25 carries a defective pathogen-like type III secretion system [66].

Table 1. Contemporary investigations

Investigation	Microcosm	Sampling and measurement	Potential variables
Experimental evolution[a] and biofilms[b.]	Glass vials containing liquid growth media.	Destructive sampling to determine diversity, fitness, biofilm growth, strength and attachment.	Nutrients, O2, physical disturbance, liquid viscosity, interspecific completion, phage and plasmid co-evolution.
Plant-specific induction of bacterial gene expression[c].	Sugar beet seedlings grown in compost-vermiculite or potting mixture.	Destructive recovery of bacteria and sequencing; re-testing to determine expression levels and fitness; Raman spectroscopy.	Plant, bacteria and soil type, temperature, water and humidity.
Fitness advantage of cellulose expression.[d]	Surface-sterilized mushroom caps.	Destructive recovery of bacteria to determine fitness.	Mushroom and bacteria type, presence of predators and competitors.
Impact of bacterial surfactants on soil hydrology.[e]	Repacked soil aggregate cores.	Destructive determination of water content.	Bacteria type and distribution, soil type, porosity, water content.
Fungal invasion of soil pore networks.[f]	Printed plastic model of real soil structure.	Non-destructive photography and X-ray CT imaging.	Structure (porosity, pore dimensions, connectivity, etc.).
Transparent soil structures.[g]	Growth of plant roots in Nafion beads.	Non-destructive optical and X-ray CT imaging; root trajectories and contact points, bacterial distribution and activity.	Plant and bacteria type, structure (porosity, pore dimensions, connectivity, etc.), Nafion surface chemistry, pore liquid chemistry and nutrients.

Investigations led by: (a), Angus Buckling, Michael Brockhurst, Rees Kassen and Paul Rainey; (b), Paul Rainey and Andrew Spiers; (c), (d) and (e), Andrew Spiers; (f) and (g), Ruth Falconer and Wilfred Otten.

Furthermore, many *P. fluorescens* strains including *Pf.* SBW25[15] produce soft rot-like symptoms in plant tissues following physical damage, suggesting opportunistic pathogen-like tendencies and a possible pathogenic origin for the species. Furthermore, the ability to colonize new environments is a characteristic associated with the pseudomonads, and may be enabled by relatively large genomes that include many sensory-regulatory elements [84, 90]. The *Pf.* SBW25 genome has been fully sequenced [83], and it can be manipulated easily using standard molecular biology techniques.

Finally, the close similarity with the opportunistic human pathogen *P. aeruginosa*, the plant pathogen *P. syringae*, and the archetypal soil isolate *P. putida*, make *Pf.* SBW25 an ideal model organism for experimental studies.

[15] Andrew Spiers, unpublished observations.

Plant Microcosms

The ability of *Pf.* SBW25 to successfully colonise leaf and root surfaces depends on the close adaptation of the bacteria to the local micro-scale chemical and physical conditions prevailing on the plant, referred to as the phyllosphere, and in the narrow layer of soil in close association with the roots, referred to as the rhizosphere. The ecological performance and fitness of *Pf.* SBW25 in these different and dynamic environments is a complex phenotype, in part explained by the ability of the bacteria to adjust gene expression patterns, enzyme activities, physiology, metabolism, and behaviour in response to environmental opportunities and signals. Various techniques have been developed to examine plant-specific induction of bacterial gene expression, and one of these, known as IVET (*in vivo* expression technology), was used by Paul Rainey's group[16] to investigate *Pf.* SBW25 gene expression on sugar beet seedlings in simple microcosms (see Figure 4) [26, 27, 69, 83]. In this work, the microcosm consisted of small plastic tubes containing vermiculite or vermiculite-compost mixtures in which individual sugar beet seeds were germinated and grown for 2 – 4 weeks. This period of growth provided a selective environment in which only those IVET constructs responding to specific, but unknown, plant signals survived.

The key to the IVET strategy was the use of *Pf.* SBW25 mutant strains that had been deleted for an essential gene, either *dapB* needed to produce diaminopimelate required for the cell wall, or *panB* required to produce the vitamin pantothenate, and a library of IVET plasmids each containing a random fragment of the *Pf.* SBW25 genome inserted immediately up-stream of a second copy of the deleted gene [26, 69]. If the genome fragment contained a promoter sequence in the correct orientation, the plasmid-born copy of the essential gene might be expressed allowing the host bacterium to survive[17]. Libraries of bacteria were used to inoculate sugar beet seeds, and bacteria were recovered from the leaves, roots and bulk soil after 2 – 4 weeks. These bacteria were tested on agar plates to exclude those plasmids containing constitutively-active promoter sequences which had no environmental relevance. The genome fragment in each IVET plasmid responding to specific environmental signals was mapped back to the *Pf.* SBW25 genome by sequence analysis to determine which genes were being expressed. Further experiments were conducted to assess the levels of gene expression and their likely function in the sugar beet environment. Examples of genes identified in this manner are those involved in nutrient acquisition, stress responses, and the expression of antibiotics, cellulose and phytohormones [26, 27, 69, 83].

Unrelated research by the Rainey group investigating the *Pf.* SBW25 mutant Wrinkly Spreader (WS) biofilm had just resulted in the identification of the cellulose biosynthesis operon (*wss*) [92] and a demonstration that *Pf.* SBW25 could expressed partially-acetylated cellulose in an air-liquid interface biofilm [92, 93] (discussed further in the following section; see also the review by Spiers et al. [91]). Both biofilm-formation and the involvement of cellulose in these structures is common amongst environmental *Pseudomonas* spp., giving rise to the suggestion that the function or ecological role of biofilms in natural environments might be to localize bacteria at the air-liquid interface in small bodies of water or liquid such as those found in soil pores, on plant surfaces, or in plant tissues [73, 89, 91, 101]. Fitness

[16] Department of Plant Sciences, University of Oxford, UK.

[17] The genome fragment might contain i) no promoter activity; ii) a promoter only active in the plant or soil environment; or iii) a promoter constitutively active in all environments including agar plates.

assays had shown that there was an advantage to cellulose-expression by wild-type *Pf.* SBW25 on sugar beet leaves and roots, but not in bulk soil [26], though this type of assay does not provide a mechanistic explanation of how cellulose might improve fitness in these environments. Recently, however, investigation of cellulose-expression in the related pseudomonad, *P. putida* mt-2, suggest that it may provide a fitness advantage in water-limiting conditions [53]. Examination of the survival and fitness advantage of a set of Brown blotch-causing pseudomonads isolated from mushrooms, plus *Pf.* SBW25 and *P. putida* KT2440 (a derivative of *Pp.* mt-2), support the view that cellulose might provide an advantage by retaining water in micro-colonies and the absorption of water directly from vapour under conditions of water stress, rather than by the formation of large biofilm structures [44, 91]. The response of *Pf.* SBW25 to plant surfaces has also been examined by single-cell Raman micro-spectroscopy [31]. This technique provides spectra reflecting the whole-cell chemical composition of bacterial cells, and provides a means of monitoring growth and metabolic status. Raman analysis is normally applied in the identification of bacteria (e.g. [46]), but it might be used in a different manner to determine changes in metabolism and physiology for bacteria growing on different nutrients or environments [33]). *Pf.* SBW25 cells grown *in vitro* in defined minimal media containing single nutrient sources, such as simple sugars, amino acids and TCA (tricarboxylic acid) cycle intermediates, were found to show significantly different Raman spectral 'fingerprints', suggesting that the technique could be used to differentiate bacterial cells growing in natural conditions on the basis of local micro-scale chemical and physical conditions, growth history and strategy. For example, this type of Raman analysis could differentiate between cells growing on fructose or glucose (or glycerol), arginine or aspartic acid (or asparagine), etc., and could be used to follow cells starving over a period of nine days [31], cells growing in high or low–O_2 conditions or in a biofilm, and cells carrying the environmental *Pseudomonas*-associated plasmid pQBR103 [36, 102].

Raman analysis could also differentiate between *Pf.* SBW25 cells growing in the sugar beet rhizosphere and bulk soil without plants, suggesting that *Pf.* SBW25 responds to different environmental signals which result in significant shifts in physiology and metabolism.

Previously, it had been suggested that a correspondence between Raman spectra obtained for bacteria growing in a natural environment and the same strain on defined growth media *in vitro* might be used to infer the metabolic status of the former [33]. *Pf.* SBW25 recovered from sugar beet leaves were found to have Raman spectral profiles more similar to *Pf.* SBW25 grown *in vitro* on fructose or aspartic acid, rather than on glucose or arginine, and where quite dissimilar to starved cells [31]. This suggests that *Pf.* SBW25 growth on the leaves of sugar beet is likely to be neither carbon-catabolite-repressed nor carbon-limited. Wei Huang et al.[18] have also demonstrated the utility of Raman analysis further by showing that it can be combined with both SIP (stable isotope probing) and FISH (fluorescence *in situ* hybridization) [32, 35]. Raman can also be combined with laser optical tweezers to trap and recover individual bacteria from solution [34, 107].

[18] Centre for Ecology and Hydrology, Oxford, UK.

Experimental Evolution and Biofilms

Experimental evolution has been used by ecologists in an attempt to understand the dynamics of diversifying and adapting populations, and more recently, in an attempt to link evolutionary dynamics, fitness, and niche specialisation, with an understanding of the mechanistic link between the underlying organismal molecular biology and environmental factors (for reviews, see [10, 41, 70]). *Pf.* SBW25 has been used as a model organism in experimental evolution studies using simple glass microcosms and was first described by Paul Rainey and Michael Travisano [72] (see Figure 4; see also Chapter 5 and references therein). When wild-type *Pf.* SBW25 is inoculated into nutrient-rich King's B liquid medium [43] the population will grow over a period of several days and accumulate mutants. One of the most visually obvious of these mutants is the Wrinkly Spreader, characterized by a wrinkled colony morphology on King's B agar plates. The Wrinkly Spreader also differs from the ancestral, wild-type *Pf.* SBW25 in that it no longer colonizes the liquid column of static King's B microcosms, but grows at the air-liquid interface by forming a robust biofilm (for a description of the evolution of the Wrinkly Spreader, see [29]). Furthermore, in static microcosms, the Wrinkly Spreader has a fitness advantage over the ancestral *Pf.* SBW25 and other non-biofilm–forming competitors [29, 92]. This advantage demonstrates that the Wrinkly Spreader is not simply one of many different random mutants that might arise during the diversification of *Pf.* SBW25 populations, but is an evolved genotype, representing a fitness or adaptive leap from the ancestral *Pf.* SBW25 and having a new niche preference for the air-liquid interface formerly not colonized by *Pf.* SBW25. In shaken microcosms where biofilms cannot form, the Wrinkly Spreader does not have a fitness advantage over wild-type *Pf.* SBW25 or other non-biofilm–forming strains [29, 92], and on agar plates, the Wrinkly Spreader is at a disadvantage and is genetically unstable [88]. Investigation of the distribution of O_2 in static microcosms by Andrew Spiers' group[19] has shown that the *Pf.* SBW25 colonisers modify the environment by creating an O_2 gradient within hours of introduction into static King's B microcosms [45]. The O_2 gradient divides the microcosm into an upper, O_2-rich zone of ~200 µm, and a lower O_2-depleted zone. These zones present the developing, diversifying *Pf.* SBW25 population with new niches to occupy. Although Wrinkly Spreaders may appear anywhere in the liquid column, they are more likely to appear in the O_2-rich zone as this supports faster growth; once they appear and localize to the air-liquid interface, they begin to produce a biofilm which will intercept O_2 diffusing into the liquid column from the air above. By intercepting this O_2, Wrinkly Spreader cells at the air-liquid interface will grow faster than the ancestral wild-type *Pf.* SBW25 and other non-biofilm–forming mutants lower down in the liquid column, thus explaining the fitness advantage of the Wrinkly Spreader [45]. As the Wrinkly Spreader biofilm develops, there is opportunity for further evolution as the O_2 gradient now subdivides the biofilm itself into an O_2-rich surface layer of ~100 µm and a lower O_2-depleted zone.

In a similar air-liquid interface biofilm produced by *Gluconacetobacter xylinus* (formerly known as *Acetobacter xylinum*), the opposing O_2 and nutrient gradients combine to define an optimal growth zone 50 – 100 µm deep, where there is sufficient O_2 diffusing down from the air above and nutrients diffusing upwards from the liquid column [103]. Recent experiments by the Spiers' group suggest that the fitness advantage of the Wrinkly Spreader in static

[19] The SIMBIOS Centre, University of Abertay Dundee, UK.

King's B microcosms also depends on the relative availability of O_2 and nutrients, as well as on the relative expense of biofilm-formation versus the cost of maintaining position at the air-liquid interface by swimming motility. Growth in O_2-rich conditions, and in a biofilm rather than as individual free-swimming planktonic cells, has a big impact on the metabolic and physiological status of bacteria, as shown by single cell Raman analysis of *Pf.* SBW25 [36] and a similar analysis of a different *P. fluorescens* strain investigated by ATR–FTIR (attenuated total reflection – Fourier transform infrared spectroscopy) [67]. The relative ease in distinguishing Wrinkly Spreader colonies from wild-type *Pf.* SBW25 and other mutant classes on King's B agar plates has meant that studying diversification and adaptation is relatively simple[20]. For example, the impact on physical disturbance, nutritional complexity, and the presence of bacteriophage[21] have all been examined using this simple microcosm system [8, 9, 40, 62]. The molecular biology underlying the WS (Wrinkly Spreader) phenotype, including the colony morphology and biofilm, has also been examined in detail [7, 92, 93, 94]. Using a mini-transposon mutagenesis approach, a number of mini-Tn*5* mutants of the archetypal Wrinkly Spreader producing wild-type *Pf.* SBW25–like colonies and unable to form biofilms, were isolated and the position of the mini-transposon located on the genome determined by sequencing. This approach and subsequent testing determined that the WS phenotype required the expression of partially-acetylated cellulose and an unidentified pili-like attachment factor [92, 93, 94], and that it was activated by a single amino residue change in a regulatory sub-unit of a membrane-associated chemoreceptor [7]. This mutation activated a diguanylate cyclase known as WspR, to produce cyclic-*di*-GMP (cyclic *di*-3',*5*'-guanylate) which then activated the cellulose synthase complex and the expression of the attachment factor [7, 48] (for a more detailed description of the WS phenotype see [29]; for a review of cellulose-expression and biofilm-formation amongst the pseudomonads, see [91]; and for a review of cyclic-*di*-GMP signalling in bacteria, see [38]).

SIMBIOS and Soil Research

The Scottish Informatics, Mathematics, Biology and Statistics (SIMBIOS) Centre was established at the University of Abertay Dundee to support a range of interdisciplinary research activities, including investigations of the micro-scale structure of soil and the use of modelling approaches, to understand how spatial heterogeneity at the microscopic scale affects biophysical behaviour at larger scales. Key to this work has been the use of high resolution X-ray CT (micro-X-ray computed tomography) to non-destructively visualize and quantify soil pore networks, resolving features down to 3 µm resolution and differentiating between materials of the basis of electron density (reviewed by [97]). A 2-D (two-dimensional) image of the physical structure of a soil aggregate, and 3-D (three-dimensional) images of a soil sample visualized by X-ray CT are provided in Figure 5 (images such as these are usually manipulated on screens where they can be rotated in 3-D space allowing the viewer an excellent impression of pore spaces and networks). SIMBIOS uses X-ray CT to investigate micro-habitat structures in natural soil and repacked soil aggregates, and are

[20] Experimental evolution is studied using other bacteria which do not produce Wrinkly Spreader-like mutants. In these systems, more laborious or expensive procedures must be used to distinguish between mutants.

[21] A bacterial virus.

developing in parallel new statistical and image analysis tools required for this type of work [54, 56]. They are also combining the 3-D microtomographs of soil structure with other techniques, such as aggregate sampling and thin sectioning used to investigate bacterial colonization (e.g. [55, 56]) and SEM–EDX (scanning electron microscopy – energy-dispersive X-ray spectroscopy) to map elemental distributions [30, 58]. Natural soil structures are hard if not impossible to replicate for research purposes (e.g. example, to investigate aspects of bacterial colonization, community structure and function, plant root development, and plant-bacterial interactions).

Soil microcosms are generally constructed by re-packing sieved soil aggregates (see Figure 4), and X-ray CT can be used to quantify pore structure in terms of porosity, pore dimensions and connectivity, etc., of these artificial environments. However, X-ray CT is limited by current ability to differentiate between materials of similar electron density (e.g. differentiating the air, water, organic and inorganic matter can be problematic). Under some circumstances, X-ray CT may be able to visualize water films in soil pore networks (e.g. [99]), and in the near future, it may be possible to map the spatial distribution of water within the soil pore network at the micrometre scale.

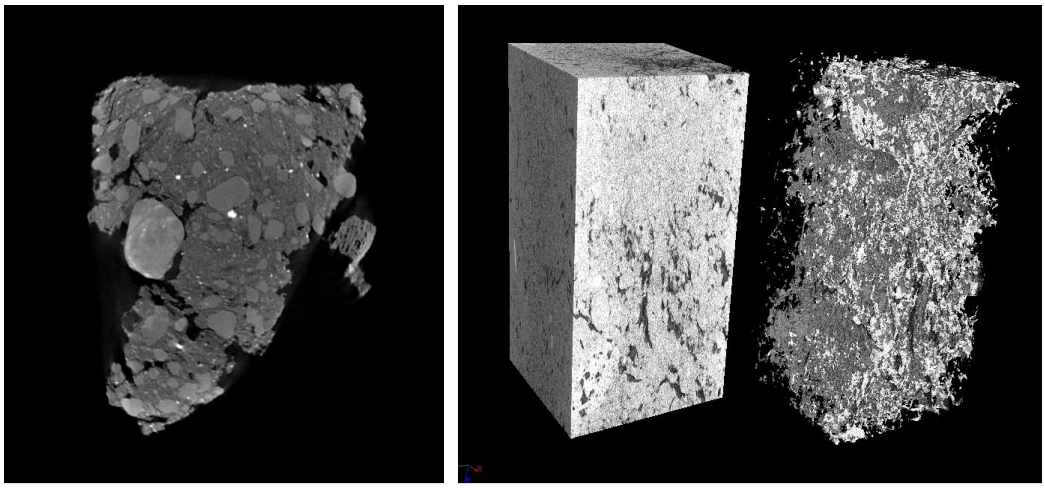

Figure 5. X-ray CT can be used to visualize the physical structure of soils. Grey-scale images are used to indicate different densities ranging from air-filled pore spaces (white) to dense aggregates (grey) and solid particles (black). (Left) A 2-D slice showing the internal structure of a soil aggregate (2 x 2 mm) at a spatial resolution of 3 µm. (Right) A 3-D projection of a soil sample (1.4 x 1.4 x 2.7 cm) is shown as a grey-scale solid and again showing only the pore spaces, at a spatial resolution of 32 µm. Images are from Wilfred Otten.

Plant roots in soil can also be visualised by X-ray CT [100], and Sonja Schmidt et al.[22] have used it to investigate the interaction between roots and soil particles at the micrometre scale, finding that the level of root-soil contact increased with decreasing particle size, and possibly also as a result of changes in particle packing around the root [80].

[22] The SIMBIOS Centre, University of Abertay Dundee, UK, and the James Hutton Institute, Invergowrie, UK.

Soil Microorganisms

The glass slides used by Cholodny [12, 13] and other early investigators to visualize soil microbiology whilst retaining some spatial detail are largely forgotten today as focus has shifted to the use of molecular techniques to investigate community function and diversity. However, there is growing recognition that there is a need to investigate microbial community function at the micrometre in the soil pore networks, where local physical and chemical conditions, and inter-species interactions are key to community function. The glass slides used by Cholodny are often viewed as problematic, insofar the slide represents a large, solid, and impermeable surface that alters soil structure and might restrict plant root and fungal development, and microbial mobility. However, these problems are reduced by using smaller sampling devices with different surface chemistries and permeabilities. Plastic films such as PET (polyethylene terephtalate) can be used instead of glass slides, and are readily cut into smaller samplers of 2 – 5 mm^2.

Olena Moshynets et al.[23] have shown that both *Pf.* SBW25 and *P. putida* KT2440 readily attach and detach from PET films *in vitro*, and pre-conditioning with soil wash suspensions can be used to modify the PET surface to increase bacterial attachment [50]. PET films buried in soil microcosms are rapidly colonized by microorganisms which could be investigated by CLSM or recovered onto agar plates; examples of this are shown in Figure 6 (like the soil landscapes produced by Winogradsky, these images are visually more exciting than the X-ray images and give a good impression of the microbiological complexity of soils at the micrometre scale). PET film samplers buried in soil microcosms can be non-destructively imaged by X-ray CT to map soil aggregate–film contact points and pore spaces [50]. In this manner, it may be possible to link specific micro-habitats identified by X-ray CT with molecular analyses conducted on the recovered film still retaining spatial detail (e.g. FISH or PCR (polymerase chain reaction) approaches to identify species and to examine gene expression patterns). However, some techniques such as Raman may not be readily applicable due to the auto-fluorescence spectrum of the PET polymer[24]. The PET film samplers have also been used to investigate bacterial colonization of bamboo tissues and the rhizosphere of *Brassica napus* (rapeseed) [51, 52]. Archana Juyal and Thilo Eickhorst[25] are investigating the dynamics of bacterial colonization of soil pore networks. They are using repacked soil aggregate microcosms inoculated with model microorganisms such as *Bacillus subtilis* and *Pf.* SBW25. These microcosms are embedded in resin and thin sections prepared for microscopy.

Two examples of the images obtained using this technique are provided in Figure 7; in the first, all microorganisms are stained using a DNA-binding fluorescent dye, and in the second, *Betaproteobacteria* cells are specifically visualized by FISH (both images are of the same region of the thin section). Although the embedding process can result in sample shrinkage, they are able to retrospectively identify the position of sliced sections in X-ray CT images of the original core, similar to the mapping of buried PET film samplers. Thilo Eickhorst is also developing CARD-FISH (catalyzed reporter deposition–FISH) for use with

[23] Institute of Molecular Biology and Genetics, National Academy of Sciences of Ukraine, Kyiv, Ukraine, and during visits to the SIMBIOS Centre, University of Abertay Dundee, UK.
[24] Wei Huang, unpublished observations, personal communication to Andrew Spiers.
[25] The SIMBIOS Centre, University of Abertay Dundee, UK, and the Institute of Soil Science, University of Bremen, Germany, respectively.

the thin sections, as this technique promises to be a more sensitive method than standard FISH or the use of fluorescent stains that bind to DNA (deoxyribonucleic acid) to detect the presence of microorganisms [5, 19, 81].

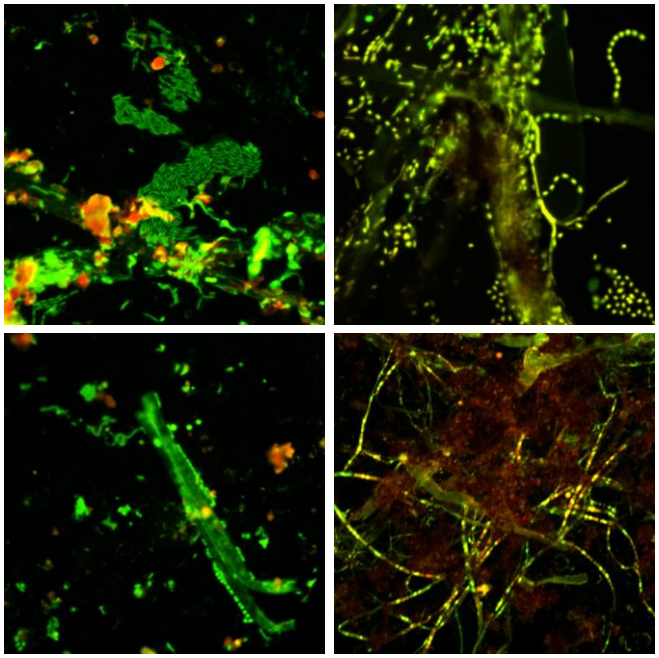

Figure 6. PET film samplers can be used to visualize the microbiological complexity of soils. Films were buried in soil for two weeks before recovery and staining with the DNA-binding fluorescent dye, Acridine orange (3,6-acridinediamine), to visualize microorganisms. Sections of film surfaces (60 x 60 µm) were inspected by CLSM (Confocal laser scanning microscopy), and in these images, many different types of microorganism can be distinguished but not identified. Images from Olena Moshynets.

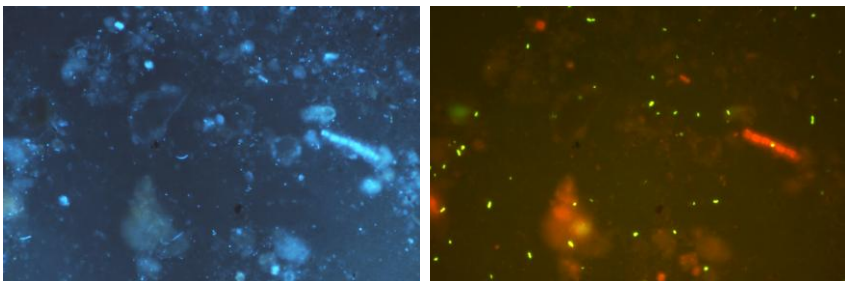

Figure 7. Bacteria can be identified in pore spaces in thin sections of soil embedded in resin. Fluorescent microscopy was used to image a region of a thin section of resin-embedded paddy soil (sandy loam) using two different techniques for the same field of view (100 x 150 µm). (Left) All microorganisms are visualized using the DNA-binding fluorescent dye, DAPI (4',6-diamidino-2-phenylindole). (Right) *Betaproteobacteria* are visualized by FISH using a specific 16S rRNA probe. Images from Thilo Eickhorst.

Although generally 16S rRNA–targeted oligonucleotide probes are used for FISH and CARD-FISH to identify microorganisms at a number of different phylogenetic levels, it is possible to use gene-specific probes that could also indicate whether individual bacteria are expressing genes involved in biological processes at the micrometre scale within soil pores. For example, the spatial clustering of bacterial nitrogen fixation genes within soil is probably due to the separation of populations across aggregates of different size classes, caused by differences in the temporal stability of aggregates as niches for microbial communities [37]. Although the identification of thin sections in the 3-D X-ray CT images of the original core were done manually, more rigorous statistical methods have been developed by Simona Hapca et al.[26] [30].

This work originated from collaboration with Clare Wilson[27] who was studying micro-spatial heterogeneity of SOC (soil organic carbon), Fe (iron) and Al (aluminum) in soils using SEM-EDX to produce two-dimensional maps which were then combined with the 3-D X-ray CT images [58].

Impact of Bacterial Surfactants on Soil Hydrology

Pf. SBW25 and other soil and plant-associated pseudomonads are known to express powerful surfactants such as the CLP (cyclic lipopeptide) viscosin, involved in a variety of roles including motility, biofilm formation, anti-bacterial activity, the inhibition of protist and nematode predation, lysis of fungi and oomycetes, and the induction of systemic resistance in plants (reviewed by [15, 68]).

However, surfactants also have a simpler impact in water where they reduce the liquid surface tension (γ) and alter the shape of liquid bodies, especially at the meniscus or the air-liquid-solid interface. The impact of reduced γ on liquid surface geometry is significant and can be illustrated by the drop collapse assay where liquids with high–γ (e.g. water) produce uniform hemispherical drops on glass slides whilst low–γ solutions produce irregular flattened shapes.

However, the ecological value to bacteria of directly modifying or manipulating water geometry through the expression of surfactants had not been considered, despite the fact that water distribution in fully and partially-saturated pores, pore-wall surface films and droplets is a key factor in bacterial colonisation and activity in soils [14, 108]. Using repacked soil aggregate microcosms (see Figure 4), the Spiers' group demonstrated that the volumetric water content of soil was significantly lowered by *Pf.* SBW25 expressing the viscosin compared to a surfactant-deficient mutant [21]. Furthermore, six of fifteen pseudomonads isolated directly from soil shown to express surfactants *in vitro* were found to have a similar impact on water content when compared to sterile microcosms [21]. These findings indicate that surfactant-expressing pseudomonads could modify local soil-water distributions within soil pore networks, and that surfactants may therefore play a significant hydrological role in soils in addition to their recognised biological activities. As X-ray CT technology develops, it may be possible to investigate bacterial surfactant-mediated changes to local soil water distribution patterns at the micrometre scale in the future.

[26] The SIMBIOS Centre, University of Abertay Dundee, UK.
[27] School of Biological and Environmental Sciences, University of Stirling, UK.

Plastic and Transparent Soils

As an extension of the experimental investigation and modelling of fungal invasion of soil pore networks [60], Ruth Falconer and Wilfred Otten[28] have employed 3-D printing techniques to produce realistic plastic soil structures using data derived from X-ray CT of native soil cores [59] (see Figure 4).

This printing technology can produce multiple replicates of the same native structure, and by transforming the data set, related structures differing in a key parameter such as total porosity can be produced for testing.

Furthermore, the plastic provides a physically and chemically homogeneous surface, allowing the effect of soil structure to be investigated without the complication of chemical heterogeneity.

However, just like the PET film samplers, the chemical surface of the plastic soils might be modified to allow subsequent investigations of physical and chemical heterogeneity in microcosms in which structure remains constant.

In some circumstances, realistic soil structure may not be a priority where research is focusing on plant root development or bacterial-root interactions. Helen Downie et al.[29] have developed OPT (optical projection tomography) to image roots and bacteria in a novel 'transparent soil' microcosm [16]. These were constructed using Nafion particles (a sulfonated tetrafluoroethylene–based fluoropolymer-copolymer) to provide a soil-like pore network that could be partially saturated with a nutrient solution to allow the growth of *Latuca sativa* (lettuce) and *Nicotiana benthamiana* (a close relative of tobacco frequently used by plant scientists) seedlings.

Immediately before visualization, the pores were saturated with a RI (refractive index)-matched solution, rendering the particles transparent and allowing the direct imaging of roots and bacteria.

The pore structure itself can be visualized using fluorescent dyes that adsorb onto the particles, while other dyes or fluorescent protein-labelling can be used to label roots or bacteria [16].

FINAL COMMENT

Winogradsky was the father of microbial ecology, developing it as a separate discipline, distinct from and as valid as medical microbiology led by the disciples of Koch. He championed the need to study soil microorganisms in their natural habitat, and pioneered the use of microcosms in which biological processes could be investigated. Winogradsky's Direct method has matured into a truly interdisciplinary research approach that is highly topical to today's environmental microbiologists and soil biophysicists. We use this approach today, employing a variety of simple microcosm systems to examine aspects of microbial ecology, and strongly encourage other microbiologists to do likewise in their own research.

[28] The SIMBIOS Centre, University of Abertay Dundee, UK.
[29] The SIMBIOS Centre, University of Abertay Dundee, UK, and the James Hutton Institute, Invergowrie, UK.

Supplementary Table 1. The professional career of S.N. Winogradsky

1877 – 1881	Entered the Department of Natural Sciences of the Physico-Mathematical Faculty, University of St. Petersburg. He then chose plant physiology as his major, working as an undergraduate research student with the botanist-physiologist Andrey Famintsyn. Awarded a Diploma of Science in 1881 and continued his research studies with Famintsyn.
1881 – 1884	**First St Petersburg research period.** Worked with Famintsyn on bacterial fermentation. Published his first research work on the nutrition and growth physiology of the yeast *Candida vini*. Awarded the degree of Master of Science in 1884.
1885 – 1888	**Strasbourg research period.** Joined the botanist and mycologist Anton DeBary at the University of Strasbourg. He investigated the sulfur-oxidising bacterium *Beggiatoa*, proving the monomorphism of so-called 'high bacteria'. Discovered the autotrophic assimilation of CO_2 by bacteria and formulated the theory of chemolithotrophy. Developed selective (elective) conditions for bacteria cultivation.
1888 – 1891	**Zurich research period.** He developed his chemistry skills with Ernst Schultz and Otto Roth at the Swiss Polytechnic Institute in Zurich, where he investigated sulfur and iron bacterium, and bacterial nitrification. Isolated pure cultures of *Nitrosomonas* and *Nitrobacter*. Lectured at the Zurich Polytechnic Institute. He rejected an offer to join the Pasteur Institute in 1891, preferring to return to Russia.
1891 – 1905	**Second St Petersburg research period.** Became the Head of the General Microbiology Department of the Imperial State Institute of Experimental Medicine at St. Petersburg (resigned as Director in 1905 but remained a member until 1912). Corresponding Member of the Academy of Sciences of France (1902). In 1903 he and Omeliansky organized the Russian Microbiological Society, where he was a director for two years. Participated in the development of anti-plague measures in Russia. In 1894 he proved the existence of anaerobic nitrogen-fixing bacteria, isolated and described *Clostridium pasteurianum*.
1905 – 1920	Due to health problems he left St. Petersburg and returned to his estate in Gorodok, Ukraine. Honorary Member of the German Botanical Society (1907). Foreign Member of the Royal Academy of Agriculture of Sweden (1908). Corresponding Member of the Academy of Medicine of Torino (1909). Honorary Member of the Russian Microbiological Society (1910). Corresponding Member of the Microbiological Society of Holland (1911). Honorary Member of the Polytechnic Institute of Riga (1912). In 1916 he moved to Odessa. Foreign member of the Royal Society in London (1918). In 1920 he left Odessa following the Russian Revolution by French warship as a Corresponding Member of the French Academy of Sciences.
1921 – 1922	Joined the Agricultural Institute of the University of Belgrade, Yugoslavia. Member of the Czechoslovak Botanical Society and a Professor of the University of Belgrade (1921). In 1922 he accepted an invitation from Emil Roux, director of the Pasteur Institute and moved to Paris.
1923 – 1953	**Paris research period.** Continued working on nitrogen-fixation in bacteria and soils; he was the first to study soils as an environment. Developed his Direct method to investigate the biological, chemical and physical characteristics of soil, beginning the modern disciplines of ecological microbiology and soil microbiology. Head of the Laboratory of Agricultural Microbiology of the Pasteur Institute in Brie-Comte-Robert (Paris). Honorary Member of the Academy of Sciences of the USSR (1923). Member of the Institute of France as a Foreign member of the Academy of Science, Foreign Member of the English Royal Society and a Honorary Member of the International Society of Soil Sciences (1924). Foreign Member of the Academy of Sciences of France (1925). Corresponding Member of the American Microbiological Society (1926). Honorary Member of the Biological Society of France (1929). Member of the Scientific Society of Italy (1931). Member of the Royal Academy of Science in Amsterdam (1932). Foreign Member of the Royal Academy of Science of Sweden (1934). Awarded the Leeuwenhoek Medal (1935). Honorary President of the IV International Botanical Congress in Amsterdam (1935). Honorary Member of the Society of Biological Chemists of India and the Society of American Bacteriologists (1936). Honorary Vice-President of the II International Microbiological Congress in London (1936). Awarded a Diploma of Ministry of New Jersey (1936). Honorary President of the International Botanical Congress in Stockholm (1940) and the IV International Microbiological Congress in Copenhagen (1947). Honorary Member of the Society of Soil Sciences of Florida (1950). Honorary Member of the Society of General Microbiologists of the UK (1952).
1953	Died in Brie-Comte-Robert.

This is not a comprehensive list of Winogradsky's research career or accomplishments.

ACKNOWLEDGMENTS

We thank Dmitry Musolin, St. Petersburg State Forest Technical University and St. Petersburg State University, and Grozdilova Ludmila, Institute of Zoology of the Russian Academy of Sciences, St. Petersburg, for their assistance in our search of the literature. We also thank Dmitry Irodov and Oleksy Burlak for their assistance accessing some of the early publications and photography of the columns, and members of SIMBIOS who provided images and comments on the developing manuscript. Andrew Spiers is a member of SAGES (Scottish Alliance for Geoscience Environment and Society), and is supported by the SIMBIOS Centre and the University of Abertay Dundee. The University of Abertay Dundee is a charity registered in Scotland, No: SC016040.

REFERENCES

[1] Ackert, L.T. (2006). The role of microbes in agriculture: Sergei Vinogradskii's discovery and investigation of chemosynthesis, 1880–1910. *J. History Biol.* 39: 373–406.

[2] Ackert, L.T. (2007). The ''Cycle of Life'' in ecology: Sergei Vinogradskii's soil microbiology, 1885–1940. *J. History Biol.* 40: 109–145.

[3] Ackert, L. (2013). Sergi Vinogradskii and the Cycle of Life. In: Archimedes 34: New Studies in the History and Philosophy of Science and Technology. Buchwald, J.Z. (Series Ed.), Springer, Dordrecht Heidelberg New York London.

[4] Acot, P. (1997). The Lamarckian cradle of scientific ecology. *Acta Biotheoretica* 45: 185–193.

[5] Amann, R. and Fuchs, B.M. (2008). Single-cell identification in microbial communities by improved fluorescence *in situ* hybridization techniques. *Nature Rev. Microbiol.* 6: 339 – 348.

[6] Anderson, D.C. and Hairston, R.V. (1999). The Winogradsky column and biofilms models for teaching nutrient cycling and succession in an ecosystem. *Amer. Biol. Teacher* 61: 453–459.

[7] Bantinaki, B., Kassen, R., Knight, C.G., Robinson, Z., Spiers, A.J. and Rainey, P.B. (2007). Adaptive divergence in experimental populations of *Pseudomonas fluorescens.* III. Mutational origins of Wrinkly Spreader diversity. *Genetics* 176: 441–453.

[8] Brockhurst, M.A., Habets, M.G.J.L., Libberton, B., Buckling, A. and Gardner, A. (2010). Ecological drivers of the evolution of public-goods cooperation in bacteria. *Ecology* 91: 334–340.

[9] Buckling, A., Kassen, R., Bell, G. and Rainey, P.B. (2000). Disturbance and diversity in experimental microcosms. *Nature* 408: 961 – 964.

[10] Buckling, A., Maclean, C.R., Brockhurst, M.A. and Colegrave, N. (2009). The Beagle in a bottle. *Nature* 457: 824–829.

[11] Canfield, D.E., Glazer, A.N. and Falkowski, P.G. (2010). The evolution and future of Earth's nitrogen cycle. *Science* 330: 192–196.

[12] Cholodny, N. (1930). Uber eine neue Methode zur Untersuchung der Bodenmikroflora. *Arch. Microbiol.* 1: 620–652.

[13] Cholodny, N.G. (1934). A soil chamber as a method for the microscopic study of the soil microflora. *Arch. Microbiol.* 5: 148–156.

[14] Crawford, J.W., Harris, J.A., Ritz, K. and Young, I.M. (2005). Towards an evolutionary ecology of life in soil. *TRENDS Ecol. Evol.* 20: 81–87.

[15] D'aes, J., De Meyer, K., Pauwelyn, E. and Höfte, M. (2010). Biosurfactants in plant-*Pseudomonas* interactions and their importance to biocontrol. *Environ. Microbiol. Reports* 2: 359-372.

[16] Downie, H., Holden, N., Otten, W., Spiers, A.J., Valentine, T.A. and Dupuy, L.X. (2012). Transparent soil for imaging the rhizosphere. *PLoS ONE* 7: e44276.

[17] Dworkin, M. (2012). Sergei Winogradsky: a founder of modern microbiology and the first microbial ecologist. *FEMS Microbiol. Rev.* 36: 364–379.

[18] Egunov, M.A. (1895). The sulfur bacteria of the Odessa Bay. *Arch. Sci. Biol. St. Petersburg* 3: 381–397.

[19] Eickhorst, T. and Tippkötter, R. (2008). Improved detection of soil microorganisms using fluorescence *in situ* hybridization (FISH) and catalyzed reporter deposition (CARD-FISH). *Soil Biol. Biochem.* 40: 1883–1891.

[20] Falkowski, P.G., Fenchel, T. and Delong, E.F. (2008). The microbial engines that drive Earth's biogeochemical cycles. *Science* 320: 1034–1039.

[21] Fechtner, J., Koza, A., Dello Sterpaio, P., Hapca, S.M. and Spiers, A.J. (2011). Surfactants expressed by soil pseudomonads alter local soil-water distribution suggesting a hydrological role for these compounds. *FEMS Microbiol. Ecol.* 78: 50–58.

[22] Francis, C.A., Beman, J.M. and Kuypers, M.M. (2007). New processes and players in the nitrogen cycle: the microbial ecology of anaerobic and archaeal ammonia oxidation. *ISME J.* 1: 19–27.

[23] Friedrich, C.G., Bardischewsky, F., Rother, D., Quentmeier, A. and Fischer, J. (2005). Prokaryotic sulfur oxidation. *Curr. Opin. Microbiol.* 8: 253–259.

[24] Frigaard, N.U. and Dahl, C. (2009). Sulfur metabolism in phototrophic sulfur bacteria. *Adv. Microb. Physiol.* 54: 103–200.

[25] Fuchsman, C.A., Kirkpatrick, J.B., Brazelton, W.J., Murray, J.W. and Staley, J.T. (2011). Metabolic strategies of free-living and aggregate-associated bacterial communities inferred from biologic and chemical profiles in the Black Sea suboxic zone. *FEMS Microbiol. Ecol.* 78: 586-603.

[26] Gal, M., Preston, G.M., Massey, R.C., Spiers, A.J. and Rainey, P.B. (2003). Genes encoding a cellulosic polymer contribute toward the ecological success of *Pseudomonas fluorescens* SBW25 on plant surfaces. *Mol. Ecol.* 12: 3109–3121.

[27] Giddens, S.R., Jackson, R.W., Moon, C.D., Jacobs, M.A., Zhang, X-X., Gehrig, S.M., Rainey, P.B. (2007). Mutational activation of niche-specific genes provides insight into regulatory networks and bacterial function in a complex environment. *Proc. Natl. Acad. Sci. (USA)* 104: 18247–18252.

[28] Ghosh, W. and Dam, D. (2009). Biochemistry and molecular biology of lithotrophic sulfuroxidation by taxonomically and ecologically diverse bacteria and archaea. *FEMS Microbiol. Rev.* 33: 999–1043.

[29] Green, J.H., Koza, A., Moshynets, O., Pajor, R., Ritchie, M.R. and Spiers, A.J. (2011). Evolution in a test-tube : rise of the Wrinkly Spreaders. *J. Biol. Educ.* 45: 54–59.

[30] Hapca, S.M., Wang, Z.X., Otten, W., Wilson, C. and Baveye, P.C. (2011). Automated statistical method to align 2D chemical maps with 3D X-ray computed micro-tomographic images of soils. *Geoderma* 164: 146–154.

[31] Huang, W.E., Bailey, M.J., Thompson, I.P., Whiteley, A.S. and Spiers, A.J. (2007). Single-cell Raman spectral profiles of *Pseudomonas fluorescens* SBW25 reflects *in vitro* and *in planta* metabolic history. *Microb. Ecol.* 53: 414–425.

[32] Huang, W.E., Ferguson, A., Singer, A.C., Lawson, K., Thompson, I.P., Kalin, R.M., Larkin, M.J., Bailey, M.J. and Whiteley, A.S. (2009). Resolving genetic functions within microbial populations: *in situ* analyses using rRNA and mRNA stable isotope probing coupled with single-cell Raman-fluorescence *in situ* hybridization. *Appl. Environ. Microbiol.* 75: 234–241.

[33] Huang, W.E. and Spiers, A.J. (2006). Consideration of future requirements for Raman microbiology as an examplar for the *ab initio* development of informatics frameworks for emergent OMIC technologies. *OMICS: J. Integ. Biol.* 10: 238–241.

[34] Huang, W.E., Ward, A.D. and Whiteley, A.S. (2009). Raman tweezers sorting of single microbial cells. *Environ. Microbiol. Reports* 1: 44–49.

[35] Huang, W.E., Stoecker, K., Griffiths, R., Newbold, L., Daims, H., Whiteley, A.S. and Wagner, M. (2007). Raman-FISH: combining stable-isotope Raman spectroscopy and fluorescence *in situ* hybridization for the single cell analysis of identity and function. *Environ. Microbiol.* 9: 1878–1889.

[36] Huang, W.E., Ude, S. and Spiers, A.J. (2007). *Pseudomonas fluorescens* SBW25 biofilm and planktonic cells have differentiable Raman spectral profiles. *Microb. Ecol.* 53: 471–474.

[37] Izquierdo, J.A. and Nüsslein, K. (2006). Distribution of extensive *nifH* gene diversity across physical soil microenvironments. *Microb. Ecol.* 51: 441–452.

[38] Jenal, U. and Malone, J. (2006). Mechanisms of cyclic-di-GMP signaling in bacteria. *Ann. Rev. Genet.* 40: 385–407.

[39] Johnson, D.B. and Hallberg, K.B. (2008). Carbon, iron and sulfur metabolism in acidophilic micro-organisms. *Adv. Microb. Physiol.* 54: 201–255.

[40] Kassen, R., Buckling, A., Bell, G. and Rainey, P.B. (2000). Diversity peaks at intermediate productivity in a laboratory microcosm. *Nature* 406: 508 – 512.

[41] Kassen, R. and Rainey, P.B. (2004). The ecology and genetics of microbial diversity. *Annu. Rev. Microbiol.* 58: 207–231.

[42] Kelly, D.P. (1971). Autotrophy: concepts of lithotrophic bacteria and their organic metabolism. *Annu. Rev. Microbiol.* 25: 177–210.

[43] King, E.O., Ward, M.K. and Raney, D.C. **(**1954). Two simple media for the demonstration of pyocyanin and fluorescin. *J. Lab. Clin. Med.* 44: 301–307.

[44] Koza, A. (2011). Adaptation and niche construction by *Pseudomonas fluorescens* SBW25. PhD thesis, University of Abertay Dundee, Dundee.

[45] Koza, A., Moshynets, O., Otten, W. and Spiers, A.J. (2011). Environmental modification and niche construction: developing O_2 gradients drive the evolution of the wrinkly spreader. *ISME J.* 5: 665–673.

[46] Lu, X., Al-Qadiri, H.M., Lin, M. and Rasco, B.A. (2011). Application of mid-infrared and raman spectroscopy to the study of bacteria. *Food Bioproc. Technol.* 4: 919–935.

[47] Madsen, E.L. (2011). Microorganisms and their roles in fundamental biogeochemical cycles. *Curr. Opin. Biotechnol.* 22: 456–464.

[48] Malone, J.G., Williams, R., Spiers, A.J. and Rainey, P.B. (2007). The structure-function relationship of WspR: a *Pseudomonas fluorescens* response-regulator with a GGDEF output domain. *Microbiology* 153: 980–994.

[49] Martínez-Espinosa, R.M., Cole, J.A., Richardson, D.J. and Watmough, N.J. (2011). Enzymology and ecology of the nitrogen cycle. *Biochem. Soc. Trans.* 39: 175–178.

[50] Moshynets, O.V., Koza, A., Dello Sterpaio, P., Kordium, V.A. and Spiers, A.J. (2011). Up-dating the Cholodny method using PET films to sample microbial communities in soil. *Biopol. Cell* 27: 199–205.

[51] Moshynets, O.V., Shpylova, S.P., Kordium, V.A. and Potters, G. (2012). Visualisation of endophytic bacteria in *Phyllostachys* sp. and *Fargesia* sp.. *Bamboo Sci. Culture* 25: 11–18.

[52] Moshynets, O.V., Shpylova, S.P., Spiers, A.J. and Kosakivska, I.V. (2010) The phytosphere of *Brassica napus* L.: a niche for *Pseudomonas fluorescens* SBW25. *Rep. Acad. Sci. Ukraine* 12: 150–153.

[53] Nielsen, L., Li, X. and Halverson, L.J. (2011). Cell-cell and cell-surface interactions mediated by cellulose and a novel exopolysaccharide contribute to *Pseudomonas putida* biofilm formation and fitness under water-limiting conditions. *Environ. Microbiol.* 13: 1342–1356.

[54] Nunan, N., Ritz, K., Rivers, M., Feeney, D.S. and Young, I.M. (2006). Investigating microbial micro-habitat structure using X-ray computed tomography. *Geoderma* 133: 398–407.

[55] Nunan, N., Wu, K., Young, I.M., Crawford, J.W. and Ritz, K. (2002). *In situ* patterns of soil bacterial populations, mapped at multiple scales, in an arable soil. *Microb. Ecol.* 44: 296–305.

[56] Nunan, N., Wu, K., Young, I.M., Crawford, J.W. and Ritz, K. (2006). Spatial distribution of bacterial communities and their relationships with the micro-architecture of soil. *FEMS Microbiol. Ecol.* 44: 203–215.

[57] Omelyansky, V.L. (1909). Osnovy mikrobiologii (The basics of microbiology). Publishing house of Imperial Academy of Sciences, St. Petersburg.

[58] Otten, W., Grinev, D., Baveye, P., Wang, Z., Hapca, S. and Wilson, C. (2010). Integrating physical and chemical techniques to characterise soil microsites. In: Gilkes, R.J. and Prakongkep, N. (Eds). Proceedings of the 19th World Congress of Soil Science; Soil Solutions for a Changing World. International Union of Soil Sciences, Brisbane.

[59] Otten, W., Pajor, R., Schmidt, S., Baveye, P.C., Hague, R. and Falconer, R.E. (2012). Combining X-ray CT and 3D printing technology to produce microcosms with replicable, complex pore geometries. *Soil Biol. Biochem.* 51: 53e55.

[60] Pajor, R., Falconer, R., Hapca, S. and Otten, W. (2010). Modelling and quantifying the effect of heterogeneity in soil physical conditions on fungal growth. *Biogeosci. Discuss.* 7: 3477–3501.

[61] Pasteur, L. (1868). Études sur le vinaigre, sa fabrication, ses maladies, moyens de les prévenir: nouvelles observations sur la conservation des vins par la chaleur. Gauthier-Villars, Paris.

[62] Paterson, S., Vogwill, T., Buckling, A., Benmayor, R., Spiers, A.J., Thomson, N.R., Quail, M., Smith, F., Walker, D., Libberton, B., Fenton, A., Hall, N. and Brockhurst,

M.A. (2010). Antagonistic coevolution accelerates molecular evolution. *Nature* 464: 275-278.

[63] Pearsall, J. (Ed.) (1998). The New Oxford Dictionary of English. Clarendon Press, Oxford.

[64] Peix, A., Ramírez-Bahena, M-H. and Velázquez, E. (2009). Historical evolution and current status of the taxonomy of genus *Pseudomonas*. *Infec. Genet. Evol.* 9: 1132–1147.

[65] Perfil'ev, B.V. and Gabe, D.R. (1969). Capillary methods of investigating micro-organisms. Oliver and Boyd, Edinburgh.

[66] Preston, G.M., Bertrand, N. and Rainey, P.B. (2001). Type III secretion in plant growth-promoting *Pseudomonas fluorescens* SBW25. *Mol. Microbiol.* 41: 999–1014.

[67] Quilès, F., Humbert, F. and Delille. A. (2010). Analysis of changes in attenuated total reflection FTIR fingerprints of *Pseudomonas fluorescens* from planktonic state to nascent biofilm state. *Spectrochimica Acta A* 75: 610–616.

[68] Raaijmakers, J.M., De Bruijn, I., Nybroe, O. and Ongena, M. (2010). Natural functions of lipopeptides from *Bacillus* and *Pseudomonas*: more than surfactants and antibiotics. *FEMS Microbiol. Rev.* 34: 1037–1062.

[69] Rainey, P.B. (1999). Adaptation of *Pseudomonas fluorescens* to the plant rhizosphere. *Environ. Microbiol.* 1: 243–257.

[70] Rainey, P.B., Buckling, A., Kassen, R. and Travisano, M. (2000). The emergence and maintenance of diversity: insights from experimental bacterial populations. *Trends Ecol. Evol.* 15: 243–247.

[71] Rainey, P.B. and Bailey, M.J. (1996). Physical and genetic map of the *Pseudomonas fluorescens* SBW25 chromosome. *Mol. Microbiol.* 19: 521–533.

[72] Rainey, P.B. and Travisano, M. (1998). Adaptive radiation in a heterogeneous environment. *Nature* 394: 69 –72.

[73] Robertson, M., Hapca, S.M., Moshynets, O. and Spiers, A.J. (2013). Air-liquid interface biofilm formation by psychrotrophic pseudomonads recovered from spoilt meat. *Ant. van Leeuwenhoek* 103: 251–259.

[74] Rogan, B., Lemke, M., Levandowsky, M. and Gorrell, T. (2005). Exploring the sulfur nutrient cycle using the Winogradsky column. *Amer. Biol. Teacher* 67: 348–356.

[75] Roslytsky, I. (2008). Sergiy Winogradsky – peredovyi mikrobioloh svity (Sergei Winogradskii is a world foremost microbiologist). Kyiv. Academperiodika, Kyiv.

[76] Schimel, J.P. and Schaeffer, S.M. (2012). Microbial control over carbon cycling in soil. *Front. Microbiol.* 3: 348.

[77] Schlegel, H.G. (1993). General microbiology. 7th Ed. Cambridge University Press, Cambridge.

[78] Schlegel, H.G. (1996). Winogradsky discovered a new *modus vivendi*. *Anaerobe* 2: 129-136.

[79] Schlegel, H.G. and Jannasch, H.W. (2006). Prokaryotes and their habitats. In: The Prokaryotes, Vol. 1: Symbiotic associations, Biotechnology, Applied Microbiology. 3rd Ed.. Dworkin, M., Falkow, S., Rosenberg, E., Schleifer, K.-H. and Stackebrandt, E. (Eds.). Springer, New York.

[80] Schmidt, S., Bengough, A.G., Gregory, P.J., Grinev, D.V. and Otten, W. (2012). Estimating root–soil contact from 3D X-ray microtomographs. *Eur. J. Soil Sci.* 63: 776–786.

[81] Schmidt, H., Eickhorst, T. and Tippkötter, R. (2012). Evaluation of tyramide solutions for an improved detection and enumeration of single microbial cells in soil by CARD-FISH. *J. Microbiol. Meth.* 91: 399–405.

[82] Seliber, G.L. (1960). Russkie mikrobiologi S.N. Vinogradskii i V.L. Omelianskii. Ministry of Agriculture of SSSR Press, Moscow.

[83] Silby, M.W., Cerdeño-Tárraga, A.M., Vernikos, G., Giddens, S.R., Jackson, R., Preston, G., Zhang, X-X., Godfrey, S., Spiers, A.J., Harris, S., Challis, G.L., Morningstar, A., Harris, D., Seeger, K., Murphy, L., Rutter, S., Squares, R., Quail, M.A., Saunders, E., Anderson, I., Mavromat, K., Brettin, T.S., Bentley, S., Thomas, C.M., Parkhill, J., Levy, S.B., Rainey, P.B. and Thomson, N.R. (2009). Genomic and functional analyses of diversity and plant interactions of *Pseudomonas fluorescens*. *Genome Biol.* 10: R51.

[84] Silby, M.W., Winstanley, C., Godfrey, S.A.C., Levy, S.B. and Jackson, R.W. (2011). *Pseudomonas* genomes: diverse and adaptable. *FEMS Microbiol. Rev.* 35: 652–680.

[85] Simon, J. and Klotz, M.G. (2013). Diversity and evolution of bioenergetic systems involved in microbial nitrogen compound transformations. *Biochim. Biophys. Acta*. 1827: 114–135.

[86] Skinner, C.E. and Fletcher, D.W. (1960). A review of the genus Candida. *Bacteriol. Rev.* 24: 397–416.

[87] Sorokin, Y.I. (1972). The bacterial population and the processes of hydrogen sulphide oxidation in the Black Sea. *J. Cons. Int. Explor. Mer.* 34: 423–454.

[88] Spiers, A.J. (2007). Wrinkly-spreader fitness in the two-dimensional agar plate microcosm: maladaptation, compensation and ecological success. *PLoS ONE* 2: e740.

[89] Spiers, A.J., Arnold, D.L., Moon, C.D. and Timms-Wilson, T.M. (2006). A survey of A-L biofilm formation and cellulose expression amongst soil and plant-associated *Pseudomonas* isolates. In: Microbial Ecology of Aerial Plant Surfaces. Bailey, M.J., Lilley, A.K. and Timms-Wilson, T.M. (Eds). CABI, Wallingford.

[90] Spiers, A.J., Buckling, A. and Rainey, P. (2000). The causes of *Pseudomonas* diversity. *Microbiology* 146: 2345–2350.

[91] Spiers, A.J., Deeni, Y.Y., Folorunso, A.O., Koza, A., Moshynets, O. and Zawadzki, K. (2013). Cellulose expression in *Pseudomonas fluorescens* SBW25 and other environmental pseudomonads. In: Cellulose. Van De Ven, T.G.M. and Trdine, J. (Eds). InTech, Rijeka.

[92] Spiers, A.J., Kahn, S.G., Bohannon, J., Travisano, M. and Rainey, P.B. (2002). Adaptive divergence in experimental populations of *Pseudomonas fluorescens*. I. Genetic and phenotypic bases of Wrinkly Spreader fitness. *Genetics* 161: 33–46.

[93] Spiers, A.J., Bohannon, J., Gehrig, S.M. and Rainey, P.B. (2003). Biofilm formation at the air–liquid interface by the *Pseudomonas fluorescens* SBW25 Wrinkly Spreader requires an acetylated form of cellulose. *Mol. Microbiol.* 50: 15–27.

[94] Spiers, A.J. and Rainey, P.B. (2005). The *Pseudomonas fluorescens* SBW25 Wrinkly Spreader biofilm requires attachment factor, cellulose fibre and LPS interactions to maintain strength and integrity. *Microbiology* 151: 2829–2839.

[95] Sternberg, C., Christensen, B.B., Johansen, T., Neilsen, A.T., Andersen, J.B., Givskov, M. and Molin, S. (1999). Distribution of bacterial growth activity in flow-chamber biofilms. *Appl. Environ. Microbiol.* 65: 4108-4117.

[96] Stewart, F.J. (2011). Dissimilatory sulfur cycling in oxygen minimum zones: an emerging metagenomics perspective. *Biochem. Soc. Trans.* 2011 39: 1859–1863.

[97] Taina, I.A., Heck, R.J. and Elliot, T.R. (2008). Application of X-ray computed tomography to soil science: A literature review. *Canadian J. Soil Sci.* 88: 1-19.

[98] Teske, A. and Nelson, D.C. (2006). The genera *Beggiatoa* and *Thioploca*. In: The Prokaryotes, Vol. 6: Proteobacteria: Gamma subclass. 3rd Ed.. Dworkin, M., Falkow, S., Rosenberg, E., Schleifer, K.-H. and Stackebrandt, E. (Eds.) Springer, New York.

[99] Tippkötter, R., Eickhorst, T., Taubner, H., Gredner, B. and Rademaker, G. (2009). Detection of soil water in macropores of undisturbed soil using microfocus X-ray tube computerized tomography (µCT). *Soil Tillage Res.* 105: 12–20.

[100] Tracy, S.R., Roberts, J.A., Black, C.R., McNeill, A., Davidson, R. and Mooney, S.J. (2010). The X-factor: visualizing undisturbed root architecture in soils using X-ray computed tomography. *J. Exp. Bot.* 61: 311–313.

[101] Ude, S., Arnold, D.L., Moon, C.D., Timms-Wilson, T. and Spiers, A.J. (2006). Biofilm formation and cellulose expression among diverse environmental *Pseudomonas* isolates. *Environ. Microbiol.* 8: 1997–2011.

[102] Ude, S., Bailey, M.J., Huang, W.E. and Spiers, A.J. (2007). The environmental plasmid pQBR103 alters the single-cell Raman spectral profile of *Pseudomonas fluorescens* SBW25. *Microb. Ecol.* 53: 494–497.

[103] Verschuren, P.G., Cardona, T.D., Nout, M.H.R., De Gooijer, K.D., Van den Heuvel, J.C. (2000). Location and limitation of cellulose production by *Acetobacter xylinum* established from oxygen profiles. *J. Biosci. Bioeng.* 89: 414–419.

[104] Waksman, S. (1953). Sergei N. Winogradsky: His Life and Work. Rutgers University Press, New Brunswick.

[105] Winogradsky, S. (1949). Microbiologie du sol, problèmes et méthodes; cinquante ans de recherches. (Soil Microbiology: Problems and Methods, Fifty Years of Investigations). Masson, Paris. (This book was also published elsewhere, for example, see the following reference for the Russian publication.)

[106] Winogradsky S.N (1952). Microbiologija pochvy. Problemy i metody. Pjatdesjat let issledovaniy (Soil Microbiology. Problems and Methods. Fifty Years of Investigations). Publishing house of the Academy of Science of USSR, Moscow.

[107] Xie, C., Mace, J., Dinno, M.A., Li, Y.Q., Tang, W., Newton, R.J. and Gemperline, P.J. (2005). Identification of single bacterial cells in aqueous solution using confocal laser tweezers Raman spectroscopy. *Anal. Chem.* 77: 4390–4397.

[108] Young, I.M., Crawford, J.W., Nunan, N., Otten, W. and Spiers, A. (2008) Microbial distribution in soils: physics and scaling. In: Advances in Agronomy. Vol. 100. Sparks, D.L. (Ed). Academic Press, Burlington.

[109] Zavarzin, G.A. (2006). Winogradsky and modern microbiology. *Microbiology* (ISSN 0026-2617) 75: 501–511.

[110] Zavarzin, G.A. (2006). Genius of natural science. On the 150th anniversary of the birth of honorary member of the USSR Academy of Sciences S.N. Vinogradskii. *Herald Russ. Acad. Sci.* (ISSN 1019-3316) 76: 361–369.

Анотація: *Бачення бактеріальних біоплівок як «мікробних міст» домінувало в нашому розумінні розвитку і функціонування бактеріальних скупчень протягом останніх 20 років. Весь цей час активний мул, згустки, колонії, флокули, мати, плівки, плоти, шлами, зооглеї тощо були здебільшого забуті або проігноровані. Хоча натхненна медициною розроблена модель існування біоплівок патогенів людини має переваги такі як обґрунтування розробки антибіоплівкових терапевтичних засобів, вона не пояснює зв'язків з іншими типами агрегації бактерій, які зазвичай зустрічаються в широкому діапазоні природних і антропогенних екологічних ніш. Можливо, в результаті цього екологічні мікробіологи як правило уникають терміну «біоплівка» та використовують замість нього інші терміни, наприклад «мікробні килимки», вивчення яких було започатковано більше ста років тому, зокрема, Сергія Виноградського, огляд робіт якого і інших вчених-мікробіологів цього покоління надається в окремій главі. В цій роботі ми кидаємо виклик спрощеній планктонно (незалежним і вільно плаваючим бактеріям)-біоплівковій (прикріплені та кооперативні бактерії) дихотомії і розглядаємо біоплівки в межах більшого контексту бактеріальних агрегацій. Розуміючи біоплівки в контексті континууму агрегацій або спільнот з різними абіотичними та біотичними властивостями, фундаментальними фізичними, біологічними та еволюційними екологічними процесами, які впливають на розвиток і функціонування спільноти більше не можна вважати унікальними біоплівки в вузькому біомедичному розумінні; всі ці феномени можна також спостерігати в інших агрегаціях які розвиваються в природних екологічних нішах під впливом динамічних умов. В результаті цього аналізу ми станемо краще розуміти процеси, які керують колонізацією бактерій і забезпечують їхній екологічний успіх в ширшому розумінні.*

.

РОЗДІЛ 2 Матеріали і методи досліджень

2.1. Робота з бактеріями.

2.1.1. Штами бактерій і плазміди.

Бактерії та плазміди, використані в цій роботі, перераховані в таблиці 1. Усі штами зберігали при -80°C для тривалого зберігання у середовищі із додаванням 15% (об./об.) гліцерину до нічних культур. *B. avium* 197N було придбано безпосередньо з Американської колекції типових культур (ATCC BAA-1003). Чутливість до антибіотиків оцінювали за допомогою дисків з антибіотиками (MAST, Великобританія). Чутливість до канаміцину і тетрацикліну підтверджували за допомогою планшетів із середовищем LB, що містили 100 мкг/мл канаміцину і 12,5 мкг/мл тетрацикліну, інкубованих при 28°C протягом 48 годин.

Таблиця 1.

Бактерії і плазміди, використані в роботі.

Штам або плазміда	Коментар
Bordetella avium 197N	Дикий штам (ATCC BAA-1003), Km^S, Tc^S.
B. avium 197N мутант дефіцитний по продукціїцелюлози	*Ba.* 197N::*wssB*::ISΩ-Km*/hah* сконструйований із використанням pAS296, Km^R.
Escherichia coli K12 DH5	Використовувався як щтам-хазяїн плазмід.
Escherichia coli K12 pC1-L	Використовувався як щтам-хазяїн плазмід.
Pseudomonas fluorescens SBW25	Дикий штам, що продукує низький рівень целюлози та утворює слабку біоплівку, відому як viscous mass (VM).
P. fluorescens SBW25 Wrinkly Spreader (WS) mutant	*Pf.* SBW25 *wssF* (*S301R*) суперпродуцент целюлози, утворює міцну, фізично міцну, або physically cohesive (PC) біоплівку
P. fluorescens SBW25 WS-GFP	*P. fluorescens* SBW25 wspF A901C
Klebsiella pneumoniae ATCC 10031	З національної колекції мікроорганізмів.
K. pneumoniae UHI 117	Клінічний ізолят від пацієнта.
K. pneumoniae UHI 486	Клінічний ізолят від пацієнта.
K. pneumoniae UHI 489	Клінічний ізолят від пацієнта.
K. pneumoniae UHI 509	Клінічний ізолят від пацієнта.
K. pneumoniae UHI 519	Клінічний ізолят від пацієнта.
K. pneumoniae UHI 520	Клінічний ізолят від пацієнта.
K. pneumoniae UHI 329	Клінічний ізолят від пацієнта.
K. pneumoniae UHI 1090	Клінічний ізолят від пацієнта.
K. pneumoniae UHI 1609	Клінічний ізолят від пацієнта.
K. pneumoniae UHI 1633	Клінічний ізолят від пацієнта.

K. pneumoniae UHI 1667	Клінічний ізолят від пацієнта.
Streptococcus gordonii UHI1	Клінічний ізолят від пацієнта.
S. sanguinis UHI1	Клінічний ізолят від пацієнта.
S. mitis UHI1	Клінічний ізолят від пацієнта.
Pseudomonas aeruginosa PA01	З національної колекції мікроорганізмів.
Staphylococcus aureus ATCC 29423	З національної колекції мікроорганізмів.

Таблиця 2.

Походження та фенотипи з антибіотикорезистентності окремих штамів *K.pneumoniae*.

	Не-MDR UHI ізоляти						MDR UHI ізоляти				
	117	486	489	509	519	520	329	1090	1609	1633	1667
Походження[1]											
Зразок[2]	М	Ф	Ф	Ф	Ф	Ф	Ф	Ф	Г	Г	М
Діагноз[3]	Б	Е	Е	Е	Е	Е	Е	Е	О	О	Е
Антимікробна чутливість[4]											
Амоксицилін	Р	Р	Р	Р	Р	Р	Р	Р	Р	Р	Р
Ампіцилін	Ч	Ч	Ч	Ч	Ч	Ч	Р	Р	Р	Р	Р
Амікацин	Ч	Ч	Ч	Ч	Ч	Ч	Р	Р	Р	Р	Р
Азитроміцин[5]	6	10	10	20	18	18	17	17	15	13	17
Гентаміцин	Ч	Ч	Ч	Ч	Ч	Ч	Р	Р	Р	Р	Р
Цефепім	Ч	Ч	Ч	Ч	Ч	Ч	Р	Р	Р	Р	Р
Цефоперазон-сульбактам	Ч	Ч	Ч	Ч	Ч	Ч	Р	Р	Р	Р	Р
Цефотаксім	Ч	Ч	Ч	Ч	Ч	Ч	Р	Р	Р	Р	Р
Цефтазидим	Ч	Ч	Ч	Ч	Ч	Ч	Р	Р	Р	Р	Р
Цефтріаксон	Ч	Ч	Ч	Ч	Ч	Ч	Р	Р	Р	Р	Р
Цефуроксим	Р	Ч	Ч	Ч	Ч	Ч	Р	Р	Р	Р	Р
Хлорамфенікол	Ч	Ч	Ч	Ч	Ч	Ч	Ч	Ч	Ч	Р	Ч
Ципрофлоксацин	Ч	Ч	Ч	Ч	Ч	Ч	Р	Р	Р	Р	Ч
Ертапенем	Ч	Ч	Ч	Ч	Ч	Ч	Р	Р	Р	Р	Р
Гатіфлоксацин	Ч	Ч	Ч	Ч	Ч	Ч	Р	Р	Р	Р	Ч
Іміпенем	Ч	Ч	Ч	Ч	Ч	Ч	Р	Р	Р	Р	Р
Левофлоксацин	Ч	Ч	Ч	Ч	Ч	Ч	Р	Р	Р	Р	Ч
Меропенем	Ч	Ч	Ч	Ч	Ч	Ч	Р	Р	Р	Р	Р
Офлоксацин	Ч	Ч	Ч	Ч	Ч	Ч	Р	Р	Р	Р	Ч
Піперацилін-тазобактам	Ч	Ч	Ч	Ч	Ч	Ч	Р	Р	Р	Р	Р
Поліміксин В[6]	Ч	Ч	Ч	Ч	Ч	Ч	Ч	Ч	Ч	Р	Ч
Тайгециклін	Ч	Ч	Ч	Ч	Ч	Ч	Р	Ч	Ч	І	Ч
Тобраміцин	Ч	Ч	Ч	Ч	Ч	Ч	Р	Р	Р	Р	Р
Тріметоприм	Ч	Ч	Ч	Ч	Ч	Ч	Р	Р	Р	Ч	Р

Колістин (бульон)[7]	Ч	Ч	Ч	Ч	Ч	Ч	Ч	Р	Ч	Р	Ч
Гени бета-лактамаз[8]											
NDM	-	+	+	+	+	+	+	-	-	-	+
VIM	-	-	-	-	-	-	-	-	-	-	-
KPC	-	+	-	+	-	+	-	-	-	+	+
OXA-48-подібна	+	-	-	-	-	-	-	-	-	-	-
Ферментна активність											
AmpC							+	+	+	+	-
KPC							+	-	+	+	+
MBL							+	+	+	-	-
OXA-48							+	+	+	-	-
ESBL[9]							+	+	+	+	+

[1]Штами було ізольовано від пацієнтів міських лікарень, Київ, Україна. [2]Штами були виділені з мокротиння (М), фекалій (Ф) і глотки (Г). [3]Діагноз пацієнта - бронхіальна астма (Б) або ентерит (Е) або зразки взяті з огляду при отриманні (О). [4]Чутливість до антибіотиків, визначена за допомогою диск-дифузійного методу, показана як чутлива (Ч), проміжна (чутлива, підвищений вплив) (І) або резистентна (Р). [5]Діаметри пригнічення зони росту (мм) надані для азитроміцину, оскільки немає офіційного стандарту інтерпретації за EUCAST для *K. pneumoniae*, який є «офіційно» стійким; у цих аналізах 6 мм свідчить про повну стійкість, тоді як 15–20 мм свідчить про значну чутливість. [6]Поліміксин В є офіційною альтернативою колістин/CMS для тестування дискової дифузії. [7]Аналіз мікророзведення бульйону колістину; чутливість становить ≤ 1 мг/л. [8]AmpliSens MDR KPOXA-48-FRT / MBL-FTR PCR (+, позитивний –, негативний). [9]Бета-лактамаза розширеного спектру дії (+, позитивний –, негативний). Жодних тестів для тих клітин, залишених порожніми, не проводилося.

2.1.2. Умови культивування.

Бактерії *B. avium* культивували при 20, 28, 37 і 42 °C з використанням Brain Heart Infusion (BHI; Oxoid, Великобританія), King's B (KB; 20 г протеозопептону № 3 (BD Biosciences, Великобританія), 10 г гліцерину, 5 г K2HPO4, 1,5 г MgSO4 на літр) і середовища Луріа-Бертані (LB; 10 г NaCl, 10 г триптону (Oxoid, Великобританія) і 5 г дріжджового екстракту (Merck, Великобританія) на літр) з 1,5% (мас./об.) мікробіологічного агару (Oxoid, Великобританія) для чашок Петрі і антибіотиків, доданих в середовищу за потреби. Культури, які струшували протягом ночі, використовували для забезпечення інокулята для експериментів. Мікрокосми являли собою 30 мл скляні

пробірки, що містили 6 мл поживного середовища. Плавальну рухливість оцінювали за допомогою чашок LB з м'яким агаром.

Klebsiella pneumoniae ATCC 10031 (Українська національна колекція) використовували як модельний штам для тестування утворення біоплівки та вільноживучої (планктонної) поведінки за різних обробок антибіотиками. Реакція біоплівки та планктону на лікування антибіотиками також була визначена для одинадцяти ізолятів *K. pneumoniae* від українських пацієнтів, включаючи мультирезистентні (MDR) штами UHI 329, UHI 1090, UHI 1609, UHI 1633 та UHI 166, а також штами не-MDR UHI 117 , UHI 486, UHI 489, UHI 509, UHI 519 і UHI 520. Усі штами зберігали у вигляді заморожених вихідних речовин у 25 (об./об.) % гліцерину при -80 °C.

K. pneumoniae UHI 1090, український лікарняний ізолят, спочатку був виділений у пацієнта з ентеритом і ідентифікований як штам із широкою лікарською стійкістю (XDR) за допомогою аналізів дифузії антибіотиків на дисках за EUCAST 2021 v.11.0. Картку AST-N332 використовували для підтвердження фенотипу штаму XDR за допомогою розширеної експертної системи VITEK 2. Антимікробну чутливість до поліміксину перевіряли за допомогою мікророзведення бульйону SensiTest Colistin (Liofilchem, Roseto degli Abruzzi, Італія), а результати інтерпретували відповідно до EUCAST. Було виявлено, що штам чутливий до поліміксину B і тайгецикліну, але стійкий до всіх β-лактамів, фторхінолонів і аміноглікозидів. Штам зберігали у замороженому вигляді в 25 (об./об.) % гліцерину при -80 °C.

Бактеріальні штами клебсієл культивували аеробно при 37°C у середовищі LB і на агарі Мюллера Хінтона (OXOID, Великобританія). Штами, що зберігались у стоковій колекції, було виділено із заморожених вихідних культур на чашках LB перед тим, як розпочати струшування культур протягом ночі, щоб отримати свіжий інокулят для експериментів (було виявлено, що пряма інокуляція із заморожених вихідних культур значно зменшує виробництво сидерофорів і розвиток біоплівки; неопубліковані спостереження). Щільність культури та розведення визначали вимірюванням OD625 за допомогою спектрофотометра Spectronic Helios Epsilon (Thermo Fisher Scientific, Великобританія) з кюветами з оптичним шляхом 10 мм або вимірюванням OD 570 за допомогою мікропланшетного фотометра Multiskan™ FC (Thermo Fisher Scientific, Великобританія).

Для основного дослідження використовували вісім макролідних антибіотиків, які включали азитроміцин (AZM; Pharmex Group, Україна), кларитроміцин (CLR; Abbott, Італія), еритроміцин (ERM; Вітаміни, Україна), джозаміцин (JSM; Astellas Pharma, Японія), мідекаміцин. (MID; KRKA, Словенія), рокситроміцин (ROX; Дарниця, Україна), спіраміцин (SPM; Sanofi Aventis, Італія), тилозин (TYL; Укрзооветпромпостач, Україна). Основні розчини, що містять 9 г/л кожного антибіотика, готували з використанням ДМСО як розчинника та зберігали при -20°C не більше 7 днів перед використанням. Основний розчин колістину метансульфонату (CMS) 1 г/л (Forest Laboratories, Великобританія) готували у воді та використовували протягом 30 хвилин після приготування. Диски, що містять антибіотики (HiMedia Laboratories, Індія), а також картки AST-N332 для VITEK 2 Advanced Expert System (bioMérieux, Франція) використовувалися для аналізів чутливості та чутливості до антимікробних препаратів. Диски, що містять антибіотики (HiMedia Laboratories, Індія), а також картки AST-N332 для розширеної експертної системи VITEK 2 (bioMerieux, Франція) використовувалися для аналізів сприйнятливості та чутливості до антимікробних препаратів.

2.1.3. Визначення антимікробної чутливості.

Для визначення антимікробної чутливості штамів *K. pneumoniae* UHI використовувався диск-дифузійний аналіз за Кірбі-Бауером. На чашки Петрі із середовищем Мюллера Хінтона наносили 200 мкл клітинної суспензії, приготовленої розведенням культур протягом ночі до 0,12–0,18 OD625, і давали висохнути, перш ніж застосовувати не більше п’яти дисків з різними антибіотиками на планшет. Потім чутливість визначали як діаметр (мм) інгібування після інкубації протягом двох днів та інтерпретували відповідно до наказу МОЗ України № 167 (05 квітня 2007 р.) для гатифлоксацину, технічних даних для цефоперазону/сульбактаму CFS 50/50 мкг диски від HiMedia Laboratories (лютий 2019 р.) для цефоперазону/сульбактаму та рекомендації Європейського комітету з тестування чутливості до протимікробних препаратів (EUCAST) для решти антибіотиків. Гени β-лактамаз виявляли методом ПЛР з використанням ДНК, очищеної за допомогою наборів AmpliSense DNA-sorb-B Nucleic Acid Extraction, MDR KPC OXA-48-FRT та MBL-FRT PCR kit (Медспілка, Україна). Активність β-лактамази визначали за допомогою KPC&MBL&OXA-48 та ESBL+AmpC скринінгових дисків (Liofilchem, Італія) відповідно до рекомендацій EUCAST. Карти AST-N332 також використовували з

розширеною експертною системою VITEK 2 для підтвердження фенотипів MDR-штаму. Випробування антимікробної чутливості CMS проводили за допомогою аналізу мікророзведення бульйону SensiTest™ Colistin (Liofilchem, Італія). Результати інтерпретувалися згідно з рекомендаціями EUCAST.

Аналіз результатів диск-дифузійного тесту за Кірбі-Бауером мав визначити, чи можна виявити синергетичну дію AZM і поліміксину B як для штамів UHI. Для цього в середовище MH додвалось 0, 3, 6, 9 мг/л AZM, інокулювали 200 мкл клітинної суспензії, приготованої шляхом розведення нічних культур до 0,12–0,18 OD625, і давали висохнути перед реплікацією дисків поліміксину-B PB300U (n = 3). Потім визначали чутливість як діаметр (мм) інгібування після інкубації протягом двох днів.

2.1.4. Отримання біоплівок.

Біоплівки *P. fluorescens* SBW25 отримували в скляних мікрокосмах. Мікрокосми являли собою скляні флакони об'ємом 30 мл, що містили 6 мл рідкого середовища King's B (KB; 20 г протеозопептону № 3 (BD Biosciences, Великобританія), 10 г гліцерину, 5 г K_2HPO_4, 1,5 г $MgSO_4$ на літр) і додавали 1 мМ $FeCl_3$ для індукції утворення біоплівки в'язкої маси. Бактерії інкубували при 20 °C з біоплівками, створеними в мікрокосмах, які статично інкубували протягом 24 годин або трьох днів (для зрілих біоплівок), а зразки планктону відновлювали з 24-годинних струшуваних мікрокосмів, в яких біоплівки не могли утворитися. Низькомолекулярна (LMW) ДНК сперми лосося (Fluka, Північна Кароліна, США) і високомолекулярна (HMW) ДНК насінників лосося (Sigma-Aldrich, Великобританія) були додані до мікрокосмів при 100, 300, і 600 мкг/мл, а дезоксирибонуклеаза I підшлункової залози великої рогатої худоби (DNase I) (Sigma-Aldrich, Великобританія) додана до 1 мкг/мл, щоб оцінити важливість еДНК для розвитку біоплівки, кінцевої міцності та рівнів прикріплення.

Штами *Bordetella* spp. культивували при 20, 28, 37 і 42 °C з використанням середовища Brain Heart Infusion (BHI; Oxoid, Великобританія), King's B і середовища Луріа-Бертані (LB; 10 г NaCl, 10 г триптону (Oxoid, Великобританія) і 5 г дріжджового екстракту (Merck, Великобританія) на літр з 1,5% (мас./об.) технічного агару (Oxoid, Великобританія). Культури, які струшували протягом ночі, використовували для забезпечення інокулята для експериментів. Мікрокосми являли собою 30 мл скляні пробірки, що містили 6 мл

ростового середовища. Плавальну рухливість оцінювали за допомогою чашок LB з м'яким агаром.

Штами *Klebsiella spp.* культивували аеробно при 37°C з використанням середовища LB. Штами були виділені із заморожених вихідних культур на чашках LB перед тим, як розпочати струшування культур протягом ночі, щоб отримати свіжий інокулят для експериментів (було виявлено, що пряма інокуляція із заморожених вихідних культур значно зменшує виробництво сидерофорів і розвиток біоплівки; неопубліковані спостереження). Щільність культури та розведення визначали вимірюванням OD625 за допомогою спектрофотометра Spectronic Helios Epsilon (Thermo Fisher Scientific, Великобританія) з кюветами з оптичним шляхом 10 мм.

Попередні експерименти з біоплівками показали, що біоплівки на межі поверхня-рідина, створені *K. pneumoniae, P. aeruginosa* і *S. aureus*, легко видалялися зі скляних флаконів або 96-лункових планшетів. Тому ми вирішили виготовити зразки біоплівки для аналізу ефектів різноманітних біоцидів шляхом безпосереднього використання таких стаціонарних культур, в яких розвиваються біоплівки. Ми зазначили, що, отже, зразки міститимуть частину планктонних клітин, але це матиме обмежений вплив на наші аналізи, оскільки у *K. pneumoniae* і *S. aureus* відсутні джгутики, і початковий інокулят не залишатиметься в стовпі рідини надовго, і весь наступний ріст має бути в біоплівках. Незважаючи на те, що *P. aeruginosa* здатний до плавання, опосередкованого джгутиками, він має високу аеротаксичну дію, і більшість клітин накопичуватиметься на межі повітря та рідини та в області меніска, де домінує ріст біоплівки. Для аналізу інактивації біоплівки культури LB розводили до 10% і аліквоти по 200 мкл переносили в лунки 96-лункового планшета, який інкубували при 37 °C протягом 24 годин перед аналізом інактивації біоцидом. Для КЛСМ та аналізу еДНК використовували 10% розведення для інокуляції 30 мл скляних флаконів (мікрокосмів), що містять 2–5 мл LB, які статично інкубували при 37 °C протягом 3–5 днів для отримання біоплівок. Біоплівки сушили на повітрі при кімнатній температурі протягом 14 днів перед аналізом еДНК. Для КЛСМ біоплівки вирощували в стаціонарних скляних флаконах об'ємом 5 мл, а зразки відбирали за допомогою піпетки зі зрізаними наконечниками об'ємом 200 мкл. Зразки біоплівки обережно помістили на предметне скло мікроскопа, а рідину злили за допомогою фільтрувального паперу. Потім їх обробляли розчином PHMG-Cl протягом 30 хвилин і обережно промивали водою за

допомогою піпетки, щоб видалити біоцид, але обмежити будь-які подальші фізичні пошкодження перед фарбуванням і зображенням.

2.1.5. Дослідження антибіоплівкових властивостей поверхонь.

Здатність бактерій утворювати біоплівки, пов'язані з досліджуваними металевими поверхнями, оцінювали за допомогою двох модельних штамів, що утворюють біоплівки, грамнегативної *Pseudomonas aeruginosa* PA01 і грампозитивної *Staphylococcus aureus* ATCC25923. Для цього кожен металевий зразок площею 1 $см^2$ стерилізували обробкою 96% етанолом з наступним спалюванням. Потім кожен зразок поміщали в лунку стерильного полістирольного 24-лункового планшета, в який додавали 2 мл середовища LB, інокулювавши 10 мкл нічної інокулятної культури, що містить 10^9 КУО/мл; було по три репліки на варіант. Планшет інкубували при 37 ºС протягом 72 годин. Утворення біоплівки оцінювали за допомогою конфокальної мікроскопії після трьох днів стаціонарної інкубації. Контроль інкубації проводили шляхом інкубації купонів у стерильному LB з трьома повторами. Після інкубації кожен зразок видаляли та тричі промивали для видалення планктону та погано прикріпленої біоплівки.

Стійкість до біологічного обростання, тобто характеристики антибіоплівкковості плівок PA-11/PHMG-NS, оцінювали шляхом вимірювання здатності двох модельних штамів, що утворюють біоплівки, *E. coli* K12 і *S. aureus* ATCC25923, утворювати прикріплені біоплівки на поверхні зразків полімерів після трьох днів стаціонарної інкубації. Кожну плівку PA-11/PHMG-NS розрізали на шматки по 1 $см^2$ кожен. Шматки стерилізували в автоклаві при 105 ºС протягом 30 хвилин. Оброблені водою шматки пластику готували експозицією 1 г пластикових плівок у 500 мл деіонізованої води протягом 7 днів.

Потім кожен шматочок поміщали в лунку стерильного полістирольного 24-лункового планшета, в який додавали 2 мл середовища LB, інокулювавши 10 мкл нічного інокуляту, що містить 10^9 КУО/мл; було вісім реплік на варіант. Планшет інкубували при 37 ºС протягом 72 годин. Контроль інкубації проводили шляхом інкубації плівок у стерильному LB з чотирма повторами. Після інкубації кожен шматок плівки видаляли та тричі промивали для видалення планктону та погано прикріпленої маси біоплівки.

Щоб виміряти рівень біомаси біоплівки, прикріпленої до пластику, було проведено аналіз кристалічним фіолетовим. Для цього вісім фрагментів із прикріпленими біоплівками поміщали у скляний флакон, фарбували 1 мл 0,05% розчину кристалічного фіолетового

протягом 30 хвилин і тричі промивали у воді, після чого барвник елюювали, інкубуючи шматок у 500 мкл 96% етанолу протягом години. Елюйований барвиник в кожній 200-мкл аліквоті визначали кількісно шляхом вимірювання абсорбції при 570 нм на спектрофотометрі для мікропланшетів BioTek ELx800. Чисте прикріплення біоплівки розраховували шляхом віднімання контрольних значень, що відповідають інкубації в LB.

Також було проведено метаболічний аналіз біоплівки із восьмикратним повтором. Для цього кожен шматочок поміщали у скляну пробірку з 500 мкл 0,05% розчину MTT (Sigma-Aldrich, Великобританія) та інкубували при 37 ^{o}C протягом 20 годин. Потім плівку та розчин MTT видаляли з кожного флакона та поміщали в пластикову пробірку на 1,5 мл, яку центрифугували при 13000 g протягом 15 хвилин (мікроцентрифуга Eppendorf 5424). Супернатант відкидали, а осад знову розчиняли в 500 мкл ДМСО. Знову ж таки, інтенсивність фарбування 200 мкл оцінювали за допомогою вимірювання абсорбції при 570 нм. Чисту метаболічну активність біоплівки розраховували шляхом віднімання контрольних значень, що відповідають інкубації в LB.

Токсичність плівок PA-11/PHMG-NS оцінювали на основі оптичної щільності, а також кількості колонієутворюючих одиниць планктонної культури над біоплівкою. Для цього 200 мкл планктонної культури над біоплівкою кожної обробки переносили в стерильний полістироловий 96-лунковий планшет. Оптичну щільність вимірювали спектрофотометрично при 570 нм. 100 мкл кожної надбіоплівкової планктонної культури використовували для приготування серій розведень, які потім висівали на чашки з агаром LB для визначення колонієутворюючих одиниць.

Антибіоплівкова ефективність поверхні фарби PyrC12-DBS вимірювали шляхом оцінки здатності двох модельних штамів, що утворюють біоплівки, *S. aureus* ATCC 25923 і *P. aeruginosa* PA01, утворювати прикріплені біоплівки на поверхні, покритій PP-115 і PP-115/PyrC12-DBS (16%) після двох днів стаціонарної інкубації. Для цього 1 см^2 металевих купонів, покритих PP-115 або PP-115/PyrC12-DBS (16%), стерилізували в автоклаві при 105 °C протягом 30 хв. Потім кожен купон поміщали в лунку стерильного полістирольного 24-лункового планшета, в який додавали 2 мл середовища LB, інокулювавши 10 мкл нічної інокулятної культури, що містить 10^9 КУО/мл; було шість реплік на варіант. Планшет інкубували при 37 °C протягом 48 годин. Контроль інкубації проводили шляхом інкубації плівок у стерильному LB із чотирма повторами. Після інкубації кожен шматок плівки

видаляли та тричі промивали для видалення планктону та погано прикріпленої маси біоплівки. Для вимірювання рівня загальної метаболічної активності біоплівки проводили МТТ-тест. З цією метою шість купонів із прикріпленими біоплівками для кожного штаму помістили в новий стерильний полістирольний 24-лунковий планшет, 200 мкл 0,05% МТТ (3-(4,5-диметилтіазол-2-іл)-2,5- дифенілтетразолію бромід; Sigma-Aldrich, Великобританія) у LB додавали до кожного купону площею 1 $см^2$, інкубували при 37 °C протягом 2 годин, середовище LB-МТТ осаджували при 10 000 g протягом 10 хвилин, осад ресуспендували в 200 мкл ДМСО. 200 мкл ДМСО також додавали до кожного купону. 100 мкл з кінцевих 400 мкл розчину формазану, розчиненого в ДМСО, на зразок переносили в полістирольний 96-лунковий планшет і метаболічну активність (А 570) вимірювали за допомогою мікропланшетного фотометра Multiskan FC (ThermoFisher Scientific, Waltham, MA, США).

2.1.6. Комбінований аналіз біоплівки.

Комбінований аналіз біоплівки (Combined Biofilm Assay) проводився для комплексного порівняльного аналізу біоплівок наступним чином. Біоплівки, що утворилися у мікрокосмах/флаконах послідовно досліджувалися на міцність (грами), рівнів прикріплення (фарбування кристалічним фіолетовим, А570) і загальну біомаса мікрокосмі (OD600) (тобто ріст). Біоплівки спочатку перевіряли на міцність за допомогою невеликих (~0,01 г) скляних кульок, які послідовно додавали, доки біоплівка не розірветься або не потоне (максимальна деформація або розривна маса). Слід зазначити, що хоча біоплівки Viscous Mass утворювалися під час усіх обробок, що підтверджено візуальним оглядом, вони, як правило, були настільки слабкими, що їх було важко виміряти порівняно з більш міцними біоплівками Wrinkly Spreader. Вміст флаконів мікрокосму з пошкодженими або затопленими біоплівками переносили в другий флакон, який потім енергійно перемішували протягом 30 секунд для розпаду всього матеріалу біоплівки. Потім відібрали пробу цієї суспензії для визначення оптичної щільності (OD600) за допомогою спектрофотометра Spectronic Helios Epsilon (ThermoFisher Scientific, Оксфорд, Великобританія) з кюветами з оптичним шляхом 10 мм, як вимірювання загальної біомаси мікросвіту. Потім вихідні флакони перевіряли на прикріплення клітин і біоплівки до меніска за допомогою кристалічного фіолетового. Флакони тричі промивали у воді для видалення неприкріплених клітин і матеріалу, а потім фарбували 0,05% мас./об. розчином кристалічного фіолетового протягом 2 хв і повторно промивали тричі для видалення незв’язаного барвника.

Кристалічний фіолетовий елюював 5 мл етанолу та обережно струшував протягом 1 години та відбирав пробу для визначення абсорбції (A570) як міри рівня прикріплення біоплівки до меніска. Друге елюювання 5 мл 10% об'єму оцтової кислоти протягом 1 години з подальшим вимірюванням абсорбції (A570) було використано для кількісного визначення залишку зв'язаного кристалічного фіолетового.

2.1.7. Вплив антибіотиків на біоплівку і планктон *Klebsiella spp*.

Для основного дослідження використовували вісім макролідних антибіотиків, які включали азитроміцин (AZM; Pharmex Group, Україна), кларитроміцин (CLR; Abbott, Італія), еритроміцин (ERM; Вітаміни, Україна), джозаміцин (JSM; Astellas Pharma, Японія), мідекаміцин. (MID; KRKA, Словенія), рокситроміцин (ROX; Дарниця, Україна), спіраміцин (SPM; Sanofi Aventis, Італія), тилозин (TYL; Укрзооветпромпостач, Україна). Основні розчини, що містять 9 г/л кожного антибіотика, готували з використанням ДМСО як розчинника та зберігали при -20°C не більше 7 днів перед використанням. Основний розчин колістину метансульфонату (CMS) 1 г/л (Forest Laboratories, Великобританія) готували у воді та використовували протягом 30 хвилин після приготування.

Аналізи росту планктону штамів ATCC 10031 і UHI оцінювали у флаконах із нещільно закритими кришками, які перед аналізом інкубували зі струшуванням. Флакони містили 6 мл LB і AZM, а CSM додавали до 6 мл флаконів LB до кінцевих концентрацій 0, 3, 6 і 9 мг/л AZM і 0, 2, 4, 6, 8, 12, 16, 18, 24, 28 і 32 мг/л CMS. Аліквоти нічної культури додавали до реплікаційних флаконів (n = 3) до ~5×10^6 КУО/мл і ріст визначали після 16 годин інкубації шляхом видалення 200 мкл зразків, які переносили в полістирольний 96-лунковий планшет і вимірювали OD570 за допомогою зчитувач пластин BioTek ELx800 (BioTek Instruments, Winooski, VT, США).

Попередня оцінка утворення біоплівки в скляних флаконах об'ємом 30 мл і полістирольних 96-лункових планшетах виявила, що біоплівки ATCC 10031 і UHI на інтерфейсі повітря-рідина (A-L) були дуже крихкими з відносно незначним зростанням у стовпчиках рідини. Однак ці біоплівки не могли бути надійно утримані під час промивання та фарбування кристалічним фіолетовим після звичайних процедур. Тому ми вирішили змінити наш підхід і використали прямі вимірювання OD570 необроблених 96-лункових планшетів, які фіксували як ріст біоплівки, так і клітини, суспендовані в стовпі рідини. Аліквоти 20 мкл нічної культури використовували для інокуляції повторних лунок (n = 8

для індивідуальних макролідних аналізів і n = 3 для AZM – CSM аналізів), що містили 200 мкл LB з відповідними антибіотиками (0, 1, 3, 6 і 9 мг/л макроліду для окремих макролідних аналізів, 0, 3, 6 і 9 мг/л AZM і 0, 2, 4, 6, 8, 12, 16, 18, 24, 28 і 32 мг/л CMS для AZM – аналізи CSM). Зростання (OD570) визначали після 24–48 год статичної інкубації за допомогою пристрою для зчитування планшетів BioTek ELx800. Метаболічну активність також визначали після додавання MTT (3-(4,5-диметилтіазол-2-іл)-2,5-дифенілтетразолію броміду; Sigma-Aldrich, Великобританія) до кінцевої концентрації 0,05% (об./об.) і подальша інкубація 3 год. Клітини виділяли з кожної лунки центрифугуванням при 6000 g протягом 15 хвилин з використанням мікроцентрифуги Eppendorf 5424 (Eppendorf, Гамбург, Німеччина). Клітинний осад розчиняли в 250 мкл ДМСО, 125 мкл якого переносили в полістирольний 96-лунковий планшет і вимірювали метаболічну активність (A570) за допомогою пристрою для зчитування планшетів BioTek ELx800. Ми постійно виявляли більшу варіацію у вимірюваннях A570 зростання біоплівки, ніж у вимірюваннях OD570, що свідчить про те, що аналіз MTT був технічно складнішим для виконання.

2.1.8. Дослідження виходу еДНК.

Біоциди тестували в різних концентраціях для визначення виходу еДНК. Для цього 1 мл 0,5 %, 0,1 % і 0,05 % ПГМГ-С1; 6% і 3% перекис водню; 70% етанол; 0,05% хлоргексидин; 0,25% Максан; 0,5% Арквадез-плюс; 0,5% десманол; і 0,5% Sanikon додавали до зневоднених біоплівок *P. aeruginosa* і *S. aureus* при кімнатній температурі, і суміші витримували протягом 1 години, з трьома повторами на обробку. Обробку лише водою знову використовували як позитивний контроль. еДНК екстрагували з рідкої фази кожного зразка. Білки спочатку видаляли рівним об'ємом хлороформу, а ДНК осаджували 70% етанолом і 0,3 М ацетатом натрію (pH 8,0). Потім ДНК розчиняли в буфері ТЕ. Концентрацію нуклеїнової кислоти вимірювали спектрофотометром NanoDrop 2000 (ThermoFisher Scientific, Inc., Вілмінгтон, Делавер, США). Потім зразки ДНК візуалізували за допомогою електрофорезу в 1,2% агарозному гелі та фарбування EtBr. Як маркер розміру використовували GeneRuler 1 kb DNA Ladder (Thermo Fisher Scientific, Литва).

2.1.9. Виділення еДНК біоплівки.

Біоплівки *P. aeruginosa* і *K. pneumoniae* вирощували в статичних флаконах LB об'ємом 5 мл при 37 °C протягом 5 днів. Потім біоплівки розщеплювали шляхом перемішування протягом 5 хв. Потім 5 мл суспензії біоплівки центрифугували при 13 000×g протягом 15

хвилин за допомогою мікроцентрифуги та виділили супернатант. eDNA у надосадовій рідині осаджували 70% етанолом і 0,3 М ацетатом натрію (pH 8,0), а потім розчиняли в буфері ТЕ. Концентрацію нуклеїнової кислоти вимірювали за допомогою NanoDrop.

2.1.10. Вплив ПГМГ-ГХ на еДНК і плазмідну ДНК pC1-L.

eDNA, виділену з *P. aeruginosa* 27853 і pC1-L ДНК, обробляли різними концентраціями ПГМГ-ГХ. Для цього 7 мкл (6,7 мкг) еДНК і 7 мкл (2,8 мкг) лінійної або ковалентно замкнутої кільцевої (CCC) pC1-L ДНК змішували з 3 мкл буфера для завантаження ДНК (ThermoFisher Scientific, Вільнюс, Литва) і остаточно концентрації 0,01% і 0,05% ПГМГ-ГХ. Зразки поміщали в діалізну трубку D-0530 (Sigma, Сент-Луїс, Міссурі, США), і зразки діалізували разом, щоб зменшити концентрацію ПГМГ-ГХ в 10–7 разів у буфері ТЕ. Зразки ДНК візуалізували за допомогою гель-електрофорезу.

2.2. Робота з еукаріотичними культурами.

2.2.1. Культури, що використовувались в роботі.

Лінія клітин нирки ембріона людини HEK293 отримана з банку клітинних ліній тканин людини і тварин інституту експериментальної патології, онкології та радіобіології імені Кавецького НАН України. Клітини культивували в модифікованому за Дульбекко середовищі Ігла (DMEM)/середовищі з високим вмістом глюкози (Biowest, Франція), що містило 10 % фетальної бичачої сироватки (FBS) (Sigma-Aldrich, США), 100 ОД/мл пеніциліну та 100 мг/мл стрептоміцину (Артеріум, Україна).

Мезенхімальні/стромальні стовбурові клітини жирової тканини людини використовували для визначення прикріплення еукаріотичних клітин до оброблених лазером металевих поверхонь. Клітини отримували з ліпоаспірату за допомогою колагенази. Ліпоаспірат двічі промивали PBS центрифугуванням при 400 g протягом 5 хв. Верхній шар жирової тканини видаляли і змішували зі свіжоприготованим розчином колагенази I (Gibco, Thermo Fisher Scientific, Inc.) до кінцевої концентрації 0,2% у PBS. Ферментне розщеплення проводили при 37 ºC при постійному перемішуванні протягом 1 години. Колагеназу інактивували шляхом додавання рівного об’єму середовища для культури клітин, після чого суспензію центрифугували при 400 g протягом 10 хв. Осад тричі промивали PBS, потім ресуспендували в PBS і фільтрували (розмір пор 100 мкМ), щоб видалити неперетравлені фрагменти тканини. Отриману стромально-судинну фракцію висівали в культуральні колби з середовищем DMEM-F12, що містить 10% фетальної

бичачої сироватки (Sigma Aldrich, Велика Британія) з додаванням 100 ОД/мл пеніциліну та 100 мкг/мл стрептоміцину. Культивування проводили при 37 ºС в атмосфері 5% CO2 протягом 48 годин перед видаленням неприкріплених клітин. Інкубація тривала ще 48 годин, перш ніж стовбурові клітини, отримані з жирової тканини (ADSC), були оброблені трипсином (0,20% трипсин-EDTA), промиті та використані для подальшого культивування або заморожування для зберігання. Експресія поверхневих маркерів CD 90, CD 105, CD 73 становила понад 98%, а експресія CD34 і CD45 – менше 0,5%.

2.2.2. Життєздатність еукаріотичних клітин після впливу антибіотиків.

Вплив CMS і AZM на життєздатність клітин HEK293 перевіряли за допомогою колориметричного аналізу метаболічної активності MTT. Клітини HEK293 висівали за 24 години до застосування антибіотиків. Перед додаванням будь-яких антибіотиків культуральне середовище змінювали на середовище без фетальної бичачої сироватки. Потім клітини HEK293 культивували при 37°C і 5% CO_2 в концентрації 3×10^5 клітин на лунку в 96-лунковому планшеті в присутності різних концентрацій антибіотика протягом 48 годин. Клітини, вирощені в DMEM/середовищі з високим вмістом глюкози без антибіотиків, служили групою негативного контролю. Вимірювання для кожної точки концентрації проводили в трьох повторах.

2.2.3. Вплив різних культуральних середовищ і клітин HEK293 на ріст *K. pneumoniae* UHI 1090.

$3x10^5$ клітин HEK293/лунку поміщали в 96-лунковий культуральний планшет за 24 години до бактеріальної інокуляції. HEK293 культивували в середовищі DMEM/високий вміст глюкози, що містило 10% FBS при 37°C, 5% CO2. Середовище змінювали перед інокуляцією *K. pneumoniae* на таке середовище: 1) 90% DMEM/середовище з високим вмістом глюкози, що містить 10% FBS; 2) 89,99% DMEM/середовище з високим вмістом глюкози, що містить 10% FBS, 0,01% Bacto Proteose Peptone (BD Biosciences, США); 3) 49,99% DMEM/середовище з високим вмістом глюкози, що містить 50% FBS, 0,01% Bacto Proteose Peptone (BD Biosciences, США). Контролем служили безклітинні середовища. *K. pneumoniae* UHI 1090 (10^4 КУО/лунку) інокулював, і інкубацію продовжували при 37 °C, 5% CO_2. Значення OD вимірювали через 24 години після інокуляції при 620 нм. Кожне вимірювання проводили в шести повторах.

2.2.4. Аналіз прикріплення еукаріотичної клітини.

В експериментах використовували ADSC першого пасажу. Металеві зразки, підготовлені як і раніше, поміщали в лунки 24-лункового планшета і засівали клітинами з щільністю посіву 2,6 × 10^3/см2. Купони видаляли після трьох днів інкубації, а клітини трипсинізувати та підраховувати.

2.3. Конфокальна лазерна скануюча мікроскопія.

Мікроскопію зразків біоплівки проводили відповідно до встановлених процедур. Зразки біоплівки були отримані з триденних мікрокосмів, намотавши їх на наконечники піпетки P1000, а потім розгорнувши в іншому напрямку на предметні стекла мікроскопа. Надлишок рідини зливали перед тим, як додавали аликвоти по 10 мкл кожного з необхідних барвників. eDNA фарбували 20 мкМ пропідію йодиду (Sigma-Aldrich, Велика Британія) та 1 мкМ Experimental Stain 986 у ДМСО (відділ біомедичної хімії ІМБГ, Київ, Україна). Внутрішньоклітинну ДНК з інтактних і метаболічно активних (живих) клітин фарбували 5 мкМ розчином SYTO 9 (ThermoFisher Scientific, США), а загальну ДНК (еДНК і ДНК в активних і мертвих клітинах) фарбували 2 мкг/мл броміду етідію (ThermoFisher Scientific, США). Амілоїдні фібрили фарбували 1 мкМ AmyGreen в ДМСО (Відділ біомедичної хімії ІМБГ, Київ, Україна) або 1 мкМ тіофлавіном Т (Sigma-Aldrich, Велика Британія) целюлозу 5 мкМ Calcofluor white (Sigma-Aldrich, Велика Британія), а мембрани везикул 5 мкл розчину Vybrant DiO (ThermoFisher Scientific, США). Додаткове промивання зразків біоплівки не застосовувалося, щоб мінімізувати фізичне руйнування структур біоплівки через рух рідини.

Для забарвлення везикул суспензію змішували з розплавленим 0,8% (мас./об.) агарозним гелем перед нанесенням її на предметне скло. Зразки не фіксували, і покривне скло було встановлено на місце перед візуалізаціями. Аналіз CLSM проводився за допомогою конфокальної системи Leica TCS SPE Confocal з кодованим інвертованим мікроскопом DMi8 (Leica, Wetzlar, Німеччина) та програмним забезпеченням Leica Application Suite X версії 3.4.1. Зображення були отримані за допомогою збудження при 488 нм і випромінювання, зібраного при 490–580 нм для AmyGreen, GFP, SYTO 9 і Vybrant DiO; збудження при 532 нм і випромінювання, зібране при 537–670 для броміду етидію, експериментальної фарби 986 і йодиду пропідію; і збудження при 405 нм та випромінювання, зібране при 450–500 нм для Calcofluor white.

Біоплівки, сформовані на купонах з покриттям PP-115 та PP-115/PyrC12-DBS (16%), також досліджували за допомогою конфокальної лазерної скануючої мікроскопії (CLSM). Біоплівки фарбували 1 мМ бромідом етидію (Sigma-Aldrich) і 5 мкг/мл білого розчину кальцофлуору (Sigma-Aldrich). Додаткове промивання не використовувалося, щоб обмежити фізичне руйнування структур біоплівки через рух рідини. Зразки не фіксували, а на забарвлені зразки наносили покривне скло перед зображенням. Аналіз CLSM проводився за допомогою конфокальної системи Leica TCS SPE Confocal з кодованим інвертованим мікроскопом DMi8 (Leica, Німеччина) і Leica Application Suite X (LAS X) версії 3.4.1. Зображення були отримані з використанням збудження при 405 нм і випромінювання, зібраного при 450-500 нм для калькофлуор білого, та збудження при 532 нм і випромінювання, зібраного при 537-670 для броміду етідію. Загальна кількість пікселів була розрахована за допомогою вищезгаданого програмного забезпечення.

Металеві купони з прикріпленим ADSC інкубували з 1 мМ SYBR green (Invitrogen, Пейслі, Великобританія) протягом 15 хв. Зображення були отримані з використанням довжини хвилі збудження при 488 нм і довжини хвилі випромінювання, зібраної при 490-580 нм, за допомогою конфокальної системи Leica TCS SPE з кодованим інвертованим мікроскопом DMi8 (Leica, Німеччина) з рекомендованим програмним забезпеченням LAS X 3.1.2.16221 (Leica, Німеччина) як описано вище.

2.4. Аналіз колокалізації.

Коефіцієнт кореляції Пірсона (PCC), або Pearson R, було розраховано за допомогою пакета обробки зображень з відкритим кодом Fiji на основі ImageJ. Було три зображення на варіант фарбування з п’ятьма областями інтересу, або ROI, з групами з двох-п’яти бактеріальних клітин, вибраних вручну, на зображення. Значення Pearson R було розраховано для пікселів, інтенсивність яких була вище порогового значення, щоб уникнути фонових сигналів і пікселів низької інтенсивності. Отримані дані обробляли статистично за допомогою програмного забезпечення Orogin7 та алгоритму One-way ANOVA. Значення $p < 0,05$ вважалося статистично значущим.

2.5. Флуоресцентна гібридизація *in situ* (FISH).

Аналіз зразків біоплівки за допомогою FISH проводили наступним чином. Олігонуклеотидні зонди для еубактерій, стрептококів і групи *Bacteroides–Porphyromonas–Prevotella* (BPP) були синтезовані комерційно, а 5'-кінець мічений флуорохромами (Синтол,

Росія). EUB 338 (5’-GCT GCC TCC CGT AGG AGT-3’) був 5’-мічений FAM (Ex/Em 488/491 – 575 нм) і використовувався для візуалізації еДНК бактерій. STR 405 (5’-TAG CCG TCC CTT TCT GGT-3’) був 5’-мічений Cy5.5 (Ex/Em: 635/645 – 800 нм) і використовувався для візуалізації еДНК оральних стрептококів. Зонд Bacto 1080 (5’-GCA CTT AAG CCG ACA CCT-3’) був позначений акридином (Ex/Em 405/407 – 496 нм) і використовувався для візуалізації еДНК, отриманої з групи BPP. Сецифічність олігонуклеотидного зонду перевіряли за допомогою *K. penumoniae* ATCC 10031, *S. gordonii* UHI1 та HEK-293. Зразки бактеріальних культур і клітин HEK-293 інкубували з 1 мг/мл лізоциму, отриманого з білка курячого яйця (47 000 ОД/мг, Sigma-Aldrich, Німеччина) у 0,1 М трис-HCl, 5 мМ розчині EDTA (pH 7,2) , протягом 10 хв при 37 °C, щоб забезпечити проникність клітинних мембран. Для піддясневих зразків і біоплівок, сформованих на ПЕТ-плівках, етап лізоциму був опущений, щоб обмежити проникнення зонда в клітини. Їх фіксували протягом ночі в 4% параформальдегіді у фосфатно-сольовому буфері (PBS, 130 мМ NaCl, 3 мМ $KH_2PO_4 \cdot 2H_2O$, 7 мМ $Na_2HPO_4 \cdot 12H_2O$, pH 7,2) при 4 °C, а потім промивали фосфатно-сольовим буфером і зберігали при -80 °C до гібридизації. Зразки зневоднювали серією промивок етанолом, що містили 50, 80 і 100% (об./об.) етанолу, протягом 3 хв перед інкубацією з олігонуклеотидами в концентрації 4 нг/мкл кожен у буфері для гібридизації (900 мМ NaCl, 20 мМ). Трис–HCl (pH 8), 30% (об./об.) формаміду та 0,1% (мас./об.) додецилсульфату натрію). Гібридизацію проводили в пластикових мікропробірках при 35 °C протягом ночі з використанням Dry Block Thermostat TBD-120 (Biosan SIA, Латвія), а потім зразки інкубували протягом 20 хвилин при 37 °C у промивному буфері, що містить 20 мМ Tris–HCl (pH 8) , 64 мМ NaCl і 0,1% (мас./об.) додецилсульфату натрію. Після промивання зразки аналізували за допомогою CLSM, як описано вище.

2.6. Полімеразна ланцюгова реакція (ПЛР).

ПЛР використовували для якісного та напівкількісного аналізу ключових збудників пародонту. Очищення ДНК проводили за допомогою набору AmpliSense DNA-sorb-B Nucleic Acid Extraction kit та ампліфікацію за допомогою набору Stomatoflor Real Time (ДНК-Технології, Росія) і Real-time CFX96 Touch system (BIO-RAD, США).

ПЛР використовували для визначення впливу обробки біоцидом на ДНК шляхом ампліфікації цільових послідовностей 16S рДНК, LIF і карбапенемази *Klebsiella pneumoniae* (KPC). Для ампліфікації послідовностей 16S із зразків еДНК використовували 25 мкл

реакційної суміші для ПЛР (Taq PCR Kit, New England Biolabs) з праймерами 27F (5′-AGAGTTTGATCMTGGCTCAG-3′) і 1492R (5′-TACGGYTACCTTGTTACGACTT-3′). Для ампліфікації гена LIF із зразків pC1-L використовували прямий (5'-ATGAAGGTCTTGGCGGCAGG-3') і зворотний (5'-ACCTCCTGCTAGAAGGCCTG-3') праймери. Умови ПЛР включали початкову стадію 5 хвилин при 95 °C. За цим слідували 30 циклів при 95 °C протягом 30 с, 57 °C протягом 30 с і 72 °C протягом 30 с і кінцева стадія при 72 °C протягом 5 хв. Очищену геномну ДНК використовували як позитивний контроль, а продукти ПЛР візуалізували за допомогою гель-електрофорезу. Послідовності KPC ампліфікували за допомогою набору реагентів AmpliSense MDR KPC/OXA-48-FL (AmpliSense, Росія) та системи CFX96 Touch Real-Time PCR Detection System (Bio-Rad, США).

2.7. Виділення мембранних везикул.

Мембранні везикули MV були виділені з біоплівок Wrinkly Spreader і планктонних культур центрифугуванням для видалення клітин і матриці з подальшою фільтрацією. Двісті мілілітрів 24-годинної культури та триденних біоплівок, зібраних із чотирьох 1-літрових колб, що містять 250 мл середовища KB, центрифугували при 8000 × g при 4 °C протягом 20 хвилин, а супернатант відновили. Потім їх центрифугували при 24000 × g 4 °C протягом 30 хвилин, а супернатанти пропускали через PES-фільтри з розміром пор 0,45 мкм (MDI, Гургаон, Індія). Фільтрати осаджували центрифугуванням при 60 000 × g при 4 °C протягом 2 годин і, нарешті, ресуспендували в 600 мкл PBS. MV-асоційовані білки розділяли SDS-PAGE та візуалізували за допомогою PageBlue Protein Staining Solution (ThermoFisher Scientific). Аліквоту білка Pierce™ Unstained Protein MW Marker (ThermoFisher Scientific) наносили на гель для визначення розміру. Зразки також обробляли 100 мкг/мкл ДНКази I (Sigma-Aldrich) у 20 мМ Tris-HCl pH7,4, 10 мМ MgCl2, перед тим, як ДНК екстрагували фенол-хлороформом, осадили ацетатом натрію/етанолом, як зазначено вище, і остаточно ресуспендують у буфері TE. Зразки піддавали електрофорезу на 1,3% (мас./об.) Трис-буферизованому EDTA (TBE)-агарозному гелі перед фарбуванням бромістим етидієм для візуалізації ДНК. Аліквоту сходів ДНК O'GeneRuler 1 kb (ThermoFisher Scientific) пропустили на гелі для визначення розміру.

2.8. Характеристика білків матриксу біопілівки.

Білки, асоційовані з матриксом, були виділені з біоплівок Wrinkly Spreader після центрифугування для видалення клітин і ретельного промивання матричного матеріалу для видалення незв’язаних білків. П'ять триденних біоплівок, вирощених у мікрокосмах KB об'ємом 6 мл, об'єднали, і рідину обережно видалили піпеткою. Додали десять мілілітрів деіонізованої води і біоплівки обережно перемішали перед тим, як залишити на 24 години. Цю промивку повторювали ще шість разів, перш ніж матрицю біоплівки осадили центрифугуванням при 4000 × g протягом 10 хв. Супернатант обережно видаляли піпеткою, а матрицю ресуспендували в рідині, що залишилася. 100 мкл зразків матриці біоплівки попередньо інкубували з 50 мкл деіонізованої води, 0,1% (мас./об.) SDS або 6 М сечовини при кімнатній температурі протягом 2 год перед додаванням 20 мкл SDS-PAGE буфера зразка. Зразки досліджували за допомогою SDS-PAGE, як зазначено вище.

2.9. MALDI-TOF Mac-спектометрія та ідентифікація білків.

Mac-спектрометрію зразків білка проводили відповідно до встановлених процедур. Тридцять мікролітрів зразка мембранної везикули (MV) і асоційованого з матрицею білка концентрували за допомогою SDS-PAGE для отримання доріжок шириною 5 мм. Доріжки, що містять білки, піддавали трипсинолізу в гелі та ідентифікували білки за допомогою мас-спектрометра Maxis Impact LC-QTOF (Bruker, Billerica, MA, США) з використанням бази даних NCBInr і сервера Mascot (Matrix Science, Лондон, Великобританія; http:// www.matrixscience.com), щоб ідентифікувати білки та обчислити значення експоненціально модифікованого індексу вмісту білка (emPAI). Анотація генної онтології (GO) та субклітинні розташування білків були отримані від UniProt (www.uniprot.org) (Консорціум UniProt. UniProt: універсальна база знань про білки у 2021 році. Nucl. Кислоти Res. 2021, 49, D480–D489. https://doi.org/10.1093/nar/gkaa1100).

2.10. Скануюча і трансмісійна електронна мікроскопії.

Ліофілізовані зразки покривали шаром золота товщиною 10–30 нм для покращення поверхневої провідності та досліджували морфологічні деталі за допомогою скануючих електронних мікроскопів Jeol JSM 35C та Jeol JSM 6060LA (Токіо, Японія).

Трансмісійна електронна мікроскопія (TEM) зразків біоплівки була проведена за стандартними процедурами. Десять мікролітрів суспензії везикул поміщали на сітки TEM, вкриті формваром, і сушили. Везикули фарбували 2% (мас./об.) уранілаксалату, pH 7,0,

протягом 10 хв, а потім промивали забуференим фосфатом фізіологічним розчином (PBS). ПЕМ проводили на мікроскопі JEM 1230 (Jeol, Токіо, Японія), який працював при 80 кВ.

Культуру *P. aeruginosa* протягом ночі розбавляли до 20% і додавали ПГМГ-ГХ до кінцевих концентрацій 5%, 1%, 0,5%, 0,1%, 0,05% і 0,01%. Зразки інкубували при кімнатній температурі протягом 20 хвилин, після чого 10 мкл аліквоти поміщали на сітку, покриту формваром, і сушили при кімнатній температурі. Потім 10 мкл 1% уранілацетату (Sigma-Aldrich, Великобританія) додавали на кожну сітку та висушували фільтрувальним папером. ПЕМ проводили за допомогою трансмісійного електронного мікроскопа JEM-1400 (JEOL, Токіо, Японія).

2.11. Модель ранової поверхні.

2.11.1. Підготовка колагенового матриксу.

Пористі колагенові матрикси були виготовлені з розчину бичачого ателоколагену в оцтовій кислоті з використанням наступної техніки ліофільної сушки. Коротко, розчин 20 мг/мл ателоколагену типу I, виділеного з бичачого сухожилля, готували в 0,5 М оцтової кислоти. Після цього розчин центрифугували при 2500 об/хв, +4 °C протягом 15 хвилин, щоб видалити бульбашки повітря, що утворилися під час змішування. Приготований розчин колагену потім заморожували в скляних чашках Петрі (діаметром 10 см) при -40°C і витримували протягом 18 годин у сублімаційній сушарці. Потім заморожені суспензії сублімували при температурі від -40 °C до +22 °C протягом 24 годин у вакуумі. Ателоколагенові матрикси зберігали при -20°C до подальшого використання. Перед використанням матрикси доводили до +22 °C, розрізали на прямокутники 3x4 мм під стерильною ламінарною кришкою та стерилізували УФ-опроміненням протягом 40 хв. Згодом їх врівноважували в 0,1 М HEPES (pH 8,0) при +4 °C протягом ночі. Після цього розчин HEPES замінювали середовищем DMEM/високим вмістом глюкози, що містило 10% (об'єм/об'єм) FBS, 100 ОД/мл пеніциліну та 100 мкг/мл стрептоміцину, в якому каркаси врівноважували протягом 48 годин при +37 °. С і 5% CO_2 перед посівом клітин.

2.11.2. Підготовка моделі рани.

Клітини HEK293 вирощували в модифікованому середовищі Ігглса (DMEM) Дульбекко з високим вмістом глюкози, що містило 10% (об'єм/об'єм) FBS, 100 ОД/мл пеніциліну та 100 мкг/мл стрептоміцину. Клітини розміром 2×10^5 висівали на пористий матрикс 0,3x0,4x0,2 $см^3$. Потім засіяні клітини матриксу переносили у свіже повне

культуральне середовище та інкубували при +37°C, 5% CO_2 протягом трьох днів. Перед інокуляцією *K. pneumoniae* UHI 1090 каркаси з клітинами тричі промивали в середовищі DMEM/високий вміст глюкози та інкубували в середовищі DMEM/високому вмісті глюкози, що містить 10% FBS, протягом ночі при 37°C, 5% CO_2. 200 мкл нічної культури *K. pneumoniae* UHI 1090 інокулюють у модельну систему, де кінцева концентрація бактеріальних клітин становила 10^4 КУО/мл. Інкубація тривала при 37°C в умовах високого CO_2 протягом двох днів. Після інкубації колонієутворюючі одиниці (КУО) у рідкій фазі моделі ідентифікували за допомогою класичного аналізу посіву в трьох повторах.

2.12. Біоциди, що було використано у роботі.

Крім ПГМГ-ГХ використовували сім біоцидів, а саме: 35% перекис водню (Хімпостачання, Харків, Україна); етанол 96% (УкрСпірт Трейд, Київ, Україна); 0,05% хлоргексидин (Здоров'я, Харків, Україна); Maxisan (Інтердез, Київ, Україна), який містив не менше 50% суміші чотирьох четвертинних амонієвих сполук; Арквадес-плюс (О. Л. КАР, Вінниця, Україна), що містить 10 % диметилдіалкіламоній хлориду, 5 % дидецилдиметиламоній хлориду, 2,5 % тетранатрієвої солі); Desmanol (Schülke & Mayr GmbH, Німеччина), що містить 75% ізопропанолу; та Санікон (Інтердез, Київ, Україна), що містить не менше 5,5% суміші чотирьох четвертинних амонієвих сполук.

2.13. Дослідження поверхонь на здатність бактеріальної колонізації.

2.13.1. Підготовка поверхонь і біоцидів.

Використовували купони з комерційної хірургічної нержавіючої сталі EI 711. Нержавіюча сталь зазвичай використовується в медицині для виготовлення медичних імплантатів та інших медичних пристроїв. Пластини розміром 10 x 10 мм вирізали за допомогою фемтосекундних лазерних імпульсів високої потужності (P = 20 Вт), щоб уникнути їх деформації. Потім пластини механічно полірували до шорсткості Ra = 0,01 нм. Нарешті, поліровані пластини очищали за допомогою ультразвукової ванни в етанолі.

Для синтезу полімерного біоциду ПГМГ-ГХ без додаткового очищення використовували такі хімічні речовини: гуанідину гідрохлорид 98% (Applichem, Німеччина), гексаметилендіамін (98%), 2-нафталінсульфонову кислоту, натрієву сіль (технічна чистота, Sigma-Aldrich), етанол (95%).

2.13.2. Налаштування лазера та текстурування поверхні.

Анізотропні канавки (anisotropic grooves, AG) і конічні шипи (conical spikes, CS) були віддруковані на полірованих хірургічних пластинах з нержавіючої сталі за допомогою фемтосекундної твердотільної лазерної системи Light Conversion Pharos, легованої Yb (ширина імпульсу 270 фс при довжині хвилі 1030 нм, змінна частота повторення < 1 МГц , максимальна середня вихідна потужність 20 Вт).

2.13.3. Синтез полімерного біоциду ПГМГ-ГХ.

ПГМГ-ГХ синтезували за такою методикою (схема 1).

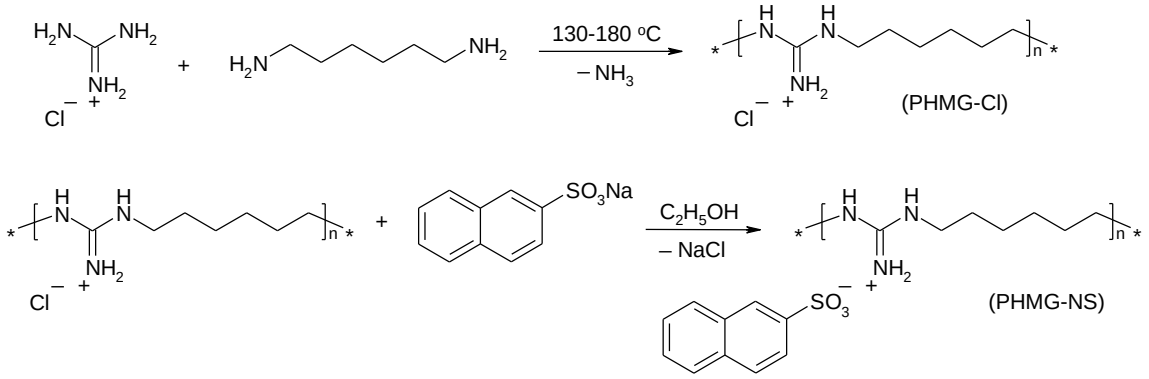

Схема 1. Синтез ПГМГ-ГХ і ПГМГ-НС.

Суміш гуанідину гідрохлориду (10 г, 0,104 моль) і гексаметилендіаміну (12 г, 0,103 моль) поміщали в круглодонну колбу (250 мл) і нагрівали при 80 °С протягом 4 годин при постійному перемішуванні. Далі реакцію проводили протягом 5 годин при 130-140 °С і 5 годин при 180 °С для отримання високов'язкого розплаву. Після охолодження реакційної суміші до кімнатної температури отримували склоподібну тверду речовину ПГМГ-ГХ. Його розчиняли у воді (200 мл) і осаджували додаванням 100 мл насиченого розчину хлориду натрію. Полімер виділяли декантацією та сушили при 140 °С протягом 24 год. Вихід продукту становив 13 г (72%). Характеристична в’язкість становила 0,09 дл/г для розчину ПГМГ-ГХ в 0,1 N NaCl при 25 °С.

До розчину ПГМГ-ГХ (10 г, 0,055 моль) у 200 мл етанолу додавали 2-нафталенсульфонат натрію (13,6 г, 0,06 моль) і суміш перемішували протягом 12 год при 60 °С. Утворився осад хлориду натрію відфільтровують і розчин виливають у воду (500 мл). Білу суспензію ПГМГ-НС відокремлювали декантацією та промивали водою. Вологий продукт сушили при 130 °С протягом 24 годин, а потім розтирали в агатовій ступці. Вихід продукту становив 16 г (87%). Сіль ПГМГ-НС має температуру плавлення 105-110 °С. Його розчинність у воді виявилася 0,24 г/л.

Дані 1H ЯМР і елементного аналізу для ПГМГ-ГХ і ПГМГ-ВБС показані у файлі додаткових даних.

2.13.4. Приготування та характеристика композитних плівок ПА-11/ПГМГ-НС.

Гранули ПА-11 розчиняли в мурашиній кислоті (98%) при 50 ºС для отримання 10% розчину. Рівний об'єм ізопропанолу додавали по краплях до перемішаного розчину для осадження порошку поліаміду. Його відфільтровували і потім послідовно промивали гідроксидом натрію (5%) і водою. Отриманий дрібнодисперсний порошок сушили у вакуумі (1 мбар) при 70 ºС протягом 12 годин. Суміш порошків ПА-11 і ПГМГ-НС розтирали протягом 3 хв в агатовій ступці з подальшим пресуванням при 240 °С. Отримано композитні поліамідні плівки (45 х 45 мм), що містять 5, 7 і 10 мас.% полімерного біоциду.

Щоб охарактеризувати хімічні властивості модифікованих плівок ПА-11, зразки спочатку поміщали на платиновий алмазний модуль ATR, а ІЧ-спектри записували за допомогою спектрометра Bruker Vertex-70V FTIR (усі Bruker Optics Inc., Еттлінген, Німеччина) оснащений детектором дейтерованого тригліцинсульфату, легованого L-аланіном (DLaDTGS). Спектри були отримані з роздільною здатністю 2 см-1 в спектральній області від 400 до 5000 см-1 як сумісне додавання 100 сканувань. Отримання цих спектрів було виконано за допомогою програмного забезпечення Bruker OPUS (версія 6.5).

Механічні випробування зразків поліаміду проводили на універсальній машині для розтягування П-50 («Мілаформ», Росія) зі швидкістю деформування 10 мм/хв. Отримані плівки розрізали на зразки розміром 40х10х0,15 мм. Середнє значення (зі стандартним відхиленням) міцності на розрив було отримано з трьох зразків кожної плівки.

Вимірювання контактного кута проводили за допомогою Drop Shape Analyzer DSA25E (Krüss, Німеччина) методом сидячої краплі. Кут контакту був оцінений за допомогою програмного забезпечення CAM як дотична нормаль до краплі води (3 мл) на перетині між сидячою краплею та поверхнею полімеру. Усі зазначені контактні кути є середнім значенням принаймні п’яти вимірювань, зроблених у різних місцях на поверхні полімеру.

Поверхневу густину заряду плівок ПА-11/ ПГМГ-НС визначали безконтактним індуктивним методом. Поверхневий заряд зразків визначали шляхом порівняння амплітуд напруги конденсатора з плівками ПА-11 і конденсатора з відомим каліброваним

електретом. Вимірювання проводили одразу після розміщення зразків у вимірювальному вузлі, а також через 5 хв для оцінки зміни заряду поверхні з часом.

Дані термогравіметричного аналізу (TGA) для зразків полімерного біоциду та модифікованого РА-11 були отримані за допомогою TGA Q500 (TA Instruments). Близько 10 мг кожного зразка нагрівали від 30 °C до 700 °C зі швидкістю нагрівання 10 °C/хв в атмосфері повітря.

Розчинність чистого ПГМГ-НС у воді визначали перемішуванням 1 г порошку полімерного біоциду в 100 мл води протягом 24 годин при кімнатній температурі. Потім розчин фільтрували і випарювали. Визначали масу твердого залишку.

Вивільнення ПГМГ-НС із плівки ПА-11 досліджували за допомогою спектрофотометричного аналізу в УФ-видимому діапазоні на спектрометрі Jenway 6850 (Великобританія). Калібрувальний графік був отриманий шляхом вимірювання абсорбції водних розчинів ПГМГ-НС в діапазоні концентрацій 10^{-5} – $5x10^{-5}$ моль/л при 227 нм, що є характерним піком нафталінового кільця. Для оцінки швидкості вимивання полімерного біоциду 2 г плівки ПА-11/ ПГМГ-НС (7%) помістили в закриту конічну колбу об'ємом 1 л, що містить 750 мл деіонізованої води. Зразок витримували при 37 ^{o}C при постійному перемішуванні. Періодично відбирали 3 мл кожного розчину та аналізували шляхом вимірювання поглинання на згаданій довжині хвилі для визначення концентрації вивільненого біоциду. Коефіцієнт виділення біоциду визначали як відсоток ПГМГ-НС, що вивільнився в розчин, від його загальної кількості в плівці. Кожне вимірювання було повторено тричі.

2.13.5. Синтез катіонного біоциду 1-додецилпіридинію додецилбензолсульфоната (PyrC12-DBS).

Піридин (99%), 1-хлорододекан (97%), додецилбензолсульфонат натрію (технічний), метиленхлорид, гексан, етилацетат (98%), гідрат метиленового синього (95%), перекис водню (35%), залізо (II) гептагідрат сульфату (99%) були придбані у Sigma-Aldrich і використані без додаткового очищення.

Для виготовлення захисних покриттів використовувалася комерційна фарба ПП-115 (Україна). Фарба містить суміш пігментів і наповнювачів (карбонат кальцію, діоксид титану, оксид заліза) в алкідному (пентафталевому) лаку. Масова частка нелетких речовин близько 60±10%.

1-додецилпіридиній хлорид (PyrC12-Cl) синтезували за схемою 2.

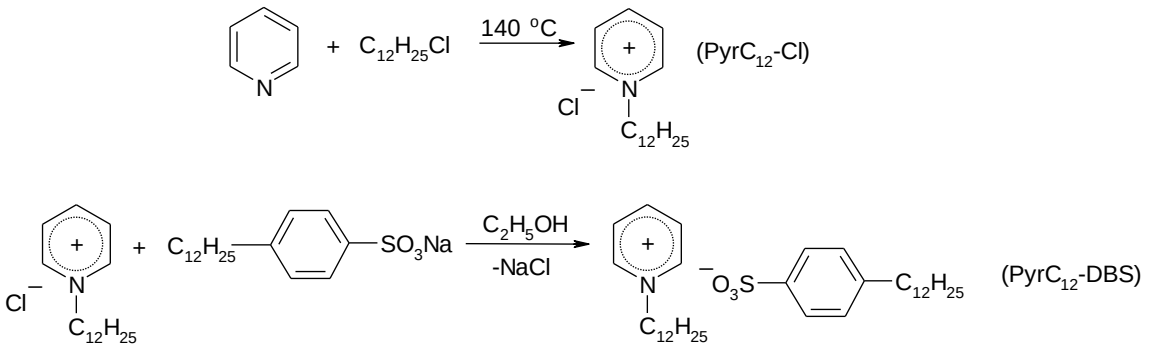

Схема 2. Синтез 1-додецилпіридиній хлориду (PyrC12-Cl).

Суміш піридину (20 г, 0,24 моль) і 1-хлорододекану (59 г, 0,29 моль) перемішували при 140 ºС протягом 24 год. Отриманий твердий продукт очищали перекристалізацією із суміші етилацетат-гексан (1:2 об./об.). Вихід: 72% (48 г), біла тверда речовина, т.пл. 92-94 °С.

1Н ЯМР (400 МГц, DMSO-D6): δ = 0,84 (т, 3Н, CH3), 1,24 (м, 18Н, CH3(CH2)9), 1,9 (м, 2Н, NCH2CH2), 4,6 (т, 2Н, NCH2), 8,2 (т, 2Н, C3-H, C5-H), 8,6 (т, 1Н, C4-H), 9,2 (д, 2Н, C2-H, C6-H).

До перемішаного розчину PyrC12-Cl (20 г, 0,07 моль) у 200 мл води додавали водний розчин додецилбензолсульфоната натрію (24 г/300 мл). Суміш перемішували протягом 1 години і потім продукт екстрагували метиленхлоридом (2 х 250 мл). Об'єднаний розчин сушили над сульфатом натрію. Метиленхлорид потім переганяли, а залишковий розчинник видаляли під вакуумом (10 мбар) при 50 °С протягом 12 годин. Катіонний біоцид PyrC12-DBS готували у вигляді світло-коричневого напівтвердого продукту.

1Н ЯМР (400 МГц, CDCl3): δ = 0,86 (т, 6Н, CH3); 1,23 (м, 32Н, CH2); 1,47-1,57 (м, 4Н, Ar-CH2CH2); 1,89 (м, 2Н, NCH2CH2); 4,76 (т, 2Н, NCH2); 7,1 (д, 2Н, C3, C5-Ar-H); 7,76 (д, 2Н, C2-Ar-H, C6-Ar-H,); 8,0 (т, 2Н, C3-H, C5-H); 8,36 (т, 1Н, C4-H); 9,2 (д, 2Н, C2-H, C6-H).

2.13.6. Підготовка антиобрастаючого покриття.

Купони з нержавіючої сталі (8 х 2,5 х 0,02 $см^3$) використовували як модельні купони для випробування покриття проти обростання. Катіонний біоцид PyrC12-DBS додавали до комерційної суднової фарби РР-115 (5% і 10% (мас./мас.) до вологої фарби або 8% і 16%

(мас./мас.) до сухого покриття) і суміш подрібнювали за допомогою цирконієвого шліфувального засібу протягом 30 хв. Потім модифіковану фарбу фільтрували та використовували для фарбування сталевих купонів за допомогою валика. Після сушіння протягом 48 год на повітрі зразки покривали другим шаром. Загальна товщина покриття становила близько 300±10 мкм. Загальна вага покриття визначалася різницею ваги між пофарбованими та акуратними сталевими купонами. Контрольні зразки покривали двома шарами фарби PP-115.

2.13.7. Характеристика готових покриттів.

Вібраційні властивості захисних покриттів досліджували на інфрачервоному (FT-IR) спектрометрі Vertex-70 Bruker (Німеччина) з детектором DTGS. Полімерні плівки встановлювали в контакт з алмазним кристалом ATR (Attenuated Total Reflection) з одноразовим відображенням, і спектри збирали в діапазоні 400–4000 см−1 з роздільною здатністю 1 $см^{-1}$.

Щоб вивчити поверхневі хімічні модифікації покриттів з вищою просторовою роздільною здатністю, вимірювання комбінаційного розсіювання проводили при кімнатній температурі за допомогою конфокального раманівського спектрометра WITec Alpha 300R (WITec GmbH, Ульм, Німеччина). Спектри комбінаційного розсіяння були отримані за допомогою зворотного розсіювання під мікроскопом з об'єктивом Zeiss EC Epiplan-Neofluar® 100X (числова апертура 0,9), фокусуючи лінію 532 нм твердотільного сапфірового лазера (Coherent INC., Санта-Клара, США) з потужністю лазера. на вибірці 8 мВт і часі інтегрування, встановленому на 1 с. Спектрометр, оснащений моторизованим скануючим столиком, записав 1600 спектрів з області картування 40 × 40 мкм2 (розмір кроку 2D карти 1 мкм). Спектральний аналіз проводили за допомогою програмного забезпечення WITec Project plus (версія 5.248, WITec GmbH, Німеччина).

Адгезію покриття до підкладок визначали відповідно до ASTM D 3359, метод B. На готові покриття наносили гратчасті надрізи з наступною візуальною оцінкою їх стану. Адгезія для всіх покриттів становила 1 бал (5 B). Краї зрізів були абсолютно гладкими, і на всіх краях решітки не було ознак розшарування.

Вимірювання статичного контактного кута проводили за допомогою аналізатора форми краплі DSA25E (Krüss, Німеччина) методом сидячої краплі. Значення контактного кута оцінювали за допомогою програмного забезпечення CAM як нормаль дотичної до

краплі води (3 мл) на перетині між сидячою краплею та поверхнею полімерного покриття. Усі зазначені контактні кути є середнім значенням принаймні п’яти вимірювань, зроблених у різних місцях на поверхні полімеру.

Тривимірну топографію поверхні покриттів вивчали за допомогою профайлера S-NEOX конфокального оптичного зображення білого світла (Sensofar-Tech S.L., Барселона, Іспанія). Площа розміром 340 × 284 мкм2 була зібрана за допомогою об’єктива Nikon 50 X DI (числова апертура 0,8). Дані були проаналізовані за допомогою відкритого програмного забезпечення Gwyddion (версія 2.60).

Диференціальну скануючу калориметрію (ДСК) проводили від -90 до 150 ºC на калориметрі TA Q2000 зі швидкістю нагріву 20 ºC/хв.

Вивільнення PyrC12-DBS з покриттів досліджували за допомогою спектрофотометричного аналізу в УФ-видимому діапазоні за допомогою спектрометра Jenway 6850 (Великобританія). Калібрувальний графік був отриманий шляхом вимірювання абсорбції при 259 нм (характерний пік катіону піридинію44) водних розчинів PyrC12-Cl в діапазоні концентрацій 1,5 x 10^{-5} – 1,5 x 10^{-4} моль/л. Для оцінки швидкості вимивання катіонного біоциду кожен пофарбований сталевий брусок (купон) (3 зразки) поміщали в закриту конічну колбу, що містить 1 л деіонізованої води. Зразки зберігали при 25 ºC. Періодично відбирали 3 мл кожного розчину та аналізували шляхом вимірювання поглинання при згаданій довжині хвилі для визначення концентрації вивільненого біоциду. Кожне вимірювання було повторено тричі.

2.13.8. Вплив пластикової поверхні, обробленої ПГМГ-ГХ, на еДНК.

Спочатку 10 мкл 1%, 0,5%, 0,1% і 0,05% ПГМГ-ГХ поміщали в лунки 96-лункових полістирольних планшетів з трьома повторами на обробку. Потім плашетам давали висохнути при кімнатній температурі і залишали на 4, 8, 11, 15, 20, 25 і 28 днів при тих же умовах. Нарешті, 10 мкл 880 нг/мкл еДНК з біоплівок *P. aeruginosa* додавали до лунок і суміш інкубували при кімнатній температурі протягом 1 години, перш ніж концентрації нуклеїнових кислот вимірювали за допомогою NanoDrop і візуалізували за допомогою гель-електрофорезу.

2.14. Синтез C6-HSL.

L-гомосерину лактон гідрохлорид був синтезований за модифікованою методикою (схема 3).

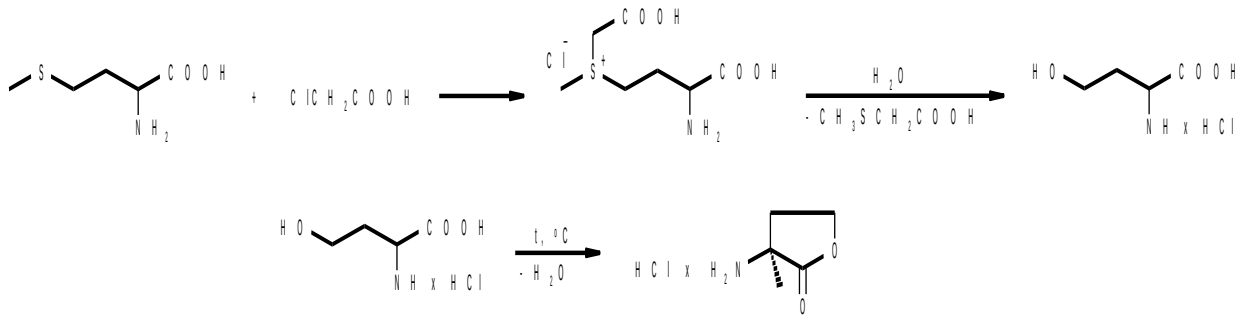

Схема 3. Синтез L-гомосерину лактон гідрохлориду.

30 г L-метіоніну, 120 мл води, 120 мл ізопропанолу і 50 мл крижаної оцтової кислоти додавали в 1-літрову круглодонну колбу, обладнану магнітною мішалкою. Додавали 20,8 г хлороцтової кислоти і суспензію перемішували протягом 12 годин при 70°C. Отриманий прозорий розчин кип'ятили зі зворотним холодильником протягом 3 год і розчинники відганяли при зниженому тиску. Для перетворення гомосерину в його лактон твердий залишок нагрівали протягом 6 годин при 100-110°C і зниженому тиску 15-20 мбар. Продукт розчиняли в 50 мл води, а потім додавали 250 мл ізопропанолу та осаджували протягом ночі при 4°C. Кристалічна тверда речовина відфільтровували, промивали 100 мл ізопропанолу та сушили у вакуумі протягом 12 годин при 40°C і 1 мбар. У цій процедурі вихід L-гомосерину лактону гідрохлориду становив 65%. Отримано спектр протонного ядерного магнітного резонансу (1H ЯМР, 300 МГц, ДМСО-D6) кінцевого продукту з наступними характеристиками: 1H ЯМР (ДМСО-D6): δ 2,37 (1H, м, 4α-H), 2,56 (1H). , m, 4β-H), 4,31 (2H, m, 5α-H, 3-H), 4,34 (1H, td, 5β-H), 9,05 (3H, уш. c, NH).

Другий етап синтезу N-гексаноіл-L-гомосерин лактону (C6-HSL) проводився за методом (схема 4).

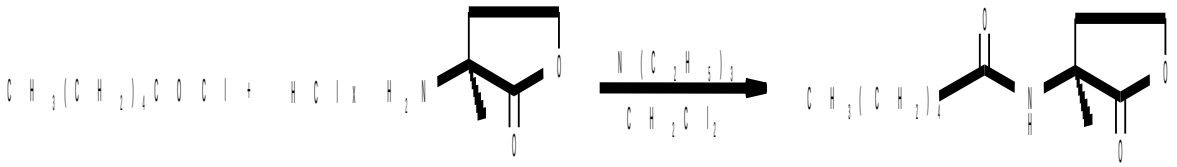

Схема 4. Синтез синтезу N-гексаноіл-L-гомосерин лактону (C6-HSL).

8,7 г триметиламіну додавали до перемішаної суспензії 5 г гідрохлориду L-гомосерин лактону в 70 мл метиленхлориду при 0°C. Суміш перемішували протягом 30 хвилин, а потім додавали по краплях 4,9 г гексаноілхлориду протягом 10 хвилин. Отримана реакція тривала протягом 1 години при 0–5°C, а потім при кімнатній температурі ще 4 години. Суміш двічі промивали 50 мл насиченого розчину гідрокарбонату натрію, двічі 50 мл 1 М розчину гідросульфату калію, а потім 70 мл насиченого розчину хлориду натрію. Розчин C6-HSL в метиленхлориді сушили над сульфатом натрію і розчинник видаляли дистиляцією. Білий твердий залишок додатково очищали шляхом перекристалізації в етилацетаті. У цій процедурі вихід C6-HSL становив 60%. Отримано спектр протонного ядерного магнітного резонансу (1H ЯМР, 300 МГц, ДМСО-D6) кінцевого продукту з такими характеристиками: 1H ЯМР (ДМСО-D6): δ 0,89 (3H, т, CH3), 1,31 (4H, м , CH3(CH2)2), 1,64 (2H, м, CH2CH2CO), 2,17 (1H, м, 4 α-H), 2,25 (2H, т, CH2CO), 2,79 (1H, м, 4 β-H), 4,29 (1H, м, 5α-H), 4,46 (1H, td, 5 β-H), 4,64 (1H, м, 3-H), 6,5 (1H, d, NH).

2.15. Робота з рослинами.

2.15.1. Сорти озимої пшениці.

Два сорти озимої пшениці (*Triticum aestivum* L.) Володарка та Ятрань 60, які широко культивуються в Лісостепу та Поліссі України і розроблені Інститутом фізіології рослин і генетики НАН України та Миронівським інститутом пшениці ім. В. М. Ремесла УААН. Володарка — низькочерешковий сорт з високою врожайністю та хорошою морозостійкістю та посухостійкістю, а Ятрань 60 — низькочерешковий середньоранній сорт з хорошою жаро- та посухостійкістю.

2.15.2. Підготовка насіння.

Насіння праймували в розчині 100 нг/мл C6-HSL (3 кг насіння / 10 л; приблизно 9 нг C6-HSL на насіння) протягом 3 годин, а потім сушили протягом 72 годин при 24–25 °C до вмісту води. 12 – 14% (мас./мас.). Контрольне насіння без ґрунтування обробляли водою перед сушінням. Потім насіння пелетували гранулювальною сумішшю AREAL BS-05 (містить полісахаридну суміш, полівініловий спирт, діоксид титану, мінералізований тальк, органічні та неорганічні пігменти та має pH розчину 7-8; компанія «Легіон Лтд», Україна) перед посівом. Насіння було зібрано з рослин, вирощених із праймованного насіння в 2015-16 роках (насіння F1), і використано в подальших тестах.

2.15.3. Дослідження схожості насіння.

Вплив праймування насіння на схожість досліджували відповідно до стандартів Міжнародної асоціації тестування насіння (ISTA). П’ятнадцять зразків по 20 насінин кожного сорту та обробки пророщували в темряві при 24°C протягом 24 годин у чашках Петрі, що містять живильний розчин Кнопа, щоб визначити рівень схожості. Паралельно три зразки по 20 насінин кожного сорту та обробки пророщували на вологому фільтрувальному папері та визначали довжину колеоптиля та корінців через 2 дні.

2.15.4. Дослідження посівів

На полігоні «Феофанія» (Інститут ботаніки ім. М. Г. Холодного НАН України, 50°20'59.7"N 30°29'16.1"E) протягом двох поспіль вегетаційних періодів (вересень 2015 р. – липень 2016 р. та серпень 2016 р. – липень 2017 р.) висаджували та збирали посіви озимої пшениці. Поля представлені сірим лісовим опідзоленим ґрунтом і сильно суглинистим чорноземом (pH KCl 5,7, загальний вміст гумусу 4,1 %, фосфору 138 мг/кг, калію 90 мг/кг). Насіння висаджували з густотою 600 насінин/м^2 на глибину 3,5 – 4 см і протягом вегетації вносили добрива (145 кг/га азоту, 90 кг/га фосфору, 90 кг/га калію). Погодні умови фіксувалися Гідрометцентром Центральної геофізичної обсерваторії Б.І. Срезневського в Києві, приблизно в 6 км від Феофанії.

Морфологічні параметри, що описують урожай рослин і насіння, вимірювали для 100 рослин кожного сорту в 2015 – 2016 роках і 50 рослин на сорт у 2016 – 2017 роках. Якість насіння оцінювали візуально як «нормальну» (добре сформовану, більшу і жирнішу морфологію) або «поганий» (деформований, дрібний і тонкий) і частка нормального насіння, визначена для трьох зразків по 100 насінин. П'ять зразків по 10 насінин кожного типу зважували для отримання середньої маси насінин. Зразки рослин відбирали для оцінки росту, морфології рослин і врожайності насіння.

2.15.5. Дослідження рівнів хлорофілу та каротиноїдів

Посіви озимої пшениці висаджували за описаними вище дослідами (серпень 2016 р. – липень 2017 р.) на полігоні Глеваха (Інститут фізіології рослин і генетики НАН України; географічні координати 50°15'37.3"N 30° 17'12.8"E) приблизно в 15 км від Феофанії із подібним типом ґрунту. Рівні хлорофілу (a і b) і каротиноїдів вимірювали після екстракції ацетоном. Було виготовлено п’ять екстрактів із матеріалу, зібраного з п’яти рослин на кожній із стадій загортання, цвітіння, молочної та молочно-воскової стиглості.

2.15.6. Мікробіологічна характеристика

Кількість асоційованих із ризосферою хемоорганотрофних, азотфіксуючих, денітрифікуючих та амілолітичних бактерій, що адгизують до коренів пшениці, визначали за допомогою підрахунку життєздатних колоній. Коріння 125 2-місячних рослин 2015-2016 рр. промивали стерильним 0,9% (мас./об.) фізіологічним розчином і аліквоти серійних розведень розподілили на поживний агар (HiMedia, Індія), який інкубували при 24°C протягом 5 днів для визначення хемоорганотрофна кількість бактерій. Середовище Ешбі з додаванням 2% (мас./об.) сахарози було використано для визначення кількості азотфіксуючих бактерій з колоніями, повторно ізольованими тричі в рідкому середовищі, щоб відрізнити азотфіксатори від олігонітрофільних бактерій. Нітрифікуючі бактерії виділяли в рідкі середовища Ватсона і Менделя та інкубували протягом 20 днів. Денітрифікуючі бактерії виділяли за допомогою середовища Гілтая (pH 6,8 – 7,2) в атмосфері інертного аргону за методом Hangeit при 24°C протягом 5 днів, кількість життєздатних визначали за допомогою методу найбільш імовірних чисел з 3-трубним варіантом. Денітрифікуючі бактерії були ідентифіковані на підставі підлужнення середовища, підвищення оптичної щільності, газоутворення та відсутності нітратів. Кількість амілолітичних бактерій визначали за допомогою 2% (мас./об.) крохмальних планшетів, інкубованих при 28°C протягом 3 днів, промиваних 0,1% (мас./об.) йоду для візуалізації очищеного ореолу навколо колоній.

2.16. Біоінформатичний аналіз.

Гомологи субодиниці синтази бактеріальної целюлози були ідентифіковані в повних геномах *Proteobacteria* за допомогою NCBI TBLASTN і Pf. SBW25 WssA – Послідовності запитів білка J (номер доступу AAL71841 – AAL71850). Гомолог WspR був ідентифікований у Ba. 197N геному з використанням Pf. SBW25 WspR (AAL71852). Філогенетичні дерева були створені з використанням інструменту множинного вирівнювання послідовностей NCBI COBALT і методу з'єднання сусідів (NJ). Дані про вміст генів і геномів GC були отримані з бази даних геному Pseudomonas (www.pseudomonas.com) і NCBI Genbank. Точкові графіки ДНК були створені за допомогою інструменту пошуку геномної подібності YASS (bioinfo.lifl.fr).

2.17. Молекулярний докінг-аналіз.

Молекулярний докінг проводили за допомогою модельного додекамера ДНК (CGCGATATCGCG), що використовується для вивчення ДНК-зв'язуючих сполук (RCSB

Protein Data Bank 1DNE: https://www.rcsb.org/structure/1dne, доступ 1 березня 2021 р.). Ланцюги A і B використовували для докінгу, а молекули води і ліганд видаляли з кристалічної структури за допомогою Accelrys DS 4.0. AutoDock Tools (ADT) 1.5.6 використовувався для створення димерного ліганду ПГМГ і додавання полярних атомів водню до ДНК. Метод noBondOrder використовувався для перенумерації всіх атомів, включаючи нові атоми водню, а метод Гаштайгера використовувався для розрахунку зарядів. ChemAxon Marvin Sketch 5.3.735 використовувався для оптимізації структури димеру ПГМГ. Мінімізація енергії та оптимізація димерного ліганду ПГМГ була виконана MO-PAC2016 за допомогою інструменту автоматичної оптимізації (силове поле MMFF94s). Часткові заряди та торсійні кути ліганду змінювали за допомогою ADT. Структура ДНК і димер ПГМГ були використані для молекулярного докінгу AutoDock Vina 1.1.2. Використовували сітку розміром 30 × 30 × 30 точок з відстанню 1 Å. Аналіз та візуалізацію взаємодій проводив Accelrys DS.

2.18. Статистичні методи.

Кількісні аналізи проводили з повторами, і середнє значення зі стандартними помилками (SE) показано, де це необхідно. Дані аналізували за допомогою статистичного програмного забезпечення JMP v12 (SAS Institute Inc., США). Підхід загальної лінійної моделі (GLM) використовувався для дослідження значення штаму, тестового середовища, росту та прикріплення (впливу) на міцність (відповідь) біоплівки за допомогою комбінованого набору даних аналізу біоплівки. Рівні прихильності також були змодельовані як відповідь. Значні ефекти досліджували за допомогою t-тесту Стьюдента LSMeans Differences та тестів Tukey HSD, а зв’язки досліджували за допомогою попарних кореляцій. Відмінності між середніми значеннями також перевіряли за допомогою ANOVA, t-тестів і тестів Turkey-Kramer HSD.

Експерименти проводилися з повторами, а середні значення зі стандартними помилками (SE) показані, де це необхідно. Статистичний тест і значення p округлюються до двох знаків після коми, а значимі результати повідомляються для $\alpha = 0,05$ або коли $p \leq 0,05$. Для аналізу даних використовували статистичне програмне забезпечення JMP Version 12 (SAS Institute Inc., Cary, NC, USA). По-перше, було досліджено залишки та визначено відповідність нормального розподілу за допомогою тесту Shapiro–Wilk W, щоб вирішити, чи продовжувати параметричний тест, чи застосувати непараметричний підхід. Загальні

лінійні змішані моделі (GLMM) були використані для дослідження комбінованих даних аналізу біоплівки та визначення значущих ефектів і взаємодій, з LSMeans Differences Tukey HSD (α = 0,05) використовувався для визначення суттєвих відмінностей між середніми значеннями. Для порівняння середніх значень також використовували Т-тести та моделі дисперсійного аналізу з ретроспективними тестами Tukey–Kramer HSD (α = 0,05). У відповідних випадках, а не для видалення викидів, використовувався непараметричний підхід з використанням тесту Kruskal–Wallis (рангові суми) та порівняння кожного середнього за методом Wilcoxon. Для визначення кореляції використовувався Rho Спірмена. Таблиці непередбачуваності та тести $\chi 2$ використовувалися для оцінки незалежності джерела білка × кількості та джерела білка × клітинної локалізації за допомогою калькулятора хі-квадрат (www.icalcu.com/stat/chisqtest).

Повторні дані обробляли за допомогою пакета статистичних програм OriginPro 7.0, MS Excel для Windows і MaxStat Pro 3.6 (MaxStat Software, Німеччина). Усі результати представлені як середнє ± стандартне відхилення. Значення $p < 0,05$ вважалося статистично значущим.

Були використані експериментальні повтори (n) (культури / зразки / зображення), а кількісні результати представлені як середнє ± стандартне відхилення (SD). Пакет статистичного програмного забезпечення OriginPro 7.0 використовувався для одностороннього дисперсійного аналізу, де $p < 0,05$ вважалося статистично значущим

Дані були проаналізовані за допомогою моделювання з використанням підходу найменших квадратів із ефектами (рік, ділянка, сорт пшениці, обробка насіння та експериментальна повторність), перевіреними за допомогою LSMeans Differences Student's t і Tukey HSD test (JMP v12, SAS Institute Inc. , США). Тести хі-квадрат незалежності (www.socscistatistics.com) використовували для оцінки впливу обробки насіння на ризосферні бактерії. Середні значення та стандартні помилки (SE) показані, де це необхідно.

2.19. Етичні умови.

Схвалення з питань етики було надано Комітетом з етики Національного університету охорони здоров'я України імені Шупика (протокол № 8 від 7 листопада 2022 р.) та отримано письмову інформовану згоду від усіх учасників перед включенням у дослідження.

2.20. Відбір пацієнтів з періодонтитом.

У всіх пацієнтів було виявлено хронічний періодонтит без системних розладів після клінічного обстеження, яке включало аналіз запису контролю нальоту, запис глибини зондування та рівня прикріплення в шести місцях навколо кожного зуба та оцінку резорбції альвеолярної кістки. Жоден пацієнт не мав лікування пародонту в анамнезі, і ніхто не приймав антибіотики протягом трьох місяців до базового обстеження. Відбір зразків під'ясенних цитологічних рельєфів проводили шляхом природного біологічного мікрообрастання біологічно нейтральних поліетилентерефталатних (ПЕТ) плівок (2–4 х 7 мм), поміщених у пародонтальні простори протягом п'яти днів. Кожну плівку вставляли в ясенну порожнину, де діагностували пародонтит пацієнтів із помірною та прогресуючою стадією пародонтиту. Пацієнтів проінструктували дотримуватися звичайної гігієни ротової порожнини, але їх попросили бути обережними під час чищення біля зуба з плівкою. Через п'ять днів плівки були видалені та поміщені в пластикову мікропробірку та негайно доставлені на цитологічний аналіз. За потреби 1 мг/мл ДНКази (Sigma-Aldrich), розчиненої в буфері, що містить 20 мМ Tris-HCl (pH 7,4) і 10 мМ $MgCl_2$, наносили на 20 хвилин перед фарбуванням зразків і подальшим мікроскопічним зображенням.

РОЗДІЛ 3. Структурні та екологічні особливості біоплівок грам-негативних бактерій

Біоплівка у широкому розумінні цього терміну (20) є формою бактеріальної колонізації еконіші. Структура біоплівки є відповіддю мікробної асоціації на різноманітність факторів еконіші. Така екологічна пластичність дозволяє максимально поширювати ареал розповсюдження, стійкість до різноманітних стресорів та адаптацію до динамічних умов. Джерелом такої пластичності є в тому числі і широкий потенціал штамів бактерій до будування своїх біоплівок. В структурному відношенні біоплівки складаються з двох масивів компонентів: бактерій і екзоклітинного матриксу біоплівки. Бактерії, що представляють біоплівкову субпопуляцію, знаходяться в різних метаболічних станах і координують свою метаболічну активність завдяки механізмам гормональної регуляції – почуття кворуму. Ці самі бактерії утворюють свою біоплівку завдяки синтезу різноманітних екзоклітинних полімерних молекул, які представляють собою так званий матрикс біоплівки. Співвідношення між екзополімерами матриксу та міжмолекулярні структурні зв'язки безпосередньо залежать і від синтетичних здатностей учасників біоплівки і від умов еконіші, де біоплівки будується. Саме тому біоплівки бактерій представляють собою результат комплексних просторових тривимірних молекулярних взаємодій різноманітних компонентів, які синтезуються учасниками біоплівки (22-24). До головних компонентів матриксу біоплівок грам-негативних бактерій відносяться полісахариди, так як, наприклад, PNAG у *K. pneumoniae* і *Acinetobacter baumannii* (25-26), Psl, Pel і альгінат у *P. aeruginosa* (27-28), ліпоолігосахариди і капсульні полісахариди у *A. baumannii* (29), целюлоза у *Enterobacter cloacae* та у псевдомонад (30), про що йдетиметься нижче. Інший важливий компонент матриксу біоплівок – функціональні амілоїди, наприклад, Bap і CSu пілі у *A. baumannii* (31, 32), FapC у *P. aeruginosa* (33), так звані curli фімбрії у *E. cloacae* (34, 35). Особливу роль у первинній адгезії бактерій, цементуванні матриксу біопівлівки і у депонуванні еволюційно успішної генетичної програми, вірогідно, відіграє екзоклітинна ДНК, або еДНК, яка широко представлена в біоплівках і грам-позитивних (36, 37) і грам-негативних бактерій (35, 38-41).

3.1. Роль целюлози у структурі біоплівок *Pseudomonas* spp

Вперше бактеріальна целюлоза була виділена з біоплівки, що утворилась на поверхні рідини, це так звані біоплівки інтерфазі П-Р (повітря-рідина), бактерією *Bacterium xylinum*

у 1886 році (42). Цей штам оцтовокислої бактерії, ймовірно, тепер має бути ідентифіковано як *Gluconacetobacter xylinus* (раніше *Acetobacter xylinum*) або споріднений вид. Протягом наступного століття було виявлено більше оцтовокислих бактерій та бактерію *Proteobacter* які продукують целюлозу (42, 43). До групи целюлозоутворюючих бактерій відносять різні коменсали кишечника, патогени рослин і тварин, зокрема родини *Clostridiaceae,* альфа-протеобактерії *Rhizobiaceae* і *Acetobacteraceae,* бета-протеобактерії *Alcaligenaceae* та гама-протеобактерії *Enterobacteriaceae* і *Pseudomonadaceae.* Цікаво тут те, що всі ці бактерії здатні для існування у ґрунті як у загальному вторинному середовищі існування.

Ймовірно, що целюлоза забезпечує захист від механічного впливу, хижаків або інших екологічних стресів, які можуть мати місце у вищезгаданих різноманітних середовищах. Біохімічні аспекти продукції бактеріальної целюлози широко вивчені для *Gluconacetobacter*, і це розуміння було використано як модель для дослідження механізмів продукції целюлози кишковими бактеріями і псевдомонадами (44, 45). З часом експериментальних даних, що підтверджують здатність нових бактерій до продукції целюлози стає все більше, з появою повногеномних баз даних все більшої кількості бактерій з'являються повідомлення щодо нових оперонів, які є подібними до класичного оперону синтеза целюлози *bcs* та гіпотетично також можуть відповідати за синтез целюлози. Це свідчить про те, що дедалі ширший спектр бактерій може бути здатний виробляти целюлозу.

Одним із добре досліджених продуцентів целюлози є асоційована з рослинами псевдомонада *Pseudomonas fluorescens* SBW25 (46-48). Ця бактерія також добре відома як модельна для дослідження еволюції. Підвищення продукції целюлози у цій бактерій внаслідок адаптативної еволюції призводить до появи нового адаптивного мутанту, що утворює супербіоплівки. Цей штам відомий як Wrinkly Spreader (WS).

Подальше дослідження фенотипу WS виявило присутність у біоплівці частково ацетильованої целюлоза як основного матриксного компоненту. Псевдомонади є дуже різноманітним родом (49, 50), серед представників якого багато різних видів, що мешкають в водних, ґрунтових та рослинних еконішах, в тому числі і фітопатогенів, утворюють свої біоплівки за допомогою целюлози (13). В тім, екологічна роль целюлози та переваги, які вона надає, все ще не вивчені. Аналізу особливостей продукції целюлози у псевдомонад присвячена робота автора (51).

Cellulose Expression in *Pseudomonas fluorescens* SBW25 and Other Environmental Pseudomonads

Andrew J. Spiers, Yusuf Y. Deeni, Ayorinde O. Folorunso, Anna Koza, Olena Moshynets and Kamil Zawadzki

Additional information is available at the end of the chapter

http://dx.doi.org/10.5772/53736

1. Introduction

Bacterial cellulose was first isolated from the air-liquid (A-L) interface biofilm produced by *Bacterium xylinum* in 1886 [1], an acetic acid bacterium strain which would probably now be recognised as *Gluconacetobacter xylinus* (formerly *Acetobacter xylinum*) or a related species. Over the following century, more acetic acid bacteria and additional *Proteobacter* were found to produce cellulose (reviewed in [2-3]). Cellulose-producing bacteria include a mixture of gut commensals, plant and animal pathogens (these are listed in Table 1), and all share soil as a common secondary habitat. It is likely that cellulose provides protection against physical disturbance, predation or other environmental stresses common to these diverse environments. The biochemistry of bacterial cellulose expression has been studied extensively for *Gluconacetobacter,* and this understanding has been used as a model for enteric bacteria and pseudomonads [4-5] (for a range of bacterial cellulose reviews, see [2-3, 6-9]). Experimental reports of bacteria expressing cellulose are increasing, as well as the annotation of putative cellulose synthase-like operons in bacterial whole-genome sequences, suggesting that an increasingly wider range of bacteria may be capable of producing cellulose.

Our interest in bacterial cellulose began with the experimental evolution of the soil and plant-associated pseudomonad, *Pseudomonas fluorescens* SBW25 [10-12]. This resulted in a novel biofilm–forming adaptive mutant known as the Wrinkly Spreader (WS) and shown in Figure 1. Subsequent investigation of the WS phenotype identified partially-acetylated cellulose as the main matrix component of the biofilm. The pseudomonads are a highly diverse genus (see recent reviews by [13-14]), and biofilm-formation and cellulose-expression are now known to be common amongst the water, soil, plant-associated and

INTECH
open science | open minds

© 2013 Spiers et al., licensee InTech. This is an open access chapter distributed under the terms of the Creative Commons Attribution License (http://creativecommons.org/licenses/by/3.0), which permits unrestricted use, distribution, and reproduction in any medium, provided the original work is properly cited.

plant-pathogenic environmental pseudomonads [15]. However, the ecological role of cellulose and the fitness advantage it confers to these bacteria is poorly understood.

Class	Order	Family	Genus	Key habitat
Clostridia	*Clostridales*	*Clostridiaceae*	*Sarcina*	Mammalian intestine commensals
α-Proteobacter	*Rhizobiales*	*Rhizobiaceae*	*Agrobacterium* *Rhizobium*	Plant pathogens Plant symbionts
	Rhodospirillales	*Acetobacteraceae**	*Gluconacetobacter*	Rotting fallen fruits
β-Proteobacter	*Burkholderiales*	*Alcaligenaceae*	*Alcaligenese*	Opportunistic human pathogens
γ-Proteobacter	*Enterobacteriales*	*Enterobacteriaceae†*	*Enterobacter* *Escherichia* *Salmonella*	}Mammalian } intestinal } commensals and pathogens
	Pseudomonadales	*Pseudomonadaceae*	*Pseudomonas*	Water, soil and plant-associated, including plant, fungal and animal pathogens

Adapted from [2-3]. ***,** Also known as the acetic acid bacteria; **†,** Referred to here as the enteric bacteria.

Table 1. Cellulose-expressing bacterial genera

Here we provide a review of our work focussing on biofilm-formation and cellulose expression by SBW25 and other environmental pseudomonads. We do not provide an extensive list of primary literature or current reviews, but hope that the citations we have made will allow others to access the growing wealth of publications relevant to the subjects raised in this review.

2. Bacterial assemblages and biofilms

The formation of biofilms by bacteria is a key strategy in the colonisation of many environments, though biofilms are only one of a range of bacterial assemblages involved in this process. Bacterial assemblages range from isolated surface-attached bacteria, monolayers of associated bacteria forming micro-colonies, larger and more complex structures including differentiated biofilms, as well as poorly-attached or free-floating flocs and slime. At times the differences between assemblage types may be minor and will depend on local environmental conditions. These differences are frequently ignored by many who prefer the simple dichotomy of individual, free-swimming planktonic bacteria verses the structurally complex and genetically-determined biofilms. Here we use the term 'biofilm' to include

partially and fully-saturated aggregations growing on solid surfaces, as well as those that are poorly-attached or 'free-floating', after the early and broad definition of Costerton *et al.* [16].

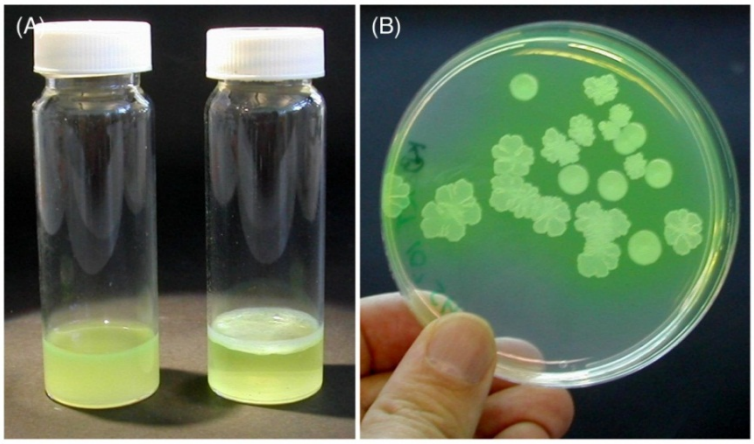

Figure 1. The Wrinkly Spreader mutant of *Pseudomonas fluorescens* SBW25. The Wrinkly Spreader (WS) mutant was isolated from evolving populations of wild-type SBW25 in static King's B microcosms. **(A)** Wild-type SBW25 (*left*) grows throughout the liquid column; in comparison, the WS (*right*) occupies the air-liquid (A-L) interface by producing a robust biofilm 1-2mm thick. **(B)** Wild-type SBW25 (smooth and rounded) and WS (wrinkled) colonies are readily differentiated on agar plates. Images from A. Spiers.

The importance of biofilms (aggregations) in nature is reflected by their prevalence in aquatic, soil, fungal, plant and animal ecosystems, and their role in many chronic human diseases and antibiotic resistance. Many natural biofilms are multi-species structures with complex interactions, and in earlier literature they were often referred to as zoogleal mats. Bacteria found within biofilms are profoundly different from those growing in suspension, differing in both gene expression and physiology and more resistant to desiccation, physical disturbance and predation. A range of biofilm reviews are provided by [16-31].

3. Archetypal 'flow-cell' biofilms

Biofilm research has largely focussed on submerged, solid-liquid (S-L) interface biofilms to provide archetypal models of biofilm structure, function and allow genetic investigation (e.g. *Pseudomonas aeruginosa* PA01 flow-cell biofilms). In these, a surface-attached exopolysaccharide (EPS) polymer matrix-based structure develops away from the solid surface, into the flow of a nutrient and O_2-rich growth medium, and where fluid flow and mass transfer affects biofilm development, structure and rheology (for reviews, see [19, 28-29]).

Biofilm formation begins when planktonic bacterial cells initiate attachment to a solid surface. Attached bacteria start to move across the surface, grow and form micro-colonies, which then develop slowly into the mature biofilm structure in which bacterial cells are embedded in an exopolysaccharide polymer matrix. When conditions become unfavourable within the biofilm, single bacteria or large lumps of biofilm material detach

and move away to colonise new surfaces in more favourable environments (reviewed in [22]). Biofilms of mixed bacterial communities and of individual species that develop on solid surfaces exposed to a continuous flow of nutrients form a thick layer generally described as consisting of differentiated mushroom and pillar-like structures separated by water-filled spaces.

A defining feature of many biofilms is the exopolysaccharide polymer 'slime' that encapsulate the bacteria and provide the main structural component or matrix of the biofilm [20, 22, 24-25]. Although generally assumed to be primarily composed of polysaccharides, e.g. alginate, PEL (a glucose-rich polymer) and PSL (a repeating pentasaccharide containing d-mannose, d-glucose and l-rhamnose) produced by *P. aeruginosa* PA01, PIA (a 28 kDa soluble linear β(1-6)-N-acetylglucosamine) and related PNAG polymer produced by *Staphylococcus aureus* MN8m and *S. epidermidis* 13-1, and PIA-like polymers produced by *Escherichia coli* K-12 MG1655, biofilm matrices can also contain proteins and nucleic acids having significant structural roles (reviewed in [30]). Exopolysaccharides are typically viewed as a shared resource that provides a benefit to the biofilm community by maintaining structure, facilitating signalling, and protecting residents from predation, competition, and environmental stress [20, 22, 32-35].

A second characteristic common to many S-L interface biofilms has been the involvement of quorum sensing in micro-colony development, exopolysaccharide expression, and dispersal. For example, the quorum signalling molecule, acyl-homoserine lactone (AHL), functions as a signal for the development of *P. aeruginosa* PA01 and *Pseudomonas fluorescens* B52 biofilms [36-37]. However, mathematical models based on O_2 and nutrient transport (diffusion) limitation result in similar biofilm architecture (reviewed in [38]), suggesting biofilm development is equally sensitive to environmental conditions as it may be to genetically-determined regulation. Although quorum sensing is important in the development of some biofilms, the bacterial community will exploit all available mechanisms to adapt to local environmental conditions. In order to further understand the development and role of biofilms, the local environment should be considered in terms of ecological landscape theory in which the spatial configuration of the biofilm biomass is shaped by multiple physical and biological factors [39]. It is therefore likely that biofilm formation is the net result of many independent interactions, rather than the result of a unique pathway initiating attachment and terminating with dispersal of mature biofilm communities.

4. Air-liquid (A-L) interface biofilms

In contrast to the archetypal S-L interface biofilms, bacterial biofilms also form at the air-liquid (A-L) interface of static liquids and are sometimes referred to as 'pellicles' [30]. Perhaps the earliest experimental observations of these were made for *Bacterium aceti* and *B. xylinum* in 1886 [1, 40]. Both bacteria were isolated from beer undergoing acetic fermentation in which alcohol is converted into acetic acid. *B. aceti*, an acetic acid bacterium whose modern name is unclear, was found to produce a greasy-looking biofilm which varied in thickness from an 'almost invisible film' to a paper-thick structure

depending on the growth medium [40]. In contrast, the *B. xylinum* isolate, which would probably now be recognised as a *Gluconacetobacter* spp. produced a 'vinegar plant' described as a jelly-like transparent mass at the bottom of the liquid, but under favourable conditions it could also produce a robust gelatinous A-L interface biofilm up to 25 mm thick [1].

Vinegar plants are generally a consortia of acetic acid bacteria and yeasts which produce a zoogleal mat or mixed-species biofilm, and were traditionally used to produce vinegar from beer, cider or wine. Acetic fermentation is initiated by a starter culture known as the 'mother' and obtained from a previous vinegar in a process known as back-slopping [41]. A similar starter often referred to as a 'tea fungus' is used today to produce Kombucha, a carbonated cider-like drink from a sugary solution containing black tea (see the description given in [42]). Acetic acid bacteria, including *Gluconacetobacter* spp., can be isolated from these and similar consortia where they are responsible for the cellulose matrix-based biofilm (see an early review of the acetic acid bacteria by [43]). These artificially-maintained *Gluconacetobacter* spp. are probably better adapted to growth in static liquid conditions than environmental isolates recovered from rotting fallen fruit [44] and under the right conditions, some can produce a gelatinous 'plug' up to 20 mm deep in 10-12 days [45]. In these, cellulose expression and probably growth, is restricted to a thin 50-100 μm deep zone at the top, where it is limited by O_2 diffusing from above and nutrients diffusing through the mature biofilm from below [45]. The growing biofilm is maintained in position by the accumulation of small CO_2 bubbles and by pressing against the walls of the container as it develops.

We expect that smaller-scale A-L interface biofilms might also occur in a wide range of natural environments, such as the partially-saturated fluid-filled pore networks of soils, in temporary puddles collecting on plants and other surfaces after rainfall, water-logged leaf tissues, or in small protected bodies of water such as ponds where the surface is not disturbed by wind or currents. In these environments, biofilm development would be restricted by a combination of nutrient availability, O_2 diffusion, physical disturbance, as well as microbial competition and predation by protists and nematodes.

A-L interface biofilms are readily produced in experimental static liquid-media microcosms [5, 11, 15], and an example of the *P. fluorescens* SBW25 Wrinkly Spreader A-L interface biofilm is shown in Figure 1. In a survey of environmental pseudomonads using nutrient-rich liquid King's B microcosms, we categorised A-L interface biofilms on the basis of phenotype and physical robustness into the physically cohesive (PC), floccular mass (FM), waxy aggregate (WA) and viscous mass (VM)-class biofilms [15, 46]. The characteristics of these biofilm-types are summarised in Table 2 (see also Figure 2). A-L interface biofilm formation appears to be an evolutionary deep-rooted ability amongst bacteria, presumably with significant ecological advantages. In experimental microcosms, increases in competitive fitness of biofilm-formers have been observed compared to non-biofilm–forming strains, whilst the cost to being a biofilm-forming mutant in an environment not suited to these structures is also measurable [5, 47-49].

	Waxy aggregate (WA)	Floccular mass (FM)	Physically cohesive (PC)	Viscous mass (VM)
Occurrence	Rare	Common	Common	Common
Structure	Single-piece rigid and brittle structure	Multiple flocs	Single-piece flexible and elastic structure	Large viscous mass
Strength	Strong	Medium	Strong	Weak
Resilience	Good, disruption produces smaller fragments	Good, disruption produces flocs that are hard to destroy	Very good, hard to break into smaller fragments	Very poor, disruption solubilises the structure
Attachment	High	Medium	High	Poor
Matrix	No evidence for EPS, possible cell-to-cell interactions	Observed	Observed	Observed

Biofilm attributes compiled from [15, 46, 73]. Strength, ability to withstand weight applied to the top of the biofilm; Resilience, response to applied physical disturbance such as gentle or vigorous mixing; Attachment, connection to the microcosm vial walls in the meniscus region; Matrix, evidence of EPS from behaviour of samples during microscopy; Cellulose, evidence from Calcofluor-staining and fluorescent microscopy.

Table 2. Different classes of air-liquid (A-L) interface biofilms produced by environmental pseudomonads

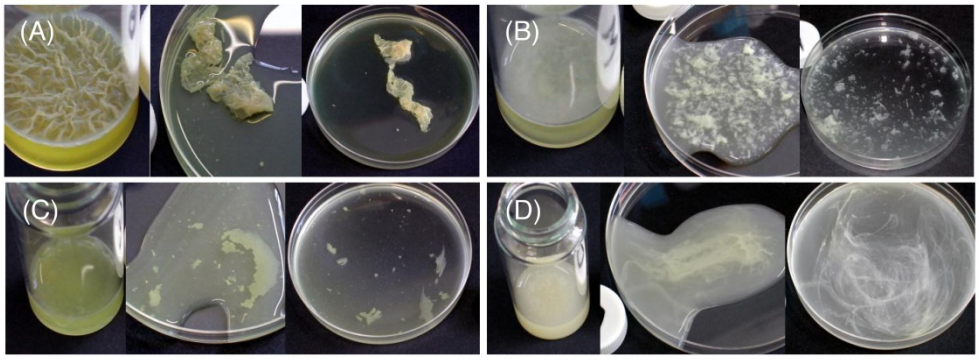

Figure 2. Air-liquid (A-L) interface biofilms. A-L interface biofilms produced by environmental pseudomonads can be categorised into four biofilm types according to visual phenotype, robustness and resistance to physical disturbance. These are the **(A)** Physically cohesive (PC), **(B)** Floccular mass (FM), **(C)** Waxy aggregate (WA), and **(D)** Viscous mass (VM) types. Shown are biofilms in static King's B microcosms *(left)*, after pouring into petri dishes (*middle*), and after vigorous mixing (*right*). Figure adapted from [15].

5. Experimental evolution and the Wrinkly Spreader

Many aspects of the ecological and mechanistic bases of evolution have been investigated by the experimental evolution of bacteria (reviewed in [50-52]). The adaptive radiation of the soil and plant-associated pseudomonad, *P. fluorescens* SBW25 [10, 12], has been investigated in some detail using experimental King's B microcosms (see Figure 1) following the first report by Rainey and Travisano [11]. These can be incubated with shaking to provide a homogenous environment, or statically without physical disturbance to provide a heterogeneous environment. The initial wild-type SBW25 colonists of static microcosms rapidly establish a gradient in which O_2 drops to < 0.05% of normal levels below a depth of 200μm [53]. This gradient produces heterogeneity in the microcosm and defines three niches for colonisation and adaptation: the A-L interface, the liquid column, and the vial bottom. In contrast, microcosms subject to constant and vigorous mixing do not develop an O_2 gradient or different niches. Wild-type SBW25 rapidly radiates to produce a range of phenotypically distinguishable mutants (morphs or morphotypes) to occupy the different niches [11]. This diversification is reproducible and occurs rapidly, typically within ~100 generations and 1-3 days. The main morphotypes recovered from evolving populations of wild-type SBW25 in static microcosms include the Wrinkly Spreaders (WS) which produce a wrinkled colony morphology and colonise the A-L interface through the formation of a biofilm (Figure 1); the Smooth (SM) morphs, including wild-type SBW25, which produce round, smooth colonies and colonise the liquid column, and the Fuzzy Spreaders (FS) which are characterised by fuzzy-topped colonies and colonise the anoxic bottom of static microcosms [11].

In an effort to understand the mechanistic basis of the adaptive leap of wild-type SBW25 from the liquid column-colonising SM-morph to the WS A-L interface niche specialist, the underlying molecular biology of the WS phenotype was investigated. This work, described in the following section, ultimately showed that the evolutionary innovation was the use of cellulose to produce a physically robust and resilient biofilm which allowed the colonisation of the A-L interface. Competitive fitness experiments have demonstrated that the WS has a significant fitness advantage over non-biofilm–forming strains in static microcosms [5, 11, 49]. Simplistically, WS cells were able to intercept O_2 diffusing across the A-L interface from the atmosphere before non-biofilm–forming competitors could do so lower down the liquid column, and as a result, WS populations could grow more rapidly than non-WS populations [53]. In contrast however, the WS do not enjoy a fitness advantage in shaken microcosms where the O_2 concentrations are uniform or on agar plates where the WS phenotype is unstable [5, 48-49].

6. Cellulose expression in *P. fluorescens* SBW25

In order to understand the underlying mechanistic basis of the WS phenotype, a mini-transposon screening approach using mini-Tn*5* was adopted to identify critical genes and pathways [5]. Mini-transposon insertions typically destroy the function of the targeted gene, and the disruption of critical genes in the WS would be expected to result in mutants that produced rounded, smooth (SM)-like colonies rather than the typical WS colony. Plates

containing hundreds or thousands of WS colonies could be easily screened for a few SM-like colonies which could then be isolated for further examination.

This approach allowed the identification and sequencing of the SBW25 *wss* operon containing ten genes (*wssA-J*) required for the WS phenotype and is shown in Figure 3 (*wss* is an acronym for WS structural locus, responsible for the production of the main structural component required for the WS phenotype) [5]. Overall, the *wss* operon showed strong similarity to the cellulose biosynthetic clusters originally identified as the *acs* operon in *Gluconacetobacter hansenii* (formerly *Acetobacter xylinus*) ATCC 23769 [54] and subsequently annotated as the *yhj* operon in the whole-genome sequence of *Escherichia coli* K-12 [55]. Most *acs* (*Acetobacter* cellulose-synthesizing) homologues are now referred to as *bcs* (bacterial cellulose synthesizing) genes as we do here (*yhj* has no meaning). The degree of homology between the *wss*, *bcs* and *yhj* genes at the amino acid level strongly suggested that the SBW25 *wss* operon encoded a functional cellulose synthase, and the predicted functions of the Wss proteins are listed in Table 3.

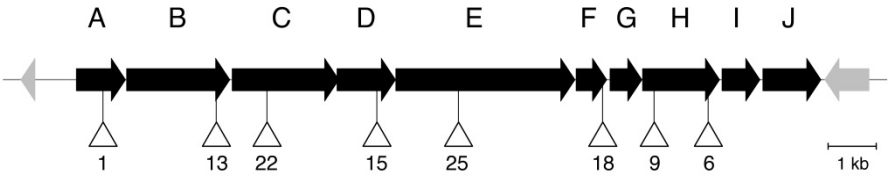

Figure 3. Structure of the cellulose biosynthesis operon. The *Pseudomonas fluorescens* SBW25 cellulose synthase is encoded by the *wss* operon (*wssA-J*, black arrows). The core synthase is composed of WssBCDE subunits and the associated acetylation activity produced by WssFGHI. WssA and WssJ may be involved in the correct cellular localisation of the Wss complex, though WssJ is functionally redundant. The locations of key mini-Tn*5* transposon insertions are indicated (open triangles). WS-1, 13, 22, 15 & 25 mutants are unable to express cellulose. WS-18, 9 & 6 mutants express un-acetylated cellulose. Upstream of the *wss* operon is $tRNA^{Thr}$ and downstream a hypothetical protein of unknown function (grey arrows). Scale bar: 1 kb. Figure adapted from [5].

However, the SBW25 *wss* operon showed two notable differences to the *G. xylinus bcs* and *E. coli yhj* operons. First, the *wss* operon contains two MinD-like homologues, WssA and WssJ, not previously recognised as having a role in cellulose synthesis. WssJ shows 51% identity at the amino acid level with WssA, but only short sections of similarity at the nucleotide level and does not appear to be a simple repeat of the *wssA* gene sequence. As MinD is involved in cell division and determining cell polarity [56], WssA and WssJ were proposed to ensure the correct spatial localization of the cellulose synthase complex at the cell poles [5]. Subsequently, the WssA-homologue, YhjQ (BcsQ), has been shown to be essential for this in *E. coli* K-12 [57]. Secondly, the *wss* operon includes three genes, *wssGHI*, that shares homology with the alginate acetylation proteins of *P. aeruginosa* FRD1, AlgFIJ [58].

In order to demonstrate that the SBW25 *wss* operon encoded a functional cellulose synthase, and to determine the role of the alginate acetylation-like *wssGHI* genes, cellulose expression in the WS and mini-Tn*5* mutants was examined by a variety of techniques, including Congo

red colony staining, fluorescent microscopy, enzymatic digestion and structural analysis of purified matrix material [5, 59-60].

Protein (synonyms)	Function (Accession No.)
WssA (BcsQ, YhjQ)	Cellulose synthase-associated positioning subunit (CAY46577.1): MinD–like ATPase involved in the appropriate spatial localisation of the cellulose synthase complex.
WssB (BcsA, YhjO)	Cellulose synthase subunit (CAY46578.1): catalytically-active subunit responsible for the polymerisation of UDP-Glucose into cellulose. Predicted integral transmembrane protein, contains conserved D residue, QXXRW, HAKAGN and QTP motifs, a PilZ domain. Binds c-*di*-GMP.
WssC (BcsB, YhjN)	Cellulose synthase subunit (CAY46579.1): unknown function (originally thought to bind c-*di*-GMP). Often fused with WssB.
WssD (Orf1, YhjM)	Cellulose synthase subunit (CAY46580.1): Endo-1,4-D-glucanase (D-family cellulase).
WssE (BcsC/S, YhjI)	Cellulose synthase subunit (CAY46581.1): unknown function. Includes a putative signal peptide.
WssF (BcsX)	Cellulose synthase-associated acetylation subunit (CAY46582.1): suggested function is to present acyl groups to WssGHI.
WssG	Cellulose synthase-associated acetylation subunit (CAY46583.1): AlgF-like protein involved in the acetylation of cellulose. Includes a putative signal peptide.
WssH	Cellulose synthase-associated acetylation subunit (CAY46584.1): AlgI-like protein involved in the acetylation of cellulose. Predicted integral transmembrane protein.
WssI	Cellulose synthase-associated acetylation subunit (CAY46585.1): AlgJ-like protein involved in the acetylation of cellulose. Localised to the periplasm.
WssJ	Cellulose synthase-associated positioning subunit (CAY46586.1): MinD-like ATPase like WssA but apparently functionally redundant.

G. xylinus Bcs and *E. coli* Yhj synonyms are provided in parentheses. Function suggested from Wss experiments and Wss homologue investigations. AlgFIJ homologues are from *P. aeruginosa* FRD1 [58].

Table 3. Predicted functions of the *Pseudomonas fluorescens* SBW25 Wss proteins

The diazo dye, Congo red (CR), had been used previously to stain bacterial colonies expressing cellulose [61], and we used this technique to show that WS, WS-18, WS-6 and WS-9, but not WS-1, WS-13, WS-22, WS-15 and WS-25 mutants, appeared to express cellulose on King's B plates [5, 59]. WS and WS-18 biofilm material were subsequently stained with the more specific fluorescent dye, Calcofluor, and examined by fluorescent microscopy (Figure 4). This showed that the biofilm was dominated by an extensive network of extracellular cellulose, with fibres ranging from 0.02 μm to over 100 μm thick. In

places, the fibres appeared to form large clumps of material and in other places forming thin films, with bacterial cells associated with the fibres and found within the voids [59]. In comparison, in colonies the cellulose fibres appear to collect above the mass of the colony (Figure 5). Scanning electron microscopy images of WS biofilms suggest a lattice-work of pores (Figure 6) which might be the result of constant growth at the top surface of the biofilm which slowly displaces older strata deeper into the liquid column [53]. Rough calculations of the density of WS biofilms suggest that they were > 97% liquid, which is in agreement with the finding that microbial amorphous celluloses are very hydrophilic, with gels having a water holding capacity of 148 – 309 g water / g dry cellulose [62-63]. Recent rheological tests have shown that the WS biofilm structure is a classic viscoelastic solid (gel-like) material (AK & AJS, unpublished observations). The structural integrity of WS biofilms could be destroyed by incubation with cellulase, adding support to initial conclusions that the major matrix component of the WS biofilm, expressed by the *wss* operon, was cellulose or a cellulose-like polymer [5, 59].

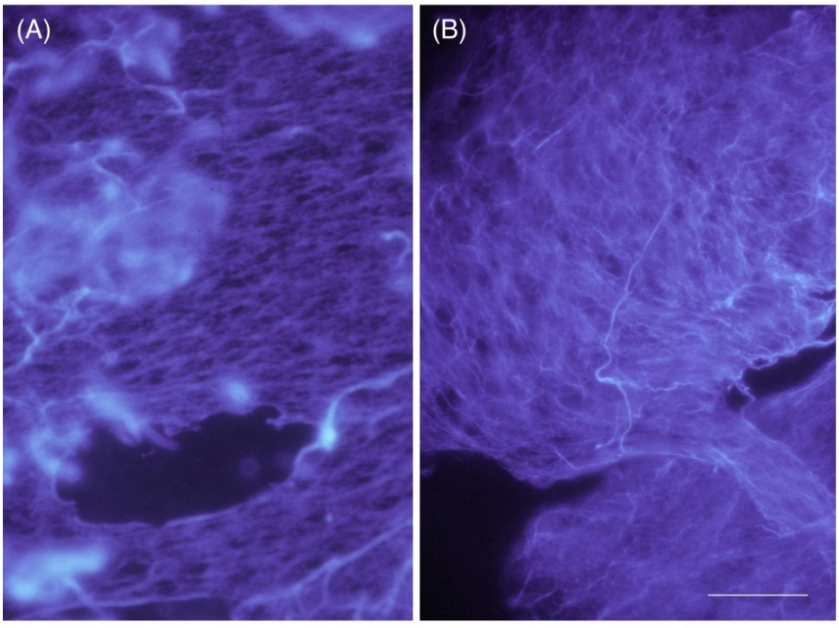

Figure 4. Fluorescent microscopy of WS biofilms. The cellulose fibre matrix of the Wrinkly Spreader (WS) biofilm can be visualised by staining with Calcofluor and fluorescent microscopy. Shown are two images showing the highly hydrated and fibrous nature of the WS biofilm. Scale bar: 100 μm. Images from A. Spiers.

WS and WS-18 biofilms were subsequently purified in order to determine the chemical identity of the matrix component. Carbohydrate analysis indicated that both samples contained ~75% glucose (Glu) and ~25% rhamnose (Rha) [59]. The latter could be explained as coming from contaminating Rha-containing A-band LPS which is highly conserved amongst the pseudomonads [64]. Linkage analyses of derivatized WS samples by GC-MS

identified a major peak corresponding to 4-Glu, and minor peaks corresponding to 2,4-Glu, 3,4-Glu and 4,6-Glu, which is consistent with a β(1-4)-linked glucose polymer, i.e. cellulose. In contrast, the WS-18 material did not contain 2,4-Glu, 3,4-Glu or 4,6-Glu derivatives, suggesting that the *wss* alginate acetylation-like genes were responsible for the acetylation of glucose residues at the 2, 3, and 6 Carbon positions. This was further supported by [^{1}H]-NMR analysis which confirmed the presence of acetylated hexose residues in the WS extract, with 14% of the glucose residues estimated to be modified with one acetyl group [59]. Although cellulose is readily acetylated by chemical treatment, we are not aware of any other reports of biologically-produced acetylated cellulose.

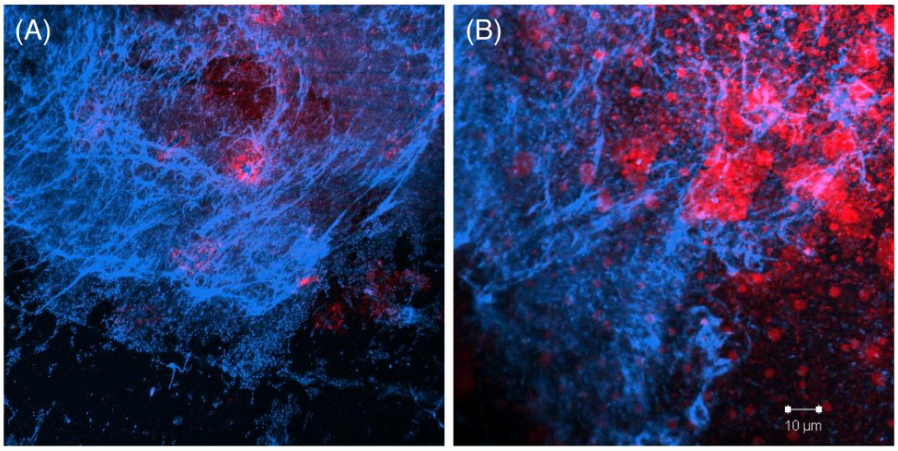

Figure 5. Inducing cellulose expression with c-*di*-GMP. An increase in c-*di*-GMP levels can induce cellulose expression in some pseudomonads. Shown are confocal laser scanning microscopy (CLSM) images of colony material from **(A)** *Pseudomonas fluorescens* SBW25 and **(B)** *P. syringae* DC3000 expressing the constitutively-active DGC response regulator WspR19 *in trans* which increases c-*di*-GMP levels, visualised with Calcofluor for cellulose (blue) and ethidium bromide for bacteria (red). Scale bar: 10 µm. Images from O. Moshynets.

The partial acetylation of the cellulose fibres expressed by the WS clearly had an impact on colony morphology and biofilm strength. Colonies produced by WS-18 were readily differentiated from WS and wild-type SM-like colonies, whilst the WS-18 biofilm was ~ 4*x* weaker than the partially-acetylated structure produced by the WS, suggesting that acetylation increased the connectivity of cellulose fibres within colonies and the biofilm matrix [59-60]. Incubation with EDTA reduced WS-18 biofilm strength, whilst incubation with some diazo dyes increased WS-18 biofilm strength compared to WS biofilms, suggesting that fibre interactions could be altered by sequestering Mg^{2+} and coating cellulose fibres with dyes [60]. A lipopolysaccharide-deficient mutant which produces a very weak biofilm compared to both WS-18 and WS, was also affected by EDTA and diazo dyes, indicating that the partially-acetylated cellulose fibres also interacted with the lipopolysaccharide on the surface of cells or associated with cell debris to further strengthen the biofilm structure [60].

Individual cellulose polymers can also interact directly to produce a number of different forms or allomorphs. *G. xylinus* produces two crystalline allomorphs, known as cellulose I and II, which requires the cellulose synthase-associated BcsD subunit that couples cellulose polymerisation and crystallization [54, 65]. However, SBW25 lacks a BcsD homologue and therefore can only produce non-crystalline amorphous cellulose.

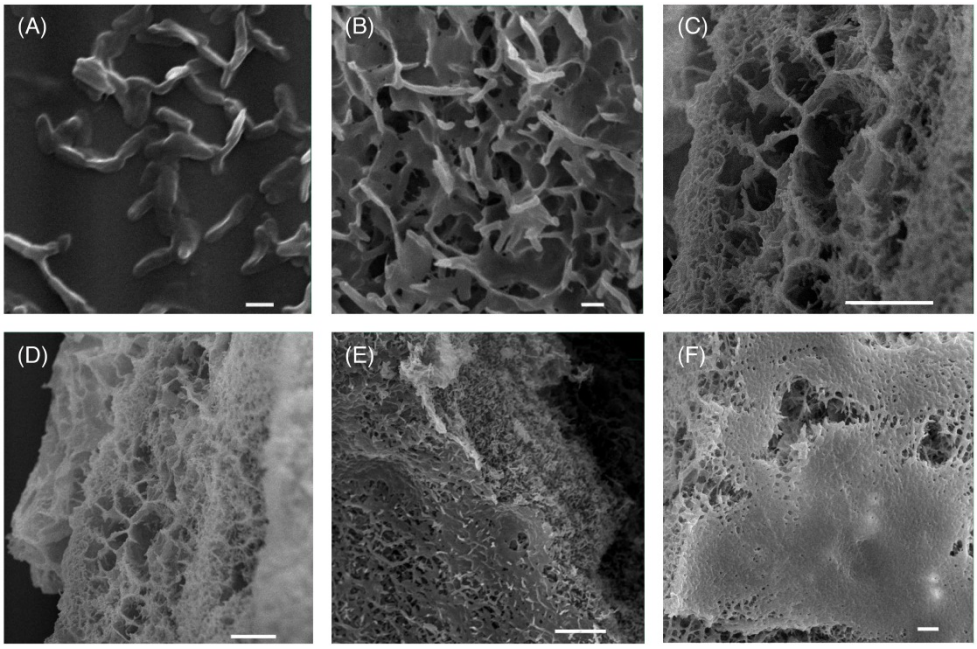

Figure 6. WS biofilm ultrastructure. Scanning electron microscopy (SEM) images of Wrinkly Spreader (WS) biofilms suggest a porous but robust structure. Shown here are a series of SEM images of decreasing magnification, from **(A)** single cells to **(F)** large pieces of biofilm. Images were obtained after freeze-drying and shadowing with gold. Scale bars: A & B, 1μm; C – F, 10 μm. Images from O. Moshynets.

Following the analysis of the WS mini-Tn*5* mutants, a further round of mini-transposon mutagenesis was undertaken using IS*phoA*/hah [66]. This mini-transposon allowed both the impact of polar and non-polar insertions to be assessed; the former destroy the function of the disrupted gene as well as any down-stream expression, whilst the latter destroys gene function but leaves down-stream expression unaffected (this is possible after Cre-mediated deletion of the central portion of the IS*phoA*/hah cassette which leaves a 63-codon in-frame insertion). WS IS*phoA*/hah mutants were recovered for each of the *wss* genes, except *wssJ*. Each of the polar IS*phoA*/hah insertions and corresponding non-polar Cre-deletions in *wssA-E* resulted in the loss of cellulose expression, whilst polar and non-polar mutants in *wssF-I* resulted in a WS-18–like phenotype [47, 59]. Finally, a WS *wssJ* deletion mutant was constructed and shown to have no impact on cellulose expression, suggesting that the final gene of the *wss* operon might be functionally redundant [47].

Examination of other mini-Tn*5* mutants also lead to the identification of the *wsp* regulatory operon of seven genes, *wspA-E & R* (*wsp* is an acronym for WS phenotype locus, responsible for the regulation of the WS phenotype) [67]. The function of these have been modelled on the *Escherichia coli* Che chemosensory system (reviewed in [68]) to provide a mechanistic explanation of the induction of the WS phenotype [67] (a schematic of this is shown in Figure 7). In this the methyl-accepting chemotaxis protein (MCP) WspA forms a membrane-bound complex with two scaffold proteins, WspB and WspD, plus the histidine kinase WspE. In the absence of an appropriate environmental signal, the complex is silent and does not activate the associate response regulator, WspR, by phosphorylation. The system is controlled by a negative feedback loop mediated by the WspC methyltransferase and WspF methylesterase. WspC constitutively antagonises WspF, and in wild-type SBW25 the activities of the two are balanced, preventing the activation of WspR and allowing the Wsp complex to oscillate between active and inactive states. WspR is a di-guanylate cyclase (DGC) response regulator, and the phosphorylated active form, WspR-P, synthesizes c-*di*-GMP (bis-(3'-5')-cyclic dimeric guanosine monophosphate) from GTP [69]. In this model, we hypothesised that mutations in WspR which stimulated DGC activity without requiring phosphorylation, or mutations inhibiting WspF function, would result in an increase in c-*di*-GMP production. This would then lead to the activation of the WS phenotype through the direct stimulation of the cellulose synthase complex, rather than up-regulated *wss* transcription [5] (the second component required for the WS phenotype, the pilli-like attachment factor, has not yet been identified and it is not known how it might be regulated by c-*di*-GMP). Several mutants of WspR had been engineered, and the effect of the constitutively-active mutant WspR19 [70] on cellulose expression by wild-type SBW25 is shown in Figure 5.

This model for the activation of the WS phenotype has been confirmed through the identification and testing of WspF mutations found in a number of independently-isolated Wrinkly Spreaders [67]. Interestingly, no naturally occurring WspR mutants have been identified yet, despite the fact that engineered WspR mutants like WspR19 were found to show the predicted phenotype [60, 69-71]. Mutations in other operons leading to the activation of the AwsR and MwsR DGCs can also induce the WS phenotype [47, 72]. These different routes activating the WS phenotype can be seen as an example of parallel evolution leading to new A-L interface biofilm-forming genotypes in static microcosms [72].

During the molecular investigation of the WS phenotype, the non-biofilm–forming wild-type SBW25 was modified by the insertion of a constitutive promoter to increase the levels of *wss* operon transcription. This mutant, JB01, was found to produce a very weak biofilm, poorly attached to the microcosm vial walls and to express similar amounts of cellulose as the WS [5, 60]. Subsequently, we found that wild-type SBW25 could be non-specifically induced by exogenous Fe to produce a phenotypically-similar biofilm referred to as the VM biofilm [73] (see below for a description of Viscous mass (VM)-class biofilms). However, VM biofilm-formation was not the result of an increase in *wss* transcription, and as yet, no link has been identified between Fe regulation and cellulose expression. We speculate that the induction of the VM biofilm is due to a minor perturbation of the Wsp system or the cellulose synthase complex itself that allows activation despite sub-critical levels of c-*di*-GMP.

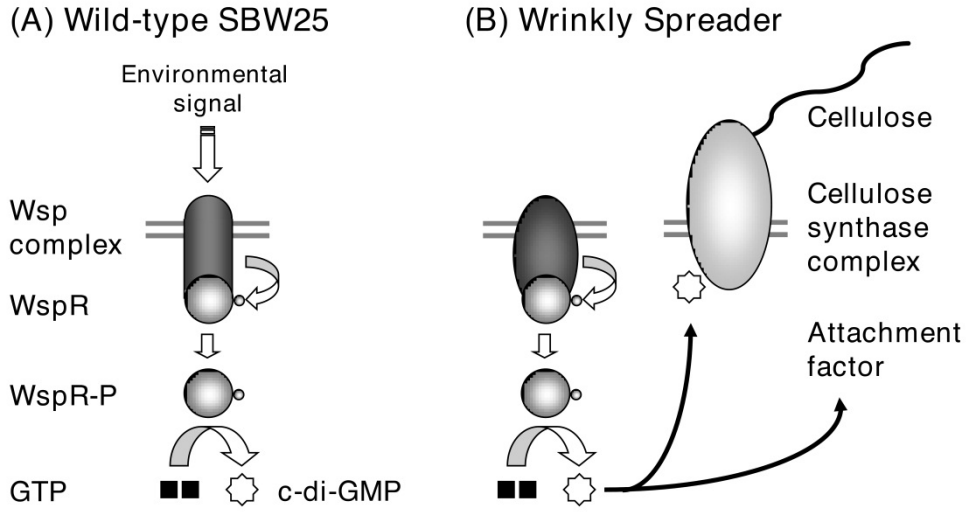

Figure 7. Activation of the WS phenotype. The Wrinkly Spreader (WS) phenotype is controlled by the membrane-associated Wsp complex and associated DGC response regulator WspR. **(A)** In wild-type *Pseudomonas fluorescens* SBW25, when an appropriate environmental signal is received the Wsp complex phosphorylates WspR which then results in the production of c-*di*-GMP. However, in the absence of signal, the Wsp complex is silent and c-*di*-GMP levels remain low. **(B)** In the Wrinkly Spreader a mutation in a Wsp subunit (WspF) alters the sensitivity of the Wsp complex such that it activates WspR in the absence of the environmental signal. The resulting increase in c-*di*-GMP activates the membrane-associated cellulose synthase complex to produce cellulose, and also activates the unidentified attachment factor that is also required for the WS phenotype.

7. Biofilm formation and cellulose expression amongst other pseudomonads

Having discovered that *P. fluorescens* SBW25 could express cellulose in the WS biofilm (and subsequently in the VM biofilm), we were interested to see if related environmental pseudomonads could produce similar cellulose-matrix–based A-L interface biofilms. We therefore undertook a survey of environmental pseudomonads, including water, soil, plant-associated and plant pathogenic isolates (we did not include human or other animal pathogens in this survey) [15]. The ability of each to produce an A-L interface biofilm was assessed in static King's B liquid media microcosms. Importantly, this assay did not differentiate between isolates that constitutively produced biofilms, with those that might utilise quorum sensing-like signalling to initiate biofilm-formation, or those that had mutated into a biofilm-forming genotype. Of the 185 environmental pseudomonads tested, 76% were found to produce observable biofilms within 15 days incubation. The phenotypes of these were variable, with biofilm strengths ranging 1500*x*, but could be categorised into the physically-cohesive (PC), floccular mass (FM), waxy aggregate (WA) and viscous mass (VM)-class biofilms described in Table 2 (see also Figure 2) [15, 46].

Calcofluor-fluorescent microscopy identified cellulose as the matrix component of 20% of the biofilm-forming isolates, indicating that at least seven *Pseudomonas* species were capable of expressing cellulose under the conditions tested. These included *P. corrugata* (tomato pathogens), *P. fluorescens* (plant-associated isolates), *P. marginalis* (alfalfa and parsnip pathogens), *P. putida* (rhizosphere and soil isolates), *P. savastanoi* (olive pathogens), *P. stutzeri* (represented by a single clinical isolate), and *P. syringae* (celery, cucumber, tobacco, and tomato isolates or pathogens) (isolates from another eleven *Pseudomonas* spp. were tested, including *P. aeruginosa* PA01 and PA14, and were not found to produce cellulose). For two of the cellulose-expressing isolates, *P. putida* KT2440 and *P. syringae* DC3000, the whole genome sequences were available and SBW25 *wss*-like cellulose synthase operons had been annotated [74-75], though no experimental reports of either expressing cellulose had been made.

Many environmental pseudomonads can also be induced to form A-L interface biofilms and to express cellulose using WspR19. When expressed *in trans* in wild-type SBW25 it produces the WS phenotype [60, 70], though in other pseudomonads the impact was found to be more variable. In a test of 16 pseudomonads known to form biofilms and express cellulose, WspR19 was found to significantly increase biofilm attachment, strength, and cellulose expression in *P. fluorescens* 54/96, *P. syringae* DC3000, *P. syringae* T1615 and *P. syringae* 6034 [15] (WspR19 induction of cellulose production by SBW25 and DC3000 is shown in Figure 5). WspR19 also induced a WS-like phenotype in *P. putida* KT2440, despite the fact that biofilm-formation or cellulose expression in this pseudomonad had not been observed in the initial survey (cellulose expression was subsequently reported for both wild-type and WspR19-carrying strains under different experimental conditions by [76]). Similarly, nine of ten non-biofilm–forming and non-cellulose expressing *P. syringae* isolates were found to produce biofilms when induced with WspR19, and two of these also expressed detectable levels of cellulose [15]. These findings suggest that biofilm-formation and cellulose expression in pseudomonads closely related to *P. fluorescens* SBW25 are probably controlled by the same c-*di*-GMP–mediated regulatory system or are sensitive to non-specific increases in c-*di*-GMP levels.

Habitat (sample size)	A-L interface biofilms	Evidence of cellulose
Plant pathogens (n = 57)	6%	26%
Plant & soil associated (n = 28)	82%	39%
Scottish soil (n = 73)[a]	95%	76%*
River (n = 57)	82%	5%
Indoor & outdoor ponds (n = 50)[b]	94%	56%
Pitcher plants (*Sarracenia* spp.) (n = 50)[c]	74%	68%
Spoilt cold-stored meat (n = 60)[d]	77%	28%
Mushroom pathogens (n = 26)[e]	77%	69%

* Estimated from a sub-sample of 25 isolates. Data compiled from [15] and unpublished research from **a,** R. Ahmed, AK & AJS; **b,** B. Varun, AK & AJS; **c,** D.S. Kumar, AK & AJS; **d,** M. Robertson & AJS; and **e,** AK & AJS.

Table 4. Prevalence of A-L interface biofilm formation and cellulose expression amongst environmental pseudomonads

We have conducted additional surveys of pseudomonads isolated from other habitats, including pond water, pitcher plant (*Sarracenia* spp.) deadfall trap-water, spoilt cold-stored meat and mushrooms (Table 4). These confirm the wide-spread ability of environmental pseudomonads to form A-L interface biofilms and to express cellulose under the experimental conditions used previously [15]. It is also evident that pseudomonads are capable of producing a wide range of EPS in addition to cellulose, including alginate, levan, marginalan, PEL, PSL, and a number of other polymers, which may be utilised as biofilm matrix components [77-80].

8. Distribution of *wss*-like cellulose synthase operons amongst the proteobacteria

We are undertaking a bioinformatics analysis of all publicly-available fully-sequenced bacterial genomes in order to determine the phylogenetic distribution and structural variation of *P. fluorescens* SBW25 *wss*-like cellulose biosynthetic operons amongst the proteobacteria. Protein (TBLASTN) homology searches were run against the GenBank complete genome database [81] using the SBW25 Wss proteins as the query sequences in October of 2011. From this, we have identified over 50 bacteria with gene clusters that showed significant protein sequence homology (≥ 25% ID) to three or more Wss proteins, including a minimum of two key cellulose synthase subunits, WssB, WssC, or WssE. Putative SBW25 *wss*-like operons were then manually curated for accuracy to provide Wss homologue protein sequences and operon structures. Phylogentic trees were constructed using the multiple sequence alignment program ClustalW 2.0 [82], and neighbour-joining and minimal evolution methods implemented by Geneious 5.5.5 (Biomatters Ltd, NZ).

Although this bioinformatics analysis is on-going and the final results expected to be published elsewhere, we make the following preliminary observations. First, whilst *wssB* tends to be followed by *wssC* in the *wss*-like cellulose synthase operons as found previously [5, 8, 83], there are examples within the *Burkholderia* and in *Cupriavidus metallidurans* CH34 where *wssB* is separated from the rest of the operon. Second, we note that only the *P. fluorescens* SBW25 and *P. syringae* DC3000 *wss* operons include the *wssG-I* alginate acetylation-like genes, but not the closely-related pseudomonad *P. putida* KT2440. This suggests that DC3000 may also be able to express partially-acetylated cellulose, and that *wssF-I* genes may be narrowly restricted to the *P. fluorescens–syringae* complex. Third, there is considerable variation in cellulose synthesis operon structure amongst the *Enterobacteriacea*, with many having two clusters of genes (e.g. *Erwinia billingiae* Eb66, *Klebsiella pneumoniae* MGH78578, *Pantoea* sp. At-9b). Many enteric bacteria also include the additional genes *bcsEFG* which have no *wss* homologues (e.g. *Escherichia coli* K-12 MG1655, *Salmonella enterica* Typhimurium LT2, *Vibrio fisheri* MJ11). These have been reported to be associated with cellulose production in *Salmonella enteritidis* 3934 [4]. However, *Escherichia coli* K-12 DH10B contains only *bcsFG*, raising the possibility that *bcsE-G* are not essential for cellulose production in these bacteria. Although the *Gluconacetobacter* are not closely related to the enteric bacteria, we note that *G. xylinus* NBRC 3288 has a small *wssBCE* operon plus a larger *wssDBCE* operon. It is possible that such duplications might enable higher levels of

cellulose expression under some environmental conditions, or that such gene duplications may persist for some time before deletion.

Finally, the clustering of WssB homologue sequences (Figure 8) generally follows the 16S phylogenetic relationships between bacteria. However, we are surprised to find that *P. fluorescens* SBW25 and *P. syringae* DC300 cluster with many of the *Burkholderia* and *Xanthomonas*, whilst *P. putida* and *P. stutzeri* strains cluster with the enteric bacteria. We have yet to compare the clustering patterns of the WssC, WssD and WssE homologues, where conserved patterns may reflect different functional roles for cellulose and host lifestyles, whilst aberrant placements of single proteins might reflect the random mutation of a phenotype no longer of functional value or under positive selection.

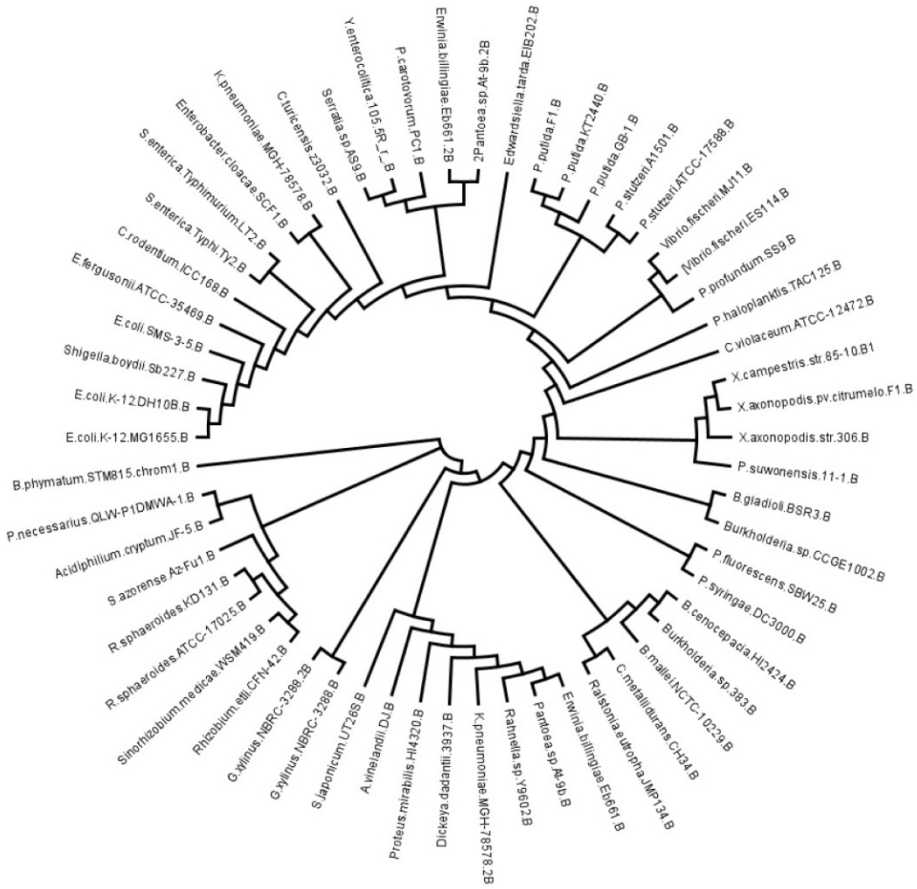

Figure 8. Cladogram of WssB homologues. The structure of the WssB cladogram is similar to that constructed using 16s rRNA sequences, with the enteric bacteria and pseudomonads forming two distinct clusters. Within the pseudomonads, the *P. fluorescens-syringae* complex has diverged earlier than the *P. putida-stutzeri* group. The cladogram was constructed using Geneious 5.5.5 (Biomatters Ltd, NZ) default parameters after multiple sequence alignment of 58 WssB proteins by ClustalW 2.0 [82].

9. Ecological role and fitness advantage of cellulose

Attempts to understand the importance of cellulose expression by *P. fluorescens* SBW25 in soil and the phytosphere have involved investigation of the regulators controlling *wss* operon transcription [5, 84], and measurement of fitness advantage using plant microcosms [85]. Cellulose expression is clearly regulated at two levels in SBW25. First, the activity of the cellulose synthase complex is regulated by c-*di*-GMP levels, but it is not known what environmental signals control WspR, other DGCs or their antagonists, though c-*di*-GMP is known to be involved in a range of surface colonisation and pathogenicity systems in a variety of bacteria (reviewed in [86-87]). Second, cellulose expression is regulated at the level of *wss* operon transcription, with mini-transposon analysis identifying AlgR, AwsR and WspR as positive regulators, and AmrZ and FleQ as negative regulators [5, 84].

AwsXR was a previously unrecognised regulatory system, first identified in SBW25 where the mutational activation of the DGC AwsR results in the WS phenotype [47, 72], though the normal means of regulating AwsR activity remains unknown. FleQ is a c-*di*-GMP–responsive transcriptional regulator, and in *P. aeruginosa* PA01 it controls the hierarchical regulatory cascade for flagella biosynthesis and the repression of the PEL biosynthesis genes [88-89]. AlgR and AmrZ (also referred to as AlgZ) are transcription factors involved in the regulation of a number of systems including alginate biosynthesis and twitching motility [79, 90]. It is possible that AlgR, AmrZ, and AwsR directly repress SBW25 *wss* transcription, whilst AwsX, FleQ, and WspR act indirectly to regulate transcription and therefore cellulose expression [84]. However, no environmental signals have been identified that induce cellulose expression via these repressors.

Sugar beet (*Beta vulgaris*) seedlings have been used to determine the competitive fitness advantage cellulose-expression may provide wild-type SBW25 compared to a cellulose-deficient mutant [85]. In these experiments, seeds were first inoculated with a mixture of wild-type SBW25 and SM-13, a mutant containing a mini-Tn*5* insertion cassette derived from WS-13 [5]. These were then germinated and grown for four weeks in an artificial soil substrate. Bacteria were then recovered from the stems and leaves (the phyllosphere), from roots and adherent vermiculite (the rhizosphere), and from un-planted containers ('bulk soil') to allow the calculation of competitive fitness (W) [91] (we report W for SM-13 *cf* wild-type SBW25 here for clarity). In the phyllosphere and rhizosphere, SBW25 was found to have a significant fitness advantage over SM-13, with $W \approx 1.8$ and $W \approx 1.11$, respectively, but not in bulk soil where $W \approx 1.05$. These findings suggest that the appropriately-controlled expression of cellulose by wild-type SBW25 provides some benefit on plant surfaces. It is possible that the mechanistic nature of this benefit may be an improved tolerance to water-limiting conditions rather than resistance to physical disturbance and predation, as the seedlings were watered using a tray rather than from a sprinkler, and vermiculite was used instead of natural soil.

Comparisons of the survival of wild-type SBW25 and a cellulose-deficient mutant similar to SM-13 under water-limiting conditions have shown that the loss of cell viability is faster for the mutant than for wild-type SBW25 (A Koza & A Spiers, unpublished observations). A

similar observation has been made for *P. putida* mt-2 (the progenitor of KT2440) where water stress was also found to increase cellulose expression [76]. Many bacteria respond to desiccation by producing exopolysaccharides, many of which are hygroscopic and retain water entropically [92], and amorphous cellulose is more hygroscopic and retains more liquid than crystalline cellulose [62]. Support for an anti-predation role for cellulose comes from the finding that the competitive fitness of WS genotypes in static microcosms increases in the presence of the grazing protist *Tetrahymena thermophile* [93].

10. Concluding statement

Bacterial cellulose production and air-liquid (A-L) interface biofilm-formation was first described 1886 for *Bacterium xylinum*, and subsequently observed by ourselves and colleagues in the evolution of the *Pseudomonas fluorescens* SBW25 Wrinkly Spreader (WS) some 116 years later. It is clear that this type of biofilm-formation is common-place amongst the environmental pseudomonads, many of which also utilise cellulose as the main matrix component of the biofilm. The fitness advantage of cellulose matrix-based biofilm-formation by SBW25 in static microcosms is well-proven, but the fitness in natural environments, and the true function of cellulose, is poorly researched and not yet understood. It may be that bacterial cellulose is used to form small biofilms in water bodies, acting to retain bacteria at the A-L interface or to maintain them on solid surfaces against water flow. Appositely, cellulose fibres may resist desiccation stress in water-limited environments, or even provide protection from protist and nematode predation. It is of course possible that cellulose performs a number of functions, which might explain the wide distribution of cellulose synthase operons amongst the *Proteobacter* inhabiting a diverse array of environments.

Author details

Andrew J. Spiers*, Ayorinde O. Folorunso and Kamil Zawadzki
The SIMBIOS Centre, University of Abertay Dundee, Dundee, UK

Yusuf Y. Deeni
School of Contemporary Sciences, University of Abertay Dundee, Dundee, UK

Anna Koza
Novo Nordisk Foundation Center for Biosustainability, Hørsholm, Denmark

Olena Moshynets
Laboratory of Microbial Ecology, Institute of Molecular Biology and Genetics of the National Academy of Sciences of Ukraine, Kiev, Ukraine

Acknowledgement

AJS is a member of the Scottish Alliance for Geoscience Environment and Society (SAGES) and AK was a SAGES-associated PhD student with AJS. KZ undertook his MSc research

* Corresponding Author

project with AJS. AF is currently undertaking his MSc with AJS and YYD; his preliminary bioinformatics results are presented here and will be published at a later date. Funding from the Royal Society of Edinburgh through the International Exchange Programme supported the collaboration between AJS and OM for this project. The University of Abertay Dundee is a charity registered in Scotland, No: SC016040.

11. References

[1] Brown AJ. XLIII. On an acetic ferment which forms cellulose. J Chem Soc, Trans 1886;49 432-439.

[2] Brown RM. Bacterial cellulose. In: Phillips GO, Williams PA, Kennedy JF. (eds) Cellulose: structural and functional aspects. Ellis Horwood Series in Polymer Science and Technology. UK: Ellis Horwood Ltd.; 1989. p145-151.

[3] Ross P, Mayer R, Benziman M. Cellulose biosynthesis and function in bacteria. Microbiol Rev 1991;55(1) 35-58.

[4] Solano C, García B, Valle J, Berasain C, Ghigo J.-M, Gamazo C, Lasa I. Genetic analysis of *Salmonella enteritidis* biofilm formation: critical role of cellulose. Mol Microbiol 2002;43(3) 793-808.

[5] Spiers AJ, Kahn SG, Bohannon J, Travisano M, Rainey PB. Adaptive divergence in experimental populations of *Pseudomonas fluorescens*. I. Genetic and phenotypic bases of Wrinkly Spreader fitness. Genetics 2002;161 33-46.

[6] Cannon RE, Anderson SM. Biogenesis of Bacterial Cellulose. Crit Rev Microbiol 1991;17(6) 435-447.

[7] Iguchi M, Yamanaka S, Budhiono A. Bacterial cellulose - a masterpiece of nature's arts. J Materials Sci 2000;35 261-270.

[8] Römling U. Molecular biology of cellulose production in bacteria. Res Microbiol 2002;153 205-212.

[9] Chawla PR, Bajaj IB, Survase SA, Singhal RS. Fermentative Production of Microbial Cellulose. Food Technol Biotechnol 2009;47(2) 107-124.

[10] Rainey PB, Bailey MJ. Physical map of the *Pseudomonas fluorescens* SBW25 chromosome. Mol Microbiol 1996;19(3) 521-533.

[11] Rainey PB, Travisano M. Adaptive radiation in a heterogeneous environment. Nature 1998;394 69-72.

[12] Silby MW, Cerdeño-Tárraga AM, Vernikos G, Giddens SR, Jackson R, Preston G, Zhang X-X, Godfrey S, Spiers AJ, Harris S, Challis GL, Morningstar A, Harris D, Seeger K, Murphy L, Rutter S, Squares R, Quail MA, Saunders E, Anderson I, Mavromat K, Brettin TS, Bentley S. Thomas CM, Parkhill J, Levy SB, Rainey PB, Thomson NR. Genomic and functional analyses of diversity and plant interactions of *Pseudomonas fluorescens*. Genome Biology 2009;10 R51.

[13] Peix A, Ramírez-Bahena M-H, Velázquez E. Historical evolution and current status of the taxonomy of genus *Pseudomonas*. Infect Genet Evol 2009;9 1132-1147.

[14] Silby MW, Winstanley C, Godfrey SAC, Levy SB, Jackson RW. *Pseudomonas* genomes: diverse and adaptable. FEMS Microbiol Rev 2011;35(4) 652-680.
[15] Ude S, Arnold DL, Moon CD, Timms-Wilson T, Spiers AJ. Biofilm formation and cellulose expression among diverse environmental *Pseudomonas* isolates. Environ Microbiol 2006;8(11) 1997-2011.
[16] Costerton JW, Lewandowski Z, Caldwell D, Korber D, Lappin-Scott HM. Microbial biofilms. Annu Rev Microbiol 1995;49 711-745.
[17] Costerton JW, Lewandowski Z, De Beer D, Caldwell D, Korber D, James G. Biofilms, the customized microniche. J Bacteriol 1994;176(8) 2137-2142.
[18] Stickler D. Biofilms. Curr Opin Microbiol 1999;2 270-275.
[19] Dalton HM, March PE. Molecular genetics of bacterial attachment and biofouling. Curr Opin Biotechnol 1998;9(3) 252-255.
[20] Davey ME, O'Toole, GA. Microbial biofilms: from ecology to molecular genetics. Microbiol Mol Biol Rev 2000;64(4) 847-867.
[21] Kuchma SL, O'Toole GA. Surface-induced and biofilm-induced changes in gene expression. Curr Opin Biotechnol 2000;11 429-433.
[22] Watnick P, Kolter, R. Biofilm, city of microbes. J Bacteriol 2000;182(10) 2675-2679.
[23] Stewart PS, Costerton JW. Antibiotic resistance of bacteria in biofilms. Lancent 2001;358 135-138.
[24] Sutherland IW. Biofilm exopolysaccharides: a strong and sticky framework. Microbiology 2001;147 3-9.
[25] Sutherland IW. The biofilm matrix- an immobilized but dynamic microbial environment. TRENDS Microbiol 2001;9(5) 222-227.
[26] Dunne WM. Bacterial adhesion: seen and good biofilms lately? Clinical Microbiol Rev 2002;15(2) 155-166.
[27] Morris CE, Monier J-M. The ecological significance of biofilm formation by plant-associated bacteria. Annu Rev Phytopathol 2003;41 429-453.
[28] Webb JS, Givskov M, Kjelleberg S. Bacterial biofilms: prokaryotic adventures in multicellularity. Curr Opin Microbiol 2003;6(6) 578-585.
[29] O'Toole GA. To build a biofilm. J Bacteriol 2003;185(9) 2687-2689.
[30] Branda SS, Vik A, Friedman L, Kolter R. Biofilms: the matrix revisited. TRENDS Microbiol 2005;13(1) 20-26.
[31] Hall-Stoodley L, Stoodley P. Evolving concepts in biofilm infections. Cellular Microbiol 2009;11(7) 1034-1043.
[32] West SA, Diggle SP, Buckling A, Gardner A, Griffin AS. The Social Lives of Microbes. Ann Rev Ecol Evol S 2007;38 53-77.
[33] Xavier JB, Foster KR. Cooperation and conflict in microbial biofilms. PNAS (USA) 2007;104(3) 876-881.
[34] Kolter R, Greenberg EP. Microbial sciences: the superficial life of microbes. Nature 2006;441 300-302.

[35] Chang WS, Van De Mortel M, Nielsen L, Nino De Guzman G, Li X, Halverson LJ. Alginate production by *Pseudomonas putida* creates a hydrated microenvironment and contributes to biofilm architecture and stress tolerance under water-limiting conditions. J Bacteriol 2007;189(22) 8290-8299.

[36] Allison DG, Ruiz B, Carmen S, Jaspe A, Gilbert P. Extracellular products as mediators of the formation and detachment of *Pseudomonas fluorescens* biofilms. FEMS Microbiol Lett 1998;167(2) 179-184.

[37] Davies DG, Parsek MR, Pearson JP, Iglewski BH, Costerton JW, Greenberg EP. The Involvement of cell-to-cell signals in the development of a bacterial biofilm. Science 1998;280(5361) 295-298.

[38] Van Loosdrecht MCM, Heijnen JJ, Eberl H, Kreft J, Picioreanu C. Mathematical modelling of biofilm structures. Antonie van Leeuwenhoek 2002;81 245–256.

[39] Battin T, Sloan WT, Kjelleberg S, Daims H, Head IM, Curtis TP, Eberl L. Microbial landscapes: new paths to biofilm research. Nature Rev Microbiol 2007;5 76-81.

[40] Brown AJ. XIX. The chemical action of pure cultivations of *Bacterium aceti*. J Chem Soc Trans 1886;49 172-187.

[41] Holzapfel WH. (1997). Use of starter cultures in fermentation on a household scale. Food Control 1997;8(5) 241–258.

[42] Greenwalt CJ, Steinkraus KH, Ledford, RA. Kombucha, the fermented tea: microbiology, composition, and claimed health effects. J Food Protection 2000;63(7) 976-981.

[43] Raghavendra MRR. Acetic acid bacteria. Annu Rev Microbiol 1957;11 317-338.

[44] Nguyen VT, Flanagan B, Gidley MJ, Dykes GA. Characterization of cellulose production by a Gluconacetobacter xylinus strain from Kombucha. Curr Microbiol 2008;57 449-453.

[45] Verschuren, PG, Cardona TD, Nout MHR, De Gooijer KD, Van Den Heuvel JC. Location and limitation of cellulose production by *Acetobacter xylinum* established from oxygen profiles. J Biosc Bioeng 2000;89(5) 414-419.

[46] Spiers AJ, Arnold DL, Moon CD, Timms-Wilson TM. A survey of A-L biofilm formation and cellulose expression amongst soil and plant-associated *Pseudomonas* isolates. In: Bailey MJ, Lilley AK, Timms-Wilson TM. (eds.) Microbial Ecology of Aerial Plant Surfaces. UK, CABI; 2006. p121-132.

[47] Gehrig SM. Adaptation of *Pseudomonas fluorescens* SBW25 to the air-liquid interface: a study in evolutionary genetics. DPhil thesis. University of Oxford; 2005.

[48] Spiers AJ. Wrinkly-Spreader fitness in the two-dimensional agar plate microcosm: maladaptation, compensation and ecological success. PLoS ONE 2007;2(8) e740.

[49] Green JH, Koza A, Moshynets O, Pajor R, Ritchie MR, Spiers AJ. Evolution in a test tube: rise of the Wrinkly Spreaders. J Biol Educ 2011;45(1) 54–59.

[50] Rainey PB, Buckling A, Kassen R, Travisano M. The emergence and maintenance of diversity: insights from experimental bacterial populations. Trends Ecol Evol 2000;15(6) 243-247.

[51] Buckling A, Wills MA, Colegrave N. Adaptation limits diversification of experimental bacterial populations. Science 2003;302(5653) 2107-2109.

[52] Buckling A, Maclean CR, Brockhurst MA, Colegrave N. The Beagle in a bottle. Nature 2009;457 824-829.

[53] Koza A, Moshynets O, Otten W, Spiers AJ. Environmental modification and niche construction: Developing O_2 gradients drive the evolution of the Wrinkly Spreader. ISME J 2011;5(4) 665-673.

[54] Saxena IM, Kudlicka K, Okuda K, Brown RM. Characterization of genes in the cellulose-synthesizing operon (*acs* operon) of *Acetobacter xylinum*: implications for cellulose crystallization. J Bacteriol 1994;176(18) 5735-5752.

[55] Blattner FR, Plunkett G. Bloch CA, Perna NT, Burland V, Riley M, Collado-Vides J, Glasner JD, Rode CK, Mayhew GF, Gregor J, Davis NW, Kirkpatrick HA, Goeden MA, Rose DJ, Mau B, Shao Y. The complete genome sequence of *Escherichia coli* K-12. Science 1997;277(5331) 1453-1462.

[56] Sullivan SM, Maddock JR. Bacterial division: finding the dividing line. Curr Biol 2000;10(6) R249-252.

[57] Le Quéré B, Ghigo JM. BcsQ is an essential component of the *Escherichia coli* cellulose biosynthesis apparatus that localizes at the bacterial cell pole. Mol Microbiol 2009;72(3) 724-740.

[58] Franklin MJ, Ohman DE. Identification of *algI* and *algJ* in the *Pseudomonas aeruginosa* alginate biosynthetic gene cluster which are required for alginate O acetylation. J Bacteriology 1996;178(8) 2186-2195.

[59] Spiers AJ, Bohannon J, Gehrig SM, Rainey PB. Biofilm formation at the air–liquid interface by the *Pseudomonas fluorescens* SBW25 wrinkly spreader requires an acetylated form of cellulose. Mol Microbiol 2003;50(1) 15-27.

[60] Spiers AJ, Rainey PB. The *Pseudomonas fluorescens* SBW25 wrinkly spreader biofilm requires attachment factor, cellulose fibre and LPS interactions to maintain strength and integrity. Microbiology 2005;151(9) 2829-2839.

[61] Zevenhuizen LP, Bertocchi C, Van Neerven AR. Congo red absorption and cellulose synthesis by *Rhizobiaceae*. Antonie Van Leeuwenhoek 1986;52(5) 381-386.

[62] Hoshino E, Wada Y, Nishizawa K. Improvements in the hygroscopic properties of cotton cellulose by treatment with an endo-type cellulase from *Streptomyces* sp. KSM-26. J Biosci Bioeng 1999;88(5) 519-525.

[63] Schrecker ST, Gostomski PA. Determining the water holding capacity of microbial cellulose. Biotechnol Lett 2005;27(19) 1435-1438.

[64] Rocchetta HL, Burrows LL, Lam JS. Genetics of O-antigen biosynthesis in *Pseudomonas aeruginosa*. Microbiol Molec Biol Rev 1999;63(3) 523-553.

[65] Benziman M, Haigler CH, Brown RM, White AR, Cooper KM. Cellulose biogenesis: polymerization and crystallization are coupled processes in *Acetobacter xylinum*. PNAS (USA) 1980;77(11) 6678-6682.

[66] Bailey J, Manoil C. Genome-wide internal tagging of bacterial exported proteins. Nat Biotechnol 2002;20(8) 839-842.

[67] Bantinaki B, Kassen R, Knight CG, Robinson Z, Spiers AJ, Rainey PB. Adaptive divergence in experimental populations of *Pseudomonas fluorescens.* III. Mutational origins of Wrinkly Spreader diversity. Genetics 2007;176(1) 441-453.

[68] Bren A, Eisenbach M. How signals are heard during bacterial chemotaxis: protein-protein interactions in sensory signal propagation. J Bacteriol 2000;182(24) 6865-6873.

[69] Malone JG, Williams R, Christen M, Jenal U, Spiers AJ, Rainey PB. The structure–function relationship of WspR, a *Pseudomonas fluorescens* response regulator with a GGDEF output domain. Microbiology 2007;153(4) 980-994.

[70] Goymer PJ. The role of the WspR response regulator in the adaptive evolution of experimental populations of *Pseudomonas fluorescens* SBW25. DPhil thesis. University of Oxford; 2002.

[71] Goymer P, Kahn SG, Malone JG, Gehrig SM, Spiers AJ, Rainey PB. Adaptive divergence in experimental populations of *Pseudomonas fluorescens*. II. Role of the GGDEF regulator WspR in evolution and development of the Wrinkly Spreader phenotype. Genetics 2006;173(2) 515-526.

[72] McDonald MJ, Gehrig SM, Meintjes PL, Zhang X, Rainey PB. Adaptive Divergence in experimental populations of *Pseudomonas fluorescens*. IV. Genetic constraints guide evolutionary trajectories in a parallel adaptive radiation. Genetics 2009;183(3) 104-1053.

[73] Koza A, Hallett PD, Moon CD, Spiers AJ. Characterization of a novel air–liquid interface biofilm of *Pseudomonas fluorescens* SBW25. Microbiology 2009;155(5) 1397-1406.

[74] Nelson KE, Weinel C, Paulsen IT, Dodson RJ, Hilbert H, Martins Dos Santos VA, Fouts DE, Gill SR, Pop M, Holmes M, Brinkac L, Beanan M, Deboy RT, Daugherty S, Kolonay J, Madupu R, Nelson W, White O, Peterson J, Khouri H, Hance I, Chris Lee P, Holtzapple E, Scanlan D, Tran K, Moazzez A, Utterback T, Rizzo M, Lee K, Kosack D, Moestl D, Wedler H, Lauber J, Stjepandic D, Hoheisel J, Straetz M, Heim S, Kiewitz C, Eisen JA, TImmis KN, Düsterhöft A, Tümmler B, Fraser CM. Complete genome sequence and comparative analysis of the metabolically versatile *Pseudomonas putida* KT2440. Environ Microbiol 2002;4(12) 799-808.

[75] Buell CR, Joardar V, Lindeberg M, Selengut J, Paulsen IT, Gwinn ML, Dodson RJ, Deboy RT, Durkin AS, Kolonay JF, Madupu R, Daugherty S, Brinkac L, Beanan MJ, Haft DH, Nelson WC, Davidsen T, Zafar N, Zhou L, Liu J, Yuan Q, Khouri H, Fedorova N, Tran B, Russell D, Berry K, Utterback T, Van Aken SE, Feldblyum TV, D'Ascenzo M, Deng WL, Ramos AR, Alfano JR, Cartinhour S, Chatterjee AK, Delaney TP, Lazarowitz SG, Martin GB, Schneider DJ, Tang X, Bender CL, White O, Fraser CM, Collmer A. The complete genome sequence of the Arabidopsis and tomato pathogen *Pseudomonas syringae* pv. *tomato* DC3000. PNAS (USA) 2003;100(18) 10181-10186.

[76] Nielsen L, Li X, Halverson LJ. Cell-cell and cell-surface interactions mediated by cellulose and a novel exopolysaccharide contribute to *Pseudomonas putida* biofilm

formation and fitness under water-limiting conditions. Environ Microbiol 2011;13(5) 1342-1356.

[77] Fett WF, Osman SF, Dunn MF. Characterization of exopolysaccharides produced by plant-associated fluorescent pseudomonads. Appl Envir Microbiol 1989;55(3) 579-583.

[78] Friedman L, Kolter R. Genes involved in matrix formation in *Pseudomonas aeruginosa* PA14 biofilms. Molec Microbiol 2004;51(3) 675-690.

[79] Ramsey DM, Wozniak DJ. Understanding the control of *Pseudomonas aeruginosa* alginate synthesis and the prospects for management of chronic infections in cystic fibrosis. Molec Microbiol 2005;56(2) 309-322.

[80] Byrd MS, Sadovskaya I, Vinogradov E, Lu H, Sprinkle AB, Richardson SH, Ma L, Ralston B, Parsek MR, Anderson EM, Lam JS, Wozniak DJ. Genetic and biochemical analyses of the *Pseudomonas aeruginosa* Psl exopolysaccharide reveal overlapping roles for polysaccharide synthesis enzymes in Psl and LPS production. Mol Microbiol 2009;73(4) 622-638.

[81] National Center for Biotechnology Information (USA). http://www.ncbi.nlm.nih.gov.

[82] Larkin MA, Blackshields G, Brown NP, Chenna R, McGettigan PA, McWilliam H, Valentin F, Wallace IM, Wilm A, Lopez R, Thompson JD, Gibson TJ, Higgins DG. Clustal W and Clustal X version 2.0. Bioinformatics 2007;23(21) 2947-2948.

[83] Kimura S, Chen HP, Saxena IM, Brown RM, Itoh T. Localization of c-*di*-GMP-binding protein with the linear terminal complexes of *Acetobacter xylinum*. J Bacteriol 2001;183(19) 5668-5674.

[84] Giddens SR, Jackson RW, Moon CD, Jacobs MA, Zhang X-X, Gehrig SM, Rainey PB. Mutational activation of niche-specific genes provides insight into regulatory networks and bacterial function in a complex environment. PNAS (USA) 2007;104(46) 18247-18252.

[85] Gal M, Preston GM, Massey RC, Spiers AJ, Rainey PB. Genes encoding a cellulosic polymer contribute toward the ecological success of *Pseudomonas fluorescens* SBW25 on plant surfaces. Molec Ecol 2003;12(11) 3109-3121.

[86] Jenal U, Malone J. Mechanisms of cyclic-di-GMP signaling in bacteria. Ann Rev Genet 2006;40 385-407.

[87] Hengge R. Principles of c-*di*-GMP signalling in bacteria. Nat Rev Microbiol 2007;7(4) 263-273.

[88] Dasgupta N, Ferrell EP, Kanack KJ, West SE, Ramphal R. *fleQ*, the gene encoding the major flagellar regulator of *Pseudomonas aeruginosa*, is sigma70 dependent and is downregulated by Vfr, a homolog of *Escherichia coli* cyclic AMP receptor protein. J Bacteriol 2002;184(19) 5240-5250.

[89] Hickman JW, Harwood CS. Identification of FleQ from *Pseudomonas aeruginosa* as a c-*di*-GMP-responsive transcription factor. Mol Microbiol 2008;69(2) 376-389.

[90] Baynham PJ, Ramsey DM, Gvozdyev BV, Cordonnier EM, Wozniak DJ. The *Pseudomonas aeruginosa* ribbon-helix-helix DNA-binding protein AlgZ (AmrZ) controls twitching motility and biogenesis of type IV pili. J Bacteriol 2006;188(1) 132-140.

[91] Lenski RE, Rose MR, Simpson SC, Tadler SC. Long-term experimental evolution in *Escherichia coli*. I. Adaptation and divergence during 2,000 generations. Am Nat 1991;138(6) 1315-1341.

[92] Flemming H-C, Wingender J. The biofilm matrix. Nat Rev Microbiol 2010;8(9) 623-633.

[93] Meyer R, Kassen R. The effects of competition and predation on diversification in a model adaptive radiation. Nature 2007;446(7134) 432-435.

Анотація: *Виробництво бактеріальної целюлози та утворення біоплівки на інтерфейсі повітря-рідина було вперше описано у 1886 році для Bacterium xylinum. Через 116 років ми все вивчаємо особливості бактеріальної целюлози в, зокрема, еволюційному аспекті у Pseudomonas fluorescens SBW25 Wrinkly Spreader (WS). Зрозуміло, що цей тип утворення біоплівки є звичайним явищем серед вільноіснуючих псевдомонад, багато з яких також використовують целюлозу як основний компонент матриксу біоплівки. Адаптивна перевага утворення біоплівки на основі целюлозного матриксу SBW25 у статичних мікрокосмах добре вивчена, але її ефективність у природних середовищах і справжня функція целюлози мало досліджена і ще не зрозуміла. Можливо, бактеріальна целюлоза використовується для утворення невеликих біоплівок у водоймах, утримуючи бактерії інтерфейсу повітря-рідина або для утримання їх на твердих поверхнях проти течії води. Целюлозні волокна можуть протистояти стресу висихання в середовищах з обмеженим вмістом води або навіть забезпечувати захист від хижаків протистів і нематод. Звичайно можливо, що целюлоза виконує ряд функцій, якими можна пояснити широке поширення оперону синтезу целюлози серед Proteobacter, які мешкають у різноманітних середовищах.*

3.2. Роль целюлози у структурі біоплівок *Bordetella* spp.

Bordetella avium - збудник бордетеллезу (трахеобронхіт), який викликає дуже заразне захворювання верхніх дихальних шляхів хвороб домашніх і диких птахів (52-54). *B. avium* також є умовно-патогенним мікроорганізмом людини, який також може бути пов'язаний з муковісцидозом (55-57). Він філогенетично відрізняється від *Bordetella bronchiseptica, Bordetella parapertussis* та *Bordetella pertussis*, які є респіраторними збудниками ссавців, хоча *B. avium* експресує подібні фактори вірулентності, а також продукує біоплівки. Однак, хоча полісахарид (Bps) бордетели було ідентифіковано як головний матриксовий біополімер *у B. bronchiseptica* RB50 і *B. pertussis* 536 (58, 59), у біоплівці *B. avium* його не булознайдено. Також не було знайдено *bps*-подібний оперон у геномі вірулентного ізоляту з індика *B. avium* 197N (60, 61). Таким чином, питання який матриксовий полімер є головним при утворенні біоплівки бордетелою під час інфікування господаря або при колонізації інших транзиторних екологічних ніш залишається відкритим.

Нами було з'ясовано, що в анотованому геномі *B. avium* 197N (62) є потенційна бактеріальна синтаза целюлози (*bcs*) оперон (гени BAV2632-2623). Оперони *Bcs* були ідентифіковані в геномах широкого спектру протеобактерій, але експресія целюлози була підтверджена для відносно небагатьох штамів, серед яких патогени і коменсали шлунково-кишкового тракту людини, а також псевдомонади, що асоційовані із ґрунтами і рослинами (51, 63, 64). Функціональна роль целюлози у поведінці бактерій вивчена недостатньо (51). Відомо, що целюлоза важлива для утворення біоплівки в епітелії кишечника та для інвазії епітеліальних клітин і макрофагів (64). Також відомо, що целюлоза може бути важливою при колонізації ґрунтів і рослин, де вона може допомогти зменшити стрес від дефіциту води (65-67). Вірогідно, целюлоза може сприяти виживаності у природному середовищі під час передачі штаму між господарями (63).

В нашій роботи ми намагались з'ясувати чи не використовує *B. avium* 197N целюлозу як один з інструментів екологічної стратегії виживання в різноманітних середовищах існування. Цікаво, що субодиниці оперону *bcs* у *B. avium* 197N демонструють близьку амінокислотну послідовність з тими, що містяться в псевдомонадах, зокрема штамом *Pseudomonas fluorescens* SBW25, що асоційований із ґрунтом і рослинами (анотований як *wssA-J*, PFLU0300-0309), незважаючи на те, що *Bordetellae* і *Pseudomonas* віддалено споріднені роди. Оперони *B. avium* 197N і *P. fluorescens* SBW25 *bcs* також подібні через включення субодиниць, що відповідають за ацетилювання целюлози. Такі субодиниці спочатку описані для *P. fluorescens* SBW25 (WssF-I). Повідомляється, що бідки, що відповідають за ацетилювання, впливають на морфологію колонії та біоплівки інтерфейсу П-Р, які розвиваються в статичному мікрокосму (45). Ці субодиниці загалом рідко

зустрічаються у природі, але вони інколи присутні серед патогенів рослин, включаючи *Pseudomonas syringae* pv. *tomato* DC3000, але не в *Pseudomonas putida* KT2440, яка колонізує споріднену еконішу (51).

Також повідомлялося, що *B. avium* 197N виробляє обмежену біоплівку в зоні меніска у статичних середовищах (68). Тому нами було вирішено використати підхід статичного мікросвіту для дослідження біолівок *B. avium* 197N. Через те, що ми спостерігали низький рівень експресії целюлози у зразках біоплівки *B. avium* 197N дикого типу та в агаризованих колонія, ми сконструювали мутант з дефіцитом продукції целюлози (CD) і продемонструвати, що целюлоза не є критичним компонентом матриксу біоплівки, що свідчить про те, що *B. avium* 197N використовує для цієї мети інший неідентифікований екзополімер.

Основні результати, отримані в цьому підрозділі дисертації опубліковані в роботі автора (69).

Research in Microbiology 168 (2017) 419–430
www.elsevier.com/locate/resmic

Original Article

Biofilm formation and cellulose expression by *Bordetella avium* 197N, the causative agent of bordetellosis in birds and an opportunistic respiratory pathogen in humans

Kimberley McLaughlin [a,2], Ayorinde O. Folorunso [a,2], Yusuf Y. Deeni [a], Dona Foster [b], Oksana Gorbatiuk [c], Simona M. Hapca [a], Corinna Immoor [a], Anna Koza [a,1], Ibrahim U. Mohammed [a], Olena Moshynets [c], Sergii Rogalsky [d], Kamil Zawadzki [a], Andrew J. Spiers [a,*]

[a] *School of Science, Engineering and Technology, Abertay University, Bell Street, Dundee DD1 1HG, UK*
[b] *Department of Biological and Life Sciences, Oxford Brookes University, Gipsy Lane, Headington, Oxford OX3 0BP, UK*
[c] *Institute of Molecular Biology and Genetics of the National Academy of Sciences of Ukraine, 150 Zabolotnoho Street, Kiev 03680, Ukraine*
[d] *Institute of Bioorganic Chemistry and Petrochemistry of the National Academy of Sciences of Ukraine, 50 Kharkivske Schose, Kiev 02160, Ukraine*

Received 17 November 2016; accepted 16 January 2017
Available online 26 January 2017

Abstract

Although bacterial cellulose synthase (*bcs*) operons are widespread within the *Proteobacteria* phylum, subunits required for the partial-acetylation of the polymer appear to be restricted to a few γ-group soil, plant-associated and phytopathogenic pseudomonads, including *Pseudomonas fluorescens* SBW25 and several *Pseudomonas syringae* pathovars. However, a *bcs* operon with acetylation subunits has also been annotated in the unrelated β-group respiratory pathogen, *Bordetella avium* 197N. Our comparison of subunit protein sequences and GC content analyses confirms the close similarity between the *B. avium* 197N and pseudomonad operons and suggests that, in both cases, the cellulose synthase and acetylation subunits were acquired as a single unit. Using static liquid microcosms, we can confirm that *B. avium* 197N expresses low levels of cellulose in air–liquid interface biofilms and that biofilm strength and attachment levels could be increased by elevating c-*di*-GMP levels like the pseudomonads, but cellulose was not required for biofilm formation itself. The finding that *B. avium* 197N is capable of producing cellulose from a highly-conserved, but relatively uncommon *bcs* operon raises the question of what functional role this modified polymer plays during the infection of the upper respiratory tract or survival between hosts, and what environmental signals control its production.
© 2017 Institut Pasteur. Published by Elsevier Masson SAS. All rights reserved.

Keywords: Air–liquid interface; Biofilm; *Bordetella avium*; c-*di*-GMP; Cellulose; Microcosm

1. Introduction

Bordetella avium is the causative agent of bordetellosis (tracheobronchitis), a highly contagious upper respiratory disease of domesticated and wild birds [1–3], as well as an opportunistic human pathogen that may also be associated with cystic fibrosis [4–6]. It is phylogenetically distinct from *Bordetella bronchiseptica*, *Bordetella parapertussis*, and *Bordetella pertussis*, which are respiratory pathogens of mammals, though *B. avium* expresses similar virulence factors

* Corresponding author. School of Science, Engineering and Technology, Abertay University, Bell Street, Dundee DD1 1HG, UK.
E-mail address: a.spiers@abertay.ac.uk (A.J. Spiers).
[1] Current address: Technical University of Denmark, Novo Nordisk Foundation Center for Biosustainability, Kemitorvet, Building 220, 2800 Kgs. Lyngby, Denmark.
[2] Contributed equally to this work and are the co-first authors.

http://dx.doi.org/10.1016/j.resmic.2017.01.002
0923-2508/© 2017 Institut Pasteur. Published by Elsevier Masson SAS. All rights reserved.

and also produces biofilms. However, whilst *Bordetella* polysaccharide (Bps) has been identified as the primary matrix component in *B. bronchiseptica* RB50 and *B. pertussis* 536 biofilms [7,8], it has not been reported for *B. avium* biofilms, nor has a *bps*-like operon been found in the genome of the virulent turkey isolate *B. avium* 197N [9–11]. This raises the question of what extracellular polymeric substance (EPS) or substances are used as the biofilm matrix during host infection or colonisation of other environments during transmission between hosts.

We have noted that the *B. avium* 197N genome [11] has been annotated with a potential bacterial cellulose synthase (*bcs*) operon (genes BAV2632-2623) (Fig. 1). *Bcs* operons have been identified in the genomes of a wide range of *Proteobacteria*, but cellulose expression per se has been reported for relatively few strains, including human gastrointestinal commensals and pathogens, and soil and plant-associated pseudomonads [12–14]. Although the functional role and fitness value of cellulose is poorly understood [13–15], it is associated with biofilm formation in the intestinal epithelium and invasion of epithelial cells and macrophages [14], and provides a fitness advantage in soils and plant environments where it may help reduce water stress [16–19]. More generally, cellulose may promote survival in natural environments during transmission between hosts [12].

We are interested in determining whether *B. avium* 197N is capable of expressing cellulose as part of a greater understanding of the functional role of cellulose in a range of environments and life strategies. Unusually, the *B. avium* 197N *bcs* operon subunits show close amino acid sequence homology with those found in pseudomonads, particularly the soil and plant-associated *Pseudomonas fluorescens* SBW25 (annotated as *wssA–J*, PFLU0300-0309 [20], Fig. 1), despite the fact that the *Bordetellae* and *Pseudomonas* are distantly related genera.

The *B. avium* 197N and *P. fluorescens* SBW25 *bcs* operons are further linked by the inclusion of cellulose acetylation-associated subunits originally described for *P. fluorescens* SBW25 (WssF–I), which affects colony morphology and air–liquid (A–L) interface biofilms that develop in static microcosms [20,21]. These subunits are rarely seen, but are present in a number of plant pathogens, including *Pseudomonas syringae* pv. *tomato* DC3000, but not, for example, the closely-related soil-associated *Pseudomonas putida* KT2440 [13,21,22] (Fig. 1). Cellulose is also expressed by *P. putida* KT2400 and *P. syringae* DC3000 in similar conditions [19,23], and static microcosms have been used to investigate biofilm-formation more widely amongst the pseudomonads [23,24] where biofilms can be quantitatively measured by combined growth, strength and attachment assays [24,25].

B. avium 197N has also been reported to produce limited biofilms at the meniscus of static liquids [26,27]. We therefore decided to use a static microcosm approach to characterise *B. avium* 197N biofilm formation more fully under a range of growth conditions. Although low levels of cellulose expression was observed in wild-type *B. avium* 197N biofilm samples and colonies, we constructed a cellulose-deficient (CD) mutant to demonstrate that cellulose was not an essential matrix component for biofilm-formation, suggesting that *B. avium* 197N utilises another but unidentified EPS for this purpose.

2. Materials and methods

2.1. Bioinformatics

Bacterial cellulose synthase subunit homologues were identified in *Proteobacteria* complete genomes using NCBI

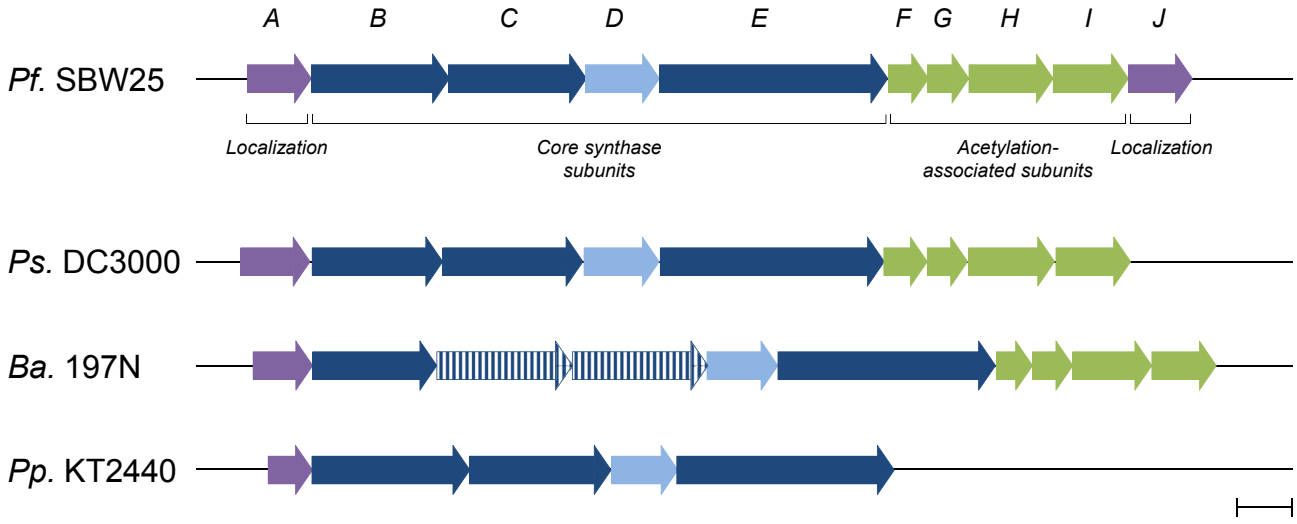

Fig. 1. **Bacterial cellulose synthase (*bcs*) operon structures**. *Bcs* operons have been identified in the whole-genome sequences of a wide range of bacteria. In *P. fluorescens* SBW25 the genes are annotated as *wssA–J* and are predicted to form the core cellulose synthase complex (dark blue) including an endoglucanase (light blue) and associated acetylation subunits (green), and to be involved in the localization of the complex at the periplasmic membrane (mauve) (top section). Shown also are the *bcs* operons of *P. putida* KT2400, *P. syringae* DC3000 and *B. avium* 197N, which also contains a duplication of a truncated version of *wssC* (blue stripes). The scale bar indicates 1 kb. (For interpretation of the references to colour in this figure legend, the reader is referred to the web version of this article.)

TBLASTN and *P. fluorescens* SBW25 WssA–J protein query sequences (Accession numbers AAL71841–AAL71850) following the selection criteria described in Supplementary Methods. A WspR homologue was identified in the *B. avium* 197N genome using *P. fluorescens* SBW25 WspR (AAL71852). Phylogenetic trees were produced using the NCBI COBALT multiple sequence alignment tool and the Neighbour Joining (NJ) method (see Suppl. Methods). Gene and whole genomic GC content data were obtained from the *Pseudomonas* Genome Database (www.pseudomonas.com) and NCBI Genbank. DNA dot plots were produced using the YASS Genomic Similarity Search Tool (bioinfo.lifl.fr).

2.2. Bacteria and plasmids

Bacteria and plasmids used in this work are listed in Table 1. All strains were kept at −80 °C for long-term storage, and stocks produced by adding 15% (v/v) glycerol to over-night cultures. *B. avium* 197N was acquired directly from the American Type Culture Collection (ATCC BAA-1003). Antibiotic susceptibility was assessed using antibiotic disks (MAST, UK). Kanamycin (Km) sensitivity [10] was confirmed using LB plates containing 100 μg ml^{-1} Km incubated at 28 °C for 48 h.

2.3. Culturing conditions

Bacteria were cultured at 20, 28, 37, and 42 °C using Brain Heart Infusion (BHI; Oxoid, UK), King's B (KB; 20 g proteose peptone No. 3 (BD Biosciences, UK), 10 g glycerol, 5 g K_2HPO_4, 1.5 g $MgSO_4$ per litre) and Luria–Bertani (LB; 10 g NaCl, 10 g tryptone (Oxoid), and 5 g yeast extract (Merck, UK) per litre) media with 1.5% (w/v) Agar Technical (Oxoid) for plates and antibiotics added as required. Overnight shaken cultures were used to provide inocula for experiments. Microcosms were 30 ml glass tubes containing 6 ml growth media [23]. Swimming motility was assessed using soft-agar LB plates (see Suppl. Methods).

2.4. Biofilm formation in static microcosms

Microcosms inoculated with 100 μl aliquots of culture and incubated statically were inspected daily for up to 5 days for signs of A–L interface biofilm-formation, and then by pouring out into Petri dishes to assess strength and attachment [23]. Biofilms were quantitatively characterised using the combined biofilm assay in which replicate microcosms ($n = 8$) were tested for biofilm strength (grams) using small glass balls, biofilm attachment to the tube walls by staining with crystal violet (A_{570}) and total growth by OD_{600} measurements [24,25]. These assays were conducted for a number of strains, media and temperatures, and data sets analysed using a general linear model (GLM) approach.

2.5. Cellulose expression

Cellulose was assessed using Congo red plates and by fluorescent microscopy. Congo red plates were BHI, KB, and LB (without NaCl) plus 0.001% (w/v) Congo red [21], and were drop-inoculated with 5 μl aliquots of culture and incubated for 2–3 days. Images were taken using a Nikon D3200 DSLR camera. Samples of colonies and biofilm material were stained with 10 μg ml^{-1} calcofluor for 1 h before viewing at 10×–40× magnification using a Leica DMR fluorescent microscope and imaging with an AxioCam MRc digital camera [21,28]. Semi-purified biofilm matrix samples were investigated by ELISA using a cellulose binding domain-containing (SPA-CBD) fusion protein [29] as

Table 1
Bacteria and plasmids.

Strains and plasmids	Comment	Source/reference
Bordetella avium 197N	Wild-type strain (ATCC BAA-1003), Km^S, Tc^{Sa}	ATCC [9,10]
Ba. 197N cellulose deficient (CD) mutant	*Ba.* 197N::*wssB*::ISΩ-Km/hah constructed using pAS296, Km^R	This work
Escherichia coli K12 DH5α	Standard host for maintaining plasmids	Gibco-BRL, UK
Pseudomonas fluorescens SBW25	Wild-type strain expressing low-levels of cellulose and producing a weak, viscous mass (VM)-class biofilm	[42]
Pf. SBW25 wrinkly spreader (WS) mutant	*Pf.* SBW25 *wssF* (S301R) over-expressing cellulose and producing a robust, physically cohesive (PC)-class biofilm	[20]
pAS296	Suicide plasmid designed to disrupt *Pf.* SBW25 *wss*-like *bcs* operons derived from pNR9.3, Km^R	This work
pNR9.3	A self-replicating *wssB*::IS-Ω-Km/hah mini-transposon construct, Km^R	S. Giddens
pVSP61-Tc	A modified version of the pVSP61 broad host-range cloning vector, Km^R and Tc^R	[28,41]
pVSP61-WspR9-Tc	pVSP61-Tc expressing the dominant-negative diguanylate cyclase mutant, WspR9 (G296R), Km^R and Tc^R	[41]
pVSP61-WspR12-Tc	pVSP61-Tc expressing the wild-type diguanylate cyclase, WspR12, Km^R and Tc^R	[28,41]
pVSP61-WspR19-Tc	pVSP61-Tc expressing the constitutively-active diguanylate cyclase mutant, WspR19 (R129C), Km^R and Tc^R	[28,41]

All plasmids were maintained in *Ec.* K12. ATCC, American Type Culture Collection. Km and Tc were used at 50 and 12.5 μg ml^{-1}, respectively, to select for plasmids in *Ec.* K12, and at 100 and 12.5 μg ml^{-1} for *Ba.* 197N strains, respectively.

[a] Antibiotic susceptibility using MASTRING M13, M14, and M51 disks was determined for *Ba.* 197N (S, Sensitive; R, Resistant): Ampicillin (R), Cephalexin (R), Cephalthin (R), Chloramphenicol (S), Ciprofloxacin (R), Coliston sulphate (S), Cotrimoxazole (R), Erythromycin (R), Fusidic acid (R), Gentamycin (S), Nalidixic acid (R), Nitrofurantoin (R), Novobiocin (R), Oxacillin (R), Penicillin (R), Streptomycin (S), Tetracycline (S), Trimethoprim (R) (these are in agreement with [33]).

described in the Suppl. Methods. Biofilm samples were also investigated by Fourier transform infrared spectroscopy (FTIR) and visualised by scanning electron microscopy (SEM) (see Suppl. Methods).

2.6. Construction of pAS296 and the cellulose-deficient (CD) mutant

The suicide plasmid pAS296 was designed to disrupt *bcs* operons by homologous recombination of a *P. fluorescens* SBW25 mini-transposon *wssB*::IS-Ω-Km/hah (Km^R) cassette (the insertion is located 1693 bp from the start of the 2219 bp *wssB* gene). This was integrated into the *B. avium* 197N chromosome following kanamycin selection to produce the cellulose-deficient (CD) mutant (see Suppl. Methods).

2.7. Statistical analyses and modelling

Quantitative assays were undertaken with replicates, and means with standard errors (SE) are shown where appropriate. Data were analysed using JMP v12 (SAS Institute Inc., USA) statistical software. A general linear model (GLM) approach was used to investigate the significance of strain, test media, growth and attachment (effects) on biofilm strength (response) using the combined biofilm assay dataset. Attachment levels were also modelled as response. Significant effects were examined by LSMeans Differences Student's *t*-test and Tukey HSD tests, and associations examined by pairwise correlations. Differences between means were also tested by ANOVA, *t*-tests and Turkey-Kramer HSD tests.

3. Results and discussion

3.1. Bacterial cellulose synthase (bcs) operons within the Proteobacteria

We identified over 100 bacterial whole genome sequences likely to contain fully functional *bcs* operons based on amino acid sequence homologies to the core cellulose synthase subunits of *P. fluorescens* SBW25 (Fig. 1 and data not shown), and it is noteworthy that such a poorly reported or tested phenotype such as the ability to express cellulose is so commonly annotated amongst the *Proteobacteria*. Within this phylum, species from one α-group, two β-group and ten γ-group genera were found to have convincing *bcs* operons (see Suppl. Table S1). As expected, the organisation of these operons, in terms of gene order and orientation, was highly variable [14], though phylogenetic-based clustering at the genus or family levels was seen in Neighbour-Joining (NJ) trees constructed using core subunit sequences. An example of one NJ tree generated using WssB homologues (see Suppl. Table S2) and rooted using α-group *Proteobacteria* is given in Fig. 2. The phylogenetic-based clustering of homologues seen here suggests that most sequence variation in core subunits is probably acquired through vertical transmission. However, the close branching of distantly related genera such as the *Bordetellae* and *Pseudomonas* in these trees suggests that *bcs* operons may have been horizontally transmitted at an early stage in the radiation of the *Proteobacteria*.

We note the increasing number of plant pathogens including *Burkholderia* (β-group), *Dickeya*, and *Pseudomonas* (γ-group) spp., and animal pathogens including *Bordetella* (β-group), *Escherichia*, *Klebsiella*, *Salmonella* and *Shigella* (γ-group) spp., encode *bcs* operons and are likely to express cellulose (Suppl. Table S1). Although these pathogens have diverse hosts and survive in a wide range of environments, cellulose might play a common role in single cell attachment, microcolony and biofilm formation, and protection against predation, disturbance or stress [13,14].

3.2. The bcs operon in B. avium 197N

Following our survey of *bcs* operons within the *Proteobacteria*, we shifted our attention to the operon annotated in the *B. avium* 197N genome. The link between this avian and opportunistic human respiratory pathogen [9–11] and the soil- and plant-associated pseudomonads is intriguing, because of the high levels of *bcs* subunit homology with *P. fluorescens* SBW25 and the presence of the rarely seen cellulose acetylation-associated subunits apparently restricted to *P. fluorescens* SBW25 and a number of related plant pathogens, including *P. syringae* DC3000 [21,22].

The *B. avium* 197N *bcs* operon is also notable, as in NJ trees, the WssBCDE homologues from *B. avium* 197N, *P. fluorescens* SBW25 and *P. syringae* DC3000 were always clustered together, but distant from the *P. putida* KT2400 homologues (see also [22]). A representative NJ tree for WssB homologues is shown in Fig. 2 and a comparison of WssA–I homologues provided in Table 2.

However, the *B. avium* 197N *bcs* operon differs significantly from the *P. fluorescens* SBW25, *P. putida* KT2400 and *P. syringae* DC3000 operons by the duplication of WssC (annotated as WssC1 and WssC2), which challenges our presumption that this bacterium could express cellulose. Although the duplication is apparent in an alignment of the *B. avium* 197N and *P. fluorescens* SBW25 genomic sequences, WssC1 and WssC2 are not direct copies of one another and share only 47% identity at the protein level (97% coverage, 0.0 E value) (see Suppl. Fig. S1). Furthermore, WssC1 and WssC2 branch separately in a NJ tree containing *P. fluorescens* SBW25, *P. putida* KT2400 and *P. syringae* DC3000 WssC homologues (Suppl. Fig. S1). The alignment of *B. avium* 197N and *P. fluorescens* SBW25 sequences also indicates that the two genomes do not share significant levels of homology beyond the boundaries of the *bcs* operons, suggesting that one or the other acquired the operon by a limited lateral gene transfer event.

A comparison of the GC content of the *bcs* genes indicates that the *B. avium* 197N, *P. fluorescens* SBW25, *P. putida* KT2400 and *P. syringae* DC3000 operons are more similar to one another than they are to the *P. putida* KT2400 operon ($\alpha = 0.05$) (Fig. 3). The mean GC contents of the *bcs* genes of *P. fluorescens* SBW25, *P. putida* KT2400 and *P. syringae* DC3000 were also significantly different from their whole

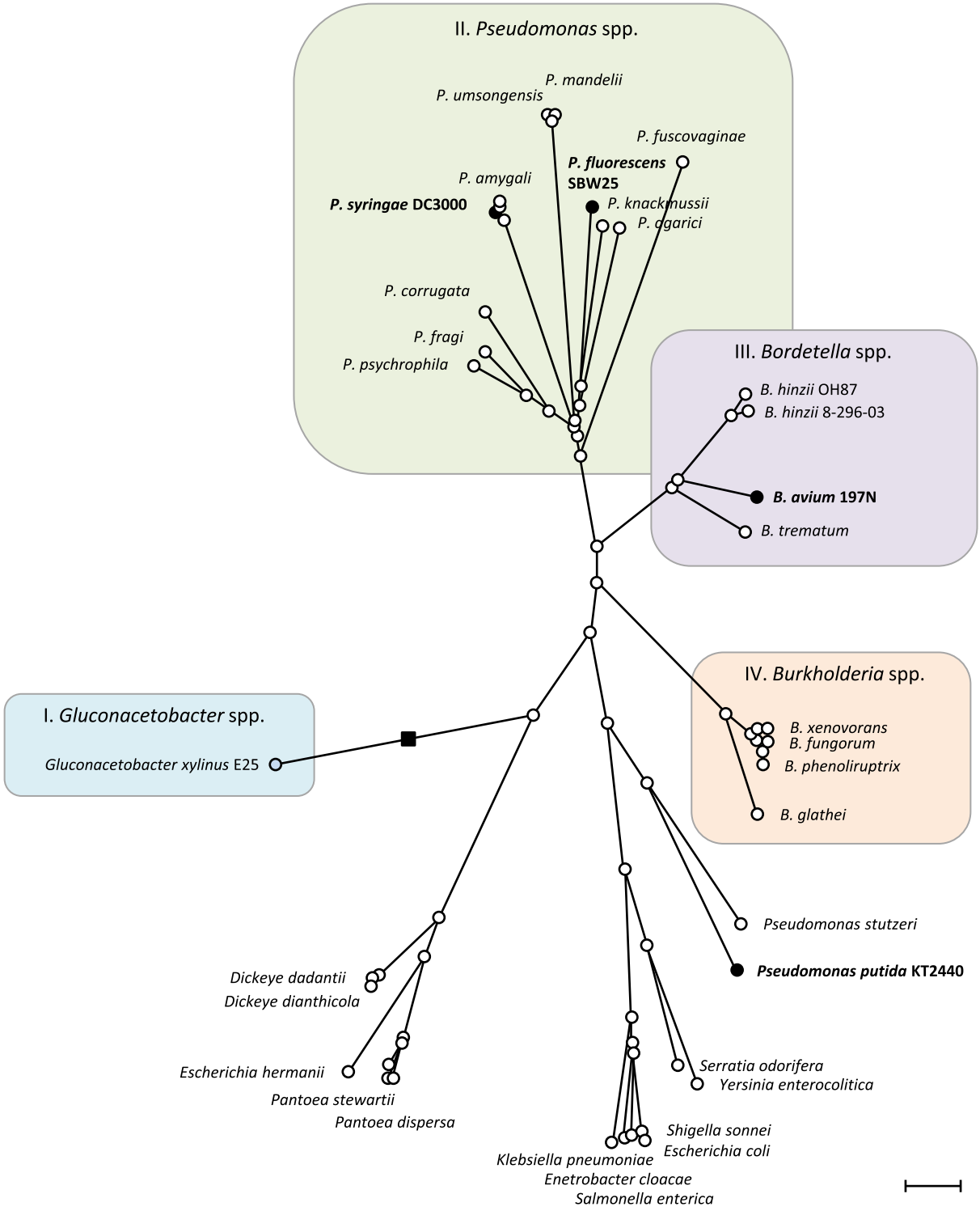

Fig. 2. **Phylogenetic analyses of representative WssB homologues**. Shown here is a phylogenetic tree showing the relationships between WssB proteins from the key strains *B. avium* 197N, *P. fluorescens* SBW25, *P. putida* KT2400 and *P. syringae* DC3000 (bold), as well as a number of other bacteria in which *wss*-like *bcs* operons have been identified. A number of *Komagataeibacter* spp. sequences were used to root the tree (indicated by the black square), and these α-group sequences represented by *Gluconacetobacter xylinus* E25 (light blue) were found to cluster separately from the other β and γ-group sequences. Most γ-group *Pseudomonas* spp. sequences clustered together (light green). Although the β-group sequences root at the base of the *Pseudomonas* spp. cluster, the *Bordetella* spp. sequences including *B. avium* 197N (purple) clustered separately from the *Burkholderia* spp. (light orange). This NJ tree is based on COBALT multiple alignments of the coding sequences listed in Table 1. Some sequences have not been labelled in the tree for clarity. The distance bar indicates 0.1 units. (For interpretation of the references to colour in this figure legend, the reader is referred to the web version of this article.)

Table 2
Homology between *Pf.* SBW25 Wss-like bacterial cellulose synthase (Bcs) complex subunits.

	Feature	Localisation	Core synthase subunits				Acetylation-associated subunits				Localisation
		WssA	WssB	WssC	WssD	WssE	WssF	WssG	WssH	WssI	WssJ
Pseudomonas fluorescens SBW25	PFLU	0300	0301	0302	0303	0304	0305	0306	0307	0308	0309
	Length	344	739	755	436	1279	221	221	468	374	324
	GC content	62.7	63.0	62.0	62.8	63.2	59.8	63.1	62.4	64.5	61.1
Compared with: *Bordetella avium* 197N	BAV	2632	2631	2630/2629[a]	2628	2627	2626	2625	2624	2623	NP
	Length	255	733	764/753	398	1323	221	222	469	389	
	% Identity	36	60	44/51	47	42	56	50	66	51	
	E value	3e−42	0	0/0	9e−116	0	3e−80	3e−52	0	5e−112	
	GC content	61.7	60.4	63.9/61.7	64.3	64.8	58.9	65.2	60.6	63.6	
Pseudomonas putida KT2440	PP	2634	2635	2636	2637	2638	NP	NP	NP	NP	NP
	Length	235	865	760	370	1172					
	% Identity	28	56	34	38	25					
	E value	0.007	0	5e−122	2e−75	3e−44					
	GC content	65.7	64.9	64.3	66.1	65.7					
Pseudomonas syringae DC3000	PSPTO	1026	1027	1028	1029	1030	1031	1032	1033	1034	NP
	Length	381	739	751	403	1230	221	224	471	383	
	% Identity	37	69	57	54	52	71	53	85	62	
	E value	5e−69	0	0	6e−147	0	9e−110	2e−66	0	2e−155	
	GC content	61.0	60.3	61.7	65.0	63.9	60.5	62.5	62.0	63.8	

The following features of the proteins listed are: genome coding sequence (PFLU, BAV, PPU and PSPTO), protein length (amino acids), BLAST % amino-acid identity and E values compared to the *Pf.* SBW25 protein, and GC content of the gene.
[a] *Ba.* 197N has a duplication of *wssC* which is annotated as *wssC2* (BAV2630) and *wssC1* (BAV2629). NP, No homologue present in that gene cluster/operon.

genome GC content ($p \leq 0.0003$), suggesting that these bacteria had acquired the *bcs* operons relatively recently and before much amelioration of divergent sequences could occur. In contrast, no significant difference was observed between the *B. avium* 197N *bcs* genes and whole genome GC content ($p = 0.2033$), suggesting that the transfer event occurred much earlier in this bacterium or that the ancestral *bcs* donor was more similar to the *Bordetellae* than to the pseudomonads. As the GC content of intergenic regions and coding sequences are frequently correlated in bacterial genomes [30], a direct comparison between the GC content of the *bcs* genes with the GC content of all other chromosomally encoded genes is unlikely to produce a substantially different result. However, we have not yet investigated the regions surrounding each of the *bcs* operons, which may show significant differences from the rest of the chromosomes.

Finally, no significant differences were observed between the GC content of core synthase and acetylation-associated genes within operons ($p \geq 0.5085$), and no significant correlations found between GC content and gene order ($p > 0.05$). This suggests that the acetylation-associated genes had been transferred and maintained with the core synthase genes, rather than as subsequent and independently acquired functions.

3.3. B. avium *197N biofilm formation in static microcosms*

Given the close protein homologies and conserved operon structures seen between the *B. avium* 197N *bcs* operon and the *P. fluorescens* SBW25, *P. putida* KT2400 and *P. syringae* DC3000 *bcs* operons, we were interested in determining whether *B. avium* 197N expressed cellulose despite the WssC duplication, and whether it also played a role in A–L interface biofilm formation, as it does for some pseudomonads. As *B. avium* 197N has been reported to form limited biofilms at the meniscus of static liquids [26,27], we decided to use the static microcosm approach we had previously developed to investigate A–L interface biofilm formation by *P. fluorescens* SBW25 and other pseudomonads [13,23,24]. In these, competition for O_2 which is otherwise growth-limiting in the liquid column drives biofilm formation at the liquid surface [31], even in the absence of host-derived factors or environmental signals that might normally regulate such activity, including the expression of biofilm-associated EPS.

In order to determine whether *B. avium* 197N could form biofilms in static microcosms, a range of media and incubation temperatures (BHI, KB and LB; 20–42 °C) were tested, as although *B. avium* 197N is routinely grown in BHI at 37 °C, phenotypic differences have been noted under other conditions [9,10,32,33]. We found clear visual evidence of growth (i.e. culture turbidity) and A–L interface biofilm formation, including culture turbidity, films extending across the A–L interface and sunken debris within three days of incubation under all conditions tested (Fig. 4). The biofilms formed in KB microcosms were particularly obvious and robust, and were characterised as physically cohesive (PC)-class/air–liquid–solid surface (A–L–S) interface-type biofilms [23,24]. In contrast, BHI biofilms were almost transparent with white flecks of material, and LB biofilms were very thin and fragile.

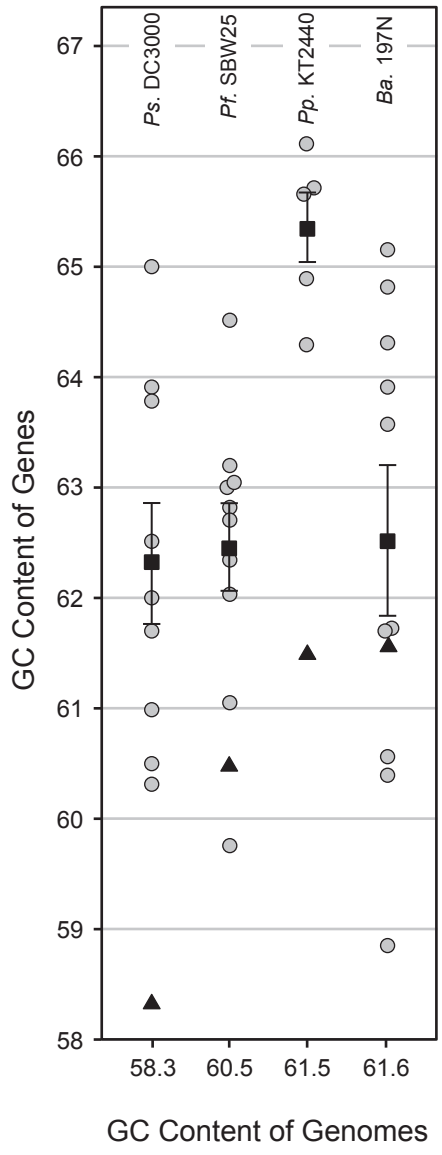

Fig. 3. **GC content of the *bcs* operons**. An analysis of the *bcs* operons from *B. avium* 197N, *P. fluorescens* SBW25, *P. putida* KT2400 and *P. syringae* DC3000 reveals substantial variation in gene GC content within operons. The GC contents of individual genes (grey circles), the mean with SE bars for each operon (squares) and each genome (triangles) are shown. See the main results section for statistical comparisons.

We recovered biofilm material from microcosms and spread it onto plates to investigate colony morphologies. In *P. fluorescens* SBW25 populations, radiation (i.e. mutation) results in significant numbers of biofilm-forming "wrinkly spreaders" (WSs) identifiable by an altered colony morphology [34]. However, only wild-type colony morphologies were observed from 3 day-old *B. avium* 197N biofilm samples, and no other signs of radiation were seen in KB microcosms incubated for up to 15 days (e.g. in siderophore production, colouration, motility, etc.). This suggests that the biofilm formation we observed in experimental static microcosms is the result of a normal physiological response by *B. avium* 197N, rather than the activity of biofilm-producing mutants. Further testing using modified media containing avian tissue-derived signal compounds, cell cultures, tracheal rings or lung tissue will be required to determine whether biofilm formation is a behaviour more specifically associated with host infection or the colonisation of water, plants, and soils during transmission between hosts.

3.4. Quantitative characterisation of the B. avium *197N biofilm*

In order to place *B. avium* 197N A–L interface biofilm formation in static microcosms into context, we compared *B. avium* 197N with wild-type *P. fluorescens* SBW25 and the *P. fluorescens* SBW25 WS mutant using a range of media and a quantitative combined biofilm assay measuring microcosm growth, biofilm strength and attachment levels [24]. Wild-type *P. fluorescens* SBW25 was included, as it produces a poorly attached, fragile biofilm referred to as the VM biofilm [35], whilst the WS produces a robust, well-attached biofilm in KB microcosms [20,21,28,34].

We modelled biofilm strength using a GLM approach, and both strain and medium were found to be significant ($p \leq 0.0001$, see Suppl. Table S3, Model 1); representative data for KB microcosms are shown in Fig. 5. Although the VM and WS biofilms were significantly different from one another, the *B. avium* 197N biofilms were of intermediate strength (Fig. 5B) and could not be differentiated from either the VM or WS biofilms ($\alpha = 0.05$). The strongest *B. avium* 197N biofilms were produced in KB microcosms, and across all three strains, KB biofilms could be differentiated from BHI and LB biofilms ($\alpha = 0.05$) which suggests that biofilm formation was influenced by media composition. Overall growth and biofilm attachment levels were not found to have significant effects on biofilm strength ($p > 0.05$) across the three strains tested in these microcosms. However, in previous work, the VM biofilm has been shown to have significantly lower attachment levels than the WS biofilm [35]. Finally, we also modelled biofilm attachment levels, as biomass at the meniscus is often used as a measure of biofilm growth in microtitre plate-based assays [36]. In this, the strain effect was found to be weakly insignificant ($p = 0.0501$, Suppl. Table S3, Model 2), with the *B. avium* 197N biofilm differentiated from the VM biofilm, but neither from the WS biofilm ($\alpha = 0.05$).

3.5. Cellulose expression by B. avium *197N*

We used the cellulose-binding dye calcofluor and fluorescent microscopy to demonstrate that cellulose fibres were present in *B. avium* 197N colonies and biofilm samples (Fig. 6A). However, relatively little cellulose was observed compared to that reported for VM and WS biofilms [21,35], and none was observed in samples from a cellulose-deficient (CD) mutant we produced by disrupting the *B. avium* 197N *bcs* operon with a *P. fluorescens* SBW25 *wssB*::IS-**Ω**-Km/hah cassette. Additional evidence to support the presence of cellulose at low levels in biofilms was obtained by ELISA using a cellulose binding-domain-containing (SPA-CBD) fusion protein [29]. This showed a 2.5× increase in cellulose levels in

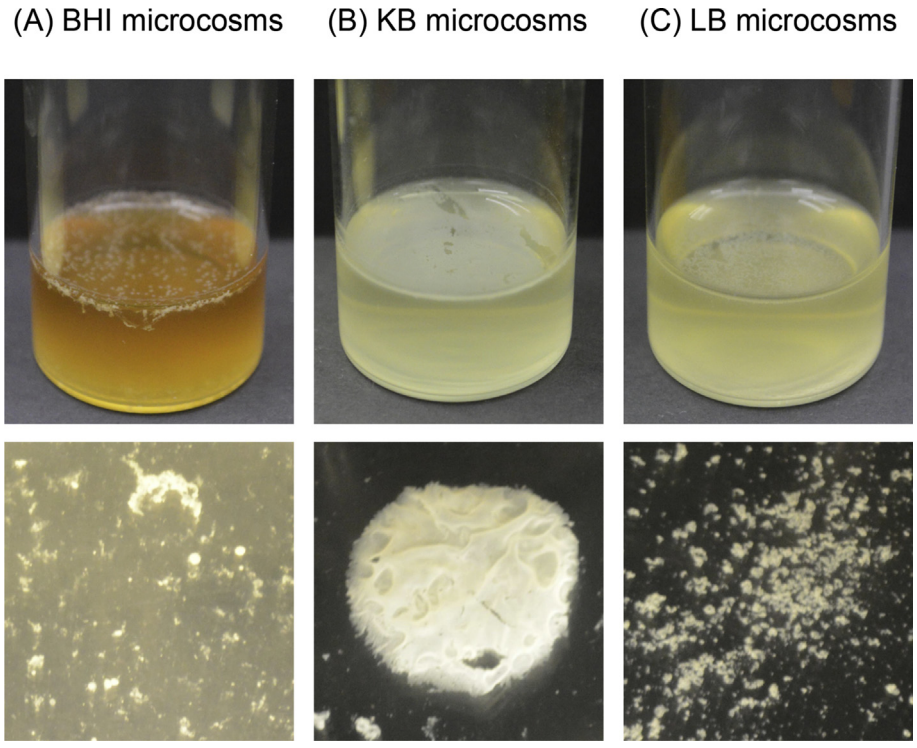

Fig. 4. ***B. avium* 197N forms biofilms at the air–liquid (A–L) interface of static microcosms**. Shown are representative images of *B. avium* 197N biofilms *in* situ in BHI, KB and LB microcosms (A–C, top row) and of biofilm material after pouring into petri dishes (bottom row). Biofilms become progressively more robust with longer incubation periods, but tend to detach from the meniscus region and sink to the bottom of the vials. Microcosms were incubated at 20 °C for three days before imaging.

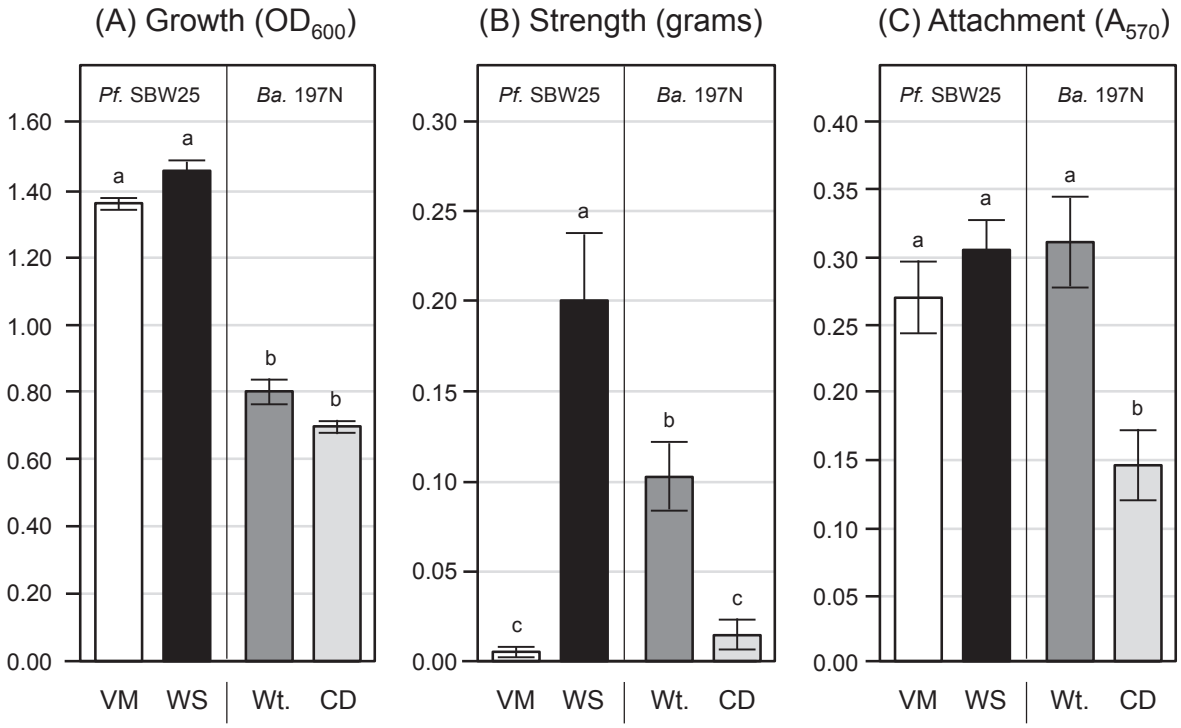

Fig. 5. **The *B. avium* 197N biofilm is intermediate in strength but with high levels of attachment**. Biofilm formation in static microcosms can be quantified by using a combined biofilm assay in which microcosm growth (A), biofilm strength (B) and attachment levels (C) are determined. Shown here are data for *P. fluorescens* SBW25 which produces the VM biofilm (white bars), the WS which produces the WS biofilm (black), *B. avium* 197N (indicated by 'Wt' for wild-type, dark grey), and the *B. avium* 197N cellulose-deficient (CD) mutant (light grey) incubated in KB microcosms at 20 °C for three days before assay. Means and SE are shown. Significant differences between means were observed for growth ($p < 0.0001$), strength ($p < 0.0001$) and attachment ($p = 0.0005$); means within assays not connected by the same letter are significantly different ($\alpha = 0.05$).

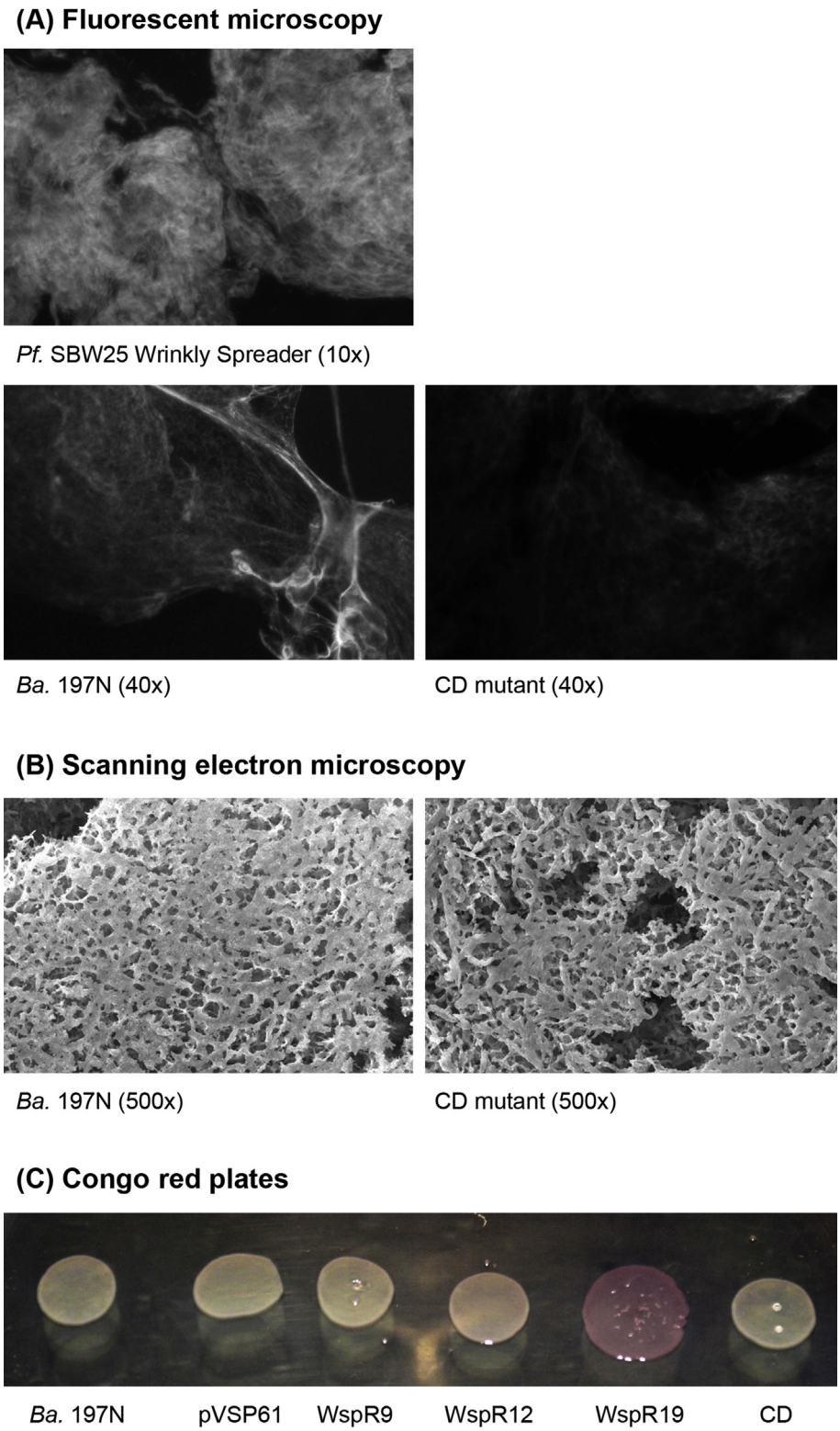

Fig. 6. **Cellulose is expressed by *B. avium* 197N but is not essential for biofilms**. Cellulose fibres forming the matrix of the *P. fluorescens* SBW25 WS mutant are readily visualised by fluorescent microscopy after staining with calcofluor (A). In comparison, only low levels of cellulose expression can be detected in *B. avium* 197N biofilm samples and none in the cellulose-deficient (CD) mutant even at higher magnification. Qualitative comparison of scanning electron microscope images of *B. avium* 197N and CD mutant biofilm samples show no obvious differences in structure (B), suggesting that the presence of cellulose has little apparent impact on biofilm structure. Congo red, which also binds cellulose and other compounds, including proteinaceous attachment factors, stains colonies of *B. avium* 197N expressing the constitutively active diguanylate cyclase WspR19 mutant *in trans* (C). However, little staining is apparent in colonies of wild-type *B. avium* 197N, *B. avium* 197N transformed with pVSP61 (the control plasmid), pVSP61-WspR9, pVSP61-WspR12 or the CD mutant. (For interpretation of the references to colour in this figure legend, the reader is referred to the web version of this article.)

semi-purified biofilm matrix samples samples compared to the CD mutant, though this assay was unreplicated and may need further testing. However, cellulose levels were insufficient for detection by FTIR (see Suppl. Fig. S2). Despite this, significant differences in biofilm strength and attachment levels were found between the *B. avium* 197N and CD mutant biofilms ($\alpha = 0.05$) (Fig. 5). These changes may not necessarily be due to the loss of cellulose in the biofilm per se, but might result from the loss of the cellulose synthase complex which effects other regulatory systems involved in the expression of biofilm matrix components and attachment factors.

We suggest that the low levels of cellulose seen in *B. avium* 197N biofilms produced under the conditions tested here may be the result of either the unusual *wssC* duplication, which might reduce *wss* operon transcription or cellulose synthase complex assembly, or the result of leaky transcriptional or synthase regulation in the absence of the normal signals required to express cellulose. It is possible that host-specific factors are required to induce cellulose expression to higher levels during invasion of avian tissues, or that other environmental signals are required for expression during transmission between hosts for survival in water, soils or plants. Future analysis will require transcriptional analyses of the *wss* operon, plus quantitative measurements of cellulose production, to better understand how and when cellulose production is controlled by this bacterium.

It remains unclear what EPS is being utilised by *B. avium* 197N as the primary biofilm matrix in these microcosms, as *B. avium* 197N lacks a *bps*-like operon required to express the Bps polymer produced by other *Bordetellae* [7,8,11]. SEM imaging of wild-type *B. avium* 197N and CD mutant biofilm samples appear very similar (Fig. 6B) and are like those produced by *B. bronchiseptica* RB50 and *B. pertussis* Bp536, for which Bps is required for biofilm formation [26,27]. *B. avium* 197N biofilms may utilise a similar polysaccharide, eDNA or a proteinaceous attachment factor or adhesin as the primary biofilm matrix component, but further biochemical and genetic analyses will be required to identify the nature of this EPS.

3.6. Involvement of c-di-GMP in B. avium 197N in colony morphology and biofilms

Biofilm formation and cellulose expression in *P. fluorescens* SBW25 is primarily controlled by c-*di*-GMP levels regulated by WspR and other diguanylate cyclases (DGCs) [34]. DGCs are found in other pseudomonads and *Bordetellae*, and we have noted a close homologue in *B. avium* 197N (WP_012416712; 336 aa, with 63% ID and an E value of 1e−149). In order to determine whether c-*di*-GMP levels may also play a role in *B. avium* 197N biofilm formation or cellulose expression, we tested the effect of overexpression of a constitutively active and dominant WspR19 mutant that induces a phenotype indistinguishable from the WS in *P. fluorescens* SBW25 [28,37]. As WspR19 is functional in other pseudomonads and in more distantly related bacteria such as *Caulobacter crescentus* CB15 [23,38,39], it might also have an impact on the phenotype of *B. avium* 197N regardless of the activity of WP_012416712.

We first tested whether WspR19 affected *B. avium* 197N swimming motility [10], as the expression of a similar DGC in *B. bronchiseptica* 9.73 was found to repress swimming motility through the elevation of c-*di*-GMP levels [40]. WspR19 was found to partially repress swimming to 11−18% % of the levels shown by *B. avium* 197N carrying the control plasmid ($p \leq 0.0001$). We then investigated whether WspR and WspR mutants affected colony morphology, including the uptake of Congo red stain used to assess cellulose and attachment factor expression [20,21,28,35]. WspR19 was found to have a consistent impact on *B. avium* 197N colony morphology, resulting in larger and slightly rougher colonies with higher levels of Congo red staining compared to wild-type *B. avium* 197N and the CD mutant (Fig. 6C). In comparison, *B. avium* 197N colonies expressing the wild-type WspR protein (WspR12) [28,41] were only slightly stained by Congo red, and colonies expressing the dominant-negative WspR9 mutant [41] were indistinguishable from *B. avium* 197N, the CD mutant and the plasmid control colonies. Although more cellulose could be observed by fluorescent microscopy in colony material produced by *B. avium* 197N expressing WspR19 compared to either *B. avium* 197N with the control plasmid or the CD mutant (data not shown), it is unclear whether the changes in colony morphology are the result of minor increases in cellulose levels or changes in other EPS or attachment factors which also bind Congo red.

The expression of WspR mutants in *B. avium* 197N also affected biofilm strength, with strain, medium and growth all found to have significant effects ($p \leq 0.0001$, Suppl. Table S3, Model 3). In particular, strains could be differentiated into three groups, with *B. avium* 197N carrying the control plasmid or expressing WspR9 having the least effect on strength, WspR12 having an intermediate effect, and WspR19 having the greatest effect on strength ($\alpha = 0.05$). The strongest biofilms were produced in KB microcosms by *B. avium* 197N expressing WspR19 which were significantly stronger than the plasmid control (2.5×, $p = 0.0353$), though growth was significantly reduced (0.6×, $p = 0.0002$). This suggests that WspR19 has a negative pleiotropic effect when expressed in *B. avium* 197N, as it does in *P. fluorescens* SBW25 [37]. Although the strain was weakly insignificant ($p < 0.0727$) when attachment was modelled (Suppl. Table S3, Model 4), it seems likely that biofilm formation by *B. avium* 197N in static microcosms under the conditions tested here is regulated to some degree by c-*di*-GMP levels.

In conclusion, bacterial cellulose synthase *bcs* operons are common amongst the *Proteobacteria*, though acetylation-associated genes are rare and have only been identified in a select group of pseudomonads and a few other species including *B. avium* 197N. In this work, we confirm that *B. avium* 197N is able to express cellulose at low levels, though it was not necessary for the formation of A−L interface biofilms in static microcosms, and further investigation is required to identify the primary matrix components utilised by *B. avium* 197N under the conditions tested here and to identify the

environmental signals and regulatory mechanisms which control expression under natural conditions. Although cellulose might be used during infection of the upper respiratory tract of hosts, it may also be important for survival between hosts in water, soil or on plant surfaces, and this might explain why *bcs* operons are carried by environmental bacteria as well as pathogenic and commensal intestinal bacteria.

Conflict of interests

The authors declare that there is no conflict of interests regarding the publication of this paper.

Author's contributions

KMcL and AOF contributed equally to this work as first co-authors. KMcL, OM and AJS designed the experiments. AOF, KZ, DF and AJS carried out the bioinformatics analyses. KMcL, CI, AK, IUM, OM and SR carried out the experiments. KMcL, SMH and AJS analysed the data. AJS and OM prepared the manuscript with comments from all authors. AJS, YD and OM were responsible for the management of this project, with AJS leading.

Appendix A. Supplementary data

Supplementary data related to this article can be found at http://dx.doi.org/10.1016/j.resmic.2017.01.002.

References

[1] Hinz KH, Glünder G. Occurrence of *Bordetella avium* sp. nov. and *Bordetella bronchiseptica* in birds. Berl Munch Tierarztl Wochenschr 1985;98:369–73 [in German].

[2] Raffel TR, Register KB, Marks SA, Temple L. Prevalence of *Bordetella avium* infection in selected wild and domesticated birds in the eastern USA. J Wildl Dis 2002;38:40–6.

[3] Grespan A, Camera O, Knöbl T, Gomes CR, Felizardo MR, Ferreira TSP, et al. Virulence and molecular aspects of *Bordetella avium* isolated from cockatiel chicks (*Nymphicus hollandicus*) in Brazil. Vet Microbiol 2012; 160:530–4.

[4] Spilker T, Liwienski AA, LiPuma JJ. Identification of *Bordetella* spp. in respiratory specimens from individuals with cystic fibrosis. Clin Microbiol Infect 2008;14:504–6.

[5] Harrington AT, Castellanos JA, Ziedalski TM, Clarridge JE, Cookson BT. Isolation of *Bordetella avium* and novel *Bordetella* strain from patients with respiratory disease. Emerg Infect Dis 2009;15:72–4.

[6] Bos AC, Beemsterboer P, Wolfs TFW, Versteegh FGA, Arets HGM. *Bordetella* species in children with cystic fibrosis: what do we know?: The role in acute exacerbations and chronic course. J Cyst Fibros 2011; 10:307–12.

[7] Sloan GP, Love CF, Sukumar N, Mishra M, Deora R. The *Bordetella* Bps polysaccharide is critical for biofilm development in the mouse respiratory tract. J Bacteriol 2007;189:8270–82.

[8] Conover MS, Sloan GP, Love CF, Sukumar N, Deora R. The Bps polysaccharide of *Bordetella pertussis* promotes colonization and biofilm formation in the nose by functioning as an adhesion. Mol Microbiol 2010;77:1439–55.

[9] Gentry-Weeks CR, Cookson BT, Goldman WE, Rimler RB, Porter SB, Curtiss R. Dermonecrotic toxin and tracheal cytotoxin, putative virulence factors of *Bordetella avium*. Infect Immunol 1988;56:1698–707.

[10] Temple LA, Weiss AA, Walker KE, Barnes HJ, Christensen VL, Miyamoto DM, et al. *Bordetella avium* virulence measured *in vivo* and *in vitro*. Infect Immun 1998;66:5244–51.

[11] Sebaihia M, Preston A, Maskell DJ, Kuzmiak H, Connell TD, King ND, et al. Comparison of the genome sequence of the poultry pathogen *Bordetella avium* with those of *B. bronchiseptica*, *B. pertussis*, and *B. parapertussis* reveals extensive diversity in surface structures associated with host interaction. J Bacteriol 2006;188:6002–15.

[12] Römling U. Molecular biology of cellulose production in bacteria. Res Microbiol 2002;153:205–12.

[13] Spiers AJ, Deeni YY, Folorunso AO, Koza A, Moshynets O, Zawadzki K. Cellulose expression in *Pseudomonas fluorescens* SBW25 and other environmental pseudomonads. In: Van De Ven TGM, Godbout L, editors. Cellulose. Rijeka, Croatia: InTech; 2013.

[14] Römling U, Galperin MY. Bacterial cellulose biosynthesis: diversity of operons, subunits, products, and functions. Trends Microbiol 2015;23: 545–57.

[15] Augimeri R, Varley AJ, Strap JL. Establishing a role for bacterial cellulose in environmental interactions: lessons learned from diverse biofilm-producing *Proteobacteria*. Front Microbiol 2015;6:1282.

[16] Gal M, Preston GM, Massey RC, Spiers AJ, Rainey PB. Genes encoding a cellulosic polymer contribute toward the ecological success of *Pseudomonas fluorescens* SBW25 on plant surfaces. Mol Ecol 2003;12: 3109–21.

[17] White AP, Gibson DL, Kim W, Kay WW, Surette MG. Thin aggregative fimbriae and cellulose enhance long-term survival and persistence of *Salmonella*. J Bacteriol 2006;188:3219–27.

[18] Gualdi L, Tagliabue L, Bertagnoli S, Ieranò T, De Castro C, Landini P. Cellulose modulates biofilm formation by counteracting curli-mediated colonization of solid surfaces in *Escherichia coli*. Microbiology 2008; 154:2017–24.

[19] Nielsen L, Li X, Halverson LJ. Cell–cell and cell–surface interactions mediated by cellulose and a novel exopolysaccharide contribute to *Pseudomonas putida* biofilm formation and fitness under water-limiting conditions. Environ Microbiol 2011;13:1342–56.

[20] Spiers AJ, Kahn SG, Bohannon J, Travisano M, Rainey PB. Adaptive divergence in experimental populations of *Pseudomonas fluorescens*. I. Genetic and phenotypic bases of wrinkly spreader fitness. Genetics 2002; 161:33–46.

[21] Spiers AJ, Bohannon B, Gehrig SM, Rainey PB. Biofilm formation at the air–liquid interface by the *Pseudomonas fluorescens* SBW25 wrinkly spreader requires an acetylated form of cellulose. Mol Microbiol 2003; 50:15–27.

[22] Arrebola E, Carrion VJ, Gutierrez-Barranquero JA, Perez-Garcia A, Rodriguez-Palenzuela P, Cazorla FM, et al. Cellulose production in *Pseudomonas syringae* pv. *syringae*: a compromise between epiphytic and pathogenic lifestyles. FEMS Microbiol Ecol 2015;91: fiv071.

[23] Ude S, Arnold DL, Moon CD, Timms-Wilson T, Spiers AJ. Biofilm formation and cellulose expression among diverse environmental *Pseudomonas* isolates. Environ Microbiol 2006;8:1997–2011.

[24] Robertson M, Hapca SM, Moshynets O, Spiers AJ. Air–liquid interface biofilm formation by psychrotrophic pseudomonads recovered from spoilt meat. Antonie van Leeuwenhoek 2013;103:251–9.

[25] Udall YC, Deeni Y, Hapca SM, Raikes D, Spiers AJ. The evolution of biofilm-forming wrinkly spreaders in static microcosms and drip-fed columns selects for subtle differences in wrinkleality and fitness. FEMS Microbiol Ecol 2015;91:fiv057.

[26] Mishra M, Parise G, Jackson KD, Wozniak DJ, Deora R. The BvgAS signal transduction system regulates biofilm development in *Bordetella*. J Bacteriol 2005;187:1474–84.

[27] Parise G, Mishra M, Itoh Y, Romeo T, Deora R. Role of a putative polysaccharide locus in *Bordetella* biofilm development. J Bacteriol 2007;198:750–60.

[28] Spiers AJ, Rainey PB. The *Pseudomonas fluorescens* SBW25 wrinkly spreader biofilm requires attachment factor, cellulose fibre and LPS interactions to maintain strength and integrity. Microbiology 2005;151: 2829–39.

[29] Gorbatiuk OB, Tsapenko MV, Pavlova MV, Okunev OV, Kordium VA. Bioaffinity sorbent based on immobilized protein A *Staphylococcus aureus*: development and application. Biopolym Cell 2012;28:141–8.
[30] Brocchieri L. The GC content of bacterial genomes. J. Phylogen Evol Biol 2014;2:1.
[31] Koza A, Moshynets O, Otten W, Spiers AJ. Environmental modification and niche construction: developing O_2 gradients drive the evolution of the wrinkly spreader. ISME J 2011;5:665–73.
[32] Loker SB, Temple LM, Preston A. The *Bordetella avium BAV1965-1962* fimbrial locus is regulated by temperature and produces fimbriae involved in adherence to Turkey tracheal tissue. Infect Immun 2011;79:2423–9.
[33] Beach NM, Thompson S, Mutnick R, Brown L, Kettig G, Puffenbarger R, et al. *Bordetella avium* antibiotic resistance, novel enrichment culture, and antigenic characterization. Vet Microbiol 2012;160:189–96.
[34] Spiers AJ. A mechanistic explanation linking adaptive mutation, niche change and fitness advantage for the wrinkly spreader. Int J Evol Biol 2014;2014:10. Article ID 675432.
[35] Koza A, Hallett PD, Moon CD, Spiers AJ. Characterization of a novel air–liquid interface biofilm of *Pseudomonas fluorescens* SBW25. Microbiology 2009;155:1397–406.
[36] O'Toole GA, Kolter R. Initiation of biofilm formation in *Pseudomonas fluorescens* WCS365 proceeds via multiple, convergent signalling pathways: a genetic analysis. Mol Microbiol 1998;28:449–61.
[37] Goymer P, Kahn SG, Malone JG, Gehrig SM, Spiers AJ, Rainey PB. Adaptive divergence in experimental populations of *Pseudomonas fluorescens*. II. Role of the GGDEF regulator WspR in evolution and development of the wrinkly spreader phenotype. Genetics 2006;173:515–26.
[38] D'Argenio DA, Calfee MW, Rainey PB, Everett C, Pesci EC. Autolysis and autoaggregation in *Pseudomonas aeruginosa* colony morphology mutants. J Bacteriol 2002;184:6481–9.
[39] Aldridge P, Paul R, Goymer P, Rainey P, Jenal U. Role of the GGDEF regulator PleD in polar development of *Caulobacter crescentus*. Mol Microbiol 2003;47:1695–708.
[40] Sisti F, Ha DG, O'Toole GA, Hozbor D, Fernández J. Cyclic-di-GMP signalling regulates motility and biofilm formation in *Bordetella bronchiseptica*. Microbiology 2013;159:869–79.
[41] Goymer PJ. The role of the WspR response regulator in the adaptive evolution of experimental populations of Pseudomonas fluorescens SBW25 [D.Phil. thesis]. Oxford: University of Oxford; 2002.
[42] Rainey PB, Bailey MJ. Physical and genetic map of the *Pseudomonas fluorescens* SBW25 chromosome. Mol Microbiol 1996;19:521–33.

Анотація. *Хоча оперони бактеріальної целюлозосинтази (*bcs*) широко поширені в типі* Proteobacteria*, субодиниці, необхідні для часткового ацетилювання полімеру, здається, обмежені кількома ґрунтовими, асоційованими з рослинами та фітопатогенними псевдомонадами групи ɣ, включаючи* Pseudomonas fluorescens *SBW25 та кілька патоварів* Pseudomonas syringae*. Однак оперон* bcs *із субодиницями ацетилювання також анотований у неспорідненому респіраторному патогені b-групи* Bordetella avium *197N. Наше порівняння послідовностей білків субодиниць і аналіз вмісту GC підтверджує велику подібність між* B. avium *197N і оперонами псевдомонад, що дає змогу припустити, що в обох випадках субодиниці синтази целюлози та субодиниці ацетилювання були придбані як одна одиниця. Використовуючи статичні рідкі мікрокосми, ми можемо підтвердити, що* B. avium *197N експресує низькі рівні целюлози в біоплівках, що утворюються на повітряно-рідинному інтерфейсі, і що міцність біоплівки та рівень прикріплення можна збільшити шляхом підвищення рівнів c-di-GMP, як у псевдомонад, але целюлоза не потрібна для утворення самої біоплівки. Виявлення того, що* B. avium *197N здатний виробляти целюлозу за допомогою висококонсервативного, але відносно рідкісного оперону* bcs*, ставить питання про те, яку функціональну роль цей модифікований полімер відіграє під час інфікування верхніх дихальних шляхів або виживання між хазяїнами, і які сигнали зовнішнього середовища регулюють виробництво целюлози.*

3.3. Роль екзоклітинної ДНК, амілоїдних фібрил і мембранних везикул у біоплівці *P. fluorescens* SBW25

Як вже повідомлялось вище, бактеріальні біоплівки є складними структурами, що використовують різні полімери в якості структурних елементів - так званого матриксу біопівлки. До матриксу досліджених біоплівок грам позитивних і грам-негативних бактерій майже завжди входить екзоклітинна ДНК (35-41, 70). еДНК бере участь у клітинній адгезії на ранніх стадіях розвитку біоплівки та відіграє ключову структурну роль у зрілих біоплівках (14-18). еДНК в біоплівці вперше була візуалізована в занурених в рідину біоплівках, асоційованих з поверхнею (Р-Т інтерфейс), створених умовно-патогенним штамом *P. aeruginosa* PA01 (71). Повідомляється, що тут еДНК сприяє початковій адгезії клітин до поверхонь, сприяє агрегації клітин і взаємодіє з іншими екзополімерами матриксу, утворюючи волокноподібні мережі, що стабілізують біоплівку (72-74).

Раніше ми досліджували П-Р біоплівки, що утворюються штамом Wrinkly Spreader, який є адаптативним мутантом вільноіснуючої та рослино-асоційованої модельної псевдомонади *P. fluorescens* SBW25, яку часто використовують для еволюційних досліджень (75), що окремо описали в оглядовій статті (76). Біоплівки П-Р інтерфейсу іноді називають плівками, а біоплівка Wrinkly Spreader технічно не плаває, а утримується на поверхні стовпчика рідини шляхом прикріплення до стінок флакону на меніску та завдяки гідрофобності (77, 78). Біоплівка Wrinkly Spreader є дуже міцною в'язкопружною структурою в порівнянні із слабшою біоплівкою Viscous Mass, яка утворюється диким типом *P. fluorescens* SBW25 (79, 80). Така більша міцність може бути пов'язана із тим фактом, що у біоплівці Wrinkly Spreader целюлозні волокна взаємодіють з ліпосахаридом і невідомим фактором прикріплення, яким, можливо, є полі-N-ацетилглюкозамін (PNAG) та/або амілоїдні волокна Fap (81, 82). Р. *fluorescens* SBW25 також виробляє альгінат і, можливо, має потенціал для виробництва інших полімерів (83).

Відомо, що в різноманітних біоплівках амілоїдні волокна, PNAG та інші екзополімери взаємодіють з еДНК (14-17, 72). Внутрішні рідини в біоплівці також насичеін різноманітними білками, джгутиками, фімбріями та пілями, а також мембранними везикулами, які виробляється метаболічно активними, стресовими або лізованими клітинами (17, 72, 84-87).

Роль еДНК в біоплівках Wrinkly Spreader є недослідженою попри те, що сама біоплівка вивчається вже протягом багатьох років. Відомо, що кілька інших видів псевдомонад продукують еДНК, серед них, *P. chlororaphis* 30–84 (88), *P. putida* KT2440, яка утворює целюлозну П-Р біоплівку, подібну до біоплівки Wrinkly Spreader (89), *Pseudomonas* sp. FW1, яка утворює Р-Т біоплівку (90) та *P. fluorescens* B/S 1000 у слизу (91).

Тож завданням цього розділу було краще зрозуміти склад матриксу біоплівок Wrinkly Spreader та визначити, чи містить вона також амілоїдні волокна та еДНК. Наші результати підтверджують наявність амілоїдних волокон і еДНК в біоплівках *P. fluorescens* SBW25. Обробка ДНКазою I демонструє, що еДНК, ймовірно, є важливою на ранніх стадіях розвитку біоплівки. Використовуючи ТЕМ ми візуалізували мембранні везикули з планктонної та біоплівкової популяції бактрій. MALDI-TOF було використано для ідентифікації та порівняльного аналізу білків матриксу та двох фракцій мембранних везикул.

Основні результати, отримані в цьому підрозділі дисертації опубліковані в роботах автора (44, 76).

International Journal of
Molecular Sciences

MDPI

Article

eDNA, Amyloid Fibers and Membrane Vesicles Identified in *Pseudomonas fluorescens* SBW25 Biofilms

Olena V. Moshynets [1], Ianina Pokholenko [1], Olga Iungin [1,2], Geert Potters [3,4,*] and Andrew J. Spiers [5]

[1] Institute of Molecular Biology and Genetics, National Academy of Sciences of Ukraine, 03143 Kyiv, Ukraine
[2] Department of Biotechnology, Leather and Fur, Kyiv National University of Technologies and Design, 01011 Kyiv, Ukraine
[3] Antwerp Maritime Academy, 2030 Antwerp, Belgium
[4] Department of Bioscience Engineering, University of Antwerp, 2000 Antwerp, Belgium
[5] School of Applied Sciences, Abertay University, Dundee DD1 1HG, UK
* Correspondence: geert.potters@hzs.be

Abstract: *Pseudomonas fluorescens* SBW25 is a model soil- and plant-associated bacterium capable of forming a variety of air–liquid interface biofilms in experimental microcosms and on plant surfaces. Previous investigations have shown that cellulose is the primary structural matrix component in the robust and well-attached Wrinkly Spreader biofilm, as well as in the fragile Viscous Mass biofilm. Here, we demonstrate that both biofilms include extracellular DNA (eDNA) which can be visualized using confocal laser scanning microscopy (CLSM), quantified by absorbance measurements, and degraded by DNase I treatment. This eDNA plays an important role in cell attachment and biofilm development. However, exogenous high-molecular-weight DNA appears to decrease the strength and attachment levels of mature Wrinkly Spreader biofilms, whereas low-molecular-weight DNA appears to have little effect. Further investigation with CLSM using an amyloid-specific fluorophore suggests that the Wrinkly Spreader biofilm might also include Fap fibers, which might be involved in attachment and contribute to biofilm strength. The robust nature of the Wrinkly Spreader biofilm also allowed us, using MALDI-TOF mass spectrometry, to identify matrix-associated proteins unable to diffuse out of the structure, as well as membrane vesicles which had a different protein profile compared to the matrix-associated proteins. CLSM and DNase I treatment suggest that some vesicles were also associated with eDNA. These findings add to our understanding of the matrix components in this model pseudomonad, and, as found in other biofilms, biofilm-specific products and material from lysed cells contribute to these structures through a range of complex interactions.

Keywords: air–liquid interface; amyloid fibers; biofilm; eDNA; EPS; outer-membrane vesicles; *Pseudomonas*

check for updates

Citation: Moshynets, O.V.; Pokholenko, I.; Iungin, O.; Potters, G.; Spiers, A.J. eDNA, Amyloid Fibers and Membrane Vesicles Identified in *Pseudomonas fluorescens* SBW25 Biofilms. *Int. J. Mol. Sci.* **2022**, *23*, 15096. https://doi.org/10.3390/ijms232315096

Academic Editors: Antonella Piozzi and Iolanda Francolini

Received: 29 October 2022
Accepted: 26 November 2022
Published: 1 December 2022

Publisher's Note: MDPI stays neutral with regard to jurisdictional claims in published maps and institutional affiliations.

Copyright: © 2022 by the authors. Licensee MDPI, Basel, Switzerland. This article is an open access article distributed under the terms and conditions of the Creative Commons Attribution (CC BY) license (https://creativecommons.org/licenses/by/4.0/).

1. Introduction

Bacterial biofilms are complex structures using a variety of polymers as structural elements (matrix), including polysaccharides (EPS), proteins, and extracellular DNA [1]. eDNA is involved in cell adhesion during the early stages of biofilm development and plays a key structural role in mature biofilms [2–6]. eDNA was first visualized in solid surface–liquid (S–L) interface (i.e., submerged) biofilms produced by the opportunistic human pathogen, *Pseudomonas aeruginosa* PA01 [7], where it aids the initial adhesion of cells to surfaces, promotes cell aggregation, and interacts with EPS to form fiber-like networks stabilizing the biofilms forming at different interfaces [8–10]. eDNA is now known to be produced by a range of benign and pathogenic species, including *Bacillus subtilis* [11], *Escherichia coli* [12], *Salmonella enterica* [13], *Staphylococcus aureus* and *S. epidermis* [14,15], *Streptococcus mutans* and *S. pneumoniae* [16,17], etc., and is widespread in aquatic environments, sediments, and soil [4]. However, the origin of eDNA is varied [3,4] and here we do not infer whether eDNA secretion or release is deliberate at the single-cell or population

level (i.e., is produced), or whether it is an indirect and advantageous consequence of cell death and lysis.

We were involved in the early description of the air–liquid (A–L) interface biofilm produced by the Wrinkly Spreader, a novel biofilm-forming mutant of the model soil- and plant-associated pseudomonad, *P. fluorescens* SBW25, isolated from experimental evolution microcosms [18,19]. A–L interface biofilms are sometimes referred to as pellicles [10] and the Wrinkly Spreader biofilm is not technically floating but is retained at the surface of the liquid column by attachment to the vial walls at the meniscus and hydrophobicity [20,21]. The Wrinkly Spreader biofilm is a very robust viscoelastic structure compared to the weaker Viscous Mass biofilm produced by wild-type *P. fluorescens* SBW25 when induced with exogenous Fe^{3+} [22,23], though both utilize partially acetylated cellulose as the primary structural matrix component [20–24]. In the Wrinkly Spreader biofilm, cellulose fibers interact with liposaccharide (LPS) and an unidentified attachment factor, possibly poly-N-acetylglucosamine (PNAG) and/or Fap amyloid fibers [19,25,26], to contribute to the biofilm structure and distinctive colony morphology [21]. *P. fluorescens* SBW25 also produces alginate [27,28] and possibly has the potential to produce other EPS, but these have not yet been implicated in biofilm formation. In other biofilms, amyloid fibers, PNAG, and other EPS are known to interact with eDNA [1–5,8], and interstitial fluids also include a variety of proteins, flagella, fimbriae, and pili, as well as membrane vesicles (MVs) produced by metabolically active, stressed, or lysed cells [1,5,6,8,9,29–32].

Although our description of the Wrinkly Spreader biofilm was contemporaneous with the first report of biofilm eDNA [7], we have never investigated *P. fluorescens* SBW25 biofilms for the presence of eDNA. Several other pseudomonad species are known to produce eDNA, such as *P. chlororaphis* 30–84 [33] and *P. putida* KT2440 [34] in A–L interface biofilms. *P. putida* KT2440 also produces cellulose matrix-based biofilms and Wrinkly Spreader-like mutants [35–39], as does *Pseudomonas* sp. FW1 [40] in a S-L interface biofilm, and *P. fluorescens* B/S_{1000} in a slime [41]. Fourier-transform infrared spectroscopy spectra suggest eDNA, besides nanocellulose, may be in other pseudomonad A–L interface biofilms, e.g., [42–44]. However, we are not aware of any other reports of eDNA for other *P. fluorescens* model strains, including CHA0, Pf0-1 and Pf5, or for the plant pathogen, *P. syringae* DC3000, which is capable of producing cellulose matrix-based A–L interface biofilms [35,43]. Both the *Pseudomonas* genus and *P. fluorescens* species are highly diverse [44–48], and the expression of biofilm EPS by pseudomonads is also highly varied [6,8,49], so it is possible that eDNA is not a common feature of these biofilms.

The aim of this work was to better understand the matrix composition of the Wrinkly Spreader biofilm and to determine whether it also included amyloid fibers and eDNA which have reported for other pseudomonad biofilms [7,25,33,34,40,41,50]. Although the Viscous Mass biofilm produced by wild-type *P. fluorescens* SBW25 is considerably more difficult to work with because it is such a fragile structure [22,23], we have included it in our investigation to see how varied the matrix composition might be within this pseudomonad strain. Our results confirm the presence of amyloid fibers and eDNA, and DNase I treatments demonstrate that eDNA is likely to be important during the early stages of biofilm development. Using MALDI-TOF, we have also visualized Wrinkly Spreader membrane vesicles and identified proteins from the matrix, as well as biofilm and planktonic vesicles. These findings have advanced our understanding of the matrix composition of this important model biofilm system and demonstrate that *P. fluorescens* SBW25 biofilms are structurally more complex than originally reported [20–24].

2. Results

2.1. Visualization of eDNA in Viscous Mass and Wrinkly Spreader Biofilms

Confocal laser scanning microscopy (CLSM) was used to determine whether Viscous Mass biofilms produced by wild-type *P. fluorescens* SBW25 and Wrinkly Spreader mutant biofilms included eDNA as part of the matrix. We used the membrane-impermeable DNA-binding stain, propidium iodide, to visualize eDNA, plus the membrane-permeable coun-

terstain, SYTO9, to visualize intracellular DNA from metabolically active (live) cells (the propidium iodide/SYTO9 combination is the basis of the 'live/dead' staining method [51], and Calcofluor white to visualize the cellulose matrix previously identified in Viscous Mass and Wrinkly Spreader biofilms [20,22,24,52]. CLSM images clearly showed the presence of eDNA in both biofilms, where it appeared to co-localize with cellulose above dense regions of active cells (Figure 1). Like cellulose, eDNA was present in thinner films and large, denser structures, but it is not clear whether the two are intermixed or occupy separate volumes above the surface of the cells, or whether eDNA and cellulose retain physical links with the secreting and/or lysing cells.

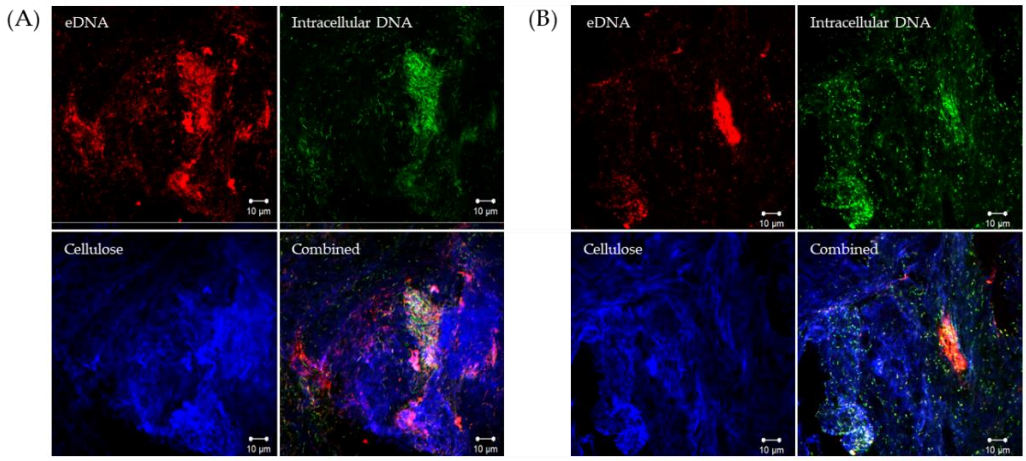

Figure 1. *P. fluorescens* SBW25 biofilms include eDNA. Confocal laser scanning microscopy (CLSM) was used to visualize eDNA, intracellular DNA, and cellulose in 24 h biofilms. Shown here are single-channel and combined CLSM images from Viscous Mass (**A**) and Wrinkly Spreader (**B**) biofilms. Propidium iodide (red channel) was used to visualize eDNA, CYTO9 (green channel) to visualize the intracellular DNA of live cells, and Calcofluor white (blue channel) to visualize cellulose, respectively, and all three channels are combined in the bottom-right image. The scale bars indicate 10 µm.

We obtained further evidence of eDNA in Wrinkly Spreader biofilms using a Green fluorescent protein (GFP) labeled Wrinkly Spreader mutant (WS-GFP [52]), instead of SYTO9, to mark live cells and avoid any possible contribution by intracellular DNA in dead, but intact, cells to the eDNA signal (GFP and SYTO9 signals have been shown to co-localize, e.g., [53]). CLSM images of these GFP–WS biofilms confirmed the presence of eDNA and supported our impression that both cellulose and eDNA were accumulating above the active cells (Figure 2). Further work would be needed to determine differences in eDNA spatial distribution and heterogeneity between the two biofilm types.

Although Propidium iodide/SYTO9 counterstaining or similar combinations, such as Propidium iodide/GFP or Propidium iodide/SYBR Green, is commonly used to visualize eDNA in biofilms (e.g., [34,51,54]), it is not always clear whether the eDNA signal is coming from extracellular DNA or from DNA within damaged or lysed cells, especially when cells may be stressed. We therefore sought confirmation of eDNA using two complementary approaches. First, we isolated eDNA from planktonic cultures and biofilms by removing cells and cellulose by centrifugation, with eDNA levels measured by spectrometry (A_{260}) [55]. We were able to detect significantly higher levels of eDNA from Wrinkly Spreader biofilms compared to planktonic cultures (1.6×; Tukey–Kramer HSD, $\alpha = 0.05$) (Figure 3A). Although the eDNA levels in Wrinkly Spreader biofilms were significantly higher than in Viscous Mass biofilms (2.3×), no significant difference in eDNA levels were observed between Viscous Mass biofilms and planktonic cultures (Tukey–Kramer HSD, $\alpha = 0.05$), perhaps because it was harder to separate free eDNA from the more fragile biofilm [22,23] and/or less eDNA is produced in this biofilm.

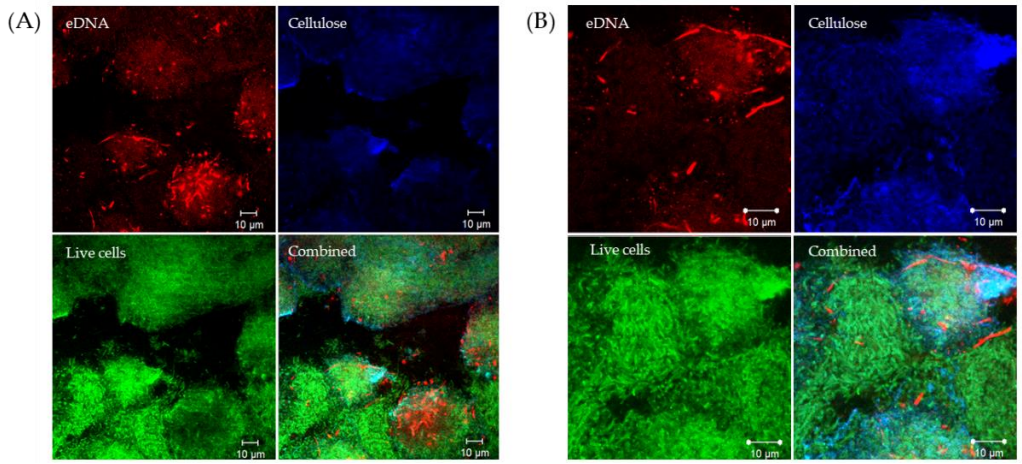

Figure 2. eDNA and cellulose accumulate above masses of cells in *P. fluorescens* SBW25 biofilms. Confocal laser scanning microscopy (CLSM) was used to visualize eDNA and cellulose against a backdrop of GFP-expressing metabolically active Wrinkly Spreader (WS-GFP) mutant cells in three-day-old biofilms. Shown here are single-channel and combined CLSM images of two sections of a Wrinkly Spreader biofilm (**A**,**B**). Propidium iodide (red channel) was used to visualize eDNA, GFP (green channel) to visualize live cells, and Calcofluor white (blue channel) to visualize cellulose, respectively, and all three channels are combined in the bottom-right image. The scale bars indicate 10 μm.

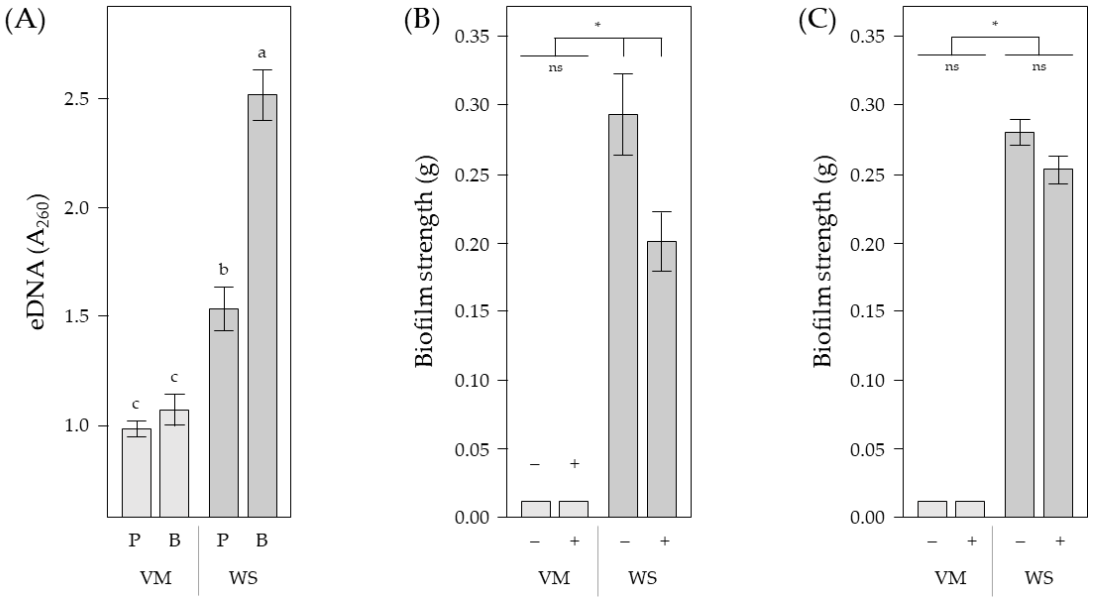

Figure 3. Quantitative measurements of eDNA and the impact it has on biofilm strength. Spectrometry was used to measure eDNA recovered from planktonic cultures and biofilms, and small glass balls to determine biofilm strength. Shown here are eDNA (A_{260}) levels (**A**) in 24 h planktonic and three-day-old biofilm samples (B, biofilm sample; P, planktonic (shaken) culture sample; VM, Viscous Mass; WS, Wrinkly Spreader). Biofilm strengths (grams) are shown (**B**) for three-day-old biofilms which developed in microcosms with DNase I before assay, and (**C**) for three-day-old biofilms treated with DNase I for 3 h before assay (+, with; −, without). Means (n = 6–8) ± SE are shown. Differences between means (**A**) were determined for each set of measurements by one-way ANOVA and post hoc Tukey–Kramer HSD tests. Means sharing the same letter are not significantly different (α = 0.05). Differences between means (**B**,**C**) were determined by the Wilcoxon method. Means linked by an asterisk are significantly different ($p < 0.05$) (ns, not significantly different).

2.2. Role of eDNA in Biofilm Strength and Attachment Levels

We then assessed the impact DNase I treatment (after [34,40,56] etc.) might have on strength with the expectation that it might contribute to the strength of mature biofilms, and/or was important for biofilm development, perhaps at the early stage of cell attachment to the microcosm vial walls. As the Viscous Mass and Wrinkly Spreader biofilms cover the air–liquid (A–L) interface, strength measurements (grams), which form part of the combined biofilm assay [57], are readily undertaken by placing a series of small glass balls on the upper surface until the biofilm rips apart or sinks. Using this approach, we found a significant reduction in the strength of Wrinkly Spreader biofilms when they were allowed to develop over three days in the presence of DNase I (1.5×; Wilcoxon, $p = 0.02$) (Figure 3B) (younger biofilms are simply too weak to be able to measure). Again, no significant difference was seen in Viscous Mass biofilm strength (Wilcoxon, $p = 1.00$) (Figure 3C), though it is difficult to measure the strength of these comparatively fragile biofilms [22,23]. It was also notable that the treatment of mature Wrinkly Spreader biofilms with DNase I for three hours did not significantly reduce strength (Wilcoxon, $p = 0.12$), suggesting that eDNA may only play an important role during the early phases of biofilm development, and/or it is more protected by the binding of proteins or interactions with other EPS in mature biofilms.

We added exogenous low-molecular-weight (LMW) and high-molecular-weight (HMW) DNA to microcosms (after [58]) to investigate the impact this might have on the development of Viscous Mass and Wrinkly Spreader biofilms over three days. In addition to the biofilm strength assay we previously used, we also determined biofilm attachment using crystal violet dye to stain bacterial cells adhering to the microcosm vial walls at the meniscus ([20,57], adapted from the procedure established by [59]). After washing to remove excess dye, crystal violet was then eluted with ethanol and absorbance (A_{570}) measured to determine attachment levels. Finally, we measured final biomass levels using optical density (OD_{600}) measurements to check whether our experimental treatments affected growth, as biofilm strength and attachment levels might be correlated with growth (i.e., faster growing cultures produce stronger and better attached biofilms).

We use a general linear mixed modelling approach to model biofilm strength, attachment levels, and final microcosm biomass (i.e., growth) as response variables with *biofilm type* (Viscous Mass and Wrinkly Spreader), *DNA treatment* (Controls with no exogenous DNA, LMW, and HMW), *DNA concentration* (0, 100, 300, and 600 µg/mL), and *replicate* as effects, and *biofilm type* × *DNA treatment* as an interaction (see Table S1 for model details and effects tests). This identified *biofilm type* as a significant effect ($p < 0.01$), as expected, because the Wrinkly Spreader biofilm is a stronger and better-attached structure, which supports a greater number of cells at the A–L interface and a higher microcosm biomass than the Viscous Mass biofilm. *DNA treatment* was also a significant effect ($p < 0.01$), but not *DNA concentration* ($p = 0.21$–0.92), suggesting that exogenous DNA added to the microcosms had an effect across treatments. Microcosms containing HMW DNA had final biomass levels 1.1× higher, but 0.6× lower biofilm strengths and 0.5× lower attachment levels than the control microcosms or those with LMW DNA (LSMeans Differences Tukey HSD, $\alpha = 0.05$). The lack of a significant *DNA concentration* effect suggests that 100 µg/mL exogenous DNA saturated all binding sites and/or formed a sufficient gel-like network, and that additional DNA made no significant difference. Finally, we note that the *biofilm type* × *DNA treatment* interaction was significant in all models ($p < 0.01$).

As no significant DNA concentration effect was seen in our models, we pooled the exogenous DNA treatments together (i.e., controls with no exogenous DNA, HMW DNA and LMW DNA) and used an analysis of variance (ANOVA) approach with post hoc Tukey–Kramer HSD tests to determine differences in final microcosm biomass, biofilm strength, and attachment levels (Figure 4). This confirmed our modelling results and shows more clearly the differences in response to exogenous DNA by the Wrinkly Spreader and Viscous Mass biofilms. We interpret these findings to mean that HMW DNA negatively affects the development of Wrinkly Spreader biofilms by reducing strength and attachment

levels, without affecting final biomass levels. In contrast, HMW DNA increases the final biomass of Viscous Mass microcosms, perhaps by supporting greater levels of biofilm development, though this is not supported by significantly increased measurements of biofilm strength or attachment levels. However, increases in attachment and strength may be very hard to quantify given the very fragile nature of the Viscous Mass biofilm.

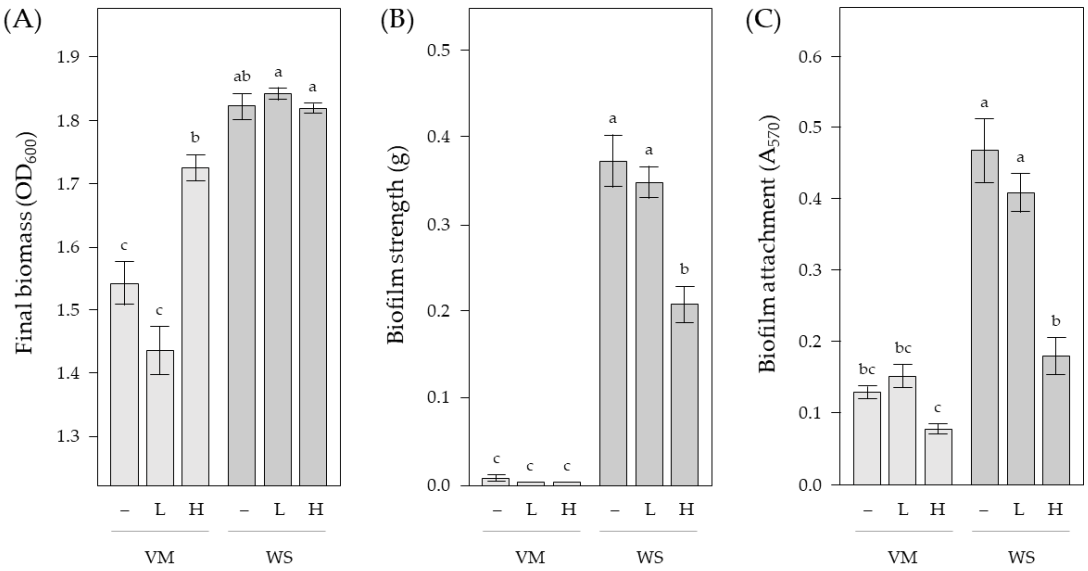

Figure 4. Exogenous DNA affects *P. fluorescens* SBW25 biofilm development. Low-molecular-weight (LMW) and high-molecular-weight (HMW) DNA was added to microcosms and Viscous Mass (VM) and Wrinkly Spreader (WS) biofilms allowed to develop for three days before assay. Shown here are the final microcosm biomass (OD_{600}) (**A**), biofilm strength (grams) (**B**), and attachment (A_{570}) (**C**) measurements (–, no exogenous DNA added; L, LMW DNA added; H, HMW DNA added). Means (n = 8–24) ± SE are shown. Differences between means were determined for each set of measurements by one-way ANOVA and post hoc Tukey–Kramer HSD tests. Means sharing the same letter are not significantly different (α = 0.05).

During the biofilm attachment assays, we noticed that Wrinkly Spreader microcosms containing LMW DNA retained considerably more crystal violet after the elution stage compared to the control microcosms or those with HMW DNA added (Figure S1A) (this retention of dye is not the result of limited washing, e.g., [60]; after staining, we wash the microcosm vials three times before elution with ethanol, which normally removes all of the dye from the meniscus region). The retention of the crystal violet stain may reflect a ring of densely attached cells at the meniscus which absorbs more dye and releases it more slowly than is normally the case. We investigated this with a second elution stage using acetic acid (a commonly used alternative to elution with ethanol [61]) followed by absorbance measurements. This allowed us to determine that Wrinkly Spreader biofilms developing in microcosms with LMW DNA release more crystal violet in the acetic acid elution than either the control microcosms or those with HMW DNA (2.0 and 2.4×, respectively; Wilcoxon, $p < 0.01$) (Figure S1B). Similarly, significantly more stain was also eluted from Viscous Mass microcosms incubated with LMW DNA with acetic acid compared to microcosms with HMW DNA (1.2×; Wilcoxon, $p < 0.01$), though there was no significant difference compared to the control microcosms (Wilcoxon, $p = 0.18$).

The additional elution of crystal violet with acetic acid does not change our understanding of the impact of HMW DNA on the attachment levels of Viscous Mass and Wrinkly Spreader biofilms, but it does reveal a more significant role for LMW DNA which was missed in our earlier attachment assays. LMW DNA appears to enhance bacterial cell attachment to the microcosm vial walls at the meniscus, allowing greater levels of attach-

ment, and/or the development of a denser layer of attached cells from which the A–L interface biofilms then develop out over the liquid surface. However, we do not know why LMW and HMW DNA have such different effects. Interestingly, we have observed large pockets of eDNA, visualized by CLSM in preliminary experiments with Experimental Stain 986, a tetrahydronaphthalenylidene-benzothiazolium derivative, in Wrinkly Spreader biofilms incubated with LMW DNA (Figure S2), but not with HMW DNA, which suggests that the physical properties of the exogenous DNA underlie the differences seen in bacterial attachment.

2.3. Viscous Mass and Wrinkly Spreader Biofilms include Amyloid Fibers

We used CLSM and the fluorescent β-ketoenole AmyGreen dye [62,63] to investigate whether Fap fibrils were produced in Viscous Mass and Wrinkly Spreader biofilms. In both biofilms (Figure 5), a strong AmyGreen signal was observed and appears to be co-localized with the ethidium bromide signal used to visualize total DNA as a proxy for cell numbers, rather than with cellulose which stretches across rips seen in the Wrinkly Spreader sample. An analysis of the total pixel sums for each of the AmyGreen, Calcofluor white, and ethidium bromide channels (n = 3 images) suggests no significant difference in amyloid fibers or cell numbers between biofilms (t-tests, p = 0.31 and 0.42, respectively) though cellulose levels in the Wrinkly Spreader biofilm were significantly higher than in the Viscous Mass biofilm (4×, t-test, p = 0.04). However, the relative production of amyloid fibers requires further corroboration with the use of *fap* deletion mutants and the testing of samples from the early attachment stage to mature biofilms.

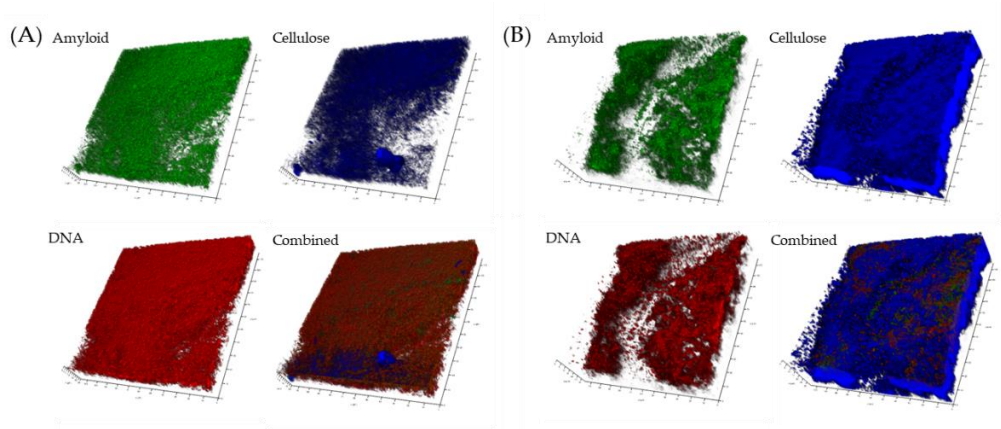

Figure 5. *P. fluorescens* biofilms include amyloid fibers. Confocal laser scanning microscopy (CLSM) was used to visualize amyloid fibers in three-day-old Viscous Mass and Wrinkly Spreader and biofilms. Shown here are single-channel and combined CLSM images of Viscous Mass (**A**) and Wrinkly Spreader (**B**) three-day-old biofilms. AmyGreen (green channel) was used to visualize amyloid fibers, Calcofluor white (blue channel) to visualize cellulose, and ethidium bromide (red channel) to visualize total DNA as a proxy for live cells, respectively, and all three channels are combined in the bottom-right images. Note the low signal region running down the Wrinkly Spreader image. The dimensions of the images are 115 × 115 × 20/35 µm.

2.4. Biofilm Membrane Vesicles and Matrix-Associated Proteins

The biofilm interstitial fluid is also known to contain membrane vesicles (MVs) and proteins secreted from metabolically active cells or released by stressed and/or dying cells [29,30,32]. Biofilm vesicles and matrix-associated proteins are generally investigated by removing cells and large debris by centrifugation, with vesicles isolated by filtration, and matrix-associated proteins by pelleting the matrix with further centrifugation, resuspension, and solubilization in an appropriate buffer (after [17] etc.). Although we were interested in comparing vesicles and matrix-associated proteins from both Wrinkly Spreader and Viscous Mass biofilms, this was only practical for the Wrinkly Spreaders which produced sufficiently

robust biofilms to allow handling and a clear separation of cells from the biofilm matrix and vesicles (similarly, cells could be separated from vesicles from planktonic samples).

We were able to isolate vesicles from three-day-old Wrinkly Spreader biofilms and 24 h planktonic cultures using centrifugation, followed by passage through a 0.2 μm pore-size filter to select for vesicles [17]. Although considerable variation in shape and size was observed, transmission electron microscopy (TEM) images suggested a diameter of ~50 nm for the more circular structures, and in the higher magnification images, double membranes were clearly seen (Figure 6). Further analysis of biofilm vesicle samples by CLSM indicates a co-localization of DNA-staining ethidium bromide and membrane-specific Vybrant DiO [64] signals, and DNase I treatment of these preparations removes all DNA, suggesting that it is associated with the outer surface of the MVs and is not internalized (Figure S3).

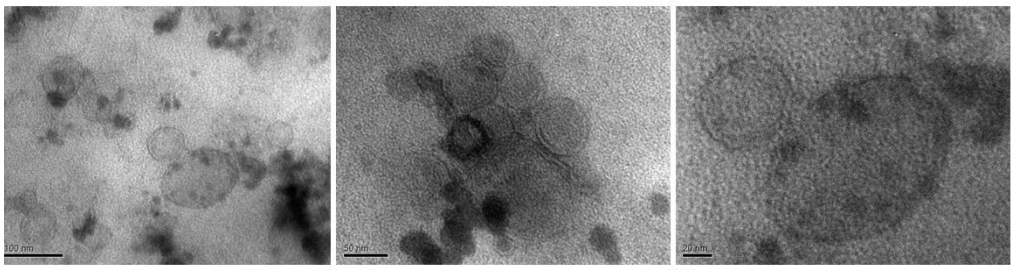

Figure 6. *P. fluorescens* SBW25 Wrinkly Spreader biofilms contain membrane vesicles. Shown here are three transmission electron microscopy (TEM) images of increasing magnification of membrane vesicles (MVs) isolated from three-day-old Wrinkly Spreader biofilms. The scale bars indicate 100 nm, 50 nm, and 20 nm (**left** to **right**).

We also investigated Wrinkly Spreader biofilm matrix-associated proteins by repeatedly washing three-day-old biofilms over seven days to remove soluble and poorly attached proteins, and pre-incubating samples with SDS and urea to release strongly attached proteins before SDS-PAGE (Figure S4). This demonstrated that significant amounts of protein are retained by the matrix and are prevented from freely diffusing out of the structure (we were unable to extract Viscous Mass biofilm proteins in a similar manner, as any physical disturbance reduces the biofilm to a viscous liquid that cannot then be manipulated).

We then used MALDI-TOF mass spectrometry to identify the most abundant proteins with emPA1 $\geq$ 1 in the Wrinkly Spreader biofilm matrix, and biofilm and planktonic membrane vesicle samples. This identified 94 proteins from the biofilm matrix (52 of 319 proteins with emPA1s of 0.03–10.9), biofilm vesicles (31 of 222 proteins with emPA1s of 0.03–5.36) and planktonic vesicles (13 of 166 proteins with emPA1s of 0.07–2.28) (see Table S2 for all identified proteins). Although some of these are homologs of proteins found in *P. aeruginosa* PA01 biofilms and vesicles (e.g., [29,65–67]), we are primarily interested in determining whether the protein profiles differ significantly between these samples. For each protein we extracted the GO functional annotation and predicted localization from UniProt, with details summarized in Figure 7. The source of the proteins and top 15 functional annotations are not independent (3×15 contingency table, χ^2, $p < 0.02$), and pairwise tests confirm that, in each case, protein profiles differed between biofilm matrix, biofilm vesicle, and plankton vesicle samples (2×15 contingency tables, χ^2, $p \leq 0.01$). Similarly, protein source and the top five predicted localizations are not independent (3×5 and 2×5 contingency tables, χ^2, $p \leq 0.03$). Proportionally, the biofilm matrix appears to contain more cellular and ribosomal proteins than either of the two vesicle samples, suggesting that most matrix proteins are released by cell lysis rather than by a more controlled process, as is the case of membrane vesicle biogenesis. The biofilm vesicles also appear to contain proportionally more cellular proteins and fewer proteins associated with external structures or secreted proteins than the planktonic vesicles. However, further

work would be needed to be able to establish which proteins might be unique to certain types of membrane vesicle or only associated with the biofilm matrix.

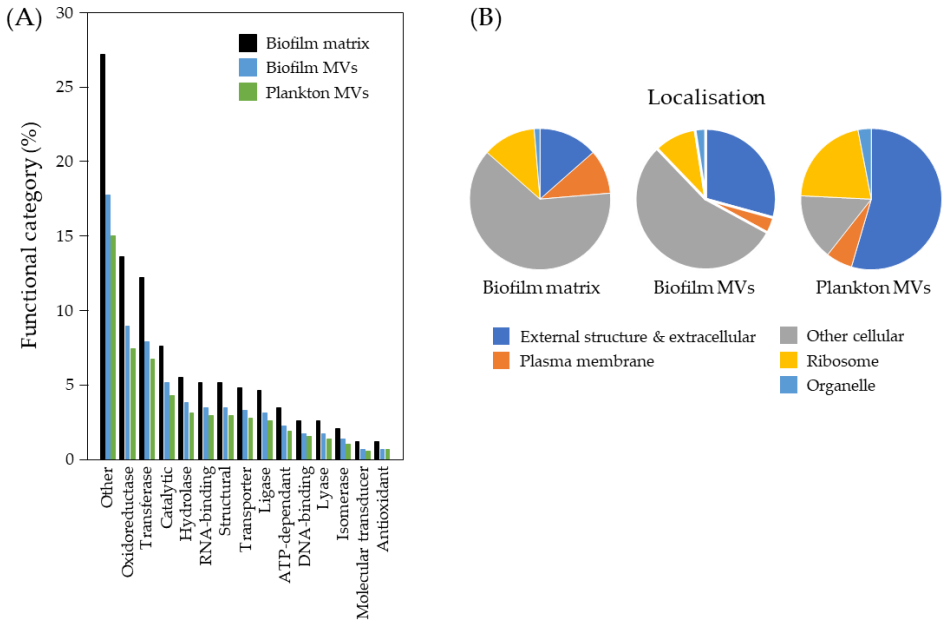

Figure 7. *P. fluorescens* SBW25 Wrinkly Spreader biofilm matrix and membrane vesicles have different protein profiles. Proteins associated with the biofilm matrix and membrane vesicles (MVs) isolated from biofilms and plankton (shaken cultures) were identified by MALDI-TOF mass spectrometry and categorized according to GO functional activities and predicted localization. Shown here (left) are the top 15 functional (**A**) and five cellular localization (**B**) categories for proteins identified from biofilm matrix samples, biofilm vesicle and planktonic vesicle samples.

3. Discussion

The Wrinkly Spreader biofilm was the first to be reported for a pseudomonad utilizing cellulose as the main matrix component [20,24]. Although cellulose production is now known to be common amongst the pseudomonads, especially in the fluorescent species which also readily form air–liquid (A–L) interface biofilms [35], biofilm literature is dominated by a relatively few *P. aeruginosa* strains, producing liquid–solid surface (L–S) interface biofilms utilizing multiple EPS. Here, we demonstrate that eDNA and amyloid fibers are present in the matrix of Viscous Mass and Wrinkly Spreader biofilms, and that eDNA has a structural role, at least in the physically more robust Wrinkly Spreader biofilm.

We have used confocal laser scanning microscopy (CLSM) with propidium iodide to visualize eDNA in Viscous Mass and Wrinkly Spreader biofilms following standard protocols, and confirmed the presence of eDNA using a GFP-labelled Wrinkly Spreader mutant to visualize metabolically active cells, rather than CYTO9 to stain intracellular DNA. DNase I treatments indicate eDNA plays a structural role in the Wrinkly Spreader biofilm, though the fragile nature of the Viscous Mass biofilm did not allow us to confirm a similar structural role in this biofilm.

Earlier research has shown that the Wrinkly Spreader biofilm and phenotype is dependent on the production of partly acetylated cellulose and an unidentified attachment factor, possibly PNAG and/or Fap amyloid fibers, and on interactions with liposaccharide (LPS), cells, and debris [19–21,24–26]. Since a cellulose-deficient Wrinkly Spreader mutant does not produce a biofilm in experimental microcosms [24], we can conclude that eDNA is not the only critical component of biofilm formation. Similarly, cellulose matrix–based A–L interface biofilms produced by *P. putida* that also contain eDNA still develop even after DNase I treatment [34]. Nonetheless, we have shown that the addition of exogenous DNA affects Wrinkly Spreader biofilm development, with LMW and HMW DNA having

different impacts on biofilm attachment levels. eDNA absorbs to the surface of cells in long loop-like structures [2] and forms a conditioning layer on glass [68]. Although we do not know the basis for the different impact of exogenous LMW and HMW DNA, DNA entanglement might favor LMW DNA to produce relatively small but dense network structures which aid cell attachment and the early development of the biofilm. In contrast, HMW DNA might produce looser but larger structures which are more sensitive to physical disturbance and distort or break away from the main body of the biofilm. The presence of non-canonical Hoogsteen base-pairing and G-quadruplex (square planar) structures in the eDNA of *P. aeruginosa* PA01 RSCV mutant biofilms [69] illustrates just how complex eDNA networks become in maturing biofilms (Holliday junction recombination intermediates have also been observed in other eDNA [70]). DNase I treatment of developing Wrinkly Spreader biofilms substantially reduces biofilm strength suggesting that eDNA is important early in biofilm formation but has little impact on mature biofilms where it might also be protected from degradation by non-canonical base pairing and association with EPS fibers, proteins, and other matrix components.

The importance of eDNA during the early stages of biofilm development is supported by our exogenous DNA experiments which suggest that LMW DNA increases cell–wall or cell–cell attachment at the meniscus, though the addition of HMW DNA reduces both biofilm attachment levels and biofilm strength. eDNA release events determine the sites for microcolony development [71] which might be mimicked by LMW DNA, leading to biofilm formation, and it is likely that the role of eDNA changes with biofilm development and the spatial heterogeneity in eDNA distributions and interactions with other matrix components add further complexity, as seen for *P. aeruginosa* PA01 [72]. In these biofilms, eDNA interacts with Pel and Psl EPS, forming cationic bridges to overcome electrostatic repulsion and allowing adhesion to surfaces, cell aggregation, and stabilizing the biofilm by forming a fiber-like network [9]. It is notable that eDNA is not restricted to S–L interface biofilms; it has been also associated with *P. aeruginosa* PA01 streamers [56] and clusters of planktonic cells [53] and therefore is not a biofilm-specific matrix component.

eDNA in bacterial biofilms is also known to promote the formation of amyloid fibers which are also critical for cell aggregation and attachment to surfaces. *P. fluorescens* SBW25 contains a Fap amyloid operon [25] and here we provide the first evidence using CLSM and AmyGreen [62,63] demonstrating that amyloid fibers are present in both Viscous Mass and Wrinkly Spreader biofilms, adding yet another layer of complexity to the matrix composition of these biofilms. Although our CLSM images suggest Fap fibers are present at equal levels in both biofilms, further work is required to confirm this using *fap* mutants which need to be produced for each of the wild-type and Wrinkly Spreader mutant strains, and to determine whether Fap levels change as the biofilms mature. As Fap fibers have been shown to increase cell aggregation and the surface hydrophobicity of *Pseudomonas* sp. UK4 cells [50,73] (Fap fibers are also produced by *P. aeruginosa* PA01, *P. fluorescens* Pf-5, and *P. putida* FI [25]), we might expect to find that Fap levels in the Wrinkly Spreader biofilm are higher, providing an explanation for the increased hydrophobic nature of Wrinkly Spreader cells and the dry nature of the top surface of Wrinkly Spreader biofilms. A direct comparison of *fap*, *pga*, and *wss* mutants in wild-type and Wrinkly Spreader backgrounds would also address the relative importance of Fap fibers, PNAG, and cellulose, respectively, in surface attachment and biofilm strength in this model system. *P. putida* KT2440 biofilms are likely to be even more complex, as this strain is also likely to produce Fap [25] and is known to produce alginate, cellulose, Pea and Peb EPS [35,38,39], as well as eDNA [34].

We have yet to start investigating the distribution of cellulose, eDNA, and Fap fibers in VM and WS biofilms, but expect differences in the distribution and quantity of matrix material, metabolically active and possibly motile cells, flagella, fimbriae, pili, LPS, etc., as well as lysing cells and cell debris, to contribute to spatial heterogeneity and larger-scale viscoelastic properties which differentiate Viscous Mass and Wrinkly Spreader biofilms [23]. It is clear from our DNase I treatments that eDNA has a greater role in early biofilm development, while our CLSM images suggest cellulose and eDNA aggregate into larger structures

separate from the layer of producing cells. Earlier epifluorescent microscopy illustrated well the network of cellulose fibers seen in Viscous Mass and Wrinkly Spreader biofilms and encompassing large voids filled with bacteria [20,22,35]. Wild-type *P. fluorescens* SBW25 and Wrinkly Spreader mutant cells are capable of swimming motility and capable of aerotaxic migration that would allow them to colonize any part of the A–L interface biofilm [74], with fitness assays suggesting that the preferred Goldilocks' zone for growth is at the top of the A–L interface [19] (CLSM suggests that the top-most layer of active cells is just below the exposed surface of the Wrinkly Spreader biofilm [52]). *P. fluorescens* SBW25 can utilize exogenous intermolecular agar networks and polyethylene glycol intermolecular friction to quickly colonize the A–L interface [74] suggesting that any viscous or viscoelastic matrix can be used as the basis for biofilm formation. It is likely therefore that cellulose and eDNA network structures or scaffolds might be colonized by motile cells to produce extensions from the original biofilm or new initial biofilm formation on uncolonized surfaces. *P. aeruginosa* PA01 eDNA-based planktonic cell clusters [53] may represent a surface-colonizing adaptation if survival and attachment rates are better than for single cells, in which case *P. fluorescens* SBW25 and other biofilm forming pseudomonads would also be expected to produce similar planktonic clusters.

There is also growing interest in other matrix components, such as membrane vesicles and proteins, which may play roles in biofilm structure and function [1,5,8,9,29–32]. The physically robust nature of the Wrinkly Spreader biofilm allowed us to readily separate cells and matrix material from the interstitial fluid, and we were able to visualize vesicles and demonstrate that eDNA was associated with these, as has been seen for *P. aeruginosa* PA01 [75,76]. *P. aeruginosa* PA01 membrane vesicles are produced by different mechanisms and have different compositions and functions [29,65,66,77]. We were able to demonstrate differences in protein profiles for biofilm matrix-associated proteins, biofilm vesicles and planktonic vesicles, which also suggest different origins and possible functions for these in the Wrinkly Spreader biofilm. We note that although membrane vesicles may diffuse away from cell surfaces, they spend more time at the liquid–bacterial membrane interface [78], raising the question of how significant their role might be in biofilms beyond regions with densely packed cells.

Although the underlying molecular biology of the *P. fluorescens* SBW25 Wrinkly Spreader biofilm was determined almost 20 years ago [18,19], we have felt that our understanding of this and the related Viscous Mass biofilm needed revision as progress has been made for other model systems where eDNA and amyloid fibers have been found to contribute to biofilm development and structure. Here, we demonstrate that eDNA and Fap amyloid fibers are also present in *P. fluorescens* SBW25 A–L interface biofilms, and eDNA plays a structural role in early development at least in the physically more robust Wrinkly Spreader biofilm. However, unlike *P. aeruginosa* S–L interface biofilms where eDNA is primarily responsible for the viscoelastic properties [69], eDNA plays a secondary role to cellulose which is the primary matrix and structural component of these *P. fluorescens* SBW25 biofilms.

4. Materials and Methods

4.1. Bacteria and Culturing Conditions

Wild-type *Pseudomonas fluorescens* SBW25 [24], which produces the Viscous Mass biofilm [22], and the archetypal Wrinkly Spreader (WS) mutant (*P. fluorescens* SBW25 *wspF* A901C) [21,79] and GFP-expressing WS-GFP strain (WS::miniTn7(Gm)$_{PAI/04/03}$ *gfp*.ASV-a) [52], which produce the Wrinkly Spreader biofilm [24,79], were examined in this work. Microcosms were 30 mL glass vials containing 6 mL King's B (KB) [80] liquid medium and supplemented with 1 mM $FeCl_3$ to induce Viscous Mass biofilm-formation [22]. Bacteria were incubated at 20 °C with biofilms produced in microcosms incubated statically for 24 h or three days (for mature biofilms), and planktonic samples recovered from 24 h shaken microcosms in which biofilms could not form. Low-molecular-weight (LMW) salmon sperm DNA (Fluka, Charlotte, NC, USA) and high-molecular-weight (HMW) salmon testis

DNA (Sigma-Aldrich, Dorset, UK) were added to microcosms at 100, 300, and 600 μg/mL, and Bovine pancreas deoxyribonuclease I (DNase I) (Sigma-Aldrich) added to 1 μg/mL to assess the importance of eDNA to biofilm development, final strength, and attachment levels.

4.2. Combined Biofilm Assay

Biofilms were quantitatively measured using the combined biofilm assay [57] based on earlier work [20,21,35] in microcosm vials which involves the serial measurement of biofilm strength (grams), attachment levels (crystal violet staining, A_{570}), and total microcosm biomass (OD_{600}) (i.e., growth). Biofilms were first assayed for strength using small (~0.01 g) glass balls which were sequentially added until the biofilm broke or sank (the maximum deformation or breaking mass [20,21,35]). It should be noted that although Viscous Mass biofilms developed in all treatments, confirmed by visual inspection, they were generally so weak that they could not easily be measured compared to the more robust Wrinkly Spreader biofilms [23]. The contents of the microcosm vials with damaged or sunken biofilms were transferred to a second vial which was then vigorously mixed for 30 s to disintegrate all biofilm material. This suspension was then sampled to determine optical density (OD_{600}) using a Spectronic Helios Epsilon spectrophotometer (ThermoFisher Scientific, Oxford, UK) with 10 mm optical-path cuvettes, as a measure of total microcosm biomass. The original vials were then assayed for the attachment of cells and biofilm at the meniscus using crystal violet [20] (after [59], etc.). The vials were washed three times in water to remove non-attached cells and material, and then stained with 0.05% *w/v* crystal violet for 2 min and rewashed three times to remove unbound dye. The crystal violet was eluted with 5 mL ethanol and gentle shaking for 1 h and sampled to determine absorbance (A_{570}) as a measure of biofilm attachment levels at the meniscus. A second elution with 5 mL 10% *v/v* acetic acid (after [61] etc.) for 1 h followed by absorbance (A_{570}) measurements was used to quantify the remaining bound crystal violet.

4.3. Spectrophometric Measurement of eDNA

Quantitative measurements of eDNA levels in three-day-old biofilms were made by spectrometry [55]. Five hundred and fifty microliter samples were recovered from microcosms and the biofilms disrupted by vortexing for 10 min before cells and debris were pelleted by centrifugation at 12,000× *g* for 15 min and 500 μL of cell-free supernatant transferred to a new tube. DNA was precipitated with 50 μL 3 M sodium acetate (pH 5.2) and 1 mL 96% (*v*/*v*) ethanol at −20 °C overnight before centrifugation at 13,000× *g* for 15 min. The pelleted DNA was washed with 1 mL 70% (*v*/*v*) ethanol and subjected to centrifugation at 13,000× *g* for 15 min before being air-dried at room temperature. Samples were dissolved in 200 μL Tris-EDTA (TE) buffer and eDNA concentration measured using a NanoDrop 2000 spectrometer (ThermoFisher Scientific).

4.4. Confocal Laser Scanning Microscopy (CLSM) and Transmission Electron Microscopy (TEM)

Microscopy of biofilm samples was undertaken following established procedures [52]. Biofilm samples were recovered from three-day-old microcosms by spooling them onto P1000 pipettor tips and then rolling them out in the other direction onto microscope slides. Excess liquid was drained off before 10 μL aliquots of each of the required stains were added. eDNA was stained with 20 μM propidium iodide (Sigma-Aldrich) and 1 μM Experimental Stain 986 in DMSO (Department of Biomedicinal Chemistry, IMBG, Kyiv, Ukraine). Intracellular DNA from intact and metabolically active (live) cells was stained with 5 μM SYTO 9 solution (ThermoFisher Scientific), and total DNA (eDNA and DNA in active and dead cells) stained with 2 μg/mL ethidium bromide (ThermoFisher Scientific). Amyloid fibers were stained with 1 μM AmyGreen in DMSO (Department of Biomedicinal Chemistry), cellulose with 5 μM Calcofluor white (Sigma-Aldrich), and vesicle membranes with 5 μL Vybrant DiO solution (ThermoFisher Scientific). No additional washing was applied to the biofilm samples to minimize the physical disruption of biofilm structures through liquid movement. To stabilize vesicles, the suspension was mixed with molten

0.8% (*w*/*v*) agarose gel before applying it to the glass slide. Samples were not fixed, and a cover slip was put into position before imaging. CLSM analysis was undertaken using a Leica TCS SPE Confocal system with a coded DMi8 inverted microscope (Leica, Wetzlar, Germany) and Leica Application Suite X Version 3.4.1 software. Images were acquired using excitation at 488 nm and emission collected at 490–580 nm for AmyGreen, GFP, SYTO 9, and Vybrant DiO; excitation at 532 nm and emission collected at 537–670 for ethidium bromide, Experimental Stain 986, and propidium iodide; and excitation at 405 nm and emission collected at 450–500 nm for Calcofluor white.

Transmission electron microscopy (TEM) of biofilm samples was undertaken following standard procedures. Ten microliters of vesicle suspension were placed onto formvar-coated TEM grids and dried. Vesicles were stained with 2% (*w*/*v*) uranyl oxalate, pH 7.0, for 10 min and then washed with phosphate buffered saline (PBS). TEM was performed on a JEM 1230 (Jeol, Tokyo, Japan) microscope operated at 80 kV.

4.5. Membrane Vesicle (MV) Preparation

MVs were isolated from Wrinkly Spreader biofilms and planktonic cultures by centrifugation to remove cells and matrix followed by filtration (after [17] etc.). Two hundred milliliters of 24 h culture and three-day biofilms pooled from four 1 L flasks containing 250 mL KB medium were centrifuged at 8000× *g* at 4 °C for 20 min and the supernatant recovered. These were then centrifuged at 24,000× *g* 4 °C for 30 min and the supernatants passed through 0.45 µm pore-size PES filters (MDI, Gurgaon, India). The filtrates were pelleted by centrifugation at 60,000× *g* at 4 °C for 2 h and finally resuspended in 600 µL PBS. MV-associated proteins were separated by SDS-PAGE and visualized with PageBlue Protein Staining Solution (ThermoFisher Scientific). An aliquot of Pierce™ Unstained Protein MW Marker (ThermoFisher Scientific) was run on the gel for sizing. Samples were also treated with 100 µg/µL DNase I (Sigma-Aldrich) in 20 mM Tris-HCl pH7.4, 10 mM $MgCl_2$, before the DNA was extracted with phenol-chloroform, precipitated with sodium acetate/ethanol as above, and finally resuspended in TE buffer. Samples were electrophoresed on a 1.3% (*w*/*v*) Tris-buffered EDTA (TBE)-agarose gel before being stained with ethidium bromide to visualize the DNA. An aliquot of O'GeneRuler 1 kb DNA ladder (ThermoFisher Scientific) was run on the gel for sizing.

4.6. Matrix-Associated Proteins

Matrix-associated proteins were recovered from Wrinkly Spreader biofilms after centrifugation to remove cells and extensive washing of the matrix material to remove unbound proteins. Five three-day biofilms grown in 6 mL KB microcosms were pooled, and the liquid carefully removed with a pipettor. Ten milliliters of deionized water were added and the biofilms gently mixed before leaving for 24 h. This washing was repeated a further six times before the biofilm matrix was pelleted by centrifugation at 4000× *g* for 10 min. The supernatant was carefully removed with a pipettor, and the matrix resuspended in the remaining liquid. 100 µL of biofilm matrix samples were pre-incubated with 50 µL deionized water, 0.1% (*w*/*v*) SDS, or 6 M urea at room temperature for 2 h before 20 µL SDS–PAGE sample buffer was added. Samples were investigated by SDS-PAGE as above.

4.7. MALDI-TOF Mass Spectometry and Protein Identification

Mass spectrometry of protein samples were undertaken following established procedures. Thirty microliters of membrane vesicle (MV) sample and matrix-associated protein were concentrated by SDS-PAGE to obtain lanes of 5 mm width. The lanes containing proteins were subjected to in-gel trypsinolysis and proteins identified by Maxis Impact LC-QTOF mass spectrometer (Bruker, Billerica, MA, USA) using the NCBInr database and Mascot server (Matrix Science, London, UK; http://www.matrixscience.com) to identify proteins and calculate exponentially modified protein abundance index (emPAI) values. Gene Ontology (GO) Annotation and protein subcellular locations were obtained from UniProt (www.uniprot.org) [81].

4.8. Statistical Analyses

Experiments were performed with replicates and means with standard errors (SE) are shown where appropriate. Statistical test and p values are rounded up to two decimal places, and significant results reported for $\alpha = 0.05$ or when $p \leq 0.05$. JMP Version 12 (SAS Institute Inc., Cary, NC, USA) statistical software was used to analyze data. First, residuals were investigated and the goodness of fit of a normal distribution determined using Shapiro–Wilk W test to decide whether to proceed with a parametric test or adopt a non-parametric approach. General linear mixed models (GLMM) were used to investigate combined biofilm assay data and determine significant effects and interactions, with LSMeans Differences Tukey HSD ($\alpha = 0.05$) used to determine significant differences between means. *T*-tests and ANOVA models with post hoc Tukey–Kramer HSD tests ($\alpha = 0.05$) were also used to make comparisons between means. Where appropriate and rather than to delete outliers, a non-parametric approach was followed using the Kruskal–Wallis (Rank Sums) test and comparisons of each mean made using the Wilcoxon method. Spearman's Rho was used to determine correlations. Contingency tables and χ^2 tests were used to assess the independence of *protein source* × *abundance* and *protein source* × *cellular localization* using the Chi-Square Calculator (www.icalcu.com/stat/chisqtest.html, last accessed on 30 November 2022).

Supplementary Materials: The following supporting information can be downloaded at: https://www.mdpi.com/article/10.3390/ijms232315096/s1.

Author Contributions: Conceptualization, O.V.M. and A.J.S.; formal analysis, A.J.S.; investigation, I.P., O.I., O.V.M. and A.J.S.; writing—original draft preparation, O.V.M., G.P. and A.J.S.; writing—review and editing, O.V.M., G.P. and A.J.S. All authors have read and agreed to the published version of the manuscript.

Funding: This research was partially funded by NATO SPS grant 'Fighting maritime corrosion and biofouling with task-specific ionic compounds' (984834).

Data Availability Statement: All data have been included in this manuscript (figures).

Acknowledgments: The authors thank Sergiy M. Yarmoluk, Department of Biomedicinal Chemistry, Institute of Molecular Biology and Genetics of the National Academy of Sciences of Ukraine, and his team for providing the Experimental Stain 986. O.V.M. thanks The Krzysztof Skubiszewski Foundation, and Marcin Skubiszewski personally, for their support through the financial aid program to scholars who are war victims. O.V.M. also thanks Elena Trizna and Airat Kayumov for their cooperation and support.

Conflicts of Interest: The authors declare no conflict of interest.

References

1. Flemming, H.-C.; van Hullebusch, E.D.; Neu, T.R.; Nielsen, P.H.; Seviour, T.; Stoodley, P.; Wingender, J.; Wuerts, S. The biofilm matrix: Multitasking in a shared space. *Nat. Rev. Microbiol.* **2022**, 1–17. [CrossRef] [PubMed]
2. Okshevsky, M.; Meyer, R.L. The role of extracellular DNA in the establishment, maintenance and perpetuation of bacterial biofilms. *Crit. Rev. Microbiol.* **2015**, *41*, 341–352. [CrossRef] [PubMed]
3. Jakubovics, N.S.; Shields, R.C.; Rajarajan, N.; Burges, J.G. Life after death: The critical role of extracellular DNA in microbial biofilms. *Lett. Appl. Microbiol.* **2013**, *57*, 467–475. [CrossRef] [PubMed]
4. Ibáñez de Aldecoa, A.L.; Zafra, O.; González-Pastor, J.E. Mechanisms and regulation of extracellular DNA release and its biological roles in microbial communities. *Front. Microbiol.* **2017**, *8*, 1390. [CrossRef]
5. Campoccia, D.; Montanaro, L.; Aricola, C.R. Extracellular DNA (eDNA). A major ubiquitous element of the bacterial biofilm architecture. *Int. J. Mol. Sci.* **2021**, *22*, 9100. [CrossRef]
6. Vandana, S.D. Genetic regulation, biosynthesis and applications of extracellular polysaccharides of the biofilm matrix of bacteria. *Carbohydr. Polym.* **2022**, *291*, 119536. [CrossRef] [PubMed]
7. Whitchurch, C.B.; Tolker-Nielsen, T.; Ragas, P.C.; Mattick, J.S. Extracellular DNA required for bacterial biofilm formation. *Science* **2002**, *295*, 1487. [CrossRef] [PubMed]
8. Mann, E.E.; Wozniak, D.J. *Pseudomonas* biofilm matrix composition and niche biology. *FEMS Microbiol. Rev.* **2012**, *36*, 893–916. [CrossRef]
9. Jiang, Z.; Nero, T.; Mukherjee, S.; Olson, R.; Yan, J. Searching for the secret of stickiness: How biofilms adhere to surfaces. *Front. Microbiol.* **2021**, *12*, 686793. [CrossRef]

10. Moshynets, O.V.; Spiers, A.J. Viewing biofilms within the larger context of bacterial aggregations. In *Microbial Biofilms–Importance and Applications*; Dhanasekaran, D., Thajuddin, N., Eds.; InTechOpen: London, UK, 2016; pp. 3–22. [CrossRef]
11. Peng, N.; Cai, P.; Mortimer, M.; Wu, Y.; Gao, Y.; Huang, Q. The exopolysaccharide–eDNA interaction modulates 3D architecture of *Bacillus subtilis* biofilm. *BMC Microbiol.* **2020**, *20*, 115. [CrossRef]
12. Wu, J.; Xi, C. Evaluation of different methods for extracting extracellular DNA from the biofilm matrix. *Appl. Environ. Microbiol.* **2009**, *75*, 5390–5395. [CrossRef] [PubMed]
13. Wang, H.; Huang, Y.; Wu, S.; Li, Y.; Ye, Y.; Zheng, Y.; Huang, R. Extracellular DNA inhibits *Salmonella enterica* serovar Typhimurium and *S. enterica* serovar Typhi biofilm development on abiotic surfaces. *Curr. Microbiol.* **2014**, *68*, 262–268. [CrossRef] [PubMed]
14. Rice, K.C.; Mann, E.E.; Endres, J.L.; Weiss, E.C.; Cassat, J.E.; Smeltzer, M.S.; Bayles, K.W. The *cidA* murein hydrolase regulator contributes to DNA release and biofilm development in *Staphylococcus aureus*. *Proc. Natl. Acad. Sci. USA* **2007**, *104*, 8113–8118. [CrossRef]
15. Qin, Z.; Ou, Y.; Yang, L.; Zhu, Y.; Tolker-Nielsen, T.; Molin, S.; Qu, D. Role of autolysin-mediated DNA release in biofilm formation of *Staphylococcus epidermidis*. *Microbiology* **2007**, *153*, 2083–2092. [CrossRef] [PubMed]
16. Hall-Stoodley, L.; Nistico, L.; Sambanthamoorthy, K.; Dice, B.; Nguyen, D.; Mershon, W.J.; Johnson, C.; Hu, F.Z.; Stoodley, P.; Ehrlich, G.D.; et al. Characterization of biofilm matrix, degradation by DNase treatment and evidence of capsule downregulation in *Streptococcus pneumoniae* clinical isolates. *BMC Microbiol.* **2008**, *8*, 173. [CrossRef] [PubMed]
17. Liao, S.; Klein, M.I.; Heim, K.P.; Fan, Y.; Bitoun, J.P.; Ahn, S.-J.; Burne, R.A.; Koo, H.; Jeannine Brady, L.; Wen, Z.T. *Streptococcus mutans* extracellular DNA is upregulated during growth in biofilms, actively released via membrane vesicles, and influenced by components of the protein secretion machinery. *J. Bacteriol.* **2014**, *196*, 2355–2366. [CrossRef] [PubMed]
18. Spiers, A.J. A mechanistic explanation linking adaptive mutation, niche change, and fitness advantage for the Wrinkly Spreader. *Int. J. Evol. Biol.* **2014**, *2014*, 675432. [CrossRef] [PubMed]
19. Koza, A.; Kuśmierska, A.; McLaughlin, K.; Moshynets, O.; Spiers, A.J. Adaptive radiation of *Pseudomonas fluorescens* SBW25 in experimental microcosms provides an understanding of the evolutionary ecology and molecular biology of A-L interface biofilm formation. *FEMS Microbiol. Lett.* **2017**, *364*, fnx109. [CrossRef] [PubMed]
20. Spiers, A.J.; Bohannon, J.; Gehrig, S.M.; Rainey, P.B. Biofilm formation at the air–liquid interface by the *Pseudomonas fluorescens* SBW25 wrinkly spreader requires an acetylated form of cellulose. *Mol. Microbiol.* **2003**, *50*, 15–27. [CrossRef]
21. Spiers, A.J.; Rainey, P.B. The *Pseudomonas fluorescens* SBW25 wrinkly spreader biofilm requires attachment factor, cellulose fibre and LPS interactions to maintain strength and integrity. *Microbiology* **2005**, *151*, 2829–2839. [CrossRef]
22. Koza, A.; Hallett, P.D.; Moon, C.D.; Spiers, A.J. Characterization of a novel air–liquid interface biofilm of *Pseudomonas fluorescens* SBW25. *Microbiology* **2009**, *155*, 1397–1406. [CrossRef] [PubMed]
23. Koza, A.; Jerdan, R.; Cameron, S.; Spiers, A.J. Three biofilm types produced by a model pseudomonad are differentiated by structural characteristics and fitness advantage. *Microbiology* **2020**, *166*, 707–716. [CrossRef] [PubMed]
24. Spiers, A.J.; Kahn, S.G.; Bohannon, J.; Travisano, M.; Rainey, P.B. Adaptive divergence in experimental populations of *Pseudomonas fluorescens*. I. Genetic and phenotypic bases of Wrinkly Spreader fitness. *Genetics* **2002**, *161*, 33–46. [CrossRef] [PubMed]
25. Dueholm, M.S.; Søndergaard, M.T.; Nilsson, M.; Christiansen, G.; Stensballe, A.; Overgaard, M.T. Expression of Fap amyloids in *Pseudomonas aeruginosa*, *P. fluorescens*, and *P. putida* results in aggregation and increased biofilm formation. *MicrobiologyOpen* **2013**, *2*, 365–382. [CrossRef] [PubMed]
26. Lind, P.A.; Farr, A.D.; Rainey, P.B. Evolutionary convergence in experimental *Pseudomonas* populations. *ISME J.* **2017**, *11*, 589–600. [CrossRef] [PubMed]
27. Lien, S.K.; Sletta, H.; Ellingsen, T.E.; Valla, S.; Correa, E.; Goodacre, R.; Vernstad, K.; Borgos, S.E.; Bruheim, P. Investigating alginate production and carbon utilization in *Pseudomonas fluorescens* SBW25 using mass spectrometry-based metabolic profiling. *Metabolomics* **2013**, *9*, 403–417. [CrossRef]
28. Ertesvåg, H.; Sletta, H.; Senneset, M.; Sun, Y.-Q.; Klinkenberg, G.; Konradsen, T.A.; Ellingsen, T.E.; Valla, S. Identification of genes affecting alginate biosynthesis in *Pseudomonas fluorescens* by screening a transposon insertion library. *BMC Genom.* **2017**, *18*, 11. [CrossRef]
29. Tashiro, Y.; Uchiyama, H.; Nomura, N. Multifunctional membrane vesicles in *Pseudomonas aeruginosa*. *Environ. Microbiol.* **2012**, *14*, 1349–1362. [CrossRef]
30. Toyofuku, M.; Nomura, N.; Eberl, L. Types and origins of bacterial membrane vesicles. *Nat. Rev. Microbiol.* **2019**, *17*, 13–24. [CrossRef]
31. Karygianni, L.; Ren, Z.; Koo, H.; Thurnheer, T. Biofilm matrixome: Extracellular components in structured microbial communities. *Trends Microbiol.* **2020**, *28*, 8. [CrossRef]
32. Mozeheb, N.; Mingeot-Leclercq, M.-P. Membrane vesicle production as a bacterial defense against stress. *Front. Microbiol.* **2020**, *11*, 600221. [CrossRef] [PubMed]
33. Wang, D.; Yu, J.M.; Dorosky, R.J.; Pierson, L.S.; Pierson, E.A. The phenazine 2-hydroxy-phenazine-1-carboxylic acid promotes extracellular DNA release and has broad transcriptomic consequences in *Pseudomonas chlororaphis* 30–84. *PLoS ONE* **2016**, *11*, e0148003. [CrossRef] [PubMed]
34. D'Alvise, P.W.; Sjøholm, O.R.; Yankelevich, T.; Jin, Y.; Wuertz, S.; Smets, B.F. TOL plasmid carriage enhances biofilm formation and increases extracellular DNA content in *Pseudomonas putida* KT2440. *FEMS Microbiol. Lett.* **2010**, *312*, 84–92. [CrossRef] [PubMed]

35. Ude, S.; Arnold, D.L.; Moon, C.C.; Timms-Wilson, T.; Spiers, A.J. Biofilm formation and cellulose expression among diverse environmental *Pseudomonas isolates*. *Env. Microbiol.* **2006**, *8*, 1997–2011. [CrossRef] [PubMed]
36. Hansen, S.K.; Haagensen, J.A.J.; Gjernmansen, M.; Jørgensen, T.M.; Tolker-Nielsen, T.; Molin, S. Characterization of a *Pseudomonas putida* rough variant evolved in a mixed-species biofilm with *Acinetobacter* sp. strain C6. *J. Bacteriol.* **2007**, *189*, 4932–4943. [CrossRef] [PubMed]
37. Lee, Y.; Oh, S.; Park, W. Inactivation of the *Pseudomonas putida* KT2440 *dsbA* gene promotes extracellular matrix production and biofilm formation. *FEMS Microbiol. Lett.* **2009**, *297*, 38–48. [CrossRef]
38. Nielsen, L.; Li, X.; Halverson, L.J. Cell–cell and cell-surface interactions mediated by cellulose and a novel exopolysaccharide contribute to *Pseudomonas putida* biofilm formation and fitness under water limiting conditions. *Environ. Microbiol.* **2011**, *13*, 1342–1356. [CrossRef]
39. Nilsson, M.; Chiang, W.-C.; Fazli, M.; Gjermansen, M.; Givskov, M.; Tolker-Nielsen, T. Influence of putative exopolysaccharide genes on *Pseudomonas putida* KT2440 biofilm stability. *Environ. Microbiol.* **2011**, *13*, 1357–1369. [CrossRef]
40. Tang, L.; Schramm, A.; Neu, T.R.; Revsbech, N.P.; Meyer, R.L. Extracellular DNA in adhesion and biofilm formation of four environmental isolates: A quantitative study. *FEMS Microbiol. Ecol.* **2013**, *86*, 394–403. [CrossRef]
41. Catlin, B.W.; Cunningham, L.S. Studies of extracellular and intracellular bacterial deoxyribonucleic acids. *J. Gen. Microbiol.* **1958**, *19*, 522–539. [CrossRef]
42. Haque, M.M.; Mosharaf, M.K.; Khatun, M.; Haque, M.A.; Biswas, M.S.; Islam, M.S.; Islam, M.M.; Shozib, H.B.; Uddian Miah, M.M.; Molla, A.H.; et al. Biofilm producing rhizobacteria with multiple plant growth-promoting traits promote growth of tomato under water-deficit stress. *Front. Microbiol.* **2020**, *11*, 542053. [CrossRef] [PubMed]
43. Haque, M.M.; Haque, M.A.; Mosharaf, M.K.; Islam, M.S.; Islam, M.M.; Hasan, M.; Molla, A.H.; Haque, M.A. Biofilm-mediated decolorization, degradation and detoxification of synthetic effluent by novel biofilm-producing bacteria isolated from textile dyeing effluent. *Environ. Pollut.* **2022**, *314*, 120237. [CrossRef]
44. Haque, M.; Biswas, M.; Mosharaf, M.K.; Islam, M.; Nahar, K.; Shozib, H.B. Halotolerant biofilm-producing rhizobacteria mitigate seawater-induced salt stress and promote growth of tomato. *Sci. Rep.* **2022**, *12*, 5599. [CrossRef] [PubMed]
45. Farias, G.A.; Olmedilla, A.; Gallegos, M.-T. Visualization and characterization of *Pseudomonas syringae* pv. tomato DC3000 pellicles. Microbial Technol. *Microbial. Biotechnol.* **2019**, *12*, 688–702. [CrossRef] [PubMed]
46. Garrido-Sanz, D.; Meier-Kolthoff, J.P.; Göker, M.; Martín, M.; Rivilla, R.; Redondo-Nieto, M. Genomic and genetic diversity within the *Pseudomonas fluorescens* complex. *PLoS ONE* **2016**, *11*, e0150183. [CrossRef] [PubMed]
47. Peix, A.; Ramírez-Bahena, M.-H.; Velázquez, E. The current status on the taxonomy of *Pseudomonas* revisited: An update. *Infect. Genet. Evol.* **2018**, *J57*, 106–116. [CrossRef]
48. Passarelli-Araujo, H.; Franco, G.R.; Venancio, T.M. Network analysis of ten thousand genomes shed light on *Pseudomonas* diversity and classification. *Microbiol. Res.* **2022**, *254*, 126919. [CrossRef]
49. Blanco-Romero, E.; Garrido-Sanz, D.; Durán, D.; Rivilla, R.; Redondo-Nieto, M.; Martín, M. Regulation of extracellular matrix components by AmrZ is mediated by c-di-GMP in *Pseudomonas ogarae* F113. *Sci. Rep.* **2022**, *12*, 11914. [CrossRef]
50. Dueholm, M.S.; Petersen, S.V.; Sønderkær, M.; Larsen, P.; Christiansen, G.; Hein, K.L.; Enghild, J.J.; Nielsen, J.L.; Nielsen, K.L.; Nielsen, P.H.; et al. Functional amyloid in *Pseudomonas*. *Mol. Microbiol.* **2010**, *77*, 1009–1020. [CrossRef]
51. Boulos, L.; Prévost, M.; Barbeau, B.; Coallier, J.; Desjardins, R. LIVE/DEAD BacLight: Application of a new rapid staining method for direct enumeration of viable and total bacteria in drinking water. *J. Microbiol. Methods* **1999**, *37*, 77–86. [CrossRef]
52. Koza, A.; Moshynets, O.; Otten, W.; Spiers, A.J. Environmental modification and niche construction: Developing O_2 gradients drive the evolution of the Wrinkly Spreader. *ISME J.* **2011**, *5*, 665–673. [CrossRef] [PubMed]
53. Schleheck, D.; Barraud, N.; Klebensberger, J.; Webb, J.S.; McDougald, D.; Rice, S.A.; Kjelleberg, S. *Pseudomonas aeruginosa* PAO1 preferentially grows as aggregates in liquid batch cultures and disperses upon starvation. *PLoS ONE* **2009**, *4*, e5513. [CrossRef] [PubMed]
54. Lehtinen, J.; Nuutila, J.; Lilius, E.M. Green fluorescent protein-propidium iodide (GFP-PI) based assay for flow cytometric measurement of bacterial viability. *Cytom. Part A* **2004**, *60*, 165–172. [CrossRef] [PubMed]
55. Moshynets, O.; Bardeau, J.-F.; Tarasyuk, O.; Makhno, S.; Cherniavska, T.; Dzhuzha, O.; Potters, G.; Rogalsky, S. Antibiofilm activity of Polyamide 11 modified with thermally stable polymeric biocide polyhexamethylene guanidine 2-naphtalenesulfonate. *Int. J. Mol. Sci.* **2019**, *20*, 348. [CrossRef]
56. Secchi, E.; Savorana, G.; Vitale, A.; Eberl, L.; Stocker, R.; Rusconi, R. The structural role of bacterial eDNA in the formation of biofilm streamers. *Proc. Natl. Acad. Sci. USA* **2022**, *119*, e2113723119. [CrossRef] [PubMed]
57. Robertson, M.; Hapca, S.M.; Moshynets, O.; Spiers, A.J. Air-liquid interface biofilm formation by psychrotrophic pseudomonads recovered from spoilt meat. *Antonie Leeuwenhoek* **2013**, *103*, 251–259. [CrossRef]
58. Chiang, W.-C.; Nilsson, M.; Jensen, P.Ø.; Høiby, N.; Nielsen, T.E.; Givskov, M.; Tolker-Nielsen, T. Extracellular DNA shields against Aminoglycosides in *Pseudomonas aeruginosa* biofilms. *Antimicrob. Agents Chemother.* **2013**, *57*, 2352–2361. [CrossRef] [PubMed]
59. O'Toole, G.A.; Pratt, L.A.; Watnick, P.I.; Newman, D.K.; Weaver, V.B.; Kolter, R. Genetic approaches to study of biofilms. *Methods Enzymol.* **1999**, *310*, 91–109. [CrossRef]
60. Koreňová, J.; Lopašovská, J.; Kuchta, T. Comparison of three microtitre plate-based methods for quantification of biofilm formation ability of bacteria contaminating food technologies. *J. Food Nutr. Res.* **2008**, *47*, 100–104.
61. O'Toole, G.A. Microtiter dish biofilm formation assay. *JoVE J. Vis. Exp.* **2011**, *47*, e2437. [CrossRef]

62. Moshynets, O.; Chernii, S.; Chernii, V.; Losytskyy, M.; Karakhim, S.; Czerwieniec, R.; Pekhnyo, V.; Yarmoluk, S.; Kovalska, V. Fluorescent β-ketoenole AmyGreen dye for visualization of amyloid components of bacterial biofilms. *Methods Appl. Fluoresc.* **2020**, *8*, 035006. [CrossRef] [PubMed]
63. Chernii, S.; Gerasymchuk, Y.; Losytskyy, M.; Szymański, D.; Tretyakova, I.; Łukowiak, A.; Pekhnyo, V.; Yarmoluk, S.; Chernii, V.; Kovalska, V. Modification of insulin amyloid aggregation by Zr phthalocyanines functionalized with dehydroacetic acid derivatives. *PLoS ONE* **2021**, *16*, e0243904. [CrossRef] [PubMed]
64. Wu, M.-Y.; Leung, J.-K.; Kam, C.; Chou, T.Y.; Wang, J.-L.; Zhao, X.; Feng, S.; Chen, S. A near-infrared plasma membrane-specific AIE probe for fluorescence lifetime imaging of phagocytosis. *Sci. China Chem.* **2022**, *65*, 979–988. [CrossRef]
65. Couto, N.; Schooling, S.R.; Dutcher, J.R.; Barber, J. Proteome profiles of outer membrane vesicles and extracellular matrix of *Pseudomonas aeruginosa* biofilms. *J. Proteome Res.* **2015**, *14*, 4207–4222. [CrossRef] [PubMed]
66. Toyofuku, M.; Roschitzki, B.; Riedel, K.; Eberl, L. Identification of proteins associated with the *Pseudomonas aeruginosa* biofilm extracellular matrix. *J. Proteome Res.* **2012**, *11*, 4906–4915. [CrossRef]
67. Choi, D.-S.; Kim, D.-K.; Choi, S.J.; Lee, J.; Choi, J.-P.; Rho, S.; Park, S.-H.; Kim, Y.-K.; Hwang, D.; Gho, Y.S. Proteomic analysis of outer membrane vesicles derived from *Pseudomonas aeruginosa*. *Proteomics* **2011**, *11*, 3424–3429. [CrossRef] [PubMed]
68. Vilain, S.; Pretorius, J.M.; Theron, J.; Brözel, V.S. DNA as an adhesin: *Bacillus cereus* requires extracellular DNA to form biofilms. *Appl. Environ. Microbiol.* **2009**, *75*, 2861–2868. [CrossRef] [PubMed]
69. Seviour, T.; Winnerdy, F.R.; Wong, L.L.; Shi, X.; Mugunthan, S.; Foo, Y.H.; Castaing, R.; Adav, S.S.; Subramoni, S.; Kohli, G.S.; et al. The biofilm matrix scaffold of *Pseudomonas aeruginosa* contains G-quadruplex extracellular DNA structures. *NPJ Biofilms Microbiomes* **2021**, *7*, 27. [CrossRef]
70. Devaraj, A.; Buzzo, J.R.; Mashburn-Warren, L.; Gloag, E.S.; Novotny, L.A.; Stoodley, P.; Bakaletz, L.O.; Goodman, S.D. The extracellular DNA lattice of bacterial biofilms is structurally related to Holliday junction recombination intermediates. *Proc. Natl. Acad. Sci. USA* **2019**, *116*, 25068–25077. [CrossRef]
71. Hynen, A.L.; Lazenby, J.J.; Savva, G.M.; McCaughey, L.C.; Turnbull, L.; Nolan, L.M.; Whitchurch, C.B. Multiple holins contribute to extracellular DNA release in *Pseudomonas aeruginosa* biofilms. *Microbiology* **2021**, *167*, 000990. [CrossRef]
72. Hunter, R.C.; Beveridge, T.J. High-resolution visualization of *Pseudomonas aeruginosa* PAO1 biofilms by freeze-substitution transmission electron microscopy. *J. Bacteriol.* **2005**, *187*, 7619–7630. [CrossRef] [PubMed]
73. Zeng, G.; Vad, B.S.; Dueholm, M.S.; Christiansen, G.; Nilsson, M.; Tolker-Nielsen, T.; Nielsen, P.H.; Meyer, R.L.; Otzen, D.E. Functional bacterial amyloid increases *Pseudomonas* biofilm hydrophobicity and stiffness. *Front. Microbiol.* **2015**, *6*, 1099. [CrossRef] [PubMed]
74. Jerdan, R.; Cameron, S.; Donaldson, E.; Iungin, O.; Moshynets, O.V.; Spiers, A.J. Community biofilm-formation, stratification and productivity in serially-transferred microcosms. *FEMS Microbiol. Lett.* **2020**, *367*, fnaa187. [CrossRef]
75. Kadurugamuwa, J.L.; Beveridge, T.J. Virulence factors are released from *Pseudomonas aeruginosa* in association with membrane vesicles during normal growth and exposure to gentamicin: A novel mechanism of enzyme secretion. *J. Bacteriol.* **1995**, *177*, 3998–4008. [CrossRef] [PubMed]
76. Renelli, M.; Matias, V.; Lo, R.Y.; Beveridge, T.J. DNA-containing membrane vesicles of *Pseudomonas aeruginosa* PAO1 and their genetic transformation potential. *Microbiology* **2004**, *150*, 2161–2169. [CrossRef] [PubMed]
77. Cooke, A.C.; Nello, A.V.; Ernst, R.K.; Schertzer, J.W. Analysis of *Pseudomonas aeruginosa* biofilm membrane vesicles supports multiple mechanisms of biogenesis. *PLoS ONE* **2019**, *14*, e0212275. [CrossRef] [PubMed]
78. Bos, J.; Cisneros, L.H.; Mazel, D. Real-time tracking of bacterial membrane vesicles reveals enhanced membrane traffic upon antibiotic exposure. *Sci. Adv.* **2021**, *7*, eabd1003. [CrossRef]
79. Bantinaki, E.; Kassen, R.; Knight, C.G.; Robinson, Z.; Spiers, A.J.; Rainey, P.B. Adaptive divergence in experimental populations of *Pseudomonas fluorescens*. III. Mutational origins of wrinkly spreader diversity. *Genetics* **2007**, *176*, 441–453. [CrossRef]
80. King, E.O.; Ward, M.K.; Raney, D.E. Two simple media for the demonstration of pyocyanin and fluorescin. *J. Lab. Clin. Med.* **1954**, *44*, 301–307. [PubMed]
81. The UniProt Consortium. UniProt: The universal protein knowledgebase in 2021. *Nucleic Acids Res.* **2021**, *49*, D480–D489. [CrossRef]

FEMS Special Edition on Pseudomonas

MiniReview : Revised manuscript with changes to text shown in blue.

Adaptive radiation of *P. fluorescens* SBW25 in experimental microcosms provides an understanding of the evolutionary ecology and molecular biology of A-L interface biofilm-formation

Anna Koza[1,2], Anna Kuśmierska[1,3], Kimberley McLaughlin[1,4], Olena Moshynets[5] & Andrew J. Spiers[1*]

1 School of Science, Engineering and Technology, Abertay University, United Kingdom.

2 Current address : Technical University of Denmark, Novo Nordisk Foundation Center for Biosustainability, Denmark.

3 Current address : Department of Industrial Microbiology and Biotechnology, Faculty of Biology and Environmental Protection, University of Łódź, Poland.

4 Current address : Australian Institute of Tropical Health and Medicine, James Cook University, Australia.

5 Institute of Molecular Biology and Genetics of the National Academy of Sciences of Ukraine, Ukraine.

* Corresponding Author : Andrew J. Spiers

School of Science, Engineering and Technology, Abertay University, Bell Street, Dundee, DD1 1HG, United Kingdom. Tel : +44(0) 1382 308730 Email : a.spiers@abertay.ac.uk

ORCID Author identifiers –

Anna Koza	0000-0001-9713-5232
Anna Kuśmierska	0000-0003-1214-4549
Kimberley McLaughlin	0000-0002-6018-4310
Olena Moshynets	0000-0002-2209-8681
Andrew Spiers	0000-0003-0463-8629

Abstract (200 / 200 words)

Combined experimental evolutionary and molecular biology approaches have been used to investigate the adaptive radiation of *Pseudomonas fluorescens* SBW25 in static microcosms leading to the colonisation of the air-liquid interface by biofilm–forming mutants such as the Wrinkly Spreader. In these microcosms, the ecosystem engineering of the early wild-type colonists establish the niche space for subsequent WS evolution and colonisation. Random WS mutations occurring in the developing population that de-regulate diguanylate cyclases and c-*di*-GMP homeostasis result in cellulose-based biofilms at the air-liquid interface. These structures allow Wrinkly Spreaders to intercept O_2 diffusing into the liquid column and limit the growth of competitors lower down. As the biofilm matures, competition increasingly occurs between WS lineages, and niche divergence within the biofilm may support further diversification before system failure when the structure finally sinks. A combination of pleiotropic and epistasis effects, as well as secondary mutations, may explain variations in WS phenotype and fitness. Understanding how mutations subvert regulatory networks to express intrinsic genome potential and key innovations providing a selective advantage in novel environments is key to understanding the versatility of bacteria, and how selection and ecological opportunity can rapidly lead to substantive changes in phenotype and in community structure and function.

One sentence summary : (29 / 30 words) The *Pf.* SBW25 experimental system has revealed the evolutionary dynamics and molecular biology of the adaptive biofilm-forming Wrinkly Spreader, providing an insight into bacterial adaptability, radiation and competitive fitness.

Keywords : Adaptive radiation, biofilms, competitive fitness, ecological opportunity, intrinsic potential, key innovation.

Introduction

Experimental studies of microbial evolution have been used to investigate adaptive radiation, a key element in the development of ecological diversity within expanding lineages, and ultimately, in the creation of new species (see Schluter (2000) and reviews by, e.g. MacLean 2005; Buckling *et al*. 2009; Losos and Mahler, 2010; Dettman *et al.* 2012; Bailey and Bataillon 2016; Dykhuizen 2016). In particular, the use of bacterial populations in simple laboratory microcosms has allowed the rapid establishment of links between evolutionary dynamics and the molecular biology underlying adaptive genotypes and key innovations (i.e. changes in phenotype that facilitate improvement in fitness).

One very successful experimental system uses the soil and plant-associated pseudomonad *P. fluorescens* SBW25 (Rainey and Bailey, 1996) in static liquid microcosms where it gives rise to adaptive Wrinkly Spreader (WS) mutants that colonise the air-liquid (A-L) interface through the formation of a cellulose matrix-based biofilm (the key innovation). The nature of WS mutations, phenotype and fitness can now be explained by integrating evolutionary dynamics with an understanding of the underlying molecular biology (reviewed by Spiers, 2014), and involves a deterministic connection between mutations that subvert regulatory systems to induce biofilm–formation, and more stochastic fitness measurements based on population dynamics sensitive to environmental conditions and initial conditions (see **Table 1** for the key challenges and opportunities for *Pf.* SBW25 colonisation of the A-L interface in static microcosms). We believe there are key insights that can be drawn from this model system with links to fundamental microbial biology often overlooked by molecular biologists, relevant to our understanding of the versatility of bacteria and their ability to colonise new environments in the context of pathogenicity, natural and engineered microbial communities.

Radiation in static microcosms and the colonisation of the air-liquid interface

The adaptive radiation of *Pf.* SBW25 has been studied using microcosms (small glass vials) containing nutrient-rich King's B growth medium which are typically initiated with a founding population of ~10^4 cells and incubated over three to five days under static conditions (Rainey and Travisano 1998; Spiers *et al.* 2002; Green *et al*. 2011). During this period the population increases to ~10^{10} cells, and evidence for radiation or diversification can be seen in the appearance of mutant genotypes distinguishable through altered colony morphologies (for this reason they are often also referred to as morphotypes). The establishment of such diversity within the developing population is influenced by spatial structure, nutrients and patterns of physical disturbance (environmental heterogeneity or grains), resource competition and productivity (e.g. Rainey and Travisano 1998; Buckling *et al.* 2000; Kassen *et al.* 2004; Buckling *et al.* 2007; Venail *et al.* 2011; Armitage 2015). One class of mutants, known as the Wrinkly Spreaders (**Figure 1**), also shows an altered niche preference when re-introduced to static microcosms where they colonise the A-L interface through the formation of robust biofilms, in contrast to the wild-type or ancestral *Pf.* SBW25 which grows throughout the liquid column (see Ferguson *et al.* 2013 for a description of another biofilm–forming morphotype known as the Fuzzy Spreaders). The Wrinkly Spreaders have a competitive fitness advantage when at low frequencies compared to the numerically dominant non-biofilm–forming competitors in static microcosms, but not in shaken microcosms where biofilms cannot form or on

agar plates where the Wrinkly Spreader (WS) phenotype is a costly disadvantage (e.g. Rainey and Travisano 1998; Spiers *et al.* 2002; Spiers 2007; Green *et al*. 2011; McDonald *et al.* 2011; Lind *et al.* 2015).

Whilst most biofilm research is focussed on the formation of liquid-solid surface (L-S) interface biofilms in flow cells or micro-titre plates, the ability to produce A-L interface biofilms in static microcosms is common amongst environmental *Pseudomonas* spp., including water and soil isolates, plant-associated and plant pathogenic strains, mushroom pathogens, and psychrotrophic pseudomonads recovered from spoilt meat (Ude *et al*. 2006; Koza 2011; Nielsen *et al*. 2011; Robertson *et al*. 2013) as well as in the opportunistic human pathogen *P. aeruginosa* (Friedman and Kolter 2004). Other examples of A-L interface biofilm–formation may exist where staining of biofilm material attached to vial walls has been measured but where no description of growth over the liquid surface is provided, e.g. in microtitre plates or Calgary biofilm devices in which it is difficult to view biofilms *in situ* (A-L interface biofilms are sometimes also referred to as pellicles, but see the opinion piece by Moshynets and Spiers 2016). Although substantial variation has been observed amongst pseudomonad A-L interface biofilms, they can be categorised into classes and types (Ude *et al*. 2006; Robertson *et al*. 2013), and further differentiated using a combined biofilm assay measuring biofilm strength, attachment levels and total microcosm growth (Robertson *et al*. 2013). This approach, alongside fitness measurements and assays quantifying additional aspects of the WS phenotype, (collectively known as wrinkeality), demonstrate significant WS variation (**Figure 2**) and suggests that Wrinkly Spreaders arise through mutation of a number of different loci that are linked to a common pathway which establishes the WS phenotype *sensu stricto* (i.e. a wrinkled colony morphology on plates and biofilm-formation in static microcosms) (e.g. MacLean *et al.* 2004; McDonald *et al.* 2009; Green *et al.* 2011; Lind *et al.* 2015; Udall *et al*. 2015).

A key insight we draw from this section is that developing populations have the potential to diversify and produce adaptive genotypes that might out-compete the original colonists or colonise new niches. This has significance in the development of infections, natural and engineered microbial communities, where genotypes may change over time effecting host-pathogen interactions, community structure and function.

Underlying molecular biology of the Wrinkly Spreader

The WS phenotype results from mutations in genes expressing proteins involved in the homeostasis of the intracellular signalling compound c-*di*-GMP, with mutations commonly found in the methylesterase WspF subunit of the chemosensory signal-transduction–like Wsp system that lead to the activation of the associated diguanylate cyclase (DGC) WspR, increased levels of c-*di*-GMP and

the expression of cellulose required for the WS biofilm (**Figure 3 A&B**) (Spiers *et al.* 2002; Spiers *et al.* 2003; Bantinaki *et al*. 2007; McDonald *et al*. 2009; McDonald *et al*. 2011; Udall *et al*. 2015). For example, in the archetypal Wrinkly Spreader the *wspF* mutation is a single nucleotide A – C transition which results in a serine – arginine change at position 301 of the protein (*wspF* S310A). This mutant subunit is predicted to show reduced methylesterase activity based on the crystal structure of the homologous CheB from *Salmonella typhimurium* (West *et al.* 1995) that results in the de-repression of WspR and the synthesis of c-*di*-GMP (Bantinaki *et al.* 2007). Allele exchange experiments swapping *wspF* mutations in Wrinkly Spreaders to the wild-type sequence, and vice versa, have demonstrated that these are sufficient for the WS phenotype and fitness (Bantinaki *et al.* 2007).

Increased levels of c-*di*-GMP lead to the over-expression of partially-acetylated cellulose through the allosteric activation of the cellulose synthase complex (Spiers *et al.* 2002; Spiers *et al.* 2003). Although cellulose expression is common amongst pseudomonads and other bacteria (Ude *et al*. 2006; Nielsen *et al*. 2011; Robertson *et al*. 2013; Arrebola *et al.* 2015; reviewed by Spiers *et al.* 2013; Römling and Galperin 2015), the modification of this polymer by *Pf.* SBW25 using alginate acetylation–like subunits is rare and has only been reported for several phytopathogenic pseudomonads including *P. syringae* pv *tomato* DC3000 and the distantly-related *Bordetella avium* 197N (Arrebola *et al*. 2015; McLaughlin *et al*. 2017). Cellulose is the primary matrix component of the WS biofilm, although a Congo red-binding attachment factor induced by high c-*di*-GMP levels and lipopolysaccharide (LPS) are also required for the WS phenotype (Spiers *et al.* 2002; Spiers *et al*. 2003; Spiers and Rainey 2005). The WS attachment factor has been genetically identified as PGA or PNAG (poly-beta-1,6-N-acety-D-glucosamine) encoded by PFLU0143 – 0146 (Gehrig, 2005; Lind *et al.* 2015), though attachment may also involve amyloid fibrils encoded by the conserved *fapA-F* genes identified in the genome of *Pf.* SBW25 (PFLU2701 – 2696) and a range of other pseudomonads (Dueholm *et al.* 2013).

The hydrophobicity of either PGA or fibrils would allow WS cells and the biofilm matrix to break the A-L interface, suspending the biofilm from above and attaching the periphery of the biofilm directly to the vial walls (after de Jong *et al*. 2009). Like many other biofilms, the WS biofilm is likely to be chemically complex with multiple extracellular polymeric substances (EPS) including cellulose and PGA, LPS, appendages such as pili and flagella, as well as cell debris, all contributing to biofilm strength and attachment (Spiers and Rainey 2005). For example, our recent investigations of biofilm samples has identified extracellular DNA (eDNA) in line with previous observations of *P. aeruginosa* PA01 biofilms (Whitechurch *et al.* 2002) and a homologue of the major outer membrane porin OrpF (PFLU4612) from *P. aeruginosa* PA01 which affects cell surface properties and adhesive capabilities and is linked to c-*di*-GMP regulation (Bouffartigues *et al.* 2015) (Olena Moshynets, Airat Kayumov, Svitlana Rymar and Andrew Spiers, unpublished observations).

The *Pf.* SBW25 c-*di*-GMP regulatory network is likely to be complex as 39 putative DGCs including WspR have been identified in the genome (Silby *et al.* 2009), and a combination of c-*di*-GMP, transcriptional and metabolic systems probably control the expression of cellulose on plant surfaces under natural conditions (Gal *et al.* 2003; Giddens *et al.* 2007; Huang *et al.* 2007b). However, in static microcosms mutations occurring in only a few DGCs or related genes appear to be able to act independently to produce sufficiently high levels of c-*di*-GMP required for the WS phenotype (Bantinaki *et al.* 2007; McDonald *et al*. 2009; McDonald *et al*. 2011; Lind *et al*. 2015; Lind *et al.*, 2017). There are striking similarities between the small suite of DGCs or related genes which lead to the WS phenotype in *Pf.* SBW25 and those producing small colony variant (SCV) morphologies in *P. aeruginosa* isolates from Cystic fibrosis lungs (Smith *et al*. 2006; Malone *et al*. 2012; Malone 2015), and that in *P. aeruginosa* PA01, the overproduction of Pel and Psl EPS is also associated with mutations in *wspF* and increased c-*di*-GMP levels (Starkey *et al.* 2009).

The WS phenotype-activating mutations are examples of adaptive mutations activating intrinsic genome potential resulting in the expression of a key innovation (i.e. biofilm–formation allowing the colonisation of the A-L interface; here we use 'genome potential' to refers to sequences that provide some functionality when expressed under certain circumstances, but which could be expressed in under different conditions where that function or a modification of that function might provide a novel advantage). Although key innovations might arise through the creation of new genes *de novo* or through duplication and divergence of existing sequences (i.e. the innovation–amplification–divergence model), the re-deployment of existing pathways through disruption of regulatory systems allows phenotype divergence and fitness increases to occur more readily and with greater impact (Behe 2010; Andersson *et al*. 2015).

A key insight we draw from this section is that regulatory systems can be subverted by random mutations to activate extant but unexpressed or otherwise–repressed pathways and express complex adaptive phenotypes. This has significance in pathogenicity and the exploitation of natural and engineered microbial communities, where substantive phenotype changes may cause problems in treatment and community structure and function, or provide new opportunities in processing and production.

Ecosystem engineering and the creation of niche space

The static microcosm initially represents an unstructured or homogeneous environment for colonisation, with a uniform O_2 concentration down the liquid column (Koza *et al.* 2011) (**Figure 3 C**). However, this is rapidly degraded by the metabolic activity of the first *Pf.* SBW25 colonists which

establish an O_2 gradient within hours that differentiates the microcosms into an O_2-rich layer ~200 µm deep at the top of the liquid column and an O_2-depleted zone below. The ecosystem engineering of the colonists and the radiation of the population as it develops provides both an ecological opportunity (in the form of a new niche space) as well as the adaptive Wrinkly Spreaders who are able to exploit this modification of the environment (**Figure 3 D&E**) (similarly, *Pf.* SBW25 also modifies the growth medium to which subsequent genotypes adapt, Callahan *et al*. 2014). Ecological opportunity and adaptive radiation are interlinked and include growth and selection feedback mechanisms, as the parameters of the new niche space and the requirements of the adaptive genotype need to be well-matched for successful colonisation (Losos and Mahler, 2010; Yoder *et al.* 2010; Odling-Smee *et al.* 2013; Matthews *et al*., 2014; Steenackers *et al.* 2016). Changes which effect O_2 and nutrient levels, or the physical dimensions of the microcosm, all impact on WS fitness and confirm the link between the O_2-rich niche and the WS adaptive genotype (Koza *et al.* 2011; Kuśmierska and Spiers 2016).

The competitive advantage of the Wrinkly Spreader compared to non-biofilm–forming genotypes is negative frequency-dependent (e.g. Rainey and Travisano 1998; Meyer and Kassen 2007). The basis for Wrinkly Spreader success appears to be the rapid domination of the A-L interface by a thin biofilm that intercepts O_2 diffusion into the liquid column and limits the growth of other competitors lower down (nutrient levels are comparatively high in King's B microcosms and only begins to limit growth when diluted to very low levels) (Koza *et al.* 2011; Kuśmierska and Spiers 2016). Access to high levels of O_2 alters cellular physiology and allows increased growth, final population sizes and biofilm thickness (Spiers et al. 2003; Huang *et al.* 2007b; Koza *et al.* 2011; Kuśmierska and Spiers 2016), and at an early stage of biofilm–formation, most competitive interactions are between the thin layer of Wrinkly Spreaders and the larger non-biofilm–forming population. The adaptive radiation of *Pf.* SBW25 follows the parapatric niche divergence of the high-O_2 layer from the lower region which becomes progressively O_2-depleted, though there is no physical barrier to migration between these two sections of the microcosm (**Figure 3 D&E**). The Wrinkly Spreaders have a significant impact on this niche divergence, as shallower O_2 gradients are formed by populations lacking Wrinkly Spreaders (Loudon *et al*. 2016).

As the WS biofilm matures and deepens, it too divides into a physically-structured upper high-O_2 layer and a lower O_2-depeleted region. During this period competition increasingly occurs between diversifying WS lineages rather that between Wrinkly Spreaders and non-biofilm–forming competitors. This situation is reminiscent of the Red Queen hypothesis (Liow *et al.* 2011) in which constant competition and adaptation is required for continued Wrinkly Spreader success. This may be mediated or modified by a variety of other evolutionary processes operating within the static microcosms. Kin selection may help develop physically or metabolically-defined niche spaces where cell dispersal is limited (West *et al.* 2006), and an ancestor's inhibition effect may also where parental

cells are suffocated by layers of daughter cells growing above them (Xavier and Foster 2007). Furthermore, the continued development of the biofilm will be effected by the increasing number of cheaters no longer contributing to the construction or maintenance of the biofilm (e.g. Rainey and Rainey 2003; Brockhurst *et al*. 2006; Brockhurst 2007). The development of environmental heterogeneity and genotype diversification in these static microcosms (**Figure 3 D&E**) is predicted by dissipative systems theory where O_2 supply is effectively considered a free energy gradient (Loudon *et al*. 2016), and the complexity of the biofilm community will continue to develop until limited by resources or by physical disturbance causing the structure to sink (this event can be considered a systems failure despite the fact that King's B microcosms have sufficient nutrients to allow the development of a second-generation biofilm if allowed, Spiers *et al*. 2003).

A key insight we draw from this section is that populations change local conditions which may favour the development of adaptive genotypes, and such cycles of change and selection are the basis of ecological succession. This has significance in pathogenicity, especially in chronic infections and gastro-intestinal tract disorders, as well as in natural and engineered microbial communities, where the original consortia may be invaded by new members that alter community structure and function.

Influence of the environment on adaptive radiation

The linkage between ecological opportunity and adaptive radiation suggest that WS evolution, wrinkeality and fitness should all be sensitive to environmental conditions. Indeed, the diversification of *Pf.* SBW25 populations and the maintenance of diversity is effected by structure, physical disturbance, and resources including O_2 and nutrients, and variation in WS fitness has been observed within different collections of isolates (e.g. Buckling *et al.* 2000; Kassen *et al.* 2004; Bantinaki *et al.* 2007; Koza *et al.* 2011; Lind *et al.* 2015; Armitage 2015; Kuśmierska and Spiers 2016). Manipulation of physical parameters including A-L interface surface area – volume ratios and the presence or absence of the high-O_2 meniscus 'trap' all impact on WS biofilm–formation and fitness (Kuśmierska and Spiers 2016), whilst a comparison of Wrinkly Spreaders isolated from static microcosms and glass bead columns has demonstrated differences in wrinkeality and fitness attributable to origin (Udall *et al.* 2015).

However, correlations between WS phenotype and fitness are poor, suggesting that measurements of microcosm growth, biofilm strength and attachment levels may not effectively capture those aspects of the WS phenotype selected for in static King's B microcosms which also explain competitive fitness advantages (Udall *et al.* 2015). Furthermore, our attempts to differentiate between twenty-four Wrinkly Spreaders on the basis of wild-type or mutant *wspF* alleles (Bantinaki *et al.* 2007; McDonald *et al*., 2011) using phenotype data we have since collected has not proved successful (Andrew Spiers,

unpublished observations), and this suggests that the WS genotype to phenotype (G-P) map is likely to be equally difficult to establish.

Phenotypic variation is not random but is regulated by internal and external factors (Sharov 2014). Although allele replacement experiments have confirmed the importance of mutations in DGCs or related genes for the WS phenotype and fitness (Bantinaki *et al.* 2007; McDonald *et al.* 2009), internal factors such as antagonistic pleiotropic (and epistasis) effects may differ between Wrinkly Spreader mutations and produce variation within the WS phenotype *sensu stricto*. The multiple DGCs identified in the *Pf.* SBW25 genome suggests the complex and dynamic regulation of c-*di*-GMP homeostasis, with functional DGC redundancy upstream and c-*di*-GMP–sensitive pleiotropy downstream. Perturbation of c-*di*-GMP homeostasis may lead to variation in substrate utilisation patterns and fitness changes (MacLean and Bell 2003; MacLean *et al.* 2004), and the archetypal Wrinkly Spreader *wspF* S310A mutation results in proteomic changes in metabolic pathways not linked with the WS phenotype that might nonetheless be associated with fitness-reducing effects (Knight *et al.* 2006). Although homeostasis may appear to restrict phenotypic variation, the mutation of complex regulatory networks allows the adjustment and multi-tasking of functions, and the establishment of new connections between regulatory components and functions which may result in diversifying phenotypic effects (Sharov 2014). Additional mutations outwith these networks will add further phenotypic complexity, and in Wrinkly Spreaders isolated from aging or multiple-transfer populations such secondary mutations may ameliorate the antagonistic pleiotropic effects of the initial WS mutation, or add more elements to the developing WS phenotype.

A key insight we draw from this section is that small changes in initial conditions can have a big impact on subsequent population growth and diversification, and on the phenotype and success of any adaptive lineages that may appear. This is a central tenant of Chaos theory (the ‘butterfly’ effect), and has significance in natural and engineered microbial communities where the complexity of interactions will restrict the predictability of adaptive radiation.

Alternative routes to the colonisation of the A-L interface by biofilm-formation

Despite the competitive success of the Wrinkly Spreader in diversifying population of *Pf.* SBW25 in static microcosms, the intrinsic genome potential exploited by this class of adaptive mutants is not the only means by which the A-L interface can be colonised. *Pf.* SBW25 is known to produce at least five different biofilms which can be differentiated by mutation, biofilm matrix components and phenotype. These include the true Wrinkly Spreaders and the Viscous mass (VM) biofilm produced by wild-type

Pf. SBW25 when induced with $FeCl_3$ (Koza *et al.* 2009) which utilise cellulose as the primary biofilm matrix, WS-like mutants derived from cellulose-deficient (Δ*wss*) strains including CBFS 2.1 (Gehrig, 2005) and the PWS mutants that use PGA instead (Lind *et al.* 2017), disrupted LPS–associated Fuzzy Spreaders (FS) (Ferguson *et al.* 2013), and matrix-independent cell–chaining (CC) phenotypes (Lind *et al.* 2017).

Comparison of WS, VM and CBFS 2.1 biofilms including quantitative measurements of biofilm strength, attachment levels, and rheology, plus measurements of competitive fitness including the ability to invade a larger population when numerically rare, clearly differentiate these structures and their ecological success in static microcosms, with the WS biofilm being the most robust and providing the greatest fitness benefit in pair-wise competitions (Koza 2011; Anna Koza and Andrew Spiers, unpublished observations). Similarly, fitness and invasion assays have been used to differentiate WS, FS, PWS and CC mutants (Rainey and Travisano 1998; Ferguson *et al.* 2013; Lind *et al*. 2017).

These different routes to the colonisation of the A-L interface by *Pf.* SBW25 is an example of evolutionary convergence and underscores the strong selection in static microcosms for access to O_2. Significantly, mutation of three key DGCs or associated regulators result in the expression of cellulose or PGA through the disruption of c-*di*-GMP homeostasis, and if these genes are deleted, there are a further thirteen mutational pathways that will still activate the WS or WS-like phenotype (Bantinaki *et al.* 2007; McDonald *et al.* 2009; McDonald *et al.* 2011; Lind *et al.* 2015; Lind *et al*. 2017). It would appear that the pleiotropic effects associated with mutations altering c-*di*-GMP homeostasis and the expression of cellulose and PGA collectively determine the fitness cost to biofilm–formation, whereas the growth advantage offered by access to higher O_2 levels provides the fitness benefit in colonising the A-L interface in static microcosms (MacLean *et al.* 2004; Koza 2011; Lind *et al*. 2017).

A key insight we draw from this section is that where there is sufficiently strong selection, multiple mutational pathways may be used to activate unexpressed or otherwise–repressed genome potential in order to allow bacteria to exploit new ecological opportunities with subtly differing phenotypes determined by pleiotropic effects. This has significance in pathogenicity, as isolates producing similar symptoms may have significantly different responses to pharmaceutical treatments such as antibiotics.

Concluding comment

The use of simple experimental microcosms to investigate adaptive radiation and the ecological success associated with complex phenotypes is often regarded by microbiologists as having little

relevance to the colonisation of natural environments by bacteria and the functioning of the communities they establish, or indeed, of the value of such approaches to assess the evolutionary or ecological significance of particular pathways of interest. However, we believe that the key insights we have drawn from this model system have relevance in a range of areas, including pathogenicity, especially in the treatment of chronic infections and long-term gastro-intestinal disorders where both pathogen populations and host communities will change over time and with medical intervention, and in natural and engineered communities such as those used for biocontrol, bioremediation, and biotechnology processes to convert biomass, produce chemicals or energy, where communities and key members will also change in response to environmental conditions. In each of these, bacteria should be seen as being enormously adaptable and able to rapidly access intrinsic genome potential through simple mutations. As populations grow, they will modify ecosystems, diversify and adapt, and this will drive ecological succession and change community functions in a manner not predictable if bacteria are considered to be cellular automatons with limited and unchanging response to abiotic and biotic factors.

Acknowledgements

We acknowledge the involvement of Airat Kayumov (Kazan Federal University, Russia) and Svitlana Rymar (Institute of Molecular Biology and Genetics of the National Academy of Sciences of Ukraine, Ukraine) who worked with Olena Moshynets in the identification of PFLU4612 which we cited as unpublished observations in this review. We thank the ERASMUS and IAESTE Student Exchange Programmes, Royal Society of Edinburgh, Abertay University Graduate School and Abertay University for their support of Anna Koza, Anna Kuśmierska and Kimberley McLaughlin, and our continued research collaborations. Andrew Spiers is also member of the Scottish Alliance for Geoscience Environment and Society (SAGES), and Anna Koza was a SAGES-associated PhD student.

References

Andersson DI, Jerlström-Hultqvist J, Näsvall J. Evolution of new functions de novo and from pre-existing genes. Cold Spring Harb Perspect Biol 2015;**7:**a017996.

Armitage DW. Experimental evidence for a time-integrated effect of productivity on diversity. *Ecology Lett* 2015;**18:**1216–25.

Arrebola E, Carrión VJ, Gutiérrez-Barranquero JA, *et al.* Cellulose production in *Pseudomonas syringae* pv. *syringae*: a compromise between epiphytic and pathogenic lifestyles. FEMS *Microbiol Ecol* 2015;**91:**fiv071.

Bailey SF, Bataillon T. Can the experimental evolution programme help us elucidate the genetic basis of adaptation in nature? *Mol Ecol* 2016;**25:**203–18.

Bantinaki E, Kassen R, Knight C, *et al*. Adaptive divergence in experimental populations of *Pseudomonas fluorescens*. III. Mutational origins of wrinkly spreader diversity. *Genetics* 2007;**176:**441–53.

Behe MJ. Experimental evolution, loss-of-function mutations, and the first rule of adaptive radiation". *Q Rev Biol* 2010:85:419–45.

Bouffartigues E, Moscoso JA, Duchesne R, *et al*. The absence of the *Pseudomonas aeruginosa* OprF protein leads to increased biofilm formation through variation in c-di-GMP level. *Front Microbiol* 2015;**6:**630.

Brockhurst MA. Population bottlenecks promote cooperation in bacterial biofilms. *PLoS ONE* 2007;e634.

Brockhurst MA, Hochberg ME, Bell T, *et al.* Character displacement promotes cooperation in bacterial biofilms. *Curr Biol* 2006;**16:**2030–4.

Buckling A, Brockhurst MA, Travisano M, *et al*. Experimental adaptation to high and low quality environments under different scales of temporal variation. *J Evol Biol* 2007;**20:**296–300.

Buckling A, Kassen R, Bell G, *et al.* Disturbance and diversity in experimental microcosms. Nature 2000;**408:**961–4.

Buckling A, Maclean RC, Brockhurst MA, *et al*. The Beagle in a bottle. *Nature* 2009;**457:**824–9.

Callahan BJ, Fukami T, Fisher DS. Rapid evolution of adaptive niche construction in experimental microbial populations. *Evolution* 2014;**68:**3307–16.

de Jong W, Wösten HA, Dijkhuizen L, *et al.* Attachment of *Streptomyces coelicolor* is mediated by amyloidal fimbriae that are anchored to the cell surface via cellulose. *Mol Microbiol* 2009;**73:**1128–40.

Dettman JR, Rodrigue N, Melnyk AH, *et al.* Evolutionary insight from whole-genome sequencing of experimentally evolved microbes. *Mol Ecol* 2012;**21:**2058–77.

Dueholm MS, Otzen D, Nielsen PH. Evolutionary insight into the functional amyloids of the pseudomonads. *PLoS ONE* 2013;**8:**e76630.

Dykhuizen D. Thoughts toward a theory of natural selection: the importance of microbial experimental evolution. *Cold Spring Harb Perspect Biol* 2016;a018044.

Ferguson GC, Bertels F, Rainey PB. Adaptive divergence in experimental populations of *Pseudomonas fluorescens*. V. Insight into the niche specialist Fuzzy Spreader compels revision of the model *Pseudomonas* radiation. *Genetics* 2013;**195:**1319–35.

Flohr RC, Blom CJ, P. B. Rainey PB, *et al.* Founder niche constrains evolutionary adaptive radiation. *PNAS (USA)* 2013;**110:**20663–8.

Friedman L, Kolter R. Genes involved in matrix formation in *Pseudomonas aeruginosa* PA14 biofilms. *Mol Microbiol* 2004;**51:**675–90.

Gal M, Preston GM, Massey RC, *et al.* (2003). Genes encoding a cellulosic polymer contribute toward the ecological success of *Pseudomonas fluorescens* SBW25 on plant surfaces. *Mol Ecol* 2003;**12:**3109–21.

Gehrig, S. Adaptation of *Pseudomonas fluorescens* SBW25 to the air-liquid interface: a study in evolutionary genetics. DPhil thesis, University of Oxford, Oxford, UK, 2005.

Giddens SR, Jackson RW, Moon CD, *et al.* Mutational activation of niche-specific genes provides insight into regulatory networks and bacterial function in a complex environment. *PNAS (USA)* 2007;**104:**18247–52.

Güvener ZT, Harwood CS. Subcellular location characteristics of the *Pseudomonas aeruginosa* GGDEF protein, WspR, indicate that it produces cyclic-*di*-GMP in response to growth on surfaces. Mol Microbiol 2007;**66:**1459–73.

Green JH, Koza A, Moshynets O, *et al*. Evolution in a Test-tube : Rise of the Wrinkly Spreaders. *J Biological Education* 2011;**45:**54–9.

Huang WE, Bailey MJ, Thompson IP, *et al*. Single-cell Raman spectral profiles of *Pseudomonas fluorescens* SBW25 reflects *in vitro* and *in planta* metabolic history. *Microbial Ecol* 2007a;**53:**414–25.

Huang WE, Ude S, Spiers AJ. *Pseudomonas fluorescens* SBW25 biofilm and planktonic cells have differentiable Raman spectral profiles. *Microbial Ecol* 2007b;**53:** 471–4.

Kassen R, Llewellyn M, Rainey PB. Ecological constraints on diversification in a model adaptive radiation. *Nature* 2004;**431:**984–8.

Knight CG, Zitman N, Prabhakar P, *et al.* Unravelling adaptive mutation: how a single point mutation affects the protein coregulation network. *Nature Genetics* 2006;**38:**1015–22.

Koza A. Adaptation and niche construction by *Pseudomonas fluorescens* SBW25. DPhil thesis, Abertay University, Dundee, UK, 2011.

Koza A, Hallett PD, Moon CD, *et al.* (2009). Characterisation of a novel air–liquid interface biofilm of *Pseudomonas fluorescens* SBW25. *Microbiol* 2009;**155:**1397–406.

Koza A, Moshynets O, Otten W, *et al.* Environmental modification and niche construction: Developing O_2 gradients drive the evolution of the Wrinkly Spreader. *ISME J* 2011;**5:**665–73.

Kuśmierska A, Spiers AJ. New insights into the effects of several environmental parameters on the relative fitness of a numerically dominant class of evolved niche specialist. *Int J Evolutionary Biol* 2016; Article ID 4846565.

Lind PA, Farr AD, Rainey PB. Experimental evolution reveals hidden diversity in evolutionary pathways. eLife 2015;**4:**07074.

Lind PA, Farr AD, Rainey PB. Evolutionary convergence in experimental *Pseudomonas* populations. *ISME J* 2017;**11:**589–600

Liow LH, Van Valen L, Stenseth NC. Red queen: from populations to taxa and communities. *Trends Ecol Evol* 2011;**26:**349–58.

Loudon CM, Matthews B, Sevilgen DS, *et al.* Experimental evidence that evolution by niche construction affects dissipative ecosystem dynamics. *Evol Ecol* 2016;**30:** 221–34.

Losos JB, Mahler DL. Adaptive radiation: the interaction of ecological opportunity, adaptation, and speciation. In: Bell MA, Futuyma DJ, Eanes WF, *et al.* (eds.). *Evolution Since Darwin: The First 150 Years*. Sunderland: Sinauer Associates, 2010, 381–420.

MacLean RC. Adaptive radiation in microbial microcosms. *J Evol Biol* 2005;**18:**1376–86.

MacLean RC, Bell G. Divergent evolution during an experimental adaptive radiation. *Proc Biol Sci* 2003;**270:**1645–50.

MacLean RC, Bell G, Rainey PB. The evolution of a pleiotropic fitness tradeoff in *Pseudomonas fluorescens*. *PNAS (USA)* 2004;**101:**8072–7.

Malone JG, Jaeger T, Manfredi P, *et al*. The YfiBNR signal transduction mechanism reveals novel targets for the evolution of persistent *Pseudomonas aeruginosa* in cystic fibrosis airways. *PloS Pathog* 2012;**8:**e1002760.

Malone JG. Role of small colony variants in persistence of *Pseudomonas aeruginosa* infections in cystic fibrosis lungs. *Infect Drug Resist* 2015;**8:**237–47.

Matthews B, De Meester L, Jones CG, *et al.* Under niche construction: an operational bridge between ecology, evolution and ecosystem science. *Ecol Monogr* 2014; **84:**245–63.

McDonald MJ, Gehrig SM, Meintjes PL, *et al.* Adaptive divergence in experimental populations of *Pseudomonas fluorescens*. IV. Genetic constraints guide evolutionary trajectories in a parallel adaptive radiation. *Genetics* 2009;**183:**1041–53.

McDonald MJ, Cooper TF, Beaumont HJE, *et al.* The distribution of fitness effects of new beneficial mutations in *Pseudomonas fluorescens*. *Biol Lett* 2011;**7:**98–100.

McLaughlin K, Folorunso AO, Deeni YY, *et al*. Biofilm formation and cellulose expression by *Bordetella avium* 197N, the causative agent of bordetellosis in birds and an opportunistic respiratory pathogen in humans. *Res Microbiol* 2017 (In press).

Meyer JR, Kassen R. The effects of competition and predation on diversification in a model adaptive radiation. *Nature* 2007;**446:**432–5.

Moshynets OV, Spiers AJ. Viewing biofilms within the larger context of bacterial aggregations. In: Dhanasekaran D, Thajuddin N (eds.). *Microbial biofilms – Importance and applications.* Rijeka: InTech Publishers, 2016, 3–22.

Nielsen L, Li X, Halverson LJ. Cell–cell and cell–surface interactions mediated by cellulose and a novel exopolysaccharide contribute to *Pseudomonas putida* biofilm formation and fitness under water-limiting conditions. *Environ Microbiol* 2011;**13:**1342-56.

Odling-Smee FJ, Erwin D, Palkovacs E, *et al.* (2013) Niche construction theory: a practical guide for ecologists. *Q Rev Biol* 2013;**88:**3–28.

Rainey PB, M. Travisano M. Adaptive radiation in a heterogeneous environment. *Nature* 1998;**394:**69–72.

Rainey PB, Bailey MJ. Physical and genetic map of the *Pseudomonas fluorescens* SBW25 chromosome. *Mol Microbiol* 1996;**19:**521–33.

Rainey PB, Rainey K. Evolution of cooperation and conflict in experimental bacterial populations. *Nature* 2003;**425:**72–4.

Robertson M, Hapca SM, Moshynets O, *et al*. Air-liquid interface biofilm formation by psychrotrophic pseudomonads recovered from spoilt meat. *Antonie van Leeuwenhoek* 2013;**103:**251–9.

Römling U, Galperin MY. Bacterial cellulose biosynthesis: diversity of operons, subunits, products, and functions. *Trends Microbiol* 2015;**23:**545–57.

Schluter D. *The ecology of adaptive radiation.* Oxford: Oxford University Press, 2000.

Sharov AA. Evolutionary constraints or opportunities? *BioSystems* 2014;**123:**9–18.

Silby MW, Cerdeño-Tárraga AM, Vernikos G, *et al*. Genomic and genetic analyses of diversity and plant interactions of *Pseudomonas fluorescens*. *Genome Biol* 2009;**10:**R51.

Smith EE, Buckley DG, Wu Z, *et al.* Genetic adaptation by *Pseudomonas aeruginosa* to the airways of cystic fibrosis patients. *PNAS (USA)* 2006;**103:**8487–92.

Spiers AJ. Wrinkly-Spreader fitness in the two-dimensional agar plate microcosm: maladaptation, compensation and ecological success. *PLoS ONE* 2007;**2:**e740.

Spiers AJ. A mechanistic explanation linking adaptive mutation, niche change and fitness advantage for the Wrinkly Spreader. *Int J Evolutionary Biol* 2014; Article ID 675432.

Spiers AJ, Bohannon J, Gehrig S, *et al*. Biofilm formation at the air–liquid interface by the *Pseudomonas fluorescens* SBW25 Wrinkly Spreader requires an acetylated form of cellulose. *Mol Microbiol* 2003;**50:**15–27.

Spiers AJ, Deeni YY, Folorunso AO, *et al*. Cellulose expression in *Pseudomonas fluorescens* SBW25 and other environmental pseudomonads. In: Van De Ven TGM, Godbout L (eds.). *Cellulose - Medical, Pharmaceutical and Electronic Applications.* Rijeka: InTech Publishers, 2013, 1–26.

Spiers AJ, Kahn SG, Travisano M, *et al*. Adaptive divergence in *Pseudomonas fluorescens*. 1. Determinants of Wrinkly Spreader fitness and the cause of an evolutionary transition. *Genetics* 2002;**161:**33–46.

Spiers AJ, Rainey PB. The *Pseudomonas fluorescens* SBW25 Wrinkly Spreader biofilm requires attachment factor, cellulose fibre and LPS interactions to maintain strength and integrity. *Microbiol* 2005;**151:**2829–39.

Starkey M, Hickman JH, Ma L, *et al. Pseudomonas aeruginosa* rugose small-colony variants have adaptations that likely promote persistence in the Cystic Fibrosis lung. *J Bacteriol* 2009;**191:**3492–503.

Steenackers HP, Parijs I, Foster KR, *et al.* Experimental evolution in biofilm populations. *FEMS Microbiol Rev* 2016;**40:**373–97.

Udall YC, Deeni Y, Hapca SM, *et al* (2015). The evolution of biofilm-forming Wrinkly Spreaders in static microcosms and drip-fed columns selects for subtle differences in wrinkleality and fitness. *FEMS Microbiol Ecol* 2015;**91:**fiv057.

Ude S, Arnold DL, Moon CD, *et al.* Biofilm formation and cellulose expression among diverse environmental *Pseudomonas* isolates. *Environmental Microbiol* 2006;**8:**1997–2011.

Venail PA, Kaltz O, Olivieri I, *et al.* Diversification in temporally heterogeneous environments: effect of the grain in experimental bacterial populations. *J Evol Biol* 2011;**24:** 2485-95.

West SA, Griffin AS, Gardner AG, *et al.* Social evolution theory for microorganisms. *Nat Reviews Microbiol* 2006;**4:**597–607.

West AH, Martinez-Hackert E, Stock AM. Crystal structure of the catalytic domain of the chemotaxis receptor methylesterase, CheB. *J Mol Biol* 1995;**250**:276–90.

Whitechurch CB, Tolker-Nielsen T, Ragas PC, *et al.* (2002) Extracellular DNA required for bacterial biofilm formation. *Science* 2002;**295:**1487.

Xavier JB, Foster KR. Cooperation and conflict in microbial biofilms. *PNAS (USA)* 2007;**104:**876–81.

Yoder JB, Clancey E, Des Roches S, *et al.* Ecological opportunity and the origin of adaptive radiations. *J Evolutionary Biol* 2010;**23:**1581–96.

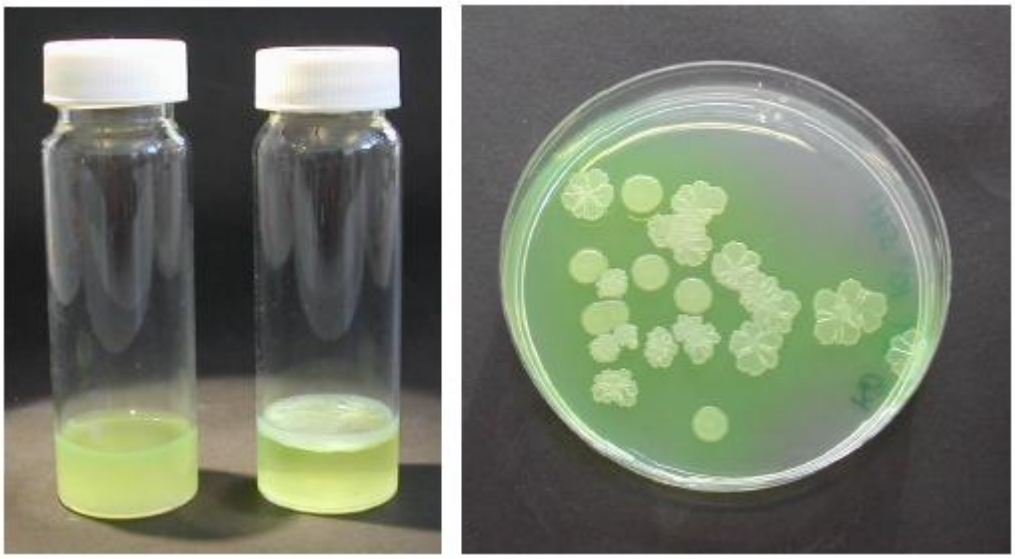

Figure 1. The adaptive Wrinkly Spreader genotype.

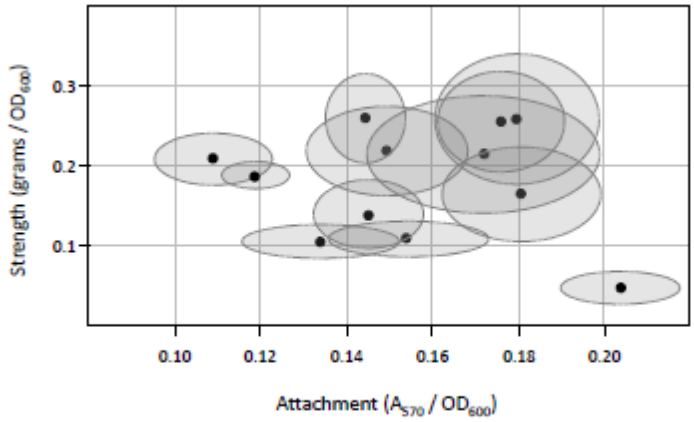

Figure 2. Wrinkly Spreader isolates show considerable variation in wrinkeality.

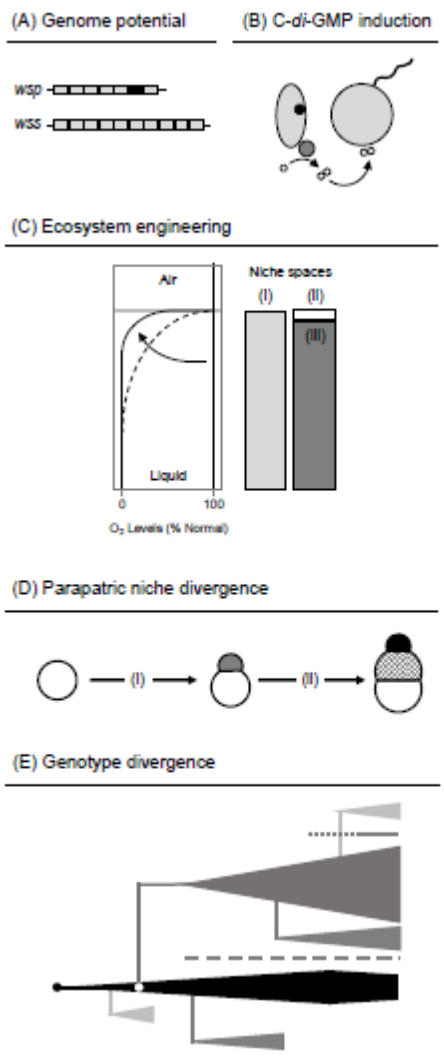

Figure 3. Elements of adaptive radiation in static microcosms.

Table 1. Challenges and opportunities for adaptive radiation of *Pf.* SBW25 in static microcosms and the colonisation of the A-L interface by biofilm–formation.

Initial conditions	*Evolvability of the ancestor* : *Pf.* SBW25 has intrinsic genome potential : a complex c-*di*-GMP regulatory system with multiple DGCs linked to the expression of EPS that can be used as biofilm matrix components
	Limiting factors in the environment : O_2 is the primary resource restricting growth rate and final population sizes in static microcosms. Cells are subject to constant movement by random diffusion and micro-currents within the liquid column and microcosms are subject to random physical disturbance (sufficient to dislodge and sink biofilms).
	Potential for adaptation : Overcoming limiting factors to achieve faster growth rates and higher final population sizes.
Ecological opportunity	*Ecosystem engineering* : Colonists change the initial environment by establishing an O_2 gradient in which flux through the A-L interface is balanced by uptake by individuals in the liquid column. This creates a high-O_2 niche space at the top of the liquid column available for colonisation.
	Parapatric niche divergence : Conditions in both niches develop as the biofilm matures and populations continue to diversify. O_2 will be further depleted in the liquid column whilst the O_2-rich region at the top will become shallower as the biofilm matures. The developing biofilm will provide physical structure and increased metabolic activity which may influence cell distributions, nutrient and waste diffusion.
Fitness concerns	*Physical structure* : The biofilm secures access to high–O_2 levels by retaining cells at the A-L advantage interface in a cost-effective manner. If costs increase, WS fitness will be reduced.
	Competitors : Establishment of the biofilm reduces O_2 available to competitors lower down in the liquid column, restricting growth rate and final population sizes. WS fitness is initially high when competition is largely between Wrinkly Spreaders and non-biofilm–forming genotypes, but decreases as Wrinkly Spreaders begin to dominate numerically.
Future developments	*Increased systems complexity* : Wrinkly Spreader competition within the biofilm, continued population diversification and complexity niche divergence, will add multiple niches defined by physical space and metabolic opportunities.
	System collapse : Random physical disturbance generally causes biofilms to sink within 5 – 7 days, and although biofilm-formation may be re-initiated, physical disturbance and nutrient levels will ultimately determine system productivity.

Анотація: *Біоплівки Pseudomonas fluorescens SBW25 є популярною моделлю для досліджень в області експериментальної еволюції та молекулярної біології. З'ясовано, що адаптивна колонізація у статичних мікрокосмах призводить до утворення мутантного штаму-суперпродуценту біоплівки Wrinkly Spreader (WS), який колонізує зону меніску (інтерфаза повітря-рідина). В такому модельному статичному мікрокосмі екосистемна інженерія перших диких колоністів створює нову екологічну нішу для подальшої еволюції популяції і її більш успішної колонізації. На молекулярному рівні до утворення суперпродуценту WS призводять випадкові мутації, які шляхом відбору призводять до селекції мутантів, що накопичують вторинний клітинних месенджер c-di-GMP, що призводить по посиленого синтезу целюлози і утворення міцної біоплівки а зоні меніску. Це у свою чергу дозволяє штаму WS перехоплювати більше O_2, що дифундує в стовп рідини, і обмежують зростання конкурентів нижче. Головним структурним компонентом біоплівки WS є целюлоза, але як саме фібрили целюлози інтегруються в успішний матрикс біоплівки було невідомо. В нашій роботі ми з'ясували, що еДНК може мати значення в утворенні біоплівкового матриксу особливо на первинних стадіях утворення біоплівки. Також було продемонстровано, що амілоїди також відіграють певну структурну роль в біоплівці WS та досліджені мембранні везикули і їхній білковий склад.*

3.4. Роль амілоїдогенезу в біоплівках грам-негативних бактерій

Амілоїди це високовпорядковані білкові агрегати з нерозгалуженою ниткоподібною структурою. Морфологічно, як правило, вони мають спіральний масив β-ланцюгів, упакованих ортогонально до вісі у вигляді довгого волокна (92). Функціональний амілоїдогенез треба відрізняти від патологічного амілоїдогенезу, який виникає внаслідок неконтрольованої агрегації білків і пептидів в амілоїдні фібрили, що призводить до таких нейродегенеративних патологій як губчаста енцефалопатія (93, 94) та ненейропатичних захворювань як цукровий діабет II типу та різні форми амілоїдозу (95).

Функціональний амілоїдогенез є широко поширеним серед і вже доведений для багатьох родин бактерій, наприклад *Bacteroidetes, Firmicutes, Actinobacteria* та *Gammaproteobacteria* (96-98). Ці функціональні амілоїди присутні в бактеріальних біоплівках, де вони сприяють початковому прикріпленню та агрегації і, нарешті, формування матриксу біоплівки (99-100). Різниця між процесами утворення патологічного та функціонального амілоїдів полягає у набагато більшій організованості утворення останніх.

Через низьку чутливість класичних амілоїд-чутливих барвників thioflavin T і congo red (101, 102) нами було розроблено і досліджено новий амілоїд-чутливий барвник AmyGreen. Цим новим цитохімічним флуоресцентним барвником було досліджено амілоїдний компонент у матриксі низки грам-негативних біоплівок, зокрема, в біоплівках *E. coli* K12, *K. pneumoniae* ATCC10031, колекції патогенних диких ізолятів *K. pneumoniae*, *P. aeruginosa* ATCC 27853 (A) і *B. avium* 61.

Основні результати, отримані в цьому підрозділі дисертації опубліковано в роботі автора (103).

Methods and Applications in Fluorescence

PURPOSE-LED PUBLISHING™

PAPER

Fluorescent β-ketoenole AmyGreen dye for visualization of amyloid components of bacterial biofilms

To cite this article: Olena Moshynets *et al* 2020 *Methods Appl. Fluoresc.* **8** 035006

View the article online for updates and enhancements.

You may also like

- Studies on the potential risk of amyloidosis from exposure to silk fibroin
Satomi Tsukawaki, Tomoaki Murakami, Kazuhiko Suzuki et al.
- Morphology and mechanical properties of multi-stranded amyloid fibrils probed by atomistic and coarse-grained simulations
Gwonchan Yoon, Myeongsang Lee, Kyungwoo Kim et al.
- Nanomechanical properties of single amyloid fibrils
K K M Sweers, M L Bennink and V Subramaniam

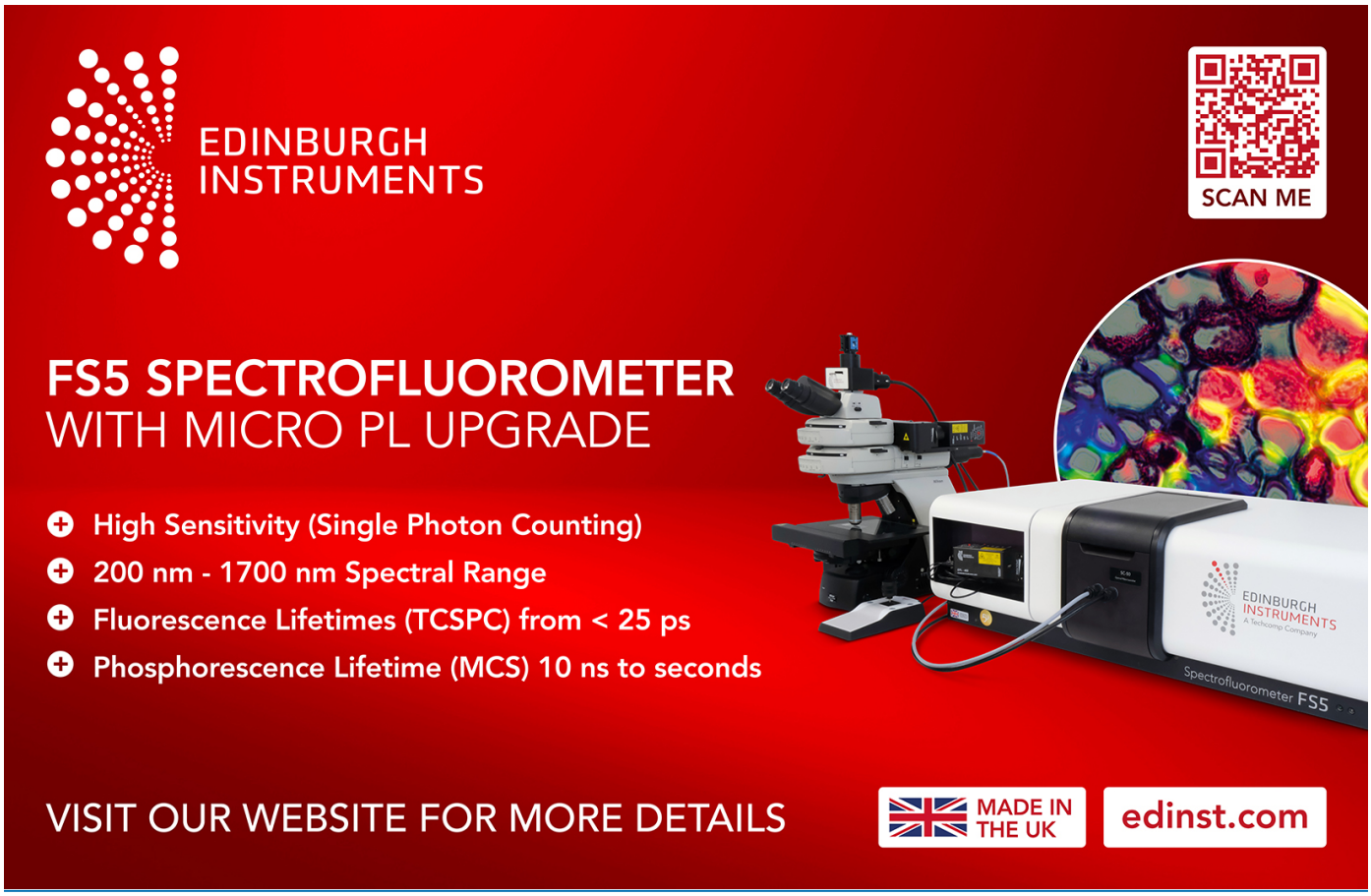

This content was downloaded from IP address 157.193.240.134 on 16/09/2024 at 10:52

Methods and Applications in Fluorescence

RECEIVED
5 March 2020

REVISED
13 April 2020

ACCEPTED FOR PUBLICATION
6 May 2020

PUBLISHED
14 May 2020

PAPER

Fluorescent β-ketoenole AmyGreen dye for visualization of amyloid components of bacterial biofilms

Olena Moshynets[1], Svitlana Chernii[1], Viktor Chernii[2], Mykhaylo Losytskyy[1], Serhii Karakhim[3], Rafal Czerwieniec[4], Vasyl Pekhnyo[2], Sergiy Yarmoluk[1] and Vladyslava Kovalska[1,5]

[1] Institute of Molecular Biology and Genetics NASU, 150 Zabolotnogo St., 03143 Kyiv, Ukraine
[2] V.I. Vernadskii Institute of General and Inorganic Chemistry NASU, 32/34 Palladin Av., 03080 Kyiv, Ukraine
[3] O. V. Palladin Institute of Biochemistry NASU, Leontovicha Str., 9, 02000 Kyiv, Ukraine
[4] Regensburg University, Universitätsstraße 31, 93053 Regensburg, Germany
[5] Scientific Services Company Otava Ltd, 150 Zabolotnogo St., 03143 Kyiv, Ukraine

E-mail: v.kovalska@gmail.com

Keywords: fluorescent detection, β-ketoenole dye, functional amyloids, bacterial biofilm, laser scanning confocal microscopy

Supplementary material for this article is available online

Abstract

Green-emitting water-soluble amino-ketoenole dye AmyGreen is proposed as an efficient fluorescent stain for visualization of bacterial amyloids in biofilms and the detection of pathological amyloids *in vitro*. This dye is almost non-fluorescent in solution, displays strong green emission in the presence of amyloid fibril of proteins. AmyGreen is also weakly fluorescent in presence to biomolecules that are components of cells, extracellular matrix or medium: nucleic acids, polysaccharides, lipids, and proteins. Thus, the luminescence turn-on behavior of AmyGreen can be utilized for visualization of amyloid components of bacterial biofilm extracellular matrix. Herein we report the application of AmyGreen for fluorescent staining of a number of amyloid-contained bacteria biofilms produced by *Escherichia coli*, *Klebsiella pneumoniae, Pseudomonas aeruginosa*, *Bordetella avium*, and *Staphylococcus aureus*. The effectiveness of AmyGreen was compared to traditional amyloid sensitive dye Thioflavine T. The main advantage of AmyGreen (concentration 10^{-5} M) is a higher sensitivity in the visualization of amyloid biofilm components over Thioflavine T (10^{-4} M) as it was revealed when staining *E. coli* and *K. pneumoniae* bacterial biofilms. Besides, AmyGreen displays lower cross-selectivity to nucleic acids as demonstrated both in in-solution experiments and upon staining of eukaryotic human mesenchymal stem cells used as amyloid-free negative control over amyloid-rich bacterial biofilms. The results point to a lower risk of false-positive response upon determination of amyloid components of bacterial biofilm using AmyGreen. Co-staining of biofilm by AmyGreen and cellulose sensitive dye Calcofluor White show difference in their staining patterns and localization, indicating separation of polysaccharide-rich and amyloid-rich regions of investigated biofilms. Thus, we suggest the new AmyGreen stain for visualization and differentiation of amyloid fibrils in bacterial biofilms to be used solely and in combination with other stains for confocal and fluorescence microscopy analysis.

Introduction

Amyloids are highly ordered protein aggregates with an unbranched filamentous morphology, typically featuring a helical array of β-strands packed orthogonally to the long fiber axis [1] (figure 1(a)). Pathological amyloids appear due to a non-controlled aggregation of proteins and peptides into amyloid fibrils and are connected with pathogenesis of numerous disorders determined as conformational or misfolding diseases. Among these pathologies, prominent examples are neurodegenerative ones like spongiform encephalopathies [2, 3] and nonneuropathic diseases such as type II diabetes and different forms of amyloidosis [4].

Despite the fact that amyloids are often associated with pathogenies, the formation of so-called functional amyloids under environmental conditions to make some advantage for living organisms is widely

© 2020 IOP Publishing Ltd

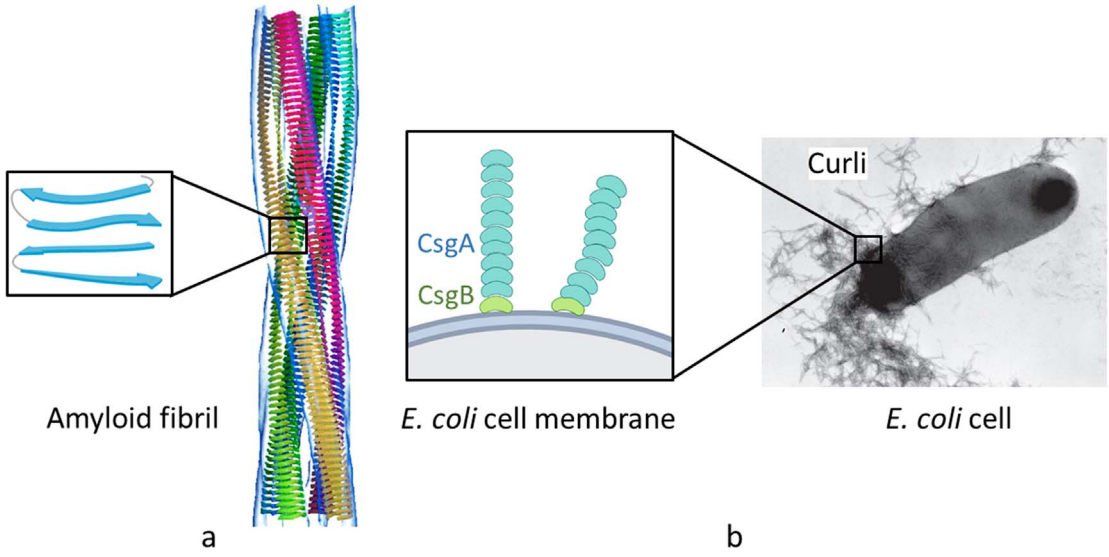

Figure 1. (a)—the model structure of insulin amyloid fibril; (b)—functional amyloids called curli on *E. coli* cell surface: scheme of localization and electron microscopic photo; CsgA and CsgB are the major protein subunits involved in curli formation. Amyloid fibril model was adapted from [5], Copyright (2002) National Academy of Sciences, USA. The electron microscopic photo of *E. coli* was adapted from [6], Copyright (2007) National Academy of Sciences, USA.

spread and already proved for many bacteria families, for example *Bacteroidetes*, *Firmicutes*, *Actinobacteria* and *Gammaproteobacteria* [7–9] (figure 1(b)). So-called functional amyloids are present in bacterial biofilms where they contribute to attachment, initial aggregation and, finally, biofilm matrix formation [10, 11]. The difference between processes of pathological and functional amyloids formation is the high regulation of second ones [12].

Due to the importance of monitoring of bacterial biofilms in health care as well as in nature and technical processes, their identification and quantification are of high interest [13, 14]. Biofilms mitigate antibiotic effects by providing a suitable environment for the enhancement of antibiotic resistance and infection persistence. Thus, bacterial biofilm formation in unwanted environments remains one of the major health threats for humans and domesticated animals [15]. Fast and selective visualization of bacterial aggregations, or biofilms, formed on biogenic and abiogenic surfaces [16] may provide means for the control of biofilm spread. Since common antimicrobial compounds in many cases cannot destroy biofilms *in vivo* and *in vitro*, there is a major need to develop tools for bacteria imaging to study alternative agents against biofilms [14]. Bacterial endogenous imaging has also been proposed for clinical detection of bacterial colonization during infections [17]. Amyloid fibrils as one of the essential components of the biofilm matrix are thus considered as a suitable visualization target.

For visualization of amyloids in bacterial aggregates such as bacterial agar colonies and biofilms, different microscopy techniques have been applied [11, 18–20]. Fluorescence microscopy is now one of the most essential approaches to confirm the presence of amyloids in bacterial aggregates as well as to investigate their spatial distribution with respect to other biofilm matrix components and cells. Thus, a fluorescent dye targeting amyloids needs to be characterized by high selectivity of the response to amyloids in order to avoid nonspecific co-staining of other extracellular polymers strongly contributing to biofilm matrices such as polysaccharides, extracellular NA (nuclei acids) or non-amyloid proteins.

Fluorescent dyes are widely used for detection of various intracellular and extracellular components, such as nucleic acids, organelles, and polysaccharides [21–25]. In microbiology, there are two main methodological approaches used to detect amyloid aggregates in bacterial extracellular matrix: Congo Red plates and fluorescence microscopy following Thioflavin (figure 2) derivatives treatment [11, 18, 19, 26]. Despite the fact that these two approaches are 'gold standard' methods, they suffer from significant disadvantages related to low specificity of the both dyes towards amyloids. In particular, Congo Red (figure 2) also binds cellulose and other compounds, including proteinaceous attachment factor, while Thioflavins bind to nucleic acids [27, 28]. Additionally, the fluorescence of the most commonly uded Thioflavin T (ThT) is strongly affected by the presence of lipid vesicles [29]. Among fluorescent molecules, CDy11 (figure 2) sensitive to amyloid fibrils has been proposed for biofilms imaging *in vitro* and *in vivo* [30], and red fluorescent dye ProteoStat can detect the presence of intracellular amyloid-like deposits in living bacterial cells with high specificity shown by confocal microscopy [31]. Curcumin (figure 2) was also reported as an amyloid-specific dye in *E. coli* that binds to curliated whole cells and isolated curli amyloid fibers

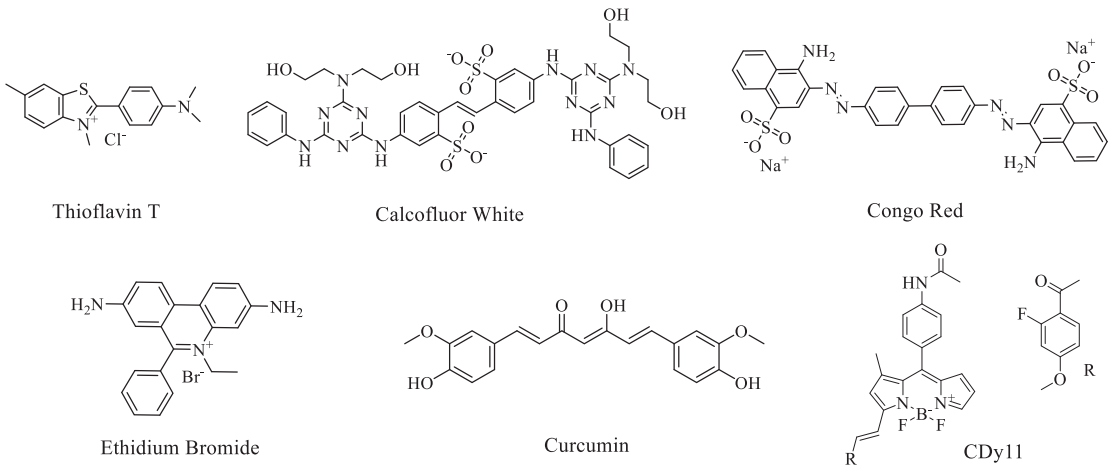

Figure 2. Chemical formulas of fluorescent dyes used for the detection and staining of intracellular and extracellular components.

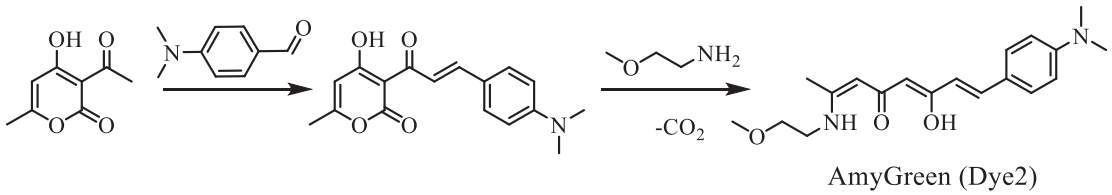

Scheme 1. Scheme of synthesis and chemical structure of AmyGreen.

[32]. Fluorescent conjugated oligothiophenes were proposed for effective *in situ* detection and differentiation of salmonella extracellular matrix (ECM) components curli and cellulose [33]. Calcofluor White is used as a fluorescent standard dye for staining polysaccharide polymers in biomedical practice.

Recently, we have reported on fluorescent sensitivity of β-ketoenole dyes to amyloid fibrils [34, 35]. Organic dyes of this kind are low-fluorescent when free and in the presence of native proteins, but they display strong emission in presence of fibrils of insulin and lysozyme. For the ketoenole dye AmyGreen (scheme 1, reported in [35] as Dye2), good concentrations range of fibril detection (0.8–100 μg ml^{-1}) and applicability for real-time monitoring of *in vitro* amyloid fibrils formation was shown. Apart of these photophysical advantages, ketoenoles are easily accessible synthetically from low-cost starting materials and simple purification [35].

The aim of this work was to study the high-efficient amyloid-sensitive β-ketoenole dye AmyGreen (figure 2) as a stain for specific visualization of amyloid components of the extracellular matrix of bacterial biofilms. For this purpose, we characterized the fluorescence response of model human amyloids formed from two proteins insulin and lysozyme *in vitro* (these proteins are known to give aggregates upon human pathological states [36, 37]), and studied *in vitro* fluorescent sensitivity of this dye to different biomolecules which are major components of cells, ECM or medium for cultivation: nucleic acids, polysaccharides, lipids, and proteins. The efficiency visualization of amyloid-producing biofilm by AmyGreen was explored on model *Escherichia coli* K12 bacteria and strains of pathogenic bacteria *Klebsiella pneumoniae* in co-staining with nucleic acid stain Ethidium Bromide (figure 2). AmyGreen was also used to visualize different amyloid-containing biofilms produced by both gram-negative and gram-positive bacteria, namely *Pseudomonas aeruginosa* ATCC 27853, *Bordetella avium* 61 and *Staphylococcus aureus* ATCC25923. Co-staining of AmyGreen with cellulose-specific dye Calcofluor White was used to study dye ability to visualize polysaccharides that are main component of ECM. (figure 2). To estimate the ability of the dye to penetrate into cells and to stain intercellular components, the staining of human mesenchymal stem cells as amyloid fibrils-free model was carried out. The amyloid-containing biofilms of *E. coli* K12 were stained by both AmyGreen and ThT to compare the effectiveness and specificities of both dyes when applied in fluorescence microscopy analysis. It was noticed that AmyGreen dye shown more advantages in detection sensitivity and selectivity for amyloid components in bacterial biofilms.

Materials and methods

Synthesis

AmyGreen was prepared according to the two step procedure.

(E)-3-(3-(4-(dimethylamino)phenyl)acryloyl)-4-hydroxy-6-methyl-2H-pyran-2-one. 14.9 g (0.1 mol) of 4-(dimethylamino)benzaldehyde was added to 16.8 g (0.1 mol) of dehydroacetic acid in 150 ml of n-butanol and was heated up to boiling temperature. 10 drops of a mixture of pyridine and piperidine (1:1 by volume) were added to the boiling homogeneous solution and boiled for 4 h. The half of the solvent was distilled, cooled down and filtered from fell out crystals. The product was washed twice on the filter with small amount of isopropanol and recrystallized from DMF-isopropanol system. After that the product was filtered, washed on the filter with isopropanol, twice with hot water and air dried. Yield 18.6 g (62%). M. p. = 208 °C–210 °C. Found, %: C 65.53; H 5.41. Anal. Calcd. (%) for $C_{17}H_{17}NO_4$: C 65.45; H 5.49. ^{1}H NMR (400 MHz, DMSO-d_6) δ: 18.57 (s, 1H), 7.95 (s, 2H), 7.59 (d, J = 9.0 Hz, 2H), 6.79 (d, J = 9.0 Hz, 2H), 6.22 (s, 1H), 3.34 (s, 6H), 2.25 (s, 3H). IR cm^{-1} (KBr): 3432 (m), 3080(s), 3063(s), 2913(s), 2856(s), 2802(s), 2643 (s), 2544(s), 1717(w), 1650(w), 1600(w), 1591(w), 1521 (w), 1461(w), 1434(w), 1362(w), 1332(w), 1287(m), 1238(m), 1213(s), 1183(w), 1163(w), 1118(w), 1073 (w), 1045(s), 1024(s), 1002(m), 982(s), 946(s), 895(m), 869(s), 823(m), 818(m), 781(s), 747(w), 735(w), 631 (s), 595(s), 525(s).

(2E,5Z,7E)-8-(4-(dimethylamino)phenyl)-6-hydroxy-2-(2-methoxyethylamino)octa-2,5,7-trien-4-one (AmyGreen). 1.5 g (5 mmol) of (E)-3-(3-(4-(dimethylamino)phenyl)acryloyl)-4-hydroxy-6-methyl-2H-pyran-2-one in 5 ml of dimethylformamide was heated to 130 °C. A small excess 0.4 g (5.3 mmol) 2-methoxyethan-1-amine was added to this solution and kept for 3–5 min until the release of carbon dioxide ceased. A change in the color of the reaction mixture from yellow to red was observed. After cooling, the reaction mixture was precipitated with water (15 ml). The resulting solid was filtered, washed with water (3 × 10 ml) and crystallized from EtOH or DMF-EtOH mixture (7:3 vol.:vol.). The crystals were collected by vacuum filtration and washed with EtOH (2 × 10 ml) and water (2 × 10 ml) and dried. Yield 1.06 g (64%). M.p.: 118 °C–121 °C. Found, (%): C, 69.10; H, 7.87; N, 8.42. Anal. Calcd. (%) for $C_{19}H_{26}N_2O_3$: C, 69.06; H, 7.93; N, 8.48. ^{1}H NMR (300 MHz, $CDCl_3$–d) δ: 15.20 (s, 1H), 10.89, 10.34 (t + t, J = 5.0 Hz, 1H), 7.45, 7.38 (d + d, J = 8.9 Hz, 2H), 7.59, 7.31 (d + d, J = 15.7 Hz, 1H), 6.67 (d, J = 3.0 Hz, 2H), 6.63, 6.24 (d + d, J = 15.7 Hz, 1H), 5.21, 4.78 (s + s, 1H), 5.07, 3.59 (s + s, 1H), 3.57–3.41 (m, 4H), 3.40, 3.37 (s + s, 3H), 3.02, 2.99 (s + s, 6H), 1.98, 1.94 (s + s, 3H). IR cm^{-1} (Cryst. powd.): 3359 (w), 3195(w), 2923(w), 2851(w), 1635(w), 1605(m), 1558(s), 1418(m), 1366(m), 1303(m), 1230(w), 1186 (w), 1146(m), 1122(m), 973(w), 937(w), 856(w), 817 (w), 728(w), 650(w), 558(w), 517(w), 495(w), 434(w).

Materials

ThT (from Sigma-Aldrich) and AmyGreen stock solutions were prepared in DMSO at the concentration 2 mM. Human insulin (Sigma-Aldrich) was dissolved at 340 μM (2 mg ml^{-1}) concentration in 0,1 M water solution of HCl (pH 2). Lysozyme (Sigma-Aldrich) was dissolved at 1 mM (14.3 mg ml^{-1}) concentration in 0.1 mM water solution of HCl (pH 2). Stock solutions of dsDNA and RNA were prepared by dissolving these nucleic acids in Tris-HCl buffer (50 mM, pH 7.9) at the concentration of 6.15 mM b.p. for DNA and 12.3 mM b.p. for RNA (dsDNA was 4 mg ml^{-1}, RNA was 8 mg ml^{-1}). Calculations for dsDNA: with respect to base pairs, b.p.; for RNA: with respect to bases, b. Stock solution of bovine serum albumin (BSA) was 0.2 mg ml^{-1} in 50 mM Tris-HCl buffer (pH 7.9). Stock solution of soybean lecithin was 4 mg ml^{-1} dissolved in distilled water. Stock solution of starch was 4 mg ml^{-1} dissolved in distilled water with 10% of DMSO.

Insulin and lysozyme fibril formation

Fibrils of human insulin were formed by incubating the protein solution (340 μM in 0,1 M HCl) in the Environmental Shaker-Incubator ES-20 (Biosan) at 65 °C for about 5 h. Fibrils of lysozyme were formed by incubating the protein solution (1 mM in 0,1 M HCl) in the Environmental Shaker-Incubator ES-20 (Biosan) at 65 °C for about 24 h.

Spectral measurements

Fluorescence excitation and emission spectra were collected on a Cary Eclipse fluorescence spectrophotometer (Varian). The excitation light wavelength was set set to be equal to the lowest-energy band maximum in the respective excitation spectrum. All measurements were performed in standard 10 mm quartz cuvettes at room temperature.

Working solutions of free dyes were prepared by dilution of the dye stock solution with Tris-HCl buffer (pH 7.9) to the concentration of 2 μM (for all measurements). The working solutions of dye/protein mixtures were prepared by adding the aliquot of stock solution of monomer insulin or fibrillar insulin/lysozyme aggregates to the 2 μM dye solution. Insulin concentration in the working solution was 3.4 μM, lysozyme concentration in the working solution was 4 μM. The working solutions of dye/NA mixtures were prepared by mixing together 2 μM of dye and an aliquot of DNA or RNA stock solutions in Tris-HCl buffer (final concentration of dsDNA was 61.5 μM b.p. and RNA was 123 μM b.p.).

The working solution of dye/BSA mixture was prepared by addition the dye to 3 μM BSA solution (dye concentration in working solution was 2 μM).

The working solution of dye/lecithin mixture was prepared by addition of lecithin aliquot to 2 μM working solution of dye (final lecithin concentration was 0.04 mg ml^{-1}). The working solution of dye/starch mixture was prepared by addition of starch aliquot to 2 μM working solution of dye (final starch concentration was 0.04 mg ml^{-1}).

Emission quantum yields of dyes bound to insulin fibrils were determined with a Hamamatsu photonic multichannel analyzer C10027 equipped with a Spectralon® integrating sphere using samples with the dye concentration of 2 μM.

Bacteria, biofilm formation and sample preparation

E. coli K12 was used as a model strain to study curli visualization in a biofilm. *P. aeruginosa* ATCC 27853, *S. aureus* ATCC25923, *B. avium* 61 [38], *K. pneumoniae* ATCC10031 and a number of *K. pneumonia* hospital isolates, specifically, UHI 117, UHI 496, UHI 509, UHI 519, UHI 520, UHI 742 obtained from Ukrainian patients were used to obtained biofilms.

Bacteria were cultured aerobically at 37 °C and liquid cultures were cultured in the classical Luria-Bertani (LB) medium shaking to provide inocula [39]. Overnight cultures of all the strains were used to produce biofilms in stationary LB or No Salt LB media microcosms containing 5 ml each. All biofilms were obtained at 28 °C or 37 °C and harvested in one or three days. Solid-liquid biofilms formed onto a bottom surface of each microcosm were sampled and put on microscopic glass slides for the following staining with Thioflavine T (ThT), AmyGreen, 5 μg ml^{-1} of Calcofluor White (CW) and 2 μg ml^{-1} of Ethidium Bromide (EtBr).

Eukaryotic cell staining

Mesenchymal stem cells were obtained like it was done before [40]. After transferring the slides to room temperature, the medium was removed. The cells were fixed on microscope slides at room temperature, and incubated with fluorescent dyes for 30 min. The washed cell samples were covered with a cover slip.

Confocal laser scanning microscopy analysis (CLSM)

CLSM analysis of the samples was done using Leica TCS SPE Confocal system with coded DMi8 inverted microscope (Leica, Germany). Images were acquired using excitation at 488 nm and emission collected at 510–605 nm for AmyGreen and ThT, excitation at 405 nm and emission collected at 450–500 for CW, and excitation at 532 nm and emission collected at 600–740 for EtBr.

Colocalization analysis

The Pearson Correlation Coefficient (PCC), or Pearson's R, was calculated using the open source image processing package Fiji based on ImageJ. There were three images per staining variant with five regions of interest, or ROI, with groups of two-five bacterial cells chosen manually, per image. The Pearson's R was calculated for pixels whose intensity was above a threshold value in order to avoid background signals and low-intensities pixels as it was recommended in [41]. The obtained data were processed statistically using the Orogin7 software and the One-way ANOVA algorithm. A value of $p < 0.05$ was considered statistically significant.

Table 1. Luminescence properties of AmyGreen and ThT in the presence of different biomolecules.

	AmyGreen			ThT		
	λ_{ex}	λ_{em}	PLQY	λ_{ex}	λ_{em}	PLQY
free dye	410	528	<0.02	444	526	<0.02
native insulin	423	532	<0.02	442	520	<0.02
fibrillar insulin	454	541	**0.45**	448	483	**0.20**
native lysozyme	430	536	<0.02	442	517	<0.02
fibrillar lysozyme	442	532	**0.49**	448	477	**0.17**
BSA	432	526	<0.02	433	490	<0.02
BSA-SDS (0.05%)	433	558	<0.02	436	510	<0.02
DNA	415	525	<0.02	446	488	**0.06**
RNA	417	527	<0.02	451	486	**0.14**
soybean lecithin	434	509	<0.02	415	480	<0.02
Starch	424	564	<0.02	426	500	<0.02

λ_{ex}, λ_{em} - maximum wavelength of excitation, emission spectrum, nm.

PLQY—fluorescence quantum yield; emission of each sample was excited at the wavelength of corresponding excitation maxima.

Results and discussion

Response of AmyGreen to various biomolecules *in vitro*

Amy Green shows strong green fluorescence in presence of fibrillar proteins that contrasts with only very weak emission in solution, which is easily rationalized by suppretion of nonradiative relaxations of electronically excited dye molecules in rigid local environments inside a fibril as compared to a bulk solvent [35]. This enhancement of fluorescence quantum yield, and thus intensity, induced by fibrillar proteins is the basis of the turn-on fluorescence detection of amyloid structures by use of AmyGreen.

The specificity of this response of AmyGreen to amyloid fibrils was investigated in comparison of the response to fibrillary proteins *in vitro* with the response to other biomolecules: nucleic acids, albumin, starch (as a model polysaccharide), soybean lecithin and BSA micelles with sodium dodecyl sulfate (BSA-SDS) (as membrane models). As reference commonly used amyloid sensitive fluorescent dye ThT was also tested in parallel. The results are collected in table 1 and representative exemplary emission and excitation spectra are shown in the figure 3.

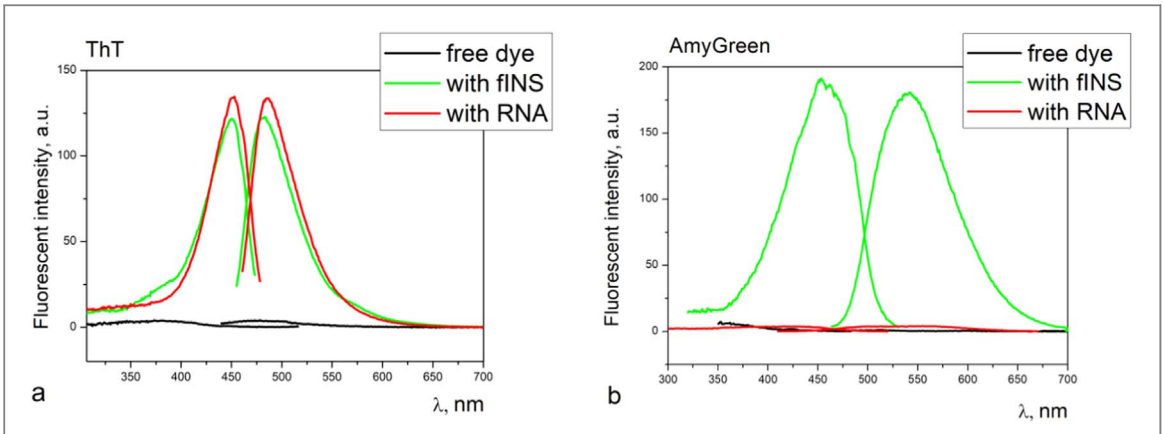

Figure 3. Fluorescence excitation (left) and emission (right) spectra of the dye **ThT** (a) and **AmyGreen** (b) free, in presence of fibrillar insulin (fINS) and RNA in 50 mM TRIS-HCl buffer (pH 7.9).

Both dyes ThT and AmyGreen, in a free state and in the presence of biomolecules, absorb light in the blue spectral region with the lowest-energy exciatation maxima between 410 and 452 nm in the case of AmyGreen and 415 and 451 nm in the case of ThT, respectively. The small spectral shifts are caused by different microenvironments when the dye molecules are bound with particular biomolecules. The both compounds emit (fluoresce) green light with the measured emission maxima between 509 and 564 nm for AmyGreen and 477 and 526 nm for ThT, respectively. The emission in the most media is very weak. The fluorescence quantum yields do not overcome the value of 2%. Only in presence of fibrillar proteins, produced by chemical denaturation of insulin and lysozyme, the fluorescence signal of AmyGreen is significantly stronger than in biomolecule-free solution. The measured fluorescence quantum yields with PLQY = 45% for fibrillar insulin and 49% for fibrillar lysozyme, respectively, are higher than for the free dye by a factor of at least 20. Thus, AmyGreen displays strong fluorescence enhancement in presence of fibrillar proteins and no significant response to any other common biomolecules tested. The reference compound ThT shows similar turn-on response to fibrillar proteins with the respective PLQY values of 20% (fibrillar insulin) and 17% (fibrillar lysozyme) being at least one order of magnitude higher than for the free dye. However, interactions with nucleic acids DNA and RNA also enhance the ThT fluorescence. The measured PLQY values are 6% and 14%, respectively.

The latter effect results from the known affinity of ThT to nucleic acids which has also been utilized, in particular, for detection of G-quadruplexes [42] and monitoring of RNA metabolism [28]. Such a high sensitivity of ThT to nucleic acids (NA) could result in decreased specificity to amyloid- components of bacterial biofilm extracellular matrix.

Thus, AmyGreen represents a promising candidate as fluorescence probe for amyloid-containing structures, for instance in bacteria biofilms. Compared with the reference amyloid marker ThT, it also offers improved selectivity in terms of the lack of false positive response to nucleic acids that are ubiquitous in biological samples.

2. The efficiency of visualization of *E. coli* K12 biofilm by AmyGreen

Herein a thin layer of 3-day low-density *E. coli* K12 biofilm was used to determine the ability of AmyGreen to visualize amyloids associated with sessile individual cells. This strain is a well-known standard producer of curli amyloid fibrils that contributed substantially to the biofilm matrix [43], they have been shown to bind amyloid-specific dyes (Congo Red or ThT).

Both amyloid-sensitive dyes AmyGreen and ThT in two concentrations 10^{-4} M and 10^{-5} M were used to stain one and three day old K12 biofilms, NA-specific dye EtBr was used for co-staining for cells visualization (figure 4, Suppl. figure S1 is available online at stacks.iop.org/MAF/8/035006/mmedia). As seen from the figure S1, both AmyGreen and ThT dyes are green-emitted, and they efficiently visualize the bacterial cells and cellular structures in a biofilm at 10^{-4} M concentration.

The overlapping of the objects stained by ThT (figures 4(A), (B)) with those stained by EtBr is high, and a number of objects giving green (ThT), but not red (EtBr) staining are negligible. The partial overlapping of objects stained by both EtBr and AmyGreen or ThT was observed supporting the fact of cell-associated curli formation. However, for AmyGreen (comparing to ThT) the overlapping with EtBr is lower, and more objects are stained only green (AmyGreen). The number of spot-like or elongated shape objects probably attributed to amyloid fibers were clearly visualized by AmyGreen and not stained by EtBr (figures 4(C)–(D)), that also points on different 'visualization targets' for those dyes. Here we suggest that ketoenole dye stains amyloid structures localized on the surface of cells and also separated from the cells in ECM, while ThT stains both amyloids and cells.

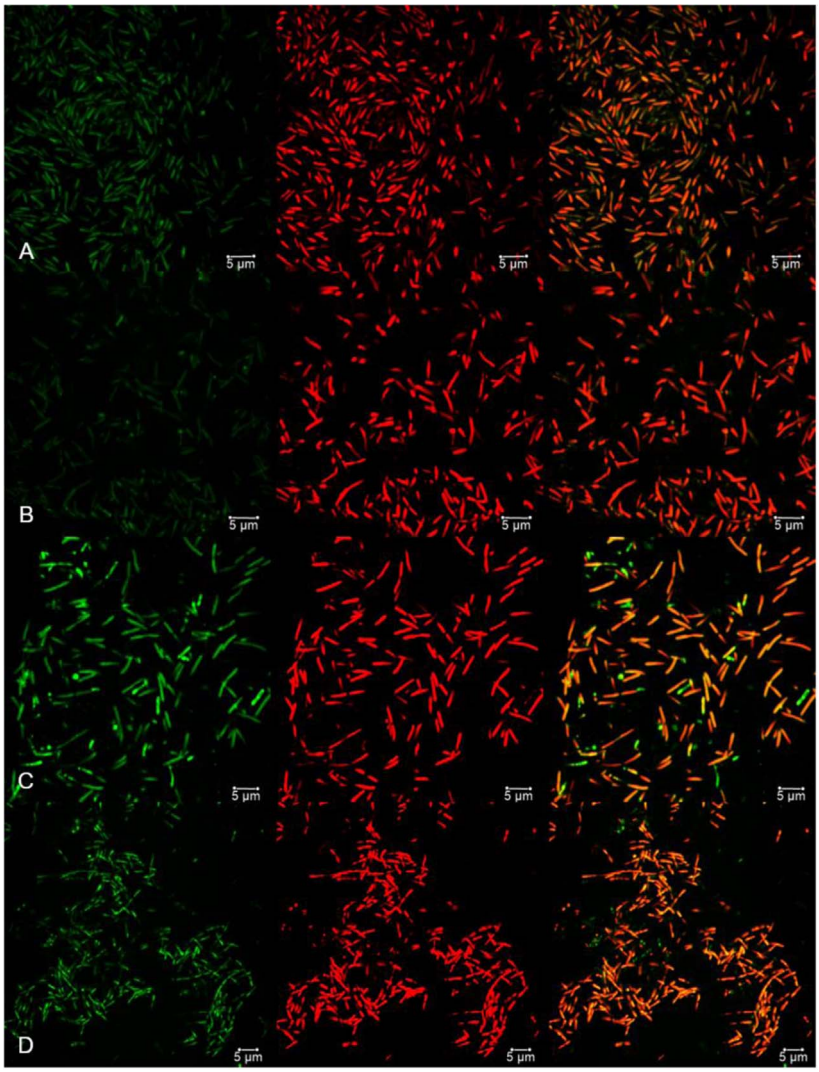

Figure 4. Fragments with sessile individual cells from three-day old E. coli K12 biofilms. Staining with EtBr and (A) ThT with concentration 10^{-4} M; (B) ThT with concentration 10^{-5} M; (C) AmyGreen with concentration 10^{-4} M; (D) AmyGreen with concentration 10^{-5} M. Left column corresponds to green signal emission (ThT or AmyGreen), middle column corresponded to red signal emission (EtBr), right column corresponded to merged signals (CLSM). Three-day old E. coli K12 biofilm was cultured aerobically at 28 °C.

Indeed, the subsequent colocalization analysis shown that the average Pearson's Rs for ThT/EtBr at 10^{-4} M and 10^{-5} M were 0,60333 ± 0,09585 and 0,505 ± 0,22039 which means that there was a positive correlation between ThT and EB signals on the images (figures 4(A), (B)). On the contrary, Pearson's Rs for AmyGreen/EtBr at 10^{-4} M and 10^{-5} M were 0,38833 ± 0,17498 and 0,07625 ± 0,07347 respectfully which were significantly lower and confirmed that AmyGreen-stained objects poorly colocalized (when 10^{-4} M concentration) and did not colocalized (when 10^{-5} M concentration) with EtBr-stained objects. This observation might be explained by the high fluorescent response of ThT on NA (table 1, figure 3). Since EtBr stains NA a high signal colocalization was observed for ThT/EtBr. Remarkably, the reduction in ThT concentration did not affect specificity and shown equally high Pearson's R. Alternatively, the one-fold reduction in AmyGreen concentration decreases it colocalization with EtBr (figure 5) and thus increase specificity of visualization of amyloid components.

Practically, in the case of lower 10^{-5} M concentration of the dyes, the image visualized by AmyGreen staining remains rather bright (figure 4(D)) and the objects are well distinguished. As for ThT (figure 4(B)) at 10^{-5} M concentration, the staining intensity is rather weak, and objects are distinguished poorly.

This suggested higher staining efficiency and specificity for amyloid-containing bacterial biofilm visualization provided by AmyGreen over ThT.

The efficiency of visualization of various *K. pneumoniae* biofilms by AmyGreen

It has been shown that clinical isolates of *K. pneumoniae* were able to produce amyloid curli [44]; however, within biofilms of some isolates of *K. pneumoniae*, the curli component was not detected [45]. Besides, in *K.*

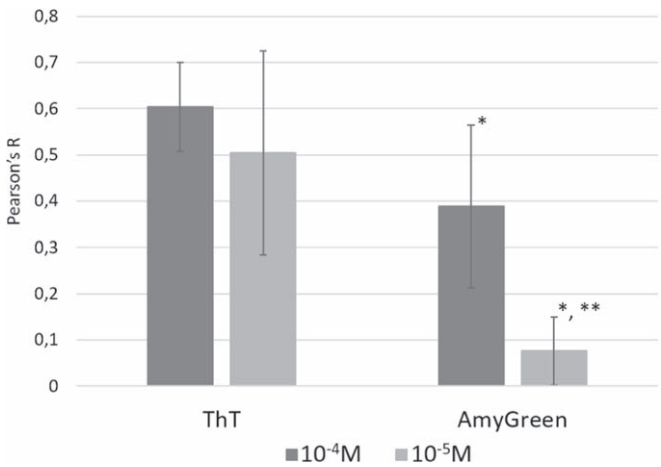

Figure 5. Pearson's R plot representing the colocalization between ThT and EtBr signals (ThT columns) and AmyGreen and EtBr signals (AmyGreen columns) at two concentrations 10^{-4} M and 10^{-5} M. Values represent the mean ± SD.* statistical significance compared to an alternative stain at a corresponding concentration; ** statistical significance compared to the same stain at a different concentration.

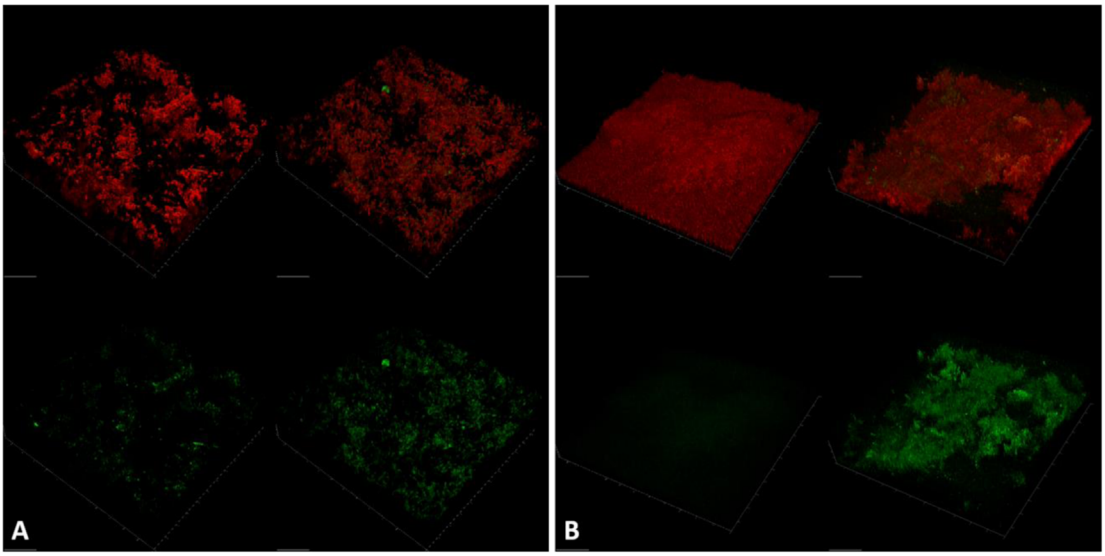

Figure 6. (A)—*K. pneumoniae* ATCC 10031 one-day-old biofilm, stained with EtBr / ThT (left) and EtBr/AmyGreen (right). (B)—Hospital isolate of K. pneumoniae UHI 117 one-day-old biofilm, stained with EB/ThT (left) and EB/AmyGreen (right). Concentration of ThT and AmyGreen dyes was 10^{-5} M. Red color is the emission of EtBr, green one is that of AmyGreen or ThT. K. pneumoniae biofilms were cultured aerobically at 37 °C.

pneumoniae the channel-forming bacteriocin Microcin E492 could exist in fibrillar form [46]. Herein, Klebsiella biofilms was used as a model of pathological biofilm to study the specificity of the new amyloid-sensitive dye.

One-day biofilms formed by different *K. pneumoniae* strains, specifically, a typical strain from the ATCC collection and a hospital isolate UHI 117, were stained using AmyGreen stain and ThT at concentration 10^{-5} M together with EtBr (figure 6). The AmyGreen has different staining patterns in the typical ATCC 10031 and pathogenic isolates. The hospital strain has shown more intensive staining that points on higher intensity of amyloids production. In contrast, ThT stains biofilms weakly, especially in the hospital bacterial strain, which is characterized by dim and dot-like staining pattern.

Thus, the AmyGreen dye was shown as a more effective stain comparing to ThT upon the visualization of the biofilms of different *K. pneumoniae* strains.

In addition, three-day-old biofilms of different hospital strains of *K. pneumoniae* were stained with AmyGreen and EtBr (figure 7). Brighter staining of *ATCC10031* and UHI 117 biofilms was observed as compared to corresponding one-day biofilms, which is explained by higher content of functional amyloids that was produced during longer incubation. AmyGreen application revealed that *K. pneumoniae* strains demonstrated a high variation in intensity of functional amyloid production in their biofilms.

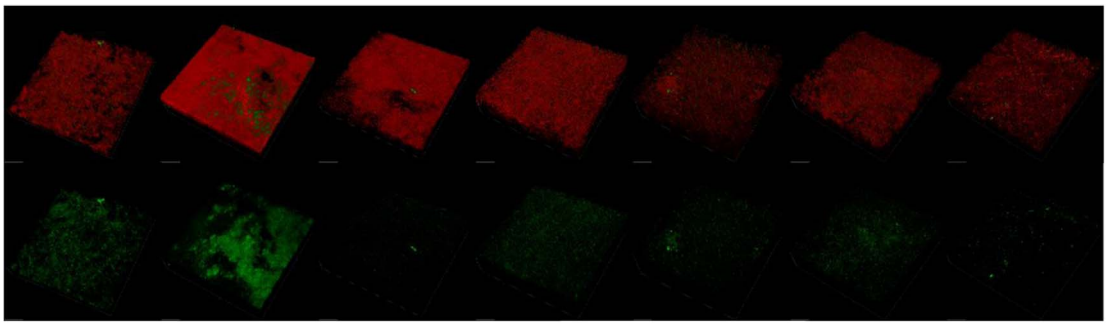

Figure 7. Three-day-old biofilms of different K. pneumoniae strains, stained with EtBr (top) and AmyGreen 10^{-4} M (bottom). Left to right: K. pneumoniae ATCC10031, UHI 117, UHI 496, UHI 509, UHI 519, UHI 520, UHI 742. K. pneumoniae biofilms were cultured aerobically at 37 °C.

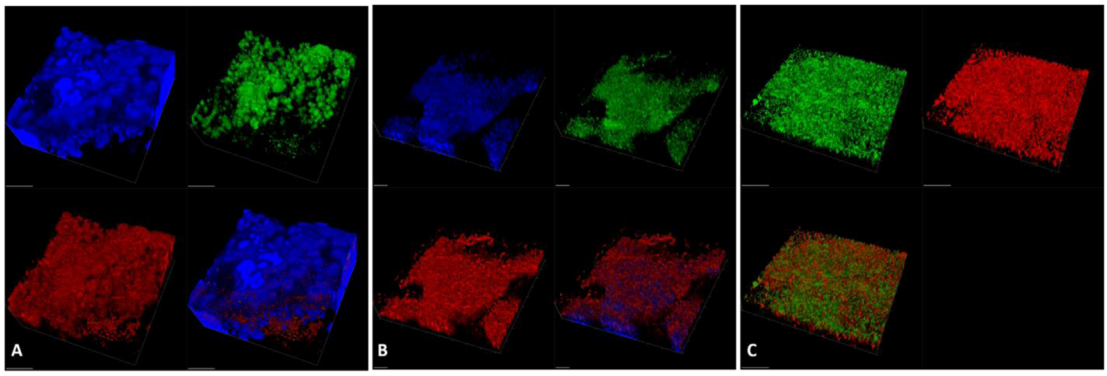

Figure 8. 5-day (A), (B) and 2-day (C) biofilms of P. aeruginosa ATCC 27853 (A), B. avium 61 (B) and S. aureus ATCC 25923 (C) stained with CW (Blue), 10^{-4} M of AmyGreen (Green) and ThBr (Red). Scale bar corresponds to 20 μm. For each sample, separate images for different stains and a merged image of all stains are presented. The biofilms were cultured aerobically at 37 °C for S. aureus ATCC 25923 and at 28 °C for P. aeruginosa ATCC 27853 and B.avium 61.

The efficiency of visualization of different bacteria biofilms by AmyGreen

Amyloid fibrils are a widely spread bacterial strategy to attach initially to a surface and build up a biofilm [16]. Examples of extracellular amyloid fibrils with structural and functional similarity to curli fimbriae of *E. coli* have been described in various species of *Pseudomonas*, *Salmonella*, *Citrobacter*, and *Enterobacter* [8, 9]. For example, Fap fimbriae of *P. aeruginosa* and *P. fluorescens* showed the presence of an extensive β-sheet structure, as well as binding to the ThT dye [44]. The visualization AmyGreen of biofilms of various gram-positive and negative bacteria that produce functional aggregates has also been studied on *P. aeruginosa* ATCC 27853, *B. avium* 61 and *S. aureus* ATCC25923. For this purpose, biofilms were stained by AmyGreen at 10^{-4} M concentration together with EtBr and CW (figure 8). Polysaccharides are poorly produced by *S. aureus ATCC 25923*, so CW was not used for co-staining for this biofilm.

It could be seen from the figure 7 that AmyGreen was able to visualize amyloid-based cell-associated structures in biofilms produced by gram-negative *P. aeruginosa* ATCC 27853, *B. avium* 61 [38] and gram-positive *S. aureus* ATCC25923. Biofilms of different bacteria were co-stained with AmyGreen, EtBr, and CW dyes. The noticeable distinction between localization of AmyGreen and CW was observed, which indicates the structural separation of polysaccharides and amyloids in the biofilm matrix. (figure 8(A)).

AmyGreen has shown effective visualization of biofilms of both gram-negative and gram-positive amyloid-producing bacteria with separate staining patterns over CW and EtBr and we can suggest that dye binded amyloid-reach regions of biofilm.

Visualization of biofilm polysaccharides by AmyGreen

Polysaccharides are considered to be the main extracellular component of many bacterial biofilm matrixes [47, 48]. Thus, it is important property for the amyloid-sensitive probe to give a low fluorescent response on polysaccharide in ECM. The intensive visualization of both ECM matrix components, amyloids and polysaccharides, was reported for conjugated oligothiophenes [33]. Extracellular polysaccharides and curli were visualized in 3-day-old mature *E. coli* biofilm grown at 28 °C to achieve a high polysaccharide production in the culture. The dye AmyGreen was applied together with the cellulose sensitive dye CW

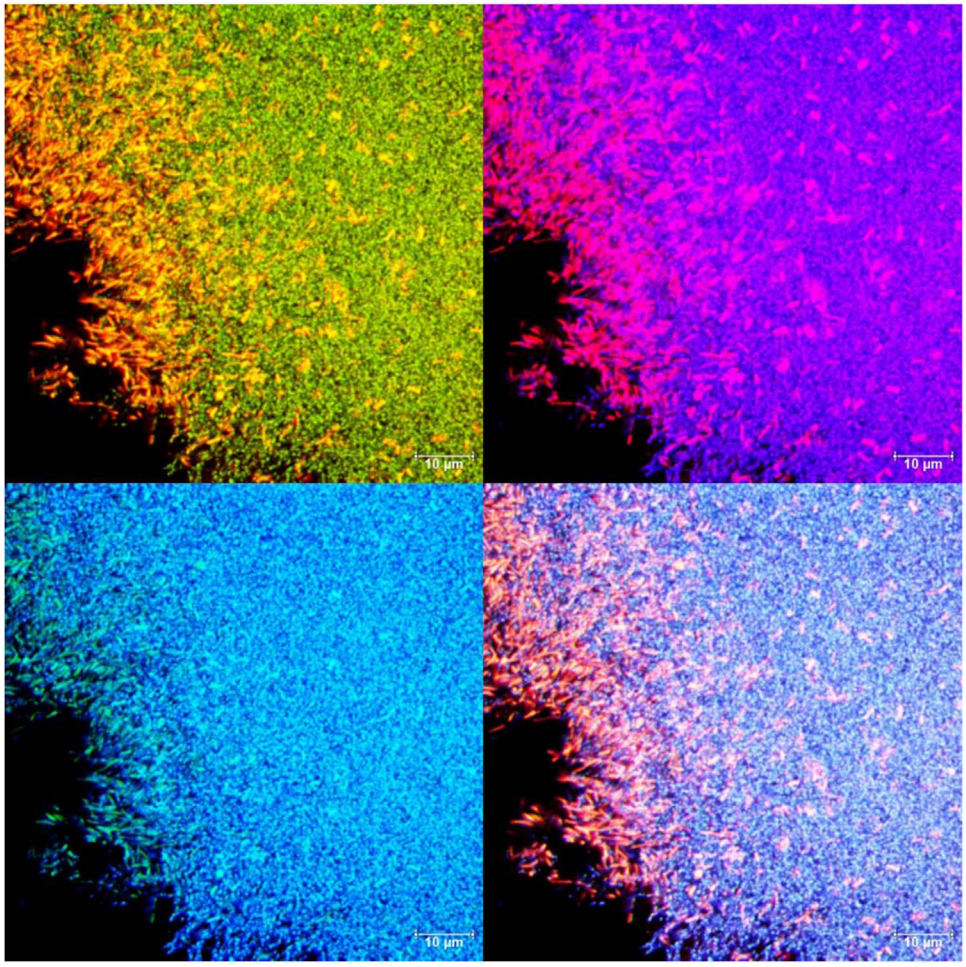

Figure 9. 2D images of three-day-old *E. coli* K12 biofilm stained with AmyGreen (concentration 10^{-5} M; green signal, CW (blue signal; corresponding to polysaccharides), and EtBr (red signal; corresponding to intracellular nucleic acids for bacterial cells visualization). Above: left—co-staining by AmyGreen with EtBr, right—co-staining by EtBr with CW; below: left—co-staining by AmyGreen with CW, right—co-staining by AmyGreen and EtBr with CW. The biofilm was cultured aerobically at 28 °C.

(blue staining) to study whether AmyGreen visualizes polysaccharides, and co-staining with EtBr was used to visualize cells location (figure 9, Suppl. figure S2).

The green-staining by AmyGreen was observed through the whole biofilm, which points on the presence of amyloid structures. Two locations of amyloids were observed: some of the fibrils were associated with cells and were thus co-stained with EtBr, while other amyloids formed spot-like extracellular clusters (figure 9, Suppl. figure S2).

For the main component of *E. coli* functional amyloid (CsgA subunit), the ability to form toxic oligomers and seed self-aggregation has been shown, as well as heterologous amyloid aggregation [49, 50]. We can assume that AmyGreen visualizes not only functional amyloid fibers attached to the cell surface, but also amyloid knots recognized as clusters in the volume of the biofilm, which are not associated with cells.

Polysaccharide-specific CW staining has shown an intensive blue signal through the whole ECM, which suggests a high content of polysaccharides. The colocalization analysis shown the average moderate colalization value for the CW signal with the AmyGreen signal (the average Pearson's R is 0,50429 $\pm$ 0,18972). This suggests the different visualized targets for these dyes which, however, can be associated since the Pearson's R varied in the wide range from 0,27 to 0,75 dependently from analyzed sector of biofilm (raw data is not shown). The effect of amyloid-polysacharide association in the biofilm extracellular matrix was described before [51].

Visualization of mesenchymal stem cells by AmyGreen

To compare the cell permeability of AmyGreen and ThT and their ability to visualize cell components, the amyloid-free mesenchymal stem cells (used as negative control) were stained by these dyes in concentration 10^{-4} M (figures 10(A), (B)). EtBr that stains nucleic acids in the cytoplasm, penetrates nuclei and visualizes nuclei components was used for co-staining.

It is seen from the figure 10 that both dyes AmyGreen and ThT were able to penetrate through the cellular membrane and visualize components of the stem cells; however, AmyGreen possessed different visualization pattern compared to ThT.

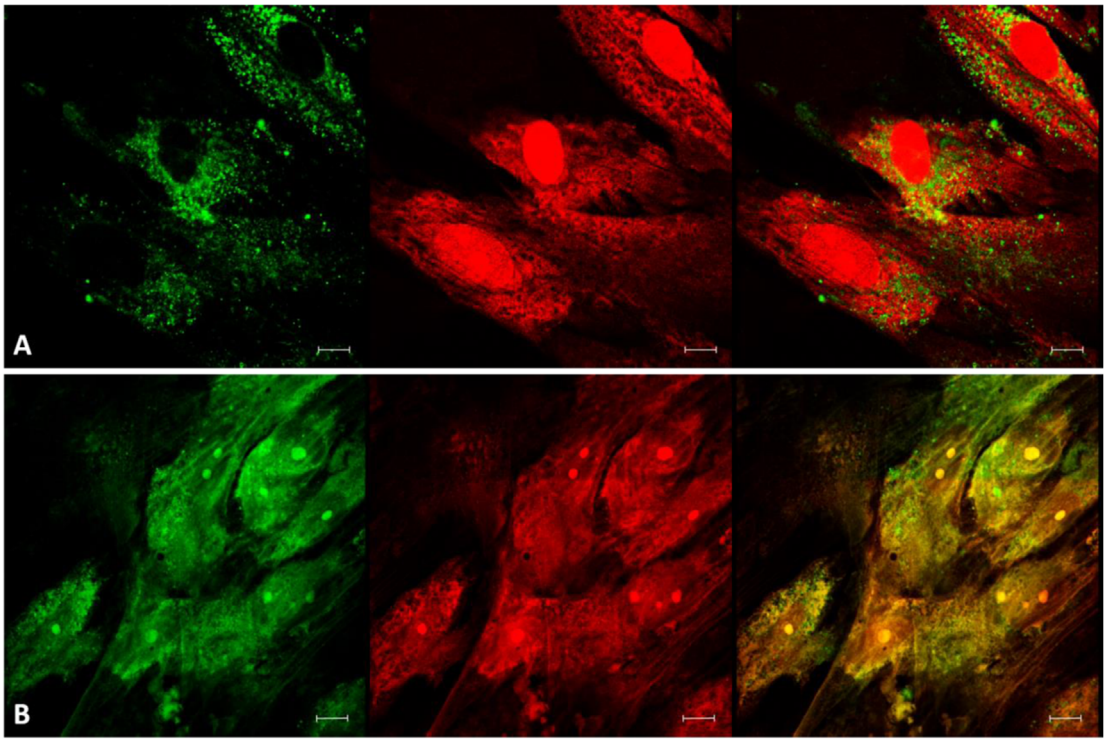

Figure 10. (A) - Mesenchymal stem cells, stained by AmyGreen (concentration 10^{-4}) and EtBr (left—AmyGreen, middle—EtBr, right—merged); (B) - Mesenchymal stem cells, stained by ThT (concentration 10^{-4}) and EtBr (left—ThT, middle—EtBr, right—merged). Scale bar corresponds to 10 μm.

AmyGreen stained vacuole-like organelles in the cytoplasm and did not penetrate into the nuclei; its staining pattern essentially differs from that of EtBr, which strongly penetrated the cell nucleus, but seems not to stain vacuole-like organelles in the cytoplasm. We suggest that AmyGreen incorporates into bi-layer lipid membrane of organelles (probably mitochondria); this correlates with the ability of this dye to increase the emission intensity in the presence of lipid-containing fraction—soybean lecithin (table 1), however, this fluorescent signal was unstable and bleached quite fast.

The staining patterns observed for EtBr and ThT significantly overlap (figure 10(B), right, yellow color at merged image), so both dyes stained the same cell components. Similarly to EtBr, ThT stains RNA is cytoplasm, penetrates into nuclei and visualizes nucleoli. Strong fluorescent sensitivity to nucleic acids, especially to RNA, by ThT was also shown by *in vitro* studies (table 1). Besides, certain areas of predominantly green staining by ThT could be attributed to vacuole-like organelles in cytoplasm.

Thus, AmyGreen was shown to penetrate into cells and be able to visualize cell components in amyloid-free cells. However, observed intensity of the cells staining is lower for AmyGreen than for referent ThT, which brightly stains nucleic acids-containing components. Hence, we suggest that AmyGreen provides more specific visualization of amyloid-containing structures in bacteria biofilms comparing to ThT.

Conclusion

Here we proposed green-emitted AmyGreen dye (alkylamino β-ketoenole) as an efficient fluorescent probe able to visualize bacterial amyloids in biofilms as well as detect pathological amyloids (*in vitro*).

In solution, AmyGreen increases its emission intensity in dozens of times in the presence of amyloid fibrils and gives the low fluorescent response in the presence of different biomolecules, such as nucleic acids, albumin, starch, soybean lecithin, and BSA-SDS micelles.

AmyGreen provides fluorescent staining of amyloids in *E. coli* K12 and *K.pneumonia* biofilms visualizing bacteria cells together with out-of-cells components that are suggested to have amyloid structure. The higher intensity of fluorescent staining and possibility of using lower dye concentration over referent dye ThT was established for AmyGreen. The higher signal-to-background ratio provided by AmyGreen upon staining allows visualizing the amyloid components of biofilms with higher resolution. Besides, difference in the *E. coli* K12 biofilm staining patterns of AmyGreen over cellulose sensitive dye Calcofluor White was shown.

AmyGreen provides high fluorescence quantum yield when bound to amyloid fibrils (up to 0.5), while its fluorescence response on other model biomolecules is much lower (less than 0.02). This gives the possibility to use the lower concentrations of dye for fibril

visualization and this way to decrease the background staining intensity and to achieve better contrasting. In the case of ThT, the quantum yields of dye bound to amyloid fibrils (up to 0.2) and RNA (up to 0.16) are rather close, this gives low possibility to decrease background staining intensity by decrease of concentration.

Besides, in amyloid-free live steam cells (used as negative control) AmyGreen non-intensively stains vacuole-like organelles in the cell cytoplasm; however, this fluorescent signal was prone to bleach. In opposite, referent dye ThT intensively stains intercellular cytoplasm and nuclei. Thus fluorescent staining of bacteria biofilms provided by AmyGreen is suggested to be more specific to amyloid-like structures comparing to ThT which was also confirmed by the colocalization assay where AmyGreen staining shown low colocalization to NA-staining with EtBr unlike ThT.

AmyGreen can be applied for imaging of amyloids in biofilms of various gram-positive and gram-negative bacteria. It was successfully used for amyloid visualization in biofilms of different amyloid-produced bacterial strains *E. coli* K12, *P. aeruginosa* KP ATCC 27853, *S. aureus* ATCC25923, *B.avium* 61, *K. pneumoniae ATCC 10031* and a collection of hospital klebsiellas.

Acknowledgments

V Ch and V P thank to NASU Program of Fundamental Research 'New Functional Substances and Materials for Chemical Engineering' No 17–20 for support of the synthesis of beta-ketoenole dyes.

O M acknowledges Kyiv National University of Technologies and Design (Kyiv, Ukraine) research grant 0120U101290 'Development of a complex preparation of combined action based on collagen derivatives for the treatment of wound surfaces' as well NATO SPS grant 984834 'Fighting maritime corrosion and biofouling with task-specific ionic compounds' for the support for laser scanning confocal microscopy studies.

The authors have declared that no conflicting interests exist.

ORCID iDs

Olena Moshynets https://orcid.org/0000-0002-2209-8681
Mykhaylo Losytskyy https://orcid.org/0000-0003-3721-5606
Vladyslava Kovalska https://orcid.org/0000-0001-8305-9398

References

[1] Eisenberg D and Sawaya M 2017 *Annu. Rev. Biochem.* **86** 69–95
[2] Verma A 2016 *Ann Indian Acad Neurol.* **19** 169–74
[3] Le N, Narkiewicz J, Aulić S, Salzano G, Tran H, Scaini D, Moda F, Giachin G and Legname G 2015 *Virus Res.* **207** 25–37
[4] Mukherjee A, Morales-Scheihing D, Butler P and Soto C 2015 *Trends Mol. Med.* **21** 439–49
[5] Jimenez J, Nettleton E, Bouchard M, Dobson C, Robinson C and Saibil H 2002 *Proc. Natl Acad. Sci. USA* **99** 196–201
[6] Hammer N, Schmidt J and Chapman M 2007 *Proc. Natl Acad. Sci. USA* **104** 12494–9
[7] Larsen P, Nielsen J, Otzen D and Nielsen P 2008 *Appl. Environ. Microbiol.* **74** 1517–26
[8] Zogaj X, Bokranz W, Nimtz M and Römling U 2003 *Infect. Immun.* **71** 4151–8
[9] Dueholm M, Søndergaard M, Nilsson M, Christiansen G, Stensballe A, Overgaard M, Givskov M, Tolker-Nielsen T, Otzen D and Nielsen P 2013 *Microbiologyopen.* **2** 365–82
[10] Dueholm M, Otzen D and Nielsen P 2013 *PLoS One* **8** e76630
[11] Serra D, Richter A, Klauck G, Mika F and Hengge R 2013 *mBio.* **4** e00103–13
[12] Bergman P, Roan N, Römling U, Bevins C and Münch J 2016 *J Intern Med.* **280** 139–52
[13] Grohmann E and Vaishampayan A 2017 Biofilms in Plant and Soil Health. *Techniques in Studying Biofilms and Their Characterization: Microscopy to Advanced Imaging System in vitro and in situ.* ed I Ahmad and M Husain (Hoboken, NJ: John Wiley & Sons Ltd) 215–30
[14] Tolker-Nielsen T 2014 *APMIS Suppl.* **138** 1–51
[15] Welling M, Hensbergen A, Bunschoten A, Velders A, Scheper H, Smits W, Roestenberg M and van Leeuwen F 2019 *Clinical and Translational Imaging.* **7** 125–38
[16] Hobley L, Harkins C, Macphee C and Stanley-Wall N 2015 *FEMS Microbiol. Rev.* **39** 649–69
[17] Rennie M, Lindvere-Teene L, Tapang K and Linden R 2017 *J Wound Care.* **26** 452–60
[18] Larsen P, Nielsen J, Dueholm M, Wetzel R, Otzen D and Nielsen P 2007 *Environ. Microbiol.* **9** 3077–90
[19] Larsen P, Olesen B, Nielsen P and Nielsen J 2008 *Biofouling.* **24** 241–50
[20] Moshynets O, Babenko L, Rogalsky S, Iungin O, Foster J, Kosakivska I, Potters G and Spiers A 2019 *PLoS One* **14** e0209460
[21] Soh K and Wallace P 2018 *Methods Mol Biol.* **1678** 49–77
[22] Kuperman M, Snihirova Y, Kryvorotenko D, Losytskyy M, Kovalska V and Yarmoluk S 2018 *Biopolym. Cell.* **34** 374–86
[23] Biancalana M and Koide S 2010 *Biochim. Biophys. Acta* **1804** 1405–12
[24] McLennan M, Ringoir D, Frirdich E, Svensson S, Wells D, Jarrell H, Szymanski C and Gaynor E 2008 *J. Bacteriol.* **190** 1097–107
[25] Kovalska V, Kuperman M, Varzatskii O, Kryvorotenko D, Kinski E, Schikora M, Janko C, Alexiou C, Yarmoluk S and Mokhir A 2017 *Methods. Appl. Fluoresc.* **5** 045002
[26] Romero D and Kolter R 2014 *Int Microbiol.* **17** 65–73
[27] Liu S, Peng P, Wang H, Shi L and Li T 2017 *Nucleic Acids Res.* **45** 12080–9
[28] Sugimoto S, Arita-Morioka K, Mizunoe Y, Yamanaka K and Ogura T 2015 *Nucleic Acids Res.* **43** e92
[29] Liu L, Komatsu H, Murray I and Axelsen P 2008 *J. Mol. Biol.* **377** 1236–50
[30] Kim J *et al* 2016 *J. Am. Chem. Soc.* **138** 402–7
[31] Navarro S and Ventura S 2014 *Biotechnol. J.* **9** 1259–66
[32] Choong F, Bäck M, Fahlén S, Johansson L, Melican K, Rhen M, Nilsson P and Richter-Dahlfors A 2016 *Biofilms and Microbiomes.* **2** 16024
[33] McCrate O, Zhou X and Cegelski L 2013 *Chem. Commun.* **49** 4193
[34] Kovalska V, Chernii S, Losytskyy M, Dovbii Y, Tretyakova I, Czerwieniec R, Chernii V, Yarmoluk S and Volkov S 2016 *Dyes Pigm.* **132** 274–81
[35] Kovalska V, Chernii S, Losytskyy M, Tretyakova I, Dovbii Y, Gorski A, Chernii V, Czerwieniec R and Yarmoluk S 2018 *New J. Chem.* **42** 13308–18

[36] Gupta Y, Singla G and Singla R 2015 *Indian J Endocrinol Metab.* **19** 174–7
[37] Booth D *et al* 1997 *Nature* 27 **385** 787–93
[38] McLaughlin K *et al* 2017 *Res. Microbiol.* **168** 419–30
[39] Sambrook J, Fritsch E and Maniatis T 1989 *Molecular Cloning: A Laboratory Manual* 2nd edn (Cold Spring Harbor, N.Y.: Cold Spring Harbor Laboratory Press)
[40] Shuvalova N and Kordium V 2016 *Biopolymers and Cell.* **32** 262–70
[41] Dunn K, Kamocka M and McDonald J 2011 *Am. J. Physiol Cell Physiol.* **300** C723–42
[42] de la Faverie A, Guédin A, Bedrat A, Yatsunyk L and Mergny J 2014 *Nucleic Acids Res.* **42** e65
[43] Smith D, Price J, Burby P, Blanco L, Chamberlain J and Chapman M 2017 *Biomolecules.* **7** 75
[44] Dueholm M *et al* 2010 *Mol. Microbiol.* **77** 1009–20
[45] Chaudhary M and Payasi A 2012 *Journal of Antibioticsvolume.* **65** 631–3
[46] Shahnawaz M and Soto C 2012 *J. Biol. Chem.* **287** 11665–76
[47] Limoli D, Jones C and Wozniak D 2015 *Microbiol Spectr.* **3** MB-0011-2014
[48] Maunders E and Welch M 2017 *FEMS Microbiol. Lett.* **364** fnx120
[49] Sivanathan V and Hochschild A 2012 *Genes & Development.* **26** 2659–67
[50] Blanco L, Evans M, Smith D, Badtke M and Chapman M 2012 *Trends in Microbiology.* **20** 66–73
[51] de Jong W, Wosten H, Dijkhuizen L and Claessen D 2009 *Mol. Microbiol.* **73** 1128–40

Анотація: *Зелений випромінюючий водорозчинний амінокетоенольний барвник AmyGreen пропонується як ефективне флуоресцентне фарбування для візуалізації бактеріальних амілоїдів у біоплівках та виявлення патологічних амілоїдів in vitro. Цей барвник майже не флуоресціює у розчині, але дає яскраве зелене випромінювання в присутності амілоїдних фібрил білків. AmyGreen теж є слабо флуоресцентним в присутності біомолекул, які є компонентами клітин, екзоклітинного матриксу або середовища, зокрема в присутності нуклеїнових кислот, полісахаридів, ліпідів, білків. Таким чином, флуоресценцію AmyGreen можна використовувати для візуалізації амілоїдних компонентів екзоклітинного матриксу в біоплівках бактерій. Відповідно, із застуванням AmyGreen ми дослідили включення амілоїдів в біоплівках Escherichia coli, K. pneumoniae, P. aeruginosa, B. avium і S. aureus. Ефективність AmyGreen порівнювали з традиційним чутливим до амілоїду барвником Thioflavine T. З'ясувалось, що основною перевагою AmyGreen (концентрація 10^{-5} М) є більш висока чутливість для візуалізації амілоїдних компонентів в біоплівкіх у порівнянні з Thioflavine T (10^{-4} М). Крім того, AmyGreen має меншу селективність до нуклеїнових кислот, що було продемонстровано як в експериментах у розчині, так і при фарбуванні еукаріотичних мезенхімальних стовбурових клітин людини, які було використано як негативний контроль. Таким чином, новий барвник має менший ризик хибнопозитивної відповіді при визначенні амілоїдних компонентів бактеріальних біоплівок. Комбіноване фарбування біоплівки барвником AmyGreen і чутливим до целюлози барвником Calcofluor White демонструє диференційне забарвлення та різну локалізацію забарвлених компонентів, що вказує різноманітність локалізацій полісахаридів та амілоїдів у досліджених біоплівках.*

3.5. Фізіологічна роль почуття кворуму у *P. fluorescens* SBW25

Утворення біоплівок є прикладом співпраці асоціації бактерій, хоча співпраця завжди врівноважується динамічною конкуренцією всередині асоціації (104, 105). Утворення біоплівки включає координоване прикріплення клітин-засновників до відповідної поверхні та виробництво важливих екзоклітинних полімерів, які утворюють матрикс біоплівки. У контексті бактеріальної соціальної еволюції екзополімери вважається виробленим «суспільним товаром» («public goods»), який виробляється за ціною окремого виробника, але який надає загальну користь для суспільства в цілому. В багатьох випадках було показано, що утворення біоплівки контролюється регуляцією почуття кворуму (ПК), який представляє собою форма бактеріальної комунікації через малі дифузійні сигнальні молекули, в яких усі члени спільноти інвестують і отримують користь однаковою мірою (9, 10, 106, 107).

Однак бувають випадки, при яких фізіологічний сигнал або генетична мутація активує утворення біоплівки, а клональне розмноження таких або індукованих клітин дикого типу, або мутантних клітини призводять до подальшого розвитку біоплівки. В цьому сценарії перевага утворення біоплівки перевищує витрати на виробництво, що призводить до переваги стратегії, яка обирає індуковані клітини дикого типу або мутантні клітин, що продукують біоплівки, над іншими небіоплівкотворними клітинами, включаючи потенційних шахраїв-опортуністів. Крім того, кооперативна поведінка в наслідок ПК, фізіологічної індукції або мутації також важливі при утворенні інших різноманітних бактеріальних агрегацій типу колоній, флокул, слизу та біоплівок *in vitro*, які зазвичай вивчають за допомогою проточних систем або мікропланшетів (20).

В цьому розділі роботи ми розглядаємо мутантний штам Wrinkly Spreaders (WS) як клас адаптивних мутантів, який виникає під час експериментальної еволюції популяції *P. fluorescens* SBW25 у статичному мікрокосмі (47). Wrinkly Spreaders виробляють біоплівки на основі целюлозного матриксу в П-Р інтерфейсі, що забезпечу учасникам біоплівки кращий доступ до кисню, швидші темпи зростання та покращену фізичну форма в порівнянні з небіоплівкотворними конкурентами (76).

Основні молекулярні механізми функціонування Wrinkly Spreaders добре зрозумілі. Вони пов’язані із мутаціями, що викликають збільшення внутрішньоклітинного c-di-GMP,

що призводить до посиленого виробництва целюлози та посилення утворення біоплівки. Дотепер роль ПК у розвитку біоплівок P. *fluoescens* SBW25 була нез’ясована.

Існують данні про зв'язок між c-di-GMP і ПК в інших псевдомонадах (108-110), що спонукало нас до повторного дослідження геному *P. fluorescens* SBW25 для пошуку потенційно ПК-споріднених генів та можливих сигнальних молекул.

Основні результати, отримані в цьому підрозділі дисертації опубліковані в роботі автора (111).

UDC 579.22 + 279.26 doi: https://doi.org/10.15407/ubj90.03.017

EXAMINING c-di-GMP AND POSSIBLE QUORUM SENSING REGULATION IN *Pseudomonas fluorescens* SBW25: LINKS BETWEEN INTRA- AND INTER-CELLULAR REGULATION BENEFITS COMMUNITY COOPERATIVE ACTIVITIES SUCH AS BIOFILM FORMATION

O. V. MOSHYNETS[1], D. FOSTER[2], S. A. KARAKHIM[3], K. McLAUGHLIN[4], S. P. ROGALSKY[5], S. Y. RYMAR[1], G. P. VOLYNETS[1], A. J. SPIERS[4]✉

[1]Institute of Molecular Biology and Genetics, National Academy of Sciences of Ukraine, Kyiv;
e-mail: moshynets@gmail.com; galina.volinetc@gmail.com
[2]Nuffield Department of Medicine, University of Oxford, John Radcliffe Hospital, United Kingdom;
e-mail: dona.foster@ndm.ox.ac.uk;
[3]Palladin Institute of Biochemistry, National Academy of Sciences of Ukraine, Kyiv;
e-mail: laserlab@biochem.kiev.ua;
[4]School of Science, Engineering and Technology, Abertay University, United Kingdom;
e-mail: mclaughlinkimberley@gmail.com;
✉e-mail: a.spiers@abertay.ac.uk;
[5]Institute of Bioorganic Chemistry and Petrochemistry, National Academy of Sciences of Ukraine, Kyiv;
e-mail: sergey.rogalsky@gmail.com

Bacterial success in colonizing complex environments requires individual response to micro-scale conditions as well as community-level cooperation to produce large-scale structures such as biofilms. Connecting individual and community responses could be achieved by linking the intracellular sensory and regulatory systems mediated by bis-(3'-5')-cyclic dimeric guanosine monophosphate (c-di-GMP) and other compounds of individuals with intercellular quorum sensing (QS) regulation controlling populations. There is growing evidence to suggest that biofilm formation by many pseudomonads is regulated by both intra and intercellular systems, though in the case of the model Pseudomonas fluorescens SBW25 Wrinkly Spreader in which mutations increasing c-di-GMP levels result in the production of a robust cellulose-based air-liquid interface biofilm, no evidence for the involvement of QS regulation has been reported. However, our recent review of the P. fluorescens SBW25 genome has identified a potential QS regulatory pathway and other QS–associated genes linked to c-di-GMP homeostasis, and QS signal molecules have also been identified in culture supernatants. These findings suggest a possible link between c-di-GMP and QS regulation in P. fluorescens SBW25 which might allow a more sophisticated and responsive control of cellulose production and biofilm formation when colonising the soil and plant-associated environments P. fluorescens SBW25 normally inhabits.

K e y w o r d s: cyclic dimeric guanosine monophosphate (c-di-GMP), acyl homoserine lactone (AHL), bacterial cellulose, biofilms, Pseudomonas, quorum sensing (QS).

The formation of biofilms is often considered an exemplar of cooperation within bacterial communities, though cooperation is always balanced by competition within the developing community [1, 2]. Biofilm formation involves the co-ordinated attachment of founder cells to an appropriate

© 2018 Moshynets O. V. et al. This is an open-access article distributed under the terms of the Creative Commons Attribution License, which permits unrestricted use, distribution, and reproduction in any medium, provided the original author and source are credited.

surface and the production of valuable extracellular polysaccharides (or extracellular polymeric substances, EPS) which forms the matrix of the biofilm structure. In the context of bacterial social evolution theory, EPS is considered a 'public goods' produced at a cost to the individual producer but providing an over-all benefit to the community as a whole. In many cases, biofilm formation has been shown to be controlled by quorum sensing (QS) regulation, a form of bacterial communication mediated by small diffusible signalling molecules [3-6], in which all members of the community invest and benefit equally and the community simultaneously protected against cheaters. However, there are cases in which physiological signals or genetic mutation activates biofilm formation, and the clonal expansion of the induced wild-type or mutant cells results in the developing structure. In this scenario, the benefit of biofilm formation outweighs the costs of production, resulting in a fitness advantage that selects for the induced wild-type or mutant cells over other non-biofilm–forming competitors including potential cheaters (in some cases the benefits of EPS production may be preferentially directed at the producing cells and be relatively un-exploitable by cheaters [7]). Furthermore, cooperative behaviours resulting from QS, physiological induction or mutation would be expected to play a part in the of a development and success broader continuum of bacterial aggregations which includes colonies, flocs, slimes, etc., as well as the in vitro biofilms commonly studied using flow cells or microtitre plates [8].

In this article, we review the Wrinkly Spreaders (WS), one class of adaptive mutants which arise during the experimental evolution of populations of *Pseudomonas fluorescens* SBW25 in static liquid microcosms [9]. Wrinkly Spreaders produce a cellulose matrix-based biofilm at the air-liquid (A-L) interface, providing better access to oxygen, faster growth rates and improved fitness compared to the ancestor and other non-biofilm–forming competitors [10, 11]. The underlying molecular biology of the Wrinkly Spreaders is well understood, with mutations causing an increase in c-di-GMP (bis-(3′-5′)-cyclic dimeric guanosine monophosphate) levels resulting in enhanced cellulose production and stronger biofilm formation. Most notably for a pseudomonad, however, was that QS regulation was not found to be directly involved in this process though QS has yet to be systematically examined in *P. fluorescens* SBW25.

Recently a linkage has been reported between c-di-GMP and QS regulation in other pseudomonads [12-14] and other bacteria (e.g. Burkholderia and Vibrio [15, 16]), and this has driven us to re-examine the *P. fluorescens* SBW25 genome for potential QS-related genes and culture supernatants for QS signals. Here we suggest how *P. fluorescens* SBW25 might use QS regulation to further refine cellulose production and biofilm formation in natural environments (as opposed to *in vitro* microcosms), and consider more generally the benefits of linking the sensory and regulatory systems of individuals with the QS-based cooperative activity of populations and communities.

Pseudomonas fluorescens SBW25 and the rise of the Wrinkly Spreaders

P. fluorescens SBW25 is a soil and plant-associated pseudomonad originally isolated from a sugar beet (*Beta vulgaris*) leaf [17], and is able to colonise the leaf and root surfaces of a range of different cultivated plants and weeds. The 6.7 Mbp genome was initially mapped by Southern analysis before the complete genome sequence was obtained [17-19]. *P. fluorescens* SBW25 has been used to investigate plant and soil-microbe interactions, regulation and metabolism, biofilm formation and experimental evolution studies [10, 11, 20-22]. In the latter, bacterial populations are grown in artificial environments known as microcosms and subject to varied selective pressures [20, 23-25]. One aim of this is to provide mechanistic explanations linking adaptive mutation and the underlying molecular biology of an organism with the fitness improvements of 'evolved' mutants compared to the ancestral strain.

Wild-type *P. fluorescens* SBW25 produces smooth round colonies on agar plates, and will grow throughout the liquid column of static microcosms over a period of several days. However, during this time the expanding population will radiate and accumulate a variety of mutants including WS [10, 11]. These are a class of mutants characterised by a flattened, wrinkled colony morphology and the ability to produce a robust and well-attached biofilm at the A-L interface of static microcosms (these characteristics are collectively known as the WS phenotype) (Fig. 1). Although most biofilm research has focussed on liquid-solid surface (L-S) interface biofilms formed by bacteria in laminar flow cells or in micro-titre plates [26-28], the ability to form biofilms at the A-L interface is common amongst

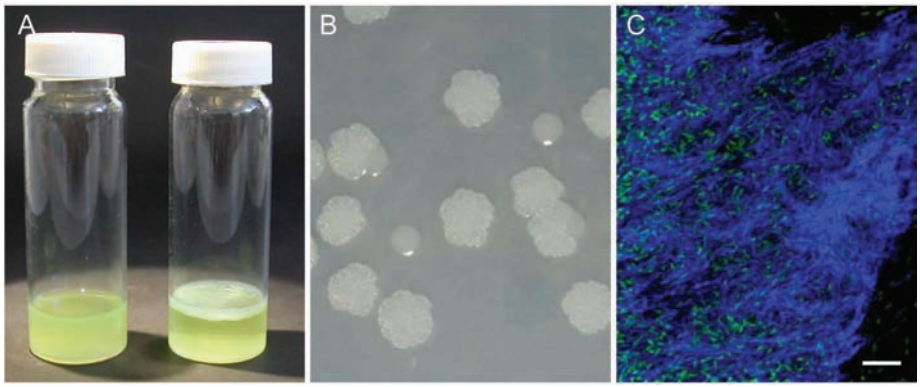

Fig. 1. The Wrinkly Spreader produces a biofilm in static microcosms and wrinkled colonies on agar plates. Developing populations of P. fluorescens SBW25 in static microcosms will radiate and produce a number of mutants including the Wrinkly Spreaders (WS). ***(A)*** *Wild-type P. fluorescens SBW25 grows in the liquid column of static microcosms (left) whereas Wrinkly Spreaders produce a robust biofilm at the air-liquid (AL) interface. The microcosms are 30 ml Universal glass vials with 6 ml liquid growth medium and are typically incubated for 3 days to allow biofilm-formation. (**B**) The Wrinkly Spreader forms wrinkled colonies readily distinguished from wild-type round and smooth colonies on agar plates. (**C**) Both the WS biofilm and colony contain extensive networks of extracellular cellulose fibres. Shown here is a confocal laser scanning microscopy (CLSM) image of a WS biofilm sample stained with Calcofluor show visualise cellulose (blue) surrounding green fluorescent protein (GFP)-expressing WS cells (green). These images were taken using a Carl Zeiss LSM-510 CLSM and the scale bar indicates 5 μm*

environmental pseudomonads [29-32]. Many abiotic and biotic factors influencing L-S and A-L interface biofilm–formation are the same and probably impact on other types of bacterial aggregation too [8].

Wrinkly Spreaders are adaptive mutants in static microcosms containing King's B (KB) liquid growth medium [33], and show improved competitive fitness (W) compared to the wild-type *P. fluorescens* SBW25 ancestor and other non-biofilm–forming competitors (W = 1.5 – 2.5 [9, 34, 35]) (W is the ratio of Malthusian parameters for continuously growing populations and by definition, adaptive mutants will have a competitive fitness (W) advantage over the ancestor, i.e. W > 1; when W = 1, the two strains are neutral with respect to one another, and when W < 1 the mutant is at a disadvantage). However, in shaken microcosms where biofilms cannot form, or on agar plates where the WS phenotype is unstable, the fitness of Wrinkly Spreaders is much reduced and at times even lower than the ancestor (W = 0.1 – 1.0 [34-36]).

The evolutionary and ecological success of the Wrinkly Spreader is explained by the ability to rapidly colonise the A-L interface of static microcosms by biofilm–formation, allowing it to intercept oxygen (O_2) diffusing into the liquid from the air above [37, 38]. *P. fluorescens* SBW25 is an aerobe that grows more slowly under micro-aerobic conditions. The initial colonists of static microcosms rapidly establish a strong O_2 gradient through the up-take of O_2, effectively dividing their environment into an O_2-rich zone at the A-L interface and an O_2-depleted zone below (in this respect, wild-type P. fluorescens SBW25 is responsible for niche construction [11, 39]). Since growth is O_2-limited in these microcosms, bacteria located at the A-L interface will grow faster than those below. As Wrinkly Spreaders can colonise the A-L interface without the constant need for swimming by biofilm–formation, better access to O_2 and higher growth rates provide the fitness advantage, allowing them to outcompete the ancestor and other non-biofilm–forming competitors [37]. Growth at the A-L interface clearly impacts on metabolism, as bacteria recovered from within and underneath biofilms can be differentiated by Raman spectroscopy [40]. In ecological terms, the A-L interface can also be thought of as unoccupied niche and colonisation of this space by biofilm–forming Wrinkly Spreaders would avoid the constant competition between the wild-type *P. fluorescens* SBW25 ancestor and other non-biofilm–forming competitors in the O_2-depleted niche below.

Wrinkly Spreader lineages (i.e. subpopulations) arise in communities, founded by wild-type *P. fluo-*

rescens SBW25 and containing numerous other mutant lineages, in which there is both inter-lineage and intra-lineage completion. This type of complex interaction is described by the Red Queen hypothesis in which all genotypes are locked into constant competition against one another [41]. In this type of community, the Wrinkly Spreader fitness advantage is negative-frequency dependent: at low relative numbers they have a significant advantage and are largely competing against non-biofilm–forming lineages. In this situation the cooperative activity within the WS lineage that forms the biofilm might be better explained by the Black Queen hypothesis where genotypes are mutually dependent [42]. However, as Wrinkly Spreader numbers grow, completion within the WS lineage increases, reducing the fitness advantage for all Wrinkly Spreaders.

In bacterial social evolution theory, biofilms are considered common or public goods in which individual bacteria are expected contribute to the costly EPS matrix through cooperative social behaviour [1, 2, 43, 44]. However, this apparent cooperation might actually result from one or more of three mechanisms, including the response of individual bacteria to environmental stimuli, a community response to QS regulation, and mutation overriding normal regulatory systems (Fig. 2). This cooperation is explained by Hamilton's inclusive fitness (or kin selection theory) which states that cooperation evolves between genetically related individuals [44], and could be facilitated by commonality of sensory systems and QS regulation in which all sufficiently-related individuals respond to the same signals, or to the clonal expansion of a single mutant lineage.

Unlike many other pseudomonads, *P. fluorescens* SBW25 has not been shown to use QS regulation and therefore appears inquorate. Perhaps uniquely, biofilm-formation by Wrinkly Spreaders has been shown to be the result of genetic mutation and clonal expansion, rather than by the cooperative effort of a community.

Unravelling the underlying molecular biology of the Wrinkly Spreader

Mini-transposon mutagenesis of the archetypal Wrinkly Spreader, a particular WS isolate also known as the Large Spreading Wrinkly Spreader (LSWS) and strain PR1200, was used to identify the key genes and regulatory pathways responsible for the WS phenotype [10, 34, 35]. Two key operons, referred to as *wss* (WS structural operon) and *wsp* (WS phenotype regulatory operon), were found to be essential for the WS phenotype.

The ten gene *wss* operon (*wssA–J*) encodes a bacterial cellulose synthase, with the core subunits encoded by WssB, WssC, WssD, and WssE [34]. Cellulose was first reported to be produced by *Acetobacter xylinus* (now known as *Gluconacetobacter hansenii*) in a thick, buoyant biofilm, and it is also

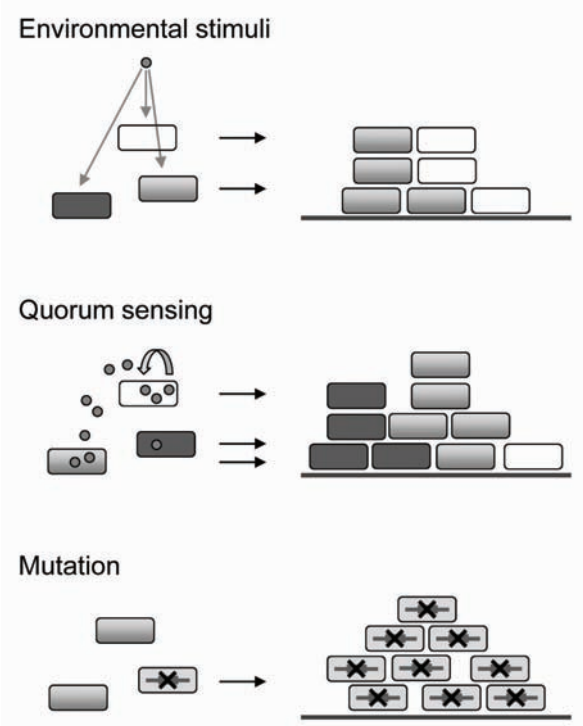

Fig. 2. Three routes leading to the formation of biofilms. Biofilms might be the result of communities of bacteria all responding to the same environmental stimuli (top), quorum sensing (QS) regulation (middle), or mutation (bottom). The initiation of biofilm-formation might be the result of the detection of a signal by all individuals indicating that conditions are appropriate for settlement and growth. Alternatively, QS signals produced by a few individuals might then commit the entire community to biofilm–formation, or mutation in one individual could induce the appropriate behaviour. In the first two situations, variation within the community (from minor genotype differences between lineages or subpopulations to species differences, indicated by white, grey and black fillings) will result in a heterogeneous biofilm-founding population. However, in the case of mutation, the biofilm will be produced by the clonal expansion of the mutant lineage with no heterogeneity in the early stages of biofilm-formation

produced in substantially lower amounts by enteric bacteria such as *Escherichia coli* K-12 and *Salmonella enteritidis* 3934 [32, 46, 47]. In *Escherichia, Gluconacetobacter* and *Salmonella* spp., the genes required for cellulose production are contained within bacterial cellulose synthase (*bcs*) operons similar to the *P. fluorescens* SBW25 *wss* operon [34], though *bcs* operon duplications and other rearrangements are common [48]. Unlike most *bcs* operons however, the *P. fluorescens* SBW25 *wss* operon also encodes proteins involved in the acetylation of cellulose (*WssF–I*) [34, 49, 50] which are also found in several closely-related *Pseudomonas* plant pathogens as well as in the bird pathogen *Bordetella avium* 197N [49, 51, 52]. This unusual modification of the polymer by *P. fluorescens* SBW25 was proven by purifying EPS from WS biofilms and subsequent chemical composition and linkage analysis [49].

Cellulose fibres and clumps could also be visualised in WS biofilm samples by fluorescent or confocal laser scanning microscopy [32, 49, 53] (Fig. 1). Mini-transposon insertions in *wssA–E* abolished cellulose production and the WS phenotype, whereas insertions in *wssF–I* resulted in the production of un-acetylated cellulose and a partial WS phenotype [34, 45 ,49, 54]. In contrast, mutation of *wssJ* had no impact, suggesting that the last gene in the *wss* operon may be redundant [45]. Furthermore, like several other pseudomonad biofilms, the WS biofilm contains extracellular DNA which may also contribute to biofilm strength and resilience (O. Moshynets et al. unpublished observations; to be published elsewhere).

The seven gene *wsp* operon (*wspA–F, R*) encodes a chemosensory-like complex in which the receipt of an unknown environmental signal results in the activation of WspR, a GGDEF-domain containing diguanylate cyclase (DGC) response regulator [34, 55, 56]. Activated WspR synthesises c-di-GMP from GTP [57]. C-di-GMP had been earlier identified as a regulator of cellulose synthase activity in *Gluconacetobacter* spp. [58] and is an important intracellular regulator found in many bacterial species. Intracellular concentrations of c-di-GMP is mediated by the opposing actions of two types of enzymes: DGCs containing GGDEF-domains that synthesize c-di-GMP, and phosphodiesterases (PDEs) containing EAL or HD-GYP domains that degrade c-di-GMP. Levels of c-di-GMP influence a wide range of phenotypes including cellular responses that effect pathogenesis, motility, secretion, cytotoxicity, synthesis of secondary metabolites and environmental stress adaptation as well as QS [59-62]. Many of these phenotypes are also regulated by the Gac/Rsm master regulon, and recently links between the c-di-GMP and Gac/Rsm networks have been identified in *P. aeruginosa* PAK [63] (the Gac/Rsm regulon is also present in *P. fluorescens* SBW25 [64]). Modulation of c-di-GMP is also associated with control of motility, biofilm formation through adhesion and EPS production, including cellulose, and other social behaviours.

The nature of the Wsp complex and the link to cellulose production through c-di-GMP suggested a model explaining the WS phenotype [56]. In this, mutations in Wsp subunits that increased WspR activation in the absence of the normal environmental signal were predicted to result in the expression of the WS phenotype (Fig. 3). The model was confirmed by the identification of a *wspF* (S301R) mutation in the archetypal Wrinkly Spreader, close to the active site and predicted to reduce the methylesterase activity of the subunit required to limit WspR activation. Allelic replacement experiments in which the *wspF* mutation was changed to the wild-type sequence and *vice versa* confirmed that this mutation was sufficient to explain the WS phenotype [56]. Further analysis of other independently-isolated Wrinkly Spreaders identified additional mutations in *wspF* and *wspE*, as well as in several other DGCs or DGC-associated loci (*aws* and *mws*), all of which are predicted to result in increased levels of c-di-GMP and the expression of the WS phenotype [56, 65, 66] (exogenous Fe can non-specifically induce cellulose production by *P. fluorescens* SBW25 and the formation of a weak, poorly attached biofilm [67]). A total of 39 GGDEF-domain containing proteins have been identified in *P. fluorescens* SBW25 genome [18], and the activation of some of these by intra- and intergenic mutations in negative regulators of the DGC or the DGCs themselves can also activate the WS phenotype in a Δ*aws* Δ*mws* Δ*wsp* triple-deletion mutant [68] (loss of function mutations often lead to bacterial adaptation to new conditions [69]). This strongly suggests that the c-di-GMP connection between the Wsp chemosensory-like complex and the Wss cellulose synthase is not unique, and any mutation occurring in radiating populations of P. *fluorescens* SBW25 in static microcosms that up-regulates c-di-GMP levels might result in Wrinkly Spreaders (mutations will arise and fix with a frequency corresponding to their ease of occurrence and fitness relative to other Wrinkly Spreader competitors).

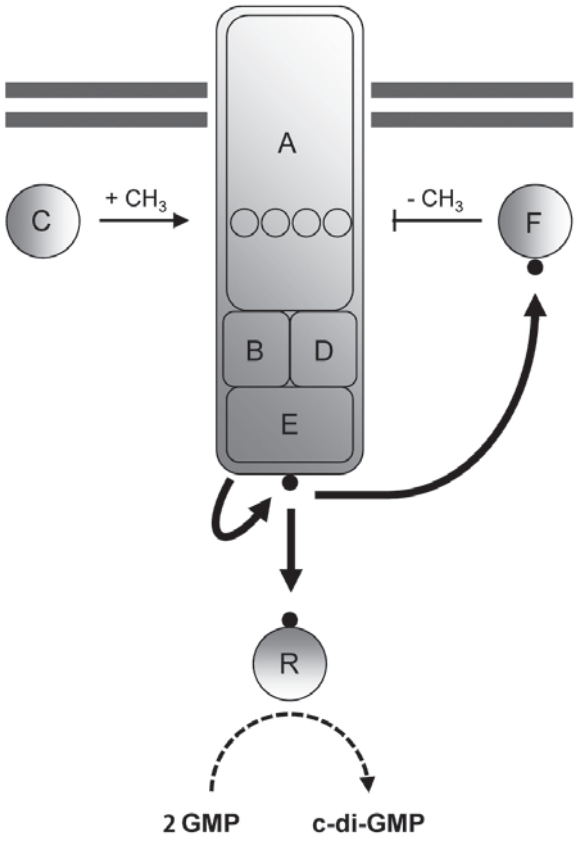

Fig. 3. The Wsp chemosensory complex is responsible for the synthesis of cyclic-di-GMP and the activation of the Wrinkly Spreader (WS) phenotype. A schematic showing the functioning of the Wsp complex is shown. The methyl-accepting chemotaxis protein (WspA), scaffold proteins (WspB and WspD) and histidine kinase (WspE) form a membrane-associated receptor-signalling complex. In the absence of an appropriate environmental signal, the complex is silent. Upon activation by phosphorylation (indicated by the black circles), the di-guanylate cyclase (DGC) response regulator (WspR) synthesizes c-di-GMP from GTP. The system is controlled by the opposing activities of a methyltransferase (WspC) and methylesterase (WspF), which add and remove, respectively, methyl (CH_3) groups on the signalling domain of WspA (circles). In wild-type P. fluorescens SBW25, the activities of the two are balanced, preventing the activation of WspR and allowing the Wsp complex to oscillate between active and inactive states. In many WS, mutations inhibiting WspF function or activating WspE kinase activity result in the activation of WspR and the production of c-di-GMP. Increased levels of c-di-GMP then lead to the expression of the WS phenotype. This figure is adapted from [9]

The WS model is not appropriate for the regulation of cellulose production by *P. fluorescens* SBW25 in natural environments

Although the WS phenotype, including both competitive fitness and wrinkleality, is variable amongst independently-isolated Wrinkly Spreaders [70], it appears that WS activating mutations are binary in nature and result in the unregulated overproduction of cellulose and biofilm formation. In the soil and plant-associated environments colonised by *P. fluorescens* SBW25, greater responsiveness to environmental stimuli and flexibility in behaviour is required, and both cellulose production and biofilm formation are expected to be controlled by a complex network of regulatory systems. Some of these have been identified with wss operon transcription regulated by the DGCs AwsR and WspR, as well as by the master regulators of alginate (AlgR) and flagella (FleQ), during the colonisation of the Sugar beet rhizosphere where the ability to produce cellulose provides a fitness advantage for P. *fluorescens* SBW25 [71, 72]. However, the environmental stimuli these systems respond to have yet to be identified, and it is notable that QS regulation, involved in the regulation of EPS production and biofilm formation in many pseudomonads, has not been reported in *P. fluorescens* SBW25, nor have QS genes been identified in the analysis of Wrinkly Spreaders or *P. fluorescens* SBW25 rhizosphere colonisation.

Challenging the view that *P. fluorescens* SBW25 is inquorate

Recently, a link between QS regulation and c-di-GMP has been identified in pseudomonads [12-14]. It is generally assumed that the primary quorum signalling molecules or autoinducers that bind their cognate receptors to directly or indirectly activate gene expression used by Gram-negative bacteria are N-acyl-homoserine lactones (AHLs) [3-6]. Pseudomonads have been reported to produce a variety of different AHLs controlling the production of virulence factors, EPS, and motility that are important for bacterial adaptation and colonisation in a range of environments [73-76]. In *P. aeruginosa* PA14, the QS regulator LasR induces the expression of TpbA which in turn represses the DGC activity of TpbB, resulting in lowered c-di-GMP levels [77] (a slightly different TpbB analogue known as YfiR has also been investigated in *P. aeruginosa* PA01 [78]). This link drove us to examine the *P. fluorescens* SBW25

genome for QS components which might also be linked to c-di-GMP homeostasis and therefore to cellulose synthesis and biofilm–formation (this analysis will be published elsewhere).

We have identified a potential AHL synthase homologue (PFLU0008), as well as homologues of LasR (PFLU1386) and TpbA (PFLU0050) in *P. fluorescens* SBW25, and hypothesize that they may form a QS regulatory pathway acting through WspR or other DGCs to repress cellulose production (Fig. 4). First, the presence of a HdtS-like AHL synthase homologue [73] suggests that *P. fluorescens* SBW25 might produce AHLs under the right conditions, and in preliminary experiments, we have detected at least two different AHL molecules in culture extracts using a standard AHL bio-reporter assay [79, 80]. Secondly, although *P. fluorescens* SBW25 was not originally annotated as having a LasR homologue [19], PFLU1386 is a putative regulator belonging to the same LuxR family of transcriptional regulators. Despite a poor level of homology (32% ID, amino-acid level sequence identity), it has been possible to model the 3D structure of PFLU1386 using a LasR–AHL co-crystal template and dock several AHLs including DHL (N-dodeconyl-L-homoserine lactone, C12-HSL) and 3-O-DHL (N-(3-oxo-dodecanoyl)-L-homoserine lactone, 3-O-C12-HSL) (Fig. 5). This suggests that PFLU1386 might bind AHLs and induce the transcription of as-yet unidentified QS-dependent genes. Finally, the 3D structure of PFLU0050 can also be modelled using a TpbA crystal template [81], suggesting that these two proteins share a high degree of structural similarity, and that PFLU0050 may also show AHL-dependent tyrosine phosphatase activity and regulate a cognate TpbB-like DGC. Using the *P. aeruginosa* PA14 TpbB amino-acid sequence, we identified a possible TpbB homologue, PFLU5210 (62% ID), which had previously been identified as AwsR which regulates wss operon transcription [65, 72]. PFLU0050 may also regulate the activity of AwsR as well as more distantly-related DGCs (e.g. WspR which shares 35% ID with TpbB) to control c-di-GMP levels.

Our analysis of the *P. fluorescens* SBW25 genome has identified several other proteins that might play a role in QS regulation including some associated with alpha-hydroxy ketones (AHKs) which we have detected *P. fluorescens* SBW25 culture extracts using the Janthinobacterium sp. bio-reporter assay [82]. We have identified two potential AHK synthases (PFLU5220 and PFLU5614) and an AHK sensory protein (PFLU1736) in the *P. fluorescens* SBW25 genome, but have not identified a potential AHK-dependent regulator. This suggests that the potential *P. fluorescens* SBW25 AHK pathway is more similar to the Vibrio pathway which also lacks a regulator, than for example, the Legionella pathway which includes one [83].

Linking individual behaviour with community action

Although biofilm-formation can result from mutation and the clonal expansion of adaptive mutant lineages, or through QS regulation, there are benefits in linking individual (intracellular) regulatory networks with community-based decision and

Fig. 4. P. fluorescens SBW25 may utilise QS to regulate cellulose production. A bioinformatics analyses of P. fluorescens SBW25 proteins has identified potential homologues which may act together to produce a QS regulatory pathway that might reduce the activity of the Wss cellulose synthase by modulating c-di-GMP levels. The homologue of HdtS (PFLU0008) is predicted to synthesize AHLs which then bind to the LasR homologue (PFLU1386) in a QS manner. Bound PFLU1386 is predicted to induce transcription of the PFLU0050 gene resulting in the expression of a DGC regulator homologous to TpbA. PFLU0050 may then regulate the activity of the TpbB homologue (AwsR, PFLU5210). PFLU0050 might also repress the activity of other DGCs, possibly even WspR, to reduce c-di-GMP levels and repress cellulose production

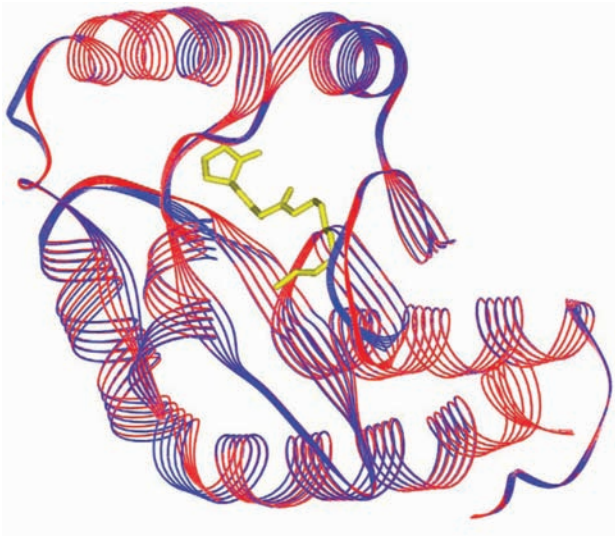

Fig. 5. PFLU1386 can be modelled to show AHL binding. The 3D structure of the P. fluorescens SBW25 PFLU1386 LasR homologue can be modelled using as a template the structure determined for the P. aeruginosa LasR–3-O-DHL (N-(3-oxododecanoyl)-L-homoserine lactone) co-crystal (Molecular modeling database (MMDB) ID: 76777). Shown here is the superposition of the PFLU1386 homology model (blue) with the LasR (red) and 3-O-DHL (yellow) co-crystal showing the high degree of structural similarity between the two proteins and relative position of the ligand-binding site. Both 3-O-DHL and DHL (N-dodeconyl-L-homoserine lactone) can be docked into the corresponding active site in the PFLU1386 model, suggesting that either might be ligands for this protein

enforcement (Table). Bacteria have multiple and interacting regulatory networks which allow the appropriate response to environmental factors. For example, in pseudomonads, Fe-repressible and anaerobically (low O_2)-induced small RNA (sRNA) repressors interact with QS regulation, whilst other sRNAs sequester RNA-binding proteins that regulate global translational repressors, including central elements controlling motility, biofilm-formation, QS regulation, the expression of virulence factors, and the utilisation of carbon sources, some of which are also regulated by c-di-GMP levels [4, 13, 84]. Although bacteria within a fairly uniform environment might be expected to show the same behaviour, micro-heterogeneity in local conditions, variation in cellular status and stochastic responses would lead to phenotypic heterogeneity within populations [85] and mean that not all individuals would be in an appropriate condition to invest in community effort or to benefit from the results of such endeavours. Indeed, if all individuals do not benefit, cooperation can breakdown leading to a public goods dilemma: in both *P. aeruginosa* PA01 and Wrinkly Spreader populations, the presence of cheaters reduces overall fitness, growth and biofilm formation [86, 87] (though not in all cases, e.g. [7]).

However, links between intracellular regulators such as c-di-GMP with community-based (intercellular) QS regulation provide a mechanism allowing individuals to opt-in and opt-out of cooperative activity. In particular, individual sensing and decision allows opting in to the early stages of biofilm formation when benefits might be expected in the future (i.e. providing a fitness benefit to that particular lineage), and opting out when biofilms mature or are damaged, when further benefits to cooperative activity are no longer likely. One example of the need for an opt-out might be found in Ancestor's inhibition, where the constant production of EPS and growth at the surface of a biofilm pushes earlier generations into the middle of the structure where conditions may no longer be adequate [88,89]. In *Escherichia coli* K12, an oxygen-sensing phosphodiesterase and associated diguanylate cyclase have been described [81], suggesting a mechanism allowing O_2-stressed individuals in biofilms to stop EPS production and de-repress mobility by altering c-di-GMP levels; in *P. aeruginosa* PA01, the anaerobic regulator Anr may also interact with QS regulation in response to altering O_2 levels [91]. Finally, QS regulation may impose a direct cost under some conditions, as many environmental and clinical isolates of *P. aeruginosa* have been found to have defective QS regulatory systems [92].

Concluding statement

Our desire to understand the underlying molecular biology of the novel biofilm–forming Wrinkly Spreader, an adaptive mutant isolated from radiating populations of *P. fluorescens* SBW25 in static microcosms, uncovered a pathway linking mutations affecting c-di-GMP levels to the production of cellulose which forms the main matrix component of the biofilm. Although this analysis was aided by availability of the genome sequence, our current review of the coding potential of the genome suggests that *P. fluorescens* SBW25 may also have QS regulation capability. The interaction between intracellular regulatory networks involving key regulators such as

T a b l e. Benefits of linking individual regulatory networks with community-based decision and enforcement for the production of biofilms

Individual sensing and decision	To integrate various environmental chemical and physical signals to confirm that individual bacteria are in the appropriate circumstances and position for attachment and biofilm formation. C-di-GMP homeostasis linked to other networks to integrate oxygen sensing, metabolic status, energy reserves, nutrient availability, etc. Although individual bacteria can express biofilm matrix components, there is no defence against competitors (cheaters) using these and avoiding the cost of production.
Community decision and control	To implement the cooperative investment of all appropriately-positioned bacteria in the formation of a biofilm for mutual benefit. As the initial expression of quorum signals within a population of bacterial cells is stochastic, and if the population is also heterogeneous in terms of cell position and status, there is the chance that QS will force some members to cooperate when they might otherwise decide not to do so.
Individual and Community interaction	Regulatory interactions allow for the fine-tuning of individual and community decisions. Interactions allow individual bacteria to opt-in to community activity when they are ready and can benefit from this investment. Poorly-positioned or stressed bacteria can also opt-out from the inappropriate demands of the comfortable majority during the initiation of biofilm formation and in developed structures when individuals may no longer occupy optimal positions. Depending on the relative strengths of the individual and community regulatory systems, the interaction might also allow the adjustment of individual investment resulting from altered conditions, new construction costs resulting from damage, and prevent the development of cheaters.

c-di-GMP with intracellular QS regulation provides additional benefits to both individual bacteria and communities during biofilm–formation. The acquisition of genome sequences is commonplace today and is often the starting point in investigating complex bacterial regulatory networks and behaviours. However, retrospective inspection of genomes can reveal additional elements which were not considered earlier, adding to our understanding of how bacteria interact with their environment and with each other.

The new challenge in understanding biofilm–formation by *P. fluorescens* SBW25 and related pseudomonads is to determine the relative importance of environmental signals, QS regulation and mutation in the colonisation of new environments and adaptation over evolutionarily-relevant time scales. A better understanding of this will be of particular relevance to medical microbiology, where bacteria are able to colonise tissues in chronic infections by overcoming the immune system and avoiding antibiotics through biofilm–formation and mutation.

Acknowledgments. This work was supported by Abertay University; A.J. Spiers is also member of the Scottish Alliance for Geoscience Environment and Society (SAGES). O.V. Moshynets was also supported by NATO SPS 984834. We cordially thank the Directors of the Institute of Molecular Biology and Genetics of NAS of Ukraine and the Zabolotny Institute of Microbiology and Virology of NAS of Ukraine for their assistance in the preparation of this review and their support of on-going collaborative research with Abertay University.

АНАЛІЗ c-di-GMP І МОЖЛИВОГО ПОЧУТТЯ КВОРУМУ В *Pseudomonas fluorescens* SBW25: ЗВ'ЯЗОК МІЖ ВНУТРІШНЬО- І МІЖКЛІТИННОЮ РЕГУЛЯЦІЄЮ СПРИЯЄ КООПЕРАТИВНІЙ ПОВЕДІНЦІ В УГРУПОВАННІ І ФОРМУВАННЮ БІОПЛІВКИ

О. В. Мошинець[1], Д. Фостер[2], С. О. Карахім[3], К. МакЛохлін[4], С. П. Рогальський[5], С. Ю. Римар[1], Г. П. Волинець[1], Е. Д. Спайрс[4]✉

[1]Інститут молекулярної біології і генетики НАН України, Київ;
e-mail: moshynets@gmail.com;
e-mail: galina.volinetc@gmail.com
[2]Оксфордський університет, Госпіталь ім. Джона Редкліфа, Велика Британія;
e-mail: dona.foster@ndm.ox.ac.uk;
[3]Інститут біохімії ім. О. В. Палладіна, НАН України, Київ;
e-mail: laserlab@biochem.kiev.ua;
[4]Школа науки, інжинірингу і технологій, Абертейський університет, Велика Британія;
e-mail: mclaughlinkimberley@gmail.com;
✉e-mail: a.spiers@abertay.ac.uk;
[5]Інститут біоорганічної хімії і нафтохімії НАН України, Київ;
e-mail: sergey.rogalsky@gmail.com

Успішність бактеріальної колонізації складних еконіш вимагає індивідуальної відповіді на зміни умов на мікрорівні так само як і кооперацію на рівні угруповання для продукції таких великомасштабних структур як біоплівки. Координація індивідуальних відповідей і відповідей угруповання може бути досягнута шляхом зв'язування внутрішньоклітинних сенсорних і регуляторних систем, опосередкованих біс-(3′,5′)-циклічним димерним гуанозинмонофосфатом (c-di-GMP) та іншими сполуками індивідуумів із міжклітинною регуляцією – почуттям кворуму (ПК), що контролює популяцію. Накопичується все більше доказів того, що формування біоплівки багатьма псевдомонадами регулюється як внутрішньоклітинними, так і міжклітинними регуляторними системами, хоча в разі модельної *Pseudomonas fluorescens* SBW25 Wrinkly Spreader, у котрій мутації, що підвищують рівні c-di-GMP, призводять до створення міцної целюлозної біоплівки на кордоні розділу фаз повітря–рідина, не було виявлено ніякого свідоцтва залучення кворумзалежної регуляції. Проте наш недавній огляд геному *P. fluorescens* SBW25 виявив потенційний ПК-залежний регуляторний шлях та інші ПК-залежні гени, пов'язані з гомеостазом c-di-GMP, а молекули ПК-сигналінгу було ідентифіковано в культурі. Ці дані свідчать про можливий зв'язок між c-di-GMP-регуляцією і ПК у *P. fluorescens* SBW25, що дозволяє проводити більш складний і гнучкий контроль продукції целюлози і утворення біоплівки за колонізації ґрунтів і еконіш, асоційованих з рослинами, – природними середовищами існування *P . fluorescens* SBW25.

Ключові слова: циклічний димерний гуанозинмонофосфат (c-di-GMP), ацилгомосеринлактон (AHL), бактеріальна целюлоза, біоплівки, *Pseudomonas*, почуття кворуму.

АНАЛИЗ c-di-GMP И ВОЗМОЖНОГО ЧУВСТВА КВОРУМА У *Pseudomonas fluorescens* SBW25: СВЯЗЬ МЕЖДУ ВНУТРИ- И МЕЖКЛЕТОЧНОЙ РЕГУЛЯЦИЕЙ СПОСОБСТВУЕТ КООПЕРАТИВНОМУ ПОВЕДЕНИЮ В СООБЩЕСТВЕ И ФОРМИРОВАНИЮ БИОПЛЁНКИ

Е. В. Мошинец[1], Д. Фостер[2], С. А. Карахим[3], К. МакЛохлин[4], С. П. Рогальский[5], С. Е. Рымарь[1], Г. П. Волынец[1], Э. Д. Спайрс[4]✉

[1]Институт молекулярной биологии и генетики НАН Украины, Киев;
e-mail: moshynets@gmail.com;
e-mail: galina.volinetc@gmail.com
[2]Оксфордский университет, Госпиталь им. Джона Редклифа, Великобритания;
e-mail: dona.foster@ndm.ox.ac.uk;
[3]Институт биохимии им. А. В. Палладина НАН Украины, Киев;
e-mail: laserlab@biochem.kiev.ua;
[4]Школа науки, инжиниринга и технологий, Абертейский университет, Великобритания;
e-mail: mclaughlinkimberley@gmail.com;
✉e-mail: a.spiers@abertay.ac.uk;
[5]Институт биоорганической химии и нефтехимии НАН Украины, Киев;
e-mail: sergey.rogalsky@gmail.com

Успешность бактериальной колонизации сложных эконишь требует индивидуального ответа на изменения условий на микроуровне рав-

но как и кооперацию на уровне сообщества для продукции таких крупномасштабных структур как биоплёнки. Координация индивидуальных ответов и ответов сообщества может быть достигнута путем связывания внутриклеточных сенсорных и регуляторных систем, опосредованных бис-(3′,5′)-циклическим димерным гуанозинмонофосфатом (c-di-GMP) и другими соединениями индивидуумов с межклеточной регуляцией – чувством кворума (ЧК), контролирующем популяцию. Накапливается всё больше доказательств того, что формирование биопленки многими псевдомонадами регулируется как внутриклеточными, так и межклеточными регуляторными системами, хотя в случае модельной *Pseudomonas fluorescens* SBW25 Wrinkly Spreader, у которой мутации, повышающие уровни c-di-GMP, приводят к созданию прочной целлюлозной биоплёнки на границе раздела фаз воздух–жидкость, не было обнаружено никакого свидетельства вовлечения кворумзависимой регуляции. Однако наш недавний обзор генома *P. fluorescens* SBW25 выявил потенциальный ЧК-зависимый регуляторный путь и другие ЧК-зависимые гены, связанные с гомеостазом c-di-GMP, а молекулы ЧК-сигналинга были идентифицированы в культуре. Эти данные свидетельствуют о возможной связи между c-di-GMP-регуляцией и ЧК у *P. fluorescens* SBW25, что позволяет проводить более сложный и гибкий контроль продукции целлюлозы и образования биопленки при колонизации почв и экониш, ассоциированных с растениями, – естественными средами обитания *P. fluorescens* SBW25.

Ключевые слова: циклический димерный гуанозинмонофосфат (c-di-GMP) ацилгомосеринлактон (AHL), бактериальная целлюлоза, биоплёнки, *Pseudomonas*, чувство кворума.

References

1. Nadell CD, Xavier JB, Foster KR. The sociobiology of biofilms. *FEMS Microbiol Rev.* 2009; 33(1): 206-224.
2. Nadell CD, Drescher K, Foster KR. Spatial structure, cooperation and competition in biofilms. *Nat Rev Microbiol*. 2016; 14(9): 589-600.
3. Galloway WR, Hodgkinson JT, Bowden SD, Welch M, Spring DR. Quorum sensing in Gram-negative bacteria: small-molecule modulation of AHL and AI-2 quorum sensing pathways. *Chem Rev.* 2011; 111(1): 28-67.
4. Coggan KA, Wolfgang MC. Global regulatory pathways and cross-talk control *Pseudomonas aeruginosa* environmental lifestyle and virulence phenotype. *Curr Issues Mol Biol.* 2012; 14(2): 47-70.
5. Stacy AR, Diggle SP, Whiteley M. Rules of engagement: defining bacterial communication. *Curr Opin Microbiol.* 2012; 15(2): 155-161.
6. Garg N, Manchanda G, Kumar A. Bacterial quorum sensing: circuits and applications. *Antonie Van Leeuwenhoek*. 2014; 105(2): 289-305.
7. Irie Y, Roberts AEL, Kragh KN, Gordon VD, Hutchison J, Allen RJ, Melaugh G, Bjarnsholt T, West SA, Diggle SP. The *Pseudomonas aeruginosa* PSL Polysaccharide Is a Social but Noncheatable Trait in Biofilms. *MBio.* 2017; 8(3). pii: e00374-17.
8. Moshynets OV, Spiers AJ. Viewing biofilms within the larger context of bacterial aggregations, in: Microbial biofilms – Importance and applications, Dhanasekaran D, Thajuddin N (Eds), InTech Publishers, Rijeka, Croatia, 2016.
9. Rainey PB, Travisano M. Adaptive radiation in a heterogeneous environment. *Nature*. 1998; 394(6688): 69-72.
10. Spiers AJ. A mechanistic explanation linking adaptive mutation, niche change, and fitness advantage for the wrinkly spreader. *Int J Evol Biol*. 2014; 2014: 675432.
11. Koza A, Kusmierska A, McLaughlin K, Moshynets O, Spiers AJ. Adaptive radiation of *Pseudomonas fluorescens* SBW25 in experimental microcosms provides an understanding of the evolutionary ecology and molecular biology of A-L interface biofilm formation. *FEMS Microbiol Lett*. 2017; 364(12).
12. Kirisits MJ, Parsek MR. Does *Pseudomonas aeruginosa* use intercellular signalling to build biofilm communities? *Cell Microbiol*. 2006; 8(12): 1841-1849.
13. Williams P, Cámara M. Quorum sensing and environmental adaptation in *Pseudomonas aeruginosa*: a tale of regulatory networks and multifunctional signal molecules. *Curr Opin Microbiol*. 2009; 12(2): 182-191.

14. Haussler S, Fuqua C. Biofilms 2012: new discoveries and significant wrinkles in a dynamic field. *J Bacteriol*. 2013; 195(13):2947-2958.
15. Waters CM, Lu W, Rabinowitz JD, Bassler BL. Quorum sensing controls biofilm formation in Vibrio cholerae through modulation of cyclic di-GMP levels and repression of vpsT. *J Bacteriol*. 2008; 190(7): 2527-2536.
16. Schmid N, Suppiger A, Steiner E, Pessi G, Kaever V, Fazli M, Tolker-Nielsen T, Jenal U, Eberl L. High intracellular c-di-GMP levels antagonize quorum sensing and virulence gene expression in *Burkholderia cenocepacia* H111. *Microbiology*. 2017; 163(5): 754-764.
17. Rainey PB, Bailey MJ. Physical and genetic map of the *Pseudomonas fluorescens* SBW25 chromosome. *Mol Microbiol*. 1996; 19(3): 521-533.
18. Spiers AJ, Field D, Bailey M, Rainey PB. Notes on designing a partial genomic database: The PfSBW25 Encyclopaedia, a sequence database for *Pseudomonas fluorescens* SBW25. *Microbiology*. 2001; 147(Pt 2): 247-249.
19. Silby MW, Cerdeño-Tárraga AM, Vernikos GS, Giddens SR, Jackson RW, Preston GM, Zhang XX, Moon CD, Gehrig SM, Godfrey SA, Knight CG, Malone JG, Robinson Z, Spiers AJ, Harris S, Challis GL, Yaxley AM, Harris D, Seeger K, Murphy L, Rutter S, Squares R, Quail MA, Saunders E, Mavromatis K, Brettin TS, Bentley SD, Hothersall J, Stephens E, Thomas CM, Parkhill J, Levy SB, Rainey PB, Thomson NR. Genomic and genetic analyses of diversity and plant interactions of *Pseudomonas fluorescens*. *Genome Biol*. 2009; 10(5): R51.
20. Spiers AJ. Bacterial evolution in simple microcosms, in: Microcosms: Ecology, Biological Implications and Environmental Impact, Microbiology Research Advances Series, C.H. Harris (Ed), Nova Publishers, Hauppauge, NY, USA, 2013.
21. Campilongo R, Fung RKY, Little RH, Grenga L, Trampari E, Pepe S, Chandra G, Stevenson CEM, Roncarati D, Malone JG. One ligand, two regulators and three binding sites: How KDPG controls primary carbon metabolism in Pseudomonas. *PLoS Genet*. 2017; 13(6): e1006839.
22. Grenga L, Chandra G, Saalbach G, Galmozzi CV, Kramer G, Malone JG. Analyzing the Complex Regulatory Landscape of Hfq - an Integrative, Multi-Omics Approach. *Front Microbiol*. 2017; 8: 1784.
23. Buckling A, Craig Maclean R, Brockhurst MA, Colegrave N. The Beagle in a bottle. *Nature*. 2009; 457(7231): 824-829.
24. Lenski RE. Evolution in action: a 50,000-generation salute to Charles Darwin. *Microbe*. 2011; 6(1): 30-33.
25. Kawecki TJ, Lenski RE, Ebert D, Hollis B, Olivieri I, Whitlock MC. Experimental evolution. *Trends Ecol Evol*. 2012; 27(10): 547-560.
26. Mann EE, Wozniak DJ. *Pseudomonas* biofilm matrix composition and niche biology. *FEMS Microbiol Rev*. 2012; 36(4): 893-916.
27. Häussler S. Multicellular signalling and growth of *Pseudomonas aeruginosa*. *Int J Med Microbiol*. 2010; 300(8): 544-548.
28. Wolcott R, Costerton JW, Raoult D, Cutler SJ. The polymicrobial nature of biofilm infection. *Clin Microbiol Infect*. 2013; 19(2): 107-112.
29. Spiers AJ, Arnold DL, Moon CD, Timms-Wilson TM. A survey of A-L biofilm formation and cellulose expression amongst soil and plant-associated *Pseudomonas* isolates, in: Bailey MJ, Lilley AK, Timms-Wilson TM, editors. Microbial ecology of aerial plant surfaces. CABI: 121-131.
30. Ude S, Arnold DL, Moon CD, Timms-Wilson T, Spiers AJ. Biofilm formation and cellulose expression among diverse environmental Pseudomonas isolates. *Environ Microbiol*. 2006; 8(11): 1997-2011.
31. Robertson M, Hapca SM, Moshynets O, Spiers AJ. Air-liquid interface biofilm formation by psychrotrophic pseudomonads recovered from spoilt meat. *Antonie Van Leeuwenhoek*. 2013; 103(1): 251-259.
32. Spiers AJ, Deeni YY, Folorunso AO, Koza A, Moshynets O, Zawadzki K. Cellulose expression in *Pseudomonas fluorescens* SBW25 and other environmental pseudomonads. In: Van De Ven TGM, Godbout L, editors. Cellulose - Medical, Pharmaceutical and Electronic Applications, 2013. InTech Publishers: 1-26.
33. King EO, Ward MK, Raney DE. Two simple media for the demonstration of pyocyanin and fluorescin. *J Lab Clin Med*. 1954; 44(2): 301-307.
34. Spiers AJ, Kahn SG, Bohannon J, Travisano M, Rainey PB. Adaptive divergence in experimental populations of *Pseudomonas fluorescens*.

I. Genetic and phenotypic bases of wrinkly spreader fitness. *Genetics.* 2002; 161(1): 33-46.
35. Green JH, Koza A, Moshynets O, Pajor R, Ritchie MR, Spiers AJ. Evolution in a test tube: rise of the Wrinkly Spreaders. *J Biol Educ.* 2011;45(1): 54-59.
36. Spiers AJ. Wrinkly-Spreader fitness in the two-dimensional agar plate microcosm: maladaptation, compensation and ecological success. *PLoS One.* 2007; 2(8): e740.
37. Koza A, Moshynets O, Otten W, Spiers AJ. Environmental modification and niche construction: developing O_2 gradients drive the evolution of the Wrinkly Spreader. *ISME J.* 2011; 5(4): 665-673.
38. Kuśmierska A, Spiers AJ. New Insights into the Effects of Several Environmental Parameters on the Relative Fitness of a Numerically Dominant Class of Evolved Niche Specialist. *Int J Evol Biol.* 2016; 2016: 4846565.
39. Day RL, Laland KN, Odling-Smee FJ. Rethinking adaptation: the niche-construction perspective. *Perspect Biol Med.* 2003; 46(1): 80-95.
40. Huang WE, Ude S, Spiers AJ. *Pseudomonas fluorescens* SBW25 biofilm and planktonic cells have differentiable Raman spectral profiles. *Microb Ecol.* 2007; 53(3): 471-474.
41. Van Valen L. A new evolutionary law. *Evolution Theory.* 1973; 1: 1-30.
42. Morris JJ, Lenski RE, Zinser ER. The Black Queen Hypothesis: evolution of dependencies through adaptive gene loss. *MBio.* 2012; 3(2). pii: e00036-12.
43. Parsek MR, Greenberg EP. Sociomicrobiology: the connections between quorum sensing and biofilms. *Trends Microbiol.* 2005; 13(1): 27-33.
44. West SA, Griffin AS, Gardner A, Diggle SP. Social evolution theory for microorganisms. *Nat Rev Microbiol.* 2006; 4(8): 597-607.
45. Gehrig SM. Adaptation of Pseudomonas fluorescens SBW25 to the air-liquid interface: a study in evolutionary genetics. DPhil thesis, University of Oxford, Oxford, UK, 2005.
46. Römling U. Molecular biology of cellulose production in bacteria. *Res Microbiol.* 2002; 153(4): 205-212.
47. Saxena IM, Brown RM Jr. Cellulose biosynthesis: current views and evolving concepts. *Ann Bot.* 2005; 96(1): 9-21.
48. Römling U, Galperin MY. Bacterial cellulose biosynthesis: diversity of operons, subunits, products, and functions. *Trends Microbiol.* 2015; 23(9): 545-557.
49. Spiers AJ, Bohannon J, Gehrig SM, Rainey PB. Biofilm formation at the air-liquid interface by the *Pseudomonas fluorescens* SBW25 wrinkly spreader requires an acetylated form of cellulose. *Mol Microbiol.* 2003; 50(1): 15-27.
50. Franklin MJ, Douthit SA, McClure MA. Evidence that the algI/algJ gene cassette, required for O acetylation of *Pseudomonas aeruginosa* alginate, evolved by lateral gene transfer. *J Bacteriol.* 2004; 186(14): 4759-4773.
51. Arrebola E, Carrión VJ, Gutiérrez-Barranquero JA, Pérez-García A, Rodríguez-Palenzuela P, Cazorla FM, de Vicente A. Cellulose production in *Pseudomonas syringae* pv. syringae: a compromise between epiphytic and pathogenic lifestyles. *FEMS Microbiol Ecol.* 2015; 91(7). pii: fiv071.
52. McLaughlin K, Folorunso AO, Deeni YY, Foster D, Gorbatiuk O, Hapca SM, Immoor C, Koza A, Mohammed IU, Moshynets O, Rogalsky S, Zawadzki K, Spiers AJ. Biofilm formation and cellulose expression by *Bordetella avium* 197N, the causative agent of bordetellosis in birds and an opportunistic respiratory pathogen in humans. *Res Microbiol.* 2017; 168(5): 419-430.
53. Moshynets OV, Koza A, Dello Sterpaio P, Kordium VA, Spiers AJ. Up-dating the Cholodny method using PET films to sample microbial communities in soil. *Biopolym Cell.* 2011; 27(3): 199-205.
54. Spiers AJ, Rainey PB. The *Pseudomonas fluorescens* SBW25 wrinkly spreader biofilm requires attachment factor, cellulose fibre and LPS interactions to maintain strength and integrity. *Microbiology.* 2005; 151(Pt 9): 2829-2839.
55. Goymer P, Kahn SG, Malone JG, Gehrig SM, Spiers AJ, Rainey PB. Adaptive divergence in experimental populations of *Pseudomonas fluorescens*. II. Role of the GGDEF regulator WspR in evolution and development of the wrinkly spreader phenotype. *Genetics.* 2006; 173(2): 515-526.
56. Bantinaki E, Kassen R, Knight CG, Robinson Z, Spiers AJ, Rainey PB. Adaptive divergence in experimental populations of *Pseudomonas fluorescens*. III. Mutational origins of wrinkly spreader diversity. *Genetics.* 2007; 176(1): 441-453.

57. Malone JG, Williams R, Christen M, Jenal U, Spiers AJ, Rainey PB. The structure-function relationship of WspR, a *Pseudomonas fluorescens* response regulator with a GGDEF output domain. *Microbiology.* 2007; 153(Pt 4): 980-994.
58. Ross P, Weinhouse H, Aloni Y, Michaeli D, Weinberger-Ohana P, Mayer R, Braun S, de Vroom E, van der Marel GA, van Boom JH, Benziman M. Regulation of cellulose synthesis in *Acetobacter xylinum* by cyclic diguanylic acid. *Nature*. 1987; 325(6101): 279-281.
59. Römling U, Gomelsky M, Galperin MY. C-di-GMP: the dawning of a novel bacterial signalling system. *Mol Microbiol*. 2005; 57(3): 629-639.
60. Jenal U, Malone J. Mechanisms of cyclic-di-GMP signaling in bacteria. *Annu Rev Genet*. 2006; 40: 385-407.
61. Hengge R. Principles of c-di-GMP signalling in bacteria. *Nat Rev Microbiol*. 2009; 7(4): 263-273.
62. Lin Chua S, Liu Y, Li Y, Jun Ting H, Kohli GS, Cai Z, Suwanchaikasem P, Kau Kit Goh K, Pin Ng S, Tolker-Nielsen T, Yang L, Givskov M. Reduced intracellular c-di-GMP content increases expression of quorum sensing-regulated genes in *Pseudomonas aeruginosa*. *Front Cell Infect Microbiol*. 2017; 7: 451.
63. Moscoso JA, Jaeger T, Valentini M, Hui K, Jenal U, Filloux A. The diguanylate cyclase SadC is a central player in Gac/Rsm-mediated biofilm formation in *Pseudomonas aeruginosa*. *J Bacteriol*. 2014; 196(23): 4081-4088.
64. Cheng X, de Bruijn I, van der Voort M, Loper JE, Raaijmakers JM. The Gac regulon of *Pseudomonas fluorescens* SBW25. *Environ Microbiol Rep.* 2013; 5(4): 608-619.
65. McDonald MJ, Gehrig SM, Meintjes PL, Zhang XX, Rainey PB. Adaptive divergence in experimental populations of *Pseudomonas fluorescens.* IV. Genetic constraints guide evolutionary trajectories in a parallel adaptive radiation. *Genetics*. 2009; 183(3): 1041-1053.
66. McDonald MJ, Cooper TF, Beaumont HJ, Rainey PB. The distribution of fitness effects of new beneficial mutations in *Pseudomonas fluorescens*. *Biol Lett*. 2011; 7(1): 98-100.
67. Koza A, Hallett PD, Moon CD, Spiers AJ. Characterization of a novel air-liquid interface biofilm of *Pseudomonas fluorescens* SBW25. *Microbiology*. 2009; 155(Pt 5): 1397-1406.
68. Lind PA, Farr AD, Rainey PB. Experimental evolution reveals hidden diversity in evolutionary pathways. *eLife*. 2015; 4: e07074.
69. Hottes AK, Freddolino PL, Khare A, Donnell ZN, Liu JC, Tavazoie S. Bacterial adaptation through loss of function. *PLoS Genet*. 2013; 9(7): e1003617.
70. Udall YC, Deeni Y, Hapca SM, Raikes D, Spiers AJ. The evolution of biofilm-forming Wrinkly Spreaders in static microcosms and drip-fed columns selects for subtle differences in wrinkleality and fitness. *FEMS Microbiol Ecol*. 2015; 91(6). pii: fiv057.
71. Gal M, Preston GM, Massey RC, Spiers AJ, Rainey PB. Genes encoding a cellulosic polymer contribute toward the ecological success of *Pseudomonas fluorescens* SBW25 on plant surfaces. *Mol Ecol*. 2003; 12(11): 3109-3121.
72. Giddens SR, Jackson RW, Moon CD, Jacobs MA, Zhang XX, Gehrig SM, Rainey PB. Mutational activation of niche-specific genes provides insight into regulatory networks and bacterial function in a complex environment. *Proc Natl Acad Sci USA*. 2007; 104(46): 18247-18252.
73. Laue BE, Jiang Y, Chhabra SR, Jacob S, Stewart GS, Hardman A, Downie JA, O'Gara F, Williams P. The biocontrol strain *Pseudomonas fluorescens* F113 produces the Rhizobium small bacteriocin, N-(3-hydroxy-7-cis-tetradecenoyl) homoserine lactone, via HdtS, a putative novel N-acylhomoserine lactone synthase. *Microbiology*. 2000; 146(Pt 10): 2469-2480.
74. Elasri M, Delorme S, Lemanceau P, Stewart G, Laue B, Glickmann E, Oger PM, Dessaux Y. Acyl-homoserine lactone production is more common among plant-associated *Pseudomonas* spp. than among soilborne *Pseudomonas* spp. *Appl Environ Microbiol.* 2001; 67(3): 1198-1209.
75. Bassler BL, Losick R. Bacterially speaking. *Cell*. 2006; 125(2): 237-246.
76. Wagner VE, Iglewski BH. P. aeruginosa Biofilms in CF Infection. *Clin Rev Allergy Immunol*. 2008; 35(3): 124-134.
77. Ueda A, Wood TK. Connecting quorum sensing, c-di-GMP, pel polysaccharide, and biofilm formation in *Pseudomonas aeruginosa* through tyrosine phosphatase TpbA (PA3885). *PLoS Pathog.* 2009; 5(6): e1000483.
78. Malone JG, Jaeger T, Spangler C, Ritz D, Spang A, Arrieumerlou C, Kaever V, Landmann R,

Jenal U. YfiBNR mediates cyclic di-GMP dependent small colony variant formation and persistence in *Pseudomonas aeruginosa*. *PLoS Pathog.* 2010; 6(3): e1000804.
79. Cha C, Gao P, Chen YC, Shaw PD, Farrand SK. Production of acyl-homoserine lactone quorum-sensing signals by gram-negative plant-associated bacteria. *Mol Plant Microbe Interact.* 1998; 11(11): 1119-1129.
80. Farrand SK, Qin Y, Oger P. Quorum-sensing system of Agrobacterium plasmids: analysis and utility. *Methods Enzymol.* 2002; 358: 452-484.
81. Koveal D, Clarkson MW, Wood TK, Page R, Peti W. Ligand binding reduces conformational flexibility in the active site of tyrosine phosphatase related to biofilm formation A (TpbA) from *Pseudomonas aeruginosa*. *J Mol Biol.* 2013; 425(12): 2219-2231.
82. Hornung C, Poehlein A, Haack FS, Schmidt M, Dierking K, Pohlen A, Schulenburg H, Blokesch M, Plener L, Jung K, Bonge A, Krohn-Molt I, Utpatel C, Timmermann G, Spieck E, Pommerening-Röser A, Bode E, Bode HB, Daniel R, Schmeisser C, Streit WR. The *Janthinobacterium* sp. HH01 genome encodes a homologue of the *V. cholerae* CqsA and *L. pneumophila* LqsA autoinducer synthases. *PLoS One*. 2013; 8(2): e55045.
83. Tiaden A, Spirig T, Hilbi H. Bacterial gene regulation by α-hydroxyketone signaling. *Trends Microbiol.* 2010; 18(7): 288-297.
84. Sonnleitner E, Haas D. Small RNAs as regulators of primary and secondary metabolism in Pseudomonas species. *Appl Microbiol Biotechnol*. 2011; 91(1): 63-79.
85. Ackermann M. A functional perspective on phenotypic heterogeneity in microorganisms. *Nat Rev Microbiol.* 2015; 13(8): 497-508.
86. Rainey PB, Rainey K. Evolution of cooperation and conflict in experimental bacterial populations. *Nature*. 2003; 425(6953): 72-74.
87. Popat R, Crusz SA, Messina M, Williams P, West SA, Diggle SP. Quorum-sensing and cheating in bacterial biofilms. *Proc Biol Sci*. 2012; 279(1748): 4765-4771.
88. Xavier JB, Foster KR. Cooperation and conflict in microbial biofilms. *Proc Natl Acad Sci USA.* 2007; 104(3): 876-881.
89. Baquero F, Lemonnier M. Generational coexistence and ancestor's inhibition in bacterial populations. *FEMS Microbiol Rev.* 2009; 33(5): 958-967.
90. Tuckerman JR, Gonzalez G, Sousa EH, Wan X, Saito JA, Alam M, Gilles-Gonzalez MA. An oxygen-sensing diguanylate cyclase and phosphodiesterase couple for c-di-GMP control. *Biochemistry.* 2009; 48(41): 9764-9774.
91. Hammond JH, Dolben EF, Smith TJ, Bhuju S, Hogan DA. Links between Anr and Quorum Sensing in *Pseudomonas aeruginosa* Biofilms. *J Bacteriol.* 2015; 197(17): 2810-2820.
92. Heurlier K, Dénervaud V, Haas D. Impact of quorum sensing on fitness of Pseudomonas aeruginosa. *Int J Med Microbiol.* 2006; 296(2-3): 93-102.

Received 05.01.2018

Анотація: *Успішність бактеріальної колонізації складних еконіш вимагає індивідуальної відповіді на зміни умов на мікрорівні так само як і кооперацію на рівні угруповання для продукції таких великомасштабних структур як біоплівки. Координація індивідуальних відповідей і відповідей угруповання може бути досягнута шляхом зв'язування внутрішньоклітинних сенсорних і регуляторних систем, опосередкованих біс-(3',5')-циклічним димерним гуанозинмонофосфатом (с-di-GMP) та іншими сполуками індивідуумів із міжклітинною регуляцією – почуттям кворуму (ПК), що контролює популяцію. Накопичується все більше доказів того, що формування біоплівки багатьма псевдомонадами регулюється як внутрішньоклітинними, так і міжклітинними регуляторними системами, хоча в разі модельної* P. fluorescens *SBW25 Wrinkly Spreader, у котрій мутації, що підвищують рівні с-di-GMP, призводять до створення міцної целюлозної біоплівки на кордоні розділу фаз повітря–рідина, не було виявлено ніякого свідоцтва залучення кворумзалежної регуляції. Проте наш огляд геному* P. fluorescens *SBW25 виявив потенційний ПК-залежний регуляторний шлях та інші ПК-залежні гени, пов'язані з гомеостазом с-di-GMP, а молекули ПК-сигналінгу було ідентифіковано в культурі. Ці дані свідчать про можливий зв'язок між с-di-GMP-регуляцією і ПК у* P. fluorescens *SBW25, що дозволяє проводити більш складний і гнучкий контроль продукції целюлози і утворення біоплівки за колонізації ґрунтів і еконіш, асоційованих з рослинами, – природними середовищами існування* P . fluorescens *SBW25.*

РОЗДІЛ 4. Роль біоплівок у розвитку інфекційних ускладнень

Утворення біоплівки є бактеріальною стратегією колонізації різноманітних екологічних ніш (20). Як вже зазначалося, біоплівки це тривимірні структури, де прикріпленні та нерухливі клітини бактерій захищені біоплівковим матриксом, який складається з екзополімерів, які синтезуються самими клітинами. Така конструкція суттєво підвищує стійкість бактерій до різноманітних зовнішніх стресів через утворення в біоплівці більш стабільних умов (69, 111). Утворення біоплівок є центральним етапом у розвитку багатьох інфекційних процесів.

Оскільки саме біоплівки є природньою формою існування бактерій, біоплівки мають бути об'єктом дослідження ефективності різних антибактеріальних препаратів (73). Більш того, сама біоплівка може бути терапевтичною мішенню у новій комбінації антибіотиків проти антибіотикорезистентних грам-негативних бактерій. Зокрема, є повідомлення про ефективність макролідних антибіотиків у пригніченні біоплівки *P. aeruginosa*, яка є біологічно стійкою до макролідів (112). Така комбінована терапія включатиме анти-біопілівковий антибіотик у комбінації із антибактеріальним, що може показати терапевтичну ефективність в умовах відсутності ефективних антибіотиків антибіотикорезистентних інфекціях.

Такі інфекційні біоплівки додатково ускладнюють взаємодією з імунною відповіддю господаря, що сприяє хронізації запалення та персистуванню збудника.

4.1. Патогенез опосередкований біоплівками як результат взаємодії патогенів з імунною системою хазяїна при пародонтиті

Захворювання пародонту визнано наслідком інфекції та запалення ясен і кісткової тканини, що асоційована із зубами (CDC, 10 липня 2013 р.; www.cdc.gov/oralhealth/conditions/periodontal-disease, на 13 листопад 2023 р.). Вважається, що пародонтит відбувається в тісній асоціації з агресивною колонізацією бактерій і патогенними утворення біоплівки такими родами бактерій як *Escherichia, Enterococcus, Klebsiella, Lactococcus, Pseudomonas, Staphylococcus* і *Streptococcus* (113-115), при чому, патологічність процесу посилюється більш патогенними вторинними колонізаторами *Aggregatibacter actinomycetemcomitans, Fusobacterium nucleatum, Porphyromonas gingivalis,*

Tannerella forsythia та *Treponema denticola* (116-119). Разом, ці мікробні асоціації утворюють над'ясневі біоплівки та зубний наліт (117, 120).

Відповідно до над'ясенних патологічних процесів, вважається, що розвитку пародонтиту починається із утворення патогенної біоплівки в під'ясенному просторі. Втім, це залишає багато питань. По-перше, поки не зрозуміло, чому бактеріальна мікрофлора в ясенних кишенях здорових людей і пацієнтів, хворих на пародонтит, є практично однаковою (121-123). По-друге, під'ясенні біоплівки також присутні у здорових людей, але вони знаходяться у динамічній рівновазі із імунною системою хазяїна. Вважається, що саме зміна цієї динамічноїрівноваги призводить до активації інфламмасоми, яка і призводить до прояву пародонтиту (124, 125).

При дослідженні над'ясенних біоплівках було встановлено, що ці біоплівки складається з представників дев'яти таксонів, які радіально утворюють структуру навколо навколо нитчастих коринебактерій (120). Кадиди також було знайдено в структурі біоплівок ротової порожнини та в патогенних біоплівках, що пов'язані із захворюваннями пародонту (126). Було досліджено і складку структуру матриксу над'ясенних біоплівок. Показано, що лойого складу входять різноманітні полімери, зокрема, секретовані і поверхнево-асоційовані амілоїдні фібрили, інші білки та полісахариди, а також бактеріальна екзоклітинна ДНК (eDNA) (126, 127). Для кращого розуміння просторових взаємодій цих різноманітних компонентів у складі біоплівки за умов патологічного процесу та для дослідження джерела еДНК та встановлення ролі еДНК господаря в утворенні патогенних біоплівок було запропоновано адаптацію модифікованого методу Холодного із використанням біологічно нейтрального поліетилентерефталатної плівки (128). Використання нової модифікації методу Холодного дозволило дослідити реальні цитологічні (мікро) ландшафти, які розвиваються при активному пародонтиті.

Основні результати, отримані в цьому підрозділі дисертації опубліковані в роботі автора (129).

frontiers | Frontiers in Cellular and Infection Microbiology

TYPE Original Research
PUBLISHED 08 May 2024
DOI 10.3389/fcimb.2024.1374817

Check for updates

OPEN ACCESS

EDITED BY
J Christopher Fenno,
University of Michigan, United States

REVIEWED BY
Alexander James Webb,
Imperial College London, United Kingdom
Michelle B. Visser,
University at Buffalo, United States

*CORRESPONDENCE
Olena Moshynets
moshynets@gmail.com

†These authors have contributed equally to this work

RECEIVED 22 January 2024
ACCEPTED 09 April 2024
PUBLISHED 08 May 2024

CITATION
Slobodianyk-Kolomoiets M, Khlebas S, Mazur I, Rudnieva K, Potochilova V, Iungin O, Kamyshnyi O, Kamyshna I, Potters G, Spiers AJ and Moshynets O (2024) Extracellular host DNA contributes to pathogenic biofilm formation during periodontitis.
Front. Cell. Infect. Microbiol. 14:1374817.
doi: 10.3389/fcimb.2024.1374817

COPYRIGHT
© 2024 Slobodianyk-Kolomoiets, Khlebas, Mazur, Rudnieva, Potochilova, Iungin, Kamyshnyi, Kamyshna, Potters, Spiers and Moshynets. This is an open-access article distributed under the terms of the Creative Commons Attribution License (CC BY). The use, distribution or reproduction in other forums is permitted, provided the original author(s) and the copyright owner(s) are credited and that the original publication in this journal is cited, in accordance with accepted academic practice. No use, distribution or reproduction is permitted which does not comply with these terms.

Extracellular host DNA contributes to pathogenic biofilm formation during periodontitis

Mariana Slobodianyk-Kolomoiets[1†], Svitlana Khlebas[1], Iryna Mazur[1], Kateryna Rudnieva[2,3], Viktoria Potochilova[4], Olga Iungin[5,6], Olexandr Kamyshnyi[7], Iryna Kamyshna[7], Geert Potters[8,9], Andrew J. Spiers[10] and Olena Moshynets[5*†]

[1]Department of Dentistry, Shupyk National Healthcare University of Ukraine, Kyiv, Ukraine, [2]Central Clinical Diagnostic Laboratory, Kyiv Regional Clinical Hospital, Kyiv, Ukraine, [3]Department of Microbiology, Virology and Immunology, Bogomolets National Medical Academy, Kyiv, Ukraine, [4]Bacteriological laboratory, Kyiv City Maternity Hospital № 2, Kyiv, Ukraine, [5]Biofilm Study Group, Department of Cell Regulatory Mechanisms, Institute of Molecular Biology and Genetics, National Academy of Sciences of Ukraine, Kyiv, Ukraine, [6]Department of Biotechnology, Leather and Fur, Faculty of Chemical and Biopharmaceutical Technologies, Kyiv National University of Technologies and Design, Kyiv, Ukraine, [7]Microbiology, Virology and Immunology Department, I. Horbachevsky Ternopil National Medical University, Ternopil, Ukraine, [8]Antwerp Maritime Academy, Antwerp, Belgium, [9]Department of Bioscience Engineering, University of Antwerp, Antwerp, Belgium, [10]School of Applied Sciences, Abertay University, Dundee, United Kingdom

Introduction: Periodontal diseases are known to be associated with polymicrobial biofilms and inflammasome activation. A deeper understanding of the subgingival cytological (micro) landscape, the role of extracellular DNA (eDNA) during periodontitis, and contribution of the host immune eDNA to inflammasome persistence, may improve our understanding of the mechanisms underlaying severe forms of periodontitis.

Methods: In this work, subgingival biolfilms developing on biologically neutral polyethylene terephthalate films placed in gingival cavities of patients with chronic periodontitis were investigated by confocal laser scanning microscopy (CLSM). This allowed examination of realistic cytological landscapes and visualization of extracellular polymeric substances (EPS) including amyloids, total proteins, carbohydrates and eDNA, as well as comparison with several single-strain *in vitro* model biofilms produced by oral pathogens such as *Klebsiella pneumoniae*, *Pseudomonas aeruginosa*, *Staphylococcus aureus*, *Streptococcus gordonii*, *S. sanguinis* and *S. mitis*. Fluorescence *in situ* hybridization (FISH) analysis was also used to identify eDNA derived from eubacteria, streptococci and members of the *Bacteroides–Porphyromonas–Prevotella* (BPP) group associated with periodontitis.

Results: Analysis of subgingival biofilm EPS revealed low levels of amyloids and high levels of eDNA which appears to be the main matrix component. However, bacterial eDNA contributed less than a third of the total eDNA observed, suggesting that host-derived eDNA released in neutrophil extracellular traps may be of more importance in the development of biofilms causing periodontitis.

Discussion: eDNA derived from host immunocompetent cells activated at the onset of periodontitis may therefore be a major driver of bacterial persistence and pathogenesis.

KEYWORDS

periodontitis, subgingival biofilms, eDNA, biofilm structure, FISH

Introduction

Biofilm formation is a bacterial strategy allowing the colonization of an ecological niche (econiche) (Moshynets and Spiers, 2016). Biofilms are three-dimensional structures where sessile cells reside and are protected by self-produced matrix of extracellular polymeric substances (EPS). These structures make bacteria less susceptible to different environmental stressors and help them to communicate with each other, to coordinate their metabolism, and to better adapt to the changing environment (McLaughlin et al., 2017; Moshynets et al., 2018). Moreover, biofilms are central to a wide range of infection processes, as any bacterial infection eventually involves biofilm formation which is further confounded by interactions with the host immune response.

Periodontal diseases have been recognized as the result of infection and inflammation of the gums and bone that surround and support the teeth (CDC, July 10, 2013; www.cdc.gov/oralhealth/conditions/periodontal-disease, accessed on 13 November 2023). They are considered to occur in close association with aggressive bacterial colonization and pathogenic biofilm formation, and include *Escherichia, Enterococcus, Klebsiella, Lactococcus, Pseudomonas, Staphylococcus* and *Streptococcus* species (Ansiliero et al., 2021; Emery et al., 2021; Espíndola et al., 2022), plus the more pathogenic, secondary-colonizing *Aggregatibacter actinomycetemcomitans*, *Fusobacterium nucleatum*, *Porphyromonas gingivalis*, *Tannerella forsythia*, and *Treponema denticola* species (Kuboniwa and Lamont, 2010; Zijnge et al., 2010; Könönen et al., 2019; Diaz and Valm, 2020) in diverse communities where spatial interactions are important in supragingival biofilms as well as in plagues formed above the gum (Mark Welch et al., 2016; Zijnge et al., 2010).

While the generally acknowledged process explaining the onset and development of periodontitis considers the role of pathogenic biofilm persistence, there are a number of questions that remain unanswered, and our understanding of how pathogenic multispecies biofilms interact with the host immune system is incomplete. Firstly, it is not yet understood why the bacterial community in the dental pocket of healthy people and periodontitis patients are essentially the same (van Winkelhoff et al., 2002; Casado et al., 2011; Naginyte et al., 2019). Secondly, subgingival biofilms are also present in healthy individuals and are in a balanced relationship with the host and it is only when this equilibrium is altered that the inflammasome is activated which leads to periodontitis manifestation (Ding et al., 2020; Esparbès et al., 2021). There is also a measure of heritability with up to a third of the variance of periodontitis due to genetic factors, with higher heritability for more severe disease (Nibali et al., 2019). Finally, little is understood about how the spatial structure of subgingival and supragingival biofilms might differ despite developing in significantly different econiches. In supragingival biofilms, the dental plaque community was shown to consist of a radial nine-taxon structure organized around filamentous corynebacteria with individual taxa spatially distributed at the micrometer scale according to their functional niche (Mark Welch et al., 2016). As well as bacteria, yeast such as Candida have also been found in oral biofilms and associated with periodontal disease (Jakubovics et al., 2021). The matrix of supragingival biofilms is also complex with a range of EPS including secreted and surface-associated amyloid fibers, other proteins and polysaccharides, as well as cellular debris, and bacterial extracellular DNA (eDNA) (Tawakoli et al., 2017; Jakubovics et al., 2021). However, a better spatial understanding of how these components might interact in oral and subgingival biofilms is required, and what role host eDNA released due to neutrophil extracellular traps (NET) activation (NETosis) and autoimmune reaction (Palaniyar et al., 2005; Oveisi et al., 2019) may have in biofilm formation and persistence.

Here we present an adaptation of the modified Cholodny method using biologically neutral polyethylene terephthalate (PET) films to sample real cytological (micro) landscapes which develop during active periodontitis (Moshynets et al., 2011). This method allows for a spatial analysis of both matrix components and cell-cell interactions in subgingival biofilms, and points towards a number of biological conditions guiding the development of periodontitis.

Materials and methods

Ethics statement

Ethics approval was granted by the Ethics Committee of from the Shupyk National Healthcare University of Ukraine (protocol No 8 dated by 7 November 2022) and written informed consent obtained from all participants before inclusion in the study.

Sample collection

All patients were identified as having chronic periodontitis with no systemic disorders after clinical examination which included analysis of the plaque-control record, recording the probing depth and attachment level at six sites around each tooth, and assessment of alveolar bone resorption. No patient had a history of periodontal treatment and none had taken antibiotics in the three months prior to the baseline examination. Sampling of subgingival cytological landscapes was performed by allowing natural biofouling of biologically neutral polyethylene terephthalate (PET) films (2 – 4 x 7 mm) placed in periodontal spaces for five days. Briefly, each film was inserted in a gingival cavity where periodontitis of patients having moderate to advanced periodontitis stage was diagnosed. The patients were instructed to follow their normal oral hygiene but were requested to take care when brushing near the tooth with the film. After five days, the films were removed and placed in a plastic micro-tube and immediately delivered for cytological analysis. When needed, 1 mg/ml DNase (Sigma-Aldrich), dissolved in a buffer containing 20 mM Tris-HCl (pH 7.4) and 10 mM $MgCl_2$ (Sambrook et al., 1989), was applied for 20 min before staining the samples and subsequent microscopy imaging.

Bacteria and culturing conditions

Escherichia coli K12, *Klebsiella penumoniae* ATCC 10031, *Pseudomonas aeruginosa* PA01, *P. fluorescens* SBW25, and *Staphylococcus aureus* ATCC 29423, were obtained from laboratory stock collections (Moshynets et al., 2020; Chernii et al., 2021; Moshynets et al., 2022b; Volynets et al., 2022). The Ukrainian hospital isolates *K. pneumoniae* UHI 489 and UHI 117 were from previous work (Moshynets et al., 2022a) and three oral streptococcal opportunistic pathogenic isolates, *Streptococcus gordonii* UHI1, *S. sanguinis* UHI1 and *S. mitis* UHI1, were isolated from samples collected from patients of the Maxillofacial Surgery Department of the Kyiv Regional clinical hospital with purulent-inflammatory processes and identified using a Bacteriological Analyzer Vitek 2 Compact v9 (bioMérieux, France). Bacteria were incubated aerobically at 37°C except for *P. fluorescens* SBW25 which was cultured at 28°C. Over-night shaken Luria-Bertani (LB) liquid cultures provided 300 µl inocula for biofilm assays which were undertaken in static 30 ml microcosms containing 5 ml media. These were incubated at 28°C or 37°C and biofilms harvested after three days. Solid-liquid interface biofilms formed on the bottom surface of microcosms, except for *Pf* SBW25 where air-liquid interface biofilms were formed (Moshynets et al., 2022c).

Microscopic analysis

Biofilm and cytological analysis was performed using confocal laser scanning microscopy (CLSM). Biofilm samples obtained from microcosms, cytological samples obtained with a spoon excavator, and subgingival biofilms formed on biologically neutral polyethylene terephthalate (PET) films, were transferred to microscopic glass slides prior to staining. Fluorescent stains were used to visualize intracellular DNA (iDNA) and extracellular DNA (eDNA), amyloids, total protein, and Candida cells. Stain combinations were based on complementary excitation/emission (Ex/Em) wavelengths which allowed individual stains to be visualized using separate CLSM channels.

iDNA was visualized with 5 µM SYBR Green solution (Thermo Fisher Scientific) which can be used to stain live cells with an intact membrane or dead cells or those with a damaged membrane and was used as a proxy for bacterial cells. 2 µg/ml Ethidium bromide solution (Sigma-Aldrich, UK) was also used to visualize iDNA because under the conditions we used, the eDNA signal was found to be very diffused compared to the signals coming from intact cells. eDNA was visualised with 20 µg/ml Propidium iodide in water, or 1 mM of the experimental stain 986 (Moshynets et al., 2022c) (supplied by SM Yarmoluk) in DMSO, which do not penetrate

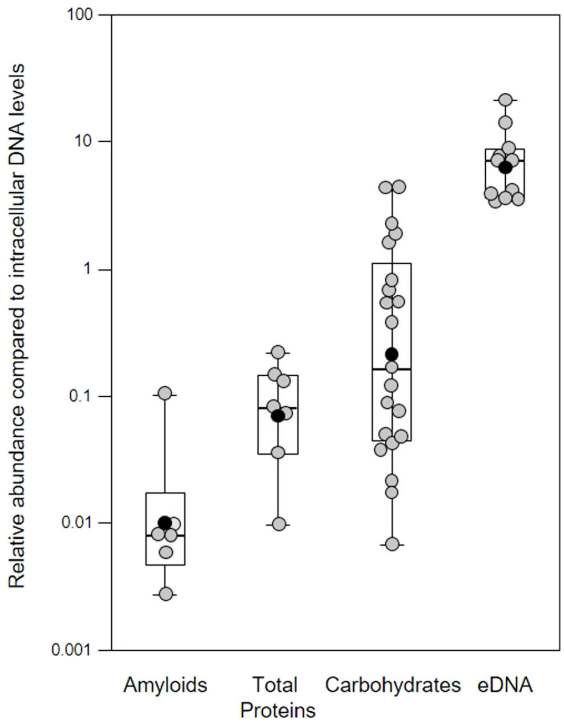

FIGURE 1
Quantification of extracellular polymeric substances in subgingival biofilms using multiple fluorescent stains. Shown here are the relative abundance of amyloids, total protein, carbohydrates and Candidia cells, and eDNA compared to intracellular DNA (iDNA) levels determined from CLSM images of subgingival biofilms sampled from four patients. Samples were further divided into subsamples to allow staining with multiple dyes. Amyloids stained with AmyGreen, total protein with Thiazine Red R, carbohydrates and Candidia with Calcofluor White, eDNA with Propidium iodide, and iDNA with Ethidium bromide or SYBR Green. Dye mixtures were chosen to avoid overlapping excitation/emission characteristics and subsamples were stained with either AmyGreen, Calcofluor White and Ethidium bromide, Cacofluor White, SYBR Green and Thiazine Red R, or Calcofluor White, Propidium iodide and SYBR Green. Whisker boxplots are shown with the median, mean (black circles) and individual ratios (grey circles). For each material at least three images were quantified from subsamples obtained from patients attending the clinic at different times (pseudo-replicates, n = 6 – 21).

intact cells. Double-staining eDNA with Propidium iodide and SYBR Green is not possible as this dye combination results in fluorescence resonance energy transfer (FRET) reducing SYBR Green fluorescence and increasing Propidium iodide fluorescence (Barbesti et al., 2000). Amyloids were visualised with 1 mM AmyGreen solution [of our own synthesis (Moshynets et al., 2020)] in DMSO and total proteins with 0.5 μg/ml Thiazine Red R (Sigma) in 0.1% acetic acid. Carbohydrates (β(1-3) glucans) and Candida cells (β(1-4) glucan, i.e., chitin) were visualised with 2 μg/ml Calcofluor White (Sigma-Aldrich, UK) in water (Domenech et al., 2013; Rezende et al., 2019).

No additional washing after staining was performed in order to limit the physical disruption of samples during preparation, and a cover slip was placed over the samples before imaging. CLSM analysis was undertaken using a Leica TCS SPE Confocal system with coded DMi8 inverted microscope (Leica, Germany) and Leica Application Suite X (LAS X) v3.4.1. Representative images were acquired using a maximum of three channels for SYBR Green or AmyGreen (Ex/Em 488/490 – 580 nm), Ethidium bromide, 986, Propidium iodide or Thiazine Red R (532/537 – 670 nm), and Calcofluor White (405/450 – 500 nm), with total pixel numbers determined for each stain (channel) using LAS X. Data are shown as total abundance or as the relative abundance compared to iDNA levels.

Fluorescence *in situ* hybridization

Analysis of biofilm samples by FISH followed earlier work (Hannig et al., 2007). Oligonucleotide probes for eubacteria, streptococci and the *Bacteroides–Porphyromonas–Prevotella* (BPP) group were synthesized commercially, and 5'-end labelled with fluorochromes (Syntol, Russia). EUB 338 (5'-GCT GCC TCC CGT AGG AGT-3') was 5' labelled with FAM (Ex/Em 488/491 – 575 nm) and used to visualize bacterial eDNA (Amann et al., 1990). STR 405 (5'-TAG CCG TCC CTT TCT GGT-3') was 5' labelled with Cy5.5 (Ex/Em: 635/645 – 800 nm) and used to visualize eDNA from oral streptococci (Paster et al., 1998). The Bacto 1080 probe (5'-GCA CTT AAG CCG ACA CCT-3') was labelled with Acridine (Ex/Em 405/407 – 496 nm) and was used to visualize eDNA derived from the BPP group (Doré et al., 1998). Samples were incubated with 1 mg/ml of lysozyme derived from chicken egg white (47,000 U/mg, Sigma-Aldrich, Germany) in 0.1 M Tris–HCl, 5 mM EDTA (pH 7.2) solution, for 10 min at 37°C, in order to permeabilize cell membranes. For subgingival samples and biofilms formed on PET films, the lysozyme step was omitted to limit probe penetration of cells. These were fixed overnight in 4% paraformaldehyde in phosphate-buffered saline (PBS, 130 mM NaCl, 3 mM $KH_2PO_4{\cdot}2H_2O$, 7 mM $Na_2HPO_4{\cdot}12H_2O$, pH 7.2) at 4°C and then washed with phosphate-buffered saline and stored at -80°C until

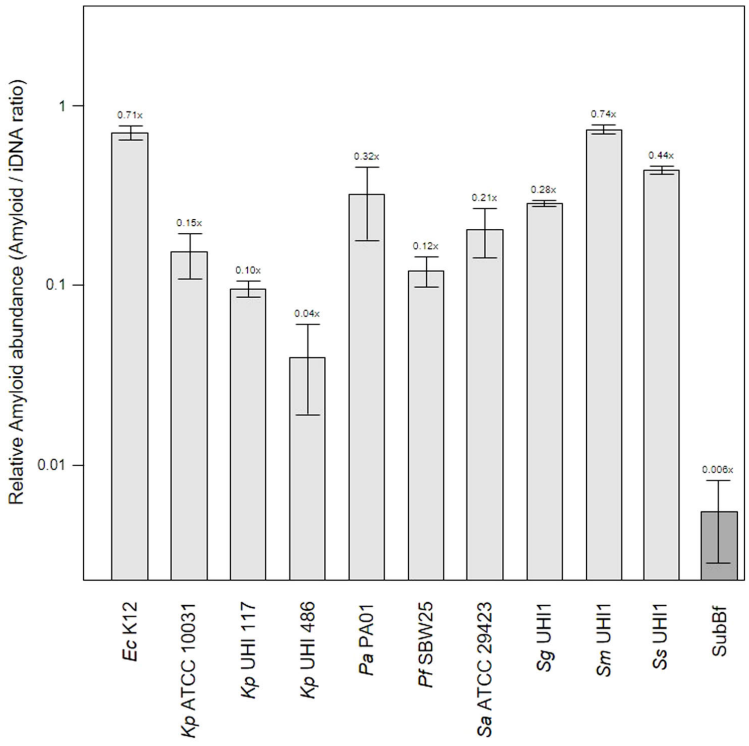

FIGURE 2
Amyloid levels are high in single-species biofilms compared to subgingival biofilms. Shown here is the relative abundance of amyloids to iDNA determined from CLSM images of three-day old single-species biofilms produced by *Escherichia coli* K12, *Klebsiella pneumoniae* ATCC 10031 and two hospital-acquired *K. pneumoniae* isolates UHI 117 and UHI 486, *Pseudomonas aeruginosa* PA01, *Pseudomonas fluorescens* SBW25, *Staphylococcus aureus* ATCC 29423, *Streptococcus gordonii* UHI1, *Streptococcus sanguinis* UHI1, *Streptococcus mitis* UHI1. The relative amyloid levels from a subgingival multispecies biofilm (SuBf) sampled from a patient also presented in Figure 1 is shown for comparison. Amyloids were stained with AmyGreen and iDNA with Ethidium bromide and relative abundance calculated from the channel pixel sums as amyloid/iDNA. The relative ratio is also indicated above each bar showing means ± SD (n = 3 views from one biofilm sample per strain).

hybridization. Samples were dehydrated with a series of ethanol washes containing 50, 80 and 100% (v/v) ethanol, for 3 min each before incubation with oligonucleotides at a concentration of 4 ng/μl each in hybridization buffer (900 mM NaCl, 20 mM Tris–HCl (pH 8), 30% (v/v) formamide and 0.1% (w/v) sodium dodecyl sulphate). Hybridization was conducted in plastic microtubes at 35° C overnight using a Dry Block Thermostat TBD-120 (Biosan SIA, Latvia) and samples were then incubated for 20 min at 37°C in wash buffer containing 20 mM Tris–HCl (pH 8), 64 mM NaCl and 0.1% (w/v) sodium dodecyl sulphate. After washing, samples were analyzed by CLSM as described above.

Identification of peridontal pathogens

The Vitacell Clinical Laboratory (Ukraine) was used to identify *Actinobacillus actinomycetemcomitans*, *Porphyromonas gingivalis*, *Prevotella intermedia*, *Tannerella forsythus* (*Bacteroides forsythus*), and *Treponema denticola* in subgingival biofilm samples using a Stomatoflor Real Time kit (DNK-Technologia, Russia) (Volinska and Bondarchuk, 2016) and Real-time CFX96 Touch system (BIO-RAD, USA).

Statistical analyses

Experimental replicates (*n*) were used and quantitative results presented using whisker plots with the median and mean indicated or as bar plots with the mean and standard deviation (SD). One-Way ANOVA using (www.originlab.com) where $p < 0.05$ was considered statistically significant.

Results and discussion

Composition of subgingival-associated biofilms during periodontal disease

Different extracellular polymeric substances (EPS) provide structural integrity to biofilms and a variety of EPS including extracellular DNA (eDNA) contribute to polymicrobial supragingival biofilms (Jakubovics et al., 2021). However, in comparison little is known about the biofilm matrix in the subgingival region during periodontitis. As part of our preliminary investigation, we sampled biofilms from patients with periodontitis with a spoon excavator, stained with different

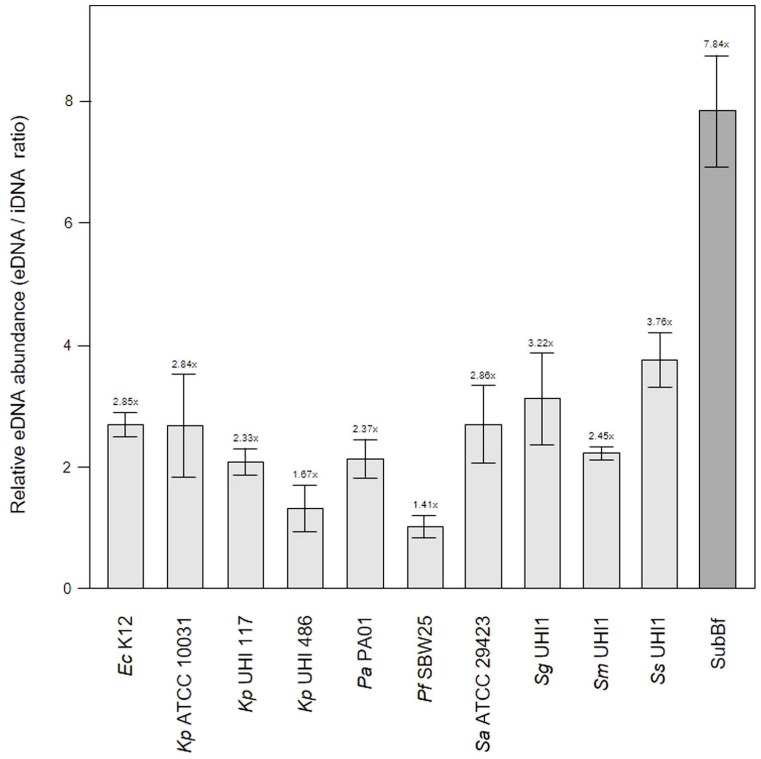

FIGURE 3
Extracellular DNA (eDNA) is a significant component in single-species biofilms and subgingival biofilms. Shown here is the relative abundance of eDNA to iDNA determined from CLSM images of three-day old single-species biofilms produced by *Escherichia coli* K12, *Klebsiella pneumoniae* ATCC 10031 and two hospital-acquired *K. pneumoniae* isolates UHI 117 and UHI 486, *Pseudomonas aeruginosa* PA01, *Pseudomonas fluorescens* SBW25, *Staphylococcus aureus* ATCC 29423, *Streptococcus gordonii* UHI1, *Streptococcus sanguinis* UHI1, *Streptococcus mitis* UHI1. The relative eDNA levels from a subgingival multispecies biofilm (SuBf) sampled from a patient also presented in Figure 1 is shown for comparison. eDNA was stained with SYBR green and iDNA with Propidium iodide and relative abundance calculated from the channel pixel sums as eDNA/iDNA. The relative ratio is also indicated above each bar showing means ± SD (*n* = 3 views from one biofilm sample per strain).

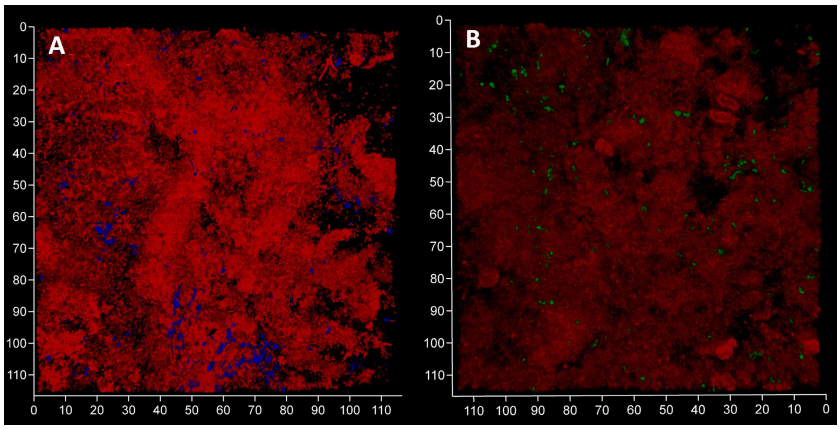

FIGURE 4
Subgingival biofilms sampled by spoon excavator are dominated by bacterial cells and eDNA. Shown here are representative CLSM images of iDNA from metabolically active and inactive bacterial cells visualized with Ethidium bromide (red channel) and Candida cells with Calcofluor White (blue channel) **(A)** and eDNA visualized with Propidium iodide (red channel) and iDNA in metabolically active cells with SYBR Green (green channel; but note the FRET effect hides the SYBR Green signal when eDNA is also bound by Propidium iodide) **(B)**. The biofilm sample was subdivided in two and stained separately for the images shown here. The axes show 110 µm.

combinations of fluorescent dyes (McLaughlin et al., 2017; Moshynets et al., 2020; Moshynets et al., 2022c), and quantified amyloids, total protein, carbohydrates and Candidia cells, and eDNA relative to intracellular DNA (iDNA) levels (Figure 1). This demonstrates the variation seen in biofilm EPS components and the difficulty in establishing normal compositions which may vary within and between patients, and changes resulting from disease progression and possible changes in community composition. While we note variation in total proteins and carbohydrates and Candidia cells in our biofilm samples, we feel the relative abundance of eDNA and amyloids is more interesting, as eDNA is a common matrix component of biofilms encompassing cells within a physical network of fibers, and amyloids interact with eDNA and surfaces to promote attachment (Gallo et al., 2015; Schwartz et al., 2016; Tursi et al., 2017).

In our samples, the mean relative eDNA levels compared to iDNA was 7.75x, suggesting substantial amounts of eDNA matrix surround bacterial cells in these biofilms, and this is supported by CLSM biofilm images (see later figures) where eDNA and iDNA are spatially differentiated. However, some caution is also required in interpreting these results, as normalizing data across biofilm samples using iDNA levels may not always be appropriate (e.g., mature biofilms may have a higher microbial load compared to the eDNA matrix compared to younger biofilms; higher levels of host

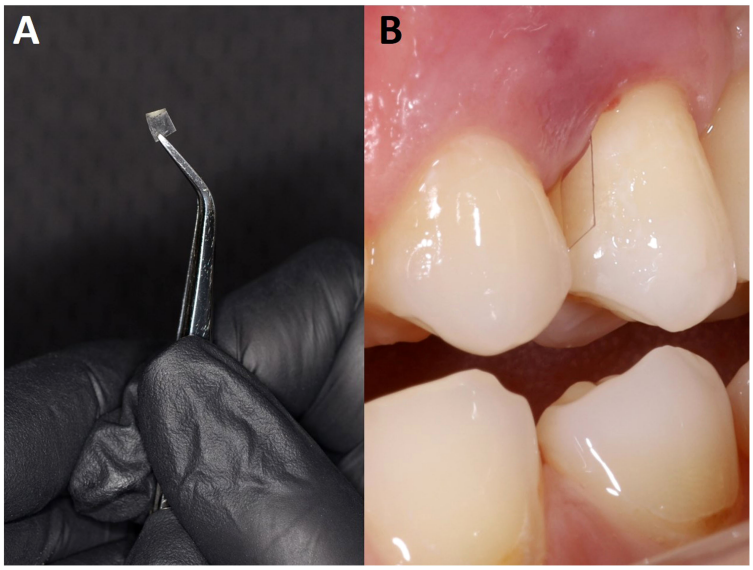

FIGURE 5
Polyethylene terephthalate (PET) films used to sample subgingival biofilm development. Shown here is a PET film (2 – 4 x 7 mm) **(A)** positioned in the periodontal space next to T24 **(B)**.

immune response might have lysed more cells without altering the matrix, etc.).

Functional amyloids (i.e., amyloid fibers) are produced by a number of periodontal pathogens including *Streptococcus mutans* and representatives of the red complex of periodontal pathogens (Besingi et al., 2017). One of these, *Porphyromonas gingivalis*, was shown to utilize amyloids for biofilm formation, with at least six variants of amyloid-like fimbrillin (FimA) being produced by this species (Amano et al., 2004; Cueno et al., 2015). Another member of the red complex, *Tannerella forsythia*, also produces the leucine-rich repeat protein BspA, which is potentially amylogenic as predicted by the Waltz algorithm, and is an important adhesin for host receptors such as glycoprotein 340 (Loimaranta et al., 2009). In our samples, the mean relative amyloid level was 0.007x suggesting very low levels of these fibers were present in the biofilms. We investigated this further by determining amyloid levels in single-species *in vitro* biofilm produced by *Klebsiella pneumoniae*, *Pseudomonas aeruginosa*, *Staphylococcus aureus*, and three oral-associated streptococci including *Streptococcus gordonii*, *S. sanguinis* and *S. mitis*, recognized as the early tooth surface colonizers (Rickard et al., 2003), with *Escherichia coli* and an environmental isolate of *Pseudomonas fluorescens* included as additional biofilm reference strains (Figure 2).

Amyloid levels relative to iDNA in the single-species biofilms varied from 0.04x for the weak producer *Kp* UHI 486 we have

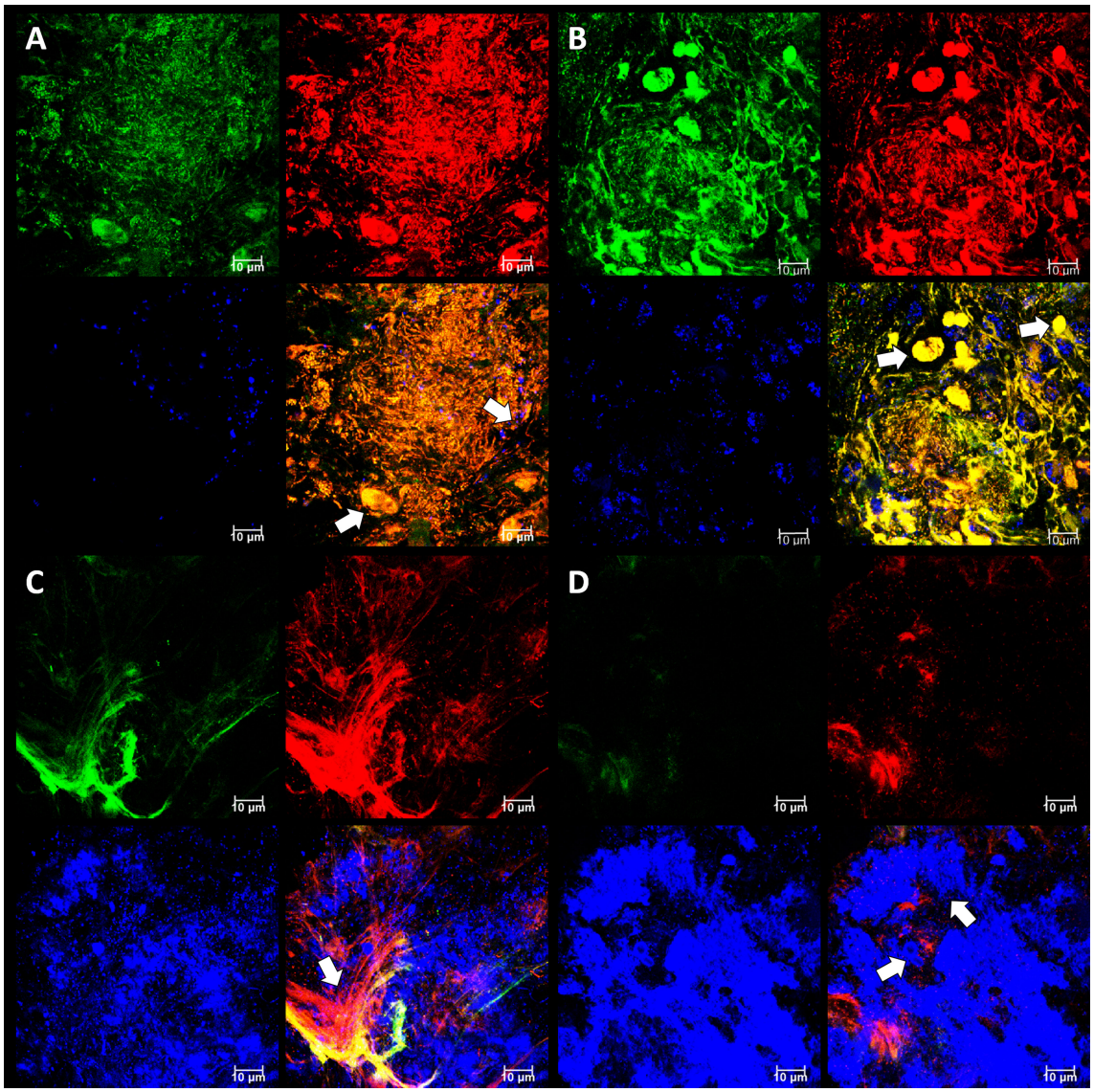

FIGURE 6
Subgingival micro-landscapes seen developing on PET films during periodontitis. Shown here are representative CLSM images with DNA stained with SYBR Green (green channel), eDNA stained with Propidium iodide (red channel), and Candida cells stained with Calcofluor White (blue channel) of sites with moderate **(A)** and strong inflammation **(B–D)**. The image shown in **(A)** is of a biofilm 12 µm thick with a slice taken 3.3 µm from the plastic surface, and arrows indicate leukocyte and Candida cells. The image shown in **(B)** is of a biofilm 11 µm thick with a slice taken at 7.5 µm and arrows indicate numerous leukocytes. The image shown in **(C)** is of a biofilm 10 µm thick with a slice taken at 1.85 µm and the arrow indicating a fibrin clot. The image shown in **(D)** is from the same position as **(C)**, but the slice is taken at 4 µm and arrows indicate Candida cells. Scale bars show 10 µm.

characterized before (Moshynets et al., 2022a) up to 0.71x and 0.74x for amyloid-superproducers *Ec* K12 and *Sm* UHI1. *Sa* ATCC 29423, *Sg* UHI1 and *Ss* UHI, also known to produce considerable amounts of amyloids and are early colonizers of teeth (Ximénez-Fyvie et al., 2000; Larsen and Fiehn, 2017), had similarly high relative levels of amyloids in these single-species biofilms. Interestingly, we note that the two pathogenic *K. pneumoniae* isolates tested here produced lower levels of amyloids compared to the ATCC reference strain that may now be laboratory-adapted.

The relatively low level of amyloids in our subgingival biofilms might be explained by a low number of amyloid producers or by downregulation of amyloid genesis to avoid or mitigate the immune response, as described for BspA in the *T. forsythia* infection model (Inagaki et al., 2005). Further evidence of an immunogenic effect of amyloid fibers in biofilms has been seen when bound to eDNA (Gallo et al., 2015; Tursi et al., 2017). However, we found lower eDNA levels relative to iDNA in our mature single-species biofilms of 1.41 – 3.76x compared to the subgingival biofilm samples we had sampled earlier with eDNA levels of 7.84x (Figure 3). Interestingly, amyloids are known to stabilize eDNA in biofilms and, reciprocally, eDNA promotes amyloid expression in *Enterobacteriaceae* (Schwartz et al., 2016; Taglialegna et al., 2016; Yan et al., 2020). However, this may not occur or be as relevant in subgingival biofilms as we have observed high levels of eDNA and low levels of amyloid. This in turns raises the question of whether all of the eDNA we have identified is of bacterial origin or if some of it is derived from host cells.

One of the leading eDNA producers is *P. aeruginosa* which utilizes eDNA for the initiation and maturation of biofilms (Subendu, 2020; Campoccia et al., 2021; Moshynets et al., 2022b) and is also capable of recruiting host eDNA during maturation (Walker et al., 2005). As our subgingival biofilms contained even more eDNA than that seen in our *Pa* PA01 biofilms or biofilms produced by other reference strains, it is likely that subgingival biofilm development also incorporates host eDNA during development. eDNA is a common component of natural dental plaque formation (Rostami et al., 2017) and is probably also common in the subgingival niche where the most obvious source are neutrophils attracted by an inflammasome during periodontal diseases. A number of studies have described the role of extracellular DNA traps (NETs) produced by neutrophils during periodontitis (Vitkov et al., 2009; Yousefi et al., 2020). However, the

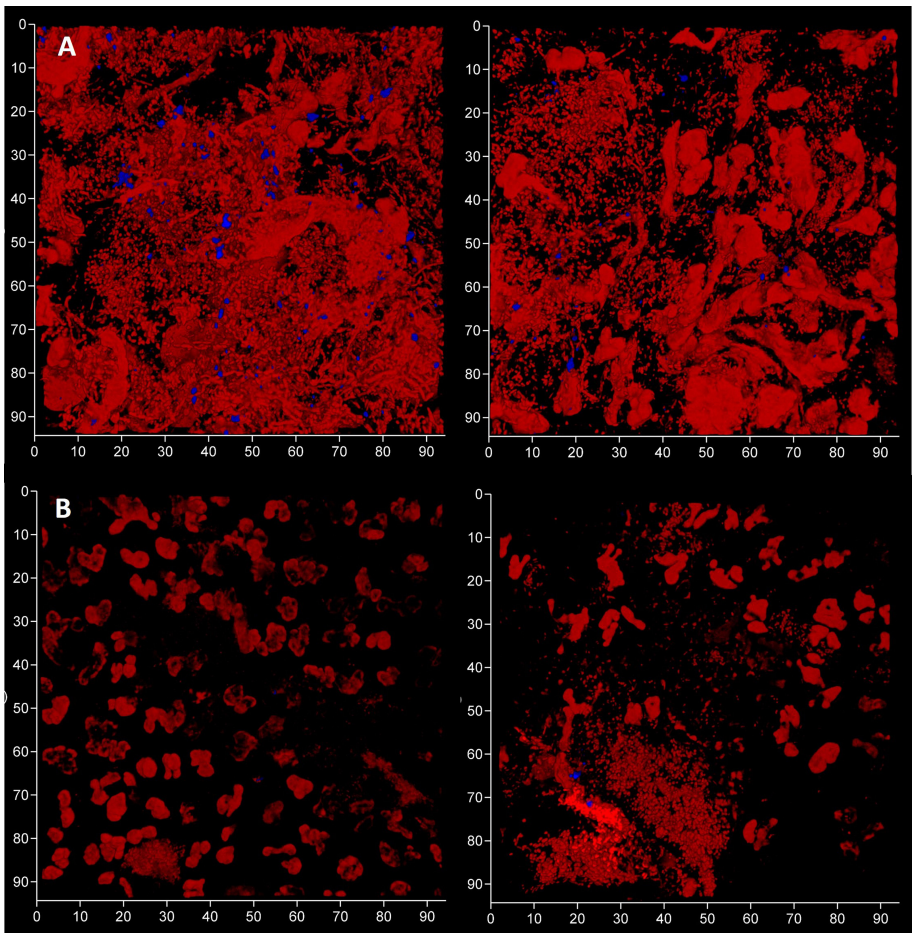

FIGURE 7
Subgingival micro-landscapes developing on PET films during periodontitis are sensitive to DNAse treatment. Shown here are two sites (left and right) of a subgingival biofilm recovered using a PET film and imaged by CLSM with total DNA stained with Ethidium bromide and Propidium iodide (red channel) and Candida cells with Calcofluor White (blue channel) before **(A)** and after treatment with DNAse **(B)**. The axes show 90 µm.

contribution of host eDNA derived from NETs to the development and persistence of pathogenic biofilms in periodontitis remains unclear.

Subgingival biofilms developing during periodontal disease

The importance of local environmental conditions and the econiche for biofilm development and community function has been recognized since the pioneering work in microbial ecology by Winogradsky (Moshynets et al., 2013). However, the modern understanding of biofilm structure, development, and function, has emerged largely from investigations of *in vitro* model systems using a variety of stationary microcosms (Koza et al., 2011; Robertson et al., 2013; Koza et al., 2017) or dynamic flow chambers (Chin et al., 2006; Tolker-Nielsen and Sternberg, 2011). Naturally occurring biofilms develop during colonization of an appropriate surface by multiple species assembling from the local environment and selected by niche physical-chemistry and topography, available resources, competition and predation. This process can be investigated by direct sampling and might reveal important interactions not seen when investigating single-species biofilms using *in vitro* systems, and was first attempted by Cholodny in the 1930s using a glass-slide sampling procedure for soil and subsequently modified by us to use PET films more suitable for modern microscopy techniques (Moshynets et al., 2011; Moshynets et al., 2012). Similar to soil biofilms, the architecture and spatial arrangement of pathogenic biofilms is also an important factor in understanding their persistence and impact on the host. Dental-associated biofilms form on tooth and soft-tissue surfaces following bacterial colonization and can result in complex heterogenic multispecies communities (Rickard et al., 2003). Polytetrafluoroethylene (PTFE, Teflon) carriers have been previously used to sample subgingival bacterial plaque (Wecke et al., 2000).

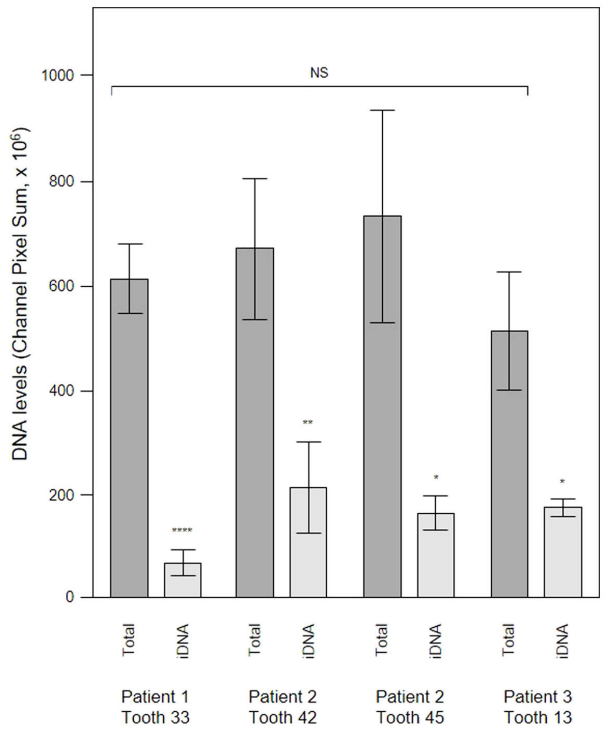

FIGURE 8
DNAse treatment demonstrates that a significant proportion of the DNA visualized in subgingival biofilms is extracellular DNA (eDNA). Shown here are DNA levels determined from CLSM images of subgingival multispecies biofilms developing in tooth pockets on PET films (Total) which were then treated with DNAse iDNA). DNA removed by DNAse treatment is exposed DNA, i.e., eDNA. DNA levels were calculated from the channel pixel sums. Bars show means ± SD (n = 3 views from one biofilm sample per tooth). *p < 0.05, **p < 0.01, and ****p < 0.001; NS, not significantly different at p < 0.05. Patient (P) and tooth (T) numbers are provided in parentheses.

Dental-associated biofilms can be readily sampled though the procedures used may damage the structure and underlying relationships between host and microbial cells, matrix, and substratum (Wood et al., 2000), and there is little information on pathogenic biofilm structure *in situ* largely because of this issue. The relationship between the biofilm and host cells and substratum is of particular interest since any effective treatment should be developed based on a realistic understanding of the cytological landscape. Although microbial diversity has been reported for subgingival biofilms, limited information is available for spatial structure (Rickard et al., 2003; Ansiliero et al., 2021) and analysis of crevicular exudate from patients with periodontitis has confirmed the importance of neutrophil extracellular traps (NET)-derived eDNA in pathological processes (Vitkov et al., 2009).

We expected to observe a standard cytological picture of inflammation when sampling periodontal subgingival biofilms from patients using a spoon excavator. However, our CLSM images suggest that these were dominated by bacterial cells and relatively few leukocyte-like cells (Figure 4) and suggests that we sampled the top surface of the biofilm rather than the substratum where more leukocytes might be expected to be found. Visualisation of eDNA and iDNA suggested a degree of heterogeneity in the samples with both dense and relatively sparse regions of cells and/or eDNA evident. We also noted the presence of Candidia cells stained with Calcofluor White (Figure 4A) and that relatively few metabolically-active bacterial cells were observed in these subgingival samples (Figure 4B).

In order to image undamaged subgingival biofilms, we placed PET films in dental pockets of patients and left them there for five days before recovery (Figure 5). This approach is similar to the use of PFTE or enamel fragments to sample dental plaque (Wecke et al., 2000; Wood et al., 2000) but our films are easier to prepare as it does not require a rigid mount and has no biorisks associated with the use of donated material. The PET film will be rapidly coated in a pre-conditioning layer of host and bacterial material, and it also provides a surface for migratory leucocytes which transform into terminal-effector cells such as neutrophils in infection sites. Once colonized the PET film develops a 3D micro-landscape structure representative of host-biofilm interactions in the subgingival niche during periodontitis. As expected, the micro-landscape was dependent upon inflammation intensity and depth of observation

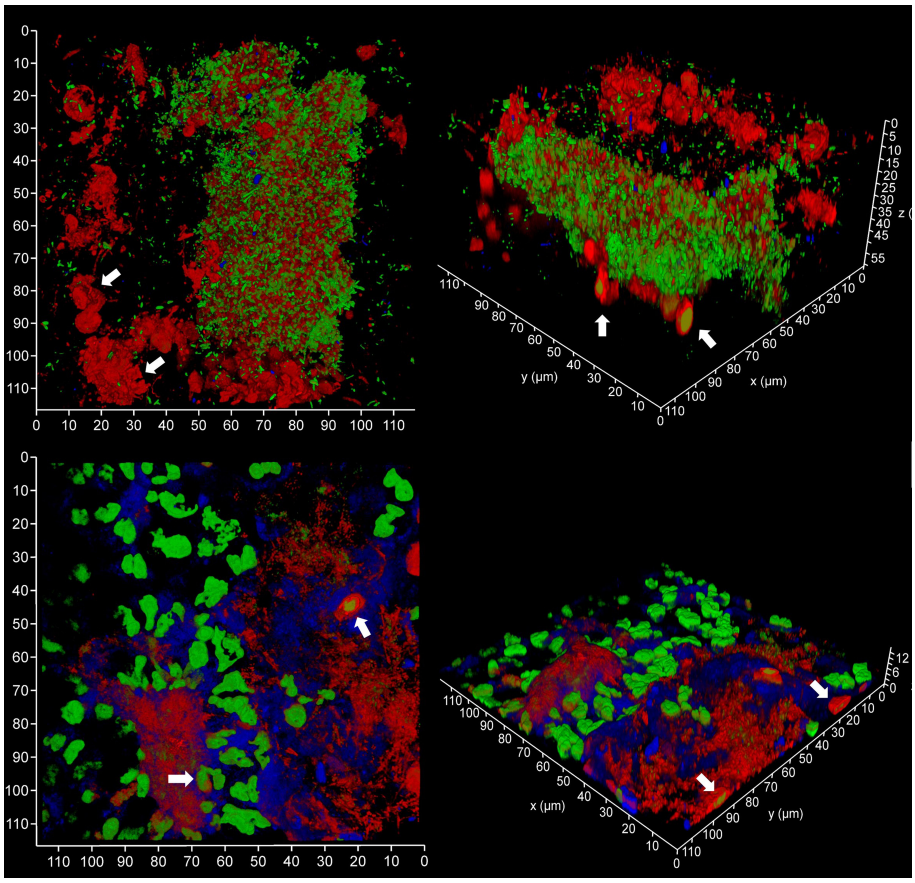

FIGURE 9
Subgingival micro-landscapes on sampling films during periodontitis. Shown here are two subgingival biofilms recovered using PET film and imaged by CLSM with iDNA stained with SYBR Green (green channel), eDNA with Propidium iodide (top images, red channel) and experimental stain 986 (bottom images, red channel), and Candida cells with Calcofluor White (blue channel). The arrows indicate leukocytes. The *x-y* axes show 110 µm.

(Figure 6). More bacteria and a broader morpho-diversity and fewer leukocytes were observed when inflammation was moderate and fewer bacteria and a lot of fibrin-embedded eDNA were observed when the inflammation was strong as was observed earlier (Krautgartner et al., 2010). Candida cells dominated the landscape when the inflammation intensity was high and were generally found at superficial locations (Figure 6D).

To evaluate the contribution of eDNA to the pathological micro-landscape, PET films were applied to four dental pockets of three patients with initial periodontitis. After five days the films were recovered and cut in half, with one piece treated with DNAse for 30 minutes before staining for total DNA and Candida cells and visualization by CLSM. Representative images from one patient clearly show a substantial reduction of the total DNA signal following DNAse treatment (Figure 7) suggesting that most of the signal was exposed eDNA. It is also notable that far fewer Candida cells remained after treatment, suggesting that eDNA helped retain these yeast close to the surface of the tooth. DNA levels were quantified for each of the four PET samples (Figure 8) and suggests that eDNA contributes up to ~70% of the DNA visualised using this technique. As the total DNA levels determined for the four micro-landscapes visualised here on PET films were not significantly different, we suggest that they are representative of subgingival multispecies biofilms developing normally in patient's teeth.

A new, experimental, super-heavy DNA-specific stain called "986" with low penetration through intact and damaged membranes specifically developed to visualize eDNA (Moshynets et al., 2022c) was tested using a PET film subgingival micro-landscape (Figure 9). eDNA was mainly associated with the biofilm matrix and a superficial surface of leukocytes, and implies that any leukocyte-associated eDNA released at these sites contributes to the bacterial eDNA and the developing biofilm. Previous work using *in vitro* biofilms has shown that neutrophils were able to settle onto *P. aeruginosa* biofilms where they became immobilized, degranulated and transformed their membranes following bacteria direction (Jesaitis et al., 2003). Similar effects where neutrophils activated their functional phagocytosis when attacking *S. aureus* and *S. epidermidis* biofilms have also been observed (Günther et al., 2009; Guenther et al., 2009). Neutrophils sensibilization toward bacterial antigens leads to elevated production of reactive oxygen species, antimicrobial peptides and lactoferrin (Arslan et al., 2009; Stroh et al., 2011; Sol et al., 2013), and when associated with periodontitis results in elevated expression of a Cluster of differentiation (CD) markers panel which leads to a neutrophil phenotype change from parainflammatory in the healthy state to proinflammatory in the diseased patient (Oveisi et al., 2019). This

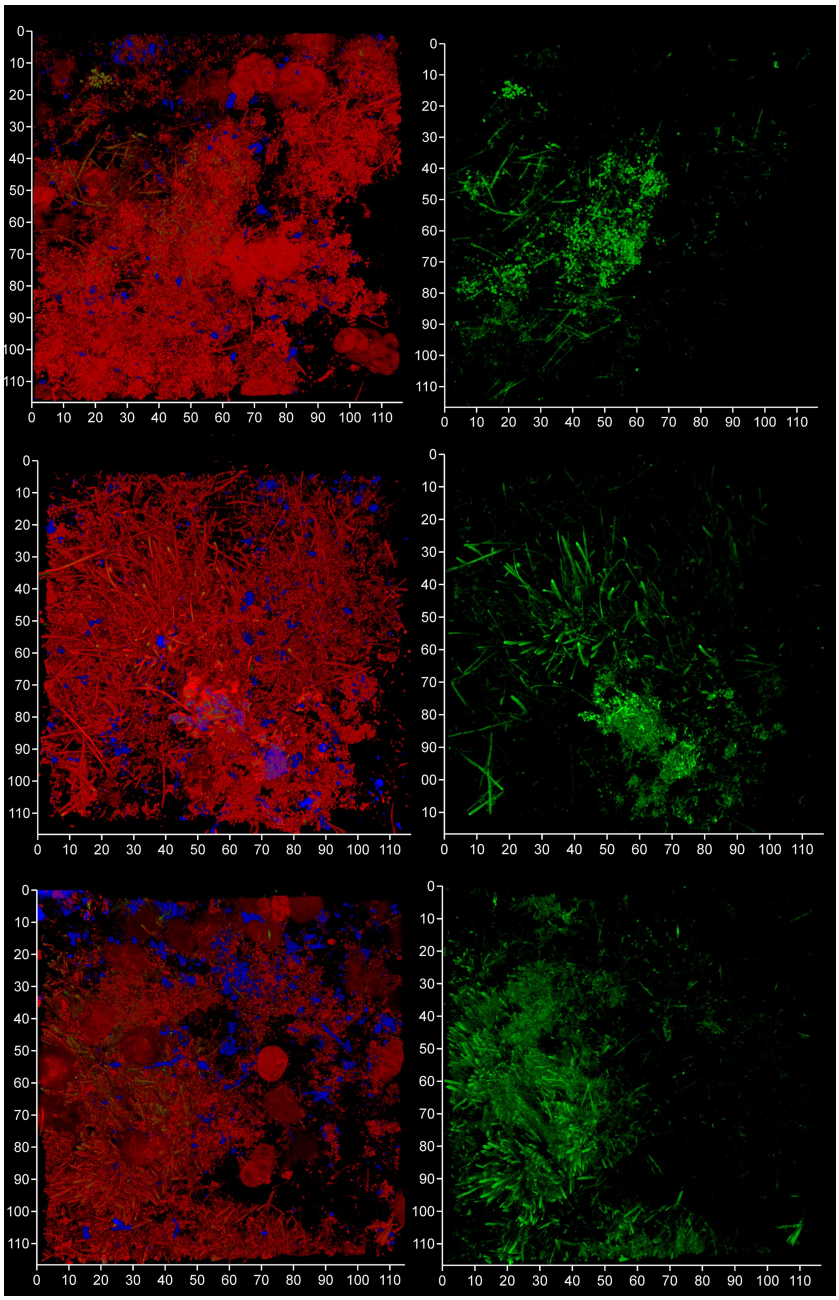

FIGURE 10
FISH probes can be used to identify bacterial eDNA. Shown here are three subgingival biofilms recovered using PET film and imaged by CLSM after staining eDNA with Propidium iodide (red channel), bacterial eDNA with FISH EUB 338 probe tagged with FITC (green channel), and Candida cells with Calcofluor White (blue channel). The images on the left show all three channels merged while the images on the right show only the green channel. The scale bars show 110 µm.

results in phagocytosis, degranulation and neutrophil extracellular traps (NET) activation (NETosis) as a strategy to combat or control pathogenic biofilm development. Such a super-activation of the neutrophils can contribute to the pathogenesis of periodontitis (Kornman, 2008) and might potentially enhance biofilm formation and biofilm-associated phenotypic resistance by periodontal pathogens as seen *in vitro* for *P. aeruginosa* (Yousefi et al., 2020).

The mechanisms of host eDNA elaboration during NET activation has been recently reviewed (Vitkov et al., 2021). The main NETos activators were bacterial outer membrane vesicles heavily loaded with bacterial LPS (Vanaja et al., 2016) and gingipain cysteine proteases produced by periodontal pathogens including *P. gingivalis* (Bryzek et al., 2019) [blood monocytes are also capable of extracellular trap release in response to different stimuli (Granger et al., 2017)]. NETs formed during periodontitis lack bactericidal activity due to the proteolytic activity of the gingipains and do not control pathogenic biofilm development. However, periodontitis-associated NETs are able to stimulate periodontal pathogen growth and possibly biofilm development (Bryzek et al., 2019).

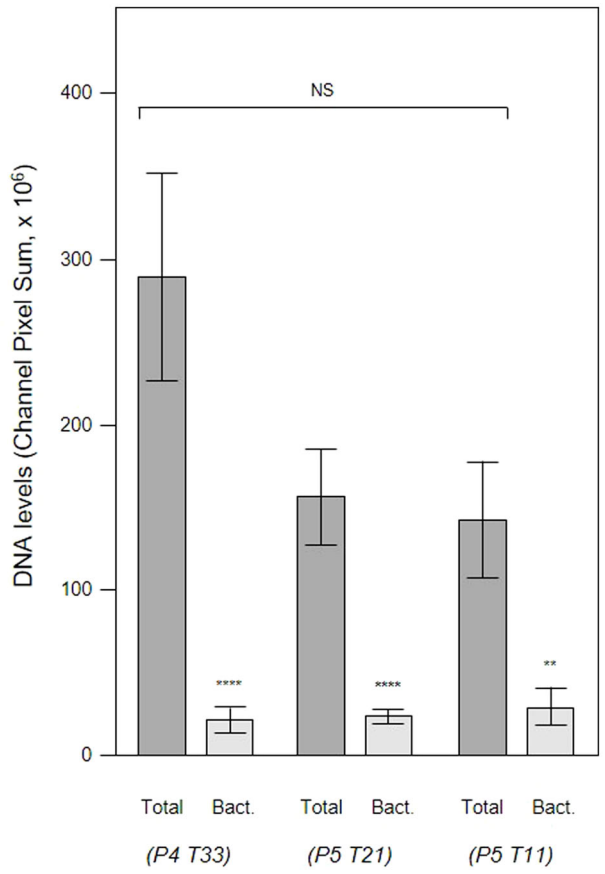

FIGURE 11
Total eDNA and bacterial eDNA levels in subgingival biofilms. Shown here are the total eDNA and bacterial eDNA (Bact.) levels determined from CLSM images of three subgingival biofilms recovered using PET films stained with propidium iodide and EUB 338. Bars show means ± SD (n = 7 views from one biofilm sample per tooth). **p < 0.01 and ****p < 0.001; NS, not significantly different at p < 0.05. Patient (P) and tooth (T) numbers are provided in parentheses.

Host eDNA dominates the microlandscape during periodontal disease

In order to evaluate the contribution of host and bacteria-derived eDNA, we undertook fluorescent *in situ* hybridization (FISH) of PET films using the EUB 338 bacteria-specific probe (Figure 10). Analysis of three samples of subgingival micro-landscapes from two patients shows that bacterial eDNA may contribute 8 – 21% to the total eDNA with the majority derived from host cells activated following periodontitis (Figure 11). It is therefore possible that the release of host DNA is responsible for the consistent persistence and pathology chronization.

eDNA from the *Bacteroides–Porphyromonas–Prevotella* group might be a major bacterial eDNA source in the microlandscape during periodontal disease

We analyzed a randomly-chosen clinical case of periodontitis (patient 5) to determine the origin of bacterial eDNA involved in subgingival biofilm formation by real time PCR and CLSM. The PCR analysis confirmed the presence of pathologically significant periodontal pathogens including *Actinobacillus actinomycetemcomitans*, *Porphyromonas gingivalis*, *Tannerella forsythensis*, *Treponema denticola* and *Candida albicans*. FISH analysis of PET films using the Bacto 1080 probe for the *Bacteroides–Porphyromonas–Prevotella* (BPP) group and the STR 405 probe for the oral streptococci group suggest that these might not be dominant in the subgingival micro-landscape, and as before host eDNA was more abundant than bacterial eDNA (Figure 12). We noticed a difference in the subgingival micro-landscape close to a fibrin clot which are commonly found during periodontitis (Figure 13). No streptococci were present near the clot although an increased number of anaerobic bacteria were found instead. This might be explained by the antibacterial effects of host eDNA and associated

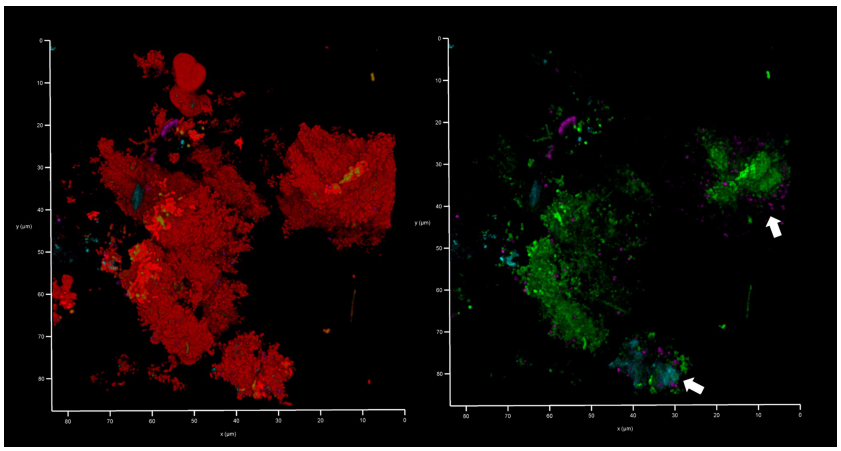

FIGURE 12
Bacteroides–Porphyromonas–Prevotella and oral streptococci group eDNA. Shown here is a subgingival biofilm recovered using a PET film and imaged by CLSM after staining eDNA with Propidium iodide (red channel), bacterial eDNA with EUB 338 probe tagged with FITC (green channel), *Bacteroides–Porphyromonas–Prevotella* group with Bacto 1080 probe tagged with modified Acridine (blue channel), and the oral streptococci group with STR 405 probe with Cy5.5 (purple channel). The left image shows all four channels merged while the right image shows the green, blue and purple channels merged. Arrows point at a *Bacteroides–Porphyromonas–Prevotella* and streptococcal microcolonies. The axes show 80 µm.

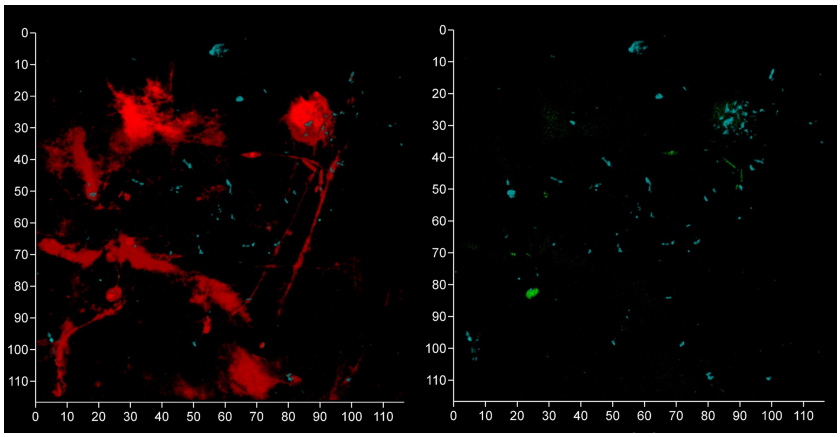

FIGURE 13
Oral streptococci group bacteria are less common near a fibrin clot. Shown here is a subgingival biofilm near a fibrin clot recovered using a PET film and imaged by CLSM after staining eDNA with Propidium iodide (red channel), bacterial eDNA with EUB 338 probe tagged with FITC (green channel), *Bacteroides–Porphyromonas–Prevotella* group with Bacto 1080 probe tagged with modified Acridine (blue channel), and the oral streptococci group with STR 405 probe with Cy5.5 (purple channel). The left image shows all four channels merged while the right image shows the green, blue and purple channels merged. The axis show 110 µm.

proteins which contribute to the clot when the fibrinogen polymerized. Representatives of the BPP group can neutralize the antibacterial activity of NET-associated host defense proteins using gingipain cysteine proteases (Bryzek et al., 2019) which cannot be done by other colonizers or by streptococci in particular. Analysis of the probe signals allowed us to compare the contribution of eDNA derived from both the BPP group and the oral streptococci group with the total bacterial eDNA which suggest that the anaerobes and streptococci may be the main biofilm-producers in the subgingival niche during periodontitis (Figure 14).

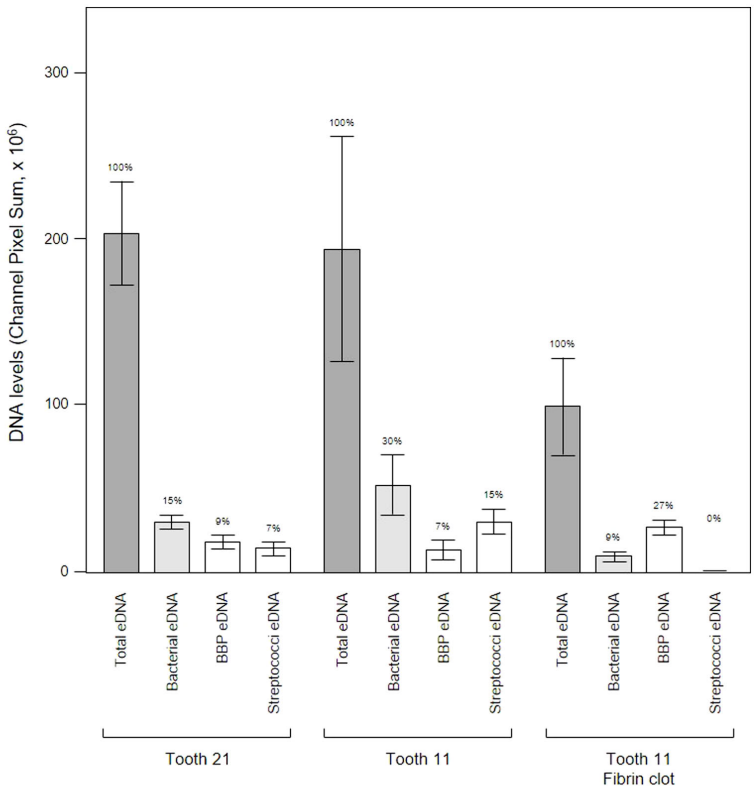

FIGURE 14
Bacterial eDNA origins differ between teeth and proximity to a fibrin clot. Shown here are the total, bacterial, *Bacteroides–Porphyromonas–Prevotella* group (BPP) and oral streptococci group eDNA levels determined from CLSM images of three subgingival biofilms recovered using PET films stained with Propidium iodide and FISH probes. Bars show means ± SD (n = 5 views from one biofilm sample per tooth) and percentage of total eDNA for each site is shown above the error bars.

Conclusion

Microbiologically induced inflammation processes underlying periodontitis take place in the subgingival niche. However, most investigations of periodontitis including dental calculus analysis have focused on the supragingival region and there is little information on the subgingival niche and the structure of the micro-landscapes during periodontitis. In this work, we undertook a comparative analysis of the EPS composition of subgingival-associated biofilms and microcosm-grown *in vitro* single-species biofilms including three isolates of oral streptococci. Amyloid genesis was found to be downregulated in the subgingival biofilms and eDNA revealed to be the main biofilm matrix component. Subsequent comparative analysis confirmed that the amount of eDNA in subgingival biofilms was higher than the bacterial biofilms normally generated including the leading eDNA producer *P. aeruginosa* PA01. FISH analysis of subgingival micro-landscapes sampled during periodontal disease revealed that host eDNA was dominant with only 8 – 21% of the total produced by periodontal pathogens. The main source of the host eDNA appears to be immunocompetent cells activated following periodontitis and is therefore a major factor of persistence and pathogenesis while eDNA from the *Bacteroides–Porphyromonas–Prevotella* and oral streptococci groups suggest that these may be the most important biofilm-formers during periodontal disease.

Data availability statement

The raw data supporting the conclusions of this article will be made available by the authors, without undue reservation.

Ethics statement

The studies involving humans were approved by the Ethics Committee of from the Shupyk National Healthcare University of Ukraine. The studies were conducted in accordance with the local legislation and institutional requirements. The participants provided their written informed consent to participate in this study.

Author contributions

MSK: Conceptualization, Data curation, Formal analysis, Funding acquisition, Investigation, Writing – original draft. OM: Conceptualization, Data curation, Formal analysis, Funding acquisition, Methodology, Project administration, Resources, Supervision, Validation, Writing – original draft, Visualization, Writing –review & editing. SK: Investigation, Writing – original draft. IM: Investigation, Writing – original draft. KR: Investigation, Writing – original draft. VP: Investigation, Writing – original draft. OI: Investigation, Writing – original draft. OK: Investigation, Writing – original draft. IK: Investigation, Writing – original draft. GP: Visualization, Writing – review & editing, Writing – original draft. AJS: Visualization, Writing – review & editing, Writing – original draft.

Funding

The author(s) declare that no financial support was received for the research, authorship, and/or publication of this article. OM was individually supported with the individual research grant #2008-VSE by STCU.

Acknowledgments

OM thanks STCU and Dr Mykola Lubiv and for their individual research grant #2008-VSE "Etiology of extracellular DNA in pathogenic biofilms associated with periodontitis" founded by the Virtual Scientist Engagement Fellowship Program for Ukrainian Scientists. OM also thanks the Krzysztof Skubiszewski Foundation and Dr Marcin Skubiszewski for their support through the program for financial aid to scholars who are victims of the ongoing aggression of Russia and Belarus against Ukraine. The authors thank Prof. Sergiy M. Yarmoluk, Department of Biomedicinal Chemistry, Institute of Molecular Biology and Genetics, National Academy of Sciences of Ukraine, for samples of Experimental Stain 986. During the manuscript revision, our co-author, collaborator, and dear friend Dr. Andrew Spiers unexpectedly passed away on March 19. We deeply appreciate the time he dedicated to us. OM expresses gratitude to Dr. Spiers for 18 years of mentoring, supervision, training, motivation, productive scientific discussions, outstanding projects, and the significant impact he had on her life.

Conflict of interest

The authors declare that the research was conducted in the absence of any commercial or financial relationships that could be construed as a potential conflict of interest.

Publisher's note

All claims expressed in this article are solely those of the authors and do not necessarily represent those of their affiliated organizations, or those of the publisher, the editors and the reviewers. Any product that may be evaluated in this article, or claim that may be made by its manufacturer, is not guaranteed or endorsed by the publisher.

Supplementary material

The Supplementary Material for this article can be found online at: https://www.frontiersin.org/articles/10.3389/fcimb.2024.1374817/full#supplementary-material

References

Amann, R. I., Binder, B. J., Olson, R. J., Chisholm, S. W., Devereux, R., and Stahl, D. A. (1990). Combination of 16S rRNA-targeted oligonucleotide probes with flow cytometry for analyzing mixed microbial populations. *Appl. Environ. Microbiol.* 56, 1919–1925. doi: 10.1128/aem.56.6.1919-1925.1990

Amano, A., Nakagawa, I., Okahashi, N., and Hamada, N. (2004). Variations of *Porphyromonas gingivalis* fimbriae in relation to microbial pathogenesis. *J. Periodontal. Res.* 39, 136–142. doi: 10.1111/j.1600-0765.2004.00719.x

Ansiliero, R., Gelinski, J. M. L. N., Samistraro, Q. L., Baratto, C. M., Almeida, C. A., and Locatelli, C. (2021). Pathogenic microbial profile and antibiotic resistance associated with periodontitis. *Indian J. Microbiol.* 61, 55–65. doi: 10.1007/s12088-020-00914-2

Arslan, S. Y., Leung, K. P., and Wu, C. D. (2009). The effect of lactoferrin on oral bacterial attachment. *Oral. Microbiol. Immunol.* 24, 411–416. doi: 10.1111/j.1399-302X.2009.00537.x

Barbesti, S., Citterio, S., Labra, M., Baroni, M. D., Neri, M. G., and Sgorbati, S. (2000). Two and three-color fluorescence flow cytometric analysis of immunoidentified viable bacteria. *Cytometry* 40, 214–218. doi: 10.1002/1097-0320(20000701)40:3<214::AID-CYTO6>3.0.CO;2-M

Besingi, R. N., Wenderska, I. B., Senadheera, D. B., Cvitkovitch, D. G., Long, J. R., Wen, Z. T., et al. (2017). Functional amyloids in *Streptococcus mutans*, their use as targets of biofilm inhibition and initial characterization of SMU_63c. *Microbiology* 163, 488–501. doi: 10.1099/mic.0.000443

Bryzek, D., Ciaston, I., Dobosz, E., Gasiorek, A., Makarska, A., Sarna, M., et al. (2019). Triggering NETosis via protease-activated receptor (PAR)-2 signaling as a mechanism of hijacking neutrophils function for pathogen benefits. *PloS Pathog.* 15, e1007773. doi: 10.1371/journal.ppat.1007773

Campoccia, D., Montanaro, L., and Arciola, C. R. (2021). Extracellular DNA (eDNA). A major ubiquitous element of the bacterial biofilm architecture. *Int. J. Mol. Sci.* 22, 9100. doi: 10.3390/ijms22169100

Casado, P. L., Otazu, I. B., Balduino, A., de Mello, W., Barboza, E. P., and Duarte, M. E. (2011). Identification of periodontal pathogens in healthy periimplant sites. *Implant. Dentistry.* 20, 226–235. doi: 10.1097/ID.0b013e3182199348

Chernii, S. V., Moshynets, O. V., Aristova, D. I., Kryvorotenko, D. V., Losytskyy, M., Iungin, O. S., et al. (2021). Benzoxazole styrylcyanine dye as a fluorescent probe for functional amyloid visualization in *Staphylococcus aureus* ATCC25923 biofilm. *Biopolym. Cell.* 37, 447–458. doi: 10.7124/bc.000A6A

Chin, M. Y., Busscher, H. J., Evans, R., Noar, J., and Pratten, J. (2006). Early biofilm formation and the effects of antimicrobial agents on orthodontic bonding materials in a parallel plate flow chamber. *Eur. J. Orthod.* 28, 1–7. doi: 10.1093/ejo/cji094

Cueno, M. E., Nagano, K., Imai, K., Tamura, M., Yoshimura, F., and Ochiai, K. (2015). *Ab initio* modeling approach towards establishing the structure and docking orientation of the *Porphyromonas gingivalis* FimA. *J. Mol. Graph. Model.* 55, 65–71. doi: 10.1016/j.jmgm.2014.11.001

Diaz, P. I., and Valm, A. M. (2020). Microbial interactions in oral communities mediate emergent biofilm properties. *J. Dent. Res.* 99, 18–25. doi: 10.1177/0022034519880157

Ding, P. H., Yang, M. X., Wang, N. N., Jin, L. J., Dong, Y., Cai, X., et al. (2020). *Porphyromonas gingivalis*-induced NLRP3 inflammasome activation and its downstream interleukin-1β release depend on caspase-4. *Front. Microbiol.* 11. doi: 10.3389/fmicb.2020.01881

Domenech, M., García, E., Prieto, A., and Moscoso, M. (2013). Insight into the composition of the intercellular matrix of *Streptococcus pneumoniae* biofilms. *Environ. Microbiol.* 15, 502–516. doi: 10.1111/j.1462-2920.2012.02853.x

Doré, J., Sghir, A., Hannequart-Gramet, G., Corthier, G., and Pochart, P. (1998). Design and evaluation of a 16S rRNA-targeted oligonucleotide probe for specific detection and quantitation of human faecal *Bacteroides* populations. *Syst. Appl. Microbiol.* 21, 65–71. doi: 10.1016/S0723-2020(98)80009-X

Emery, D. C., Cerajewska, T. L., Seong, J., Davies, M., Paterson, A., Allen-Birt, S. J., et al. (2021). Comparison of blood bacterial communities in periodontal health and periodontal disease. *Front. Cell Infect. Microbiol.* 10. doi: 10.3389/fcimb.2020.577485

Esparbès, P., Legrand, A., Bandiaky, O. N., Chéraud-Carpentier, M., Martin, H., Montassier, E., et al. (2021). Subgingival microbiota and cytokines profile changes in patients with periodontitis: a pilot study comparing healthy and diseased sites in the same oral cavities. *Microorganisms* 9, 2364. doi: 10.3390/microorganisms9112364

Espíndola, L. C. P., Picão, R. C., Mançano, S. M. C. N., Martins do Souto, R., and Colombo, A. P. V. (2022). Prevalence and antimicrobial susceptibility of Gram-negative bacilli in subgingival biofilm associated with periodontal diseases. *J. Periodontol.* 93, 69–79. doi: 10.1002/JPER.20-0829

Gallo, P. M., Rapsinski, G. J., Wilson, R. P., Oppong, G. O., Sriram, U., Goulian, M., et al. (2015). Amyloid-DNA composites of bacterial biofilms stimulate autoimmunity. *Immunity* 42, 1171–1184. doi: 10.1016/j.immuni.2015.06.002

Granger, V., Faille, D., Marani, V., Noël, B., Gallais, Y., Szely, N., et al. (2017). Human blood monocytes are able to form extracellular traps. *J. Leukoc. Biol.* 102, 775–781. doi: 10.1189/jlb.3MA0916-411R

Guenther, F., Stroh, P., Wagner, C., Obst, U., and Hänsch, G. M. (2009). Phagocytosis of staphylococci biofilms by polymorphonuclear neutrophils: S. aureus and *S. epidermidis* differ with regard to their susceptibility towards the host defense. *Int. J. Artif. Organs.* 32, 565–573. doi: 10.1177/039139880903200905

Günther, F., Wabnitz, G. H., Stroh, P., Prior, B., Obst, U., Samstag, Y., et al. (2009). Host defence against *Staphylococcus aureus* biofilms infection: phagocytosis of biofilms by polymorpho- nuclear neutrophils (PMN). *Mol. Immunol.* 46, 1805–1813. doi: 10.1016/j.molimm.2009.01.020

Hannig, C., Hannig, M., Rehmer, O., Braun, G., Hellwig, E., and Al-Ahmad, A. (2007). Fluorescence microscopic visualization and quantification of initial bacterial colonization on enamel *in situ*. *Arch. Oral. Biol.* 52, 1048–1056. doi: 10.1016/j.archoralbio.2007.05.006

Inagaki, S., Kuramitsu, H. K., and Sharma, A. (2005). Contact-dependent regulation of a *Tannerella forsythia* virulence factor, BspA, in biofilms. *FEMS Microbiol. Lett.* 249, 291–296. doi: 10.1016/j.femsle.2005.06.032

Jakubovics, N. S., Goodman, S. D., Mashburn-Warren, L., Stafford, G. P., and Cieplik, F. (2021). The dental plaque biofilm matrix. *Periodontol. 2000.* 86, 32–56. doi: 10.1111/prd.12361

Jesaitis, A. J., Franklin, M. J., Berglund, D., Sasaki, M., Lord, C. I., Bleazard, J. B., et al. (2003). Compromised host defense on *Pseudomonas aeruginosa* biofilms: characterization of neutrophil and biofilm interactions. *J. Immunol.* 171, 4329–4339. doi: 10.4049/jimmunol.171.8.4329

Könönen, E., Gursoy, M., and Gursoy, U. K. (2019). Periodontitis: A multifaceted disease of tooth-supporting tissues. *J. Clin. Med.* 8, 1135. doi: 10.3390/jcm8081135

Kornman, K. S. (2008). Mapping the pathogenesis of periodontitis: a new look. *J. Periodontol.* 79, 1560–1568. doi: 10.1902/jop.2008.080213

Koza, A., Kusmierska, A., McLaughlin, K., Moshynets, O., and Spiers, A. J. (2017). Adaptive radiation of P. fluorescens SBW25 in experimental microcosms provides an understanding of the evolutionary ecology and molecular biology of A-L interface biofilm-formation. *FEMS Microbiol. Lett.* 364. doi: 10.1093/femsle/fnx109

Koza, A., Moshynets, O., Otten, W., and Spiers, A. J. (2011). Environmental modification and niche construction: Developing oxygen gradients in static liquid microcosms drives the evolution of the biofilm-forming Wrinkly Spreader. *ISME. J.* 5, 665–673. doi: 10.1038/ismej.2010.156

Krautgartner, W. D., Klappacher, M., Hannig, M., Obermayer, A., Hartl, D., Marcos, V., et al. (2010). Fibrin mimics neutrophil extracellular traps in SEM. *Ultrastruct. Pathol.* 34, 226–231. doi: 10.3109/01913121003725721

Kuboniwa, M., and Lamont, R. J. (2010). Subgingival biofilm formation. *Periodontol. 2000.* 52, 38–52. doi: 10.1111/j.1600-0757.2009.00311.x

Larsen, T., and Fiehn, N. E. (2017). Dental biofilm infections - an update. *APMIS* 125, 376–384. doi: 10.1111/apm.12688

Loimaranta, V., Hytönen, J., Pulliainen, A. T., Sharma, A., Tenovuo, J., Strömberg, N., et al. (2009). Leucine-rich repeats of bacterial surface proteins serve as common pattern recognition motifs of human scavenger receptor gp340. *J. Biol. Chem.* 284, 18614–18623. doi: 10.1074/jbc.M900581200

Mark Welch, J. L., Rossetti, B. J., Rieken, C. W., Dewhirst, F. E., and Borisy, G. G. (2016). Biogeography of a human oral microbiome at the micron scale. *Proc. Natl. Acad. Sci. U.S.A.* 113, E791–E800. doi: 10.1073/pnas.1522149113

McLaughlin, K., Folorunso, A. O., Deeni, Y. Y., Foster, D., Gorbatiuk, O., Hapca, S. M., et al. (2017). Biofilm formation and cellulose expression by *Bordetella avium* 197N, the causative agent of bordetellosis in birds and an opportunistic respiratory pathogen in humans. *Res. Microbiol.* 168, 419–430. doi: 10.1016/j.resmic.2017.01.002

Moshynets, O. V., Baranovskyi, T. P., Cameron, S., Iungin, O. S., Pokholenko, I., Jerdan, R., et al. (2022a). Azithromycin possesses biofilm–inhibitory activity and potentiates non-bactericidal colistin methanesulfonate (CMS) and polymyxin B against *Klebsiella pneumonia*. *PloS One* 17, e0270983. doi: 10.1371/journal.pone.0270983

Moshynets, O. V., Baranovskyi, T. P., Iungin, O. S., Kysil, N. P., Metelytsia, L. O., Pokholenko, I., et al. (2022b). eDNA inactivation and biofilm inhibition by the polymeric biocide polyhexamethylene guanidine hydrochloride (PHMG-Cl). *Int. J. Mol. Sci.* 23, 731. doi: 10.3390/ijms23020731

Moshynets, O., Boretska, M., and Spiers, A. J. (2013). "From Winogradsky's column to contemporary research using bacterial microcosms," in *Microcosms: Ecology, Biological Implications and Environmental Impact, April*. Ed. C. C. Harris (Nova Publisher), 1–27.

Moshynets, O., Chernii, S., Chernii, V., Losytskyy, M., Karakhim, S., Czerwieniec, R., et al. (2020). Fluorescent β-ketoenole AmyGreen dye for visualization of amyloid components of bacterial biofilms. *Methods Appl. Fluoresc.* 8, 035006. doi: 10.1088/2050-6120/ab90e0

Moshynets, O. V., Foster, D., Karakhim, S. A., McLaughlin, K., Rogalsky, S. P., Rymar, S. Y., et al. (2018). Examining c-di-GMP and possible QS regulation in *Pseudomonas fluorescens* SBW25: links between intra and inter-cellular regulation benefits community cooperative activities such as biofilm formation. *Ukr. Biochem. J.* 90, 17–31. doi: 10.15407/ubj90.03.017

Moshynets, O., Koza, A., Dello Sterpaio, P., Kordium, V., and Spiers, A. J. (2011). Up-dating the Cholodny method using PET films to sample microbial communities in soil. *Biopolym. Cell.* 27, 199–205. doi: 10.7124/bc.0000BA

Moshynets, O. V., Pokholenko, I., Iungin, O., Potters, G., and Spiers, A. J. (2022c). eDNA, amyloid fibers and membrane vesicles identified in *Pseudomonas fluorescens* SBW25 biofilms. *Int. J. Mol. Sci.* 23, 15096. doi: 10.3390/ijms232315096

Moshynets, O. V., Shpylova, S. P., Kordium, V. A., and Potters, G. (2012). Visualisation of endophytic bacteria in *Phyllostachys* sp. and *Fargesia* sp. *Bamboo. Sci. Culture.* 25, 11–18.

Moshynets, O. V., and Spiers, A. J. (2016). "Viewing biofilms within the larger context of bacterial aggregations," in *Microbial Biofilms - Importance and Applications*. Eds. D. Dhanasekaran and N. Thajuddin (InTech Press). doi: 10.5772/62912

Naginyte, M., Do, T., Meade, J., Devine, D. A., and Marsh, P. D. (2019). Enrichment of periodontal pathogens from the biofilms of healthy adults. *Sci. Rep.* 9, 5491. doi: 10.1038/s41598-019-41882-y

Nibali, L., Bayliss-Chapman, J., Almofareh, S. A., Zhou, Y., Divaris, K., and Vieira, A. R. (2019). What is the heritability of periodontitis? A systematic review. *J. Dent. Res.* 98, 632–641. doi: 10.1177/0022034519842510

Oveisi, M., Shifman, H., Fine, N., Sun, C., Glogauer, N., Senadheera, D., et al. (2019). Novel assay to characterize neutrophil responses to oral biofilms. *Infect. Immun.* 87, e00790–e00718. doi: 10.1128/IAI.00790-18

Palaniyar, N., Clark, H., Nadesalingam, J., Shih, M. J., Hawgood, S., and Reid, K. B. (2005). Innate immune collectin surfactant protein D enhances the clearance of DNA by macrophages and minimizes anti-DNA antibody generation. *J. Immunol.* 174, 7352–7358. doi: 10.4049/jimmunol.174.11.7352

Paster, B. J., Bartoszyk, I., and Dewhirst, F. E. (1998). Identification of oral streptococci using PCR-based, reverse-capture, checkerboard hybridization. *Methods Cell Sci.* 20, 223–231. doi: 10.1023/A:1009715710555

Rezende, G., Arthur, R. A., Lamers, M. L., and Hashizume, L. N. (2019). Structural organization of dental biofilm formed *in situ* in the presence of sucrose associated to maltodextrin. *Braz. Dent. J.* 30, 36–42. doi: 10.1590/0103-6440201902183

Rickard, A. H., Gilbert, P., High, N. J., Kolenbrander, P. E., and Handley, P. S. (2003). Bacterial coaggregation: an integral process in the development of multi-species biofilms. *Trends Microbiol.* 11, 94–100. doi: 10.1016/s0966-842x(02)00034-3

Robertson, M., Hapca, S. M., Moshynets, O., and Spiers, A. J. (2013). Air-liquid interface biofilm formation by psychrotrophic pseudomonads recovered from spoilt meat. *Antonie. van. Leeuwenhoek.* 103, 251–259. doi: 10.1007/s10482-012-9796-x

Rostami, N., Shields, R. C., Yassin, S. A., Hawkins, A. R., Bowen, L., Luo, T. L., et al. (2017). A critical role for extracellular DNA in dental plaque formation. *J. Dent. Res.* 96, 208–216. doi: 10.1177/0022034516675849

Sambrook, J., Fritsch, E. F., and Maniatis, T. (1989). *Molecular Cloning: A Laboratory Manual. 2nd ed* (New York: Cold Spring Harbor Laboratory Press).

Schwartz, K., Ganesan, M., Payne, D. E., Solomon, M. J., and Boles, B. R. (2016). Extracellular DNA facilitates the formation of functional amyloids in Staphylococcus aureus biofilms. *Mol. Microbiol.* 99, 123–134. doi: 10.1111/mmi.13219

Sol, A., Ginesin, O., Chaushu, S., Karra, L., Coppenhagen-Glazer, S., Ginsburg, I., et al. (2013). LL-37 opsonizes and inhibits biofilm formation of *Aggregatibacter actinomycetemcomitans* at sub-bactericidal concentrations. *Infect. Immun.* 81, 3577–3585. doi: 10.1128/IAI.01288-12

Stroh, P., Günther, F., Meyle, E., Prior, B., Wagner, C., and Hänsch, G. M. (2011). Host defence against *Staphylococcus aureus* biofilms by poly- morphonuclear neutrophils: oxygen radical production but not phagocytosis depends on opsonisation with immunoglobulin G. *Immunobiology* 216, 351–357. doi: 10.1016/j.imbio.2010.07.009

Subendu, S. (2020). Release mechanisms and molecular interactions of *Pseudomonas aeruginosa* extracellular DNA. *Appl. Microbiol. Biotechnol.* 104, 6549–6564. doi: 10.1007/s00253-020-10687-9

Taglialegna, A., Lasa, I., and Valle, J. (2016). Amyloid structures as biofilm matrix scaffolds. *J. Bacteriol.* 198, 2579–2588. doi: 10.1128/JB.00122-16

Tawakoli, P. N., Neu, T. R., Busck, M. M., Kuhlicke, U., Schramm, A., Attin, T., et al. (2017). Visualizing the dental biofilm matrix by means of fluorescence lectin-binding analysis. *J. Oral. Microbiol.* 9, 1345581. doi: 10.1080/20002297.2017.1345581

Tolker-Nielsen, T., and Sternberg, C. (2011). Growing and analyzing biofilms in flow chambers. *Curr. Protoc. Microbiol.* doi: 10.1002/9780471729259.mc01b02s21. Chapter 1:Unit 1B.2.

Tursi, S. A., Lee, E. Y., Medeiros, N. J., Lee, M. H., Nicastro, L. K., Buttaro, B., et al. (2017). Bacterial amyloid curli acts as a carrier for DNA to elicit an autoimmune response via TLR2 and TLR9. *PloS Pathog.* 13, e1006315. doi: 10.1371/journal.ppat.1006315

Vanaja, S. K., Russo, A. J., Behl, B., Banerjee, I., Yankova, M., Deshmukh, S. D., et al. (2016). Bacterial outer membrane vesicles mediate cytosolic localization of LPS and caspase-11. *Activation. Cell* 165, 1106–1119. doi: 10.1016/j.cell.2016.04.015

van Winkelhoff, A. J., Loos, B. G., van der Reijden, W. A., and van der Velden, U. (2002). *Porphyromonas gingivalis, Bacteroides forsythus* and other putative periodontal pathogens in subjects with and without periodontal destruction. *Clin. Periodontol.* 29, 1023–1028. doi: 10.1034/j.1600-051x.2002.291107.x

Vitkov, L., Klappacher, M., Hannig, M., and Krautgartner, W. D. (2009). Extracellular neutrophil traps in periodontitis. *J. Periodontal. Res.* 44, 664–672. doi: 10.1111/j.1600-0765.2008.01175.x

Vitkov, L., Muñoz, L. E., Schoen, J., Knopf, J., Schauer, C., Minnich, B., et al. (2021). Neutrophils orchestrate the periodontal pocket. *Front. Immunol.* 12. doi: 10.3389/fimmu.2021.788766

Volinska, T. B., and Bondarchuk, O. V. (2016). Clinical experience of the use of the test-system Stomatoflor for the evaluation of microbiota of periodontal pocket with a PCR method in a real-time. *Implantol. Periodontol. Osteol.* 2, 84–89.

Volynets, G. P., Barthels, F., Hammerschmidt, S. J., Moshynets, O. V., Lukashov, S. S., Starosyla, S. A., et al. (2022). Identification of novel small-molecular inhibitors of *Staphylococcus aureus* sortase A using hybrid virtual screening. *J. Antibiot.* 75, 321–332. doi: 10.1038/s41429-022-00524-8

Walker, T. S., Tomlin, K. L., Worthen, G. S., Poch, K. R., Lieber, J. G., Saavedra, M. T., et al. (2005). Enhanced *Pseudomonas aeruginosa* biofilm development mediated by human neutrophils. *Infect. Immun.* 73, 3693–3701. doi: 10.1128/IAI.73.6.3693-3701.2005

Wecke, J., Kersten, T., Madela, K., Moter, A., Göbel, U. B., Friedmann, A., et al. (2000). A novel technique for monitoring the development of bacterial biofilms in human periodontal pockets. *FEMS Microbiol. Lett.* 191, 95–101. doi: 10.1111/j.1574-6968.2000.tb09324.x

Wood, S. R., Kirkham, J., Marsh, P. D., Shore, R. C., Nattress, B., and Robinson, C. (2000). Architecture of intact natural human plaque biofilms studied by confocal laser scanning microscopy. *J. Dent. Res.* 79, 21–27. doi: 10.1177/00220345000790010201

Ximénez-Fyvie, L. A., Haffajee, A. D., and Socransky, S. S. (2000). Comparison of the microbiota of supra- and subgingival plaque in health and periodontitis. *J. Clin. Periodontol.* 27, 648–657. doi: 10.1034/j.1600-051x.2000.027009648.x

Yan, Z., Yin, M., Chen, J., and Li, X. (2020). Assembly and substrate recognition of curli biogenesis system. *Nat. Commun.* 11, 241. doi: 10.1038/s41467-019-14145-7

Yousefi, S., Simon, D., Stojkov, D., Karsonova, A., Karaulov, A., and Simon, H. U. (2020). *In vivo* evidence for extracellular DNA trap formation. *Cell Death Dis.* 11, 300. doi: 10.1038/s41419-020-2497-x

Zijnge, V., van Leeuwen, M. B., Degener, J. E., Abbas, F., Thurnheer, T., Gmür, R., et al. (2010). Oral biofilm architecture on natural teeth. *PloS One* 5, e9321. doi: 10.1371/journal.pone.0009321

Анотація: *Відомо, що захворювання пародонту пов'язані з полімікробними біоплівки та активацією запалення. Більш глибоке розуміння підясенного цитологічного (мікро) ландшафту, ролі езоклітинної ДНК (еДНК) при пародонтиті та розуміння ролі імунної еДНК господаря в запаленні при пародонтиті може покращити наше розуміння механізмів важких форм пародонтиту. Аналіз під'ясенної біоплівки за допомогою модифікованого методу Холодного виявив низький вміст бактеріальних амілоїдів та високий рівень еДНК в пародонтних біоплівках. Встановлено, що еДНК бактерій становить менше третини загальної еДНК в цитологічному ландшафті при пародонтиті. Вірогідно, що переважна кількість еДНК при пародонтиті вивільняється з нейтрофільних позаклітинних пасток і може мати велике значення у розвитку біоплівок, що викликають пародонтит. Таким чином, еДНК активованих імунокомпетентних клітин господаря може бути основним фактором персистенції бактерій і розвитку патологічного запалення при пародонтиті*.

4.2. Біоплівки *Klebsiella pneumoniae* як форма інфекційного процесу та комбінована анти-біоплівкова терапія клебсієльозів

Резистентність до антибіотиків є однією з найсерйозніших загроз людству. У всьому світі зростає ризик зараження бактеріальними інфекціями, стійкими до багатьох препаратів або цілком резистентних до них під час або після перебування в лікарні. За даними ВООЗ (2009), загалом інфекції, пов'язані з наданням медичної допомоги, у Європі призводять до смерті принаймні в 2,7% випадків і спричиняють 135 000 смертей на рік. ECDC інформують про принаймні 135 000 смертей від антибіотикорезистеності щорічно. За даними Національної експертної групи з інфекційного контролю (https://negic.ua/), в Україні щороку реєструється до 1 мільйона випадків внутрішньолікарняних інфекцій і 50 000 смертей (4). Війни часто призводять до епідеміологічних спалахів стійкості до антибіотиків (130-132). Війна в Україні також суттєво вплинула на локальне та глобальне поширення антимікробної резистентності (133-135). Війна кидає складний виклик системі охорони здоров'я, який є особливо важкими в умовах поширення антибіотикорезистентості (134, 136-137).

Російська війна проти України різко вплинула на антибіотикорезистентність на місцевому та національному рівнях, та вплинуло на поширення антибіотикорезистентності глобально (133, 138-140). Одним із драматичних наслідків російсько-української війни є поява суперрезистентних бактерій, або супербактерій, в тому числі майже повністю резистентних, або XDR (extensively drug-resistant) штамів, та резистентних до всіх лікарських засобів – так звані PDR (pandrug resistant) штами. PDR бактерії є стійкими до всіх доступних антибіотиків, тому інфекції, які вони викликають, не мають стандартних терапевтичних підходів для лікування. Це не тільки становить серйозну загрозу життю госпіталізованих пацієнтів, але також є викликом для інфекційного контролю та в цілому системі охорони здоров'я (133, 141). Крім того, висока вартість резервних антибіотиків далі загострює проблеми, з якими стикається медична система (133, 142). В 2021 р. ВООЗ оновила класифікацію антибіотиків AWaRe; в неї включено вісім резервних антибіотиків для лікування XDR патогенів. До цієї групи резервних антибіотиків відносять сефідерокол (cefiderocol), цефтазидим/авібактам, колістин, фосфоміцин, лінезолід, меропенем/ваборбактам, плазоміцин і поліміксин B (2021 AWaRe classification (who.int)). Проте їх відсутність і високі ціни перешкоджають їх доступності, особливо в

умовах конфлікту з обмеженими ресурсами. Зокрема, наразі в Україні відсутні сефідерокол, парентеральна форма фосфоміцину, меропенем/ваборбактам, плазоміцин; лінезолід є антибіотиком для грам-позитивної флори; колістин є антибіотиком із дуже слабкою терапевтичною ефективністю (4), доступність поліміксин В є дуже обмеженою, крім того, резистентність на поліміксини, до яких відносять колістин і поліміксин В, вже не є рідкістю в українських госпітальних ізолятах, а цефтазидим/авібактам є високовартісним і через це недоступним для широкого використання. Цей дефіцит потенційно ефективних антибіотиків додає ще один рівень складності лікування бойових травмам та підвищує на максимальний рівень загрозу здоров'ю госпіталізованих пацієнтів.

В таких жорстких умовах критичного дефіциту ефективних антибіотиків і розвитку панрезистентності єдиним практичним рішенням є пошук нових терапевтичних підходів на основі комбінацій антибіотиків, що є доступними для терапії. Саме тому вже близько 10 років триває робота по вивченню терапевтичної ефективності різноманітних комбінації на основі колістину (143), карбапенемів і тайгецикліну (144) і порівняння мототерапії і комбінацій, в тому числі і з новітнім сефідероколом (145). Daikos et al., 2014 довели, що за умов XDR/PDR фенотипу інфекції, що викликає сепсис, кращий відсоток виживання дає саме комбінаційна терапія (27,2%), в той час як монотерапія призводила до смертності у 44,4%. Терапія комбінацією антибіотиків при лікуванні XDR грам-негативних інфекцій новим і поки що недоступним в Україні антибіотиком сефідероколом вочевидь також не стане ефективним рішенням, особливо у випадку українських повоєнних госпітальних ізолятів (133, 146).

Принциповою новизною результатів цього підрозділу є встановлення і дослідження нових унікальних властивостей азитроміцину як антибіоплівкого антибіотику у складі комплексної терапії XDR/PDR грам-негативних бактерій, зокрема, клебсієльозів.

Основні результати, отримані в цьому підрозділі дисертації опубліковані в роботах автора (4, 135, 147, 148).

PLOS ONE

RESEARCH ARTICLE

Azithromycin possesses biofilm–inhibitory activity and potentiates non-bactericidal colistin methanesulfonate (CMS) and polymyxin B against *Klebsiella pneumonia*

Olena V. Moshynets[1]*, Taras P. Baranovskyi[2,3], Scott Cameron[4], Olga S. Iungin[1,5], Ianina Pokholenko[1], Robyn Jerdan[4], Aleksandr Kamyshnyi[6], Alexey A. Krikunov[7], Viktoria V. Potochilova[3], Kateryna L. Rudnieva[3], Andrew J. Spiers[4]*

1 Institute of Molecular Biology and Genetics of the National Academy of Sciences of Ukraine, Kyiv, Ukraine, **2** Shupyk National Healthcare University of Ukraine, Kyiv, Ukraine, **3** Kyiv Regional Clinical Hospital, Kyiv, Ukraine, **4** School of Applied Sciences, Abertay University, Dundee, United Kingdom, **5** Kyiv National University of Technologies and Design, Kyiv, Ukraine, **6** I. Horbachevsky Ternopil National Medical University, Ternopil, Ukraine, **7** Amosov National Institute of Cardiovascular Surgery, Kyiv, Ukraine

* moshynets@gmail.com (OVM); a.spiers@abertay.ac.uk (AJS)

Check for updates

OPEN ACCESS

Citation: Moshynets OV, Baranovskyi TP, Cameron S, Iungin OS, Pokholenko I, Jerdan R, et al. (2022) Azithromycin possesses biofilm–inhibitory activity and potentiates non-bactericidal colistin methanesulfonate (CMS) and polymyxin B against *Klebsiella pneumonia*. PLoS ONE 17(7): e0270983. https://doi.org/10.1371/journal.pone.0270983

Editor: Iddya Karunasagar, Nitte University, INDIA

Received: March 4, 2022

Accepted: June 21, 2022

Published: July 1, 2022

Copyright: © 2022 Moshynets et al. This is an open access article distributed under the terms of the Creative Commons Attribution License, which permits unrestricted use, distribution, and reproduction in any medium, provided the original author and source are credited.

Data Availability Statement: All relevant data are within the article and its Supporting Information files.

Funding: OMV received the research grant 'Development of combined therapy for severe Klebsiella pneumoniae-associated nosocomial infections to overcome the antibiotic resistance' (2020.02/0246) from the National Research Foundation of Ukraine (https://nrfu.org.ua/en/). The funder had no role in study design, data collection

Abstract

Novel antibiotic combinations may act synergistically to inhibit the growth of multidrug-resistant bacterial pathogens but predicting which combination will be successful is difficult, and standard antimicrobial susceptibility testing may not identify important physiological differences between planktonic free-swimming and biofilm-protected surface-attached sessile cells. Using a nominally macrolide-resistant model *Klebsiella pneumoniae* strain (ATCC 10031) we demonstrate the effectiveness of several macrolides in inhibiting biofilm growth in multi-well plates, and the ability of azithromycin (AZM) to improve the effectiveness of the antibacterial last-agent-of-choice for *K. pneumoniae* infections, colistin methanesulfonate (CMS), against biofilms. This synergistic action was also seen in biofilm tests of several *K. pneumoniae* hospital isolates and could also be identified in polymyxin B disc-diffusion assays on azithromycin plates. Our work highlights the complexity of antimicrobial-resistance in bacterial pathogens and the need to test antibiotics with biofilm models where potential synergies might provide new therapeutic opportunities not seen in liquid culture or colony-based assays.

Introduction

Gram-negative infections are recognised as a serious global health problem with multi- and pan-drug resistant (M/PDR) strains included in the World Health Organisation's list of antibiotic-resistant 'priority pathogens' that pose the greatest threat to human health. This includes *Klebsiella pneumoniae* which is a leading nosocomial causative agent of Gram-negative bacterial infections in Ukraine [1, 2] and the frequency of M/PDR stains associated with a high mortality rate is increasing in eastern Europe and worldwide [3–5] and poses a significant challenge for the treatment of *K. penumoniae* infections.

and analysis, decision to publish, or preparation of the manuscript.

Competing interests: The authors have declared that no competing interests exist.

An antibacterial last-agent-of-choice for M/PDR GNB strains is colistin methanesulfonate (CMS) (also known as colistimethate sodium and polymyxin E) which is an improved version of colistin sulfate [6, 7]. CMS is generally regarded as a 'weak antibiotic' with a low bactericidal activity and clinical failure of 79% against colistin-sensitive strains at 14 days, and 43% mortality at 28 days [8]. However, CMS has the advantage of reduced kidney toxicity compared to colistin sulfate, allowing higher concentrations to be used and overcoming the poor bioavailability of the active form colistin (COL). Increasing CMS dosage can raise serum COL levels to ~6 mg/L [9–12], but the minimum inhibitory concentration (MIC) breakpoint for COL-susceptible GNB is 2 mg/L and commonly used dosage CMS regimes have sub-optimal maximum serum concentration (C_{max}) / MIC ratios. An alternative to increasing C_{max} is to use antibiotic combinations such as COL-carbapenem, COL-tigecycline and COL-aminoglycoside, which are more effective against carbapenemase-producing GNB [5, 13] than monotherapy. The potentiation of weak antibiotics such as CMS with other antimicrobials may provide new therapeutic opportunities for the treatment of M/PDR Gram-negative bacterial infections.

However, not all antibiotic combinations make pharmaceutical sense and predictions made of the efficacy of antimicrobials acting alone may not be true when antibiotics are delivered in combination. More tests are needed to identify potential synergistic activity in antibacterial combinations using physiologically relevant concentrations. Antimicrobial susceptibility tests such as the Kirby-Bauer disc-diffusion assay [14, 15] which can be extended to identify synergistic actions between antibiotics [16–18] rely on colony growth across the surface of agar and may not accurately reflect the physiological and metabolic state of liquid culture (planktonic) bacterial cells or those encased in protective biofilms and adhered to surfaces. Biofilm-formation underlies the survival and persistence of many pathogens, providing phenotypic resistance or tolerance to therapy when genetic resistance might be restricted [19, 20]. However, there are some reports of antimicrobials such as azithromycin (AZM) which are effective against *Pseudomonas aeruginosa* biofilms but not against colonies or liquid cultures [21–24], suggesting that new therapeutic opportunities for the treatment of M/PDR Gram-negative bacterial infections might also be found in re-testing antimicrobials using a biofilm model system rather than conventional agar plate or liquid-culture–based assays.

K. pneumoniae and *P. aeruginosa* share some common characteristics including the ability to form biofilms as well as similar macrolide resistance mechanisms [25]. We therefore hypothesized that AZM or other macrolides which have no effect against *K. pneumoniae* liquid cultures or colonies [26], might instead be effective against biofilm-forming *K. pneumoniae* cells (the ability to form biofilms is common among *K. pneumoniae* isolates (e.g., 63–94% [27–29]) and MDR and biofilm-formation appear unlinked [29]). Moreover, we suggest that AZM or other macrolides acting as an anti-biofilm therapeutic agent might enhance the bactericidal effectiveness of CMS in a combined anti-*Klebsiella* therapy, as macrolides have been shown to potentiate CMS against both *K. pneumoniae* and *P. aeruginosa* [30]. Previously we have discussed the range of different aggregations bacteria form and key differences between classical biofilms, colonies, and liquid cultures [31]. In light of this and the recognition of the growing importance of biofilms in infections, the aims of our study were to evaluate the effectiveness of different macrolides in supressing biofilm growth by a model *K. pneumoniae* strain (ATCC 10031) [32–34] test the most effective macrolide suppressor in combination with CMS used in a range of physiologically-relevant concentrations, and then to test this combination using a collection of *K. pneumoniae* hospital isolates to evaluate the potential therapeutic benefit offered by a macrolide-CMS combination against *K. pneumoniae* biofilm–associated infections.

Materials and methods

Klebsiella strains

Klebsiella pneumoniae ATCC 10031 (Ukrainian National Collection ATCC) was used as a model strain for testing biofilm formation and free-living (planktonic) behaviour under different antibiotic treatments. Biofilm and planktonic responses to antibiotic treatment was also determined for eleven *K. pneumoniae* isolates from Ukrainian patients, including the multi-drug (MDR) strains UHI 329, UHI 1090, UHI 1609, UHI 1633 and UHI 166, and the non-MDR strains UHI 117, UHI 486, UHI 489, UHI 509, UHI 519 and UHI 520 [32] (see **S1 Table** for strain origins and antibiotic sensitivities; strains were selected without knowing whether they could form biofilms or not). All strains were stored as frozen stocks in 25 (v/v) % glycerol at -80˚C.

Culturing and antibiotics

Klebsiella were cultured aerobically at 37˚C using Luria-Bertani (LB) medium (10 g/L peptone, 5 g/L yeast extract and 10 g/L sodium chloride; 12 g/L agar added for plates [35]) and Muller Hinton Agar (OXOID, UK). Strains were recovered from frozen stocks on LB plates before initiating over-night shaken cultures to provide fresh inocula for experiments (direct inoculation from frozen stocks was found to reduce siderophore production and biofilm development considerably; unpublished observations). Culture densities and dilutions were determined by OD_{625} measurements using a Spectronic Helios Epsilon spectrophotometer (Thermo Fisher Scientific, UK) with 10 mm optical-path cuvettes.

Eight macrolide antibiotics were used for the main study and included Azithromycin (AZM; Pharmex Group, Ukraine), Clarithromycin (CLR; Abbott, Italy), Erythromycin (ERM; Vitaminy, Ukraine), Josamycin (JSM; Astellas Pharma, Japan), Midecamycin (MID; KRKA, Slovenia), Roxithromycin (ROX; Darnitsa, Ukraine), Spiramycin (SPM; Sanofi Aventis, Italy), and Tylosin (TYL; Ukrzoovetprompostach, Ukraine). Stock solutions containing 9 g/L of each antibiotic were prepared using DMSO as solvent and kept at -20˚C for no longer than 7 days before use. A 1 g/L stock solution of colistin methanesulfonate (CMS) (Forest Laboratories, UK) was prepared in water and used within 30 minutes of preparation. Discs containing antibiotics (HiMedia Laboratories, India) as well as AST-N332 cards for the VITEK 2 Advanced Expert System (bioMérieux, France) were used for antimicrobial susceptibility and sensitivity assays listed in **S1 Table**.

Confirming antimicrobial susceptibilities of the UHI strains

The Kirby-Bauer disc-diffusion assay [14, 15] was used to determine the antimicrobial susceptibility of the *K. pneumoniae* UHI strains. Mueller Hinton plates were spread with 200 μL of cell suspension prepared by diluting over-night cultures to 0.12–0.18 OD_{625} and allowed to dry before no more than five discs with different antibiotics per plate were applied. Susceptibility was then determined as the diameter (mm) of inhibition after incubation for two days and interpreted according to European Committee on Antimicrobial Susceptibility Testing (EUCAST) guidelines [26], HiMedia (for Cefoperazone/Sulbactam [36]), and the Ministry of Health of Ukraine (for Gatifloxacin [37]). β-lactamase genes were detected by PCR using DNA purified using AmpliSense DNA-sorb-B Nucleic Acid Extraction, MDR KPCOXA-48-FRT and MBL-FRT PCR kits (InterLabService, Russia). β-lactamase activity was determined with KPC&MBL&OXA-48 and ESBL+AmpC screen disc kits (Liofilchem, Italy) according to EUCAST guidelines [38]. AST-N332 cards were also used with the VITEK 2 Advanced Expert System to confirm the MDR strain phenotypes. Antimicrobial susceptibility testing of CMS

was performed with the broth microdilution assay SensiTest™ Colistin (Liofilchem, Italy) results interpreted according to EUCAST guidelines [26].

The Kirby-Bauer disc-diffusion assay was also used to determine whether an AZM and polymyxin B synergistic action could be detected for UHI. Mueller Hinton plates supplemented with 0, 3, 6, 9 mg/L AZM were spread with 200 μL of cell suspension prepared by diluting over-night cultures to 0.12–0.18 OD_{625} and allowed to dry before replicate polymyxin-B PB300U discs (n = 3) were applied. Susceptibility was then determined as the diameter (mm) of inhibition after incubation for two days.

Planktonic and biofilm growth assays

Planktonic growth assays of ATCC 10031 and the UHI strains was assessed in loosely lidded 30 ml glass vials which were incubated with shaking before assay. AZM and CSM were added to 6 mL LB vials to final concentrations of 0, 3, 6 and 9 mg/L AZM and 0, 2, 4, 6, 8, 12, 16, 18, 24, 28 and 32 mg/L CMS. Aliquots of over-night culture were added to replicate vials (n = 3) to ~5 x 10^6 CFU/mL and growth determined after 16 h incubation by removing 200 μL samples which were transferred to a polystyrene 96-well plate and OD_{570} measured using a BioTek ELx800 (BioTek Instruments, Winooski, VT, USA) plate reader.

In a preliminary assessment of biofilm formation in vials and polystyrene 96-well plates, ATCC 10031 and UHI solid-liquid (S-L) interface biofilms were observed. These were very fragile and there was no growth occurring in the liquid column and no visible sediment formed from the initial inoculum. However, these biofilms could not be reliably retained during washing and Crystal violet staining following standard procedures (e.g., [29]). We therefor decided to modify our approach and used direct OD_{570} measurements of biofilms in situ in unprocessed 96-well plates. 20 μL aliquots of over-night culture were used to inoculate replicate wells (n = 8 for individual macrolide assays and n = 3 for AZM–CSM assays) containing 200 μL LB with the appropriate antibiotics (0, 1, 3, 6 and 9 mg/L macrolide for the for individual macrolide assays, 0, 3, 6 and 9 mg/L AZM and 0, 2, 4, 6, 8, 12, 16, 18, 24, 28 and 32 mg/L CMS for the AZM–CSM assays). Growth (OD_{570}) was determined after 24–48 h static incubation using a BioTek ELx800 plate reader. Metabolic activity was also determined after adding MTT (3-(4,5-dimethylthiazol-2-yl)-2,5-diphenyltetrazolium bromide; Sigma-Aldrich, UK) to a final concentration of 0.05% (v/v) and a further incubation of 3 h (after [39]). Cells were recovered from each well by centrifugation at 6000 g for 15 minutes using an Eppendorf 5424 Microcentrifuge (Eppendorf, Hamburg, Germany). The cell pellet was dissolved in 250 μL of DMSO, 125 μL of which was transferred to a polystyrene 96-well plate and metabolic activity (A_{570}) measured using a BioTek ELx800 plate reader. We consistently found greater variation in A_{570} measurements of biofilm growth than in OD_{570} measurements which suggest that the MTT assay was the technically more difficult assay to perform.

Statistical analyses

Experiments were performed with replicates (n) and data examined using JMP v12 statistical software (SAS Institute Inc.). Means ± standard errors are shown, and degrees of freedom (DF), test statistics, alpha and p-values provided. A mixed-effects modelling approach was used to investigate the effect of treatments on relative planktonic and biofilm growth and colony inhibition. The Restricted Maximum Likelihood (RML) method with unbounded variance components was used with experimental replicate included as a random effect in all models, and antibiotics, antibiotic concentrations, strain type (MDR and non-MDR), and strain nested in type (strain[type]), as fixed effects. Models were run iteratively with the residuals inspected and outliers removed until normality was attained as determined by Shapiro-Wilks tests

($p < 0.05$). Model robustness was monitored by RSquare and the retention of degrees of freedom with concentration ranges limited to avoid singularities. Effects and interactions were investigated using Least-Squares Means (LSMeans) Differences Student's and Tukey HSD tests (alpha = 0.05).

For clarity, individual mixed-effects models were run with antibiotic concentration as an effect to differentiate treatments and the results of the LSMeans Tukey HSD tests are shown in the figures. Spearman's (rho) coefficient was used to test for correlations between mean OD_{570} and A_{570} data. Some difficulty was encountered in analysing the relative inhibition data for individual strains using a mixed-effects modelling approach where normality could not be achieved (some data were too discrete) and one strain was omitted from the combined mixed-effects model as there was no variation in relative inhibition across AZM concentrations. For some, a general linear modelling (GLM) approach was successful with replicate and antibiotic concentration included as effects. However, two strains could not be analysed using GLMs or one-way ANOVA, so differences between key treatments were investigated with Wilcoxon (Rank sums) tests using a one-way test Chi-Square approximation. Rho was used to test for correlations between relative inhibition diameter and antibiotic concentration. Similarities in the effects of macrolides and the response of strains to antibiotics were visualised by Hierarchical Cluster Analysis using the Ward method and with equal weightings of factors. A Chi-Square test was used to test the independence of HCA clusters and MDR and non-MDR strain types (iCalcu.com).

Results and discussion

Biofilm growth by a model *Klebsiella* and suppression by macrolide antibiotics

K. pneumonia ATCC 10031 was found to form solid-liquid (S-L) interface biofilms [31] at the bottom of static LB microcosms within 24 h as had been reported earlier under different culture conditions [32–34]. As the liquid columns remained transparent with bacteria localised in the biofilm (*K. pneumoniae* is non-motile [40]), we used multi-well plates in which optical density measurements are made vertically up through the plate bottom and liquid column to record biofilm growth. This had the advantage of being able to quantify very weak biofilms that might not be retained during washing and elution of Crystal violet as noted in other cases [41] (ATCC 10031 produces weak biofilms compared to those produced by *Pseudomonas aeruginosa* and *Staphylococcus aureus* [33] or *Bordetella avium* [42]). We used this approach with *K. pneumonia* ATCC 10031 to evaluate the effect of eight macrolides, AZM, CLR, ERM, JSM, MID, ROX, SPM and TYL. These were tested over a concentration range of 0–9 mg/L and relative biofilm growth (OD_{570}) determined after 24 h in comparison with a no-antibiotic control (**Fig 1**). Of the eight macrolides, AZM and JSM showed high levels of inhibition of 2.5 – 5x with 3–9 mg/L of each antibiotic. CLR, ERM, MID and SPM showed moderate levels of inhibition of 1.2–1.7x over the same range, while ROX and TYL had little or no significant impact under the conditions tested here (LSMeans Differences Tukey HSD, alpha = 0.05 for individual macrolide mixed-effects models of relative OD_{570}). Further analysis of all macrolides in a combined mixed-effects model of relative OD_{570} confirmed macrolide-type and concentration effects (*macrolide*, $F_{7,7} = 126$, p = 0.01; *concentration*, $F_{3,3} = 290$, p = 0.01; no-macrolide control omitted to avoid singularities), as well as a significant synergistic interaction between macrolides and macrolide concentration (*macrolide x concentration*, $F_{21,21} = 13$, p = 0.01). These findings demonstrate that *K. pneumonia* ATCC 10031 biofilm growth is differentially affected by both the type of macrolide and the concentrations tested in this assay.

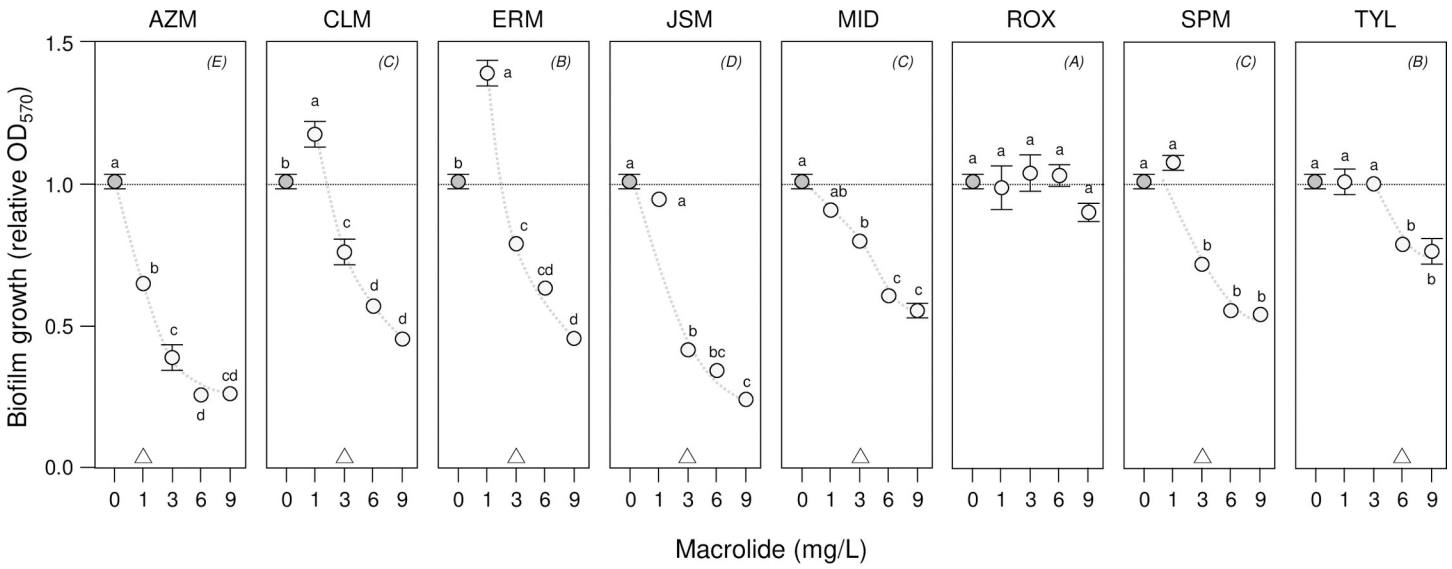

Fig 1. Optical density measurements of *K. pneumonia* biofilm growth show inhibition by macrolides. The inhibition of *K. pneumonia* ATCC 10031 biofilm growth by eight macrolides was investigated by biofilm assays with optical density (OD_{570}) measurements after 24 h incubation. Mean relative OD_{570} ± SE (n = 3) is shown, with the no-macrolide (control) treatment indicated by dark circles and 1–9 mg/L macrolide treatments by light circles (trends are suggested by dashed curves). Means not connected by the same letters within panels are significantly different (LSMeans Differences Tukey HSD, alpha = 0.05 for individual macrolide mixed-effects models; note no significant differences for ROX). Triangles at the bottom of panels indicate biofilm minimum inhibitory concentrations (MIC) where relative OD_{570} was first significantly reduced by macrolide treatment. Macrolides not connected by the same letters indicated in parentheses in the top-right of each panel are significantly different (LSMeans Differences Tukey HSD, alpha = 0.05 for combined macrolide mixed-effects model of relative OD_{570}).

https://doi.org/10.1371/journal.pone.0270983.g001

These findings were confirmed using MTT and relative absorbance measurements (A_{570}) to determine metabolic activity as a measure of biofilm growth (Fig 2). We chose to use this complementary approach to measuring biofilms, as the colorimetric MTT assay depends on metabolically-active cells to reduce MTT to purple-coloured formazan and is not affected by biofilm extracellular polysaccharides leading to cell-clumping or undamaged but dead cells that might affect optical density–based measurements. Significant levels of inhibition were seen for AZM and JSM and no effect for ROX and TYL (LSMeans Differences Tukey HSD, alpha = 0.05 for individual macrolide mixed-effects models of relative A_{570}). Macrolide-type, concentration effects and the synergistic interaction were confirmed in a combined mixed-effects model of relative A_{570} (*macrolide*, $F_{7,7}$ = 20, p = 0.01; *concentration*, $F_{3,3}$ = 41, p = 0.01; *macrolide x concentration*, $F_{21,21}$ = 2, p = 0.03; no-macrolide control omitted to be consistent with the relative OD_{570} model). Relative A_{570} treatment means were positively correlated with the relative OD_{570} means of the first assay (rho = 0.80, p = 0.01), demonstrating that the optical density and metabolic measurements of biofilm growth were in agreement. Hierarchical cluster analysis using relative A_{570} and OD_{570} means also grouped macrolides according to inhibition levels, with AZM and JSM clustered together and distal to both ROX and TYL (see S1 Fig for the HCA dendrogram). As AZM is available in both peroral and parenteral forms for treatment, it was selected for further testing with CMS as a combined therapy against biofilm associated *Klebsiella* infections.

Antibacterial activity of AZM and CMS in combination against planktonic and biofilm–forming ATCC 10031 cells

The synergistic action of AZM and CMS on *K. pneumonia* ATCC 10031 was investigated using both planktonic and biofilm assays, because we hypothesized that lifestyle differences

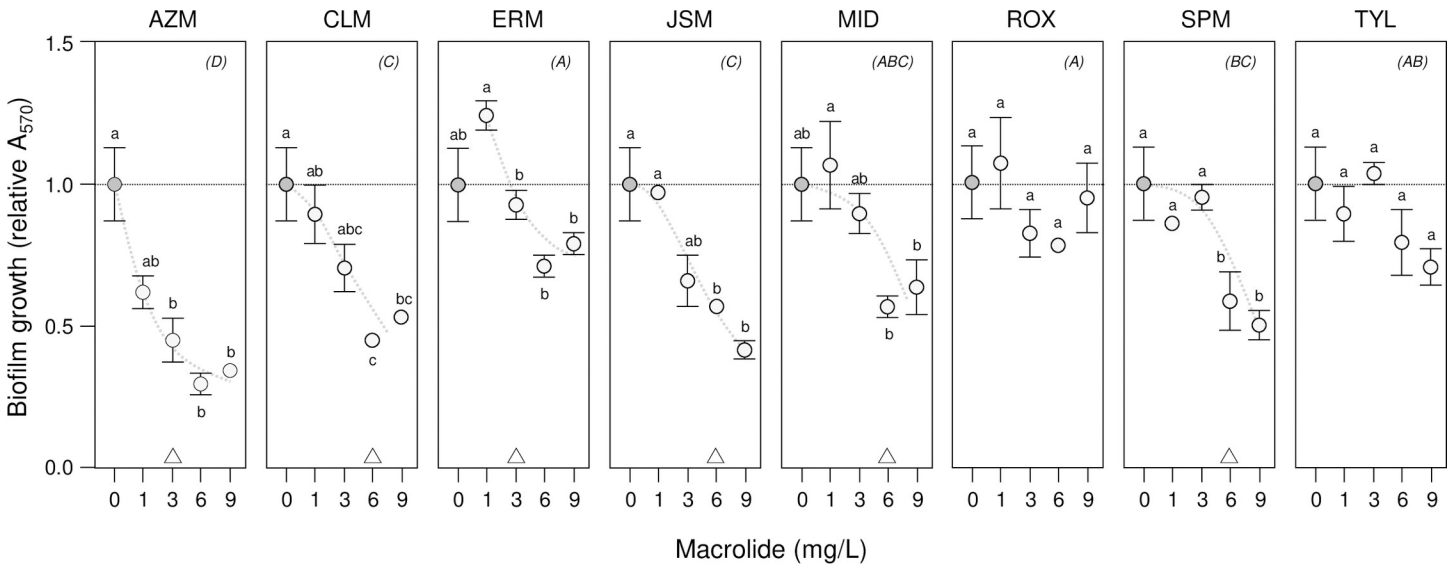

Fig 2. MTT assays of *K. pneumonia* biofilm growth show inhibition by macrolides. The inhibition of *K. pneumonia* ATCC 10031 biofilm growth by eight macrolides was investigated by biofilm assays using the metabolic indicator dye MTT with absorbance (A_{570}) measurements after 24 h incubation. Mean relative A_{570} ± SE (n = 3) is shown, with the no-macrolide (control) treatment indicated by dark circles and 1–9 mg/L macrolide treatments by light circles (trends are suggested by dashed curves). Means not connected by the same letters within panels are significantly different (LSMeans Differences Tukey HSD, alpha = 0.05 for individual macrolide mixed-effects models). Triangles at the bottom of panels indicate biofilm minimum inhibitory concentrations (MIC) where relative A_{570} was first significantly reduced by macrolide treatment. Macrolides not connected by the same letters indicated in parentheses in the top-right of each panel are significantly different (LSMeans Differences Tukey HSD, alpha = 0.05 for combined macrolide mixed-effects model of relative OD_{570}; note no significant differences for ROX and TYL).

https://doi.org/10.1371/journal.pone.0270983.g002

affect antibiotic sensitivities, and because infections involve both lifestyles [43, 44]. CMS had no impact on planktonic growth when tested alone but inhibited growth at 6 mg/L with 3 mg/L AZM and at 2 mg/L with 9 mg/L AZM (Fig 3A). A significant synergistic interaction between AZM and CMS was found in a mixed-effects model of relative OD_{570} (*AZM x CMS*, $F_{12,12}$ = 170, p = 0.01) confirming the synergistic action of AZM and CMS on planktonic growth, as well as significant concentration effects (*AZM*, $F_{2,2}$ = 3464, p = 0.01; *CMS*, $F_{6,6}$ = 314, p = 0.01; data limited to 0–16 mg/L CMS to avoid singularities as higher-concentration treatments were highly correlated). In comparison, CMS was found to have an inhibitive effect on biofilm growth without AZM and inhibited growth at a lower concentration (2 mg/L) with 3 mg/L AZM (Fig 3B) (growth of the initial inoculum in these assays was fully suppressed by 9 mg/L AZM). Once again, a significant synergistic interaction was found in a mixed-effects model of relative OD_{560} (*AZM x CMS*, $F_{12,12}$ = 176, p = 0.01) as well as significant concentration effects (*AZM*, $F_{2,2}$ = 1786, p = 0.01; *CMS*, $F_{6,6}$ = 354, p = 0.01; data limited to be consistent with the planktonic model).

The effect of AZM and CMS on biofilm growth was further confirmed by MTT assays (Fig 4) where a significant synergistic interaction was found in a mixed-effects model of relative A_{570} (*AZM x CMS*, $F_{12,12}$ = 134, p = 0.01) as well as significant concentration effects (*AZM*, $F_{2,2}$ = 2663, p = 0.01; *CMS*, $F_{6,6}$ = 299, p = 0.01; data limited to 0–16 mg/L CMS to be consistent with the relative OD_{570} models). Again, relative A_{570} and OD_{570} treatment means were positively correlated (rho = 0.82, p = 0.01), demonstrating that the optical density and metabolic measurements of biofilm growth were in agreement. Finally, the combined AZM and CMS treatment was found to inhibit further growth of established biofilms by 0.8x (LSMeans Differences Tukey HSD, alpha = 0.05; see S2 Fig for effect of combined AZM and CMS treatment on further ATCC 10031 biofilm growth) and a significant AZM effect and synergistic interaction were found in a mixed-effects model of relative A_{570} (*AZM*, $F_{1,1}$ = 362, p = 0.01; *AZM x*

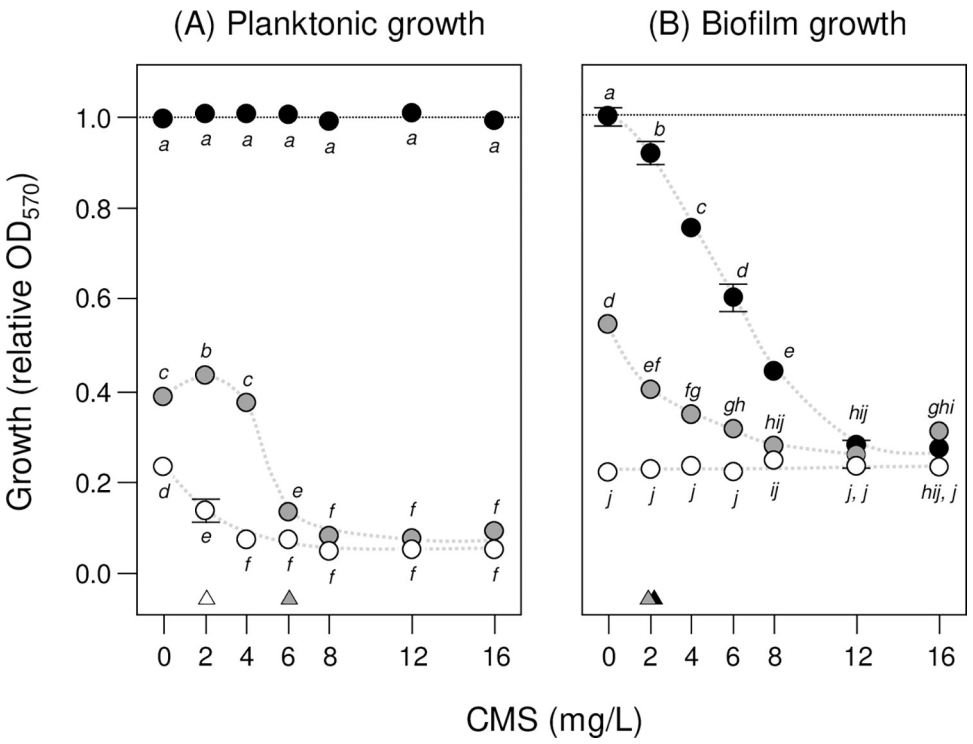

Fig 3. AZM and CMS synergistically inhibit *K. pneumonia* planktonic and biofilm growth. The effect of azithromycin (AZM) and colistin methanesulfonate (CMS) on *K. pneumonia* ATCC 10031 (A) planktonic and (B) biofilm growth was investigated by optical density (OD_{570}) measurements after 16 h and 24 h incubation, respectively. Data are shown as mean relative OD_{570} ± SE (n = 3), with no-AZM (control) treatments indicated by dark circles, 3 mg/L AZM by grey circles and 9 mg/L AZM by white circles (trends are suggested by dashed curves). Means not connected by the same letters are significantly different (LSMeans Differences Tukey HSD, alpha = 0.05 for planktonic and biofilm growth mixed-effects models of relative OD_{570}). Small triangles indicate planktonic and biofilm minimum inhibitory concentrations (MIC) where relative OD_{570} was first significantly reduced by CMS for each AZM treatment.

https://doi.org/10.1371/journal.pone.0270983.g003

CMS, $F_{2,2}$ = 74, p = 0.01) but not a CMS effect (*CMS*, $F_{2,2}$ = 0.2; p = 0.79). Our initial expectations were that CMS would have little effect on either planktonic or biofilm growth of *K. pneumonia* and that AZM is not considered an appropriate treatment for such infections. However, collectively our findings suggest that AZM and CMS have a synergistic activity on the planktonic growth of ATCC 10031 cells as well as on biofilm–formation. This suggests that an AZM-CMS combination therapy might be effective in treating biofilm–based Klebsiella hospital infections.

AZM and CMS in combination inhibits biofilm growth of *K. pneumonia* hospital isolates

As there are often significant differences between potentially laboratory-adapted model strains and recent hospital isolates, we investigated whether the synergistic action of AZM and CMS inhibiting the biofilm growth of *K. pneumonia* ATCC 10031 might also occur with hospital isolates. To investigate this, we chose five multiple drug resistant (MDR) and six non-MDR *K. pneumonia* Ukrainian hospital isolate (UHI) strains as *K. pneumonia* is the leading nosocomial gram-negative pathogen in Ukraine [1, 2], and all of which were found to produce S-L interface biofilms under the conditions used here. The origins of the UHI strains as well as their antibiotic sensitivities are listed in **S1 Table** (note that although UHI 1090 was found to be sensitive to polymyxin B in the disc-diffusion assay, it was resistant to COL in the broth dilution

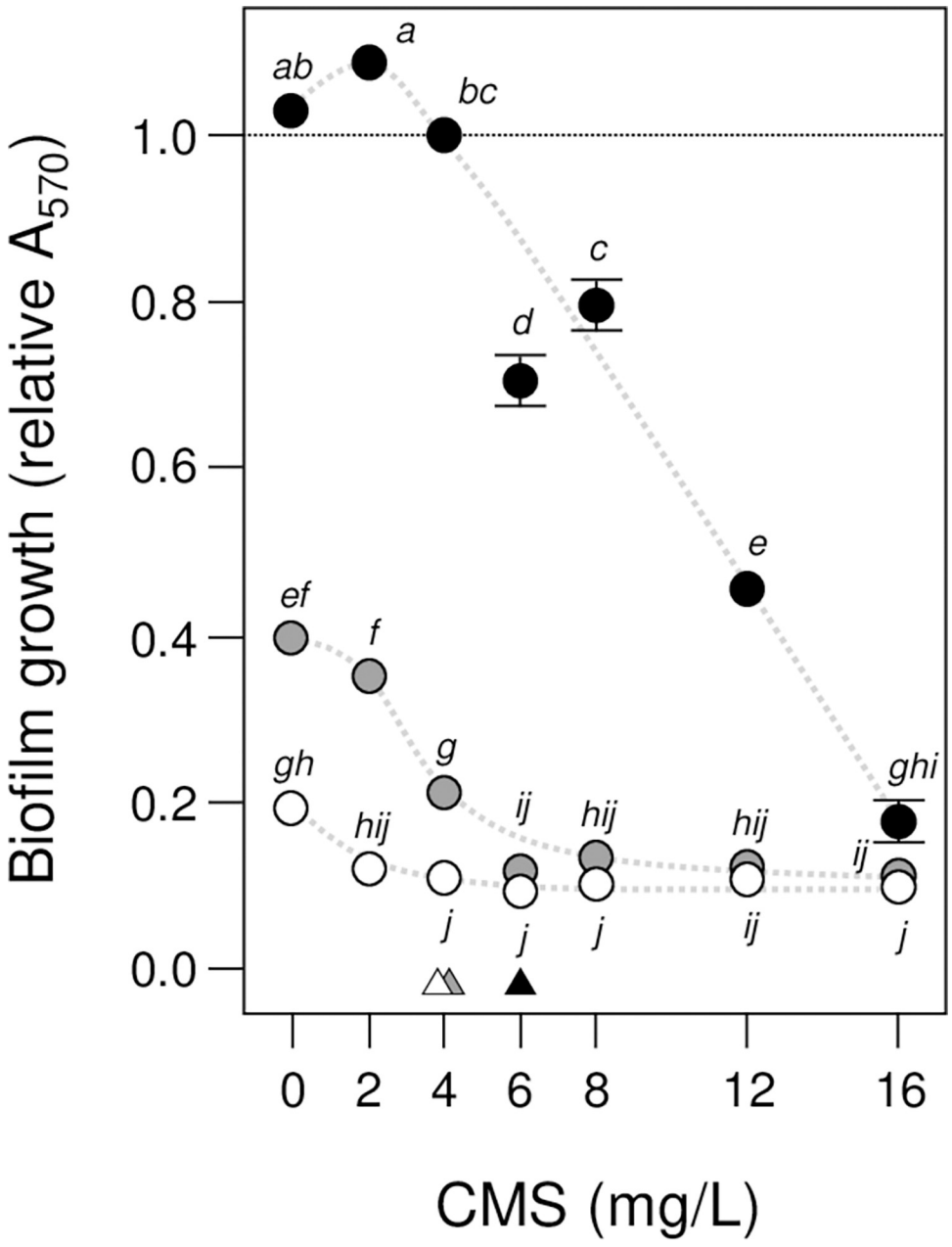

Fig 4. MTT assays of *K. pneumonia* biofilm growth confirms synergistic action of AZM and CMS. The effect of azithromycin (AZM) and colistin methanesulfonate (CMS) on *K. pneumonia* ATCC 10031 biofilm growth was investigated using the metabolic indicator dye MTT with absorbance (A_{570}) measurements after 24 h incubation. Mean relative A_{570} ± SE (n = 3) is shown, with no-AZM (control) treatments indicated by dark circles, 3 mg/L AZM by grey circles and 9 mg/L AZM by white circles (trends are suggested by dashed curves). Means not connected by the same letters are significantly different (LSMeans Differences Tukey HSD, alpha = 0.05 for mixed-effects model of relative A_{570}). Small triangles indicate planktonic and biofilm minimum inhibitory concentrations (MIC) where relative A_{570} was first significantly reduced by CMS for each AZM treatment.

https://doi.org/10.1371/journal.pone.0270983.g004

assay whereas UHI 1633 was resistant in both assays). We then tested the inhibitory effect of AZM on the biofilm growth of these strains. Hierarchical cluster analysis based on antibiotic susceptibly clearly grouped these strains by MDR/non-MDR type (see S3 Fig for the HCA dendrogram). Significant inhibition of biofilm growth was seen for four MDR strains and all

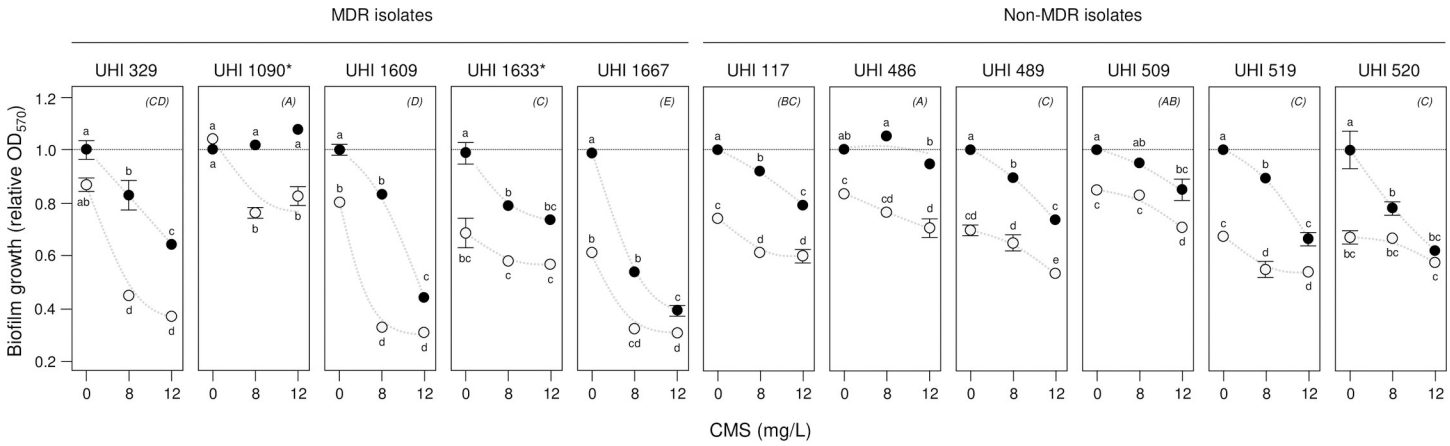

Fig 5. AZM and CMS synergistically inhibit biofilm growth of *K. pneumonia* hospital strains. The effect of azithromycin (AZM) and colistin methanesulfonate (CMS) on biofilm growth of multiple-drug resistant (MDR) and non-MDR *K. pneumonia* Ukrainian Hospital Isolate (UHI) strains was investigated using biofilm assays and with optical density (OD_{570}) measurements after 24 h incubation. Mean relative OD_{570} ± SE (n = 3) is shown, with no-AZM (control) treatments indicated by dark circles and 9 mg/L AZM treatments by light circles, (trends are suggested by dashed curves). Means not connected by the same letters are significantly different (LSMeans Differences Tukey HSD, alpha = 0.05 for individual UHI strain mixed-effects models of relative OD_{570}). Strains not connected by the same letters indicated in parentheses in the top-right of each panel are significantly different (LSMeans Differences Tukey HSD, alpha = 0.05 for combined UHI strain mixed-effects model of relative OD_{570}). *, UHI 1090 and UHI 1633 were found to be resistant to COL in the broth dilution assay.

https://doi.org/10.1371/journal.pone.0270983.g005

non-MDR strains (LSMeans Differences Tukey HSD, alpha = 0.05 for individual mixed-effects models of OD_{570}; see S4 Fig for the effect of AZM on UHI strain biofilm growth). A combined mixed-effects model of OD_{570} with all strains confirmed significant strain and AZM effects (*MDR/non-MDR type*, $F_{1,1}$ = 12, p = 0.01; *strain[type]*, $F_{9,9}$ = 26, p = 0.01; *AZM*, $F_{2,2}$ = 221, p = 0.01). Despite the MDR/non-MDR division seen earlier, a hierarchical cluster analysis using these OD_{570} treatment means was found to cluster strains independently of strain type (Chi-square, $DF_{4,2}$ = 4.95, p = 0.18; see S3 Fig for the HCA dendrogram). The differences seen in biofilm response to AZM indicates that this small collection of strains was diverse and suggests that it could be used to test whether the synergistic action of AZM and CMS occurs more widely amongst *K. pneumonia* hospital isolates.

The effect on relative biofilm growth (OD_{570}) of the MDR and non-MDR UHI strains by CMS in combination with AZM was then investigated (Fig 5). A mixed-effects model of relative OD_{570} found significant strain effects (MDR & non-MDR type, $F_{1,1}$ = 53, p = 0.3; strain [type], $F_{9,9}$ = 28, p = 0.01) as well as a synergistic interaction across strains (AZM *x* CMS, $F_{2,2}$ = 7, p = 0.01). Individual strain mixed-effects models of relative OD_{570} confirmed the synergistic interaction in all but UHI 1633 and 509 (UHI 1633, $F_{2,2}$ = 2, p = 0.20; UHI 509, $F_{2,2}$ = 0.4, p = 0.70) where it appears that the effects of AZM and CMS are simply additive. This test of UHI strains strongly suggests that the synergistic action of AZM and CMS is likely to be seen for other MDR and non-MDR *K. pneumonia* hospital isolates.

Polymyxin B disc-diffusion inhibition of colony growth of *K. pneumonia* hospital isolates on AZM plates also shows synergistic action

We were interested in determining whether the synergistic action of AZM and CMS was also evident in antibiotic disc-diffusion assays which involve the inhibition of colony growth rather than biofilms. As CMS is not readily available in discs, we used the related antibiotic polymyxin B which is the preferred alternative for antimicrobial susceptibility testing when CMS is used in treatments (EUCAST recommendations [45]) (Polymyxin B and CMS (polymyxin E) are largely equivalent with the main differences associated with formulation and

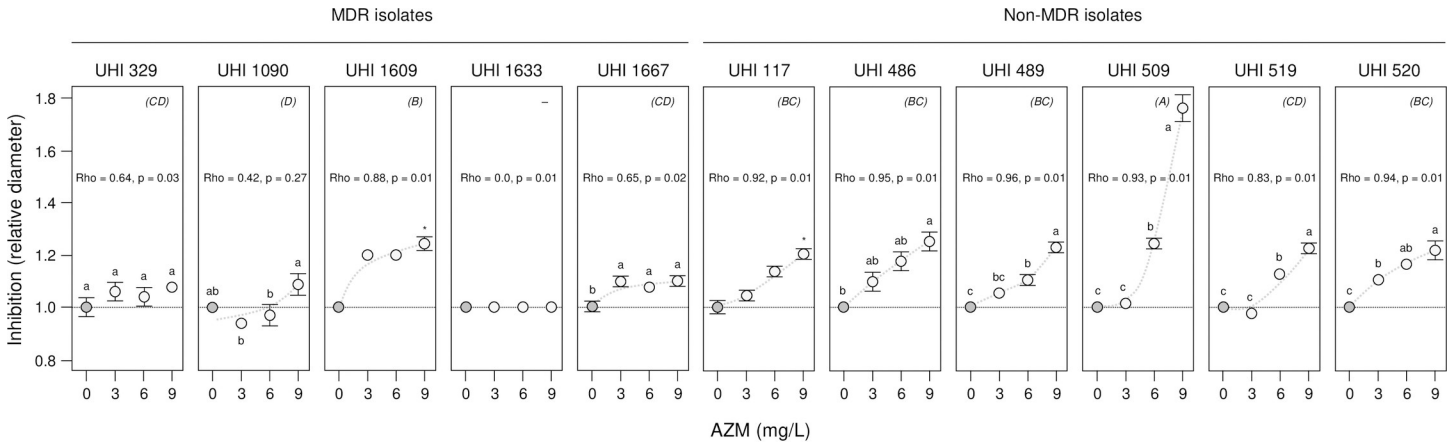

Fig 6. Synergistic inhibition of colony growth of *K. pneumonia* hospital strains by AZM and polymyxin B. The inhibition of colony growth of multiple-drug resistant (MDR) and non-MDR *K. pneumonia* Ukrainian Hospital Isolate (UHI) strains was investigated using polymyxin B disks on azithromycin (AZM) plates with colony inhibition zone measurements after 48 h incubation. Mean relative inhibition (mm) ± SE (n = 3) is shown, with no-AZM (control) treatments indicated by dark circles and 3–9 mg/L AZM treatments by light circles (trends are suggested by dashed curves). Means not connected by the same letters within panels are significantly different (LSMeans Differences Tukey HSD, alpha = 0.05 for individual mixed-effects models of relative inhibition for UHI 329, 509, 520, 1090 & 1667; individual general linear models for UHI 486, 489, 509, 519 & 1633; asterisk indicates significant difference between no AZM and 9 mg/L AZM treatments; Wilcoxon, UHI 117, ChiSquare, DF_1 = 4.1, p = 0.04; UHI 1609, ChiSquare DF_1 = 4.5, p = 0.03). Spearman's correlation (Rho) between relative inhibition and AZM concentration is provided for each strain. Strains not connected by the same letters indicated in parentheses in the top-right of each panel are significantly different (LSMeans Differences Tukey HSD, alpha = 0.05 for combined UHI strain mixed-effects model of relative inhibition; UHI 1633 was omitted from this analysis as there was no variation in relative inhibition across AZM concentrations and was resistant to polymyxin B).

https://doi.org/10.1371/journal.pone.0270983.g006

administration [46]). Although others have used Epsilometer test (E-test) strips [15] to deliver the first antibiotic over a range of concentrations onto an agar plate containing the second antibiotic to test for synergistic action (e.g., [47]), we found it easier and more accurate to measure colony inhibition using single-concentration discs placed on a range of plates with different concentrations of the second antibiotic. We measured the zone of colony inhibition (mm) surrounding polymyxin B discs on 0, 3, 6, 9 mg/L AZM plates spread with MDR and non-MDR *K. pneumonia* hospital isolates (AZM did not prevent colony growth at any concentration; **Fig 6**). Significant increases in sensitivity to polymyxin B were seen with increasing AZM levels for most strains except UHI 329 and UHI 1663 (LSMeans Differences Tukey HSD, alpha = 0.05 for individual strain mixed-effects models but see **Fig 6** legend for further details) and the synergistic activity confirmed by positive correlations between relative inhibition and AZM concentration for these strains (rho = 0.64–0.96, p = 0.01–0.03). The synergistic activity was the highest for UHI 509 with the inhibition zone diameter around the polymyxin B discs increasing 1.8x on 9 mg/L AZM plates, with the majority of strains only showing a 1.2x increase, and UHI 329, 1090, 1663 and 1667 showing little or no change (UHI 329, 1090 and 1667 had previously been shown to be sensitive polymyxin B while UHI 1663 was resistant, **S1 Table**; in this case there was no inhibition of colony growth next to the polymyxin discs on any of the AZM plates). Finally, a mixed-effects model of relative inhibition confirmed strain effects (*MDR & non-MDR type*, $F_{1,1}$ = 27, p = 0.01; *strain[type]*, $F_{8,8}$ = 13, p = 0.01) in agreement with the earlier finding that there is diversity within this collection of MDR and non-MDR UHI hospital isolates, as well as an AZM effect across strains (*AZM*, $F_{3,3}$ = 85, p = 0.01).

Conclusions

The development of combination therapies based on the synergistic activities between antibiotics to overcome resistance is of growing interest to combat GNB pathogens such as *Klebsiella pneumoniae* [8, 13]. This has involved the exploration of unusual combinations

contraindicated by current treatment guidelines, and further opportunities in developing effective therapies may also be found in recognising that susceptibility testing and efficacy in patient treatments may be sensitive to bacterial lifestyles, as free-swimming planktonic and sessile biofilm-encased cells are known to have different physiology and resistance to stress and antibiotics. For example, most susceptibility testing in hospitals is based on the Kirby-Bauer disc-diffusion assay (sometimes using E-test strips) [14, 15] in which colony (lawn) development is inhibited, but it is unclear whether this more closely resembles planktonic or biofilm growth (the disc diffusion assays are often followed by broth-dilution tests [15]). Furthermore, bacteria are known to grow in a continuum of aggregations which range from a few closely associated cells to highly densely packed structures in liquids, viscous environments and on surfaces [31], which suggests that bacterial growth is more nuanced, and the term 'biofilm' is often used without sufficient definition [31, 48]. We have found that biofilm growth by a model *Klebsiella pneumoniae* strain (ATCC 10031) as well as hospital isolates can be inhibited by several macrolides including azithromycin (AZM), and that AZM can improve the effectiveness of colistin methanesulfonate (CMS), currently the last-agent-of-choice for *Klebsiella* infections [8]. However, in our investigation of ATCC 10031 and both MDR and non-MDR hospital isolates, we have found discrepancies suggesting that disc-diffusion and broth growth-based assays may not be good predictors of antibiotic susceptibility in biofilms. Better choices of combination therapies might be made if simple biofilm assays were used when determining which antibiotics to use in patient treatment.

Supporting information

S1 Dataset. Experimental data sets. This file lists the quantitative replicate data used in the statistical analyses and figures presented in this work.
(DOCX)

S1 Fig. Macrolides differentially effect *K. pneumonia* biofilm growth. Macrolides show different levels of inhibition of *K. pneumonia* ATCC 10031 biofilm growth and can be visualised by Hierarchical cluster analysis that group strains according to similarity. Dendrograms were constructed using mean relative (A) optical density (OD_{570}) and (B) metabolic activity (A_{570}) measurements of biofilm growth after 24 h. Macrolides linked to the same node (small circles) are more similar than those linked by deeper nodes, and the arbitrary root for this dendrogram is indicated by the dashed circle.
(PPTX)

S2 Fig. Combined AZM and CMS treatment supresses further *K. pneumonia* biofilm growth. The effect of azithromycin (AZM) and colistin methanesulfonate (CSM) on established *K. pneumonia* ATCC 10031 biofilms was investigated by optical density (OD_{570}) measurements after 24 h incubation. Mean relative OD_{570} ± SE (n = 3) is shown, with no-AZM (control) treatments indicated by dark circles and 9 mg/L AZM treatments by light circles (trends are suggested by dashed curves). Means not connected by the same letters are significantly different (LSMeans Differences Tukey HSD, alpha = 0.05 for mixed-effects model of relative OD_{570}).
(PPTX)

S3 Fig. *K. pneumonia* hospital strains are differentiated by antibiotic susceptibility and AZM inhibition of biofilm growth. The phenotypic diversity among the multiple-drug resistant (MDR) and non-MDR Ukrainian Hospital Isolate (UHI) strains can be visualised by Hierarchical cluster analysis that group strains according to similarity of (A) antibiotic susceptibility and (B) the effect of azithromycin (AZM) on biofilm growth in dendrograms

with different topologies. The dendrogram on the left was constructed using disc-diffusion assay data for those antibiotics listed in S1 Table and the one on the right using mean relative optical density (OD_{570}) measurements of biofilm growth with AZM after 24 h. MDR strains are indicated by dark circles and non-MDR strains by light circles. Strains linked to the same node (small circles) are more similar than those linked by deeper nodes, and the arbitrary roots for these dendrograms are indicated by the dashed circle.
(PPTX)

S4 Fig. AZM inhibits biofilm growth of *K. pneumonia* hospital strains. The effect of azithromycin (AZM) on biofilm growth of multiple-drug resistant (MDR) and non-MDR *K. pneumonia* Ukrainian Hospital Isolate (UHI) strains was investigated by biofilm assays with optical density (OD_{570}) measurements after 24 h incubation. Data are shown as mean OD_{570} ± SE (n = 3) (trends are suggested by dashed curves). Means not connected by the same letters are significantly different (LSMeans Differences Tukey HSD, alpha = 0.05 for individual UHI strain mixed-effects models of OD_{570}; no significant effect for UHI 329, p = 0.06). Strains not connected by the same letters indicated in parentheses in the top-left of each panel are significantly different (LSMeans Differences Tukey HSD, alpha = 0.05 for combined UHIO strains mixed-effects model of relative inhibition).
(PPTX)

S1 Table. Origin and antibiotic susceptibility of the UHI *Klebsiella pneumoniae* strains used in this work. This table lists the origins and antibiotic susceptibility of the UHI strains used in this work.
(DOCX)

Acknowledgments

We thank Viktoria Savchenko and the IMD Medical Laboratory, Galyna Filonenko, Centre for Paediatric Cardiology and Cardiac Surgery, Kyiv, and Olga Balko, Zabolotny Institute of Microbiology and Virology of the National Academy of Sciences of Ukraine, for their support. OVM also thanks I. Gilbert and D. Purves, Wellcome Centre for Anti-Infectives Research, University of Dundee, for their support to participate in the 'Setting our sights on infectious diseases' conference in 2019, and to L. Silver, LL Silver Consulting, New Jersey, USA, for productive discussions.

Author Contributions

Conceptualization: Olena V. Moshynets, Andrew J. Spiers.

Formal analysis: Olena V. Moshynets, Andrew J. Spiers.

Investigation: Olena V. Moshynets, Taras P. Baranovskyi, Scott Cameron, Olga S. Iungin, Ianina Pokholenko, Robyn Jerdan, Aleksandr Kamyshnyi, Alexey A. Krikunov, Viktoria V. Potochilova, Kateryna L. Rudnieva, Andrew J. Spiers.

Methodology: Olena V. Moshynets, Taras P. Baranovskyi, Scott Cameron, Olga S. Iungin, Ianina Pokholenko, Robyn Jerdan, Aleksandr Kamyshnyi, Alexey A. Krikunov, Viktoria V. Potochilova, Kateryna L. Rudnieva, Andrew J. Spiers.

Project administration: Olena V. Moshynets, Andrew J. Spiers.

Supervision: Robyn Jerdan, Andrew J. Spiers.

Visualization: Andrew J. Spiers.

Writing – original draft: Olena V. Moshynets, Taras P. Baranovskyi, Scott Cameron, Olga S. Iungin, Ianina Pokholenko, Aleksandr Kamyshnyi, Alexey A. Krikunov, Viktoria V. Potochilova, Kateryna L. Rudnieva, Andrew J. Spiers.

Writing – review & editing: Olena V. Moshynets, Taras P. Baranovskyi, Scott Cameron, Olga S. Iungin, Ianina Pokholenko, Aleksandr Kamyshnyi, Alexey A. Krikunov, Viktoria V. Potochilova, Kateryna L. Rudnieva, Andrew J. Spiers.

References

1. Lazoryshynetz VV, Spysarenko SP, Krykunov AA, Malysheva TA. Antibiotic resistance in the current realities of cardiac surgery. Ukrainian J Cardiovascular Surgery 2017; 1:110–114.
2. Loban GA, Hancho OV, Chapala AN, Fedorchenko VI, Sivovol VN. Spectrum of pathogens causing purulent inflammatory diseases in surgical patients. Actualni problemi suchanoi medetsini: Vistnyk ukrainskoi medichnoi akademii 2021; 1:97–100.
3. Tumbarello M, Viale P, Viscoli C, Trecarichi EM, Tumietto F, Marchese A, et al. Predictors of mortality in bloodstream infections caused by Klebsiella pneumoniae carbapenemase-producing *K. pneumoniae*: importance of combination therapy. Clin Infect Dis. 2012; 55:943–950. https://doi.org/10.1093/cid/cis588 PMID: 22752516
4. Albiger B, Glasner C, Struelens M, Grundmann H, Monnet D, the European Survey of Carbapenemase-Producing Enterobacteriaceae (EuSCAPE) working group. Carbapenemase-producing *Enterobacteriaceae* in Europe: assessment by national experts from 38 countries, May 2015. Euro Surveill. 2015; 20:30062.
5. Oliva A, Mascellino MT, Cipolla A, D'Abramo A, De Rosa A, Savinelli S, et al. Therapeutic strategy for pandrug-resistant *Klebsiella pneumoniae* severe infections: short-course with colistin increases the *in vivo* and *in vitro* activity of double carbapenem regimen. Int J Infect Diseases 2015; 33:132–134. https://doi.org/10.1016/j.ijid.2015.01.011 PMID: 25597275
6. Michalopoulos AS, Falagas ME. Colistin: resent data on pharmacodynamics properties and clinical efficacy in critically ill patients. Ann Intensive Care 2011; 1:30. https://doi.org/10.1186/2110-5820-1-30 PMID: 21906382
7. Michalopoulos AS, Karatza DC, Gregorakos L. Pharmacokinetic evaluation of colistin sodium. Expert Opin Drug Metab Toxicol. 2011; 7:245–255. https://doi.org/10.1517/17425255.2011.541439 PMID: 21128824
8. Paul M, Daikos GL, Durante-Mangoni E, Yahav D, Carmeli Y, Dishon Benattar Y, et al. Colistin alone versus colistin plus meropenem for treatment of severe infections caused by carbapenem-resistant Gram-negative bacteria: an open-label, randomised controlled trial. Lancet Infect Dis. 2018; 18:391–400. https://doi.org/10.1016/S1473-3099(18)30099-9 PMID: 29456043
9. Plachouras D, Karvanen M, Friberg LE, Papadomichelakis E, Antoniadou A, Tsangaris I, et al. Population pharmacokinetic analysis of colistin methanesulfonate and colistin after intravenous administration in critically ill patients with infections caused by gram-negative bacteria. Antimicrob Agents Chemother. 2009; 53:3430–3436. https://doi.org/10.1128/AAC.01361-08 PMID: 19433570
10. Daikos GL, Skiada A, Pavleas J, Vafiadi C, Salatas K, Tofas P, et al. Serum bactericidal activity of three different dosing regimens of colistin with implications for optimum clinical use. J Chemother. 2010; 22:175–178. https://doi.org/10.1179/joc.2010.22.3.175 PMID: 20566422
11. Imberti R, Cusato M, Villani P, Carnavale L, Iotti GA, Langer M, et al. Steady-state pharmacokinetics and bronchoalveolar lavage concentration of colistin in critically ill patients after intravenous colistin methanesulphonate administration. Chest J. 2010; 138:1333–1339.
12. Karvanen M, Plachouras D, Friberg LE, Paramythiotou E, Papadomichelakis E, Karaiskos I, et al. Colistin methanesulfonate and colistin pharmacokinetics in critically ill patients receiving continuous venovenous hemodiafiltration. AAC 2013; 57:668–671. https://doi.org/10.1128/AAC.00985-12 PMID: 23147733
13. Daikos GL, Tsaousi S, Tzouvelekis LS, Anyfantis I, Psichogiou M, Argyropoulou A, et al. Carbapenemase-producing *Klebsiella pneumoniae* bloodstream infections: lowering mortality by antibiotic combination scheme and the role of carbapenems. Antimicrob Agents Chemother. 2014; 58:2322–2328. https://doi.org/10.1128/AAC.02166-13 PMID: 24514083
14. Bauer AW, Kirby WMM, Sherris JC, Turck M. Antibiotic susceptibility testing by a standardized single disk method. Amer J Clin Pathol. 1966; 45: 493–496.

15. Benkova M, Soukup O, Marek J. Antimicrobial susceptibility testing: currently used methods and devices and the near future in clinical practice. J Appl Microbiol. 2020; 129: 806–822. https://doi.org/10.1111/jam.14704 PMID: 32418295

16. Galani I, Orlandou K, Moraitou H, Petrikkos G, Souli M. Colistin/daptomycin: an unconventional antimicrobial combination synergistic *in vitro* against multidrug-resistant *Acinetobacter baumannii*. Int J Antimicrob Agents 2014; 43:370–374. https://doi.org/10.1016/j.ijantimicag.2013.12.010 PMID: 24560919

17. Tagliaferri E, Tascini C, Leonildi A, Cuillo I, Amadori F, Menichetti F. Easy synergism for colistin-resistant KPC-producing *Klebsiella pneumoniae*: the E-test with supplemented agar. Clin Microbiol Infections 2015; 21:e7–e8. https://doi.org/10.1016/j.cmi.2014.08.016 PMID: 25682280

18. Kali A, Bhuvaneshwar D, Charles PMV, Seetha KS. Antibacterial synergy of curcumin with antibiotics against biofilm producing clinical bacterial isolates. J Basic Clin Pharm. 2016; 7:93–96. https://doi.org/10.4103/0976-0105.183265 PMID: 27330262

19. Mah TF. Biofilm–specific antibiotic resistance. Fut Microbiol. 2012; 7:1061–1072.

20. Olsen I. Biofilm-specific antibiotic tolerance and resistance. Eur J Clin Microbiol Infect Dis. 2015; 34:877–886. https://doi.org/10.1007/s10096-015-2323-z PMID: 25630538

21. Saiman L, Marshall BC, Mayer-Hamblett N, Burns JL, Quittner AL, Cibene DA, et al. Azithromycin in patients with cystic fibrosis chronically infected with *Pseudomonas aeruginosa*. JAMA 2003; 290:1749–1756. https://doi.org/10.1001/jama.290.13.1749 PMID: 14519709

22. Gillis RJ, Iglewski BH. Azithromycin retards *Pseudomonas aeruginosa* biofilm formation. J Clin Microbiol. 2004; 42:5842–5845. https://doi.org/10.1128/JCM.42.12.5842-5845.2004 PMID: 15583321

23. Imperi F, Leoni L, Visca P. Antivirulence activity of azithromycin in *Pseudomonas aeruginosa*. Front Microbiol. 2014; 5:178. https://doi.org/10.3389/fmicb.2014.00178 PMID: 24795709

24. Swatton JE, Davenport PW, Maunders EA, Griffin JL, Lilley KS, Welch M. Impact of azithromycin on the quorum sensing-controlled proteome of *Pseudomonas aeruginosa*. PLoS One 2016; 1:e0147698. https://doi.org/10.1371/journal.pone.0147698 PMID: 26808156

25. Stoodley P, Jørgensen F, Williams P, Lappin-Scott HM. The role of hydrodynamics and AHL signalling molecules as determinants of the structure of *Pseudomonas aeruginosa* biofilms. In: Bayston R, Brading M, Gilbert P, Walker J, Wimpenny JWT, editors. Biofilms: the good, the bad, and the ugly. BioLine; 1999. pp. 323–330.

26. European Committee on Antimicrobial Susceptibility Testing. Breakpoint tables for interpretation of MICs and zone diameters. Version 11.0, 2021. Available from: http://www.eucast.org.

27. Yang D, Zhang Z. Biofilm-forming *Klebsiella pneumoniae* strains have greater likelihood of producing extended-spectrum beta-lactamases. J Hosp Infect. 2008; 68:369–371. https://doi.org/10.1016/j.jhin.2008.02.001 PMID: 18353499

28. Seifi K, Kazemian H, Heidari H, Rezagholizadeh F, Saee Y, Shirvani F, et al. Evaluation of biofilm formation among *Klebsiella pneumoniae* isolates and molecular characterization by ERIC-PCR. Jundishapur J Microbiol. 2016; 9:e30682. https://doi.org/10.5812/jjm.30682 PMID: 27099694

29. Nirwati H, Sinanjung K, Fahrunissa F, Wijaya F, Napitupulu S, Hati VP, et al. Biofilm formation and antibiotic resistance of *Klebsiella pneumoniae* isolated from clinical samples in a tertiary care hospital, Klaten, Indonesia. BMC Proceedings 2019; 13:20. https://doi.org/10.1186/s12919-019-0176-7 PMID: 31890013

30. Tapalski DV, Petrovskaya TA, Kozlova AI, Edelstein MV. Potentiation of antimicrobial activity of colistin with antibiotics of different groups against multidrug- and extensively drug-resistant strains of *Klebsiella pneumoniae*, *Acinetobacter baumannii* and *Pseudomonas aeruginosa*. KMAX 2020; 22: cmac.2020.2.128–136.

31. Moshynets OV, Spiers AJ. Viewing biofilms within the larger context of bacterial aggregations. In: Dhanasekaran D, Thajuddin N, editors. Microbial Biofilms—Importance and Applications. InTechOpen; 2016. pp. 3–22.

32. Moshynets O, Chernii S, Chernii V, Losytskyy M, Karakhim S, Czerwieniec R, et al. Fluorescent β-ketoenole AmyGreen dye for visualization of amyloid components of bacterial biofilms. Meth Appl Fluoresc. 2020; 8:035006. https://doi.org/10.1088/2050-6120/ab90e0 PMID: 32375137

33. Tutar U, Çelik C, Ataş M, Tunç T, Gözel MG. Evaluation of biofilm formation activity of standard microorganism strains. J Clin Exper Invest. 2015; 6:135–139.

34. Mohsen A., Gomaa A., Mohamed F., Ragab R., Eid M., Ahmed A., et al. Antibacterial, Anti-biofilm activity of some non-steroidal anti-inflammatory drugs and N-acetyl cysteine against some biofilm producing uropathogens. Amer J Epidemiol Infect Dis. 2015; 3, 1–9.

35. Sambrook J, Fritsch EF, Maniatis T. Molecular Cloning: A Laboratory Manual. 2nd ed. Cold Spring Harbor: Cold Spring Harbor Laboratory Press; 1989.

36. HiMedia Laboratories. Technical Data Sheet SD259 for Cefoperazone/Sulbactam. 2019. Available from: https://www.himedialabs.com.

37. Ministry of Health of Ukraine. Order No 167 for Gatifloxacin. 2007. Available from: https://zakononline.com.ua.

38. European Committee on Antimicrobial Susceptibility Testing. EUCAST guidelines for detection of resistance mechanisms and specific resistances of clinical and/or epidemiological importance Version 2.0, 2017. Available from: http://www.eucast.org.

39. Lalitha C, Raman T, Rathore SS, Ramar M, Munusamy A, Ramakrishnan J. ASK2 bioactive compound inhibits MDR *Klebsiella pneumoniae* by antibiofilm activity, modulating macrophage cytokines and opsonophagocytosis. Front Cell Infect Microbiol. 2017; 7:346. https://doi.org/10.3389/fcimb.2017.00346 PMID: 28824881

40. Brisse S, Grimont F, Grimont PAD. The genus *Klebsiella*. In: Dworkin M, Falkow S, Rosenberg E, Schleifer K-H, Stackebrandt E, editors. Prokaryotes. Vol 6: Proteobacteria: Gamma subclass. 3rd edition. New York: Springer-Verlag New York; 2006. pp. 159–196.

41. Azeredo J, Azevedo NF, Briandet R, Cerca N, Coenye T, Costa AR, et al. Critical review on biofilm methods. Crit. Rev. Microbiol. 2017; 43:313–351. https://doi.org/10.1080/1040841X.2016.1208146 PMID: 27868469

42. McLaughlin K, Folorunso AO, Deeni YY, Foster D, Gorbatiuk O, Hapca SM, et al. Biofilm formation and cellulose expression by *Bordetella avium* 197N, the causative agent of bordetellosis in birds and an opportunistic respiratory pathogen in humans. Res. Microbiol. 2017; 168:419–430. https://doi.org/10.1016/j.resmic.2017.01.002 PMID: 28131895

43. Ceri H, Olson ME, Stremick C, Read RR, Morck D, Buret A. Calgary biofilm device: New technology for rapid determination of antibiotic susceptibilities of bacterial biofilms. J Clin Microbiol. 1999; 37:1771–1776. https://doi.org/10.1128/JCM.37.6.1771-1776.1999 PMID: 10325322

44. Müsken M, Klimmek K, Sauer-Heilborn A, Donnert M, Sedlacek L, Suerbaum S, et al. Towards individualized diagnostics of biofilm-associated infections: a case study. NPJ Biofilms Microbiomes 2017; 3:22. https://doi.org/10.1038/s41522-017-0030-5 PMID: 28970943

45. European Committee on Antimicrobial Susceptibility Testing. EUCAST (2010). Colistin: Rationale for the clinical breakpoints. Version 1.0, 2010. Available from: http://www.eucast.org.

46. Cai Y, Lee W, Kwa AL. Polymyxin B versus colistin: an update. Expert Rev Anti-infective Therapy 2015; 10.1586/14787210.2015.1093933. https://doi.org/10.1586/14787210.2015.1093933 PMID: 26488563

47. Orhan G, Bayram A, Zer Y, Balci I. Synergy tests by E test and Checkerboard methods of antimicrobial combinations against *Brucella melitensis*. J Clin Microbiol. 2005; 43:140–143. https://doi.org/10.1128/JCM.43.1.140-143.2005 PMID: 15634962

48. Flemming H-C., Baveye P., Neu T.R., Stoodley P., Szewzyk U., Wingender J., et al. (2021). Who put the film in biofilm? The migration of a term from wastewater engineering to medical and beyond. Biofilms Microbiomes 7, s41522-020-00183-3.

antibiotics

MDPI

Article

Therapeutic Potential of an Azithromycin-Colistin Combination against XDR *K. pneumoniae* in a 3D Collagen-Based In Vitro Wound Model of a Biofilm Infection

Olena V. Moshynets [1,*], Taras P. Baranovskyi [2], Olga S. Iungin [1,3], Alexey A. Krikunov [4], Viktoria V. Potochilova [5], Kateryna L. Rudnieva [6,7], Geert Potters [8,9,*] and Ianina Pokholenko [10,11]

1 Biofilm Study Group, Department of Cell Regulatory Mechanisms, Institute of Molecular Biology and Genetics, National Academy of Sciences of Ukraine, Zabolotnoho Str. 150, 03680 Kyiv, Ukraine
2 CeMM, Research Center for Molecular Medicine of the Austrian Academy of Sciences, Lazarettgasse 14, A-1090 Vienna, Austria
3 Department of Biotechnology, Leather and Fur, Faculty of Chemical and Biopharmaceutical Technologies, Kyiv National University of Technologies and Design, Nemyrovycha-Danchenka Street 2, 01011 Kyiv, Ukraine
4 National Amosov Institute of Cardio-Vascular Surgery Affiliated to National Academy of Medical Sciences of Ukraine, Amosov Str. 6, 02000 Kyiv, Ukraine
5 Kyiv City Maternity Hospital № 2, Mostytska 11, 02000 Kyiv, Ukraine
6 Kyiv Regional Clinical Hospital, Baggovutovskaya Str. 1, 04107 Kyiv, Ukraine
7 Department of Microbiology, Virology and Immunology, Bogomolets National Medical University, Shevchenka Blvd. 13, 01601 Kyiv, Ukraine
8 Antwerp Maritime Academy, Noordkasteel Oost 6, 2030 Antwerp, Belgium
9 Department of Bioscience Engineering, University of Antwerp, Groenenborgerlaan 171, 2020 Antwerp, Belgium
10 Department of Cell Regulatory Mechanisms, Institute of Molecular Biology and Genetics, National Academy of Sciences of Ukraine, 150 Zabolotnoho Str., 03680 Kyiv, Ukraine
11 The Polymer Chemistry & Biomaterials Group, Department of Organic and Macromolecular Chemistry, Ghent University, Krijgslaan 281, S4-Bis, 9000 Ghent, Belgium
* Correspondence: moshynets@gmail.com (O.V.M.); geert.potters@hzs.be (G.P.)

Abstract: A therapeutic combination of azithromycin (AZM) and colistin methanesulfonate (CMS) was shown to be effective against both non-PDR and PDR *Klebsiella pneumoniae* biofilms in vitro. These anti-biofilm effects, however, may not correlate with effects observed in standard plate assays, nor will they representative of in vivo therapeutic action. After all, biofilm-associated infection processes are also impacted by the presence of wound bed components, such as host cells or wound fluids, which can all affect the antibiotic effectiveness. Therefore, an in vitro wound model of biofilm infection which partially mimics the complex microenvironment of infected wounds was developed to investigate the therapeutic potential of an AZM-CMS combination against XDR *K. pneumoniae* isolates. The model consists of a 3D collagen sponge-like scaffold seeded with HEK293 cells submerged in a fluid milieu mimicking the wound bed exudate. Media that were tested were all based on different strengths of Dulbecco's modified Eagles/high glucose medium supplemented with fetal bovine serum, and/or Bacto Proteose peptone. Use of this model confirmed AZM to be a highly effective antibiofilm component, when applied alone or in combination with CMS, whereas CMS alone had little antibacterial effectiveness or even stimulated biofilm development. The wound model proposed here proves therefore, to be an effective aid in the study of drug combinations under realistic conditions.

Keywords: MDR/XDR/PDR Gram-negative infection; *Klebsiella pneumonia*; biofilms; wound model; colistin methanesulfonate; azithromycin; combined antibacterial therapy

check for updates

Citation: Moshynets, O.V.; Baranovskyi, T.P.; Iungin, O.S.; Krikunov, A.A.; Potochilova, V.V.; Rudnieva, K.L.; Potters, G.; Pokholenko, I. Therapeutic Potential of an Azithromycin-Colistin Combination against XDR *K. pneumoniae* in a 3D Collagen-Based In Vitro Wound Model of a Biofilm Infection. *Antibiotics* **2023**, *12*, 293. https://doi.org/10.3390/antibiotics12020293

Academic Editor: Marc Maresca

Received: 28 December 2022
Revised: 20 January 2023
Accepted: 28 January 2023
Published: 1 February 2023

Copyright: © 2023 by the authors. Licensee MDPI, Basel, Switzerland. This article is an open access article distributed under the terms and conditions of the Creative Commons Attribution (CC BY) license (https://creativecommons.org/licenses/by/4.0/).

1. Introduction

Lately, difficult-to-treat multi-drug resistant (MDR), extensively drug-resistant (XDR) and pandrug-resistant (PDR) gram-negative bacterial (GNB) infections are occurring more frequently all over the world, putting pressure on health care personnel to use so-called last-resort antibiotic compounds. Different forms of polymyxins belong to this group of last-resort agents. These compounds had been in use until the 1980s, but over the last decades, they were recently put forward again, in response to increased numbers of MDR/XDR/PDR GNB-associated infections [1–3].

In particular, two pharmacological types of these therapeutic polymyxins are currently in use as last-resort antibacterial agents for the treatment of XDR and PDR GNB strains: one of them is colistin sulfate (COL), and the other is colistin methanesulfonate (CMS, also known as colistimethate sodium), an improved version of colistin [4,5]. CMS is considered a prodrug of COL and transforms, upon uptake into an organism, into an active polymyxin cation, though with an unknown ratio and uncertain pharmacodynamics and with low effectiveness [4–6]. Generally, CMS might be considered a "weak antibiotic" with a 28-day patient mortality of about 43% [7]. On the other hand, CMS is less toxic to patients compared with COL; however, the compound is also less effective against bacteria and has poor bioavailability, i.e., low concentration in the pleural cavity, bronchoalveolar lavage (BAL), lung parenchyma, bones, and the cerebrospinal fluid, where the colistin distribution may correspond to 15–25% of the plasma concentration or even remain undetectable [5,6,8].

Nevertheless, the effectiveness of even these weaker antibiotics may be synergistically enhanced when applied therapeutically in combination with antibiotics with a different mode of action. Macrolides, for example, may present themselves as an option for a combined treatment with CMS or COL. While they are usually not a proper option for the treatment of GNB, because these bacteria are considered inherently resistant against this class of antibiotics [9], a combination of CMS and azithromycin (AZM) has been shown to have a synergistic antibacterial effect on both planktonic growth and biofilm development of a standard *K. pneumoniae* ATCC 10031 culture, in a physiological concentration range [10]. Moreover, this holds for non-MDR, MDR, and colistin-resistant PDR *K. pneumoniae* hospital isolates as well [10].

Interestingly, this synergy between CMS and AZM in a standard agar-diffusion assay did not match the effects observed in the corresponding biofilm models, possibly because biofilms are natural aggregates while agar colonies are artificial ones due to the unnatural conditions under which they are grown [11]. One might even say that the existence of such discrepancies suggests that disc-diffusion and broth growth-based assays may not be good predictors of antibiotic susceptibility in biofilms, and that biofilm-based tests are better models to evaluate antibiotic effectiveness. Moreover, even biofilms are not the best in vitro test systems to test antibiotic effectiveness, since they lack the eukaryotic (host) component of the infection. Both the microbial pathogens and key wound bed components (an extracellular matrix, the presence of cells from the host and the fluids in the wound milieu) are critical, each in their own specific way, for biofilm-associated infection development. These factors should therefore be taken into account when biomimetic in vitro models are being studied [12].

One of these components is the extracellular matrix protein collagen. It is the most abundant component of the extracellular matrix and provides tensile strength, regulates cell adhesion, supports chemotaxis and migration, and directs tissue development [13]. At present, collagen can be extracted from various natural animal sources or be obtained from recombinant production systems in bacteria, plants, etc. [14–17]. Due to the role of the extracellular matrix in infection development, collagen-based gel matrices have been used extensively as a substrate for the in vitro culture of biofilms [18]. Secondly, the introduction of host cells into the model allows for a better description of the mechanisms of the interactions between the cells and the bacteria, as well as of the involvement in biofilm development and protection of the bacteria from being killed by antibiotics. Thirdly, the medium environment used in the model to reproduce wound fluid milieu, affects antibiotic

behavior. For instance, AZM seemed to have a stronger antibacterial effect on some GNB in eukaryotic media [9,19–21]. This might be associated with the cell wall rebuilding due to OprM downregulation [19] which may potentially improve the antibacterial effects of other antibiotics used in combination with AZM [20,21]. This might also influence the CMS susceptibility in a biofilm culture, since a synergistic effect between CMS and AZM was already observed [10,20].

To produce a better model to evaluate the treatment efficiency of a combination of antibiotics against wound infections, three biomimetic wound surface models were constructed with collagen-based 3D scaffolds and seeded with epithelial-like cells. These wound surface models were then used to investigate the therapeutic potential of CMS-AZM combinations against XDR *K. pneumoniae* isolates.

2. Results

2.1. The Influence of Different Culture Media and the Presence of HEK293 on the Growth of K. pneumoniae UHI 1090

In order to construct a working model imitating a wound, both the scaffolding on which the cells can develop, and the liquid phase, which mimics the wound fluids, should be chosen carefully. The liquid phase should contain serum, red blood cells, plasma, and a source of hydrolyzed proteins, such as brain heart infusion media or peptones [22]. At the same time, the medium components should potentiate microbial growth as well as biofilm formation and should not demonstrate any inhibitory effect. To evaluate this, different modifications of the liquid phase content have been studied, following their effects on the *K. pneumoniae* UHI 1090 culture. A total of three modifications of the general growth medium of the bacterial culture were chosen to be seeded with or without the mammalian HEK293 cells: (1) 90% DMEM/high glucose, 10% fetal bovine serum (FBS); (2) 89.9% DMEM/high glucose, 10% FBS, 0.01% Bacto Proteose Peptone; (3) 49.9% DMEM/high glucose, 50% FBS, 0.1% Bacto Proteose Peptone. The data obtained revealed that all culture media supported the growth of *K. pneumoniae* UHI 1090 (Figure 1). An increase in optical density during 24 h in culture was more pronounced in variants that contained the HEK293 cells (Figure 1a).

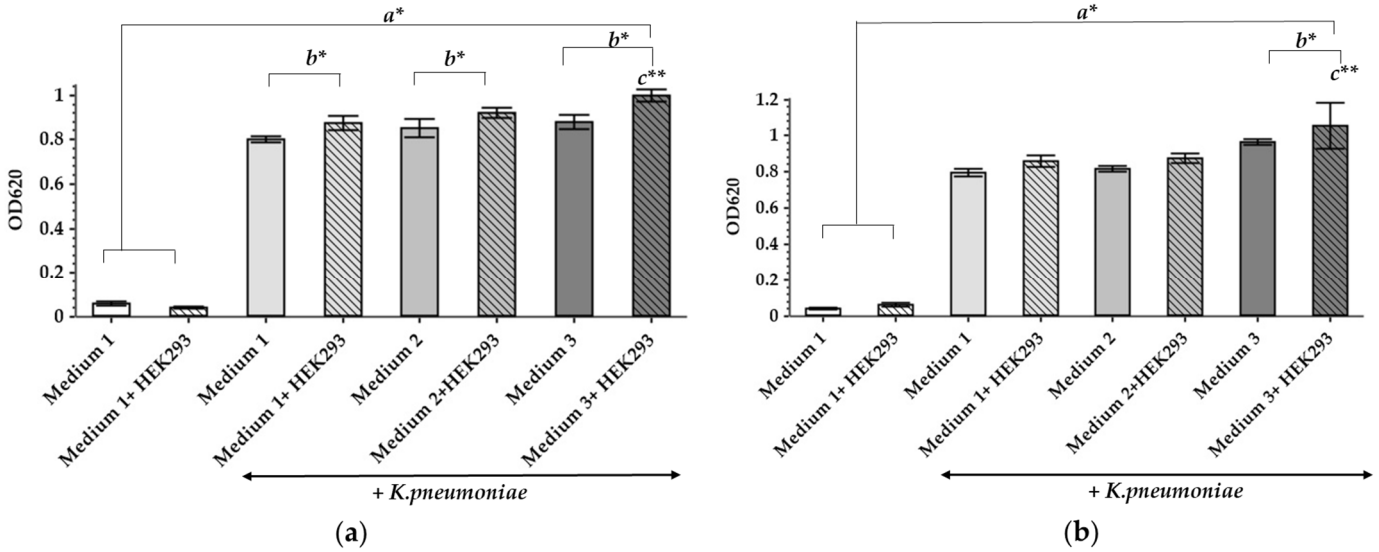

Figure 1. The influence of culture medium and HEK293 cells on the growth of *K. pneumoniae* UHI 1090. Growth shown under static conditions, after 24 h (**a**) and 48 h (**b**) of incubation. Data are expressed as mean values (n = 6). Error bars represent standard deviations. Data were analyzed by one-way ANOVA with a Barlette post hoc test. * Represents significant differences at $p < 0.05$, ** represents significant differences at $p < 0.001$. a–as compared to the control groups incubated without bacteria; b–as compared between the samples incubated with or without HEK293; c–as compared to all other groups.

Addition of HEK293 cells to each of the media promoted microbial growth within 24 h of cultivation (Figure 1a) and even within 48 h for the third medium (49.9% DMEM/high glucose, 50% FBS, 0.1% Bacto Proteose Peptone) (Figure 1b). The high FBS content in the third medium emulates the bed wound exudate, the presence of which can stimulate bacterial culture development. As demonstrated previously, *K. pneumoniae* may induce cytotoxic effects in lung epithelial cells in vitro, as a kind of predatory effect, and the cytotoxicity was highly dependent on the presence and properties of capsule polysaccharides [23]. Since *K. pneumoniae* UHI 1090 is a hospital pathogenic isolate, it is quite possible that it has similar cytotoxic effects on the HEK293 cells. Also, this third culture medium has the highest content of proteins as well as their hydrolysis products, and the presence of HEK293 cells was linked to the most pronounced stimulation of bacterial growth during 48 h in culture. Since all media tested here showed good microbial tolerance, these culture media were selected for further studies.

2.2. AZM and CMS Effects on the Viability of HEK293 Cells In Vitro

Some antibiotics may not only influence bacterial cells but have also a general toxic effect on eukaryotic cells by causing mitochondrial dysfunction, or by generating abnormally high levels of oxygen reactive species, which leads to oxidative damage to the cells [24]. This prompted the need to study the effects of AZM and CMS on the metabolic activity of the HEK293 cells (Figure 2).

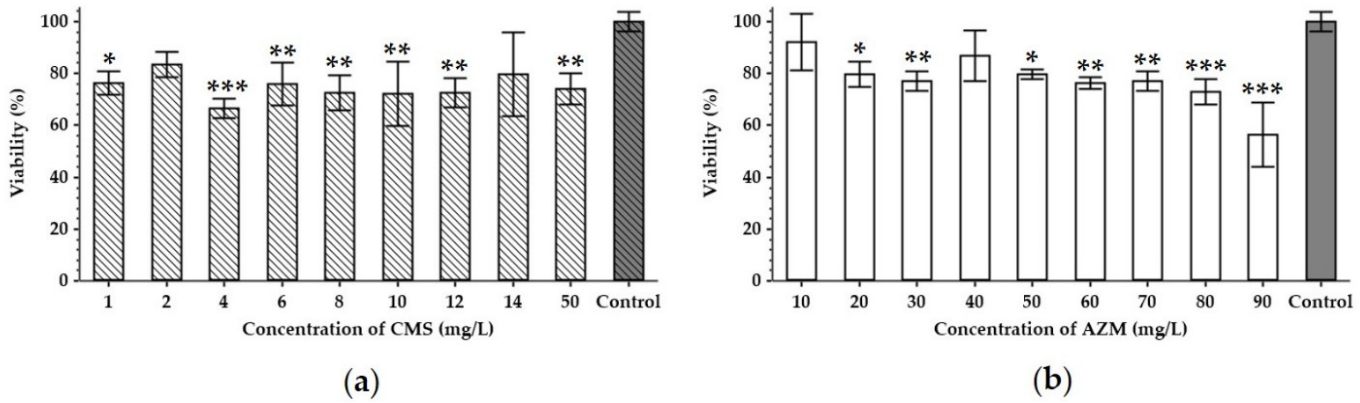

Figure 2. Cytotoxicity of colistin methanesulfonate (**a**) and azithromycin (**b**). The viability of HEK293 (human embryonal kidney) cell line treated with different concentrations of antibiotics for 48 h was analyzed using an MTT assay. Data are expressed as mean values (n = 3). Error bars represent SD. Control represents the HEK293 cultured without the addition of antibiotics. Data were analyzed by the Mann–Whitney U-test; * represents significant differences at $p < 0.05$, ** represents significant differences at $p < 0.01$, *** represents significant differences at $p < 0.001$, each time as compared to the control samples incubated without the addition of antibiotics.

CMS seems to decrease the metabolic activity of the HEK293 cells by 17–34% in a range from 1 to 50 mg/L compared to the non-treated controls (Figure 2a). As the HEK293 cell line was derived from the human embryonal kidney, this cytotoxicity of the CMS can be associated with the nephrotoxicity known to be induced by polymyxins [25,26]. AZM also exhibited cytotoxic effects towards HEK293, however, in a clear dose-dependent manner. In concentrations of 20–90 mg/L, it induced a 9–44% reduction in the cell's metabolic activity with the maximum effect at the highest dose tested (Figure 2b), while at 10 mg/L of AZM, the lowest concentration in the test, it did not cause any significant decrease in metabolic activity.

According to pharmacokinetic literature, the maximum serum concentration of CMS (C_{max}) corresponds to 10–12 mg/L [27,28]. Therefore, only concentrations lower than this C_{max} should be tested, as higher concentrations are not physiologically relevant. Serum C_{max} for AZM varies from 1 to 9 mg/L with tissue concentrations 10–50-fold higher and

a 24–34% increase in infected/inflamed tissues [29,30]. Our cytotoxicity assays, however, suggest that 5 mg/L of CMS and 10 mg/L of AZM, which both fall into the physiological range, would not impose a significant effect on the eukaryotic cell viability (Figure 2). These amounts could therefore, be expected in patients' sera and tissues following a standard dosage regime.

2.3. Development and Characterization of a Porous Collagen Scaffold for a 3D Collagen-Based Wound Model In Vitro

A porous 3D collagen-based matrix colonized with the epithelial-like HEK293 cells, and immersed in culture media that mimic wound exudate, has been selected to develop an in vitro model which maximally mimics the tissue-specific parameters during a wound-like infection during which bacterial biofilms form on the soft tissues. Type I collagen was selected for the development of the 3D scaffold because it is one of the main components of the derma. The matrices were developed by freeze-drying a solution of bovine collagen type I. The data received by SEM revealed that scaffolds had pores with an average pore diameter of 117 $\pm$ 57 µm (Figure 3). The internal microstructure of the scaffolds consisted of multi-layered porous sheets (as seen from the cross-section SEM image in Figure 3a) with an average distance between the layers of 91 $\pm$ 50 µm. The porous structure of the developed 3D scaffolds facilitates cell migration inside the scaffold, ensures the exchange of the culture medium as well as gases and allows for the removal of cell metabolism products.

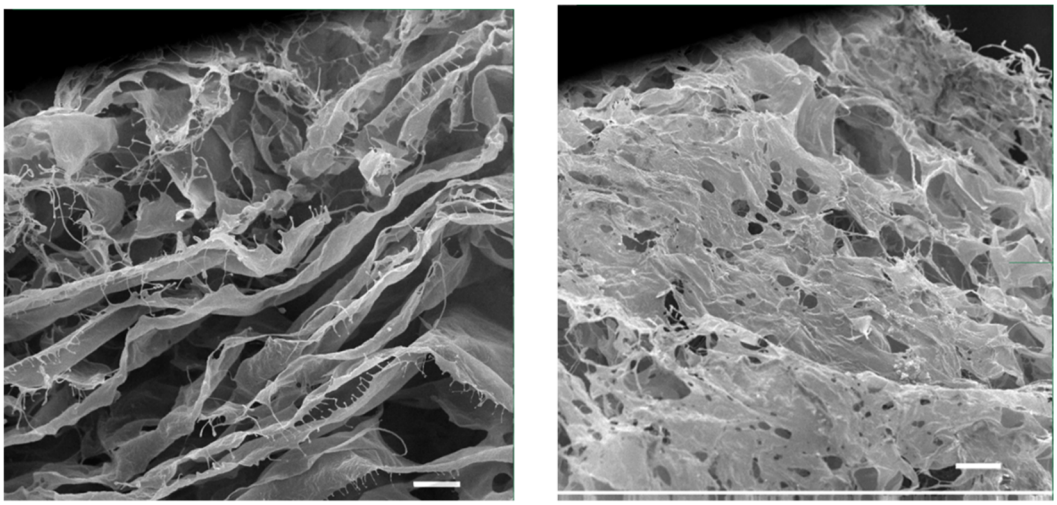

Figure 3. Scanning electron micrographs of a 3D collagen scaffold (scale bar corresponds to 100 µm). (**a**) cross-section; (**b**) the surface of the scaffold.

This collagen scaffold was tested to see whether it could be colonized by the epithelial-like cell line HEK293, as well as by a XDR hospital isolate of *K. pneumoniae* UHI 1090. To evaluate whether HEK293 could colonize the developed collagen scaffold, 2×10^5 HEK293 cells were seeded onto a collagen scaffold of approximately 0.024 cm^3 in volume, immersed in DMEM/high glucose medium containing 10% FBS. After three days, colonization could be confirmed (Figure 4).

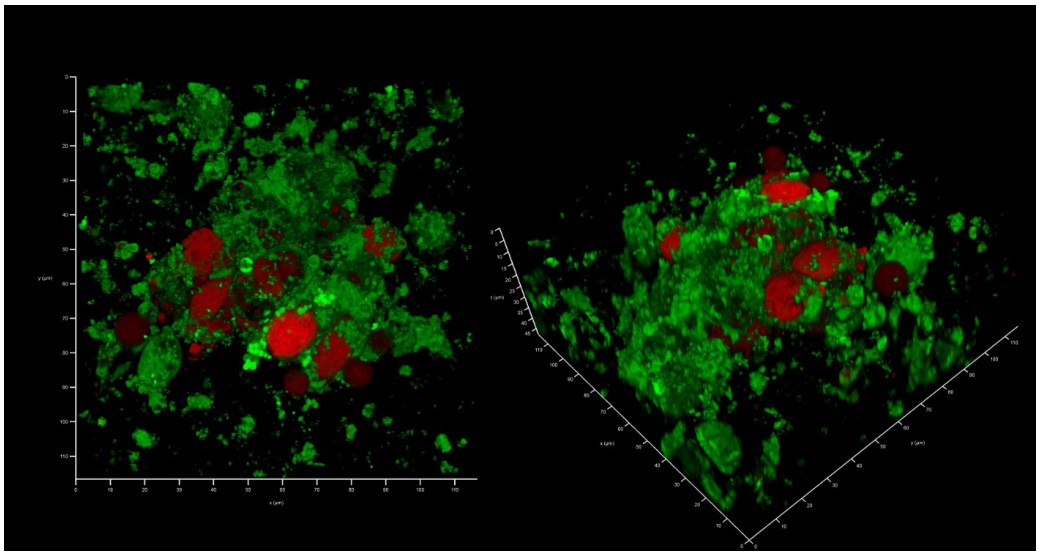

Figure 4. In vitro wound model of a 3D collagen scaffold seeded with HEK293 cells line after three days of incubation. Confocal laser scanning microscopy imaging, 120 µm × 120 µm × 35 µm, 10 µm per division. AmyGreen was used to stain collagen (green signal) and ethidium bromide was used to stain eukaryotic nuclei (red signal).

Interestingly, *K. pneumoniae* UHI 1090 failed to develop biofilms on this collagen scaffold if it was not colonized with HEK293 (Figure 5). Briefly, when 10^4 CFU/mL of the bacterial culture was inoculated, there were no bacterial biofilms observed following 48 h of incubation. Instead, individually attached bacterial cells were found on the collagen surface, and no CFU was found in the liquid medium, suggesting that no planktonic bacterial subpopulation had developed.

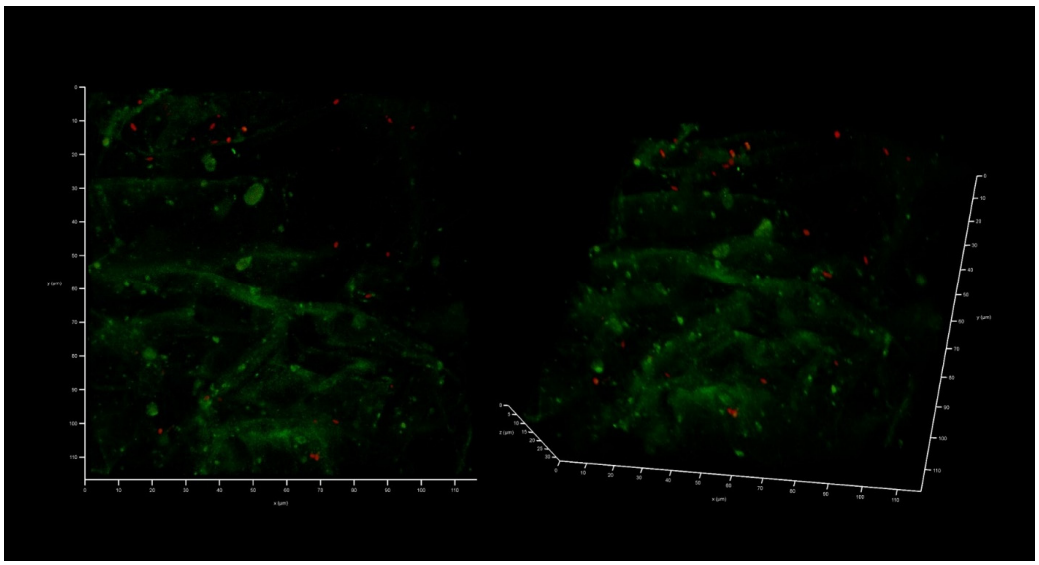

Figure 5. A 48-h old *K. pneumoniae* UHI 1090 culture developed on a 3D collagen scaffold. The scaffold was not seeded with HEK293 cells, but fetal bovine serum was added as a source of blood proteins (medium No. 1). Confocal laser scanning microscopy imaging, 120 µm × 120 µm × 35 µm, 10 µm per division. AmyGreen was used to stain collagen (green signal), and ethidium bromide was used to stain the bacterial cells (red signal).

Thus, to mimic the conditions under which these can be observed in vivo, the presence of eukaryotic cells might be specifically important to allow pathogenic isolates to develop both their biofilms and planktonic subpopulations.

2.4. AZM and CMS Effects on Biofilm Development by K. pneumoniae UHI 1090 in a 3D Collagen-Based In Vitro Model

The first model, developed in medium No. 1, demonstrated well-developed biofilms in a control where no eukaryotic cells remained and even better biofilm biomass where CMS was added (Figure 6). The level of CFU in the liquid medium phase correlated with the biofilm biomass present and was 10^7 for control and 10^8 CFU/mL for the CMS microcosm correspondingly, which demonstrated a stimulatory effect of CMS instead of the expected antibacterial action. In the AZM-containing microcosm, the *Klebsiella* CFU was 10^2 per mL and the eukaryotic cells were mostly preserved and the biofilms did not develop with only one field of view where a few attached bacterial cells were found (Figure 6, right image). Both antibiotics had strong antibacterial effects and inhibited the development of the biofilm on the wound model, however, with ten bacterial cells/mL as a planktonic subpopulation.

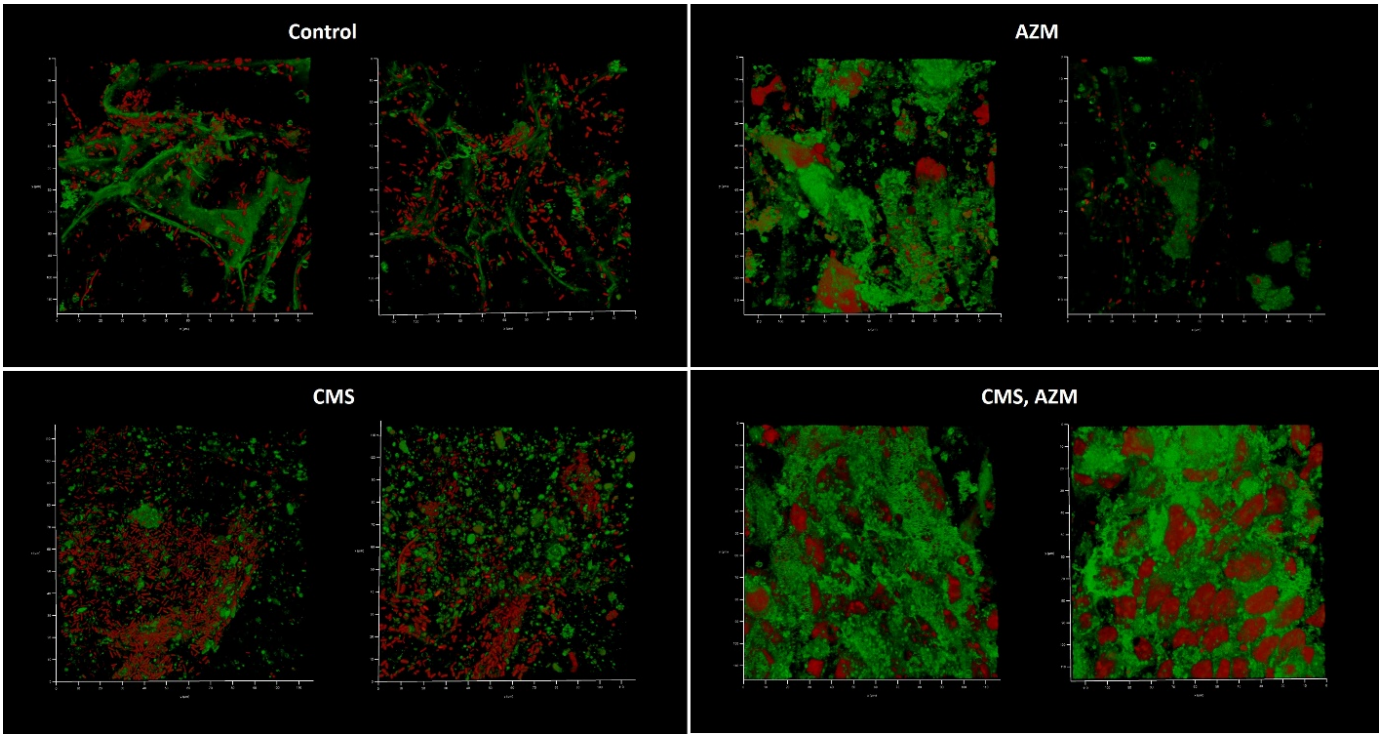

Figure 6. In vitro wound model of a *K. pneumoniae* UHI 1090 biofilm exposed to colistin methanesulfonate and azithromycin. Images were taken after 48 h of biofilm development on a 3D collagen scaffold seeded with the epithelial-like cell line HEK293 in medium No. 1 (90% DMEM/high glucose, 10% fetal bovine serum), supplemented with 5 mg/L colistin methanesulfonate (**CMS**) or 10 mg/L of azithromycin (**AZM**), or both colistin methanesulfonate and azithromycin (**CMS, AZM**), or without (**control**). Confocal laser scanning microscopy imaging, 120 µm × 120 µm × 35 µm, 10 µm per division. AmyGreen was used to stain collagen (green signal) and ethidium bromide was used to stain eukaryotic nuclei and bacteria (red signal).

Interestingly, bacterial functional amyloids were observed to be associated with *Klebsiella* cells when medium No. 1 was applied (Figure 7). Previously, we demonstrated that AmyGreen visualizes functional bacterial amyloids more effectively than the classical Thioflavine T [31,32]. However, amyloidogenesis was repressed when AZM was used.

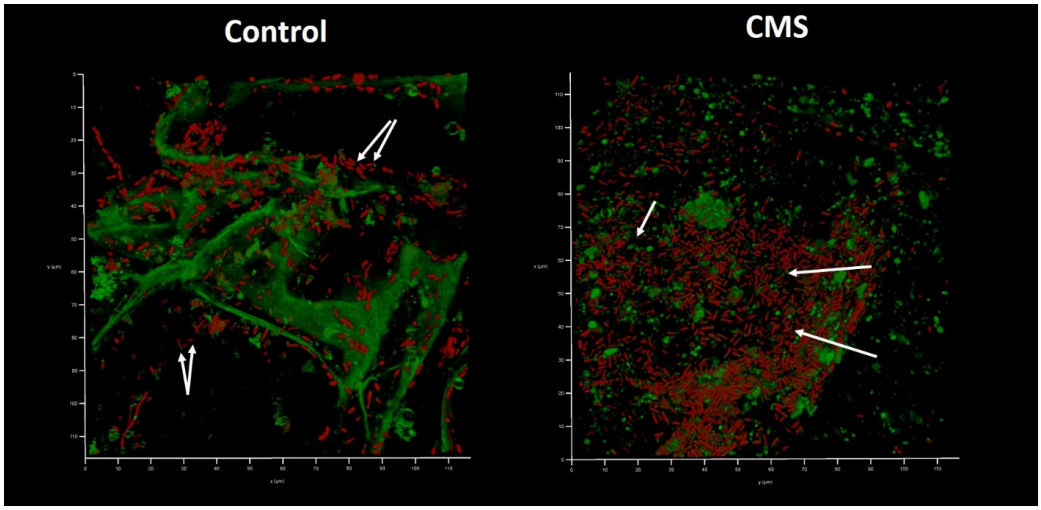

Figure 7. In vitro wound model of a *K. pneumoniae* UHI 1090 biofilm exposed to colistin methanesulfonate (enlarged details of parts of Figure 6). Images were taken after 48 h of biofilm development on a 3D collagen scaffold seeded with the epithelial-like cell line HEK293 in medium No. 1 (90% DMEM/high glucose, 10% FBS) supplemented with 5 mg/L colistin methanesulfonate (**CMS**) or without (**control**). Confocal laser scanning microscopy imaging, 120 µm × 120 µm × 35 µm, 10 µm per division. AmyGreen was used to stain collagen and bacterial amyloid fibers (green signal) and ethidium bromide was used to stain eukaryotic nuclei and bacteria (red signal). Arrows point to amyloid fibers associated with bacterial cells.

The second model was based on medium No. 2. This model proved to be less effective than the previous one although neither medium No. 1 nor No. 2 demonstrate any differences in the plate-based assay (Figure 8). Upon application of medium No. 2, biofilms were only observed under control conditions, where no antibiotics had been added. The corresponding planktonic subpopulations were also suppressed: the control had 10^5 CFU/mL, whereas no CFU were observed in antibiotic-containing variants.

Medium No. 3 was used in the third model. Like in the first model, biofilm development and absence of eukaryotic nuclei were observed in control and CMS-containing variants when AZM and AZM + CMS variants demonstrated partially preserved initial model structure with some individual bacterial cells attached (Figure 9). Plating assays confirmed the cytological observations: planktonic cell concentrations of 10^8 CFU/mL were observed in control and CMS-supplemented variants, while concentrations of 10^2 CFU/mL were observed in AZM and AZM + CMS variants, which suggests that CMS did not show any antibacterial effect even though *K. pneumoniae* UHI 1090 was sensitive to polymyxin. On the contrary, AZM demonstrated strong antibacterial effects against planktonic and biofilm subpopulations.

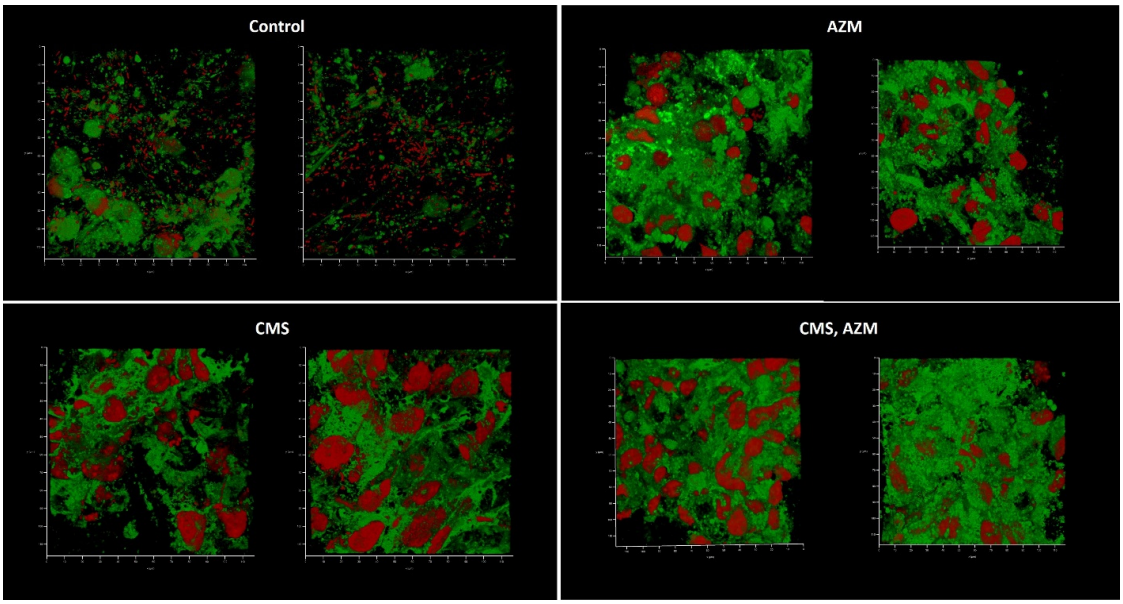

Figure 8. In vitro wound model of a *K. pneumoniae* UHI 1090 biofilm exposed to colistin methanesulfonate and azithromycin. Images were taken after 48 h of biofilm development on a 3D collagen scaffold seeded with the epithelial-like cell line HEK293, in medium No. 2 (89.9% DMEM/high glucose, 10% FBS, 0.01% Bacto Proteose Peptone), supplemented with 5 mg/L colistin methanesulfonate (**CMS**) or 10 mg/L of azithromycin (**AZM**), or both colistin methanesulfonate and azithromycin (**CMS, AZM**), or without (**control**). Confocal laser scanning microscopy imaging, 120 µm × 120 µm × 35 µm, 10 µm per division. AmyGreen was used to stain collagen (green signal) and ethidium bromide was used to stain eukaryotic nuclei and bacteria (red signal).

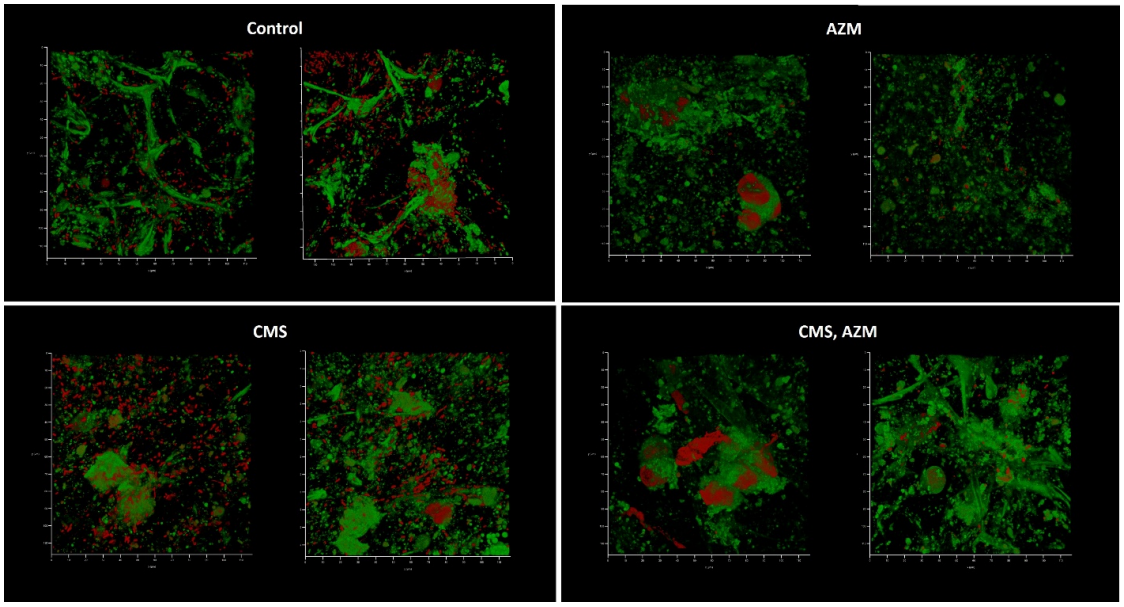

Figure 9. In vitro wound model of a *K. pneumoniae* UHI 1090 biofilm exposed to colistin methanesulfonate and azithromycin. Images were taken after 48 h of biofilm development on a 3D collagen scaffold seeded with the epithelial-like cell line HEK293, in medium No. 3 (49.9% DMEM/high glucose, 50% fetal bovine serum, 0.1% Bacto Proteose Peptone) supplemented with 5 mg/L colistin methanesulfonate (**CMS**) or 10 mg/L of azithromycin (**AZM**), or both colistin methanesulfonate and azithromycin (**CMS, AZM**), or without (**control**). Confocal laser scanning microscopy imaging, 120 µm × 120 µm × 35 µm, 10 µm per division. AmyGreen was used to stain collagen (green signal) and ethidium bromide was used to stain eukaryotic nuclei and bacteria (red signal).

3. Discussion

Polymyxin antibiotics demonstrate an extremely narrow therapeutic index of 2–4 mg/L [33]. This reduces the application of colistin considerably: an antibacterial effect may overlap with the nephrotoxic dose regimen [26]. Thus, since the introduction of polymyxins in the 1950s, the most effective therapeutic regime has been debated [8,33,34]. As the overall success of CMS therapy stands at approximately 50%, there is a prediction that better balanced regime might improve the therapeutic outcome. This can be achieved by increasing the C_{max} up to the MIC and beyond. However, increasing the dosage does not help to achieve this goal. Even 3 million units (MU) i/v every 8 h does not provide a needed C_{max}:MIC ratio for COL-susceptible GNB with MIC $\leq$ 2 (2022 EUCAST Clinical Breakpoints; European Committee on Antimicrobial Susceptibility Testing). Particularly, 2 MU of CMS i/v every 8 h resulted in a COL concentration of 0.92 $\pm$ 0.46 mg/L or 1.03 $\pm$ 0.69 mg/L in another study, when 3 MU i/v every 8 h corresponded to 0.6–2.3 mg/L of COL [8,27,35]. In another study, the C_{max} of COL concentration in plasma following i/v administration of 3 MU of CMS every 8 h, 4.5 MU every 12 h and 9 MU every 24 h corresponded to 3.34 +/− 0.35, 2.98 +/− 0.27 and 5.63 +/−0.87 mg/L, respectively [36]. Moreover, all serum samples containing more than 4 mg/L COL eliminated *P. aeruginosa*, whereas complete bacterial eradication was only achieved in 40% of the samples containing less than 4 mg/L COL [36]. Since the MIC breakpoint for COL-susceptible GNB corresponds to 2 mg/L, the widely used dosage regimes of CMS are associated with suboptimal C_{max}:MIC ratios, which still need to be determined. Still, based on [36] we can conclude that the empirical C_{max}:MIC-ratio would have to be more than two, or that C_{max} has to be more than 4 mg/L for GNB. Taking this into account, several approaches for a colistin dosing regimen have been adopted, such as the application of a loading dose followed by a maintenance dose, a higher dose as per patient renal function and targeted steady-state concentrations of colistin, local administration (intraventricular or inhaled), and antibiotic combination therapy [37]. Following their systematic review, Haseeb et al. [33] concluded that a loading dose of 9 MU of CMS followed by a maintenance dose of 4.5 MU every 12 h was considered the most appropriate dosing strategy to optimize the safety and efficacy of treatment and improve clinical outcomes. Katip et al. [38] also concluded that the loading dose of 9 MU should be used to increase the opportunity for patients to achieve favorable outcomes. However, an increase in nephrotoxicity was found to be associated with the 9 MU loading dose application [38].

Another way to optimize the CMS therapy might be an approach to decrease the MIC of COL/CMS by applying a synergistic antibiotic with another mechanism of action, presumably one which can decrease metabolic activity and biofilm formation to reduce phenotypic resistance. Macrolides correspond to such requirements. Even though none of the macrolides are officially recommended to treat Gram-negative infections due to their natural genetic resistance, there is some evidence that some macrolides have anti-biofilm and anti-virulence effects on *P. aeruginosa* [9,39–42], which could be associated with protein synthesis inhibition due to the formation of a ribosomal-macrolide complex [43,44]. This results in an inhibition of the general metabolic activity of a cell albeit without a lethal effect due to drug efflux. Thus, any of the macrolides with the same mode of action may be effective in metabolic suppression and, as a result, have anti-biofilm efficacy. Indeed, two out of eight macrolides repressed biofilm formation by *K. pneumoniae*, with azithromycin effectively suppressing ATCC, hospital acquired MDR/PDR and non-MDR *K. pneumoniae* isolates [10]. It was quite surprising not to see both erythromycin and clarithromycin as effective anti-biofilm macrolides, as both antibiotics were described as effective as azithromycin in the treatment of *P. aeruginosa*-related infections [44–48]. Also, it was unexpected to find josamycin as effective as azithromycin to suppress *K. pneumoniae* biofilm development as several studies reported that josamycin was absolutely not effective against *P. aeruginosa* [44,48,49]. That might suggest that effects of different macrolides on Gram-negative bacteria are independent of the number of lactone rings, as was suggested by the above-mentioned authors, but are, on the contrary species dependent.

Recently we have investigated and described a synergistic effect of CMS and AZM applied together against planktonic populations and biofilms of XDR/PDR and non-MDR *K. pneumoniae* hospital isolates [10]. In order to investigate how the same combination of antibacterial compounds can act against XDR (sensitive to colistin) *K. pneumoniae* infection, three modifications of the in vitro wound model based on a collagen scaffold seeded with epithelial-like cell line HEK293 were used. All the models differed only with respect to the liquid phase in which the scaffold with eukaryotic cells was submerged. Even though none of the liquid phases showed significant differences in their ability to support bacterial growth, the models were considerably different in terms of bacterial behavior and antibiotic effectiveness. The second model was less favorable for the modulation of the infection process since the control variant (no antibiotic added) demonstrated weak bacterial growth (10^5 CFU/mL). The first and the third models were more effective: the first model was able to stimulate the appearance of bacterial amyloid fibrils, and both of the models confirmed the absence of antibacterial activity of CMS (in a 5 mg/L concentration), as was expected.

Intriguingly, as was already discussed by [9], a significant difference was observed in the effects of AZM and CMS on *K. pneumoniae* UHI 1090, where 9 mg/L of AZM was able to reduce biofilm development by 7% in a *K. pneumoniae* UHI 1090 biofilm model (Figure 10, adapted from Figure 5 in [10]) and the in vitro wound model used in this study.

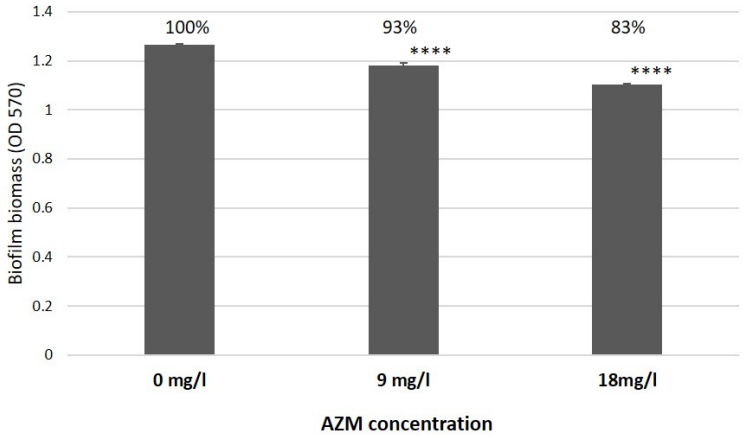

Figure 10. The effect of azithromycin on biofilm growth by *K. pneumoniae* UHI 1090 investigated using biofilm assays and optical density (OD) measurements at 570 nm after 24 h incubation (adapted from Figure 5 in [10]). Statistical differences were determined between media with azithromycin versus control media without; **** $p < 0.001$.

In our in vitro wound model, AZM considerably suppressed the biofilm formation and reduced CFU from 10^7–10^8 CFU/mL up to 10^2 CFU/mL, which confirmed a considerable improvement of antibacterial efficiency of AZM against GNB in the physiologically relevant environment as observed before [9,19–21]. Moreover, the synergistic action of AZM and CMS observed in a biofilm model, as mentioned before (Figure 11, [10]), also considerably improved. Briefly, a combined application of 8 mg/L CMS and 9 mg/L AZM reduced biofilm development by 18% compared to the control. In our models, lower concentrations of CMS (5 mg/L) and 10 mg/L AZM, demonstrated a bactericidal effect in model No. 1 and a considerable bacterial suppression in model No. 3, illustrated by weak bacterial growth (100 CFU/mL) and a partial retention of the model structure.

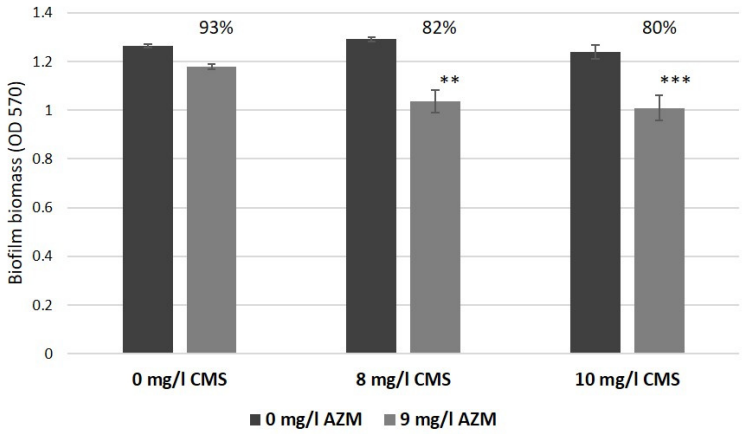

Figure 11. The effect of azithromycin and colistin methanesulfonate on biofilm growth by *K. pneumoniae* UHI 1090 investigated using biofilm assays and with optical density (OD 570) measurements after 24 h incubation (adapted from Figure 5 in [10]). Statistical differences were determined between media with azithromycin versus control media without; ** $p < 0.01$, *** $p < 0.005$.

Analysis of the effects of AZM in model No. 1 and model No. 3 demonstrates a strong bactericidal effect of AZM against XDR *K. pneumoniae* UHI, which was not observed in a biofilm model used before [10]. On the contrary, CMS did not demonstrate any antibacterial (model No. 3) or even a growth-stimulating effect (model No. 1). It is well known that CMS interacts with the negatively charged phosphate groups of Lipid A on the outer membrane of gram-negative bacteria [50], leading to the impairment of the three-dimensional LPS structure. However, the interaction of LPS with the chromosomal DNA that was released from the dying HEK293 cells could possibly block the binding of colistin to its cellular target. Also, DNA can serve as a scavenger for the CMS molecules. It was demonstrated previously that polymyxin B could bind the chromosomal DNA of mammalian cells [51]. The increased bacterial growth on the less nutritious culture medium 1 in the presence of CMS could be explained by the early release of additional nutrients from HEK293 stimulated by the cytotoxic action of CMS on these cells. On the other side, sub-MIC concentrations of CMS were shown to enhance biofilm formation by upregulating 197 genes responsible for the formation of extracellular polymeric substances, the production of homoserine lactone and the expression of amyloid, as well as to slow down cell metabolism by downregulating 88 genes in *Acinetobacter baumannii* [52]. Both the stimulation effect as well as the enhancement of amyloid production observed in Figure 7 might therefore be a direct response to a sub-MIC regime of CMS.

4. Materials and Methods

4.1. Bacterial Strain and Culture Conditions

Klebsiella pneumoniae UHI 1090, a Ukrainian hospital isolate, was originally recovered from a patient with enteritis and identified as an extensively drug-resistant (XDR) strain using antibiotic disc diffusion assays and EUCAST 2021 v.11.0 breakpoints [10]. An AST-N332 card was used to confirm the XDR strain phenotype with the VITEK 2 Advanced Expert System. Antimicrobial susceptibility to polymyxin was tested with a SensiTest Colistin (Liofilchem, Roseto degli Abruzzi, Italy) broth microdilution assay and the results were interpreted according to EUCAST breakpoints. The strain was found to be sensitive to polymyxin B and tigecycline but resistant to all β-lactams, fluoroquinolones and aminoglycosides (details of which can be found at https://doi.org/10.1371/journal.pone.0270983.s006) (accessed on 28 December 2022). The strain was stored as frozen stocks in 25 (*v*/*v*) % glycerol at −80 °C.

4.2. Mammalian Cell Lines

The human embryonal kidney cell line HEK293 was obtained from the Bank of Cell Lines from Human and Animal Tissues of the Kavetsky Institute of Experimental Pathology, Oncology and Radiobiology of the National Academy of Science of Ukraine. The cells were cultured in Dulbecco's modified Eagles medium (DMEM)/high glucose culture medium (Biowest, Nuaillé, France), containing 10% fetal bovine serum (FBS) (Sigma-Aldrich, Saint Louis, MO, USA), 100 U/mL of penicillin, and 100 mg/mL of streptomycin (Arterium, Kyiv, Ukraine).

4.3. Viability of Eukaryotic Cells after Antibiotic Treatment

The influence of CMS and AZM on the viability of HEK293 cells was tested with the colorimetric MTT metabolic activity assay. HEK293 cells were seeded 24 h prior to the application of the antibiotics. Before any antibiotics were added, the culture medium was changed to a medium without fetal bovine serum. HEK293 cells were then cultured at 37 °C and 5% CO_2, at a concentration of 3×10^5 cells per well in a 96-well plate, in the presence of varying concentrations of the antibiotic for 48 h. Cells grown in DMEM/high glucose medium without antibiotics served as a negative control group. The assay was performed according to [53]. Measurements for each concentration point were performed in triplicate.

4.4. Effects of Different Culture Media and HEK293 Cells on the Growth of K. pneumoniae UHI 1090

A total of 3×10^5 HEK293 cells/well were plated into 96-well culture plate 24 h before bacterial inoculation. The HEK293 cells were cultivated in DMEM/high glucose medium, containing 10% FBS at 37 °C, 5% CO_2. The medium was changed before inoculation of *K. pneumoniae* to the following media: (1) 90% DMEM/high glucose medium, containing 10% FBS; (2) 89.99% DMEM/high glucose medium, containing 10% FBS, 0.01% Bacto Proteose Peptone (BD Biosciences, Franklin Lakes, NJ, USA); (3) 49.99% DMEM/high glucose medium, containing 50% FBS, 0.01% Bacto Proteose Peptone (BD Biosciences, Franklin Lakes, NJ, USA). Cell-free media served as control. *K. pneumoniae* UHI 1090 (10^4 CFU/well) was inoculated, and the incubation was prolonged at 37 °C, 5% CO_2. OD values were measured 24 h after inoculation at 620 nm. Each measurement was performed in six replicates.

4.5. Cultivation of Bacteria and Antibiotic Treatments

The bacterial strains were cultured aerobically at 37 °C in Luria–Bertani (LB) medium (10 g/L peptone, 5 g/L yeast extract and 10 g/L sodium chloride, with 12 g/L agar added when solid media were needed [54]) and on Muller Hinton Agar (OXOID, Basingstoke, UK). The strain was recovered from frozen stocks on LB plates before initiating overnight shaken cultures to provide fresh inoculum for experiments (direct inoculation from frozen stocks was found to reduce siderophore production and biofilm development considerably; unpublished observations). Culture densities and dilutions were determined by OD 570 measurements using a Multiskan™ FC Microplate Photometer (Thermo Fisher Scientific, Waltham, MA, USA). A 10 g/L AZM (Pharmex Group, Boryspil, Ukraine) stock solution was prepared using DMSO as a solvent, while a 1 g/L stock solution of CMS (Forest Laboratories, Barnstaple, UK) was prepared in water. Both stocks were used within 30 min of preparation. Discs containing antibiotics (HiMedia Laboratories, Mumbai, India) as well as AST-N332 cards for the VITEK 2 Advanced Expert System (bioMerieux, Marcy l'Étoile, France) were used for antimicrobial susceptibility and sensitivity assays as listed in [10].

4.6. Collagen Scaffold Preparation

Porous collagen scaffolds were produced from a solution of bovine atelocollagen in acetic acid using the following freeze-drying technique. Briefly, a solution of 20 mg/mL

of type I atelocollagen, isolated from a bovine tendon, was prepared in 0.5 M acetic acid. Afterwards, the solution was centrifuged at 2500 rpm, +4 °C for 15 min to remove air bubbles formed during mixing. The prepared collagen solution was then frozen in glass Petri dishes (10 cm in diameter) at −40 °C and held for 18 h inside a freeze-dryer. The frozen suspensions were subsequently sublimed at −40 °C to +22 °C for 24 h under a vacuum. The atelocollagen scaffolds were stored at −20 °C until further use. Prior to usage, the scaffolds were brought to +22 °C, cut into 3 × 4 mm rectangles under a sterile laminar hood, and sterilized by UV-exposure for 40 min. Subsequently, they were equilibrated in 0.1 M HEPES (pH 8.0) at +4 °C overnight. Afterwards, the HEPES solution was changed with DMEM/high glucose medium, containing 10% (*v*/*v*) FBS, 100 U/mL penicillin and 100 μg/mL streptomycin, in which the scaffolds were equilibrated for 48 h, at +37 °C and 5% CO_2, before cell seeding.

4.7. Preparation of the Wound Model

HEK293 cells were grown in Dulbecco's modified Eagle's medium (DMEM)/high glucose, containing 10% (*v*/*v*) FBS, 100 U/mL penicillin and 100 μg/mL streptomycin. The 2×10^5 cells were seeded on $0.3 \times 0.4 \times 0.2$ cm^3 porous scaffold. The cell-seeded scaffolds were then transferred into fresh full culture medium and incubated at +37 °C, 5% CO_2 for three days. Prior to *K. pneumoniae* UHI 1090 inoculation, the scaffolds with cells were washed three times in DMEM/high glucose medium and incubated in DMEM/high glucose containing 10% FBS overnight at 37 °C, 5% CO_2. 200 μL of an overnight culture of *K. pneumoniae* UHI 1090 was inoculated into a model system where the final concentration of the bacterial cells was 10^4 CFU/mL. The incubation lasted at 37 °C under high CO_2 conditions for two days. Upon incubation, colony forming units (CFU) in the liquid phase of a model were identified by a classical plating assay in triplicate.

4.8. Confocal Laser Scanning Microscopy (CLSM)

Samples taken from the wound model cultures were placed onto glass slides and stained with 2 μg/mL ethidium bromide (ThermoFisher Scientific, Waltham, MA, USA) and 1 μM AmyGreen (Department of Biomedicinal Chemistry, Institute of Molecular Biology and Genetics, Kyiv, Ukraine) in DMSO (Sigma-Aldrich, Saint Louis, MO, USA) without being washed, to limit the physical disruption of biofilm structures through liquid movement. The samples were not fixed, and a cover slip was placed over the stained samples before imaging. CLSM analysis was undertaken using a Leica TCS SPE Confocal system with a coded DMi8 inverted microscope (Leica, Mannheim, Germany) and Leica Application Suite X (LAS X) Version 3.4.1 (Leica Microsystems CMS, GmbH, Wetzlar, Germany). Images were acquired using an excitation wavelength of 488 nm and with emissions collected at 490–580 nm for AmyGreen and excitation at 532 nm and at 537–670 nm for ethidium bromide.

4.9. Scanning Electron Microscopy (SEM)

Freeze-dried samples of developed matrices were coated with a 10–30 nm thick gold-metal layer to improve the surface conductivity and examined for morphological details with the Jeol JSM 35C and Jeol JSM 6060LA scanning electron microscopes (Tokyo, Japan).

4.10. Statistical Analysis

Replicate data were processed using the statistical software package OriginPro 7.0 (OriginLab Corporation, Northampton, MA, USA), MS Excel for Windows and MaxStat Pro 3.6 (MaxStat Software, Jever, Germany). All results are presented as the mean ± standard deviation. A value of $p < 0.05$ was considered statistically significant.

5. Conclusions

An effective combined antibacterial therapy against XDR and PDR *K. pneumoniae* infections which is effective for most of the hospital isolates, can be a good alternative to

the synergy tests or other time- and cost-consuming assays which have not been introduced widely into clinic practice. AZM demonstrated effective antibacterial and antibiofilm activities against *K. pneumoniae* UHI 1090 biofilm infections in in vitro wound models based on a 3D collagen scaffold seeded with epithelial-like cell line HEK293. CMS did not have a promising antibacterial effect in combination with AZM, except for a slight improvement as observed in one model. On the other hand, CMS applied alone, either had no effect on the *Klebsiella* population or even stimulated bacterial growth.

Author Contributions: Conceptualization, O.V.M., A.A.K. and I.P.; methodology, O.V.M. and I.P.; validation, O.V.M. and I.P.; formal analysis, O.V.M. and I.P.; investigation, O.V.M., T.P.B., O.S.I., A.A.K., V.V.P., K.L.R. and I.P.; resources, O.V.M. and I.P.; data curation, O.V.M.; writing—original draft preparation, O.V.M., I.P. and G.P.; writing—review and editing, O.V.M., I.P. and G.P.; visualization, O.V.M. and I.P.; supervision, O.V.M.; project administration, O.V.M.; funding acquisition, O.V.M. All authors have read and agreed to the published version of the manuscript.

Funding: This research was funded by the National Research Foundation of Ukraine (https://nrfu.org.ua/en/) (accessed on 17–18 September 2022, protocol No 21) within the frame of the project "Development of combined therapy for severe *Klebsiella pneumoniae*–associated nosocomial infections to overcome the antibiotic resistance" (2020.02/0246).

Institutional Review Board Statement: Not applicable.

Informed Consent Statement: Not applicable.

Data Availability Statement: All data have been incorporated into this manuscript.

Acknowledgments: The authors would like to express their sincere thanks towards the Ukrainian Army and the Ukrainian engineers for their fantastic support in defending the country and its energy infrastructure, so that scientific research can continue to progress and be published.

Conflicts of Interest: The authors declare no conflict of interest. The funders had no role in the design of the study; in the collection, analyses, or interpretation of data; in the writing of the manuscript; or in the decision to publish the results.

References

1. Karakonstantis, S.; Kritsotakis, E.I.; Gikas, A. Pandrug-resistant Gram-negative bacteria: A systematic review of current epidemiology, prognosis and treatment options. *J. Antimicrob. Chemother.* **2019**, *75*, 271–282. [CrossRef] [PubMed]
2. Higgins, P.G.; Hagen, R.M.; Podbielski, A.; Frickmann, H.; Warnke, P. Molecular Epidemiology of Carbapenem-Resistant *Acinetobacter baumannii* Isolated from War-Injured Patients from the Eastern Ukraine. *Antibiotics* **2020**, *9*, 579. [CrossRef]
3. Voidazan, S.; Albu, S.; Toth, R.; Grigorescu, B.; Rachita, A.; Moldovan, I. Healthcare Associated Infections-A New Pathology in Medical Practice? *Int. J. Environ. Res. Public Health* **2020**, *17*, 760. [CrossRef] [PubMed]
4. Michalopoulos, A.S.; Falagas, M.E. Colistin: Resent data on pharmacodynamics properties and clinical efficacy in critically ill patients. *Ann. Intensive Care* **2011**, *1*, 30. [CrossRef] [PubMed]
5. Michalopoulos, A.S.; Karatza, D.C.; Gregorakos, L. Pharmacokinetic evaluation of colistin sodium. *Expert Opin. Drug Metab. Toxicol.* **2011**, *7*, 245–255. [CrossRef]
6. Li, J.; Turnidge, J.; Milne, R.; Nation, R.L.; Coulthard, K. In vitro pharmacodynamics properties of colistin and colistin methanesulfonate against *Pseudomonas aeruginosa* isolates from patients with cystic fibrosis. *Antimicrob. Agents Chemother.* **2001**, *45*, 781–785. [CrossRef]
7. Paul, M.; Daikos, G.L.; Durante-Mangoni, E.; Yahav, D.; Carmeli, Y.; Benattar, Y.D.; Skiada, A.; Andini, R.; Eliakim-Raz, N.; Nutman, A.; et al. Colistin alone versus colistin plus meropenem for treatment of severe infections caused by carbapenem-resistant Gram-negative bacteria: An open-label, randomized controlled trial. *Lancet Infect Dis.* **2018**, *18*, 391–400. [CrossRef]
8. Imberti, R.; Cusato, M.; Villani, P.; Carnavale, L.; Iotti, G.A.; Langer, M.; Regazzi, M. Steady-state pharmacokinetics and bronchoalveolar lavage concentration of colistin in critically ill patients after intravenous colistin methanesulphonate administration. *Chest* **2010**, *138*, 1333–1339. [CrossRef]
9. Karakonstantis, S. Macrolides: An underappreciated option for treatment of *Pseudomonas aeruginosa* infections (and potentially other gram-negative pathogens)? *Clin. Microbiol. Infect.* **2022**, *28*, 1665–1666. [CrossRef]
10. Moshynets, O.V.; Baranovskyi, T.P.; Cameron, S.; Iungin, O.S.; Pokholenko, I.; Jerdan, R.; Kamyshnyi, A.; Krikunov, A.A.; Potochilova, V.V.; Rudnieva, K.L.; et al. Azithromycin possesses biofilm-inhibitory activity and potentiates non-bactericidal colistin methanesulfonate (CMS) and polymyxin B against *Klebsiella pneumonia*. *PLoS ONE* **2022**, *2022 17*, e0270983. [CrossRef]
11. Moshynets, O.V.; Spiers, A.J. Viewing biofilms within the larger context of bacterial aggregations. In *Microbial Biofilms-Importance and Applications*; Dhanasekaran, D., Thajuddin, N., Eds.; InTech Press: London, UK, 2016; pp. 3–22. [CrossRef]

12. Vyas, H.K.N.; Xia, B.; Mai-Prochnow, A. Clinically relevant in vitro biofilm models: A need to mimic and recapitulate the host environment. *Biofilm* **2022**, *4*, 100069. [CrossRef] [PubMed]
13. Frantz, C.; Stewart, K.M.; Weaver, V.M. The extracellular matrix at a glance. *J. Cell Sci.* **2010**, *123*, 4195–4200. [CrossRef] [PubMed]
14. Stein, H.; Wilensky, M.; Tsafrir, Y.; Rosenthal, M.; Amir, R.; Avraham, T.; Ofir, K.; Dgany, O.; Yayon, A.; Shoseyov, O. Production of Bioactive, Post-Translationally Modified, Heterotrimeric, Human Recombinant Type-I Collagen in Transgenic Tobacco. *Biomacromolecules* **2009**, *10*, 2640–2645. [CrossRef] [PubMed]
15. Ramshaw, J.A.M.; Werkmeister, J.A.; Glattauer, V. Recent progress with recombinant collagens produced in *Escherichia coli*. *Curr. Opin. Biomed. Eng.* **2019**, *10*, 149–155. [CrossRef]
16. Matinong, A.M.E.; Chisti, Y.; Pickering, K.L.; Haverkamp, R.G. Collagen Extraction from Animal Skin. *Biology* **2022**, *11*, 905. [CrossRef]
17. Maistrenko, L.; Iungin, O.; Pikus, P.; Pokholenko, I.; Gorbatiuk, O.; Moshynets, O.; Okhmat, O.; Kolesnyk, T.; Potters, G.; Mokrousova, O. Collagen Obtained from Leather Production Waste Provides Suitable Gels for Biomedical Applications. *Polymers* **2022**, *14*, 4749. [CrossRef]
18. Slade, E.A.; Thorn, R.M.S.; Young, A.; Reynolds, D.M. An in vitro collagen perfusion wound biofilm model; with applications for antimicrobial studies and microbial metabolomics. *BMC Microbiol.* **2019**, *19*, 310. [CrossRef]
19. Buyck, J.M.; Plésiat, P.; Traore, H.; Vanderbist, F.; Tulkens, P.M.; Van Bambeke, F. Increased susceptibility of *Pseudomonas aeruginosa* to macrolides and ketolides in eukaryotic cell culture media and biological fluids due to decreased expression of oprM and increased outer-membrane permeability. *Clin. Infect. Dis.* **2012**, *55*, 534–542. [CrossRef]
20. Lin, L.; Nonejuie, P.; Munguia, J.; Hollands, A.; Olson, J.; Dam, Q.; Kumaraswamy, M.; Rivera, H., Jr.; Corriden, R.; Rohde, M.; et al. Azithromycin Synergizes with Cationic Antimicrobial Peptides to Exert Bactericidal and Therapeutic Activity Against Highly Multidrug-Resistant Gram-Negative Bacterial Pathogens. *eBioMedicine* **2015**, *2*, 690–698. [CrossRef]
21. Dillon, N.; Holland, M.; Tsunemoto, H.; Hancock, B.; Cornax, I.; Pogliano, J.; Sakoulas, G.; Nizet, V. Surprising synergy of dual translation inhibition vs. Acinetobacter baumannii and other multidrug-resistant bacterial pathogens. *eBioMedicine* **2019**, *46*, 193–201. [CrossRef]
22. Kadam, S.; Nadkarni, S.; Lele, J.; Sakhalkar, S.; Mokashi, P.; Kaushik, K.S. Bioengineered Platforms for Chronic Wound Infection Studies: How Can We Make Them More Human-Relevant? *Front. Bioeng. Biotechnol.* **2019**, *7*, 418. [CrossRef]
23. Cano, V.; Moranta, D.; Llobet-Brossa, E.; Bengoechea, J.A.; Garmendia, J. *Klebsiella pneumoniae* triggers a cytotoxic effect on airway epithelial cells. *BMC Microbiol.* **2009**, *9*, 156. [CrossRef]
24. Kalghatgi, S.; Spina, C.S.; Costello, J.C.; Liesa, M.; Morones-Ramirez, J.R.; Slomovic, S.; Molina, A.; Shirihai, O.S.; Collins, J.J. Bactericidal antibiotics induce mitochondrial dysfunction and oxidative damage in mammalian cells. *Sci. Transl. Med.* **2013**, *5*, 192ra85. [CrossRef]
25. Zavascki, A.P.; Nation, R.L. Nephrotoxicity of Polymyxins: Is There Any Difference between Colistimethate and Polymyxin B? *Antimicrob. Agents Chemother.* **2017**, *61*, e02319-16. [CrossRef]
26. Nation, R.L.; Rigatto, M.H.P.; Falci, D.R.; Zavascki, A.P. Polymyxin Acute Kidney Injury: Dosing and Other Strategies to Reduce Toxicity. *Antibiotics* **2019**, *8*, 24. [CrossRef]
27. Karvanen, M.; Plachouras, D.; Friberg, L.E.; Paramythiotou, E.; Papadomichelakis, E.; Karaiskos, I.; Tsangaris, I.; Armaganidis, A.; Cars, O.; Giamarellou, H. Colistin methanesulfonate and colistin pharmacokinetics in critically ill patients receiving continuous venovenous hemodiafiltration. *Antimicrob. Agents Chemother.* **2013**, *57*, 668–671. [CrossRef]
28. Instruction for Colomycin. Available online: https://compendium.com.ua/dec/266344/378710/ (accessed on 27 December 2022).
29. Foulds, G.; Shepard, R.M.; Johnson, R.B. The pharmacokinetics of azithromycin in human serum and tissues. *J. Antimicrob. Chemother.* **1990**, *25*, 73–82. [CrossRef]
30. Instruction for Azithromycin. Available online: https://compendium.com.ua/dec/337677/ (accessed on 27 December 2022).
31. Moshynets, O.; Chernii, S.; Chernii, V.; Losytskyy, M.Y.; Karakhim, S.; Czerwieniec, R.; Pekhnyo, V.; Yarmoluk, S.; Kovalska, V. Fluorescent β-ketoenole AmyGreen dye for visualization of amyloid components of bacterial biofilms. *Methods Appl. Fluoresc.* **2020**, *8*, 035006. [CrossRef]
32. Moshynets, O.V.; Pokholenko, I.; Iungin, O.; Potters, G.; Spiers, A.J. eDNA, Amyloid fibers and membrane vesicles identified in *Pseudomonas fluorescens* SBW25 biofilms. *Int. J. Mol. Sci.* **2022**, *23*, 15096. [CrossRef]
33. Haseeb, A.; Faidah, H.S.; Alghamdi, S.; Alotaibi, A.F.; Elrggal, M.E.; Mahrous, A.J.; Almarzoky Abuhussain, S.S.; Obaid, N.A.; Algethamy, M.; AlQarni, A.; et al. Dose Optimization of Colistin: A Systematic Review. *Antibiotics* **2021**, *10*, 1454. [CrossRef]
34. Fekety, F.R.; Norman, P.S.; Cluff, L.E. The treatment of gram-negative bacillary infections with colistin. *Ann. Intern. Med.* **1962**, *57*, 214–229. [CrossRef] [PubMed]
35. Plachouras, D.; Karvanen, M.; Friberg, L.E.; Papadomichelakis, E.; Antoniadou, A.; Tsangaris, I.; Karaiskos, I.; Poulakou, G.; Kontopidou, F.; Armaganidis, A.; et al. Population pharmacokinetic analysis of colistin methanesulfonate and colistin after intravenous administration in critically ill patients with infections caused by gram-negative bacteria. *Antimicrob. Agents Chemother.* **2009**, *53*, 3430–3436. [CrossRef] [PubMed]
36. Daikos, G.L.; Skiada, A.; Pavleas, J.; Vafiadi, C.; Salatas, K.; Tofas, P.; Tzanetou, K.; Markogiannakis, A.; Thomopoulos, G.; Vafiadi, I.; et al. Serum bactericidal activity of three different dosing regimens of colistin with implications for optimum clinical use. *J. Chemother.* **2010**, *22*, 175–178. [CrossRef] [PubMed]

37. Vardakas, K.Z.; Mavroudis, A.D.; Georgiou, M.; Falagas, M.E. Intravenous colistin combination antimicrobial treatment vs. monotherapy: A systematic review and meta-analysis. *Int. J. Antimicrob. Agents* **2018**, *51*, 535–547. [CrossRef]
38. Katip, W.; Uitrakul, S.; Oberdorfer, P. Clinical Efficacy and Nephrotoxicity of the Loading Dose Colistin for the Treatment of Carbapenem-Resistant *Acinetobacter baumannii* in Critically Ill Patients. *Pharmaceutics* **2022**, *14*, 31. [CrossRef]
39. Saiman, L.; Marshall, B.C.; Mayer-Hamblett, N.; Burns, J.L.; Quittner, A.L.; Cibene, D.A.; Coquillette, S.; Feiberg, A.Y.; Accurso, F.J.; Campbell, P.W. Azithromycin in patients with cystic fibrosis chronically infected with *Pseudomonas aeruginosa*. *JAMA* **2003**, *290*, 1749–1756. [CrossRef]
40. Gillis, R.J.; Iglewski, B.H. Azithromycin retards *Pseudomonas aeruginosa* biofilm formation. *J. Clin. Microbiol.* **2004**, *42*, 5842–5845. [CrossRef]
41. Imperi, F.; Leoni, L.; Visca, P. Antivirulence activity of azithromycin in *Pseudomonas aeruginosa*. *Front. Microbiol.* **2014**, *5*, 178. [CrossRef]
42. Swatton, J.E.; Davenport, P.W.; Maunders, E.A.; Griffin, J.L.; Lilley, K.S.; Welch, M. Impact of azithromycin on the quorum sensing-controlled proteome of *Pseudomonas aeruginosa*. *PLoS ONE* **2016**, *1*, e0147698. [CrossRef]
43. Kohler, T.; Dumac, J.L.; Van Delden, C. Ribosome protection prevents azithromycin-mediated quorum-sensing modulation and stationary-phase killing of *Pseudomonas aeruginosa*. *Antimicrob. Agents Chemother.* **2007**, *51*, 4243–4248. [CrossRef]
44. Tateda, K.; Ishii, Y.; Matsumoto, T.; Kobayashi, T.; Miyazaki, S.; Yamaguchi, K. Potential of macrolide antibiotics to inhibit protein synthesis of *Pseudomonas aeruginosa*: Suppression of virulence factors and stress response. *J. Infect. Chemother.* **2000**, *6*, 1–7. [CrossRef]
45. Hirakata, Y.; Kaku, M.; Mizukane, R.; Ishida, K.; Furuya, N.; Matsumoto, T.; Tateda, K.; Yamaguchi, K. Potential effects of erythromycin on host defense systems and virulence of *Pseudomonas aeruginosa*. *Antimicrob. Agents Chemother.* **1992**, *36*, 1922–1927. [CrossRef]
46. Kawamura-Sato, K.; Iinuma, Y.; Hasegawa, T.; Horii, T.; Yamashino, T.; Ohta, M. Effect of subinhibitory concentrations of macrolides on expression of flagellin in *Pseudomonas aeruginosa* and *Proteus mirabilis*. *Antimicrob. Agents Chemother.* **2000**, *44*, 2869–2872. [CrossRef]
47. Wolter, J.; Seeney, S.; Bell, S.; Bowler, S.; Masel, P.; McCormack, J. Effect of long term treatment with azithromycin on disease parameters in cystic fibrosis: A randomized trial. *Thorax* **2002**, *57*, 212–216. [CrossRef]
48. Yanagihara, K.; Tomono, K.; Imamura, Y.; Kaneko, Y.; Kuroki, M.; Sawai, T.; Miyazaki, Y.; Hirakata, Y.; Mukae, H.; Kadota, J.I.; et al. Effect of clarithromycin on chronic respiratory infection caused by *Pseudomonas aeruginosa* with biofilm formation in an experimental murine model. *J. Antimicrob. Chemother.* **2002**, *49*, 867–870. [CrossRef]
49. Tateda, K.; Ishii, Y.; Kimura, S.; Horikawa, M.; Miyairi, S.; Yamaguchi, K. Suppression of *Pseudomonas aeruginosa* quorum-sensing systems by macrolides: A promising strategy or an oriental mystery? *J. Infect. Chemother.* **2007**, *13*, 357–367. [CrossRef]
50. Andrade, F.F.; Silva, D.; Rodrigues, A.; Pina-Vaz, C. Colistin Update on Its Mechanism of Action and Resistance; Present and Future Challenges. *Microorganisms* **2020**, *8*, 1716. [CrossRef]
51. Yun, B.; Zhang, T.; Azad, M.A.K.; Wang, J.; Nowell, C.J.; Kalitsis, P.; Velkov, T.; Hudson, D.F.; Li, J. Polymyxin B causes DNA damage in HK-2 cells and mice. *Arch. Toxicol.* **2018**, *92*, 2259–2271. [CrossRef]
52. Shenkutie, A.M.; Zhang, J.; Yao, M.; Asrat, D.; Chow, F.W.N.; Leung, P.H.M. Effects of sub-minimum inhibitory concentrations of imipenem and colistin on expression of biofilm-specific antibiotic resistance and virulence genes in *Acinetobacter baumannii* Sequence Type 1894. *Int. J. Mol. Sci.* **2022**, *23*, 12705. [CrossRef]
53. Denizot, F.; Lang, R. Rapid colorimetric assay for cell growth and survival. Modifications to the tetrazolium dye procedure giving improved sensitivity and reliability. *J. Immunol. Methods* **1986**, *89*, 271–277. [CrossRef]
54. Sambrook, J.; Fritsch, E.F.; Maniatis, T. *Molecular Cloning: A Laboratory Manual*, 2nd ed.; Cold Spring Harbor Laboratory Press: New York, NY, USA, 1989.

Disclaimer/Publisher's Note: The statements, opinions and data contained in all publications are solely those of the individual author(s) and contributor(s) and not of MDPI and/or the editor(s). MDPI and/or the editor(s) disclaim responsibility for any injury to people or property resulting from any ideas, methods, instructions or products referred to in the content.

frontiers | Frontiers in Medicine

TYPE Case Report
PUBLISHED 22 September 2023
DOI 10.3389/fmed.2023.1264492

Check for updates

OPEN ACCESS

EDITED BY
Amir Sasan Mozaffari Nejad,
Jiroft University of Medical Sciences, Iran

REVIEWED BY
Mohammad Reza Arabestani,
Hamadan University of Medical Sciences, Iran
Prasanth Manohar,
Texas A&M University, United States

*CORRESPONDENCE
Olena Moshynets
✉ moshynets@gmail.com

RECEIVED 20 July 2023
ACCEPTED 28 August 2023
PUBLISHED 22 September 2023

CITATION
Kryzhevskyi V, Strokous V, Lifshyts Y, Rybianets Y, Oberniak A, Krikunov A, Iungin O, Potochilova V, Rudnieva K, Petakh P, Kamyshnyi A and Moshynets O (2023) Case report: Azithromycin-meropenem combination therapy as a low-cost approach to combat PDR gram-negative infections of war wounds in Ukraine.
Front. Med. 10:1264492.
doi: 10.3389/fmed.2023.1264492

COPYRIGHT
© 2023 Kryzhevskyi, Strokous, Lifshyts, Rybianets, Oberniak, Krikunov, Iungin, Potochilova, Rudnieva, Petakh, Kamyshnyi A and Moshynets. This is an open-access article distributed under the terms of the Creative Commons Attribution License (CC BY). The use, distribution or reproduction in other forums is permitted, provided the original author(s) and the copyright owner(s) are credited and that the original publication in this journal is cited, in accordance with accepted academic practice. No use, distribution or reproduction is permitted which does not comply with these terms.

Case report: Azithromycin-meropenem combination therapy as a low-cost approach to combat PDR gram-negative infections of war wounds in Ukraine

Vadym Kryzhevskyi[1], Viktor Strokous[1], Yurii Lifshyts[2], Yurii Rybianets[1], Artem Oberniak[3,4], Alexey Krikunov[5], Olga Iungin[6,7], Viktoria Potochilova[8], Kateryna Rudnieva[9], Pavlo Petakh[10,11], Aleksandr Kamyshnyi[10] and Olena Moshynets[6]*

[1]Kyiv City Clinical Hospital No 6, Kyiv, Ukraine, [2]Oxford Medical Clinic, Kyiv, Ukraine, [3]Bila Tserkva City Hospital No 2, Bila Tserkva, Ukraine, [4]Shupyk National Healthcare University of Ukraine, Kyiv, Ukraine, [5]Amosov National Institute of Cardiovascular Surgery, Kyiv, Ukraine, [6]Biofilm Study Group, Department of Cell Regulatory Mechanisms, Institute of Molecular Biology and Genetics, National Academy of Sciences of Ukraine, Kyiv, Ukraine, [7]Department of Biotechnology, Leather and Fur, Faculty of Chemical and Biopharmaceutical Technologies, Kyiv National University of Technologies and Design, Kyiv, Ukraine, [8]Kyiv City Maternity Hospital No 2, Kyiv, Ukraine, [9]Bogomolets National Medical University, Kyiv, Ukraine, [10]Department of Microbiology, Virology, and Immunology, I. Horbachevsky Ternopil National Medical University, Ternopil, Ukraine, [11]Department of Biochemistry and Pharmacology, Uzhhorod National University, Uzhhorod, Ukraine

Antimicrobial resistance recognised as a major global health problem and it poses a significant challenge in conflict zones, such as the Russia-Ukraine war. This case study focuses on a 32-year-old soldier who sustained combat-related injuries, including extensive wound infections caused by multidrug-resistant and pan-resistant bacteria and was successfully treated with azithromycin-meropenem combination therapy. The emergence of pan-resistant bacteria, particularly a pandrug-resistant strain of *Pseudomonas aeruginosa*, highlights the severity of the problem and the limited treatment options available. Additionally, the financial burden posed by reserve antibiotics further complicates the management of these infections. The case study demonstrates the effectiveness of including azithromycin-meropenem combination therapy in the treatment regimen, which resulted in improvements in the patient's condition and the eradication of the resistant strains. The findings underscore the need for effective antimicrobial stewardship, infection control measures, and alternative treatment strategies to combat antimicrobial resistance in conflict zones.

KEYWORDS

MDR, PDR, XDR gram-negative infections, low-cost therapy, pandrug resistance, hospital infection, war wounds, Russia-Ukraine war

Introduction

Antimicrobial resistance is one of the most serious global public health threats. Wars are often associated with antibiotic resistance outbreaks, and, consequently, the conflict in Ukraine has significantly impacted the local and global spread of antimicrobial resistance (1–3). Combat-related injuries often present complex and challenging medical scenarios that require rapid and comprehensive treatment to ensure the best possible outcomes. In the context of conflict, such as the Russia-Ukraine war, healthcare systems face unique challenges (4–7). Consequently, the Russian war against Ukraine dramatically influenced on antibiotic resistance local and global spread (8–12).

One of the alarming consequences of the Russia-Ukraine war is the emergence of super-resistant bacteria, or superbugs, including pandrug-resistant (PDR) strains. Pan-resistant bacteria are resistant to all available antibiotics, leaving healthcare providers without standard treatment options. This not only possess a significant threat to the lives of war-wounded patients but also presents a challenge in terms of infection control and public health (12, 13).

Furthermore, the high cost of reserve antibiotics further exacerbates the challenges faced by healthcare providers (12, 14). In 2021, the WHO updated the AWaRe classification of antibiotics; this included eight reserve antibiotics for the treatment of multidrug-resistant pathogens. It contains cefiderocol, ceftazidime + avibactam, colistin, fosfomycin, linezolid, meropenem + vaborbactam, plazomicin, and polymyxin B (15) (cited July 7, 2023). However, their limited availability and high prices hinder their accessibility, particularly in resource-constrained conflict settings. This scarcity of effective antibiotics adds another layer of complexity to the management of combat-related injuries, jeopardizing the already precarious health outcomes for patients.

This case report focuses on the treatment of a 32-year-old soldier who sustained substantial injuries during battle in Ukraine. By examining the patterns of antimicrobial resistance observed in a war-wounded patient from Ukraine, this case study aims to shed light on the difficulties associated with pan-resistant bacteria in the context of conflict and suggests a new therapeutic approach that may be applied when PDR Gram-negative infection. Following the CARE checklist, this report aims to provide a thorough analysis of the case, ensuring transparency and adherence to established reporting guidelines (https://www.care-statement.org/, accessed on July 15, 2023).

Patient information

A 32-year-old male soldier received a penetrating abdominal injury after a fight in the Donbas. Initial medical care was provided by the advanced surgical group of the reinforcement in Druzkivka; following stabilization the patient was transferred to the Dnipro Regional Clinical Hospital by I. I. Mechnikov the same day. Upon admission, the patient's condition was critical. He was under medical sedation and had a plaster cast on his left hand. Breathing assistance was provided through an endotracheal tube connected to a transport ventilator, initially through a Maquet respirator in Synchronized Intermittent Mandatory Ventilation (SIMV) mode. Hemodynamics were stable with normal blood pressure. Heart sounds were muffled. The patient's abdomen was tense, and no peristalsis was audible. Abdominal bandages showed saturation with blood. Urinary output was managed through a Foley urinary catheter, and central venous catheters had been inserted in the right and left subclavian vein.

Clinical findings

The patient presented with a series of significant clinical findings:

1. Gunshot shrapnel blind penetrating abdominal injury with damage to the small and large intestine.
2. Hemoperitoneum, indicating the presence of blood in the peritoneal cavity.
3. Entrapment of the small intestine, complicating the patient's condition.
4. Significant soft tissue defect of the anterior abdominal wall.
5. Gunshot fracture of the 3rd finger at the level of the middle phalanx.
6. Open fracture of the 2nd and 5th fingers at the level of the distal phalanx of the left hand with a foreign body.

Timeline

On April 20, 2023, the patient was admitted to the Dnipro Regional Clinical Hospital by I. I. Mechnikov. A laparotomy was performed, and the damaged small intestine was sutured. The colon underwent obstructive resection, and an abdominal tamponade was applied as part of damage control surgery. Additionally, the patient received primary surgical treatment for the left-hand wound, including removal of a foreign body and application of a plaster cast.

The following day, April 21, 2023, a relaparotomy was conducted, along with an abdominal cavity revision. The small intestine and descending colon were resected, and a side-to-side entero-enteroanastomosis was performed. An ileostomy was created, and abdominal tamponade was implemented.

On April 24, 2023, another relaparotomy was carried out to inspect the abdominal cavity. A descending-sigmoid anastomosis was performed, and the large cap was resected. Tampons were removed, and a necrectomy of the anterior abdominal wall wound was performed. A Vacuum-Assisted Closure (VAC) system was installed to aid in wound healing.

A lower tracheostomy was performed on April 26, 2023, followed by a removal of the VAC system on April 27, 2023. A relaparotomy was performed to revise the abdominal cavity, suture the small intestine defect, and reinstall the VAC system.

The patient stayed in the Dnipro Regional Clinical Hospital by I. I. Mechnikov for eight days before he was transferred to Kyiv City Clinical Hospital No 6 in Kyiv. During these eight days, there was no microbiological investigation performed with, however, empirical antibiotic therapy with ceftazidim (20–23 of April), meropenem (23–28 of April), linezolid (20–28 of April), metronidazole (20–28 of April), and clindamycin (25–28 of April).

Diagnostic assessment

Upon arrival at Kyiv City Clinical Hospital No 6 the diagnostic assessments performed on the patient included a CT scan of the chest and abdominal cavities, a clinical blood count, leukocyte count, and measurement of procalcitonin levels. The CT scan revealed multiple fragments in the abdominal cavity. The clinical blood count assessed various blood cell counts. Procalcitonin levels were measured as a biomarker for bacterial infections.

Microbiology analyses were carried out on sputum, wound, urine samples and blood catheters regularly to monitor microbial infections. The samples underwent laboratory testing to determine the specific microorganisms present and assess their susceptibility to a range of antibiotics. The antibiotic susceptibility testing was performed using the disk-diffusion method in accordance with the guidelines set by the European Committee on Antimicrobial Susceptibility Testing (EUCAST) (Version 13.0, 2023, for all of the antibiotics except tigecycline where Version 8.0, 2018, was used. http://www.eucast.org, accessed on July 15, 2023).

The wound samples obtained from the patient revealed the presence of multidrug-resistant (MDR) strains of *Escherichia coli* and *Klebsiella pneumoniae*. Furthermore, extensively drug-resistant (XDR) strains of *E. coli*, *K. pneumoniae* and *Acinetobacter baumannii* were also isolated from the wound. Notably, a pandrug resistant (PDR) strain of *P. aeruginosa* was identified, indicating resistance to a wide range of antimicrobial agents.

Similarly, the sputum samples (due to a ventilation associated pneumonia, VAP) collected from the patient exhibited the presence of MDR strains of *E. coli* and *A. baumannii*. Additionally, a PDR strain of *P. aeruginosa*, as well as XDR strains of *K. pneumoniae* and *A. baumannii* were isolated from the sputum (Supplementary material).

Therapeutic intervention

The following medications were administered during treatment in Kyiv City Clinical Hospital No 6 (Figure 1): sodium colistimethate (colistin) was prescribed at a dosage of 2 MO every 8 h IV from the 1st to the 16th day of treatment. 50 mg tigecycline was given IV every 12 h from day 1 to 19 and from day 32 to 31. Azithromycin, a macrolide antibiotic, was included in the treatment plan. The patient received a dosage of 500 mg of azithromycin every 8 h IV from the 10th to the 37th day. Meropenem, a carbapenem antibiotic, was prescribed at a dosage of 2 g every 8 h IV from the 17th to the 37th day of treatment.

Outcomes

The introduction of azithromycin into the treatment regimen on day 10 resulted in notable improvements in the patient's condition. Procalcitonin level, which serve as a marker for bacterial infection, showed a consistent decline over the course of treatment (Figure 1). On day 10, the procalcitonin level was measured at 1.69 ng/mL. Within 7 days (by day 17) it decreased to 0.8 ng/mL during which the same antibiotics were given as since the beginning of the therapy (colistin and tigecycline). By day 23 it had decreased to 0.307 ng/mL, and further decreased to 0.18 ng/mL by day 36.

The appearance of a PDR *P. aeruginosa* isolate correlated with the increase in WBC and NLR indicating a considerable immunogenicity of the *P. aeruginosa* isolate found the same day in both wound and sputum samples. A significant NLR increase occurred three days from the moment when PDR *P. aeruginosa* was detected, and azithromycin therapy was started. A considerable dynamic reduction in stabs and PCT started on the 7th day when both colistin and tigecycline were replaced with meropenem even though all of the detected isolates were resistant to this antibiotic. Interestingly, the PDR *P. aeruginosa* isolate was replaced with a non-MDR *P. aeruginosa* isolate sensitive to five antibiotics which were ineffective against the previous *P. aeruginosa* isolate (Supplementary material). The meropenem added on the 7th day since the azithromycin therapy started (day 17th of the treatment in Kyiv), considerably improved PCT, WBC, stabs dynamics and resulted in a complete normalization by day 36. The subsequent monitoring and treatment strategy led to the complete eradication of the PDR/non-MDR *P. aeruginosa* strains by day 31. This successful outcome demonstrates the effectiveness of the implemented therapeutic interventions in targeting and eliminating the PDR *P. aeruginosa* -associated infection.

Furthermore, encouraging progress was observed in the healing of the stoma wound. The wound underwent a process of granulation, which involves the formation of new tissue, and exhibited signs of healing. This positive development suggests that the combination of the prescribed medications and wound care measures facilitated the healing process (Figure 2).

Systemic antimicrobial therapy was stopped on the 37th day, when the patient was stable, with no recurrence of the sepsis markers and a PCT not higher that 0.25 ng/mL for the following two weeks and he finally was released from the intensive care unit.

Discussion

Sepsis caused by super-resistant multi-infection was diagnosed in the patient. Until transportation to Kyiv City Clinical Hospital No 6 and within the first 8 days, only MDR gram-negative isolates were detected. It is important to emphasize that all these four isolates were sensitive to tigecycline, and they hypothetically may be still sensitive to colistin, as colistin-resistance is still not so often encountered in Ukrainian hospital isolates, as demonstrated before (16) or as demonstrated by other authors (17). However, despite this rational combined antimicrobial therapy with colistin and tigecycline, the condition of the patient decreased: he had hypothermia, anemia, underwent two blood transfusions, his bilirubin level was increased and PCT varied from 3.247 to 1.698 ng/mL (Figure 3). All this indicated that phenotypic resistance to both colistin and tigecycline developed following biofilm formation during infection process despite the confirmed genetic sensitivity to one antibiotic and expected sensitivity to another. The phenotypic resistance should always be suspected if a recommended rational therapy does not improve the condition of a patients within three days.

The newly suggested therapy was focused on anti-biofilm therapy and included azithromycin which was effective against gram-negative XDR/PDR Ukrainian Hospital Isolates as shown before (16, 18). The combination therapy with azithromycin and meropenem was suggested based on own previous experimental and clinical data which confirmed that both antibiotics demonstrated a strong synergistic effect *in vivo* against diverse gram-negative hospital

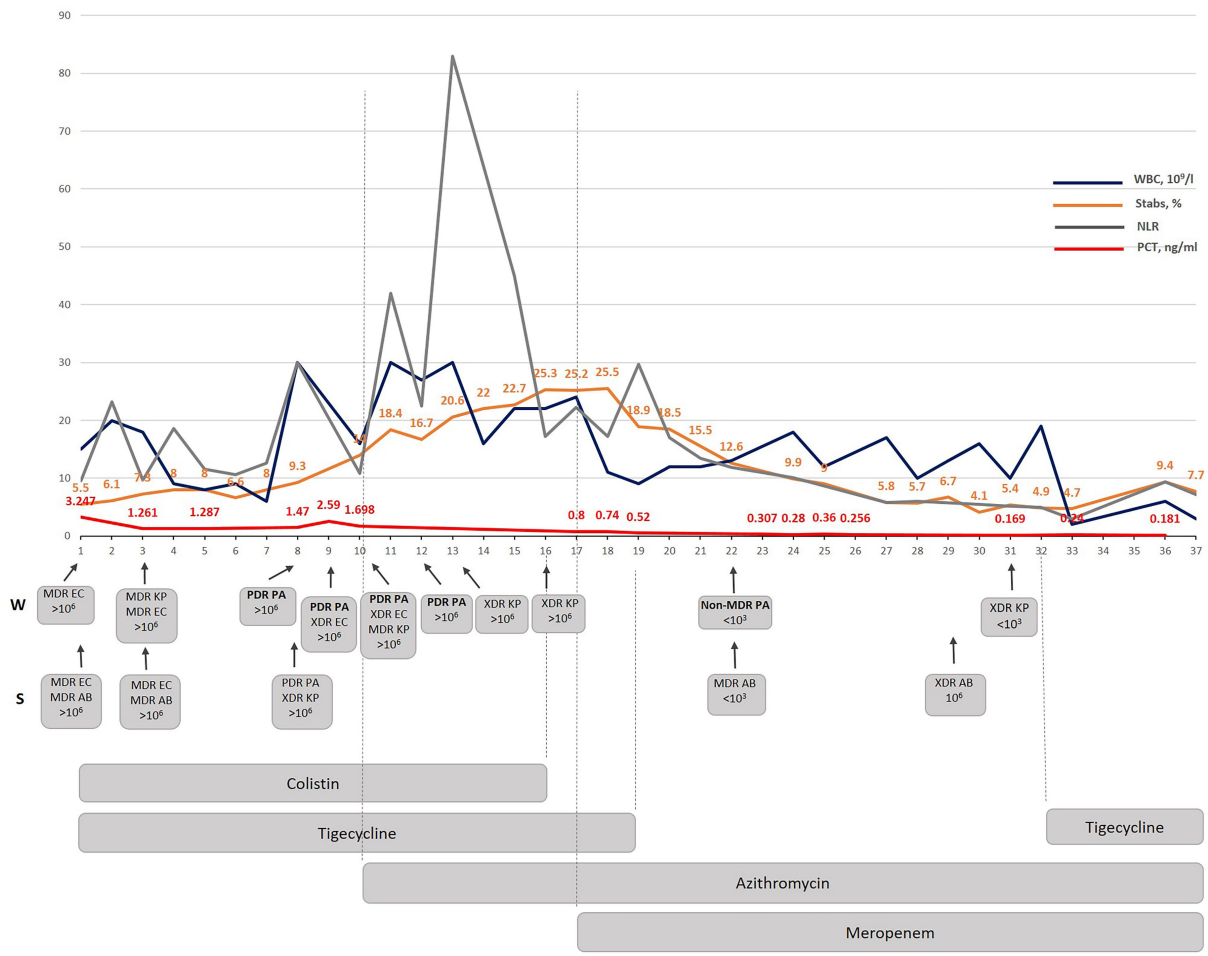

FIGURE 1
The dynamic correlation of some inflammatory markers as well as WBC and stabs during antibacterial treatment performed in Kyiv City Clinical Hospital No 6. WBC-white blood cells; NLR- a neutrophil lymphocyte ratio; PCT – procalcitonin; W-wound; S – sputum; MDR – multidrug-resistant; XDR – extensively drug-resistant; PDR – pandrug resistant; EC – *E. coli*; AB – *A. baumannii*; KP – K. *pneumoniae*; PA – *P. aeruginosa*.

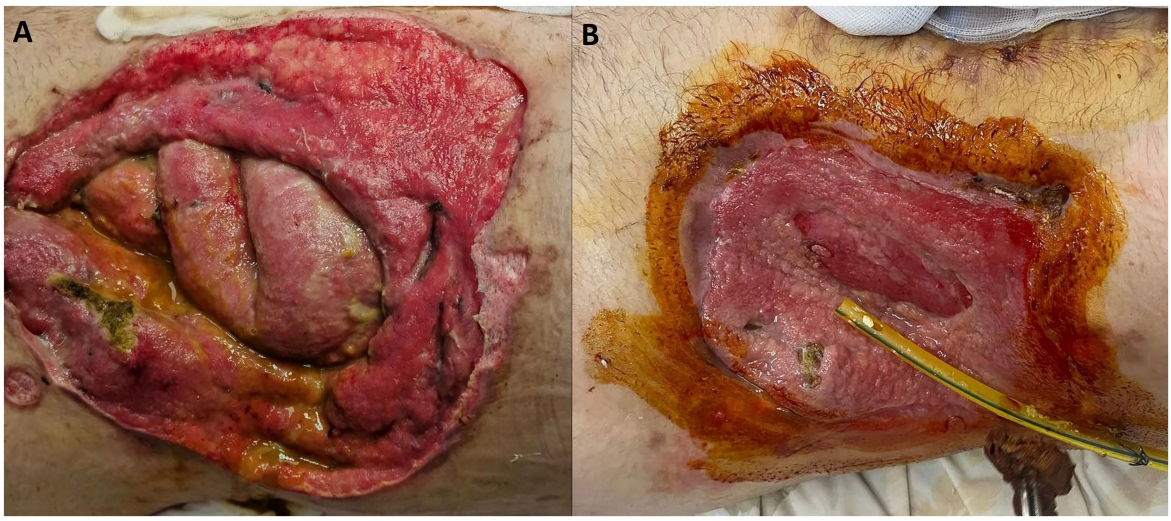

FIGURE 2
The 9-day old **(A)** and the same wound on day 36 **(B)**.

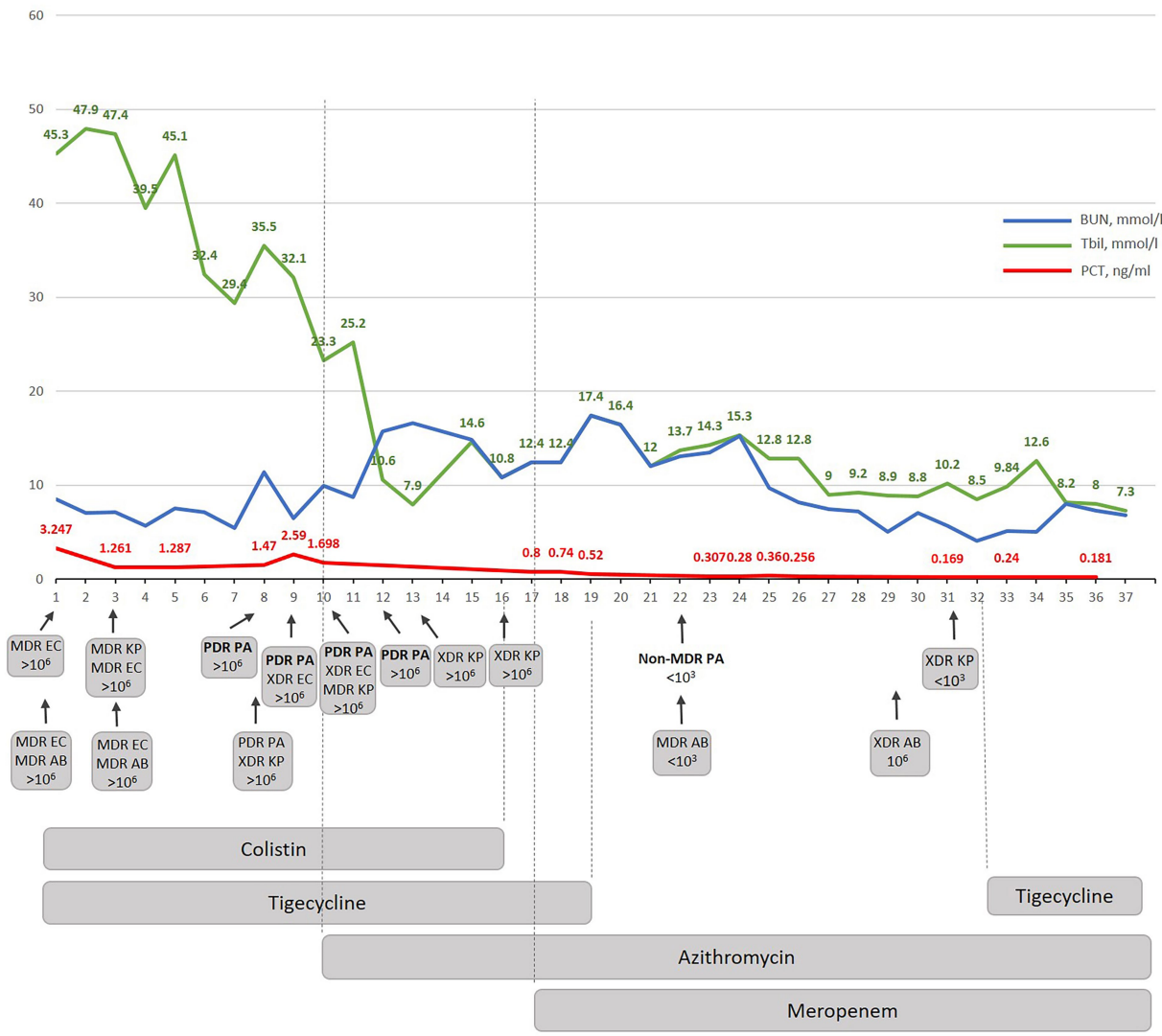

FIGURE 3
The dynamic correlation of some biochemical markers during antibacterial treatment performed in Kyiv City Clinical Hospital No 6. BUN-blood urea nitrogen; Tbil-total bilirubin; PCT – procalcitonin; W-wound; S – sputum; MDR – multidrug-resistant; XDR – extensively drug-resistant; PDR – pandrug resistant; EC – *E. coli*; AB – *A. baumannii*; KP – *K. pneumoniae*; PA – *P. aeruginosa*.

isolates. Moreover, this synergism cannot be observed for individual isolates in the standard recommended *in vitro* assays as it is biofilm dependent and specific *in vivo* due to enhanced bactericidal efficacy of AZM in a physiologically relevant environment. In other words, when the infection is caused by gram-negative bacteria with the XDR/PDR phenotype, azithromycin-meropenem can be used without additional synergism testing. Indeed, the beginning of the azithromycin therapy provoked immunostimulation (quick rise of NLR and stabs) but a decrease in PCT (0.8 ng/mL) (Figure 1). Since colistin therapy demonstrated nephrotoxicity (BUN increased up to 18 mmoL/L) (Figure 3) and because our new experimental data demonstrates that the adaptation to azithromycin mitigates PDR phenotype and restores sensitivity to meropenem in PDR *K. pneumoniae* (Abstract No 03094, Poster No P04461 presented as a poster during ECCMID 2023) colistin and tigecycline were replaced with meropenem (19). This resulted in fast normalization of PCT (from 0.8 to less than 0.25 ng/mL), normalization of WBS, stabs and NLR. Interestingly, as predicted in our research, PDR *P. aeruginosa* restores the sensitivity to meropenem, but not only to that. In general, PDR *P. aeruginosa* was replaced with non-MDR *P. aeruginosa* sensitive to five antibiotics on day 12 of azithromycin therapy and following 5 days of therapy with meropenem (Supplementary material). 1,500 mg of azithromycin daily was nicely tolerated; the only observed side effect was the appearance of individual myelocytes and blast cells in peripheral blood which might be explained by the inhibition of nuclear factor kappa B (NF-kB) by azithromycin (20) which it turn promotes myelogenesis (21). Atypical cells disappeared within three days after completion of the azithromycin therapy.

The successful use of azithromycin-meropenem combination demonstrates a low-cost approach for combating XDR/PDR in multiple gram-negative infections of war wounds in Ukraine. Another approach such as cefiderocol is unlikely to be effective in Ukraine due to its high price and fast resistance development (12). Berger (12) also suggests to use a combination of ceftazidime/avibactam and aztreonam, as this would restore the sensitivity to NDM-producing gram-negative hospital isolates. The latter are present in up to 99% of the Ukrainian hospital

isolates (even carbapenem-sensitive, unpublished data), However, this may not be effective in Ukraine due to the low quality of the available aztreonam (personal observation).

Data availability statement

The raw data supporting the conclusions of this article will be made available by the authors, without undue reservation.

Ethics statement

The studies involving humans were approved by Institute of Molecular Biology and Genetics. The studies were conducted in accordance with the local legislation and institutional requirements. The participants provided their written informed consent to participate in this study. Written informed consent was obtained from the individual(s) for the publication of any potentially identifiable images or data included in this article. Written informed consent was obtained from the participant/patient(s) for the publication of this case report.

Author contributions

KV: Formal analysis, Data curation, Methodology, Resources. SV: Data curation, Formal analysis, Methodology, Resources, Visualization. LY: Data curation, Formal analysis, Methodology, Resources. RY: Data curation, Formal analysis, Methodology, Resources. OA: Formal analysis, Methodology. KrA: Conceptualization, Investigation, Methodology. IO: Investigation, Methodology. PV: Investigation, Methodology. RK: Investigation, Methodology. PP: Formal analysis, Writing – original draft, Writing – review & editing. KaA: Formal analysis, Conceptualization, Writing – original draft, Writing – review & editing. OM: Data curation, Formal analysis, Funding acquisition, Investigation, Methodology, Project administration, Resources, Supervision, Validation, Visualization, Writing – original draft, Writing – review & editing.

Funding

The author(s) declare financial support was received for the research, authorship, and/or publication of this article. This research was funded by the National Research Foundation of Ukraine (https://nrfu.Org.ua/en/) (accessed on 17–18 September 2020, protocol No 21) within the frame of the project "Development of combined therapy for severe Klebsiella pneumoniae–associated nosocomial infections to overcome the antibiotic resistance" (2020.02/0246).

Acknowledgments

The authors would like to express their sincere thanks towards the Ukrainian Army and the Ukrainian engineers for their fantastic support in defending the country. The authors thank Geert Potters for his constant invaluable support of the Ukrainian researchers. OM personally thanks to her friend Anton Solomin who became the first volunteer to successfully undergo an experimental treatment of PDR *P. aeruginosa/A. baumannii* – associated infection with only the azithromycin-meropenem combination which inspired her for further research and broader applied medical practice.

Conflict of interest

The authors declare that the research was conducted in the absence of any commercial or financial relationships that could be construed as a potential conflict of interest.

Publisher's note

All claims expressed in this article are solely those of the authors and do not necessarily represent those of their affiliated organizations, or those of the publisher, the editors and the reviewers. Any product that may be evaluated in this article, or claim that may be made by its manufacturer, is not guaranteed or endorsed by the publisher.

Supplementary material

The Supplementary material for this article can be found online at: https://www.frontiersin.org/articles/10.3389/fmed.2023.1264492/full#supplementary-material

References

1. Älgå A, Karlow Herzog K, Alrawashdeh M, Wong S, Khankeh H, Stålsby LC. Perceptions of healthcare-associated infection and antibiotic resistance among physicians treating Syrian patients with war-related injuries. *Int J Environ Res Public Health*. (2018) 15:2709. doi: 10.3390/ijerph15122709

2. Jakovljevic M, Al Ahdab S, Jurisevic M, Mouselli S. Antibiotic resistance in Syria: a local problem turns into a global threat. *Front Public Health*. (2018) 6:212. doi: 10.3389/fpubh.2018.00212

3. Yaacoub S, Truppa C, Pedersen TI, Abdo H, Rossi R. Antibiotic resistance among bacteria isolated from war-wounded patients at the weapon traumatology training Center of the International Committee of the red cross from 2016 to 2019: a secondary analysis of WHONET surveillance data. *BMC Infect Dis*. (2022) 22:257. doi: 10.1186/s12879-022-07253-1

4. Kardas P, Babicki M, Krawczyk J, Mastalerz-Migas A. War in Ukraine and the challenges it brings to the polish healthcare system. *Lancet Reg Health Eur*. (2022) 15:100365. doi: 10.1016/j.lanepe.2022.100365

5. Shkodina AD, Chopra H, Singh I, Ahmad S, Boiko DI. Healthcare system amidst the war in Ukraine. *Ann Med Surg (Lond)*. (2022) 80:104271. doi: 10.1016/j.amsu.2022.104271

6. Petakh P, Kamyshnyi A. Risks of outbreaks: the health concerns of internally displaced persons in Transcarpathia, Ukraine. *New Microbes New Infect*. (2023) 52:101106. doi: 10.1016/j.nmni.2023.101106

7. Petakh P, Kamyshnyi A, Tymchyk V, Armitage R. Infectious diseases during the Russian-Ukrainian war – morbidity in the Transcarpathian region as a marker of epidemic danger on the EU border. *Public Health Pract*. (2023) 6:100397. doi: 10.1016/j.puhip.2023.100397

8. Kondratiuk V, Jones BT, Kovalchuk V, Kovalenko I, Ganiuk V, Kondratiuk O, et al. Phenotypic and genotypic characterization of antibiotic resistance in military hospital-associated bacteria from war injuries in the eastern Ukraine conflict between 2014 and 2020. *J Hosp Infect*. (2021) 112:69–76. doi: 10.1016/j.jhin.2021.03.020

9. Melwani M. How war is spreading drug resistant superbugs across Ukraine and beyond. *BMJ*. (2022) 379:o2731. doi: 10.1136/bmj.o2731

10. Murray CJL, Ikuta KS, Sharara F, Swetschinski L, Robles Aguilar G, Gray A, et al. Global burden of bacterial antimicrobial resistance in 2019: a systematic analysis. *Lancet*. (2022) 399:629–55. doi: 10.1016/S0140-6736(21)02724-0

11. Organization WHO. *WHO response to the Ukraine crisis: March 2023 bulletin*. Regional Office for Europe: World Health Organization (2023).

12. Berger FK, Schmartz GP, Fritz T, Veith N, Alhussein F, Roth S, et al. Occurrence, resistance patterns, and management of carbapenemase-producing bacteria in war-wounded refugees from Ukraine. *Int J Infect Dis*. (2023) 132:89–92. doi: 10.1016/j.ijid.2023.04.394

13. Magiorakos AP, Srinivasan A, Carey RB, Carmeli Y, Falagas ME, Giske CG, et al. Multidrug-resistant, extensively drug-resistant and pandrug-resistant bacteria: an international expert proposal for interim standard definitions for acquired resistance. *Clin Microbiol Infect*. (2012) 18:268–81. doi: 10.1111/j.1469-0691.2011.03570.x

14. Majumder MAA, Rahman S, Cohall D, Bharatha A, Singh K, Haque M, et al. Antimicrobial stewardship: fighting antimicrobial resistance and protecting global public health. *Infect Drug Resist*. (2020) 13:4713–38. doi: 10.2147/IDR.S290835

15. *AWaRe classification* (2021). Geneva: World Health Organization. Available at: https://www.who.int/publications/i/item/2021-aware-classification

16. Moshynets OV, Baranovskyi TP, Cameron S, Iungin OS, Pokholenko I, Jerdan R, et al. Azithromycin possesses biofilm–inhibitory activity and potentiates non-bactericidal colistin methanesulfonate (CMS) and polymyxin B against Klebsiella pneumonia. *PLoS One*. (2022) 17:e0270983. doi: 10.1371/journal.pone.0270983

17. Mc Gann PT, Lebreton F, Jones BT, Dao HD, Martin MJ, Nelson MJ, et al. Six extensively drug-resistant bacteria in an injured soldier, Ukraine. *Emerg Infect Dis*. (2023) 29:1692–5. doi: 10.3201/eid2908.230567

18. Moshynets OV, Baranovskyi TP, Iungin OS, Krikunov AA, Potochilova VV, Rudnieva KL, et al. Therapeutic potential of an azithromycin-colistin combination against XDR *K. pneumoniae* in a 3D collagen-based in vitro wound model of a biofilm infection. *Antibiotics (Basel)*. (2023) 12:293. doi: 10.3390/antibiotics12020293

19. Moshynets O, Baranovskyi T, Iungin O, Pokholenko I, Potochilova V, Krikunov A, et al. *Adaptation to azithromycin mitigates PDR phenotype and restores sensitivity to meropenem in PDR Klebsiella pneumonia*. 33rd. Copenhagen, Denmark: ECCMID (2023) Abstract No 03094, Poster No P0461.

20. Iwamoto S, Kumamoto T, Azuma E, Hirayama M, Ito M, Amano K, et al. The effect of azithromycin on the maturation and function of murine bone marrow-derived dendritic cells. *Clin Exp Immunol*. (2011) 166:385–92. doi: 10.1111/j.1365-2249.2011.04480.x

21. Reikvam H. Inhibition of NF-κB signaling alters acute myelogenous leukemia cell transcriptomics. *Cells*. (2020) 9:1677. doi: 10.3390/cells9071677

Journal of Infection 89 (2024) 106224

Contents lists available at ScienceDirect

Journal of Infection

journal homepage: www.elsevier.com/locate/jinf

Review

Conflict and catastrophe-related severe burn injuries: A challenging setting for antimicrobial decision-making

Scott JC Pallett [a,b,*], Rakhee Mistry [c], Zoe L Lambert [d], Stephen D Woolley [a,e,f], Aula Abbara [g], Aodhan O Breathnach [h,i], Lucy E Lamb [f,j], Andrew Williams [k], Nabeela Mughal [b], Olena Moshynets [l], Stephen J Hughes [c], Matthew K O'Shea [a,f,m], Luke SP Moore [b,n]

[a] Centre of Defence Pathology, Royal Centre for Defence Medicine, Queen Elizabeth Hospital, Birmingham, UK
[b] Clinical Infection Department, Chelsea and Westminster Hospital NHS Foundation Trust, SW10 9NH London, UK
[c] Department of Pharmacy, Chelsea and Westminster Hospital NHS Foundation Trust, SW10 9NH London, UK
[d] Britannia Royal Navy College Dartmouth, College Way, Dartmouth, Devon TQ6 0HJ, UK
[e] Department of Clinical Sciences, Liverpool School of Tropical Medicine, Liverpool, Merseyside, UK
[f] Academic Department of Military Medicine, Royal Centre for Defence Medicine, Queen Elizabeth Hospital, Birmingham, UK
[g] Faculty of Medicine, Department of Infectious Diseases, Imperial College Praed Street, London W2 1NY, UK
[h] Infection Care Group, St George's University Hospitals NHS Foundation Trust, Blackshaw Road, London SW17 0QT, UK
[i] International Health Regulations Strengthening Project, UK Health Security Agency, South Colonnade Canary Wharf, London E14 4PU, UK
[j] Infectious Diseases Department, Royal Free Hospital, Pond Street, London NW3 2QG, UK
[k] Burns Unit, Chelsea and Westminster Hospital NHS Foundation Trust, SW10 9NH London, UK
[l] Institute of Molecular Biology and Genetics of National Academy of Sciences of Ukraine, Kyiv 03143, Ukraine
[m] Institute of Immunology and Immunotherapy, College of Medical & Dental Sciences, University of Birmingham, Birmingham, UK
[n] National Institute for Health Research Health Protection Research Unit in Healthcare Associated Infections and Antimicrobial Resistance, Imperial College London, Hammersmith Campus, London, UK

ARTICLE INFO

Article history:
Accepted 4 July 2024
Available online 8 July 2024

Keywords:
Antimicrobial stewardship
Multidrug resistance
Antimicrobial resistance
Conflict
Disaster medicine

SUMMARY

Severe burns are a major component of conflict-related injuries and can result in high rates of mortality. Conflict and disaster-related severe burn injuries present unique challenges in logistic, diagnostic and treatment options, while wider conflict is associated with driving local antimicrobial resistance. We present a targeted review of available literature over the last 10 years on the use of systemic antimicrobial antibiotics in this setting and, given limited available data, provide an expert consensus discussion. While international guidelines do not tend to recommend routine use of prophylactic systemic antibiotics, the challenges of conflict settings and potential for polytrauma are likely to have ongoing impacts on antimicrobial decision-making and use. Efforts must be made to develop a suitable evidence base in this unique setting. In the interim, a pragmatic approach to balancing selective pressures of antimicrobial use with realistic access is possible.
© 2024 Published by Elsevier Ltd on behalf of The British Infection Association. This is an open access article under the CC BY-NC-ND license (http://creativecommons.org/licenses/by-nc-nd/4.0/).

Background

Conflict drivers of antimicrobial resistance (AMR) are a global health risk of increasing significance.[1] While limited, reports of high-rates of multidrug resistant infections among hospital patients with combat-related wounds from Ukraine are deeply concerning, with recognition of spread throughout Europe,[1] and the recent outbreak of conflict in Gaza presents additional concerns.[2] Together, these and other crisis situations (e.g. the recent earthquakes in Turkey) demonstrate major challenges to addressing the development and spread of AMR among healthcare facilities both locally and cross-border.

Within conflict, burns are common injuries, and subsequent sepsis due to infection is a major cause of mortality.[3] Where post-burn infections occur within the first couple of days, they tend to be with Gram positive organisms with later infections driven by Gram negative organisms.[4] International guidelines, primarily intended for use in civilian/non-disaster settings, do not routinely support immediate prophylactic antibiotics for burns citing a lack of available evidence.[3,5,7] The International Society for Burns Injuries Practice

* Corresponding author at: Clinical Infection Department, Chelsea and Westminster Hospital NHS Foundation Trust, SW10 9NH London, UK.
E-mail address: scott.pallett@nhs.net (S.J. Pallett).

https://doi.org/10.1016/j.jinf.2024.106224
0163-4453/© 2024 Published by Elsevier Ltd on behalf of The British Infection Association. This is an open access article under the CC BY-NC-ND license (http://creativecommons.org/licenses/by-nc-nd/4.0/).

Guidelines do however acknowledge in resource poor settings, where microbiology monitoring may be difficult, use of prophylactic antibiotics by burn specialists may see a lowered threshold given concerns for sepsis as a leading cause of death.[3] Systematic reviews used to inform these guidelines tend to draw on small numbers of studies across several decades, with practice changing considerably over the time period.[3] A 2013 Cochrane analysis likewise concluded unclear effects of early systemic antibiotic prophylaxis on burn wound infections.[8] Perhaps more relevant for disaster settings, Médecins Sans Frontières and the evidence-based review Prevention of Combat-Related Infections Guidelines likewise do not advise systemic antimicrobial therapy for isolated severe burn injuries in the absence of signs of systemic infection while highlighting the importance of early debridement, topical antibiotics and rigorous infection prevention and control.[9,10] The 2017 Guidelines for Burn Care in Austere Environments broadly recommend avoiding prophylactic antibiotics due to a lack of definitive evidence.[6] In contrast, a 2010 meta-analysis concluded a potential for beneficial effect of prophylactic antibiotics in severe burns but likewise acknowledged methodological data as weak,[11] while a large nationwide Japanese study from 2017 suggested a potential benefit in those with severe burns needing mechanical ventilation in the first 48 h.[12]

In some conflict scenarios, however, the possibility of considerable delay (≥24 h) to first debridement, co-existent polytrauma (e.g. open fracture), environmental contamination with potential for multidrug-resistant organisms, or mass-casualty limiting opportunity for detailed examinations may occur,[5] which may impact early antimicrobial decision making. While broad-spectrum antimicrobial use is a selective pressure for AMR,[13] the choice of agent in conflict and catastrophe scenarios has multiple influencers, not least logistical challenges. Disruption to diagnostic pathways, drug supply chain insecurity, increased economic cost of reserve antibiotics, delay to initial surgery, and limited remote diagnostics could all understandably increase the likelihood of early prophylactic antimicrobial prescribing and selection of a broad-spectrum agent. The development of antimicrobial resistance in conflict-related infected wounds has resulted in the need to consider novel antibiotic combinations to manage late-stage infections.[14] Given the time since the publication of guidelines and limited available evidence, we undertook a review of the recent literature for conflict and/or disaster-related use of antibiotics in severe burn injuries. We then offer expert advice on considerations to limit broad-spectrum use of early systemic antibiotics, where they may be indicated, given associated challenges.

Review of the literature

Available data on outcomes in choice of antimicrobial agent for early prophylaxis of contaminated burns injuries is limited. Medline and Cochrane database searches were conducted for articles published in the last 10 years using terms 'burn' and 'conflict' or 'war' or 'combat' or 'catastrophe' or 'disaster' and 'antibiotic' or 'antimicrobial'. 1089 articles were returned (Supplementary Figure 1). Abstracts were reviewed by two independent investigators for articles that considered the use of early systemic prophylactic antibiotics in a conflict or disaster setting. Articles were excluded if they did not consider the use of prophylactic systemic antibiotics in a conflict or disaster setting. 34 articles were selected for full review by two independent investigators, and eight met the inclusion criteria (Supplementary Figure 1).[15–22]

Of the eight articles included, three reported observations of antimicrobial prophylaxis use in the context of burns following a mass casualty incident.[15–17] Two separate papers reported on the same 33 adult patients involved in an outdoor dust explosion,[15–17] and a further reported on 16 adult patients involved in a gas tanker explosion near eastern China.[17] One of these articles considered directly the benefit of prophylactic antibiotic use, showing a reduction in infection rates against time and no mortalities but was limited by a lack of control group and recommended the need for a randomised control trial in the setting of a major burn incidents.[16] All three reported potential benefits in considering early systemic prophylactic antibiotics for severe burns following a mass casualty incident, but recognise considerable limitations in sample sizes and study design.[15–17]

Parrish and Seda, summarising the special consideration of radiation burns, highlight a triage approach to burns patients that includes special consideration of early systemic prophylactic antibiotics following exposures greater than 2 Gy.[18] A summary of antimicrobial use for battlefield injuries managed in French military facilities mentions simple burns, for which they do not recommend any antimicrobial prophylaxis but do not directly comment on severe burns, although do recommend prophylaxis in cases of multiple trauma (first line intravenous amoxicillin-clavulanate).[19] The final articles represented clinical guidelines for use in combat-related injuries,[20] in military prolonged field care settings,[21] and the report of the World Health Organisation (WHO) technical working group on mass casualty burns where systemic prophylactic antibiotics were not routinely advised,[20–22] albeit with recognition of the potential for the need to provide cover for concomitant wounds (e.g. open fractures),[21,22] and with a recommendation to carry appropriate antibiotics in case of evidence of early infection.[21] The US Clinical Practice Guideline recommended only topical antimicrobials in the context of superficial, deep partial or full-thickness burns.[20] There is also guidance provided however for situations of expected delay to reach surgical care, which recommended moxifloxacin or ertapenem as first-line oral and intravenous/intramuscular options respectively.[20] In short, evidence for the benefit of systemic prophylactic antibiotics in conflict or disaster-related severe burn injuries remains limited and unclear. However, the chaotic nature of conflicts and disasters, with the potential for gross contamination and polytrauma, means that their use is likely to continue. Recognition of high rates of AMR associated with conflict in general, but over the last two years, particularly with conflict-related wounds in Ukraine,[1] is then likely to impact the antimicrobial agent of choice, with the temptation to select a broader agent. More thorough data on pre-injury carriage rates of AMR could help reassure in this situation.

In lieu of adequate evidence available now, and given the concurrent risk of conflict-related burns and evolving multi-drug resistance in Ukraine and other major conflict areas, we assembled an Expert Advisory Group to consider burns in conflict settings and discuss options in these circumstances. The assembled group was selected using snowball sampling to gather appropriate expertise in civilian medical microbiology and infectious diseases, military medical microbiology and infectious diseases, global public health (in the context of AMR), antimicrobial pharmacy, antimicrobial stewardship, humanitarian medicine, burns and plastic surgery and hold associated academic and/or national or international advisory roles. After review of the literature and expert discussions, antimicrobial agents included for discussion were selected based on available agents licensed for appropriate systemic Gram-positive antimicrobial cover in Europe (including newer agents) or supported by knowledge of current agents being employed in areas of ongoing European conflict.[20] Antimicrobials were excluded if considered prohibitively expensive for widespread use. Key points discussed included (i) common causes of early infection in severe burns, (ii) potential ideal properties of an antimicrobial agent for use in conflict settings, (iii) potential value, and limitations, of AMR surveillance repositories in these settings, (iv) potential advantages and disadvantages of available antimicrobial agents and (v) potential future work of benefit. The outcome of discussions and a summary table of considerations for potential antimicrobial agents in this scenario are presented.

Table 1
Potential antimicrobial considerations for early prophylaxis in conflict-related severe burns injuries subject to delayed initial debridement.

Agent	Spectrum						Route	Dosing	AMS	Cost	Advantages	Limitations of use	
Drug	Pathogens			Commensal*			*IV (intravenous); B (bolus) or I (infusion) / IM (intramuscular) / PO (oral)*	*Frequency of dosing*	*Risk of selective pressure on multi-drug resistant Gram negative pathogens*	*£(< €20/d) / ££ (€20-40d) / £££(> €40/d)*	*NS (narrow spectrum), WA (widely available), LA (long acting)*	*AMR (selective pressure on G negative resistance), MDD (multiple daily dosing)*	*WHO AWaRe category*
	MSSA	*MRSA*	*Group A Strep*	*Pseudomonas sp.*	*Acinetobacter sp.*	*Enterobacterales*							
Cefazolin	+	-	+	-	-	±	IV(B&I) / IM	8 hourly	Moderate	£	NS, WA	MDD	Access
Ceftaroline fosamil	+	+	+	-	-	+	IV (B&I)	12 hourly	Moderate - high	£££	Anti-MRSA	Limited availability, AMR (ESBL and CRO risk)	Reserve
Ceftriaxone	+	-	+	-	-	+	IV(B&I) / IM	24 hourly	Moderate – high	£	WA, LA	AMR (ESBL and CRO risk)	Watch
Dalbavancin	+	+	+	-	-	-	IV infusion	Stat / weekly	Low	£££	NS, anti-MRSA, LA	Infusion only, limited availability	Reserve
Daptomycin	+	+	+	-	-	-	IV (B&I)	24 hourly	Low	£££	Anti-MRSA, NS, LA	Fridge storage only	Reserve
Delafloxacin	+	+	+	+	-	+	IV (I) / PO	12 hourly	Moderate	£££	Oral administration	Limited availability	Watch
Ertapenem	+	-	+	-	-	+	IV (I) / IM	24 hourly	Moderate - high	££	WA, LA	AMR risk for CRO	Watch
Flucloxacillin	+	-	+	-	-	-	IV(B&I) / IM / PO	6 hourly	Low	£	NS, WA,	MDD	Access
Linezolid	+	+	+	-	-	-	IV (I) / oral	12 hourly	Low	£	Anti-MRSA, NS, oral administration	Prescribing cautions with concomitant medications Potential for driving resistance in tuberculosis	Reserve
Levofloxacin	+	+	+	+	-	+	PO / IV(I)	12-24 hourly	Moderate	£	Oral administration	Potential for driving resistance in tuberculosis	Watch
Moxifloxacin	+	+	+	-	-	+	PO / IV(I)	24 hourly	Moderate	£ (PO)-£££ (IV)	Oral administration, LA	Limited availability of IV Potential for driving resistance in tuberculosis	Watch
Teicoplanin	+	+	+	-	-	-	IV(B&I) / IM	12-24 hourly	Low	£	NS, anti-MRSA, LA	Weight-based dosing	Watch
Tigecycline	+	+	+	-	+	+	IV(I)	12 hourly	Moderate	££	Anti-MRSA, LA	Broad-spectrum, nausea common, infusion only	Reserve

*CRO = carbapenem resistant organism, AMR = antimicrobial resistance, ESBL = extended spectrum beta lactamase, MRSA = methicillin-resistant S. aureus, MSSA = methicillin-susceptible S. aureus. *In the context of early causes of infection following a severe burn, Gram-negative organisms are commonly found but less likely to be the cause of infection. Potential antimicrobial options to cover common skin and soft-tissue pathogens in early infection of severe burns are listed, and characteristics for use in conflict or natural disaster scenarios are considered. Individual countries provide licensing for the use of antimicrobial agents in different infection scenarios. As an example, listed antimicrobials are approved by the European Medicines Agency for use in (i) skin and soft tissue AND bone and joint infection (ceftriaxone, teicoplanin), (ii) skin and soft tissue but NOT bone and joint infection (ceftaroline, dalbavancin, daptomycin, delafloxacin, tigecycline, tedizolid) or (iii) neither (ertapenem, except in the context of diabetic foot infections). For the remaining, the UK Medicines Health Research Authority have licensed flucloxacillin for use in bone and joint infections, moxifloxacin and levofloxacin for use in complicated skin and soft-tissue infections, and cefazolin for use in skin and soft tissue AND bone and joint infections. World Health Organisation Access, Watch, Reserve classification is provided as per the latest 2023 guidelines.*[28] Further information, including references for product information, is available in Supplementary data, Table 1.

Expert consensus

Severe burn injuries are associated with longer hospital stays, higher rates of antimicrobial exposure and severe sepsis that can be difficult to distinguish from burns pro-inflammatory pathophysiology in the early phase.[4] Review of casualties from modern conflicts highlights a rising incidence of burn injuries, in both military and civilian populations.[23] Mortality rates are associated, among other factors, with total body surface area (TBSA) burned, with 24% mortality rates in those with > 30% TBSA involvement seen in Ukraine even prior to the outbreak of conflict.[24] After initial resuscitation, sepsis is considered the leading cause of death.[25] Early causes of infection are typically with Gram positive organisms such as *Staphylococcus aureus,* with Gram negative organisms colonising the wound within the first 5–7 days and often being responsible for later episodes of infection.[26] If used, therefore, early antimicrobials must be optimised while acknowledging the challenges above to provide suitable cover against common Gram-positive organisms while reducing antimicrobial selective pressure on late (often Gram negative) infections as much as possible. This is particularly important in the context of extensive, conflict-related injuries with severe burns that often require a protracted course of healing.

Where a decision is made to prescribe an antimicrobial for patients who have experienced severe burn injuries in conflict settings, desirable properties may include agents that (i) are deliverable via intravenous bolus (rather than infusion) and/or intramuscular injection (or ideally a highly bioavailable oral agent), (ii) have a long half-life requiring minimal daily (or less frequent) dosing, (iii) have a good spectrum of Gram-positive organism activity, (iv) are cost-effective and (v) have a reliable drug supply chain without the need for cold chain storage (Table 1).

Pre-conflict antimicrobial surveillance data may help guide the initial selection of prophylactic agents. However, often, due to the concurrent conflict there is significant disruption to these surveillance systems, therefore limiting their ability to guide these selections. Current data sets should however be interpreted with caution, with recognition of considerable variability across surveillance repositories for key organisms, including *Staphylococcus aureus*, evident over recent years.[27] Moreover, key international observatories, such as the World Health Organization's Global Antimicrobial Use and Surveillance System, tend to derive data from countries in conflict from a limited number of hospital samples, making generalisation to a population at the point-of-wounding inappropriate.[28] Data for Ukraine for example, held in the Central Asian and European Antimicrobial Surveillance repository pre-conflict, suggests 30.1% of (n = 176, 2021) invasive *Staphylococcus aureus* samples were reported as methicillin resistant.[28] Despite this, there have been reports from Ukraine of good outcomes with ceftriaxone at the point-of-wounding,[29] suggesting caution must be applied in interpreting these limited data among the general population.

Several potential agents exist that may provide appropriate options for early systemic prophylaxis and treatment of infection in those who have also experienced severe burn injuries while limiting AMR selective pressures. Where delays or multiple injuries may occur, Table 1 describes potential options for pre-debridement antimicrobial prophylaxis in severe conflict-associated burn injuries, being cognizant of the location of the patient in the evacuation pathway, the severity and location of burn, time to initial debridement, potential concurrent injuries and considering posological aspects of the different agents in this setting. When selecting an antibiotic, it is also worth noting WHO AWaRe (access, watch, reserve) classifications that consider individual agent's potential impact on antimicrobial resistance as well as current safety notices (Table 1).[30] Fluoroquinolones for example, may be associated with selecting out porin producing *Pseudomonas aeruginosa,* impacting a range of antimicrobial classes and have been the focus of safety notices aimed at restricting their use.[31,32] These may be relevant considerations if treatment courses beyond a single dose were considered.

While conflict presents challenges to all levels of antimicrobial stewardship, efforts must be made to balance broad selective antimicrobial pressures against appropriate antimicrobial access. Without such, we risk increasing levels of AMR associated with nosocomial infections and further limiting options for late-stage treatment of infected patients. Reporting of data on outcomes, including early microbiological results and incidence of post-injury blood-stream infection underpinned by reliable diagnostics and the impact of IPC programmes in different settings (e.g. field hospitals vs urban hospitals) will be paramount in helping build a suitable evidence base for antimicrobial decision making in the context of conflict or catastrophe-related severe burn injuries.

Author contributions

All authors contributed significantly to pre-draft discussions for this work. SJCP, RM, SH and LSPM drafted the initial manuscript. SJCP, ZL, and SDW conducted the literature search. SH prepared the manuscript table. RM prepared the Supplementary data file. All authors contributed significantly to revisions and preparation of the final draft.

Funding

There was no specific funding associated with this work.

Declaration of Competing Interest

LSPM has consulted for or received speaker fees from bioMerieux (2013–2024), Eumedica (2016–2022), Pfizer (2018–2024), Sumitovant (2021–2023), Shionogi (2021–2024), Qiagen (2023), and Gilead (2024) and received research grants from the National Institute for Health Research (2013–2024), CW+ Charity (2018–2024), North West London Pathology (2022–2024), LifeArc (2020–2022), Shionogi (2024), and the Healthcare Infection Society (2024). SJCP has received research grants from the Hospital Infection Society, John Muir Trust and the Drummond Foundation not in connection with this work. All other authors have no conflicts of interest to declare.

Appendix A. Supporting information

Supplementary data associated with this article can be found in the online version at doi:10.1016/j.jinf.2024.106224.

References

1. Pallett SJC, Boyd SE, O'Shea MK, Martin J, Jenkins DR, Hutley EJ. *The contribution of human conflict to the development of antimicrobial resistance. Commun Med* 2023;**3**(1):153. https://doi.org/10.1038/s43856-023-00386-7
2. Moussally K, Abu-Sittah G, Gomez FG, Fayad AA, Farra A. *Antimicrobial resistance in the ongoing Gaza war: a silent threat. Lancet* 2023;**402**(10416):1972–3. https://doi.org/10.1016/S0140-6736(23)02508-4
3. International Society for Burns Injuries Practice Guidelines Committee. *ISBI practice guidelines for burn care. Burns* 2016;**42**(5):953–1021. https://doi.org/10.1016/j.burns.2016.05.013
4. Zhang P, Zou B, Liou YC, Huang C. *The pathogenesis and diagnosis of sepsis post burn injury. Burns Trauma* 2021;**9**:tkaa047. https://doi.org/10.1093/burnst/tkaa047
5. European Burn Association. European Practice Guidelines for Burn Care Minimum level of burn care provision in Europe; 2017. ⟨https://www.euroburn.org/wp-content/uploads/EBA-Guidelines-Version-4-2017-1.pdf⟩ [Accessed 14 April 2024].
6. American Burn Association. Guidelines for Burn Care under Austere Conditions: Introduction to Burn Disaster; 2017. ⟨https://ameriburn.org/wp-content/uploads/2020/04/1.-guidelines-for-austere-conditions-introduction-to-burn-disaster-airway-and-ventilator-2.pdf⟩ [Accessed 20 April 2024].
7. German Society of Burn Treatment. AWMF-S2K-Leitlinie. Leitlinie zur Behandlung Thermischer Verletzungen des Erwachsenen. (044–001); 2021. ⟨https://www.awmf.org/leitlinien/detail/ll/044–001.html⟩ [Accessed 20 April 2024].

8. Barajas-Nava LA, López-Alcalde J, Roqué i Figuls M, Solà I, Bonfill Cosp X. *Antibiotic prophylaxis for preventing burn wound infection. Cochrane Database Syst Rev* 2013(6):CD008738. https://doi.org/10.1002/14651858.CD008738.pub2
9. Medecins Sans Frontieres. MSF Medical Guidelines. Chapter 10: Medical and minor surgical procedures – Burns. ⟨https://medicalguidelines.msf.org/en/node/308⟩. [Accessed 20 April 2024].
10. D'Avignon LC, Chung KK, Saffle JR, Renz EM, Cancio LC, Prevention of Combat-Related Infections Guidelines Panel. *Prevention of infections associated with combat-related burn injuries. J Trauma* 2011;**71**(2 Suppl 2):S282–9. https://doi.org/10.1097/TA.0b013e318 227adc2
11. Avni T, Levcovich A, Ad-El DD, Leibovici L, Paul M. *Prophylactic antibiotics for burns patients: systematic review and meta-analysis. BMJ* 2010;**340**:c241. https://doi.org/10.1136/bmj.c241
12. Tagami T, Matsui H, Fushimi K, Yasunaga H. *Prophylactic antibiotics may improve outcome in patients with severe burns requiring mechanical ventilation: propensity score analysis of a Japanese Nationwide Database. Clin Infect Dis* 2016;**62**(1):60–6. https://doi.org/10.1093/cid/civ763
13. Karam G, Chastre J, Wilcox MH, Vincent JL. *Antibiotic strategies in the era of multidrug resistance. Crit Care* 2016;**20**(1):136. https://doi.org/10.1186/s13054-016-1320-7
14. Kryzhevskyi V, Strokous V, Lifshyts Y, Rybianets Y, Oberniak A, et al. *Case report: azithromycin-meropenem combination therapy as a low-cost approach to combat PDR gram-negative infections of war wounds in Ukraine. Front Med* 2023;**10**:1264492. https://doi.org/10.3389/fmed.2023.1264492
15. Yeong EK, Sheng WH, Hsueh PR, Hsieh SM, Huang HF, Ko AT, et al. *The wound microbiology and the outcomes of the systemic antibiotic prophylaxis in a mass burn casualty incident. J Burn Care Res* 2020;**41**(1):95–103. https://doi.org/10.1093/jbcr/irz077
16. Yeong EK, O'Boyle CP, Huang HF, Tai HC, Hsu YC, Chuang SY, et al. *Response of a local hospital to a burn disaster: contributory factors leading to zero mortality outcomes. Burns* 2018;**44**(5):1083–90. https://doi.org/10.1016/j.burns.2018.03.019
17. Jin R, Yang M, Weng T, Shao J, Xia S, Han C, et al. *Epidemiology and early bacteriology of extremely severe burns from an LPG tanker explosion in Eastern China. J Epidemiol Glob Health* 2022;**12**(4):478–85. https://doi.org/10.1007/s44197-022-00066-0
18. Parrish JS, Seda G. *Disasters resulting from radiologic and nuclear events. Crit Care Clin* 2019;**35**(4):619–31. https://doi.org/10.1016/j.ccc.2019.06.005
19. Mérens A, Rapp C, Delaune D, Danis J, Berger F, Michel R. *Prevention of combat-related infections: antimicrobial therapy in battlefield and barrier measures in French military medical treatment facilities. Travel Med Infect Dis* 2014;**12**(4):318–29. https://doi.org/10.1016/j.tmaid.2014.04.013
20. Saeed O, Tribble DR, Biever KA, Crouch HK, Kavanaugh M. *Infection prevention in combat-related injuries. Mil Med* 2018;**183**(suppl_2):137–41. https://doi.org/10.1093/milmed/usy077. PMID: 30189072.
21. Cancio LC, Powell D, Adams B, Bull K, Keller 4th AP, Gurney JM, et al. *Management of burn wounds under prolonged field care. J Spec Oper Med* 2016;**16**(4):87–98. https://doi.org/10.55460/KNX8-LXSO
22. Hughes A, Almeland SK, Leclerc T, Ogura T, Hayashi M, Mills JA, et al. *Recommendations for burns care in mass casualty incidents: WHO Emergency Medical Teams Technical Working Group on Burns (WHO TWGB) 2017-2020. Burns* 2021;**47**(2):349–70. https://doi.org/10.1016/j.burns.2020.07.001
23. Khorram-Manesh A, Goniewicz K, Burkle FM, Robinson Y. *Review of military casualties in modern conflicts – the re-emergence of casualties from armored warfare. Mil Med* 2022;**187**(3-4):e313–21. https://doi.org/10.1093/milmed/usab108
24. Fuzaylov G, Murthy S, Dunaev A, Savchyn V, Knittel J, Zabolotina O, et al. *Improving burn care and preventing burns by establishing a burn database in Ukraine. Burns* 2014;**40**(5):1007–12. https://doi.org/10.1016/j.burns.2013.11.013
25. Boehm D, Menke H. *Sepsis in burns – lessons learnt from developments in the management of septic shock. Medicina* 2021;**58**(1):26. https://doi.org/10.3390/medicina58010026
26. Lachiewicz AM, Hauck CG, Weber DJ, Cairns BA, van Duin D. *Bacterial infections after burn injuries: impact of multidrug resistance. Clin Infect Dis* 2017;**65**(12):2130–6. https://doi.org/10.1093/cid/cix682
27. Pallett SJ, Charani E, Hawkins L, Mazzella A, Anton-Vazquez V, Banerjee R, et al. *National action plans for antimicrobial resistance and variations in surveillance data platforms. Bull World Health Organ* 2023;**101**(8):501–512F. https://doi.org/10.2471/BLT.22.289403
28. World Health Organization. Central Asian and European Antimicrobial Surveillance: Antimicrobial resistance surveillance in Europe 2023 – 2021 data. ⟨https://www.who.int/europe/publications/i/item/9789289058537⟩ [Accessed 7 December 2023].
29. Quinn J, Panasenko SI, Leshchenko Y, Gumeniuk K, Onderková A, et al. *Prehospital lessons from the war in Ukraine: damage control resuscitation and surgery experiences from point of injury to role 2. Mil Med* 2024;**189**(1-2):17–29. https://doi.org/10.1093/milmed/usad253
30. World Health Organisation. WHO Access, Watch, Reserve (AWaRe) classification of antibiotics for evaluation and monitoring of use; 2023. ⟨https://iris.who.int/bitstream/handle/10665/371093/WHO-MHP-HPS-EML-2023.04-eng.xlsx?sequence=1⟩ [Accessed 20 April 2024].
31. European Medicines Agency. Fluoroquinolone antibiotics: reminder of measures to reduce the risk of long-lasting, disabling and potentially irreversible side effects. 2023. ⟨https://www.ema.europa.eu/en/news/fluoroquinolone-antibiotics-reminder-measures-reduce-risk-long-lasting-disabling-potentially-irreversible-side-effects⟩ [Accessed 29 April 2024].
32. Rees VE, Bulitta JB, Nation RL, Tsuji BT, Sörgel F, Landersdorfer CB. *Shape does matter: short high-concentration exposure minimizes resistance emergence for fluoroquinolones in Pseudomonas aeruginosa. J Antimicrob Chemother* 2015;**70**(3):818–26. https://doi.org/10.1093/jac/dku437

Анотація: *Нові комбінації антибіотиків можуть діяти синергічно, щоб призводить до пригнічення рост множинної антибіотикорезистентності. Втім, важко передбачити, яка саме комбінація антибіотиків буде успішною. Стандартний тест на антимікробну чутливість може не виявити таких синергідних ефектів через особливість інфекційного процесу. Крім того, існує фізіологічна різниця між планктонними вільно існуючими та прикріпленими, захищеними біоплівкою, бактеріальними клітинами і, відповідно, чутливість до антибіотиків у таких різних субпопуляцій теж буде відрізнятись. На прикладі номінально стійкої до макролідів бактерії* K. pneumoniae *(ATCC 10031) було продемонстровано ефективність кількох макролідів у пригніченні росту біоплівки і здатність азитроміцину підвищувати ефективність таргетного антибіотику метансульфонату колістину при біоплівкових інфекціях, спричинених* K. pneumoniae*, Ця синергетична дія також була підтверджена на колекції госпітальних ізолятів* K. pneumoniae *із високою резистентністю. Ця сама терапевтична комбінація азитроміцину і метансульфонату колістину була досліджена на розробленій модель рани in vitro. Розроблена модель складалась з тривимірної колагенової губчастої основи, засіяної епітелізованними HEK293 клітинами, яку було занурено в рідинне середовище, що імітує ексудат ранового дна. В цій моделі було підтверджено високу терапевтичну ефективність комбінації азитроміцину з метансульфонатом колістину у пригніченні високорезистентного штаму* K. pneumoniae*. Використання азитроміцину для пом'якщення важкості інфекційного процесу та у комбінації із таргетним антибіотиком було продемонстровано у лікуванні пацієнта, який отримав бойові поранення та обширні ранові інфекції, спричинені мультирезистентними та панрезистентними штамами. Зокрема, пацієнта було успішно вилікувано комбінованою терапією азитроміцином з меропенемом. Отримані результати підкреслюють необхідність пошуку нових ефективних протимікробних терапевтичних підходів як альтернативні стратегії лікування інфекцій із високою резистентністю.*

4.3. Неспецифічна біоплівко-стимулююча активність фармакологічних молекул

Зворотною стороною використання неефективних режимів терапії є стимуляція утворення біоплівки інфекційним штамом. Ця стимуляція може бути неспецифічною. Відомо, що антибіотики в субоптимальних дозах сприяють утворенню біоплівки та розвитку стійкості до антибіотиків. Так, повідомлялось про те, що субмінімальні інгібіторні концентрації (суб-МІК) іміпенему та колістину впливають на гени, пов'язані з утворенням біоплівки та резистентністю до специфічних для біоплівки антибіотиків у *A. baumannii* (5). Відомо, що підвищена регуляція генів, пов'язаних з біоплівкою, може посилити утворення біоплівки при лікуванні антибіотиками в суб-МІК режимі. В наших роботах ми також спостерігали стимулюючу активність колістину по відношенню до полірезистентного штаму *K. pneumoniae* (4, 135)

Втім, можлива і специфічна стимуляція утворення біоплівки. Зокрема, автором було досліджено стимуляція утворення біоплівки у грам-негативних бактерій новими антистафілококовими речовинами із анти-сортазною активністю. Зокрема, деякі інгібітори сортази А стафілококу, які проявляли антибіоплівкову дію по відношенню до *S. aureus,* стимулювали чотирикратний ріст біомаси біоплівки *K. pneumoniae* ATCC 10031 (149). Такий неочікуваний ефект можна пояснити відмінностями поверхневих клітинних білків клітин *K. pneumoniae* від білків стафілококу. Така відмінність може призводити до інгібування деяких регулярних або метаболічні шляхів, що пов'язані з утворенням біоплівки у *K. pneumoniae*. Зокрема, виявилось, що сортаза класу А (SrtA) у *K. pneumonia* має високу гомологію до SrtA у *S. aureus* з ідентичністю амінокислотної послідовності 40,5%.

Основні результати, отримані в цьому підрозділі дисертації опубліковано в роботі автора (149).

The Journal of Antibiotics
https://doi.org/10.1038/s41429-022-00524-8

Japan Antibiotics Research Association
The Society for Actinomycetes Japan

ARTICLE

Identification of novel small-molecular inhibitors of *Staphylococcus aureus* sortase A using hybrid virtual screening

Galyna P. Volynets[1] · Fabian Barthels[2] · Stefan J. Hammerschmidt[2] · Olena V. Moshynets[3] · Sergiy S. Lukashov[1] · Sergiy A. Starosyla[1,4] · Hanna V. Vyshniakova[5] · Olga S. Iungin[6] · Volodymyr G. Bdzhola[1] · Andrii O. Prykhod'ko[1,7] · Anatolii R. Syniugin[1] · Vladislav M. Sapelkin[1] · Sergiy M. Yarmoluk[1] · Tanja Schirmeister[2]

Received: 14 March 2022 / Revised: 30 March 2022 / Accepted: 6 April 2022
© The Author(s), under exclusive licence to the Japan Antibiotics Research Association 2022

Abstract

Staphylococcus aureus is one of the most dangerous pathogens commonly associated with high levels of morbidity and mortality. Sortase A is considered as a promising molecular target for the development of antistaphylococcal agents. Using hybrid virtual screening approach and FRET analysis, we have identified five compounds able to decrease the activity of sortase A by more than 50% at the concentration of 200 µM. The most promising compound was 2-(2-amino-3-chloro-benzoylamino)-benzoic acid which was able to inhibit *S. aureus* sortase A at the IC_{50} value of 59.7 µM. This compound was selective toward sortase A compared to other four cysteine proteases – cathepsin L, cathepsin B, rhodesain, and the SARS-CoV2 main protease. Microscale thermophoresis experiments confirmed that this compound bound sortase A with K_D value of 189 µM. Antibacterial and antibiofilm assays also confirmed high specificity of the hit compound against two standard and three wild-type, *S. aureus* hospital infection isolates. The effect of the compound on biofilms produced by two *S. aureus* ATCC strains was also observed suggesting that the compound reduced biofilm formation by changing the biofilm structure and thickness.

Introduction

Staphylococcus aureus (*S. aureus*) is one of the most common nosocomial pathogens that causes a number of hospital-acquired diseases ranging from skin infections to severe human infections associated with high levels of morbidity and mortality such as sepsis, endocarditis, osteomyelitis, necrotizing pneumonia, etc [1–3].

The main problem of staphylococcal infections treatment is the increasing emergence of multidrug resistance. Nowadays, methicillin- (MRSA) and vancomycin-resistant *S. aureus* (VISA and VRSA) strains remain serious medical and public problems worldwide since the antibiotics of the last choice such as linezolid, teicoplanin and daptomycin are not always effective and have shown a tendency to lose their effectiveness due to resistance [4–8]. Therefore, the development of novel types of antistaphylococcal agents is of great importance.

Sortase A is recognized as a promising druggable anti-virulence target [9–12]. Sortase A is a membrane-localized cysteine transpeptidase that catalyzes the attachment of surface virulence proteins to the cell wall [13], which play essential roles in infection processes by promoting bacterial

Supplementary information The online version contains supplementary material available at https://doi.org/10.1038/s41429-022-00524-8.

✉ Galyna P. Volynets
g.p.volynets@gmail.com

[1] Department of Medicinal Chemistry, Institute of Molecular Biology and Genetics, the NAS of Ukraine, 150 Zabolotnogo St, 03143 Kyiv, Ukraine

[2] Institute of Pharmaceutical and Biomedical Sciences, Johannes Gutenberg-University of Mainz, Staudinger Weg 5, 55128 Mainz, Germany

[3] Biofilm study group, Institute of Molecular Biology and Genetics, the NAS of Ukraine, 150 Zabolotnogo St, 03143 Kyiv, Ukraine

[4] RECEPTOR.AI, Boston, MA, USA

[5] L.V. Gromashevsky Institute of Epidemiology and Infectious Diseases NAMS of Ukraine, 5 Amosova St, 03038 Kyiv, Ukraine

[6] Department of Functional Genomics, Institute of Molecular Biology and Genetics, the NAS of Ukraine, 150 Zabolotnogo St, 03143 Kyiv, Ukraine

[7] Research and Development Department, Scientific Services Company Otava Ltd, 150 Zabolotnogo St, 03143 Kyiv, Ukraine

Published online: 19 April 2022

adhesion, biofilm formation, host cell entry, acquisition of important nutrients from the host, immune evasion and suppression [14, 15]. Sortase A is a promising target since it is localized on the extracellular side of the cell membrane. This enhances the bioavailability of the inhibitor due to accessibility of the target with no requirement for penetration through the bacterial cell wall. Another advantage is that the sortase A does not have human homologs hence selective inhibitors of this enzyme should possess lower toxicity. Sortase A is not crucial for bacterial growth and viability, and therefore, the inhibition of this enzyme is expected to cause lower selection pressure on resistance development [15, 16].

To date, several chemical classes of sortase A inhibitors have been reported among synthetic and natural compounds, [12, 16–21] but none of them have entered clinical trials as yet. Therefore, it is of great interest for medicinal chemistry to discover novel chemical scaffolds of sortase A inhibitors.

Materials and methods

Molecular docking

The semi-flexible receptor-ligand docking was performed with the DOCK package [22–25]. As a receptor, the crystal structure of *S. aureus* sortase A with PDB accession code:2MLM was used [26]. The ligands geometry was calculated with YFF force field [27] and the partial atomic charges were added using the Kirchhoff method [28]. Docking parameters were set as reported previously [29]. The spheres in the active site of SrtA were generated with the DOCK *sphgen* program. Grid maps were built using the *grid* program with grid spacing 0.3 Å. The all-atom model was used for protein representation. We selected "multiple anchor" parameter for molecular docking and the minimal number of atoms in the achor was 6 and the maximum number of orientations was 1000.

Visual analysis of docking complexes was carried out with Discovery Studio Visualizer 4.0 [30].

Pharmacophore modeling

Receptor-oriented pharmacophore models were generated based on the two crystal structures of *S. aureus* SrtA with the ligands. The first primary pharmacophore model was built taking into account the intermolecular bonds of the small-molecular inhibitor benzo[d]isothiazol-3-one with SrtA (PDB ID: 2MLM) [26] and the second pharmacophore model was developed based on the complex of polypeptide substrate with SrtA (PDB ID: 2KID) [31]. The excluded volumes were generated using the atoms of amino acid residues in the active site of SrtA within 5 Å of the ligand. These models were optimized in different ways: excluding several pharmacophore features, changing the radii, and scores of pharmacophore features. Therefore, a number of derivative pharmacophore models were obtained. Pharmacophore model validation was performed by screening towards a training set containing 173 known inhibitors of SrtA (cutoff of activity was 30 μM). As a result, nine pharmacophore models, which correctly predicted active and inactive compounds from the training set, were selected for pharmacophore screenings of the OTAVA compound collection [32].

Sortase A (SrtA) expression and purification

Expression of the *S. aureus* SrtA was mainly performed as described previously [33]. The SrtA-sequence containing pET23b expression construct was transformed into competent cells of the *Escherichia coli* (*E. coli*) strain BL21-Gold (DE3) (Agilent Technologies, Santa Clara, California) and grown in 100 μM ampicillin containing LB medium at 37 °C until they reached an OD_{600} of ~0.6–0.8. Expression was induced with addition of 1 mM isopropyl-D-thiogalactoside (IPTG) for 16 h at 20 °C. After harvesting by centrifugation (10 min, 10 krpm), cells were resuspended in lysis buffer (20 mM Tris, pH 6.9, 300 mM NaCl, 0.1% (v/v) $Triton_{X\text{-}100}$, DNase, lysozyme) and lysed by sonication (Sonoplus, Bandelin, Berlin, Germany). The cleared lysate (45 min, 15 krpm) was subjected to IMAC (HisTrap HP 5 ml column, GE Healthcare, Chicago, Illinois) to crudely isolate the protein. Eluted fractions containing protein were subsequently administered to a gel-filtration (size exclusion chromatography, SEC) step (HiLoad 16/60 Superdex 75 column, GE Healthcare) in the SEC/storage buffer (20 mM Tris-HCl, pH 7.5, 150 mM NaCl, 5 mM $CaCl_2$). Purified SrtA was shock frozen in liquid nitrogen and stored at −80 °C until further use. Throughout all steps, protein concentrations were measured via absorbance at 280 nm and sample purity was assessed via SDS-PAGE.

In vitro Sortase A inhibition assay

Assays of *S. aureus* SrtA transpeptidation activity were performed as previously described [12]. Briefly, recombinantly expressed SrtA (final concentration: 1 μM) was incubated in assay buffer (50 mM Tris, 150 mM NaCl, 5 mM $CaCl_2$, pH 7.5) with 25 μM of Abz-LPETG-Dap(Dnp)-OH and 0.5 mM H_2N-$(Gly)_4$-OH. Inhibitors were added from DMSO stocks. Assays were initiated by the addition of SrtA and monitored for 30 min at 30 °C in an Infinite M200 Pro plate reader with λ_{ex} 320 nm/λ_{em} 430 nm. Three technical replicates were performed for each inhibitor in flat-bottomed black 96-well plates. Enzyme inhibition was analyzed as previously described [12].

Protease inhibition selectivity

Fluorometric assays for cathepsin B, cathepsin L, and rhodesain were performed as described previously [12]. Cbz-Phe-Arg-AMC was used as the fluorogenic substrate (100 µM for cathepsin B, 6.5 µM for cathepsin L, and 10 µM for rhodesain). Fluorometric assays for SARS-CoV2 M^{pro} were performed as described previously [34]. Dabcyl-KTSAVLQSGFRKME-Edans was used as a FRET-substrate at a final concentration of 20 µM.

Microscale thermophoresis

Purified *S. aureus* sortase A was labeled with the Monolith Protein Labeling Kit RED-NHS according to the manufacturer's instructions. MST sample preparation was conducted as described by the manufacturer's standard protocols. Briefly, MST reaction mixtures consisted of 5 nM labeled sortase A in MST buffer (50 mM Tris, 150 mM NaCl, 5 mM $CaCl_2$, 0.05% (v/v) Tween-20, 10% DMSO, pH 7.50) supplemented with a 1:1 dilution series of the hit compounds (500-31 µM). MST measurements were performed with a NanoTemper Monolith NT.115 instrument (MST power of 50%, LED power of 70%, 20 s laser-on time, and 5 s laser-off time) with NanoTemper Monolith premium capillaries. Binding affinities (K_D) were determined with the Nanotemper MO Analysis Software v2.3. Response evaluation was conducted at 10 s laser-on time.

Aggregation assessment by turbidimetry

To assess the aggregation potential of the identified hit compounds, a turbidimetric analysis was conducted. Therefore, the optical density (OD_{610}) was measured over time (assay buffer, no enzyme 200 µM compound concentration). Absorption measurements were conducted in 60 kinetic cycles of each 30 s with orbital shaking (300 rpm for 5 s before readout) using a Tecan Spark 10 M plate reader. Compounds did not show significant absorbance at this wavelength spectrum, thus, any increase in OD_{610} was assumed to be caused by precipitation of the hit compound.

Strains and culturing conditions

S. aureus ATCC 25923, *S. aureus* ATCC 43300, *P. aeruginosa* PA 01, and *K. pneumoniae* ATCC 10031 (Ukrainian National Collection) were used as model strains for testing biofilm formation and free-living (planktonic) behavior under different concentrations of the tested compound. Biofilm responses to the compound were also determined for three *S. aureus* isolates from Ukrainian hospitals, including the multidrug (MDR) strains UHI 1, UHI 2, and UHI 3. The Kirby-Bauer disc-diffusion assay was used to determine the antimicrobial susceptibility of the *S. aureus* strains. Susceptibility was then determined as the diameter (mm) of inhibition or MIC value after incubation up two days and interpreted according to the European Committee on Antimicrobial Susceptibility Testing (EUCAST) guidelines [35] for the rest of the antibiotics.

Antibiotic susceptibility of the *S. aureus* strains listed in S2 Table. All strains were stored as frozen stocks in 25 (v/v) % glycerol at −80 °C.

Planktonic assay

Planktonic growth assays of *S. aureus* ATCC 25923, *S. aureus* ATCC 43300, *P. aeruginosa* PA 01, *K. pneumoniae* ATCC 10031 were assessed in loosely lidded 30 ml glass microcosms which were incubated with shaking before assay at 37 °C. The microcosms contained 5 ml Mueller-Hinton broth and the corresponding concentration of the tested compound or without. Aliquots of over-night culture were added to replicate vials ($n = 6$) to ~5×10^6 CFU ml^{-1} and growth was determined after 16 h incubation by removing 200 µl samples which were transferred to a polystyrene 96-well plate and OD620 measured using a Multiskan ™ FC Microplate Photometer (Thermo Fisher Scientific).

Biofilm assay

20 µl aliquots of over-night culture of *S. aureus* ATCC 25923, *S. aureus* ATCC 43300, *P. aeruginosa* PA01, *K. pneumoniae* ATCC 10031, and three UHI strains were used to inoculate replicate wells ($n = 5$ for each treatment) containing 200 µl Mueller-Hinton with the appropriate concentration of the tested compound or without. Growth (OD_{620}) was determined after 24–48 h static incubation at 37 °C using a Multiskan ™ FC Microplate Photometer (Thermo Fisher Scientific).

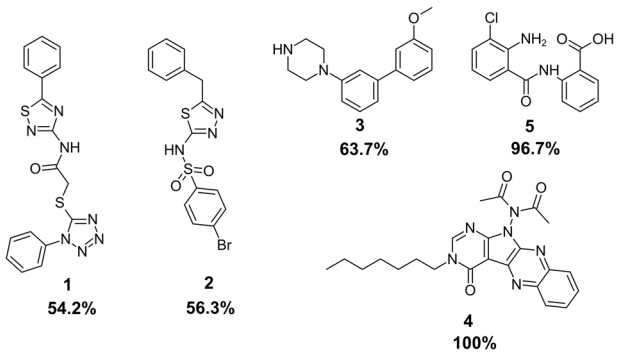

Fig. 1 Inhibitors of *S. aureus* sortase A. Chemical structure of hit compounds identified after screening at 200 µM inhibitor concentration and FRET-quenching correction

Confocal laser scanning microscopy (CLSM)

Biofilm samples were prepared in 30 ml glass microcosms containing 5 ml Mueller-Hinton broth. The biofilm was stained with 1 mM ethidium bromide (Sigma) and 3 mM AmyGreen solution (own synthesis). No additional washing was used in order to limit the physical disruption of biofilm structures through liquid movement. The samples were not fixed, and a cover slip was placed over the stained samples before imaging. CLSM analysis was undertaken using a Leica TCS SPE Confocal system with coded DMi8 inverted microscope (Leica, Germany) and Leica Application Suite X (LAS X) Version 3.4.1. Images were acquired using excitation at 488 nm and emission collected at 490-580 nm for AmyGreen, and excitation at 532 nm and emission collected at 537-670 for ethidium bromide. The total pixels were calculated by the above-mentioned software.

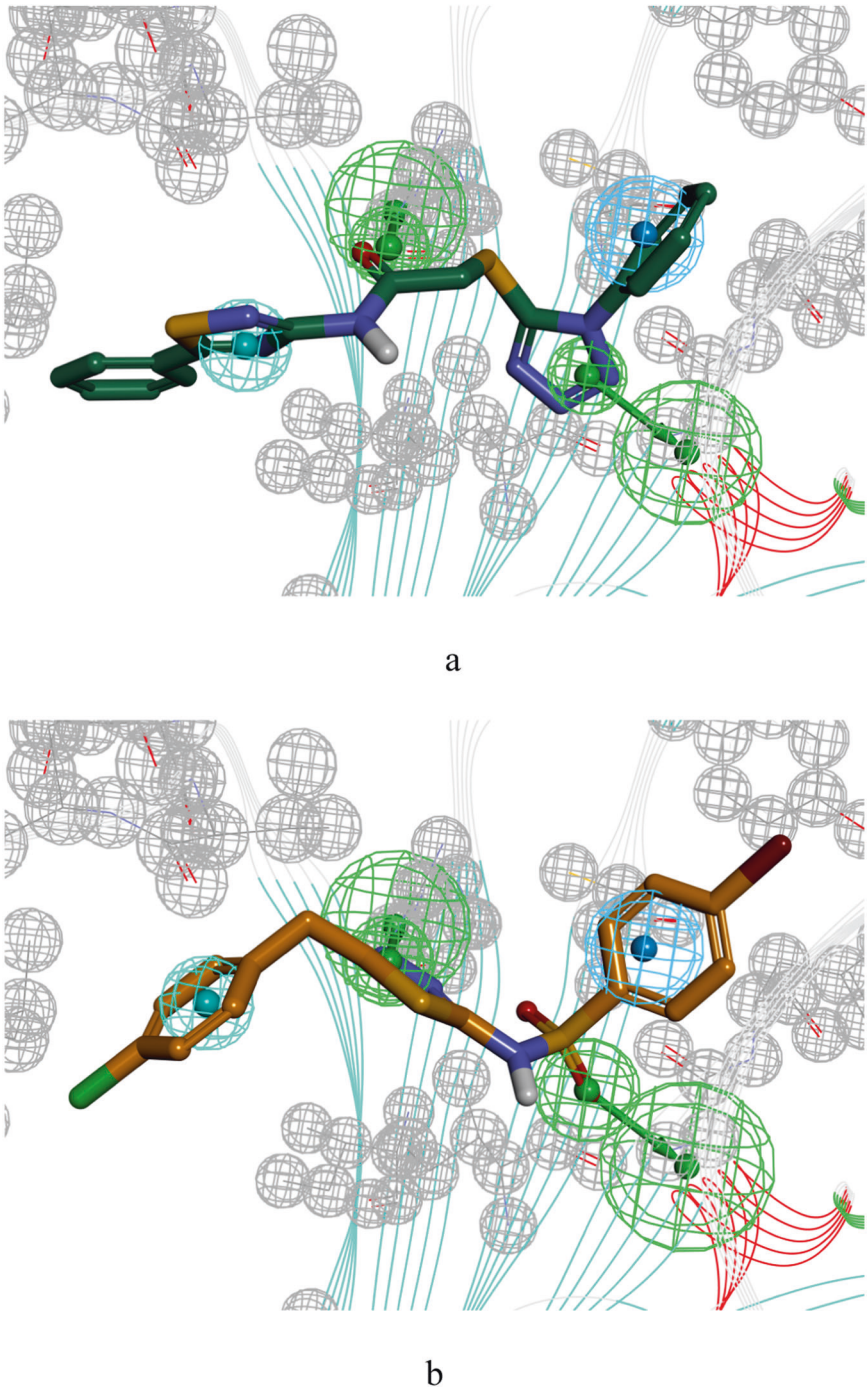

Fig. 2 *S. aureus* sortase A pharmacophore models. Mapping of compound **1** (**a**) and compound **2** (**b**) to corresponding pharmacophore models. Pharmacophore features matched with generated models are labeled with green (H-bond acceptor), cyan (hydrophobic), and azure (aromatic feature without vector) color. Excluded volumes (labeled with gray color) were built on the atoms of amino acid residues in the active site of sortase A within 5 Å around the ligand

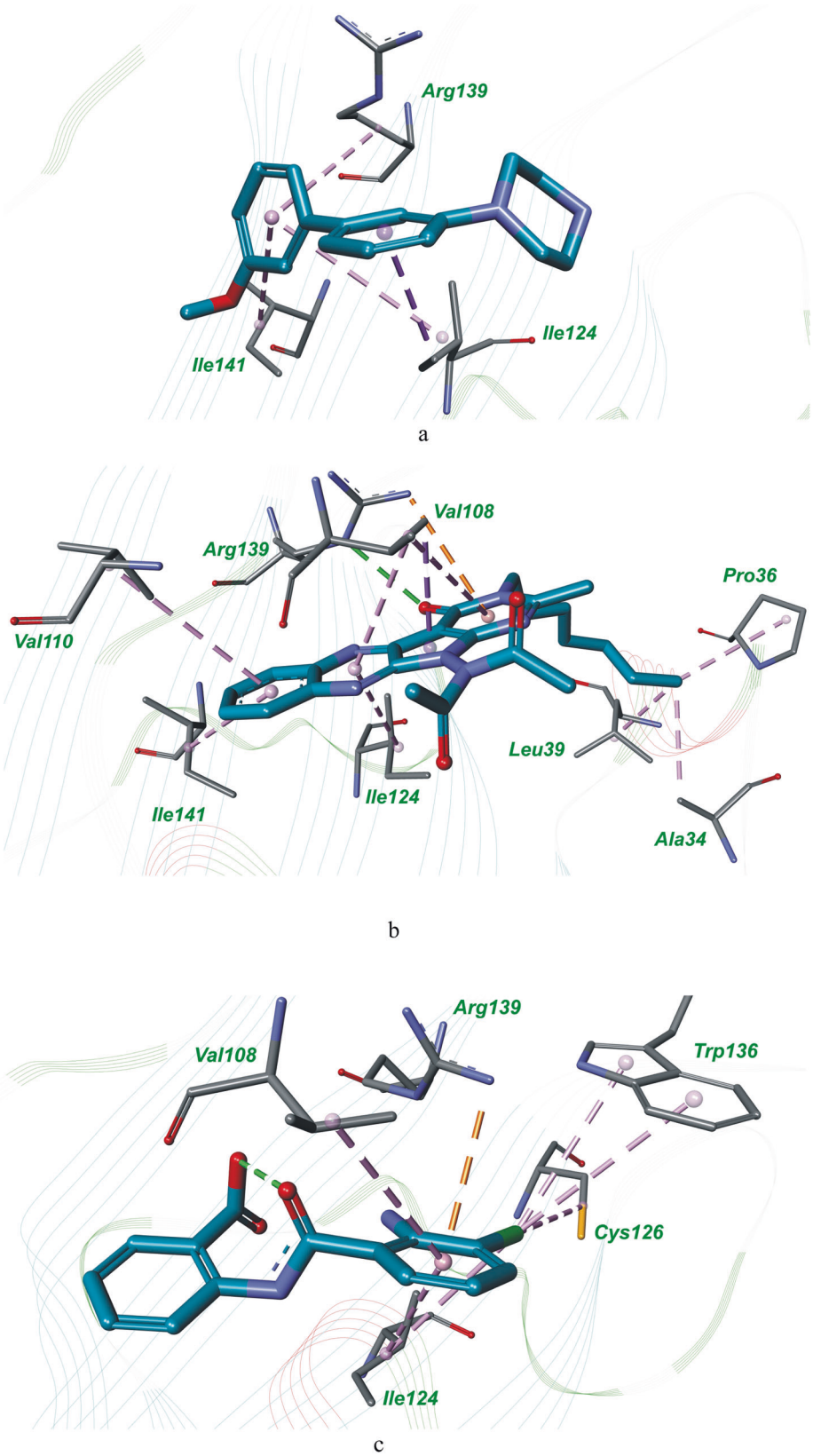

Fig. 3 The complexes of compounds **3** (**a**), **4** (**b**), and **5** (**c**) with amino acid residues in the active site of *S. aureus* sortase A, obtained with molecular docking. The hydrogen bonds are shown by green dashed lines, π-alkyl interactions are shown by yellow dashed lines, and π-cation interactions are indicated with orange dashed lines

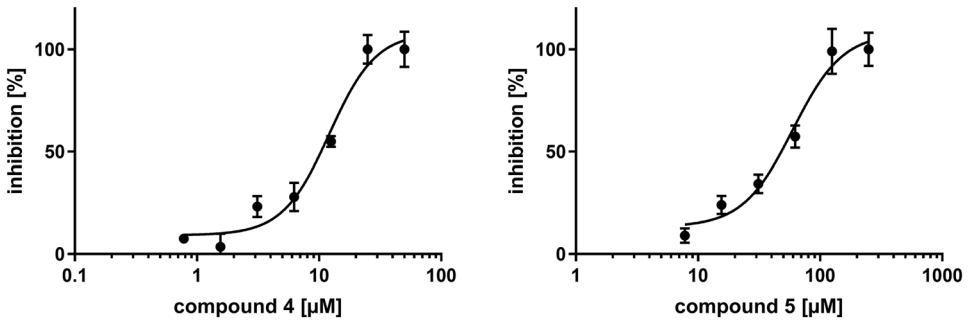

Fig. 4 Determination of IC_{50} values for compounds **4** and **5**

Table 1 Selectivity results from screening of compounds **4** and **5** against various cysteine proteases

Inhibition	sortase A	hCatL	hCatB	rhodesain	SARS-CoV2 M^{pro}
Compound **4** (25 μM)	100%	2.3%	11.8%	37.3%	36.2%
Compound **5** (125 μM)	99%	7.6%	7.1%	10.9%	16.5%

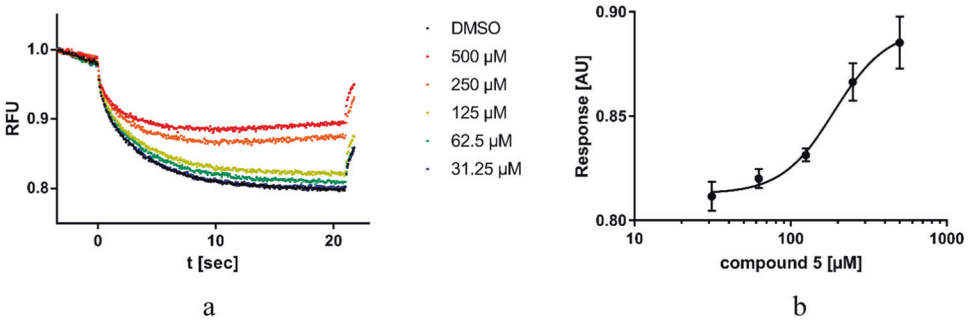

Fig. 5 Determination of the K_D value for compound **5** by MST. The normalized thermophoresis time traces (**a**) display significant bumps and a pronounced shift with higher concentrations of **5**. The sigmoidal fit of response-concentration blot after 10 s laser-on time (**b**) determined the K_D of **5** to be 189 μM

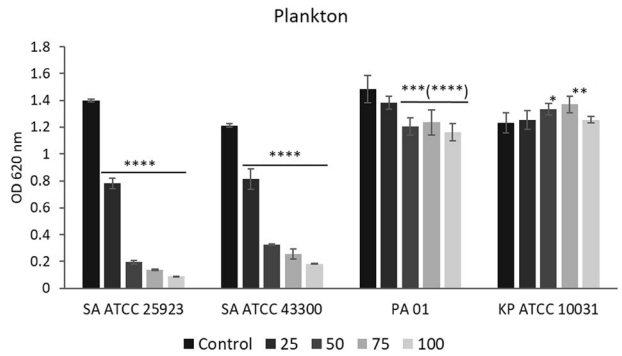

Fig. 6 The level of planktonic bacteria biomass after treatment with compound **5**. The level of planktonic biomass of S. *aureus* (SA) ATCC 25923 (MS), *S. aureus* (SA) ATCC 43300 (MR), *P. aeruginosa* (PA) PA 01, *K. pneumoniae* (KP) ATCC 10031 formed in the presence of compound **5** in a concentration of 25, 50, 75, 100 mg l^{-1} (which corresponds to 86 μM, 172 μM, 258 μM, 344 μM) or without (control) following 24 h of incubation measured as the optical density at 620 nm. Statistical significance compared to control. *$p < 0.05$, **$p < 0.01$, ***$p < 0.005$, ****$p < 0.001$

Statistical analysis

Replicate data were processed using the statistical software package OriginPro 7.0 and MS Excel for Windows. All results are presented as the mean ± standard deviation. A value of $p < 0.05$ was considered statistically significant.

Results and discussion

In order to identify novel inhibitors of *S. aureus* sortase A the molecular docking and pharmacophore screening of the OTAVA compound collection [32] containing about 250,000 compounds were performed. There were 96 compounds selected for in vitro assays following the results of virtual screenings including 39 compounds selected according to the docking assay and 57 compounds selected in the pharmacophore screening assay.

First, the 96 test compounds were screened for inhibition of sortase A in a Förster resonance energy transfer (FRET)-based enzyme assay using Abz-LPETG-Dap(dnp)-OH as a substrate. For this purpose, an initial inhibitor concentration of 200 μM was chosen in order to identify weaker inhibitors also. The inhibition data (triplicates) for all 96 compounds are available as supplementary material (Table S1). Of the 96 compounds, 17 showed inhibition of >50% at 200 μM and were chosen for further characterization. There were a number of visibly colored compounds that could potentially interfere in the FRET-based enzyme assay. The potential

quenching of the FRET-fluorophore (anthranilic acid) was determined by measuring the fluorescence of variable concentrations of anthranilic acid (1.25–10 µM) with 200 µM of each inhibitory compound. The inhibition caused by this quenching of the fluorophore was subtracted from the inhibition in the sortase A enzyme assay. As seen in Table S1, 12 of the 17 primarily identified hits were actually false-positives. However, 5 out of 96 compounds showed >50% corrected inhibition at 200 µM. The chemical structures of these compounds are shown in Fig. 1.

The compounds **1** and **2** were found with pharmacophore screening toward pharmacophore models generated based on the crystal structure of *S. aureus* sortase A with PDB accession code 2MLM [26]. The mapping of compounds **1** and **2** on corresponding pharmacophore models is shown in Fig. 2.

The compounds **3**, **4**, and **5** were identified according to molecular docking results. The complexes of these compounds with amino acid residues in the active site of *S. aureus* sortase A are presented in Fig. 3.

According to FRET analysis data, two compounds **4** and **5** demonstrated strong inhibition of > 95%. Concentration-dependent inhibition series of these two compounds were performed to calculate the IC_{50} values. The IC_{50} values for compounds **4** and **5** were determined to be 12.1 µM and 59.7 µM, respectively (Fig. 4). For the other compounds, the inhibition at 200 µM was too low to determine an IC_{50} value and testing at higher concentrations was limited by solubility.

In order to show whether the inhibition is specific for sortase A, these two compounds were tested on four additional cysteine proteases. This selectivity measurement was performed against human cathepsin L (hCatL), cathepsin B (hCatB), the cathepsin L-like parasite protease rhodesain, and the severe acute respiratory syndrome coronavirus 2 main protease (SARS-CoV2M^{pro}) at an inhibitor concentration of 25 µM for compound **4** and 125 µM for compound **5**. Only slight inhibition beyond the sortase A target was found for the two inhibitors indicating selective inhibition (Table 1).

As an orthogonal assay strategy, microscale thermophoresis (MST) experiments were performed with the identified hit compounds at 500 µM inhibitor concentration (Fig. 5). A change in the thermophoresis curves in the presence of inhibitors suggests selective binding of the compounds to sortase A. For compound **5**, the thermophoresis response changed significantly. For the other compounds, no thermophoresis changes were observed, which is either because (1) these substances do not bind selectively to sortase A or (2) the binding does not lead to a sufficient change of the hydration

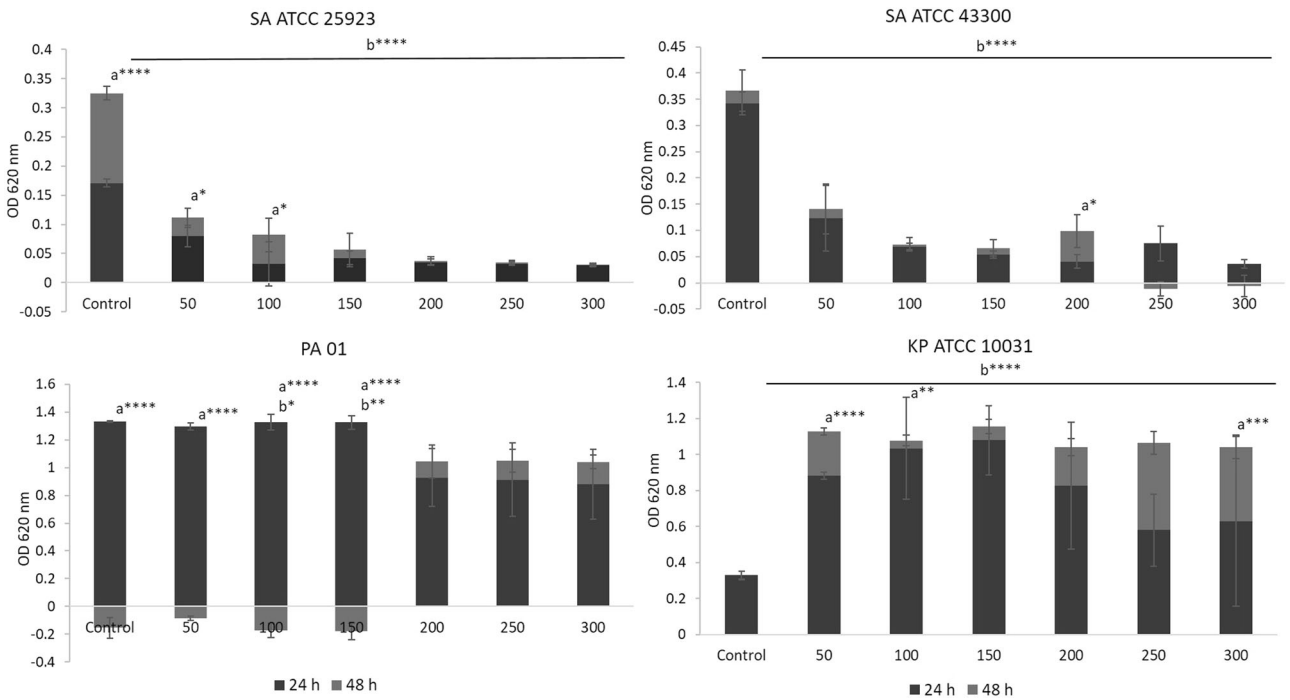

Fig. 7 The level of the total bacteria biofilm biomass after treatment with compound **5**. The level of total biofilm biomass of S. *aureus* (SA) ATCC 25923 (MS), *S. aureus* (SA) ATCC 43300 (MR), *P. aeruginosa* (PA) PA 01, *K. pneumoniae* (KP) ATCC 10031 formed in the presence of compound **5** in concentrations of 50, 100, 150, 200, 250, 300 mg l^{-1} (which corresponds to 172 µM, 344 µM, 516 µM, 688 µM, 860 µM, 1032 µM) or without (control) following the first day (dark grey, 24 h) and the second day (light grey, 48 h) of incubation measured as the optical density at 620 nm. a statistical significant differences of the second-day growth compared to the first day of incubation; b statistically significant difference compared to control. * $p < 0.05$, ** $p < 0.01$, *** $p < 0.005$, **** $p < 0.001$

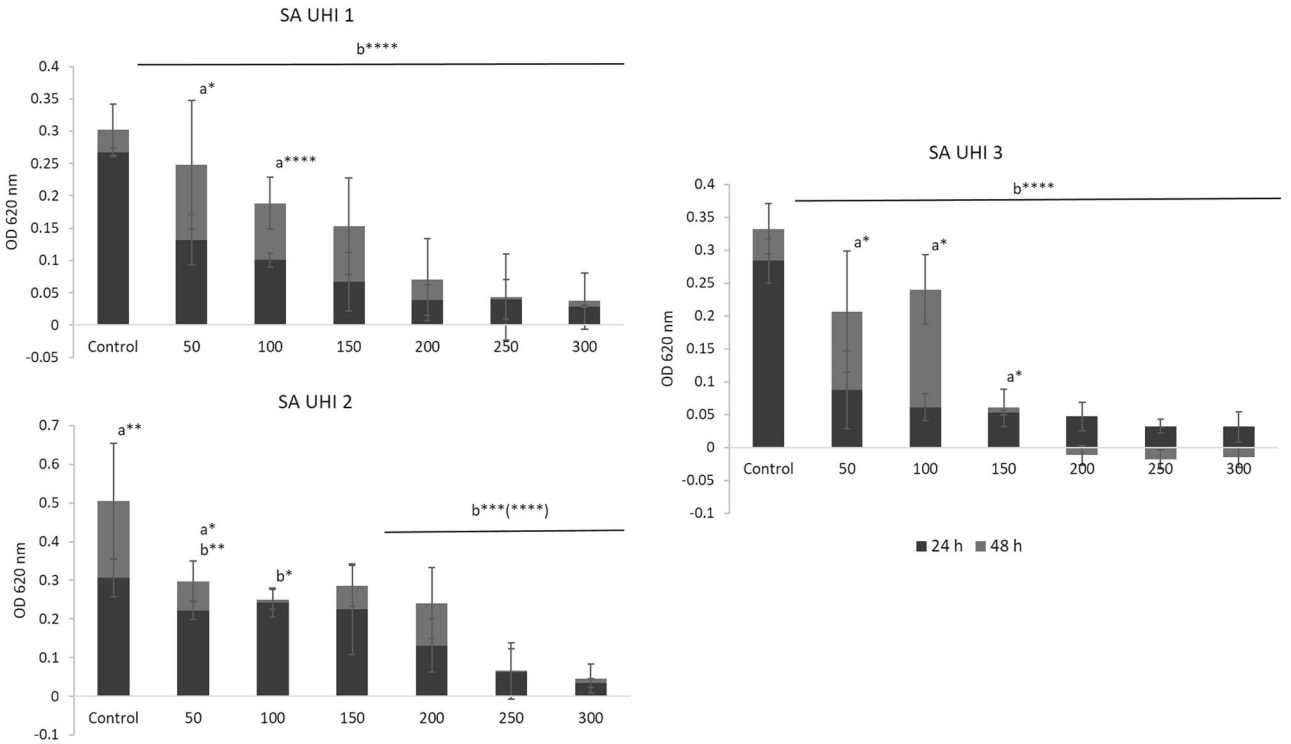

Fig. 8 The level of the total biofilm biomass of *S. aureus* strains after treatment with compound **5**. The level of the total biofilm biomass of three *S. aureus* wild type UHI strains formed in the presence of compound **5** in a concentration of 50, 100, 150, 200, 250, 300 mg l^{-1} (which corresponds to 172 µM, 344 µM, 516 µM, 688 µM, 860 µM, 1032 µM) or without (control) following the first day (dark grey, 24 h) and the second day (light grey, 48 h) of incubation measured as the optical density at 620 nm. a statistical significance of the second-day growth compared to the first day of incubation; b statistical significance compared to control. *$p < 0.05$, **$p < 0.01$, ***$p < 0.005$, ****$p < 0.001$

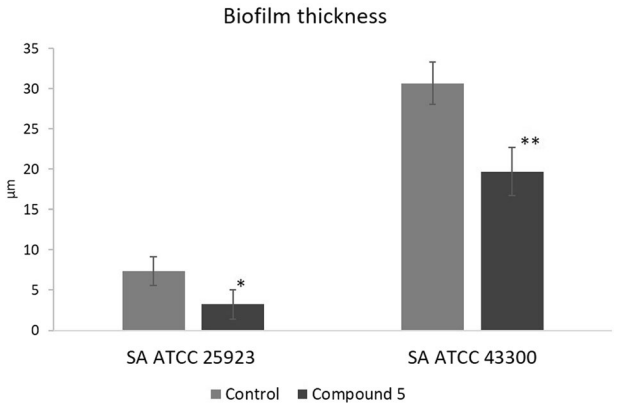

Fig. 9 The thickness of *S. aureus* biofilms. The average thickness of the two-day-old biofilms produced by two S. *aureus* strains ATCC 25923 and ATCC 43300 was observed by confocal laser scanning microscopy (CLSM). Statistical significance of compared to control. *$p < 0.05$, **$p < 0.01$

shell, or (3) the inhibitor concentrations are too low compared to the affinity. MST is also a sensitive method to identify ligand-induced protein aggregation, as expressed by bumpy thermophoresis curves. The thermophoresis curves demonstrated that compound **4** is likely to be an aggregator. The identified binder compound **5** was subsequently analyzed in a 1:1 dilution series, beginning with 500 µM by MST to determine the K_D value. For compound **5**, a K_D value of 189 µM was found (Fig. 5).

To investigate if any of the other hit structures is likely to cause assay-interfering aggregation, all hit compounds were subjected to a turbidimetry screening. The optical density (OD_{610}) was measured over time (assay buffer, 200 µM compound concentration). The optical density did increase over time for compound **4**, indicating that this substance can form microscopic aggregates in a protein-independent manner due to its high hydrophobicity. The other four hit compounds did not cause precipitation detectable by turbidimetry. These findings are in line with our MST measurements, indicating the formation of aggregates at higher concentrations of **4**.

The effects of the hit compound **5** against *S. aureus* free-living plankton and sessile attached biofilm-forming bacterial cultures were determined. The direct antibacterial effect of the compound **5** and its specificity against free-living bacteria were studied using four typical strains, specifically, methicillin-sensitive (MS) *S. aureus* ATCC 25923, methicillin-resistant (MR) *S. aureus* ATCC 43300, *Pseudomonas aeruginosa* PA 01, and *Klebsiella pneumoniae* ATCC

10031. Four concentrations, particularly, 25, 50, 75, and 100 mg l^{-1} of compound **5** were used to evaluate antibacterial effect against planktonic culture. The compound showed statistically significant reduction in plankton growth for both *S. aureus* strains for all the concentrations used. The lowest concentration of 25 mg l^{-1} reduced the population of *S. aureus* ATCC 25923 and *S. aureus* ATCC 43300 by 42% and 33%, respectively (Fig. 6). The rest of the concentration demonstrated 7- and 4-fold growth reduction for *S. aureus* ATCC 25923 and *S. aureus* ATCC 43300. Interestingly, there was no substantial effect of the compound onto *P. aeruginosa* PA 01: only 20% growth decrease was observed for 50, 75, and 100 mg l^{-1}. It was also noticed that compound **5** showed stimulative activity for *K. pneumoniae* ATCC 10031, increasing the growth by 14–16% whereas exposure to 50 and 75 mg l^{-1} had no effects. This suggests specificity of compound **5** for the target, associated with free-living *S. aureus* cells.

Bacteria colonize the econiche through biofilm formation which is the dominant form of bacterial persistence [36].

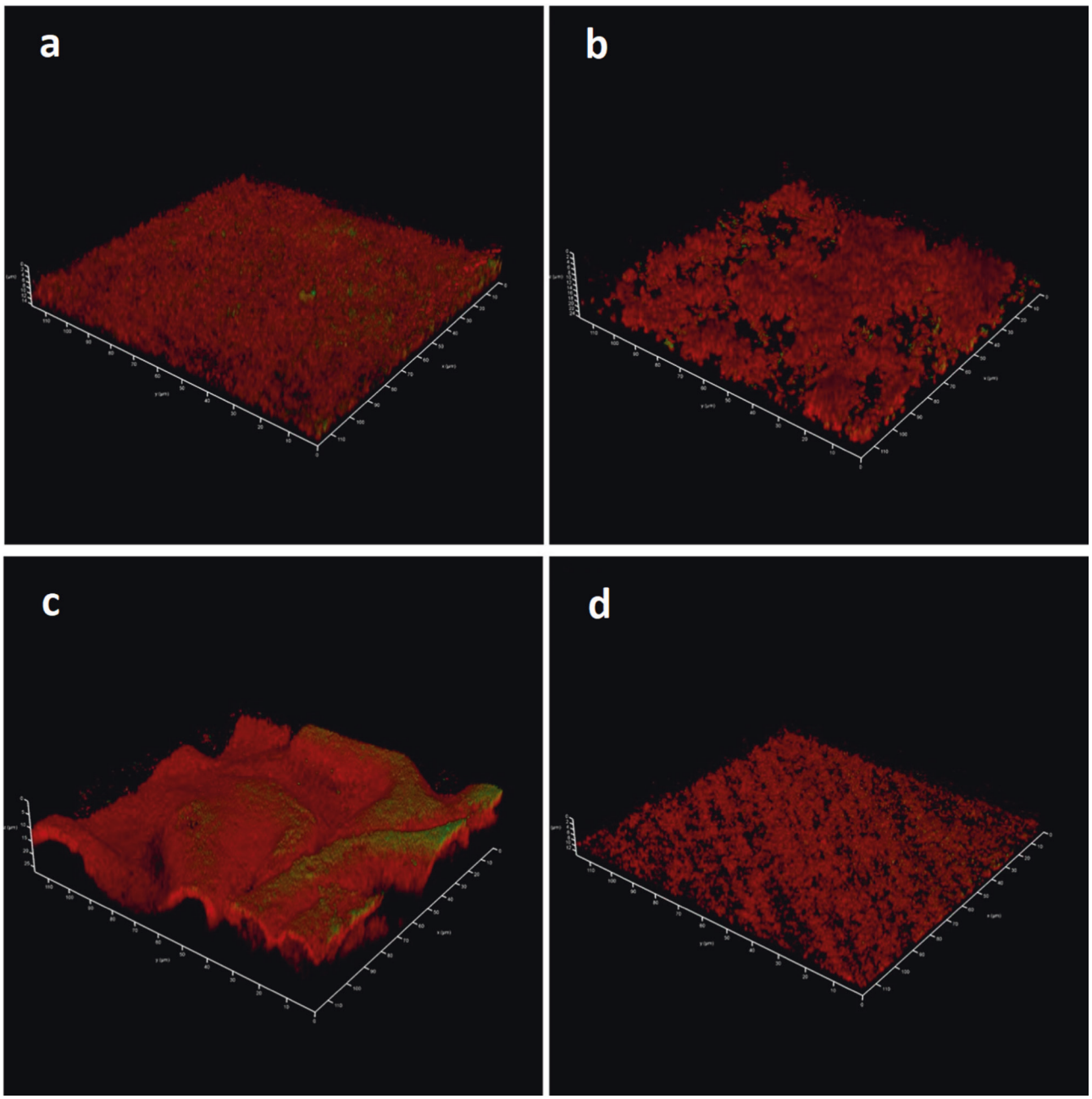

Fig. 10 Biofilm structure of *S. aureus* strains. Biofilm structure of two S. *aureus* strains, ATCC 25923 (**a**, **b**) and ATCC 43300 (**c**, **d**) following 2 days of incubation in the presence of compound **5** in a concentration of 100 mg l^{-1} (**b**, **d**) or without (**a**, **c**). Staining was performed with ethidium bromide to visualize cells and AmyGreen to visualize amyloids, CLSM

The bacterial strains used in the planktonic assay are well-known biofilm producers [37]. The biofilm formation by these four strains was measured at 24 and 48 h of incubation in presence of compound **5** in varying concentrations (50, 100, 150, 200, 250, and 300 mg l^{-1}) to observe the dynamic change in the biofilm biomass. Increase in biofilm mass was measured as difference between 24- and 48-hour biofilm biomass, measured spectrophotometrically (Fig. 7). In this biofilm formation assay, the high specificity of compound **5** for the *S. aureus*-associated target was also confirmed since all tested concentrations effectively reduced or suppressed biofilm formation in *S. aureus*. On the contrary, compound **5** did not suppress *P. aeruginosa* PA 01 biofilms and, as before, showed stimulative activity on *K. pneumoniae* ATCC 10031 stationary culture, resulting in a 4-fold increase in biofilm formation. This might be explained by differences in the surface proteins onto the outer surface of *K. pneumoniae* cells, since sortase A is a transpeptidase enzyme that is responsible for tagging many surface-associated proteins. This, in turn, might inhibit some regulatory or metabolic pathways associated with biofilm formation and disruption in *K. pneumoniae*. Indeed, we found that class A sortase (SrtA) in *K. pneumonia* beares a high homology to SrtA of *S. aureus* with an amino-acid sequence identity of 40.5%. However, there are no available data on how SrtA suppression might affect *K. pneumoniae* biofilm. We hypothesized that there might be some stimulation of the biofilm formation by *K. pneumoniae* when SrtA is repressed by an unknown mechanism.

Since biofilm formation is exacerbates bacterial infection, we wondered how pathogenic wild type *S. aureus* isolates might respond to compound **5**. To study this, three isolates from Ukrainian hospital (UHI1-3) were obtained. These isolates had extended antibiotic resistances (Table S2), which were characterized according to EUCAST (European Committee on Antimicrobial Susceptibility Testing) recommendations [35], and were used to screen for antibiofilm activity of compound **5** (Fig. 8).

It was shown that the UHI were less sensitive than the ATCC strains to compound **5**, in general, with the biofilm inhibitory activity starting from 50 mg l^{-1} as before.

It was recently shown that SrtA inhibition may be associated with biofilm suppression in *Streptococcus mutans*, *Streptococcus pneumoniae*, and *S. aureus* [38–42]. Thus, we wondered how compound **5** could influence biofilm development. For this, we measured the average thickness of the biofilms, developed by *S.aureus* ATCC strains in the presence of 100 mg l^{-1} (344 μM) of compound **5** or without (Fig. 9). We noticed that the thickness of the biofilms was reduced by compound **5** in both strains.

We also investigated the structure of biofilms produced by two ATCC strains in the presence of the studied compound (Fig. 10). As seen in the microscopy image, the spatial structure was substantially affected by the presence of the compound.

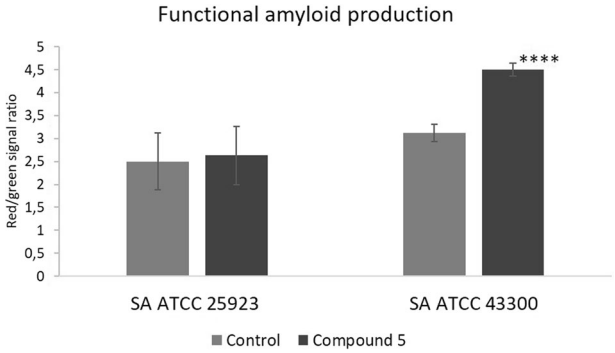

Fig. 11 The cell/amyloid biomass ratio calculated from total pixels in 3D. The cell/amyloid biomass ratio calculated from total pixels in CLSM imaging of 48 h old S.*aureus* (SA) ATCC 25923 and *S. aureus* (SA) ATCC 43300 biofilms, formed in the presence of 100 mg/L (344 μM) of compound **5** or without (control). Statistical significance compared to control. ****$p < 0.001$

In order to evaluate how compound **5** influenced functional amyloid production of both *S. aureus* strains, we calculated the ratio of the total amount of red and green pixels in the 3D imaging obtained with CLSM above. Here, the red signal corresponded to the total cell biomass amount, following ethidium bromide staining whereas the green signal, produced by the newly introduced amyloid-specific stain, specifically visualized bacterial functional amyloid fibers as we described before [37]. The ratio shows that there was no effect of compound **5** on amyloid production by the weaker biofilm-forming strain ATCC 25923 (Fig. 10a) whereas the other strain ATCC 43300, which produced stronger biofilm (Fig. 10c), demonstrated a reduction in amyloid production (Fig. 11).

Conclusions

Using a molecular docking approach, we identified the *S. aureus* sortase A inhibitor 2-(2-amino-3-chloro-benzoylamino)-benzoic acid (**5**), possessing an IC_{50} value of 59.7 μM. This compound is selective towards SrtA, compared to other four cysteine proteases–CatL, CatB, rhodesain and the SARS-CoV2 M^{pro}. Also, this compound demonstrates *S. aureus*–specific antibacterial and anti-biofilm effects by reducing planktonic cells and biofilm thickness. Compound **5** shows good specificity since it does not reduce *P. aeruginosa* and stimulates *K. pneumoniae* biofilms. This suggests that all potential SrtA inhibitors should be tested against Gram-negative bacteria due to the possibility of a stimulative effect.

Therefore, compound **5** can be a valuable candidate for further chemical optimization and biological research.

Compliance with ethical standards

Conflict of interest The authors declare no competing interests.

Publisher's note Springer Nature remains neutral with regard to jurisdictional claims in published maps and institutional affiliations.

References

1. Ericson JE, Popoola VO, Smith PB, Benjamin DK, Fowler VG, Benjamin DK JR, et al. Burden of invasive *Staphylococcus aureus* infections in hospitalized infants. JAMA Pediatr. 2015;169:1105–11.
2. Defres S, Marwick C, Nathwani D. MRSA as a cause of lung infection including airway infection, community-acquired pneumonia and hospital-acquired pneumonia. Eur Respir J. 2009;34:1470–6.
3. Ippolito G, Leone S, Lauria FN, Nicastri E, Wenzel RP. Methicillin-resistant *Staphylococcus aureus*: the superbug. Int J Infect Dis. 2010;14:S7–S11.
4. Gardete S, Alexander, Tomasz A. Mechanisms of vancomycin resistance in *Staphylococcus aureus*. J Clin Invest. 2014;124: 2836–40.
5. Kali A. Antibiotics and bioactive natural products in treatment of methicillin-resistant *Staphylococcus aureus* (MRSA): a brief review. Pharmacogn Rev. 2015;9:29–34.
6. Kaur DC, Chate SS. Study of antibiotic resistance pattern in methicillin-resistant *Staphylococcus aureus* with special reference to newer antibiotic. J Glob Infect Dis. 2015;7:78–84.
7. Arunkumar V, Prabagaravarthanan R, Bhaskar M. Prevalence of methicillin-resistant *Staphylococcus aureus* (MRSA) infections among patients admitted in critical care units in a tertiary care hospital. Int J Res Med Sci. 2017;5:2362–6.
8. McGuinness WA, Malachowa N, DeLeo FR. Vancomycin resistance in *Staphylococcus aureus*. Yale J Biol Med. 2017;90:269–81.
9. Mazmanian SK, Liu G, Ton-That H, Schneewind O. *Staphylococcus aureus* sortase, an enzyme that anchors surface proteins to the cell wall. Science 1999;285:760–3.
10. Zhang J, Liu H, Zhu K, Gong S, Dramsi S, Wang YT, et al. Antiinfective therapy with a small molecule inhibitor of *Staphylococcus aureus* sortase. Proc Natl Acad Sci USA. 2014;111:13517–22.
11. Cascioferro S, Totsika M, Schillaci D. Sortase A: an ideal target for anti-virulence drug development. Micro Pathog. 2014;77: 105–12.
12. Barthels F, Marincola G, Marciniak T, Konhäuser M, Hammerschmidt S, Bierlmeier J, et al. Asymmetric disulfanylbenzamides as irreversible and selective inhibitors of *Staphylococcus aureus* sortase A. ChemMedChem 2020;15:839–50.
13. Spirig T, Weiner EM, Clubb RT. Sortase enzymes in gram-positive bacteria. Mol Microbiol. 2011;82:1044–59.
14. Marraffini LA, Dedent AC, Schneewind O. Sortases and the art of anchoring proteins to the envelopes of gram-positive bacteria. Microbiol Mol Biol Rev. 2006;70:192–221.
15. Cascioferro S, Totsika M, Schillaci D. Sortase A an ideal target for anti-virulence drug development. Micro Pathog. 2014;77:105–12.
16. Cascioferro S, Raffa D, Maggio B, Raimondi MV, Schillaci D, Daidone G. Sortase A inhibitors: recent advances and future perspectives. J Med Chem. 2015;58:9108–23.
17. Guo Y, Cai S, Gu G, Guo Z, Long Z. Recent progress in the development of sortase A inhibitors as novel anti-bacterial virulence agents. RSC Adv. 2015;5:49880–9.
18. Ha MW, Yi SW, Paek SM. Design and synthesis of small molecules as potent *Staphylococcus aureus* sortase A inhibitors. Antibiotics 2020;9:706.
19. Alharthi S, Alavi SE, Moyle PM, Ziora ZM. Sortase A (SrtA) inhibitors as an alternative treatment for superbug infections. Drug Disco Today. 2021;26:2164–72.
20. Nitulescu G, Margina D, Zanfirescu A, Olaru OT, Nitulescu GM. Targeting bacterial sortases in search of anti-virulence therapies with low risk of resistance development. Pharmaceuticals 2021;14:415.
21. Volynets G, Vyshniakova H, Nitulescu G, Nitulescu GM, Ungurianu A, Margina D, et al. Identification of novel antistaphylococcal hit compounds targeting sortase A. Molecules 2021;26:7095.
22. Bodian DL, Yamasaki RB, Buswell RL, Stearns JF, White JM, Kuntz ID. Inhibition of the fusion-inducing conformational change of influenza hemagglutinin by benzoquinones and hydroquinones. Biochemistry 1993;32:2967–78.
23. Ewing TJ, Makino S, Skillman AG, Kuntz ID. DOCK 4.0: search strategies for automated molecular docking of flexible molecule databases. J Comput-Aided Mol Des. 2001;15:411–28.
24. Ring CS, Sun E, McKerrow JH, Lee GK, Rosenthal PJ, Kuntz ID, et al. Structure-based inhibitor design by using protein models for the development of antiparasitic agents. Proc Natl Acad Sci USA. 1993;90:3583–7.
25. Stoichet BK, Stroud RM, Santi DV, Kuntz ID, Perry KM. Structure-based discovery of inhibitors of thymidylate synthase. Science 1993;259:1445–50.
26. Zhulenkovs D, Rudevica Z, Jaudzems K, Turks M, Leonchiks A. Discovery and structure-activity relationship studies of irreversible benzisothiazolinone-based inhibitors against *Staphylococcus aureus* sortase A transpeptidase. Bioorg Med Chem. 2014;22:5988–6003.
27. Yakovenko OY, Oliferenko A, Golub A, Bdzhola V, Yarmoluk S. The new method of distribution integrals evaluations for high throughput virtual screening. Ukr Bioorg Acta. 2007;1:52–62.
28. Yakovenko O, Oliferenko AA, Bdzhola VG, Palyulin VA, Zefirov NS. Kirchhoff atomic charges fitted to multipole moments: implementation for a virtual scrrening system. J Comput Chem. 2008;29:1332–43.
29. Kovalenko OP, Volynets GP, Rybak MY, Starosyla SA, Gudzera OI, Lukashov SS, et al. Dual-target inhibitors of mycobacterial aminoacyl-tRNA synthetases among N-benzylidene-N'-thiazol-2-yl-hydrazines. Medchemcomm 2019;10:2161–9.
30. Discovery Studio Visualizer 4.0. https://www.3dsbiovia.com/products/collaborative-science/biovia-discovery-studio/visualization-download.php, (accessed May 2019).
31. Suree N, Liew CK, Villareal VA, Thieu W, Fadeev EA, Clemens JJ, et al. The structure of the *Staphylococcus aureus* sortase-substrate complex reveals how the universally conserved LPXTG sorting signal is recognized. J Biol Chem. 2009;284:24465–77.
32. We used a database of commercially available compounds (Otava Ltd., http://www.otavachemicals.com/).
33. Schmohl L, Bierlmeier J, von Kügelgen N, Kurz L, Reis P, Barthels F, et al. Identification of sortase substrates by specificity profiling. Bioorg Med Chem 2017;25:5002–7.
34. Klein P, Barthels F, Johe P, Wagner A, Tenzer S, Distler U, et al. Naphthoquinones as covalent reversible inhibitors of cysteine proteases – studies on inhibition mechanism and kinetics. Molecules 2020;252:064.
35. EUCAST guidelines for detection of resistance mechanisms and specific resistances of clinical and/or epidemiological importance, Version 1.0, December Effect of Combination l-Citrulline and Metformin Treatment on Motor Function in Patients With Duchenne Muscular Dystrophy: A Randomized Clinical Trial, JAMA network open, 2013, 2, 1914171.
36. Moshynets OV, Spiers AJ. Viewing biofilms within the larger context of bacterial aggregations. In Biofilms: InTech Press; 2016. p. 3-22.

37. Moshynets O, Chernii S, Chernii V, Losytskyy M, Karakhim S, Czerwieniec R, et al. Fluorescent β-ketoenole AmyGreen dye for visualization of amyloid components of bacterial biofilms. Methods Appl Fluoresc. 2020;8:035006.
38. Hu P, Huang P, Chen MW. Curcumin reduces *Streptococcus mutans* biofilm formation by inhibiting sortase A activity. Arch Oral Biol. 2013;58:1343–8.
39. Huang P, Hu P, Zhou SY, Li Q, Chen WM. Morin inhibits sortase A and subsequent biofilm formation in *Streptococcus mutans*. Curr Microbiol. 2014;68:47–52.
40. Wang J, Song M, Pan J, Shen X, Liu W, Zhang X, et al. Quercetin impairs *Streptococcus pneumonia* biofilm formation by inhibiting sortase A activity. J Cell Mol Med. 2018;22:6228–37.
41. Thappeta KRV, Zhao LN, Nge CE, Crasta S, Leong CY, Ng V, et al. In-silico identified new natural sortase A inhibitors disrupt *S. aureus* biofilm formation. Int J Mol Sci. 2020;21:8601.
42. Wang L, Wang G, Qu H, Wang K, Jing S, Guan S, et al. Taxifolin, an inhibitor of sortase A, interferes with the adhesion of methicillin-resistant *Staphylococcal aureus*. Front Microbiol. 2021;12:686864.

Анотація: *Пошук нових антимікробних речовин методами біомедичної хімії і раціонального драг-дизайну є перспективним напрямом подолання кризи нестачі ефективних антибактеріальних речовин. Втім треба пам'ятати, що специфічні інгібітори із антибактеріальними властивостями для обраних інфекційних штамів можуть мати неочікувані стимулюючі ефекти для інших патогенів. Більш того, такі ефекти мають бути перевірені не тільки в класичних біомедичних моделях, тобто, на рівні рідкої культури (планктонна субпопуляція) і на рівні агаризованих колоній (штучні мікробні агрегації), а і в наближених до умов реального інфекційного процесу умовах – на біоплівках. Відштовхуючись від цього уявлення було досліджено нову антистафілокову речовину. Зокрема, 2-(2-аміно-3-хлор-бензоїламіно)-бензойну кислоту, яка здатна інгібувати сортазу A* S. aureus *із папаметрами IC 50 59,7 мкМ. Ця сполука була більш селективна до сортази А порівняно з іншими чотирма цистеїновими протеазами – катепсином L, катепсином B, родезайном і SARS- CoV2 протеазою. Антибактеріальний і антибіоплівковий аналізи також підтвердили високу специфічність сполуки проти двох стандартних штамів і трьох госпітальних ізолятів* S. aureus. *Втім, було досліджено, що ця сама речовина не впливала на рівні планктону двох грам-негативних штамів, зокрема,* P. aeruginosa *PA01 і* K. pneumoniae *ATCC 10031. Цікаво, що ця речовина не впливала на розвиток біоплівки* P. aeruginosa *PA01, але стимулювали чотирикратний ріст біомаси біоплівки* K. pneumoniae *ATCC 10031. Таким чином, при дослідженні нових антимікробних речовин важливими є дослідження неочікуваних стимулюючих ефектів на альтернативні збудник інфекцій.*

РОЗДІЛ 5. Роль біоплівок як джерела генів резистому у госпітальному середовищі

У всьому світі зростає ризик зараження бактеріальними інфекціями, стійкими до багатьох препаратів та цілком резистентних до них, під час або після перебування в лікарні. Війна в Україні призвела до значних міграційних рухів, з ≥7,8 мільйонами біженців по всій Європі до грудня 2022 року (ВООЗ, 2022). Такі міграційні хвилі посприяли поширенню надзвичайно небезпечних MDR/XDR/PDR штамів в деяких країнах ЄС, включаючи Німеччину (133). Дійсно, після звіту про те, «як війна поширює стійкі до ліків супербактерії по Україні та за її межами» (139), нещодавні дані геномного спостереження підкреслили значні проблеми, пов'язані з бактеріями, що продукують карбапенемази, через війну в Україні (150). Пов'язана з війною інфекція та резистентність до антимікробних препаратів матимуть різкий вплив на здоров'я людей в країні та за її межами, створюючи величезний резервуар MDR/XDR/PDR інфекцій в Україні з потенціалом для подальшого поширення (151).

Біологічною основою фенотипу MDR/XDR/PDR у грам-негативних бактерій є їхні гени стійкості до антибіотиків (ГАР, гени антибіотикорезистентності), або резистоми. MDR/XDR/PDR неминуче вносять свої ГАР у лікарняне середовище. Це включає ГАР, розташовані в геномах бактерій (внутрішньоклітинна ДНК, вДНК), а також позаклітинні ГАР у екзоклітинній ДНК (еГАР). Мікробна еДНК поширена всюди, і її можна знайти скрізь, де є мікробне життя. Вона виділяється під час утворення біоплівки або через загибель клітин. Ця еДНК зберігає динамічний пул генів за допомогою горизонтального переносу генів (ГПГ) у спільноті біоплівок. ГАР є важливим джерелом природного ГПГ (152). ГПГ клінічно значущих еГАР (що містять, наприклад, бета-лактамази розширеного спектру дії та гени стійкості до карбапенемів), може потім трансформувати бактерії навколишнього середовища, де плазміди піддаються рекомбінації та переміщуються в новий патогенний лікарняний ізолят (153).

Не так багато відомо про епідеміологічні аспекти утримання, рекомбінації та повторного зараження еГАР у лікарняних пацієнтів. еГАР, а також вГАР (MDR/XDR/PDR бактерії) можна знайти в багатьох екологічних нішах, пов'язаних із лікарнями, наприклад, у лікарняних матеріалах (154, 155), меблях (156) та дрібних предметах, такі як стетоскопи (157), мобільні телефони (158-161). Однак лікарняні каналізаційні системи виявилися критично важливими гарячими точками для утримання та рекомбінації ГАР.

Ретроспективне епідеміологічне дослідження, проведене в лікарні в США, виявило, що більшість підтверджених спалахів, пов'язаних з bla_{KPC}, були пов'язані не з контактами між пацієнтом і пацієнтом і не з контактами пацієнта з персоналом лікарні, а з контактами між пацієнтом і лікарнею (162). Пізніше ті ж автори описали лікарняну каналізаційну систему як основне джерело стійких і рекомбінантних плазмід bla_{KPC}, які викликають внутрішньолікарняні інфекції у пацієнтів (153). Таким чином, бактеріальні біоплівкоутворюючі спільноти, що виробляють еГАР, що містить ГАР, а також еГАР, більше не пов'язані з біоплівками, становлять значну проблему в сучасному середовищі охорони здоров'я. ГАР можуть поширюватися по всій лікарняні шляхом перенесення плазмід, у геномах бактеріофагів і як вільна лінійна ДНК (152) та завдяки дії біоцидів, які регулярно використовуються в українській клінічній практиці та збагачують навколишнє середовище на еГАР (4).

5.1. Розповсюдженість генів антибіотикорезистентності в українській популяції грам-негативних госпітальних інфекцій.

Конфлікти та катастрофи все частіше визнаються рушійними силами розвитку та поширення резистентності до антибіотиків, що нещодавно було включено до ратифікованої політичної заяви на Засіданні високого рівня ООН щодо антимікробної резистентності у 2024 році. Після розширення та інтенсифікації війни в 2022 році дані епіднагляду в Україні були дуже обмежені, але звіти свідчать про зв'язок із високою множинною стійкістю у грамнегативних ранових інфекцій. Набільше інформації щодо генетичного профілю антибіотикорезистентності було отримано від пацієнтів, які отримували допомогу в інших країнах Європи. Залишається незрозумілим, на якому етапі лікування пацієнти найбільше піддаються ризику, оскільки історичні спостереження свідчать про зв'язок із затримкою першої операції, забрудненням навколишнього середовища та тривалим перебуванням у лікарні. Проте свідчення про епідеміологію антибіотикорезистентності в Україні є значно обмеженими за масштабом і обсягом. Відсутність сучасних даних з України підриває можливості для розуміння ситуації, що розвивається, та оптимізації призначення антимікробних препаратів. Завдяки спільному українсько-британському співробітництву представлено характеристику фенотипічної та молекулярної резистентності для мультирезистентних грамнегативних інфекцій конфліктних ран, виявлених в Україні на

ранніх стадіях лікування. Порівняно з раніше опублікованими даними, наші дані свідчать про значне підвищення показників резистентності до аміноглікозидів і зростання резистентності до колістину. Не було виявлено жодної різниці в моделях резистентності між зразками, взятими на ранній стадії в медичних закладах у Харкові, та тими, які були взяті пізніше на шляху лікування в Києві. Спостерігався високий рівень категоричної відповідності між методами дискової дифузії та методами розведення мікробульйону для цефідероколу при застосуванні оновлених 2024 року Європейського комітету з тестування чутливості до антимікробних засобів. Застосування нового аналізу молекулярних механізмів резистентності до 90 генів підтверджує постійну поширеність генів β-лактамаз NDM і OXA-типу, але також визначає зростаючий обсяг альтернативних генів, включаючи незвичайні знахідки NDM і KPC, які спільно продукують *P. aeruginosa*, а також як значна частина фенотипово резистентних грамнегативних організмів з н виявлено ген стійкості до карбапенемази.

Нами також було досліджено 100 карбапенем-резистентних ізолятів, ізольованих з ран протягом весни 2024 року, пов’язаних із військовими діями, ізольованих. Порівняння ізолятів, отриманих з первинних медичних закладів, протягом перших семи днів після травми, з інфекціями, що виникли пізніше на етапі лікування (та після переведення до додаткових лікувальних закладів), показало тенденцію до збільшення резистентності у інфекцій, що виникли пізніше, особливо для гентаміцину та колістину. Спостерігалась велике носійство карбапенемаз серед ізолятів, отриманих на ранніх етапах лікування після травми. Молекулярно-генетичні методи підтвердили постійну поширеність генів NDM та OXA-типу β-лактамаз, але також виявли зростаючу кількість альтернативних генів, включаючи незвичайні знахідки NDM та KPC ко-продукуючих *Pseudomonas aeruginosa* та *Acinetobacter baumanii*.

Основні результати, отримані в цьому підрозділі дисертації опубліковано в роботі автора (148, 163).

Severe conflict-associated wound infections complicated by the discovery of carbapenemase-coproducing *Pseudomonas aeruginosa* in Ukraine

We commend the report by Dennis Nurjadi and colleagues in *Lancet Microbe* of highly unusual findings of *Pseudomonas aeruginosa* coproducing *Klebsiella pneumoniae* carbapenemase (KPC) and New Delhi metallo-β-lactamase (NDM) enzymes from a patient in Viet Nam.[1] The authors rightly highlight concerns about the shifting evolution of carbapenem-resistant *P aeruginosa* in southeast Asia, and we strongly agree with the need for enhanced molecular and genomic surveillance of this development.[1]

Our work supporting Ukrainian bacterial surveillance activity in the ongoing conflict raises grave concerns about the widespread distribution of KPC-producing *P aeruginosa*, NDM-producing *P aeruginosa*, or both. Among patients with conflict-associated wound infections, we identified 12 patients with multidrug-resistant *P aeruginosa* infection across three different Ukrainian healthcare sites. Eight of the 12 patients were infected with *P aeruginosa* producing metallo-β-lactamases, including infections involving *P aeruginosa* coproducing KPC and NDM (one of eight), producing NDM only (four of eight), coproducing NDM and OXA-48-type carbapenemases (one of eight), coproducing NDM and an imipenemase-type metallo-β-lactamase (one of eight), and producing an imipenemase-type metallo-β-lactamase (one of eight).

The metallo-β-lactamases were detected using a novel 90+-target carbapenem-resistant Enterobacteriaceae (CRE) reference panel (AusDiagnostics). However, such assays require elaborate laboratory infrastructure, which could hinder their routine deployment in low-resource settings. Therefore, positive samples were repeated on the NG-test Carba-5 lateral flow immunoassay (Una Health) to confirm the initial findings. The NG-test Carba-5 immunoassay is a simple device for the rapid identification and differentiation of the five most prevalent carbapenemase families and offers a practical option for large-scale testing in more resource-challenged environments.

According to the European Committee on Antimicrobial Susceptibility Testing breakpoint guidelines,[2] all eight isolates were resistant to first-line antibiotics, one was susceptible to gentamicin, and seven were resistant to ceftazidime-avibactam. Similar to the findings of Nurjadi and colleagues, all samples were susceptible to colistin.[1] In contrast, seven of the eight samples were also susceptible to cefiderocol according to microbroth dilution, thus indicating variations in NDM expression or phenotypic resistance conferred by different NDM types.[3] Recently, aztreonam-avibactam has become available, with particular emphasis on its activity against metallo-β-lactamase-producing bacteria.[4] Given these unusual findings, the understanding of the potential of aztreonam-avibactam in cases of infections caused by *Pseudomonas* species is quite poor. Regarding its unavailability, using ceftazidime-avibactam in combination with aztreonam could offer a viable treatment option in the short term.[5]

Our findings not only support the potential evolution of carbapenemase-producing *P aeruginosa* but also strongly suggest its distribution beyond southeast Asia. Identification of these organisms in multiple patients with infection of severe bone and soft-tissue injuries is particularly concerning. Enhancing the capacity for global surveillance of carbapenemase-producing Gram-negative organisms is paramount and will most likely require suitably efficient options for use in resource-limited settings.

LSPM has consulted for or received speaker fees from bioMérieux (2013–24), Eumedica (2016–24), Pfizer (2018–24), Sumitovant (2021–23), Shionogi (2021–24), Qiagen (2023), Gilead Sciences (2024), BioNTech (2024), and Insmed (2024); and received research grants from the National Institute for Health and Care Research (2013–24), CW+ Charity (2018–24), North West London Pathology (2022–24), LifeArc (2020–22), Shionogi (2024), InfectoPharm (2022–24), the Joint Programming Initiative on Antimicrobial Resistance (2023–24), and the Healthcare Infection Society (2024). SJCP has received grants from the John Muir Trust, Drummond Foundation, and Hospital Infection Society, but not in connection with this work. SJCP has a role as a British Society for Antimicrobial Chemotherapy Parliamentary Intern to the Office of Dr Danny Chambers MP. Funding for this work was provided by the Chelsea Infectious Diseases Research Group, a part of the CW+ Charity. SJCP, MKO, LSPM, and OM devised the study. OM conducted the initial antimicrobial susceptibility testing in Ukraine and prepared samples for transport. SJCP and AM conducted testing in the UK. SJCP, LSPM, and OM drafted the initial manuscript. All authors contributed to revisions of the manuscript and agreed on the final version for submission. All authors had full access to all the data in the study and had final responsibility for the decision to submit for publication. This work is supported by a collaboration between Chelsea and Westminster Hospital, London, UK, and the Institute of Molecular Biology and Genetics of the National Academy of Sciences, Kyiv, Ukraine. The authors recognise the support of biomedical scientists at both the locations, including Viktoria Potochilova and Kateryna Rudnieva, who helped to identify and prepare suitable isolates in Ukraine for further testing; and Zoe Lambert and Vincent Sgro, who provided testing support within the UK.

Copyright © 2024 The Author(s). Published by Elsevier Ltd. This is an open access article under the CC BY-NC-ND license (http://creativecommons.org/licenses/by-nc-nd/4.0/).

*Scott J C Pallett, Anna Morkowska, Stephen D Woolley, Matthew K O'Shea, Luke S P Moore, Olena Moshynets
scott.pallett@nhs.net

Clinical Infection Department, Chelsea and Westminster Hospital National Health Service Foundation Trust, London, UK (SJCP, LSPM); Centre of Defence Pathology (SJCP, SDW, MKO) and Academic Department of Military Medicine (SDW, MKO), Royal Centre for Defence Medicine, Queen Elizabeth Hospital Birmingham, Birmingham B15 2WB, UK; North West London Pathology, Charing Cross Hospital, London, UK (AM); Department of Clinical Sciences, Liverpool School of Tropical Medicine, Liverpool, Merseyside, UK (SDW); Institute of Immunology and Immunotherapy, College of Medical and Dental Sciences, University of Birmingham, Birmingham, UK (MKO); National Institute for Health Research Imperial Biomedical Research Centre, Imperial College London, Hammersmith Campus, London, UK (LSPM); Institute of Molecular Biology and Genetics of National Academy of Sciences of Ukraine, Kyiv, Ukraine (OM)

Lancet Microbe 2024

Published Online
https://doi.org/10.1016/j.lanmic.2024.101046

See Comment https://doi.org/10.1016/j.lanmic.2024.100958

1 Nurjadi D, Nhat My T, Göpel L, Boutin S, Song LH, Velavan TP. Emergence of extensively drug-resistant *Pseudomonas aeruginosa* ST308 co-producing *Klebsiella pneumoniae* carbapenemase and New Delhi metallo-β-lactamase in Viet Nam. *Lancet Microbe* 2024; published online Aug 23. https://doi.org/10.1016/j.lanmic.2024.100958.

2 European committee on antimicrobial susceptibility testing. Clinical breakpoints–breakpoints and guidance. Clinical breakpoints v14.0. https://www.eucast.org/fileadmin/src/media/PDFs/EUCAST_files/Breakpoint_tables/v_14.0_Breakpoint_Tables.xlsx (accessed Nov 5, 2024).

3 Karakonstantis S, Rousaki M, Kritsotakis EI. Cefiderocol: systematic review of mechanisms of resistance, heteroresistance and in vivo emergence of resistance. *Antibiotics (Basel)* 2022; **11:** 723.

4 Pfizer. European Commission Approves Pfizer's EMBLAVEO® for patients with multidrug-resistant infections and limited treatment options. April 22, 2024. https://www.pfizer.com/news/press-release/press-release-detail/european-commission-approves-pfizers-emblaveor-patients#:~:text=(NYSE%3A%20PFE)%20today%20announced,associated%20pneumonia%20(VAP)%2C%20and (accessed Nov 8, 2024).

5 Rawson TM, Brzeska-Trafny I, Maxfield R, et al. A practical laboratory method to determine ceftazidime-avibactam-aztreonam synergy in patients with New Delhi metallo-beta-lactamase (NDM)-producing *Enterobacterales* infection. *J Glob Antimicrob Resist* 2022; **29:** 558–62.

Evolving antimicrobial resistance of extensively drug-resistant Gram-negative severe infections associated with conflict wounds in Ukraine: an observational study

Scott J. C. Pallett,[a,b,o,*] Anna Morkowska,[c,o] Stephen D. Woolley,[b,d,e] Viktoria V. Potochilova,[f,g] Kateryna L. Rudnieva,[f,h] Olga S. Iungin,[f,i] Vincenzo Sgro,[c] Sara E. Boyd,[j,k] Nicola Reece,[b] Zoe L. Lambert,[l] Ngee Keong Tan,[k] Nabeela Mughal,[a,c] Olena V. Moshynets,[f,o] Luke S. P. Moore,[a,c,m,o] and Matthew K. O'Shea[b,e,n,o]

[a]Clinical Infection Department, Chelsea and Westminster Hospital NHS Foundation Trust, London, UK
[b]Centre of Defence Pathology, Royal Centre for Defence Medicine, Queen Elizabeth Hospital, Birmingham, UK
[c]North West London Pathology, Charing Cross Hospital, Fulham Palace Rd, London, UK
[d]Department of Clinical Sciences, Liverpool School of Tropical Medicine, Liverpool, Merseyside, UK
[e]Academic Department of Military Medicine, Royal Centre for Defence Medicine, Queen Elizabeth Hospital, Birmingham, UK
[f]Institute of Molecular Biology and Genetics of National Academy of Sciences of Ukraine, Kyiv, 03143, Ukraine
[g]Kyiv City Maternity Hospital № 2, Mostytska 11, 02000, Kyiv, Ukraine
[h]Bogomolets National Medical University, Shevchenka Blvd. 13, 01601, Kyiv, Ukraine
[i]Kyiv National University of Technologies and Design, Mala Shiyanovska Street 2, 01011, Kyiv, Ukraine
[j]David Price Evans Global Health and Infectious Disease Research Group, University of Liverpool, Institute of Systems, Molecular & Integrative Biology, William Henry Duncan Building, Liverpool, UK
[k]Department of Medical Microbiology, South West London Pathology, St George's University Hospitals NHS Foundation Trust, London, UK
[l]Britannia Royal Navy College Dartmouth, College Way, Dartmouth, Devon, UK
[m]National Institute for Health Research Health Biomedical Research Centre, Imperial College London, Hammersmith Campus, London, UK
[n]Institute of Immunology and Immunotherapy, College of Medical & Dental Sciences, University of Birmingham, Birmingham, UK

The Lancet Regional Health - Europe 2025;52: 101274
Published Online xxx
https://doi.org/10.1016/j.lanepe.2025.101274

Summary

Background Conflict can have devastating effects on the development and spread of antimicrobial resistance. In Ukraine, early data post-injury are limited. We aim to explore extensively drug-resistant (XDR) Gram negative phenotypes and genotypes for infections arising early following conflict-associated wounds in Ukraine.

Methods Carbapenem-resistant infections following conflict-associated wounds in Ukraine (February–May 2024) underwent extended antimicrobial susceptibility testing (AST) for 19 antimicrobial agents using 2025 European Committee for Antimicrobial Susceptibility Testing breakpoints. Carbapenemase genes were identified using a novel multiplex molecular resistance assay. Infections arising in the first seven days versus those arising after seven days since injury were compared by logistic regression. Significance was set at $p < 0.05$.

Findings 100 isolates were tested (53, 53.0% *Klebsiella pneumoniae*; 16, 16.0% *other* Enterobacterales; 18, 18.0% *Acinetobacter baumanii* and 13; 13.0% *Pseudomonas aeruginosa*). Gentamicin ($p = 0.0046$) and colistin ($p = 0.049$) resistance were higher in infections arising later. Overall, resistance rates for amikacin (74/100, 74.0%), cefiderocol (44/100, 44.0%) and ceftazidime-avibactam (26/79, 67.1%) were observed. Prevalent resistance genes included NDM + OXA-48-like (24/100, 24.0%), NDM-only (24/100, 24.0%) and KPC (9/100, 9%). Others included OXA 23-like/51-like, IMP and/or mcr1. Earlier infection isolates had a higher burden of carbapenemases/isolate ($p = 0.006$).

Interpretation Extensively drug-resistant infections were observed early post-injury in Ukraine, with some trend to further resistance in those arising later in the patient pathway. A diverse presence of carbapenemase genes amid XDR Gram negative phenotypes highlights the importance of early screening for mechanisms of resistance in this setting.

Funding This study was funded by the Healthcare Infection Society and CW+ Charity.

Copyright © 2025 The Authors. Published by Elsevier Ltd. This is an open access article under the CC BY-NC-ND license (http://creativecommons.org/licenses/by-nc-nd/4.0/).

*Corresponding author. Clinical Infection Department, Chelsea and Westminster Hospital NHS Foundation Trust, London, UK.
E-mail address: scott.pallett@nhs.net (S.J.C. Pallett).
[o]Contributed equally.

Keywords: Surveillance; Antimicrobial resistance; Genotype; Phenotype

Research in context

Evidence before this study

Conflict and catastrophe are increasingly recognised as drivers for the development and spread of antimicrobial resistance (AMR), being recently included in the ratified political statement at the 2024 United Nations High Level Meeting on AMR. Since the outbreak of wider conflict in 2022, Ukraine surveillance data has been severely limited, but reports have suggested an association with highly multidrug-resistant (MDR) Gram negative wound infections. Most information however has been derived from patients receiving care elsewhere in Europe, after contact with multiple healthcare facilities. It remains unclear at which point in the treatment pathway patients are most at risk. We searched PubMED for peer reviewed papers describing Gram negative infections associated with conflict wounds and arising within Ukraine from 01 April 2022 to 31 December 2024 using the terms Ukrain* AND resis* AND infection*. No data was identified for 2024. Two studies were identified that described isolates derived from hospitals in Ukraine from 2022 to 2023 with both reporting high levels of carbapenem resistance. No studies were identified that specifically reported early sampling data from smaller hospitals near the point-of-injury.

Added value of this study

Through a joint Ukraine–UK collaboration, we present phenotypic and molecular resistance characterisation for XDR Gram-negative conflict-wound associated infections identified within Ukraine, early in the treatment pathway. Comparison of isolates derived from initial healthcare treatment facilities during the first seven days post-injury, compared with infections arising later in the treatment pathway, (and after transfer to additional treatment facilities) showed a trend to increasing resistance for infections arising later and significantly so for gentamicin and colistin. A greater burden of carbapenemases among isolates was however seen early post-injury. High levels of agreement between disc diffusion and broth microdilution methods for cefiderocol were observed. Employment of a novel molecular resistance assay affirms an ongoing prevalence of NDM and OXA-type β-lactamase genes but also identifies an increasing scope of alternative genes, including unusual findings of NDM and KPC co-producing *Pseudomonas aeruginosa* and *Acinetobacter baumanii*.

Implications of all the available evidence

Observation of XDR infections arising early post-conflict injury is highly concerning and strongly supports the need for more consistent and representative surveillance to guide treatment options, improve clinical outcomes and reduce the spread of AMR. High levels of concordance between disc diffusion and broth microdilution for cefiderocol is encouraging, with the former offering a more practical option for resource limited settings. Recognition of a broader scope of resistance genotypes than previously reported suggests evolving patterns of resistance in Ukraine. In particular, a considerable portion of phenotypically resistant isolates without an identified carbapenemase genotype, suggests the need for whole genome sequencing to support future surveillance activities.

Introduction

Antimicrobial resistance (AMR) surveillance has featured as a key global health priority for over a decade.[1] The potential for conflict and catastrophe to accelerate the development of AMR has since become increasingly apparent,[2] recently featuring as an independent consideration in the political statement following the 2024 United Nations General Assembly High-Level Meeting on AMR.[3]

Much of the recent literature in this area has focused on recognition of highly multidrug-resistant (MDR; non-susceptible to at least one agent in three or more antimicrobial categories) or extensively drug-resistant (XDR; non-susceptibility to at least one agent in all but two or fewer antimicrobial categories) Gram-negative organisms (MDRO/XDRO) complicating the healthcare management of patients from Ukraine.[4–8] Prior to the outbreak of wider conflict in 2022, Ukraine had started submitting AMR surveillance data as part of the Central Asian and European Surveillance of Antimicrobial Resistance network, which showed rising resistance patterns among key Gram-negative organisms against beta-lactams.[9] *Klebsiella pneumoniae* and *P. aeruginosa* blood-stream infections for example had reported rates of 64.4 and 78.0% resistance in 2021.[9] Since then, detection and characterisation of these MDR/XDR organisms has often relied on the screening and surveillance programmes in neighbouring European countries, primarily being derived from injured patients who have required transfer between several medical facilities or after long-hospital stays.[4–6,8,10,11] By 2022, data from within Ukraine observed *K. pneumoniae* infections to have >80% resistance across several β-lactam/β-lactamase inhibitor combination agents, as well as cefiderocol.[7] A lack of surveillance data from early in the patient care pathway restricts any understanding of risk factors for acquisition of MDR infections or effective treatments, hampering the development of targeted mitigation and antimicrobial stewardship efforts in a resource challenged setting.

Among the available evidence since 2022, a pattern of increasing resistance against reserve antimicrobial agents has emerged,[5,7] particularly with New Delhi metallo-β-lactamase (NDM) producing organisms.[5,10–12] However, there remain considerable knowledge gaps in the breadth of phenotypic and genotypic resistance patterns of conflict-associated wound infections in Ukraine, particularly during early surgical management following injury. These data are vital in informing early antimicrobial decision making and targeting infection prevention and control (IPC) measures. We therefore aim to update our understanding of the phenotype and genotype of XDR Gram negative infections following conflict-associated wounds in Ukraine during 2024. Additionally, we will compare infection phenotypes from initial infections observed shortly after injury and those later in the course of the patient care pathway, after transfer between medical facilities.

Methods

Samples were identified from patients with clinical signs of infection following conflict-associated wounds sustained in Ukraine by the treating clinicians and subsequently sent for further characterisation at the National Academy of Sciences of Ukraine (NASU) in Kyiv between February and May 2024. Gram-negative organisms that were considered extensively resistant (phenotypically resistant in all but two or less antimicrobial classes) by disc diffusion (DD) were sent for additional testing at Chelsea and Westminster Hospital and North West London Pathology (NWLP), London, UK to provide further insights to the character of prevalent resistance patterns.

Sample type

Sample types included for further testing included those collected from positive blood cultures (23), deep wound and bone (48), or other (29) endotracheal samples. Isolates were derived from infections observed at one of three different healthcare facilities including a regional hospital in Kharkiv or City Hospital in Kryvyi Rih with general surgical services or a major hospital in Kyiv with rehabilitation services and specialist surgical capabilities including management of polytrauma and burns injuries. Prior work in 2022 would broadly classify the first two as a level 2 echelon of care and the last as level 4 as per NATO standards.[13] Sites in Kharkiv and Kryvyi Rih represented the initial healthcare management facility for injured patients and these initial infections were confirmed within seven days of injury. By comparison isolates from Kyiv represent infections arising after seven days since injury and following transfer from ≥one prior facility. All isolates were independent (e.g. isolates from different locations were not derived from the same patient).

Disc diffusion phenotypic testing of XDROs

Identification of species were confirmed on receipt at NWLP by matrix-assisted laser desorption/ionization-time-of-flight (MALDI-TOF). Phenotypic testing was initially conducted by DD method and interpreted for each organism as per European Committee on Antimicrobial Susceptibility Testing (EUCAST) breakpoint guidelines.[13] Each organism underwent initial screening for DD susceptibility with ampicillin (10 μg), piperacillin-tazobactam (36 μg), cefotaxime (30 μg), ciprofloxacin (5 μg), gentamicin (10 μg), temocillin (30 μg), ceftriaxone (30 μg), ertapenem (10 μg), cotrimoxazole (25 μg), amikacin (30 μg), ceftazidime (10 μg), co-amoxiclav (30 μg), ceftazidime-avibactam (14 μg), fosfomycin (200 μg), tigecycline (15 μg), aztreonam (30 μg), cefiderocol (30 μg) and meropenem (10 μg).

Microbroth dilution susceptibility testing

All samples subsequently underwent screening for *in vitro* colistin susceptibility by broth microdilution (BMD) as per EUCAST guidelines.[14–16] Additionally, all cefiderocol results by DD methodology were repeated by BMD as per EUCAST guidelines and interpreted using 2025 EUCAST breakpoints,[14,16] except for *A. baumanii* isolates where CLSI M100 ED35:2025 guidelines were employed instead.

Molecular resistance testing of XDROs

A novel CRE reference polymerase chain reaction (PCR) molecular resistance assay for use on the AusDiagnostics Highplex or Ultraplex 3 system was performed to identify the scope and prevalence of commonly recognised beta-lactamase resistance genes (AusDiagnostics, Sydney, Australia). Pure bacterial colonies were harvested directly from purity culture plates as per manufacturer instructions. The assay has >90 gene targets which included verona integron mediated metallo-β-lactamase (VIM 1–7, 11, 19, 36–40), pan-imipenemase metallo- β-lactamase (IMP 1, 4–7, 10, 13, 26, 29, 34, 40, 42), separate IMP 14 and IMP 8, *Serratia marcescens* enzyme carbapenamase, mobilised colistin resistance gene (mcr1), β-lactamase DIM-1, *K. pneumoniae* carbapenamase (all types), KPC mutation associated with ceftazidime-avibactam resistance (D179Y), NDM 1–8, Seoul imipenemase metallo-β-lactamase 1, German imipenemase metallo- β-lactamase 1, imipenemase resistance gene (IMI 1, 2, 4, 7, 8), Sao Paulo metallo-β-lactamase 1, French imipenemase (FRI 1–4), Guiana extended spectrum β-lactamase, PER β-lactamase, OXA-23 like β-lactamases (OXA 23, 49, 73, 134, 146, 165–171, 225), OXA 24/40-like β-lactamases, β-lactamase OXA 48 group (OXA 48, 181, 204, 232, 244–245, 484), OXA 51 like β-lactamases from Acinetobacter spp. (OXA-51, 66, 69, 87, 89, 106–109, 242, 387, 404), carbapenem-hydrolysing oxacillinase (blaOXA-58) gene (OXA 58, 97), β-lactamase VEB-1.

Statistical analysis

Descriptive statistics were used to assess organism, AST phenotype and genotype prevalence. Susceptibility was determined using the 2025 EUCAST breakpoint guidelines,[14] except for *A. baumanii* with cefiderocol where EUCAST breakpoints are not available and CLSI M100 ED35:2025 guidelines were employed instead. Colistin susceptibilities were reported, acknowledging these isolates may have resistance mechanisms that are not detectable phenotypically and results must be interpreted with caution, noting clinical evidence for use as monotherapy is lacking. Agreement for susceptible and resistant results by DD and BMD were reported for cefiderocol. Clinical data, including outcomes and prior antimicrobial exposure were not reliably available and so not included in analyses. Variations in antimicrobial susceptibility rates and molecular results for samples derived from infections observed in the early post-injury phase (within 7 days of injury while still within initial admission healthcare facilities) versus those observed later (after 7 days since injury and having transferred from at least one other healthcare facility) were compared for each individual antimicrobial agent using binary logistic regression with odds ratios and 95% confidence intervals reported. Significance was set at $p < 0.05$.

Ethical approval

This work was conducted as part of routine surveillance work using residual samples through a collaboration between the Institute of Molecular Biology and Genetics of the National Academy of Sciences of Ukraine and the Clinical Infection Department of Chelsea and Westminster Hospital, United Kingdom. No patient demographic data or clinical information was included in the analysis.

Role of the funding source

Antimicrobial susceptibility testing and genotyping was funded by the Healthcare Infection Society and Chelsea Infectious Diseases Research (CINDER) Group/CW + Charity. Funders had no role in the study design, data collection, data analysis, interpretation, or writing of the report.

Results

100 isolates were identified and sent for further analysis. Of these, 69/100 (69.0%) were Enterobacterales of which 53/69 were identified as *K. pneumoniae*, 11/69 as *Escherichia coli*, 2/69 as *Enterobacter hormachei*, 2/69 as *Proteus mirabilis* and 1/69 as *Providencia stuartii*. The remaining samples were lactose non-fermenters including 18/100 (18.0%) *A. baumanii* and 13/100 (13.0%) *P. aeruginosa*. Agreement between MALDI-TOF methods was 94.0%. Where disagreements were observed this was typically between species of *Klebsiella* or *Enterobacter* with *Klebsiella aerogenes* identified by API being alternatively identified by MALDI-TOF as *K. pneumoniae* or *E. hormachei* and *Klebsiella oxytoca* being identified as *K. pneumoniae*. In addition, 6/100 isolates (6%), showed additional growth of Gram-positive species including coagulase negative Staphylococci (1/6 *S. haemolyticus*, 1/6 *S. epidermidis)* and *Enterococcus faecalis* (4/6), of unclear significance. 37/100 (100%) were derived from primary infections following initial admission (<seven days since injury) and 63/100 (63%) from later (>seven days since injury) in the patient care pathway after transfer between medical facilities. There were no missing data for antimicrobial susceptibilities.

AST phenotypes

All 100 samples underwent DD AST for 18 antimicrobial agents. Three samples (two *P.* mirabilis and one *P. aeruginosa* isolates) did not meet the XDR criteria. Of the remaining 97 isolates, meropenem susceptibility was 9/67 (13.4%) for Enterobacterales, 0/18 (0%) for *A. baumanii* and 1/12 (8.3%) for *P. aeruginosa* samples by DD (Fig. 1; a complete breakdown of species-meropenem susceptibility-genotype is provided in Supplementary Figure S1). Co-amoxiclav, ceftriaxone and ceftazidime susceptibility were each 1.5% (1/67) across all Enterobacterales. Ciprofloxacin susceptibility was 0% for all organisms tested. Gentamicin and amikacin susceptibility ranged from 1/12 (8.3%) for XDR *P. aeruginosa* for both agents, to 3/18 (16.7%) and 2/18 (11.1%) respectively for *A. baumanii* and 9/67 (13.4%) and 20/67 (29.9%) respectively for XDR Enterobacterales. For tigecycline, 10/11 (90.9%) *E. coli* isolates tested as susceptible. Overall, 56/67 (83.6%) XDR Enterobacterales were susceptible using the same EUCAST breakpoints, however there is limited data around non-*E. coli* species and only where higher doses are employed.[14] Susceptibility to ceftazidime-avibactam was 25/67 (37.3%) for XDR Enterobacterales and 1/12 (8.3%) among XDR *P. aeruginosa* while colistin susceptibility ranged from 66.6% (8/12) for XDR *P. aeruginosa* to 77.8% (14/18) for *A. baumanii* and 64.2% (43/67) among XDR Enterobacterales. The mean disc zone size for fosfomycin was 19.5 mm (IQR 14–23).

Comparison of cefiderocol testing by disc diffusion and microbroth dilution methods

For cefiderocol, susceptibility by BMD was 50.7% (34/67) for XDR Enterobacterales, 61.1% (11/18) for *A. baumanii* and 91.7% (11/12) for XDR *P. aeruginosa*. In total, 10/100 (10.0%, 9 Enterobacterales, 1 *P. aeruginosa*) were observed to be within the ATU for their respective organisms when tested by DD. Of these, 10/10 were susceptible by BMD methods. Agreement between disc diffusion and microbroth dilution was 99.0%, with a mismatch for one *P. aeruginosa* sample reported as susceptible by DD (24 mm) but resistant by BMD methods (MIC >16).

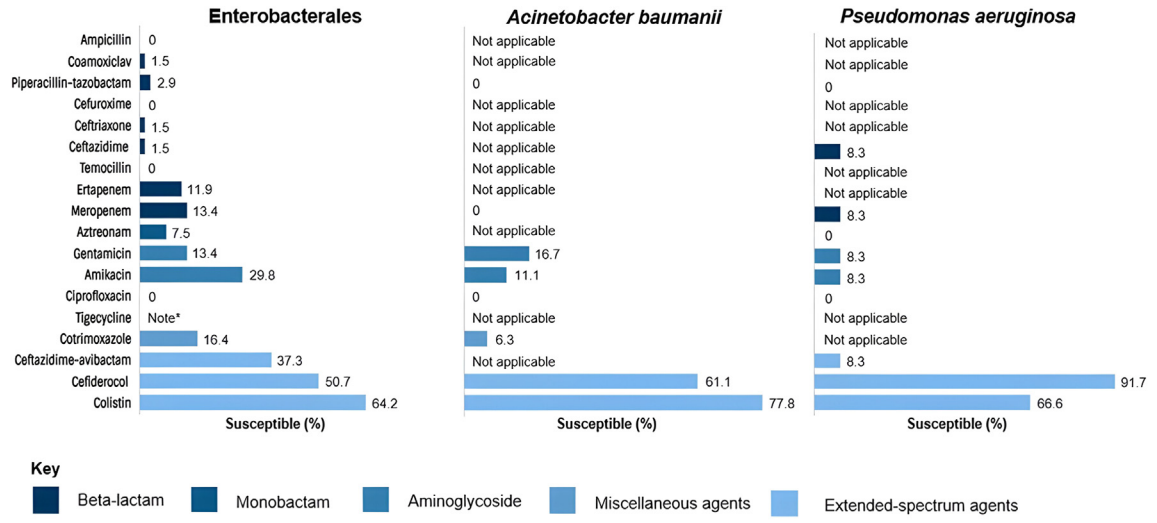

Fig. 1: **Antimicrobial susceptibility testing of severe Gram-negative infections associated with conflict-related injuries within Ukraine, 2024**. Antimicrobial tested and reported as per European Committee on Antimicrobial Susceptibility Testing (EUCAST) 2025 breakpoint guidelines, except for *A. baumanii* with cefiderocol where EUCAST guidelines are not available and so CLSI M100 ED35:2025 guidance was used. For colistin, EUCAST breakpoints are provided as a best fit, acknowledging these isolates may have resistance mechanisms that are not detectable phenotypically and noting that clinical evidence for use as monotherapy is lacking. Colistin susceptibility results presented here should be interpreted with caution. For tigecycline, 10/11 (90.9%) *E. coli* isolates tested as susceptible. Testing was conducted using disc diffusion methodology except for cefiderocol which underwent both disc diffusion and broth microdilution testing and colistin which was undertaken by broth microdilution as per EUCAST guidelines.

Molecular resistance testing results

All isolates were included in the molecular resistance testing analysis. Of the 10/100 samples that tested susceptible to meropenem, 6/10 were associated with detection of a resistance gene (3/6 NDM, 1/6 IMP, 1/6 mcr1 and 1/6 OXA-48-like). Of those isolates that were meropenem susceptible and had no gene detected, 4/4 were phenotypically resistant to third-generation cephalosporins, aztreonam and piperacillin-tazobactam. The most prevalent detected resistance genes included 24/100 (24%) of isolates with both NDM and OXA-48-like carbapenemases and 24/100 (24%) with NDM only (Fig. 2). Identified molecular resistance mechanism distribution among Gram-negative species were as follows, Enterobacterales (*n*): NDM + OXA-48-like (19), NDM (16), KPC (10), OXA-48-like (3), KPC + NDM (2), IMP (2), KPC + OXA-48-like (1), NDM + OXA 51-like (1), mcr1 (1), IMP + NDM (1), IMP + KPC (1), not detected (12); *A. baumanii*: NDM (5), OXA 23-like + OXA 51-like (3), IMP + OXA 51-like (2), OXA-48-like (2), NDM + OXA 23-like + OXA 51-like (1), IMP + KPC + OXA 51-like (1), OXA 23-like + OXA 51-like + OXA 48-like (1), not detected (3). *P.* aeruginosa; NDM (4), NDM + KPC (1), NDM + IMP (1), NDM + OXA-48-like (1), IMP (1 meeting XDR criteria, 1 not meeting XDR criteria), not detected (4) (Fig. 2).

Comparison of AST and molecular results across locations

Organisms resistant to each tested agent were identified at all three locations. There were no significant differences for most AST results (Supplementary Data, Table 1). Where significant results were detected, these trended for greater resistance in samples from infections observed later in the patient care pathway, including with WHO AWaRe classification of access for gentamicin (odds ratio 4.56, 95% CI 1.54–13.52, $p = 0.0046$) and reserve for colistin (odds ratio 2.64, 95% CI 1.00–6.93, $p = 0.049$) (Supplementary Data, Table 1).[17] When presence of each gene type was compared for results from each of the locations, those from earlier in the patient care pathway were more likely to be associated with OXA-type carbapenemases ($p = 0.0098$). Isolates from early post-injury were more likely to be associated with multiple carbapenemases than those in later in the patient care pathway (odds ratio 3.10, 95% CI 1.31–7.32, $p < 0.01$) (Supplementary Data, Table 1). No other combinations demonstrated significant differences in their prevalence.

Discussion

Our data support prior observations of high levels of beta-lactam resistance among infection associated with conflict wound infections from Ukraine, while also recognising an increasing pattern of resistance against aminoglycosides and colistin later in the patient care pathway. Additionally, use of a novel molecular resistance assay has demonstrated prevalence of a broad range of resistance genes in addition to the more commonly reported NDM-1 and/or OXA-48-type

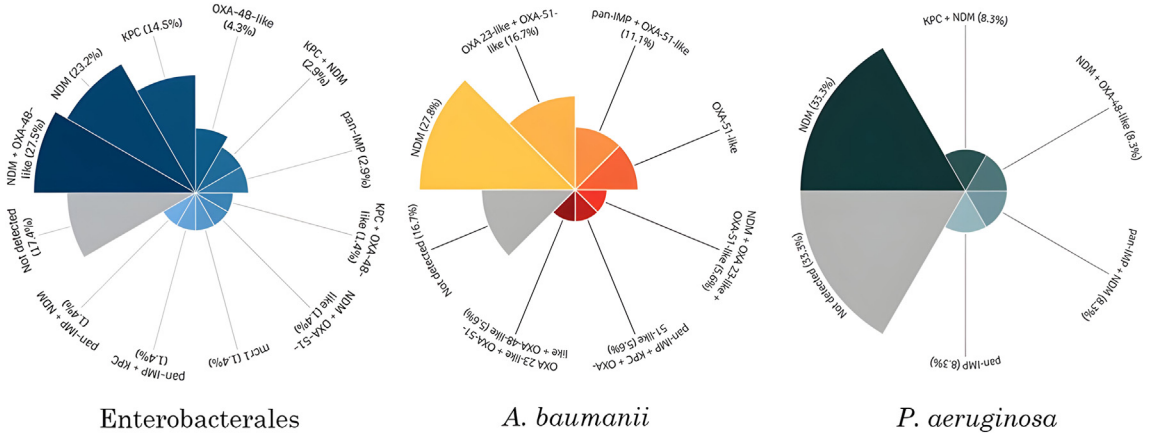

Fig. 2: **Identification of prevalent genes associated with among Gram-negative isolates from conflict-associated wound infections in Ukraine, 2024**. Each sector's radius is proportional to the prevalence of each identified genotype among tested XDR Gram-negative organisms associated with infected wounds from Ukraine. Percentages are provided in brackets for each detected gene for that organism/group. Genotype testing conducted by the 24 well CRE reference polymerase chain reaction assay (AusDiagnostics, Sydney, Australia). The pan-IMP target screens for carriage of imipenemase metallo-β-lactamases 1, 4–7, 10, 13, 26, 29, 34, 40, 42.

combinations. Of note, our data show a higher burden of carbapenemases (per patient) early following wounding from samples derived near the fighting in Kharkiv, which may reflect more limited capacity for IPC measures or early infection from contaminated wounds in contrast to those samples derived later in the patient care pathway, that may be more associated with healthcare transmission.

While previous data on XDR Gram-negative wound infections published since the onset of the wider Ukrainian conflict in 2022 have been limited, they have been consistent in reporting high levels of beta-lactam resistance.[4–8,10–12] Ceftazidime-avibactam, imipenem-relebactam and meropenem-vaborbactam were observed to have >80% resistance among 45 Enterobacterales isolates from 2022, while cefiderocol resistance was 78%.[7] Notably, colistin resistance from the same study was only 22% for Enterobacterales and 0% among 16 *P. aeruginosa* and 46 *A. baumanii* isolates,[7] considerably lower than our observations here. The reporting of aminoglycoside susceptibilities from infections within Ukraine has been less consistent. Prior to the wider conflict in 2022, aminoglycoside resistance among MDR Gram-negative clinical isolates from a multicentre study ranged from 9.2 to 25.4%,[18] while data from national blood-stream Enterobacterales infections (data considered of medium representativeness across Ukraine) reported higher rates of gentamicin resistance of 24.3–79.%.[9] Reports from the Netherlands in 2024 were more fitting with our data, observing aminoglycoside resistant of >72–94%,[19] although passage through multiple healthcare facilities and international travel had made relevance of comparison for this data for early management post-injury unclear. Our data suggests the reality of aminoglycoside resistance early following injury, when the surgical burden, use of prosthetic lines and potential for sepsis is likely to be greatest is more likely to reflect reports for Ukrainian injured patients overseas.[19] While newer beta-lactam agents, including combination agents such as aztreonam-avibactam, may offer alternatives for longer antibiotic courses, the reduced activity of aminoglycosides is highly concerning and highlights the vital importance of access to early and aggressive surgical debridement and effective IPC measures to limit the likelihood of Gram-negative infection in the early post-injury period. Likewise, the value of strict antimicrobial stewardship (AMS) programmes cannot be overstated. Where lacking, international support for AMS programme development is available through organisations such as the British Society for Antimicrobial Chemotherapy or European Society for Clinical Microbiology and Infectious Diseases and are an important consideration for reducing selective pressures on vital treatment options.[20]

Published data have suggested an association with organisms expressing NDM-1 or OXA-48-type carbapenemases but understanding the full spectra of resistance mechanisms for war wounds infected with MDRO/XDROs in Ukraine remains incomplete. Our data likewise show a high prevalence of NDM and/or OXA-48-type genes among XDR Gram-negative infections of war wounds but also suggests a considerably greater breadth of contributing mechanisms. Despite observing a rise in colistin resistance, only one sample was positive for the plasmid-mediated *mcr1* gene. It is also interesting to note that, despite using a broad 90 plus-target assay, a considerable portion of phenotypically XDR Gram-negative organisms had no detected resistance

genes. Given their XDR phenotypes, this is likely to represent alternative mechanisms of carbapenem resistance including combinations of porin expression modification,[21] extended-spectrum β-lactamase and AmpC expression,[22] efflux pumps overexpression,[23] or potentially uncommon genes of hydrolysing enzymes not included in the molecular resistance assay. The genotype findings for *P. aeruginosa* producing NDM and/or KPC are unusual, as reported by our group separately.[24] These findings highlight the evolving nature of Gram-negative carbapenemase resistance organisms in Ukraine and the vital importance of continued surveillance activity to help guide both mitigation and treatment policies. Further understanding of the full spectrum of prevalent resistance mechanisms is needed to fully inform antimicrobial decision making and stewardship strategies and is likely to require international support for surveillance and/or reporting of conflict-associated infections from Ukraine with whole genome sequencing of carbapenem-resistant isolates.

This study is limited by the small number of isolates. However, even among these a pattern of evolving resistance phenotypes and genotypes among XDR Gram-negative wound infections was evident. The study is also limited to assessment of *in vitro* phenotypes, while the addition of clinical data would allow greater understanding of the proportional impact of these infections on clinical outcomes. While such data can be difficult to obtain in this setting, future studies would benefit from more granular data on time of infection since injury, number of healthcare facilities visited, prior antibiotic exposure and clinical outcomes. This is particularly following prior recognition of an association between multiple healthcare facility transfers and resistant infections in prior conflicts.[25] While use of a broad molecular resistance assay revealed the involvement of a range of different resistance genes, observation of XDROs with no gene detected highlights the need for whole genome sequencing to support future surveillance work in this setting. Additionally, given high aminoglycoside resistance, further evaluation of 16 S rRNA methylase genes or other aminoglycoside inactivating enzymes would be of further use. Given the evolving resistance pattern observed here, further work to establish susceptibility patterns among new combination agents would have value in planning treatment approaches.

The ongoing conflict in Ukraine has been associated with MDR/XDR Gram-negative infections as a complication of conflict-associated wounds. Our data suggest evolving patterns of resistance, particularly among aminoglycosides and colistin, compared with previous studies. While NDM and OXA-48-type carbapenemases continue to predominate, a broad range of resistance genes were identified. A considerable proportion of phenotypically resistant organisms without a detectable genotype associated with resistance further suggests additional mechanisms of resistance are prevalent.

Support to infection control and surveillance in Ukraine is paramount if the evolving nature of antimicrobial resistance is to be addressed in real-time. Understanding of the full spectra of prevalent resistance mechanisms is likely to require whole genome sequencing while global efforts need to be coordinated to ensure this region has access to appropriate antimicrobial agents given the burden of infection observed.

Contributors

SJCP, SDW, SEB, MOS, LSPM and OM designed the study. VP, KR and MO conducted initial testing in Ukraine and prepared samples for transport. SJCP and NT supported transport of samples to the UK. SJCP, AM, ZL and VS conducted additional testing in the UK. SJCP, SDW accessed the data and conducted analyses. SJCP, SEB, MOS, OM and LSPM wrote the initial draft. All authors reviewed the manuscript and contributed significantly to revisions. All authors agreed on the final version for submission.

Data sharing statement

Further information is available from the corresponding author (SJCP; scott.pallett@nhs.net) on reasonable request, as long as this meets local ethical and research governance.

Declaration of interests

LSPM has consulted for or received speaker fees from bioMerieux (2013–2025), Eumedica (2016–2025), Pfizer (2018–2025), Sumitovant (2021–2023), Shionogi (2021–2025), Qiagen (2023), Gilead (2024), BioNTech (2024), Insmed (2024), & Advanz (2024–2025) and received research grants from the National Institute for Health and Care Research (2013–2025), CW + Charity (2018–2025), North West London Pathology (2022–2024), LifeArc (2020–2022), Shionogi (2024), Infectopharm (2022–2024), the Joint Programming Initiative on AntiMicrobial Resistance (2023–2025), & the Healthcare Infection Society (2024–2025). SEB has consulted for or received speaker fees for bioMerieux, Shionogi, UK Clinical Pharmacy Association, and received funding support for attending meetings from Advanz Pharma. SEB has participated on a Scientific Advisory Board for Sumitovant Biopharma and has an unpaid role as a Young Scientist Committee member for the British Society for Antimicrobial Chemotherapy Antimicrobial Susceptibility Testing Committee. SEB declares stock options as a dividend reinvestment with Scottish and Southern Energy. SJCP has received research grants from the John Muir Trust, the Drummond Foundation not in connection with this work and from the Healthcare Infection Society in connection with this work. SJCP has a role as a British Society for Antimicrobial Chemotherapy Parliamentary Intern to the Office of Dr Danny Chambers MP. All remaining authors have no potential conflicts of interest to declare.

Acknowledgements

KLR, OSI, VVP and OVM would like to thank Viktoria Savchenko and Valentia Yanovskaya from the IMD medical laboratory (Kyiv, Ukraine), Oksana Kryzska from Kharkiv Regional Hospital, Olena Denysenko from Communal non-commercial enterprise of the Kharkiv Regional Council "Regional Children's Clinical Hospital", and Karyne Sarhsian from Municipal enterprise "Kryvyi Rih City Clinical Hospital No. 2" of the Kryvyi Rih City Council for their collaboration and assistance in the collection preparation. Antimicrobial susceptibility testing and genotyping was funded by the Healthcare Infection Society and Chelsea Infectious Diseases Research (CINDER) Group/CW+ Charity.

Appendix A. Supplementary data

Supplementary data related to this article can be found at https://doi.org/10.1016/j.lanepe.2025.101274.

References

1 World Health Organization. Antimicrobial resistance: global report on surveillance. https://iris.who.int/bitstream/handle/10665/112642/9789241564748_eng.pdf?sequence=1; 2014. Accessed November 4, 2024.
2 Pallett SJC, Boyd SE, O'Shea MK, Martin J, Jenkins DR, Hutley EJ. The contribution of human conflict to the development of antimicrobial resistance. *Commun Med*. 2023;3(1):153. https://doi.org/10.1038/s43856-023-00386-7.
3 United Nations. Political declaration of the high-level meeting on antimicrobial resistance. https://www.un.org/pga/wp-content/uploads/sites/108/2024/09/FINAL-Text-AMR-to-PGA.pdf; 2024. Accessed November 4, 2024.
4 Pallett SJC, Trompeter A, Basarab M, Moore LSP, Boyd SE. Multidrug-resistant infections in war victims in Ukraine. *Lancet Infect Dis*. 2023;23(8):e270–e271. https://doi.org/10.1016/S1473-3099(23)00391-2.
5 Zwittink RD, Wielders CC, Notermans DW, et al. Multidrug-resistant organisms in patients from Ukraine in the Netherlands, March to August 2022. *Euro Surveill*. 2022;27(50):2200896. https://doi.org/10.2807/1560-7917.ES.2022.27.50.2200896.
6 Schultze T, Hogardt M, Velázquez ES, et al. Molecular surveillance of multidrug-resistant Gram-negative bacteria in Ukrainian patients, Germany, March to June 2022. *Euro Surveill*. 2023;28(1):2200850. https://doi.org/10.2807/1560-7917.ES.2023.28.1.2200850.
7 Ljungquist O, Nazarchuk O, Kahlmeter G, et al. Highly multidrug-resistant Gram-negative bacterial infections in war victims in Ukraine, 2022. *Lancet Infect Dis*. 2023;23(7):784–786. https://doi.org/10.1016/S1473-3099(23)00291-8.
8 Witteveen S, Hans JB, Izdebski R, et al. Dissemination of extensively drug-resistant NDM-producing Providencia stuartii in Europe linked to patients transferred from Ukraine, March 2022 to March 2023. *Euro Surveill*. 2024;29(23):2300616. https://doi.org/10.2807/1560-7917.ES.2024.29.23.2300616.
9 World Health Organisation. Antimicrobial resistance surveillance in Europe 2023-2021 data. https://iris.who.int/bitstream/handle/10665/366822/9789289058537-eng.pdf?sequence=1; 2023. Accessed November 4, 2024.
10 Sandfort M, Hans JB, Fischer MA, et al. Increase in NDM-1 and NDM-1/OXA-48-producing Klebsiella pneumoniae in Germany associated with the war in Ukraine, 2022. *Euro Surveill*. 2022;27(50):2200926. https://doi.org/10.2807/1560-7917.ES.2022.27.50.2200926.
11 Stein C, Zechel M, Spott R, Pletz MW, Kipp F. Multidrug-resistant isolates from Ukrainian patients in a German health facility: a genomic surveillance study focusing on antimicrobial resistance and bacterial relatedness. *Infection*. 2023;51(6):1731–1738. https://doi.org/10.1007/s15010-023-02061-4.
12 Hernández-García M, González de Aledo M, Ponce-Alonso M, et al. Simultaneous clonal spread of NDM-1-producing Pseudomonas aeruginosa ST773 from Ukrainian patients in the Netherlands and Spain. *IJID Reg*. 2024;12:100415. https://doi.org/10.1016/j.ijregi.2024.100415.
13 Kazmirchuk A, Yarmoliuk Y, Lurin I, et al. Ukraine's experience with management of combat casualties using NATO's four-tier "changing as needed" healthcare system. *World J Surg*. 2022;46(12):2858–2862. https://doi.org/10.1007/s00268-022-06718-3.
14 European Committee on Antimicrobial Susceptibility Testing. Clinical breakpoints – breakpoints and guidance. Clinical breakpoints v15.0. https://www.eucast.org/fileadmin/src/media/PDFs/EUCAST_files/Breakpoint_tables/v_14.0_Breakpoint_Tables.xlsx. Accessed November 5, 2024.
15 European Committee on Antimicrobial Susceptibility Testing. Implementation and use of the 2022 revised colistin breakpoints. https://www.eucast.org/fileadmin/src/media/PDFs/EUCAST_files/Breakpoint_tables/v_15.0_Breakpoint_Tables.xlsx. Accessed February 5, 2024.
16 European Committee on Antimicrobial Susceptibility Testing. Cefiderocol MIC broth microdilution guide. https://www.eucast.org/fileadmin/src/media/PDFs/EUCAST_files/Guidance_documents/Cefiderocol_MIC_testing_EUCAST_guidance_document_January_2024.pdf. Accessed November 5, 2024.
17 World Health Organization. The selection and use of essential medicines 2023: web annex C: WHO AWaRe (access, watch, reserve) classification of antibiotics for evaluation and monitoring of use. https://iris.who.int/handle/10665/371093; 2023. Accessed December 31, 2024.
18 Salmanov A, Shchehlov D, Artyomenko V, et al. Nosocomial transmission of multi-drug-resistant organisms in Ukrainian hospitals: results of a multi-centre study (2019-2021). *J Hosp Infect*. 2023;132:104–115. https://doi.org/10.1016/j.jhin.2022.12.008.
19 Verkaik NJ, Wielders CCH, den Boer H, et al. Participating laboratories; SWAB Working Group Surveillance of Antimicrobial Resistance. Antimicrobial susceptibility to last-resort antibiotics in carbapenemase-producing bacteria from Ukrainian patients. *Microbiol Spectr*. 2024;12(11):e0114224. https://doi.org/10.1128/spectrum.01142-24.
20 British Society for Antimicrobial Chemotherapy. BSAC launches global antimicrobial stewardship accreditation scheme (GAMSAS). https://bsac.org.uk/bsac-launches-global-antimicrobial-stewardship-accreditation-scheme-gamsas/. Accessed February 11, 2025.
21 Bialek-Davenet S, Mayer N, Vergalli J, et al. In-vivo loss of carbapenem resistance by extensively drug-resistant Klebsiella pneumoniae during treatment via porin expression modification. *Sci Rep*. 2017;7(1):6722. https://doi.org/10.1038/s41598-017-06503-6.
22 Lee YQ, Sri La Sri Ponnampalavanar S, Chong CW, et al. Characterisation of non-carbapenemase-producing carbapenem-resistant Klebsiella pneumoniae based on their clinical and molecular profile in Malaysia. *Antibiotics (Basel)*. 2022;11(11):1670. https://doi.org/10.3390/antibiotics11111670.
23 Bouganim R, Dykman L, Fakeh O, et al. The clinical and molecular epidemiology of noncarbapenemase-producing carbapenem-resistant enterobacteriaceae: a case-case-control matched analysis. *Open Forum Infect Dis*. 2020;7(8):ofaa299. https://doi.org/10.1093/ofid/ofaa299.
24 Pallett SJC, Morkowska A, Woolley SD, O'Shea MK, Moore LSPM, Moshynets O. Severe conflict-associated wound infections complicated by discovery of co-producing metallo-β-lactamase Pseudomonas aeruginosa in Ukraine. *Lancet Microbe*. 2024:101046. https://doi.org/10.1016/j.lanmic.2024.101046.
25 Tribble DR, Conger NG, Fraser S, et al. Infection-associated clinical outcomes in hospitalized medical evacuees after traumatic injury: trauma infectious disease outcome study. *J Trauma*. 2011;71(1 Suppl):S33–S42. https://doi.org/10.1097/TA.0b013e318221162e.

Анотація: *Війна, що триває в Україні, пов'язана із персистуванням мультирезистентних грамнегативних інфекцій як ускладненням травм, спричинених військовими діями. Наші дані свідчать про зміну моделей резистентності, особливо серед аміноглікозидів і колістину, порівняно з попередніми даними. У той час як карбапенемази типу NDM і OXA-48 продовжують домінувати, ідентифіковано широкий діапазон інших генів резистентності. Значна частка фенотипово резистентних організмів без виявленого генотипу, пов'язаного з резистентністю, також свідчить про те, що в популяції українських грамнегативних інфекцій домінують додаткові механізми резистентності. Підтримка інфекційного контролю та інфекційного нагляду в Україні має першорядне значення для вирішення проблеми розвитку резистентності до антибактеріальних препаратів. Розуміння повного спектру поширених механізмів резистентності, ймовірно, вимагатиме секвенування всього генома досліджуваних ізолятів, тоді як глобальні зусилля повинні бути скоординовані, щоб забезпечити Україну доступом до відповідних антимікробних агентів, враховуючи тягар інфекції, який спостерігається.*

5.2. Роль біоцидів у підтриманні пулу генів стійкості до антибіотиків у госпітальному середовищі

Мікробна еДНК поширена всюди, де існує мікробне життя. Вона вивільняється в процесі загибелі та лізису клітин та може секретуватися живими клітинами після чого може зберігатися інтактною деякий час (152). Як зазначалось вище, eDNA важлива для виживання мікробів та приймає участь в утворенні матриксу біоплівок (35, 37-41, 70). Іншою важливою екологічною функцією еДНК є збереження динамічного пулу генів внаслідок ГПГ всередині спільноти яка часто представляє собою єдиний простір біоплівки. еГАР є важливим джерелом природного ГПГ через трансдукцію, трансформацію та кон'югаці. Четвертий поки що мало досліджений механізм ГПГ включає в себе переніс генів через мембранні везикули.

Протягом останніх кількох років дослідження розповсюдження еДНК та її ролі в різних екосистеми значно збільшилися. Однак, ці дослідження в основному зосереджені на природних екосистемах типу стічних вод, тоді як розповсюдження еГАР вантропогенних нішах залишається переважно поза увагою. Наприклад, в PubMed Central (https://www.ncbi.nlm.nih.gov/pmc на 1 березня 2021 р.) містить понад 7000 посилань на «еДНК + вода» та «еДНК + лікарня», але менше 2000 посилань можна знайти для «еДНК + ген стійкості до антибіотиків» і «еДНК + ген стійкість до антибіотиків + лікарня». Тим не менш, аналіз еГАР у водних осадах і воді може потенційно надати уявлення про роль цих еГАР як частини резистому еконіші.

Основні результати, отримані в цьому підрозділі дисертації опубліковано в роботі автора (164).

International Journal of
Molecular Sciences

MDPI

Article

eDNA Inactivation and Biofilm Inhibition by the PolymericBiocide Polyhexamethylene Guanidine Hydrochloride (PHMG-Cl)

Olena V. Moshynets [1,*], Taras P. Baranovskyi [2,3], Olga S. Iungin [1,4], Nadiia P. Kysil [5], Larysa O. Metelytsia [6], Ianina Pokholenko [1], Viktoria V. Potochilova [3], Geert Potters [7,8], Kateryna L. Rudnieva [3], Svitlana Y. Rymar [1], Ivan V. Semenyuta [6], Andrew J. Spiers [9], Oksana P. Tarasyuk [6] and Sergiy P. Rogalsky [6,*]

1 Biofilm Study Group, Department of Cell Regulatory Mechanisms, Institute of Molecular Biology and Genetics, National Academy of Sciences of Ukraine, 150 Zabolotnoho Str., 03680 Kiev, Ukraine; olgaungin@gmail.com (O.S.I.); yasnenka@gmail.com (I.P.); s.y.rymar@gmail.com (S.Y.R.)
2 Department of Dermatovenerology, Allergology, Clinical and Laboratory Immunology, Shupyk National Healthcare University of Ukraine, 9 Dorohozhytska Str., 03680 Kiev, Ukraine; taras.baranovskyi@gmail.com
3 Kyiv Regional Clinical Hospital, 1 Baggovutivska Street, 04107 Kiev, Ukraine; vika.ptch@gmail.com (V.V.P.); kateryna.rudneva@gmail.com (K.L.R.)
4 Department of Biotechnology, Leather and Fur, Faculty of Chemical and Biopharmaceutical Technologies, Kyiv National University of Technologies and Design, Nemyrovycha-Danchenka Street, 2, 01011 Kiev, Ukraine
5 National Children's Specialized Hospital "Okhmatdyt", 28/1 Chornovola Str., 01135 Kiev, Ukraine; nadejda.kisel1961@gmail.com
6 V. P. Kukhar Institute of Bioorganic Chemistry and Petrochemistry, National Academy of Science of Ukraine, 50 Kharkivske Schose, 01135 Kiev, Ukraine; LarisaMetelitsa@gmail.com (L.O.M.); ivan@bpci.kiev.ua (I.V.S.); oksanatarasyuk1201@gmail.com (O.P.T.)
7 Antwerp Maritime Academy, Noordkasteel Oost 6, 2030 Antwerp, Belgium; geert.potters@hzs.be
8 Department of Bioscience Engineering, University of Antwerp, Groenenborgerlaan 171, 2020 Antwerp, Belgium
9 School of Applied Sciences, Abertay University, Bell Street, Dundee DD1 1HG, UK; a.spiers@abertay.ac.uk
* Correspondence: moshynets@gmail.com (O.V.M.); sergey.rogalsky@gmail.com (S.P.R.)

Abstract: The choice of effective biocides used for routine hospital practice should consider the role of disinfectants in the maintenance and development of local resistome and how they might affect antibiotic resistance gene transfer within the hospital microbial population. Currently, there is little understanding of how different biocides contribute to eDNA release that may contribute to gene transfer and subsequent environmental retention. Here, we investigated how different biocides affect the release of eDNA from mature biofilms of two opportunistic model strains *Pseudomonas aeruginosa* ATCC 27853 (PA) and *Staphylococcus aureus* ATCC 25923 (SA) and contribute to the hospital resistome in the form of surface and water contaminants and dust particles. The effect of four groups of biocides, alcohols, hydrogen peroxide, quaternary ammonium compounds, and the polymeric biocide polyhexamethylene guanidine hydrochloride (PHMG-Cl), was evaluated using PA and SA biofilms. Most biocides, except for PHMG-Cl and 70% ethanol, caused substantial eDNA release, and PHMG-Cl was found to block biofilm development when used at concentrations of 0.5% and 0.1%. This might be associated with the formation of DNA–PHMG-Cl complexes as PHMG-Cl is predicted to bind to AT base pairs by molecular docking assays. PHMG-Cl was found to bind high-molecular DNA and plasmid DNA and continued to inactivate DNA on surfaces even after 4 weeks. PHMG-Cl also effectively inactivated biofilm-associated antibiotic resistance gene eDNA released by a pan-drug-resistant *Klebsiella* strain, which demonstrates the potential of a polymeric biocide as a new surface-active agent to combat the spread of antibiotic resistance in hospital settings.

Keywords: eDNA; antibiotic resistance; biofilms; biocides; disinfectant; alcohols; hydrogen peroxide; quaternary ammonium compounds; polyhexamethylene guanidine

check for updates

Citation: Moshynets, O.V.; Baranovskyi, T.P.; Iungin, O.S.; Kysil, N.P.; Metelytsia, L.O.; Pokholenko, I.; Potochilova, V.V.; Potters, G.; Rudnieva, K.L.; Rymar, S.Y.; et al. eDNA Inactivation and Biofilm Inhibition by the PolymericBiocide Polyhexamethylene Guanidine Hydrochloride (PHMG-Cl). *Int. J. Mol. Sci.* **2022**, *23*, 731. https://doi.org/10.3390/ijms23020731

Academic Editors: Iolanda Francolini and Antonella Piozzi

Received: 14 November 2021
Accepted: 3 January 2022
Published: 10 January 2022

Publisher's Note: MDPI stays neutral with regard to jurisdictional claims in published maps and institutional affiliations.

Copyright: © 2022 by the authors. Licensee MDPI, Basel, Switzerland. This article is an open access article distributed under the terms and conditions of the Creative Commons Attribution (CC BY) license (https://creativecommons.org/licenses/by/4.0/).

1. Introduction

The risk of multi-drug and pan-drug-resistant bacterial infections during or after a hospital stay is increasing worldwide. According to the WHO (2009), in general, health-care-associated infections in Europe lead to death in at least 2.7% of the cases and accounts for 135,000 deaths per year. According to the National Expert Group on Infection Control (https://negic.ua/eng/, accessed on 1 September 2021), there are up to 1 million cases of hospital-acquired infections and 50,000 deaths occurring in Ukraine each year. Each drug-resistant bacterium can contribute antibiotic resistance genes (ARGs), or resistome, to the hospital environment. This includes ARGs located within bacterial genomes (intracellular DNA) as well as cell-free ARGs in extracellular DNA (eARGs).

Microbial eDNA is ubiquitous and can be found everywhere where microbial life is present. It is released by the process of cell death and lysis and may be secreted by living cells, but is not enclosed in living cells, may not remain with the cells from which it originated, and may persist for some time before it is finally degraded [1]. eDNA is involved in microbial survival, often contributes to the structure of biofilms as a matrix component [2–8], and acts to preserve a dynamic pool of genes via horizontal gene transfer (HGT) within the biofilm community. ARGs are an important source for naturally occurring HGT [9–11] via transduction and conjugation. In contrast, the spread of eARGs by transformation and outer-membrane-vesicle-associated transport seems to be underestimated [1,12].

Over the last few years, investigations of eDNA distributions and its role in various resistomes have increased considerably. However, research mainly focuses on the wastewater environmental resistome, while the source and fate of eARGs in other environments, including hospital-associated niches, remain largely overlooked. For instance, while PubMed Central (https://www.ncbi.nlm.nih.gov/pmc, accessed on 1 March 2021) contains over 7000 references for "eDNA + water" and "eDNA + hospital", less than 2000 references can be found for "eDNA + antibiotic resistant gene" and "eDNA + antibiotic resistant gene + hospital." Nevertheless, an analysis of eARGs in aquatic sediments and water can potentially provide insights into the role of these eARGs as part of the environmental antibiotic resistome. eARGs persist more easily in sediments, which makes them more available for transformation [13]. HGT of such clinically significant eARGs (containing, for example, extended-spectrum beta-lactamases and carbapenem-resistant genes) can then transform environmentally harmless bacteria into pathogens that may then pose a threat to human health. A good demonstration of the importance of HGT in the evolution of human pathogens can be found in water-borne *Vibrio cholera*, where the ability to take up eDNA (competence) is induced by chitin, which is abundant in aquatic habitats [14].

In contrast, little is known about the impact of eDNA on the hospital resistome [13]. Hospital sewage systems are the source of persistent and recombinant *bla*KPC plasmids, which cause hospital-acquired infections in patients [15]. Hospital wastewater sludge is a prime source of eARGs, with a higher abundance of eARGs than normal wastewater sludge, pharmaceutical factory waste, lake sediments, or swine manure [16]. Hospital materials [17–19]; furniture [20]; and small items, such as stethoscopes [21], mobile phones [22–25], and keyboards [26], are also known to be the source of hospital-associated infections, and even dust plays an important part in the deposition and transmission of ARGs [27] in the hospital environment. Ironically, poor or incomplete cleaning of surfaces with bacterial colonies or biofilms with biocides may release intracellular DNA, which might then persist as eDNA until it degrades or is removed by subsequent cleaning (a combination of mechanical and chemical cleaning is needed to remove dried DNA effectively from surfaces [28]). While assessments of the effectiveness of disinfectants on biofilms largely concentrate on cell survival [29], little is reported about the amount of DNA released, whether it is soluble, whether it remains associated with cell debris or complexes with compounds (including disinfectants), or its persistence in the environment post cleaning.

Bacterial-biofilm-forming communities producing eDNA containing ARGs as well as eARGs no longer associated with biofilms, therefore, pose a significant problem in modern health-care environments. ARGs can spread throughout a hospital econiche by plasmid

transfer, in the genomes of bacteriophages and as naked linear DNA [9,10]. There are only a limited number of studies in which the susceptibility of bacterial communities and eDNA to different biocides have been evaluated, and HGT may still be possible when cell-damaging biocides have been deployed but have failed to kill all bacteria in a biofilm [30,31]. The aim of our research was to evaluate the effect of different biocides on eDNA in biofilms produced by model hospital opportunistic pathogens, with a specific focus on the use of the polymeric biocide polyhexamethylene guanidine hydrochloride (PHMG-Cl) as a potential DNA-deactivating biocide.

2. Results

2.1. Effects of Different Biocides on DNA Release from PA and SA Biofilms

To investigate how much eDNA could potentially be released from biofilm contamination likely to be found in hospital environments following treatment with biocides, we used dehydrated 5-day-old *Pseudomonas aeruginosa* ATCC 27853 (PA) and *Staphylococcus aureus* ATCC 25923 (SA) biofilms to mimic dried biofilm material likely to be found on a variety of surfaces [32]. The preparation of the dehydrated samples was likely to cause some cell damage and the release of intracellular DNA, adding to the eDNA that had accumulated during the growth of the biofilms before drying. We considered both the pre-existing eDNA and freshy released DNA to be eDNA in the context of our assays, as eDNA is released by both living and dead cells [1]. Any further contribution to eDNA levels by biocides could then be assessed by comparison with water-only controls (which lacked biocide treatment). The water-only treatment might release some DNA from cells that survived the preparation of the dehydrated samples through osmotic shock, but it is more likely that in this control, DNA is solubilized from cell debris and the original eDNA of the biofilm (we note that both PA and SA are isolated from fresh and drinking water, indicating that they are adapted to hypo-osmotic conditions [33,34]).

We tested these biofilms with a number of biocides used frequently in the National Children's Specialized Hospital Okhmatdyt (Kiev, Ukraine), including hydrogen peroxide; ethanol; isopropanol-based Desmanol; 0.05% chlorhexidine; and commercially available mixtures of quaternary ammonium compounds, such as Maxisan, Arquades-plus, and Sanikon; plus the polymeric cationic biocide polyhexamethylene guanidine hydrochloride (PHMG-Cl), which we had previously used in the synthesis of a new thermally stable polymeric biocide polyhexamethylene guanidine 2-naphtalenesulfonate to modify polyamide 11 [35]. After 1 h of exposure of the biofilms to the biocide, we isolated eDNA from the biofilms and measured eDNA yields compared to a water-only control treatment (Figure 1). This demonstrated that eDNA release from biofilms (i.e., pre-existing eDNA or DNA released from biocide-damaged cells) differed depending on both the biofilm and the biocide.

We also visualized the released eDNA by gel electrophoresis, which confirmed that PHMG-Cl reduces eDNA yield from PA biofilms compared to the water-only control treatment. The eDNA was a mix of high-molecular-weight DNA, with substantial amounts remaining in the wells after electrophoresis, and highly degraded DNA. In contrast, PHMG-Cl, alcohols, quaternary ammonium compounds, and 3% hydrogen peroxide were able to reduce the eDNA yield from SA biofilms (Figure 2), in agreement with our direct measurement of eDNA concentrations.

Surprisingly, the eDNA released from the dehydrated biofilms after their exposure to biofilms was largely undamaged, as assessed by PCR of 16S rDNA (Figure 3). However, PCR amplification of the PHMG-Cl samples failed, suggesting that, in addition to reducing eDNA yield, this biocide was complexing with the eDNA to prevent the amplification of the target sequence.

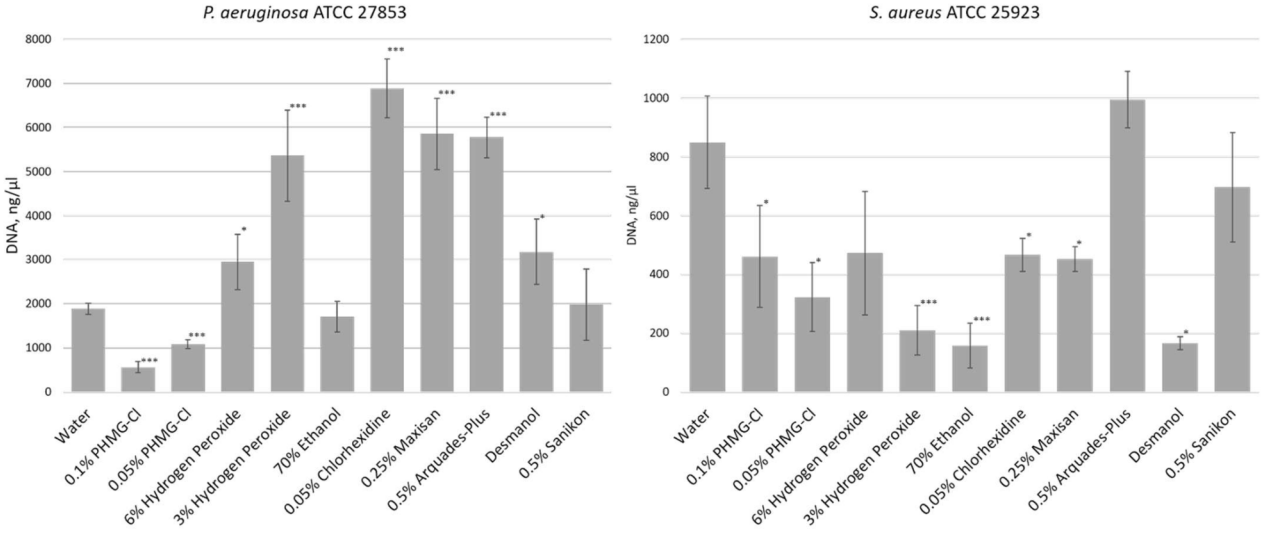

Figure 1. eDNA released from dehydrated *Pseudomonas aeruginosa* ATCC 27853 and *Staphylococcus aureus* ATCC 25923 biofilms after treatment with biocides. Shown here are eDNA yields (ng/µL) recovered from 5-day-old dehydrated biofilms after 1 h of exposure to biocides (n = 3). Statistical significance compared to water exposure (control) when * $p < 0.05$ and *** $p < 0.005$.

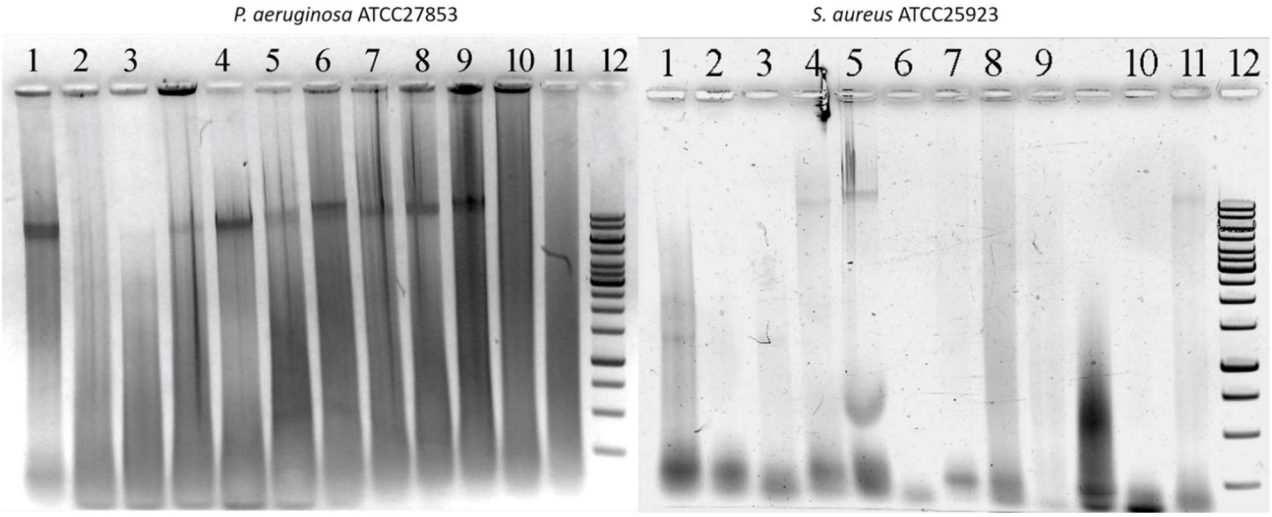

Figure 2. High-molecular-weight and degraded eDNA released from 5-day-old dehydrated *Pseudomonas aeruginosa* ATCC 27853 (PA) and *Staphylococcus aureus* ATCC 25923 (SA) biofilms after treatment with biocides. Shown here are 1.2% agarose-TA gels stained with EtBr to visualize the eDNA released from PA (left) and SA (right) biofilms after 1 h of exposure to biocides. Treatments: (1) water-only control, (2) 0.1% PHMG-Cl, (3) 0.05% PHMG-Cl, (4) 6% hydrogen peroxide, (5) 3% hydrogen peroxide, (6) 70% ethanol, (7) 0.05% chlorhexidine, (8) 0.25% Maxisan, (9) Arquades-plus, (10) Desmanol, and (11) Sanikon. A sample of GeneRuler 1 kb DNA Ladder (Thermo Fisher Scientific, Vilnius, Lithuania) is shown in the rightmost lane of each gel (12).

2.2. Anti-Biofilm Activity of PHMG-Cl against PA and SA Biofilms

Given the effectiveness of PHMG-Cl in inactivating the eDNA released from dehydrated biofilms, we tested PHMG-Cl to see if it could also suppress or inhibit the growth of PA and SA biofilms in situ. We treated 24 h old biofilms with different concentrations of PHMG-Cl and then determined metabolic activity using MTT (Figure 4). In this assay, the lowest concentration of PHMG-Cl that was not significantly different from the EtOH-treated (dead) negative control biofilm but significantly lower than the water-treated (live) positive control was biocidal. For the PA biofilm, the biocidal concentration was 0.1%, and

for the SA biofilm, it was 0.5% PHMG-Cl. Increasing concentrations of PHMG-Cl also reduced eDNA yield from biofilms (Figure 5). At 0.5% PHMG-Cl, the eDNA yield was reduced to less than a quarter of that from the water-treated positive PA control biofilm and to around one-third of that from the SA control biofilm.

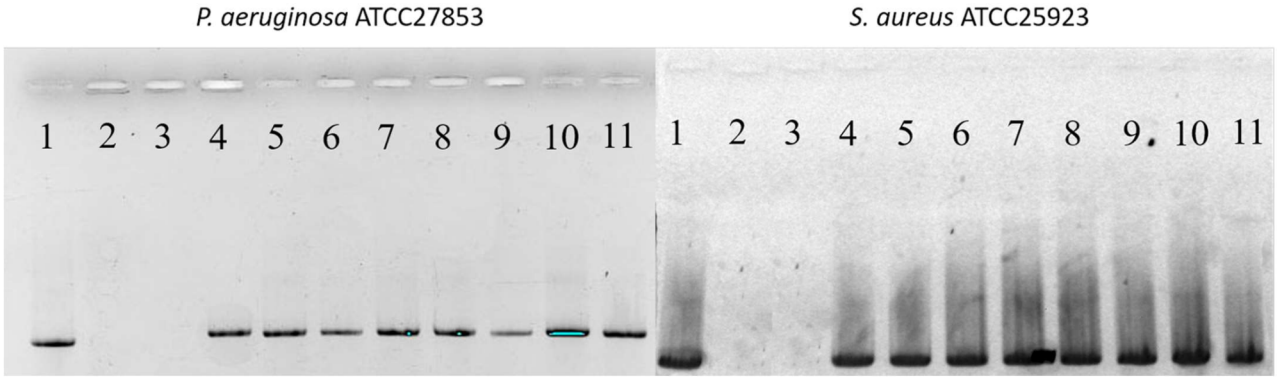

Figure 3. PHMG-Cl inhibits PCR amplification of 16S rDNA target sequences from eDNA released from 5-day-old dehydrated *Pseudomonas aeruginosa* ATCC 27853 (PA) and *Staphylococcus aureus* ATCC 25923 (SA) biofilms after treatment with biocides. Shown here are 1.2% agarose-TA gels stained with EtBr to visualize PCR products from PA (left) and SA (right) biofilms after 1 h of exposure to biocides. Treatments: (1) water-only control, (2) 0.1% PHMG-Cl, (3) 0.05% PHMG-Cl, (4) 6% hydrogen peroxide, (5) 3% hydrogen peroxide, (6) 70% ethanol, (7) 0.05% chlorhexidine, (8) 0.25% Maxisan, (9) Arquades-plus, (10) Desmanol, and (11) Sanikon. The 16S rDNA amplicons were 1420 bp.

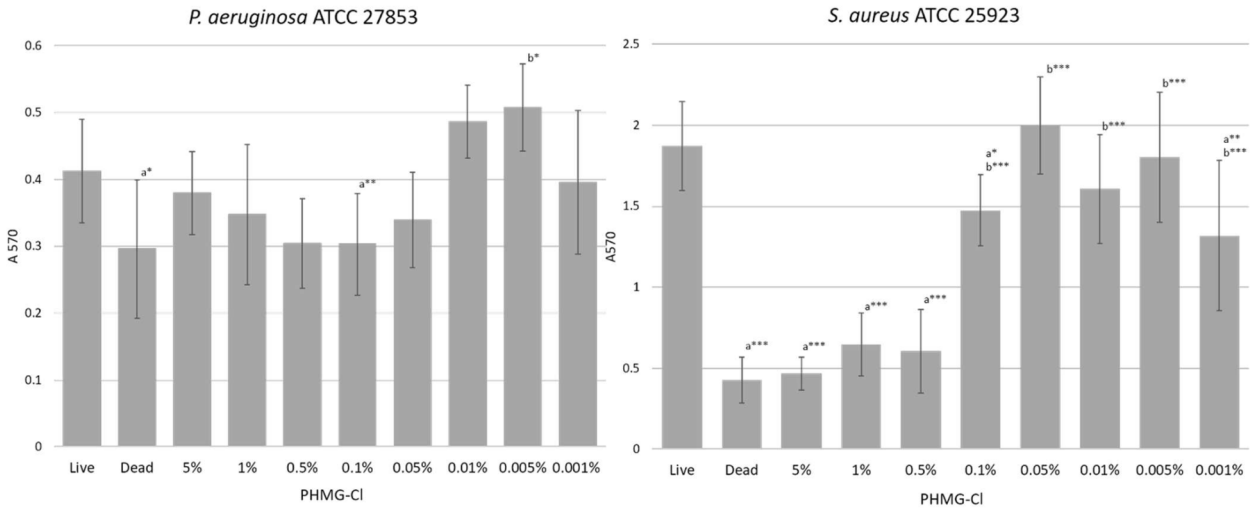

Figure 4. Metabolic assays show the biocidal activity of PHMG-Cl on *Pseudomonas aeruginosa* ATCC 27853 (PA) and *Staphylococcus aureus* ATCC 25923 (SA) biofilms growing in situ. Shown here are the metabolic activity of 24 h PA (**left**) and SA (**right**) biofilms after treatment with PHMG-Cl for 1 h (n = 8). Statistical differences are determined between treatments and the water-treated (live) positive controls (a) and the EtOH-treated (dead) negative controls (b); * $p < 0.05$, ** $p < 0.01$, and *** $p < 0.005$.

The spatial distribution of eDNA in PA and SA biofilms treated with water only and those treated with 0.5% PHMG-Cl was also investigated by CLSM, with PI used to visualize eDNA and dead cells and SYBR Green used to visualize intracellular DNA in living cells with undamaged membranes [36] (Figure 6). As was expected, the eDNA could be visualized in 3-day-old PA and SA biofilms and in these water-only controls, the DNA was specifically eDNA that had accumulated during the development of the biofilm, as no biocide treatment was applied that might have damaged cells and caused the release of intracellular DNA. However, PHMG-Cl had different effects on the biofilms, which may

reflect the differences between PA and SA biofilm structures and cell wall organization. In PA biofilms, PHMG-Cl caused substantial lysis of cells and the formation of large eDNA filaments. Conversely, in SA biofilms, PHMG-Cl caused substantial cell damage and a lot of the eDNA on the top surface of the biofilm was lost. In both biofilms, cell damage appeared to result in decompaction and an increase in biofilm thickness. We noted that the SYBR Green signal was enhanced after PHMG-Cl treatment, presumably because the damage to cell walls and membranes allowed greater penetration of the cell and binding intracellular DNA (SYBR Green has a relative MW of approx. 510, compared with 670 for PI, explaining why the PI signal did not seem to show a similar increase in strength if it could also access cells through damaged membranes).

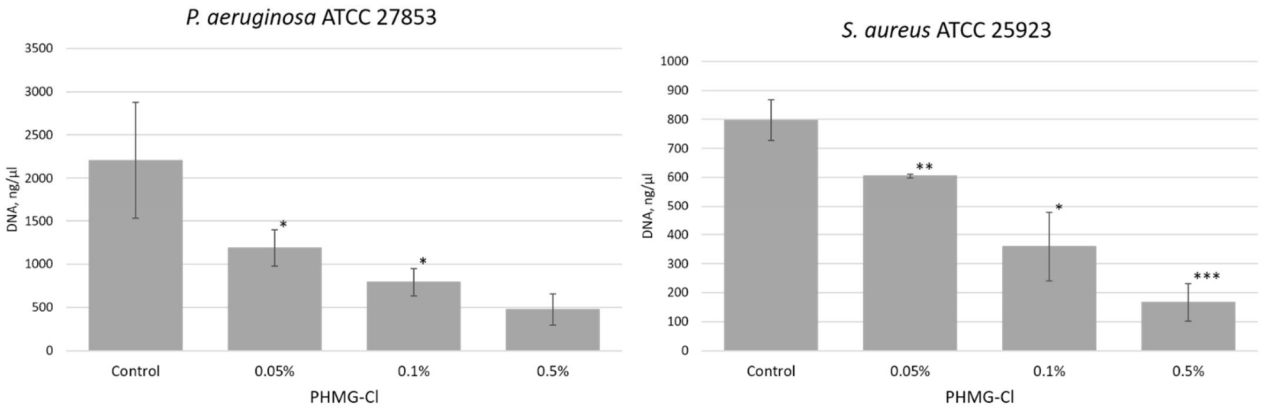

Figure 5. Increasing concentrations of PHMG-Cl reduce eDNA yield from *Pseudomonas aeruginosa* ATCC 27853 (PA) and *Staphylococcus aureus* ATCC 25923 (SA) biofilms. Shown here is the eDNA yield from 3-day old PA (**left**) and SA (**right**) biofilms after treatment with PHMG-Cl (n = 3). Statistical differences are determined between treatments and the water-treated positive controls for each of the PA and SA biofilms; * $p < 0.05$, ** $p < 0.01$, and *** $p < 0.005$.

2.3. Inactivation of DNA by PHMG-Cl

PHMG-Cl was the only biocide found to prevent the PCR amplification of 16S rDNA target sequences from eDNA samples (Figure 3). We, therefore, speculated as to how eDNA inactivation might have occurred, given that measurable quantities of eDNA could still be recovered from PHMG-Cl-treated biofilms. We first extracted eDNA from PA biofilm samples in a manner that avoided contamination by intracellular DNA and used an electrophoretic mobility assay to determine whether PHMG-Cl formed DNA complexes that might prevent PCR amplification. PA eDNA treated with 0.001–0.01% PHMG-Cl did not affect the intrinsic charge of DNA molecules, but concentrations of 0.05–0.5% PHMG-Cl effectively neutralized the DNA, which was then lost during gel electrophoresis (Figure 7). However, it is not clear from this assay whether PHMG-Cl binding was co-operative or not, but we assume that 0.05% PHMG-Cl was sufficiently saturating to bind all surface sites. Dialysis or deproteinization of the eDNA–PHMG-Cl reaction mixture had little impact on electrophoresis, suggesting that these complexes were stable and not dependent on the presence of DNA-binding proteins that may have co-isolated with the eDNA (the presence of eDNA was confirmed by NanoDrop spectrophotometry, demonstrating that DNA was not lost during processing). PHMG-Cl also complexed with covalently closed circular (CCC) and linear forms of pC1-L plasmid DNA, suggesting that this process may not be too sensitive to DNA structure. Treatment of CCC and linear pC1-L also prevented PCR amplification of the LIF gene target sequence (Figure 8). We also included a mixture of PHMG-Cl-treated pC1-L DNA with untreated pC1-L DNA in this PCR assay, which demonstrated that once complexed with DNA, PHMG-Cl could not bind new DNA (suggesting a low dissociation constant for the DNA–PHGM-Cl complex) or directly interact with the Taq polymerase to prevent PCR amplification. These assays confirmed

that treatment with 0.05% PHMG-Cl effectively inactivated a range of DNA, including eDNA as well as CCC and linear plasmid DNA.

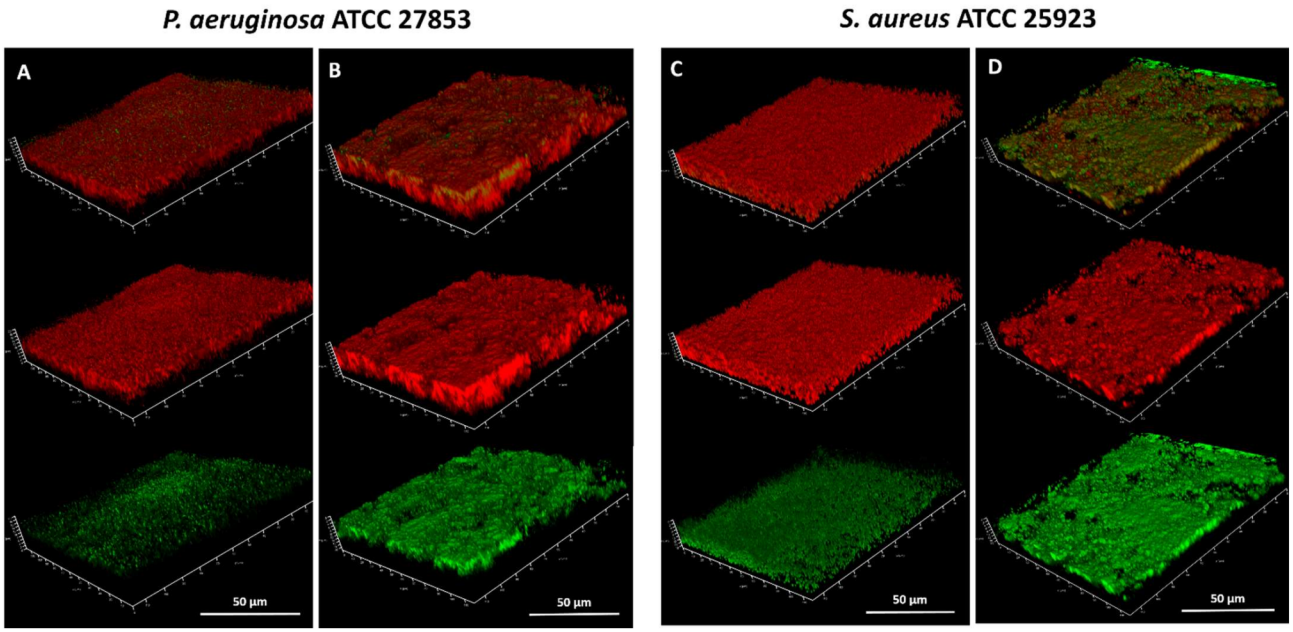

Figure 6. CLSM imaging of *Pseudomonas aeruginosa* ATCC 27853 (PA) and *Staphylococcus aureus* ATCC 25923 (SA) biofilms in situ after exposure to PHMG-Cl. Shown here are images of 3-day-old PA and SA biofilms after treatment with water (**A**,**C**) and 0.5% PHMG-Cl (**B**,**D**). PI (red signal) and SYBR Green (green signal) were used to visualize eDNA, including the eDNA released from damaged cells, and SYBR Green to visualize the intracellular DNA of living (metabolically active) cells with undamaged membranes. In each panel, the top orthogonal view shows the combined PI and SYBR Green signal. The PI signal is shown in the middle view and the SYBR Green signal in the bottom view. The red/green channel pixel sum ratios are (**A**) 1.43, (**B**) 2.28, (**C**) 2.76, and (**D**) 1.15. The SYBR Green appears enhanced after PHMG-Cl treatment (bottom view in **B** and **D**) because the biocide damages the cell wall and membrane, allowing more SYBR Green to enter the cell and bind intracellular DNA.

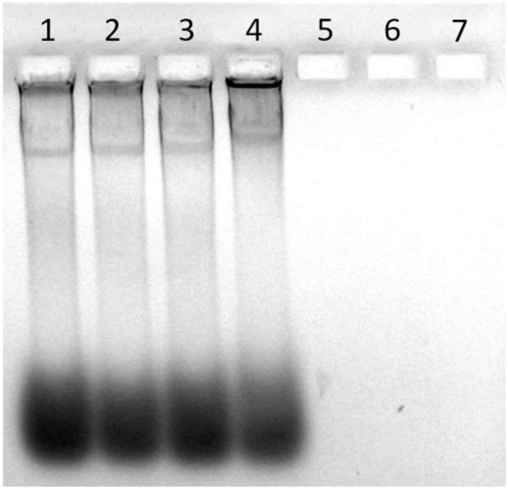

Figure 7. PHMG-1 complexes with eDNA and neutralizes the intrinsic charge of DNA molecules. Shown here is a 1.2% agarose-TA gel stained with EtBr to visualize *Pseudomonas aeruginosa* ATCC 27853 (PA) eDNA that had been treated with PHMG-Cl. Treatments: (1) water-only control, (2) 0.001%, (3) 0.005%, (4) 0.01%, (5) 0.05%, (6) 0.1%, and (7) 0.5% PHMG-Cl.

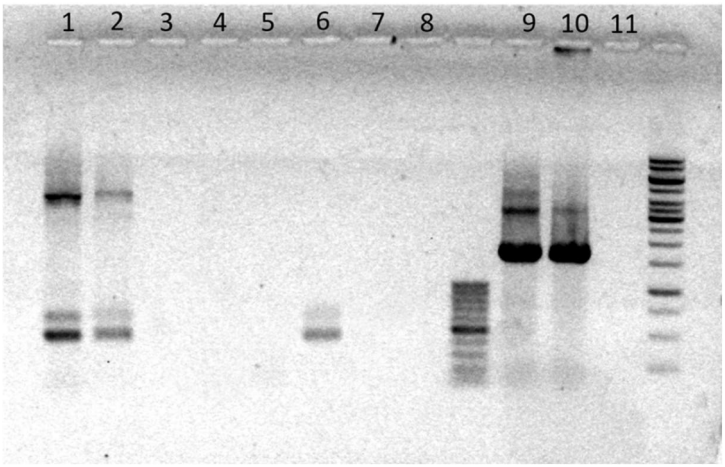

Figure 8. PHMG-Cl–DNA complexes prevent PCR amplification of target sequences in pC1-L plasmid DNA and eDNA. Shown here is a 1.2% agarose-TA gel stained with EtBr to visualize PCR products after amplification with pL1-C LIF gene or 16S-specific primers. CCC pC1-L DNA treatments: (1) water-only control, (2) control sample plus an equal volume 0.01% PHMG-Cl sample, (3) control sample plus an equal volume of 0.05% PHMG-Cl sample, (4) 0.01% PHMG-Cl, and (5) 0.05% PHMG-Cl; linear pC1-L DNA treatments: (6) water-only control, (7) 0.01% PHMG-Cl, and (8) 0.05% PHMG-Cl; eDNA treatments: (9) water-only control, (10) 0.01% PHMG-Cl, and (11) 0.05% PHMG-Cl. A sample of GeneRuler 1 kb DNA Ladder (Thermo Fisher Scientific, Vilnius, Lithuania) is shown in the rightmost lane of the gel.

2.4. Inactivation of eARG by PHMG-Cl

To confirm the direct inactivation of a model ARG in eDNA by PHMG-Cl, we extracted eDNA from biofilms of a pan-drug-resistant *Klebsiella pneumoniae* hospital isolate (UHI KP 1633). We confirmed that UHI KP 1633 was a pan-drug-resistant strain and was resistant to carbapenems and colistin and we used real-time PCR to amplify the carbapenemase (KPC) resistance gene from eDNA treated with PHMG-Cl (Figure 9). Real-time PCR was only able to detect KPC in the eDNA water-only control and samples treated with 0.001–0.005% PHMG-Cl but not in samples treated with higher concentrations of PHMG-Cl, in agreement with our earlier tests of PA eDNA and pC1-L plasmid DNA.

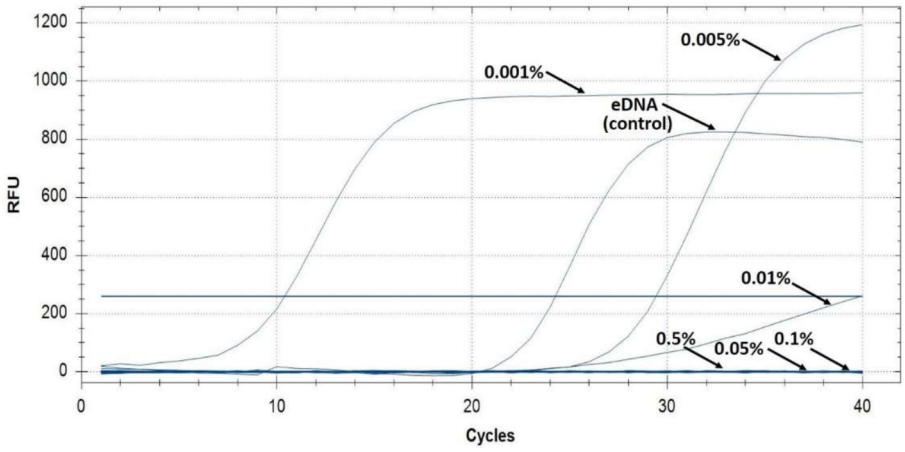

Figure 9. Real-time PCR of a model eARG is inhibited by PHMG-Cl treatment of eDNA. Shown here are the real-time PCR amplification curves of the KPC antibiotic resistance gene from UHI KP 1633 eDNA samples after PHMG-Cl treatment. The water-only control and 0.001–0.5% PHMG-Cl treatments are indicated. Note that RFU is not normalized as quantitative results were not needed and these curves are only used to indicate positive PCR amplification. The blue horizontal line is the fluorescent threshold, and Cq (not marked) is where the PCR amplification curves cross the threshold.

2.5. DNA-Inactivating Activity of PHMG-Cl Adsorbed onto Plastic Surfaces

PHMG-Cl is known to have strong absorptive properties, and slow-release from surfaces can provide long-lasting antibacterial defense [37,38]. We speculated whether the inactivation of DNA we had observed with PHMG-Cl added to dehydrated and growing biofilms and eDNA also occurred when the eDNA was allowed to dry onto plastic surfaces treated with PHMG-Cl. We treated 96-well polystyrene plates with PHMG-Cl and added PA eDNA and stored them at room temperature for up to 28 days before recovery of DNA and gel electrophoresis (Figure 10). Although the total amount of DNA recovered decreased with age, sufficient DNA remained after 28 days to demonstrate that surfaces treated with 0.5–1.0% PHMG-Cl could still inactivate eDNA and that 0.05–0.1% PHMG-Cl could also protect surfaces and inactivate eDNA for 4–8 days.

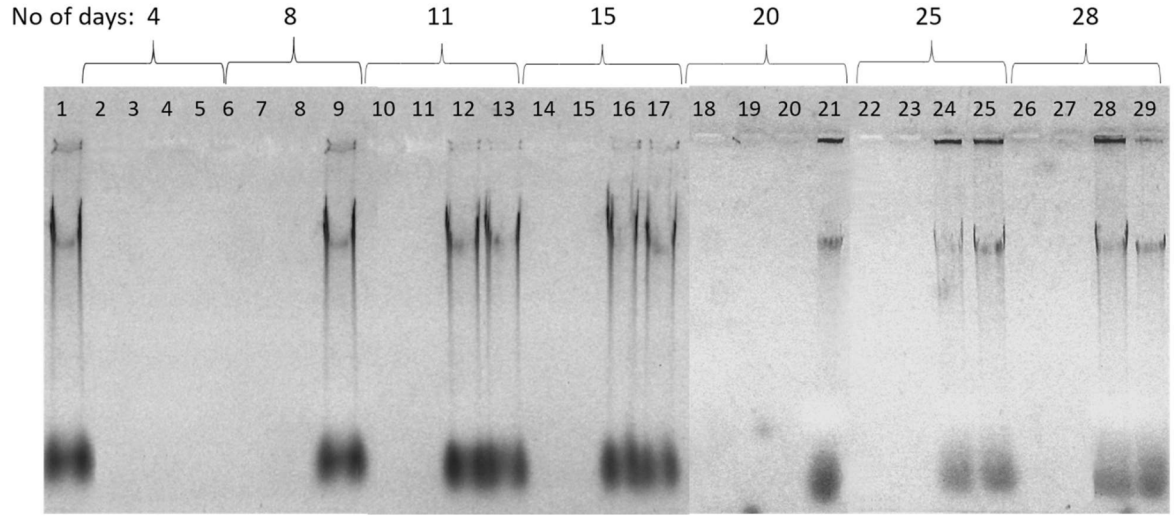

Figure 10. Plastic surface treated with PHMG-Cl inactivates eDNA. Shown here is a 1.2% agarose-TA gel stained with EtBr to visualize eDNA recovered from plastic treated with PHMG-Cl for up to 28 days. PHMG-Cl treatments (1%, 0.5%, 0.1%, and 0.05% are grouped according to the length of exposure (days). Treatments: (1) clean-surface control, (2, 6, 10, 14, 18, 22, and 26) 1% PHMG-Cl, (3, 7, 11, 15, 19, 23, and 27) 0.5% PHMG-Cl, (4, 8, 12, 16, 20, 24, and 28) 0.1% PHMG-Cl, and (5, 9, 13, 17, 21, 25, and 29) 0.05% PHMG-Cl.

2.6. DNA Docking Assay

We undertook molecular docking using the DNA oligonucleotide 1DNE to investigate the mechanism that might allow the formation of DNA–PHMG-Cl complexes. 1DNE has been previously used in several studies to investigate the interaction of various ligands with DNA [39–41]. As we were interested in identifying PHMG-Cl interactions in both AT- and CG-rich regions, we modeled PHMG-Cl as a dimer following the approach used in studying DNA–PHMB dimer interactions [42]. We obtained a 1DNE DNA–PHMG dimer complex that was stabilized by six hydrogen bonds (1.97–3.20 Å) and five electrostatic bonds (1.97–3.20 Å), with five additional longer-range electrostatic interactions (4.42–5.13 Å) occurring via the PHMG amino groups (Figure 11). The DA7, DT6, DT8, DC9, DT18, DA19, and DC21 nucleotide bases in 1DNE play a key role in stabilizing the complex. Our docking results showed the formation of the DNA–PHMG dimer complex with estimated binding energies of 7.8 kcal/mol predominantly at the AT base pair region of 1DNE.

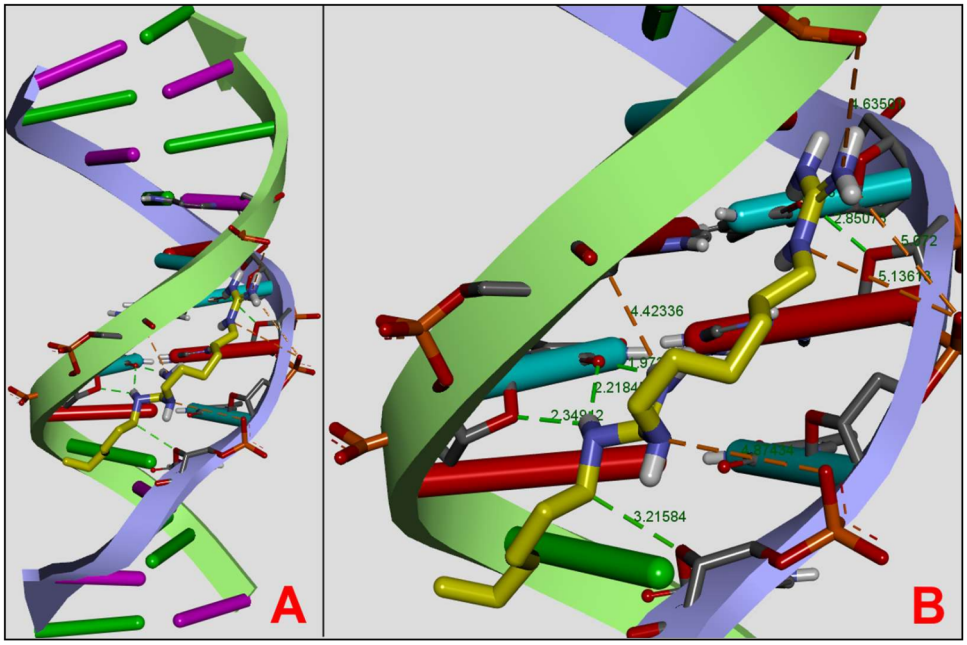

Figure 11. PHMG can dock to DNA in the minor groove and is stabilized by hydrogen and electrostatic bonds. Shown here are two views of a DNA–PHMG dimer complex produced by molecular docking studies using the model DNA oligonucleotide 1DNE. (**A**) A general view of the PHMG dimer (yellow) docking in the minor groove of DNA. (**B**) Detailed docking position including the hydrogen (green) and electrostatic (orange) bonds with bond lengths (Å) indicated.

We validated our approach by redocking the DNA intercalator Netropsin after ligand randomization [39,43] to 1DNA with an estimated binding energy of −7.7 kcal/mol after ligand randomization with an RMSD value for all atoms of 0.2 Å. The similarity between the two estimated binding energies suggests that we selected the correct docking strategy for the PHMG dimer.

3. Discussion

3.1. Impact of Biocides on eDNA

Biofilms are a form of bacterial colonization of the environment [44–47]. eDNA is an extracellular matrix polymer found in the biofilms of many important opportunists, such as *Acinetobacter baumannii*, *Enterococcus faecalis*, *Helicobacter pylori*, *P. aeruginosa*, and *Staphylococcus* spp. [2–8]. It is an important structural element and is stabilized by functional amyloids and cross-linked with polysaccharides [8,48,49]. eDNA is also a source of nutrients and provides antibacterial, antibiotic-resistant, and regulatory activities [50–52] and has good adhesive properties in *P. aeruginosa* and *Bacillus cereus* biofilms in particular [4,53]. It has been traditionally considered as an inevitable attribute of microbial contamination, and in recent years, more attention has been paid to eDNA as a source of ARGs contributing to hospital resistomes. eDNA has finally been recognized as a contaminant that should be controlled to reduce HGT intensity and resistomes [7,54,55]. Similar to other resistance factors, eDNA in biofilms can be enhanced by sublethal doses of antimicrobials [56–58] and biocides [9,59], which result in hospital contamination [16]. It is, therefore, likely that the use of some biocides in hospitals may be counter-productive in controlling biofilms, eDNA, HGT, and resistomes.

A better understanding of how biocides affect the release of eDNA from biofilms and contribute to surface and water contaminants and dust particles is required. In this research, the effect of four groups of biocides on eDNA release from dehydrated biofilms produced by two model hospital pathogens, *Pseudomonas aeruginosa* ATCC 27853 and *Staphylococcus aureus* ATCC 25923, was studied. Interestingly, almost all the biocides tested, except for PHMG-Cl and 70% ethanol, caused substantial eDNA release that was a mixture of pre-

existing eDNA accumulated during the growth of the biofilm samples and DNA freshly released from damaged cells as the result of the application of the biocide. The amount of eDNA released from these biofilms might be explained by structural differences between biofilms. PA biofilms are rich in eDNA, which plays not only a structural role but also an important physiological role, providing phenotypic resistance [48,50,51].

3.2. PHMG Blocks Biofilm Development

Cationic polymers are now being considered as a new generation of biocides due to their enhanced antimicrobial activity, as well as their low toxicity to human cells, compared to common low-molecular cationic surfactants [60,61]. A wide variety of biocidal cationic polymers comprising quaternary ammonium, pyridinium, phosphonium, and guanidinium cations in main chains or as pendant groups has been reported [60–63]. The high activity of cationic polymers against microorganisms is caused by the presence of multiple positive charges within a single molecule that are able to compensate the negative charges present on the outer cell membranes of microbes. Due to these strong electrostatic interactions, polycations are able to attack the cellular envelope and subsequently associate with the head groups of the acidic phospholipids. The presence of hydrophobic aliphatic chains in the cationic polymer structure ensures a better partition to the hydrophobic regions of the phospholipids membrane, resulting in a change in membrane permeability and lethal leakage of cytoplasmic materials [60,64]. So far, this has been the only established way of the action of polycationic antimicrobial polymers confirmed by numerous studies [60,65].

Polymeric cationic biocides incorporating guanidinium cations in the polymer backbone, such as polyhexamethylene biguanide hydrochloride (PHMB-Cl) and polyhexamethylene guanidine hydrochloride (PHMG-Cl), are often considered as cost-effective alternatives to common inorganic antimicrobial agents as they have high efficacy in killing antibiotic-resistant bacteria and fungi and low cytotoxicity [66–70]. Guanidinium-based cationic polymers are widely used as effective disinfectants in cooling systems, swimming pools, and hospitals; in personal hygiene products; as well as in the food industry [66,68,70,71].

Although bacterial-biofilm-forming communities pose a significant problem in modern healthcare environments, there are a limited number of studies investigating their susceptibility to existing biocides and cationic polymers such as PHMG-Cl have been tested on *S. aureus* in liquid cultures (planktonic state) as well as in biofilms [72] and have demonstrated an anti-biofilm activity that is significantly higher compared to that of common antimicrobial agents, including benzalkonium chloride, cetrimide, chlorhexidine, and cetylpyridinium chloride [73]. PHMG-Cl also demonstrated bactericidal advantages over chlorhexidine digluconate against ESKAPE bacteria [74].

To evaluate the biocidal effectiveness of PHMG-Cl, we measured the total metabolic activity of PA and SA biofilms, which confirmed that it is an effective antibacterial compound. Our testing again demonstrated a difference between PA and SA biofilms, with SA biofilms more resistant to PHMG-Cl, with a minimal effective anti-biofilm concentration of 0.5%, which was 5× lower than that needed for PA biofilms. However, the mechanism behind the effectivity of PHMG-Cl against biofilms or biofilm-resident cells is not yet understood for either Gram-negative or Gram-positive opportunistic pathogens. We noted that PHMG-Cl could effectively release pre-existing eDNA and DNA from damaged cells from the dehydrated biofilms that we used as a model surface contamination as well as from fully hydrated and growing biofilms, suggesting that this biocide might work well with both developing biofilms as well as biofilm residue.

3.3. PHMG Binds to DNA and Inhibits Its Functionality

Our molecular docking analysis of a PHMG dimer with a model DNA oligonucleotide suggests that the high anti-biofilm activity of PHMG-Cl may be associated with specific DNA binding in high-AT regions. DNA binding is also the likely explanation of why PHMG-Cl-treated eDNA and pC1-L plasmid did not enter agarose gels during electrophoresis and the failure of PCR to amplify target sequences. PHMG-Cl was able to

inactivate genes, including ARGs, when used at 0.01–0.05%, and plastic surfaces treated with PHMG-Cl continued to show DNA deactivation for up to 28 days after application. For high-molecular-weight and degraded eDNA, there was a direct correlation between eDNA and PHMG-Cl concentrations needed to inactivate the DNA and 0.01% PHMG-Cl also inactivated CCC and linear plasmid DNA. A similar DNA-inactivation effect was observed earlier for polyamide films containing 7–10% PHMG-NS [32], where only the PHMG at the surface of the film was actively in contact with biofilm eDNA. There are some reports that polyhexamethylene biguanidine (PHMB) might bind selectively and condense bacterial chromosomes [42,74].

Selective binding and condensation of intracellular DNA might be one more mechanism inhibiting bacterial growth [74]. To investigate this effect and the spatial distribution of both eDNA and intracellular DNA in PA and SA biofilms, we applied the classical live/dead staining routinely used in microbiology [36], with PI used to visualize eDNA and the DNA of cells with damaged membranes and the membrane permeable SYBR Green to stain all DNA. As both dyes bind in the minor groove of DNA, fluorescence resonance energy transfer (FRET) results in eDNA and dead cells fluorescing only with a red emission [75]. We observed eDNA in both PA and SA biofilms as expected and found that PHMG-Cl treatment differentially impacted eDNA and biofilm structure. PHMG-Cl caused cell lysis and the formation of large eDNA filaments, and biofilm thickness increased in areas of acute cell damage. In SA biofilms, it appeared that a lot of the eDNA from the top surface of the biofilm had been lost despite the gentle washing we used in the treatment of the samples. Finally, we noted that the effects of PHMG were not confined to eDNA only. Similar to others [76], we noticed microscopic evidence of cell wall damage after PHMG-Cl treatment (Figure 12), confirming the generally accepted model of PHMG-Cl activity in which cell walls and membranes are affected. This is confirmed by our observation that after PHMG-Cl treatment, the SYBR Green signal was enhanced because of the easier access to the intracellular DNA through damaged membranes.

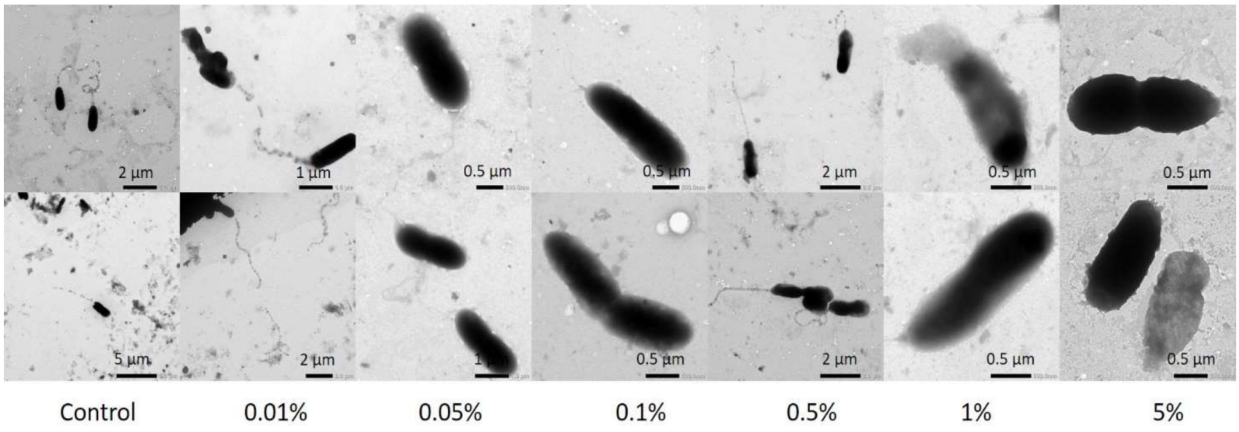

Figure 12. PHMG-Cl effects cell shape, causing damage to the cell wall and membrane. Shown here are TEM images of PA cells subjected to different PHMG-Cl concentrations.

4. Materials and Methods

4.1. Synthesis of the Polymeric Biocide Polyhexamethylene Guanidine Hydrochloride (PHMG-Cl)

A mixture of guanidine hydrochloride (20 g, 0.21 mol) and hexamethylenediamine (23.1 g, 0.2 mol) was placed in a round-bottomed flask (500 mL) equipped with a mechanical stirrer (Scheme 1). This mixture was heated to 100 °C and the melt was stirred for 4 h at this temperature. Further, the reaction was carried out for 4 h at 130–140 °C, and finally 4 h at 180 °C to obtain a highly viscous melt of PHMG-Cl. A vitreous solid was obtained after cooling the mixture to room temperature, which was then dissolved in water (200 mL), filtered, and precipitated by the addition of a saturated aqueous solution of sodium chloride (100 mL). PHMG-Cl was isolated by the decantation of the water solution and dried at

140 °C for 24 h before being powdered in a porcelain mortar. The final product had a melting point of 134–136 °C and an intrinsic viscosity of 0.09 dL/g in 0.1 N NaCl at 25 °C. The molecular weight of PHMC-Cl was calculated using the Mark–Houwink equation $[\eta] = K \times M^{\alpha}$, where $[\eta]$ is intrinsic viscosity, M is the viscosity-average molecular weight, α and K are parameters whose values depend on the nature of the polymer and the solvent. For the PHMG-Cl–water system, $K = 1.83 \times 10^{-3}$ and $\alpha = 0.38$ at 25 °C [77]. Thus, the viscosity-average molecular weight of the synthesized PHMG-Cl was found to be 28,000.

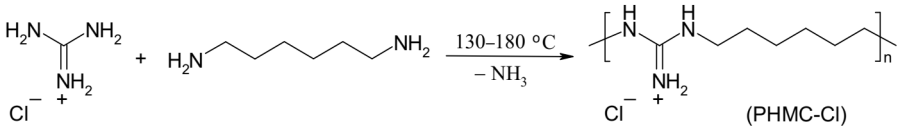

Scheme 1. Synthesis of PHMG-Cl.

NMR spectra of PHMG-Cl were recorded in DMSO-d6 on a Varian Gemini-2000 (400 MHz) spectrometer with the following results: ^{1}H NMR (400 MHz, DMSO-D6): δ = 1.32 (m, 4H, CH_2), 1.47 (m, 4H, N-CH_2CH_2), 3.16 (m, 4H, N-CH_2), and 7.1–8.1 (br s, 4H, NH); ^{13}C NMR: 25.3 (CH_2), 28.1 (N-CH_2CH_2), 40.5 (N-CH_2), and 156.6 (NH).

4.2. Biocides Used in the Assays

Seven biocides were used in addition to PHMG-Cl, i.e., 35% hydrogen peroxide (Khimpostachannia, Kharkiv, Ukraine); 96% ethanol (UkrSpirt Trade, Kiev, Ukraine); 0.05% chlorhexidine (Zdorovie, Kharkiv, Ukraine); Maxisan (Interdez, Kiev, Ukraine), which contained not less than 50% of a mix of four quaternary ammonium compounds; Arquades-plus (O. L. KAR, Vinnitsa, Ukraine), containing 10% dimethyldialkylammonium chloride, 5% didecyldimethylammonium chloride, and 2.5% tetrasodium salt); Desmanol (Schülke & Mayr GmbH, Germany), containing 75% isopropanol; and Sanikon (Interdez, Kiev, Ukraine), containing not less than 5.5% of a mix of four quaternary ammonium compounds.

4.3. Microorganisms and Culturing Conditions

Two model hospital opportunistic pathogens, *Pseudomonas aeruginosa* ATCC 27853 (PA) and *Staphylococcus aureus* ATCC 25923 (SA), were used to study the effects of biocides on established biofilms and eDNA yield. The Ukrainian hospital isolate *Klebsiella pneumoniae* 1633 (KP) was recovered from a patient and identified as a pan-drug-resistant (PDR) strain using antibiotic disc diffusion assays and EUCAST 2021 v.11.0 breakpoints. An AST-N332 card was used to confirm the PDR strain phenotype with the VITEK 2 Advanced Expert System. Antimicrobial susceptibility testing of CMS was performed by a SensiTest Colistin (Liofilchem, Roseto degli Abruzzi, Italy) broth microdilution assay and the results interpreted according to EUCAST breakpoints. Bacterial strains were cultured aerobically at 37 °C with shaking in a Luria–Bertani (LB) medium to provide inoculum [78]. Preliminary biofilm experiments showed that the surface–liquid interface biofilms produced by KP, PA, and SA were readily dislodged from glass vials or 96-well plates (this is an acknowledged problem in crystal staining biofilms) [79]. We therefore decided to produce biofilm samples for the assay without rinsing or washing. We noted that the samples will therefore contain a proportion of planktonic cells but that this will have a limited impact on our assays, as KP and SA lack flagella and the initial inoculum will not remain in the liquid column for long and all subsequent growth must be in biofilms. While PA is capable of flagella-mediated swimming, it is highly aerotaxic and most cells will accumulate at the air–liquid interface and in the meniscus region where biofilm growth dominates. We used water-only treatments to provide positive controls for some assays but do not believe these brief exposures to distilled water would lead to substantial cell lysis through hypo-osmotic shock, as both PA and SA are often isolated from fresh and drinking water and must, therefore, be able to cope with this stress [33,34]. For the biofilm inactivation assay, LB cultures were diluted to 10% and 200 µL aliquots transferred to the wells of a 96-well plate that was incubated at 37 °C for 24 h before the biocide inactivation assay. For CLSM and

the eDNA yield assay, 10% dilutions were used to inoculate 30 mL glass vials (microcosms) containing 2–5 mL LB that were incubated statically at 37 °C for 3–5 days to produce biofilms [80]. The biofilms were air-dried at room temperature for 14 days before eDNA yield analysis. For CLSM, biofilms were grown in 5 mL stationary glass vials and samples recovered using a pipetter with cut 200 µL tips. The biofilm samples were gently placed onto microscope glass slides and the liquid drained off using filter paper. They were then treated with a PHMG-Cl solution for 30 min and gently washed with water using a pipetter to remove the biocide but limit any further physical damage before staining and imaging (see below).

4.4. Plasmids Used in the Study

The pC1-L plasmid containing the human LIF gene [81] was used to investigate the effect of biocides on covalently closed circular and linear plasmid DNA.

4.5. Biofilm Metabolic Assay

Aliquots of an aqueous PHMG-Cl solution were added to the wells of a 96-well plate with 24 h PA and SA biofilm cultures at final concentrations of 5%, 1%, 0.5%, 0.1%, 0.05%, 0.01%, 0.005%, and 0.001%, with eight replicates per treatment. These were incubated for 1 h at room temperature. A negative control sample was produced using 50% ethanol and a positive (live) control produced by adding sterile distilled water. MTT solution (Sigma-Aldrich, UK) was then added to each well to a final concentration of 0.05% and the mixture incubated at 37 °C for 3 h. Biofilms were removed from each well and placed in 1.5 mL plastic tubes, which were then centrifuged at 13,000× *g* for 15 min in an Eppendorf 5424 microcentrifuge (Eppendorf, Germany). The supernatant was discarded, and the pellet dissolved in 500 µL of DMSO. Metabolic activity was evaluated using absorbance measurements at 570 nm in a BioTek ELx800 microplate spectrophotometer (BioTek Instruments, Inc., Winooski, VT, USA). Net biofilm metabolic activity was calculated by subtracting the negative control values.

4.6. eDNA Yield Assay

Biocides were tested at different concentrations to determine eDNA yields. For this, 1 mL of 0.5%, 0.1%, and 0.05% PHMG-Cl; 6% and 3% hydrogen peroxide; 70% ethanol; 0.05% chlorhexidine; 0.25% Maxisan; 0.5% Arquadez-plus; 0.5% Desmanol; and 0.5% Sanikon were added to dehydrated PA and SA biofilms at room temperature and the mixtures kept for 1 h, with three replicates per treatment. A water-only treatment was again used as the positive control. eDNA was extracted from the liquid phase of each sample. Proteins were first removed with an equal volume of chloroform and DNA precipitated with 70% ethanol and 0.3 M sodium acetate (pH 8.0). DNA was then dissolved in TE buffer. The nucleic acid concentration was measured by a NanoDrop 2000 spectrophotometer (Thermo Fisher Scientific, Inc., Wilmington, DE, USA). DNA samples were then visualized by 1.2% agarose-TA gel electrophoresis and EtBr staining. GeneRuler 1 kb DNA Ladder (Thermo Fisher Scientific, Vilnius, Lithuania) was used as a size marker.

4.7. Biofilm eDNA Isolation

PA and KP biofilms were grown in 5 mL LB static vials at 37 °C for 5 days. The biofilms were then disintegrated by agitation for 5 min. Then, 5 mL of the biofilm suspension was centrifuged at 13,000× *g* for 15 min using a microcentrifuge and the supernatant recovered. The eDNA in the supernatant was precipitated with 70% ethanol and 0.3 M sodium acetate (pH 8.0) and then dissolved in TE buffer. The nucleic acid concentration was measured by NanoDrop.

4.8. PHMG-Cl Effects on eDNA and pC1-L Plasmid DNA

The eDNA isolated from PA 27853 and pC1-L DNA was treated with different PHMG-Cl concentrations. For this, 7 µL (6.7 µg) of eDNA and 7 µL (2.8 µg) of linear or covalently

closed circular (CCC) pC1-L DNA was mixed with 3 µL of DNA loading buffer (Thermo Fisher Scientific, Vilnius, Lithuania) and final concentrations of 0.01% and 0.05% PHMG-Cl. Samples were placed in D-0530 dialysis tubing (Sigma, Saint Louis, MO, USA) and the samples dialyzed together to reduce the PHMG-Cl concentration by 10–7× in TE buffer. The DNA samples were visualized by gel electrophoresis.

4.9. PCR of 16S rDNA, LIF, and KPC Sequences

PCR was used to determine the effect of biocide treatment on DNA by amplifying 16S rDNA, LIF, and *Klebsiella pneumoniae* carbapenemase (KPC) target sequences. To amplify 16S sequences from eDNA samples, 25 µL PCR reaction mixtures (Taq PCR Kit, New England Biolabs, Ispwich, MA, USA) with 27F (5′-AGAGTTTGATCMTGGCTCAG-3′) and 1492R (5′-TACGGYTACCTTGTTACGACTT-3′) primers were used [82]. Forward (5′-ATGAAGGTCTTGGCGGCAGG-3′) and reverse (5′-ACCTCCTGCTAGAAGGCCTG-3′) primers were used to amplify the LIF gene from pC1-L samples. PCR conditions involved an initial stage of 5 min at 95 °C. This was followed by 30 cycles at 95 °C for 30 s, 57 °C for 30 s, and 72 °C for 30 s and a final stage at 72 °C for 5 min. Purified genomic DNA was used as a positive control and the PCR products visualized by gel electrophoresis. KPC sequences were amplified using the AmpliSense MDR KPC/OXA-48-FL reagent kit (AmpliSense, Moscow, Russia) and the CFX96 Touch Real-Time PCR Detection System (Bio-Rad, Hercules, CA, USA).

4.10. Effect of PHMG-Cl-Treated Plastic Surface on eDNA

First, 10 µL of 1%, 0.5%, 0.1%, and 0.05% PHMG-Cl was placed into the wells of 96-well polystyrene plates, with three replicates per treatment. Then, the plates were allowed to dry at room temperature and left for 4, 8, 11, 15, 20, 25, and 28 days under the same conditions. Finally, 10 µL of 880 ng/µL eDNA from PA biofilms was added to the wells and the mixture incubated at room temperature for 1 h before nucleic acid concentrations were measured by NanoDrop and visualized by gel electrophoresis.

4.11. Molecular Docking Assay

Molecular docking was performed using the model DNA dodecamer (CGCGATATCGCG) used to study DNA-binding compounds (RCSB Protein Data Bank 1DNE: https://www.rcsb.org/structure/1dne, accessed on 1 March 2021) [83]. Chains A and B were used for docking, and the water molecules and the ligand were removed from the crystal structure using Accelrys DS 4.0 [84]. AutoDock Tools (ADT) 1.5.6 [85] was used to make the PHMG dimer ligand and add polar hydrogens to the DNA. The noBondOrder method was used to renumber all atoms including the new hydrogen atoms, and the Gasteiger method was used to calculate charges. ChemAxon Marvin Sketch 5.3.735 [86] was used to optimize the PHMG dimer structure. Energy minimization and optimization of the PHMG dimer ligand were performed by MOPAC2016 [87] using the Auto Optimization Tool (MMFF94s force field) [88]. Partial charges and torsion angles of the ligand were changed using ADT. The DNA structure and the PHMG dimer were used for molecular docking by AutoDock Vina 1.1.2 [89]. A grid box of 30 × 30 × 30 points was used with a spacing of 1 Å. The analysis and visualization of interactions were performed by Accelrys DS.

4.12. Confocal Laser Scanning Microscopy (CLSM)

Biofilm samples were stained with 5 µL of 100× SYBR Green (Invitrogen, Waltham, MA, USA) and 1 mM propidium iodide (PI) (Sigma, Gillingham, UK). No additional washing was applied so as to limit the physical disruption of biofilm structures through liquid movement. The samples were not fixed, and a cover slip was placed over the stained samples before imaging. CLSM analysis was undertaken using a Leica TCS SPE Confocal system with a coded DMi8 inverted microscope (Leica, Mannheim, Germany) and Leica Application Suite X (LAS X) Version 3.4.1. Images were acquired using excitation at 488 nm

and emission collected at 490–580 nm for SYBR Green and excitation at 532 nm and emission collected at 537–670 for PI.

4.13. Transmission Electron Microscopy (TEM)

An overnight PA culture was diluted to 20% and PHMG-Cl added to final concentrations of 5%, 1%, 0.5%, 0.1%, 0.05%, and 0.01%. Samples were incubated at room temperature for 20 min before a 10 µL aliquot was placed onto a formvar covered grid and dried at room temperature. Then, 10 µL of 1% uranyl acetate (Sigma-Aldrich, Gillingham, UK) was dropped onto each grid and dried with filter paper. TEM was performed with a JEM-1400 transmission electron microscope (JEOL, Tokyo, Japan).

4.14. Statistical Analysis

Replicate data were processed using the statistical software package OriginPro 7.0 and MS Excel for Windows. All results are presented as the mean ± standard deviation. A value of $p < 0.05$ was considered statistically significant.

5. Conclusions

Our investigations clearly demonstrate that the biocides commonly used in hospitals can have a significant impact on the release of eDNA from bacterial biofilms. Some biocides, in particular PHMG-Cl, were found to block biofilm development and were able to complex with DNA in a manner predicted by molecular docking assays. PHMG-Cl binding to DNA altered the electrophoretic mobility of both high-molecular-weight and plasmid DNA and prevented the amplification of a target ARG gene from the eDNA isolated from a Klebsiella biofilm. PHMG-Cl was also found to inactivate DNA when used to treat plastic surfaces, up to 28 days after application. These findings demonstrate the potential of PHMG-Cl as a surface-active agent that can be used in hospital settings to help reduce the spread of antibiotic resistance by inactivating the eDNA commonly found in bacterial biofilms and by limiting the development of biofilms themselves.

Author Contributions: Conceptualization: O.V.M., S.Y.R. and N.P.K.; data curation: O.V.M.; formal analysis: O.V.M., S.P.R., S.Y.R., A.J.S. and G.P.; funding acquisition: O.V.M. and O.S.I.; investigation: O.V.M., T.P.B., O.S.I., L.O.M., I.P., V.V.P., K.L.R., S.Y.R., I.V.S., O.P.T. and S.P.R.; methodology: O.V.M., S.Y.R. and I.V.S.; project administration: O.V.M.; resources: O.V.M., S.Y.R. and S.P.R.; supervision: O.V.M.; visualization: O.V.M.; writing: O.V.M., G.P. and A.J.S. All authors have read and agreed to the published version of the manuscript.

Funding: This work was undertaken with the support of the National Research Foundation of Ukraine through the Leading and Young Scientists Research Support program and the research grant "Development of combined therapy for severe *Klebsiella pneumoniae*-associated nosocomial infections to overcome the antibiotic resistance" (2020.02/0246). O.V.M. and O.S.I. also acknowledge the Kyiv National University of Technologies and Design research grant "Development of a complex preparation of combined action based on collagen derivatives for the treatment of wound surfaces" (0120U101290) and the NATO SPS grant "Fighting maritime corrosion and biofouling with task-specific ionic compounds" (984834). O.V.M., S.Y.R. and I.P. also acknowledge the National Academy of Sciences of Ukraine research grant "Development of innovative methods for drug delivery and control of their action" (0117U002124).

Institutional Review Board Statement: Not applicable.

Informed Consent Statement: Not applicable.

Data Availability Statement: All data have been included in this manuscript (figures).

Acknowledgments: O.V.M. thanks Mykola Kovinya and OM Agro for consultation and technical support. O.V.M. also thanks I. Gilbert and D. Purves, Wellcome Centre for Anti-Infectives Research, University of Dundee, for support to participate in the "Setting our sights on infectious diseases" conference in 2019 and to L. Silver, LL Silver Consulting, NJ, USA, for productive discussions.

Conflicts of Interest: The authors declare no conflict of interest.

References

1. Sivalingam, P.; Poté, J.; Prabakar, K. Extracellular DNA (eDNA): Neglected and potential sources of antibiotic resistant genes (ARGs) in the aquatic environments. *Pathogens* **2020**, *9*, 874. [CrossRef] [PubMed]
2. Allesen-Holm, M.; Barken, K.B.; Yang, L.; Klausen, M.; Webb, J.S.; Kjelleberg, S.; Mollin, S.; Givskov, M.; Tolker-Nielsen, T. A characterization of DNA release in *Pseudomonas aeruginosa* cultures and biofilms. *Mol. Microbiol.* **2006**, *59*, 1114–1128. [CrossRef]
3. Thomas, V.C.; Hiromasa, Y.; Harms, N.; Thurlow, L.; Tomich, J.; Hancock, L.E. A fratricidal mechanism is responsible for eDNA release and contributes to biofilm development of *Enterococcus faecalis*. *Mol. Microbiol.* **2009**, *72*, 1022–1036. [CrossRef]
4. Vilain, S.; Pretorius, J.M.; Theron, J.; Brozer, V.S. DNA as an adhesion: *Bacillus cereus* requires extracellular DNA to form biofilm. *Appl. Environ. Microbiol.* **2009**, *75*, 2861–2868. [CrossRef]
5. Christner, M.; Heinze, C.; Busch, M.; Franke, G.; Hentschke, M.; Buhring, S.B.; Buttner, H.; Kotasinska, M.; Wischnewski, V.; Kroll, G.; et al. SarA negatively regylates *Staphylococcus epidermidis* biofilm formation by modulation exprtession of 1 MDa extracellular matrix binding protein and autolysis-dependent release of eDNA. *Mol. Microbiol.* **2012**, *86*, 394–410. [CrossRef]
6. Sahu, P.K.; Iyer, P.S.; Oak, A.M.; Pardesi, K.R.; Chopade, B.A. Characterization of eDNA from the clinical strain *Acinetobacter baumannii* AIIMS7 and its role in biofilm formation. *Sci. World J.* **2012**, *2012*, 973436. [CrossRef]
7. Grande, R.; Di Marcantonio, M.C.; Robuffo, I.; Pompilio, A.; Celia, C.; Di Marzio, L.; Paolino, D.; Codagnone, M.; Muraro, R.; Stoodley, P.; et al. *Helicobacter pylori* ATCC 43629/NCTC 11639 outer membrane vesicles (OMVs) from biofilm and planktonic phase associatied with extracellular DNA (eDNA). *Front. Microbiol.* **2015**, *6*, 1569. [CrossRef] [PubMed]
8. Schwartz, K.; Ganesan, M.; Payne, D.E.; Solomon, M.J.; Boles, B.R. Extracellular DNA facilitates the formation of functional amyloids in *Staphylococcus aureus* biofilms. *Mol. Microbiol.* **2016**, *99*, 123–134. [CrossRef]
9. Itzek, A.; Zheng, L.; Chen, Z.; Merritt, J.; Kreth, J. Hydrogen peroxide-dependent DNA release and transfer of antibiotic resistance genes in *Streptococcus gordonii*. *J. Bacteriol.* **2011**, *193*, 6912–6922. [CrossRef] [PubMed]
10. Hannan, S.; Ready, D.; Jasni, A.S.; Rogers, M.; Pratten, J.; Roberts, A.P. Transfer of antibiotic resistance by transformation with eDNA within oral biofilms. *FEMS Immunol. Med. Microbiol.* **2010**, *59*, 345–349. [CrossRef]
11. Nolan, L.M.; Turnbull, L.; Katrib, M.; Osvath, S.R.; Losa, D.; Lazenby, J.J.; Whitchurch, C.B. *Pseudomonas aeruginosa* is capable of natural transformation in biofilms. *Microbiology* **2020**, *166*, 995–1003. [CrossRef] [PubMed]
12. Thomas, C.M.; Nielsen, K.M. Mechanisms of, and barriers to, horizontal gene transfer between bacteria. *Nat. Rev. Genet.* **2005**, *3*, 711–721. [CrossRef]
13. Domingues, S.; Nielsen, K.M. Membrane vesicles and horizontal gene transfer in prokaryotes. *Curr. Opin. Microbiol.* **2017**, *38*, 16–21. [CrossRef] [PubMed]
14. Meibom, K.L.; Blokesch, M.; Dolganov, N.A.; Wu, C.Y.; Schoolnik, G.K. Chitin induces natural competence in *Vibrio cholerae*. *Science* **2005**, *310*, 1824–1827. [CrossRef]
15. Mathers, A.J.; Crook, D.; Vaughan, A.; Barry, K.E.; Vegesana, K.; Stroesser, N.; Parikh, H.I.; Sebra, R.; Kotay, S.; Walker, A.S.; et al. *Klebsiella quasipneumoniae* provides a window into carbapenemase gene transfer, plasmid rearrangements, and patient interactions with the hospital environment. *Antimicrob. Agents Chemother.* **2019**, *63*, e02513-18. [CrossRef] [PubMed]
16. Dong, P.; Wang, H.; Fang, T.; Wang, Y.; Ye, Q. Assessment of extracellular antibiotic resistance genes (eARGs) in typical environmental samples and the transforming ability of eARG. *Environ. Int.* **2019**, *125*, 90–96. [CrossRef]
17. Wiener-Well, Y.; Galuty, M.; Rudensky, B.; Schlesinger, Y.; Attias, D.; Yinnon, A.M. Nursing and physician attire as possible source of nosocomial infections. *Am. J. Infect. Control* **2011**, *39*, 555–559. [CrossRef]
18. Lopez, P.-J.; Ron, O.; Parthasarathy, P.; Soothill, J.; Spitz, L. Bacterial counts from hospital doctors' ties are higher than those from shirts. *Am. J. Infect. Control* **2009**, *37*, 79–80. [CrossRef]
19. Treakle, A.M.; Thom, K.A.; Furuno, J.P.; Strauss, S.M.; Harris, A.D.; Perencevich, E.N. Bacterial contamination of health care workers' white coats. *Am. J. Infect. Control* **2009**, *37*, 101–105. [CrossRef]
20. Lax, S.; Smith, D.; Sangwan, N.; Handley, K.; Larsen, P.; Richardson, M.; Taylor, S.; Landon, E.; Alverdy, J.; Siegel, J.; et al. Colonization and succession of hospital-associated microbiota. *Sci. Transl. Med.* **2017**, *9*, eaah6500. [CrossRef]
21. Marinella, M.A.; Pierson, C.; Chenoweth, C. The stethoscope. A potential source of nosocomial infection? *Arch. Intern. Med.* **1997**, *157*, 786–790. [CrossRef]
22. Brady, R.R.W.; Wasson, A.; Stirling, I.; McAllister, C.; Damani, N.N. Is your phone bugged? The incidence of bacteria known to cause nosocomial infection on healthcare workers' mobile phones. *J. Hosp. Infect.* **2006**, *62*, 123–125. [CrossRef] [PubMed]
23. Brady, R.R.W.; Verran, J.; Damani, N.N.; Gibb, A.P. Review of mobile communication devices as potential reservoirs of nosocomial pathogens. *J. Hosp. Infect.* **2009**, *71*, 295–300. [CrossRef] [PubMed]
24. Ulger, F.; Esen, S.; Dilek, A.; Yanik, K.; Gunaydin, M.; Leblebicioglu, H. Are we aware how contaminated our mobile phones with nosocomial pathogens? *Ann. Clin. Microbiol. Antimicrob.* **2009**, *8*, 7. [CrossRef] [PubMed]
25. Akinyemi, K.O.; Atapu, A.D.; Adetona, O.O.; Coker, A.O. The potential role of mobile phones in the spread of bacterial infections. *J. Infect. Dev. Ctries.* **2009**, *3*, 628–632. [CrossRef]
26. Bures, S.; Fishbain, J.T.; Uyehara, C.F.; Parker, J.M.; Berg, B.W. Computer keyboards and faucet handles as reservoirs of nosocomial pathogens in the intensive care unit. *Am. J. Infect. Control.* **2000**, *28*, 465–471. [CrossRef]
27. Li, X.; Wu, Z.; Dang, C.; Zhang, M.; Zhao, B.; Cheng, Z.; Chen, L.; Zhong, Z.; Yuhui, Y.; Xia, Y. A metagenomic-based method to study hospital air dust resistome. *Chem. Eng. J.* **2021**, *406*, 126854. [CrossRef] [PubMed]

28. Kampmann, M.-L.; Børsting, C.; Morling, N. Decrease DNA contamination in the laboratories. *Forensic Sci. Int. Genet. Suppl. Ser.* **2017**, *6*, e577–e578. [CrossRef]
29. Bridier, A.; Briandet, R.; Thomas, V.; Dubois-Brissonnet, F. Resistance of bacterial biofilms to disinfectants: A review. *Biofouling* **2011**, *27*, 1017–1032. [CrossRef]
30. Pearce, H.; Messager, S.; Maillard, J.Y. Effect of biocides commonly used in the hospital environment on the transfer of antibiotic-resistance genes in *Staphylococcus aureus*. *J. Hosp. Infect.* **1999**, *43*, 101–107. [CrossRef]
31. Jutkina, J.; Marathe, N.P.; Flach, C.F.; Larsson, D.G.J. Antibiotics and common antibacterial biocides stimulate horizontal transfer of resistance at low concentrations. *Sci. Total Environ.* **2018**, *616–617*, 172–178. [CrossRef] [PubMed]
32. Moshynets, O.; Chernii, S.; Chernii, V.; Losytskyy, M.Y.; Karakhim, S.; Czerwieniec, R.; Pekhnyo, V.; Yarmoluk, S.; Kovalska, V. Fluorescent β-ketoenole AmyGreen dye for visualization of amyloid components of bacterial biofilms. *Methods Appl. Fluoresc.* **2020**, *8*, 035006. [CrossRef] [PubMed]
33. Mena, K.D.; Gerba, C.P. Risk assessment of *Pseudomonas aeruginosa* in water. In *Reviews of Environmental Contamination and Toxicology*; Whitacre, D., Ed.; Reviews of Environmental Contamination and Toxicology (Continuation of Residue Reviews); Springer: Boston, MA, USA, 2009; Volume 201. [CrossRef]
34. Santos, G.A.C.; Dropa, M.; Rocha, S.M.; Peternella, F.A.S.; Razzolini, M.T.P. *Staphylococcus aureus* and methicillin-resistant *Staphylococcus aureus* (MRSA) in drinking water fountains in urban parks. *J. Water Health* **2020**, *18*, 654–664. [CrossRef]
35. Moshynets, O.; Bardeau, J.-F.; Tarasyuk, O.; Makhno, S.; Cherniavska, T.; Dzhuzha, O.; Potters, G.; Rogalsky, S. Anti-biofilm activity of polyamide 11 modified with thermally stable polymeric biocide polyhexamethylene guanidine 2-naphtalenesulfonate. *Int. J. Mol. Sci.* **2019**, *20*, 348. [CrossRef] [PubMed]
36. Feng, J.; Yee, R.; Zhang, S.; Tian, L.; Shi, W.; Zhang, W.-H.; Zhang, Y. A Rapid growth-independent antibiotic resistance detection test by SYBR Green/Propidium Iodide viability assay. *Front. Med.* **2018**, *5*, 127. [CrossRef]
37. Chen, S.; Li, C.; Hou, T.; Cai, Y.; Liang, L.; Chen, L.; Li, M. Polyhexamethylene guanidine functionalized chitosan nanofiber membrane with superior adsorption and antibacterial performances. *React. Funct. Polym.* **2019**, *145*, 104379. [CrossRef]
38. Wu, F.; Xu, J.; Yan, R.; Hu, B.; Li, G.; Jin, M.; Jiang, X.; Li, J.; Tang, P.; Zhu, J.; et al. In vitro and in vivo evaluation of antibacterial activity of polyhexamethylene guanidine (PHMG)-loaded TiO_2 nanotubes. *Biomed. Mater.* **2020**, *15*, 045016. [CrossRef]
39. Ricci, G.C.; Netz, P.A. Docking studies on DNA-ligand interactions: Building and application of a protocol to identify the binding mode. *J. Chem. Inf. Model.* **2009**, *49*, 1925–1935. [CrossRef]
40. Guo, Y.; Yue, Q.; Gao, B. Molecular docking study investigating the possible mode of binding of C.I. Acid Red 73 with DNA. *Int. J. Biol. Macromol.* **2011**, *49*, 55–61. [CrossRef]
41. Khosravifar, F.; Dehghan, G.; Bidoki, S.K.; Mahdavi, M. DNA-binding activity and cytotoxic and cell-cycle arrest properties of some new coumarin derivatives: A multispectral and computational investigation. *Luminescence* **2020**, *35*, 98–106. [CrossRef]
42. Sowlati-Hashjin, S.; Carbone, P.; Karttunen, M. Insights into the polyhexamethylene biguanide (PHMB) mechanism of action on bacterial membrane and DNA: A molecular dynamics study. *J. Phys. Chem. B* **2020**, *124*, 4487–4497. [CrossRef]
43. Kopka, M.L.; Yoon, C.; Goodcell, D.; Pjura, P.; Dickerson, R.E. Binding of an antitumor drug to DNA netropsin and C-G-C-G-A-A-T-T-BrC-G-C-G. *J. Mol. Biol.* **1985**, *183*, 553–563. [CrossRef]
44. Jerdan, R.; Cameron, S.; Donaldson, E.; Iungin, O.; Moshynets, O.; Spiers, A. Community biofilm-formation, stratification and productivity in serially-transferred microcosms. *FEMS Microbiol. Lett.* **2020**, *367*, fnaa187. [CrossRef]
45. Rycker, M.D.; Horn, D.; Aldridge, B.; Amewu, R.K.; Barry, C.E., III; Buckner, F.S.; Cook, S.; Ferguson, M.A.J.; Gobeau, N.; Herrmann, J.; et al. Setting our sights on infectious diseases. *ACS Infect. Dis.* **2020**, *6*, 3–13. [CrossRef] [PubMed]
46. Moshynets, O.V.; Foster, D.; Karakhim, S.A.; McLaughlin, K.; Rogalsky, S.P.; Rymar, S.Y.; Volynets, G.P.; Spiers, A.J. Examining c-di-GMP and possible QS regulation in *Pseudomonas fluorescens* SBW25: Links between intra and inter-cellular regulation benefits community cooperative activities such as biofilm formation. *Ukr. Biochem. J.* **2018**, *90*, 17–31. [CrossRef]
47. McLaughlin, K.; Folorunso, A.O.; Deeni, Y.Y.; Foster, D.; Gorbatiuk, O.; Hapca, S.M.; Immoor, C.; Koza, A.; Mohammed, I.U.; Moshynets, O.; et al. Biofilm formation and cellulose expression by *Bordetella avium* 197N, the causative agent of bordetellosis in birds and an opportunistic respiratory pathogen in humans. *Res. Microbiol.* **2017**, *168*, 419–430. [CrossRef] [PubMed]
48. Jennings, L.K.; Storek, K.M.; Ledvina, H.E.; Coulon, C.; Marmont, L.S.; Sadovskaya, I.; Secor, P.R.; Tseng, B.S.; Scian, M.; Filloux, A.; et al. Biofilm matrix composition and localization. *Proc. Natl. Acad. Sci. USA* **2015**, *112*, 11353–11358. [CrossRef]
49. Wang, S.; Liu, X.; Liu, H.; Zhang, L.; Guo, Y.; Yu, S.; Wozniak, D.J.; Ma, L.Z. The exopolysaccharide Psl-eDNA interaction enables the formation of a biofilm skeleton in *Pseudomonas aeruginosa*. *Environ. Microbiol. Rep.* **2015**, *7*, 330–340. [CrossRef]
50. Mulcahy, H.; Charron-Mazenod, L.; Lewenza, S. Extracellular DNA chelates cations and induces antibiotic resistance in *Pseudomonas aeruginosa* biofilms. *PLoS Pathog.* **2008**, *4*, e1000213. [CrossRef]
51. Wilton, M.; Charron-Mazenod, L.; Moore, R.; Lewenza, S. Extracellular DNA acidifies biofilms and induces aminoglycosaside resistance in *Pseudomonas aeruginosa*. *Antimicrob. Agents Chemother.* **2016**, *60*, 544–553. [CrossRef]
52. Sharma, D.; Misba, L.; Khan, A.U. Antibiotics versus biofilms: An emerging battleground in microbial communities. *Antimicrob. Resist. Infect. Control* **2019**, *8*, 76. [CrossRef]
53. van Schaik, E.J.; Giltner, C.L.; Audette, G.F.; Keizer, D.W.; Bautista, D.L.; Slupsky, C.M.; Sykes, B.D.; Irvin, R.T. DNA binding: A novel function of *Pseudomonas aeruginosa* Type IV Pili. *J. Bacteriol.* **2005**, *187*, 1455–1464. [CrossRef]
54. Sanderson, H.; Fricker, C.; Brown, R.S.; Majury, A.; Liss, S.N. Antibiotic resistance genes as an emerging environmental contaminant. *Environ. Rev.* **2016**, *24*, 205–218. [CrossRef]

55. Slipko, K.; Reif, D.; Wögerbauer, M.; Hufnagl, O.P.; Krampe, J.; Kreuzinger, N. Removal of extracellular free DNA and antibiotic resistance genes from water and wastewater by membranes ranging from microfiltration to reverse osmosis. *Water Res.* **2019**, *164*, 114916. [CrossRef] [PubMed]
56. Turnbull, L.; Toyofuku, M.; Hynen, A.L.; Kurosawa, M.; Pessi, G.; Petty, N.K.; Osvath, S.R.; Ca'rcamo-Oyarce, G.; Gloag, E.S.; Shimoni, R.; et al. Explosive cell lysis as a mechanism for the biogenesis of bacterial membrane vesicles and biofilms. *Nat. Commun.* **2016**, *7*, 11220. [CrossRef]
57. Yu, W.; Hallinen, K.M.; Wood, K.B. Interplay between antibiotic efficacy and druginduced lysis underlies enhanced biofilm formation at subinhibitory drug concentrations. *Antimicrob. Agents Chemother.* **2018**, *62*, e01603-17. [CrossRef] [PubMed]
58. Tahrioui, A.; Duchesne, R.; Bouffartigues, E.; Rodrigues, S.; Maillot, O.; Tortuel, D.; Hardouin, J.; Taupin, L.; Groleau, M.C.; Dufour, A.; et al. Extracellular DNA release, quorum sensing, and PrrF1/F2 small RNAs are key players in *Pseudomonas aeruginosa* tobramycin-enhanced biofilm formation. *NPJ Biofilms Microbiomes* **2019**, *5*, 15. [CrossRef] [PubMed]
59. Liu, S.-S.; Qu, H.-M.; Yang, D.; Hu, H.; Liu, W.-L.; Qiu, Z.-G.; Hou, A.-M.; Guo, J.; Li, J.-W.; Shen, Z.-Q.; et al. Chlorine disinfection increases both intracellular and extracellular antibiotic resistance genes in a full-scale wastewater treatment plant. *Water Res.* **2018**, *136*, 131–136. [CrossRef] [PubMed]
60. Siedenbiedel, F.; Tiller, J.C. Antimicrobial polymers in solution and on surfaces: Overview and functional principles. *Polymers* **2012**, *4*, 46–71. [CrossRef]
61. Carmona-Ribeiro, A.M.; de Melo Carrasco, L.D. Cationic antimicrobial polymers and their assemblies. *Int. J. Mol. Sci.* **2013**, *14*, 9906–9946. [CrossRef]
62. Strassburg, A.; Kracke, F.; Wenners, J.; Jemeljanova, A.; Kuepper, J.; Petersen, H.; Tiller, J.C. Nontoxic, hydrophilic cationic polymers—Identified as class of antimicrobial polymers. *Macromol. Biosci.* **2015**, *15*, 1710–1723. [CrossRef] [PubMed]
63. Krumm, C.; Trump, S.; Benski, L.; Wilken, J.; Oberhaus, F.; Köller, M.; Tiller, J.C. Fast-acting antibacterial, self-deactivating polyionene esters. *ACS Appl. Mater. Interfaces* **2020**, *12*, 21201–21209. [CrossRef]
64. Gilbert, P.; Moore, L.E. Cationic antiseptics: Diversity of action under a common epithet. *J. Appl. Microbiol.* **2005**, *99*, 703–715. [CrossRef] [PubMed]
65. Timofeeva, L.; Kleshcheva, N. Antimicrobial polymers: Mechanism of action, factors of activity, and applications. *Appl. Microbiol. Biotechnol.* **2011**, *89*, 475–492. [CrossRef] [PubMed]
66. Moore, K.; Gray, D. Using PHMB antimicrobial to prevent wound infection. *Wounds UK* **2007**, *3*, 96–102.
67. Kaehn, K. Polyhexadine: A safe and highly effective biocide. *Skin Pharmacol. Physiol.* **2010**, *23*, 7–16. [CrossRef] [PubMed]
68. Oulè, M.K.; Azinwi, R.; Bernier, A.M.; Kablan, T.; Maupertuis, A.M.; Mauler, S.; Koffi-Nevry, R.; Dembèlè, K.; Forbes, L.; Diop, L. Polyhexamethylene guanidine hydrochloride-based disinfectant: A novel tool to fight meticillin-resistant *Staphylococcus aureus* and nosocomial infections. *J. Med. Microbiol.* **2008**, *57*, 1523–1528. [CrossRef] [PubMed]
69. Zhou, Z.; Wei, D.; Guan, Y.; Zheng, A.; Zhong, J.-J. Extensive in vitro activity of guanidine hydrochloride polymer analogs against antibiotics-resistant clinically isolated strains. *Mater. Sci. Eng.* **2011**, *31*, 1836–1843. [CrossRef]
70. Choi, H.; Kim, K.-J.; Lee, D.J. Antifungal activity of the cationic antimicrobial polymer-polyhexamethylene guanidine hydrochloride and its mode of action. *Fungal Biol.* **2017**, *121*, 53–60. [CrossRef]
71. Zhang, Y.; Jiang, J.; Chen, Y. Synthesis and antimicrobial activity of polymeric guanidine and biguanide salts. *Polymer* **1999**, *40*, 6189–6198. [CrossRef]
72. Caballero Gómez, N.; Abriouel, H.; Grande, J.; Pulido, R.P.; Gálvez, A. Combined treatments of enterocin AS-48 with biocides to improve the inactivation of methicillin-sensitive and methicillin-resistant *Staphylococcus aureus* planktonic and sessile cells. *Int. J. Food Microbiol.* **2013**, *163*, 96–100. [CrossRef]
73. Zhou, Z.; Wei, D.; Lu, Y. Polyhexamethylene guanidine hydrochloride shows bactericidal advantages against ESKAPE bacteria. *Biotechnol. Appl. Biochem.* **2015**, *62*, 268–274. [CrossRef]
74. Chindera, K.; Mahato, M.; Sharma, A.K.; Horsley, H.; Kloc-Muniak, K.; Kamaruzzaman, N.F.; Kumar, S.; McFarlane, A.; Stach, J.; Bentin, T.; et al. The antimicrobial polymer PHMB enters cells and selectively condenses bacterial chromosomes. *Sci. Rep.* **2016**, *6*, 23121. [CrossRef] [PubMed]
75. Habtewold, T.; Duchateau, L.; Christophides, G.K. Flow cytometry analysis of the microbiota associated with the midguts of vector mosquitoes. *Parasites Vectors* **2016**, *9*, 167. [CrossRef] [PubMed]
76. Zhou, Z.; Wei, D.; Guan, Y.; Zheng, A.; Zhong, J.-J. Damage of *Escherichia coli* membrane by bactericidal agent polyhexamethylene guanidine hydrochloride: Micrographic evidences. *J. Appl. Microbiol.* **2010**, *108*, 898–907. [CrossRef] [PubMed]
77. Kamenieva, T.M.; Tarasyuk, O.P.; Derevianko, K.Y.; Aksenovska, O.A.; Shybyryn, O.V.; Metelytsia, L.O.; Rogalsky, S.P. Antioxidant activity of polymeric biocide polyhexamethylene guanidine hydrochloride. *Catal. Petrochem.* **2020**, *30*, 73–82. [CrossRef]
78. Sambrook, J.; Fritsch, E.R.; Maniatis, T. *Molecular Cloning: A Laboratory Manual*, 2nd ed.; Cold Spring Harbor Laboratory Press: Cold Spring Harbor, NY, USA, 1989.
79. Azeredo, J.; Azevedo, N.F.; Briandet, R.; Cerca, N.; Coenye, T.; Costa, A.R.; Desvaux, M.; Di Bonaventura, G.; Hébraud, M.; Jaglic, Z.; et al. Critical review on biofilm methods. *Crit. Rev. Microbiol.* **2017**, *43*, 313–351. [CrossRef]
80. Moshynets, O.; Boretska, M.; Spiers, A.J. From Winogradsky's column to contemporary research using bacterial microcosms. In *Microcosms: Ecology, Biological Implications and Environmental Impact*; Harris, C.C., Ed.; Nova Publisher: Hauppauge, NY, USA, 2013; pp. 1–27.

81. Rymar, S.Y.; Ruban, T.A.; Irodov, D.M.; Kordium, V.A. Expression and secretion of human recombinant LIF by genetically modified mammalian cells. *Biopolym. Cell* **2011**, *27*, 53–58. [CrossRef]
82. DeLong, E.F. Archaea in coastal marine environments. *Proc. Natl. Acad. Sci. USA* **1992**, *89*, 5685–5689. [CrossRef]
83. Coll, M.; Aymami, J.; Van Der Marel, G.A.; Van Boom, J.H.; Rich, A.; Wang, A.H.-J. Molecular structure of the netropsin-D(CGCGATATCGCG) complex: DNA confirmation in an alternating AT segment; conformation 2. *Biochemistry* **1989**, *28*, 310–320. [CrossRef]
84. *Dassault Systèmes BIOVIA, Discovery Studio Visualizer, v4.0.100.13345*; Dassault Systèmes: San Diego, CA, USA, 2021.
85. Sanner, M.F. Python: A programming language for software integration and development. *J. Mol. Graph. Model.* **1999**, *17*, 57–61. [PubMed]
86. ChemAxon. Marvin Sketch 5.3.735. 2017. Available online: http://www.chemaxon.com (accessed on 1 March 2021).
87. James, J.P. MOPAC2016; Stewart Computational Chemistry: Colorado Springs, CO, USA. Available online: http://OpenMOPAC.net (accessed on 1 March 2021).
88. Halgren, T.A. MMFF VI. MMFF94s option for energy minimization studies. *J. Comput. Chem.* **1999**, *20*, 720–729. [CrossRef]
89. Trott, O.; Olson, A.J. AutoDock Vina: Improving the speed and accuracy of docking with a new scoring function, efficient optimization, and multithreading. *J. Comput. Chem.* **2010**, *31*, 455–461. [CrossRef] [PubMed]

Анотація: *Вибір ефективних біоцидів, які використовуються в рутинній лікарняній практиці, повинен враховувати роль дезінфікуючих засобів у підтримці та розвитку місцевого резистому та як вони можуть впливати на перенесення генів резистентності до антибіотиків у лікарняній мікробній популяції. Наразі мало інформації як різні біоциди сприяють вивільненню еДНК, що може сприяти ГПГ та подальшому їхньому зберіганню в навколишньому середовищі. В роботі ми дослідили чим відрізняються біоциди по дії на еДНК із зрілих біоплівок двох опортуністичних модельних штамів P. aeruginosa ATCC 27853 (PA) і S. aureus ATCC 25923 (SA). Дія чотирьох груп біоцидів, зокрема, спиртів, перекису водню, сполук четвертинного амонію та полімерний біоцид полігексаметиленгуанідин гідрохлорид (PHMG-Cl), досліджували із використанням біоплівок PA та SA. Більшість біоцидів, за винятком PHMG-Cl і 70% етанолу, викликали значне вивільнення еДНК. Було показано, що PHMG-Cl блокує розвиток біоплівки при використанні в концентраціях 0,5% і 0,1%. Це може бути пов'язано з утворенням комплексів ДНК–PHMG-Cl. За допомогою аналізів молекулярного докінгу очікується зв'язування PHMG-Cl з парами основ A-T. Було виявлено, що PHMG-Cl зв'язується з високомолекулярною ДНК і плазмідною ДНК, інактивація еДНК на поверхнях продовжується навіть після 4 тижнів після обробки поверхні. PHMG-Cl також ефективно інактивував еДНК у вигляді гену стійкості до антибіотиків, пов'язаного з біоплівкою, що було знайдено в еДНК полірезистентного штаму* Klebsiella. *PHMG-Cl демонструє потенціал полімерного біоциду як нової поверхнево-активної речовини для боротьби з поширенням стійкості до антибіотиків у лікарняних умовах.*

5.3. Розробка нових матеріалів із анти-біоплівковою та анти-ДНК діями для вирішення проблем персистування генів стійкості до антибіотиків у госпітальному середовищі.

Утворення бактеріальних біоплівок на контактних поверхнях матеріалів, що контактують з водою є важливою і складною проблемою для багатьох систем, таких як, наприклад, водопровідні та каналізаційні трубопроводи, гідропоніка, сантехніка, харчова упаковка, медичні пластикові вироби, медичне обладнання тощо. Наприклад, медичні пристрої можуть мати мікробне забруднення на поверхнях. Зокрема, такі контамінації небезпечними бактеріями, грибами або вірусами може призводити до виникнення спалахів нозокоміальних опортуністичних інфекцій.

Відомо, що лікарняні матеріали, меблі та дрібні предмети, такі як стетоскопи, мобільні телефони та клавіатури комп'ютерів можуть бути джерелом внутрішньолікарняних інфекцій (156-162). Ще однієюпроблемою є інфекційне ураження імплантів та розвиток імплант-асоційованої інфекції.

Ріст бактеріальних біоплівок також створює проблеми для немедичної промисловості. Часті проблемами контамінації притаманні технологічним поверхням в індустріях обробки харчових, молочних, вино-матеріалів, в системах стічних вод, що спричиняє засміченню труб, зниженню ефективності теплообміну процесів і, зрештою, псування їжі. Нарешті, мікроорбрастання металевих поверхонь сприяють мікробіологічно-індукованій корозії, яка також пов'язана з біоплівками.

Отже, контроль розвитку біоплівки на поверхнях є важливою проблемою для багатьох індустрій. Поточні рішення, як правило, спираються на регулярну хімічну інактивацію поверхонь або додавання антибіотиків до матеріалів. Однак такі покриття часто завантажені гостротоксичними хімічними речовинами або хімічними речовинами з високою стійкістю та потенціалом до накопичення в екосистемах, що призводить до хронічного пошкодження відповідних екосистем та впливає на здоров'я людини. Саме тому нові підходи в модифікації матеріалів для зниження їхньої здатності до біообрастання може суттєво покращити екологічність матеріалів та знизити вірогідність розвитку госпітальних інфекційних ускладнень.

Основні результати, отримані в цьому підрозділі дисертації опубліковано в роботах автора (165-167).

International Journal of
Molecular Sciences

MDPI

Article

Antibiofilm Activity of Polyamide 11 Modified with Thermally Stable Polymeric Biocide Polyhexamethylene Guanidine 2-Naphtalenesulfonate

Olena Moshynets [1,*], Jean-François Bardeau [2], Oksana Tarasyuk [3], Stanislav Makhno [4], Tetiana Cherniavska [4], Oleg Dzhuzha [3], Geert Potters [5,6] and Sergiy Rogalsky [3,*]

1 Institute of Molecular Biology and Genetics of NAS of Ukraine, 03143 Kyiv, Ukraine
2 Institut des Molécules et Matériaux du Mans, UMR CNRS 6283, Université du Mans, 72085 Le Mans, France; jean-francois.bardeau@univ-lemans.fr
3 V. P. Kukhar Institute of Bioorganic Chemistry and Petrochemistry of NAS of Ukraine, 02160 Kyiv, Ukraine; oksanatarasyuk@bigmir.net (O.T.); dzhuzha.oleg@gmail.com (O.D.)
4 Chuiko Institute of Surface Chemistry of NAS of Ukraine, 03680 Kyiv, Ukraine; stmax@ukr.net (S.M.); t-cherniavska@ukr.net (T.C.)
5 Antwerp Maritime Academy, Noordkasteel Oost 6, 2030 Antwerp, Belgium; geert.potters@hzs.be
6 University of Antwerp, Groenenborgerlaan 171, 2020 Antwerp, Belgium
* Correspondence: moshynets@gmail.com (O.M.); sergey.rogalsky@gmail.com (S.R.); Tel.: +38-044-5594622 (S.R.)

Received: 9 December 2018; Accepted: 8 January 2019; Published: 16 January 2019

Abstract: The choice of efficient antimicrobial additives for polyamide resins is very difficult because of their high processing temperatures of up to 300 °C. In this study, a new, thermally stable polymeric biocide, polyhexamethylene guanidine 2-naphtalenesulfonate (PHMG-NS), was synthesised. According to thermogravimetric analysis, PHMG-NS has a thermal degradation point of 357 °C, confirming its potential use in joint melt processing with polyamide resins. Polyamide 11 (PA-11) films containing 5, 7 and 10 wt% of PHMG-NS were prepared by compression molding and subsequently characterised by FTIR spectroscopy. The surface properties were evaluated both by contact angle, and contactless induction. The incorporation of 10 wt% of PHMG-NS into PA-11 films was found to increase the positive surface charge density by almost two orders of magnitude. PA-11/PHMG-NS composites were found to have a thermal decomposition point at about 400 °C. Mechanical testing showed no change of the tensile strength of polyamide films containing PHMG-NS up to 7 wt%. Antibiofilm activity against the opportunistic bacteria *Staphylococcus aureus* and *Escherichia coli* was demonstrated for films containing 7 or 10 wt% of PHMG-NS, through a local biocide effect possibly based on an influence on the bacterial eDNA. The biocide hardly leached from the PA-11 matrix into water, at a rate of less than 1% from its total content for 21 days.

Keywords: polyamide 11; antibacterial; polymeric biocide; thermal stability; biofilm

1. Introduction

Produced from a renewable source, polyamide 11 (PA-11) is a unique thermoplastic polymer with excellent functional properties, combining high ductility and mechanical strength, dimensional stability, low density, excellent abrasion and fatigue resistance, a low friction coefficient, high barrier properties and resistance to many types of chemicals. Many industries around the world (automotive, transport, textile, oil and gas, wire and cables, and electronics) have been using PA-11 for decades [1]. PA-11 powder coatings were developed to protect metal parts from corrosion, particularly for the protection of steel in the fluid transfer industry, for example in pipes and fittings in water treatment

plants, water/hydrocarbon transportation pipelines, transport and building constructions, medical equipment, office furniture, and many other appliances [2].

It is known that the surface of polyamide plastics can be colonised rapidly by bacteria, fungi and algae, especially in a humid environment, which is then followed by the formation of biofilms/fouling. Moreover, the emerging biofilm causes contamination, staining, odours and eventually deterioration of the mechanical properties of the plastic because of the degradation of the polymer, utilising the carbon in the course of development as a nutrient [3–5]. Biofilm formation starts with the deposition of different microorganisms on the surface of the material, followed by growth and spreading of the colonies forming a highly complex structure, culminating in microbial evolution and adaptation towards a stronger resistance to antibiotics and biocides, the appearance of super-biofilm with super-mucous and super-adhesive opportunistic strains, etc. [6–10]. Bacteria foul medical devices and implants, e.g., polymeric materials used as internal or invasive devices such as catheters, components of cardiac pacemakers, artificial heart valves and joints. The formed biofilm can initiate degradation of the material, as well as hospital-acquired infections, for example of small medical devices, because of a high concentration of microorganisms. These implant-associated biofilms are often difficult to remove, even after cleaning the implants pre-operatively with oxidisers and detergents or treating them with antibiotics, and in certain situations replacement surgery may be required [6].

The introduction of antimicrobial agents into the base polymer of these articles is considered the most efficient approach to prevent the growth of biofilms on their surface. A wide variety of organic and inorganic biocides is available, whether synthetic or nature-inspired [11–15]. The choice of appropriate biocides for PA-11 is strongly limited because of the high processing temperatures of the polymer, up to 300 °C. Currently, silver-based compounds are the most widely used antimicrobial additives for PA-11 because of their excellent thermal stability [16,17], as well as their low toxicity to human cells [18]. Silver nanoparticles are regarded as the most promising biocides for polyamide resins since their high surface area ensures an efficient release of Ag^+ species into the medium [19–21]. However, it should be noted that silver nanoparticles are hard to disperse in a polymer matrix because of their strong aggregation ability [16,17,21]. Moreover, silver ions are known to interact with polyamides during melt processing and cause an undesirable discolouration of polymer articles. Therefore, many antimicrobial formulations contain silver-based compounds intercalated into inorganic anion exchangers or encapsulated using soluble ceramics [16,17].

Thus, there is a growing demand for the development of low-cost and low toxic antimicrobial agents that combine good compatibility and processability with polyamide resins, as well as high leaching resistance from polymer matrix.

Copper and its compounds have also emerged as promising antimicrobial additives for polyamides, being much cheaper than silver. Thus, a commercially available ionic copper-based additive, Plasticopper, was incorporated into the PA-11 matrix during the polymer processing stage [22]. The incorporation of 5% and 10% copper was found to have a reinforcing effect on the composites and did not adversely affect their mechanical performance. These composite systems showed long-term antimicrobial activity against Gram-negative bacteria (*E. coli*) with a reduction of the bacterial population of more than 99.99% [22].

Nowadays, cationic polymers are being considered as a new generation of biocides because of their enhanced antimicrobial activity, as well as their low toxicity to human cells, compared to common low molecular cationic surfactants [23,24]. In particular, polyhexamethylene guanidine (PHMG) salts, comprising guanidinium cations in the main chain, are receiving increasing attention since they display a broad range of antimicrobial activity against bacteria, fungi and viruses [25–31], as well as antifouling activity against macrofoulers in an aquatic environment [32,33]. It should also be noted that PHMG salts showed a much lower acute toxicity than copper-based biocides [33]. The high activity of guanidinium-based polymeric biocides against microorganisms is caused by the presence of multiple positive charges within a single molecule that are able to compensate the negative charges present on the outer cell membranes of microbes. Because of these strong electrostatic interactions,

PHMG is able to attack the cellular envelope, and subsequently associates itself with the head groups of the acidic phospholipids. The presence of hydrophobic aliphatic chains in the PHMG backbone ensures a better partition to the hydrophobic regions of the phospholipid membrane, resulting in a change of membrane permeability and lethal leakage of cytoplasmic materials [27–31].

Poorly water-soluble PHMG salts such as PHMG stearate, PHMG sulfanilate, or PHMG dodecylbenzenesulfonate (PHMG-DBS) have been reported as efficient antimicrobial additives for polycaprolactone [34], polylactide [35], polyamides [36,37] and silicones [38]. PHMG-DBS was found to have sufficient thermal stability to be melt processed with PA-11 and PA-12 resins by conventional methods [36,37]. PA-11 films containing 5–7 wt% of PHMG-DBS showed a high activity against *E. coli*, as well as an excellent resistance against leaching of the polymeric biocide [37].

Another successful approach involves the intercalation of the cationic polymer (partially aminated poly(vinylbenzyl chloride)) into a smectic clay, montmorillonite, to produce a modified organoclay containing 33 wt% of polymeric biocide [39]. Polymerically modified organoclay was found to have sufficient thermal stability for joint processing with PA-6 resin by melt extrusion. The obtained nanocomposites were active against both Gram-negative *E. coli* and Gram-positive *S. aureus* bacteria and demonstrated up to a 2-log reduction in the viable cells adhering to the material surface at an organoclay content of 5 wt%. The mode of antimicrobial action of this material was determined as contact-active because the biocide does not leach out [39].

Despite the evidence for a pronounced antibacterial and antifungal activity of contact-active polyamide composites, their activity against biofilms has not yet been studied. It is worth noting that antibiofilm characteristics do not always parallel antibacterial characteristics. There are several examples of compounds that were added to polymers and possessed antibacterial characteristics, but could not decrease fouling, and vice versa [40–42]. In the present study, a new thermally stable hydrophobic cationic polymer, polyhexamethylene guanidine 2-naphtalene sulfonate (PHMG-NS), was synthesised. In contrast to the previously reported polymeric biocide PHMG-DBS, which sticks together during storage, PHMG-NS forms a fine powder that makes it a good candidate to be applied in PA-11 based powder coating formulations. The aim of our research was to investigate the antibiofilm activity of PA-11 films modified with PHMG-NS biocide against the biofilm-forming model bacterial strains, opportunistically pathogenic *E. coli* K12 and *S. aureus* ATCC 25923.

2. Results and Discussion

2.1. FTIR Analysis of PA-11/PHMG-NS Films

Infrared spectroscopy was employed both to identify the presence of PHMG-NS inside the polymer films and reveal potential interactions between PA-11 and the biocide. Figure 1a shows infrared spectra of PHMG-Cl and PHMG-NS in the 400–4000 cm^{-1} region and Figure 1b shows infrared spectra in the 960–1830 cm^{-1} region of PA-11 and PA-11/PHMG-NS films containing 5%, 7% and 10% of PHMG-NS. As previously described for PHMG-Cl, which was the precursor compound for making PHMG-NS, the very broad bands in the region of 2600–3700 cm^{-1} are attributed to the CH_2, NH_2, and OH stretching vibrations [33]. The modification of PHMG-Cl to PHMG-NS does not change the position of vibrational modes, whose maxima are found at approximately 2856 and 2932 cm^{-1}, respectively, and attributed to the symmetric $\nu_s(CH_2)$ and asymmetric $\nu_{as}(CH_2)$ stretching vibrations of the methylene groups. However, the bands attributed to the symmetric $\nu_s(NH_2)$ and asymmetric $\nu_{as}(NH_2)$ stretching vibrations of amine groups shift to higher wavenumbers at about 3194 and 3313 cm^{-1}. The IR spectra show also strong absorption bands between 1500 and 1800 cm^{-1}, characteristic of both the C=N stretching and the NH_2 scissoring modes. The central position of these broad bands does not shift between PHMG-Cl and PHMG-NS. The strong absorption bands observed at 1177, 1090, 1030 and 673 cm^{-1} can be assigned to the sulphonic group of the 2-naphthalenesulfonate. Two of these later vibrational modes can easily be observed at 1092 cm^{-1} and 1032 cm^{-1} in Figure 1b (dashed lines) with PA-11/PHMG-NS films containing 5%, 7% and 10% of PHMG-NS, thus confirming

the presence of the biocide in the films. Overall, the IR spectra of the modified films are similar to each other revealing that the introduction of PHMG-NS does not significantly influence the vibrational bands of PA-11. However, a noticeable change can be observed in Figure 1b: the small intensity band assigned to the carbonyl (C=O) stretching vibrations for PA-11 (at 1727 cm^{-1}) shifts toward higher wavenumbers as a function of the PHMG-NS content and reaches 1734 cm^{-1} for films containing 10% of PHMG-NS (Figure 1b, black arrow). This feature suggests a modification of the specific environment of the C=O group. The guanidinium cation is known to participate in direct hydrogen bonding with backbone carbonyl groups of proteins [43], which suggests a similar interaction between the guanidinium cations of PHMG-NS and the amide carbonyl groups of PA-11.

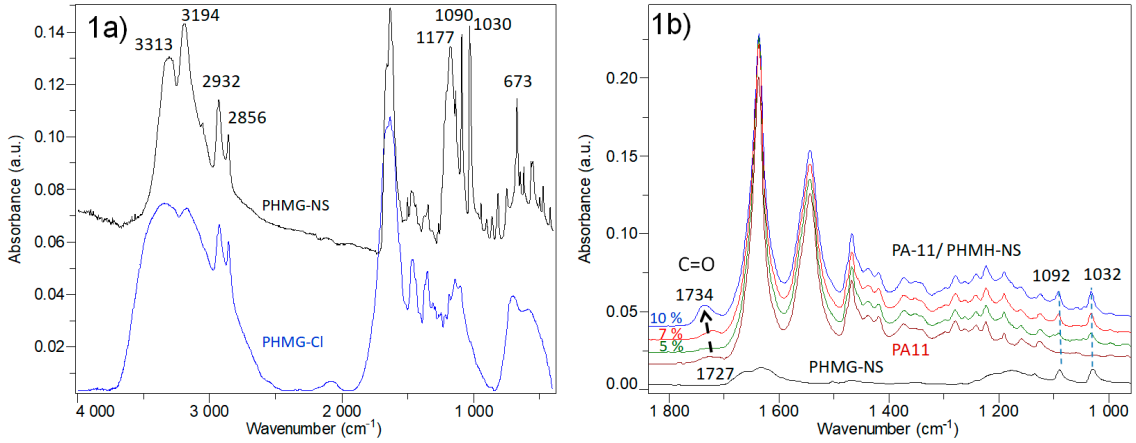

Figure 1. IR spectra: (**a**) PHMG-Cl and PHMG-NS; and (**b**) PHMG-NS, PA-11 and PA-11/PHMG-NS film with 5%, 7% and 10% of PHMG-NS.

2.2. Surface Properties of PA-11/PHMG-NS Films

According to the contact angle measurements data, an introduction of 5 wt% of PHMG-NS into a PA-11 film led to an enhanced hydrophilicity of the surface, which can be attributed to the increase of the polar functional groups on the polyamide surface. However, further increase of PHMG-NS content had little impact on the contact angle value (Table 1). The results of the electrophysical study of the PA-11/PHMG-NS films indicate a sharp increase of the positive surface charge density at a PHMG-NS content of 7 wt% and more (Table 1). Probably, it can be explained by the formation of an uncompensated positive charge of the guanidinium cations at the polymer surface because of specific interactions between the hydrophobic fragments of the PHMG-NS and the PA-11 matrix. It should be noted that both the improved hydrophilicity and the positive charge of the polymer surface are considered to be important factors that determine the antimicrobial efficacy [44–46].

Table 1. Surface properties of PA-11/PHMG-NS films.

Sample	Contact Angle (Degree)	Surface Charge Density (C/cm^2)
PA-11	80 ± 2	$(0.47 \pm 0.02) \times 10^{-10}$
PA-11/PHMH-NS (5%)	70 ± 2	$(1.2 \pm 0.1) \times 10^{-10}$
PA-11/PHMH-NS (7%)	68 ± 2	$(6.5 \pm 0.3) \times 10^{-10}$
PA-11/PHMH-NS (10%)	68 ± 2	$(27 \pm 1) \times 10^{-10}$

2.3. Mechanical and Thermal Properties of PA-11/PHMG-NS Composites

It has been established that inorganic biocides have a reinforcing effect on the polyamide matrix caused by the formation of strong interfacial interactions, leading to a reduction in the mobility of polymer chains [22,39]. For example, heterogeneous PA-11/Cu antimicrobial nanocomposites showed

an increase of the yield strength from 45 to 54 MPa when 2–10% of a copper additive was introduced [22]. The introduction of 5% of cationic biocide intercalated organoclay into PA-6 improved the yield strength by 44.6% [39].

The polymeric biocide PHMG-NS forms homogeneous composites with PA-11 because of its low melting temperature, as well as its good compatibility with the polymer matrix. Tensile testing of PA-11/PHMG-NS samples was performed to evaluate the effect of the antimicrobial additive on the mechanical properties of polyamide. PA-11 films containing 5% and 7% of PHMG-NS have tensile strength values similar to pure polyamide. A further increase of the polymeric biocide content to 10% led to a deterioration of the mechanical properties of the material (Table 2).

Table 2. Mechanical properties of PA-11/PHMG-NS composites.

Sample	Tensile Strength, MPa	Elongation at Break, %
PA-11	45 ± 2	24 ± 4
PA-11/PHMG-NS (5%)	45 ± 1	25 ± 5
PA-11/PHMG-NS (7%)	43 ± 2	15 ± 3
PA-11/PHMG-NS (10%)	27 ± 2	6 ± 2

The results of the thermal characterisation of the polymeric biocide PHMG-NS, PA-11 and PA-11/PHMG-NS containing 10 wt% of polymeric biocide are summarised in Figure 2 and Table 3. According to the TGA data, PHMG-NS has a thermal decomposition point (which was defined as the temperature of 5% weight loss ($T_{\Delta m}$ = 5%) at 357 °C. The peak mass loss temperature of PHMG-NS is 392 °C (Figure 2a). Pure PA-11 begins to decompose at 425 °C and the maximum rate of thermal degradation was observed at 431 °C (Figure 2b). The PA-11/PHMG-NS composite containing 10 wt% of PHMG-NS is thermally stable to at least 391 °C, and the peak mass loss was found at 465 °C (Figure 2c). At a lower PHMG-NS content, the thermal stability of a composite becomes closer to pure PA-11 (Table 3). Hence, PHMG-NS has excellent thermal stability and can be used for joint melt processing with polyamide resins by conventional methods, as previously reported for the polymeric biocide PHMG-DBS [36,37]. However, PHMG-NS seems to have a broader application range, due to its hydrophobic powder state, whereas PHMG-DBS has a tendency for aggregation during storage. These properties of PHMG-NS allow for its introduction into PA-11-based powder coatings for covering metal articles, by conventional methods using a fluidised bed method of air suspension of a composite material or an electrostatic spraying process.

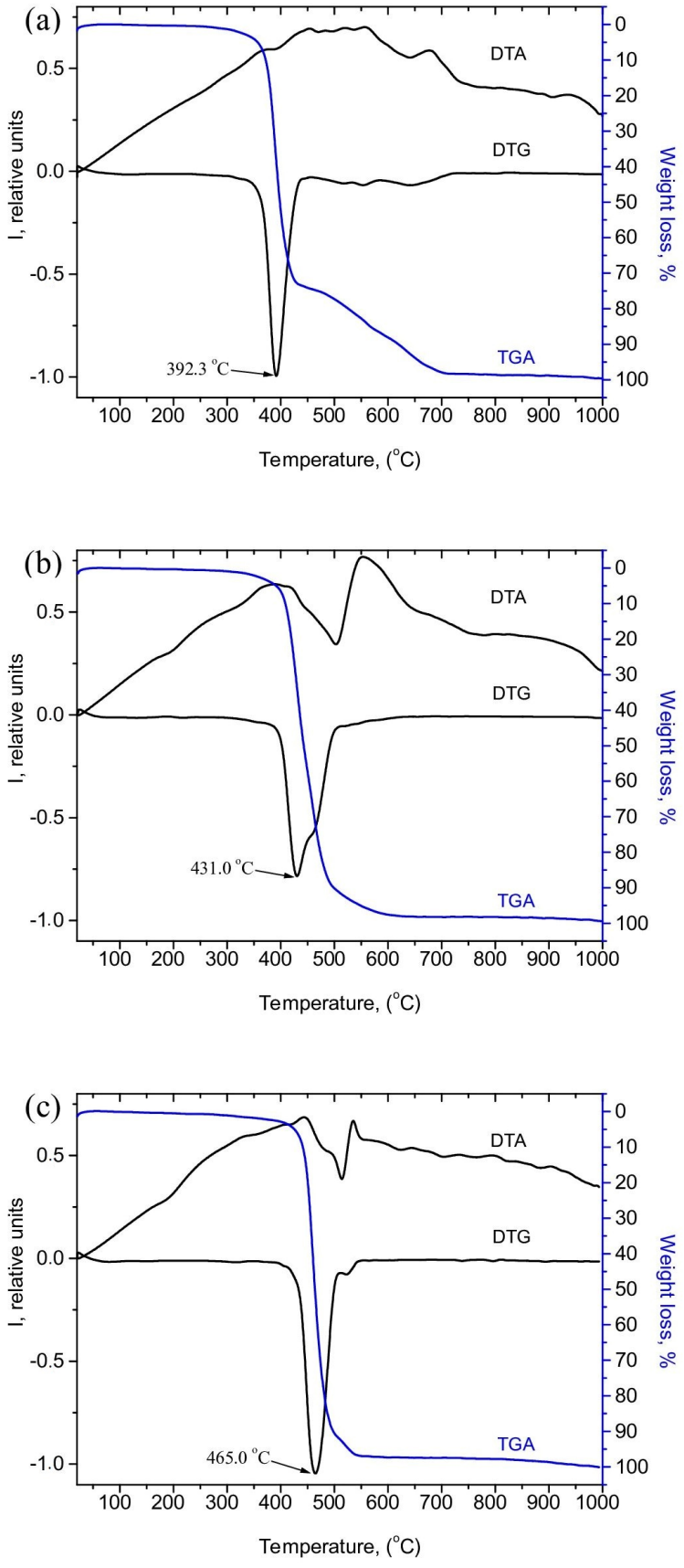

Figure 2. TGA curves in air of: PHMG-NS (**a**); PA-11 (**b**); and PA-11/PHMH-NS (10%) (**c**).

Table 3. TGA data for PHMG-NS and PA-11/PHMG-NS composite*.

Sample	$T_{\Delta m}$ = 5%, °C	$T_{\Delta m}$ = 10%, °C	$T_{\Delta m}$ = 20%, °C	$T_{\Delta m}$ = 50%, °C
PHMG-NS	357	372	381	398
PA-11	425	441	450	463
PA-11/PHMG-NS (5%)	413	434	445	456
PA-11/PHMG-NS (7%)	405	430	442	449
PA-11/PHMG-NS (10%)	391	408	420	443

* Standard error $n \pm 1$.

2.4. Antibiofilm Efficacy of PA-11/PHMG-NS Films

The antibiofilm/antifouling properties of PA-11 modified with the polymeric biocide PHMG-NS were evaluated using two opportunistic biofilm-forming model strains: the Gram-negative *E. coli* K12 belonging to the Enterobacteriaceae family [47] and the Gram-positive *S. aureus* ATCC 25923 [48]. Overall, *E. coli* has been shown to be more resistant to PHMG-containing biocides than the Gram-positive opportunists, such as methicillin-resistant *Staphylococcus aureus* [34,35,38,49]. In addition, its enzymes are more stable when in contact with PHMG derivatives [35]. Principally, both strains were able to form solid–liquid biofilms to the PA-11 films within three days of cultivation. The level of biofilm biomass attached to a PA-11 film containing 5%, 7% or 10% of PHMG-NS was found to be significantly different from those on the control PA-11 films in the Crystal Violet assay (Figure 3) [50]. The biofilm formation decreased approximately three times for the samples containing 7% and 10% of PHMG-NS.

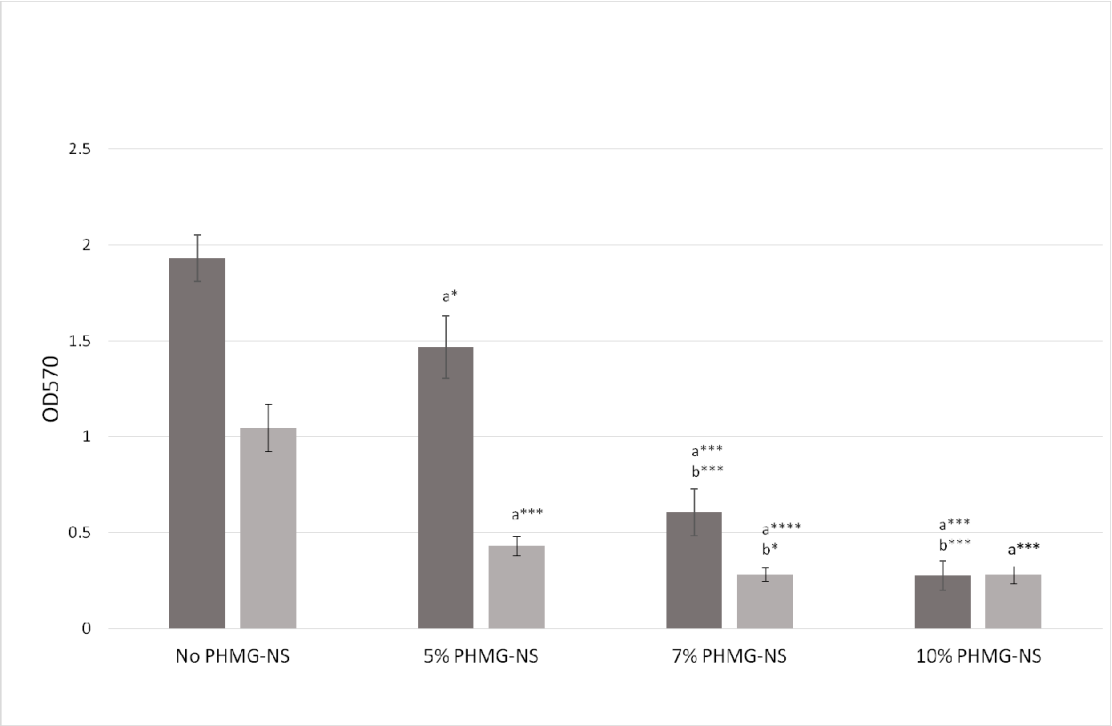

Figure 3. The level of biomass of *E. coli* K12 (dark grey) and *S. aureus* ATCC 25923 (light grey) biofilms formed onto PA-11 films containing 5%, 7% and 10% of PHMG-NS following 72 h of incubation determined by Crystal Violet staining and measured as the optical density at 570 nm (OD570). a: statistical significance compared to control (No PHMG-NS); b: statistical significance compared to 5% PHMG-NS. * $p < 0.05$, *** $p < 0.005$, **** $p < 0.001$.

The Crystal Violet assay measures the overall level of organic layers formed on a plastic surface, containing bacterial cells and numerous organic molecules integrated into the biofilm matrix. Of course, contact-active antimicrobial surfaces are often coated with a layer of dead microbes, to which newly approaching microbes can also adhere and proliferate [51]. Hence, a higher level of Crystal Violet staining does not always correspond to a higher metabolic activity of a biofilm. To assess whether the metabolic activity of the biofilm could be related to the overall number of living bacterial cells in the biofilms, an MTT test was performed in parallel [52]. In this assay, a similar tendency was revealed. All PHMG-NS-containing PA-11 films showed a significant reduction in biofilm metabolic activity (Figure 4). The level of biofilm metabolic activity was 2.5 times lower on the PA-11/PHMG-NS (5%) than on the control PA-11 films. There was a significant difference between the growth under control conditions and the growth on PA-11 containing 5%, 7% and 10% of the polymeric biocide. There was no significant difference between samples containing 5% and 7% PHMG-NS, and between PA-11/PHMG-NS (7%) and PA-11/PHMG-NS (10%). Generally, there was a fivefold decrease in the biofilm metabolic activity for polymer films containing 7% PHMG-NS compared to the control PA-11 films for both bacterial strains ($p < 0.001$ for *E. coli* and $p < 0.01$ for *S. aureus*), and there was almost no metabolic activity on films with 10% PHMG-NS inoculated with *E. coli*.

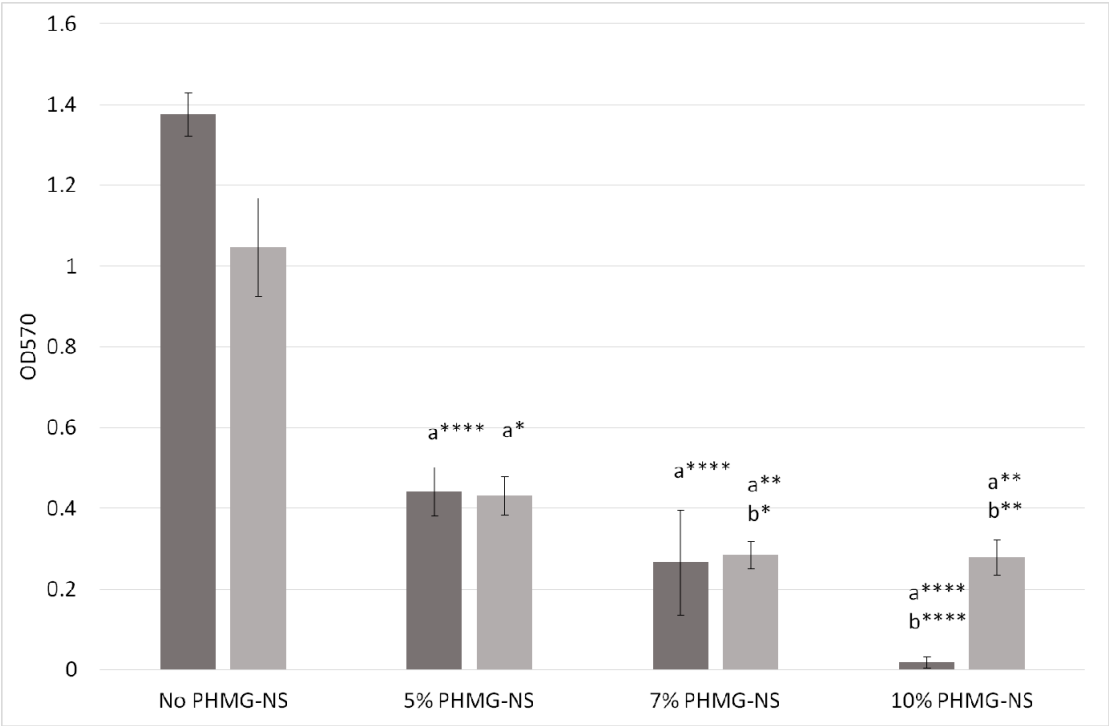

Figure 4. The level of metabolic activity of *E. coli* K12 (dark grey) and *S. aureus* ATCC 25923 (light grey) biofilms formed onto PA-11 films containing 5%, 7% and 10% of PHMG-NS following 72 h of incubation determined by MTT staining and measured as the optical density at 570 nm (OD570). a: statistical significance compared to control (No PHMG-NS); b: statistical significance compared to 5% PHMG-NS. * $p < 0.05$, ** $p < 0.01$, **** $p < 0.001$.

The bacterial toxicity of the PA-11/PHMG-NS films for the planktonic part of the bacterial culture was evaluated by measuring both the optical density and the colony forming units (CFU) count in the overbiofilm layer in 72-h stationary biofilm-forming K12 and ATCC 25923 cultures. There was no significant difference in optical density between any of the four samples (Figure 5) except a minor and possible negligible decrease of ATCC 25923 in the presence of PA-11/PHMG-NS (10%) ($p < 0.05$). The planktonic CFU numbers in the media in contact with the control and 5% PHMG-NS films were, respectively, tenfold and fivefold higher than the CFU of the plankton in contact with

the PA-11/PHMG-NS (10%) and the PA-11/PHMG-NS (7%) films for K12. There was also a tenfold decrease in plankton density in PA-11 films doped with 5% and 7% of PHMG-NS and a fivefold decrease for PA-11/PHMG-NS (10%) compared to control PA-11 for ATCC 25923. However, there was no significant difference in effect between the different polyamide films on the planktonic bacteria in a biofilm-forming culture, suggesting a low release rate of the biocide into the medium in the experimental conditions presented here.

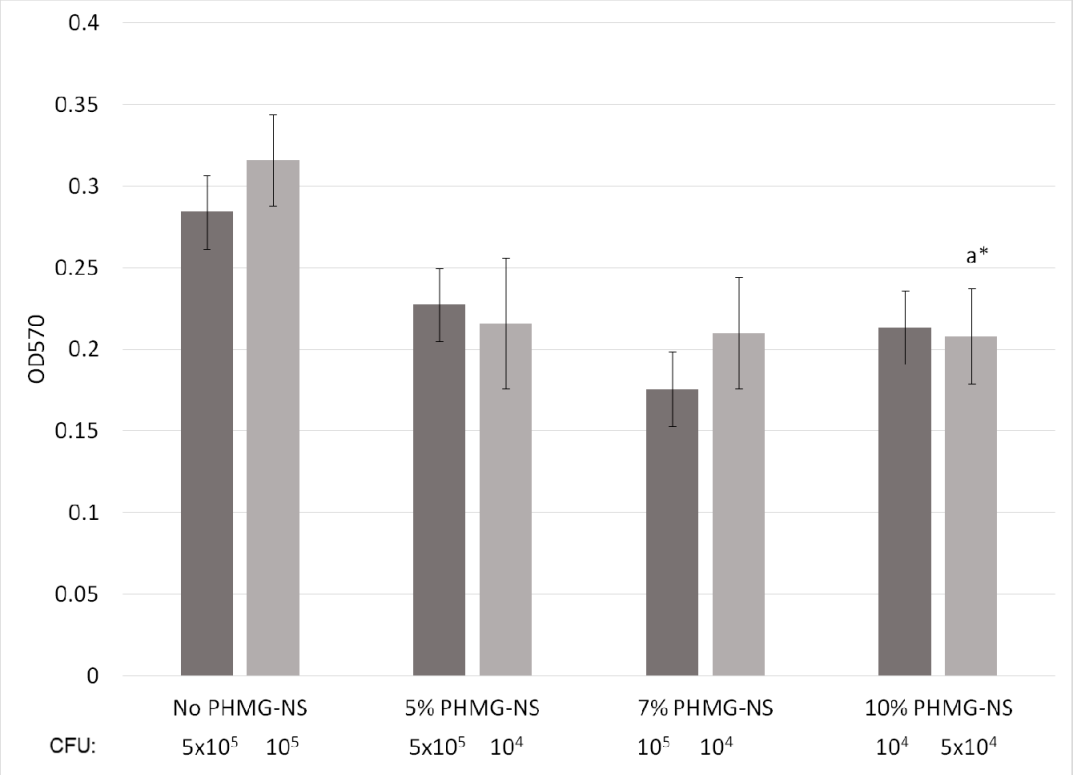

Figure 5. The level of planktonic cell biomass (overbiofilm layer indicated by the optical density at 570 nm (OD570)) of K12 (dark grey) and ATCC 25923 (light grey) in the presence of PA-11 films containing 5%, 7% and 10% of PHMG-NS following 72 h of incubation, correlated with the corresponding CFU counts. a: statistical significance compared to control (No PHMG-NS); * $p < 0.05$.

The behaviour of the planktonic part of the culture raised a question about the antibiofilm properties of the PA-11 films after water exposure. To investigate this, pieces of polymer containing 7% and 10% of PHMG-NS were exposed to water for seven days. The biofilm assay did not show any significantly different antibiofilm properties between the exposed and the non-exposed films.

Despite the absence of any significant effect of the presence of PHMG-NS in the PA-11 on the growth of planktonic cells, visual observation of the 72-h cultures revealed that the biofilm formation on the solid–liquid interface of the microcosms was unexpectedly reduced by the presence of at least 7% of PHMG-NS in the PA-11 films (direct observations). This raises a question: is there any distant effect of non-leaching PHMG-NS onto biofilm formation in a microcosm? Biofilms consist of bacterial cells embedded into a matrix of extracellular polymers composed of polysaccharides, proteins and nucleic acids (mostly DNA) [53]. Extracellular DNA (eDNA) has been known to play quite an important role in the initiation and the development of biofilms of many bacteria [54–57], among which those made by *E. coli* and *S. aureus* [58,59]. eDNA is a negatively charged molecule which might interact with the positively-charged PHMG-NS-containing PA-11. To check this hypothesis, the total eDNA content in the culture was precipitated from the solid–liquid interface biofilms formed after 72 h in the microcosms (Figure 6). There was a significant decrease in eDNA content in the biofilms formed in the presence of PA-11/PHMG-NS (7%) and PA-11/PHMG-NS (10%) for K12 ($p < 0.001$) and in the

presence of only PA-11/PHMG-NS (10%) for ATCC 25923 ($p < 0.05$ compared to the control culture and $p < 0.001$ compared to the 5% PHMG-NS treatment), each time compared to the eDNA amount found in microcosms exposed to control PA-11 and PA-11/PHMG-NS (5%), while there were no such differences in the overbiofilm layer in any of the microcosms (Figure 7). Such a decrease in eDNA in the solid–liquid interface biofilms, in contrast with the constant level in the overbiofilm culture, might suggest that at least one of the antibiofilm mechanisms of PHMG-NS-containing PA-11 is associated with eDNA reduction, which in turn may have an influence on the initial stages of bacterial biofilm formation. Moreover, decreasing the level of eDNA would hypothetically reduce an abundance of resistance genes spread horizontally in a hospital-related environment, as eDNA associated with biofilms has been considered a hotspot for deposition and recombination of antibiotic resistance genes [60,61].

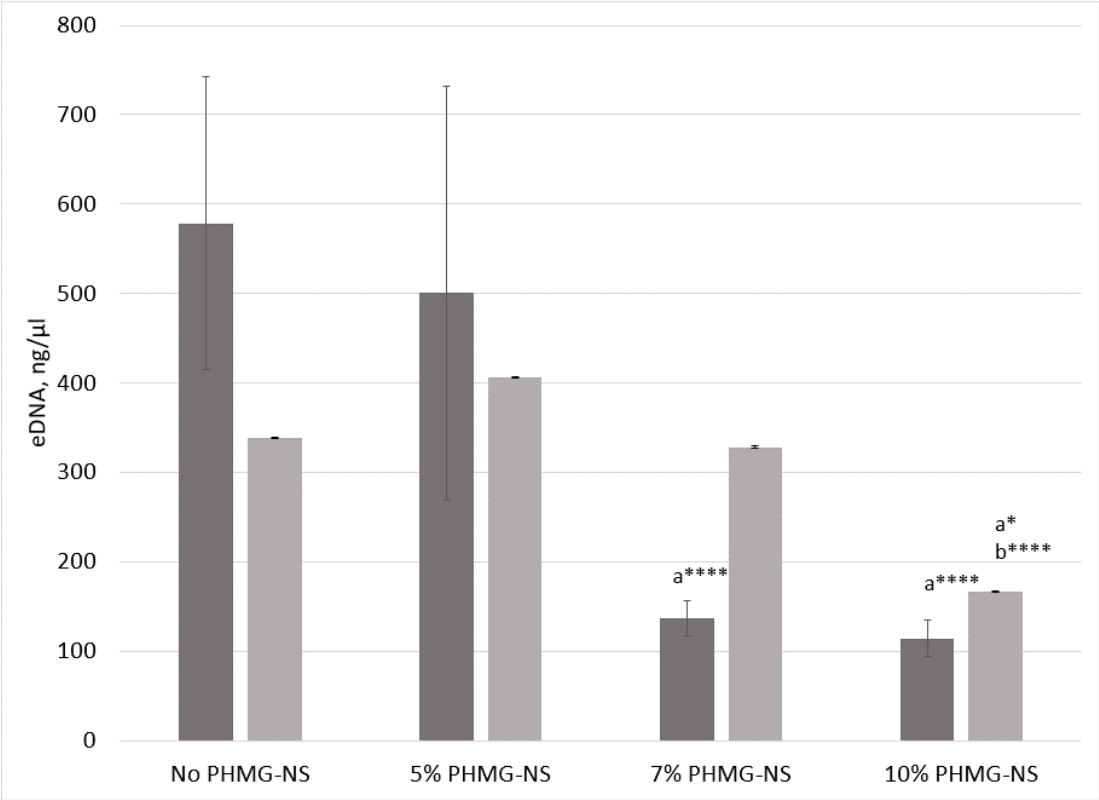

Figure 6. Amount of eDNA precipitated from a biofilm layer (solid-bottom phase) of 72-h-old biofilm-formed K12 (dark grey) and ATCC 25923 (light grey) cultures with PA-11 films containing 5%, 7% and 10% of PHMG-NS. a, statistical significance compared to control (No PHMG-NS); b: statistical significance compared to 5% PHMG-NS. * $p < 0.05$ **** $p < 0.001$.

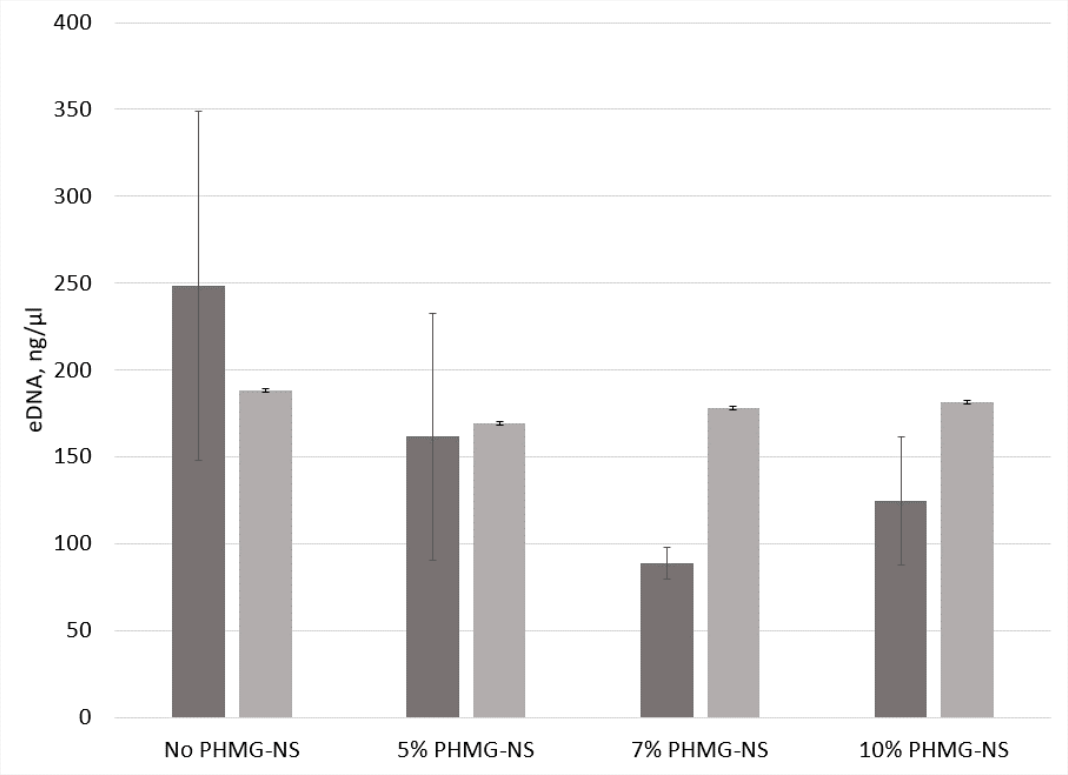

Figure 7. Amount of eDNA precipitated from overbiofilm layer (liquid plankton phase) of 72-h-old biofilms-formed K12 (dark grey) and ATCC 25923 (light grey) cultures with PA-11 films containing 5%, 7% and 10% of PHMG-NS.

It is worth noting that the reported antimicrobial polyamide composites have never before been studied for their activity against biofilms. However, polylactide films containing hydrophobic PHMG salts were found to strongly inhibit the activity of bacterial intracellular dehydrogenases, which prevented the formation of microbial biofilms on the polymer surface [35].

2.5. Leaching Resistance of PHMG-NS from PA-11 Films

The water solubility of PHMG-NS was found to be 0.24 g/L. Thus, given the possibility of a non-covalent association between the PA-11 matrix and PHMG-NS, a gradual release of polymeric biocide into the aqueous medium could be expected. Figure 8 contains UV-visible spectra of PHMG-NS (Curve 1), as well as its precursor PHMG-Cl (Curve 3), which is highly soluble in water. As one can see from these spectra, the characteristic ultraviolet absorption of the guanidyl carbon-to-nitrogen double bond of PHMG allows for a spectrophotometric analysis of either compound in aqueous solutions [62]. However, the adsorption peak of the 2-naphthalene sulfonate anion at 227 nm is the most expressive (Figure 8, Curve 2) and therefore was used for PGMG-NS detection.

After three days of contact with warm water, the PA-11/PHMG-NS (7%) film had lost less than 1% of its biocide contents (Figure 8, Curve 4). No further release of biocide was detected after 7, 14 and 21 days of exposure, which indicates that the biocide-doped polymer is highly resistant to leaching, which in turn is important for the potential durability of the antimicrobial activity of the material. It is worth noting that PA-11 has a much lower water absorption than other commercial polyamides [1], which may be a crucial factor in the determination of low biocide release rate [19]. Moreover, the cooperative hydrogen bonding of both guanidinium cations and 2-naphthalenesulfonate anions with the polar amide groups may also ensure the high retention of PHMG-NS in PA-11.

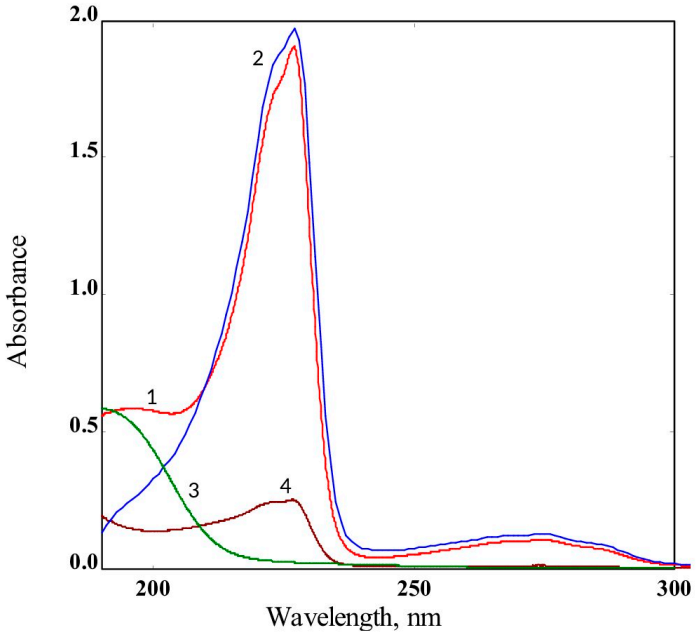

Figure 8. UV-visible spectra of: PHMG-NS (1); sodium 2-naphthalene sulfonate (2); PHMG hydrochloride (3) (C = 4.5 × 10^{-5} mol/L), and water solution after seven-day contact with PA-11/PHMG-NS (7%) film (4).

Even though the non-covalent association between the bioactive compounds and the polymer matrix has been a major advantage to optimise the antimicrobial performance [24,51], the question always remains: is the system contact-active or biocide-releasing? It was shown for antimicrobial polyamide nanocomposites containing silver- or copper-based inorganic biocides that they release Ag or Cu ions into the surrounding aqueous medium in a steady and prolonged manner [19–22]. At the same time, biocide release was detected neither for polylactides, polyamides or silicones containing hydrophobic PHMG salts [35–38] nor for PA-6 containing cationic biocide-modified organoclays [39]. Thus, the mode of antimicrobial action of these materials can be determined as contact-active because of the non-leachable form of the biocide. Bacterial membranes are known to carry a large number of negative charges and therefore can adsorb on positively charged polymer surfaces [24,46,63]. Upon adsorption on a cationic solid substrate, the electrostatic compensation of the negative charges of the bacterial envelope is provided by the cationic charges of the substrate, and the bacteria lose their natural counterions. It has been suggested that this counterion release initiates bacterial death. In the case of Gram-negative bacteria such as *E. coli*, Mg^{2+} and Ca^{2+} ions, which stabilise the outer membrane of the bacterial cell, are expelled during the adsorption of the bacteria on the charged substrate. Thus, the outer membrane is destabilised, leading to non-viable cells [24].

In our study, the low antimicrobial activity of PA-11/PHMG-NS films against planktonic bacteria may indicate that its antimicrobial action is based on contact-killing. The negligible release of polymeric biocide from polyamide matrix may also testify in favour of this assumption. As mentioned above, the antibiofilm properties of both PA-11/PHMG-NS (7%) and (10%) films were not altered after a seven-day water exposure, suggesting that the contact-killing mode of action as well as the anti-eDNA effect were the main elements in the antibiofilm/antifouling mechanism.

3. Materials and Methods

3.1. Materials

The following chemicals were used without further purification for the synthesis of the polymeric biocide: guanidine hydrochloride, 98% (Applichem, Darmstadt, Germany), hexamethylenediamine

(98%), 2-naphtalenesulphonic acid, sodium salt (technical grade, Sigma-Aldrich, Taufkirchen, Germany), and ethanol (95%). Rilsan®PA11 (granules) was supplied by Arkema (King of Prussia, PA, USA).

3.2. Synthesis of Polymeric Biocide PHMG-NS

PHMG-NS was synthesised according to the following procedure (Scheme 1).

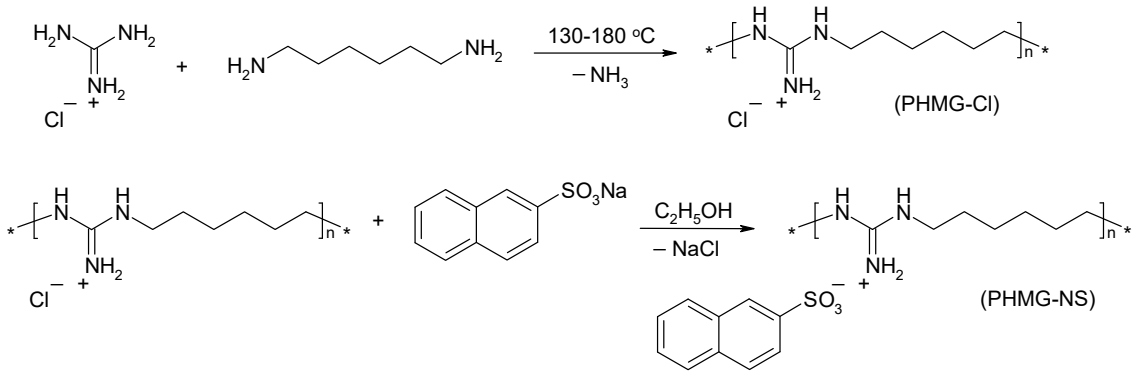

Scheme 1. Synthesis of polymeric biocide PHMG-NS.

A mixture of guanidine hydrochloride (10 g, 0.104 mol) and hexamethylenediamine (12 g, 0.103 mol) was placed into a round-bottomed flask (250 mL) and heated at 80 °C for 4 h under constant stirring. Subsequently, the reaction was carried out for 5 h at 130–140 °C and 5 h at 180 °C to obtain a highly viscous melt. After cooling the reaction mixture to room temperature, a vitreous solid PHMG-Cl was obtained. It was dissolved in water (200 mL) and precipitated by adding 100 mL of a saturated sodium chloride solution. The polymer was isolated by decantation and dried at 140 °C for 24 h. The product yield was 13 g (72%). The intrinsic viscosity was 0.09 dL/g for a PHMG-Cl solution in 0.1 N NaCl at 25 °C.

Sodium 2-naphtalenesulfonate (13.6 g, 0.06 mol) was added to the solution of PHMG-Cl (10 g, 0.055 mol) in 200 mL of ethanol and the mixture was stirred for 12 h at 60 °C (Scheme 1). The formed sodium chloride precipitate was filtered off and the solution was poured into water (500 mL). The white slurry of PHMG-NS was separated by the decantation and washed with water. The wet product was dried at 130 °C for 24 h and then powdered in an agate mortar. The product yield was 16 g (87%). The PHMG-NS salt has a melting point of 105–110 °C. Its water solubility was found to be 0.24 g/L.

The ^{1}H NMR and elemental analysis data for PHMG-Cl and PHMG-DBS are shown in the Supplementary Materials.

3.3. Preparation of PA-11/PHMG-NS Composite Films

PA-11 granules were dissolved in formic acid (98%) at 50 °C to obtain a 10 wt%. solution. An equal volume of isopropanol was added dropwise to the stirred solution to precipitate the polyamide powder. It was filtered off and then washed successively with sodium hydroxide (5%) and water. The obtained fine powder was dried in vacuum (1 mbar) at 70 °C for 12 h.

The mixture of PA-11 and PHMG-NS powders was ground for 3 min in an agate mortar followed by compression moulding at 240 °C. Composite polyamide films (45 mm × 45 mm) were obtained containing 5, 7 and 10 wt% of polymeric biocide.

3.4. Characterisation of PA-11/PHMG-NS Composite

To characterise the chemical properties of the modified PA-11 films, the samples were first placed on the Platinum diamond ATR module and IR spectra were recorded using a Bruker Vertex-70V FTIR spectrometer (all Bruker Optics Inc., Ettlingen, Germany) equipped with a L-alanine-doped deuterated triglycine sulphate (DLaDTGS) detector. Spectra were acquired with a resolution of 2 cm^{-1} in the

spectral region from 400 to 5000 cm^{-1} as the co-addition of 100 scans. Acquisition of these spectra was done with Bruker OPUS software (version 6.5, Ettlingen, Germany).

Mechanical testing of the polyamide samples was performed using a P-50 universal tensile testing machine (Milaform, Moscow, Russia) at a deformation rate of 10 mm/min. The obtained films were cut into specimens with the size of 40 mm × 10 mm × 0.15 mm. An average value (with standard deviation) for the tensile strength was obtained from three samples of each film.

Contact angle measurements were performed using a Drop Shape Analyzer DSA25E (Krüss, Hamburg, Germany) by the sessile drop method. The contact angle was estimated, using ImageJ software (version 1.50i, Bethesda, MD, USA), as the tangent normal to the water drop (3 mL) at the intersection between the sessile drop and the polymer surface. All reported contact angles are the average of at least five measurements taken at different locations on the polymer surface.

The surface charge density of the PA-11/PHMG-NS films was determined with the contactless inductive method [37]. The surface charge of the samples was determined by comparing the voltage amplitudes of the capacitor with PA-11 films and of the capacitor with a known calibrated electret. The measurements were carried out immediately after the samples were positioned into the measuring assembly, as well as 5 min later to estimate the changes of the surface charge with time.

Thermal gravimetric analysis (TGA) data for the polymeric biocide and modified PA-11 samples were obtained using a TGA Q500 (TA Instruments, Eschborn, Germany). About 10 mg of each sample were heated from 30 °C to 700 °C with a heating rate of 10 °C/min under an air atmosphere.

3.5. Biocide Release

The solubility of pure PHMG-NS in water was determined by stirring 1 g of the polymeric biocide powder in 100 mL of water for 24 h at room temperature. Then, the solution was filtered and evaporated. The weight of the solid residue was determined.

The release of PHMG-NS from the PA-11 film was investigated by UV-visible spectrophotometric analysis using a Jenway 6850 spectrometer (Stone, United Kingdom). The calibrating graph was obtained by measuring the absorbance of PHMG-NS aqueous solutions in a concentration range of 1×10^{-5}–5×10^{-5} mol/L at 227 nm, which is the characteristic peak of the naphthalene ring. For the evaluation of the leaching rate of polymeric biocide, 2 g of PA-11/PHMG-NS (7%) film was placed into a closed 1 L conical flask containing 750 mL of deionised water. The sample was kept at 37 °C at constant stirring. Three millilitres of each solution were taken periodically and analysed by measuring the absorbance at said wavelength to determine the concentration of the released biocide. The biocide release ratio was determined as the percentage of PHMG-NS released into the solution from its total quantity in the film. Each measurement has been repeated three times.

3.6. Biofilm Assay

The resistance to biofouling, i.e., the antibiofilm characteristics of the PA-11/PHMG-NS films, was evaluated by assessing the capability of two biofilm-forming model strains, *E. coli* K12 and *Staphylococcus aureus* ATCC 25923, to form attached biofilms on the surface of polymer samples following three days of stationary incubation. Each PA-11/PHMG-NS film was cut into pieces of 1 cm^2 each. The pieces were sterilised by autoclaving at 105 °C for 30 min. Water-treated pieces of plastics were prepared by exposition of 1 g of plastic films in 500 mL of deionised water for 7 days.

Each piece was then placed in a well of a sterile polystyrene 24-well plate in which 2 mL of Luria Broth (LB) medium were added, inoculated with 10 µL of an overnight inoculum culture containing 10^9 CFU/mL; there were eight replicas per variant. The plate was incubated at 37 °C for 72 h. The control for incubation was performed by incubating the films in sterile LB with four replicas. After incubation, each film piece was removed and washed three times to remove planktonic and poorly attached biofilm mass.

To measure the level of biofilm biomass attached to the plastics, a Crystal Violet assay was performed. To this end, eight pieces with attached biofilms were placed in a glass vial, stained with

1 mL of a 0.05% Crystal Violet stain solution for 30 min, and washed three times in water, after which the stain was eluted by incubating the piece in 500 µL of 96% ethanol for an hour. The eluted stain in each 200 µL aliquot was quantified by absorbance measurements at 570 nm in a BioTek ELx800 microplate spectrophotometer. Net biofilm attachment was calculated by subtracting the control values, corresponding to an incubation in LB.

A biofilm metabolic assay was performed for eight pieces as well. For this, each piece was placed in a glass vial with 500 µL of a 0.05% methylthiazolyldiphenyltetrazolium bromide (MTT) solution (Sigma-Aldrich, Taufkirchen, Germany) and incubated at 37 °C for 20 h. Then, the film and the MTT solution were removed from each vial and placed in a 1.5 mL plastic tube, which was spun down at 13,000× *g* for 15 min (Eppendorf 5424 Microcentrifuge (Fisher Scientific, Pittsburg, PA, USA). The supernatant was discarded and the sediment was dissolved again in 500 µL of DMSO. Again, staining intensities of 200 µL were evaluated using absorbance measurements at 570 nm. Net biofilm metabolic activity was calculated by subtracting the control values, corresponding to an incubation in LB.

3.7. Bacteria Toxicity Assay

The toxicity of the PA-11/PHMG-NS films was assessed on the basis of the optical density as well as the colony forming units number of the overbiofilm planktonic culture. For this, 200 µL of the overbiofilm planktonic culture of each treatment were transferred into a sterile polystyrene 96-well plate. The optical density was measured spectrophotometrically at 570 nm [64]. One hundred microlitres of each overbiofilm planktonic culture were used for preparing dilution series which were subsequently plated on LB agar plates for a colony forming units determination.

3.8. eDNA Assay

The amount of extracellular DNA (eDNA) was measured after its precipitation from cell-free supernatants. For this, 500 µL of the aforementioned biofilm culture and 550 µL of the bottom culture containing solid–liquid interface biofilms of the same microcosm, in which the PA-11/PHMG-NS films had been incubated for 72 h, were vortexed for 1 min and spun down at 13,000× *g* for 15 min (Eppendorf 5424 Microcentrifuge). Five hundred microlitres of each supernatant were removed and transferred into new 1.5 mL plastic tubes. One millilitre of chilled 96% ethanol and 50 µL of a 3 M sodium acetate solution (pH 5.2) were added to the supernatants, which were then incubated overnight at –20 °C. Then, the samples were spun down at 13,000× *g* for 15 min and the supernatants were removed. One millilitre of 70% ethanol was added into each of the tubes, which were then spun down again at 13,000× *g* for 15 min to wash the pellet. The supernatants were removed and the sediments were dried to full ethanol evaporation. Two hundred microlitres of Tris-EDTA (TE) buffer were added to dissolve each sample. eDNA concentration was measured using a NanoDrop 2000 spectrometer (Thermo Fisher Scientific, Waltham, MA, USA).

3.9. Statistical Analysis

The obtained data were processed statistically using the software package Statistica 7 or MS Excel for Windows. All results are presented as mean ± standard deviation. A value of $p < 0.05$ was considered statistically significant.

4. Conclusions

A new, thermally stable polymeric biocide polyhexamethylene guanidine 2-naphtalenesulfonate (PHMG-NS) was synthesised by anion metathesis between polyhexamethylene guanidine hydrochloride and sodium 2-naphtalenesulfonate. In dried conditions, PHMG-NS can be prepared as fine powder, which makes it suitable as an antimicrobial additive for polymer articles and protective coatings. It has a melting point of 105–110 °C and a limited water solubility of 0.024 g/L. According to thermogravimetric analysis, PHMG-NS is thermally stable to at least 357 °C, which indicates its

availability for joint melt processing with polyamide resins by common methods. Polyamide 11 (PA-11) films containing 5, 7 and 10 wt% of PHMG-NS have been obtained by compression moulding at 240 °C. The introduction of PHMG-NS into PA-11 films was found to significantly increase its surface hydrophilicity, as well as positive surface charge density. PA-11/PHMG-NS composites showed no changes of tensile strength at PHMG-NS content up to 7%, as well as high thermal decomposition point about 400 °C.

The antibiofilm properties of PA-11 modified with the polymeric biocide PHMG-NS were evaluated using the opportunistic biofilm-forming model bacterial strains *E. coli* K12 and *S. aureus* ATCC 25923. There was a substantial decrease in biofilm metabolic activity as well as in biofilm biomass for PA-11 films containing 7% and 10% of PHMG-NS for both strains. At the same time, there was no significant difference between the different PA-11/PHMG-NS films with regard to their effect on the planktonic bacteria in a biofilm-forming culture. The last fact may be due to the negligible biocide release into the medium. Indeed, the study of PHMG-NS release behaviour from the PA-11 films showed a low leaching ratio of less than 1% after 21 days, confirming its high retention in polymer matrix and maintenance its antibiofilm characteristics. Thus, it has been suggested that at least one mechanism of antibiofilm activity of PHMG-NS-containing PA-11 is associated with a reduction of eDNA, which affects the initial stages of bacterial biofilm formation and, thus, may decrease the spread of antibiotic resistance genes in a hospital-related environment.

Supplementary Materials: Supplementary materials can be found at http://www.mdpi.com/1422-0067/20/2/348/s1.

Author Contributions: O.M. designed and performed antibiofilm experiments, as well as spectrophotometric control of biocide release; J.-F.B. performed infrared analysis; O.T. synthesised polymeric biocide and prepared polymer composites; S.M. performed electrophysical investigations; T.C. performed thermal investigations; O.D. performed surface analysis; G.P. analysed the data; S.R. conceived and designed the experiments; and O.M. and S.R. wrote the paper.

Acknowledgments: The authors would like to thank NATO Science for Peace and Security multi-year project SPS 984834 "Fighting maritime corrosion and biofouling with task-specific ionic compounds" for its financial support of the project.

Conflicts of Interest: The authors declare no conflict of interest.

Abbreviations

PA-11	Polyamide 11
PHMG-Cl	Polyhexamethylene guanidine hydrochloride
PHMG-NS	Polyhexamethylene guanidine 2-naphtalenesulfonate
LB	Luria Broth
MTT	Methylthiazolyldiphenyltetrazolium bromide
eDNA	Extracellular DNA
TE buffer	Tris-EDTA buffer
CFU	colony forming units

References

1. *RILSAN®PA11: Created from a Renewable Source (Product Data Sheet)*; Arkema: Puteaux, France, 2005.
2. *Fine Powders: A Durable Coating for Durable Products (Product Data Sheet)*; Arkema: Colombes, France, 2010.
3. Klun, U.; Friedrich, Z.; Kržan, A. Polyamide 6 fibre degradation by a lignolytic fungus. *Polym. Degrad. Stab.* **2003**, *79*, 99–104. [CrossRef]
4. Tomita, K.; Ikeda, N.; Ueno, A. Isolation and characterization of a thermophilic bacterium, Geobacillus thermocatenulatus, degrading nylon 12 and nylon 66. *Biotechnol. Lett.* **2003**, *25*, 1743–1746. [CrossRef] [PubMed]
5. Chonde Sonal, G.; Chonde Sachin, G.; Raut, P.D. Studies on Degradation of synthetic polymer Nylon 6 and Nylon 6, 6 by Pseudomonas aeruginosa NCIM 2242. *IJETCAS* **2013**, *4*, 362–369. [CrossRef]

6. Kaali, P.; Strömberg, E.; Karlsson, S. Prevention of biofilm assotiated infections and degradation of polymeric materials used in biomedical applications. In *Biomedical Engineering, Trends in Material Science*; Laskovski, A.N., Ed.; In Tech: Rijeka, Slovenia, 2011; Chapter 22, pp. 513–541.
7. Moshynets, O.V.; Spiers, A.J. Viewing biofilms within the larger context of bacterial aggregations. In *Microbial Biofilms—Importance and Applications*; Dhanasekaran, D., Thajuddin, N., Eds.; InTech: Rijeka, Croatia, 2016; pp. 3–22, ISBN 978-953-2436-8.
8. Koza, A.; Kusmierska, A.; McLauglin, K.; Moshynets, O.; Spiers, A.J. Adaptive radiation of P. fluorescens SBW25 in experimental microcosms provides an understanding of the evolutionary ecology and molecular biology of A-L interface biofilm-formation. *FEMS Microbiol. Lett.* **2017**, *364*. [CrossRef]
9. McLaughlin, K.; Folorunso, A.O.; Deeni, Y.Y.; Foster, D.; Gorbatiuk, O.; Hapca, S.M.; Immoor, C.; Koza, A.; Mohammed, I.U.; Moshynets, O.; et al. Biofilm formation and cellulose expression by Bordetella avium 197N, the causative agent of bordetellosis in birds and an opportunistic respiratory pathogen in humans. *Res. Microbiol.* **2017**, *168*, 419–430. [CrossRef] [PubMed]
10. Donlan, R.M.; Costerton, J.W. Biofilms: Survival mechanisms of clinically relevant microorganisms. *Clin. Microbiol. Rev.* **2002**, *15*, 167–193. [CrossRef] [PubMed]
11. Nichols, D. *Biocides in Plastics. Rapra Review Reports*; Rapra Technology: Shrewsbury, UK, 2005; Volume 15, Report 180.
12. Rabin, N.; Zheng, Y.; Opoku-Temeng, C.; Du, Y.; Bonsu, E.; Sintim, H.O. Agents that inhibits bacterial biofilm formation. *Future Med. Chem.* **2015**, *7*, 647–671. [CrossRef] [PubMed]
13. Vitiello, G.; Pezzella, A.; Zanfardino, A.; Varcamonti, M.; Silvestri, B.; Costantini, A.; Branda, F.; Luciani, G. Titania as driving agent for DHICA polymerization: A novel strategy for the design of bioinspired antimicrobial nanomaterials. *J. Mater. Chem. B* **2015**, *3*, 2808–2815. [CrossRef]
14. Vitiello, G.; Pezzella, A.; Zanfardino, A.; Varcamonti, M.; Silvestri, B.; Giudicianni, P.; Costantini, A.; Varcamonti, M.; Branda, F.; Luciani, G. Antimicrobial activity of eumelanin-based hybrids: The role of TiO_2 in modulating the structure and biological performance. *Mater. Sci. Eng. C* **2017**, *75*, 454–462. [CrossRef]
15. Vitiello, G.; Silvestri, B.; Luciani, G. Learning from nature: Bioinspired strategies towards antimicrobial nanostructured systems. *Curr. Top. Med. Chem.* **2018**, *18*, 22–41. [CrossRef] [PubMed]
16. Kuratsuji, T.; Shimizu, H. Polyamide Based Antibacterial Powder Paint Composition. U.S. Patent 20030171452, 11 September 2003.
17. Lapeyre, A.; Ganset, C. Polyamide-Based Powder and Its Use for Obtaining an Antibacterial Coating. U.S. Patent 8303970, 4 August 2005.
18. Williams, R.L.; Doherty, P.J.; Vince, D.J.; Grashoff, G.J.; Williams, D.F. The biocompatibility of silver. *Crit. Rev. Biocompat.* **1989**, *5*, 221–223.
19. Kumar, R.; Münstedt, H. Silver ion release from antimicrobial polyamide/silver composites. *Biomaterials* **2005**, *26*, 2081–2088. [CrossRef] [PubMed]
20. Damm, C.; Münstedt, H.; Rösch, A. Long-term antimicrobial polyamide 6/silver-nanocomposites. *J. Mater. Sci.* **2007**, *42*, 6067–6073. [CrossRef]
21. Damm, C.; Münstedt, H.; Rösch, A. The antimicrobial efficacy of polyamide 6/silver-nano- and microcomposites. *Mater. Chem. Phys.* **2008**, *108*, 61–66. [CrossRef]
22. Thokala, N.; Kealey, C.; Kennedy, J.; Brady, D.B.; Farrell, J.B. Characterization of polyamide 11/copper antimicrobial composites for medical device applications. *Mater. Sci. Eng. C* **2017**, *78*, 1179–1186. [CrossRef] [PubMed]
23. Gilbert, P.; Moore, L.E. Cationic antiseptics: Diversity of action under a common epithet. *J. Appl. Microbiol.* **2005**, *99*, 703–715. [CrossRef] [PubMed]
24. Carmona-Ribeiro, A.M.; de Melo Carrasco, L.D. Cationic antimicrobial polymers and their assemblies. *Int. J. Mol. Sci.* **2013**, *14*, 9906–9946. [CrossRef]
25. Zhang, Y.M.; Jiang, J.M.; Chen, Y.M. Synthesis and antimicrobial activity of polymeric guanidine and biguanidine salts. *Polymer* **1999**, *40*, 6189–6198. [CrossRef]
26. Oulè, M.K.; Azinwi, R.; Bernier, A.M.; Kablan, T.; Maupertuis, A.M.; Mauler, S.; Koffi- Nevry, R.; Dembèlè, K.; Forbes, L.; Diop, L. Polyhexamethylene guanidine hydrochloride-based disinfectant: A novel tool to fight meticillin-resistant Staphylococcus aureus and nosocomial infections. *J. Med. Microbiol.* **2008**, *57*, 1523–1528. [CrossRef]

27. Qian, L.; Guan, Y.; He, B.; Xiao, H. Modified guanidine polymers: Synthesis and antimicrobial mechanism revealed by AFM. *Polymer* **2008**, *49*, 2471–2475. [CrossRef]
28. Zhou, Z.; Wei, D.; Guan, Y.; Zheng, A.; Zhong, J.-J. Damage of Escherichia coli membrane by bactericidal agent polyhexamethylene guanidine hydrochloride: Micrographic evidences. *J. Appl. Microbiol.* **2010**, *108*, 898–907. [CrossRef]
29. Zhou, Z.; Wei, D.; Guan, Y.; Zheng, A.; Zhong, J.-J. Extensive in vitro activity of guanidine hydrochloride polymer analogs against antibiotics-resistant clinically isolated strains. *Mater. Sci. Eng.* **2011**, *31*, 1836–1843. [CrossRef]
30. Zhou, Z.; Zheng, A.; Zhong, J. Interactions of biocidal guanidine hydrochloride polymer analogs with model membranes: A comparative biophysical study. *Acta Biochim. Biophys. Sin.* **2011**, *43*, 729–737. [CrossRef]
31. Choi, H.; Kim, K.-J.; Lee, D.J. Antifungal activity of the cationic antimicrobial polymer-polyhexamethylene guanidine hydrochloride and its mode of action. *Fungal Biol.* **2017**, *121*, 53–60. [CrossRef]
32. Han, J.-S.; Lim, K.-M.; Park, S.-J.; Song, W.-S. Polyhexamethyleneguanidine Phosphate Powder, Method of Making the Same and Antimicrobial Resin Containing the Same. Eur. Patent 1 110 948, 17 May 2001.
33. Protasov, A.; Bardeau, J.-F.; Morozovskaya, I.; Boretska, M.; Cherniavska, T.; Petrus, L.; Tarasyuk, O.; Metelytsia, L.; Kopernyk, I.; Kalashnikova, L.; et al. New promising antifouling agent based on polymeric biocide polyhexamethylene guanidine molybdate. *J. Environ. Toxicol.* **2016**, *36*, 2543–2551. [CrossRef]
34. Swiontek Brzezinska, M.; Walczak, M.; Jankiewizs, U.; Pejchalová, M. Antimicrobial activity of polyhexamethylene guanidine derivatives introduced into polycaprolactone. *J. Polym. Environ.* **2018**, *26*, 589–595. [CrossRef]
35. Walczak, M.; Richert, A.; Burkowska-But, A. The effect of polyhexamethylene guanidine hydrochloride (PHMG) derivatives introduced into polylactide (PLA) on the activity of bacterial enzymes. *J. Ind. Microbiol. Biotechnol.* **2014**, *41*, 1719–1724. [CrossRef]
36. Rogalskyy, S.; Bardeau, J.-F.; Tarasyuk, O.; Fatyeyeva, K. Fabrication of new antifungal polyamide-12 material. *Polym. Int.* **2012**, *61*, 686–691. [CrossRef]
37. Rogalsky, S.; Bardeau, J.-F.; Wu, H.; Lyoshina, L.; Bulko, O.; Tarasyuk, O.; Makhno, S.; Cherniavska, T.; Kyselov, Y.; Koo, J.H. Structural, thermal and antibacterial properties of polyamide 11/polymeric biocide polyhexamethylene guanidine dodecylbenzenesulfonate composites. *J. Mater. Sci.* **2016**, *51*, 7716–7730. [CrossRef]
38. Ghamrawi, S.; Bouchara, J.-P.; Tarasyuk, O.; Rogalsky, S.; Lyoshina, L.; Bulko, O.; Bardeau, J.-F. Promising silicones modified with cationic biocides for the development of antimicrobial medical devices. *Mater. Sci. Eng. C* **2017**, *75*, 969–979. [CrossRef]
39. Nigmatullin, R.; Gao, F.; Konovalova, V. Permanent, non-leaching antimicrobial polyamide nanocomposites based on organoclays modified with a cationic polymer. *Macromol. Mater. Eng.* **2009**, *294*, 795–805. [CrossRef]
40. Li, G.; Shen, J. A study of pyridinium-type functional polymers. IV. Behavioral features of the antibacterial activity of insoluble pyridinium-type polymers. *J. Appl. Polym. Sci.* **2000**, *78*, 676–684. [CrossRef]
41. Desai, D.G.; Liao, K.S.; Cevallos, M.E.; Trautner, B.W. Silver or nitrofurazone impregnation of urinary catheters has a minimal effect on uropathogen adherence. *J. Urol.* **2010**, *184*, 2565–2571. [CrossRef]
42. Ghatak, P.D.; Mathew-Steiner, S.S.; Pandey, P.; Roy, S.; Se, C.K. A surfactant polymer dressing potentiates antimicrobial efficacy in biofilm disruption. *Sci. Rep.* **2018**, *8*, 873. [CrossRef]
43. Shao, Q.; Fan, Y.; Yang, L.; Gao, Y.Q. Counterion effects on the denaturing activity of guanidinium cation to protein. *J. Chem. Theory Comput.* **2012**, *8*, 4364–4373. [CrossRef]
44. Jansen, B.; Peters, G. Modern strategies in the prevention of polymer-associated infections. *J. Hosp. Infect.* **1991**, *19*, 83–88. [CrossRef]
45. An, Y.H.; Friedman, R.J. Concise review of mechanisms of bacterial adhesion to biomaterial surfaces. *J. Biomed. Mater. Res.* **1998**, *43*, 338–348. [CrossRef]
46. Kügler, R.; Bouloussa, O.; Rondelez, F. Evidence of a charge-density threshold for optimum efficiency of biocidal cationic surfaces. *Microbiology* **2005**, *151*, 1341–1348. [CrossRef]
47. Reisner, A.; Haagensen, J.A.J.; Schembri, M.A.; Zechner, E.L.; Molin, S. Development and maturation of Escherichia coli K-12 biofilms. *Mol. Microbiol.* **2003**, *48*, 933–946. [CrossRef]
48. Avila-Novoa, M.G.; Iniguez-Moreno, M.; Solis-Velazquez, O.A.; Gonzalez-Gomez, J.P.; Guerrero-Medina, P.J.; Gutierrez-Lomeli, M. Biofilm formation by Staphyloccus aureus isolated from food contact surface in the dairy industry of Jalisco, Mexico. *J. Food Qual.* **2018**. [CrossRef]

49. Zhou, Z.; Wei, D.; Lu, Y. Polyhexamethylene guanidine hydrochloride bactericidal advantages over chlorhexidine bigluconate against ESKAPE bacteria. *Biotechnol. Appl. Biochem.* **2014**. [CrossRef]
50. Moshynets, O.; Koza, A.; Dello Sterpaio, P.; Kordium, V.; Spiers, A.J. Up-dating the Cholodny method using PET films to sample microbial communities in soil. *Biopolym. Cell* **2011**, *27*, 199–205. [CrossRef]
51. Siedenbiedel, F.; Tiller, J.C. Antimicrobial polymers in solution and on surfaces: Overview and functional principles. *Polymers* **2012**, *4*, 46–71. [CrossRef]
52. Wang, H.; Chen, H.; Wang, F.; Wei, D.; Wang, X. An improved 3-(4,5-dimethylthiazol-2-yl)-2,5-diphenyl tetrazolium bromide (MTT) reduction assay for evaluating the viability of *Escherichia coli* cells. *J. Microbiol. Methods* **2010**, *82*, 330–333. [CrossRef]
53. Flemming, H.C.; Wingender, J. The biofilm matrix. *Nat. Rev. Microbiol.* **2010**, *8*, 623–633. [CrossRef]
54. Allesen-Holm, M.; Barken, K.B.; Yang, L.; Klausen, M.; Webb, J.S.; Kjelleberg, S.; Molin, S.; Givskov, M.; Tolker-Neilsen, T. A characterization of DNA release in *Pseudomonas aeruginosa* cultures and biofilms. *Mol. Microbiol.* **2006**, *59*, 1114–1128. [CrossRef]
55. Thomas, V.C.; Hiromasa, Y.; Harma, N.; Thurlow, L.; Tomich, J.; Hancock, L.E. A fratricidal mechanism is responsible for eDNA release and contributes to biofilm development of *Enterococcus faecalis*. *Mol. Micriol.* **2009**, *72*, 1022–1036. [CrossRef]
56. Montanaro, L.; Poggi, A.; Visai, L.; Ravaioli, S.; Campoccia, D.; Speziale, P.; Arciola, C.R. Extracellular DNA in biofilms. *Int. J. Artif. Organs* **2011**, *34*, 824–831. [CrossRef]
57. Christner, M.; Heinze, C.; Busch, M.; Franke, G.; Hentschke, M.; Duhring, S.B.; Buttner, H.; Kotasinska, M.; Wischnewski, V.; Kroll, G.; et al. sarA negatively regulats staphylococcus epidermidis biofilm formation by modulation expression of 1 MDa extracellular matrix binding protein and autolysis-dependent release of eDNA. *Mol. Microbiol.* **2012**, *86*, 394–410. [CrossRef]
58. Wu, J.; Xi, C. Evaluation of different methods for extracting extracellular DNA from the biofilm matrix. *Appl. Environ. Microbiol.* **2009**, 5390–5395. [CrossRef]
59. Schwartz, K.; Ganesan, M.; Payne, D.E.; Solomon, M.J.; Boles, B.R. Extracellular DNA facilitates the formation of functional amyloids in Staphylococcus aureus biofilms. *Mol. Microbiol.* **2016**, *99*, 123–134. [CrossRef]
60. Hannan, S.; Ready, D.; Jasni, A.S.; Rogers, M.; Pratten, J.; Roberts, A.P. Transfer of antibiotic resistance by transformation with eDNA within oral biofilms. *FEMS Immunol. Med. Microbiol.* **2010**, *59*, 345–349. [CrossRef]
61. Itzek, A.; Zheng, L.; Chen, Z.; Merritt, J.; Kreth, J. Hydrogen peroxide-dependent DNA release and transfer of antibiotic resistance genes in *Streptococcus gordonii*. *J. Bacteriol.* **2011**, *193*, 6912–6922. [CrossRef]
62. Wei, D.; Zhou, R.; Guan, Y.; Zheng, A.; Zhang, Y. Investigation on the reaction between polyhexamethylene guanidine hydrochloride oligomer and glycidyl methacrylate. *J. Appl. Polym. Sci.* **2013**, *127*, 666–674. [CrossRef]
63. Lewis, K.; Klibanov, A.M. Surpassing nature: Rational design of sterile-surface materials. *Trends Biotechnol.* **2005**, *23*, 343–348. [CrossRef]
64. Sambrook, J.; Fritsch, E.F.; Maniatis, T. *Molecular Cloning: A Laboratory Manual*, 2nd ed.; Cold Spring Harbor Laboratory Press, Cold Spring Harbor: New York, NY, USA, 1989; Volume 3, ap. B.11 and B.23.

© 2019 by the authors. Licensee MDPI, Basel, Switzerland. This article is an open access article distributed under the terms and conditions of the Creative Commons Attribution (CC BY) license (http://creativecommons.org/licenses/by/4.0/).

J. Coat. Technol. Res., **21** (3) 939–953, 2024
https://doi.org/10.1007/s11998-023-00862-8

Preparation and characterization of new antifouling coating based on alkyd paint modified with hydrophobic cationic biocide

Sergiy Rogalsky, Olena Moshynets, Oleg Dzhuzha, Oksana Tarasyuk, Anastasiia Hubina, Alina Madalina Darabut, Yevheniia Lobko, Iryna Morozovska, Oleksandr Protasov, Jean-François Bardeau

Received: 13 June 2023 / Revised: 17 September 2023 / Accepted: 25 September 2023
© American Coatings Association 2024

Abstract New water-immiscible cationic biocide 1-dodecylpyridinium dodecylbenzenesulfonate ($PyrC_{12}$-DBS) has been synthesized and tested as potential antifouling agent for commercial alkyd paint PP-115 (Ukraine). The modified PP-115/$PyrC_{12}$-DBS coatings containing 8% and 16% (w/w) of $PyrC_{12}$-DBS were prepared by dissolution directly of the cationic biocide into the PP-115 paint. Once the stainless steel bars were painted, the surface wettability of the coating was found to be significantly increased when modified with cationic biocide. The results of scanning electron microscopy (SEM) and energy-dispersive X-ray spectroscopy (EDX) studies indicate high homogeneity of the modified coatings. Infrared analysis revealed hydrogen bonding between ester groups of alkyd resin and pyridinium cations of $PyrC_{12}$-DBS. The plasticizing effect of the cationic biocide on the alkyd binder has also been revealed by differential scanning calorimetry analysis. According to spectrophotometric analysis data, $PyrC_{12}$-DBS has excellent resistance to leaching from protective coatings into water. Antibiofilm efficiency of $PyrC_{12}$-DBS was evaluated by assessing the capability of two biofilm-forming model strains, namely *Staphylococcus aureus* ATCC 25923 and *Pseudomonas aeruginosa* PA01, to form attached biofilms on the surface coated with modified alkyd paint. A significant decrease in biofilm metabolic activity, as well as in cell biomass, was determined for PP-115/$PyrC_{12}$-DBS (16%) coatings. The antifouling activity was evaluated by exposure to experimental substrates in freshwater (Dnipro River) for 143 days. The surface of PP-115/$PyrC_{12}$-DBS (16%) coatings showed an almost 13-fold reduction of total biomass formed by Dreissenidae mussels compared with control substrates. Overall, the obtained data indicate that the contact-active protective coatings based on water-insoluble polymer matrix and water-insoluble cationic biocide may effectively resist biofouling at relatively high biocide content.

Keywords Antifouling coating, Alkyd paint, Cationic biocide, Contact active, Biofilm

Supplementary Information The online version contains supplementary material available at https://doi.org/10.1007/s11998-023-00862-8.

S. Rogalsky (✉), O. Dzhuzha, O. Tarasyuk
Laboratory of Modification of Polymers, V.P. Kukhar Institute of Bioorganic Chemistry and Petrochemistry of the NAS of Ukraine, 50, Kharkivske shose, Kyiv 02160, Ukraine
e-mail: sergey.rogalsky@gmail.com

O. Moshynets
Department of Cell Regulatory Mechanisms, Institute of Molecular Biology and Genetics of the NAS of Ukraine, 150 Zabolotnoho str., Kyiv 03680, Ukraine

A. Hubina
Department of Polymers, Faculty of Chemical Technology, University of Chemistry and Technology (UCT) Prague, Technická 5, Prague 166 28, Czech Republic

A. M. Darabut, Y. Lobko
Department of Surface and Plasma Science, Faculty of Mathematics and Physics, Charles University, V Holešovičkách 747/2, Praha 8, Prague 180 00, Czech Republic

I. Morozovska, O. Protasov
Department of Ecological Hydrology and Water Ecosystem Management, Institute of Hydrobiology of the NAS of Ukraine, 12, Volodymyra Ivasyuka Avenue, Kyiv 04210, Ukraine

J.-F. Bardeau
Institut des Molécules et Matériaux du Mans, UMR CNRS 6283, Le Mans Université, Le Mans, France

Introduction

Biofouling is known to take place on almost any solid substrate immersed into freshwater or seawater. This process begins with the colonization of solid substrates by microfoulers (bacteria, algae, and diatoms).[1–4] Biofilms formed on marine surfaces protect microorganisms from the action of adverse environmental conditions and allow the occurrence of macrofouling by bryozoans, mollusks, crustacean, polychaeta, fungi, etc.[3,4] The best known bioadhesive system is that produced by mussels. These shellfish attach by depositing a mixture of proteins which crosslink the macromolecules between them to harden the glue.[2] It is worth noting that the attachment of macrofoulers to biofilm-free surfaces can also occur. Biofouling creates severe economic problems all over the world, leading to considerably increased operational and maintenance costs of underwater equipment and constructions. Thus, it damages several marine facilities, including oil production platforms, powerplants, industrial water inlet systems, or seawater cooled systems.[5–7] In the shipping industry, fouling organisms attached to vessel hulls promote surface corrosion and increased frictional resistance, leading to fuel consumption and loss of speed. There are high costs incurred in ship hull cleaning and repainting, as well as loss of revenue when the frequency of dry-docking operations increased.[8,9] This fouling process also accumulates a large amount of toxic macrofouling waste in landfills. Furthermore, marine biofouling promotes bio-invasion of species into environments where they were not naturally present that has an extremely negative impact on global biodiversity.[1,2] Therefore, prevention of biofouling remains one of the most important challenges in marine industry and world ecology.

The common approach to inhibiting fouling of underwater constructions in both seawater and freshwater is to cover them with protective polymer coatings containing biocides. Various kinds of biocide-based antifouling coating systems exist, depending on how biocidal additives are released into the water.[1,10] Until recently, self-polishing coatings (SPCs) based on copolymers of tributyltin (TBT) acrylate and methyl methacrylate were the most commonly used since they provide efficient antifouling resistance for at least 5-7 years.[10] In SPCs, biocidal TBT groups are bonded onto the polymer backbone by an ester linkage. After immersion, slow hydrolysis of carboxyl-TBT linkage occurs on the surface and cleaves the TBT moiety from the hydrophobic polymer matrix. The partially hydrolyzed polymer backbone becomes hydrophilic, and a surface layer can then be easily eroded by the moving seawater, leading to renewal of a bioactive surface in contact with water.[10,11] However, the use of organotin additives in marine paints was banned recently by the International Marine Organization due to their severe negative impact on nontarget species, including commercially important organisms.[12]

During the last decade, significant investments have been made in the development of tin-free antifouling systems which may be classified into the following main groups. Tin-free SPCs are based on organo copper esters of poly(methacrylic acid) copolymers which have the same biocide-releasing mechanism with seawater as TBT-SPCs.[1] The Cu-acrylate coatings have been reported to be active for up to 3 years. Controlled depletion systems (CDPs) consist of soluble binder based on synthetic resins and rosin derivatives incorporating seawater-soluble cuprous oxide.[1] Once in contact with seawater, the biocides dissolve together with the soluble binder. This type of antifouling coating is less effective for up to 36 months.[1] It should also be noted that high cuprous oxide loading (more than 40% by volume) is required to permit adequate release of copper for prolonged periods.[13] Thus, the mechanism of action of common TBT-free antifouling coatings also involves gradual wasting of their components producing a thin, toxic layer which repels aquatic organisms and therefore prevents the onset of biofouling. However, the amounts of copper leached from antifouling paints were also found to be harmful for various aquatic micro- and macroorganisms.[14–16] Meanwhile, the use of copper alone is not enough to prevent marine organisms from attaching to surfaces and it is for this reason that coatings are filled with biocides (usually pesticides) to boost their effectiveness. The toxic impact of booster biocides such as Diuron, Sea-Nine 211, Irgarol®, and zinc pyrithione on nontarget species has also been established.[17–20]

Therefore, the problem still remains and there is a need to develop alternative antifouling coatings which combine both high efficiency and low environmental impact, as well as low cost. The simplest solution would be to use a polymer matrix that is insoluble in seawater and does not polish or erode after immersion. Such antifouling coatings require sufficiently high loading of biocide to permit continuous contact of toxic particles. However, the common insoluble matrix paints also include toxic antifouling agents that are released upon contact with water. The active species dissolved by the seawater penetrating into the polymer matrix have to diffuse to the surface through the interconnecting pores formed after dissolution of the soluble pigments.[1] The short life time of these coatings (12–18 months) has limited their practical applications. So, the use of insoluble matrix paints containing water-insoluble biocides seems to be the next step in the development of new environmentally friendly antifouling coatings. Potential advantages of such systems include the absence of release of biocides into the aquatic environment, as well as long-term antifouling activity.

Nowadays, contact-active antimicrobial polymer composites are considered very promising eco-friendly materials for various applications since they do not release biocides into contact medium.[21–23] The covalent surface grafting of cationic biocides to various synthetic and natural polymers is a common approach

for the formation of safe and effective antimicrobial materials.[24] Cationic biocides based on long-chain quaternary onium salts comprising tetraalkylammonium, 1,3-dialkylimidazolium, and 1-alkylpyridinium cations are known to possess broad-spectrum activity against both gram-positive and gram-negative bacteria, antifungal activity, as well as strong antibiofilm activity against a panel of pathogen microorganisms.[25–30] The mechanism of antimicrobial action of cationic biocides involves the electrostatic interaction with outermost surface of bacterial cells which are often negatively charged and association with the head groups of acidic phospholipids. The lipophilic hydrocarbon tails of the cationic amphiphilic compound then penetrate into the hydrophobic membrane core and form mixed-micelle aggregates with its components, resulting in a deformation of membrane permeability and lethal leakage of cytoplasmic materials.[27,31,32]

Moreover, 1-dodecyl-3-methylimidazolium iodide was found to have superior antibiofouling activity against dominant fouling barnacle *Amphibalanus reticulatus*.[33] It has also been found that polymeric alkylpyridinium salts (poly-APS) isolated from the Mediterranean marine sponge, Haliclona (Rhizoniera) sarai, effectively inhibit barnacle larva settlement and natural marine biofilm formation through a nontoxic and reversible mechanism.[34] Few synthetic analogs of poly-APS showed antifouling efficacy very similar to natural ones, as well as negligible toxicity.[34]

Numerous studies have shown that cationic biocides attached covalently to the polymer surface are able to kill microorganisms at the polymer–water interface similarly to free biocide molecules in water solution.[21,24,35] These sterile-surface materials have long-lasting antimicrobial activity and effectively prevent the formation of microbial biofilms. However, the covalent grafting of biocides to the surface of protective coatings is difficult to realize from a practical point of view. At the same time, recent studies reported preparation of contact-active antimicrobial materials based on synthetic polymers (i.e., polyamides, polycaprolactone, polylactides, silicone rubber) comprising hydrophobic cationic biocides as external additives.[36–40] Polymer films containing 5–7 wt% of low molecular or polymeric cationic biocides showed a high activity against both gram-positive and gram-negative bacteria,[37–40] as well as high antibiofilm activity.[36,40] It has also been found that hydrophobic cationic biocides have excellent leaching resistance due to their poor water solubility, as well as physicochemical interactions with polymer matrix.[36,37,40] Another successful approach to prepare contact-active antimicrobial composites involves the intercalation of the cationic polymer, partially aminated poly(vinylbenzyl chloride), into a smectic clay, montmorillonite, to produce a modified organoclay containing 33 wt% of polymeric biocide.[41] Polymerically modified organoclay was compounded with polyamide resin by melt extrusion. The obtained nanocomposites were active against both gram-negative *E. coli* and gram-positive *S. aureus* bacteria and demonstrated up to a 2-log reduction in the viable cells adhering to the material surface at an organoclay content of 5 wt%. The mode of antimicrobial action of this material was determined as contact-active due to the nonleachable form of biocide.[41]

Thus, water-immiscible cationic biocides seem promising candidates as antifouling additives for ship paints. Liquid long-chain onium salts are of particular interest as they dissolve easily in paints and therefore can be used in coatings. In this study, hydrophobic cationic biocide 1-dodecylpyridinium dodecylbenzenesulfonate ($PyrC_{12}$-DBS) has been synthesized by anion metathesis between 1-dodecylpyridinium chloride and sodium dodecylbenzenesulfonate. Water-soluble 1-dodecylpyridinium salts are known to possess excellent antimicrobial activity which is significantly higher compared to quaternary ammonium surfactants,[42] as well as 1-alkyl-3-dodecylimidazolium salts[26,30,43] The combination of 1-dodecylpyridinium cation with DBS anion allowed preparing water-immiscible cationic biocide which was evaluated as potential antifouling agent for industrial ship paint. The modified protective coatings containing $PyrC_{12}$-DBS were prepared and characterized in terms of morphological, surface, and thermophysical properties, antibiofilm activity, as well as antifouling activity in freshwater environment.

Materials and methods

Materials

Pyridine (99%), 1-chlorododecane (97%), sodium dodecylbenzenesulfonate (technical grade), methylene chloride, hexane, and ethyl acetate (98%) (Sigma-Aldrich) were purchased from ALSI (Ukraine) and used without further purification.

Commercial paint PP-115 (Sorbi, Ukraine) was used for the preparation of protective coatings. The paint contains a mixture of pigments and fillers (calcium carbonate, titanium dioxide, iron oxide) in an alkyd (pentaphthalic) varnish. Mass fraction of nonvolatile substances is about 60 ± 10%.

Synthesis of cationic biocide 1-dodecylpyridinium dodecylbenzenesulfonate ($PyrC_{12}$-DBS)

1-Dodecylpyridinium chloride ($PyrC_{12}$-Cl) was synthesized according to Scheme 1. The mixture of pyridine (20 g, 0.24 mol) and 1-chlorododecane (59 g, 0.29 mol) was stirred at 140°C for 24 h. The obtained solid product was purified by recrystallization from ethyl acetate–hexane mixture (1:2 v/v). Yield: 72% (48 g), white solid, mp 92–94°C.

^{1}H NMR (400 MHz, $CDCl_3$): δ = 0.75 (t, J = 6.8 Hz, 3H, CH_3), 1.14-1.41 (m, 18H, $CH_3(CH_2)_9$), 1.91 (p, J = 7.4 Hz, 2H, NCH_2CH_2), 4.87 (t, J = 7.4 Hz, 2H, NCH_2), 8.06 (t, J = 6.9 Hz, 2H, C_3–H, C_5–H), 8.39 (t,

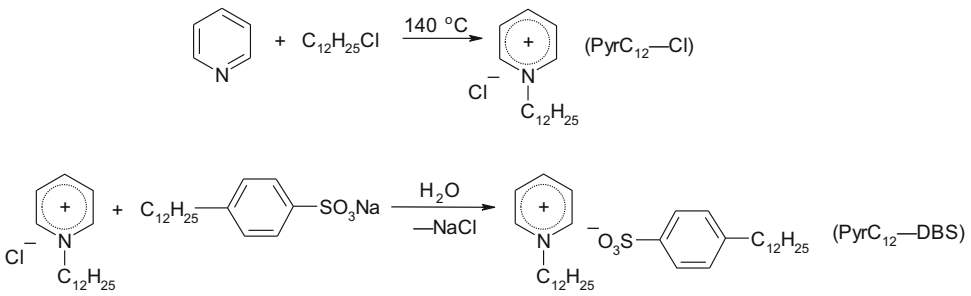

Scheme 1: Synthesis of cationic biocide $PyrC_{12}$-DBS

J = 7.8 Hz, 1H, C_4–H), 9.56 (d, J = 5.9 Hz, 2H, C_2–H, C_6–H).

To the stirred solution of $PyrC_{12}$-Cl (20 g, 0.07 mol) in 200 mL of water was added aqueous solution of sodium dodecylbenzenesulfonate (24 g/300 mL). The mixture was stirred for 1 h, and then, the product was extracted with methylene chloride (2 × 250 mL). The combined solution was dried over sodium sulfate. Methylene chloride was then distilled, and the residual solvent was removed under vacuum (10 mbar) at 50°C for 12 h. Cationic biocide $PyrC_{12}$-DBS was prepared as a light brown semi-solid product.

^{1}H NMR (400 MHz, $CDCl_3$): δ = 0.68-0.91 (m, 9H, CH_3); 0.96-1.34 (m, 32H, CH_2); 1.39-1.69 (m, 4H, CH_2); 1.89 (p, J = 7.2 Hz, 2H, NCH_2CH_2); 4.76 (t, J = 7.4 Hz, 2H, NCH_2); 7.08-7.17 (m, 2H, C_3-Ar-H, C_5–Ar–H); 7.77 (dd, J = 8.3, 1.9 Hz, 2H, C_2–Ar–H, C_6–Ar–H,); 8.0 (dd, J = 7.8, 6.4 Hz, 2H, C_3–H, C_5–H); 8.36 (t, J = 7.8 Hz, 1H, C_4–H); 9.08-9.16 (m, 2H, C_2–H, C_6-H).

Preparation of antifouling coating

Stainless steel bars (8 × 2.5 × 0.05 cm) were used as model substrates for testing the antifouling coating. Cationic biocide $PyrC_{12}$-DBS was added to the commercial ship paint PP-115 (5% and 10% (w/w) to wet paint or 8% and 16% (w/w) to dry coating), and the mixture was ground using zirconia grinding media for 30 min. The modified paint was then filtered and used to paint the steel bars using a paint roller. After drying for 48 h in air, the samples were coated with a second layer. The total coating thickness was about 300 ± 10 μm. The total weight of coating was determined by weight difference between painted and neat steel bars. The control samples were coated with two layers of paint PP-115.

Characterization of prepared coatings

The vibrational properties of protective coatings were studied using a Vertex-70 Bruker (Germany) Fourier transform infrared (FT-IR) spectrometer equipped with a DTGS detector. Coating samples were placed into contact with the single reflection diamond ATR (attenuated total reflection) crystal, and the spectra were collected over the range of 400–4000 cm^{-1} at a resolution of 1 cm^{-1}.

In order to study the surface chemical modifications of coatings with higher spatial resolution, Raman measurements were taken at room temperature using a WITec Alpha 300R confocal Raman spectrometer (WITec GmbH, Ulm Germany). Raman spectra were acquired in backscattering under a microscope with a Zeiss EC Epiplan-Neofluar® 100X objective (numerical aperture of 0.9) focusing the 532-nm line of a solid-state sapphire laser (Coherent Inc., Santa Clara, USA) with a laser power at the sample of 8 mW and an integration time set at 1 s. The spectrometer being equipped with a motorized scanning stage, 1600 spectra were recorded from a mapping area of 40 × 40 μm^2 (2D map step size of 1 μm). The spectral analysis was performed using the WITec Project plus software (version 5.248, WITec GmbH, Germany).

The adhesion of the coating onto the substrates was determined in accordance with ASTM D 3359, method B. Latticed notches were applied to the finished coatings followed by visual assessment of its condition. The adhesion for all coatings was 1 point (5 B). The edges of cuts were completely smooth, and there were no signs of delamination on all edges of the lattice.

Static contact angle measurements were taken using a Drop Shape Analyzer DSA25E (Krüss, Germany) by the sessile drop method. The contact angle values were estimated, using CAM software, as the tangent normal to the water drop (3 mL) at the intersection between the sessile drop and the polymer coating surface. All reported contact angles are the average of at least five measurements taken at different locations on the polymer surface.

The 3D surface topography of the coatings was studied using the confocal white-light optical imaging S-NEOX profiler (Sensofar-Tech S. L., Barcelona, Spain). The 340 × 284 μm^2 area was collected using a 50 X DI Nikon objective (0.8 numerical aperture). The data were analyzed by the open-source Gwyddion software (version 2.60).

Scanning electron microscopy (SEM) images were taken using a MIRA 3 (Tescan GmbH, Czech Republic) microscope operating at 10 kV electron beam energy. Chemical composition mapping analysis was carried out using energy-dispersive X-ray spectroscopy

(EDX) with a Bruker XFlash detector mounted directly into the SEM.

Differential scanning calorimetry (DSC) analyses were performed from − 90 to 100°C on a Discovery DSC250 Auto (TA Instruments, USA) with a heating rate of 10°C/min under N_2 atmosphere. The data for analysis were acquired from the second heating run.

The release of $PyrC_{12}$-DBS from the coatings was studied by UV–visible spectrophotometric analysis using a Jenway 6850 spectrometer (Great Britain). The calibrating graph was obtained by measuring the absorbance at 259 nm (characteristic peak of pyridinium cation[44]) of $PyrC_{12}$-Cl aqueous solutions in a concentration range of 1.5×10^{-5}–1.5×10^{-4} mol/L. For the evaluation of the leaching rate of cationic biocide, each painted steel bar (three samples) was placed into a closed conical flask containing 1 L of deionized water. The samples were kept at 25°C. Three milliliters of each solution was taken periodically and analyzed by measuring the absorbance at mentioned wavelength to determine the concentration of the released biocide. Each measurement was repeated three times.

Antibiofilm efficiency of $PyrC_{12}$-DBS was evaluated by assessing the capability of two biofilm-forming model strains, *Staphylococcus aureus* ATCC 25923 and *Pseudomonas aeruginosa* PA01, to form attached biofilms on the surface coated with PP-115 and PP-115/$PyrC_{12}$-DBS following two days of stationary incubation. For this, 1 cm^2 metal plates covered with either PP-115 or PP-115/$PyrC_{12}$-DBS were sterilized by autoclaving at 105°C for 30 min. Each substrate was then placed in a well of a sterile polystyrene 24-well plate in which 2 mL of Luria broth (LB) medium was added and inoculated with 10 µL of an overnight inoculum culture containing 10^9 CFU/ml; there were six replicas per variant. The plate was incubated at 37°C for 48 h. The control for incubation was performed by incubating the substrates in sterile LB with four replicas. After incubation, each sample was removed and washed three times to remove planktonic and poorly attached biofilm mass. To measure the level of total biofilm metabolic activity, MTT assay was performed. To this end, six substrates with attached biofilms for each strain were placed in a new sterile polystyrene 24-well plate, and 200 µL 0.05% MTT (3-(4,5-dimethylthiazol-2-yl)− 2,5-diphenyltetrazolium bromide; Sigma-Aldrich, UK) in LB was added to each sample and incubated at 37°C for 2 h, LB-MTT medium was sedimented at 10,000 g for 10 min, the sediment was resuspended in 200 µl DMSO, and also, 200 µL DMSO was added to each sample. Out of the final 400 µL of DMSO-dissolved formazan solution per sample, 100 µL was transferred to a polystyrene 96-well plate, and metabolic activity (A 570) was measured using a Multiskan FC Microplate Photometer (ThermoFisher Scientific, Waltham, MA, USA).

Biofilms formed onto PP-115- and PP-115/$PyrC_{12}$-DBS-coated substrates were also investigated by confocal laser scanning microscopy as it was done before.[45] The biofilms were stained with 1 mM ethidium bromide (Sigma-Aldrich) and 5 µg/mL calcofluor white solution (Sigma-Aldrich). No additional washing was used in order to limit the physical disruption of biofilm structures through liquid movement. The samples were not fixed, and a cover slip was placed over the stained samples before imaging. CLSM analysis was undertaken using a Leica TCS SPE confocal system with coded DMi8 inverted microscope (Leica, Germany) and Leica Application Suite X (LAS X) version 3.4.1. Images were acquired using excitation at 405 nm and emission collected at 450–500 nm for calcofluor white, and excitation at 532 nm and emission collected at 537–670 for ethidium bromide. The total pixels were calculated by the above-mentioned software.

Replicate data were processed using the statistical software package OriginPro 7.0 and MS Excel for Windows. All results are presented as the mean ± standard deviation. A value of $p < 0.05$ was considered statistically significant.

For biofouling testing, the painted stainless steel bars were fixed on experimental stand with the help of corrosion-resistant wire. Each series contained 12 samples. The stand with experimental substrates was dipped into water of Kaniv reservoir of the Dnipro River to a depth from 1 to 1.5 m. During the experiment sample, selections were carried out for 35 and 143 days. Removed substrates were fixed by 4% (w/w) formaldehyde solution for the following laboratory studies. The number (exemplars (ex)/m^2) and biomass (g/m^2) of hydrobionts was determined using the standard method.[46]

Results and discussion

IR analysis

Infrared spectroscopy was used both to confirm the presence of cationic biocide $PyrC_{12}$-DBS inside the coating and to reveal and identify specific interactions between PP-115 based on alkyd resin and the biocide.

In the IR spectrum of $PyrC_{12}$-DBS (Fig. 1), the strong bands in the 2800–3000 cm^{-1} region are associated with the alkyl chain of the compound. In particular, the band at 2923 cm^{-1} is attributed to the CH_2 asymmetric stretching mode and the band at 2853 cm^{-1} to CH_2 symmetric stretching mode. The two smaller intensity bands, observed at 2955 cm^{-1} and 2872 cm^{-1}, are assigned to the asymmetric and symmetric stretching vibrations of the methyl group.[47–49] The weak bands at 1635 and 1600 cm^{-1} are assigned to aromatic C=C stretching vibrations, the sharp peaks at 1489 and 1467 cm^{-1} to CH_2 bending vibrations,[47,50] and the bands at 1460 and 1377 cm^{-1} to asymmetric and symmetric bending vibrations of CH_3 groups.[48] In the region 1150–1260 cm^{-1}, the intense asymmetric broad band can reasonably be refined using five different vibrational modes assigned to aromatic C–H

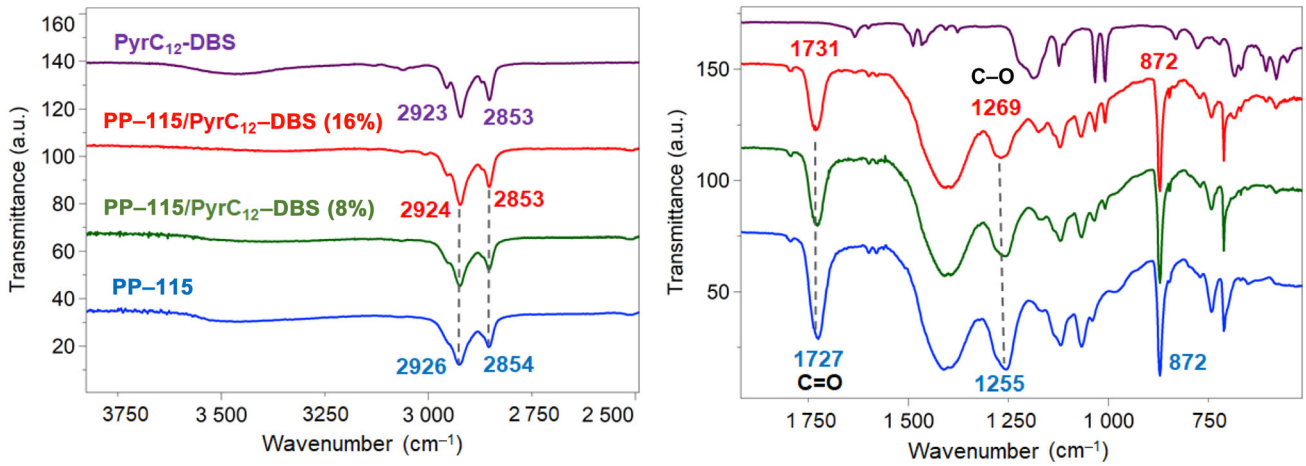

Fig. 1: IR spectra of cationic biocide and coatings based on alkyd resin

wagging (at 1227 cm^{-1}), C–N–C symmetric stretching vibrations (at 1192 cm^{-1}), asymmetric stretching vibrations of S=O group (at 1212 and 1177 cm^{-1}), and a combination of C–S stretching and alkyl C–C symmetric stretching vibrations (at 1160 cm^{-1}).[51,52] The asymmetric band at 1124 cm^{-1} is attributed to a combination of the benzene ring breathing vibration and SO_3 stretching mode.[51,52]

IR spectrum of control coating PP-115 based on alkyd resin (Fig. 1) contains a broad band with low absorption in the region 3600-3400 cm^{-1}, assigned to stretching vibrations of hydrogen-bonded hydroxyl groups.[53] This indicates the presence of a small number of unreacted OH groups of the free pentaerythritol in the polymer binder. In the high wavenumber region, the bands at 2926 and 2854 cm^{-1} are assigned to CH_2 asymmetric and symmetric stretching vibrations, respectively. The strong band at 1727 cm^{-1} is assigned to the stretching vibrations of C=O groups and the observation of an asymmetric broad bands between 1370 and 1500, and two well-defined bands at 872 cm^{-1} and 711 cm^{-1} confirm the presence of $CaCO_3$ polymorph.[54,55] These bands are commonly attributed to the asymmetric stretching modes and the asymmetric and symmetric deformations of the calcite, respectively.[56] However, the band at 711 cm^{-1} being asymmetrical with a shoulder around 700 cm^{-1}, the presence of an aragonite phase in the paint cannot be excluded. Finally, the absorption band at 1255 cm^{-1} indicates the presence of C–O stretching vibrations of ester groups, while the bands at 1120 and 1067 cm^{-1} are assigned to the stretching vibrations of C–O bonds from free OH groups.[53]

A comparison of the IR spectra of pure PP-115 paint and PP-115/$PyrC_{12}$-DBS (16%) reveals that the characteristic peak of the carbonyl band shifts by 4 cm^{-1} to higher frequencies concomitantly with a significant shift from 1255 to 1269 cm^{-1} of the C–O stretching mode of the ester groups. The peak position associated with the deformation of $CaCO_3$ not being impacted by the introduction of the cationic biocide, we compared

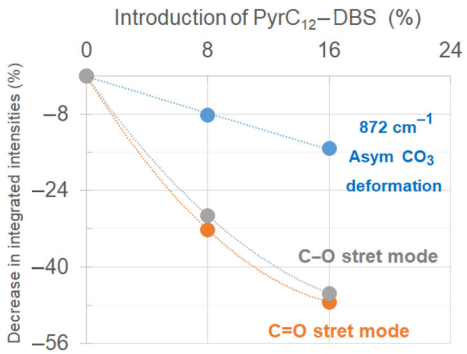

Fig. 2: Evolution of integrated intensities of asymmetric CO_3 deformation, C=O and C–O stretching modes with the introduction of $PyrC_{12}$-DBS content

the loss of integrated intensity of this mode, with those associated with the C = O and C–O stretching modes (Fig. 2). While the intensity loss follows a linear law for the $CaCO_3$ deformation mode, in accordance with the introduction of 8 and 16% of biocide, the intensity loss for the other two modes is similar and much faster, confirming strong physicochemical interactions with these functional groups. C–H bonds in ortho-position of pyridinium cation being slightly acidic due to the lowest electron density on carbon atoms,[57] hydrogen bonding may thus occur between C–H groups of $PyrC_{12}$-DBS and carbonyl oxygen of ester groups carrying partial negative charge (Scheme 2).

Morphological and surface properties

Surface roughness is known to promote water organism settlement since it creates appropriate attachment points for bioadhesion.[9] Thus, smooth surfaces are considered much more resistant to biofouling.[3,9] The 3D surface topography of the PP-115-based coatings was studied using a confocal white-light optical imag-

ing profiler (Fig. 3). The root mean square roughness Sq describes the root mean square average of height deviations taken from the mean data plane and the average roughness Sa describes the difference in height of each point compared to the arithmetical mean of the surface. These values determined on the same surface dimension (340 × 284 μm^2) are similar, which shows that the introduction of the biocide does not modify the surface roughness. Overall, the prepared PP-115/PyrC$_{12}$-DBS coatings can be considered smooth since their surface roughness is only twice that of commercial silicone-based marine coating.[3]

To quantitatively assess the variation in wettability of the surface of the films induced by the introduction of biocide, static water contact angle measurements were taken. The results are illustrated in Fig. 4. The surface of neat PP-115 coating has water contact angle (θ_ω) of 100°, which indicates high hydrophobicity.[58] Modified PP-115/PyrC$_{12}$-DBS coatings showed significantly higher wettability which is manifested by a strong decrease of θ_ω values (Fig. 4). This effect is probably due to the predominant orientation of the polar groups of the cationic biocide on the surface of the polymer matrix, thus allowing the formation of a hydration layer by means of hydrogen bonding between the water molecules and 1-dodecylpyridinium salt. This wettability is significant enough to reduce the adhesion of proteins to the surface and then the initial attachment and subsequent accumulation of fouling organisms.[59–61]

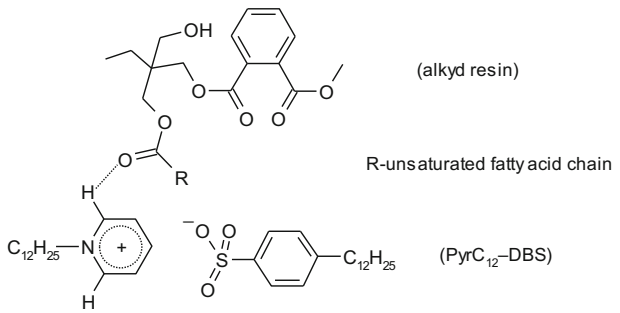

Scheme 2: Hydrogen bonding between alkyd resin and cationic biocide

Raman imaging

In order to localize the chemical modifications of the coating surfaces after introduction of the biocide, Raman spectra were recorded for each sample over an area of 40 × 40 μm^2 (2D map step of 1 μm) and a true component analysis (TCA) was performed. This dedicated tool of the WITec Project FIVE plus software helps to identify pixels in a map with similar spectral features and provide these spectral characteristics (i.e., similar chemical response) in an image of

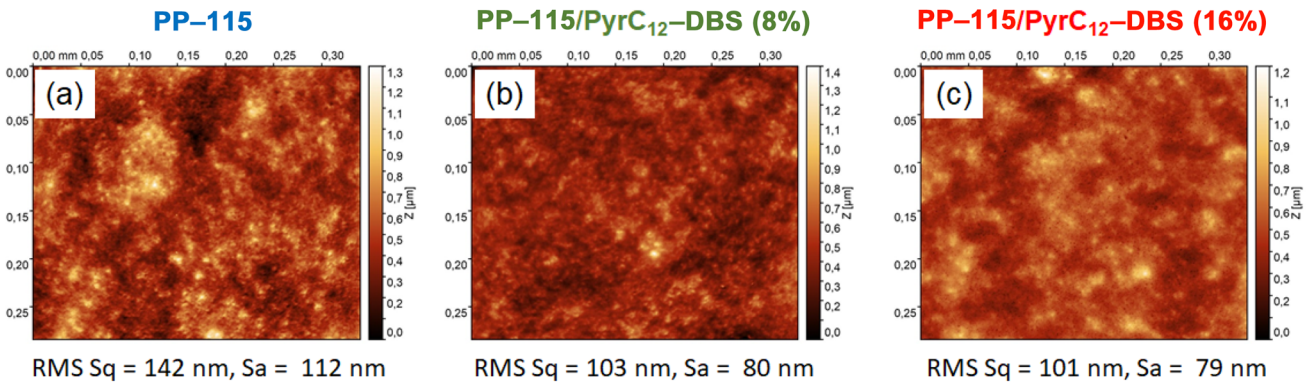

Fig. 3: 2D topographical images obtained with an optical confocal profiler: (a) control PP-115 coating, (b) modified PP-115/PyrC$_{12}$-DBS (8%) coating, and (c) modified PP-115/PyrC$_{12}$-DBS (16%) coating. The root mean square roughness (RMS) Sq and the arithmetic mean roughness Sa are given below each image

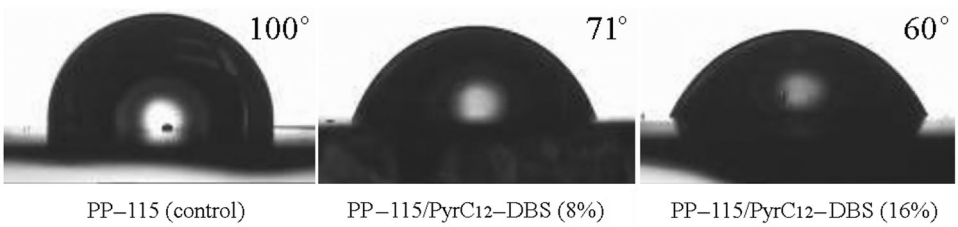

Fig. 4: Photographs of water droplets on the surface of coatings

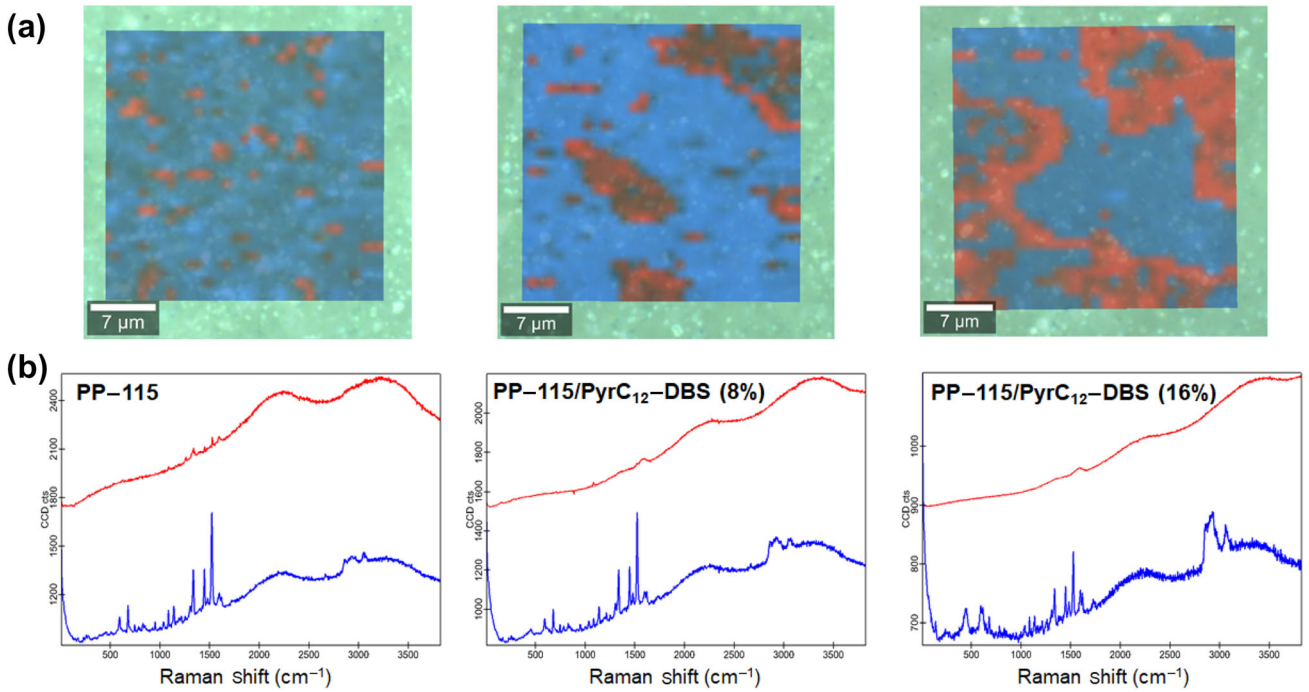

Fig. 5: Raman mapping based on 1600 spectra recoded in 40 × 40 µm^2 area. (a) True component analysis identified two major spectral components for both samples. The identified components are shown in (b). For clarity, all Raman spectra were shifted in intensity

intensity distribution (Fig. 5). The spectral signatures coded in blue (component 1) can be attributed to the average spectrum of the alkyd (pentaphthalic) varnish. The second component (coded in red) is characterized by a strong luminescence whose surface proportion increases with the introduction of the biocide. This 2D representation reveals the chemical inhomogeneity of the surface. In the case of the PP-115 paint, the red areas represent 8% of the total surface likely due to the presence of pigments and/or fillers. This proportion increases to about 20% and 40% with the introduction of 8 wt% and 16 wt% of biocide, respectively, thus suggesting that the composition of the film is not homogeneous in the thickness and that an increasing part of biocide is found on the surface during drying. This result could then explain the strong decrease in the contact angle with water when the content of biocide is increased and thus the modification of the surface properties.

EDX imaging

The distribution of the biocide in the coating was evaluated by means of energy-dispersive X-ray spectroscopy (EDX). As a reference element to evaluate the homogeneity of biocide distribution, sulfur was selected as it is present in biocide counterion and is absent in the content of neat PP-115 paint, which is confirmed by the results presented in Fig. S1 and Table S1.

Figure 6 shows the distribution of sulfur (S) in all samples. Images, as well as element analysis, show the absence of sulfur in the neat paint, while both samples with biocide demonstrate noticeable sulfur content. Overall, the results of SEM and EDX analysis indicate high homogeneity of modified coatings, as well as homogeneous distribution of the elements in the bulk of samples (Fig. S2).

DSC analysis

Influence of the $PyrC_{12}$-DBS content on the T_g value of PP-115 was investigated via DSC method. On the thermogram of the cationic biocide $PyrC_{12}$-DBS (Fig. 7a), T_g is observed at − 68°C, crystallization occurs at − 13°C, and then, melting point occurs at 5°C. PP-115 demonstrates T_g around 3°C, and also, each of the composites, PP-115/$PyrC_{12}$-DBS (8%) and PP-115/$PyrC_{12}$-DBS (16%) exhibits only one T_g, at − 10°C and − 17°C, respectively (Fig. 7b). No other phase transitions can be observed on the thermograms of the composites, which indicates that no phase separation occurred, and the paint formed with the additive a homogeneous mixture. Moreover, T_g value decreases with the growth of $PyrC_{12}$-DBS content, which shows that the additive, presumably, serves as a plasticizer.

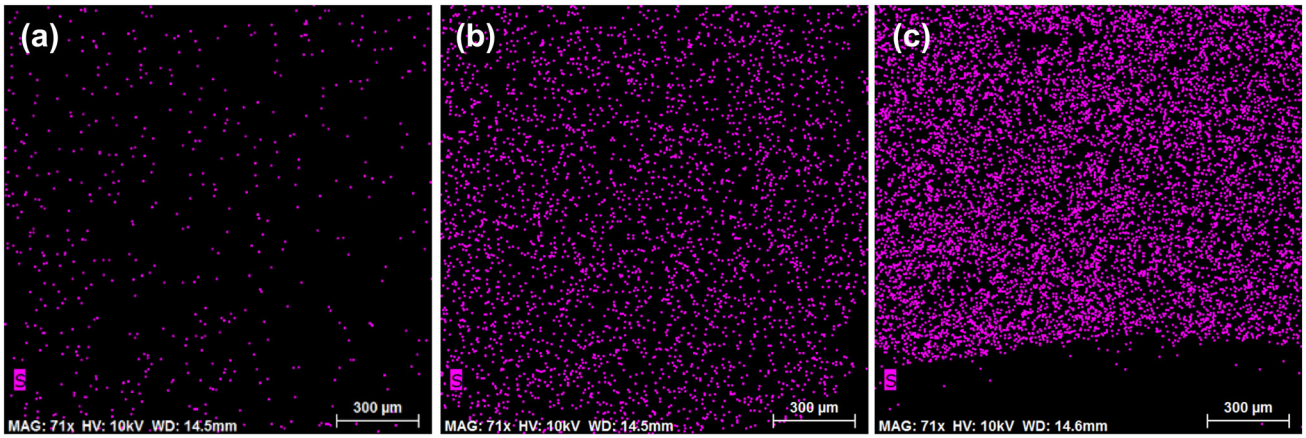

Fig. 6: Energy-dispersive X-ray spectroscopy elemental maps (S) in PP-115 (a), PP-115/PyrC$_{12}$-DBS (8%) (b), and PP-115/PyrC$_{12}$-DBS (16%) (c) coatings

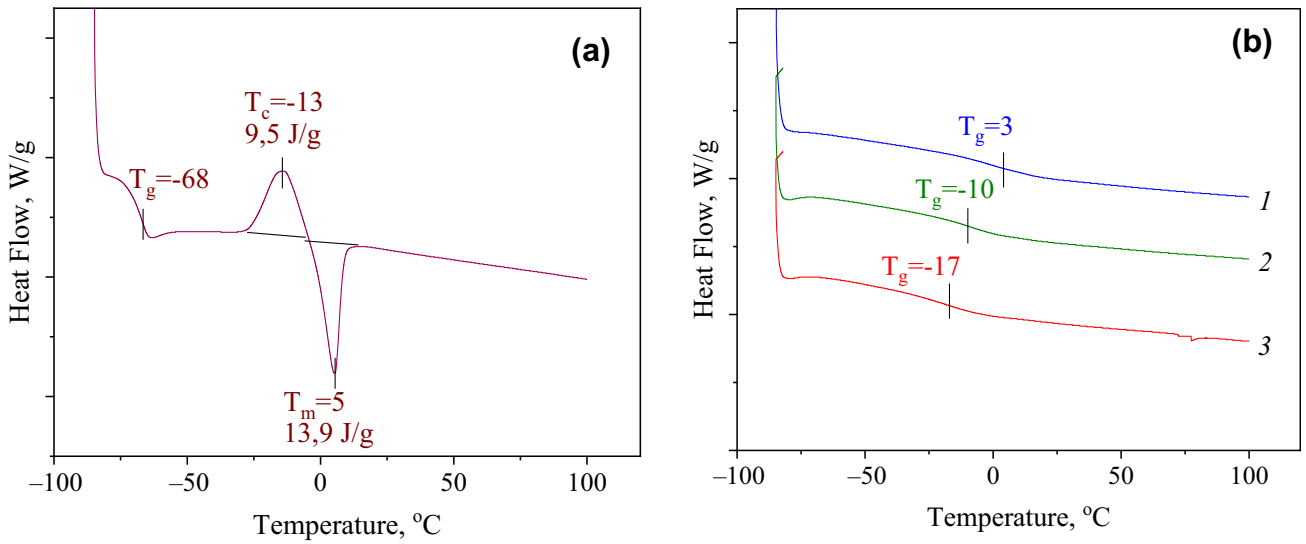

Fig. 7: DSC curves: (a) PyrC$_{12}$-DBS, (b) 1—PP-115 (control), 2—PP-115/PyrC$_{12}$-DBS (8%), 3—PP-115/PyrC$_{12}$-DBS (16%)

Leaching resistance of PyrC$_{12}$-DBS

UV–visible absorption spectroscopy is a convenient method to determine the concentrations of onium salts in water. Specifically, pyridinium salts with conjugated cation are easily detectable.[44] The results of spectrophotometric study of biocide release from PP-115 coating are illustrated in Fig. 9. UV spectrum of PyrC$_{12}$-Cl, which is water-soluble precursor for the synthesis of PyrC$_{12}$-DBS, contains two intensive peaks at 214 and 259 nm (Fig. 8, curve 1). These peaks are assigned to n–π * and π–π* electronic transitions of pyridine ring. The calibrating graph was found to be linear in the concentration range of 1.5×10^{-5}–1.5×10^{-4} mol/L at λ_{max} 259 nm. However, no signal of pyridinium cation was detected in water solution after its 60-day contact with PP-115/PyrC$_{12}$-DBS-coated steel panel (Fig. 8, curve 2). The obtained results indicate a high resistance of the cationic biocide to leaching from the protective coating which in turn is important for the potential durability of the antifouling activity of the coating, as well as for its minimal environmental impact.

Antibiofilm activity of PP-115/PyrC$_{12}$-DBS coatings

Biofilms are microbial-derived sessile communities, characterized by cells that are irreversibly attached to a surface, an interface, or to each other.[62] The microbial cells are embedded in a matrix of self-produced extracellular polymeric substances (EPS) and exhibit far more resistance to adverse environmental conditions, as well as antimicrobial agents. Therefore, understanding the mechanisms of biofilm formation is of fundamental importance to develop innovative methods to prevent biofilm growth and/or to remove

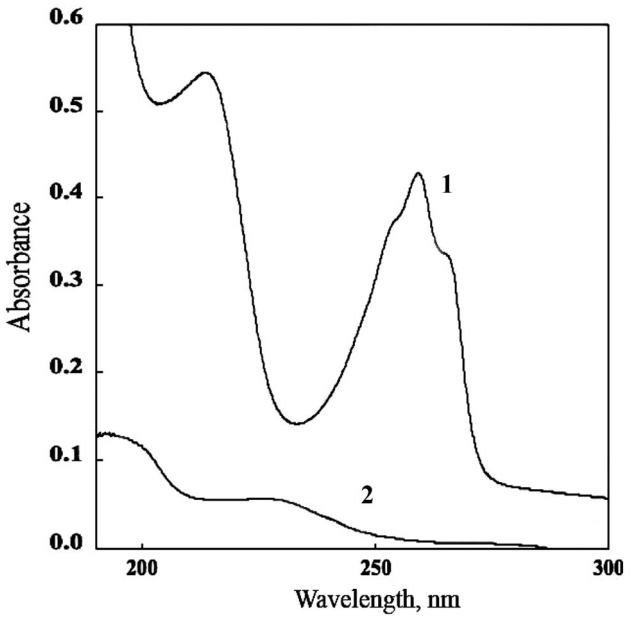

Fig. 8: UV spectra of $PyrC_{12}$-Cl (1) (C = 1 × 10^{-4} mol/L) and water solution after 60-day contact with PP-115/$PyrC_{12}$-DBS (16%)-coated substrate (2)

established biofilms. Most of the antibiofilm strategies that are currently used involve inhibition of bacterial adhesion to the surface and bacterial colonization,[3,63,64] interference with the signal molecules that modulates biofilm development,[65] and disaggregation of the biofilm matrix.[61,65] Although several strategies have been realized to deter bioadhesion, biocides, by far, still provide the most effective prevention of biofouling.[1–3]

The capability of both PP-115 and PP-115/$PyrC_{12}$-DBS to be biofouled was investigated using two standard bacterial strains *S. aureus* ATCC 25923 and *P. aeruginosa* PA 01. For this, the total metabolic activity of the 48-hour biofilms developed onto tested surfaces was measured (Fig. 9). For both gram-positive and gram-negative tested cultures, a significant drop in the metabolic activity was observed.

The decrease in biofilm metabolic activity correlated with the decrease in cell biomass observed microscopically (Figs. 10, 11). Interestingly, the $PyrC_{12}$-DBS (16%) influenced the biofilm matrix structure reducing polysaccharide content in both biofilms.

It should be noted that PP-115/$PyrC_{12}$-DBS (8%) coatings did not demonstrate noticeable antibiofilm activity (not shown in figures). Thus, the obtained results confirm the fact that the high loading of nonleaching biocide is required to prepare contact-active antibacterial surfaces.[21,35,40,41] Probably, good compatibility of $PyrC_{12}$-DBS with alkyd matrix leads to immobilization of essential part of biocide in the bulk of the resin, thus decreasing its efficient concentration at the surface.

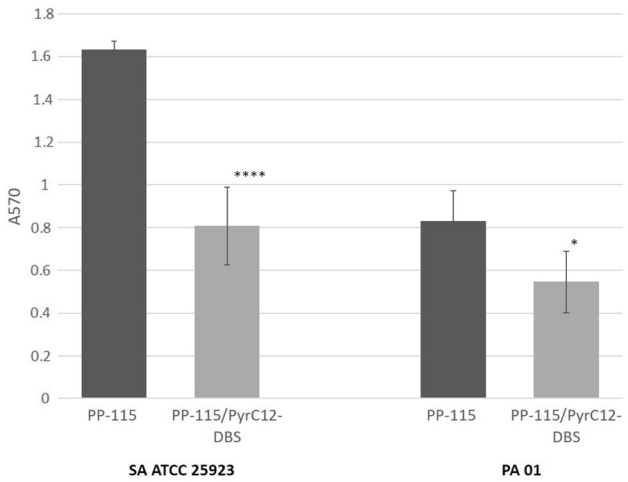

Fig. 9: The level of metabolic activity of *S. aureus* ATCC 25923 (left) and *P. aeruginosa* PA 01 (right) biofilms formed onto PP-115 (control) and PP-115/$PyrC_{12}$-DBS (16%)-coated substrate following 48 h of incubation determined by MTT staining and measured as the optical density at 570 nm (OD570). Statistical significance compared to control (no XXX added), * $p < 0.05$, **** $p < 0.001$

Antifouling activity of PP-115/$PyrC_{12}$-DBS coating

Figure 12 shows a photograph of experimental substrates after their exposure in the Dnipro River for 143 days. The surface of control coating (neat PP-115) contained 11 defined lower taxons (DLT). The total number of DLT was 52667 ± 4345 ex/m^2 which formed a biomass value of 5891 g/m^2 ± 613 g/m^2. The biofouling was determined mainly by *Dreissena polymorpha* (54% by number and 93% by mass). The surface of steel bars coated with PP-115/$PyrC_{12}$-DBS (16%) was found to have much higher biofouling resistance (Fig. 12) and contained ten DLT with a total number of 2559 ± 320 ex/m^2 and a biomass value of 430 g/m^2 ± 51 g/m^2. Similar to the control samples, *Dreissena polymorpha* formed the majority of fouling biomass (59% by number and 98% by biomass).

Thus, after 4.5-month exposure in freshwater the surface of coatings containing cationic biocide $PyrC_{12}$-DBS had more than an order of magnitude less fouling biomass compared to the control substrates. It should be noted that no difference was observed for antifouling activity of control PP-115 coatings and PP-115/$PyrC_{12}$-DBS coatings with 8% biocide content (not shown). These data agree with previously reported ones which indicate that relatively high content of water-immiscible biocide in the coating is required to impart its resistance to biofouling.[66,67] However, the question still remains about the durability of such coatings since they are often considered to be self-deactivating, because killed fouling organisms may adhere to the active layer and therefore deactivate it.[35]

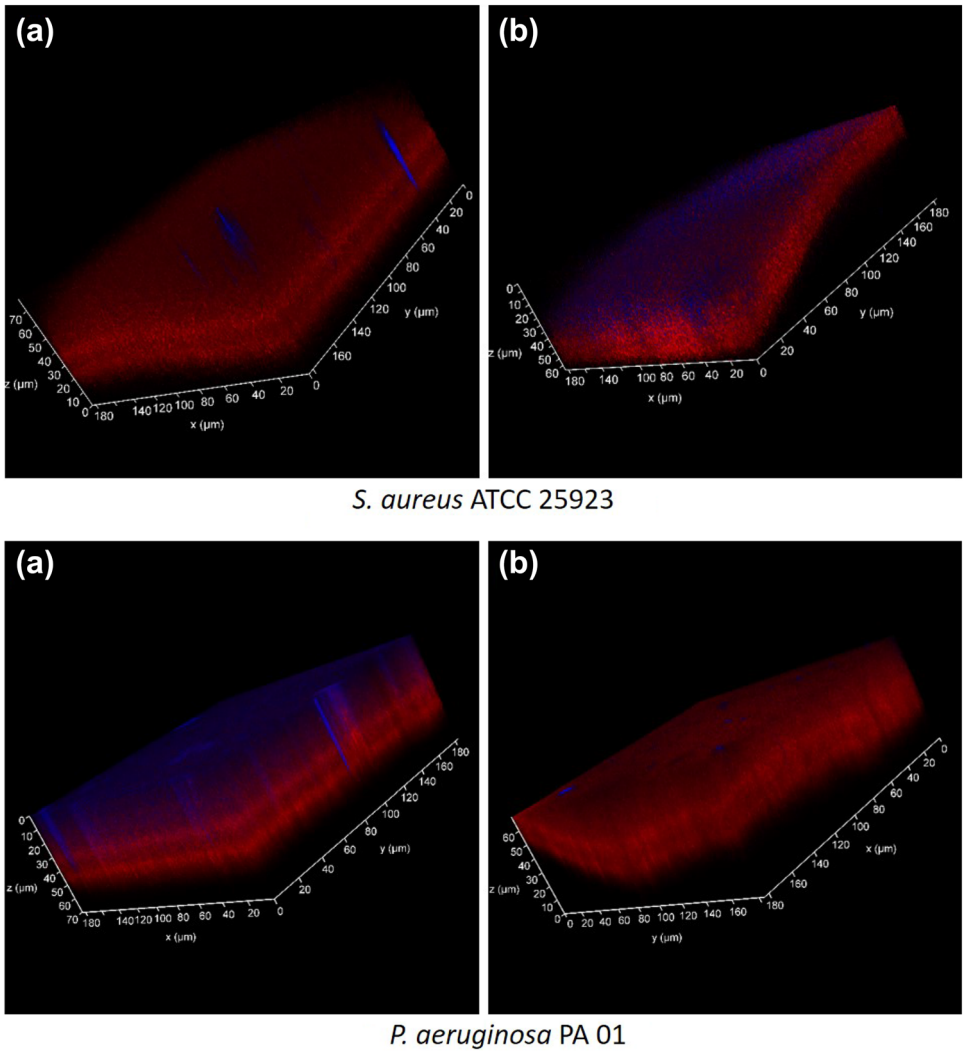

Fig. 10: CLSM imaging of *S. aureus* ATCC 25923 and *P. aeruginosa* PA 01 biofilms formed onto PP-115-coated (a) and PP-115/PyrC_{12}-DBS (16%)-coated (b) substrate following 48 h of incubation. Ethidium bromide (red signal) was used to visualize cells, and calcofluor (blue signal) was used to visualize biofilm-associated carbohydrates (Color figure online)

Conclusions

Water-immiscible cationic biocide 1-dodecylpyridinium dodecylbenzenesulfonate (PyrC_{12}-DBS) has been synthesized by anion metathesis between water-soluble precursor 1-dodecylpyridinium chloride and sodium dodecylbenzenesulfonate. PyrC_{12}-DBS has been evaluated as a potential antifouling additive for commercial alkyd paint PP-115. Thus, modified PP-115/PyrC_{12}-DBS coatings containing 8 and 16 wt% of PyrC_{12}-DBS were prepared by direct dissolution of cationic biocide in the paint followed by painting of the stainless steel bars. The results of energy-dispersive X-ray spectroscopy (EDX) study revealed homogeneous distribution of the biocide in the coatings. The analysis of 3D surface topography of the coatings by a confocal white-light optical imaging profiler has shown that the introduction of PyrC_{12}-DBS does not modify the surface roughness. The surface wettability of PP-115 coating was found to be significantly increased when modified with cationic biocide that was manifested in a sharp reduction of water contact angle. IR analysis revealed physicochemical interaction between ester groups of alkyd binder and PyrC_{12}-DBS mainly via hydrogen bonding. Moreover, the plasticizing effect of the cationic biocide on the alkyd binder has been revealed by differential scanning calorimetry. According to results of spectrophotometric analysis, no signal of 1-dodecylpyridinium cation was detected in water after 60-day contact with PP-115/PyrC_{12}-DBS coatings. This indicates excellent resistance of biocidal additive to leaching.

Antibiofilm activity of PP-115/PyrC_{12}-DBS coatings was evaluated against two biofilm-forming model strains, *Staphylococcus aureus* ATCC 25923 and *Pseudomonas aeruginosa* PA01. The decrease in biofilm metabolic activity, as well as in cell biomass attached to the surface was determined only for PP-115/PyrC_{12}-

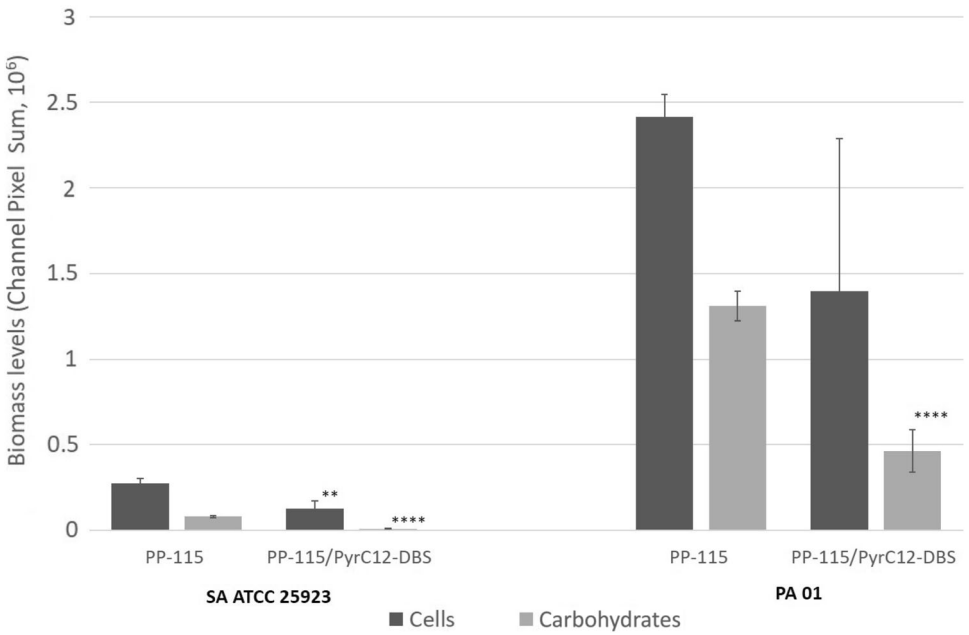

Fig. 11: The level of cell biofilm biomass (dark gray) and carbohydrate biofilm matrix (light gray) of *S. aureus* ATCC 25923 and *P. aeruginosa* PA01 biofilms formed onto PP-115-coated (control) and PP-115/PyrC$_{12}$-DBS (16%)-coated substrate following 48 h of incubation determined as the corresponding channel pixel sum calculated from the Fig. 10, where the cell biofilm biomass was tagged by ethidium bromide (red signal) and the carbohydrate biofilm matrix was tagged by calcofluor white (blue signal). Statistical significance compared to control, ** $p < 0.01$, **** $p < 0.001$

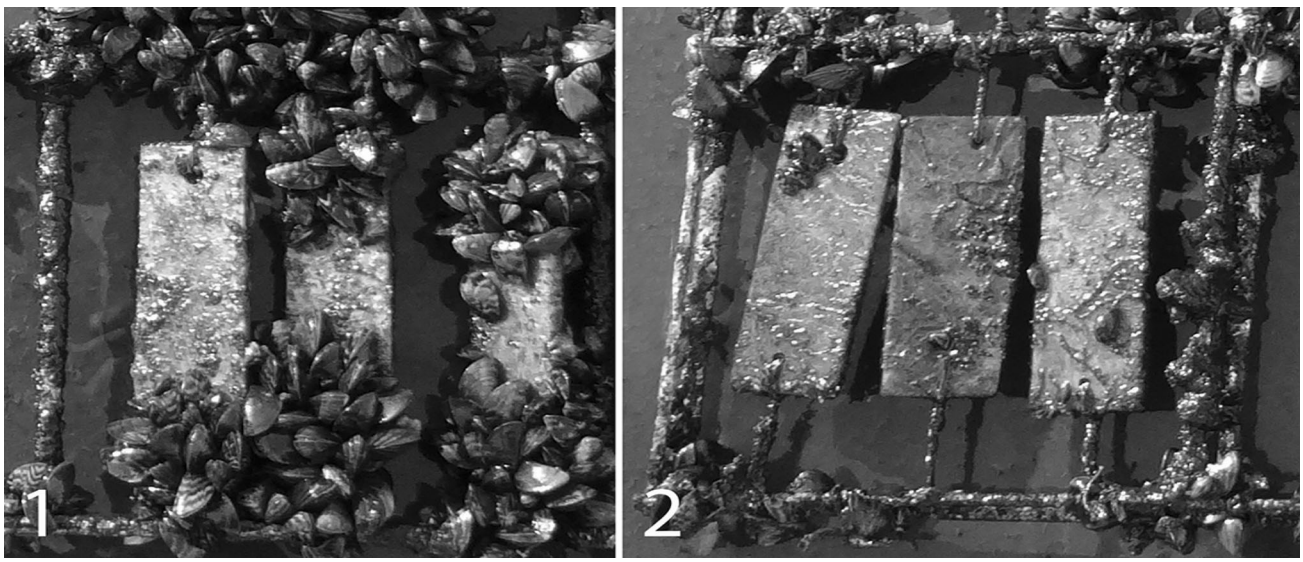

Fig. 12: Painted steel bars after 143-day exposure in the Dnipro River: 1—PP-115 (control coating), 2—PP-115/PyrC$_{12}$-DBS (16%)

DBS (16%) coatings. After 143-day exposure of experimental substrates in freshwater of the Dnipro River, the surface of PP-115/PyrC$_{12}$-DBS (16%) coatings showed almost a 13-fold reduction of total biomass formed by Dreissenidae mussels, compared with control substrates. For lower biocide content (8%), no difference in antifouling activity of modified and control coatings was detected. Overall, the obtained data indicate that the fabrication of contact-active protective coatings based on water-insoluble polymer matrix and water-insoluble biocide can be considered a promising approach to control biofouling in freshwater. However, relatively high biocide content is required to impart efficient antifouling activity to the coating.

Author contributions SR and OM were involved in conceptualization; J-FB and OP were involved in methodology and data curation; OM, J-FB, OD, OT, AH, AMD, and IM were involved in investigation; YL was involved in formal analysis; and SR and J-FB were involved in writing–original draft preparation.

Funding No funds, grants, or other support was received.

Data availability The authors declare that the data supporting the findings of this study are available within the paper. Should any raw data files be needed in another format they are available from the corresponding author upon reasonable request. Source data are provided with this paper.

Conflict of interest The authors declare that they have no conflict of interest. The authors have no competing interests to declare that are relevant to the content of this article.

References

1. Liu, D, Shu, H, Zhou, J, Bai, X, Cao, P, ''Research Progress on New Environmentally Friendly Antifouling Coatings in Marine Settings: A Review.'' *Biomimetics*, **8** (2) 200 (2023)
2. Del Grosso, CA, McCarthy, TW, Clark, CL, Cloud, JL, Wilker, JJ, ''Managing Redox Chemistry to Deter Marine Biological Adhesion.'' *Chem. Mater.*, **28** 6791–6796 (2016)
3. Faria, SI, Teixeira-Santos, R, Gomes, LC, Silva, ER, Morais, J, Vasconcelos, V, Mergulhão, FJM, ''Experimental Assessment of the Performance of Two Marine Coatings to Curb Biofilm Formation of Microfoulers.'' *Coatings*, **10** 893 (2020)
4. Tu, C, Chen, T, Zhou, Q, Liu, Y, Wei, J, Waniek, JJ, Luo, Y, ''Biofilm Formation and Its Influences on the Properties of Microplastics as Affected by Exposure Time and Depth in the Seawater.'' *Sci. Total Environ.*, **734** 139237 (2020)
5. Gormley, K, McLellan, F, McCabe, C, Hinon, C, Ferris, J, Kline, DI, Scott, BE, ''Automated Image Analysis of Offshore Infrastructure Marine Biofouling.'' *J. Mar. Sci. Eng.*, **6** 2 (2018)
6. Rao, TS, ''Biofouling in Industrial Water Systems.'' In: Amjad, Z, Demadis, KD (eds.) *Minerals Scales and Deposits*, pp. 123–140. Elsevier, New Jersey (2015)
7. Mathew, NT, Kronholm, J, Bertilsson, K, Despeisse, M, Johansson, B, ''Environmental and Economic Impacts of Biofouling on Marine and Coastal Heat Exchangers.'' In: Kishita, Y, Matsumoto, M, Inoue, M, Fukushige, S (eds.) *EcoDesign and Sustainability II. Sustainable Production, Life Cycle Engineering and Management*. Springer, Singapore (2021)
8. Liu, S, Kee, Y-H, Shang, B, Papanikolaou, A, ''Assessment of the Economic, Environmental and Safety Impact of Biofouling on a Ship's Hull and Propeller.'' *Ocean Eng.*, **285** 115481 (2023)
9. Lindholdt, A, Dam-Johansen, K, Olsen, SM, Yebra, DM, Kiil, S, ''Effects of Biofouling Development on Drag Forces of Hull Coatings for Ocean-Going Ships: A Review.'' *J. Coat. Technol. Res.*, **12** (3) 415–444 (2015)
10. Dong, M, Liu, L, Wang, D, Li, M, Yang, J, Chen, J, ''Synthesis and Properties of Self-Polishing Antifouling Coatings Based on BIT-Acrylate Resins.'' *Coatings*, **12** 891 (2022)
11. Olsen, SM, Yebra, DM, ''On the Use of the Term 'Self-Polishing' for Antifouling Paints.'' *Prog. Org. Coat.*, **76** 1699–1700 (2013)
12. Ytreberg, E, Lagerström, M, Nöu, S, Wiklund, A-K, ''Environmental Risk Assessment of Using Antifouling Paints on Pleasure Crafts in European Union Waters.'' *J. Environ. Manage.*, **281** 111846 (2021)
13. Lagerström, M, Ytreberg, E, Wiklund, A-K, ''Antifouling Paints Leach Copper in Excess–Study of Metal Release Rates and Efficacy Along a Salinity Gradient.'' *Water Res.*, **186** 116383 (2020)
14. Cima, F, Varello, R, ''Potential Disruptive Effects of Copper-Based Antifouling Paints on the Biodiversity of Coastal Macrofouling Communities.'' *Environ. Sci. Pollut. Res.*, **30** 8633–8646 (2023)
15. Miller, RJ, Adeleye, AS, Page, HM, Kui, L, Lenihan, HS, Keller, AA, ''Nano and Traditional Copper and Zinc Antifouling Coatings: Metal Release and Impact on Marine Sessile Invertebrate Communities.'' *J. Nanopart. Res.*, **22** 129 (2020)
16. Lagerström, M, Ferreira, J, Ytreberg, E, Eriksson-Wiklund, A-K, ''Flawed Risk Assessment of Antifouling Paints Leads to Exceedance of Guideline Values in Baltic Sea Marinas.'' *Environ. Sci. Pollut. Res.*, **27** 27674–27687 (2020)
17. Guardiola, FA, Cuesta, A, Meseguer, J, Esteban, MA, ''Risks of Using Antifouling Biocides in Aquaculture.'' *Int. J. Mol. Sci.*, **13** 1541–1560 (2012)
18. Onduka, T, Ojima, D, Ito, M, Ito, K, Mochida, K, Fujii, K, ''Toxicity of the Antifouling Biocide Sea-Nine 211 to Marine Algae, Crustacea, and a Polychaete.'' *Fish Sci.*, **79** 999–1006 (2013)
19. Silva, ER, Tulcidas, AV, Ferreira, O, Bayón, R, Igartua, A, Mendoza, G, Mergulhão, FJM, Faria, SI, Gomes, LC, Carvalho, S, Bordado, JCM, ''Assessment of the Environmental Compatibility and Antifouling Performance of an Innovative Biocidal and Foul-release Multifunctional Marine Coating.'' *Environ. Res.*, **198** 111219 (2021)
20. Machate, O, Dellen, J, Schulze, T, Wentzky, VC, Krauss, M, Brack, W, ''Evidence for Antifouling Biocides as One of the Limiting Factors for the Recovery of Macrophyte Communities in Lakes of Schleswig-Holstein.'' *Environ. Sci. Eur.*, **33** 57 (2021)
21. Lewis, K, Klibanov, AM, ''Surpassing Nature: Rational Design of Sterile-Surface Materials.'' *Trends Biotechnol.*, **23** (7) 343–348 (2005)
22. Cuervo-Rodríguez, R, López-Fabal, F, Gómez-Garcés, JL, Muñoz-Bonilla, A, Fernández-García, M, ''Contact Active Antimicrobial Coatings Prepared by Polymer Blending.'' *Macromol. Biosci.*, **17** 1700258 (2017)
23. Izmaylov, B, Di Gioia, D, Markova, G, Aloisio, I, Colonna, M, Vasnev, V, ''Imidazolium Salts Grafted on Cotton Fibers for Long-Term Antimicrobial Activity.'' *React. Funct. Polym.*, **87** 22–28 (2015)
24. Poverenov, E, Klein, M, ''Formation of Contact Active Antimicrobial Surfaces by Covalent Grafting of Quaternary Ammonium Compounds.'' *Colloids Surf. B: Biointerfaces*, **169** 195–205 (2018)
25. Reddy, GKK, Nancharaiah, YV, ''Alkylimidazolium Ionic Liquids for Biofilm Control: Experimental Studies on Controlling Multispecies Biofilms in Natural Waters.'' *J. Mol. Liq.*, **336** 116859 (2021)
26. Cornellas, A, Perez, L, Comelles, F, Ribosa, I, Manresa, A, ''Self-Aggregation and Antimicrobial Activity of Imida-

zolium and Pyridinium Based Ionic Liquids in Water Solutions.'' *J. Colloid Interface Sci.*, **355** 164–171 (2011)
27. Vereshchagin, AN, Frolov, NA, Egorova, KS, Seitkalieva, MM, Ananikov, VP, ''Quaternary Ammonium Compounds (QACs) and Ionic Liquids (ILs) as Biocides: From Simple Antiseptics to Tunable Antimicrobials.'' *Int. J. Mol. Sci.*, **22** 6793 (2021)
28. Bergamo, VZ, Donato, RK, Dalla Lana, DF, Donato, KJZ, Ortega, GG, Schrekker, HS, Fuentefria, AM, ''Imidazolium Salts as Antifungal Agents: Strong Antibiofilm Activity Against Multidrug-Resistant *Candida tropicalis* Isolates.'' *Lett. Appl. Microbiol.*, **60** 66–67 (2014)
29. Reddy, GKK, Nancharaiah, YV, Venugopalan, VP, ''Long Alkyl-Chain Imidazolium Ionic Liquids: Antibiofilm Activity Against Phototrophic Biofilms.'' *Colloids Surf. B. Biointerfaces.*, **155** 487–496 (2017)
30. Semenyuta, I, Trush, M, Kovalishyn, V, Rogalsky, S, Hodyna, D, Karpov, P, Xia, Z, Tetko, I, Metelytsia, L, ''Structure-Activity Relationship Modeling and Experimental Validation of the Imidazolium and Pyridinium Based Ionic Liquids as Potential Antibacterials of MDR *Acinetobacter baumannii* and *Staphylococcus aureus.*'' *Int. J. Mol. Sci.*, **22** 563 (2021)
31. Gilbert, P, Moore, LE, ''Cationic Antiseptics: Diversity of Action Under a Common Epithet.'' *J. Appl. Microbiol.*, **99** 703–715 (2005)
32. Tischer, M, Pradel, G, Ohlsen, K, Holzgrabe, U, ''Quaternary Ammonium Salts and Their Antimicrobial Potential: Targets or Nonspecific Interactions?'' *Chem. Med. Chem.*, **7** 22–31 (2012)
33. Reddy, GKK, Rajitha, K, Nancharaiah, YV, ''Antibiofouling Potential of 1-Alkyl-3-Methylimidazolium Ionic Liquids: Studies Against Biofouling Barnacle Larvae.'' *J. Mol. Liq.*, **302** 112497 (2020)
34. Piazza, V, Dragić, I, Cepčić, K, Faimali, M, Garaventa, F, Turk, T, Berne, S, ''Antifouling Activity of Synthetic Alkylpyridinium Polymers Using the Barnacle Model.'' *Mar. Drugs*, **12** 1959–1976 (2014)
35. Siedenbiedel, F, Tiller, JC, ''Antimicrobial Polymers in Solution and on Surfaces: Overview and Functional Principles.'' *Polymers*, **4** 46–71 (2012)
36. Walczak, M, Richert, A, Burkowska-But, A, ''The Effect of Polyhexamethylene Guanidine Hydrochloride (PHMG) Derivatives Introduced into Polylactide (PLA) on the Activity of Bacterial Enzymes.'' *J. Ind. Microbiol. Biotechnol.*, **41** 1719–1724 (2014)
37. Rogalsky, S, Bardeau, J-F, Wu, H, Lyoshina, L, Bulko, O, Tarasyuk, O, Makhno, S, Cherniavska, T, Kyselov, Y, Koo, JH, ''Structural, Thermal and Antibacterial Properties of Polyamide 11/Polymeric Biocide Polyhexamethylene Guanidine Dodecylbenzenesulfonate Composites.'' *J. Mater. Sci.*, **51** 7716–7730 (2016)
38. Ghamrawi, S, Bouchara, J-P, Tarasyuk, O, Rogalsky, S, Lyoshina, L, Bulko, O, Bardeau, J-F, ''Promising Silicones Modified with Cationic Biocides for the Development of Antimicrobial Medical Devices.'' *Mater. Sci. Eng. C*, **75** 969–979 (2017)
39. Swiontek Brzezinska, M, Walczak, M, Jankiewizs, U, Pejchalová, M, ''Antimicrobial Activity of Polyhexamethylene Guanidine Derivatives Introduced into Polycaprolactone.'' *J. Polym. Environ.*, **26** (2) 589–595 (2018)
40. Moshynets, O, Bardeau, J-F, Tarasyuk, O, Makhno, S, Cherniavska, T, Dzhuzha, O, Potters, G, Rogalsky, S, ''Antibiofilm Activity of Polyamide 11 Modified with Thermally Stable Polymeric Biocide Polyhexamethylene Guanidine 2-Naphtalenesulfonate.'' *Int. J. Mol. Sci.*, **20** (2) 348 (2019)
41. Nigmatullin, R, Gao, F, Konovalova, V, ''Permanent, Non-Leaching Antimicrobial Polyamide Nanocomposites Based on Organoclays Modified with a Cationic Polymer.'' *Macromol. Mater. Eng.*, **294** 795–805 (2009)
42. Inásio, ÂS, Domingues, NS, Nunes, A, Martins, PT, Moreno, MJ, Estronca, LM, Fernandes, R, Moreno, AJM, Borrego, MJ, Gomes, JP, Vaz, WLC, Vieira, OV, ''Quaternary Ammonium Surfactant Structure Determines Selective Toxicity Towards Bacteria: Mechanism of Action and Clinical Implications in Antibacterial Prophylaxis.'' *J. Antimicrob. Chemother.*, **71** 641–654 (2016)
43. Trush, M, Metelytsia, L, Semenyuta, I, Kalashnikova, L, Papeykin, O, Venger, I, Tarasyuk, O, Bodachivska, L, Blagodatnyi, V, Rogalsky, S, ''Reduced Ecotoxicity and Improved Biodegradability of Cationic Biocides Based on Ester-Functionalized Pyridinium Ionic Liquids.'' *Environ. Sci. Poll. Res.*, **26** (5) 4878–4889 (2019)
44. Cao, Y, Cen, Y, Sun, X, Mu, T, ''Quantification of Ionic Liquids Concentration in Water and Qualification of Conjugated and Inductive Effects of Ionic Liquids by UV Spectroscopy.'' *Clean Soil Air Water*, **42** 1162–1169 (2014)
45. Volynets, GP, Barthels, F, Hammerschmidt, SJ, Moshynets, OV, Lukashov, SS, Starosyla, SA, Vyshniakova, HV, Iungin, OS, Bdzhola, VG, Prykhodko, AO, Syniugin, AR, Sapelkin, VM, Yarmoluk, SM, Schirmeister, T, ''Identification of Novel Small-Molecular Inhibitors of *Staphylococcus aureus* Sortase A Using Hybrid Virtual Screening.'' *J. Antibiot.*, **75** 321–332 (2022)
46. Protasov, A, Bardeau, J-F, Morozovskaya, I, Boretska, M, Cherniavska, T, Petrus, L, Tarasyuk, O, Metelytsia, L, Kopernik, I, Kalashnikova, L, Dzhuzha, O, Rogalsky, S, ''New Promising Antifouling Agent Based on Polymeric Biocide Polyhexamethylene Guanidine Molybdate.'' *Environ. Toxicol. Chem.*, **36** (9) 2543–2551 (2017)
47. Potangale, M, Das, A, Kapoor, S, Tiwari, S, ''Effect of Anion and Alkyl Chain Length on the Structure and Interactions of N-Alkyl Pyridinium Ionic Liquids.'' *J. Mol. Liq.*, **240** 694–707 (2017)
48. Mokti, N, Borhan, A, Nur, S, Zaine, A, Fatimah, H, Zaid, M, ''Synthesis and Characterisation of Pyridinium-Based Ionic Liquid as Activating Agent in Rubber Seed Shell Activated Carbon Production for CO_2 Capture.'' *J. Adv. Res. Fluid Mech. Therm. Sci.*, **82** 85–95 (2021)
49. Bardeau, J-F, Parikh, AN, Beers, JD, Swanson, BI, ''Phase Behavior of a Structurally Constrained Organic-Inorganic Crystal: Temperature-Dependent Infrared Spectroscopy of Silver n-Dodecanethiolate.'' *J. Phys. Chem. B*, **104** 627–635 (2000)
50. Xu, ZP, Braterman, PS, ''High Affinity of Dodecylbenzene Sulfonate for Layered Double Hydroxide and Resulting Morphological Changes.'' *J. Mater. Chem.*, **13** 268–273 (2003)
51. Sperline, RP, Yuan Song, Y, Freiser, H, ''Fourier Transform Infrared Attenuated Total Reflection Linear Dichroism Study of Sodium Dodecylbenzenesulfonate Adsorption at the Al_2O_3/Water Interface Using Al_2O_3-Coated Optics.'' *Langmuir*, **10** 31–44 (1994)
52. Shishlov, NM, Khursan, SL, ''Effect of Ion Interactions on the IR Spectrum of Benzenesulfonate Ion. Restoration of Sulfonate Ion Symmetry in Sodium Benzenesulfonate Dimer.'' *J. Mol. Struct.*, **1123** 360–366 (2016)
53. Bumbac, M, Zaharescu, T, Nicolescu, CM, ''Thermal and Radiation Stability of Alkyd Based Coatings Used as Insulators in the Electrical Rotating Machines.'' *J. Sci. Arts*, **1** (38) 119–130 (2017)

54. Jones, GC, Jackson, B, *Infrared Transmission Spectra of Carbonate Minerals*. Springer, Dordrecht, Netherlands (1993)
55. White, WB, ''The Carbonate Minerals.'' In: Farmer, VC (ed.) *The Infrared Spectra of Minerals*, pp. 227–284. Mineralogical Society of London (1974)
56. Badou, A, Pont, S, Auzoux-Bordenave, S, Lebreton, M, Bardeau, J-F, ''New Insight on Spatial Localization and Microstructures of Calcite-Aragonite Interfaces in Adult Shell of *Haliotis tuberculata*: Investigations of Wild and Farmed Abalones by FTIR and Raman Mapping.'' *J. Struct. Biol.*, **214** 107854 (2022)
57. Zhang, Y, He, H, Zhang, S, Fan, M, ''Hydrogen-Bonding Interactions in Pyridinium-Based Ionic Liquids and Dimethyl Sulfoxide Binary Systems: A Combined Experimental and Computational Study.'' *ACS Omega*, **3** (2) 1823–1833 (2018)
58. Law, K-Y, ''Definitions for Hydrophilicity, Hydrophobicity, and Superhydrophobicity: Getting the Basics Right.'' *J. Phys. Chem. Lett.*, **5** 686–688 (2014)
59. Pardo, IJ, van der Ven, LGJ, van Benthem, RATM, de With, G, Esteves, ACC, ''Hydrophilic Self-replenishing Coatings with Long-term Water Stability for Anti-Fouling Applications.'' *Coatings*, **8** 184 (2018)
60. Pistone, A, Scolaro, C, Visco, A, ''Mechanical Properties of Protective Coatings Against Marine Fouling: A Review.'' *Polymers*, **13** 173 (2021)
61. Qiu, H, Feng, K, Gapeeva, A, Meurisch, K, Kaps, S, Li, X, Yu, L, Mishra, YK, Adelung, R, Baum, M, ''Functional Polymer Materials for Modern Marine Biofouling Control.'' *Prog. Polym. Sci.*, **127** 101516 (2022)
62. Moshynets, OV, Spiers, AJ, ''Viewing Biofilms Within the Larger Context of Bacterial Aggregations.'' In: Dhanasekaran, D, Thajuddin, N (eds.). *Microbial Biofilms–Importance and Applications*, pp 3-22. InTech Press (2016). https://doi.org/10.5772/61499
63. Ong, KS, Mawang, CI, Daniel-Jambun, D, Lim, YY, Lee, SM, ''Current Anti-Biofilm Strategies and Potential of Antioxidants in Biofilm Control.'' *Expert Rev. Anti-Infect. Ther.*, **16** 855–864 (2018)
64. Liu, X, Tong, W, Wu, Z, Jiang, W, ''Poly(N-vinylpyrrolidone)-Grafted Poly(dimethylsiloxane) Surfaces with Tunable Microtopography and Anti-Biofouling Properties.'' *RSC Adv.*, **3** 4716–4722 (2013)
65. Kalia, VC, ''Quorum Sensing Inhibitors: An Overview.'' *Biotechnol. Adv.*, **31** 224–245 (2013)
66. Bhattarai, HD, Ganti, VS, Paudel, B, Lee, YK, Hong, Y-K, Shin, HW, ''Isolation of Antifouling Compounds from the Marine Bacterium, *Shewanella Oneidensis* SCH0402.'' *World J. Microbiol. Biotechnol.*, **23** 243–249 (2007)
67. Bazes, A, Silkina, A, Douzenel, P, Faÿ, F, Kervarec, N, Morin, D, Berge, J-P, Bourgougnon, N, ''Investigation of the Antifouling Constituents from the Brown Alga *Sargassum Muticum* (Yendo) Fensholt.'' *J. Appl. Phycol.*, **21** 395–403 (2009)

Publisher's Note Springer Nature remains neutral with regard to jurisdictional claims in published maps and institutional affiliations.

Springer Nature or its licensor (e.g. a society or other partner) holds exclusive rights to this article under a publishing agreement with the author(s) or other rightsholder(s); author self-archiving of the accepted manuscript version of this article is solely governed by the terms of such publishing agreement and applicable law.

Nanoscale Advances

ROYAL SOCIETY OF CHEMISTRY

PAPER

View Article Online
View Journal | View Issue

Check for updates

Cite this: *Nanoscale Adv.*, 2023, **5**, 6659

Femtosecond laser modified metal surfaces alter biofilm architecture and reduce bacterial biofilm formation†

Iaroslav Gnilitskyi, *[abc] Svitlana Rymar,[d] Olga Iungin, [de] Olexiy Vyshnevskyy, [f] Pietro Parisse,[g] Geert Potters,[hi] Anatoly V. Zayats *[a] and Olena Moshynets *[d]

Biofilm formation, or microfouling, is a basic strategy of bacteria to colonise a surface and may happen on surfaces of any nature whenever bacteria are present. Biofilms are hard to eradicate due to the matrix in which the bacteria reside, consisting of strong, adhesive and adaptive self-produced polymers such as eDNA and functional amyloids. Targeting a biofilm matrix may be a promising strategy to prevent biofilm formation. Here, femtosecond laser irradiation was used to modify the stainless steel surface in order to introduce either conical spike or conical groove textures. The resulting topography consists of hierarchical nano-microstructures which substantially increase roughness. The biofilms of two model bacterial strains, *P. aeruginosa* PA01 and *S. aureus* ATCC29423, formed on such nanotextured metal surfaces, were considerably modified due to a substantial reduction in amyloid production and due to changes in eDNA surface adhesion, leading to significant reduction in biofilm biomass. Altering the topography of the metal surface, therefore, radically diminishes biofilm development solely by altering biofilm architecture. At the same time, growth and colonisation of the surface by eukaryotic adipose tissue-derived stem cells were apparently enhanced, leading to possible further advantages in controlling eukaryotic growth while suppressing prokaryotic contamination. The obtained results are important for developing anti-bacterial surfaces for numerous applications.

Received 4th August 2023
Accepted 13th October 2023

DOI: 10.1039/d3na00599b

rsc.li/nanoscale-advances

Open Access Article. Published on 17 October 2023. Downloaded on 1/25/2024 7:09:18 PM.
This article is licensed under a Creative Commons Attribution 3.0 Unported Licence.

1. Introduction

Formation of bacterial biofilms on material surfaces in contact with water is an important and difficult problem in many settings, such as water and wastewater pipelines, hydroponics plumbing, food packaging, and medical devices to name but a few. For example, medical devices may carry microbial contamination on their surfaces of bacterial, fungal or viral nature, leading to nosocomial opportunistic infections. Hospital materials,[1–3] furniture[4] and small items such as stethoscopes,[5] mobile phones[6–8] and keyboards[9] are known to be the source of hospital-associated infections. These can be pathogenic viruses, bacteria or fungi, which can quickly colonize such surfaces with subsequent formation of a biofilm that often leads to general sepsis. Implant-related infections are often caused by skin-associated microflora, such as staphylococci and other nosocomial pathogens, anaerobic bacteria on dental implants, or by *Escherichia coli* on urinary catheters.[10–14] The growth of bacterial biofilms also causes problems for non-medical industrial surfaces during processing of food, dairy, wine or wastewater, causing pipe blockages and the accumulation of water, reduction in the efficiency of heat transfer processes and eventually food spoilage.[15–17] Lastly, the problem of microbiologically induced corrosion is related to biofilms in which microbial organisms can accelerate/contribute to total corrosion.[18,19] The degradation of metallic surfaces due to atmospheric corrosion is a well-known problem for many exposed steel structures such as ships, bridges, storage tanks and pipelines.[20–22]

Managing biofilm development is a hard and costly task, due to its specific structure. Current solutions generally rely on chemical means to dispose of surface-associated pathogens by adding biocides and antibiotics to materials used in medical devices or creating specific coatings.[23] Such coatings however are often loaded with acutely toxic chemicals or chemicals with

[a]*Department of Physics and London Centre for Nanotechnology, King's College London, Strand, London WC2R 2LS, UK. E-mail: iaroslav.gnilitskyi@kcl.ac.uk; anatoly.zayats@kcl.ac.uk*
[b]*NoviNano Lab LLC, Lviv, Ukraine*
[c]*Lviv Polytechnic National University, Ukraine*
[d]*Institute of Molecular Biology and Genetics of National Academy of Sciences of Ukraine, Kyiv, Ukraine. E-mail: moshynets@gmail.com*
[e]*Kyiv National University of Technologies and Design, Kyiv, Ukraine*
[f]*M. P. Semenenko Institute of Geochemistry, Mineralogy and Ore Formation of National Academy of Sciences of Ukraine, Kyiv, Ukraine*
[g]*Istituto Officina dei Materiali (IOM)–CNR, Laboratorio TASC, I-34149 Trieste, Italy*
[h]*Antwerp Maritime Academy, Antwerp, Belgium*
[i]*Department of Bioscience Engineering, University of Antwerp, Antwerp, Belgium*

† Electronic supplementary information (ESI) available. See DOI: https://doi.org/10.1039/d3na00599b

© 2023 The Author(s). Published by the Royal Society of Chemistry

Open Access Article. Published on 17 October 2023. Downloaded on 1/25/2024 7:09:18 PM.
This article is licensed under a Creative Commons Attribution 3.0 Unported Licence.

a high persistence and biomagnification potential, leading to chronic damage to the surrounding ecosystems or to human health.[24–27] Bacteria forming biofilms become adapted to detergents, biocides and antibiotics, gradually reducing their effectiveness.[28,29]

A faster and safer solution might therefore lie in a physical surface modification rather than an addition of chemicals. Such a physical modification implies alteration of surface topography, forming nano- or microscale features of different shapes. One example of such micrometer-scale patterns in nature is the surface of the *Clanger cicada* wings bearing needle-like nanostructures, which strongly limit the contact area of a surface, accumulate surface charge, and have a drastic effect on pathogenic biological objects.[30] There are several methods of obtaining nano- and microscale features on surfaces to prevent biofilm formation, such as spraying, plasma etching, optical and physical lithography, hydrothermal etching process,[31,32] and forming liquid infused surfaces[33] and liquid-like solid surfaces.[34] However, all these methods are expensive, require multistep processing, and often offer limited flexibility with many working well only on flat surfaces and limited surface areas.

Laser-assisted surface modifications have recently emerged as a promising technique for local tailoring of surface topography and chemical and wetting properties of surfaces. Femtosecond (fs) laser surface texturing has unique properties such as the non-thermal mechanism of ablation with minimum thermal collateral damage.[35] It has also been exploited to induce laser-induced periodic surface structures (LIPSS),[36] which have already been used in holography,[37] optoelectronics,[38] medicine[39] and many other applications. Recently, LIPSS have been considered for developing antibacterial surfaces.[40,41] LIPSS reduce bacterial adhesion and the tendency to form biofilms albeit in a species-dependent manner.[40] For example, *Escherichia coli* avoids adhesion to the LIPSS, while *Staphylococcus aureus* favours colonization of these nanostructures.[41] While LIPSS nanostructures do not provide a perfect antibacterial surface, possibly due to the shallow shape of the structures, fs-laser structuring can be used for formation of a broad range of complex nano- and microstructures through tuning of the irradiation conditions. For instance, grooves or spikes of varying height and morphology can be formed on a surface by varying the number of laser pulses and tuning laser fluence.[42] Such nanostructures can be very effective against bacteria due to their topographic features, *e.g.* sharp needles and cones may prevent bacterial adhesion onto the surface.

The reduction of total biomass due to laser-based surface texturing was detected in a number of studies,[43,44] but the question remains how nano- and microstructuring of an inert metal surface is able to influence the collective and cooperative behaviour of bacterial cells. The understanding of the relation between bacterial communities and the topography of the underlying surface is important to develop and optimise laser-based surface texturing for controlling undesired and harmful biofouling on a surface. In this paper, we develop hierarchical nano-microstructured surfaces and analyse the effect of the nanostructure parameters on biofilm formation and architecture.

2. Results and discussion

2.1 Morphology of laser structured surfaces

Ultrashort laser irradiation causes formation of complex self-organised structures on metal surfaces with features that can be controlled by the irradiation parameters (Fig. 1). Two nanostructured surfaces were fabricated (Table 1). The AG surface consists of periodic microstructures with sharp conical features between them (Fig. 1b). The period between microstructures is around 40 ± 2 μm and the distance between conical features is around 3–5 microns. If the laser repetition rate, step and speed are decreased (Table 1), a different type of structure on the surface is obtained with periodically corrugated microstructures of a period of 60 ± 2 μm (Fig. 1c). They consist of irregularly arranged blunt or sharp conical surface structures with average distances and heights of up to a few tens of micrometers. The spikes have some peculiarities; for instance, each spike has a sharp conical feature on the top of it. In turn, every conical feature contains periodic nanostructures with a period of around 800 nm (Fig. 1c). The root mean square roughness of the non-treated surface (R_a) is approximately 10 ± 5 nm according to the AFM images, the AG surface has an R_a of 340 ± 20 nm and the CS surface has an R_a of 300 ± 20 nm. For both laser-structured surfaces, the surface structures appear to be homogeneously distributed. Chemical analysis (see Materials and methods) shows the increase of the oxygen content at the laser irradiated surfaces, expected from the laser irradiation of the metal in air.

The chemical properties of laser modified areas have also been characterized by energy dispersive spectroscopy (EDX). Given that the laser experiment was carried out in air, the surface was, for both laser modifications, exposed to oxidation reactions.[42] Indeed, the AG surface showed a drastic increase of oxygen as well as carbon content, up to 6.07% and 7.61% respectively, which exceed the values seen for the non-treated surface (Table S1†). However, an even stronger increase of oxygen, up to 18.23%, was observed for the CS surface, concomitant with a slight increase of C up to 8.23%.

Wetting behaviour of a material is usually described by a static contact angle θ between the water droplet and solid surface. For the untreated sample, a contact angle of $96.2° \pm 3.2°$ was measured (Fig. S4†). A significant enhancement of hydrophobic properties was observed for laser-treated AG and CS surfaces with contacts angles of $117.5° \pm 4.6°$ and $134.6° \pm 4.3°$, respectively. This can be explained by the notable increase of surface roughness and changing surface chemistry of laser modified samples, as described by the Cassie–Baxter model,[45] where surface roughness allows air to be trapped inside the cavities.

2.2 Biofilm formation

In order to investigate the antibiofilm characteristics of the modified metal surfaces, two model bacterial strains which represent Gram-positive and Gram-negative bacterial opportunists were chosen. The metal coupons were incubated in

 © 2023 The Author(s). Published by the Royal Society of Chemistry

Open Access Article. Published on 17 October 2023. Downloaded on 1/25/2024 7:09:18 PM.
This article is licensed under a Creative Commons Attribution 3.0 Unported Licence.

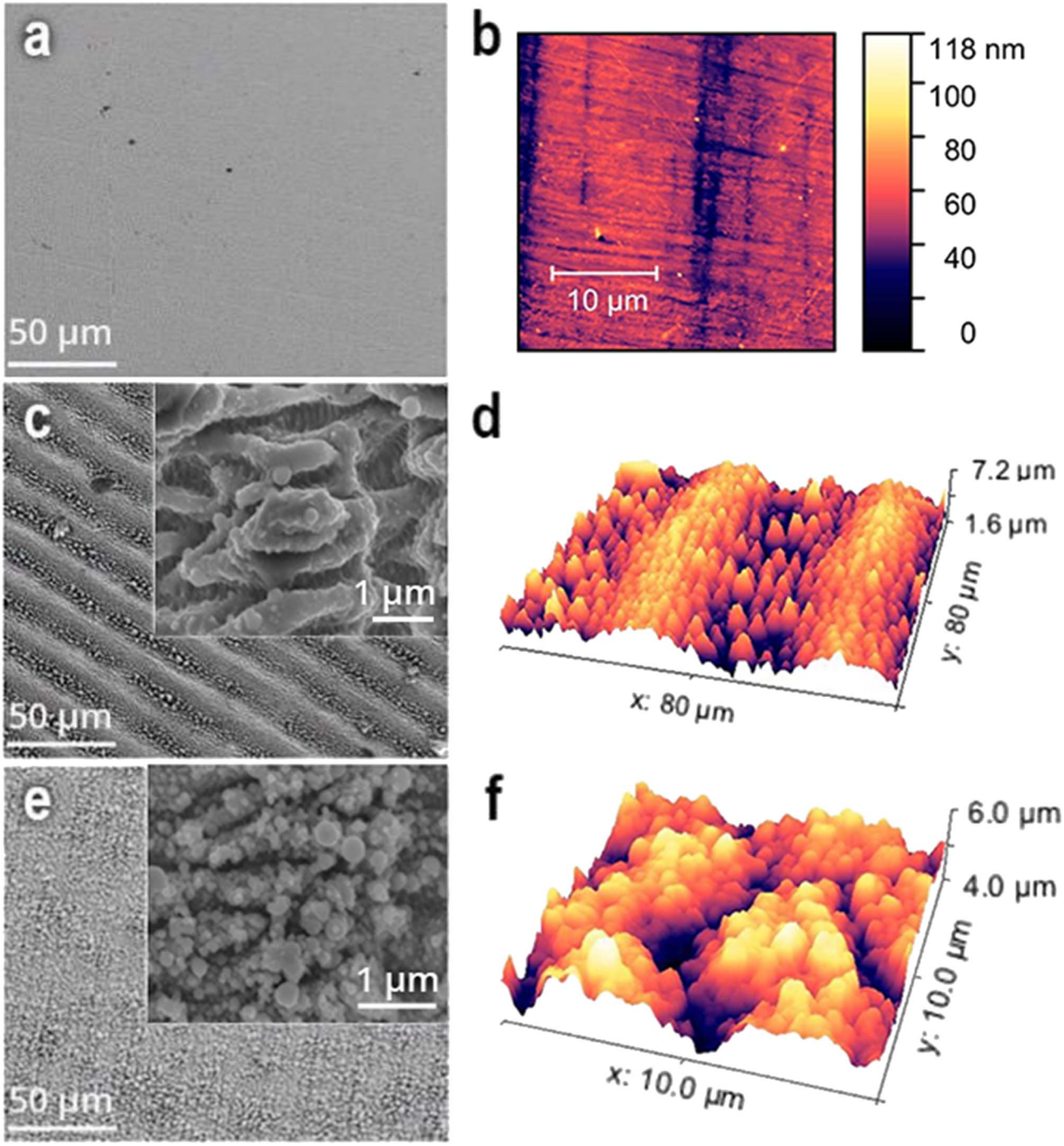

Fig. 1 (a, c, and e) SEM and (b, d, and f) AFM images of stainless-steel coupons: (a) untreated, (c and d) anisotropic grooves (AG) and (e and f) conical spikes (CS) on laser-treated surfaces. Insets in (c and e) show the respective images with higher magnifications.

Table 1 Laser parameters for generation of anisotropic grooves (AG) and conical spikes (CS)

Kind of microstructures	Power (W)	Repetition rate (Hz)	Step (μm)	Speed (mm s^{-1})	Pulse duration (fs)
AG	5	600	7.5	500	266
CS	5	100	2.5	100	266

© 2023 The Author(s). Published by the Royal Society of Chemistry

Open Access Article. Published on 17 October 2023. Downloaded on 1/25/2024 7:09:18 PM.
This article is licensed under a Creative Commons Attribution 3.0 Unported Licence.

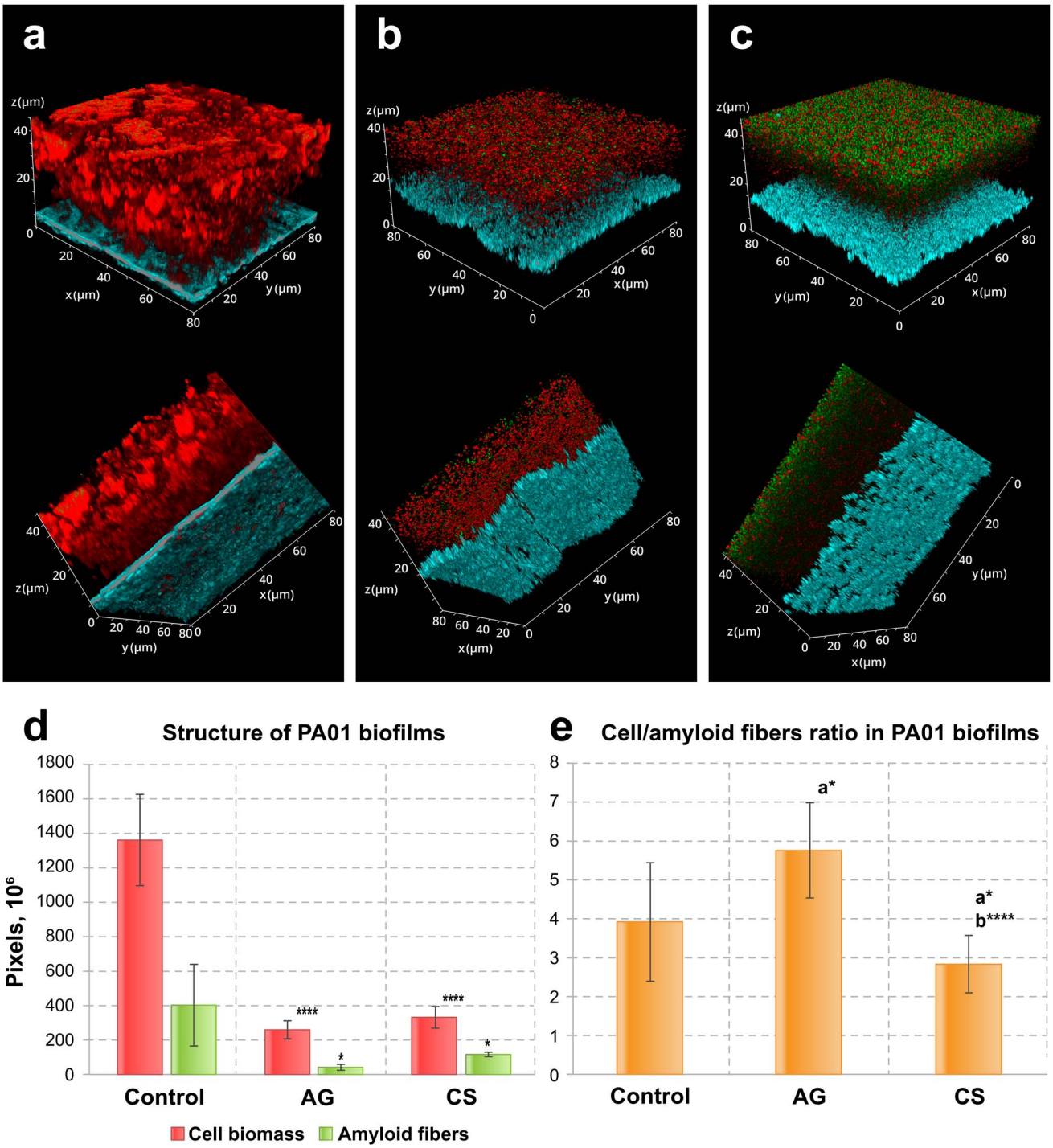

Fig. 2 Confocal laser scanning fluorescence images of three-day old biofilms of *P. aeruginosa* PA01 formed on (a) non-treated, (b) AG and (c) CS metal surfaces, (d) their structure and (e) the cell/amyloid biomass ratio. In (d and e), the *y*-axis shows the number of pixels in the signal of either the cell biomass (red) or the amyloid fibers (green), calculated after *z*-stacking serial CLSM images of biofilms; a* indicates statistical significance compared to control; b*** indicates statistical significance CS compared to AG with $*p < 0.05$, $****p < 0.001$. Staining was performed with ethidium bromide to visualize cells and eDNA (red PL signal) and AmyGreen (green PL signal) to visualize amyloids, the blue signal is the reflected excitation light from the metal surface.

stationary microcosms containing cultures of *Staphylococcus aureus* ATCC29423 and *Pseudomonas aeruginosa* PA01 for 72 hours.

After termination of the incubation, the biofilms formed on the coupon surfaces were stained with a combination of dyes, namely ethidium bromide (red PL signal) to stain bacterial cells and extracellular DNA (eDNA) and AmyGreen (green PL signal) for a comparative study of amyloid production. Both eDNA and amyloids are fundamental components of a bacterial biofilm which impact its proper formation.[46,49,50] Functional bacterial

 © 2023 The Author(s). Published by the Royal Society of Chemistry

Open Access Article. Published on 17 October 2023. Downloaded on 1/25/2024 7:09:18 PM.
This article is licensed under a Creative Commons Attribution 3.0 Unported Licence.

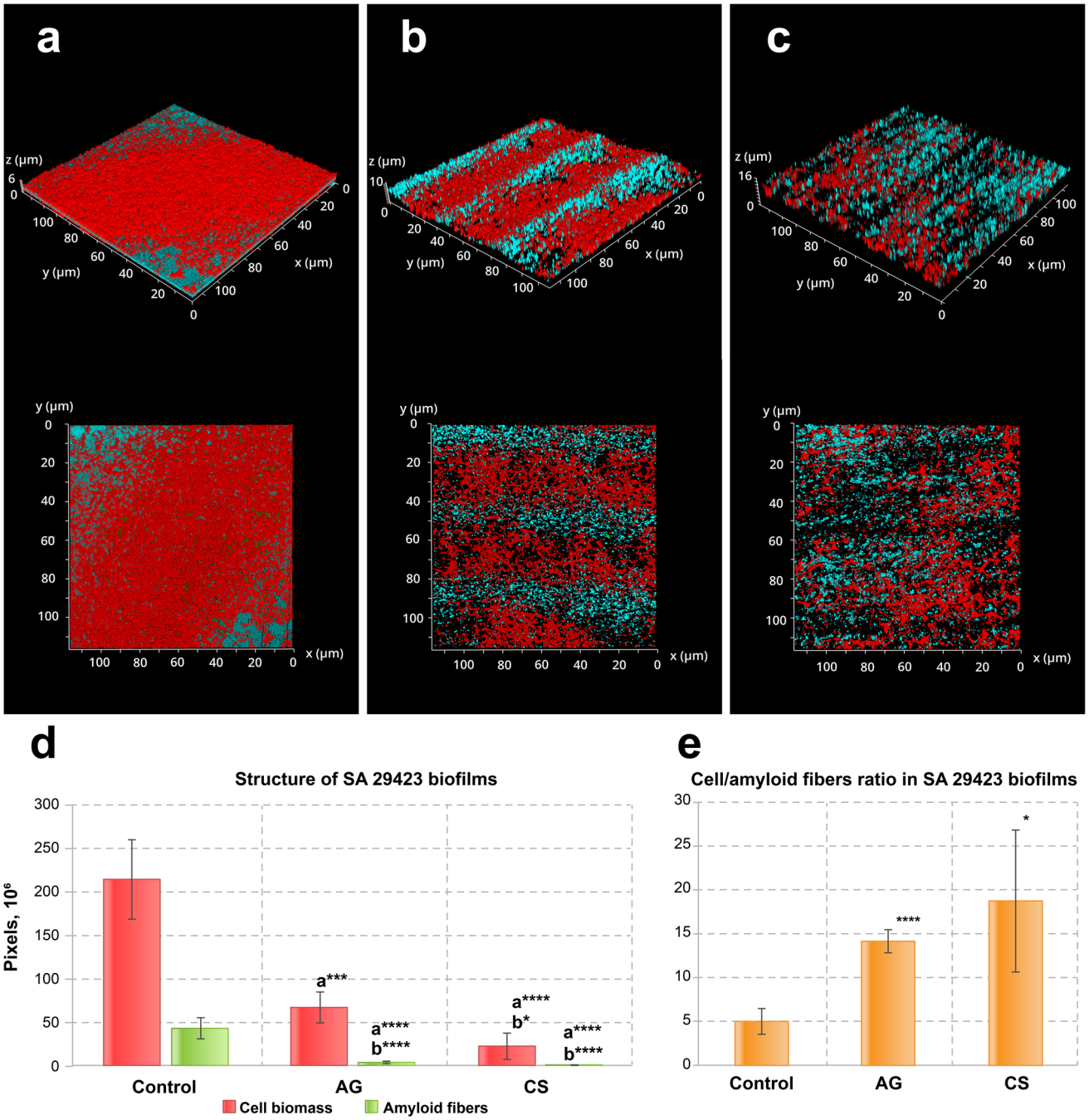

Fig. 3 CSLM fluorescence images of three-day old biofilms of *S. aureus* ATCC29423 formed on (a) non-treated, (b) AG and (c) CS metal surfaces and (d) their structure and (e) the cell/amyloid biomass ratio. In (d and e), the *y*-axis shows the number of pixels in the signal of either the cell biomass (red) or the amyloid fibers (green), calculated after *z*-stacking serial CLSM images of biofilms; a* indicates statistical significance compared to control; b*** indicates statistical significance CS compared to AG with $*p < 0.05$, $***p < 0.005$, $****p < 0.001$. Amyloid production was suppressed in biofilms formed on both laser-modified surfaces. Staining was performed with ethidium bromide to visualize cells and eDNA (red PL signal) and AmyGreen (green PL signal) to visualize amyloids, the blue signal is the reflected excitation light from the metal surface.

amyloids are highly ordered protein aggregates with an unbranched filamentous morphology, typically featuring a helical array of β-strands packed orthogonally to the long fiber axis.[51] They are widespread within the taxa *Bacteroidetes*, *Firmicutes*, *Actinobacteria* and *Gammaproteobacteria*, where they contribute to attachment, initial aggregation and, finally, biofilm matrix formation.[52–56] Moreover, amyloids physically stabilize the eDNA within the biofilm matrix.[57,58]

After three days of incubation, the biofilms on control and laser-modified surfaces demonstrated considerable differences, both in the case of *P. aeruginosa* PA01 and of *S. aureus* ATCC29423 biofilms. First, the morphology of *P. aeruginosa*

© 2023 The Author(s). Published by the Royal Society of Chemistry

Open Access Article. Published on 17 October 2023. Downloaded on 1/25/2024 7:09:18 PM.
This article is licensed under a Creative Commons Attribution 3.0 Unported Licence.

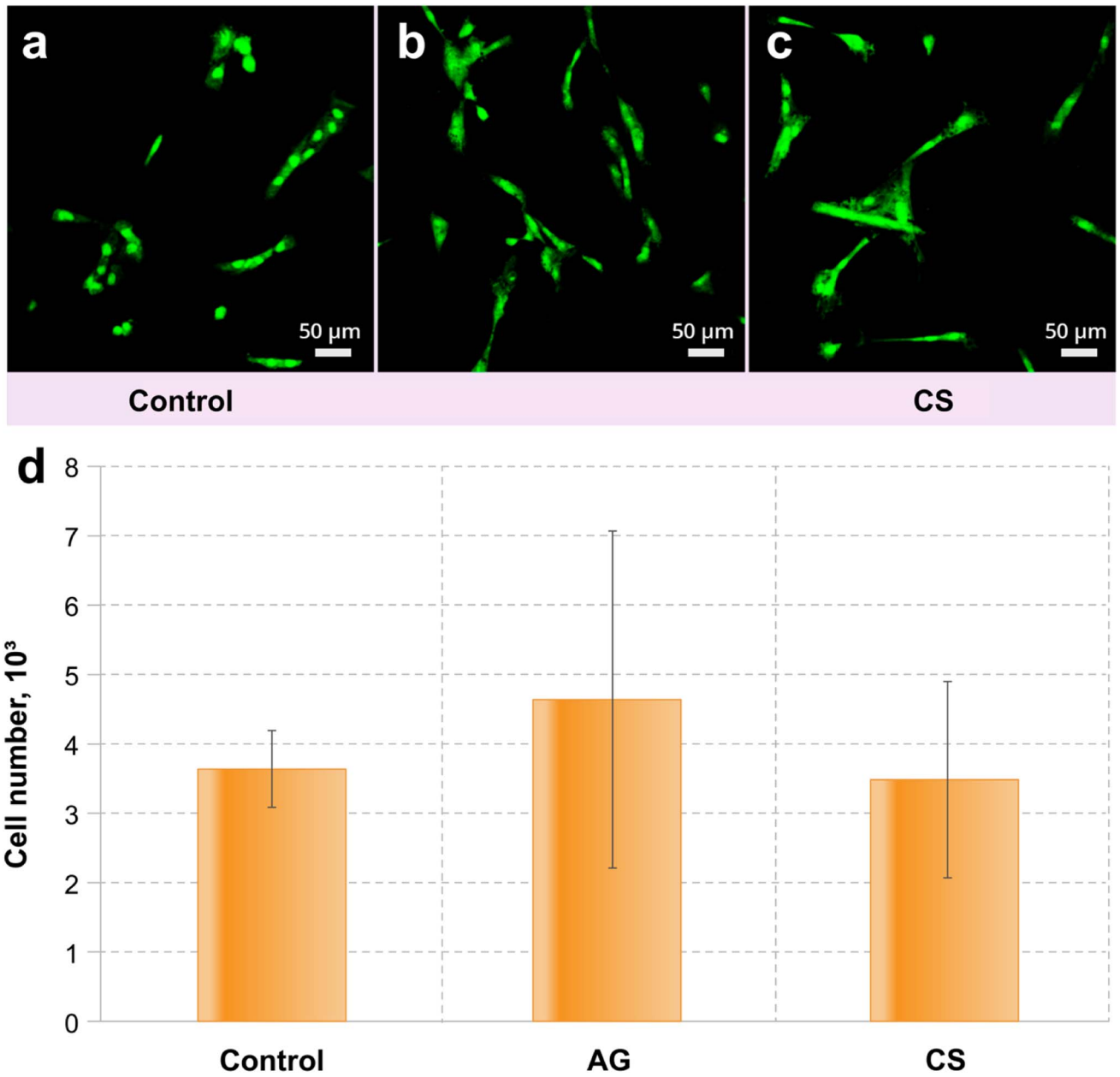

Fig. 4 CSLM fluorescence images of the colonisation level of (a) control, (b) AG and (c) CS metal surfaces with ADSC culture. (d) Statistical significance compared to control with $*p < 0.05$ (see Fig. 2 and 3, for the statistical analysis details).

PA01 biofilms differed significantly between the non-treated and treated surfaces (3(a–c)). Biofilms formed on the control surface had a thickness up to 45 μm with a rich smooth structure, while the biofilms formed on the laser-treated surfaces were mostly crumbly with a thickness around 20 μm (Fig. S2†).

These microscopical morphological changes corresponded to a statistically significant suppression of biofilms and amyloid biomass associated with laser-modified surfaces as compared to the biofilms on the control surfaces (Fig. 2d). Amyloid production was suppressed in biofilms formed on both laser-modified surfaces (Fig. 2d) but the relative amyloid production was different: it was suppressed in the case of AG surfaces, but enhanced in biofilms grown on the CS (Fig. 2e).

In the analysis of biofilm development, eDNA and amyloid contents warrant specific attention due to their high importance in the initial bacterial adhesion to inert surfaces and in the following biofilm extracellular matrix development.[34,46] In *P. aeruginosa* PA01, biofilm-associated eDNA decreased when biofilms were formed on the modified surfaces (Fig. S3†). Interestingly, in all variants, biofilm thickness remained constant, while the extracellular biofilm matrix decreased significantly in biofilms formed on laser-modified surfaces compared to non-treated. Moreover, the CS surface fully inhibits initial eDNA attachment, as demonstrated by the absence of the red peak (elsewhere corresponding to the presence of eDNA and cells) relative to the blue peak corresponding

 © 2023 The Author(s). Published by the Royal Society of Chemistry

Open Access Article. Published on 17 October 2023. Downloaded on 1/25/2024 7:09:18 PM. This article is licensed under a Creative Commons Attribution 3.0 Unported Licence.

to the metal surface (Fig. S3c†), while these red peaks were present in control and AG-surface-associated biofilms (Fig. S3a and b†).

These results demonstrate that both surface modifications reduce the total biofilm biomass as well as amyloid production but had different influences on the fine structure of the *P. aeruginosa* PA01 biofilm. Specifically, the AG surface relatively reduced amyloid production while the CS surface enhanced it. The CS surface was also able to inhibit eDNA surface adhesion which might explain why the amyloid production was stimulated: a surface with considerable hydrophobicity may favour amyloid production because amyloids are highly hydrophobic adhesins, and, alternatively, reduce the adhesion of DNA, which is fully hydrophilic.

Similar effects were observed in *S. aureus* ATCC29423 biofilms (Fig. 3a–c). As before, the biofilm biomass and amyloid production were reduced (Fig. 3d). Contrary to what could be seen for *P. aeruginosa* PA01, however, the biofilms of this bacterial species tend to grow inside the grooves of the AG topography (Fig. 3b). The *S. aureus* ATCC29423 biofilms formed on the control metal surface exhibited 7 times less biomass than in those produced by *P. aeruginosa* PA01. This may be explained by the low adhesion activity of staphylococci to neutral surfaces, *i.e.*, lacking an additional preconditioning protein layer such as collagen. Both modified surfaces inhibited amyloid protein synthesis and suppressed amyloid layer formation in the biofilms (Fig. 3d and e).

This assay demonstrates that both model bacterial strains, *P. aeruginosa* PA01 and *S. aureus* ATCC29423, considerably reduce the biofilm biomass developed on modified surfaces. Specifically, the laser-induced surface modifications evaluated in this study demonstrated biofilm biomass reduction by 3.8–5.5 times for *P. aeruginosa* PA01 and by 5.5–8.4 times for *S. aureus* ATCC29423. The fine structure of biofilms formed on modified surfaces changed considerably compared to the control: amyloid production was reduced in both strains when the relative amyloid production enhancement was observed for the *P. aeruginosa* PA01 biofilm developed on the CS surface. Importantly, the CS surface also demonstrated complete inhibition for eDNA adhesion which in turn might effectively suppress the initiation of biofilm development for strains such as *P. aeruginosa* utilizing eDNA as the primary adhesin or amyloid network stabilizer.

2.3 Eukaryotic cell attachment assay

Adipose tissue-derived stem cell (ADSC) culture was used to estimate the ability of the control and modified surfaces to be colonised by eukaryotic cells. The results demonstrated that the modification of the metal surfaces did not provide a toxic environment for the cell line.

Similar numbers of ADSC cells observed in all the samples suggest that the surfaces are not toxic for the culture (Fig. 4). The colonisation rate of the CS surface did not differ from that on the control surface, while the AG surface demonstrates a statistically better colonisation than observed in the control (Fig. 4a). Interestingly, the morphology of the ADSC is different between the non-treated and modified surfaces: cells from the control surface had an altered morphology (compared to what can normally be expected from these cells[59]) suggesting that these cells are suffering from increased physiological stress (Fig. 4b). Both modified surfaces support cells of a predominantly regular morphology (Fig. 4c and d), which suggests that the AG and CS surfaces provide more favourable conditions for colonization by eukaryotic cells.

3. Conclusion

We have shown that surface nanotexturing can be used to control bacterial fouling in a non-chemical manner using a low-cost and high-speed method based on naturally occurring self-organised formation of nanostructures upon laser irradiation. The studied complex structures on stainless steel surfaces consist of nano- and micro-structures that radically change biofilm formation due to purely geometrical effects. The biofilm matrix of both *P. aeruginosa* PA01 and *S. aureus* ATCC29423 biofilms was observed to be substantially reduced due to the interaction between the laser-induced changes in topography and the main components in the biofilm composition (*i.e.*, eDNA and amyloids). Altering the topography of the metal surface, therefore, radically diminishes biofilm development, not by reducing the surface area of bacteria coverage but by altering the biofilm architecture. At the same time, growth and colonisation of the surface by eukaryotic ADSC were apparently enhanced, leading to possible further advantages in controlling eukaryotic growth while suppressing prokaryotic contamination. The obtained results are important for developing antibacterial surfaces for numerous applications.

4. Materials and methods

4.1 Materials

Plates of commercial surgical stainless-steel EI 711 were used. Stainless steel is typically used in medicine for manufacturing medical implants and other medical devices. Plates with size 10 × 10 mm were cut by using high power femtosecond laser pulses ($P = 20$ W) in order to avoid their deformation. Then, the plates were mechanically polished to achieve roughness R_a = 0.01 μm. Finally, polished plates were cleaned using an ultrasound bath in ethanol.

4.2 Laser setup and surface texturing

Anisotropic grooves (AG) and conical spikes (CS) were imprinted on polished surgical stainless steel plates using a Light Conversion Pharos femtosecond Yb-doped solid state laser system (270 fs pulse width at a wavelength of 1030 nm, variable repetition rate <1 MHz, a maximum average output power of 20 W). Schematic of the experimental setup is shown in the ESI†.

4.3 Characterisation of surface morphology

SEM images were acquired using a JSM-6700F field emission scanning electron microscope equipped with a JED-2300 energy-dispersive spectrometer (JEOL). Surface morphology

Open Access Article. Published on 17 October 2023. Downloaded on 1/25/2024 7:09:18 PM.
This article is licensed under a Creative Commons Attribution 3.0 Unported Licence.

was imaged by atomic force microscopy (AFM) in semi-contact mode (NT-MDT Solver Pro) using commercial silicon cantilevers (NSG30). All images were analysed with the Gwyddion® software. Surface roughness (R_a, arithmetic mean height, and R_z, maximum height) was obtained by averaging five different images.

Wettability measurements on an untreated surface of stainless steel and laser modified surfaces AG and CS were carried out using a tensiometer (Biolin Scientific). Water contact angles of the 5 samples for each type of surface were evaluated by static contact angle measurements using the sessile drop method.

4.4 Biofilm formation assay

The bacterial ability to form biofilms associated with the studied surfaces was evaluated using two model biofilm-forming strains, the Gram-negative *Pseudomonas aeruginosa* PA01 and the Gram-positive *Staphylococcus aureus* ATCC25923. To this end, each metal coupon of 1 cm^2 was sterilised by treatment with 96% ethanol and subsequent burning. Each coupon was then placed in a well of a sterile polystyrene 24-well plate in which 2 mL of Luria Broth (LB) medium was added, and inoculated with 10 μL of an overnight inoculum culture containing 10^9 CFU mL^{-1}; there were three replicas per variant. The plate was incubated at 37 °C for 72 h. Biofilm formation was evaluated using confocal microscopy following three days of stationary incubation. The control for incubation was performed by incubating the coupons in sterile LB with three replicas. After incubation, each coupon was removed and washed three times to remove planktonic and poorly attached biofilm mass.

4.5 Biofilm structure assay

Biofilms were stained with 1 mM ethidium bromide (Sigma) and 3 mM AmyGreen solution.[46] No additional washing steps were performed to limit the physical disruption of biofilm structures through movement in the liquid. The samples were not fixed, but a cover slip was placed over the stained samples before imaging. Confocal laser scanning microscopy (CLSM) analysis was used to measure the total biofilm biomass as well as to visualize the metal surfaces associated with the biofilms, using a Leica TCS SPE Confocal system with a coded DMi8 inverted microscope (Leica, Germany) with recommended LAS X 3.1.2.16221 software (Leica, Germany). Images were acquired with excitation at 488 nm and emission wavelengths collected at 490–580 nm for AmyGreen, and with excitation at 532 nm and emissions collected at 537–670 nm for ethidium bromide. 635 nm laser light was used in reflection for surface visualization. The total number of pixels was calculated with the above-mentioned software.

4.6 Eukaryotic cell attachment assay

Mesenchymal/stromal stem cells of human adipose tissue were used to determine eukaryotic cell attachment to the laser treated metal surfaces. Cells were obtained from lipoaspirate using collagenase.[47] The lipoaspirate was washed twice with PBS by centrifugation at 400*g* for 5 min. The top layer of adipose tissue was removed and mixed with a freshly prepared solution of collagenase I (Gibco, Thermo Fisher Scientific, Inc.) up to a final concentration of 0.2% in PBS.[48] Enzyme digestion was carried out at 37 °C under constant stirring for 1 hour. Collagenase was inactivated by adding an equal volume of cell culture medium, after which the suspension was centrifuged at 400*g* for 10 min. The pellet was washed three times with PBS, then resuspended in PBS and filtered (100 μM pore size) to remove undigested tissue fragments. The resulting stromal-vascular fraction was seeded into culture flasks with DMEM-F12 medium containing 10% fetal bovine serum (Sigma Aldrich) with addition of 100 U per mL penicillin, and 100 μg per mL streptomycin. Cultivation was performed at 37 °C under 5% CO_2 for 48 hours before non-attached cells were removed. The incubation continued for 48 hours more before the adipose tissue-derived stem cells (ADSC) were trypsinized (0.20% trypsin-EDTA), washed, and used for further cultivation or freezing for storage. The expression of surface markers CD90, CD105, and CD73 was more than 98%, and the expression of CD34 and CD45 was less than 0.5%.

The ADSC of the first passage was used in the experiments. Metal coupons prepared as before were placed in wells of a 24-well plate and seeded with the cells at a seeding density of 2.6×10^3 cm^{-2}. The coupons were removed after three days of incubation, and the cells were trypsinized and counted.

4.7 CLSM analysis of eukaryotic cell attachment

Metal coupons with attached ADSC were incubated with 1 mM SYBR green (Invitrogen, Paisley, UK) for 15 min. PL images were acquired with an excitation wavelength of 488 nm and an emission in the spectral range 490–580 nm, using a Leica TCS SPE Confocal system with a coded DMi8 inverted microscope (Leica, Germany), controlled by AS X 3.1.2.16221 software (Leica, Germany).

Experimental replicates (cultures/samples images) were used and quantitative results were presented as mean ± standard deviation (SD). The statistical software package OriginPro 7.0 was used for the one-way ANOVA procedure, with $p < 0.05$ being considered statistically significant.

Conflicts of interest

There are no conflicts to declare.

Acknowledgements

This work has been partially performed in the framework of the Nanoscience Foundry and Fine Analysis (NFFA-MUR Italy Progetti Internazionali) facility (https://www.trieste.nffa.eu/). The work was supported in part by the NATO Science for Peace and Security multi-year project SPS G6053 "Inhibition of Bacterial Settlement and Biofilm Formation through Physical Control of the Environment (PHYBI)", UK EPSRC (EP/W017075/1) and the British Academy. The authors thank Vincent

 © 2023 The Author(s). Published by the Royal Society of Chemistry

Open Access Article. Published on 17 October 2023. Downloaded on 1/25/2024 7:09:18 PM. This article is licensed under a Creative Commons Attribution 3.0 Unported Licence.

Polewczyk for useful discussions of chemical characterization of laser modified surfaces.

References

1 D. López, H. Vlamakis, R. Losick and R. Kolter, Cannibalism enhances biofilm development in *Bacillus subtilis*, *Mol. Microbiol.*, 2009, **74**(3), 609–618.
2 A. M. Treakle, K. A. Thom, J. P. Furuno, S. M. Strauss, A. D. Harris and E. N. Perencevich, Bacterial contamination of health care workers' white coats, *Am. J. Infect. Control*, 2009, **37**(2), 101–105.
3 Y. Wiener-Well, M. Galuty, B. Rudensky, Y. Schlesinger, D. Attias and A. M. Yinnon, Nursing and physician attire as possible source of nosocomial infections, *Am. J. Infect. Control*, 2011, **39**(7), 555–559.
4 S. Lax, N. Sangwan, D. Smith, P. Larsen, K. M. Handley, M. Richardson and J. A. Gilbert, Bacterial colonization and succession in a newly opened hospital, *Sci. Transl. Med.*, 2017, **9**(391), eaah6500.
5 M. A. Marinella, C. Pierson and C. Chenoweth, The stethoscope: a potential source of nosocomial infection, *Arch. Intern. Med.*, 1997, **157**(7), 786–790.
6 L. Doyle, A. M. Brady and G. Byrne, An overview of mixed methods research, *J. Res. Nurs.*, 2009, **14**(2), 175–185.
7 F. Ulger, S. Esen, A. Dilek, K. Yanik, M. Gunaydin and H. Leblebicioglu, Are we aware how contaminated our mobile phones with nosocomial pathogens?, *Ann. Clin. Microbiol. Antimicrob.*, 2009, **8**(1), 1–4.
8 K. O. Akinyemi, A. D. Atapu, O. O. Adetona and A. O. Coker, The potential role of mobile phones in the spread of bacterial infections, *J. Infect. Dev. Countries*, 2009, **3**(08), 628–632.
9 S. Bures, J. T. Fishbain, C. F. Uyehara, J. M. Parker and B. W. Berg, Computer keyboards and faucet handles as reservoirs of nosocomial pathogens in the intensive care unit, *Am. J. Infect. Control*, 2000, **28**(6), 465–471.
10 G. Chauhan, M. J. Madou, S. Kalra, V. Chopra, D. Ghosh and S. O. Martinez-Chapa, Nanotechnology for COVID-19: therapeutics and vaccine research, *ACS Nano*, 2020, **14**(7), 7760–7782.
11 World Health Organization (WHO), *Antimicrobial Resistance*, WHO, 2021, **https://www.who.int/news-room/fact-sheets/detail/antimicrobial-resistance**.
12 G. Volynets, H. Vyshniakova, G. Nitulescu, G. M. Nitulescu, A. Ungurianu, D. Margina and S. Yarmoluk, Identification of novel antistaphylococcal hit compounds targeting sortase a, *Molecules*, 2021, **26**(23), 7095.
13 J. Ferlay, M. Colombet, I. Soerjomataram, C. Mathers, D. M. Parkin, M. Piñeros and F. Bray, Estimating the global cancer incidence and mortality in 2018: GLOBOCAN sources and methods, *Int. J. Cancer*, 2019, **144**(8), 1941–1953.
14 P. Dong, H. Wang, T. Fang, Y. Wang and Q. Ye, Assessment of extracellular antibiotic resistance genes (eARGs) in typical environmental samples and the transforming ability of eARG, *Environ. Int.*, 2019, **125**, 90–96.
15 H. Vlamakis, The world of biofilms, *Virulence*, 2011, **2**(5), 431–434.
16 S. Galie, C. García-Gutiérrez, E. M. Miguélez, C. J. Villar and F. Lombó, Biofilms in the food industry: health aspects and control methods, *Front. Microbiol.*, 2018, **9**, 898.
17 C. Carrascosa, D. Raheem, F. Ramos, A. Saraiva and A. Raposo, Microbial biofilms in the food industry—A comprehensive review, *Int. J. Environ. Res. Public Health*, 2021, **18**(04), 2014.
18 D. Xu, Y. Li, F. Song and T. Gu, Laboratory investigation of microbiologically influenced corrosion of C1018 carbon steel by nitrate reducing bacterium *Bacillus licheniformis*, *Corros. Sci.*, 2013, **77**, 385–390.
19 *Microbiologically Influenced Corrosion in the Upstream Oil and Gas Industry*, ed. T. L. Skovhus, D. Enning and J. S. Lee, CRC press, 2017.
20 B. Chugh, S. Thakur and A. K. Singh, Microbiologically influenced corrosion inhibition in oil and gas industry, in *Corrosion Inhibitors in the Oil and Gas Industry*, 2020, pp. 321–338.
21 G. Wang, J. Spencer and T. Elsayed, Estimation of corrosion rates of structural members in oil tankers, in *International Conference on Offshore Mechanics and Arctic Engineering*, 2003, pp. 253–258.
22 B. J. Little, D. J. Blackwood, J. Hinks, F. M. Lauro, E. Marsili, A. Okamoto and H. C. Flemming, Microbially influenced corrosion—Any progress?, *Corros. Sci.*, 2020, **170**, 108641.
23 S. Nundy, A. Ghosh and T. K. Mallick, Hydrophilic and superhydrophilic self-cleaning coatings by morphologically varying ZnO microstructures for photovoltaic and glazing applications, *ACS Omega*, 2020, **5**(2), 1033–1039.
24 U. Ben-David, B. Siranosian, G. Ha, H. Tang, Y. Oren, K. Hinohara and T. R. Golub, Genetic and transcriptional evolution alters cancer cell line drug response, *Nature*, 2018, **560**(7718), 325–330.
25 V. Contardo-Jara, S. Meinecke, M. Feibicke, R. Berghahn, R. Schmidt and S. Mohr, Fate, bioaccumulation and toxic effects of triclosan on a freshwater community–A mesocosm study, *Environ. Adv.*, 2021, **5**, 100100.
26 N. García-Bueno and A. Marín, Ecological management of biomass and metal bioaccumulation in fish-cage nettings: influence of antifouling paint and fiber manufacture, *Aquaculture*, 2021, **544**, 737142.
27 A. Kumar and K. R. Nayar, COVID 19 and its mental health consequences, *J. Mental Health*, 2021, **30**(1), 1–2.
28 O. V. Moshynets, T. P. Baranovskyi, O. S. Iungin, N. P. Kysil, L. O. Metelytsia, I. Pokholenko, V. V. Potochilova, G. Potters, K. L. Rudnieva, S. Y. Rymar, I. V. Semenyuta, A. J. Spiers, O. P. Tarasyuk and S. P. Rogalsky, eDNA inactivation and biofilm inhibition by the polymeric biocide polyhexamethylene guanidine hydrochloride (PHMG-Cl), *Int. J. Mol. Sci.*, 2022, **23**(2), 731.
29 O. V. Moshynets, T. P. Baranovskyi, S. Cameron, O. S. Iungin, I. Pokholenko, R. Jerdan, A. Kamyshnyi, A. A. Krikunov, V. V. Potochilova, K. L. Rudnieva and A. J. Spiers, Azithromycin possesses biofilm–inhibitory activity and potentiates non-bactericidal colistin methanesulfonate

© 2023 The Author(s). Published by the Royal Society of Chemistry

Open Access Article. Published on 17 October 2023. Downloaded on 1/25/2024 7:09:18 PM. This article is licensed under a Creative Commons Attribution 3.0 Unported Licence.

(CMS) and polymyxin B against *Klebsiella pneumonia*, *PLoS ONE*, 2022, **17**(7), e0270983.
30 S. Pogodin, J. Hasan, V. A. Baulin, H. K. Webb, V. K. Truong, T. H. P. Nguyen and E. P. Ivanova, Biophysical model of bacterial cell interactions with nanopatterned cicada wing surfaces, *Biophys. J.*, 2013, **104**(4), 835–840.
31 Y. Cao, *et al.*, Nanostructured titanium surfaces exhibit recalcitrance towards *Staphylococcus epidermidis* biofilm formation, *Sci. Rep.*, 2018, **8**, 1071.
32 C. M. Bhadra, *et al.*, Antibacterial titanium nano-patterned arrays inspired by dragonfly wings, *Sci. Rep.*, 2015, **5**, 16817.
33 Y. Zhu, G. McHale, J. Dawson, S. Armstrong, G. Wells, R. Han, H. Liu, W. Vollmer, P. Stoodley, N. Jakubovics and J. Chen, Slippery liquid-like solid surfaces with promising antibiofilm performance in both static and flow conditions, *ACS Appl. Mater. Interfaces*, 2022, **14**, 6307–6317.
34 C. Howell, A. Grinthal, S. Sunny, M. Aizenberg and J. Aizenberg, Designing liquid-infused surfaces for medical applications: a review, *Adv. Mater.*, 2018, **30**, e1802724.
35 R. Gattass and E. Mazur, Femtosecond laser micromachining in transparent materials, *Nat. Photonics*, 2008, **2**, 219–225.
36 J. Bonse, J. Krüger, S. Höhm and A. Rosenfeld, Femtosecond laser-induced periodic surface structures, *J. Laser Appl.*, 2012, **24**, 042006.
37 Y. Kotsiuba, I. Hevko, S. Bellucci and I. Gnilitskyi, Bitmap and vectorial hologram recording by using femtosecond laser pulses, *Sci. Rep.*, 2021, **11**, 16406.
38 S. V. Mamykin, I. M. Gnilitskyi, M. G. Dusheyko, T. A. DeVol and V. N. Bliznyuk, Femtosecond laser nano-structuring for surface plasmon resonance-based detection of uranium, *Appl. Surf. Sci.*, 2022, **576**, 151831.
39 I. Gnilitskyi, M. Pogorielov, R. Viter, A. M. Ferraria, A. P. Carapeto, O. Oleshko, L. Orazi and O. Mishchenko, Cell and tissue response to nanotextured Ti6Al4V and Zr implants using high-speed femtosecond laser-induced periodic surface structures, *Nanomed. Nanotechnol. Biol. Med.*, 2019, **21**, 102036.
40 A. Cunha, A.-M. Elie, L. Plawinski, A. P. Serrod, A. M. Botelho do Rego, A. Almeida, M. C. Urdaci, M.-C. Durrieu and R. Vilar, Femtosecond laser surface texturing of titanium as a method to reduce the adhesion of Staphylococcus aureus and biofilm formation, *Appl. Surf. Sci.*, 2016, **360**(Part B), 485–493.
41 N. Epperlein, F. Menzel, K. Schwibbert, R. Koter, J. Bonse, J. Sameith and J. Toepel, Influence of femtosecond laser produced nanostructures on biofilm growth on steel, *Appl. Surf. Sci.*, 2017, **418**, 420–424.
42 K. M. T. Ahmmed, C. Grambow and A.-M. Kietzig, Fabrication of micro/nano structures on metals by femtosecond laser micromachining, *Micromachines*, 2014, **5**, 1219–1253.
43 A. C. Ionescu, E. Brambilla, F. Azzola, M. Ottobelli, G. Pellegrini and L. A. Francetti, Laser microtextured titanium implant surfaces reduce *in vitro* and *in situ* oral biofilm formation, *PLoS ONE*, 2018, **13**(9), e0202262.
44 M. Koopaie, A. Bordbar-Khiabani, S. Kolahdooz, A. K. Darbandsari and M. Mozafari, Advanced surface treatment techniques counteract biofilm-associated infections on dental implants, *Mater. Res. Express*, 2020, **7**(1), 015417.
45 A. B. D. Cassie and S. Baxter, Wettability of porous surfaces, *Transitions Faraday Soc.*, 1944, **40**, 546–551.
46 O. Moshynets, S. Chernii, V. Chernii, M. Y. Losytskyy, S. Karakhim, R. Czerwieniec, V. Pekhnyo, S. Yarmoluk and V. Kovalska, Fluorescent β-ketoenole AmyGreen dye for visualization of amyloid components of bacterial biofilms, *Methods Appl. Fluoresc.*, 2020, **8**(3), 035006.
47 S. Schneider, M. Unger, M. Van Griensven and E. R. Balmayor, Adipose-derived mesenchymal stem cells from liposuction and resected fat are feasible sources for regenerative medicine, *Eur. J. Med. Res.*, 2017, **22**(1), 1–11.
48 K. Huttenlochner, C. Müller-Renno, C. Ziegler, R. Merz, B. Merz, M. Kopnarski and R. Ulber, Removing biofilms from stainless steel without changing surface properties relevant for bacterial attachment, *Biointerphases*, 2017, **12**(2), 02C404.
49 O. V. Moshynets, T. P. Baranovskyi, O. S. Iungin, N. P. Kysil, L. O. Metelytsia, I. Pokholenko, V. V. Potochilova, G. Potters, K. L. Rudnieva, S. Y. Rymar, I. V. Semenyuta, A. J. Spiers, O. P. Tarasyuk and S. P. Rogalsky, eDNA inactivation and biofilm inhibition by the polymeric biocide polyhexamethylene guanidine hydrochloride (PHMG-Cl), *Int. J. Mol. Sci.*, 2022, **23**(2), 731.
50 O. Moshynets, J. F. Bardeau, O. Tarasyuk, S. Makhno, T. Cherniavska, O. Dzhuzha and S. Rogalsky, Antibiofilm activity of polyamide 11 modified with thermally stable polymeric biocide polyhexamethylene guanidine 2-naphtalenesulfonate, *Int. J. Mol. Sci.*, 2019, **20**(2), 348.
51 D. S. Eisenberg and M. R. Sawaya, Structural studies of amyloid proteins at the molecular level, *Annu. Rev. Biochem.*, 2017, **86**(1), 69–95.
52 P. Larsen, J. L. Nielsen, D. Otzen and P. H. Nielsen, Amyloid-like adhesins produced by floc-forming and filamentous bacteria in activated sludge, *Appl. Environ. Microbiol.*, 2008, **74**(5), 1517–1526.
53 X. Zogaj, W. Bokranz, M. Nimtz and U. Römling, Production of cellulose and curli fimbriae by members of the family Enterobacteriaceae isolated from the human gastrointestinal tract, *Infect. Immun.*, 2003, **71**(7), 4151–4158.
54 A. Taglialegna, I. Lasa and J. Valle, Amyloid structures as biofilm matrix scaffolds, *J. Bacteriol.*, 2016, **198**(19), 2579–2588.
55 P. Ragonis-Bachar and M. Landau, Functional and pathological amyloid structures in the eyes of 2020 cryo-EM, *Curr. Opin. Struct. Biol.*, 2021, **68**, 184–193.
56 Ü. Akbey and M. Andreasen, Functional amyloids from bacterial biofilms–structural properties and interaction partners, *Chem. Sci.*, 2022, **13**, 6457–6477.
57 K. Schwartz, M. Ganesan, D. E. Payne, M. J. Solomon and B. R. Boles, Extracellular DNA facilitates the formation of functional amyloids in Staphylococcus aureus biofilms, *Mol. Microbiol.*, 2016, **99**(1), 123–134.

 © 2023 The Author(s). Published by the Royal Society of Chemistry

58 S. A. Tursi, E. Y. Lee, N. J. Medeiros, M. H. Lee, L. K. Nicastro, B. Buttaro and Ç. Tükel, Bacterial amyloid curli acts as a carrier for DNA to elicit an autoimmune response via TLR2 and TLR9, *PLoS Pathog.*, 2017, **13**(4), e1006315.
59 M. Skok, O. Deryabina, O. Lykhmus, O. Kalashnyk, K. Uspenska, N. Shuvalova, I. Pokholenko, I. Lushnikova, K. Smozhanyk, G. Skibo and V. Kordyum, Mesenchymal stem cell application for treatment of neuroinflammation-induced cognitive impairment in mice, *Regener. Med.*, 2022, **17**(8), 533–546.

Open Access Article. Published on 17 October 2023. Downloaded on 1/25/2024 7:09:18 PM.
This article is licensed under a Creative Commons Attribution 3.0 Unported Licence.

Анотація: *Утворення біоплівки, або мікрообростання, є основною стратегією бактерій для колонізації поверхні та може відбуватися на поверхні будь-якої природи, де присутні бактерії. Біоплівки важко знищити через матрикс в якому живуть бактерії, що складається з міцних, адгезивних і адаптивних полімерів, які виробляються учасниками біоплівки. Вплив на структуру біопілвки може бути ефективною стратегією зниження мікрообрастання поверхонь. Досліджено декілька шляхів модифікації матеріалів, які призводили до зниження мікрообрастання. Зокрема, запропоновано і досліджено новий термічно стійкий полімерний біоцид полігексаметиленгуанідин 2-нафталінсульфонат, який додано до поліаміду. Було підтверджено антибіоплівкову активність проти умовно-патогенних бактерій S. aureus та E.coli для полімерів, що містили 7 та 10 % полімерного біоциду. Ще один полімерний катіонний біоцид 1-додецилпіридинію додецилбензолсульфонат (PyrC 12-DBS) був синтезований і протестований як потенційний протибіоплівковий компонент як додаток до комерційної алкідної фарби PP-115 (Україна). Модифіковані покриття PP-115/PyrC 12 –DBS, що містили 8% і 16% PyrC 12 –DBS, проявили суттєві антибіопівлівкові властивості проти S. aureus ATCC 25923 і P. aeruginosa PA01. Також було досліджено можливості зниження мікрообрастання металевих поверхонь шляхом лазерної модифікації. Така модифікація призвела до суттєвого зниження мас біоплівок P. aeruginosa PA01 і S. aureus ATCC29423.*

РОЗДІЛ 6. Біотехнології на основі біоплівок грамнегативних бактерій для вирішення завдань у агропромисловості

Пшениця є одним із найважливіших продуктів харчування та експортних товарів в Україні, при чому приблизно 95% врожаю припадає на посіви озимої пшениці (168). Озима пшениця становить приблизно 95%, решта 5% — яра пшениця (169). Але через високу вразливість культури пшениці, через кліматичні зміни і політико-економічну нестабільність, існує потреба в розробці нових більш продуктивних та технологічних підходів у покращенні та захисті пшениці (170).

Широке застосування сільськогосподарських бактерицидів і фунгіцидів, їхня хімічна стабільність і вплив на навколишнє середовище в цілому викликає все більше занепокоєння, оскільки в усьому світі використовується велика кількість ахрохімічних сполук, наприклад, понад 284 411 тон у 2015 році (170). Їх використання можна зменшити, використовуючи бактеріальні інокулянти, що стимулюють ріст рослин а також регулятори росту рослин бактеріального походження для обробки насіння та розсади (171, 172). Такі «зелені» технології стають все більш популярними, а в деяких випадках природні фітостимулятори забезпечують більш тривалий вплив на стресостійкість посівів і підвищення продуктивності без небажаного впливу на навколишнє середовище (173).

В нашій роботі ми дослідили чи можуть бактеріальні ацилгомосеринлактони, або АГЛ, які використовуються як предпосівна обробка насіння, мати значний вплив на врожайність озимої пшениці в реальних умовах землеробства. Зокрема, було порівняно розвиток рослин, продуктивність і структуру врожайності двох українських озимих сортів пшениці після обробки насіння лактоном N-гексаноіл-L-гомосерин лактон (ГГЛ) та продемонстровано підвищення врожайності обробленої озимої пшениці протягом двох вегетаційних сезонів у 2015–17 рр.

Основні результати, отримані в цьому підрозділі дисертації опубліковано в роботі автора (174).

PLOS ONE

RESEARCH ARTICLE

Priming winter wheat seeds with the bacterial quorum sensing signal N-hexanoyl-L-homoserine lactone (C6-HSL) shows potential to improve plant growth and seed yield

Olena V. Moshynets[1☯*], Lidia M. Babenko[2☯], Sergiy P. Rogalsky[3], Olga S. Iungin[4], Jessica Foster[5], Iryna V. Kosakivska[2], Geert Potters[6,7], Andrew J. Spiers[5*]

1 Institute of Molecular Biology and Genetics, National Academy of Sciences of Ukraine, Kiev, Ukraine, **2** M. G. Kholodny Institute of Botany, National Academy of Sciences of Ukraine, Kiev, Ukraine, **3** V.P. Kukhar Institute of Bioorganic Chemistry and Petrochemistry, National Academy of Sciences of Ukraine, Kiev, Ukraine, **4** D.K. Zabolotny Institute of Microbiology and Virology, National Academy of Sciences of Ukraine, Kiev, Ukraine, **5** School of Science, Engineering and Technology, Abertay University, Dundee, United Kingdom, **6** Antwerp Maritime Academy, Antwerp, Belgium, **7** Department of Bioscience Engineering, University of Antwerp, Antwerp, Belgium

☯ These authors contributed equally to this work.
* moshynets@gmail.com (OM); a.spiers@abertay.ac.uk (AS)

Check for updates

OPEN ACCESS

Citation: Moshynets OV, Babenko LM, Rogalsky SP, Iungin OS, Foster J, Kosakivska IV, et al. (2019) Priming winter wheat seeds with the bacterial quorum sensing signal N-hexanoyl-L-homoserine lactone (C6-HSL) shows potential to improve plant growth and seed yield. PLoS ONE 14 (2): e0209460. https://doi.org/10.1371/journal.pone.0209460

Editor: Ricardo Aroca, Estacion Experimental del Zaidin, SPAIN

Received: November 29, 2018

Accepted: February 7, 2019

Published: February 25, 2019

Copyright: © 2019 Moshynets et al. This is an open access article distributed under the terms of the Creative Commons Attribution License, which permits unrestricted use, distribution, and reproduction in any medium, provided the original author and source are credited.

Data Availability Statement: All relevant data are within the manuscript.

Funding: The project was partially supported by a grant to L.M. Babenko and O.V. Moshynets (0115U004178; Development of wheat priming biotechnology based on N-Acyl Homoserine Lactones for increasing resistance and productivity, 2015-2019) provided under the National Multidisciplinary NASU Research Program

Abstract

Several model plants are known to respond to bacterial quorum sensing molecules with altered root growth and gene expression patterns and induced resistance to plant pathogens. These compounds may represent novel elicitors that could be applied as seed primers to enhance cereal crop resistance to pathogens and abiotic stress and to improve yields. We investigated whether the acyl-homoserine lactone N-hexanoyl-L-homoserine lactone (C6-HSL) impacted winter wheat (*Triticum aestivum* L.) seed germination, plant development and productivity, using two Ukrainian varieties, Volodarka and Yatran 60, in both *in vitro* experiments and field trials. *In vitro* germination experiments indicated that C6-HSL seed priming had a small but significant positive impact on germination levels (1.2x increase, $p < 0.0001$), coleoptile and radicle development (1.4x increase, $p < 0.0001$). Field trials over two growing seasons (2015–16 and 2016–17) also demonstrated significant improvements in biomass at the tillering stage (1.4x increase, $p < 0.0001$), and crop structure and productivity at maturity including grain yield (1.4–1.5x increase, $p < 0.0007$) and quality (1.3x increase in good grain, $p < 0.0001$). In some cases variety effects were observed ($p \leq 0.05$) suggesting that the effect of C6-HSL seed priming might depend on plant genetics, and some benefits of priming were also evident in F1 plants grown from seeds collected the previous season ($p \leq 0.05$). These field-scale findings suggest that bacterial acyl-homoserine lactones such as C6-HSL could be used to improve cereal crop growth and yield and reduce reliance on fungicides and fertilisers to combat pathogens and stress.

"Molecular and Cellular Biotechnology for Medicine, Industry and Agrarian Sciences". Further internal support to O.V. Moshynets and A.J. Spiers was provided by IMBG and Abertay University. There was no additional external funding received for this study.

Competing interests: The authors have declared that no competing interests exist.

Introduction

Wheat is one of the most important food staples and export commodities in Ukraine with ~95% of the harvest coming from winter wheat crops [1]. Winter wheat represents ~95% of the annual crop with the remaining 5% planted as spring wheat [2]. It is typically sown in autumn (September-October) and harvested in mid-summer (July) of the following year, however, weather conditions severely affect the quality of the crop, and frequent changes during the growing season makes it more susceptible to bacterial and fungal pathogens than spring wheat which is grown from April to August. While there are a number of intensive agricultural technologies to improve crop yield and control pathogens, the economics of wheat production is dominated by the need to keep inputs beyond pre-plant bactericide and fungicide treatment and fertilization low to be economical [3]. Therefore, there is a need to augment existing production practices with economical, yet effective seed treatments to increase crop yield and resistance to pathogens.

The large-scale use of agricultural bactericides and fungicides, their persistence and impact on the wider environment is of increasing concern, with over 284,411 tonnes used worldwide in 2015 [4]. Their use can be reduced by using plant growth-promoting bacterial inoculants as well as bacterially-derived plant growth regulators to treat seeds and seedlings [5–7]. Such 'green' technology is becoming more popular, and in some cases, natural phyto-stimulators provide a more lasting impact on crop stress tolerance and increase productivity without undesirable environmental effects [8].

One of the most effective technologies to increase crop resistance to biotic and abiotic stressors is seed priming which increases germination vigour and activates plant defence mechanisms early in plant development through induced resistance [9,10]. Plant growth can be further supported by bacterial inocula which can facilitate mineral up-take and reduce pathogens through biological competition as well as stimulate the plant defence system [11,12]. Plants are also known to respond to bacterial quorum sensing signal molecules used by bacteria to regulate gene expression and coordinate social activities [9–10, 13–15]. For example, the legume *Medicago truncatula* responds to nanomolar concentrations of acyl-homoserine lactones (AHLs) produced by its symbiont *Sinorhizobium meliloti* and the pathogen *Pseudomonas aeruginosa* with specific and extensive changes in root gene expression and protein accumulation [16]. In tomato (*Solanum lycopersicum*) the plant growth-promoting bacterium *Serratia marcescens* but not AHL-deficient mutants increase systemic resistance against the fungal leaf pathogen *Alternaria alternata* [17], and treatment of roots with synthetic AHLs enhanced the expression of defence-related genes in the leaves of tomato [18].

We are interested in determining whether bacterial AHLs used as a seed primer can have a significant impact on winter wheat crop yields under realistic agricultural conditions. Here we compare plant development, productivity and yield structure for two Ukrainian winter wheat varieties following seed priming with the AHL N-hexanoyl-L-homoserine lactone (C6-HSL) and demonstrate improved crop yields over two growing seasons in 2015–17 at the Feofaniya research site near Kiev.

Materials and methods

C6-HSL synthesis

L-homoserine lactone hydrochloride was synthesized using a modified procedure [19] (**Fig 1**). 30 g of L-methionine, 120 mL water, 120 mL isopropanol and 50 mL glacial acetic acid were added to a 1 L round-bottom flask equipped with a magnetic stirrer. 20.8 g chloroacetic acid added and the suspension stirred for 12 h at 70˚C. The resulting transparent solution was

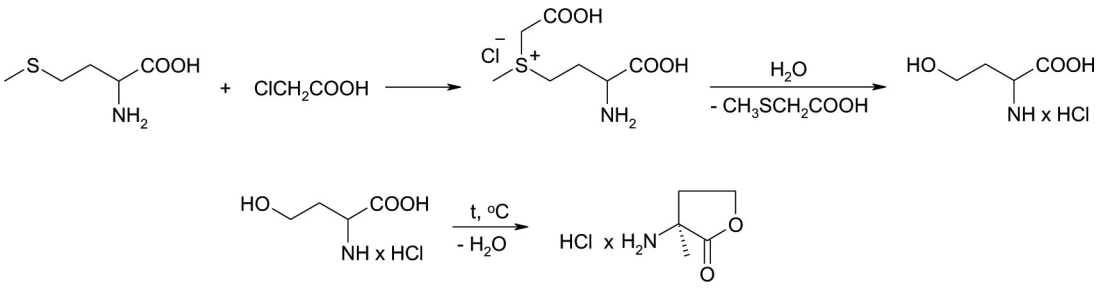

Fig 1. Synthetic route to obtain L-homoserine lactone hydrochloride.

https://doi.org/10.1371/journal.pone.0209460.g001

boiled with reflux for 3 h and the solvents distilled off at a reduced pressure. To convert the homoserine into its lactone, the solid residue was heated for 6 h at 100–110˚C and reduced pressure of 15–20 mbar. The product was dissolved in 50 mL water before 250 mL isopropanol was added and precipitated overnight at 4˚C. The crystalline solid was filtered out, washed with 100 mL isopropanol and vacuum–dried for 12 h at 40˚C and 1 mbar. In this procedure the yield of L-homoserine lactone hydrochloride was 65%. A proton nuclear magnetic resonance (^{1}H NMR, 300 MHz, DMSO-D6) spectrum of the end product with the following characteristics was obtained: ^{1}HNMR (DMSO-D6): δ 2.37 (^{1}H, m, 4α-H), 2.56 (^{1}H, m, 4β-H), 4.31 (^{2}H, m, 5α-H, 3-H), 4.34 (1H, td, 5β-H), 9.05 (3H, br s, NH).

The second-step synthesis of N-hexanoyl-L-homoserine lactone (C6-HSL) followed an earlier method [20] (**Fig 2**). 8.7 g trimethylamine was added to a stirred suspension of 5 g L-homoserine lactone hydrochloride in 70 mL methylene chloride at 0˚C. The mixture was stirred for 30 min before 4.9 g hexanoyl chloride was added dropwise within 10 min. The resultant reaction continued for 1 h at 0–5˚C and then at room temperature for a further 4 h. The mixture was washed twice with 50 mL saturated sodium hydrogen carbonate, twice with 50 mL 1 M potassium hydrogen sulfate, and then with 70 mL saturated sodium chloride. The solution of C6-HSL in methylene chloride was dried over sodium sulfate and the solvent was removed by distillation. The white solid residue was further purified by recrystallization in ethyl acetate. In this procedure the yield of C6-HSL was 60%. A proton nuclear magnetic resonance (^{1}H NMR, 300 MHz, DMSO-D6) spectrum of the end product with the following characteristics was obtained: ^{1}HNMR (DMSO-D6): δ 0.89 (3H, t, CH_3), 1.31 (4H, m, $CH_3(CH_2)_2$), 1.64 (2H, m, CH_2CH_2CO), 2.17 (1H, m, 4 α-H), 2.25 (2H, t, CH_2CO), 2.79 (1H, m, 4 β-H), 4.29 (1H, m, 5α-H), 4.46 (1H, td, 5 β-H), 4.64 (1H, m, 3-H), 6.5 (1H, d, NH).

Winter wheat varieties

Two varieties of winter wheat (*Triticum aestivum* L.), Volodarka and Yatran 60, cultivated extensively in the Lisostep and Polissye regions of Ukraine and produced by the Institute of Plant Physiology and Genetics (National Academy of Science of Ukraine) and the V.M. Remeslo Mironovka Institute of Wheat (Ukrainian Academy of Agrarian Sciences) were used in this work. Volodarka is a short-stalked variety with high yields and good resistance to frost and

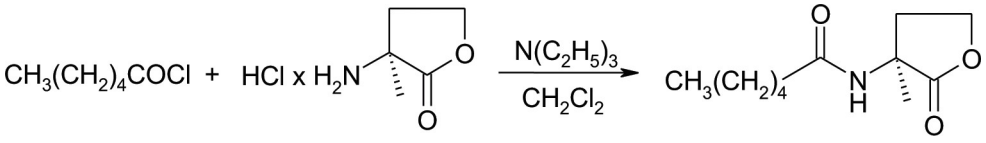

Fig 2. Synthetic route to obtain N-hexanoyl-L-homoserine lactone.

https://doi.org/10.1371/journal.pone.0209460.g002

drought while Yatran 60 is a short-stalked, medium-early variety with good resistance to heat and drought.

Seed preparation

Seeds were primed in a 100 ng/mL C6-HSL solution (3 kg seeds / 10 L; approx. 9 ng C6-HSL per seed) for 3 h before being dried for 72 h at 24–25˚C to a water content of 12–14% (w/w). Non-primed control seeds were treated with water before drying. Seeds were then coated using AREAL BS-05 pelleting mixture (containing a polysaccharide mix, polyvinyl alcohol, titanium dioxide, mineralized talcum powder, organic and nonorganic pigments, and has a solution pH of 7–8; Legion Company Ltd, Ukraine) pelleting mixture before sowing. Seeds were collected from plants grown from primed seeds in 2015–16 (F1 seeds) and used in further tests.

Seed germination assays

The effects of seed priming on germination were investigated according to the International Seed Testing Association (ISTA) standards. Fifteen samples of 20 seeds of each variety and treatment were germinated in the dark at 24˚C for 24 h in Petri dishes containing Knop's nutrient solution [21] to determine germination levels. In parallel, three samples of 20 seeds of each variety and treatment were germinated on wet filter paper and coleoptile and radicle lengths determined after 2 days.

Crop trials

Winter wheat crops were planted and harvested over two consecutive growing seasons (September 2015 –July 2016, and August 2016 –July 2017) at the Feofaniya research site (M.G. Kholodny Institute of Botany, National Academy of Science Ukraine; Geographical coordinates 50˚20'59.7"N 30˚29'16.1"E) near Kiev. The crop fields are composed of grey forest soil with ash and a very loamy chernozem (pH KCl 5.7, total humus content 4.1%, 138 mg phosphorus/kg, 90 mg potassium/kg). Seeds were planted at a density of 600 seeds/m^2 at 3.5–4 cm depth and fertilizer added during the growing season (145 kg/ha nitrogen, 90 kg/ha phosphorus, and 90 kg/ha potassium). Weather conditions (**Fig 3**) were recorded by the Meteorological Centre, Central Geophysical Observatory of B.I. Sreznevsky at Kiev, approximately 6 km from Feofaniya.

Morphological parameters describing plant and seed yield were measured for 100 plants of each variety in 2015–2016 and 50 plants per variety in 2016–2017. Seed quality was assessed visually as either 'normal' (well-shaped, larger and fatter morphology) or 'poor' (misshapen, small and thin) and the proportion of normal seeds determined for three samples of 100 seeds. Five samples of 10 seeds of each type were weighed to obtain mean seed weights. Plants were sampled to assess growth, plant morphology, and seed yield.

Chlorophyll and carotenoid levels

Winter wheat crops were planted as for the crop trials described above (August 2016 –July 2017) at the Hlevakha research site (Institute of Plant Physiology and Genetics, National Academy of Science of Ukraine; Geographical coordinates 50˚15'37.3"N 30˚17'12.8"E) approximately 15 km away from Feofaniya and having a similar soil type. Chlorophyll (a and b) and carotenoid levels were measured after acetone extraction [22]. Five extracts were prepared from material harvested from five plants at each of the booting, flowering, milk ripeness, and milk-wax ripeness stages.

Microbiological characterization

The numbers of rhizosphere-associated chemo-organotrophic, nitrogen-fixing, denitrifying, and amylolytic bacteria adhering to wheat roots were determined using viable colony counts. Roots from 125 2 month-old plants from 2015–2016 were washed in sterile 0.9% (w/v) saline and aliquots of serial dilutions spread onto Nutrient Agar (HiMedia, India) which were incubated at 24˚C for 5 days to determine chemo-organotrophic bacterial numbers. Ashby's medium supplemented with 2% (w/v) sucrose [23–24] was used to determine nitrogen-fixing bacterial numbers with colonies re-isolated three times in liquid medium to distinguish nitrogen-fixers from oligonitrophilic bacteria [23]. Nitrifying bacteria were isolated in liquid Watson and Mendel's media and incubation for 20 days [23]. Denitrifying bacteria were isolated using Gil'tai's medium (pH 6.8–7.2) in an inert argon atmosphere using a Hangeit-like technique [25] at 24˚C for 5 days, with viable numbers determined using the most probable number method [26] with 3-tube variation [27]. Denitrifying bacteria were identified based on medium alkalinisation, increasing optical density, gas production, and the absence of nitrate. Amylolytic bacterial numbers were determined using 2% (w/v) starch plates incubated at 28˚C for 3 days washed with 0.1% (w/v) iodine to visualize cleared halo around the colonies [28].

Statistical analyses

Data were analysed by modelling using a least squares approach with effects (year, plot, wheat variety, seed treatment, and experimental replicate) tested by LSMeans Differences Student's t and Tukey HSD tests ($\alpha = 0.05$) (JMP v12, SAS Institute Inc., USA). Chi-Square tests of independence (www.socscistatistics.com) were used to assess the effect of seed treatment on rhizosphere bacteria. Means and standard errors (SE) are shown where appropriate.

Results

Germination

In vitro germination assays were conducted to determine whether seed priming effected germination and seedling development (**Fig 4**). Priming had a significant positive effect on

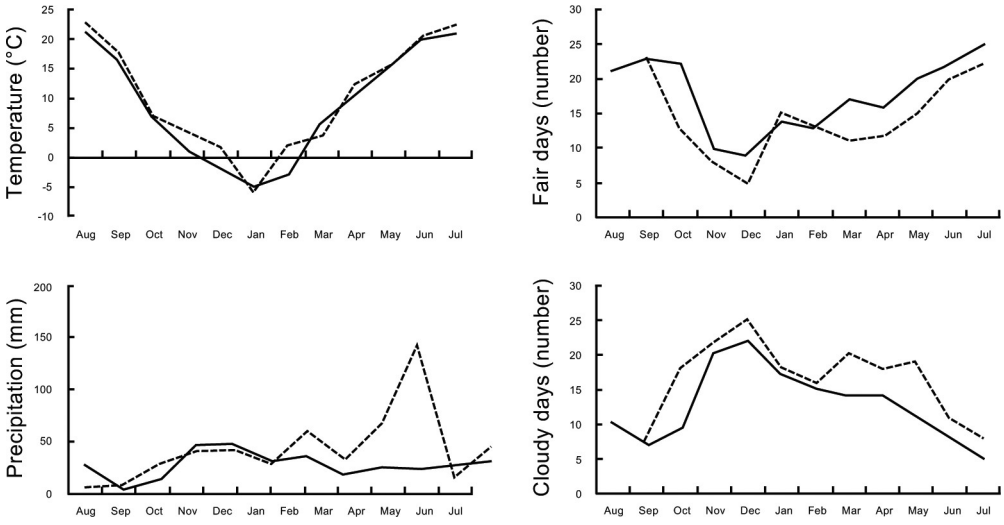

Fig 3. Meteorological conditions during crop trials. Winter wheat was planted and harvested over two consecutive growing seasons, from September 2015 –July 2016 (dashed lines) and August 2016 –July 2017 (solid lines) at the Feofaniya research site and weather conditions recorded at the nearby Meteorological Centre of the Central Geophysical Observatory of B.I. Sreznevsky.

https://doi.org/10.1371/journal.pone.0209460.g003

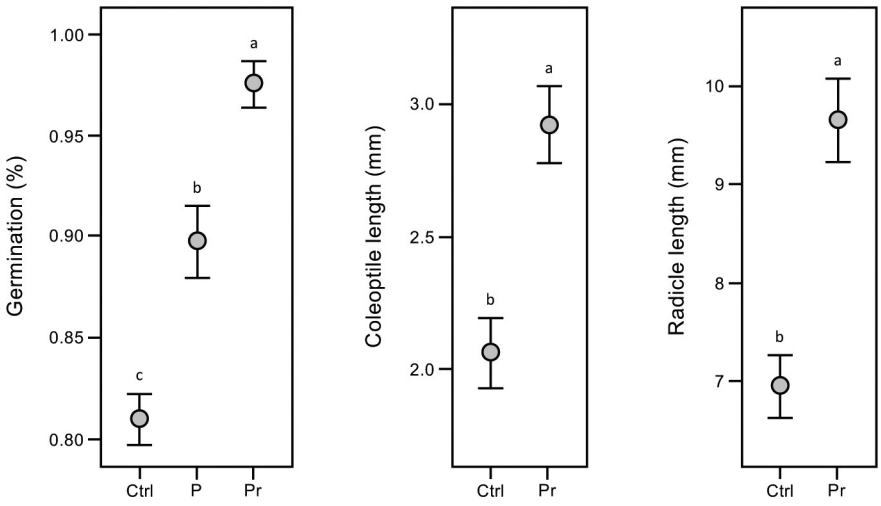

Fig 4. C6-HSL seed priming affects germination and early development. Seed treatments have small but significant effects on *in vitro* germination rates and on two day-old winter wheat seedling coleoptile (the protective sheath covering the emerging shoot) and radicle (embryonic root) lengths. Plants were grown from pelleted and primed (Pr), pelleted (P), or untreated (Ctrl) seeds. As no significant wheat variety effect was observed (p = 0.32, 0.99 and 0.48, respectively) data are pooled and means and standard errors (SE) shown. Means not connected by the same letter are significantly different (α = 0.05).

https://doi.org/10.1371/journal.pone.0209460.g004

germination with levels 1.2x greater than the untreated controls ($p < 0.0001$), and on two-day old seedling development with coleoptile (the protective sheath covering the emerging shoot) and radicle (embryonic root) lengths 1.4x greater than the untreated controls ($p < 0.0001$). However, no wheat variety effects were observed in these assays (p = 0.32, 0.99 and 0.48, respectively). These findings suggest that seed priming with C6-HSL may have a positive impact on the early development of wheat seeds.

Plant development

Two month-old plants at the tillering stage were sampled from our research field site in 2015–16 to determine whether seed priming effected plant development (Fig 5). Priming had a significant positive effect on plant growth with dried aboveground biomass 1.4x greater than the untreated controls ($p < 0.0001$), though like the *in vitro* assays, no wheat variety effects were observed (p = 0.39). This suggests that the seed priming advantage seen in better germination rates and faster embryo development also occurs in the field and continues through tillering development.

Crop structure and productivity

Mature plants with grain were harvested in mid-summer of 2015–16 and 2016–17 to determine whether seed priming effected crop structure and productivity. In our analysis of these data, a significant year effect was observed ($p < 0.05$) which may be explained by the colder conditions and lower seasonal rainfall in the second growing season (Fig 3). Priming had a significant effect on over-all plant height, tiller numbers, ear length, spikelets per ear, grains per ear, and the grain mass per plant in 2015–16 and 2016–17 ($p < 0.0001$), and a significant wheat variety effect was observed ($p < 0.0001$) with Yatran 60 generally out-performing the Volodarka variety (data for 2015–16 and 2016–17 is provided in Table 1). Priming also had a significant positive effect on crop yield (kg/m^2) with grain mass 1.4x and 1.5x greater than the untreated controls ($p < 0.0007$) in 2015–16 and 2016–17, respectively. The impact of seed

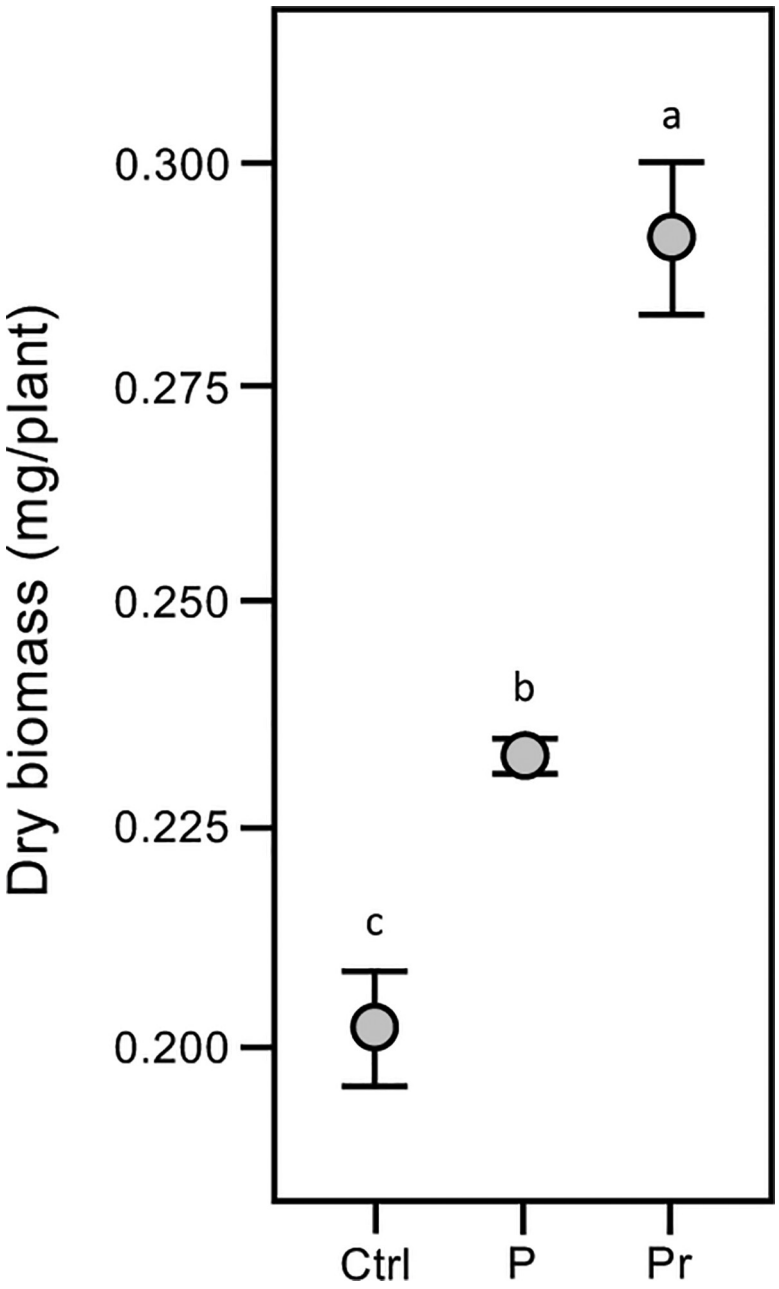

Fig 5. C6-HSL seed priming affects plant development at the tillering stage. Seed treatments have small but significant effects on total dry biomass at 2 months in winter wheat crop trials (2015–16). Plants were grown from pelleted and primed (Pr), pelleted (P) or untreated (Ctrl) seeds. As no significant wheat variety effect was observed ($p = 0.3924$) data are pooled and means and standard errors (SE) shown. Means not connected by the same letter are significantly different ($\alpha = 0.05$).

https://doi.org/10.1371/journal.pone.0209460.g005

priming with C6-HSL on crop yield is also evident by PCA of data by year and variety (Fig 6). In a separate trail at the nearby Hlevakha research site in 2016–17, priming was also found to have a significant effect on over-all chlorophyll and carotenoid levels, as did plant development stage (from booting, flowering, milk ripeness to milk-wax ripeness) ($p < 0.0001$), and for carotenoids a significant wheat variety effect was also observed ($p = 0.006$) (Table 2). These

findings suggest that the positive effect seen with seed priming with C6-HSL continues through wheat development to plant maturity and grain production.

Grain quality

Grain produced in 2016–17 was examined to determine whether seed priming effected grain quality or mean weight (Fig 7). Priming had a significant effect on grain quality with the proportion of good grain 1.3x greater than the untreated controls ($p < 0.0001$), though no wheat variety effects were observed ($p = 0.08$). A more complex range of factors including grain quality, seed treatment, and the seed quality x seed treatment and seed treatment x wheat variety interactions had significant effects on mean grain weight ($p < 0.0001$, 0.0164, 0.0002, 0.0006, respectively), though no wheat variety effect was observed ($p = 0.46$). These findings suggest that seed priming also effects grain quality and weight.

F1 plants grown from primed seed-plants

F1 grain collected from primed seed-plants grown in 2015–16 was tested to determine whether the seed priming effect was transferred to the next generation of wheat. Re-analysis of earlier experiments including F1 data showed significant differences between plants grown from F1 seeds and untreated control seeds in seven of 11 assays (Table 3) and this is also evident by PCA of crop yield data for 2016–17 by variety (Fig 8). This suggests that the seed priming effect is transferred to the following generation of wheat.

Table 1. Productivity structure (2015–16 & 2016–17).

Season	Wheat variety		Ctrl seeds	Pelleted seeds (P)	P/Ctrl ratio	Pelleted & Primed seeds (Pr)	Pr/Ctrl ratio
2015–16	Volodarka	Plant height (cm)	93.1 ± 0.3	91.6 ± 0.6	0.98	94.3 ± 0.3	1.01
		Number of tillers per plant	6.6 ± 0.1	7.1 ± 0.1	1.08	11.8 ± 0.2	1.79
		Ear length (cm)	12.2 ± 0.2	11.9 ± 0.2	0.98	13.6 ± 0.1	1.12
		Number of spikelets per ear	17.2 ± 0.2	18.4 ± 0.1	1.07	19.3 ± 0.1	1.12
		Number of grains per ear	41.0 ± 0.5	42.5 ± 0.5	1.04	52.5 ± 0.6	1.28
		Grain mass per plant (g)	1.57 ± 0.02	1.68 ± 0.02	1.07	2.18 ± 0.03	1.39
	Yatran 60	Plant height (cm)	84.7 ± 0.4	83.3 ± 0.3	0.98	86.7 ± 0.3	1.02
		Number of tillers per plant	7.3 ± 0.2	7.3 ± 0.1	1.00	12.7 ± 0.2	1.74
		Ear length (cm)	13.4 ± 0.1	13.4 ± 0.1	1.00	13.5 ± 0.1	1.01
		Number of spikelets per ear	21.0 ± 0.1	20.9 ± 0.1	1.00	21.6 ± 0.1	1.03
		Number of grains per ear	44.0 ± 0.4	45.7 ± 0.3	1.04	55.8 ± 0.3	1.27
		Grain mass per plant (g)	1.57 ± 0.03	1.68 ± 0.03	1.07	1.98 ± 0.02	1.26
2016–17	Volodarka	Plant height (cm)	85.2 ± 0.4	82.2 ± 0.3	0.97	83.4 ± 0.4	0.98
		Number of tillers per plant	2.4 ± 0.2	2.1 ± 0.1	0.88	4.5 ± 0.2	1.88
		Ear length (cm)	12.3 ± 0.2	12.2 ± 0.2	0.99	13.1 ± 0.2	1.07
		Number of spikelets per ear	17.3 ± 0.3	18.1 ± 0.1	1.05	18.8 ± 0.3	1.09
		Number of grains per ear	38.1 ± 0.4	36.4 ± 0.6	0.96	40.2 ± 0.7	1.06
		Grain mass per plant (g)	1.64 ± 0.07	1.68 ± 0.05	1.02	2.20 ± 0.08	1.34
	Yatran 60	Plant height (cm)	78.3 ± 0.3	79.4 ± 0.2	1.01	80.8 ± 0.3	1.02
		Number of tillers per plant	2.2 ± 0.1	2.0 ± 0.1	0.91	4.8 ± 0.2	2.18
		Ear length (cm)	12.8 ± 0.2	13.0 ± 0.2	1.02	13.9 ± 0.2	1.09
		Number of spikelets per ear	16.3 ± 0.2	15.2 ± 0.4	0.93	20.1 ± 0.4	1.23
		Number of grains per ear	39.6 ± 0.4	38.2 ± 0.6	0.97	46.5 ± 0.9	1.17
		Grain mass per plant (g)	1.47 ± 0.04	1.52 ± 0.05	1.03	1.84 ± 0.06	1.25

Means ± SE are shown. Ctrl, Plants grown from untreated seeds. See the main text for the statistical analyses of these data using a modelling approach.

https://doi.org/10.1371/journal.pone.0209460.t001

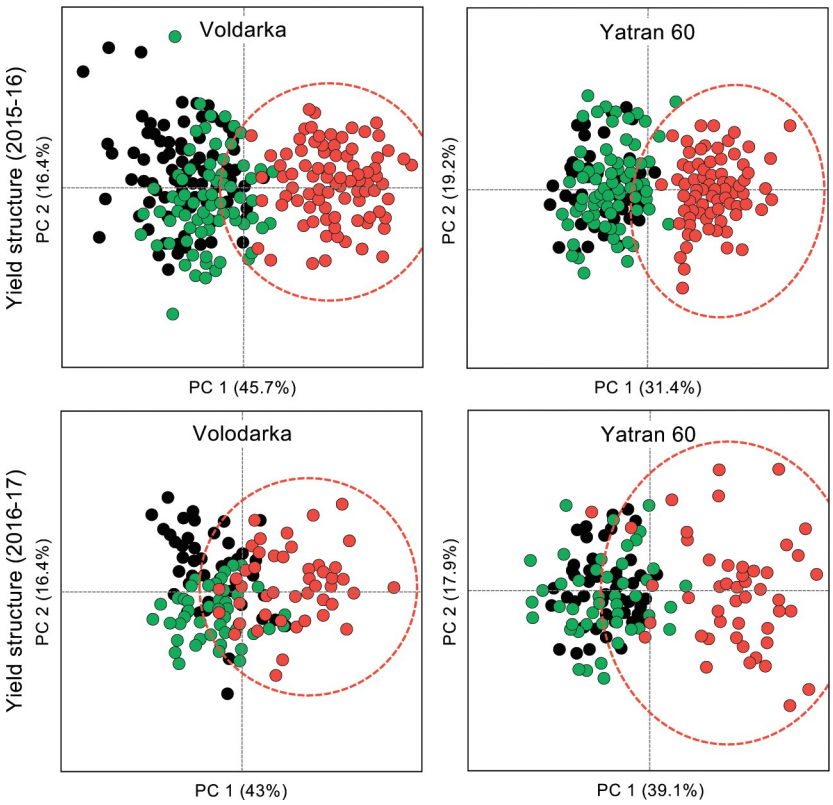

Fig 6. C6-HSL seed priming affects crop yield structure. The effect of seed treatment on winter wheat yield structure (over-all plant height, tiller numbers, ear length, spikelets per ear, grains per ear, and the grain mass per plant) can be visualised by Principal component analysis (PCA) for 2015–16 and 2016–17. Plants were grown from pelleted and primed (red and dashed oval), pelleted (green) or untreated (black) seeds. Axis scales are the same for each biplot and the cumulative percentage covariance is shown for both principal axes.

https://doi.org/10.1371/journal.pone.0209460.g006

Rhizosphere microbiology

Bacteria recovered from the roots of two month-old plants at the tillering stage in 2015–16 were characterised in a preliminary investigation to determine whether seed priming effected

Table 2. Chlorophyll and carotenoid levels (2016–17).

		Chlorophyll a			Chlorophyll b			Carotenoids		
Wheat variety	**Plant developmental stage**	**Ctrl seeds**	**Primed seeds (Pr)**	**Pr/Ctrl ratio**	**Ctrl seeds**	**Primed seeds (Pr)**	**Pr/Ctrl ratio**	**Ctrl seeds**	**Primed seeds (Pr)**	**Pr/Ctrl ratio**
Volodarka	Flowering	2.02 ± 0.01	2.27 ± 0.01	1.13	0.77 ± 0.01	0.77 ± 0.01	1.00	0.69 ± 0.01	0.69 ± 0.01	1.00
	Milk ripeness	1.99 ± 0.01	2.13 ± 0.02	1.07	0.65 ± 0.02	0.72 ± 0.01	1.11	0.59 ± 0.01	0.65 ± 0.01	1.10
	Booting	1.80 ± 0.01	2.11 ± 0.01	1.17	0.61 ± 0.01	0.77 ± 0.01	1.26	0.58 ± 0.01	0.61 ± 0.01	1.05
	Milk-wax ripeness	0.97 ± 0.01	1.01 ± 0.01	1.04	0.30 ± 0.01	0.33 ± 0.01	1.10	0.52 ± 0.01	0.46 ± 0.01	0.89
Yatran 60	Flowering	1.81 ±0.01	2.61 ± 0.01	1.44	0.67 ± 0.01	0.94 ± 0.02	1.40	0.55 ± 0.01	0.77 ± 0.01	1.40
	Milk ripeness	1.57 ± 0.01	2.44 ± 0.02	1.55	0.56 ± 0.02	0.83 ± 0.01	1.48	0.45 ± 0.01	0.68 ± 0.01	1.51
	Booting	1.52 ± 0.09	1.91 ± 0.02	1.26	0.55 ± 0.03	0.62 ± 0.02	1.13	0.44 ± 0.02	0.55 ± 0.02	1.25
	Milk-wax ripeness	1.10 ± 0.02	1.43 ± 0.01	1.30	0.31 ± 0.01	0.41 ± 0.01	1.32	0.45 ± 0.01	0.58 ± 0.01	1.29

Chlorophyll and carotenoids were measured as mg/g of fresh plant weight. Means ± SE are shown. Ctrl, Plants grown from untreated seeds. See the main text for the statistical analyses of these data using a modelling approach.

https://doi.org/10.1371/journal.pone.0209460.t002

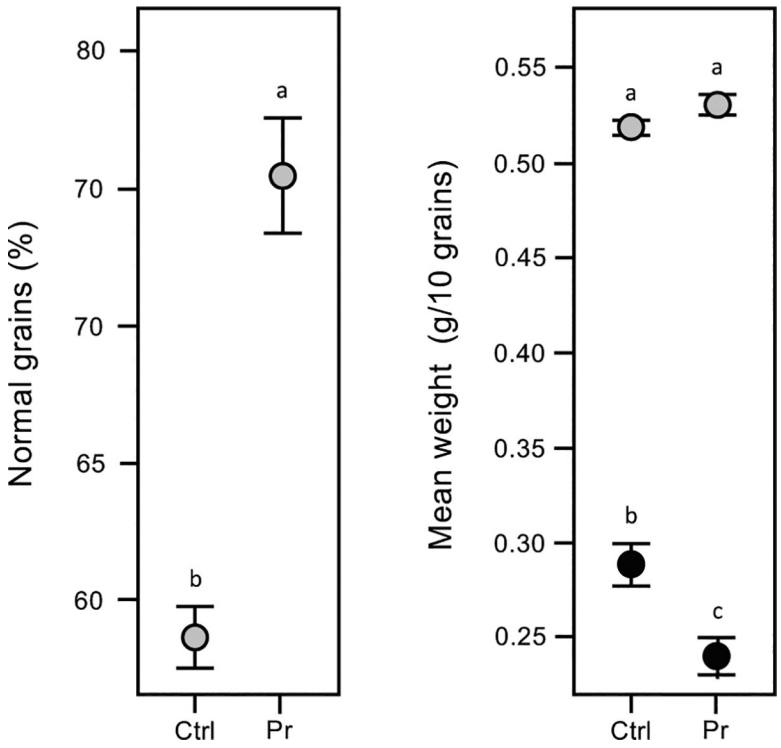

Fig 7. C6-HSL seed priming affects grain quality. Seed treatments have small but significant effects on the percentage of normal grain (grey) and on the mean weight of poor grain (black) in winter wheat crop trials (2016–17). Grain was collected from plants grown from pelleted and primed (Pr) or untreated seeds (Ctrl). As no significant wheat variety effect was observed (proportion of normal grain, p = 0.08; weight of 10 grains, p = 0.46) data are pooled and means and standard errors (SE) shown. Means not connected by the same letter are significantly different (α = 0.05).

https://doi.org/10.1371/journal.pone.0209460.g007

rhizosphere microbiology. Bacterial numbers in five functional groups (amylolytic, denitrifying, nitrifying, N-fixing, and oligonitrophilic bacteria) determined from pooled samples

Table 3. F1 characteristics (2016–17).

		Seed treatment effects & tests				
		P	**Ctrl seeds**	**Pelleted seeds**	**Pelleted & Primed seeds**	**F1 seeds**
Seedling	Coleoptile development (mm)	< 0.0001	2.1 ± 0.1^{b}		2.9 ± 0.2^{a}	2.8 ± 0.1^{a}
	Radicle development (mm)	< 0.0001	6.9 ± 0.3^{b}		9.7 ± 0.4^{a}	7.9 ± 0.3^{b}
Productivity structure	Plant height (cm)	< 0.0001	81.7 ± 0.4^{a}	80.8 ± 0.2^{b}	82.1 ± 0.3^{a}	80.2 ± 0.2^{b}
	Number of tillers per plant	< 0.0001	2.3 ± 0.1^{c}	2.1 ± 0.1^{c}	4.6 ± 0.1^{a}	3.4 ± 0.1^{b}
	Ear length (cm)	< 0.0001	12.6 ± 0.1^{b}	12.6 ± 0.1^{b}	13.5 ± 0.1^{a}	12.9 ± 0.1^{b}
	Number of spikelets per ear	< 0.0001	16.8 ± 0.2^{bc}	16.7 ± 0.3^{c}	19.4 ± 0.3^{a}	17.6 ± 0.3^{b}
	Number of grains per ear	< 0.0001	38.8 ± 0.3^{c}	37.3 ± 0.4^{c}	43.4 ± 0.6^{a}	40.7 ± 0.4^{b}
	Grain mass per plant (g)	< 0.0001	1.55 ± 0.04^{b}	1.60 ± 0.04^{b}	2.02 ± 0.05^{a}	1.67 ± 0.04^{b}
Yield structure	Total above-ground biomass (kg/m^2)	< 0.0001	0.52 ± 0.01^{b}	0.50 ± 0.01^{b}	0.78 ± 0.02^{a}	0.73 ± 0.01^{a}
	Straw biomass (kg/m^2)	0.0004	0.17 ± 0.02^{b}	0.17 ± 0.01^{b}	0.26 ± 0.02^{a}	0.30 ± 0.01^{a}
	Grain mass (kg/m^2)	< 0.0001	0.35 ± 0.01^{c}	0.34 ± 0.02^{c}	0.53 ± 0.01^{a}	0.43 ± 0.01^{b}

Main experiments were reanalysed after including F1 data. All assays with significant seed treatment effects ($p < 0.05$) are listed and pooled means ± SE are shown. Seed treatment effects are examined further by LSMeans Differences Tukey HSD tests. Treatments not connected by the same letter are significantly different ($\alpha = 0.05$). All data are from 2016–17. Ctrl, Plants grown from untreated seeds; F1, plants grown from seeds collected in 2015–16 from plants grown from pelleted and primed seeds.

https://doi.org/10.1371/journal.pone.0209460.t003

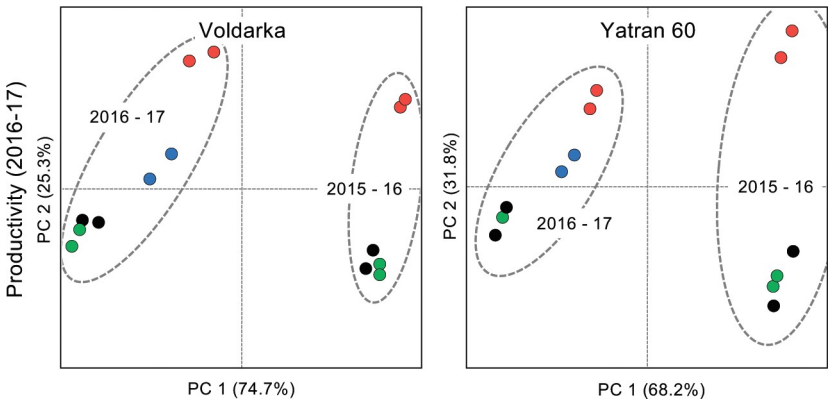

Fig 8. C6-HSL seed priming affects are transferred to the following generation. Principal component analysis (PCA) of winter wheat crop productivity (total above ground biomass, straw biomass, and grain mass) can differentiate plants grown from F1 seeds produced by pelleted and primed plants in 2015–16 and sown in 2016–17 (blue) from plants grown from pelleted and primed (red), pelleted (green) or untreated (black) seeds. In these analyses a strong *year* effect is also apparent for both wheat varieties (indicated by dashed ovals). Axis scales are the same for each biplot and the cumulative percentage covariance is shown for both principal axes.

https://doi.org/10.1371/journal.pone.0209460.g008

(Table 4) were found to be dependent on seed treatment for both wheat varieties ($p < 0.0001$). This preliminary result suggests that the seed priming effect alters the functional composition of bacterial communities around wheat roots.

Discussion

Early investigations of the effect of AHL applications on plant development and systemic resistance have focussed on *in vitro* and pot-plant experiments and reported changes in gene expression patterns, root development and systemic resistance [16–17, 29–33]. In this study, we were interested in determining whether bacterial AHLs can be used as a novel class of phyto-stimulator seed primers to improve cereal crop growth and grain yields, using winter wheat to investigate changes in seed germination *in vitro* and field trials to investigate changes in plant development and crop yield. Interestingly, the changes we have observed in C6-HSL-primed plants correspond well with those observed in wheat plants treated with the gram-negative plant growth-promoting rhizobacteria [34–36] which naturally produce AHLs to regulate gene expression and coordinate social activities [17, 37–39].

In this study, we investigate the effect of AHL applied directly to seeds before germination whereas previous research has focused on dosing or spaying seedlings or even older plants

Table 4. Rhizosphere microbiology (2015–16).

	Volodarka			Yatran 60		
Functional group	**Ctrl seeds**	**Pelleted seeds**	**Primed seeds**	**Ctrl seeds**	**Pelleted seeds**	**Primed seeds**
Amylolytic	11	32	120	10	33	23
Denitrifying	6	60	250	60	600	1
Nitrifying	9	190	19	500	1900	900
N-fixing	95	450	250	450	1500	150
Oligonitrophilic	230	480	270	440	930	1500

Numbers are 10^4 per un-replicated (pooled) rhizosphere samples. Bacterial numbers and treatments are dependent for both wheat varieties (Volodarka, $\chi^2 = 568$, $p < 0.0001$; Yatran 60, $\chi^2 = 1675$, $p < 0.0001$). Ctrl, rhizosphere samples from plants grown from untreated seeds.

https://doi.org/10.1371/journal.pone.0209460.t004

with AHL solutions [16–17, 31–33, 40–41]. We test here the effectiveness of seed priming with C6-HSL on two varieties of winter wheat as we expected to see a strong genetic effect in response to AHL treatment, but variety effects were seen in less than half of the characteristics we measured. The changes we observed in C6-HSL-primed plants suggest that the delivery of AHLs by seed priming would be successful in an agricultural context, as priming and pelleting are commonly used to apply a range of bactericides, fungicides, pesticides, herbicides, and phytostimulators, as well as fertiliser, to improve crop yields and lessen waste in a cost-effective manner.

Effect of seed priming with C6-HSL on plant development and crop yield

We have investigated the effect of seed priming with C6-HSL on the germination and early seedling development of winter wheat *in vitro* where C6-HSL was found to have a small but significant positive effect on the germination and early seedling development (**Fig 4 & Table 3**). Seed priming with C6-HSL continued to have a positive effect in field trials, with improvements seen in plant biomass at the tillering stage (**Fig 5**), chlorophyll and carotenoid levels (**Table 2**), and on plant structure and yield at maturity (**Fig 7, Tables 1 & 3**). Collectively seed priming with C6-HSL seems to produce more robust and healthy plants which results in a higher grain yield at maturity. Although we have not directly investigated whether seed priming improves plant resistance to stress, we note that the 2016–17 growing season with lower than normal seasonal rainfall (**Fig 3**) resulted in plants with reduced productivity compared to 2015–16, yet grain yield from plants grown from primed seeds remained similar in both seasons (**Table 1**). The impact of seed priming on plant health and yield might be the result of direct effects on plant development and stress resistance and/or indirect effects resulting from changes in the plant-associated microbial community.

Direct effects on plant development and stress resistance

Plants may respond directly to bacterial AHLs as they produce structurally-similar compounds including *N*-acyl ethanolamines and alkamides with likely roles in cell division and differentiation processes [28]. Bacterial AHLs are furthermore known to alter cell division in the primary root meristem, interact with G-protein and Ca^{2+} signalling, effect transpiration, and involve modulators of plant defence such as oxylipin and salicylic acid [9–10, 29, 31–32, 42], and in the context of pathogen and stress resistance, produce healthier and more robust plants. From our analyses, C6-HSL priming appears to promote faster germination and embryo development in winter wheat (**Fig 4**) which might allow seedlings to out-pace or overcome stresses which normally limit growth and yields. Alternatively, C6-HSL might affect signalling pathways to produce a response similar to the stress-induced morphogenic response (SIMR) caused by exposure to chronic, low-intensity stress [43–45]. It is possible that such 'pre-stressed' plants are better suited to subsequent growth under non-optimal conditions, and that this explains the positive impact on winter wheat plant development and yield we observed in our field trials.

We note that plants grown from seed collected from C6-HSL treated plants (i.e. second generation or F1 plants) performed significantly better than control plants (**Table 3**). Although these improvements may partially be explained by healthy plants producing better quality seeds leading to more vigorous plants in the next generation [46–47], it is also possible that the seed priming effect is acting through epistasis in which heritable changes in gene expression patterns occurring without alteration of DNA sequences [48–49] and such epigenetic changes are known to occur in plants development and as a result of environmental stress [50].

Indirect effects on plant-associated microbial communities

Rhizosphere (root) and phyllosphere (above ground) plant-associated microbial communities are known to have a direct and positive impact on plant growth and resistance to pathogens by mobilising soil nutrients, out-competing pathogens and inducing plant resistance [51–52]. It is possible that the C6-HSL carried by primed seeds might leach into the surrounding soil and stimulate plant growth-promoting (PGP) bacteria including *Bacillus* and *Pseudomonas* spp., resulting in better plant–surface colonisation and greater levels of pathogen suppression, especially during the early stages of seedling development. However, we believe that it is more likely that the direct stimulation of plant growth by C6-HSL results in greater levels of photosynthate exudate which then supports more effective PGP microbial communities. Our preliminary analysis of wheat rhizosphere community structure indicates that seed priming with C6-HSL results in functional changes (**Table 4**). We noted an increase in amylolytic bacteria which are involved in the degradation of dead root cells that promotes root growth and releases sugars for other rhizosphere bacteria, and they also effect plant defence response by provoking systemic resistance and improving the recognition of pathogenic microbes [53]. We also noted an apparent reduction in N-fixing and nitrifying bacteria which sometimes results in lower yields [54] though it might also be caused by improved N uptake by plants with better root development.

Agro-economic advantages to AHL seed priming

Plant protection is ranked high in importance for stable wheat production by growers who face a range of pathogens which can be responsible for 15–20% yield losses per annum [55–56]. However, the net returns from fungicide use are highly variable and are only profitable in years with moderate to high disease severity [57–58]. As a consequence, the adoption of a new phyto-stimulator such as C6-HSL by growers will be governed by yield (and yield stability) improvements, chemical and treatment costs, and any potential savings made by reduced bactericide and fungicide applications.

We estimate our treatment costs at €14 per 10^3 kg of seeds having synthesized C6-HSL using standard laboratory-grade reagents (analytical-grade C6-HSL costs €11 mg^{-1}) and could probably lower costs even further using Ukrainian-sourced chemicals. Seed priming of winter wheat in Ukraine is increasing, with more that 70% of seeds treated with 1.5 x 10^9 kg of fungicides in 2018 (Superagronom.com), but in order for C6-HSL seed priming to be commercially acceptable, costs need to be equal or lower than current treatments and produce the same or greater benefits. In comparison, the phyto-stimulator Raykat (Start Atlantica, Spain) and the fungicide Vitavax 200 FF (Brook Crompton, Italy), both widely used in Ukraine, cost €26 and €14.5 per 10^3 kg of seeds, respectively. The continued use and development of bactericides, fungicides, and phyto-stimulators, etc., is necessary to increase stable crop yields world-wide, reduce the ecological impact of modern intensive agriculture, and combat the spread and evolution of new pathogens driven by globalisation and climate change [57, 59–61].

Conclusions

Bacterial AHLs such as C6-HSL are known to effect plant growth and resistance to pathogens in laboratory-based experiments. Our work provides the first field-scale evidence to suggest that C6-HSL may be a viable phyto-stimulator when applied as a seed primer for winter wheat. The significant improvements seen in wheat growth, productivity and yield structure are explained by healthier and more robust plants resulting from the direct or indirect effects of C6-HSL on seed germination, plant growth and maturation. The development of new phyto-stimulators based on bacterial AHLs as a part of modern plant protection, in a combination

with new bactericides, fungicides, crop varieties, and agricultural techniques, etc., could provide a more sophisticate means of combating plant pathogens and increasing stable crop yields in the future.

Acknowledgments

We thank the Institute of Molecular Biology and Genetics, National Academy of Science of Ukraine, and Abertay University, for their continued support of the on-going collaboration between O.V. Moshynets and A.J. Spiers; A.J. Spiers is also member of the Scottish Alliance for Geoscience Environment and Society (SAGES). We thank the Director of the Institute of Plant Physiology and Genetics of the National Academy of Sciences of Ukraine, Prof. DSc. Academician V.V. Morhun for his support with the seed materials and fruitful discussions of our experimental results. We also thank the founder of Agrohub (https://agrohub.org/) and co-founder of Radar Tech (http://radartech.com.ua/) Yulia Poroshenko for her support and advice.

Author Contributions

Conceptualization: Olena V. Moshynets.

Data curation: Olena V. Moshynets, Lidia M. Babenko.

Formal analysis: Geert Potters, Andrew J. Spiers.

Funding acquisition: Olena V. Moshynets, Lidia M. Babenko.

Investigation: Lidia M. Babenko, Sergiy P. Rogalsky, Olga S. Iungin, Jessica Foster.

Methodology: Lidia M. Babenko.

Project administration: Olena V. Moshynets, Lidia M. Babenko.

Resources: Olena V. Moshynets, Lidia M. Babenko.

Supervision: Iryna V. Kosakivska.

Visualization: Andrew J. Spiers.

Writing – original draft: Olena V. Moshynets, Geert Potters, Andrew J. Spiers.

Writing – review & editing: Olena V. Moshynets, Geert Potters, Andrew J. Spiers.

References

1. Brecker-Reshef I, Vermore E, Lindeman M, Justice C. A generalized regression-based model for forecasting winter wheat yields in Kansas and Ukraine using MODIS data. Remote Sensing Environ. 2010; 114: 1312–1323. https://doi.org/10.1016/j.rse.2010.01.010
2. Kogan F, Kussul N, Adamenko T, Skakun S, Kravchenko O, Kryvobok O, et al. Winter wheat yield forecasting in Ukraine based on Earth observation, meteorological data and biophysical models. Inter J Appl Earth Obser Geoinformat. 2013; 23: 192–203. https://doi.org/10.1016/j.jag.2013.01.002
3. Tadesse W, Solh M, Braun H-J, Oweis T, Baum M. Approaches and strategies for sustainable wheat production: Tools and Guidelines; ICARDA: Beirut, Lebanon 2016; ISBN 92-9127-490-9.
4. Tissue culture techniques for horticultural crops. 1st ed. New York, London: Chapman and Hall; 1989.
5. FAOSTAT. Food and agriculture data. Food and Agriculture Organization of the United Nations. c2017 –[cited 2018 Nov 19]. Available from: http://www.fao.org/faostat/en/#data/RP.
6. Paradikovic N, Vinkovic T, Vrcek IV,Tkalec M. Natural biostimulants reduce the incidence of BER in sweet yellow pepper plants (*Capsicum annuum* L.). Agric Food Sci. 2013; 22: 307–317. https://doi.org/10.23986/afsci.7354
7. Maksimov IV, Yarullina LG, Surina OB. The effect of exogenous phytohormones on resistance of wheat calluses to *Tilletia caries* (D.C.) Tul. & C. Tul. Amer J Plant Sci. 2014; 5: 1745–1754. https://doi.org/10.4236/ajps.2014.512189

8. Tsygankova V, Shysha E, Andrusevich Y, Galkin A, Iutynsk G, Yemets A, et al. 2016. Using of new microbial biostimulants for obtaining in vitro new lines of *Triticum aestivum* L. cells resistant to nematode *H. avenae*. Eur J Biotechnol Biosci. 2016; 4: 41–53.
9. Floryszak-Wieczorek J, Arasimowicz-Jelonek M, Abramowski D. BABA-primed defence responses to *Phytophthora infestans* in the next vegetative progeny of potato. Front Plant Sci. 2015; 6: 844. https://doi.org/10.3389/fpls.2015.00844 PMID: 26528308
10. Schenk ST, Schikora A. AHL-priming functions via oxylipin and salicylic acid. Front Plant Sci. 2015; 5: 784. https://doi.org/10.3389/fpls.2014.00784 PMID: 25642235
11. Schikora A, Schenk ST, Hartmann A. Beneficial effects of bacteria-plant communication based on quorum sensing molecules of the N-acyl homoserine lactone group. Plant Mol Biol. 2016; 90: 605–612. https://doi.org/10.1007/s11103-016-0457-8 PMID: 26898296
12. Moshynets OV, Kosakivska IV. Phytosphere ecology: Plant-microbial interactions. Part 1. Structure functional characteristic of rhizo-, endo- and phytosphere. Bull Nat Kharkov Agrarian Univ. 2010; 2: 19–36.
13. Moshynets OV, Kosakivska IV. Phytosphere ecology: Plant-microbial interactions. Part 2. Phytosphere as a niche for plant-microbial interactions. Functional microbial activity and its influence of plants. Bull Nat Kharkov Agrarian Univ. 2010; 3: 6–22.
14. Klein I, von Rad U, Durner J. Homoserine lactones: do plants really listen to bacterial talk? Plants Signaling & Behavior. 2009; 4: 50–51. https://doi.org/10.4161/psb.4.1.7300
15. Papenfort K, Bassler BL. Quorum sensing signal–response systems in Gram-negative bacteria. Nat Rev Microbiol. 2016; 14: 576–588. https://doi.org/10.1038/nrmicro.2016.89 PMID: 27510864
16. Whiteley M, Diggle SP, Greenberg EP. Progress in and promise of bacterial quorum sensing research. Nature. 2017; 551: 313–320. https://doi.org/10.1038/nature24624 PMID: 29144467
17. Mathesius U, Mulders S, Gao M, Teplitski M, Caetano-Anolles G, Rolfe BG, et al. Extensive and specific responses of a eukaryote to bacterial quorum-sensing signals. Proc Natl Acad Sci USA. 2003; 100: 1444–1449. https://doi.org/10.1073/pnas.262672599 PMID: 12511600
18. Schuhegger R, Ihring A, Gantner S, Bahnweg G, Knappe C, Vog G, et al. Induction of systemic resistance in tomato by N-acyl-L-homoserine lactone-producing rhizosphere bacteria. Plant Cell Environ. 2006; 29: 909–918. https://doi.org/10.1111/j.1365-3040.2005.01471.x PMID: 17087474
19. Licciardello G, Bertani I, Steindler L, Bella P, Venturi V, Catara V. *Pseudomonas corrugata* contains a conserved N-acyl homoserine lactone quorum sensing system; its role in tomato pathogenicity and tobacco hypersensitivity response. FEMS Microbiol Ecol. 2007; 61: 222–234. https://doi.org/10.1111/j.1574-6941.2007.00338.x PMID: 17537174
20. Natelson S, Natelson EA. Preparation of D-, DL-, and L-homoserine lactone from methionine. Microchemical J. 1989; 40: 226–232. https://doi.org/10.1016/0026-265X(89)90074-X
21. Chhabra SR, Harty C, Hooi DSW, Daykin M, Williams P, Telford G, et al. Synthetic analogues of the bacterial signal (quorum sensing) molecule N-(3-Oxododecanoyl)-l-homoserine lactone as immune modulators. J Med Chem. 2003; 46: 97–104. https://doi.org/10.1021/jm020909n PMID: 12502363
22. Torres KC. Tissue culture techniques for horticultural crops. 1st ed. New York, London: Chapman and Hall; 1989.
23. Wellburn AR. The spectral determination of chlorophyll a and chlorophyll b, as well as total carotenoids, using various solvents with spectrophotometers of different resolution. J Plant Physiol. 1994; 144: 307–313. https://doi.org/10.1016/S0176-1617(11)81192-2
24. Egorov NS. Guide to practical training in microbiology: textbook. 3rd ed. Moscow: Moscow State University Press; 1995.
25. Stella M, Suhaimi M. Selection of suitable growth medium for free-living diazotrophs isolated from compost. J Trop Agric Food Sci. 2010; 38: 211–219.
26. Rosenblatt JE, Fallon A, Finegold SM. Comparison of methods for isolation of anaerobic bacteria from clinical specimens. Appl Microbiol. 1973; 25: 77–85. PMID: 4568893
27. Woomer PL. Most probable number counts. In: Weaver RW, Angle S, Bottomley P, Bezdicek D, Smith S, Tabatabai A, Wollum A, editors. Methods of Soil Analysis. Part 2. Microbiological and Biochemical Properties. Madison: Soil Science Society of America; 1994. pp. 59–79.
28. Dehority BA, Tirabasso PA, Grifo AP. Most-probable-number procedures for enumerating ruminal bacteria, including the simultaneous estimation of total and cellulolytic numbers in one medium. App Environ Microbiol. 1989; 55: 2789–2792.
29. Sjofjan O, Ardyati T. Extracellular amylase activity of amylolytic bacteria isolated from quail's (*Coturnix japonica*) intestinal tract in corn flour medium. Inter J Poultry Sci. 2011; 10: 411–415. https://doi.org/10.3923/ijps.2011.411.415

30. Ortíz-Castro R, Martínez-Trujillo M, López-Bucio J. N-acyl-L-homoserine lactones: a class of bacterial quorum-sensing signals alter post-embryonic root development in *Arabidopsis thaliana*. Plant Cell Environ. 2008; 31: 1497–1509. https://doi.org/10.1111/j.1365-3040.2008.01863.x PMID: 18657054

31. Jin G, Liu F, Ma H, Hao S, Zhao Q, Bian Z, et al. Two G-protein-coupled-receptor candidates, Cand2 and Cand7, are involved in Arabidopsis root growth mediated by the bacterial quorum-sensing signals N-acyl-homoserine lactones. Biochem Biophys Res Commun. 2012; 41: 991–995. https://doi.org/10.1016/j.bbrc.2011.12.066

32. Liu F, Bian Z, Jia Z, Zhao Q, Song S. The GCR1 and GPA1 participate in promotion of Arabidopsis primary root elongation induced by N-acyl-homoserine lactones, the bacterial quorum-sensing signals. Mol Plant Microbe Interact. 2012; 25: 677–683. https://doi.org/10.1094/MPMI-10-11-0274 PMID: 22250582

33. Palmer AG, Senechal AC, Mukherjee A, Ané JM, Blackwell HE. Plant responses to bacterial N-acyl L-homoserine lactones are dependent on enzymatic degradation to L-homoserine. ACS Chem Biol. 2014; 9: 1834–1845. https://doi.org/10.1021/cb500191a PMID: 24918118

34. Ding L, Cao J, Duan Y, Li J, Yang Y, Yang G, et al. 2016. Proteomic and physiological responses of *Arabidopsis thaliana* exposed to salinity stress and N-acyl-homoserine lactone. Physiologia Plantarum 2016; 158: 414–434. https://doi.org/10.1111/ppl.12476 PMID: 27265884

35. Khalid A, Arshad M, Zahir ZA. Screening plant growth-promoting rhizobacteria for improving growth and yield of wheat. J Appl Microbiol. 2004; 96: 473–480. https://doi.org/10.1046/j.1365-2672.2003.02161.x PMID: 14962127

36. Kizilkaya R. Yield response and nitrogen concentrations of spring wheat (*Triticum aestivum*) inoculated with *Azotobacter chroococcum* strains. Ecol Eng. 2008; 33: 150–156.

37. Shaharoona B, Naveed M, Arshad M, Zahir ZA. 2008. Fertilizer-dependent efficiency of Pseudomonads for improving growth, yield, and nutrient use efficiency of wheat, *Triticum aestivum* L. Appl Microbiol Biotechnol. 2008; 79: 147–155. https://doi.org/10.1007/s00253-008-1419-0 PMID: 18340443

38. Pierson EA, Wood DW, Cannon JA, Blachere FM, Person LS. Interpopulation signaling via N-acyl-homoserine lactones among bacteria in the wheat rhizosphere. Mol Plant Microb Inter. 1998; 11: 1078–1084. https://doi.org/10.1094/MPMI.1998.11.11.1078

39. Laue BE, Jiang Y, Chhabra SR, Jacob S, Stewart GS, Hardman A, et al. The biocontrol strain *Pseudomonas fluorescens* F113 produces the Rhizobium small bacteriocin, N-(3-hydroxy-7-cis-tetradecenoyl) homoserine lactone, via HdtS, a putative novel N-acylhomoserine lactone synthase. Microbiol. 2000; 146: 2469–2480. https://doi.org/10.1099/00221287-146-10-2469 PMID: 11021923

40. Elasri M, Delorme S, Lemanceau P, Stewart G, Laue B, Glickmann E, et al. Acyl-homoserine lactone production is more common among plant-associated *Pseudomonas* spp. than among soilborne *Pseudomonas*. Appl Environ Microbiol. 2001; 67: 1198–1209. https://doi.org/10.1128/AEM.67.3.1198-1209.2001 PMID: 11229911

41. Miao C, Liu F, Zhao Q, Jia Z, Song S. A proteomic analysis of *Arabidopsis thaliana* seedling responses to 3-oxo-octanoyl-homoserine lactone, a bacterial quorum-sensing signal. Biochem Biophys Res Commun. 2012; 427: 293–298. https://doi.org/10.1016/j.bbrc.2012.09.044 PMID: 22995300

42. Cheng F, Ma A, Zhuang G, Fray RG. Exogenous N-acyl-homoserine lactones enhance the expression of flagella of *Pseudomonas syringae* and activate defence responses in plants. Mol Plant Pathol. 2018; 19: 104–115. https://doi.org/10.1111/mpp.12502 PMID: 27756102

43. Schenk ST, Hernandez-Reyes C, Samans B, Stein E, Neumann C, Schikora M, et al. N-Acyl-homoserine lactone primes plants for cell wall reinforcement and induces resistance to bacterial pathogens via the salicylic acid/oxylipin pathway. Plant Cell 2014; 26: 2708–2723. https://doi.org/10.1105/tpc.114.126763 PMID: 24963057

44. Brodführer U. Der Einfluss einer abgestuften Dosierung von ultravioletter Sonnenstrahlung auf das Wachstum der Pflanzen. Planta 1955; 45: 1–56.

45. Potters G, Pasternak TP, Guisez Y, Palme KJ, Jansen MA. Stress-induced morphogenic responses: growing out of trouble? Trends Plant Sci. 2007; 12:, 98–105. https://doi.org/10.1016/j.tplants.2007.01.004 PMID: 17287141

46. Jansen MA, Klem K, Robson TM, Urban O. 5. UV-B-induced Morphological Changes–an Enigma. In: Jordan BR, editor. UV-B Radiation and Plant Life: Molecular Biology to Ecology. Wallingford: CABI; 2017. pp. 58–71. https://doi.org/10.1016/j.jcs.2013.12.001

47. Naylor REL. The effect of parent plant nutrition on seed size, viability and vigour and on germination of wheat and triticale at different temperatures. Ann Appl Biol. 1993; 123: 379–390. https://doi.org/10.1111/j.1744-7348.1993.tb04100.x

48. Guberac V, Martincic J, Banaj D. Influence of cereal seed size on shoot and root length. Die Bodenkultur. 1999; 50: 39–41.

49. Gutzat R, Scheid OM. Epigenetic responses to stress: triple defense? Curr Opin Plant Biol. 2012; 15: 568–573. https://doi.org/10.1016/j.pbi.2012.08.007 PMID: 22960026

50. Lämke J, Bäurle I. Epigenetic and chromatin-based mechanisms in environmental stress adaptation and stress memory in plants. Genome Biol. 2017; 18: 124. https://doi.org/10.1186/s13059-017-1263-6 PMID: 28655328

51. Kumar S. Epigenomics of plant responses to environmental stress. Epigenomes. 2018; 2: 6. https://doi.org/10.3390/epigenomes2010006

52. Lugtenberg B, Kamilova F. Plant-growth-promoting rhizobacteria. Annu Rev Microbiol. 2009; 63: 541–556. https://doi.org/10.1146/annurev.micro.62.081307.162918 PMID: 19575558

53. Lareen A, Burton F, Schäfer P. Plant root-microbe communication in shaping root microbiomes. Plant Mol Biol. 2016; 90: 575–587. https://doi.org/10.1007/s11103-015-0417-8 PMID: 26729479

54. Jones JDG, Dangl JL. The plant immune system. Nature. 2006; 444: 323–329. https://doi.org/10.1038/nature05286 PMID: 17108957

55. Hawkesford MJ. Reducing the reliance on nitrogen fertilizer for wheat production. J Cereal Sci. 2014; 59: 276–283. https://doi.org/10.1016/j.jcs.2013.12.001 PMID: 24882935

56. Macholdt J, Honermeier B. Yield stability in winter wheat production: a survey on German farmers' and advisors' views. Agronomy. 2017; 7: 45. https://doi.org/10.3390/agronomy7030045

57. Figueroa M, Hammond-Kosack KE, Solomon PS. A review of wheat diseases—a field perspective. Mol Plant Pathol. 2018; 19: 1523–1536. https://doi.org/10.1111/mpp.12618 PMID: 29045052

58. Wiik L, Rosenqvist H. The economics of fungicide use in winter wheat in southern Sweden. Crop Protection. 2010; 29: 11–19. https://doi.org/10.1016/j.cropro.2009.09.008

59. Wegulo SN, Zwingan MV, Breathnach JA, Baenzinger PS. Economic returns from fungicide application to control foliar fungal diseases in winter wheat. Crop Protection. 2011; 30: 685–692. https://doi.org/10.1016/j.cropro.2011.02.002

60. Chakraborty S. Migrate or evolve: options for plant pathogens under climate change. Global Change Biol. 2013; 19: 1985–2000. https://doi.org/10.1111/gcb.12205 PMID: 23554235

61. Bebber DP, Holmes T, Gurr SJ. The global spread of crop pests and pathogens. Global Ecol Biogeogr. 2014; 23: 1398–1407. https://doi.org/10.1111/geb.12214

Анотація: *Відомо, що кілька модельних рослин реагують на молекули бактеріального ПК, зокрема, зміненим ростом коренів і експресією генів, а також розвитком індукованої стійкість до патогенних захворювань рослин. Сполуки ПК можуть представляти нові активні речовини, які можна застосовувати як праймери для насіння рослин для підвищення стійкості зернових культур до хвороботворних мікроорганізмів та абіотичного стресу та підвищення врожайності. В нашій роботі було досліджено чи ГГЛ може мати вплив на проростання насіння пшениці озимої (*Triticum aestivum *L.), розвиток рослин та їхню продуктивність на прикладі двох українських сортів пшениці озимої Володарка та Ятрань 60. Досліди проростання in vitro показали, що праймування насіння ГГЛ мало невеликий, але значний позитивний вплив на рівень схожості (1,2 х збільшення, $p < 0,0001$), розвиток колеоптиля та корінця (1,4-кратне збільшення, $p < 0,0001$). В польових дослідженнях протягом двох вегетаційних періодів (2015–16 та 2016–17) також продемонстровано значні покращення біомаси на стадії кущіння (збільшення в 1,4 рази, $p < 0,0001$), а також покращення структури посівів. Зокрема, врожайність зерна (збільшення в 1,4–1,5 рази, $p < 0,0007$) та якість (1,3-кратне збільшення хорошого зерна, $p < 0,0001$). Ці польові результати показують, що бактеріальні АГЛ, такі як ГГЛ, можна використовувати для покращення врожаю зернових культур.*

Висновки

Отримані в роботі результати є суттєвим вкладом в розуміння структури і функціонування деяких грам-негативних бактерій, зокрема умовно-патогенних і патогенних штамів. Велику увагу приділено патогенетичній ролі біоплівки грам-негативних бактерій. Зокрема, досліджено феноменологію утворення біоплівок при пародонтиті та при інфекційних процесах, опосередкованих *K. pneumoniae.* Досліджено біоплівку як нову фармакологічну мішень при лікуванні інфекцій, спричинених грам-негативними бактеріями. Окремо розглядається роль біоплівки у підтримці пулу генів резистентності в екологічній ніші, можлива роль різноманітних біоцидів в підтримці такого локального резистому та розглядається можливість створення нових матеріалів із підвищеною стійкістю то біообрастання біоплівками. Також розглядається можливість створення нових агробіотехнологій праймування продуктивних рослин хімічними аналогами медіаторів бактеріального почуття кворуму.

1. Целюлоза є важливим структурним компонентом матриксу біоплівок багатьох *Proteobacteria*, зокрема, *P. fluorescens* SBW25, *P. syringae, B. avium*. Для всіх цих бактерій притаманна однотипність оперону продукції целюлози bcs. Для *P. fluorescens* SBW25 целюлоза є головним структурним полімером біоплівки в той час як у *B. avium* целюлоза присутня у невеликій кількості і не впливає на міцність біоплівки. Для *P. fluorescens* SBW25 адаптативна колонізація зони розподілу фаз (менісковий ріст) призводить до утворення і домінування мутантного штаму-суперпродуценту целюлозної біоплівки Wrinkly Spreader. На молекулярному рівні випадкові мутації шляхом відбору призводять до селекції мутантів, що накопичують вторинний клітинних месенджер c-di-GMP, який посилює синтез целюлози і утворює міцну біоплівку а зоні меніску. Це у свою чергу дозволяє штаму краще конкурувати та перехоплювати більше кисню.

2. Іншим важливим компонентом матриксу біоплівки грамнегативних бактерій є амілоїдні фібрили. За допомогою власного нового високочутливого амілоїд-специфічного барвника AmyGreen було візуалізовано амілоїдні компонентів екзоклітинного матриксу в біоплівках *E. coli, K. pneumoniae, P. aeruginosa, P. fluorescens* SBW25, *B. avium* і *S. aureus.*

3. еДНК – ще один важливий компонент матриксу різноманітних моно і полімікробних біоплівок. Продемонстровано, що еДНК може мати значення в утворенні біоплівкового матриксу *P. fluorescens* SBW25 WS особливо на первинних стадіях утворення біоплівки

4. Почуття кворуму є прикладом гормональної надклітинної регуляції, внаслідок якої мікробна популяція регулює роботу геномів та координує свої фізіологічні процеси, зокрема, і утворення біоплівки.

5. Біоплівки чинників інфекційних процесів завжди є активними учасниками патогенезу. Взаємодія імунної системи хазяїна із парадонтопагоненною флорою при пародонтиті призводить до посилення біоплівок, зокрема, продемонстровано, що еДНК хазяїна, джерелом якої є імунокомпетентні клітини, вбудовується в біоплівки парадонтопатогенів та становить приблизно 70% від загальної еДНК біопілівки. Таким чином, еДНК активованих імунокомпетентних клітин господаря може бути основним фактором персистенції бактерій і розвитку патологічного запалення при пародонтиті.

6. Розуміння патогенетичної ролі біоплівок інфекційних ізолятів відкриває нові фармакологічні можливості для створення альтернативних терапевтичних протоколів, заснованих на антибіоплівковій терапії. Продемонстровано, що азитроміцин пригнічує утворення біоплівок *K. pneumoniae*. Комбінація азитроміцину із таргетним антибіотиком підвищує ефективність останнього, що продемонстровано при лікуванні пацієнта із множинною генералізованою інфекцією, викликаним асоціацією повністю резистентних грам-негативних бактерій. Отримані результати підкреслюють необхідність пошуку нових ефективних протимікробних терапевтичних підходів як альтернативні стратегії лікування інфекцій із високою резистентністю.

7. Зворотною стороною використання неефективних режимів терапії є стимуляція утворення біоплівки інфекційним штамом. Показано, що специфічні інгібітори із антибактеріальними властивостями, зокрема, експериментальна протистафілококова сполука №5 стимулювала розвиток біоплівки *K. pneumoniae* ATCC 10031.

8. Досліджено роль біоплівок як джерела генів резистому у госпітальному середовищі при обороці біоплівок різноманітними біоцидами, що використовуються у практиці. З'ясовано, що всі біоциди, окрім PHMG-Cl, сприяли вивільненню еДНК.

9. Нові сконструйовані матеріали, зокрема, поліамід 11 із додаванням PHMG-NS, фарба PP-115 із додаванням PyrC 12-DBS і мікроструктуровані лазером металеві поверхні продемонстрували значні анти-біоплівкові та для деяких матеріалів – ДНК-інактивуючі дії для вирішенні проблем персистування генів стійкості до антибіотиків у госпітальному середовищі;

10. Бактеріальні гормони сприймаються сенсорними системами макроорганізмів, зокрема, рослинами, як стресорні сигнали, що призводить до активації імунної відповіді, що може бути використано для створення нових екологічних агробіотехнологій, як це демонструється на прикладі двох українських сортів озимої пшениці, які суттєво підвищили свою врожайність в наслідок праймування бактеріальної сигнальною молекулою C6-HSL.

Список літературних джерел

1. Costerton JW, Lewandowski Z, DeBeer D, Caldwell D, Korber D, James G. Biofilms, the customized microniche. *J Bacteriol*. 1994;176:2137–2142.
2. Costerton JW, Lewandowski Z, Caldwell D, Korber D, Lappin-Scott HM. Microbial biofilms. *Annu Rev Microbiol*. 1995;49:711–745.
3. Buyck JM, Plésiat P, Traore H, Vanderbist F, Tulkens PM, Van Bambeke F. Increased susceptibility of *Pseudomonas aeruginosa* to macrolides and ketolides in eukaryotic cell culture media and biological fluids due to decreased expression of oprM and increased outer-membrane permeability. *Clin Infect Dis*. 2012;55(4):534–542.
4. Moshynets OV, Baranovskyi TP, Cameron S, Iungin OS, Pokholenko I, Jerdan R, Kamyshnyi A, Krikunov AA, Potochilova VV, Rudnieva KL, Spiers AJ. Azithromycin possesses biofilm–inhibitory activity and potentiates non-bactericidal colistin methanesulfonate (CMS) and polymyxin B against *Klebsiella pneumoniae*. *PLoS ONE*. 2022;17(7):e0270983.
5. Shenkutie AM, Zhang J, Yao M, Asrat D, Chow FWN, Leung PHM. Effects of sub-minimum inhibitory concentrations of imipenem and colistin on expression of biofilm-specific antibiotic resistance and virulence genes in *Acinetobacter baumannii* Sequence Type 1894. *Int J Mol Sci*. 2022;23:12705.
6. Müsken M, Klimmek K, Sauer-Heilborn A, et al. Towards individualized diagnostics of biofilm-associated infections: a case study. *npj Biofilms Microbiomes*. 2017;3:22.
7. Thöming JG, Häussler S. *Pseudomonas aeruginosa* Is More Tolerant Under Biofilm Than Under Planktonic Growth Conditions: A Multi-Isolate Survey. *Front Cell Infect Microbiol.* 2022 Feb 28;12:851784.
8. Williams P, Cámara M. Quorum sensing and environmental adaptation in *Pseudomonas aeruginosa*: a tale of regulatory networks and multifunctional signal molecules. *Curr Opin Microbiol.* 2009;12(2):182-191.
9. Galloway WR, Hodgkinson JT, Bowden SD, Welch M, Spring DR. Quorum sensing in Gram-negative bacteria: small-molecule modulation of AHL and AI-2 quorum sensing pathways. *Chem Rev*. 2011;111(1):28-67.
10. Garg N, Manchanda G, Kumar A. Bacterial quorum sensing: circuits and applications. *Antonie Van Leeuwenhoek*. 2014;105(2):289-305.
11. Solano C, García B, Valle J, Berasain C, Ghigo J.-M, Gamazo C, Lasa I. Genetic analysis of *Salmonella enteritidis* biofilm formation: critical role of cellulose. *Mol Microbiol* 2002;43(3):793-808.

12. Zogaj X, Bokranz W, Nimtz M, Römling U. Production of cellulose and curli fimbriae by members of the family *Enterobacteriaceae* isolated from the human gastrointestinal tract. *Infect Immun*. 2003;71:4151-4158.
13. Ude S, Arnold DL, Moon CD, Timms-Wilson T, Spiers AJ. Biofilm formation and cellulose expression among diverse environmental *Pseudomonas* isolates. *Environ Microbiol* 2006;8(11):1997-2011.
14. Okshevsky M, Meyer RL. The role of extracellular DNA in the establishment, maintenance and perpetuation of bacterial biofilms. *Crit Rev Microbiol*. 2015;41:341–352.
15. Jakubovics NS, Shields RC, Rajarajan N, Burges JG. Life after death: The critical role of extracellular DNA in microbial biofilms. *Lett Appl Microbiol*. 2013;57(6):467–475.
16. Ibáñez de Aldecoa AL, Zafra O, González-Pastor JE. Mechanisms and regulation of extracellular DNA release and its biological roles in microbial communities. *Front Microbiol*. 2017;8:1390.
17. Campoccia D, Montanaro L, Aricola CR. Extracellular DNA (eDNA): A major ubiquitous element of the bacterial biofilm architecture. *Int J Mol Sci*. 2021;22(17):9100.
18. Vandana SD. Genetic regulation, biosynthesis and applications of extracellular polysaccharides of the biofilm matrix of bacteria. *Carbohydr. Polym.* 2022, 291, 119536.
19. Coenye T. Biofilm antimicrobial susceptibility testing: where are we and where could we be going? *Clin Microbiol Rev*. 2023 Dec 20;36(4):e0002423.
20. Moshynets OV, Spiers AJ. Viewing biofilms within the larger context of bacterial aggregations. In: Dhanasekaran D, Thajuddin N, editors. *Microbial Biofilms–Importance and Applications*. London, UK: InTechOpen; 2016. p. 3–22.
21. Moshynets O, Boretska M, Spiers AJ. From Winogradsky's column to contemporary research using bacterial microcosms. In: Harris CC, editor. *Microcosms: Ecology, Biological Implications and Environmental Impact*. Nova Publisher; 2013. p. 1-27.
22. Hobley L, Harkins C, MacPhee CE, Stanley-Wall NR. Giving structure to the biofilm matrix: an overview of individual strategies and emerging common themes. *FEMS Microbiol Rev*. 2015;39(5):649–669.
23. Payne DE, Boles BR. Emerging interactions between matrix components during biofilm development. *Curr Genet*. 2016;62:137–141.
24. Ruhal R, Kataria R. Biofilm patterns in gram-positive and gram-negative bacteria. *Microbiol Res.* 2021; 251:126829.
25. Chen KM, Chiang MK, Wang M, Ho HC, Lu MC, Lai YC. The role of pgaC in *Klebsiella pneumoniae* virulence and biofilm formation. *Microb Pathog*. 2014;77:89-99.

26. Singh JK, Adams FG, Brown MH. Diversity and function of capsular polysaccharide in *Acinetobacter baumannii*. *Front Microbiol*. 2019;9:3301.
27. Colvin KM, Irie Y, Tart CS, Urbano R, Whitney JC, Ryder C. The Pel and Psl polysaccharides provide *Pseudomonas aeruginosa* structural redundancy within the biofilm matrix. *Environ Microbiol*. 2012;14(7):1913-1928.
28. Irie Y, Borlee BR, O'Connor JR, Hill PJ, Harwood CS, Wozniak DJ. Self-produced exopolysaccharide is a signal that stimulates biofilm formation in *Pseudomonas aeruginosa*. *Proc Natl Acad Sci U S A*. 2012;109(51):20632–20637.
29. Singh JK, Adams FG, Brown MH. Diversity and function of capsular polysaccharide in *Acinetobacter baumannii*. *Front Microbiol*. 2019;9:3301.
30. Zogaj X, Bokranz W, Nimtz M, Römling U. Production of cellulose and curli fimbriae by members of the family Enterobacteriaceae isolated from the human gastrointestinal tract. *Infect Immun*. 2003 Jul;71(7):4151-8.
31. Goh HMS, Beatson SA, Totsika M, Moriel DG, Phan MD, Szubert J. Molecular analysis of the *Acinetobacter baumannii* biofilm-associated protein. *Appl Environ Microbiol*. 2013;79(20):6535-6543.
32. Pakharukova N, Tuittila M, Paavilainen S, Malmi H, Parilova O, Teneberg S. Structural basis for *Acinetobacter baumannii* biofilm formation. *Proc Natl Acad Sci U S A*. 2018;115:5558-5563.
33. Javed I, Zhang Z, Adamcik J, Andrikopoulos N, Li Y, Otzen DE. Accelerated amyloid beta pathogenesis by bacterial amyloid FapC. *Adv Sci*. 2020;7(24):2001299.
34. Kim SM, Lee HW, Choi YW, Kim SH, Lee JC, Lee YC. Involvement of curli fimbriae in the biofilm formation of *Enterobacter cloacae*. *J Microbiol*. 2012;50(2):175-178.
35. Qian W, Fu Y, Liu M, Zhang J, Wang W. Mechanisms of action of luteolin against single- and dual-species of *Escherichia coli* and *Enterobacter cloacae* and its antibiofilm activities. *Appl Biochem Biotechnol*. 2021;193:1397-1414.
36. Rice KC, Mann EE, Endres JL, Weiss EC, Cassat JE, Smeltzer MS. The cidA murein hydrolase regulator contributes to DNA release and biofilm development in *Staphylococcus aureus*. *Proc Natl Acad Sci U S A*. 2007;104:8113-8118.
37. Paganelli FL, de Been M, Braat JC, Hoogenboezem T, Vink C, Bayjanov J. Distinct SagA from hospital-associated Clade A1 *Enterococcus faecium* strains contributes to biofilm formation. *Appl Environ Microbiol*. 2015;81:6873-6882.
38. Allesen-Holm M, Barken KB, Yang L, Klausen M, Webb JS, Kjelleberg S. A characterization of DNA release in *Pseudomonas aeruginosa* cultures and biofilms. *Mol Microbiol*. 2006;59(4):1114-1128.

39. Mulcahy H, Charron-Mazenod L, Lewenza S. Extracellular DNA chelates cations and induces antibiotic resistance in *Pseudomonas aeruginosa* biofilms. *PLoS Pathog*. 2008;4:e1000213.
40. Sahu PK, Iyer PS, Oak AM, Pardesi KR, Chopade BA. Characterization of eDNA from the clinical strain *Acinetobacter baumannii* AIIMS 7 and its role in biofilm formation. *Sci World J*. 2012;2012: e973436.
41. Desai S, Sanghrajka K, Gajjar D. High adhesion and increased cell death contribute to strong biofilm formation in *Klebsiella pneumoniae*. *Pathogens*. 2019;8(4):277.
42. Brown AJ. XLIII. On an acetic ferment which forms cellulose. *J Chem Soc, Trans*. 1886;49:432-439.
43. Ross P, Mayer R, Benziman M. Cellulose biosynthesis and function in bacteria. *Microbiol Rev* 1991;55(1):35-58.
44. Moshynets OV, Pokholenko I, Iungin O, Potters G, Spiers AJ. eDNA, Amyloid fibers and membrane vesicles identified in *Pseudomonas fluorescens* SBW25 biofilms. *Int J Mol Sci*. 2022;23:15096.
45. Spiers AJ, Kahn SG, Bohannon J, Travisano M, Rainey PB. Adaptive divergence in experimental populations of *Pseudomonas fluorescens*. I. Genetic and phenotypic bases of Wrinkly Spreader fitness. *Genetics* 2002;161:33-46.
46. Rainey PB, Bailey MJ. Physical map of the *Pseudomonas fluorescens* SBW25 chromosome. *Mol Microbiol* 1996;19(3):521-533.
47. Rainey PB, Travisano M. Adaptive radiation in a heterogeneous environment. *Nature* 1998;394:69-72.
48. Silby MW, Cerdeño-Tárraga AM, Vernikos G, Giddens SR, Jackson R, Preston G, Zhang X-X, Godfrey S, Spiers AJ, Harris S, Challis GL, Morningstar A, Harris D, Seeger K, Murphy L, Rutter S, Squares R, Quail MA, Saunders E, Anderson I, Mavromat K, Brettin TS, Bentley S. Thomas CM, Parkhill J, Levy SB, Rainey PB, Thomson NR. Genomic and functional analyses of diversity and plant interactions of *Pseudomonas fluorescens*. *Genome Biology* 2009;10 R51.
49. Peix A, Ramírez-Bahena M-H, Velázquez E. Historical evolution and current status of the taxonomy of genus *Pseudomonas*. *Infect Genet Evol* 2009;9:1132-1147.
50. Silby MW, Winstanley C, Godfrey SAC, Levy SB, Jackson RW. *Pseudomonas* genomes: diverse and adaptable. *FEMS Microbiol Rev* 2011;35(4):652-680.
51. Spiers AJ, Deeni YY, Folorunso AO, Koza A, Moshynets O, Zawadzki K. Cellulose expression in *Pseudomonas fluorescens* SBW25 and other environmental pseudomonads. In: Van De Ven TGM, Godbout L, editors. *Cellulose*. Rijeka, Croatia: InTech; 2013.

52. Hinz KH, Glunder G. Occurrence of *Bordetella avium* sp. nov. and *Bordetella bronchiseptica* in birds. *Berl Munch Tierarztl Wochenschr*. 1985;98(10):369-373.
53. Raffel TR, Register KB, Marks SA, Temple L. Prevalence of *Bordetella avium* infection in selected wild and domesticated birds in the eastern USA. *J Wildl Dis* 2002;38:40e6.
54. Grespan A, Camera O, Knöbl T, Gomes CR, Felizardo MR, Ferreira TSP, et al. Virulence and molecular aspects of *Bordetella avium* isolated from cockatiel chicks (*Nymphicus hollandicus*) in Brazil. *Vet Microbiol*. 2012;160(3-4):530-534.
55. Spilker T, Liwienski AA, LiPuma JJ. Identification of *Bordetella* spp. in respiratory specimens from individuals with cystic fibrosis. *Clin Microb Infect* 2008;14:504e6.
56. Harrington AT, Castellanos JA, Ziedalski TM, Clarridge JE, Cookson BT. Isolation of *Bordetella avium* and novel *Bordetella* strain from patients with respiratory disease. *Emerg Infect Dis*. 2009;15(1):72-74.
57. Bos AC, Beemsterboer P, Wolfs TFW, Versteegh FGA, Arets HGM. Bordetella species in children with cystic fibrosis: what do we know? The role in acute exacerbations and chronic course. *J Cyst Fibros*. 2011;10(4):307-12.
58. Sloan GP, Love CF, Sukumar N, Mishra M, Deora R. The *Bordetella* Bps polysaccharide is critical for biofilm development in the mouse respiratory tract. *J Bacteriol* 2007;189:8270e82.
59. Conover MS, Sloan GP, Love CF, Sukumar N, Deora R. The Bps polysaccharide of *Bordetella pertussis* promotes colonization and biofilm formation in the nose by functioning as an adhesion. *Mol Microbiol*. 2010;77(6):1439-1455.
60. Gentry-Weeks CR, Cookson BT, Goldman WE, Rimler RB, Porter SB, Curtiss R. Dermonecrotic toxin and tracheal cytotoxin, putative virulence factors of *Bordetella avium*. *Infect Immunol*. 1988;56(7):1698-1707.
61. Temple LA, Weiss AA, Walker KE, Barnes HJ, Christensen VL, Miyamoto DM, et al. *Bordetella avium* virulence measured in vivo and in vitro. *Infect Immun* 1998;66:5244e51.
62. Sebaihia M, Preston A, Maskell DJ, Kuzmiak H, Connell TD, King ND, et al. Comparison of the genome sequence of the poultry pathogen *Bordetella avium* with those of *B. bronchiseptica*, *B. pertussis*, and *B. parapertussis* reveals extensive diversity in surface structures associated with host interaction. *J Bacteriol* 2006;188:6002e15.
63. Romling U. Molecular biology of cellulose production in bacteria. *Res Microbiol* 2002;153:205e12.
64. Romling U, Galperin MY. Bacterial cellulose biosynthesis: diversity of operons, subunits, products, and functions. *Trends Microbiol* 2015;23:545e57.

65. Gal M, Preston GM, Massey RC, Spiers AJ, Rainey PB. Genes encoding a cellulosic polymer contribute toward the ecological success of *Pseudomonas fluorescens* SBW25 on plant surfaces. *Mol Ecol*. 2003;12(10):3109–3121.
66. White AP, Gibson DL, Kim W, Kay WW, Surette MG. Thin aggregative fimbriae and cellulose enhance long-term survival and persistence of *Salmonella*. *J Bacteriol* 2006;188:3219e27. Paganelli
67. Gualdi L, Tagliabue L, Bertagnoli S, Ierano T, De Castro C, Landini P. Cellulose modulates biofilm formation by counteracting curli-mediated colonization of solid surfaces in *Escherichia coli*. *Microbiology*. 2008;154(7):2017–2024.
68. Mishra M, Parise G, Jackson KD, Wozniak DJ, Deora R. The BvgAS signal transduction system regulates biofilm development in *Bordetella*. *J Bacteriol*. 2005;187:1474–1484.
69. McLaughlin K, Folorunso AO, Deeni YY, Foster D, Gorbatiuk O, Hapca SM, Immoor C, Koza A, Mohammed IU, Moshynets O, Rogalsky S, Zawadzki K, Spiers AJ. Biofilm formation and cellulose expression by *Bordetella avium* 197N, the causative agent of bordetellosis in birds and an opportunistic respiratory pathogen in humans. *Res Microbiol*. 2017 Jun;168(5):419-430.
70. Paganelli FL, de Been M, Braat JC, Hoogenboezem T, Vink C, Bayjanov J. Distinct SagA from hospital-associated Clade A1 *Enterococcus faecium* strains contributes to biofilm formation. *Appl Environ Microbiol*. 2015;81:6873-6882.
71. Whitchurch CB, Tolker-Nielsen T, Ragas PC, Mattick JS. Extracellular DNA required for bacterial biofilm formation. *Science*. 2002;295:1487.
72. Mann EE, Wozniak DJ. Pseudomonas biofilm matrix composition and niche biology. *FEMS Microbiol Rev*. 2012;36(6):893–916.
73. Moshynets OV, Spiers AJ. Viewing biofilms within the larger context of bacterial aggregations. In: Dhanasekaran D, Thajuddin N, editors. *Microbial Biofilms–Importance and Applications*. London, UK: InTechOpen; 2016. p. 3–22.
74. Jiang Z, Nero T, Mukherjee S, Olson R, Yan J. Searching for the secret of stickiness: How biofilms adhere to surfaces. *Front Microbiol*. 2021;12:686793.
75. Spiers AJ. A mechanistic explanation linking adaptive mutation, niche change, and fitness advantage for the Wrinkly Spreader. *Int J Evol Biol*. 2014;2014:675432.
76. Koza A, Kuśmierska A, McLaughlin K, Moshynets O, Spiers AJ. Adaptive radiation of *Pseudomonas fluorescens* SBW25 in experimental microcosms provides an understanding of the evolutionary ecology and molecular biology of A-L interface biofilm formation. *FEMS Microbiol Lett*. 2017;364(23):fnx109.

77. Spiers AJ, Bohannon J, Gehrig SM, Rainey PB. Biofilm formation at the air–liquid interface by the *Pseudomonas fluorescens* SBW25 wrinkly spreader requires an acetylated form of cellulose. *Mol Microbiol*. 2003;50:15–27.
78. Spiers AJ, Rainey PB. The *Pseudomonas fluorescens* SBW25 wrinkly spreader biofilm requires attachment factor, cellulose fibre and LPS interactions to maintain strength and integrity. *Microbiology*. 2005;151:2829–2839.
79. Koza A, Hallett PD, Moon CD, Spiers AJ. Characterization of a novel air-liquid interface biofilm of *Pseudomonas fluorescens* SBW25. *Microbiology (Reading)*. 2009 May;155(Pt 5):1397-1406;
80. Koza A, Jerdan R, Cameron S, Spiers AJ. Three biofilm types produced by a model pseudomonad are differentiated by structural characteristics and fitness advantage. *Microbiology (Reading).* 2020 Aug;166(8):707-716. Dueholm et al., 2013;
81. Lind PA, Farr AD, Rainey PB. Evolutionary convergence in experimental *Pseudomonas* populations. *ISME J*. 2017;11(3):589–600.
82. Ertesvåg H, Sletta H, Senneset M, Sun Y-Q, Klinkenberg G, Konradsen TA, Ellingsen TE, Valla S. Identification of genes affecting alginate biosynthesis in *Pseudomonas fluorescens* by screening a transposon insertion library. *BMC Genom*. 2017;18(1):11.
83. Tashiro Y, Uchiyama H, Nomura N. Multifunctional membrane vesicles in *Pseudomonas aeruginosa*. *Environ. Microbiol.* 2012, 14, 1349–1362.
84. Toyofuku M, Nomura N, Eberl L. Types and origins of bacterial membrane vesicles. *Nat. Rev. Microbiol.* 2019, 17, 13–24.
85. Karygianni L, Ren Z, Koo H, Thurnheer T. Biofilm matrixome: Extracellular components in structured microbial communities. *Trends Microbiol*. 2020;28(1):8-20.
86. Mozeheb N, Mingeot-Leclercq MP. Membrane vesicle production as a bacterial defense against stress. *Front Microbiol*. 2020;11:600221.
87. Wang D, Yu J.M., Dorosky R.J., Pierson L.S., Pierson E.A. The phenazine 2-hydroxy-phenazine-1-carboxylic acid promotes extracellular DNA release and has broad transcriptomic consequences in *Pseudomonas chlororaphis* 30–84. *PLoS ONE* 2016, 11, e0148003.
88. D'Alvise PW, Sjøholm OR, Yankelevich T, Jin Y, Wuertz S, Smets BF. TOL plasmid carriage enhances biofilm formation and increases extracellular DNA content in *Pseudomonas putida* KT2440. *FEMS Microbiol Lett*. 2010;312(1):84–92.
89. Tang L, Schramm A, Neu TR, Revsbech NP, Meyer RL. Extracellular DNA in adhesion and biofilm formation of four environmental isolates: A quantitative study. *FEMS Microbiol. Ecol.* 2013, 86, 394–403.

90. Catlin BW, Cunningham LS. Studies of extracellular and intracellular bacterial deoxyribonucleic acids. *J Gen Microbiol*. 1958;19(3):522–539.
91. Eisenberg DS, Sawaya MR. Structural studies of amyloid proteins at the molecular level. *Annu Rev Biochem*. 2017 Jun 20;86:69-95.
92. Verma A. Prions, prion-like prionoids, and neurodegenerative disorders. *Ann Indian Acad Neurol.* 2016 Apr-Jun;19(2):169-74.
93. Le NT, Narkiewicz J, Aulić S, Salzano G, Tran HT, Scaini D, Moda F, Giachin G, Legname G. Synthetic prions and other human neurodegenerative proteinopathies. *Virus Res*. 2015 Sep 2;207:25-37.
94. Mukherjee A, Morales-Scheihing D, Butler PC, Soto C. Type 2 diabetes as a protein misfolding disease. *Trends Mol Med*. 2015 Jul;21(7):439-49.
95. Zogaj X, Bokranz W, Nimtz M, Römling U. Production of cellulose and curli fimbriae by members of the family *Enterobacteriaceae* isolated from the human gastrointestinal tract. *Infect Immun.* 2003;71:4151-4158.
96. Larsen P, Nielsen JL, Otzen D, Nielsen PH. Amyloid-like adhesins produced by floc-forming and filamentous bacteria in activated sludge. *Appl Environ Microbiol*. 2008 Mar;74(5):1517-1526.
97. Dueholm MS, Otzen D, Nielsen PH. Evolutionary insight into the functional amyloids of the pseudomonads. *PLoS One*. 2013 Oct 7;8(10):e76630.
98. Dueholm MS, Søndergaard MT, Nilsson M, Christiansen G, Stensballe A, Overgaard MT. Expression of Fap amyloids in *Pseudomonas aeruginosa*, *P. fluorescens*, and *P. putida* results in aggregation and increased biofilm formation. *MicrobiologyOpen*. 2013;2(3):365–382.
99. Serra DO, Richter AM, Klauck G, Mika F, Hengge R. Microanatomy at cellular resolution and spatial order of physiological differentiation in a bacterial biofilm. *mBio.* 2013 Mar 19;4(2):e00103-13.
100. Sugimoto S, Arita-Morioka K, Mizunoe Y, Yamanaka K, Ogura T. Thioflavin T as a fluorescence probe for monitoring RNA metabolism at molecular and cellular levels. *Nucleic Acids Res.* 2015 Aug 18;43(14):e92.
101. Liu S, Peng P, Wang H, Shi L, Li T. Thioflavin T binds dimeric parallel-stranded GA-containing non-G-quadruplex DNAs: a general approach to lighting up double-stranded scaffolds. *Nucleic Acids Res*. 2017 Dec 1;45(21):12080-12089.
102. Moshynets O, Chernii S, Chernii V, Losytskyy MY, Karakhim S, Czerwieniec R, Pekhnyo V, Yarmoluk S, Kovalska V. Fluorescent β-ketoenole AmyGreen dye for visualization of amyloid components of bacterial biofilms. *Methods Appl Fluoresc*. 2020;8(3).

103. Nadell CD, Xavier JB, Foster KR. The sociobiology of biofilms. *FEMS Microbiol Rev*. 2009;33(1):206-224.
104. Nadell CD, Drescher K, Foster KR. Spatial structure, cooperation and competition in biofilms. *Nat Rev Microbiol*. 2016;14(9):589-600.
105. Coggan KA, Wolfgang MC. Global regulatory pathways and cross-talk control *Pseudomonas aeruginosa* environmental lifestyle and virulence phenotype. *Curr Issues Mol Biol*. 2012;14(2):47-70.
106. Stacy AR, Diggle SP, Whiteley M. Rules of engagement: defining bacterial communication. *Curr Opin Microbiol.* 2012;15(2):155-161.
107. Kirisits MJ, Parsek MR. Does *Pseudomonas aeruginosa* use intercellular signalling to build biofilm communities? *Cell Microbiol*. 2006;8(12):1841-1849.
108. Williams P, Cámara M. Quorum sensing and environmental adaptation in *Pseudomonas aeruginosa*: a tale of regulatory networks and multifunctional signal molecules. *Curr Opin Microbiol.* 2009;12(2):182-191.
109. Haussler S, Fuqua C. Biofilms 2012: new discoveries and significant wrinkles in a dynamic field. *J Bacteriol*. 2013;195(13):2947-2958.
110. Moshynets OV, Foster D, Karakhim SA, McLaughlin K, Rogalsky SP, Rymar SY, Volynets GP, Spiers AJ. Examining c-di-GMP and possible QS regulation in *Pseudomonas fluorescens* SBW25: links between intra and inter-cellular regulation benefits community cooperative activities such as biofilm formation. *Ukr Biochem J*. 2018;90(3):17-31.
111. Gillis RJ, Iglewski BH. Azithromycin retards *Pseudomonas aeruginosa* biofilm formation. *J Clin Microbiol*. 2004 Dec;42(12):5842-5845.
112. Ansiliero R, Gelinski JMLN, Samistraro QL, Baratto CM, Almeida CA, Locatelli C. Pathogenic microbial profile and antibiotic resistance associated with periodontitis. *Indian J Microbiol*. 2021;61(1):55–65.
113. Emery DC, Cerajewska TL, Seong J, Davies M, Paterson A, Allen-Birt SJ, et al. Comparison of blood bacterial communities in periodontal health and periodontal disease. *Front Cell Infect Microbiol*. 2021;10:542.
114. Espíndola LCP, Picão RC, Mançano SMCN, Martins do Souto R, Colombo APV. Prevalence and antimicrobial susceptibility of Gram-negative bacilli in subgingival biofilm associated with periodontal diseases. *J Periodontol*. 2022;93(1):69–79.
115. Kuboniwa M, Lamont RJ. Subgingival biofilm formation. *Periodontol 2000*. 2010;52(1):38–52.
116. Zijnge V, van Leeuwen MB, Degener JE, Abbas F, Thurnheer T, Gmür R, et al. Oral biofilm architecture on natural teeth. *PLoS One*. 2010;5:e9321.

117. Könönen E, Gursoy M, Gursoy UK. Periodontitis: A multifaceted disease of tooth-supporting tissues. *J Clin Med*. 2019;8(7):1135.
118. Diaz PI, Valm AM. Microbial interactions in oral communities mediate emergent biofilm properties. *J Dent Res*. 2020;99(1):18–25.
119. Welch MJL, Rossetti BJ, Rieken CW, Dewhirst FE, Borisy GG. Biogeography of a human oral microbiome at the micron scale. *Proc Natl Acad Sci U S A*. 2016;113:E791–E800.
120. van Winkelhoff AJ, Loos BG, van der Reijden WA, van der Velden U. *Porphyromonas gingivalis*, *Bacteroides forsythus* and other putative periodontal pathogens in subjects with and without periodontal destruction. *Clin Periodontol*. 2002;29:1023–1028.
121. Casado PL, Otazu IB, Balduino A, de Mello W, Barboza EP, Duarte ME. Identification of periodontal pathogens in healthy periimplant sites. *Implant Dent*. 2011;20(3):226–235.
122. Naginyte M, Do T, Meade J, Devine DA, Marsh PD. Enrichment of periodontal pathogens from the biofilms of healthy adults. *Sci Rep*. 2019;9:5491.
123. Ding PH, Yang MX, Wang NN, Jin LJ, Dong Y, Cai X, et al. *Porphyromonas gingivalis*-induced NLRP3 inflammasome activation and its downstream interleukin-1β release depend on caspase-4. *Front Microbiol*. 2020;11:2192.
124. Esparbès P, Legrand A, Bandiaky ON, Chéraud-Carpentier M, Martin H, Montassier E, et al. Subgingival microbiota and cytokines profile changes in patients with periodontitis: a pilot study comparing healthy and diseased sites in the same oral cavities. *Microorganisms*. 2021;9(11):2364.
125. Jakubovics NS, Goodman SD, Mashburn-Warren L, Stafford GP, Cieplik F. The dental plaque biofilm matrix. *Periodontol 2000*. 2021;86:32-56.
126. Tawakoli PN, Ragnarsson KT, Rechenberg DK, Mohn D, Zehnder M. Effect of endodontic irrigants on biofilm matrix polysaccharides. *Int Endod J*. 2017 Feb;50(2):153-160.
127. Moshynets O, Koza A, Dello Sterpaio P, Kordium V, Spiers AJ. Up-dating the Cholodny method using PET films to sample microbial communities in soil. *Biopolym Cell*. 2011;27:199-205.
128. Slobodianyk-Kolomoiets M, Khlebas S, Mazur I, Rudnieva K, Potochilova V, Iungin O, Kamyshnyi O, Kamyshna I, Potters G, Spiers AJ, Moshynets O. Extracellular host DNA contributes to pathogenic biofilm formation during periodontitis. *Front Cell Infect Microbiol.* 2024 May 8;14:1374817.
129. Älgå A, Karlow Herzog K, Alrawashdeh M, Wong S, Khankeh H, Stålsby Lundborg C. Perceptions of Healthcare-Associated Infection and Antibiotic Resistance among Physicians Treating Syrian Patients with War-Related Injuries. *Int J Environ Res Public Health*. 2018 Dec 1;15(12):2709.

130. Jakovljevic M, Al Ahdab S, Jurisevic M, Mouselli S. Antibiotic resistance in Yaacoub S, Truppa C, Pedersen TI, Abdo H, Rossi R. Antibiotic resistance among bacteria isolated from war-wounded patients at the Weapon Traumatology Training Center of the International Committee of the Red Cross from 2016 to 2019: a secondary analysis of WHONET surveillance data. *BMC Infect Dis.* 2022 Mar 14;22(1):257.
131. Berger FK, Schmartz GP, Fritz T, Veith N, Alhussein F, Roth S, Schneitler S, Gilcher T, Gärtner BC, Pirpilashvili V, Pohlemann T, Keller A, Rehner J, Becker SL. Occurrence, resistance patterns, and management of carbapenemase-producing bacteria in war-wounded refugees from Ukraine. *Int J Infect Dis*. 2023 Jul;132:89-92.
132. Petakh P, Kamyshnyi A, Tymchyk V, Armitage R. Infectious diseases during the Russian-Ukrainian war - Morbidity in the Transcarpathian region as a marker of epidemic danger on the EU border. *Public Health Pract (Oxf).* 2023 Jun 17;6:100397.
133. Moshynets OV, Baranovskyi TP, Iungin OS, Krikunov AA, Potochilova VV, Rudnieva KL, Potters G, Pokholenko I. Therapeutic potential of an azithromycin-colistin combination against XDR K. pneumoniae in a 3D collagen-based in vitro wound model of a biofilm infection. *Antibiotics*. 2023;12:293.
134. Kardas P, Babicki M, Krawczyk J, Mastalerz-Migas A. War in Ukraine and the challenges it brings to the Polish healthcare system. *Lancet Reg Health Eur*. 2022 Mar 15;15:100365.
135. Shkodina AD, Chopra H, Singh I, Ahmad S, Boiko DI. Healthcare system amidst the war in Ukraine. *Ann Med Surg (Lond).* 2022 Jul 31;80:104271.
136. Kondratiuk V, Jones BT, Kovalchuk V, Kovalenko I, Ganiuk V, Kondratiuk O, Frantsishko A. Phenotypic and genotypic characterization of antibiotic resistance in military hospital-associated bacteria from war injuries in the Eastern Ukraine conflict between 2014 and 2020. *J Hosp Infect*. 2021 Jun;112:69-76.
137. Melwani M. How war is spreading drug resistant superbugs across Ukraine and beyond. *BMJ*. 2022 Nov 22;379:o2731.
138. Ljungquist O, Nazarchuk O, Kahlmeter G, Andrews V, Koithan T, Wasserstrom L, Dmytriiev D, Fomina N, Bebyk V, Matuschek E, Riesbeck K. Highly multidrug-resistant Gram-negative bacterial infections in war victims in Ukraine, 2022. *Lancet Infect Dis*. 2023 Jul;23(7):784-786.
139. Magiorakos AP, Srinivasan A, Carey RB, Carmeli Y, Falagas ME, Giske CG, Harbarth S, Hindler JF, Kahlmeter G, Olsson-Liljequist B, Paterson DL, Rice LB, Stelling J, Struelens MJ, Vatopoulos A, Weber JT, Monnet DL. Multidrug-resistant, extensively drug-resistant and pandrug-resistant bacteria: an international expert proposal for interim standard definitions for acquired resistance. *Clin Microbiol Infect*. 2012 Mar;18(3):268-281.

140. Majumder MAA, Rahman S, Cohall D, Bharatha A, Singh K, Haque M, Gittens-St Hilaire M. Antimicrobial Stewardship: Fighting Antimicrobial Resistance and Protecting Global Public Health. *Infect Drug Resist*. 2020 Dec 29;13:4713-4738.
141. Paul M, Daikos GL, Durante-Mangoni E, Yahav D, Carmeli Y, Benattar YD, Skiada A, Andini R, Eliakim-Raz N, Nutman A, Zusman O, Antoniadou A, Pafundi PC, Adler A, Dickstein Y, Pavleas I, Zampino R, Daitch V, Bitterman R, Zayyad H, Koppel F, Levi I, Babich T, Friberg LE, Mouton JW, Theuretzbacher U, Leibovici L. Colistin alone versus colistin plus meropenem for treatment of severe infections caused by carbapenem-resistant Gram-negative bacteria: an open-label, randomised controlled trial. *Lancet Infect Dis.* 2018 Apr;18(4):391-400.
142. Daikos GL, Tsaousi S, Tzouvelekis LS, Anyfantis I, Psichogiou M, Argyropoulou A, Stefanou I, Sypsa V, Miriagou V, Nepka M, Georgiadou S, Markogiannakis A, Goukos D, Skoutelis A. Carbapenemase-producing Klebsiella pneumoniae bloodstream infections: lowering mortality by antibiotic combination schemes and the role of carbapenems. Antimicrob Agents Chemother. 2014;58(4):2322-8.
143. Jones N, Mitchell J, Cooke P, Baral S, Arjyal A, Shrestha A, King R. Gender and Antimicrobial Resistance: What Can We Learn From Applying a Gendered Lens to Data Analysis Using a Participatory Arts Case Study? Front Glob Womens Health. 2022 May 27;3:745862.
144. Pallett SJC, Trompeter A, Basarab M, Moore LSP, Boyd SE. Multidrug-resistant infections in war victims in Ukraine. *Lancet Infect Dis.* 2023 Aug;23(8):e270-e271.
145. Kryzhevskyi V, Strokous V, Lifshyts Y, Rybianets Y, Oberniak A, Krikunov A, Iungin O, Potochilova V, Rudnieva K, Petakh P, Kamyshnyi A, Moshynets O. Case report: Azithromycin-meropenem combination therapy as a low-cost approach to combat PDR gram-negative infections of war wounds in Ukraine. *Front Med*. 2023;10:1264492.
146. Pallett SJ, Mistry R, Lambert ZL, Woolley SD, Abbara A, Breathnach AO, Lamb LE, Williams A, Mughal N, Moshynets O, Hughes SJ, O'Shea MK, Moore LS. Conflict and catastrophe-related severe burn injuries: A challenging setting for antimicrobial decision-making. J Infect. 2024 Sep;89(3):106224.
147. Volynets GP, Barthels F, Hammerschmidt SJ, Moshynets OV, Lukashov SS, Starosyla SA, Vyshniakova HV, Iungin OS, Bdzhola VG, Prykhod'ko AO, Syniugin AR, Sapelkin VM, Yarmoluk SM, Schirmeister T. Identification of novel small-molecular inhibitors of *Staphylococcus aureus* sortase A using hybrid virtual screening. *J Antibiot*. 2022;75:321–332.
148. Sandfort M, Hans JB, Fischer MA, Reichert F, Cremanns M, Eisfeld J, Pfeifer Y, Heck A, Eckmanns T, Werner G, Gatermann S, Haller S, Pfennigwerth N. Increase in NDM-1 and

NDM-1/OXA-48-producing *Klebsiella pneumoniae* in Germany associated with the war in Ukraine, 2022. *Euro Surveill.* 2022 Dec;27(50):2200926.

149. Petrosillo N, Petersen E, Antoniak S. Ukraine war and antimicrobial resistance. *Lancet Infect Dis.* 2023 Jun;23(6):653-654.
150. Itzek A, Zheng L, Chen Z, Merritt J, Kreth J. Hydrogen peroxide-dependent DNA release and transfer of antibiotic resistance genes in *Streptococcus gordonii*. *J Bacteriol*. 2011 Dec;193(24):6912-6922.
151. Mathers AJ, Crook D, Vaughan A, Barry KE, Vegesana K, Stoesser N, Parikh HI, Sebra R, Kotay S, Walker AS, Sheppard AE. *Klebsiella quasipneumoniae* Provides a Window into Carbapenemase Gene Transfer, Plasmid Rearrangements, and Patient Interactions with the Hospital Environment. *Antimicrob Agents Chemother*. 2019 May 24;63(6):e02513-18.
152. Lopez PJ, Ron O, Parthasarathy P, Soothill J, Spitz L. Bacterial counts from hospital doctors' ties are higher than those from shirts. *Am J Infect Control*. 2009 Feb;37(1):79-80.
153. Treakle AM, Thom KA, Furuno JP, Strauss SM, Harris AD, Perencevich EN. Bacterial contamination of health care workers' white coats. *Am J Infect Control.* 2009 Mar;37(2):101-5.
154. Lax S, Sangwan N, Smith D, Larsen P, Handley KM, Richardson M, Guyton K, Krezalek M, Shogan BD, Defazio J, Flemming I, Shakhsheer B, Weber S, Landon E, Garcia-Houchins S, Siegel J, Alverdy J, Knight R, Stephens B, Gilbert JA. Bacterial colonization and succession in a newly opened hospital. Sci Transl Med. 2017 May 24;9(391):eaah6500.
155. Marinella MA, Pierson C, Chenoweth C. The stethoscope. A potential source of nosocomial infection? *Arch Intern Med*. 1997 Apr 14;157(7):786-790.
156. Brady RR, Wasson A, Stirling I, McAllister C, Damani NN. Is your phone bugged? The incidence of bacteria known to cause nosocomial infection on healthcare workers' mobile phones. *J Hosp Infect*. 2006 Jan;62(1):123-5.
157. Brady RR, Verran J, Damani NN, Gibb AP. Review of mobile communication devices as potential reservoirs of nosocomial pathogens. *J Hosp Infect*. 2009 Apr;71(4):295-300.
158. Ulger F, Esen S, Dilek A, Yanik K, Gunaydin M, Leblebicioglu H. Are we aware how contaminated our mobile phones are with nosocomial pathogens? *Ann Clin Microbiol Antimicrob.* 2009 Mar 6;8:7. doi: 10.1186/1476-0711-8-7. Erratum in: *Ann Clin Microbiol Antimicrob.* 2009;8:31.
159. Akinyemi KO, Atapu AD, Adetona OO, Coker AO. The potential role of mobile phones in the spread of bacterial infections. *J Infect Dev Ctries*. 2009 Sep 15;3(8):628-32.
160. Sheppard AE, Stoesser N, Wilson DJ, Sebra R, Kasarskis A, Anson LW, Giess A, Pankhurst LJ, Vaughan A, Grim CJ, Cox HL, Yeh AJ; Modernising Medical Microbiology (MMM)

Informatics Group; Sifri CD, Walker AS, Peto TE, Crook DW, Mathers AJ. Nested Russian Doll-Like Genetic Mobility Drives Rapid Dissemination of the Carbapenem Resistance Gene *blaKPC*. *Antimicrob Agents Chemother.* 2016 May 23;60(6):3767-78.

161. Pallett SJC, Morkowska A, Woolley SD, O'Shea MK, Moore LSP, Moshynets O. Severe conflict-associated wound infections complicated by the discovery of carbapenemase-coproducing *Pseudomonas aeruginosa* in Ukraine. *Lancet Microbe.* 2024.
162. Moshynets OV, Baranovskyi TP, Iungin OS, Kysil NP, Metelytsia LO, Pokholenko I, Potochilova VV, Potters G, Rudnieva KL, Rymar SY, Semenyuta IV, Spiers AJ, Tarasyuk OP, Rogalsky SP. eDNA inactivation and biofilm inhibition by the polymeric biocide polyhexamethylene guanidine hydrochloride (PHMG-Cl). *Int J Mol Sci*. 2022;23(2):731.
163. Moshynets O, Bardeau JF, Tarasyuk O, Makhno S, Cherniavska T, Dzhuzha O, Potters G, Rogalsky S. Antibiofilm activity of polyamide 11 modified with thermally stable polymeric biocide polyhexamethylene guanidine 2-naphtalenesulfonate. *Int J Mol Sci*. 2019;20:348.
164. Gnilitskyi I, Rymar S, Iungin O, Vyshnevskyy O, Parisseg P, Potters G, Zayats AV, Moshynets O. Femtosecond laser modified metal surfaces alter biofilm architecture and reduce bacterial biofilm formation. *Nanoscale Adv*. 2023;5(23):6659–6669.
165. Rogalsky S, Moshynets O, Dzhuzha O, Tarasyuk O, Hubina A, Darabut AM, Lobko Y, Morozovska I, Protasov O, Bardeau JF. Preparation and characterization of new antifouling coating based on alkyd paint modified with hydrophobic cationic biocide. *J Coat Technol Res*. 2024.
166. Brecker-Reshef I, Vermore E, Lindeman M, Justice C. A generalized regression-based model for forecasting winter wheat yields in Kansas and Ukraine using MODIS data. *Remote Sensing Environ*. 2010;114(7):1312–1323.
167. Kogan F, Kussul N, Adamenko T, Skakun S, Kravchenko O, Kryvobok O, et al. Winter wheat yield forecasting in Ukraine based on Earth observation, meteorological data and biophysical models. *Inter J Appl Earth Obser Geoinformat*. 2013;23:192–203.
168. Tadesse W, Solh M, Braun H-J, Oweis T, Baum M. Approaches and strategies for sustainable wheat production: Tools and Guidelines; ICARDA: Beirut, Lebanon 2016; ISBN 92-9127-490-9.
169. Paradikovic N, Vinkovic T, Vrcek IV, Tkalec M. Natural biostimulants reduce the incidence of BER in sweet yellow pepper plants (*Capsicum annuum* L.). *Agric Food Sci.* 2013; 22: 307–317.
170. Maksimov IV, Yarullina LG, Surina OB. The effect of exogenous phytohormones on resistance of wheat calluses to *Tilletia caries* (D.C.) Tul. & C. Tul. *Amer J Plant Sci*. 2014;5:1745–1754.

171. Tsygankova V, Shysha E, Andrusevich Y, Galkin A, Iutynsk G, Yemets A, et al. Using new microbial biostimulants for obtaining in vitro new lines of *Triticum aestivum* L. cells resistant to nematode *H. avenae*. *Eur J Biotechnol Biosci.* 2016; 4: 41–53.
172. Moshynets O, Babenko L, Rogalsky S, Iungin O, Foster J., Kosakivska I, Potters G, Spiers A Priming winter wheat seeds with the bacterial quorum sensing signal N-hexanoyl-L-homoserine lactone (C6-HSL) shows potential to improve plant growth and seed yield. *PLoS ONE*. 2019, 14(2):e0209460.

ДОДАТОК 1

СПИСОК ПУБЛІКАЦІЙ ЗДОБУВАЧА

Наукові праці, що розкривають основні наукові результати дисертації:

1. Pallett S.J.C., Morkowska A., Woolley S.D., Potochilova V.V., Rudnieva K.L., Iungin O.S., Sgro V., Boyd S.E., Reece N., Lambert Z.L., Tan N.K., Mughal N., Moshynets O.V., Moore L.S.P., O'Shea M.K. Evolving antimicrobial resistance of extensively drug-resistant Gram-negative severe infections associated with conflict wounds in Ukraine: an observational study. Lancet Regional Health - Europe. 2025 Mar 20;52:101274. https://doi: 10.1016/j.lanepe.2025.101274 **[IF 13,6; SCOPUS, WoS; SCImago Q1 – 2024 Public Health, Environmental and Occupational Health]** (Особистий внесок здобувача: збір колекції ізолятів, обговорення результатів, написання рукопису).
2. Pallett S.J.C., Morkowska A., Woolley S.D., O'Shea M.K., Moore L.S.P., Moshynets O. Severe conflict-associated wound infections complicated by the discovery of carbapenemase-coproducing *Pseudomonas aeruginosa* in Ukraine. Lancet Microbe. 2024 Dec 6:101046. https://doi.org/10.1016/j.lanmic.2024.101046 **[IF 20,9; SCOPUS, WoS; SCImago Q1 – 2023 Infectious diseases, Microbiology (medical)]** (Особистий внесок здобувача: збір колекції ізолятів, обговорення результатів, написання рукопису).
3. Pallett S.J., Mistry R., Lambert Z.L., Woolley S.D., Abbara A., Breathnach A.O., Lamb L.E., Williams A., Mughal N., **Moshynets O.**, Hughes S.J., O'Shea M.K., Moore L.S. (2024) Conflict and catastrophe-related severe burn injuries: A challenging setting for antimicrobial decision-making. Journal of Infection 89 (3): 106224. https://doi.org/10.1016/j.jinf.2024.106224 **[IF 14,3; SCOPUS, WoS; SCImago Q1 – 2023 Infectious diseases]** (Особистий внесок здобувача: аналіз національних підходів у веденні опікових пацієнтів в Україні).
4. Slobodianyk-Kolomoiets M., Khlebas S., Mazur I., Rudnieva K., Potochilova V., Iungin O., Kamyshnyi O., Kamyshna I., Potters G., Spiers A.J., **Moshynets O**. (2024) Extracellular host DNA contributes to pathogenic biofilm formation during periodontitis. Frontiers in Cellular and Infection Microbiology 14: 1374817. https://doi.org/10.3389/fcimb.2024.1374817 **[IF 4,6; SCOPUS, WoS; SCImago Q1 – 2023 Infectious diseases]** (Особистий внесок здобувача:

концептуалізація, планування та адміністрування роботи, аналіз літератури, проведення лабораторних досліджень, аналіз результатів, написання рукопису).

5. Rogalsky S., **Moshynets O**., Dzhuzha O., Tarasyuk O., Hubina A., Darabut A.M., Lobko Y., Morozovska I., Protasov O., Bardeau J.F. (2024) Preparation and characterization of new antifouling coating based on alkyd paint modified with hydrophobic cationic biocide. Journal of Coatings Technology and Research 21: 939-953. https://doi.org/10.1007/s11998-023-00862-8 **[IF 2,3; SCOPUS; SCImago Q2 – 2023 Surfaces, coatings and films]** (Особистий внесок здобувача: проведення антибіоплівкових досліджень, аналіз результатів, написання рукопису).

6. Gnilitskyi I., Rymar S., Iungin O., Vyshnevskyy O., Parisseg P., Potters G., Zayats A.V., **Moshynets O**. (2023) Femtosecond laser modified metal surfaces alter biofilm architecture and reduce bacterial biofilm formation. Nanoscale Advance 5(23): 6659–6669. https://doi.org/10.1039/D3NA00599B **[IF 4,6; SCOPUS, WoS; SCImago Q1 – 2023 Materials Science]** (Особистий внесок здобувача: проведення антибіоплівкових досліджень, проведення мікроелементного аналізу, скануюча електронна мікроскопія зразків, аналіз результатів, написання рукопису).

7. Kryzhevskyi V., Strokous V., Lifshyts Y., Rybianets Y., Oberniak A., Krikunov A., Iungin O., Potochilova V., Rudnieva K., Petakh P., Kamyshnyi A., **Moshynets O.** (2023) Case report: Azithromycin-meropenem combination therapy as a low-cost approach to combat PDR gram-negative infections of war wounds in Ukraine. Frontiers in Medicine, 10:1264492. https://doi.org/10.3389/fmed.2023.1264492 **[IF 3,1; SCOPUS, WoS; SCImago Q1 – 2023 Medicine]** (Особистий внесок здобувача: концептуалізація, аналіз літератури, ведення пацієнта, аналіз результатів, графічне представлення динаміки показників, написання рукопису).

8. **Moshynets O.V**., Baranovskyi T.P., Iungin O.S., Krikunov A.A., Potochilova V.V., Rudnieva K.L., Potters G., Pokholenko I. (2023) Therapeutic potential of an azithromycin-colistin combination against XDR *K. pneumoniae* in a 3D collagen-based in vitro wound model of a biofilm infection. Antibiotics 12: 293. https://doi.org/10.3390/antibiotics12020293 **[IF 4,3; SCOPUS, WoS; SCImago Q1 – 2023 Pharmacology]** (Особистий внесок здобувача: концептуалізація, аналіз літератури, планування та адміністрування роботи, дослідження

біоплівок в умовах моделі ранової інфекції, порівняльний аналіз антибіоплівкової дії антибіотиків, аналіз результатів, написання рукопису).

9. **Moshynets O.V.**, Baranovskyi T.P., Cameron S., Iungin O.S., Pokholenko I., Jerdan R., Kamyshnyi A., Krikunov A.A., Potochilova V.V., Rudnieva K.L., Spiers A.J. (2022) Azithromycin possesses biofilm–inhibitory activity and potentiates non-bactericidal colistin methanesulfonate (CMS) and polymyxin B against *Klebsiella pneumonia*. PLoS ONE 17(7): e0270983. https://doi.org/10.1371/journal.pone.0270983 **[IF 3,7; SCOPUS, WoS; SCImago Q1 – 2022 Multidisciplinary]** (Особистий внесок здобувача: концептуалізація, аналіз літератури, планування та адміністрування роботи, дослідження біоплівок, порівняльний аналіз антибіоплівкової дії антибіотиків, порівняльний аналіз синергідної дії антибіотиків за методом Кірбі-Бауера, аналіз результатів, написання рукопису).

10. **Moshynets O.V**., Pokholenko I., Iungin O., Potters G., Spiers A.J. (2022) eDNA, Amyloid fibers and membrane vesicles identified in *Pseudomonas fluorescens* SBW25 biofilms. International Journal of Molecular Sciences 23: 15096. https://doi.org/10.3390/ijms232315096 **[IF 4,9; SCOPUS, WoS; SCImago Q2 – 2022 Molecular biology]** (Особистий внесок здобувача: концептуалізація, планування та адміністрування роботи, проведення комбінованого дослідження біоплівок, мікроскопічні дослідження біоплівок, виділення мембранних везикул, проведення трансмісійної електронної мікроскопії зразків везикул, спектрофотометричні дослідження, виділення і аналіз білків матриксу біоплівок і білків мембранних везикул, аналіз отриманих результатів, написання рукопису).

11. **Moshynets O.V.**, Baranovskyi T.P., Iungin O.S., Kysil N.P., Metelytsia L.O., Pokholenko I., Potochilova V.V., Potters G., Rudnieva K.L., Rymar S.Y., Semenyuta I.V., Spiers A.J., Tarasyuk O.P., Rogalsky S.P. (2022) eDNA inactivation and biofilm inhibition by the polymeric biocide polyhexamethylene guanidine hydrochloride (PHMG-Cl). International Journal of Molecular Sciences 23(2):731. https://doi.org/10.3390/ijms23020731 **[IF 4,9; SCOPUS, WoS; SCImago Q2 – 2022 Molecular biology]** (Особистий внесок здобувача: концептуалізація, аналіз літератури, планування та адміністрування роботи, отримання моделей біоплівок, підбір біоцидів для порівняльних досліджень, виділення ДНК, спектрофотометричний аналіз, аналіз якості ДНК, аналіз пролонгованості дії полімерного біоциду ПГМГ-ГХ, аналіз результатів, написання рукопису).

12. Volynets G.P., Barthels F., Hammerschmidt S.J., **Moshynets O.V**., Lukashov S.S., Starosyla S.A., Vyshniakova H.V., Iungin O.S., Bdzhola V.G., Prykhod'ko A.O., Syniugin A.R., Sapelkin V.M., Yarmoluk S.M., Schirmeister T. (2022) Identification of novel small-molecular inhibitors of *Staphylococcus aureus* sortase A using hybrid virtual screening. Journal of Antibiotics 75: 321–332. https://doi.org/10.1038/s41429-022-00524-8 **[IF 2,1; SCOPUS; SCImago Q2 – 2022 Drug discovery]** (Особистий внесок здобувача: проведення досліджень на біоплівках, аналіз результатів, написання рукопису).

13. **Moshynets O.**, Chernii S., Chernii V., Losytskyy M.Y., Karakhim S., Czerwieniec R., Pekhnyo V., Yarmoluk S., Kovalska V. (2020) Fluorescent β-ketoenole AmyGreen dye for visualization of amyloid components of bacterial biofilms. Methods and Applications in Fluorescence 8(3). DOI 10.1088/2050-6120/ab90e0 **[IF 2,3; SCOPUS; SCImago Q1 – 2020 Instrumentation]** (Особистий внесок здобувача: проведення мікроскопічних досліджень на біоплівках, аналіз результатів, написання рукопису).

14. **Moshynets O.**, Bardeau J.F., Tarasyuk O., Makhno S., Cherniavska T., Dzhuzha O., Potters G., Rogalsky S. (2019) Antibiofilm activity of polyamide 11 modified with thermally stable polymeric biocide polyhexamethylene guanidine 2-naphtalenesulfonate. International Journal of Molecular Sciences 20: 348. https://doi.org/10.3390/ijms20020348 **[IF 4,9; SCOPUS, WoS; SCImago Q1 – 2019 Organic chemistry]** (Особистий внесок здобувача: проведення антибіоплівкових досліджень, аналіз результатів, написання рукопису).

15. **Moshynets O**., Babenko L., Rogalsky S., Iungin O., Foster J., Kosakivska I., Potters G., Spiers A. (2019) Priming winter wheat seeds with the bacterial quorum sensing signal N-hexanoyl-L-homoserine lactone (C6-HSL) shows potential to improve plant growth and seed yield. PLoS ONE, 14 (2): e0209460. https://doi.org/10.1371/journal.pone.0209460 **[IF 3,7; SCOPUS, WoS; SCImago Q1 – 2022 Multidisciplinary]** (Особистий внесок здобувача: концептуалізація, планування та адміністрування роботи, проведення мікробіологічних досліджень, курація польових і лабораторних досліджень, обрахунок результатів, аналіз результатів, написання рукопису).

16. **Moshynets O.V.,** Foster D., Karakhim S.A., McLaughlin K., Rogalsky S.P., Rymar S.Y., Volynets G.P., Spiers A.J. (2018) Examining c-di-GMP and possible QS regulation in *Pseudomonas fluorescens* SBW25: links between intra and inter-cellular regulation benefits community cooperative activities such as biofilm formation. Ukrainian Biochemical Journal 90(3):

17-31. doi: https://doi.org/10.15407/ubj90.03.017 **[SCOPUS; SCImago Q4 – 2018 Biochemistry]** (Особистий внесок здобувача: концептуалізація, аналіз літератури, біоінформатичний аналіз, написання рукопису).

17. McLaughlin K., Folorunso A.O., Deeni Y.Y., Foster D., Gorbatiuk O., Hapca S.M., Immoor C., Koza A., Mohammed I.U., **Moshynets O.**, Rogalsky S., Zawadzki K., Spiers A.J. (2017) Biofilm formation and cellulose expression by *Bordetella avium* 197N, the causative agent of bordetellosis in birds and an opportunistic respiratory pathogen in humans. Research in Microbiology 168: 419-430. https://doi.org/10.1016/j.resmic.2017.01.002 **[IF 2,5; SCOPUS, WoS; SCImago Q3 – 2019 Microbiology]** (Особистий внесок здобувача: дослідження структури біоплівок штамів *B. avium*, аналіз отриманих результатів, написання рукопису).

18. Koza A., Kusmierska A., McLauglin Kimberley, **Moshynets O**., Spiers A.J. (2017) Adaptive radiation of *P. fluorescens* SBW25 in experimental microcosms provides an understanding of the evolutionary ecology and molecular biology of A-L interface biofilm-formation. FEMS Microbiology Letters 364 (12). **[IF 2,2; SCOPUS, WoS; SCImago Q3 – 2017 Microbiology]** (Особистий внесок здобувача: аналіз літературних джерел, написання рукопису).

19. **Moshynets O.V.,** Spiers A.J. (2016) Viewing biofilms within the larger context of bacterial aggregations. In "Biofilms", p. 3-22, InTech Press. DOI: 10.5772/62912. (Особистий внесок здобувача: аналіз літератури, концептуалізація, написання рукопису та підготовка глави монографії до друку).

20. **Moshynets O.**, Boretska M., Spiers A.J. (2013) From Winogradsky's column to contemporary research using bacterial microcosms. In Harris C.C. (eds.) "Microcosms: Ecology, Biological Implications and Environmental Impact"; p. 1-27, April, Nova Publisher. (Особистий внесок здобувача: аналіз літератури, концептуалізація, підготовка і проведення досліджень, підготовка ілюстративного матеріалу, написання рукопису та підготовка глави монографії до друку).

21. Spiers A.J., Deeni Y., Folorunso A.O., Koza A., **Moshynets O.,** Zawadzki K. (2013) Cellulose expression in *Pseudomonas fluorescens* SBW25 and other environmental pseudomonads. In: van de Ven T. & Godbout L. (eds.) "Cellulose – Medical, Pharmaceutical and Electronic Applications", p. 1-26, InTech Press, 2013. – 304 p. DOI: 10.5772/53736 (Особистий

внесок здобувача: аналіз літератури, написання рукопису та підготовка глави монографії до друку).

Публікації, що засвідчують апробацію матеріалів дисертації:

1. **Moshynets O.,** Slobodianyk-Kolomoiets M., Khlebas S., Mazur I., Rudnieva K., Potochilova V., Iungin O., Potters G., Spiers A. J. Extracellular host DNA contributes to pathogenic biofilm formation during periodontitis. Eurobiofilms 2024, oral presentation O-14, Copenhagen, Denmark, 24-29 June 2024. (Особистий внесок здобувача: тези і доповідь засновані на результатах отриманих здобувачем або під його керівництвом, здобувач написав тези конференції та безпосередньо представив усну доповідь).
2. **Moshynets O.**, Gnilitskyi I., Rymar S., Iungin O., Vyshnevskyy O., Potters G. Laser modification of metal surfaces alters biofilm architecture and reduce bacterial biofilm formation. Eurobiofilms 2024, poster presentation PG2-62, Copenhagen, Denmark, 24-29 June 2024. (Особистий внесок здобувача: тези і доповідь засновані на результатах отриманих здобувачем або під його керівництвом, здобувач написав тези конференції та безпосередньо представив стендову доповідь).
3. **Moshynets O**., Iungin O., Rymar S., Gnilitskyi I., Potters G. Nano-microstructured metal surfaces demonstrated alteration in biofilm architecture and reduction in biofilm formation. The 9th Thesinge biofilm meeting on biomaterial-associated infections May 13-14, 2024, Thesinge, The Netherlands. (Особистий внесок здобувача: тези і доповідь засновані на результатах отриманих здобувачем або під його керівництвом, здобувач написав тези конференції та безпосередньо представив стендову доповідь).
4. **Moshynets O.**, Iungin O., Potochilova V., Rudnieva K. Azithromycin mitigates PDR phenotype and improves sensitivity to meropenem in PDR *Klebsiella pneumoniae* biofilms. 34th European Congress of Clinical Microbiology & Infectious Diseases ESCMID-Global, Abstract/ePoster Number: 4227/P0182, 27 – 30 April 2024, Bacelona, Spain. (Особистий внесок здобувача: тези і доповідь засновані на результатах отриманих здобувачем або під його керівництвом, здобувач написав тези конференції та безпосередньо представив стендову доповідь).

5. **Moshynets O.**, Kryzhevskyi V., Strokous V., Lifshyts Y., Rybianets Y., Oberniak A., Iungin O., Potochilova V., Rudnieva K. The alternative low-cost approach to combating PDR gram-negative infections of war injuries in Ukraine using a combination of azithromycin-meropenem. 34th European Congress of Clinical Microbiology & Infectious Diseases ESCMID-Global, Abstract/ePoster Number: 06182/P4128, 27 – 30 April 2024, Bacelona, Spain. (Особистий внесок здобувача: тези і доповідь засновані на результатах отриманих здобувачем або під його керівництвом, здобувач написав тези конференції та безпосередньо представив стендову доповідь).

6. **Moshynets O**., Baranovskyi T., Iungin O., Pokholenko I., Potochilova V., Krikunov A., Spiers A., Rudnieva K. Adaptation to azithromycin mitigates PDR phenotype and restores sensitivity to meropenem in PDR *Klebsiella pneumoniae*. 33rd European Congress of Clinical Microbiology & Infectious Diseases, Abstract/ePoster Number: 3094/P0461, 15 – 18 April 2023, Copenhagen, Denmark. (Особистий внесок здобувача: тези і доповідь засновані на результатах отриманих здобувачем або під його керівництвом, здобувач написав тези конференції та безпосередньо представив стендову доповідь).

7. **Moshynets O**., Rudnieva K., Potochilova V., Iungin O., Baranovskyi T., Spiers A., Krikunov A., Pokholenko I. Biomimetic wound surface model using collagen-based 3D scaffolds seeded with HEK293 cells show azithromycin-colistin combination treatment highly effective against XDR K. pneumoniae infection. 33rd European Congress of Clinical Microbiology & Infectious Diseases, Abstract/ePoster Number: 2720/P1021, 15 – 18 April 2023, Copenhagen, Denmark. (Особистий внесок здобувача: тези і доповідь засновані на результатах отриманих здобувачем або під його керівництвом, здобувач написав тези конференції та безпосередньо представив стендову доповідь).

8. **Moshynets O**. Azithromycin in a combined application of antibacterials against PDR *K. pneumoniae*: does it influence antibiotic bioavailability and permeability?", "Molecular basis of antibiotic permeability in Gram-negative bacteria" Workshop, 21-24 June 2022, Hamburg, Germany. (Особистий внесок здобувача: тези і доповідь засновані на результатах отриманих здобувачем або під його керівництвом, здобувач написав тези конференції та безпосередньо представив усну доповідь).

9. **Moshynets O**., Rudnieva K., Baranovskyi T., Potochilova V., Iungin O., Pokholenk I., Spiers A.J. Azithromycin reveals biofilm–inhibitory activity and potentiates non-bactericidal

colistin methanesulfonate against *Klebsiella pneumonia*. Proceedings of the All-Ukrainian Conference on Molecular and Cell Biology with international participation, dedicated to the heroic struggle of the Ukrainian people against the Russian invaders, p. 61, 15-17 June 2022, Kyiv, Ukraine. (Особистий внесок здобувача: тези і доповідь засновані на результатах отриманих здобувачем або під його керівництвом, здобувач написав тези конференції та безпосередньо представив усну доповідь).

10. Pokholenko I., Rudnieva K., Baranovskyi T., Potochilova V., Iungin O., Spiers A., Krikunov A. A., **Moshynets O.** Biomimetic 3D model to reproduce wound-associated biofilm-related infectious process *in vitro*. Proceedings of the All-Ukrainian Conference on Molecular and Cell Biology with international participation, dedicated to the heroic struggle of the Ukrainian people against the Russian invaders, p. 53, 15-17 June 2022, Kyiv, Ukraine. (Особистий внесок здобувача: тези і доповідь засновані на результатах отриманих здобувачем або під його керівництвом, здобувач написав тези конференції та безпосередньо представив усну доповідь).

11. **Moshynets O.V.**, Baranovskyi T.P., Iungin O.S., Kysil N.P., Metelytsia L.O., Pokholenko I., Potochilova V.V., Potters G., Rudnieva K.L., Rymar S.Y., Semenyuta I.V., Spiers A.J., Tarasyuk O.P., Rogalsky S.P. Biocides contribute to antibiotic resistance spread by increase eDNA release from biofilms. – 00365. The 32nd European Congress of Clinical Microbiology and Infectious Diseases, No 365, 23 - 26 April 2022, Lisbon, Portugal. (Особистий внесок здобувача: тези і доповідь засновані на результатах отриманих здобувачем або під його керівництвом, здобувач написав тези конференції та безпосередньо представив усну доповідь).

12. **Moshynets O**., Krykunov O., Iungin O., Jerdan R., Filonenko G., Spiers A. Azithromycin possesses biofilm-inhibitory activity against Klebsiella pneumonia and potentiates colistin to combat klebsiella-associated infection. - 051-DKMP. 6 th Joint Conference of DGHM & VAAM, 8-11 March 2020, Leipzig, Germany. (Особистий внесок здобувача: тези і доповідь засновані на результатах отриманих здобувачем або під його керівництвом, здобувач написав тези конференції та безпосередньо представив стендову доповідь).

13. **Moshynets O**., Chernii S., Snihirova Y., Czerwieniec R., Chernii V., Yarmoluk S., Kovalska V. AmyGreen is a new amyloid-sensitive stain for biofilm research - 101-MCBP. 6 th Joint Conference of DGHM & VAAM, 8-11 March 2020, Leipzig, Germany. (Особистий внесок здобувача: тези і доповідь засновані на результатах отриманих здобувачем або під його

керівництвом, здобувач написав тези конференції та безпосередньо представив стендову доповідь).

14. **Moshynets O**., Iungin O., De Baere K., Meskens R., Leyn M., Bardeau J.F., Tarasyuk O., Makhno S., Cherniavska T., Dzhuzha O., Potters G., Rogalsky S. Polyhexamethylene guanidine salts as an effective biofouling and DNA inhibitor for polymeric articles and protective coatings. 8th Congress of European Microbiologists, July 7-11, 2019, Glasgow, UK. (Особистий внесок здобувача: тези і доповідь засновані на результатах отриманих здобувачем або під його керівництвом, здобувач написав тези конференції та безпосередньо представив стендову доповідь).

15. **Moshynets O**., Spiers A. Identification of extracellular DNA in *P.fluorescens* SBW25 air-liquid interface biofilms. 8th Congress of European Microbiologists, July 7-11, 2019, Glasgow, UK. (Особистий внесок здобувача: тези і доповідь засновані на результатах отриманих здобувачем або під його керівництвом, здобувач написав тези конференції та безпосередньо представив стендову доповідь).

16. **Moshynets O.V**., Vodianyk A.A., Krykunov O.A., Spiers A.J. Azithromycin-colistin as a new combination therapy against carbapenem-resistant *Klebsiella pneumoniae* infection: anti-biofilm activity and treatment effectiveness. Setting our sights on infectious diseases Conference, 12-15 May 2019, University of Dundee, UK. (Особистий внесок здобувача: тези і доповідь засновані на результатах отриманих здобувачем або під його керівництвом, здобувач написав тези конференції та безпосередньо представив усну доповідь).

17. **Moshynets O.,** Spiers A., Krykunov A. Azithromycin-colistin as a new combination therapy against carbapenem resistant *Klebsiella pneumonia* esepsis: anti-biofilm activity and treatment effectiveness. – P2461. The 29th Congress of Clinical Microbiology & Infectious Diseases, 13-16 April 2019, Amsterdam, the Netherlands. (Особистий внесок здобувача: тези і доповідь засновані на результатах отриманих здобувачем або під його керівництвом, здобувач написав тези конференції та безпосередньо представив стендову доповідь).

18. **Moshynets O**., Babenko L., Foster, J., Kosakivska I., Iungin O., Potters G., Rogalsky S., Jerdan R., Bamanga, R, Spiers A. The quorum-signal N-hexanoyl-L-homoserine lactone applied as a winter wheat seed primer has a phytostimulative effect. – 166 B. 17th Symposium of International Society on Microbial Ecology, ISME, 12-17 August 2018, Leipzig, Germany. (Особистий внесок здобувача: тези і доповідь засновані на результатах отриманих

здобувачем або під його керівництвом, здобувач написав тези конференції та безпосередньо представив стендову доповідь).

19. **Moshynets O.,** Bardeau J.F., Tarasyuk O., Makhno S., Cherniavska T., Dzhuzha O., Rogalsky S. Antibiofilm activity of polyamide 11 modified with cationic biocide. – P2085. The 28th European Congress of Clinical Microbiology and Infectious Diseases, 21 - 24 April 2018, Madrid, Spain. (Особистий внесок здобувача: тези і доповідь засновані на результатах отриманих здобувачем або під його керівництвом, здобувач написав тези конференції та безпосередньо представив стендову доповідь).

20. **Moshynets O**., Babenko L., Foster, J., Kosakivska I., Iungin O., Potters G., Rogalsky S., Jerdan R., Bamanga R, Spiers A. The quorum-sensing molecule N-hexanoyl-L-homoserine lactone applied in seed priming effects phytosphere microflora, chlorophyll levels and crop yield of winter wheat. – EMV30. Annual Conference 2018 of the Association for General and Applied Microbiology, VAAM 2018, March 17-20, Wolfsburg, Germany. (Особистий внесок здобувача: тези і доповідь засновані на результатах отриманих здобувачем або під його керівництвом, здобувач написав тези конференції та безпосередньо представив стендову доповідь).

21. **Moshynets O**., Rogalsky S., Iungin O., Voychuk S., Tarasyuk O., Potters G. Cationic biocides as potential antifouling agents for polymeric coatings/plastic systems. Annual Conference 2018 of the Association for General and Applied Microbiology, VAAM 2018, March 17-20, Wolfsburg, Germany. (Особистий внесок здобувача: тези і доповідь засновані на результатах отриманих здобувачем або під його керівництвом, здобувач написав тези конференції та безпосередньо представив стендову доповідь).

22. **Moshynets O.,** Babenko L., Karakhim S., Kharkhota M., Kosakivska I., Rogalsky S., Shcherbatiuk M., Suslova O., Spiers A. N-acyl-L-homoserine lactones are inter-kingdom signalling molecules controlling quorum sensing in the Gram-negative bacteria and priming plants increasing stress adaptation. P.5.4-035, Abstract of the 42-nd Congress of Federation of European Biochemical Societies, Jerusalem, Israel; 10–14 September 2017. (Особистий внесок здобувача: тези і доповідь засновані на результатах отриманих здобувачем або під його керівництвом, здобувач написав тези конференції та безпосередньо представив стендову доповідь).

23. **Moshynets O.,** Rogalsky S., Irodov D., Karakhim S., Tarnavsky S., Kharhota M., Volynets G., Spiers A. *Pseudomonas fluorescens* SBW25 uses N-octanoyl-L-homoserine lactone as a quorum sensing molecule. Abstract No 691 of the 7th Congress of European Microbiologists, July

9-13, 2017, Valencia, Spain. (Особистий внесок здобувача: тези і доповідь засновані на результатах отриманих здобувачем або під його керівництвом, здобувач написав тези конференції та безпосередньо представив стендову доповідь).

24. Babenko L.M., Rogalsky S.P., Suslova O.S., Shcherbatiuk M.M., Kosakivska I.V., **Moshynets O.V.** The quorum-sensing molecule N-hexanoyl-L-homoserine lactone used for presowing wheat seed priming reveals phytostimulated activity and affects the rhizosphere microflora. Book of Abstracts of the 14th Symposium on Bacterial Ecology and Genetics, 4-8 June 2017, Aberdeen, UK. – P.102-103. (Особистий внесок здобувача: тези і доповідь засновані на результатах отриманих здобувачем або під його керівництвом, здобувач написав тези конференції та безпосередньо представив стендову доповідь).

25. **Moshynets O.V**., Rymar S.Y., Rogalsky S.P., Kisyl N.P., Spiers A.J. Biocides as a causative agent of the emergence of pan-drug resistance: biocidal effects on DNA structure and biological activity. The 27th European Congress of Clinical Microbiology and Infectious Diseases, 22 - 25 April 2017, Vienna, Austria. (Особистий внесок здобувача: тези і доповідь засновані на результатах отриманих здобувачем або під його керівництвом, здобувач написав тези конференції та безпосередньо представив стендову доповідь).

26. **Moshynets O.V.,** Rogalsky S., Karakhim S.O. Spiers A.J. Evidence of quorum sensing in the biofilm-forming soil and plant-associated *Pseudomonas fluorescens* SBW25. Biofilms 7, 26-28 June 2016, Porto, Portugal – P1: 62. (Особистий внесок здобувача: тези і доповідь засновані на результатах отриманих здобувачем або під його керівництвом, здобувач написав тези конференції та безпосередньо представив стендову доповідь).

27. Protasov A., Bardwau J.F., MorozovskayaI., Guryanova G., Metelytsia L., Kalashnikova L., Kopernyk I., Kipnis L., Tarasyuk O., **Moshynets O**., Rogalsky S. New antifouling coating containing polymeric biocide polyhexamethylene guanidine molybdate. 18th International Congress on Marine Corrosion and Fouling, 19-24 June 2016, Toulon, France – P.219. (Особистий внесок здобувача: тези і доповідь засновані на результатах отриманих здобувачем або під його керівництвом, здобувач написав тези конференції та безпосередньо представив стендову доповідь).

28. **Moshynets O.V**., Rogalsky S.P., Babenko L.M., Shcherbatiuk M.M., Spiers A.J. Quorum sensing in Gram-negatives: from a biofilm to the plant immunity. II International Scientific Conference “Microbiology and Immunology – the development outlook in the 21st century”, 14-

15 April 2016, Kiev, Ukraine. (Особистий внесок здобувача: тези і доповідь засновані на результатах отриманих здобувачем або під його керівництвом, здобувач написав тези конференції та безпосередньо представив стендову доповідь).

29. **Moshynets O**., Rogalsky S., Bellenberg S., Boretska M., Irodov D., Kararhim S., Spiers A. *Pseudomonas fluorescens* SBW25 uses two signaling pathways utilizing N-acylhomoserine lacton and alpha-hydroxy ketones. Proceedings of the 6th FEMS2015, 7-11 June 2015, Maastricht, The Nitherlands. – FEMS-1379 (Особистий внесок здобувача: тези і доповідь засновані на результатах отриманих здобувачем або під його керівництвом, здобувач написав тези конференції та безпосередньо представив стендову доповідь).

30. **Moshynets O.**, Rogalsky S., Pokholenko J., Irodov D., Kararhim S., Spiers A.J. *Pseudomonas fluorescens* SBW25 reveals AHL-dependent quorum sensing behaviour in culture and biofilms. Proceedings of the Biofilms 6, International Conference on Microbial Biofilms, 11-13 May 2014, Vienna, Austria. – P. 46.